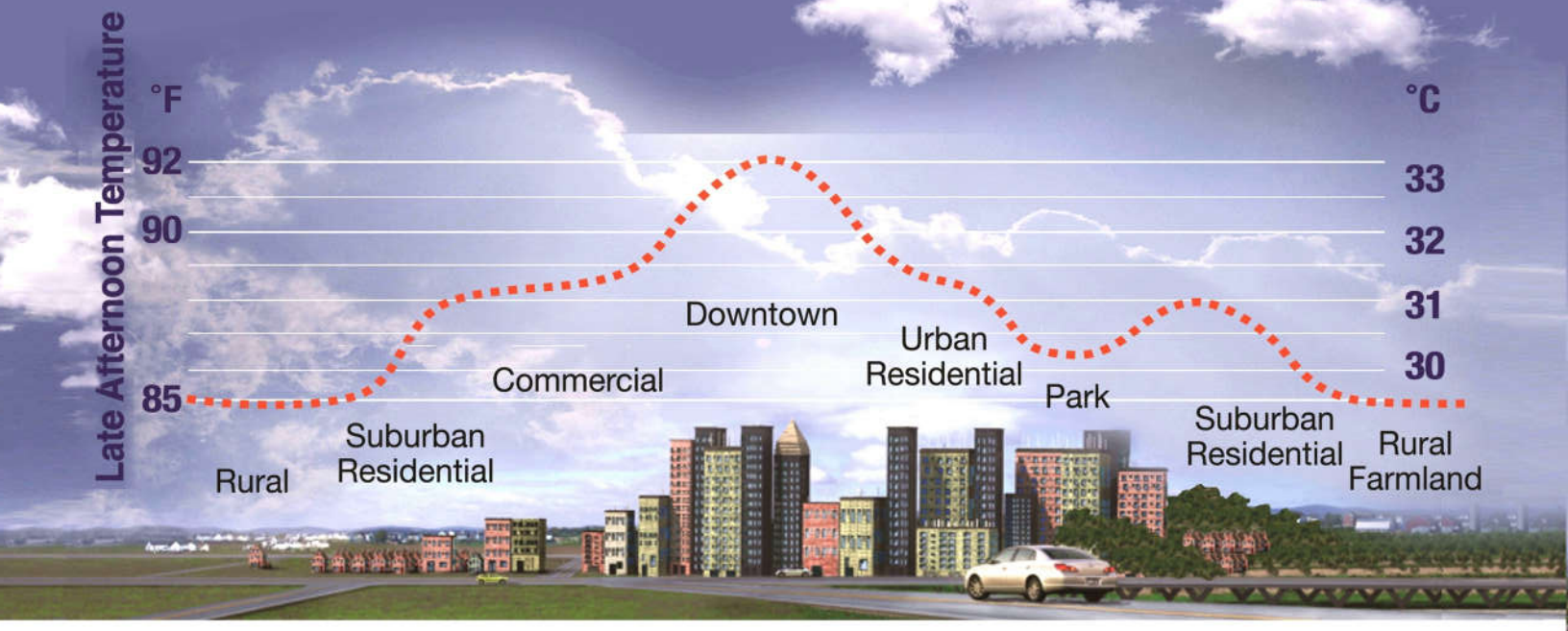
5th International Conference on Countermeasures to Urban Heat Islands

02-04 December 2019

Conference Proceedings



IC2UHI 2019

International Institute of Information Technology Hyderabad
Hyderabad

Editors: Hashem Akbari, Vishal Garg, Jyotirmay Mathur, Vaibhav Rai Khare

Conference Proceedings of
5th International Conference on Countermeasures to Urban Heat Islands (IC2UHI 2019)

December 2-4, 2019

Editors:

Hashem Akbari

Vishal Garg

Jyotirmay Mathur

Vaibhav Rai Khare

Organized by:

International Institute of Information Technology,

Professor CR Rao Rd, Gachibowli,

Hyderabad, Telangana 500032.

Conference Proceedings of 5th International Conference on Countermeasures to Urban Heat Islands (IC2UHI 2019)

No part of this publication may be reproduced, stored in a retrieval system, or transmitted, in any form or by any means, without prior permission. The views and contents of this book are solely of the authors. Moreover, in the event, the authors have been unable to track any source and if any copyright have been inadvertently infringed, please notify the publisher in written for corrective action.

© Cover page Image credit "Heat Island Group, Lawrence Berkeley National Laboratory"

Disclaimer

The publisher and Organisers do not claim any responsibility for the accuracy of the data, statements made, and opinions expressed by authors. The authors are solely responsible for the contents published in the paper.

International Standard Book Number:

***Published by*:**

BS Publications

A unit of **BSP Books Pvt., Ltd.**
4-4-309/316, Giriraj Lane,
Sultan Bazar, Hyderabad - 500 095.
Phone :040 - 23445688
e-mail :info@bspbooks.net
www.bspbooks.net

© 2019 International Institute of Information Technology Hyderabad, India

Editors

Hashem Akbari is a professor in Building, Civil, and Environmental Engineering at Concordia University, Canada. Before joining Concordia University, he was a senior scientist and the leader of the Heat Island Group at the Environmental Energy Technologies Division of Lawrence Berkeley National Laboratory (LBNL). He is a founder of the Urban Heat Island (UHI) group, where he worked in the areas of heat-island quantification, mitigation, and novel techniques in the analysis of energy use in buildings and industry. Prof. Akbari mostly deals with roofs, meteorology, urban heat island, reflective surfaces, and environmental engineering. He has done ground-breaking research on the potential for cool roofing and paving materials to reduce the urban heat islands effect and quantified the effect of cool roofs on cooling the globe. He is one of the founding organizers of the Global Cool Cities Alliance (vice-Chairman of the Board, Technical committee chair), the Cool Roof Rating Council (CRRC), and the European Cool Roof Council (ECPR).

Vishal Garg is a professor and head of the Center for IT in Building Science at the International Institute of Information Technology (IIIT), Hyderabad, India. His current research interests are in the areas of energy simulation and cool roofs. He teaches building automation and controls, energy simulation, and lighting design and technology. He has conducted several national and international workshops on intelligent buildings, green buildings, and energy simulation. He holds a BTech (Hons.) degree in civil engineering from MBM Engineering College, Jodhpur, India, and a Ph.D. from the Indian Institute of Technology, Delhi, India. Prof. Garg is actively involved in the green building movement and in developing eTools for advancing energy efficiency in buildings and energy efficiency building code and its implementation. He was the founding president of the Indian chapter of the International Building Performance Simulation Association (IBPSA) and chaired the organizing committee of the International Conference for Building Simulation 2015. He is a fellow of IBPSA and received the inaugural Arthur H. Rosenfeld Urban Cooling Achievement Award in 2018.

Jyotirmay Mathur is a professor of mechanical engineering and the founding head of the Centre for Energy and Environment at Malaviya National Institute of Technology, Jaipur, India. He has done postgraduate work in energy studies at the Indian Institute of Technology, Delhi, India, and has received a doctorate in energy systems from the University of Essen, Germany. Prof. Mathur has supervised 20 Ph.D. theses, published more than 100 research papers in referred international journals and has presented more than 150 papers/talks in international conference, besides authoring/editing 8 books in the field of energy, besides holding two patents for his innovations in the field of energy. Prof. Mathur works in the field of energy planning & modelling, codes and standards, energy conservation in buildings, passive cooling, adaptive thermal comfort, and building integrated photovoltaic systems.

Vaibhav Rai Khare is working as a Manager at Environmental Design Solutions, New Delhi. His work experience includes in different sectors of energy including energy modelling and CFD simulation, passive cooling, thermal comfort, and energy policy advocacy. He is post graduate in Energy Engineering from MNIT Jaipur and has published several research publications in international journals and conferences. Vaibhav is also focused on sustainability education and delivered several lectures and training. He worked as a scientific and organizing committee in various prestigious international conferences such as IBPSA BS2015, and INSPIRE2017. Vaibhav is acting as a secretary of ISHRAE Technical group 'Thermal Comfort' and a founder & board member of the Indian chapter of the International Building Performance Simulation Association (IBPSA) society.

Executive Scientific Committee

Hashem Akbari (Chair)	Concordia University, Canada
Jyotirmay Mathur (Co-Chair)	Malaviya National Institute of Technology Jaipur, India
Afroditi Synnefa	UNSW Sydney NSW, Australia
Alberto Muscio	Università di Modena e Reggio Emilia, Italy
Anna Laura Pisello	Università degli Studi di Perugia, Perugia, Italy
Costas Cartalis	University of Athens, Greece
Denia Kolokotsa	Technical University of Crete, Kounoupidiana
Edward Ng	Chinese University of Hong Kong, China
Elena Morini	Università degli Studi di Perugia
Federico Rossi	University of Perugia, Italy
Haley Gilbert	Consultant, USA
Hee Joo Poh	Institute of High-Performance Computing, Singapore
Hideki Takebayashi	Kobe University, Japan
Krishna Prapoorna Billigiri	Indian Institute Technology - Tirupati, India
Kurt Shickman	Global Cool Cities Alliance, USA
Manju Mohan	Indian Institute Technology - Delhi, India
Masayuki Ichinose	Tokyo Metropolitan University, Japan
Mat Santamouris	University of New South Wales, Australia
Michele Zinzi	National Agency for New Technologies, Italy
Mohd Fairuz Shahidan	Universiti Putra Malaysia
Nyuk Hien Wong	National University of Singapore, Singapore
Paul Osmond	University of New South Wales, Australia
Rajan Rawal	CEPT University, India
Ronnen Levinson	Lawrence Berkeley National Laboratory, USA
Shady Attia	University of Liège, Belgium
Sheikh Ahmad Zaki	Universiti Teknologi, Malaysia
Steffen Lehmann	Curtin University, Australia
Steve Kardinal Jusuf	Singapore Institute of Technology, Singapore
Vishal Garg	International Institute of Information Technology Hyderabad, India
Wan Man Pun	Nanyang Technological University, Singapore
Yasunobu Ashie	Building Research Institute, Japan
Yupeng Wang	Xi'an Jiaotong University, China

Organizing Committee

Conference Chair:
Prof. Hashem Akbari,
Concordia University, Montreal, Canada

Organizing Chair:
Prof. Vishal Garg,
International Institute of Information Technology Hyderabad, India

Scientific Co-chair:
Prof. Jyotirmay Mathur,
Malaviya National Institute of Technology Jaipur, India

Secretary - Organizing Committee:
Ms. Sraavani Gundepudi,
International Institute of Information Technology Hyderabad

Secretary - Scientific Committee:
Mr. Vaibhav Rai Khare,
Environmental Design Solutions, New Delhi

Members:

Ashok Lall	Ashok B Lall Architects, New Delhi
Anubhav Tiwari	CIE, International Institute of Information Technology, Hyderabad
Aviruch Bhatia	TERI School of Advanced Studies, New Delhi
Hema Rallapalli	Geetam University, Hyderabad
Krishan Kumar	Jawaharlal Nehru University, Delhi
M Anand	Indian Green Building Council, Hyderabad
Neetu Jain	Panache Green, Ahmedabad
Rajan Rawal	CEPT University, Ahmedabad
Rajashree Kotharkar	Visvesvaraya National Institute of Technology, Nagpur
Rajkiran Bilolikar	Administrative Staff College of India, Hyderabad
Sam Babu Godithi	International Institute of Information Technology, Hyderabad
Shivraj Dhaka	Indian Green Building Council, Jaipur
Srinivas Cherukupalli	Dupont, Hyderabad
Shrishty Srivastava	Jawaharlal Nehru Architecture and Fine Arts University, Hyderabad
Tanmay Tathagat	Environmental Design Solutions, New Delhi

Hosted by:
IIIT Hyderabad, India
Venue: IIIT Hyderabad, Gachibowli, India

Preface

An urban heat island (UHI) is an urban area that is significantly warmer than its surrounding rural areas due to human activities. The temperature difference is usually larger at night than during the day and is most apparent when winds are weak. This UHI leads to an increase in energy consumption, elevated emissions of air pollutants and adversely impacts human health and comfort, especially of urban poor.

This conference proceedings contains the accepted version of papers presented during the fifth International Conference on Countermeasures to Urban Heat Islands (IC2UHI 2019), which was held at International Institute of Information Technology Hyderabad, India during December 2-4, 2019. Earlier conferences were held in Tokyo, Berkeley (California), Venice, and Singapore. This conference was devoted to science, engineering, and public policies to help relieve the excess heat and air pollution of Summers in hot cities. The objective of the conference was to bring the academicians, researchers, industrialists, and experts under one roof to present and discuss the latest research on countermeasures to urban heat islands.

The conference was inaugurated by Mr. Arvind Kumar, IAS, Principal Secretary, Municipal Administration & Urban Development (MA&UD). Mr. Kumar shared some of Telangana government's countermeasures for reducing urban heat islands, such as the Ministerial Act whereby each of the State's 33 districts shall have a year-wise green action plan for all urban local bodies (ULB) within the district for the next 5 years. Each ULB should have a nursery, and 10 % of the budget has been earmarked for green budget as the first charge, should conduct water audits and reduce non-revenue water to its minimum. Also, town planning has been taking necessary action to fix traffic and infrastructure and the State is encouraging the setting up and development of integrated townships. He also stressed the importance of every individual to be personally invested in countering urban heat islands and doing their bit for the environment.

This conference brought together around 120 delegates from different parts of the world. There was significant participation from students in the conference. During the conference, 3 distinguished keynote speakers had delivered their research works and insights in various fields of UHI. There were 95 oral presentations and 6 case studies presented over ten different tracks in four parallel sessions which brought a great opportunity to share the knowledge and research work among each other.

There were 3 keynote addresses by distinguished speakers from the USA and India. Prof. David Sailor, Arizona State University, USA presented a keynote lecture on "Moving beyond UHI - Is the urban heat island concept too limiting to solve urban climate changes". The second keynote lecture was given by Dr. Ronnen Levinson, LBNL, USA on "Seizing the decade - Cool initiatives for the 2020s from the Berkeley heat island group". The third keynote lecture was presented by Mr. Tanmay Tathagat, Environmental Design Solutions, India on "Policy and programs for mitigating UHI - Perspective from India".

Apart from the paper presentations, two panel discussions on 'Identifying and bridging UHI countermeasure technology gaps' and 'Creating better spaces - Conversations on climate change and health' followed by one open session on 'UHI mitigation initiatives in India' was conducted during the conference. The open session included an international case study from Los Angeles on cool pavements, session on UHI mitigation initiatives in India and a panel discussion on UHI implementation challenges in India.

The presented papers covered topics including Analysis and modelling of UHI; Vegetation; Outdoor thermal comfort; Cool materials; Policies, rating & labelling programs for UHI. A summary of the number of presented papers from different tracks are presented below:

Tracks	**No. of Papers**
Analysis of UHI and its effect across scales	20
Cool material development and characteristics	10
Implementation on urban heat mitigation strategies	10
Measurement techniques and standards	5
Modelling and forecasting urban climate and weather	5
Outdoor comfort and health in the urban environment	17
Policies, rating & labelling Programs with UHI mitigation strategies	3
Remote sensing of cities and urban climates	5
Resilient design of buildings in response to changing climates	5
Urban economy	5
Urban vegetation and greenery	10

Some presented papers have been selected for the submission of special issues for two journals 'Urban Climate' and 'Energy & Buildings' based on the quality, novelty, and context. Both journals are peer reviewed Scopus indexed journals which target the scientific and research communities related to urban climate conditions, technological & environmental dynamics, and global change. Total number of 25 original research papers are published under both special issues out of which 19 papers are an extended version of conference papers and the rest of the papers were directly submitted into the special issue. The papers selected in these special issues are from the areas of Cool materials; Outdoor thermal comfort; Policies, rating & labelling programs for UHI; and Implementation of UHI mitigation strategies.

The papers in the conference proceedings are categorized as per the conference tracks. Papers which got published in the journal special issue are not included in the conference proceedings. Only abstract and the link of such papers have been included. We would like to thank 'Energy and Buildings' and 'Urban Climate' journals and Elsevier publisher for publishing special issues into their journals and allowing us to reproduce the abstract in this conference proceedings.

At the end, we would like to thank all participants for their contributions to the Conference program and for their contributions to these Proceedings. Our special thanks go to the scientific committee for their devoted assistance to reviewing the paper in the conference.

From:

Hashem Akbari
Vishal Garg
Jyotirmay Mathur
Vaibhav Rai Khare

Editors, IC2UHI2019 Conference Proceedings

List of Papers

Manuscript Title	Pages
Track - Analysis of UHI and its Effect across Scales	
Effects of Heat Island Mitigation on Heat-Related Mortality in Montreal during Heat Wave Periods of 2005, 2011 and 2018 *Zahra Jandaghian, Hashem Akbari*	2-11
Urban heat island and bioclimate studies in Freiburg, Germany *Andreas Matzarakis*	12-21
Study on appropriate ground cover configuration of open spaces to mitigate urban heat island effect *Yuvraj P. Meshram, Shirish A. Deshpande, Sheeba Valsson*	22-34
Improving the accuracy of simplified urban canopy models for arid regions using site-specific prior information *Afshin Afshari, Nicolas Ramirez*	35
Assessment of surface urban heat island and urban cooling effect based on downscaled LST, a case study of Fukuoka prefecture, Japan *Wangchongyu Peng, Rui Wang, Wei Chen, Lilei Zhou, Weijun Gao, Yingjun Ruan*	36-45
Urban features at neighborhood scale to assess and mitigate the heat island in arid Mendoza, Argentina *María Belén Sosa, Erica Correa, Michele Zinzi*	46-56
Development and Application of “Shadow Ratio” for Evaluating Urban Thermal and Wind Environment - Take a Site of Xi 'an West Street as an Example *Yuheng Lyu, Dian Zhou, Yupeng Wang*	57-67
Thermal Studies of a mid-latitude Urban Environment *Roger Clay, Huade Guan*	68-77
Monitoring the urban heat island effect and the efficacy of future countermeasures in the Los Angeles Basin *Ronnen Levinson, George Ban-Weiss, Sharon Chen, Haley Gilbert, Howdy Goudey, Joseph Ko, Yun Li, Arash Mohegh, Angie Rodriguez, Jonathan Slack, Haider Taha, Tianbo Tang, Jiachen Zhang*	78-87
Impact Analysis of Deep Static Blue space on Urban Heat Island: Case of Chandigarh *Aditya Rahul, Mahua Mukherjee*	88-97
Evaluating urban heat island due to built morphology in Pune city *Shruti Khandelwal, Namrata Dhamankar, Sujata Karve*	98-108
Heat Vulnerability Index for Urban Heat wave Risk Adaptation for Indian Cities: A Case Study of Akola *Rajashree Kotharkar, Sahil Aneja, Aveek Ghosh*	109-130
Extent vs. Impact: A modeling study of Targeted Heat Mitigation Strategies *David J. Sailor, Peter J. Crank, Jannik Heusinger, Masayuki Hara*	131-141
Conceptual Framework for Environmental City Planning Tool with an Intelligent System based on BIM and GIS Technology *Shinji Yamamura, Liyang Fan, Yupwng Wang, Dian Zhou*	142-151

Manuscript Title	**Pages**
Characteristics of micro weather stations distributions for urban heat island monitoring and corresponding thermal mapping *Tzu-Ping Lin, Taiwan Yu-Cheng Chen*	152-162
Assessment of variation in Intra Canopy Layer Urban Heat Island Intensity in Residential areas --- A case study of Nagpur City *Sujata Godbole, Ravikumar Bhargava*	163-173
Satellite based observations for Surface level Urban Heat Island over Bhubaneswar: A case study *Dudam Bharath Kumar*	174-182
Land surface temperature variations: Case study Bhopal (M.P.) *Pallavi Tiwari, Arka Kanungo*	183-192
Evaluation of sleep disorder caused by urban heat island based on the Pittsburgh Sleep Quality Index *Tomohiko Ihara, Daisuke Narumi, Sanae Fukuda, Hiroaki Kondo*	193-202
Evaluation of the Daily Cycle of UHI using Multi-site Measurements in a Central European Capital City *Rita Pongrácz, Judit Bartholy, Zsuzsanna Dezső, Csenge Dian, Dóra Incze, Eötvös Loránd, Máté Kurcsics*	203-210
Track - Cool Material Development and Characteristics	
Quantum Dots: A New Generation of Fluorescent Materials for UHI Mitigation *Samira Garshasbi, Shujuan Huang, Mat Santamouris*	212-220
The evaporative cooling and its impact on the urban climate: study of the influence of road covering materials *Sophie Parison, Martin Hendel, Arnaud Grados, Laurent Royon*	221-230
Development of heterogeneous directionally reflective materials for building facade and measurements of their reflective properties *Chiara Ferrari, Riccardo Paolini, Alberto Muscio, Mat Santamouris*	231-241
Potential of switching cool materials to optimize the thermal response of residential buildings in the Mediterranean region *Michele Zinzi, Stefano Agnoli, Giulia Ulpiani, Benedetta Mattoni*	242
Black Titanium Dioxide: An Innovative Material to minimize the Urban Heat Island Effects in Walled city of Jaipur *Prasanna Bhangdia, Tarush Chandra, Pooja Nigam*	243-252
Analysis of the heat budget of standard, cool and watered pavements under lab heat-wave conditions *Sophie Parison, Martin Hendel, Arnaud Grados, Laurent Royon*	253
Numerical Analysis of Human Thermal Load Affected by Solar Reflection Characteristics of Vertical Wall in Street Space *Shinichi Kinoshita, Atsumasa Yoshida*	254-260
Harnessing benefits of pervious concrete pavements: A novel UHI mitigation strategy *Poornachandra Vaddy, Avishreshth Singh, Prasanna Venkatesh Sampath, Krishna Prapoorna Biligiri*	261-269
Cool Roof initiatives in India: An evaluation of the existing conditions and lessons to be learnt from global best practices. *Hema Sree Rallapalli, Janmejoy Gupta*	270-279

Manuscript Title	**Pages**
Development of an online calculator for cool roof and green roof *Shanmukh Dontu, Vishal Garg*	280-289
Track - Implementation on Urban Heat Mitigation Strategies	
Increasing urban albedo to reduce heat-related mortality in Toronto and Montreal, Canada *Zahra Jandaghian, Hashem Akbari*	291
Potential of switching cool materials to optimize the thermal response of residential buildings in the Mediterranean region *Michele Zinzi, Stefano Agnoli, Giulia Ulpiani, Benedetta Mattoni*	292
A pavement-watering thermal model validation for SOLENE-microclimate: application to the Buire street *Marie-Hélène Azam, Auline Rodler, Marjorie Musy, Sihem Guernouti*	293-302
The Oasis Project: UHI mitigation strategies applied to Parisian schoolyards *Ghid Karam, Martin Hendel, Cécilia Bobée, Alexandre Berthe, Patricia Bordin, Laurent Royon*	303-311
Impact of Urban Heat Island formation on electricity consumption over Delhi region *Priyanka Kumari, Vishal Garg, Krishan Kumar*	312-322
Outdoor thermal comfort improvements due to innovative solar awning solutions: An experimental campaign *Federico Rossi, Marta Cardinali, Alberto Maria Gambelli, Mirko Filipponi, Beatrice Castellani, Andrea Nicolini*	323
Physical and geographic analysis of the urban cooling potential *Martin Hendel, Sophie Parison, Laurent Royon*	324-333
Effect of surface treatment and built form on thermal profile of open spaces: A case of Mumbai, India *Surabhi Mehrotra, Divya Subramanian, Ronita Bardhan, Arnab Jana*	334
Effect of UHI and Building Geometry on Pollution Dispersion in an Urban Street Canyon *Udayraj*	335-344
Controlled experiment for estimating the energy-saving potential and indoor thermal comfort improvement by the use of high albedo surfaces on pitched concrete roofs *Vishal Garg, Sraavani Gundepudi, Aviruch Bhatia, Rathish Arumugum, Sasank Bethapudi*	345-354
Track - Measurement Techniques and Standards	
IMPACT ZONATION AND MITIGATION OF UHI (……. through remote sensing & development of blue green infrastructure network) *Atul Kumar, Jagrati Sehgal, Mahua Mukherjee, Ajanta Goswami*	356-365
Green Infrastructure Strategies as Countermeasures to Urban Heat Islands with particular reference to the Bangalore Metropolitan Area *Reshmi Manikoth Kollarath, Vasseem Anjum Sheriff*	366-376
Microclimate analysis of UHI affected areas through wearable monitoring systems: the case study of New York City *Benedetta Pioppi, Ilaria Pigliautile, Anna Laura Pisello*	377

Manuscript Title	**Pages**
Local Climate Zone Classification and Seasonal Variation by using Land Surface Temperature: A case of National Capital Territory, Delhi, India *Manoj Panwar, Avlokita Agrawal, Varuvel Devadas*	378-389
"Inverted" Surface UHI: An artefact of relying solely on Satellite Remote Sensing data for measuring the Urban Heat Island Phenomenon *Prasad Pathak, Raja Sengupta, Bakul Budhiraja*	390-399
Track - Modelling and Forecasting Urban Climate and Weather	
Improving the Accuracy of Simplified Urban Models Using Actual Radiation Parameters *Afshin Afshari, Nicolas Ramirez*	401-411
Urban Heat Island Minimization, Local Climate Zones and Parametric Optimization: A "Grasshopper" Based Model *Madhuranga K.K.K.D.R.., Perera, N. G. R.*	412-421
Modeling potential air temperature reductions yielded by cool roofs and urban irrigation in the Kansas City Metropolitan Area *Seongeun Jeong, Dev Millstein, Ronnen Levinson*	422
Envelope heat load characteristics of the building cluster considering radiate heat exchange process in an urban district *Yasunobu Ashie*	423-428
Minimizing the inconsistencies of urban building energy simulations through strong microclimate coupling *Georgios – Evrystheas Kyriakodis, Emmanuel Bozonnet, Peter Riederer*	429-438
Track - Outdoor Comfort and Health in the Urban Environment	
Effect and Development of Cool Roofs: A Review *Meng ZHEN, Ru JIA, Qishu ZOU, Wei DING, Weihan ZOU, Ling WANG*	440-449
Outdoor Thermal Sensation and Thermal Comfort in Xi'an *Meng ZHEN, Ru JIA, Weihan ZOU, Wei DING, Ling WANG*	450-460
Heat Health Warning System in Germany – Implementation of city issues *Andreas Matzarakis, Stefan Muthers*	461-468
Thermal sensation and thermal load of human body in irradiated hot environment *Atsumasa Yoshida, Takuma Naka, Narihisa Chigusa, Shinichi Kinoshita*	469
Comprehensive evaluation of the influence of outdoor temperature change on health around the urban area *Daisuke Narumi, Tomohiko Ihara, Sanae Fukuda, Yoshiyuki Shimoda*	470-479
The effects of commuter travel behavior on transportation heat and pollution emissions *Man Li, Yupeng Wang, Jun Zhou*	480-489
Quantitative outdoor thermal comfort assessment of street: A case in a warm and humid climate of India *Brinda Deevi, Faiz Ahmed Chundeli*	490
Outdoor Thermal Comfort Implications of Planning and Building Regulation Induced Canyon Geometry *Hepsheba, J. J., Perera, N. G. R.,Emmanuel, R.*	491-500

Manuscript Title	**Pages**
Study on the Microclimate Effect of Water Body Form in Urban Square *Ziyu Tong, Cong Zhang, Juelun Zhou*	501-510
Urban micro-climate and spatial promotion for creating the historical streets' sustainability *Zheyang Fei, Yupeng Wang, Man Li*	511-521
Modelling the influence of high-rise urban geometry on outdoor thermal comfort in Singapore *Juan Angel Acero, Elliot J.Y. Koh, Lea A. Ruefenacht, Leslie K. Norford*	522
Experimental evaluation of thermal comfort improvement due to innovative solutions for tensile structures *Federico Rossi, Mirko Filipponi, Beatrice Castellani, Andrea Nicolini, Marta Cardinali, Alberto Maria Gambelli*	523-531
Local scale climate change assessment for preservation of cultural heritage sites and their resilience, the case study of Gubbio medieval city in Italy *Benedetta Pioppi, Ilaria Pigliautile, Mauro Felli, Cristina Piselli, Anna Laura Pisello, Franco Cotana*	532-541
Effectiveness of UHI mitigation strategies for outdoor thermal comfort enhancement *Ilaria Pigliautile, Anna Laura Pisello, Elie Bou-Zeid*	542-549
Effects of the Green Façade on Thermal Comfort in the Transitional Spaces: Field Measurements in Munich, Germany *Hankun Lin, Ata Chokhachian, Florian Musso, Yiqiang Xiao*	550-559
Summertime Thermal Comfort Assessment for Compact Local Climate Zone *Rajashree Kotharkar, Shweta Deshmukh*	560-571
Effect of urban morphology on urban microclimate: a case of Vijayawada *Ar.Madhavan Rajan, D.Kannamma*	572-578
Track - Policies, Rating & Labelling Programs with UHI Mitigation Strategies	
Solar-reflective "cool" walls: benefits, technologies, and implementation *Ronnen Levinson, George Ban-Weiss, Paul Berdahl, Sharon Chen, Hugo Destaillats, Nathalie Dumas, Haley Gilbert, Howdy Goudey, Sébastien Houzé de l'Aulnoit, Jan Kleissl, Benjamin Kurtz, Yun Li, Yan Long, Arash Mohegh, Matteo Pizzicotti, Pablo Rosado, Marion Russell, Jonathan Slack, Xiaochen Tang, Jiachen Zhang, Weilong Zhang*	580-590
Review of heat wave studies and related urban policies in South Asia *Rajashree Kotharkar, Aveek Ghosh*	591
A Big Picture of Urban Heat Island Mitigation Strategies and Recommendation for India *Vaibhav Rai Khare, Akash Vajpai, Durva Gupta*	592
Track - Remote Sensing of Cities and Urban Climates	
Assessment of urban cooling effect based on downscaled land surface temperature: A case study for Fukuoka, Japan *Wangchongyu Peng, Xin Yuan, Weijun Gao, Rui Wang, Wei Chen*	594
Urban surfaces analysis with remote sensing data for the evaluation of UHI mitigation scenarios *Francesca Despini, Chiara Ferrari, Giulia Santunione, Stefano Tommasone, Alberto Muscio, Sergio Teggi*	595
Relationship Between Urban Land Use Dynamics and Land Surface Temperature: Current and Future Scenario Modeling *Nimish G., Chandan M. C., Bharath H. A*	596-606

Manuscript Title	**Pages**
Land surface temperature responses to land use dynamics across the agro-climatic zones of Karnataka *Ramachandra TV, Bharath Setturu, Madhumita Dey*	607-615
Spatial and Temporal Nature of Urban Heat Island in Roorkee *Siva Ram Edupuganti, Arjun Satheesh, Mahua Mukherjee*	616-629
Track - Resilient Design of Buildings in Response to Changing Climates	
Study of adaptive city by Osaka Heat Island Countermeasure Technology Consortium *Hideki Takebayashi, Masakazu Moriyama*	631-640
"Cradle to Gate" assessment of material related embodied carbon: A design stage stratagem for mid-rise housing in Sri Lanka *Ashan S Jayawardana, Narein G R Perera, L S Ranjith Perera*	641
The resilient design for traditional residential building in Northern Shaanxi of China *Sunwei Liu, Yupeng Wang, Yitong Kang*	642-651
The Resilient Design for Small Commercial Building – A Case in City Center of Gifu, Japan *Yitong Kang, Dian Zhou, Yupeng Wang, Sunwei Liu*	652-661
Assessing resilience to summertime overheating in modern low energy flats in UK *Rajat Gupta*	662-671
Track - Urban Economy	
Health and energy benefits of urban overheating mitigation counteracting climate change *Riccardo Paolini, Samira Garshasbi, Shamila Haddad, Mattheos Santamouris*	673-682
Use Urban Green as a Mitigation Strategy to Combat Urban Heat Island Effect: A Case of Puri-Cuttack Road, Bhubaneswar, Odisha *Sukanya Dasgupta, Nilanjana Roy, Dudam Bharath Kumar*	683-692
Spatiotemporal Characteristics of Anthropogenic Heat and Its Impact on Outdoor Thermal Environment in a University in Chongqing *Zhongyu Hao*	693-702
Climate-Informed Decision-Making for Urban Design: Assessing the Impact of Urban Morphology on Urban Heat Island *Luis G. R. Santos, Ido Nevat, Gloria Pignatta, Leslie K. Norford*	703
Climate change and infrastructure risk: Indoor heat exposure during a concurrent heat wave and blackout event in Phoenix, Arizona *Brian Stone, Evan Mallen, Mayuri Rajput, Ashley Broadbent, E. Scott Krayenhoff, Godfried Augenbroe, Matei Georgescu*	704
Track - Urban Vegetation and Greenery	
Influence of urban green on human thermal bioclimate – Application of thermal indices and micro scale models *Andreas Matzarakis, Marcel Gangwisch, Dominik Fröhlich*	706-715
Assessment of terrace gardens as modifiers of building microclimate *Chitra Chidambaram, Pranjali Varshney, Sakshi Kumar, Surabhi S. Nath*	716-724

Manuscript Title	**Pages**
The seasonal thermal environment in urban park and surrounding urban spaces: A case study in Xi'an, China *Dixuan Ma, Yupeng Wang, Zongzhou Zhu*	725-735
Study of the thermal behaviour of unplanted extensive green roof sample according to the nature of the substrat *Chaumont Maxime, Parison Sophie, Hendel Martin, Royon Laurent*	736-744
Study Of Urban Morphology and Its Impact on Microclimate of Surrounding Area Case Study – S.B. Road, Pune *Prathama Jhaveri, Namrata Dhamankar, Sujata Karve*	745-754
A study on Park Cooling Island Effect on Surrounding Urban Area, in urban design perspective *Tong Wu, Shuowen Chi, Youpei Hu*	755-768
Surface temperature reduction by tree shade: Influence of tree characteristics *Andrew Speak, Leonardo Montagnani, Camilla Wellstein, Stefan Zerbe*	769-779
Sustainable Landscaping Initiatives in Three Educational Institutions in India *Mohan Kotamrazu*	780-788
High albedo plant selection for mitigation of the urban heat island *Giulia Santunione, Chiara Ferrari, Alberto Muscio*	789-799
A Comparative empirical assessment of native deciduous and evergreen trees on carbon stock potential for regulating ecosystem services in tropical dry evergreen forest, Coromandel coast, Tamil Nadu, India *Parisutha Rajan Alphonse Marianadin, Minakshi Jain, Abdul Razak Mohamad*	800-806

ANALYSIS OF UHI AND ITS EFFECT ACROSS SCALES

Effects of Heat Island Mitigation on Heat-Related Mortality in Montreal during Heat Wave Periods of 2005, 2011 and 2018

Zahra Jandaghian, Research Assistant at Ryerson University
Hashem Akbari[1], Professor at Concordia University (Canada)

ABSTRACT

Heat-related mortality (HRM) is increasing as a result of climate change leading to extreme heat events. Increasing surface reflectivity is applied to mitigate the effects of heat island and high temperature in urban areas. The Weather Research and Forecasting model (WRF) is coupled with a multi-layer of the Urban Canopy Model (ML-UCM) to investigate the effects of heat island mitigation strategy during the 2005, 2011 and 2018 heat wave periods in the Greater Montreal Area (GMA). Three indicators are applied to translate the effects of extreme heat events and the potential of albedo enhancement on HRM rates: air mass type, air temperature and apparent temperature changes for each day of simulations. Using the Spatial Synoptic Classification (SSC) indicates that the moist tropical plus and dry tropical weather have the highest rank in HRM. The non-accidental mortality data during summer period are employed. The heat-induced mortality correlations are defined on daily basis based on consecutive days of the heat wave events, the day in summer season and apparent temperature in ^{o}C. The albedo of roofs, walls and ground increased from 0.2 by 45%, 40% and 25%, respectively. The beneficial contributions of albedo enhancement are a decrease in daily averaged temperature by nearly 1°C and an increase in daily averaged dew point temperature by 0.4^{o}C. Heat island strategy shift days into less oppressive air masses by 50%. The heat-related death will decrease by at least 3 to 5%, meaning that seven to twelve lives could be saved during these heat wave events.

INTRODUCTION

The rate of heat-related mortality is increasing in urban areas because of the impacts of heat island phenomenon. Climate change poses extreme heat events and magnifies the frequency and duration of urban heat island (UHI). Urban heat island intensity causes an increase in morbidity and mortality (Jenkins et al., 2014; Horton et al., 2014 and Hajat et al., 2010). The combination of extreme heat wave events and UHI leads to higher ambient temperatures, causing heat stress for urban dwellers. High temperature is responsible for the heat-related mortality increments in cities around the globe (Basu 2009). In North America, around 700 deaths are categorized as directly linked to high temperatures annually (Center for Disease Control and Prevention 2013). But it is presumed that the total number of heat-related death is even higher because mortality can also be classified under other natural causes, for instant air pollution. The indirect effect of UHI is to increase photochemical reaction rates and thus worsen air quality.

Epidemiological studies show a positive correlation between extreme air temperature and mortality (Diaz et al., 2002 and O'Neill et al., 2009; Jandaghian and Akbari, 2016). Urban areas absorb and trap heat because of high thermal mass and low ventilation, and thus the residence is at great risk (Diaz et al., 2002). Heat-related mortality is increased by 4.5% per degree Celsius and by 0.4% per day in heat wave periods in North America (Anderson and Bell, 2009). In another study, mortality increases by 3.6% per degree Celsius increase in temperature in the United State

[1]Corresponding Author: Hashem.Akbari@Concordia.ca, Heat Island Group, Building, Civil and Environmental Engineering Department, Concordia University Montreal, QC H3G 1M8, Canada.

(Zanobetti et al., 2014) and by 4.6% per degree Celsius rise in apparent temperature (Basu and Samet, 2002). A research indicated that the mortality rates rise as temperatures reach beyond human comfort zone and in the future with the advance of heat wave events the number of heat-death will increase more comparing to cold-death (McMichael et al., 2006).

To mitigate the adverse effects of heat waves and heat island in urban areas, increasing surface albedo can be applied in local and global scales (Akbari et al., 2009; Oleson et al., 2011; Ban-Weiss et al., 2015; Taha 2009). The albedo of roofs or pavements range from 0.1 to 0.2 but can be even higher because of the use of reflective materials (Akbari et al., 2002 and 2016). Jandaghian et al. (2017) showed that by increasing surface albedo, air temperature decreases by 0.2°C, wind speed slightly increases, relative humidity and precipitation respectively decrease by 2.8% and 0.2 mm in Greater Montreal Area (GMA) in 2009. Jandaghian and Akbari (2018a) also showed that increasing surface albedo in Sacramento, Houston and Chicago result in a decrease in air temperature by 2.3°C in urban areas and 0.7°C in suburban areas; a slight increase in wind speed; an increase in relative humidity (3%) and dew point temperature (0.3°C), respectively.

The Statistics Canada reveals that heat-related death reached to 158-people over a decade. The Canadian Environment Health Atlas (CEHA, 2018) estimates that in Montreal 121 people die each year because of high temperature. In another study, the number of heat-related deaths was estimated to be 209 people during the July 2010 heat wave period in Montreal (Bustinza et al., 2013). More than 90 heat-related death is linked to three consecutive days in 2018 heat wave period in Montreal. In addition, high temperature is known to be responsible for increasing the rate of heart stock, kidney failure and cause many other issues as facing lack of fresh drinkable water that is excluded in this study (Jandaghian and Akbari, 2018b). The intention of this study is to investigate the impacts of extreme heat events and heat island on meteorological parameters and heat-related death over the Greater Montreal Area during three heat wave periods in 2005, 2011 and 2018. We applied the fully coupled online Weather Research and Forecasting model (WRF) with a multi-layer of the Urban Canopy Model (ML-UCM). The second objective is to assess the effects of albedo enhancement on air temperature, wind speed, dew point temperature and changes on air mass type and heat-related death.

METHODOLOGY

Heat-related mortality (HRM) can be magnified in urban areas because of the urban heat island (UHI) effects. UHI intensity and duration cause an increase in mortality. To fight the heat island effects, increasing urban albedo is applied. To investigate the effects of albedo enhancement on heat-related deaths, meteorological simulations are conducted.

Heat-Related Mortality Estimation

Three indicators are applied to translate the effects of extreme heat events and the potential of increasing surface reflectivity on heat-related mortality rates: air mass type, air temperature, and apparent temperature changes for each day during heat wave periods. The air temperature and apparent temperature are calculated based on simulation results. As this research focuses on heat, the summer period of June, July and August (JJA) in the GMA is being analyzed. Vanos et al. (2014) classified weather types into Spatial Synoptic Classification (SSC) (Sheridan, 2002) for 12 cities in Canada. The meteorological data applied to classify weather types into SSC was collected from airport weather stations maintained by the Meteorological Service of Canada. They estimated the heat-related mortality based on daily non-accidental mortality data that were collected across the city's metropolitan area from the Canadian Vital Statistics databases at Statistics Canada over 20 years (1981–2000).

The number of deaths related to each air mass classification is estimated based on the rate above the mean anomalous daily mortality in Montreal per 100,000 people. The Statistics Canada Census estimated the population of Montreal as 4.027,100 people in 2016. The Dry Moderate (DM) weather type, that includes mild and dry air in the summer season, is the most common type in the GMA. The highest rate of mortality during summer periods corresponds to the hotter and more humid air mass type (MT+), while the dry tropical condition (DT) places second (Vanos et al., 2014). Table 1 and Figure 1 represent the specific air mass classification, the summertime frequencies (JJA, %), and heat-related mortality in the GMA (Vanos et al., 2014; Martel B et al., 2010). The Canadian Environment Health Atlas (CEHA) estimates that in Montreal 121 people die each year because of high temperature.

Table 1. Summertime mortality rate for GMA within five weather types (1981–2000): weather type frequency for June, July, and August and relative mortality (the averaged anomalous number of heat-related death above baseline value for mean daily mortality). The standard deviation is presented. [Mortality rate per 100,000 people, calculated based on Statistics Canada 2011 Census as 3,824,221 people in GMA] (Source: Vanos et al., 2014)

Synoptic weather category	Frequency (%)	Deaths	SD	~ Number of deaths based on 2011 Census
DM	32.2	1.96	±0.36	75
DT	1.30	2.27	±0.53	87
MM	24.0	1.95	±0.36	75
MT	22.0	2.13	±0.42	81
MT+	4.40	2.38	±0.59	91
TR	16.1	0	0	0

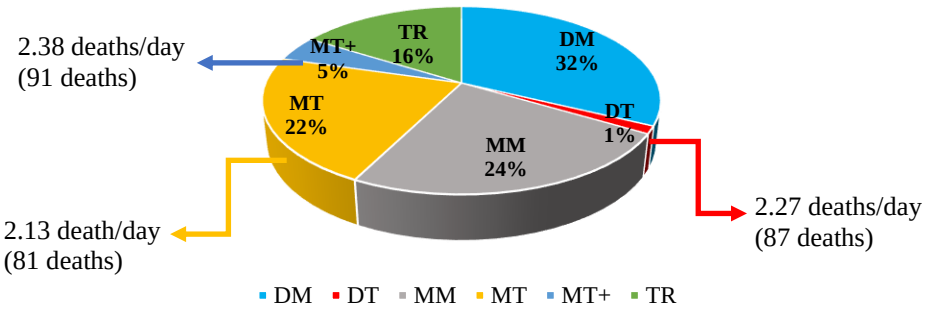


Figure 1. The number of deaths corresponding to each synoptic weather type during summer time (JJA). Dry Moderate (DM): mild and dry air; Dry Tropical (DT): the hottest and driest conditions; Moist Moderate (MM): warmer and more humid conditions; Moist Tropical (MT): warm and very humid; Moist Tropical Plus (MT+): hotter and more humid subset of MT; Transition (TR): days in which one weather type yields to another (Source: Sheridan, 2002)

Two categories are considered regarding the air mass classifications for heat-related mortality estimation: dry tropical (DT) and moist tropical / moist tropical plus (MT/MT+). Since the heat-related deaths corresponding to the frequency of DT are significant, the positive weighting factor for the day in sequences (DIS) is only defined for this air mass category. The DIS factor means that for each consecutive day within the DT air mass type, the estimated mortality increases by 1.07. Another weighting factor is for apparent temperature, 0.339, derived from the simulation results and presents the effects of temperature (T2) and dew point temperature (DPR). The other factor is time of season (TOS), derived from Kalkstein et al.'s (2013) HRM correlations for DT

and MT/MT+ in the District of Columbia. Accordingly, the daily heat-related mortality calculation for Dry Tropical (DT) that represents the hottest and driest condition is Eq. (1):

$$\mathrm{HRM_D} = -4.32 + 1.07\mathrm{DIS} - 0.066\mathrm{TOS} + 0.339\ \mathrm{AT} \quad (1)$$

and for Moist Tropical (MT) and Moist Tropical Plus (MT+) that represent very warm and humid condition is Eq. (2):

$$\mathrm{HRM_D} = 2.70 - 0.016\mathrm{TOS} + 0.339\mathrm{AT} \quad (2)$$

Simulation Setups

The NCAR Weather Research and Forecasting Model (WRFV3.6.1) (Skamarock et al., 2008) is applied within a multi-layer of the Urban Canopy Model (ML-UCM) (Chen et al., 2011) to simulate the meteorological interactions in the urban atmosphere. Montreal is the second largest city in Canada and is centered at the ~45.5ºN and ~73.6ºW. The horizontal domain of the simulations is composed of four two-way nested domains. Figure 2 shows the inner domain with the horizontal resolution of 0.333 km. Three simulations are conducted during the heat wave periods in July of 2005 (10th-12th), 2011 (20th- 23rd) and 2018 (2nd-5th). The NOAH land-surface model employed to provide boundary conditions for the meteorological model. The planetary boundary layer is simulated by the Mellor-Yamada-Janjic scheme. For radiation, microphysics and cumulus models, we respectively applied the Rapid Radiative Transfer Model, Lin scheme and Grell 3D. Two sets of scenarios are defined for each period of the simulation (Jandaghian and Akbari, 2018a, 2018b and 2018c). The base case, where the fraction of urban albedo is assumed to be 0.2 (hereafter referred to as CTRL) and albedo case, where the reflectivity of roofs, walls and grounds are increased by 45%, 40% and 25%, respectively (hereafter referred to as ALBEDO).

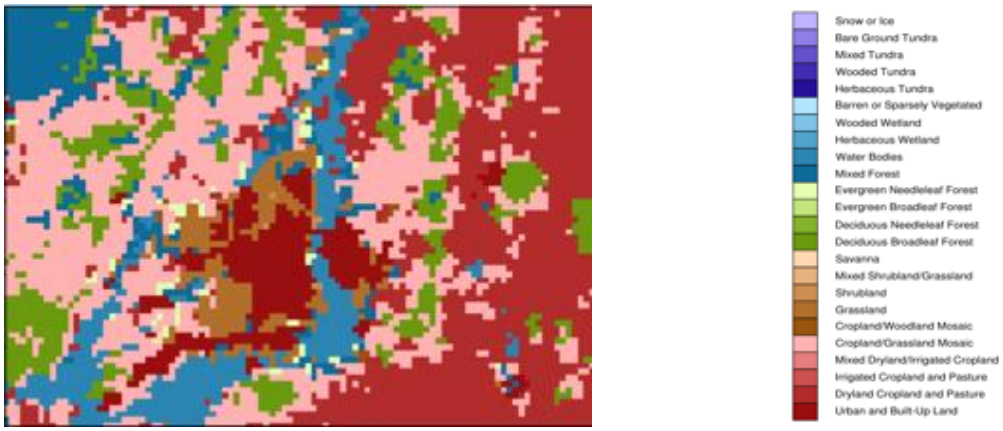


Figure 2. Simulation domain and Land Use Land Cover (LULC) of GMA

RESULTS

Model Performance Evaluation

The Mean Bias Error (MBE), Mean Absolute Error (MAE) and Root Mean Square Error (RMSE) are calculated for 2-m air temperature (T2), 10-m wind speed (WS10), and dew point temperature (DPT) of CTRL results compared with the measurements from four weather stations: McTavish (MT, location:45.50ºN, 73.58ºW), Pierre Elliott Trudeau Intl (PET, location:45.47ºN, 73.75ºW), Montreal/St-Hubert (SH, location: 45.52ºN, 73.42ºW) and Ste-Anne-de-Bellevue (SAB, location: 45.43ºN,~73.93ºW) (Jandaghian and Akbari, 2018a, 2017a, and 2017b). Table 2

presents the MBE, MAE and RSME of aforementioned parameters. Figure 3 shows the comparisons between simulated and measured air temperature for one day of each simulation in 2005, 2011 and 2018.

The model, on average, well predicts air temperature, slightly underestimates wind speed and dew point temperature. The reason is because the effects of micro scale parameters cannot be captured in mesoscale models precisely. The heat emission from buildings and transportation sectors is miscalculated in model estimation. Jandaghian et al. (2017) run a sensitivity analysis of physical parameterizations in WRF for urban climate simulations in Greater Montreal Area for 3 consecutive days in 2009. The results indicated the mean absolute error (MAE) of the 2-m air temperature, wind speed, relative humidity, and precipitation are approximately 1.4ºC, 1 m/s, 16% and 2mm, respectively. In other studies, the comparison of thermal components of WRF and the Fifth-Generation NCAR/Penn State Mesoscale Model (MM5) indicated that both models have the MBE of T2 as almost -3.8ºC to 0.2ºC during a year. (Gilliam et al., 2006 and Wang et al., 2012). Thus, the performance of WRF is generally consistent with the measurements and the results are well reliable for further investigations.

Table 2. The Mean Bias Error (MBE), Mean Absolute Error (MAE) and Root Mean Square Error (RMSE) of 2-m air temperature (oC), 10-m wind speed (m/s) and dew point temperature (oC) simulation results in CTRL case vs. measurements obtained from weather stations over the Greater Montreal Are during the 2005, 2011 and 2018 heat wave periods

Station	Air temperature (ºC) in 2005			Air temperature (ºC) in 2011			Air temperature (ºC) in 2018		
	MBE	MAE	RMSE	MBE	MAE	RMSE	MBE	MAE	RMSE
MT	0.08	1.50	1.76	0.07	1.51	1.91	0.11	1.01	1.33
PET	-0.62	1.20	1.44	-0.88	1.37	1.83	-0.30	0.80	1.01
SH	0.02	1.19	1.50	-0.94	1.30	1.70	0.22	1.10	1.47
SAB	1.07	1.28	1.65	0.03	1.10	1.47	0.19	1.12	1.30
Average	0.12	1.25	1.53	-0.43	1.32	1.73	0.06	1.01	1.28
Station	Wind speed (m/s) in 2005			Wind speed (m/s) in 2011			Wind speed (m/s) in 2018		
	MBE	MAE	RMSE	MBE	MAE	RMSE	MBE	MAE	RMSE
MT	1.66	1.82	2.30	-0.61	0.85	0.91	1.8	1.90	2.11
PET	-0.63	1.88	2.11	-2.17	2.25	2.40	0.87	1.22	1.87
SH	-0.13	2.38	2.21	-2.83	3.11	2.11	0.34	1.19	1.49
SAB	0.54	1.88	2.11	-0.33	1.25	2.81	1.05	1.70	2.18
Average	0.36	1.99	2.18	-0.93	1.86	2.05	1.01	1.50	1.91
Station	Dew point temperature (ºC) in 2005			Dew point temperature (ºC) in 2011			Dew point temperature (ºC) in 2018		
	MBE	MAE	RMSE	MBE	MAE	RMSE	MBE	MAE	RMSE
MT	0.82	0.83	0.90	0.52	0.58	0.71	0.21	0.54	0.69
PET	0.33	0.55	0.61	0.71	0.74	0.91	0.51	0.30	0.41
SH	-0.19	0.51	0.61	0.47	0.48	0.61	0.22	0.48	0.64
SAB	-0.16	0.38	0.52	0.93	0.93	1.01	0.30	0.61	0.67
Average	0.21	0.56	0.44	0.65	0.68	0.81	0.31	0.48	0.62

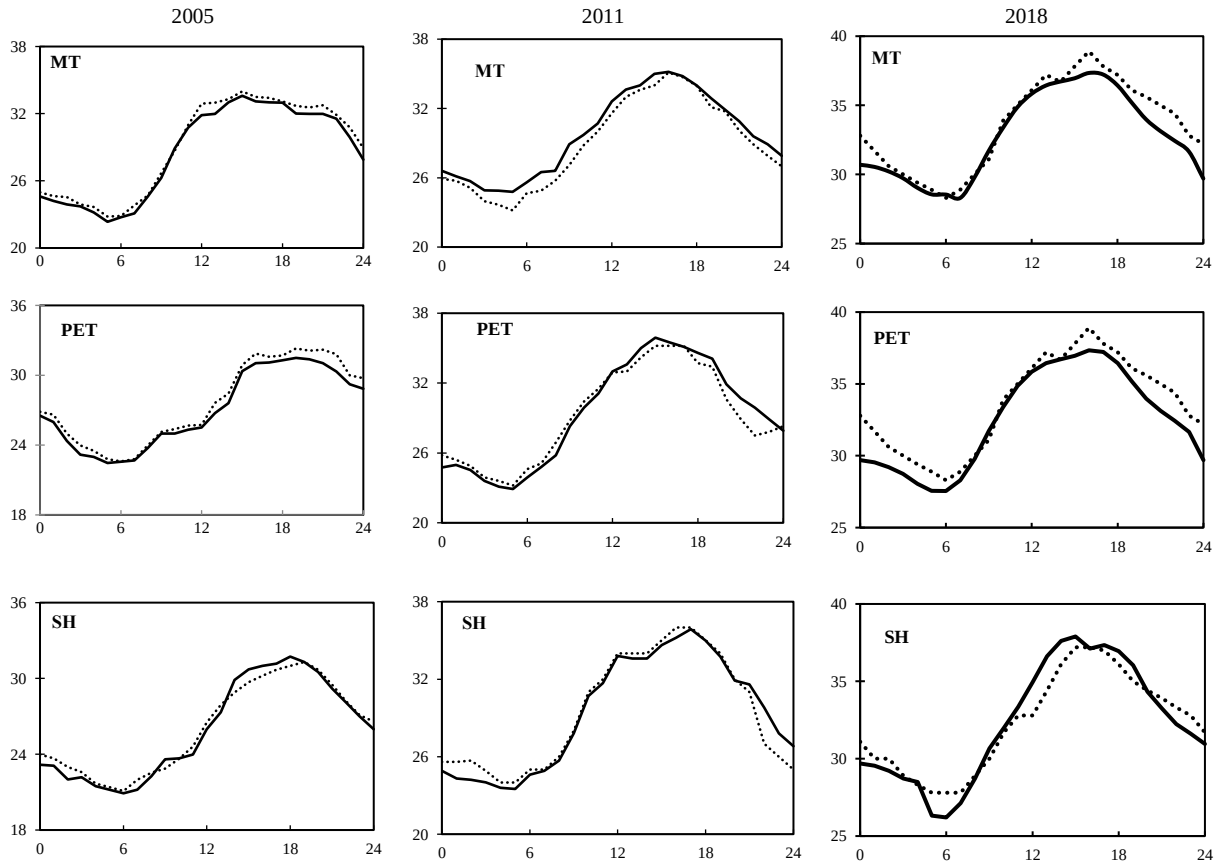
Note: The definitions of statistical measurements are as follows Jandaghian et al. (2018c) [51]: $\mathrm{MBE} = \frac{1}{\mathrm{N}}\sum_1^{\mathrm{N}}(\mathrm{C_M} - \mathrm{C_O})$, $\mathrm{MAE} = \frac{1}{\mathrm{N}}\sum_1^{\mathrm{N}}|\mathrm{C_M} - \mathrm{C_O}|$, $\mathrm{RMSE} = \left[\frac{1}{\mathrm{N}}\sum_1^{\mathrm{N}}(\mathrm{C_M} - \mathrm{C_O})^2\right]^{1/2}$, C_M and $\mathrm{C_O}$ are modeled and observed concentrations, respectively and N is the total number of model and observation pairs.

Albedo Enhancement Effects

The albedo of roofs, walls and grounds increased from 0.2 in CTRL scenarios to 0.65, 0.60, and 0.45 in ALBEDO scenarios, respectively. Table 3 represents the averaged 2-m air temperature,

10-m wind speed and dew point temperature differences between CTRL and ALBEDO scenarios. The averaged 2-m air temperature decreased by nearly 1°C in urban areas (MT and PET) and by 0.5^{o}C in rural areas (SH and SAB). The simulation results indicate that the T2 reduces less at 12 p.m. compared to 6 p.m. because of the heat that is absorbed by the ground surface during sunlight and then released at sunset and thus added up to the air temperature in the evening. The averaged 10-m wind speed differences between CTRL and ALBEDO scenarios indicate that an increase in surface albedo causes a slight increase in the wind speed. The increase in wind assists the decrease in air temperature in those areas. The averaged dew point temperature differences between these scenarios show a slight decrease in air humidity by nearly 0.3^{o}C.

The results indicate that an increase in surface albedo causes a decrease in apparent temperature and discomfort indices that makes the environment more preferable and suitable for urban dwellers during summer time and therefore reduces the risk of heat-related morbidity and mortality. We applied two indicators; 2-m air temperature and dew point temperature that extracted from ALBEDO simulation results in these estimations. The consequences of albedo increments show that the Discomfort Index (DI) improved by nearly 3-5% and the Apparent Temperature (AT) decreased by nearly 3°C in urban area.



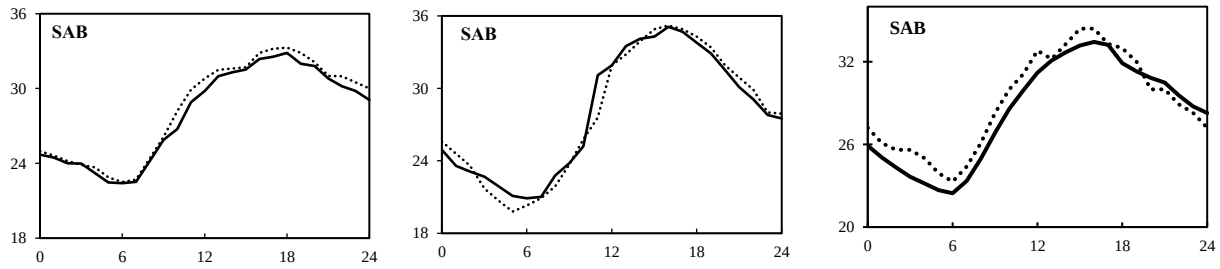


Figure 3. Simulation results averaged diurnal cycle of 2-m air temperature (oC) in CTRL [solid line] vs. measurements [dashed line] from four weather stations: MT (McTavish), PET (Pierre Elliott Trudeau Intl), SH (St-Hubert), SAB (Ste-Anne-de-Bellevue) over Greater Montreal Area during the 2005 [left], 2011 [middle] and 2018 [right] heat wave periods

Table 3. Averaged 3-day differences of 2-m air temperature(oC), 10-m wind speed(km/h) and dew point temperature(oC) between CTRL and ALBEDO scenarios in Greater Montreal Area during 2005, 2011 and 2018 heat wave periods

CTRL-ALBEDO	Heat-wave	MT	PET	SH	SAB
ΔT2 (°C)	2005	0.7	0. 5	0.2	0.7
	2011	0.8	0.7	0.2	0.6
	2018	0.9	0.8	0.4	0.7
ΔWS_{10} (m/s)	2005	-0.2	-0.05	-0.01	-0.01
	2011	-0.3	-0.09	-0.02	0.01
	2018	-0.4	-0.2	-0.01	-0.04
ΔDPT (°C)	2005	0.19	0.27	0.18	0.25
	2011	0.28	0.38	0.13	0.29
	2018	0.22	0.29	0.21	0.31

Heat-Related Mortality Changes

The synoptic air mass classifications are defined for each day of the simulation based on meteorological changes such as air temperature, dew point temperature, and wind velocity over the GMA. Table 4 shows the changes in air mass type during the 2005, 2011 and 2018 heat wave periods for CTRL and ALBEDO scenarios. The moist tropical plus air mass type is improved to moist tropical because of the mitigation strategy and surface modification that leads to a decrease in air temperature and dew point temperature. The dry tropical classification has also transformed to dry moderate, which is a more benign condition. These changes cause a decrease in heat-related mortality during these three heat wave events in the Greater Montreal Area.

Table 4. Air mass classifications on each day during 2005, 2011 and 2018 heat wave periods in GMA, the bold entries show changes in air mass type resulted in increasing surface albedo

Scenario	CTRL	ALBEDO
10-Jul-2005	DT	DT
11-Jul-2005	MT+	MT
12-Jul-2005	DT	DT
21-Jul-2011	MT+	MT
22-Jul-2011	MT	MT
23-Jul-2011	DT	DM

03-Jul-2018	MT+	MT
04-Jul-2018	DT	DM
05-Jul-2018	MT+	MT

The results of heat-related mortality estimations are presented in Table 5 in CTRL and ALBEDO scenarios for the three heat wave periods in the GMA. The consequences of albedo enhancement indicate that there would be around 3%, 4% and 5% reduction in heat-related mortality in the 2005, 2011 and 2018 heat events, respectively. Accordingly, as the air mass classification shifted from oppressive condition (e.g., DT) to a benign situation (e.g., DM), a reduction in HRM is more noticeable.

Table 5. Daily heat-related mortality estimation per 100,000 population based on HRM calculations for DT, MT and MT+ during the 2005, 2011 and 2018 heat wave periods. For human lives, the numbers are shown with 1 decimal

Mortality Estimations		
Scenario	**CTRL**	**ALBEDO**
10-Jul-2005	4.9	4.8
11-Jul-2005	13.9	13.6
12-Jul-2005	7.8	7.6
Total HRM	~ 27	~ 26
Average Mortality	8.9	8.7
Averaged Reduction (%)		**2.7%**
21-Jul-2011	13.9	13.8
22-Jul-2011	13.6	13.4
23-Jul-2011	7.3	6.2
Total HRM	~ 35	~ 33
Average Mortality	11.6	11.2
Averaged Reduction (%)		**3.7%**
03-Jul-2018	20.9	17.1
04-Jul-2018	19.9	18.1
05-Jul-2018	18.7	18.5
Total HRM	~ 60	~ 54
Average Mortality	19.8	17.5
Averaged Reduction (%)		**4.7%**

CONCLUSIONS

The effects of increasing surface albedo are assessed on heat-related mortality in Greater Montreal Area during three heat wave periods in 2005, 2011 and 2018. Numerical simulations were conducted using the online WRF coupled with a ML-UCM. A series of metrics calculation are employed to evaluate the model performance and compared the simulation results with the measurements obtained from four weather stations over the domain. The comparisons of the base case simulations indicated that the model on average well predicts the meteorological variables.

The albedo of roofs, walls and grounds were increased by 45%, 40% and 25%, respectively. The average daily 2-m air temperature reduced by nearly 0.8 to 1°C in urban areas during heat wave events, whereas this reduction in rural area was around 0.2-0.6^{o}C. The albedo enhancement caused a slight increase in wind speed in urban areas that increase the convection heat transfer and thus decrease the skin temperature. A higher wind speed reduces the effects of heat and ambient temperature and produces a more pleasant condition for urban dwellers. It should be noted that increasing surface albedo is a region-specific strategy and needs to be evaluated over any interested area because it depends on urban characteristics and morphology.

Here, three indicators are applied to translate the effects of extreme heat events and the potential of increasing surface reflectivity on heat-related mortality rates: air mass type, air temperature and apparent temperature changes for each day during heat-wave periods. The results of surface modifications indicated that the moist tropical plus and dry tropical air mass types are shifted to moist tropical and dry moderate, respectively. These changes cause a decrease in heat-related mortality during these three heat wave events. Three of the six heat wave days showed air mass changes from more to less oppressive conditions. The beneficial outcome is a reduction in heat-related death by approximately 3-5% during heat wave periods, meaning that seven to twelve lives (out of 3,82 million) could be saved during these periods. It should be noted that by reducing ambient temperature, the pollutants emission from biogenic and anthropogenic sources and thus photochemical reaction rates will reduce. So, the death related to air quality will also reduce. In addition, increasing surface reflectivity shift days into less oppressive air masses by 50%.

The heat-related mortality estimation is based upon some assumptions and limitations. The effects of air pollution, radiation budget changes, human physical characteristics, such as age, gender, economic and educational status, have not been taken into account. This study shows that increasing surface reflectivity contributes to a reduction in ambient temperature in urban area. It illustrates that cooling temperature to even less than a degree can lead to air mass category changes, reduce the adverse effects of elevated temperature, thus improving human comfort and decreasing heat-related mortality to some noticeable extent. Albedo enhancement will not decrease the rate of heat death by a significant number but saving even one human life and improving the level of comfort for inhabitants are, as always, important that requires rapid action.

ACKNOWLEDGMENT

The funding for this research provided by the National Science and Engineering Research Council of Canada under discovery program.

REFERENCES

Akbari H., Menon S., Rosenfeld A. 2009. Global cooling: increasing world-wide urban albedos to offset CO2. Climatic Change, 94 (3-4): 275-286.

Akbari H., Kolokotsa D. 2016. Three decades of urban heat islands and mitigation technologies research. Enbuild. 133: 834-842.

Anderson B.G., Bell M.L. 2009. Weather-related mortality: how heat, cold, and heat waves affect mortality in the United States. Epidemiology. 20(2): 205–213.

Basu R. 2009. High ambient temperature and mortality: a review of the epidemiologic studies from 2001 to 2008. Enviro Health. 8: 40-48.

Basu R., Samet J.M. 2002. Relation between elevated ambient temperature and mortality: a review of the epidemiologic evidence. Epidemio Rev. 24(2):190–202.

Ban-Weiss G.A., Woods J., Levinson R. 2014. Using remote sensing to quantify albedo of roofs in seven California cities, Part 1: Methods. Sol Energy. 115: 777-790.

Chen F., Kusaka H., Bornstein R., Ching J., Grimmond C. S. B., Grossman-Clarke S., Loridan T., Manning K.W., Martilli A., Miao S., Sailor D., Salamanca F.P., Taha H., Tewari M., Wang X., Wyszogrodzkia A.A, Zhang C.

2011. The integrated WRF/urban modelling system: development, evaluation, and applications to urban environmental problems. Int. J. Climatol. 31: 273-288.

Diaz J., Jordan A., García R., Lopez C., Alberdi J., Hernandez E., Otero A. 2002. Heat waves in Madrid 1986-1997: effects on the health of the elderly. Int. Arch. Occup. Environ. Health. 75 (3): 163-170.

Grell G.A, Devenyi D. 2002. A generalized approach to parameterizing convection combining ensemble and data assimilation techniques. Geophysical Research Letters. 29 (14): 31-38.

Gilliam R.C., Hogrefe C., Rao S.T. 2006. New methods for evaluating meteorological models used in air quality applications. Atmos. Environ. 40: 5073–5086.

Horton D.E., Skinner C.B., Singh D., Diffenbaugh N.S. 2014. Occurrence and persistence of future atmospheric stagnation events. Nat Clim Change Lett. 4: 698-703.

Hajat S., O'Connor M., Kosatsky T. 2010. Health effects of hot weather: from awareness of risk factors to effective health protection. Lancet. 375(9717): 856–863.

Environment Canada, (2017). Online: http://climate.weather.gc.ca/historical_data/search_historic_data_e.html

IPCC. 2014. Summary for policymakers. In: Climate Change 2014. Impacts, Adaptation, and Vulnerability. Part A: Global and Sectoral Aspects. Contribution of Working Group II to the Fifth Assessment Report of the Intergovernmental Panel on Climate Change. 1-32, New York (NY), USA.

Jenkins K., Hall J., Glenis V., Kilsby C., McCarthy C., Goodess D., Smith N., Malleson M. 2014. Probabilistic spatial risk assessment of heat impacts and adaptations for London, Clim. Change 124: 105–117.

Jandaghian, Z., Touchaei, G.A., and Akbari, H. 2017. Sensitivity analysis of physical parameterizations in WRF for urban climate simulations and heat island mitigation in Montreal. Urban Climate. 24: 577-599.

Jandaghian, Z., and Akbari, H. 2018a. The effects of increasing surface reflectivity on heat-related mortality in Greater Montreal Area, Canada. Urban Climate. 25: 135-151.

Jandaghian, Z., and Akbari, H. 2018b. The effects of increasing surface albedo on urban climate and air quality: a detailed study for Sacramento, Houston and Chicago. Climate. 6: 2-27.

Jandaghian, Z., and Akbari, H. 2019. Effects of increasing surface reflectivity on aerosol, radiation and cloud interactions in urban atmosphere. Submitted to a Journal.

Jandaghian, Z., and Akbari, H. Urban Heat Island and Human Health. 4th International Conference on Countering Urban Heat Island (UHI) and Climate Change Through Mitigation and Adaptation, May- 2016.

Kalkstein L., Sailor D., Shickman K., Sherdian S., Vanos J. 2013. Assessing the health impacts of urban heat island reduction strategies in the District of Columbia. Report DDOE ID#2013-10-OPS, Global Cool Cities Alliance.

Martel B., Giroux J.X., Gosselin P., Chebana F., Ouarda T.B.M.J., Charron C. 2010. Indicateurs et seuils météorologiques pour les systèmes de veille-avertissement lors de vagues de chaleur au Québec. Québec: Institut national de santé publique du Québec. ISBN 978-2-550-59896-1.

McMichael A., Woodruff R.E., Hales S. 2006. Climate change and human health: present and future risks. 367(9513):859-69.

O'Neill M.S., Ebi K.L. 2009. Temperature extremes and health: impacts of climate variability and change in the United States. J Occup Environ Med 51: 13–25.

Oleson K.W., Bonan G.B., Feddema J., Jackson T. 2011. An examination of urban heat island characteristics in a global climate model, Int. J. Climatol. 31(12): 02-22

Skamarock W.C., Klemp J.B., Dudhia J, Gill D.O., Barker D.M., Duha M.G., Huang X.Y., Wang W., Powers J.G., 2008. A Description of the Advanced Research WRF Version 3. National Center for Atmospheric Research: Boulder, CO, USA.

Sheridan S.C. 2002. The redevelopment of a weather-type classification scheme for North America. Int J Climatol 22(1):51–68.

Taha H., 2009. In: Mesoscale and Meso-urban Meteorological and Photochemical Modeling of Heat Island Mitigation in California: Results and Regulatory Aspects Conference on Countermeasures to UHI, Berkeley (CA) USA.

Vanos J.K., Hebbern C., Cakmak S. 2014. Risk assessment for cardio- vascular and respiratory mortality due to air pollution and synoptic meteorology in 10 Canadian cities. Environ Pollut 185:322–332.

Wang X.Y., Barnett A.G., Yu W., FitzGerald G., Tippett V., Aitken P., Neville G., McRae D., Verrall K., Tong S. 2012. The impact of heatwaves on mortality and emergency hospital admissions from non-external causes in Brisbane, Australia. Occup. Environ. Med. 69 (3), 163-169.

Zanobetti A., Luttmann-Gibson H., Horton E.S., Cohen A., Coull B.A., Hoffmann B., Schwartz J.D., Mittleman M.A., Li Y., Stone P.H., de Souza C., Lamparello B., Koutrakis P., Gold D.R., 2014. Brachial artery responses to ambient pollution, temperature, and humidity in people with type 2 diabetes: a repeated- measures study. Environ. Health Perspect. 122 (3), 242.

Urban heat island and bioclimate studies in Freiburg, Germany

Andreas Matzarakis[1], *Research Centre Human Biometeorology, German Meteorological Service (Germany)*

ABSTRACT

The city of Freiburg has a long tradition in urban climate issues because of the specific perception of the population on climate by the local wind system developed by the complex surrounding topography. The first comprehensive climate analysis were performed in the beginning of the seventies of the 20th century, where car traverses have been implemented in the analysis and the beginning of the development of climate function maps. In the following decades only specific modifications the area of the city have been analyzed like the development of new residential areas or the increase of the site of the football stadium or the new railway station. In the beginning of the 21st century the Freiburg city council begun to update the city's master plan and to adjust it for the year 2020. Local climate and air pollution were considered in this scheme through the application of a spatial urban climate analysis of the entire area. The analysis has built the basis for future analyses of individual areas in the context of building applications in the meantime. After 2015 the city of Freiburg decided to implement the issue of climate change for a vulnerability analysis.

Introduction

Freiburg belongs to one of the warmest cities in Germany because of its geographical location in the upper Rhine valley (Nübler 1979). More than 30 days with heat stress can be detected each year (REKLIP 1995). During extreme summers like the one in 2003, the number of days with heat stress is much higher. Air pollutants are dominantly produced by car traffic due to the absence of industrial emissions (UMEG 2003). Freiburg is located at the foothills or plains of the Black Forest, specifically at the exit of the Dreisam valley. In general, during cloudless and less windy weather conditions, a mountain breeze is formed. During the daylight hours, air masses move in the direction of the Black Forest and an air mass exchange is produced. During the night time hours, cold airflows from the slopes of the valleys are formed, and the induced cold air flows to the city of Freiburg from the east, affecting the climate conditions there. This local wind system called "Höllentäler" is very well known and is accompanied with the ventilation of parts of the city of Freiburg (Parlow 1983; Nübler 1979). The cold airflows depend on the synoptic conditions with a diverse intensity and range. In the Dreisam valley the local wind system occurs during 65% of the night hours per year (Parlow 1983).

Therefore, Freiburg has a specific role because of its location in the south of Germany and its complex topography. It combines many relevant aspects of climate and the effects of urbanization and topographical effects, not only due to the Black Forest, but also due to its location in the upper Rhine valley.

[1] Corresponding Author: andreas.matzarakis@dwd.de, +49 69 8062 9610, Research Centre Human Biometeorology, German Biometeorological Service, Stefan-Meier-Str. 4, D-79104 Freiburg, Germany.

Nevertheless, since the 1960s, several studies concerning local climates and urban effects in the city have been conducted in the vicinity of Freiburg. In the 70s, a whole approach for the quantification of the urban climate in Freiburg was conducted and was the basis for the authorities and decision makers of the city. This was followed by specific urban climate studies and had effects on diverse projects, i.e. new building areas or the modification of sport facilities were only limited in terms of single effects concerning wind conditions. At the start of the 21st century, the municipality realised the importance (not only because of climate change issues) of urban climate and demanded a new integral climate analysis for Freiburg (Röckle et al. 2003; Matzarakis et al. 2008; Matzarakis 2013).

Method

In order to obtain and quantify the distribution of the climatological and air pollution conditions, several approaches based on measurements and modelling have been performed and applied (VDI, 1988; Helbig, Baumüller, and Kerschgens 1999). Several factors, e.g. air temperature, wind, human bioclimate, and air pollutants have been aggregated and summarised into maps (Röckle et al. 2003; Matzarakis et al. 2008).

In detail, the following methods and results have been applied:

- Measurements
  - Thermal imaging by airplanes
  - Thermal mapping (day and night)
  - Screen level measurement campaigns
  - Tracer gas experiments
- Modelling
  - Cold air drainage flow simulation
  - Ventilation analysis
  - Analysis of thermal bioclimate
  - Analysis of air pollution situation
  - Affect analysis
- Maps
  - Climate function map
  - Planning advices map.

The aforementioned methods and data were the basis for the development of an integral analysis of the urban climate conditions of Freiburg. The aim of the study was that the produced results were based on the latest scientific methods and findings and are applicable in the urban planning process in Freiburg.

Measurements and Results

In this chapter the most relevant information for the production of the final maps are described. First, an inventory of existing data was performed and all data was considered for the study. In addition, required data was obtained through measurements and models. This chapter is divided into measured and modelled data.

Thermal Imaging

Thermal imaging to acquire spatial information about the thermal situation of a surface at a very high resolution has been applied. In order to detect day and night dynamics, two flights for the period with the highest heating of the surface (8th July 2002, afternoon) and highest surface cooling (9th July 2002, before sunrise) during high pressure weather conditions were carried out. The delivered result is not the surface temperature but the radiation received by the detector of the airplane. Despite lower radiation temperatures during the night (an average of about 17°C in contrast to the daytime of 26°C), the urbanised areas are significantly warmer than the surrounding areas; the inner city area is significantly dominated by warmer conditions in the nocturnal thermal image. Streets and buildings are heated from the short wave radiation during the day and release their heat as long wave radiation to the air during the night.

Screen Level Measurement Campaign

In addition to the thermal images measurements on the 8th and 9th of July 2002, a 24-hour screen level measurement campaign was carried out. Its aim was to record the meteorological variables: wind direction, wind speed, air temperature, and air humidity. These were the basic measurements required in order to have basic variables for estimating the thermal bio-climate of the whole area of Freiburg. The analysis of measured data shows the locations and times at which the highest air temperatures are observed in the investigation area. During times of maximum air temperature e.g. at the main center of Freiburg, the air temperature is about 2.5°C warmer than in green areas in the west of Freiburg. By contrast, during the times of minimum of air temperature the difference is about 5.5°C, showing that the highest intensity of the urban heat island takes place during the night.

Tracer Gas Experiments

Using tracer gas (SF6) experiments at six specific locations, the dispersion of gas in the evening and night hours was detected. The dispersion experiments show both the course of the cold air drainage flow and the degree of influence at these specific sites. The results of the tracer gas experiments are in accordance with the cold air flow simulations by modelling.

Modelling and Results

Cold Air Drainage Flow Simulations

For the cold air drainage flow for the whole area during the nocturnal flow, a numerical simulation model (Röckle 1992) for a typical weather situation with less wind and radiation was conducted and a 50m spatial resolution was applied. During the night, the area of Freiburg is dominated by a local wind system called “Höllentäler”. Such an effect is present not only in the eastern parts of Freiburg, which are affected by the Black Forest, but also in the northern parts. The local wind system is evident outside of the small valleys of the Black Forest for some hours after sunset. In the early evening hours, the local cold air flows coming from several small- and

medium-sized valleys dominate the wind flow conditions. They fit the huge east-west flow and are affected strongly by this flow.

Ventilation Analysis

A ventilation analysis was performed with a numerical wind flow model (Röckle and Richter 1998). The basis for the analysis was the information on the buildings of the city of Freiburg, allowing for a high spatial resolution of 5m; the 5m resolution was aggregated to 20m for a more appropriate overview. The analysis shows the areas in which the wind fields near the surface are modified the most. The analyses were performed for the main wind directions and allow the detection of ventilation paths, i.e. railway tracks or river areas. The inner part of the city is less ventilated because of the relatively tall and compact buildings. Similar conditions can be also found in other dense areas such as trade districts (Röckle et al. 2003).

Analysis of Thermal Bioclimate

In applied climatology and biometeorology, thermal comfort is described by using thermal indices, which include the combination of air temperature and/or air humidity or wind speed. Thermal perception and thermal comfort can not only be expressed by air temperature, but also by the influence of radiation conditions (depending on the diurnal and annual variation of solar radiation, shade of buildings and vegetation, infrared radiation of buildings, etc.), wind speed, and also air humidity (VDI 1998; Matzarakis 2001). Urban climate is usually characterised by a modified climate and expressed by the urban heat island, which can also be expressed in an urban bioclimate island for humans. This leads to pronounced additional heat stress, which usually occurs during the afternoon hours. In contrast, during the night, the thermal bioclimatic conditions are lower in rural areas due to the course of air temperature and the absence of solar radiation (Fig. 1). For the evaluation of the thermal component of urban climate, this can be also expressed as thermal bioclimate indices, based on the energy exchange of the human body; the Physiologically Equivalent Temperature (PET) is used (Höppe 1999; Matzarakis et al. 1999; 2007). The calculations are based on different land use information (representing the building mass and other urban characteristics), elevation, measurements from campaigns, and thermal imaging data. A summer day was selected for the construction of maps and the background data used; the PET was calculated for 1500 CET by using the radiation and bioclimate model RayMan (Matzarakis, Rutz, and Mayer 2007; 2010).

The highest PET values are found in locations with increased sealing factors and lower green percentages. The suburban parts of the rural areas are exposed to heat stress, which can be explained by the low buildings that are not able to produce shadows like the taller buildings in the inner parts of the city. In the higher areas of the Black Forest, there is no heat stress. During the nighttime hours especially at 0300 CET, PET values range between 6 and 11°C, meaning that people are affected by a slight cold stress during that time.

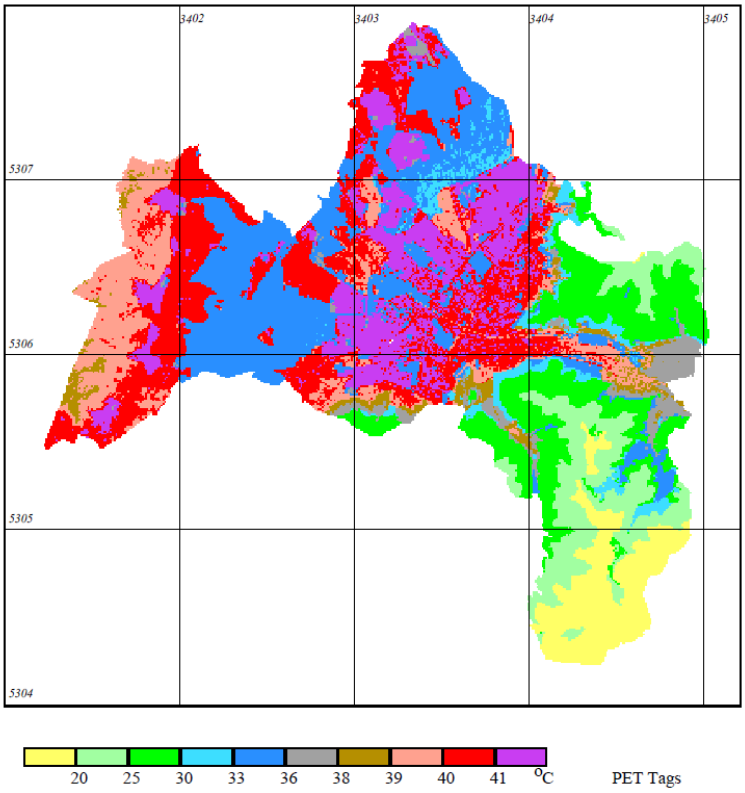


Figure 3. Map of PET. Source: Matzarakis et al. 2015

Analysis of the Air Pollution Situation

The air pollution situation in Freiburg, due to the absence of large emission sources, is primarily dominated by car traffic (Matzarakis, Röckle, and Mayer 2015). Estimations for NO_2, Benzene, and particulate matter (PM10) were performed for this source group. For the consideration of the complex topography of the area, five different meteorological dispersion classes were calculated (Richter and Röckle 1995). The estimated time horizon was fixed to the year 2005. It is assumed that emissions will be reduced by 2020 because of the specific reductions of air pollutants by cars. The highest estimated concentrations occur, as expected, along the highway (Autobahn A5), at the crossing points of the highway, and in the portal of the traffic tunnels in the eastern part of Freiburg. The limit values for NO_2 can sometimes be exceeded. Based on the estimated values of Benzene, NO_2, and PM10, an air pollution index for the human-biometeorological quantification was applied (Mayer et al. 2002). Most of the areas of Freiburg are less loaded by air pollutants, apart from the streets and their affected areas. During winterly inversions, air polluted situations are more pronounced, in contrast to the heat stress conditions in summer, as air exchange is limited.

Results and hints for urban planning

Affect Analysis

For the assessment of thermal stress or air pollution situation, the intensity as well as the number of people who are affected by these conditions is of importance. For this reason, two maps of affect analysis for day and night were made. During the day, the inner part of the city is characterized by strong heat stress. During the night, the areas in the west of Freiburg with a high density of buildings are related to thermal load. The most urbanized areas are usually found in the "moderate" and "strong" class of heat stress during the day and night. The thermal classes "low" and "very low" are less frequently found in the urban area. In general, Freiburg shows 'high problem areas', which are a result of thermal stress. Based on that, the importance of green- and free areas has to be considered and assessed. In the inner city, most of the areas are characterized by 'high problem areas', especially during the summer. Aside from the daytime situation, the night-time situation is also of importance because of the absence of cooling effects for regeneration from the climatic point of view (cooling of building mass and transportation of polluted air and warm air masses). In this context the ventilation possibilities and especially the cold airflow with less polluted air should not be reduced (Röckle et al. 2003).

Urban Planning Maps

A climate function map as well as a planning advices map was produced based on the information derived above and the knowledge from previous investigations (e.g. Nübler 1979; Rudloff 1993; Friedrich 2000). The spatial dimension of climate information is a possibility for the quantification of the recent and future effects of the structure plan concerning the local climate and air pollution situation in a city.

Planning Oriented Maps

Climate Function Map

Climate function maps are focused on the spatial and detailed distribution of the present thermal and air pollution conditions (Matzarakis, Röckle, and Mayer 2015). Focus is also placed on the autochthonous weather conditions, i.e. weather situations with high solar radiation and less wind exchange. With the consideration of air paths or ventilation paths based on the long term wind conditions of the area, a more realistic mean condition approach is reached. Finally, a climate function map is based on a general assessment of several existing climate factors (i.e. slope aspect of topography, land use, etc.), measured climate information (i.e. air temperature, wind, radiation properties of the surfaces, air quality), and results from modelling approaches (ventilation, cold air drainage flow, bioclimate). In the climate function map only atmospheric processes are included, which occur at the screen level considered, so the interactions between different climate relevant areas (climatopes) are not sharply separated (VDI 1997), i.e. the areas have to be seen as transitions areas. In addition, the signatures or legends used have a symbolic character without including exact and quantitative information about, for instance, the range or intensity of flows. The climatopes included in the climate function and planning advices maps

are based on the VDI-guideline 3787, Part 1: Environmental meteorology: Climate and air pollution maps for cities and regions (VDI 1997).

Planning Advices Map

The aforementioned and -explained climatic properties and characteristics are part of the climate function maps. Based on the climate function maps, which are somewhat static, and under the consideration of existing air pollution data (measured and modelled) and the affect analysis maps, a detailed planning advices maps has been constructed (Figure 2). In contrast to the climate function map, where the information is not assessed by specific spaces or areas, information is indicated with a specific value: free spaces based on their climatic/air pollution function and urban structures concerning their sensibility in relation to higher urban density. The urban air paths are separated into polluted and non-polluted quantities (Mayer et al. 1994). Air polluted areas are expressed based on their traffic load. The extracted information is prepared with emphasis on planning advices for the level of city planning.

The most relevant and important findings in the planning advices map are summarised as follows: Urban areas are classified into areas of low, medium, and high sensibility in relation to urban development or extension based on the affect value (for the thermal and air pollution situation) and their importance to the surrounding areas. For Freiburg, the free spaces in west to east and north to south directions are conspicuous. Mostly located in the east and south of Freiburg are areas with very high climatic and air quality compensation potential. This means, that from those areas cooler or less polluted air is transported to areas with higher thermal load or higher air-pollution (Matzarakis, Röckle, and Mayer 2015). This is an effect of the local wind system formed by the topographical properties of the nearby valley in the Black Forest. This local wind classified as a cool mountain breeze is of importance during specific weather situations and is responsible for the ventilation of the city area, therefore, the source area (forest areas in the southeast and east of Freiburg) of the wind systems is classified as a high priority area. Areas near the river and the small valleys in the eastern and south-eastern part are also classified with the highest climatic priority. Free spaces on the slopes in the south are also of specific climatic relevance, as is the airport area in the north-east and the forest areas in the west of Freiburg. Inner city areas like cemeteries and other green areas have a high climatic potential and are classified by the highest category of positive effects. Free spaces with low and moderate building densities are classified as having improved climatic and air pollution compensation functions. Moderate compensation function concerning climate have less residential buildings density or moderate trade/industrial areas during weather situations with heat stress. Spaces with no particular cold air production and areas with no residential relation are classified in the category of low climatic-air pollution compensation function, but this category does not exist in Freiburg.

Aside from the assessment of free and residential areas, the planning advices maps also include several elements of the air exchange. The effect of mountain breezes from two different directions during the night and day including the cold air drainage flow of the mountain breeze play an important role in the regional and local significance of the wind conditions in the urban climate conditions of the city of Freiburg. They are an important issue in the planning advices map and are indicated and quantified by polluted and unpolluted urban air paths. Urban air paths are areas with less roughness, sufficient length and width, and preferably straight courses

contributing to the ventilation of urban areas (Mayer, Beckröge, and Matzarakis 1994). Regional urban air paths are of importance because of the transport of unpolluted air masses from rural environments to city areas. Local urban air paths contribute to the air exchange in urban areas. The efficiency of urban air paths is dependent on the dominant wind direction of a region and/or area.

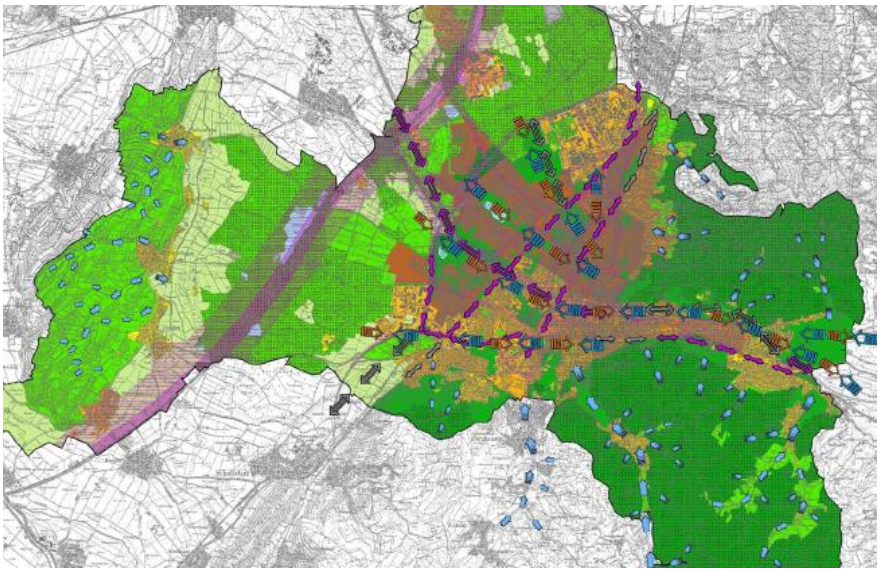


Figure 2. Planning advices map. Source: Röckle etal. 2003; Matzarakis, Röckle, and Mayer 2015.

Discussion and conclusion

The general and specific aim of assessing areas for future or planned urban development was quantified by an ecological risk analysis. The impact of an area modified by a microclimate is dependent on:

a) Intensity, range, and direction of the effect,
b) Sensitivity and value (significance) of the area in contrast to a specific effect of the modification planned.

For the quantification, the frequency of use by humans (estimated from the land use), the human biometeorological thermal stress (here quantified by PET), and the air pollution situation have been considered. It is a fact that after building up an area, the physical properties of that area are modified and changed (i.e. heat balance, ventilation, air pollution, and so on). The range of effects on surrounding areas depends on the transport of these properties by synoptic, regional, local wind conditions. Concerning human thermal bioclimate, a separation between diurnal and nocturnal conditions has to be performed because of different air exchange conditions during hot days and especially in areas (such as cities) embedded in complex topographies, where local wind systems can be developed. All of the modified conditions have to be estimated based on the microclimatic effects (including bioclimate and air pollution) and the sensitivity of the area of interest.

The final climatic consequences for planners can be summarised as follows (Matzarakis et al. 2008):

1. Maintenance of urban climate relevant air paths (for fresh- and cold air) transport,
2. Micro-scale climate manipulations to avoid diurnal heating of buildings. Possibilities include planting trees with broad leaves (spending shade), or the surface management of materials with a high reflectance of short wave radiation (albedo management).

Furthermore, for an improved outdoor quality of life, high climate diversity is of an advantage, preferably in short spatial and temporal accessibility. This can be performed by considering affect factors and analysis. It has to be noted that it is less meaningful to analyse and assess separate and single urban structures. A master analysis under consideration of climatic factors and conditions should be included in any master plan analysis.

The analysis of the specific climate of urban structures and cities should not be an alibi, but the possibility of solid appreciation of values for decision makers should be assessed and known. This is especially valid for cities, which are under expansion pressure and are increasing in the density of their urban structures. The climatic properties in cities are going to be more important not only because of climate change discussion but also as a factor of quality of life. Finally, urban structures and cities in general can use urban climate modifications and manipulations as a possibility for mitigation and adaptation strategies facing climate change (Matzarakis 2013).

The update of the described analysis and approach is under investigation. For this specific issue the Municipality of Freiburg run at the moment two additional analysis a) urban climate analysis including climate change factors in a similar spatial resolution and also identifying recent and future hot spots b) vulnerability analysis for the identification and development of adaptation strategies.

References

Helbig, A., Baumüller, J., Kerschgens, M. J. (1999). Stadtklima und Luftreinhaltung. 2. vollständig überarbeitete und ergänzte Auflage. Berlin, Springer-Verlag.

Höppe, P. (1999). The physiological equivalent temperature – a universal index for the biometeorological assessment of the thermal environment. Int. J. Biometeorol. 43, 71-75.

Matzarakis, A. (2001). Die thermische Komponente des Stadtklimas. Ber. Meteor. Inst. Univ. Freiburg Nr. 6.

Matzarakis, A., 2013. Stadtklima vor dem Hintergrund des Klimawandels. Gefahrstoffe – Reinhaltung der Luft 73, 115-118.

Matzarakis, A., Mayer, H. and Iziomon, M., (1999). Applications of a universal thermal index: physiological equivalent temperature. Int. J. Biometeorol. 43, 76-84.

Matzarakis, A., Rutz, F., and Mayer, H. (2007). Modelling Radiation fluxes in simple and complex environments – Application of the RayMan model. Int. J. Biometeorol. 51, 323-334.

Matzarakis, A., Rutz, F. and Mayer, H., (2010). Modelling Radiation fluxes in simple and complex environments – Basics of the RayMan model. Int. J. Biometeorol. 54, 131-139.

Matzarakis, A., Röckle, R., Richter, C.J., Höfl, H.C., Steinicke, W., Streifeneder, M. and Mayer, H., (2008). Planungsrelevante Bewertung des Stadtklimas – Am Beispiel von Freiburg im Breisgau. Gefahrstoffe – Reinhaltung der Luft 68, 334-340.

Matzarakis, A., Röckle, R., Mayer, H., 2015: Urban climatic map studies in Germany: Freiburg. In: Ng, E., Ren, C. (Ed.) The urban climatic map for sustainable planning. Earthsacan by Routledge. Chapter 26, 369-379.

Mayer, H., Beckröge, W. and Matzarakis, A. (1994). Bestimmung von stadtklimarelevanten Luftleitbahnen. UVP-Report 5/94, S. 265-268.

Mayer, H., Kalberlah, F., Ahrens, D. and Reuter, U. (2002). Analyse von Indizes zur Bewertung der Luft. Gefahrstoffe – Reinhalt. der Luft 62, 177-183.

Nübler, W. (1979). Konfiguration und Genese der Wärmeinsel der Stadt Freiburg. Freiburger Geographische Hefte, 16, Freiburg.

Parlow, E. (1983). Geländeklimatologische Untersuchungen im Bereich der Staufener Bucht unter besonderer Berücksichtigung lokaler Ausgleichsströmungen. Freiburger Geographische Hefte, 20, Freiburg.

REKLIP (1995). Klimaatlas Oberrhein Mitte-Süd. Hrsg. Trinationale Arbeitsgemeinschaft REGIO-KLIMA-PROJEKT. Vdf Hochschulverlag, Zürich – IFG, Offenbach – Editions Coprus, Straßburg.

Richter, C.-J., Röckle, R. (1995). Methode zur Ermittlung von Kfz-bedingten Schadstoffkonzentrationen in bebauten Gebieten. UVP-Report 5, 233-235.

Röckle, R. (1992). Einsatz mikroskaliger Strömungsmodelle bei Planungsfragen. Annalen der Meteorologie, 28, 43 – 45.

Röckle, R., Richter, C.-J. (1998). Ausbreitung von Geruchsstoffen in Kaltluftabflüssen - Messungen und Modellrechnungen. VDI-Berichte 1373, 249 - 259.

Röckle, R., Richter, C.-J., Höfl, H.-C., Steinicke, W., Streifeneder, M. and Matzarakis, A. (2003). Klimaanalyse Stadt Freiburg. Auftraggeber Stadtplanungsamt der Stadt Freiburg. November 2003.

VDI (1988). Stadtklima und Luftreinhaltung. Berlin, Springer-Verlag.

VDI (1997). Umweltmeteorologie: Klima- und Lufthygienekarten für Städte und Regionen. VDI-Richtlinie 3787, Blatt 1.

VDI (1998). Methoden zur human-biometeorologischen Bewertung von Klima und Lufthygiene für die Stadt- und Regionalplanung, Teil I: Klima. VDI-Richtlinie 3787 Blatt 2.

Study On Appropriate Ground Cover Configuration of Open Spaces to Mitigate Urban Heat Island Effect

***Prof. Yuvraj P. Meshram*[1]**
Ph.D. Research Scholar, Associate Professor and Principal,
Radhikatai Pandav Institute of Architecture, Nagpur (M.S.), India.

***Prof. Shirish A. Deshpande*[2]**
Ph.D. Guide, Retd. Professor and HOD,
Visvesvaraya National Institute of Technology, Nagpur (M.S.), India.

***Dr. Sheeba Valsson*[3]**
Ph.D. Guide, Professor and Principal
Shri. Datta Meghe College of Architecture, Nagpur (M.S.), India.

ABSTRACT

Natural landscapes are continuously being built over at the cost of concrete jungle / hard surfaces as buildings, roads, paved areas act as barriers for the proper dissipation of heat energy to the retention capacities. This calls for monitoring of temperature changes, especially in urban areas. There is a steady increase in global temperature in association with climate changes in the past 150 years, and at least partially this is a direct result of mankind's activities such as "Urban Heat Island" (UHI).

UHI is characterized by amplification of temperature values, lower relative humidity values and moderation of wind velocity, can create unpleasant micro-climatic conditions for human. On the other hand, green areas within the urban space can create a cooling effect, lowering temperatures and increasing relative humidity. The cooling effect of urban park creates a "Park Cool Island" (PCI), and is most prominent in an urban area that has developed a UHI.

Materials that are used within private or public spaces, included ground surfaces and building materials determine the micro-climate and affect the energy consumption, thermal and visual comfort as well as the thermal balance. Generally, utilization of high reflectivity materials in the buildings, as well as the covered urban surfaces reduces the absorbed solar radiation and preserves the coolness of the surfaces. These materials are also known as "Cool materials". Specification of the proper structural and cladding materials in the cities and buildings is considered to be one of the most promising mitigation techniques concerning improvement of the urban micro-climate.

Micro-climatic conditions in parks are influenced by both Pervious - soft surfaces and Impervious – hard surfaces and their physical properties. Vegetation and plantation, particularly in the presence of high moisture level, plays a vital role in the regulation of air temperature. The aim of this paper is to evaluate the impact of Cool pavements with variation in percentage of perforations, and by exploring the possibilities of vegetation configuration to maximize the cooling effect in urban open spaces of Nagpur city.

Key words: - *Open space, micro-climate, cool material, pervious, impervious, vegetation.*

Introduction

There is a shift from the traditional rural community to the modern urban community resulting in urban drift. In India, 31.16% of the total population is living in urban areas (Census 2011), which is 3.35% greater than in 2001 (27.81%). There is a remarkable degradation of urban habitats due to the rapid change in urban environment. In Central India, the most common problem that cities have been facing in recent years is the continuous increase in temperature. Drastically expansion of urban areas affects its local and regional climate and the quality of life (Luck, 2002). The urban spaces are found to be generally warmer than the surrounding rural areas (Oke, 1982) and this phenomenon called **"Urban Heat Island"** effect. There is an extensive need of the hour for regular monitoring of temperature changes in urban areas, has been already prioritized for mitigating measures by many governments and cities in the world**.** However in India we are lagging behind in this respect.

In urban areas, the natural landscapes and vegetation are continuously being built upon by the paved surfaces (typically paved road and building surface) act as barriers for the proper dissipation of heat energy to the surrounding environment. These paved surfaces have higher heat absorption and retention capacities. There is continuous change of the land surface in the urban area and the replacement of vegetation by expansively built surface is the main reasons of forming UHI (Voogt, 1989).

During summer, the extenuated temperature from urban heat island could influence a community's environment and quality of life (Akbari and Konopacki, 2004 & 2005). Therefore there is an extreme need to estimate strategies that may mitigate the impacts of Urban Heat Islands in urban areas (Givoni, 1991); (Gill et al., 2007). Thus, it is necessary to understand the importance of open spaces and their design aspects so that the associated microclimate might be improved.

Need?

Environmental problems in cities - To meet the demands of Urbanization there is a steady loss of open spaces and unfortunately there are very few existing open spaces which are not well maintained and lack of vegetation, as a result adversely affecting the micro-climate of the city.

Impact of urbanization upon climate change and environmental distress - Vast growth of cities is leading to increased carbon release in atmosphere and accelerates the climate change.

Degrading quality of life - Pollution, noise, overcrowding, lack of open spaces and vegetation, safety, and many of such reasons have led to degrading social life and quality of life in cities.

Planning policies - There is lack of research based scientific town planning process. Planning has been undertaken in isolation without overlapping the socio-cultural-economical-political-legal aspects (Ramanathan S., 2015).

Literature Review

Open Space

Open space is defined as an area, forming an integral part of the site, left open to sky. Commonly, urban open spaces such as parks or squares, outdoor sport areas, public spaces etc. (Urban Development Plan Formulation and Implementation guidelines)

Climate

According to Chandler, (1989), under the influence of local regional geographic factors different climatic effects occur within a general pattern. These in turn can fabricate a climate influenced by buildings and their immediate elements within the urban setting. Chandler classified climate into different level; viz:

Macro-climate: Climate obtained by using data from a number of identical sites over a large area such as region, country, continent by oceans.

Micro-climate: Encompasses large area with reasonably uniform situation which are influenced by air masses moving over earth surface within parameters that characterize a localized area with a geographic scale ranges from $1m^2$ to $100m^2$. The main factors that influence microclimate include surface temperature, air temperature, relative humidity, wind velocity, solar radiation and precipitation.

Mitigation of UHI

Role of vegetation in controlling micro-climate - Degree of "Greenery" (Green space factor) is usually calculated as the percentage of total urban area that is dedicated to open green spaces. Higher the percentage of green area covers the greener that particular city becomes. The green spaces assist to reduce urban heat island effect and improve the air quality by regulating the temperature. (Lin., T., A. Matzarkis and R.Hway, 2010).

Research Gap

To deal with the Urban Heat Island effect, steps would have to be taken at macro and micro levels. Design of the open spaces (parks and gardens) in the cities would be one of the most efficient levels in which this can be achieved. However, the universal strategies for mitigating Urban Heat Island effects are reasonably well known, specific guidelines and standards for mitigation of adverse effects of impervious (hard) paved areas on the urban microclimate have not been established.

Standards like LEED, GRIHA etc. specify that greenery should be maintained at a certain level; however the outcome of maintaining these standards on the microclimate and temperature have not been recognized or stipulated so far. Some research has been done pertaining to building, roofing, paving, construction materials, etc. usually by the industry which has developed such materials, with the aim to promote these materials. However, such studies and standards are available pertaining to surface temperatures of these materials in controlled and built environment like research labs. Standards related to the resultant ambient air temperature as an effect of a variety of commonly used paving materials in combination with vegetation in various percentages have not been established yet.

By establishing such standards, it should be possible to predict the effect of ground cover configuration on ambient air temperature and micro-climate within the planned open space; based on the known properties of the surface treatment like solar radiation, solar absorption, emissivity etc. Such standards would be a useful tool for designing and rating of open spaces having desirable temperature and micro-climate within it.

Aim

The present study aims to understand and establish this relationship through the comparison between recorded and predicted Ambient Air Temperatures by applying Grass pavers with variations in percentage of perforation which can be used for prediction of ambient air temperature obtained from designed ground cover configuration. The present study focuses on this Research Gap.

Research Area - Nagpur City

Nagpur is one of the prominent cities of Maharashtra state in Central India, which faces exceptionally hot summer. Open Spaces in Nagpur city provide ideal settings and scopes for bridging the identified research gap, i.e. to study effects of various types of surface treatments in combination with vegetation cover and variations in percentage of perforations on corresponding ambient air temperature.

Climatic behaviour of Nagpur city- In general, Nagpur has a Composite Climate; Temperature during the month of March, April, May and June is on the elevated side beyond the comfort zone. The winter (November to February) in general is quiet. The annual rainfall (based on 30 years data) is about 1161.5 mm. The climatic study of Temperature is considered by using 42 years data for the period 1969-2010. Nagpur climate witness an extremely hot weather during summer. It reaches the peak in the month of May.

Table 1: Extreme Temperatures at Nagpur (1969-2010)

Season	Months	Maximum Temperature				Minimum Temperature			
		Highest	Date	Lowest	Date	Highest	Date	Lowest	Date
Summer	March	42.5	23,24/2010	20.6	11/ 2006	28.0	29 /1996	10.1	10 /1979
	April	47.1	30/ 2009	30.8	19 /2000	31.9	23 /1973	16.2	02 /1996
	May	47.6	23/ 2005	24.8	13 /1990	34.3	15 /1970	20.4	06 /1997

Source: Climate of Nagpur, Regional Meteorological Centre, Airport, Nagpur, M.S., India Meteorological Dept.

The highest maximum temperature of 45° C or more was most frequent during most of the years during summer for the period from 1969 to 2010 is shown in Table 1.1. May is the hottest and most uncomfortable month during the summer season with maximum highest and minimum highest temperature is 47.6° C (23/05/2005) and 34.3° C (15/05/1970) respectively. However, extreme recorded maximum temperature is 47.7° C on 26/05/1954.

Identification of study areas - The selection of all the open spaces are based upon Location within Nagpur Municipal limits - in and around Residential areas of different Zones such as, North, South, East and West having approx. area of 1.00 Hect. to 2.50 Hect.(Refer Fig.-1).

Field Surveys has been carried out in the selected Developed parks (Four Nos.) and Un-developed open spaces (Four Nos.) as listed below...

Developed Open Spaces

1) Dr. Ambedkar Park, Vaishali Nagar - 27239.39 Sq.m (Pilot Study)
2) Dayanand Park, Jaripatka – 25253.33 Sq.m.
3) Shivaji Nagar Park – 14449.75 Sq.m.
4) NIT Park, Suyog Nagar – 27149.49 Sq.m.

Un- Developed Open Spaces

1) Buddha Park, Buddha Nagta –21074.28 Sq.m. (Pilot Study)
2) Ganesh Park, Vaishali Nagar – 10635.32 Sq.m.
3) NIT Park, Ramnagar – 13747.25 Sq.m.
4) NIT Park, Bagadganj – 20161.00 Sq.m.

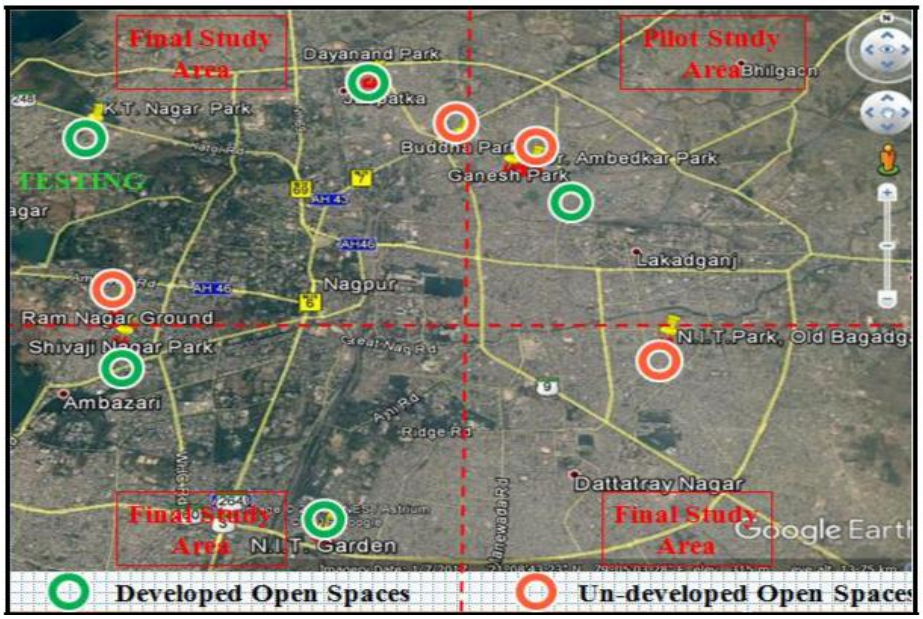


Figure 1: Identification of Study Areas. *Source*: Researcher

Schematic Framework for Data Collection and Analysis

Preparation of detail measured drawings and method of data collection - Measured drawings were prepared accurately, in which all types of surface treatments – paving materials and built structures as well as all types of vegetation were observed and documented. All surface areas were calculated in each park.

Testing and calibration of instruments - For primary data collection, 4 nos. calibrated Digital 4 in 1 Anemometer (Lutron-L8000A) instruments are used for recording temperature, (error factor +/- 1^0 C) and humidity (error factor +/- 4%).

a) Temperatures were recorded during summer and winter at 8.00 A.M. in the morning, 2.00 P.M. in the afternoon and 8.00 P.M. in the evening in all the parks. The temperatures were recorded at 2 meters above the ground level as per the standard practice and about 20 meters apart from each other on an east-west transect line in the middle of the parks along the length of the park.

b) Surface area analysis included the area calculation of each type of surface cover in each 20 meter diameter circle and then application of following parameters to each surface area in the circle.
c) The parameters which were applied to each surface area in the current study were Solar reflectance (albedo), Solar Absorption and Emissivity, for each type of material including soft permeable (soil / vegetation) surfaces. These parameters directly affect the temperature and the same are very much predictable and can be standardized.

Analysis of Surface Treatment area and configuration of each study area was done in detail for each data station for Developed Parks. On this analysis direct correlation between the surface treatment at the data station and resultant ambient air temperature is established at each location. This correlation data is used for Statistical analysis to arrive at the final regression equation by using Statistical Package for the Social Sciences (SPSS).

Role of Cool Materials

Materials that are used within private or public spaces, included building materials determine the microclimate and affect the energy consumption, as well as the thermal and visual comfort. Materials embodied in the surfaces receive the incident solar radiation. Part of this radiation is absorbed and the rest is reflected. Generally, utilization of high reflectivity materials in the buildings, as well as the covered urban surfaces reduces the absorbed solar radiation and preserves the coolness of the surfaces. These materials are also known as **"cool materials".** The temperature reduction depends on two factors:

- Reduction of the thermal gains
- Increase of thermal losses

Characteristics of Cool Materials (Pavements)

- High solar reflectance
- Faster release of heat
- Lower surface temperature
- Less heat penetrates into the building
- Less heat transferred to ambient air

The aforementioned properties are expressed in values ranging from zero to one. The greater is the value, the more "cool" is the surface and the more reduced is the surface temperature.

- When wet, these pavements can lower temperatures through evaporative cooling. The water passes through the voids and into the soil or supporting materials below.
- Moisture within the pavement structure evaporates as the surface heats, thus drawing heat out of the pavement, similar to evaporative cooling from vegetated land cover.
- Some permeable pavement systems contain grass or low-lying vegetation, which can stay particularly cool because the surface temperature of well-hydrated vegetation is lower than the ambient air temperature.
- When dry, the extent to which permeable pavements can influence temperatures is more complex and uncertain. For example, the larger air voids in permeable pavements increase the available surface area. These conditions may limit heat transfer to the lower

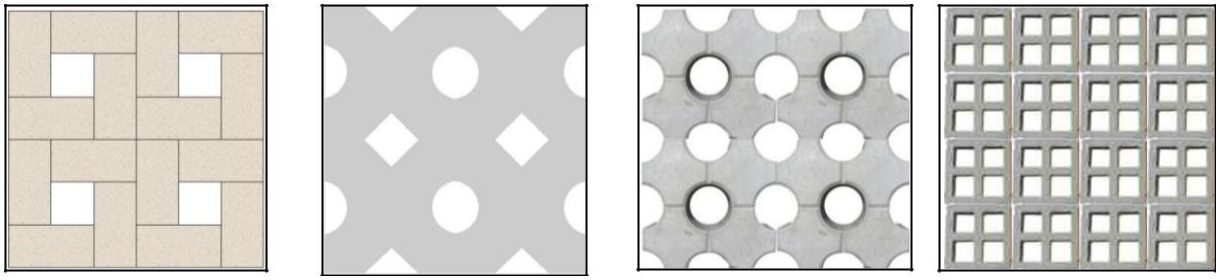
pavement structure and soils, keeping heat at the pavement's surface (and increasing daytime surface temperatures), but reducing bulk heat storage (reducing release of heat at nighttime). Overall, the limited transfer of heat to the pavement subsurface layers would reduce the release of heat during the nighttime. Release of stored heat from materials is a significant contributor to the nighttime Urban Heat Island effect.

Comparative measurements of cool material, regarding their thermal behavior, have shown to exhibit a surface temperature up to 12 ^{0}C lower than common materials. It was established that during the summer period, an increase of surface reflectivity of 40% can reduce the air temperature by 0.5-1.5 ^{0}C, whilst an increase of 65% reduces the temperature by 1-2 ^{0}C.

Numerous studies have been carried out in order to assess thermal and optical characteristics of various materials searching for the most suitable for the urban environment. Besides the lack of vegetation, the high solar radiation absorption by urban surfaces is another reason contributing to urban microclimate distortion.

Application of the Research Outcome

Grass Pavements with Variations in Percentage of Perforations



Option – A **(11.11%)** Option – B **(25%)** **Option – C (40%)** **Option – D (50%)**

Figure 2: Grass Pavers with variations in percentage of perforations available in the market which are used for examining the research outcome - Regression Equation. *Source:* Researcher

Case Study: 1 - Dr Ambedkar Park, Vaishali Nagar

Table 2: Comparison between recorded and predicted Ambient Air Temperatures by applying Grass pavers with variations in percentage of perforation for Dr Ambedkar Park, Vaishali Nagar

Points	Recorded Temp.	50% Shaded	11.11%	25%	40%	50%
		Predicted Temp.	Predicted Temp.	Predicted Temp.	Predicted Temp.	Predicted Temp.
A	40.6	36.8	37.5	37.1	36.8	36.5
B	40.8	36.0	36.3	36.2	36.0	35.9
C	40.4	35.9	36.1	36.0	35.9	35.8
D	41.8	35.9	36.2	36.0	35.9	35.8
E	40.7	35.9	36.1	36.0	35.9	35.8
F	39.3	35.6	35.7	35.7	35.6	35.6
G	41.2	35.7	35.8	35.8	35.7	35.6
H	44.9	37.1	37.9	37.5	37.1	36.8
I	41.5	37.0	37.5	37.2	36.8	36.6
X	36.3	36.1	36.2	36.1	35.9	35.8
Y	36.8	36.2	36.2	36.0	35.9	35.8

Source: Researcher

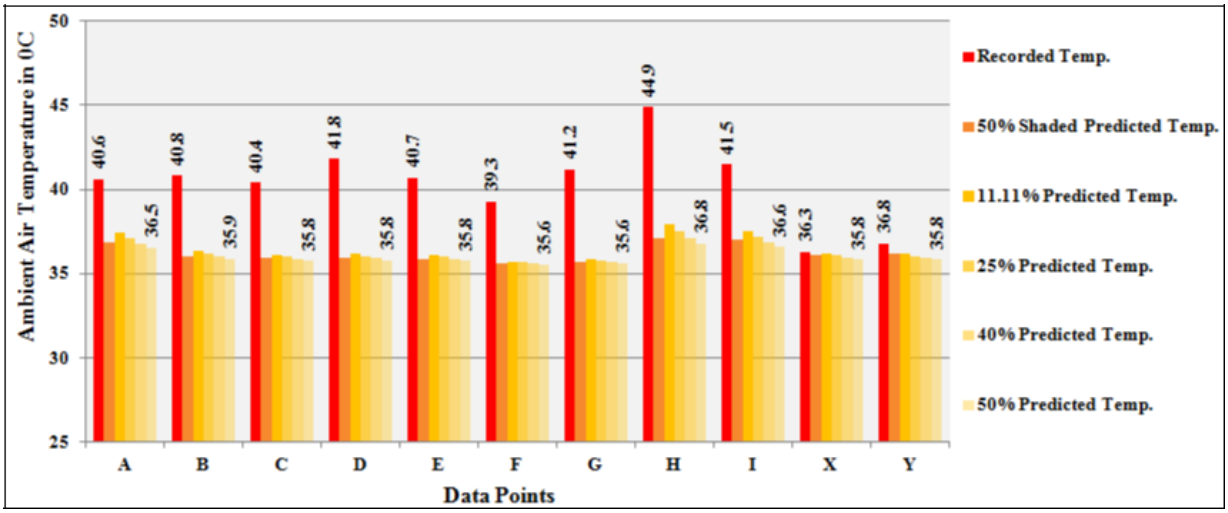


Figure 3: Column Chart showing Comparison between recorded and predicted Ambient Air Temperatures by applying Shading or Grass pavers with variations in percentage of perforation for Dr. Ambedkar Park, Vaishali Nagar. *Source*: Researcher

Step:1 - 50% Impervious (hard) area was proposed to be shaded without any change in permeability. By applying the regression equation it was found that the temperature difference would be 4.2^{o}C.
Step:2 - Impervious (hard) area was replaced by various cool / grass pavers giving 11.11%, 25%, 40% and 50% permeability as shown above without changing the shading area.
The varying but significant results of both these steps are shown. Various such combinations are possible which can all give corresponding results.

Similarly, observations were carried out for all the open spaces in steps 1 and 2;

Case Study: 2 - Dayanand Park, Jaripatka

Table 3: Comparison between recorded and predicted Ambient Air Temperatures by applying Grass pavers with variations in percentage of perforation for Dayanand Park, Jaripatka

Points	Recorded Temp.	50% Shaded	11.11%	25%	40%	50%
		Predicted Temp.	Predicted Temp.	Predicted Temp.	Predicted Temp.	Predicted Temp.
A	42.7	36.8	37.4	37.0	36.7	36.5
B	40.2	36.3	36.5	36.3	36.1	36.0
C	39.2	35.4	35.4	35.4	35.4	35.4
D	38.9	35.4	35.4	35.4	35.4	35.4
E	39.2	35.4	35.4	35.4	35.4	35.4
F	39	35.4	35.4	35.4	35.4	35.4
G	39.1	35.4	35.4	35.4	35.4	35.4
H	37.3	36.2	36.4	36.2	36.1	35.9
I	38.2	36.5	36.9	36.6	36.4	36.2
X	38.5	36.6	36.5	36.3	36.1	36.0
Y	41.8	36.3	36.6	36.4	36.2	36.0

Source: Researcher

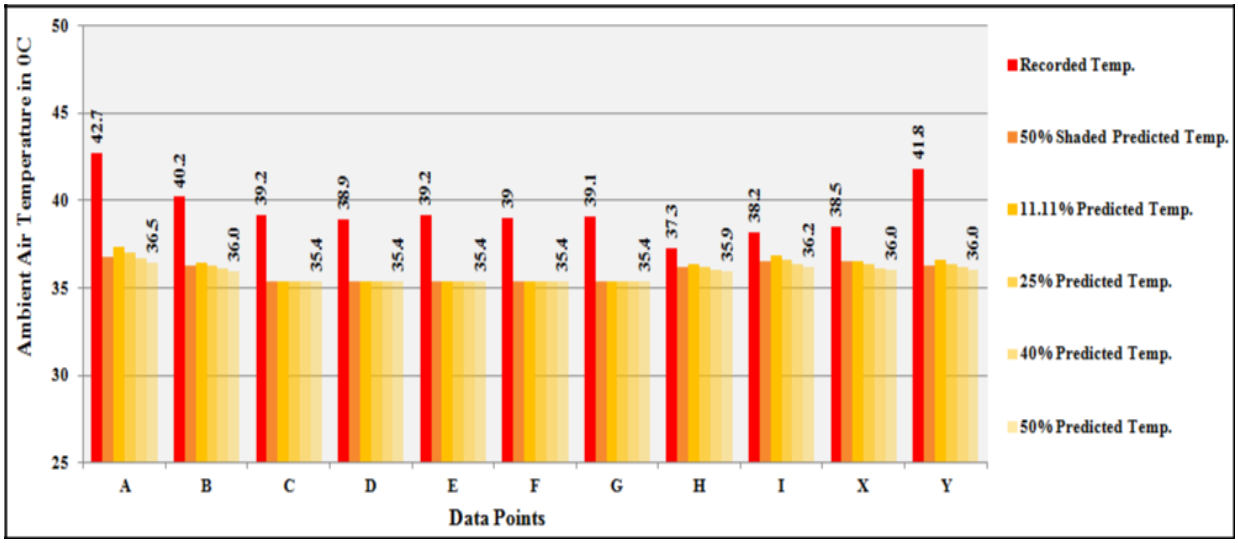


Figure 4: Column Chart showing Comparison between recorded and predicted Ambient Air Temperatures by applying Shading or Grass pavers with variations in percentage of perforation for Dayanand Park, Jaripatka.
Source: Researcher

Temperature difference would be 3.6^{o}C.

Case Study: 3 - Shivaji Nagar Park, Shivaji Nagar

Table 4: Comparison between recorded and predicted Ambient Air Temperatures by applying Grass pavers with variations in percentage of perforation for Shivaji Nagar Park

Points	Recorded Temp.	50% Shaded	11.11%	25%	40%	50%
		Predicted Temp.	Predicted Temp.	Predicted Temp.	Predicted Temp.	Predicted Temp.
A	39.7	36.4	36.8	36.6	36.3	36.2
B	39.3	35.5	35.5	35.5	35.5	35.5
C	36.4	35.8	35.9	35.8	35.7	35.6
D	39.1	36.5	37.0	36.7	36.5	36.3
E	37.1	36.4	36.7	36.5	36.3	36.1
F	37.3	36.1	36.4	36.2	36.1	35.9
G	42.9	37.1	37.9	37.5	37.0	36.8
H	37.5	36.4	36.9	36.7	36.4	36.2
I	43.4	37.5	38.4	37.9	37.4	37.1
X	38.8	36.3	36.6	36.4	36.2	36.1
Y	37.8	36.3	36.6	36.4	36.2	36.1

Source: Researcher

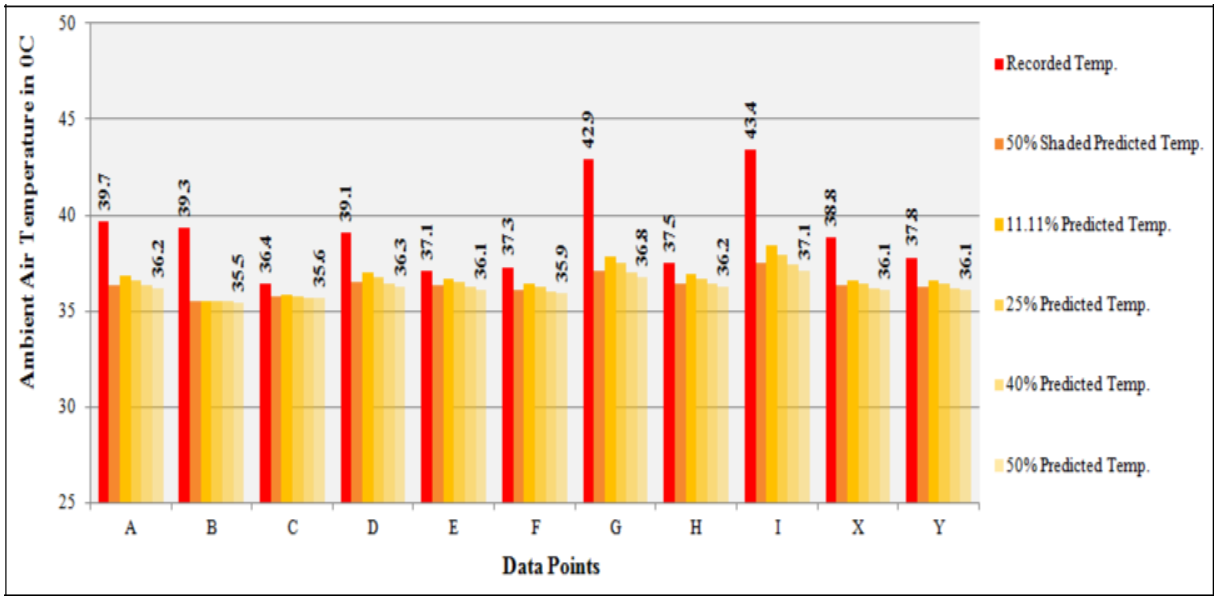


Figure 5: Column Chart showing Comparison between recorded and predicted Ambient Air Temperatures by applying Shading or Grass pavers with variations in percentage of perforation for Shivaji Nagar Park, Shivaji Nagar
Source: Researcher

Temperature difference would be 2.6^{o}C.

Case Study: 4 - NIT Park, Suyog Nagar

Table 5: Comparison between recorded and predicted Ambient Air Temperatures by applying Grass pavers with variations in percentage of perforation for N. I. T. Park, Suyog Nagar

Points	Recorded Temp.	50% Shaded	11.11%	25%	40%	50%
		Predicted Temp.	Predicted Temp.	Predicted Temp.	Predicted Temp.	Predicted Temp.
A	37.7	37.1	36.9	36.7	36.4	36.2
B	43.1	37.4	38.2	37.7	37.3	36.9
C	37.9	36.2	36.6	36.4	36.2	36.0
D	39.4	35.4	35.4	35.4	35.4	35.4
E	41.1	36.2	36.4	36.2	36.1	35.9
F	41.4	36.2	36.4	36.3	36.1	36.0
G	39.7	35.4	35.4	35.4	35.4	35.4
H	39.5	35.4	35.4	35.4	35.4	35.4
I	38.3	35.9	36.0	35.9	35.8	35.7
X	37.3	36.9	36.7	36.5	36.3	36.1
Y	40.6	36.8	37.2	36.9	36.6	36.4

Source: Researcher

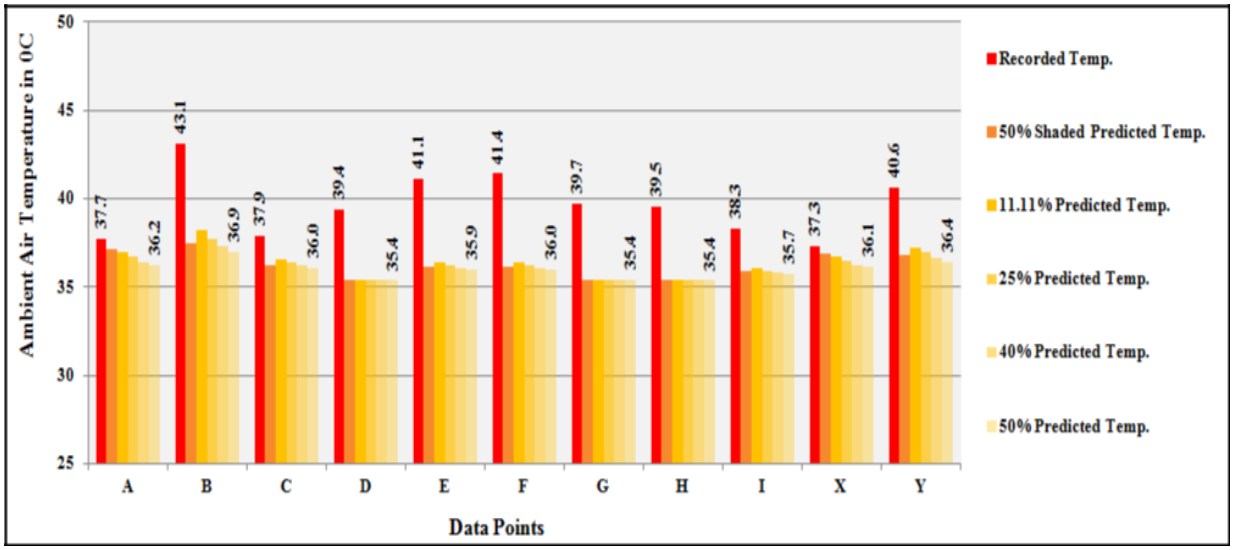


Figure 6: Column Chart showing Comparison between recorded and predicted Ambient Air Temperatures by applying Shading or Grass pavers with variations in percentage of perforation for N.I.T. Park, Suyog Nagar. *Source*: Researcher

Temperature difference would be 3.3^{o}C.

Comparison between Recorded and Predicted Ambient Air Temperatures by applying Shading or Grass Pavers with Variations in Percentage of Perforation in all Study Areas

Table 6: Comparison between recorded and predicted Ambient Air Temperatures by applying Shading and Grass pavers with variations in percentage of perforation in all study areas

Description	Dr. Ambedkar Park	Dayanand Park	Shivaji Nagar Park	N.I.T. Park, Suyog Nagar
Recorded Temp.	40.4	39.5	39.0	39.6
50% Shaded	36.2	35.9	36.4	36.3
Less by 11.11%	36.5	36.1	36.8	36.4
Less by 25%	36.3	36.0	36.6	36.3
Less by 40%	36.1	35.8	36.3	36.1
Less by 50%	36.0	35.8	36.2	36.0
Max. Temp. Reduction	**4.4**	**3.7**	**2.8**	**3.6**

Source: Researcher

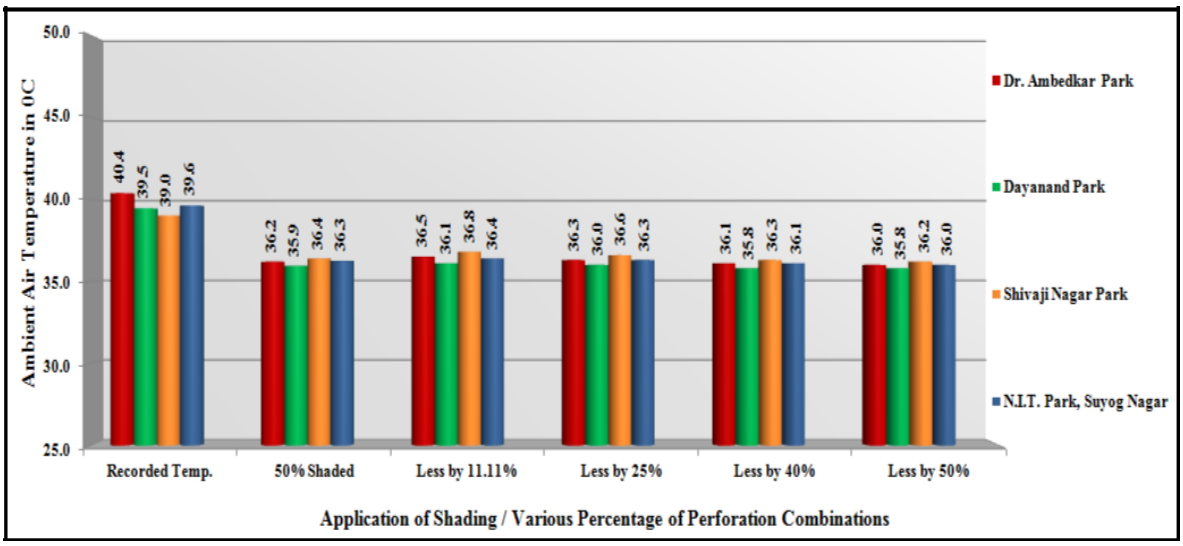


Figure 7: Column Chart showing Comparison between recorded and predicted Ambient Air Temperatures by applying Shading or Grass pavers with variations in percentage of perforation in all study areas. *Source*: Researcher

Analysis and Conclusion:

- Overall, it can be seen that by applying shading to 50% of the Impervious (hard) areas, significant temperature reduction (2.6^{o}C to 4.2^{o}C) can be achieved.
- By changing the permeability of paver blocks by 50%, again significant temperature reduction can be achieved (2.8^{o}C to 4.4^{o}C). Variable permeability (11.11% or 25% 0r 40%) gives proportionate temperature reduction. In all these cases, shading and application of grass pavers are considered separately and independent of each other.
- Percentage Distribution of Ground Cover Configuration (Impervious-hard and Permeable-soft surfaces) of Open Spaces has a direct co-relation with Ambient Air Temperature is found to be correct.
- A statistical relationship is established between Percentage Distribution of Ground Cover Configuration and Ambient Air Temperature which can be used as an effective tool for designing of parks which can provide predictable temperature moderation.
- Appropriate surface treatment results in reducing the thermal stress. However, such measures cannot be taken unless the parks are properly developed.
- Various permutations and combinations are possible for a designer by applying grass pavers in combination with shading to achieve even more significant results as per requirements.

References

Abreu, L. V. and L. C. Labaki. (2010): "Different arboreal species provides spedific influence radius in microclimate." 3rd International Conference on Passive and Low Energy Cooling for the Built Environment (PALENC). Rhodes, Greece.

Akbari, H. and Konopacki, S.(2005): "Calculating energy saving potentials of heat-island reduction strategies." Energy Policy 33 721-756.

Akbari, H. and Konopacki, S..(2004): "Energy effects of heat-island reduction strategies in Toronto, Canada." Energy 29,191-210.

ANSI/ASHRAE (2004): "Thermal Environmental Conditions for Human Occupacy, Atlanta." American society of heating, refrigerating, and air-conditioning engineers, 55. Atmospheric Environment 25: 289–299.

Chandler, I. (1989): Building Technology 2, Performance Construction Technology and Management, published in Association with Chattered Institute of Building (CIOB), III Series ISBN 0.7134-5248-x

Development Control Regulation. (DCR) of Nagpur city, 2012.

Emmanuel Rohinton M., An Urban Approach to Climate-Sensitive Design, Strategies for Tropics, Taylor & Francis Group, Spon Press, Great Britain

Gill, S.E.; Handley, J.F.; Ennos, A.R.; Pauleit, S. (2007): Adapting cities for climate change: The role of the green infrastructure. Built Environment, 33, 115–133.

Gillespie, R. Brown and T. (1995): "Microclimate Landscape Design: Creating Thermal Comfort and Energy Efficiency." John Wiley & Sons, New York..

Givoni, B. (1991): "Impact of planted areas on urban environmental quality: a review."

Givoni, B., (1976) : Man, Climate and Nature, Second edition, Applied Science Publishers Ltd. U.K. 1976

Government Circulars from Nagpur Improvement Trust (NIT) and Nagpur Municipal Corporation (NMC).
June 2015, from Jana Urban Space Foundation: http://www.janaagraha.org/content/pages/white-paper-sustainable urbanization-india-janaagraha

Krishen A., et. Al. (2001) , Climate Responsive Architecture, Edited by Tata- Mc Grawl- Hill.

Koenigsberger et. Al, (1973) Manual of Tropical Housing and Builings, Orient Longman,

Lin, T., A. Matzarkis and R. Hwang,. 2010): "Shading effect on long-term outdoor thermal comfort, Building and Environment." Building and Environment, 45, 213-221.

Luck, M. and J. Wu. (2002): "A gradient analysis of urban landscape pattern: A Case study from the Phoenix metropolitan region, Arizona,." Landscape Ecology, 327-339.

M.Tech. II Sem., Urban Planning, VNIT, Nagpur Student's Academic Report Under Guidance of Prof. Vidya Ghuge (2012-2014) : Open Space Development Strategy of Nagpur, India Madras.

Oke, T.R. (1989): "The micrometeorology of the urban forest." B: Biological Sciences 324, Philosophical Transactions of the Royal Society, 335–349.

Oke, TR. (1982) "The energetic basis of the urban heat island." Quarterly Journal of the Royal Meteorological Society 108: 1–24.

Ramanathan, S. (2015): White Paper on Sustainable Urbanization In India. Retrieved

Urban Development Plan Formulation and Implementation Guideline, (UDPFI,Guideline) www.nitnagpur.

Voogt, J. (1989): "Urban Heat Island." Encyclopedia of Global Environmental Change, 660-666.

Improving the accuracy of simplified urban canopy models for arid regions using site-specific prior information

Afshin Afshari, Fraunhofer Institute of Building Physics, Germany
Nicolas Ramirez, Engie Solutions Middle East, United Arab Emirates

ABSTRACT

An overly complex urban climate/energy model would not be of much practical use in a decision support setting where a large number of year-long simulations are often necessary. While detailed modeling of urban momentum/energy exchanges can be attempted via Computational Fluid Dynamics (CFD) or mesoscale modeling, conducting multiple full year simulations in a design optimization or sensitivity analysis context is practically impossible. Furthermore, CFD models often do not consider climate/building energy exchanges. To address these limitations, standalone Urban Canopy Models (UCMs) have been developed, attempting to replace the full-fledged atmospheric representation with a computationally light equivalent. In this study, we investigate the impact of several modifications to a standalone Single-Layer Urban Canopy Model (SLUCM) for an arid region based on the prior availability of site-specific information. The suggested improvements are portable to SLUCM schemes incorporated within mesoscale models. The SLUCM will undergo several improvements and each variant will be evaluated based on its ability to predict UHI intensity and air-conditioning energy demand. Three original SLUCM improvements are covered in the present study. (1) We use actual radiation parameters instead of those generated for idealized geometries. It is shown that, in the absence of this improvement, standard UCMs can underestimate the average urban heat island intensity by 5% if using the Town Energy Balance (TEB) radiation scheme or overestimate it by 7% if using the Square Prism Urban Canopy (SPUC) radiation scheme. (2) We use the results of a prior steady-state RANS (Reynolds-Averaged Numerical Simulation) simulation to replace some of the default morphological parameters of the UCM by the more accurate values derived from the RANS results. It is shown that, in the absence of this improvement, standard UCMs using default empirical relations can overestimate the average urban heat island intensity by up to 22%. (3) Instead of using the empirically calculated default value of the urban canyon wind speed, we estimate it directly from the concomitant rural value using a regression model trained by historical measurements. It is shown that, in the absence of this improvement, standard UCMs can underestimate the average canyon wind velocity by more than 12%, although the other indicators (UHI, cooling demand) are not significantly affected.

Special Issue Journal	:	Urban Climate
DoI	:	https://doi.org/10.1016/j.uclim.2020.100722
Citation	:	Afshari, A., & Ramirez, N. (2021). Improving the accuracy of simplified urban canopy models for arid regions using site-specific prior information. Urban Climate, 35, 100722.

Assessment of surface urban heat island and urban cooling effect based on downscaling LST, a case study of Fukuoka prefecture, Japan

Wangchongyu Peng[1], the University of Kitakyushu (Japan)
Rui Wang, the University of Kitakyushu (Japan)
Wei Chen. Xi'an Jiaotong University (China)
Lilei Zhou, Chongqing University (China)
Weijun Gao, the University of Kitakyushu (Japan)
Yingjun Ruan, Tongji University (China)

ABSTRACT

The phenomenon of urban areas becoming warmer than surrounding rural areas, known as urban heat island, is one of the biggest urban issues due to human activities. The study adopts remote sensing data from Moderate-Resolution Imaging Spectroradiometer (MODIS) sensor to assess the surface urban heat island effect for summer and winter (daytime and nighttime) of two cities in Fukuoka Prefecture, Japan, Fukuoka and Kitakyushu, in 2005 to 2015. The land surface temperature (LST) images were first downscaled to 250 m spatial resolution based on Random Forest Regression (RFR). The study first identified the surface urban heat island intensity (SUHII) based on downscaled LST images. Then the interrelationship between SUHII and distribution of population, the distance to the sea, and land use and land cover (LULC) were studied. The results show that the SUHII in summer daytime is the biggest while in winter nighttime is the smallest, and SUHII in Fukuoka city is bigger than that in Kitakyushu city suggesting city size has a positive impact on UHI. Through zonal statistics, population distribution was strongly correlated to SUHII in Fukuoka prefecture, and the sea has the strongest urban cooling effect (UCE).

Introduction

Built-up areas are mainly artificial structures such as pavements, parking lots, industrial areas, building roofs. Numerous studies have found that built-up areas have great effect on environment and urban quality (Wang et al., 2014). Along with the rapid urbanization and modernization, built-up areas replaced with natural landscapes, and thus many environmental problems occurred, such as water and air pollution, increase in greenhouse gas, increase in fossil fuel energy consumption, and urban heat islands (Zhou et al., 2004, Zhu et al., 2012, Foley et al., 2005). The most important effect of urbanization is the urban heat island (UHI) in which the atmospheric or surface temperature of an urban area is significantly higher than its surrounding rural areas due to artificial land cover and anthropogenic heat.

The traditional method of observing meteorological data has the limitation that the local meteorological observation points are not able to represent the whole study region. On the contrary, remote sensing (RS) and GIS technologies enable large-scale research of the UHI which are increasing used in recent UHI studies (dos Santos et al., 2017). Moderate Resolution Imaging Spectroradiometer (MODIS) images have become an increasingly important source for its high temporal resolution (per day). However, the MODIS thermal data which provide land surface temperature (LST) images with 1 km spatial resolution can only provide a generalized LST

[1] Wangchongyu Peng: pengwcy@gmail.com +818090635540.

condition and spatial pattern and is hard to compute the detailed UHI distribution. Hence, downscaling of spatial resolution of MODIS LST images is essential. Traditional downscaling methods such as Temperature Sharpening (TsHARP) (Agam et al., 2007) bases on linear correlation between vegetation indices and LST, and Multiple Linear Regression (MLR) bases on correlation between LST and surface reflectance or land use and land cover (LULC). Meanwhile, various Machine Learning (ML) methods such as Support Vector Regression (SVR), and Random Forests Regression (RFR) have been applied to downscaling LST and have better performance compared to the traditional methods (Mukherjee et al., 2014).

Fukuoka prefecture, Japan was selected as the study area which is the most urbanized area in Kyushu islands in west Japan. Fukuoka prefecture has a population of approximately 5.1 million and covers an area of approximately 4986.4 km^2. The main objective of this study are downscaling MODIS LST product (MOD11A2) into 250 m LST based on RFR, comparing the UHI differences between 2005 and 2015, summer and winter, daytime and nighttime, and study the interrelationship between UHI intensity and population distribution and LULC.

Study area, data, and methods

Study area

Fukuoka prefecture, Japan is chosen as the study area which is located in the west of Japan and domain ranging from 130.0°N, 33.0°E to 131.19°N, 33.97°E, with an approximate area of 5010 km^2 (Figure 1 (a)). Fukuoka city and Kitakyushu city are two coastal cities on the Japan Sea with a population of 2.6 million (Japan National Population Census 2015). Fukuoka city and Kitakyushu city are two government ordinance cities in Fukuoka prefecture, which delegated more functions than other cities, including civil affairs, urban planning, culture and education, and other public administrative affairs. Densely Inhabited Districts (DID) are the urban areas designated based on the statistical data since the Japan National Population Census in 1960. The urban boundaries of Fukuoka city and Kitakyushu city were extracted based on distribution of the DID in Fukuoka prefecture (Figure 1(b)), (Japan National Land Numerical Information (http://nlftp.mlit.go.jp/ksj/)). Japan has witnessed a rapid rate of urbanization in the 1970s and 1980s and the process of the urbanization has been slowed since the 21st century. The population of Fukuoka city increased from 1.34 million to 1.57 million, however, Kitakyushu city has drained a population of 50 thousand since 2000 (Figure 2).

Data

MODIS LST data were used to calculate the SUHII in the study area. The 8-day composite (MOD11A2) MODIS LST products in 2005 and 2015 at 1 km (960.3 m) spatial resolution were downloaded from the NASA EARTHDATA website (https://search.earthdata.nasa.gov/). The daytime (local time 10:30) LST and nighttime (local time 22:30) LST layers were reprojected into WGS 1984 Transverse Mercator projection and resampled to 1km resolution. The day/night and summer/winter SUHII in 2005 and 2015 were calculated in the 2 cities. In Fukuoka prefecture, Summer was the period from June to August and winter was the period from December to February. The 8-day LST images with fewer missing pixels were composited seasonal LST images.

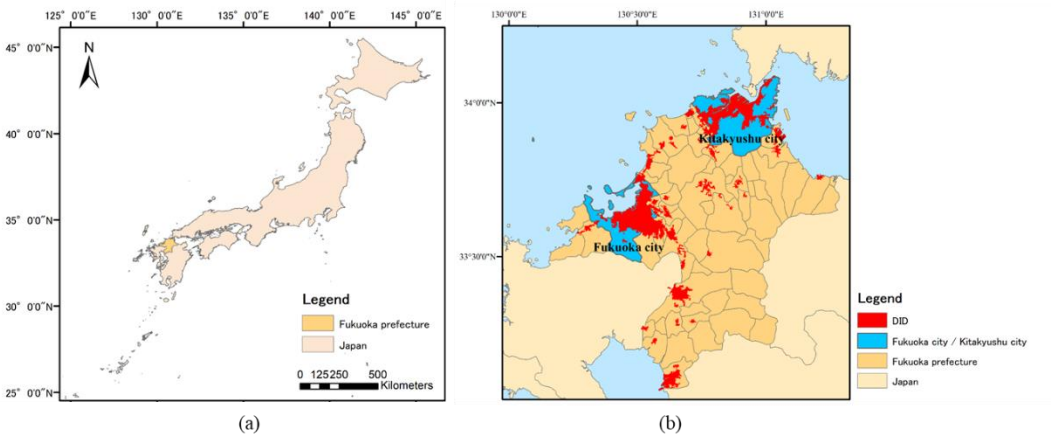


Figure 1. (a) Location of Fukuoka prefecture, (b) Location of Fukuoka city and Kitakyushu city and DID distribution in Fukuoka prefecture

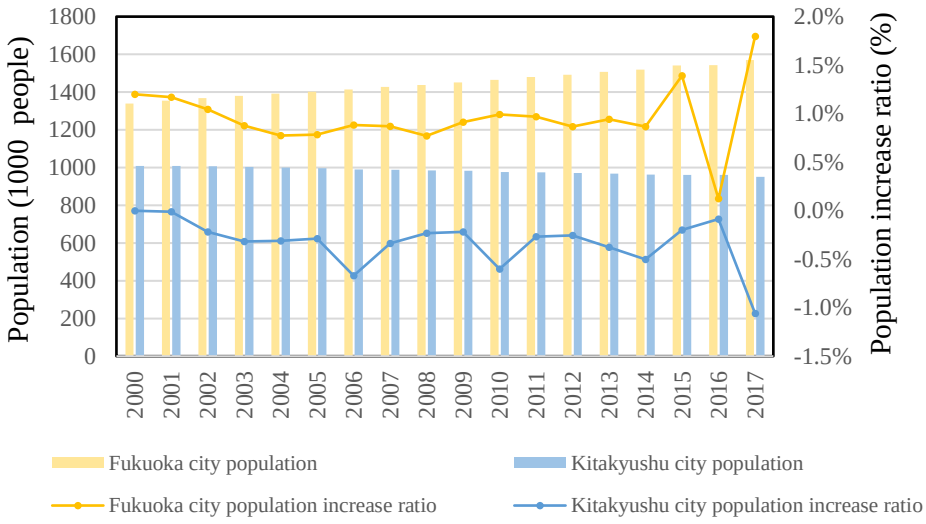


Figure 2. Fukuoka city and Kitakyushu city population and population increase ratio (2000-2017)

The 16-day composite (MOD13Q1) MODIS images with NDVI data and surface reflectance data at 250 m spatial resolution were also downloaded from the EARTHDATA website (https://search.earthdata.nasa.gov/). The land use and land cover of Fukuoka prefecture in 2006 and 2016 at 100 m spatial resolution were download form Japan National Land Numerical Information website (http://nlftp.mlit.go.jp/ksj/) (Figure 3). The digital elevation data with 30 m spatial resolution were downloaded from the Advanced Spaceborne Thermal Emission and Reflection Radiometer (ASTER) Global Digital Elevation Model Version 2 (GDEM V2). These data are all reprojected to WGS 1984 and resampled to 250 m spatial resolution for downscaling MODIS LST images. In addition, to find interrelationship between population with UHI, population distribution data with 250 m spatial resolution in 2005 and 2015 based on Japan

National Population Census in 2005 and 2015 were collected from Japanese Government Statistics Website (https://www.e-stat.go.jp/) (Figure 4).

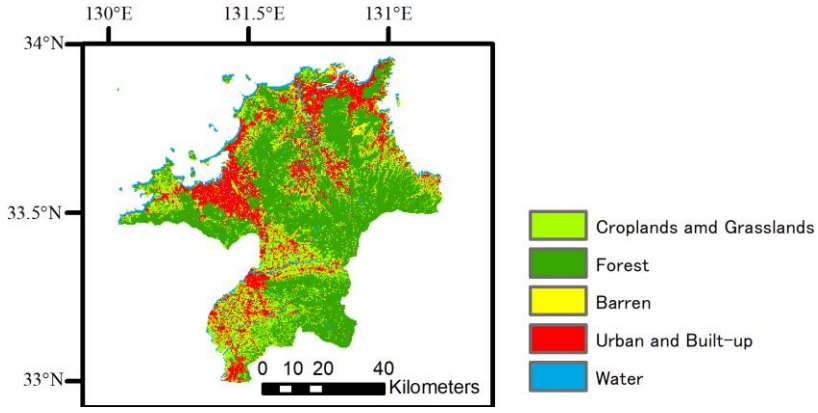


Figure 3. Land use and land cover of Fukuoka prefecture in 2016

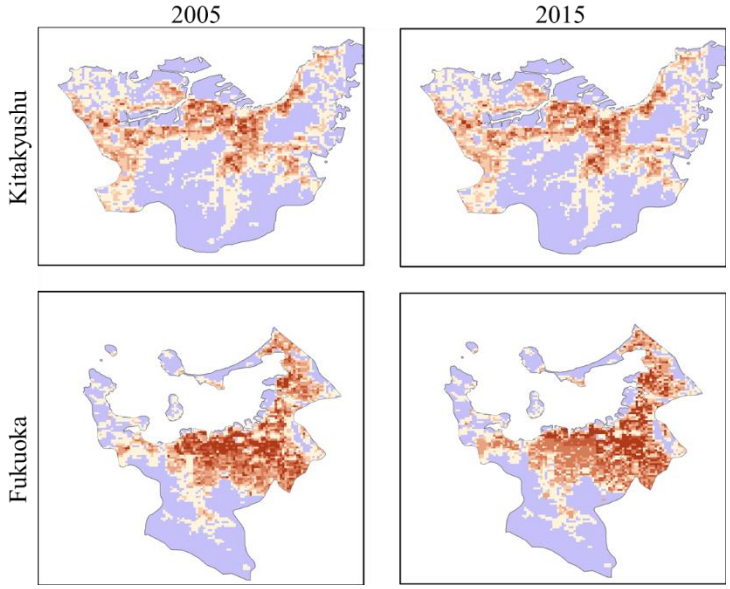


Figure 4. Population distribution in Kitakyushu and Fukuoka in 2005 and 2015

Method

Random forest based downscaling method

The RF method is a widely used ensemble machine learning method for classification, regression, and other tasks. The method constructs large numbers of decision trees during the training time, and output the mean prediction of the individual trees. RF has the advantage in modeling the complex nonlinear relationships between responding variable and predictive variables. Compared to the TsHARP method, the MRM, and other ML methods, the RF based downscaling method has higher precision (Hutengs et al., 2016). In this study, coordinate, digital elevation, NDVI, surface reflectance, and LULC were selected as the predictive variables, each decision tree is built from a bootstrap sample contains 70% of the input data. Based on a number

of testing results, the number of variables selected at each split each was set to 4, and the number of trees was set to 1000.

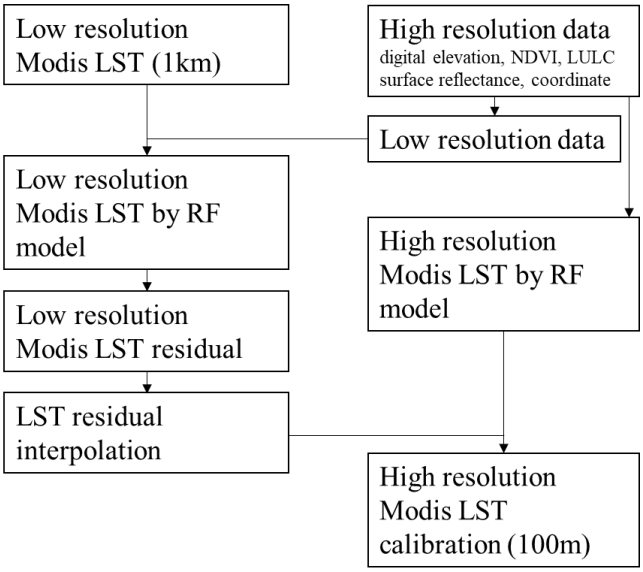


Figure 5. Flow chart of downscaling MODIS LST products based on RF

Figure 5 shows the downscaling process. Firstly, all predictive variables were resampled to 1 km spatial resolution to match the MODIS LST data. Secondly, the prediction of low resolution LST data based on the RF regression was conducted and the residual between real MODIS LST data and prediction was calculated. Thirdly, the high resolution (250 m) LST data were predicted based on the RF regression and corrected with the spline interpolated residual. The correlation coefficients and the root mean square error (RMSE) were calculated for downscaling accuracy assessment.

Surface urban heat island intensity

In this study, surface urban heat island intensity (SUHII) was defined as the average urban LST subtracts the average LST of surrounding rural areas. The urban areas of the 2 cities were extracted by the DID distribution. 3 km buffer zones surrounding the DID in the two cities were selected as the urban boundary area. Zonal statistics were used to calculate the mean LST value of the urban boundary area. The SUHII is the difference between the LST of the pixel in the urban area and the mean LST value of the urban boundary area, shown as Eq.1.

$$SUHII_{(i,j)} = \overline{LST}_{boundary} - LST_{(i,j)} \quad (1)$$

Data analysis

Zonal statistics were conducted to study the relationship between the SUHII and population distribution and the LULC. We studied the correlation between the mean SUHII and the increasing Euclidean distance to each LULC type to evaluate the urban cooling effect potential of each LULC type.

Results and discussions

Downscaling LST results

Figure 6 shows the downscaled LST images. The accuracy of the downscaling LST based on RF regression is presented in Table 1 for Fukuoka prefecture in 2005, and 2015. In general, the results show that good performance of RF regression. Especially in summer daytime, summer nighttime, and winter daytime the overall R^2 varied from 0.73 to 0.88, and the overall RMSE varied from 0.45 to 1.05 °C. However, relatively poor correlation in winter nighttime was found that the R^2 of winter nighttime in 2005 and 2015 were 0.57 and 0.54. Figure 5 shows the downscaling MODIS LST results in Fukuoka. The thermal environment is similar in the same season in 2005 and 2015. Specifically, the UHI effect exists during the study period for the high LST in the urban area. However, the LST of the coastal area in the north part of Fukuoka prefecture is low in the daytime and high in nighttime both in summer and winter shows the urban cooling effect (UCE) potential. The SUHII in summer daytime is the highest both of the two cities, while in winter nighttime, the SUHII is the lowest varied from 0.69 °C to 1.11 °C. Meanwhile, the UHI effect is more significant in Fukuoka city and the biggest difference exist in summer daytime that the mean SUHII of Fukuoka city is about 1.7 °C higher than Kitakyushu city.

SUHII variation and UCE intensity

In this study, we combined population distribution data and LULC data and the downscaled SUHII data for Fukuoka city and Kitakyushu city in the summer and winter of 2005 and 2015 (day/night). We calculated the average SUHII for the population distribution (gradient 10 people), and Euclidean distance to each LULC type (gradient 100 m). The results of the SUHII variation and UCE intensity and distance is shown in Figure 7. The determination coefficient R^2 are shown in Table 2.

Table 1. Downscaling LST results based on RF regression, R^2 is the determination coefficient, RMSE is the root-mean-square error (°C), a is the slope, b is the intercept between predict and actual value. SUHII are calculated based on Eq. 1

	R^2	RMSE (°C)	a	b	Fukuoka SUHII (°C)	Kitakyushu SUHII (°C)
2005						
summer daytime	0.80	0.92	0.91	3.51	6.91	4.71
summer nighttime	0.77	0.45	0.82	2.54	2.82	2.24
winter daytime	0.73	0.82	0.72	2.18	2.79	2.36
winter nighttime	0.57	0.71	0.55	1.18	1.11	0.69
2015						
summer daytime	0.88	1.05	0.98	0.84	6.98	4.16
summer nighttime	0.82	0.55	0.92	0.45	2.01	1.48
winter daytime	0.86	0.63	1.01	0.05	2.94	2.40
winter nighttime	0.54	0.51	1.08	0.12	0.69	0.72

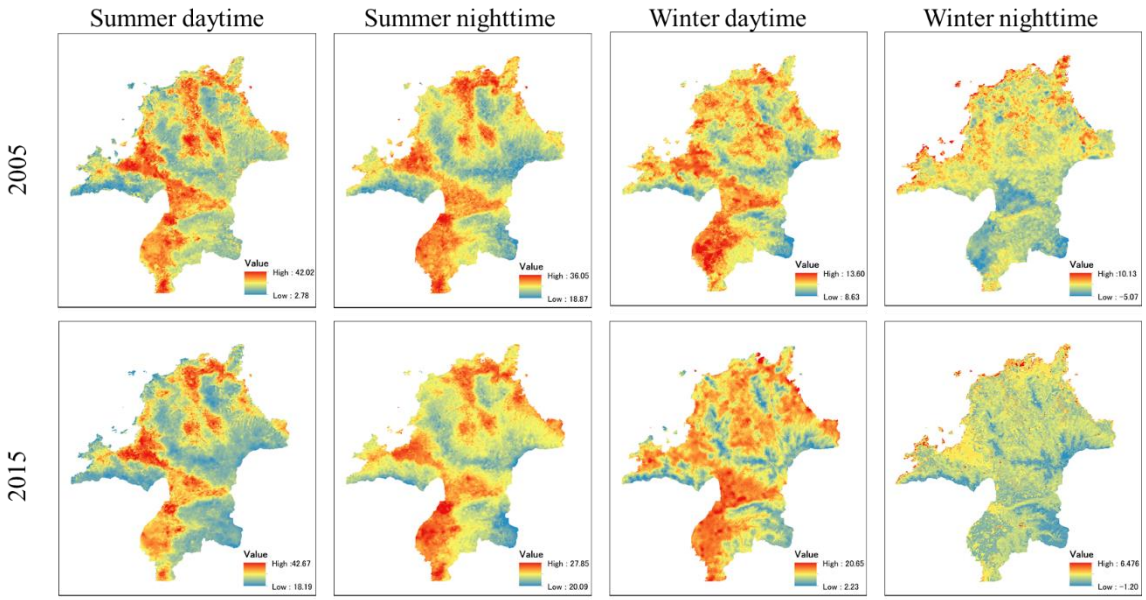


Figure 6. Downscaled LST using RFR

The mean SUHII variation on the population density shows the strong correlation between urban population and urban thermal environment. The mean SUHII increased rapidly first then slowed down when the population reaches about 600. In addition, the SUHII increases in Fukuoka city are more obvious than that in Kitakyushu city. However, the population effect on SUHII is not obvious in winter nighttime, which might due to the effect of the high LST of the coastal areas in the two cities. Previous study found a strong connection between NDVI and LST (Yuan et al. 2007, Chen et al., 2006), however, the NDVI interval in urban areas range from -0.2 to 0 approximately, while there is a wide LST range in the urban areas. As a result, the accuracy of downscaling MODIS LST images based on predictive parameters including NDVI in the urban built-up areas is smaller than that in the rural and green areas.

The mean SUHII decreases when the distance to the urban area increases and the mean SUHII is dropped to 0 when it is about 800 m to the urban area. When the mean SUHII is dropped below -1 °C in the summer daytime, the variation of mean SUHII is not obvious. The change curves in other period are similar to that in summer daytime. The only different curve is shown in Fukuoka city in 2005 in winter nighttime, which could explain by the high LST in the coastal areas.

In general, the UCE of the sea is the biggest, the UCE of the forest comes second, then comes to UCE of green area and river. The results for the sea show that in daytime, the mean SUHII of the offshore area is low, and the UCE of the sea is the biggest for the mean SUHII change occurring at about 2.5 km in Fukuoka city in the summer daytime, which is the farthest turning point. The R^2 are approximately 0.88 in 2005 and 0.91 in 2015 during the summer daytime. Meanwhile, the mean SUHII of the offshore area is high in the nighttime, the UCE distance varies from 600 m to 1 km during the summer nighttime and winter nighttime. The UCE distance of the river is about 300 m during the four study periods. The R^2 varies from 0.8 to 0.95 during the summer daytime, 0.9 to 0.97 during the summer nighttime, 0.81 to 0.98 during the winter daytime, and 0.56 to 0.89 during the winter nighttime. The daytime characteristics for the SUHII variation for the forest is similar to the sea while the nighttime characteristics are the opposite. The mean

SUHII change occurring at about 1 km to the forest area with about 6 °C SUHII variation in the summer daytime, 2 °C SUHII variation in the summer nighttime and winter daytime, 0.5 °C SUHII variation in the winter nighttime. The UCE distance of green areas variance from 300 m to 900m. However, the UCE is relatively small with a small changing scale of the SUHII variation and flat fitting curve.

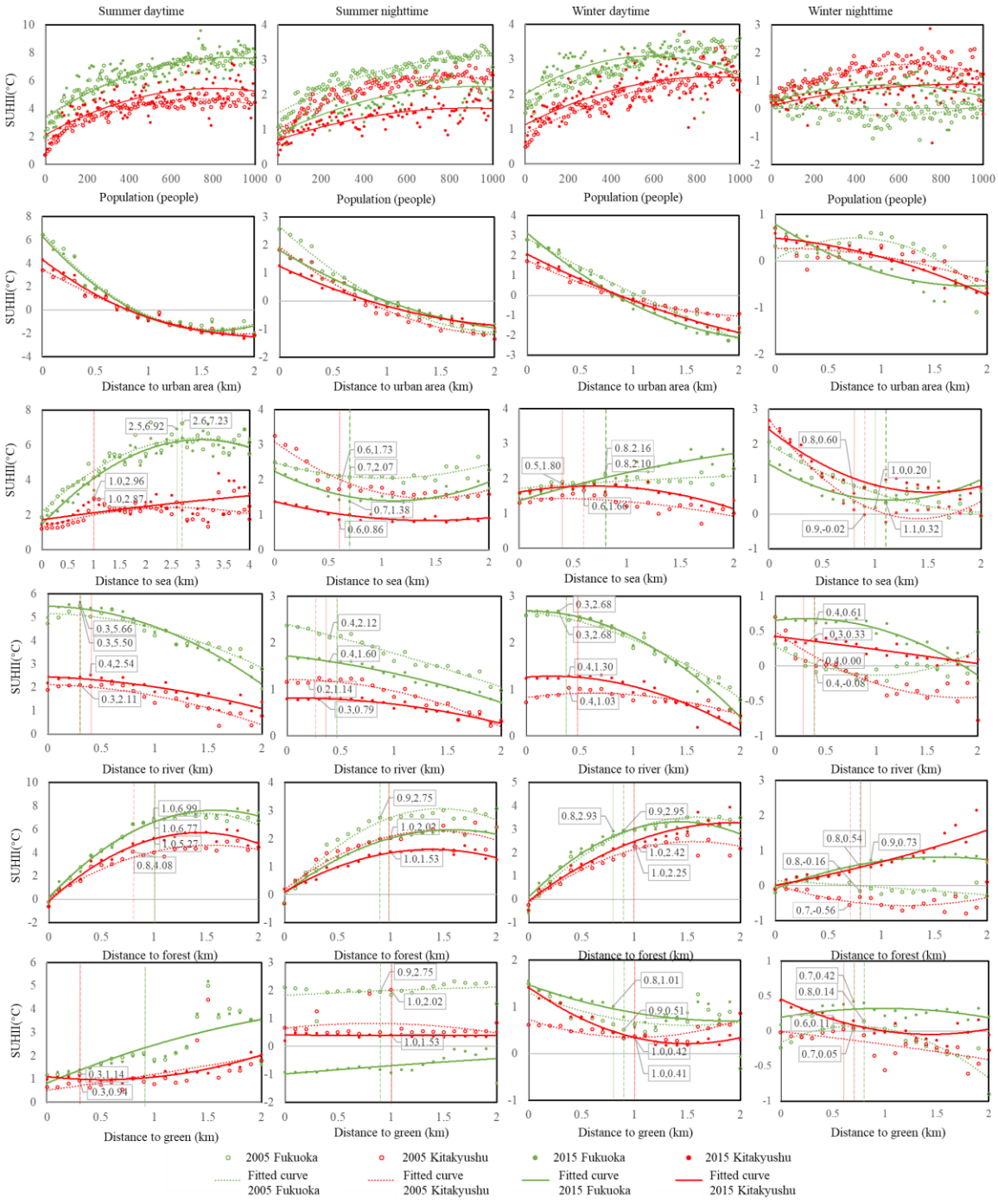


Figure 7. Relationship between mean SUHII and population and distance to each LULC type, vertical lines and curve lines represent turning points of SUHII and fitting curves.

Previous studies have intensively focus on the UCE of the urban green areas and urban rivers (Xue et al., 2019, Park et al., 2019). In addition, based on remote sensing technology, a number of the UHI studies introduced NDVI which is easy to calculate from remote sensing data as an evaluation index for the UHI. However, in a highly dense urban area, the UHI study should give priority to the effect of artificial heat source, aerodynamic roughness length, wind speed, and sky view factor.

Table 2. Determination coefficient R^2 between SUHII and population and distance to each LULC type

	Summer daytime SUHII				Summer nighttime SUHII				Winter daytime SUHII				Winter nighttime SUHII			
	Fukuoka		Kitakyushu		Fukuoka		Kitakyushu		Fukuoka		Kitakyushu		Fukuoka		Kitakyushu	
R^2	2005	2015	2005	2015	2005	2015	2005	2015	2005	2015	2005	2015	2005	2015	2005	2015
Population	0.89	0.70	0.83	0.56	0.89	0.68	0.88	0.55	0.85	0.48	0.82	0.41	0.23	0.12	0.55	0.18
Distance to urban area	0.96	0.98	0.98	0.98	0.99	0.98	0.98	0.99	0.98	0.99	0.98	0.99	0.69	0.84	0.59	0.95
Distance to sea	0.88	0.91	0.33	0.35	0.57	0.84	0.89	0.86	0.48	0.89	0.55	0.76	0.95	0.68	0.95	0.89
Distance to river	0.90	0.80	0.95	0.86	0.96	0.97	0.92	0.90	0.98	0.97	0.81	0.91	0.56	0.89	0.80	0.83
Distance to forest	0.97	0.98	0.94	0.98	0.95	0.97	0.84	0.95	0.98	0.95	0.91	0.93	0.37	0.96	0.50	0.75
Distance to green	0.59	0.55	0.27	0.88	0.01	0.29	0.09	0.05	0.32	0.50	0.68	0.97	0.78	0.27	0.45	0.79

Conclusion

We analyzed the spatial characteristics of the UHI of Fukuoka city and Kitakyushu city in Fukuoka prefecture, Japan in 2005 and 2015 during summer and winter. The results show that the SUHII in summer daytime is the biggest while in winter nighttime is the smallest. The SUHII of Fukuoka city is bigger than that in Kitakyushu city, suggesting a positive correlation between the UHI effect and the city size. The relationship between the SUHII variation and the urban population distribution shows the population density has a strong correlation with the UHI in the two study cities. Furthermore, the sea has the biggest UCE. The UCE distance of the sea is about 2.5 km in Fukuoka city in the summer daytime. The UCE of the forest comes second, the UCE distance is about 1 km over the study period. The UCE of the river and the green areas are relatively small and the UCE distances vary from 300 m to 1 km.

References

Zhou, L., Dickinson, R. E., Tian, Y., Fang, J., Li, Q., Kaufmann, R. K., ... & Myneni, R. B. (2004). Evidence for a significant urbanization effect on climate in China. Proceedings of the National Academy of Sciences, 101(26), 9540-9544.

Zhu, H. M., You, W. H., & Zeng, Z. F. (2012). Urbanization and CO2 emissions: A semi-parametric panel data analysis. Economics Letters, 117(3), 848-850.

Agam N, Kustas W P, Anderson M C, et al. A vegetation index based technique for spatial sharpening of thermal imagery[J]. Remote Sensing of Environment, 2007, 107(4): 545-558

Chen X L, Zhao H M, Li P X, et al. Remote sensing image-based analysis of the relationship between urban heat island and land use/cover changes[J]. Remote sensing of environment, 2006, 104(2): 133-146.

dos Santos, A. R., de Oliveira, F. S., da Silva, A. G., Gleriani, J. M., Gonçalves, W., Moreira, G. L., ... & Juvanhol, R. S. (2017). Spatial and temporal distribution of urban heat islands. Science of the Total Environment, 605, 946-956.

Foley, J. A., DeFries, R., Asner, G. P., Barford, C., Bonan, G., Carpenter, S. R., ... & Helkowski, J. H. (2005). Global consequences of land use. science, 309(5734), 570-574

Mukherjee S, Joshi P K, Garg R D. A comparison of different regression models for downscaling Landsat and MODIS land surface temperature images over heterogeneous landscape[J]. Advances in Space Research, 2014, 54(4): 655-669.

Park C Y, Lee D K, Asawa T, et al. Influence of urban form on the cooling effect of a small urban river[J]. Landscape and Urban Planning, 2019, 183: 26-35.

Wang, S., Ma, H., & Zhao, Y. (2014). Exploring the relationship between urbanization and the eco-environment—A case study of Beijing–Tianjin–Hebei region. Ecological Indicators, 45, 171-183.

Xue Z, Hou G, Zhang Z, et al. Quantifying the cooling-effects of urban and peri-urban wetlands using remote sensing data: Case study of cities of Northeast China[J]. Landscape and Urban Planning, 2019, 182: 92-100.

Yuan F, Bauer M E. Comparison of impervious surface area and normalized difference vegetation index as indicators of surface urban heat island effects in Landsat imagery[J]. Remote Sensing of environment, 2007, 106(3): 375-386.

Urban features at neighbourhood scale to assess and mitigate the heat island in arid Mendoza, Argentina

María Belén Sosa, Instituto de ambiente, hábitat y energía - CONICET (Argentina)
Erica Correa, Instituto de ambiente, hábitat y energía - CONICET (Argentina)
Michele Zinzi[1]*, ENEA (Italy)*

ABSTRACT

In arid and hot climate cities, urban heat island (UHI) phenomenon reductions represent a major challenge. Nowadays, climate-sensitive urban planning strategies are useful in order to reduce the UHI in arid cities. The presented study was carried out in the arid Metropolitan Mendoza Area (MMA), Argentina. The study measures the thermal improvement of apply high-albedo's roof materials and analyses its effectiveness in different neighbourhood´s layouts forms. To carry out the study, three low-density neighbourhoods that have analogous urban features but different layouts forms (multi-azimuthal, rectangular and Cul-de-Sac) were selected. Also, the downtown and four MMA´s boundaries points were assessed. The study cases were micro-climate monitored, and the three neighbourhoods were modelled and adjusted with ENVI-met software. The results show that reductions in diurnal air temperatures could be achieved by using cool roofs strategy. These findings validate the researches that indicate that this UHI mitigation strategy has a higher diurnal cooling impact. Regarding the neighbourhood form, the rectangular and multi-azimuthal layouts forms remain cooler. This highlights that suitable urban planning decisions in arid cities could helps reduce the UHI phenomenon and improves the liveability of outdoor and indoor spaces.

Introduction

Global warming and urban development are generating several environmental impacts at different climatic scales. At city scale, urban heat island (UHI) is the most noticeable phenomenon, worldwide observed and measured (Suman et al. 2018; Leal Filho et al. 2017; Tsoka Tsikaloudaki and Theodosiou 2017; Yan and Dong 2015; Mills et al. 2010; Jusuf, Wong and Hagen 2007; Collier 2006; Oke 1982). UHI impacts on outdoor and indoor thermal conditions decreasing thermal comfort and increasing the energy consumption for air condition demand (Salamanca et al. 2014; Lin, Matzarakis and Hwand 2011; Kovats and Akhtar 2008).

Particularly in arid and hot climate cities, reduce the UHI represents a major challenge because of the extreme weather conditions during summertime. In addition, hot climates areas have higher urbanization rates and population growth compared to other climates (United

[1] Corresponding Author: michele.zinzi@enea.it.

Nations 2015). According to *Keitsch (2012)* an unfavourable outdoor and indoor climate can be prevented or mitigated through the application of climate-sensitive urban and building design, which refers to measures that adapt the urban landscape to the site, the region, and the climate. In relating to this, there exists a wide range of strategies to reduce and mitigate the UHI that urban planners could implement. *Kleerekoper, Van Esch and Salcedo (2012)* summarize and cluster the strategies in four categories: (i) built form, (ii) material, (iii) vegetation, and (iv) water.

Regarding the built form many studies suggest that a well-planned neighbourhood, which considers the layout, street and block proportions and orientations can reduce the impacts on the micro-climate (Hu, White and Ding 2016; Jusuf, Wong and Hagen 2007). In this sense, *Middel et al. (2014)* have demonstrated, at neighbourhood scale, that the urban form has a larger impact on daytime temperatures than urban greening. Taking into account the materials, high-albedo urban surfaces are an effective strategy to counterbalance the UHI impacts, particularly in cities with sunny climates, high solar radiation and external air temperature (Baniassadi et al. 2018; Kolokotroni et al. 2018; Santamouris 2014). High-albedo roofs in the southwest U.S. reported a 0.3°C decrease in summertime average ambient temperature in urban areas per 0.1 increases of average albedo of urban surfaces (Santamouris 2014). Also, *Sproul et al. (2014)* reported that cool roofs are the most cost-effective energy saving strategy when it comes to rooftops. According to incorporate vegetation, *Declet-Barreto et al. (2013)*, showed that increasing vegetation have the potential to cool the air by as much as 1.9 °C by modelled air temperatures through the creation of park cool islands in inner-city neighbourhoods in Phoenix. Finally, the incorporation of water bodies and fountains into cities with arid climates is not considered a sustainable planning policy, because of this resource scarcity. *Jenerette et al. (2011)* underscores the paradox of water conservation and UHI mitigation through evapotranspirational cooling in arid regions. The implementation of these strategies depends on the availability for that purpose of natural, economic, industrial, and social resources in each city.

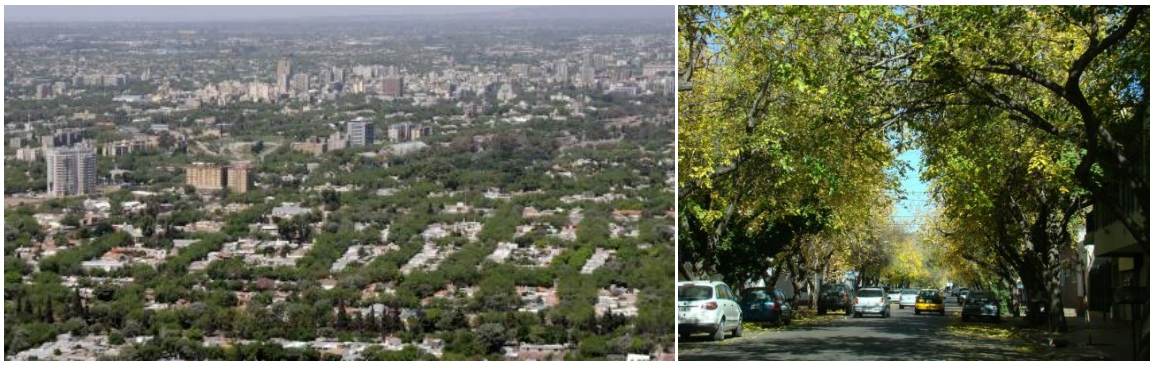


Figure 1. Mendoza Metropolitan Area - Argentina

The presented study was carried out in the Metropolitan Mendoza Area (MMA), Argentina 32º53’S latitude, 68º51’W longitude, 750m.a.s.l. The MMA has most of its streets forested, being this a particular characteristic regarding it arid climate context, see Figure 1. As

the street trees are already considered an effective UHI mitigation strategy, evaluate the outdoor air temperatures improvement by taking into account others features at neighbourhood scale is considered a suitable urban planning recommendation. For the exposed, the study aims to analyse the thermal performance by applying high-albedo roofs in three low-density neighbourhoods, which are forested and have different layouts form. Also, analyse if the effectiveness of the strategy dependent on the urban grid form.

Methodology

The method implemented for the present work consists of three main stages.

Study cases

The selected three neighbourhoods have different layout grids —multi-azimuthal, rectangular and Cul-de-Sac— but similar features —houses typology, materials, street trees and LCZ class— that allows contrasting their thermal behaviour. The selection criteria and characterization was described in *Sosa, Correa and Cantón (2017)*. The three neighbourhoods have their streets forested with second magnitude trees, streets widths of 16 and 20m, houses height of 3m, albedo's of 0.2 in roofs, 0.3 in façades, 0.5 as a combined average value between side-walks and streets materials, and LCZ class 6_b (open-low rise class with scattered trees subclass). Also, these neighbourhoods are located in different areas of the MMA around 6.5 and 4.8km distance to the downtown.

In order to analyse the UHI impact in the MMA, four boundaries points (North, South, East and West sectors) and a point in the MMA downtown were monitored. The selected boundaries points are coincident with the MMA urbanization limits, sparsely built areas (LCZ class 9). The study cases are show in Figure 2.

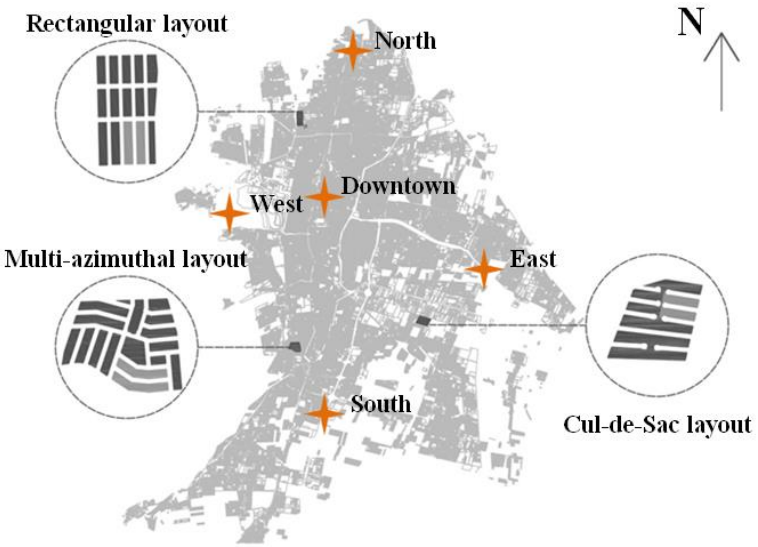


Figure 2. Study cases located in the MMA

Micro-climatic data monitoring

The thermal behaviours were monitored with HOBO® data-loggers (model H08-003-02; measure range -20°C to +70°C; accuracy ±0.7°C at +21°C; resolution 0.4°C at +21°C) set up every 15 minutes. They were installed into a solar radiation shield at 2m height, a total of eight fix-sensors were used simultaneously during the summer period from January 8th to February 6th 2014. The monitored points are presented in Figure 2.

Micro-climate simulation

In a second stage, three urban scenarios were numerically simulated in order to analysed the cool roof´s effectiveness at neighbourhood scale. ENVI-met software version 3.1 (Bruse 2004) was used. ENVI-met requires two main input files: the area input file (.IN file), and the configuration file (.CF file). The .IN file specifies the geometry of the model environment such as buildings, plants or soils in detail. In this study the scenarios were modelled within a horizontal area of 258 × 258m that comprised of 86 × 86 cell grids of 3 × 3m. Each cell grid was 3m in height, and there were 30 such grids (i.e., the spatial height of each model is 90m).

Table 1. ENVI-met input parameters after model adjustment

Meteorological	
Mean wind speed 10 m from the ground (m/s, Airport meteorological station)	2.5
Prevailing wind direction (Airport meteorological station)	140º
Roughness length	0.1
Solar adjustment factor	1.3
Initial atmospheric temperature (K) (University of Wyoming, station 87418 Mendoza)	300
Specific humidity at 2500 m (g/kg-1)	2.8
Relative humidity at 2 m (%)	37
Building	
Indoor temperature (K)	297
Heat Transmission Walls (W/m^{2}K)	2
Heat Transmission Roofs (W/m^{2}K)	0.78
Walls albedo	0.3
Roofs albedo	0.2
Soil	
Initial upper soil layer (0-20 cm) temperature (K)	292
Initial upper soil layer (20-50 cm) temperature (K)	292
Initial deeper soil layer (below 50 cm) temperature (K)	290
Upper soil layer (0-20 cm) moisture content (%)*	20
Upper soil layer (20-50 cm) moisture content (%)*	35
Deeper soil layer (below 50 cm) moisture content (%)*	60

To represent street trees, the “Tb” model was selected from the ENVI-met PLANTS database, which was based on a field survey and observation of the vertical configurations of

trees (a height of 10m and LAD between 0.80 and 2.00m²/m³ were used for calculation). Also, the SVF values of each urban canyon where the data-logger was installed were adjusted with those generated by the ENVI-met model. The soils data represent the real condition of the study cases that have concrete streets, side-walks with tiles and grass areas in the patios of the houses. Also, the positions of receptors were designed in this file. To ensure numerical stability and minimize boundary effects that may affect the output data, three (9m) nesting grids were set around the main model area (Morakinyo et al. 2017). The .CF file defines the settings for the simulation to run, for example, the name for the area .IN file, the meteorological settings or the name of the output files. Table 1 shows the .CF ENVI-met input parameters that were used.

Validation of the models and data calibration

A calibration procedure was made for each neighbourhood layout, by comparing the series of air temperature measurements from January 18th with the corresponding simulated values. Then the three scenarios were statistically evaluated using a set of indices that describe the magnitude of the difference between the observation and prediction (R^2, RMSE, MAE and MBE). After made several simulations adjustments the scenarios achieved a good statically accuracy. Based on statistical index values that were accepted in previous ENVI-met evaluation studies, the models can reliably simulate micro-climates (Tsoka, Tsikaloudaki and Theodosiou 2017). The adjustment values for the three models are shown in Table 2.

Table 2. Models adjustment and statistical indicators for validation

	Rectangular	Multi-azimuthal	Cul-de-Sac
MAE	0.5	0.6	0.5
RSME	1.7	0.4	1.1
MBE	-1.0	-0.2	-0.3
R^2	0.91	0.99	0.95

Cool roofs scenarios modelling

With the three adjusted models, the high-albedo material where apply at roofs scale (original value 0.2, improved value 0.7). This albedo material value has a strong reflective capability and potentials to lower surface temperature, so its colour tends to be light (Santamouris 2013; Synnefa et al. 2011). The high-albedo value used follows the recommendations of a previous study conducted in the MMA (Alchapar and Correa 2015). The albedo values of walls and pavements were maintained at same from the original neighbourhood materials (walls 0.3, pavements 0.5).

Results

Figure 3 shows the thermal performance of the four boundaries points (North, South, East and West) and the MMA downtown. The North sector registered the lowest minimum air

temperature (21.5 °C). The downtown point registered the coolest maximum air temperature (36.8 °C) and the highest minimum (26.3 °C). These behavioural differences between the boundaries and downtown are a result of several factors, including but not limited to the amount of built-up areas and the anthropogenic heat generation (e.g., transportation and air conditioning use) that exists within a city (Ahmed et al. 2013). In terms of habitability, the downtown behaviour is positive. However, at night, this area suffers from the worst scenario of UHI.

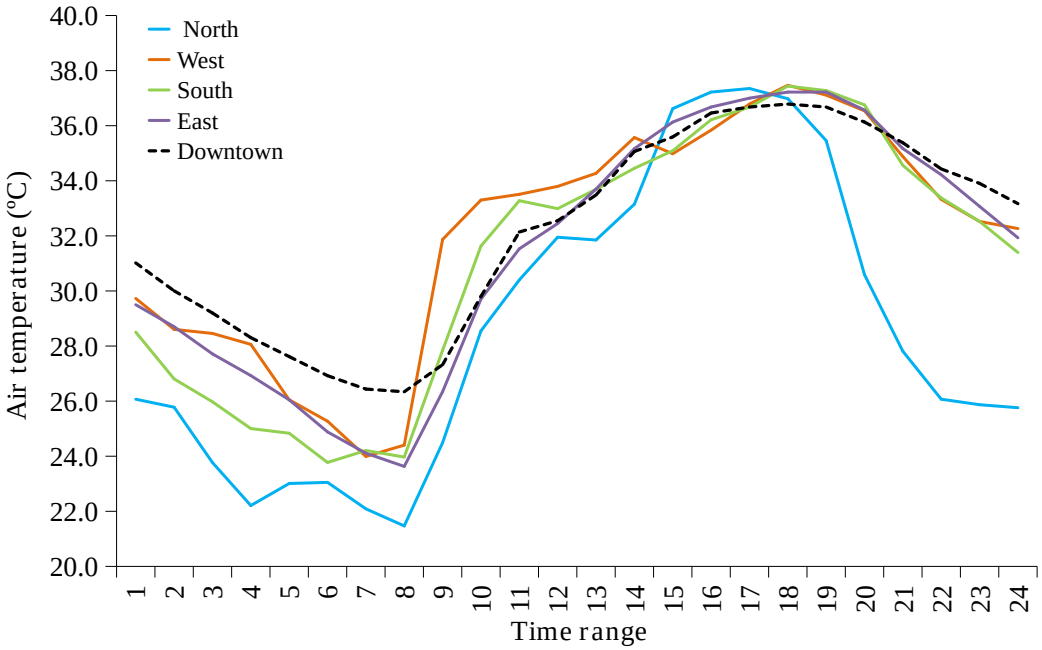


Figure 3. Thermal performance of each monitored point

The monitoring data were used the calibrate the model. Figure 4 and Table 3 shows the thermal performance by applying high-albedos roof in the three neighbourhood layouts. By analysing the impact in each neighbourhood layout we can see that:

- The rectangular layout neighbourhood achieved the lowest maximum and average air temperatures (37.5ºC and 30.6ºC), but the highest minimum temperature (25.1ºC).
- The multi-azimuthal layout neighbourhood achieved the lowest minimum air temperature (23.2ºC), and similar maximum and average air temperatures with the rectangular layout (37.8ºC and 30.9ºC).
- The Cul-de-Sac layout neighbourhood achieved the highest maximum and average air temperatures (38.4ºC and 31.1ºC), and similar minimum air temperature with the multi-azimuthal layout (23.5ºC).
- These observations follow the thermal performance trend of the original neighbourhood, where the rectangular and multi-azimuthal layouts forms remains cooler. Also, the maximum and average air temperatures decrease in all the neighbourhoods but the minimum air temperatures have not significant reductions. These findings are in concordance with researches that have been demonstrating a higher diurnal cooling

performance than the nocturnal cooling performance (Qi et al. 2019; Li and Norford 2016).

Table 3. Thermal performance of the study cases

Study cases	Tº maximum (ºC)	Tº minimum (ºC)	Tº average (ºC)
R.O	38.6	25.4	33.0
R.I	37.5	25.1	30.6
Δ	1.1	0.3	2.4
M.O	39.5	23.2	31.9
M.I	37.8	23.2	30.9
Δ	1.7	0	1.0
C.O	40.8	24.1	32.8
C.I	38.4	23.5	31.1
Δ	2.4	0.6	1.7

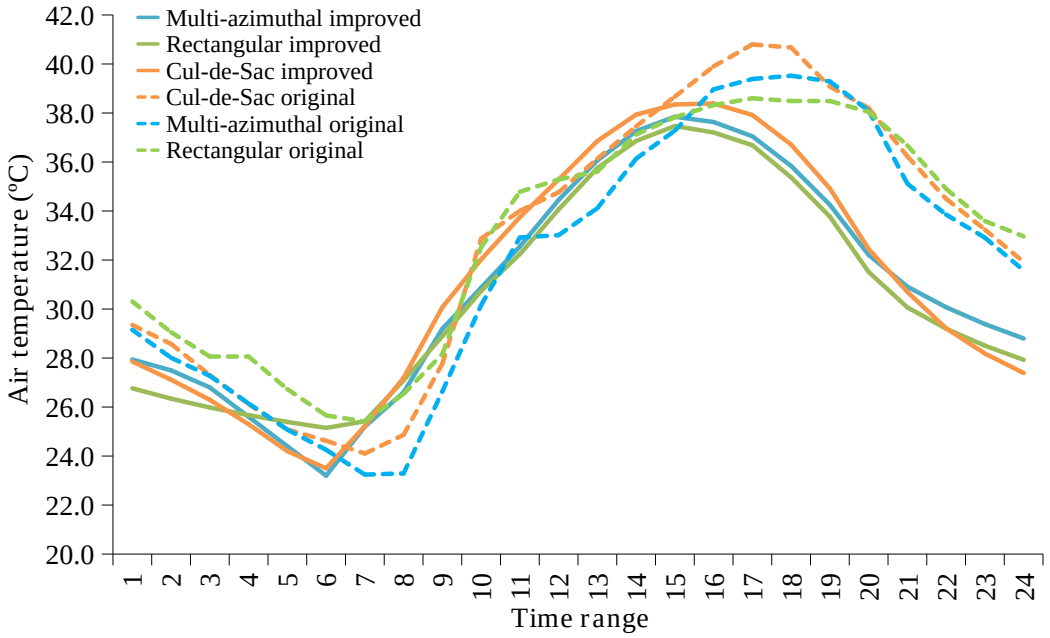


Figure 4. Ambient temperature profile of the study cases

Regarding the relationship between the layout form and the thermal performance, the rectangular neighbourhood achieved the lowest maximum air temperature by the North-South streets orientation (south hemisphere). On the other hand, the minimum air temperature is the highest. This could be because the distribution of the street trees in the canyon.

Conclusions

The study presents and analysed the outdoor air temperature performance of three MMA`s low-density neighbourhoods by applying high-albedo materials at roof scale. Each study case has different layout form but maintain similar other urban features. The study cases were modelled in ENVI-met in order to measure the thermal impact of the application of the cool roof as an UHI mitigation strategy. The results show that air temperatures reductions could be achieved in the daytime. These findings validate the researches that indicate that this UHI mitigation strategy has a higher diurnal cooling impact. Regarding the neighbourhood form, the rectangular and multi-azimuthal layouts remain cooler in both stages, original and improved.

These findings highlight that suitable neighbourhood layouts, that incorporates cool materials, could help to decrease the UHI phenomenon in arid cities. Also in order to avoid this phenomenon extension, cool surfaces should be used in entire city districts. For that, the cool roof application needs to be further analysed in a bigger area of intervention in order to measure the expected temperature improvements. This strategy is feasible to apply in climate-sensitive planning regulations and policies at neighbourhood scale by promoting mitigation measures into new developments as well as during retrofitting and maintenance.

Acknowledgments

This work was supported by the Agencia Nacional de Promoción Científica y Tecnológica; and the Consejo Nacional de Investigaciones Científicas y Técnicas (CONICET).

References

Ahmed, B., Kamruzzaman, M., Zhu, X., Shahinoor Rahman, Md., & Keechoo, C. (2013). Simulating land cover changes and their impacts on land surface temperature in Dhaka, Bangladesh. Remote Sensing, 5, 5969–5998.

Alchapar, N., & Correa, E. (2015). Comparison the Performance of Different Facade materials for Reducing Building Cooling needs. Eco-efficient materials for Mitigating Building Cooling Needs, Woodhead Publishing, Cambridge, 155-194.

Baniassadi, A., Sailor, D. J., Crank, P. J., & Ban-Weiss, G. A. (2018). Direct and indirect effects of high-albedo roofs on energy consumption and thermal comfort of residential buildings. Energy and Buildings 178, 71-83.

Bruse, M. (2004). ENVI-met website. Available from: http://www.envi-met.com/

Collier, C. (2006). The impact of urban areas on weather. Quarterly Journal of the Royal Meteorological Society, 132, 1-25.

Correa, E., de Rosa, C., & Lesino, G. (2008). Urban heat island effect on heating and cooling degree day's distribution in Mendoza's metropolitan area. Environmental costs. Proceedings of the EUROSUN 2: 951-958, Lisbon from 7-10 October.

Declet-Barreto, J., Brazel, A., Martin, C., Chow, W., & Harlan, S. (2013). Creating the park cool island in an inner-city neighborhood: heat mitigation strategy for Phoenix, AZ. Urban Ecosystem, 16, 617-635.

Hu, Y., White, M., & Ding, W. (2016). An Urban Form Experiment on Urban Heat Island Effect in High Density Area." Procedia Engineering, 169, 166-174.

Jenerette, G., Harlan, S., Stefanov, W., & Martin, C. (2011). Ecosystem services and urban heat riskscape moderation: water, green spaces, and social inequality in Phoenix, USA. Ecol Appl, 21, 2637-2651.

Jusuf, S., Wong, N., & Hagen, E. (2007). The influence of land use on the urban heat island in Singapore. Habitat International, 31, 232-242.

Keitsch, M. (2012). Sustainable architecture, design and housing. Sustainable Development, 20, 141-145.

Kleerekoper, L., Van Esch, M., & Salcedo, T. (2012). How to make a city climate-proof, addressing the urban heat island effect. Resources, Conservation and Recycling, 64, 30-38.

Kolokotroni, M., Shittu, E., Santos, T., Ramowski, L., Mollard, A., Rowe, K., Wilson, E., Pereira de Brito Filho, J., & Novieto, D. (2018). Cool roofs: High tech low cost solution for energy efficiency and thermal comfort in low rise low income houses in high solar radiation countries. Energy and Buildings, 176, 58-70.

Kovats, S., & Akhtar, R. (2008). Climate, climate change and human health in Asian cities. Environ Urban, 20, 165-175.

Leal Filho, W., Echevarria, F., Emanche, V., & Al-Amin, Q. A. (2017). An Evidence-Based Review of Impacts, Strategies and Tools to Mitigate Urban Heat Islands. *I*nt. J. Environ. Res. Public Health, 14, 1600.

Li, X., & Norford, L. K. (2016). Evaluation of cool roof and vegetations in mitigating urban heat island in a tropical city, Singapore. Urban Climate, 16, 59-74.

Lin, T.P., Matzarakis, A., &Hwand, R.L. (2011). Shading effect on long-term outdoor thermal comfort. Building and Environment, 45, 213-211.

Middel, A., Häb, K., Brazel, A. J., Martin, C. A., & Guhathakurta, S. (2014). Impact of urban form and design on mid-afternoon microclimate in Phoenix Local Climate Zones. Landscape and Urban Planning, 122, 16-28.

Mills, G., Cleugh, H., Emmanuel, R., Endlicher, W., Erell, E., McGranahan, G., Ng, E. Nickson, A., Rosenthal, J., & Steemer, K. (2010). Climate Information for Improved Planning and Management of Mega Cities (Needs Perspective). Procedia Environmental Sciences I, 228-246.

Morakinyo, T., Kong, L., Lau, K., Yuan, C., & Ng, E. (2017). A study on the impact of shadow cast and tree species on in canyon and neighborhood's thermal comfort. Building and Environment, 115, 1-17.

Oke., T. R. (1982). The energetic basis of the urban heat island. Quarterly Journal Royal Meteorological Society, 108, 1-24.

Qi, J., He, B., Wang, M., Zhu, J., & Fu, W. (2019). Do grey infrastructures always elevate urban temperature? No, utilizing grey infrastructures to mitigate urban heat island effects. Sustainable Cities and Society, 46, 101-392.

Salamanca, F., Georgescu, M., Mahalov, A., Moustaoui, M., & Wang, M. (2014). Anthropogenic heating of the urban environment due to air conditioning. J. Geophys. Res. Atmos., 119, 1-17.

Santamouris, M. (2013). Using cool pavements as a mitigation strategy to fight urban heat island—A review of the actual developments. Renewable and Sustainable Energy Reviews, 26, 224-240.

Santamouris, M. (2014). Cooling the cities – A review of reflective and green roof mitigation technologies to fight heat island and improve comfort in urban environments. Solar Energy, 103, 682-703.

Sosa, M. B., Correa, E. N., & Cantón, M. A. (2017). Urban grid forms as a strategy for reducing heat island effects in arid cities. Sustainable Cities and Society, 32, 547-556.

Sproul, J., Wan, M.P., Mandel, B.H., & Rosenfeld, A.H. (2014). Economic comparison of white, green, and black flat roofs in the United States. Energy and Buildings, 71, 20-27.

Suman, P., Satiprasad, S., Pulak, M., & Subhash Chandra, M. (2018). Impacts of urbanization on land use /cover changes and its probable implications on local climate and groundwater level. Journal of Urban Management, 7, 70-84.

Synnefa, A., Karlessi, T., Gaitani, N., Santamouris, M., Assimakopoulos, D.N., & Papakatsikas, C. (2011). Experimental testing of cool colored thin layer asphalt and estimation of its potential to improve the urban microclimate. Building and Environment, 46 (1), 38-44.

Tsoka, S., Tsikaloudaki, K., & Theodosiou, T. (2017). Urban space's morphology and microclimatic analysis: a study for a typical urban district in the Mediterranean city of Thessaloniki, Greece. Energy and Buildings, 156, 96-108.

United Nations. (2015). World Urbanization Prospects: The 2014 Revision, New York: United Nations.

Yan, H., & Dong, L. (2015). The impacts of land cover types on urban outdoor thermal environment: the case of Beijing, China. Journal of Environmental Health Science & Engineering, 13, 1-7.

Development and Application of "Shadow Ratio" for Evaluating Urban Thermal and Wind Environment - Take a Site of Xi 'an West Street as an Example

Yuheng Lyu [1], Department of Architecture Xi'an JiaoTong University (China)
Dian Zhou [2], Department of Architecture, Xi'an JiaoTong University (China)
Yupeng Wang [3] , Department of Architecture, Xi'an JiaoTong University (China)

ABSTRACT

The development of urban economy and society, especially the advancement of urbanization greatly facilitates human life, and also deteriorates the living environment of cities to a certain extent. The urban environment is closely related to citizens' well-being. Therefore, the continuous improvement of living standards, creating a livable city space environment is particularly important. Urban wind environment and thermal environment are elements of urban microclimate and are playing an important role in optimizing urban living environment. Shadow from the buildings have an important influence on urban microclimate, because it affects the heat and wind environment to a great extent.

This paper proposed the concept of "Shadow Ratio" and its derivative concept of "Continuous Shadow Ratio", which could be used to indicate the spatial morphology of urban thermal environment and wind environment. The importance of using sunlight shadow to prevent heat in buildings in cold region is analyzed, and the relationship between sunlight shadow and building thermal environment and wind environment is indicated. ENVI-met software is used to simulate and evaluate the urban environment in a 300m×300m scale in the central area of Xi 'an city, calculated the shadow ratio of the site at 7 time points in the day and compares the calculated results with the environmental simulation data, and carried out coupling analysis. This paper developed and demonstrated the application value of "Shadow Ratio" for urban building environment evaluation.

1.Introduction

Cities in cold regions like Xi'an should try to improve the thermal comfort of the urban environment as much as possible in winter and should consider heat prevention in summer. Increasing solar radiation in winter can improve thermal comfort. In summer, shade can be used to reduce the heat at human level. Therefore, the use of shadows in cold regions like Xi'an is of great significance for heat mitigation in summer. Related researches have demonstrated that Shadows are formed when opaque objects block direct sunlight. And shadow in a city may come from (1): the shadow of topography; (2): architectural shadow; (3): the shadow of the vegetation. Shadow has an important influence on the thermal environment and wind environment around the buildings. Cities that are hot in summer can alleviate the heat caused by solar radiation by shading, while cities that are cold in winter can improve the thermal comfort by increasing the sunshine radiation. Shadow plays an important role in improving the urban thermal and wind environment and improving the comfort in summers.

[2]Corresponding Author: [dianz_lab@163.com]

In the 1990s, Arnfield (A.J) proposed the solar energy utilization coefficient, which represents the potential use of solar energy by a certain urban ground. Givoni.b proposed the shadow coefficient in the microclimate of seville, Spain.

Sunlight shadow and the thermal environment of residential area have a close relationship, which is one of the important factors to deal with the microclimate environment of residential area. Cities in hot-summer and cold-winter zone are sunny and have strong radiation, causing the outdoor temperature is higher. If we can make full use of the shadows generated by buildings in the planning and design process of residential districts to reduce the direct sunlight on the ground and external walls of buildings, it will be conducive to improve the thermal environment and save the energy consumption of air conditioning buildings.

The purpose of this paper is to propose a concept of “Shadow Ratio” to describe space environment. Numerical simulation is used for demonstrating this concept and proving the relationship between shadow ratio and urban environment such like thermal environment and wind environment. Considering that the concept of shadow ratio lacks time universality as an indicator of urban morphology, in order to better apply this concept to the study of urban microenvironment, the concept of "Continuous Shadow Ratio" is further proposed. The main research method used in this paper is to simulate the 24-hour climate of summer solstice day (June 21) in an area near the central area of Xi’an city with ENVI-met software then put the results, such as temperature, wind speed together with the shadow ratio to make a coupling calculation to prove that the shadow ratio is valuable for the study of urban thermal and wind environment.

2. Research Methodology

The area of 300m×300m in the central district of Xi'an is selected for simulation and analysis. Summer solstice day of 2017 (June 21) is selected, and the 24-hour thermal environment and wind environment simulation results are carried out by using the environment simulation software which is called ENVI-met to complete the 24 hours simulation. A site and building model were built in Sketchup software to simulate and calculate the shadow ratio of 7 time points in the day on 21 June. The data of temperature, wind speed and shadow ratio in the simulation results were analyzed by linear regression, and then the conclusion was drawn.

In order to better apply this concept as an indicator in the study of urban morphology, the author calculated the "Continuous Shadow Ratio" of the region. According to the regulations of Japanese building standards on building shadow, the author uses Tianzheng software to analyze the sunshine in this area from 8:00 a.m. to 4:00 p.m. on the winter solstice day. The area of continuous shadow area exceeding 4 hours is regarded as "continuous shadow area". The result of "continuous shadow area" is obtained by calculating the data of "continuous shadow area" and the floor area of the building, the total area of the study area, etc.

ENVI-met is a software for microclimate simulation of the scale of city blocks, which can be used to build an overall three-dimensional and non-static model, so as to simulate the interaction of surface-plant-air. Therefore, it is often used to simulate the environment of the city. It is designed to have a typical horizontal resolution of 0.5 to 5 meters and a microscale simulation of typical time frames of 24 to 48 hours with a time step of 1 to 5 seconds.

3. Definition and Calculation of the Shadow Ratio (SR) and Continuous Shadow Ratio (CSR)

3.1 Definition of Shadow Ratio (SR)

The ratio of the total area shaded by buildings or other obstructions in the area and the floor area of the building to the total area of the site is called the shadow ratio. And the calculation formula is shown as follows:

$$\mathrm{SR} = \frac{A_S + A_B}{A}$$

Where SR represents the shadow ratio, A_S represents the shadow area, A_B represents the floor area of the building, A represents the total area of the study area.

3.2 Definition of Continuous Shadow Ratio (CSR)

Because the concept of shadow ratio varies with time and in many cases a universal indicator is needed to evaluate urban morphology. In order to better apply this concept as an indicator to the study of urban microclimate, the author proposed a derivative concept of "Shadow Ratio": "Continuous Shadow Ratio". According to Article 56 of the Building Standard Law of Japan, the allowable hours of shadows in different land-use zones are indicated by shadow restrictions, to restrict the building heights for different neighborhoods. The standard time for environmental shadow evaluation is on the winter solstice, from 8 am to 4 pm. On average, 2-hour shadows are restricted 10 m away from buildings, and 4-hour shadows are restricted 5 m away from buildings. In this paper, 4-hour shadows are taken as the calculation criteria. Taking 8 am to 4 pm. on the winter solstice as the calculation range of shadow area, the ratio of the total area shaded by buildings or other obstructions in the area for more than 4 hours and the floor area of the building to the total area of the site is called the continuous shadow ratio. And the calculation formula is shown as follows:

$$\mathrm{CSR} = \frac{A_{CS} + A_B}{A}$$

Where CSR represents the continuous shadow ratio, A_{CS} represents the shadowed area lasting more than 4 hours from 8 am to 4 pm on winter solstice, A_B represents the floor area of the building, A represents the total area of the study area.

3.3 Study Area and the Model

The central area of Xi'an city was selected as the research area, and the map is shown in Figure 1. Xi'an is located in the cold region of China with cold and dry winters and the summers are hot with large daily temperature range of which the sunshine is relatively abundant. Therefore, the study of urban building shadow plays an important role in summer cooling and improving human comfort. And as shown in Figure 1, according to the Baidu map information, a simplified site and building model is established in Sketchup software to facilitate calculation and environmental simulation. The highest building in the area is 64m, and the lowest building height is 4m. Moreover, the plane form is diversified, including enclosed, semi-enclosed and open space.

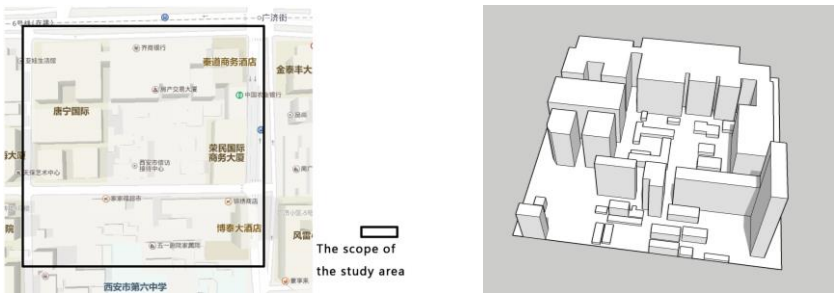
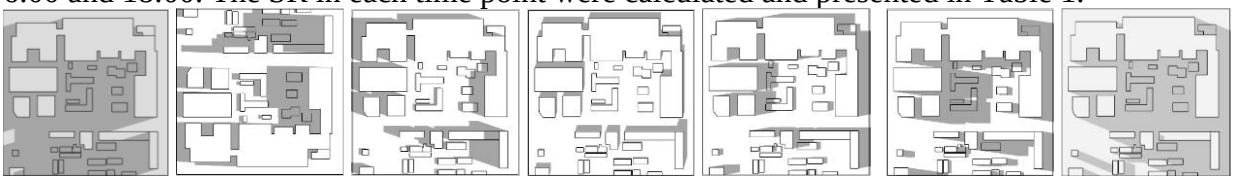


FIG 1. The Baidu map (left side) and the simulation model (right side) of the study area

3.4 Calculation of the Shadow Ratio (SR) and the Continuous Shadow Ratio (CSR)

The effect of shadow on urban environment is mainly reflected in the cooling effect during the summer heat period. Therefore, the summer solstice day (June 21, 2017) was selected as a typical example for the study in this paper. In order to make a comprehensive analysis of the whole summer day, SR in every two hours from 6:00 (7 time points) were calculated using Sketchup software. Then the plane graphs were exported separately to obtain the shadow distribution results as shown in Figure 2. As shown in the shadow simulation results, the minimum shadow area was observed at 12:00, and the largest shadow areas were observed at 6:00 and 18:00. The SR in each time point were calculated and presented in Table 1.



6:00 8:00 10:00 12:00 14:00 16:00 18:00

FIG 2. Shadow simulation results

Table 1. SR in 7 time points in June 21, 2017

Time	**6:00**	**8:00**	**10:00**	**12:00**	**14:00**	**16:00**	**18:00**
SR	0.85	0.68	0.62	0.54	0.60	0.69	0.82

The sunshine from 8 am to 4 pm on the winter solstice of 2017 was simulated by Tianzheng software. As shown in Figure 3, the area with less than 4 hours of sunshine in the figure can be considered as the area covered by shadows for more than 4 hours, thus selecting elements in Photoshop and calculating the shadowed area lasting more than 4 hours from 8 am to 4 pm on winter solstice day, floor area and the total area of the study area , so as to calculate the continuous shadow ratio (CSR). Therefore after calculation the CSR in this area is 0.87.

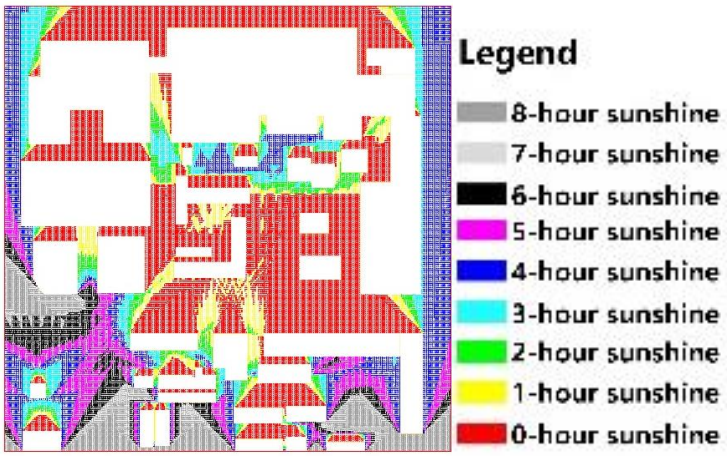


FIG 3. Shadow simulation results

3.5 Modeling and Setting of Boundary Conditions

The basic setting of ENVI-met model : x-grids of 60, y-grids of 60, z-grids of 30, the grid size of X and Y axes are 5m and the Z axes is 7m. The actual height of the buildings and the distribution of vegetation are measured by Baidu map street view and used in this simulation model. The simulation started from 18:00 at June 20, 2017, reserved six hours for the "preheating" of model, the total simulation time is 30 hours. Practical and effective data is from 0:00 to 24:00 of June 21, 2017. Initial temperature and humidity values for simulation was set according to the actual conditions from the Shaanxi provincial meteorological station. The highest temperature was 32 ℃ occurred at 15:00 and the lowest temperature was 23 ℃ occurred at 5:00. The highest humidity was 75% at 19:00, and the lowest humidity is 35% at 17:00.

In order to carry out the analysis more accurately, 3 measuring points in the study area were selected. The 3 location points are presenting enclosed urban form that is surrounded by buildings (A), semi-enclosed urban form with buildings in the north and south side (B) and open urban form with no buildings close by (C). (FIG. 4)

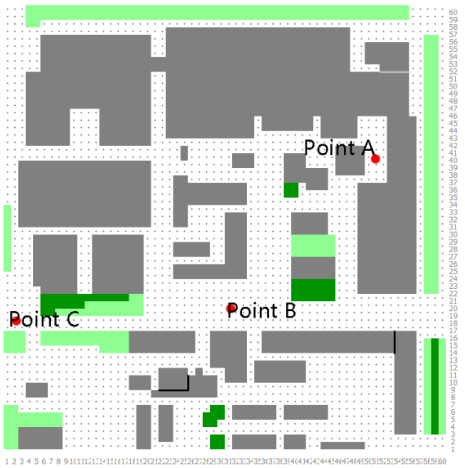


FIG 4. Image of simulation model and the location of measuring points

4. Research Results

4.1 Environmental Simulation

The simulation results of the temperature distribution are shown in Figure 5. Simulation results show that the whole day's temperatures range from 23.04 ℃ to 32.38 ℃. The lowest temperature appears at 6:00 while the highest temperature appears at 16:00. The whole day's temperature changes from 6:00 to 16:00 showed an upward trend, and after 16:00 the temperature began to decrease.

The simulation results of wind speed distribution are shown in Figure 6. The simulation results show that the wind speed ranges from 0.41m/s to 4.41m/s. The lowest wind speed is below 0.39m/s occurring from 12:00 to 18:00. And the highest wind speed is 3.86m/s appearing at 6:00. The whole day's wind speed changes from 6:00 to 16:00 showed a downward trend and increased from 16:00 to 18:00.

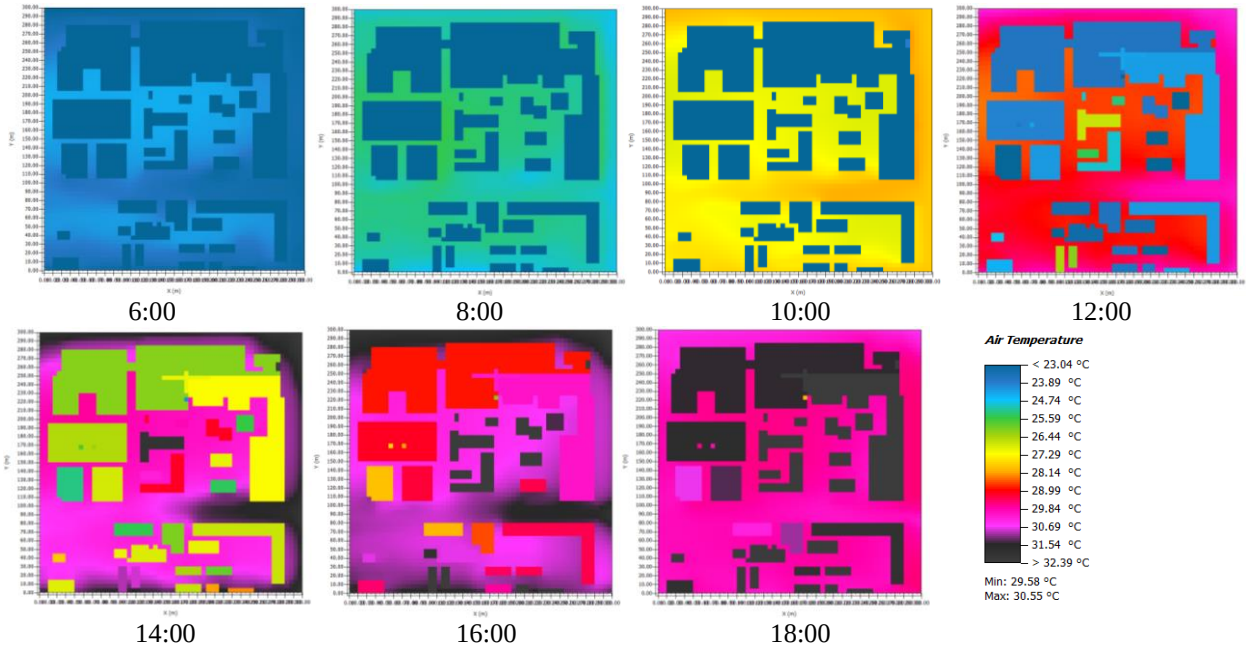
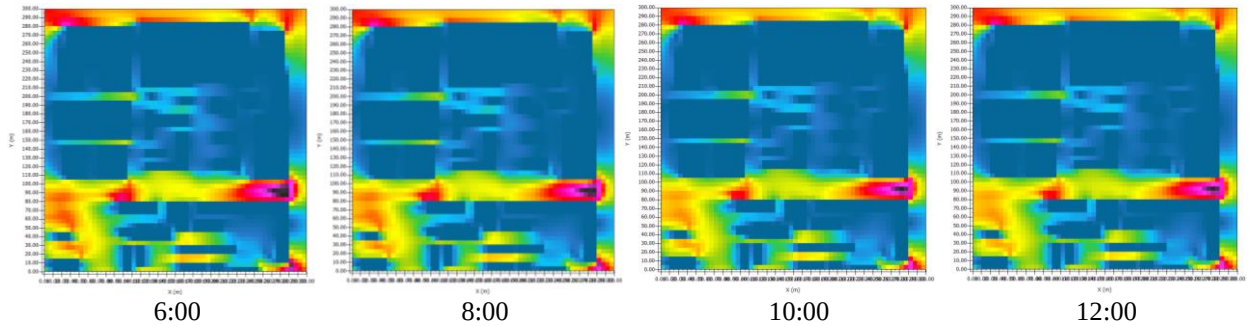


FIG 5. Temperature distribution at 1.5m height in June 21, 2017



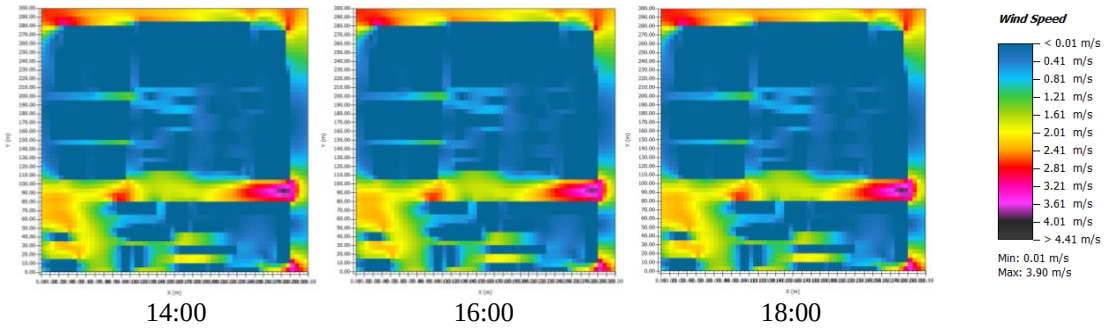


FIG 6. Wind speed distribution at 1.5m height in June 21, 2017

4.2 Linear Regression Analysis of SR and Urban Environments

As shown in Figure 7, the three measuring points all reached the maximum shadow ratio at 6:00 and 18:00 and 6:00 was also the lowest temperature. The lowest shadow ratio occurs at 12:00, the highest temperature appears at 16:00. The lowest shadow ratio does not exactly match the highest temperature but it can be seen that the shadow ratio and temperature does exist a certain negative correlation. The correlation between SR and temperature need further correlation analysis to prove.

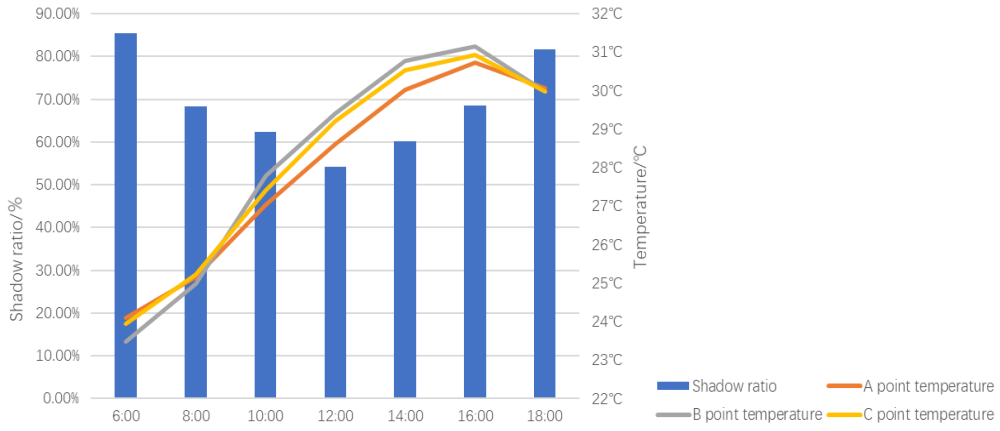
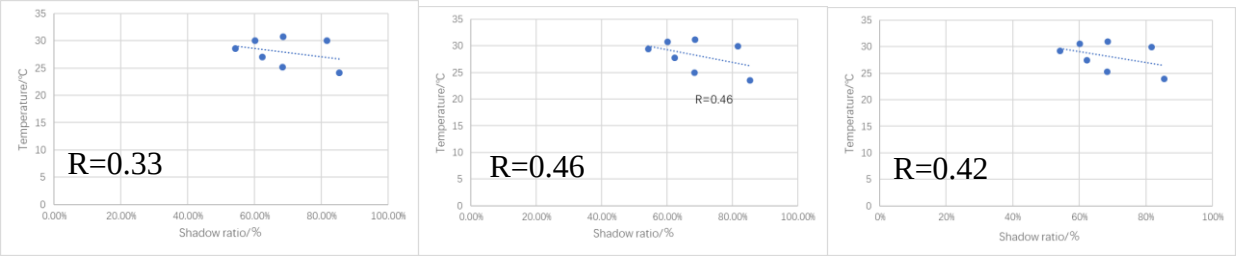


FIG 7. Statistic chart of measurement point temperature and shadow ratio

Figure 8 shows the correlation analysis between the temperature and SR in the three measurement points at each time point. The temperature and shadow ratio data of three measuring points at each time point were input into Excel software to generate scatter plots, then trend lines are generated, and then the correlation coefficients were calculated by a linear regression method. The coefficient of correlation between temperature and shadow ratio of the three measuring points are 0.33 (point A), 0.46 (point B) and 0.42 (point C). The average correlation coefficient is 0.40 in these 3 points. This is to say the temperature is related to the SR in each measuring point.



(a) Point A (b) Point B (c) Point C

FIG 8. Regression analysis of measuring point temperature and shadow ratio

Figure 9 shows the wind speed and shadow ratio of the three measuring points at 7 time points in a day. The three measuring points all reached the maximum shadow ratio at 6:00 and 18:00, while the maximum wind speed appeared at 6:00 in the morning. From 6:00 to 12:00 the proportion of shadow is decreasing and the wind speed is decreasing. Except point A, the shadow ratio between 16:00 and 18:00 showed an upward trend, and the wind speed also showed an upward trend. There may be a correlation between SR and wind speed, which needs further correlation analysis to prove.

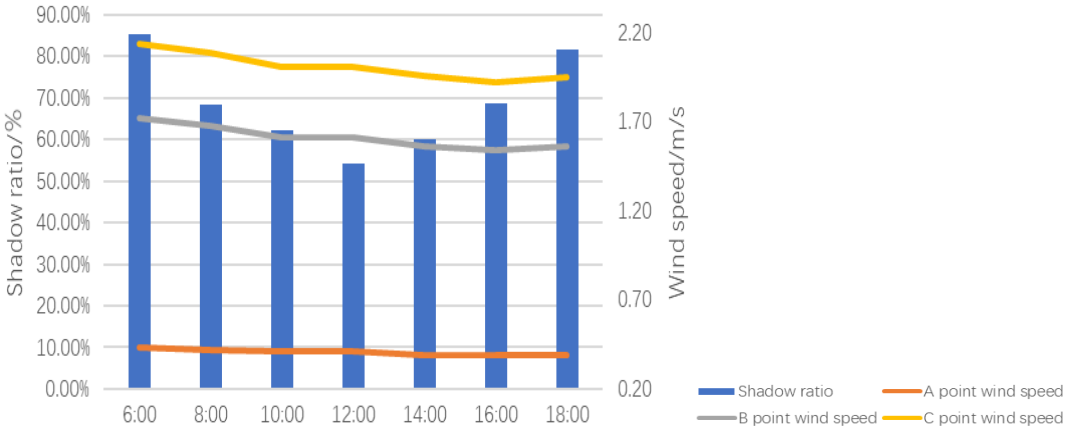
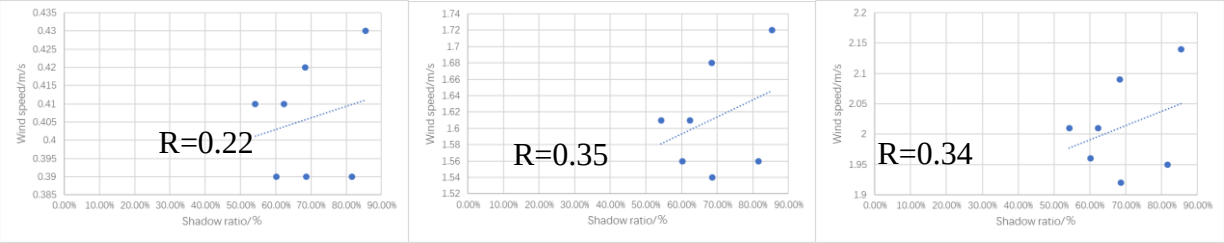


FIG 9. Statistics of wind speed and shadow ratio at measurement points

Figure 10 shows correlations between wind speed and shadow ratio of the three measurement points at each time point. The coefficient of correlation between temperature and shadow ratio of the three measuring points are 0.22 (point A), 0.35 (point B) and 0.34 (point C). The average coefficient of correlation is 0.30. The reason why point A has a low correlation may be that point A is a completely enclosed measurement point and buildings on the east and south sides are relatively high and urban wind is largely blocked here. The point A is likely to be insensitive to changes in wind speed. It can be concluded that the wind speed of the measurement point is related to SR, when the influence of the measurement point A is weakened.



(a) Point A (b) Point B (c) Point C

FIG 10. Regression analysis of wind speed and shadow ratio at measurement points

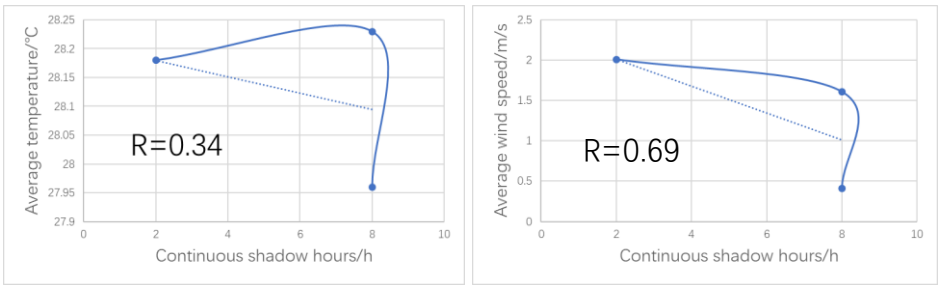
4.3 Analysis of the Relation between CSR and Urban Environment

CSR is a concept with time universality, so it is difficult to make a regression analysis of CSR at multiple time points with its corresponding temperature or wind speed like SR. Since continuous shadow hour is an important factor in CSR, we can study the relationship between CSR and environment by analyzing the relationship between continuous shadow hour and urban environment. Table 2 shows the continuous shadow hours at three measuring points and the average temperature and wind speed at each point. We will continue to study the correlation between continuous shadow hours and urban environment by regression analysis.

Table 2. Continuous shadow hours, average temperature and wind speed of 3 measuring points

Measuring points	**Point A**	**Point B**	**Point C**
Continuous shadow hours	8	8	2
Average temperature	27.96	28.23	28.18
Average wind speed	0.41	1.61	2.01

Figure 11 shows the linear regression relationship between the average temperature of summer solstice day and the continuous shadow hours of 8 am to 4 pm on winter solstice day at each point and the linear regression relationship between the average wind speed and the continuous shadow hours. The coefficient of correlation between the average temperature and the continuous shadow hours is 0.34 while the coefficient of correlation between the average wind speed and the continuous shadow hours is 0.69. This is to say that there is a correlation between continuous shadow hours and the average temperature and between continuous shadow hours and the average wind speed. Since continuous shadow hour is an important factor in CSR, we can conclude that there is a certain correlation between CSR and urban temperature. Similarly, there is a certain correlation between CSR and urban wind speed



(a) (b)

FIG 11. Regression analysis of continuous shadow hours and average temperature (a) and Regression analysis of continuous shadow hours and average wind speed (b)

4.4 Application of SR and CSR

The difference between SR and CSR is that SR is a time-varying indicator, while CSR is a fixed indicator. Generally speaking, CSR is used to compare the shadow condition in different sites, while SR is used to compare the shadow condition at different moment in a site. SR and CSR are mainly used to quantify the shadows of an area. Controlling SR or CSR in a reasonable range can improve the thermal comfort of buildings in the process of Architectural design. At the same time, SR and CSR can also be used as reference indicators for evaluating the quality of architectural design. There is also a correlation between the overall urban shadow and the urban heat island effect. The relationship between SR and CSR can be used to guide urban design in order to reduce urban heat island effect if they are applied to larger scale, such as urban scale.

5. Conclusion

As an important factor of urban spatial environment, shadow has an important influence on microclimate of city. This paper proposed the concept of SR and its derivative concept of CSR and simulated the environmental simulation data of a 300m*300m site in the near central area of Xi 'an city on June 21, 2017 using ENVI-met software. By coupling the data of thermal environment and wind environment with the SR data calculated by Skectup software, the correlation between this concept and thermal and wind environment of city has been proved. Compared with other spatial morphological indicators, the concept of SR proposed in this paper has the following characteristics: (1) Calculation of SR is different from that of traditional index of space such as intensity, height, maintenance coefficient factor, street height to width ratio, etc. After completion of the planning and design of city, intensity and height values are fixed and unique. But for buildings and the surrounding environment, the SR varies with the seasons and different times of the day, so that the shadow ratio has a characteristic that changes with date and time. At the same time, the CSR has the universality of time, which is convenient for quantitative research as an indicator of urban morphology. (2) SR can be used as an indicator to describe the spatial form. Through simulation and regression analysis, this paper proved the thermal environment and wind environment in the city are correlated to SR, especially with thermal environment, which can be described as a spatial morphological index for studying thermal environment and wind environment of city. (3) SR is easy to quantitative research. It is simple to calculate SR, and there is a situation that can directly characterize the distribution of shadow in

the research site and it is suitable for using in the quantitative description of the spatial morphology to facilitate further research and analysis.

And the concept has the following advantages: (1) The concept of SR has been proposed to reflect the sunshine and shadow of the city in the cold region better so as to optimize the thermal environment and wind environment design of the city better and to improve the living environment. Evaluating the spatial shape of the region by SR will be conducive to improve the urban environmental quality. (2) SR is closely related to the thermal and wind environment of the area. In the area where is hot in summer, if the shadow of the building can be fully utilized to reduce the direct sunlight, the thermal environment will be improved.

In general, the paper proved that SR has a strong correlation with thermal environment and the wind environment. And it proved that the concept is very valuable to the study of thermal and wind environment of city, which can be used in the study of urban thermal and wind environment. In the cold areas represented by Xi 'an, there is a need to utilize the solar radiation rationally in winter to improve the thermal comfortableness of the human body and to use the shadow to cool down and prevent heat in the summer. The shadow is of great significance for optimizing the thermal and wind environment of the city. The concept of SR for the quantitative study of the microclimate in the cold regions is of great value.

Reference

Sun Xin. Thermal environment of the city and the space form the coupling research [D]. Southeast University, 2015.

Arnfield A J, Grimmond C S B. An urban canyon energy budget model and its application to urban storage heat flux modeling[J]. Energy & Buildings, 1998, 27(1):61-68.

Givoni B. Man, climate and architecture[M]// Climate and architecture. Госстройиздат, 1969.

Li Jiancheng, Wang Ling, Li Peng. Thermal environment of the city and the space form the coupling research [J]. Journal of Xi'an University Of Architecture And Technology (NATURAL SCIENCE EDITION), 2001, 33(4):387-391.

Liao Xiao Qin. Study on the equivalent solar radiation absorption coefficient of the underlying surface in outdoor thermal environment analysis [D]. South China University of Technology, 2013.

Thermal Studies of a Mid-latitude Urban Environment

Roger Clay[1]*, School of Physical Sciences, University of Adelaide (Australia)*
Huade Guan, National Centre from Groundwater Research and Training, College of Science & Engineering, Flinders University (Australia)

ABSTRACT

Urban Heat Island (UHI) studies have been carried out over a number of years in the City of Adelaide. Adelaide is a coastal city with a Mediterranean climate and is noteworthy in having a central business district (CBD) which is surrounded by substantial parklands. Studies have been made of the Adelaide UHI both with a fixed system of temperature and humidity sensors, and through night-time traverses monitoring temperature, humidity, and infra-red sky temperatures. A summary of the measured UHI properties of Adelaide will be presented to discuss relevant urban distance scales, the effect of varying sky view factors, and the effects of incorporating small open spaces in an urban environment.

Introduction

The urban heat island (UHI) of Adelaide has been studied for a decade using a large array of fixed sensors and mobile vehicular traverses. Some of the accumulated data are reviewed here and deal with the effect of wind on the UHI, particularly in the central city regions, derivations of the spatial scales which are relevant for UHI, the effect of parks and the park-urban boundary, and the role of humidity in the UHI and the study of its properties.

Methods

Fixed Sensor Array

The Adelaide Urban Heat Island Monitoring Network (Guan et al. 2016) consists of multiple logging temperature and humidity sensors, fixed at a height of 4 m, located through the central urban area and surrounding suburbs (Figure 1). These sensors can be used to create temperature contour maps over the studied area at 15 minute intervals, as in the example shown in figure 2. Figure 2 shows a rather extreme UHI period but UHI excesses are commonly found in the range 2° to 5° C for this location.

Mobile Vehicular Traverses

Vehicular traverses were made with screen temperature (1.5 m above ground), relative humidity, and infra-red temperatures (most recently with two radiometers) being logged at 10 s intervals (Clay et al. 2016). The screen temperature was calibrated to 0.1 ^{o}C and the response time was ~130 ms. When travelling at central city speeds, this technique introduces a

[1] Corresponding Author: [roger.clay@adelaide.edu.au], [+61 83135046].

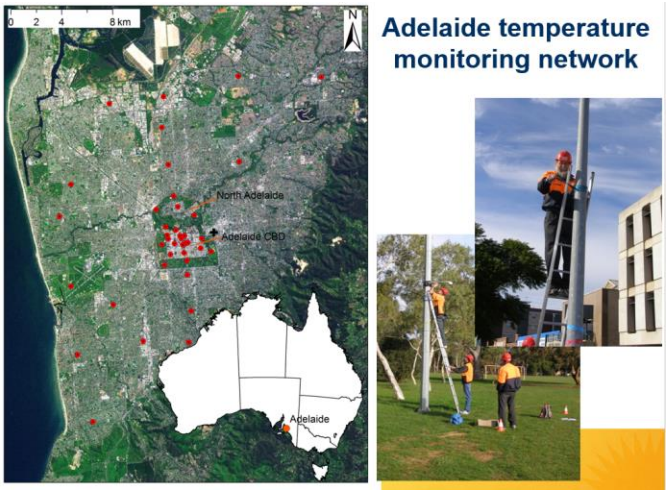


Fig. 1. Showing the location (and installation) of the sensors of the Adelaide Urban Heat Island Monitoring Network within Adelaide and its suburbs.

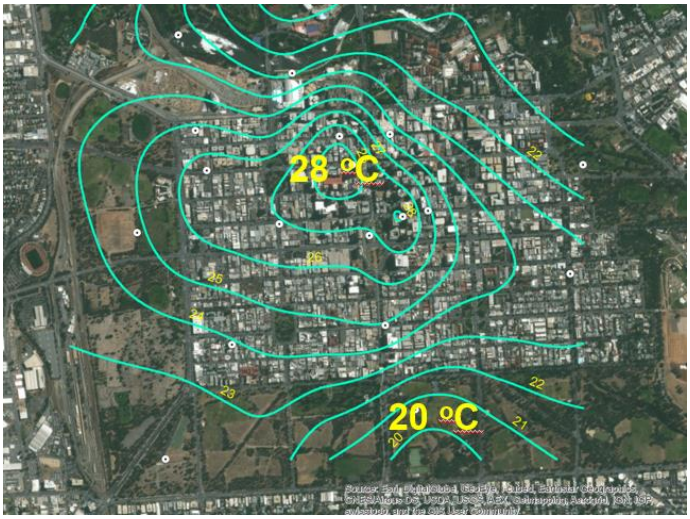


Fig. 2. Showing a temperature contour map (superimposed on a Google Map image of the City of Adelaide and its "parklands") produced from data recovered from sensors in the Adelaide Urban Heat Island Monitoring Network.

characteristic spatial uncertainty of order 50 m in general, although important spatial points were usually recorded with better resolution whilst the vehicle was travelling very slowly or was stationary at traffic lights. Traverses took place typically between 4 a.m. and 6 a.m., always well before sunrise. Figure 3 shows data for four transits for a common route through the central city area at times of different wind speeds. Those transits began and ended at the outside of the "parklands" which surround the central City of Adelaide with an area of approximately 5 km^2 (see figure 2). The transits begin and end in the parklands and the UHI effect can be seen as an increased temperature between the parklands. However, there is also a clear decrease in the fine structure of the UHI as the wind speed increases.

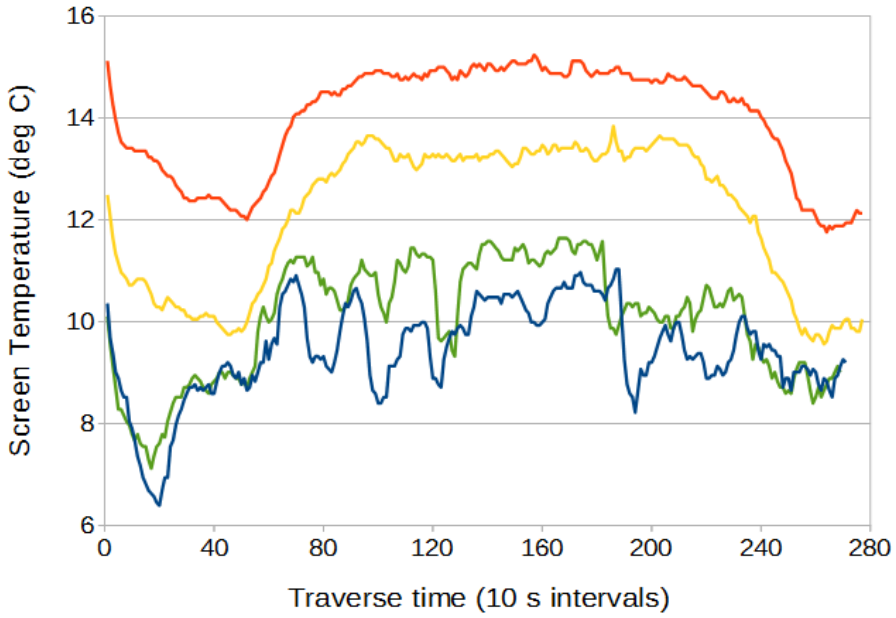


Fig. 3. Temperature measurements along a traverse route centered on the Adelaide CBD. The horizontal axis is in units of 10 s intervals. The time-scale and route are the same in each case. The traverses were for clear sky conditions at times when there was wind. The colors yellow, red, green, blue are from transits with wind speeds (at a Bureau of Meteorology site 1 km distant) of 6, 5, 2, 1 ms^{-1} respectively.(from Clay et al. 2016)

Sky View Factor, UHI Intensity, and Effective Surface Areas

Within an urban area dominated by impervious surfaces, the UHI associated with urban canyons is strongly dependent on the depth of the canyons. This can be measured by the fraction of the possible sky hemisphere which is actually visible from within a canyon, known as the sky view factor. That factor also needs to take into account the physics of the net infra-red energy transport from within the canyon, which depends on the infra-red 'temperature' of the sky. The latter depends on the density of greenhouse gases in the clear atmosphere but, to a first approximation, is dominated by the presence or absence of cloud cover (overcast skies are typically 20° warmer in the infra-red than clear skies). Figure 4 diagrammatically shows the relationship between the strength of UHI and the (effective-including infra-red effects) sky view factor (esvf). There is a clear increase of the UHI intensity as the effective sky view factor decreases, with the esvf being substantially lower at times with overcast skies (Zhu et al. 2013).

In those urban areas, air temperature correlates with the average infra-red surface brightness temperature and this correlation maximizes when block sizes of ~ 150 x 150 m^2 are considered (this depends a little on whether or not roof pixels (infra-red) are included) (Guan et al. 2015). This result is compatible with data from Nichol and Wong 2008.

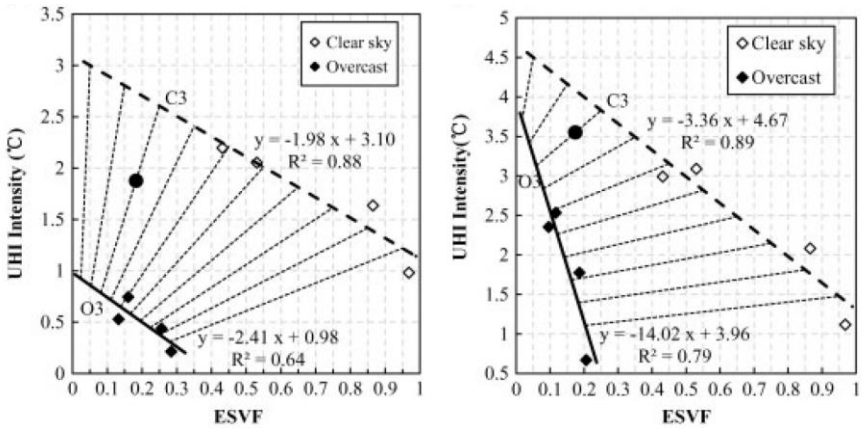


Fig. 4. Scatter diagram (points) between effective sky view factor (esvf) and UHI intensity for clear and overcast skies. Black dotted lines connect the estimated twin esvf and UHI intensity points by setting esvf at clear skies to 0.5-0.95 in intervals of 0.1. (a) summer (b) winter (from Zhu et al. 2013)

Wind and the UHI

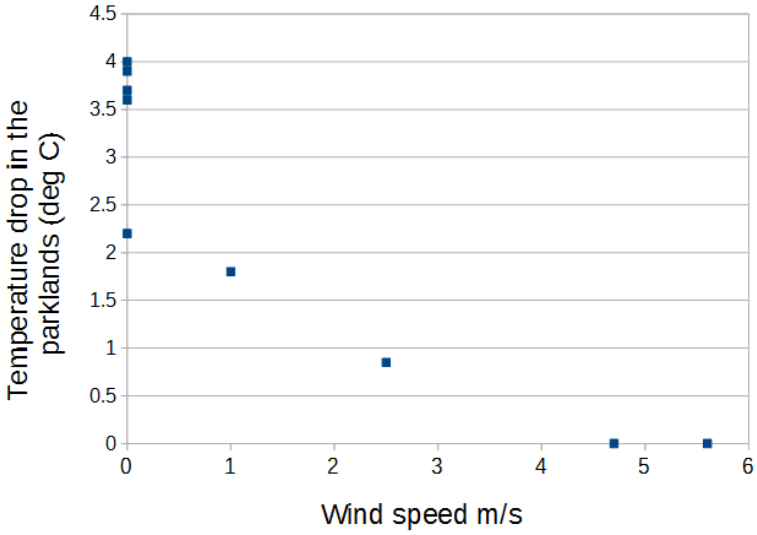


Fig. 5. The effect of changing wind speed on the structure which is found in the UHI. In this case, the structure is the drop in temperature when the traverse leaves the CBD and enters the "South Parklands". This figure is for traverses under clear skies. Data for individual traverses are shown.(from Clay et al. 2016)

We saw in figure 3 that structure in the UHI, and even its existence, depends on the strength of the wind. The level of the UHI as a function of wind speed can be quantified as in fig. 5 (Clay et al. 2016). As well as affecting the strength of the UHI effect, wind can affect its spatial distribution as can be seen when there is cool air drainage from the hills to the east of Adelaide (fig. 6) and the variation of wind with time can be important such as at times in the summer when a sea breeze develops (fig. 7).

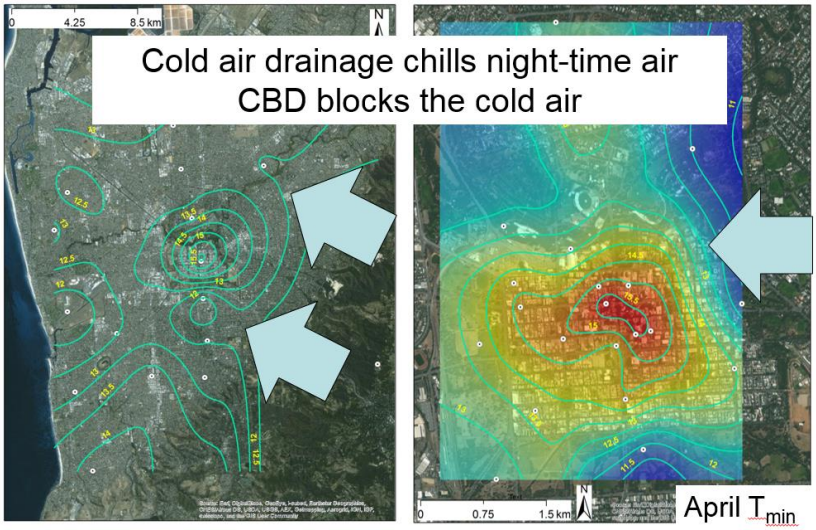


Fig. 6. The effect of wind and the structure of the urban landscape on the spatial distribution of the UHI.

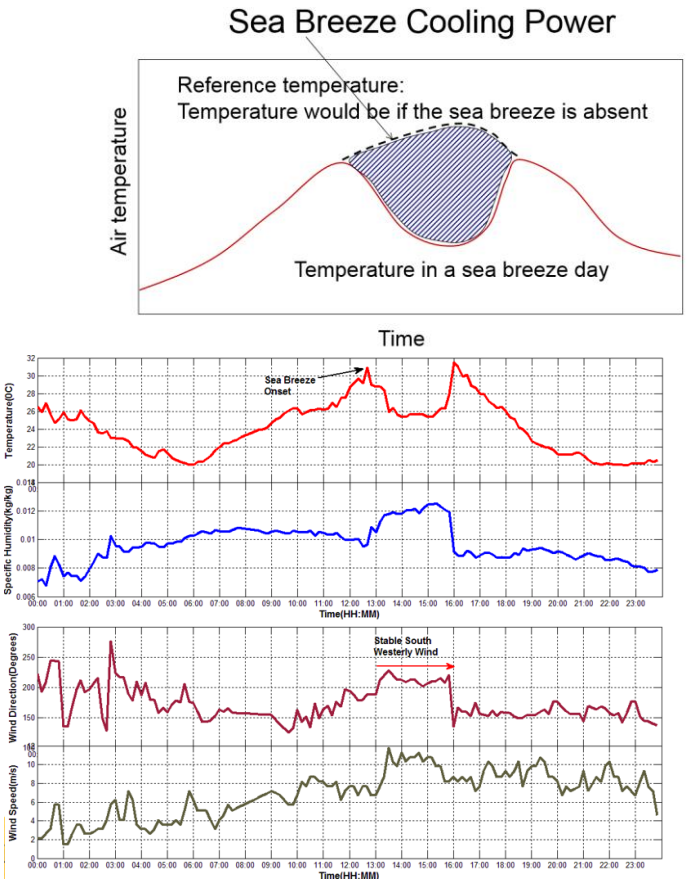


Fig. 7. The effect of the development of a sea breeze on the UHI intensity. A schematic of the effect is shown together with transect data for 25 January 2012.

Humidity

An expected characteristic of parks is that they would have a higher environmental humidity when compared to urban areas which have substantial impervious surfaces. Figure 8 shows data for a traverse through the Adelaide parklands (returning through them) and the central urban area. There is an inverse relationship between temperature and water vapor content of the air (vapor density). We will argue below, using average diurnal temperature and humidity data) that evapotranspiration is playing a key cooling role in cooling the parklands.

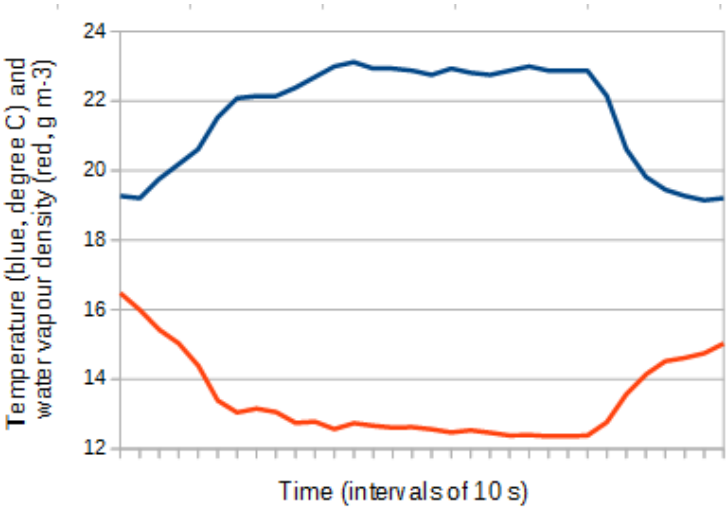


Fig. 8. Data from a traverse through parklands into the urban city area, and then out, returning into parklands. The screen temperature and the calculated water vapour density (from temperature and relative humidity recordings) are shown. (from Clay and Guan 2019)

The UHI Boundary

The urban heat island can have structure which depends on time of day, as physical conditions progressively change (figure 9). However, there is always temperature structure associated with the boundary of an urban area. In the context of the City of Adelaide, this is most clearly associated with the area of parks which surround the central urban area, known as the "parklands". We have made detailed studies of that transition. Many vehicular traverses have crossed the parklands and selected data (for clear skies and different wind speeds) are shown in fig. 10. In fig. 10, all traverses covered the same route, leaving the urban area into the parklands at time marker 7. When wind speeds are low, the transition occurs within one marker of passing the urban/parkland boundary (50 m resolution). Furthermore, there is no evidence of an extension of the cooler parkland air into the urban area at time of low wind speed. At higher wind speeds (e.g. 10 kph in the figure), it is possible to see cooling entering the urban area for up to ~1 km and this may be consistent with data of Yan et al. 2018 for a large Beijing park.

We can also look at that boundary through data from the fixed sensor Adelaide Urban Heat Island Monitoring Network (Guan et al. 2016). Figures 11 and 12 show average data (over days including all meteorological conditions) for 24 hour periods, derived from four sensor sites.

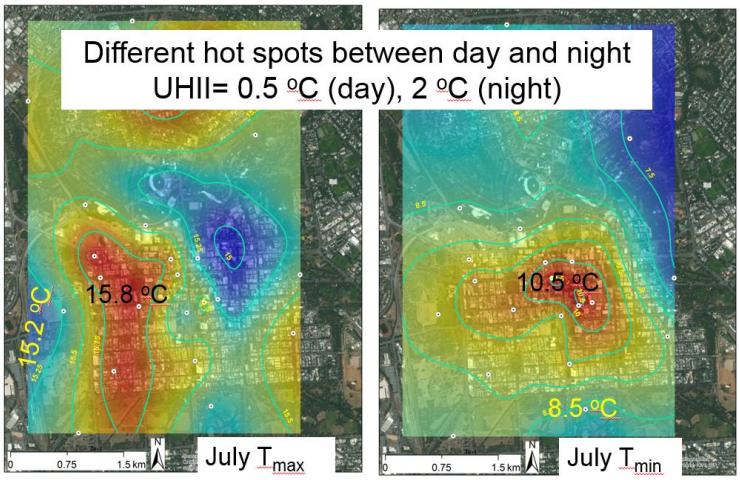


Fig. 9. Illustrating the changing structure of the UHI over a day/night period.

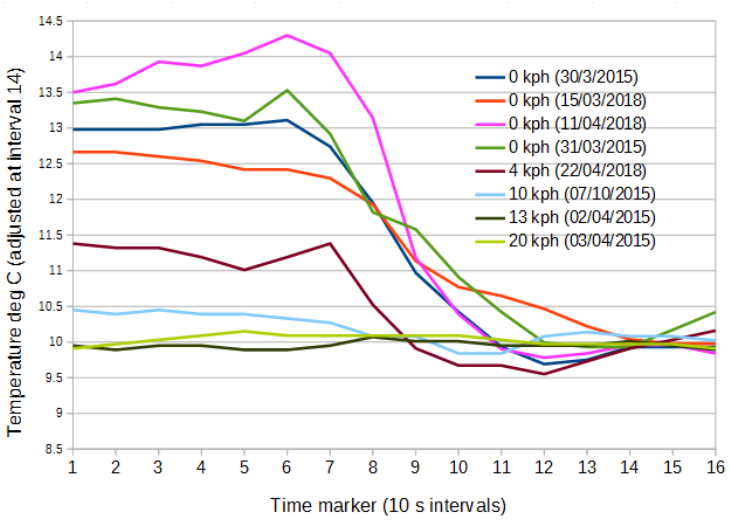


Fig. 10. Traverse temperature measurements ('y' axis) a fixed path (at 10 s intervals) through the southern urban/parkland boundary of the City of Adelaide (from Clay and Guan 2019 – in preparation). The local wind speeds recorded by the Bureau of Meteorology are noted. Temperature measurements for each traverse are have fixed temperatures added to agree at time marker 14. (from Clay and Guan 2019)

One site is in the parkland (site 1, 345 m from the boundary), one at the boundary (site 2) and two are within the urban area (sites 3 and 4). Temperature data show that the parkland site (site1) is consistently cooler than the urban sites (including the boundary). The temperature difference is greatest between the hours of 10:00 and 16:00 local standard time. The humidity (specific humidity, g/kg) data show related features but, in this case, the data at the boundary follow those in the parkland. In the period between 10:00 and 16:00, there is a substantial difference between the humidity data for the parkland (and the boundary) and the data from the urban sites. We take this to be due to evapotranspiration being strongest in the parklands at those times, leading to extra cooling in the parkland environment. We speculate that humid air from

the parkland penetrates into the urban area through diffusion and wind but that this air quickly reaches thermal equilibrium with the local surfaces to result in the contrasting temperature and humidity structures.

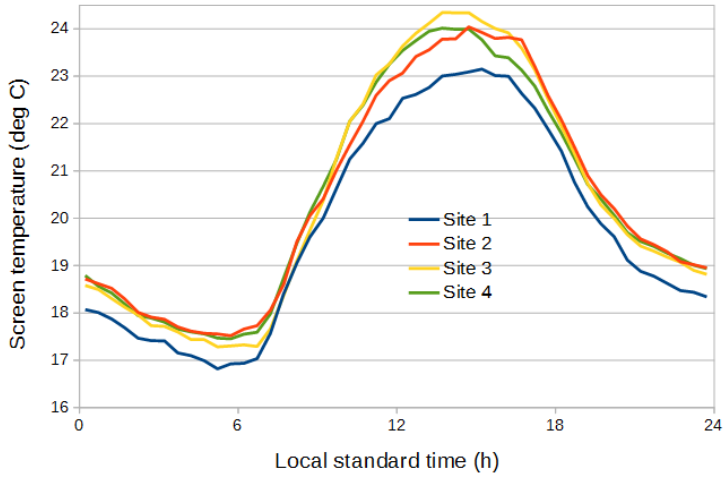


Fig. 11. Temperature variations over one day at four fixed sites (blue - parkland (345 m from the city boundary); red – boundary between the parkland and the city; yellow and green – progressively further inside the city area) (from Clay and Guan 2019)

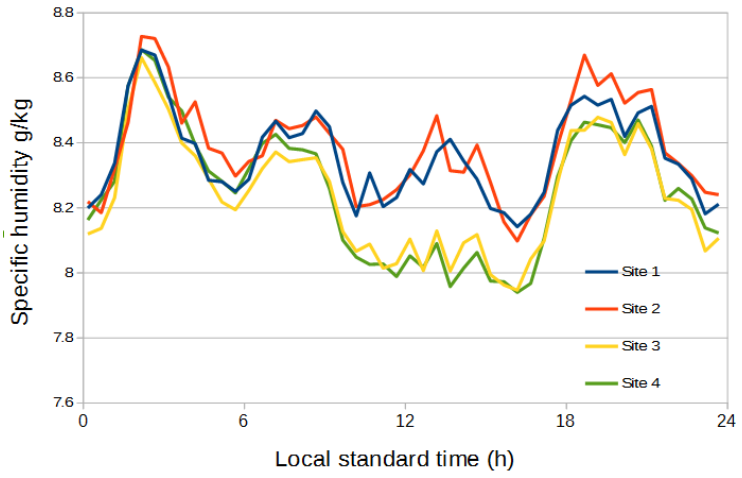


Fig. 12. The 24 h variation in specific humidity at the four sites whose temperatures are shown in figures 5 and 10. (blue - parkland (345 m from the city boundary); red – boundary between the parkland and the city; yellow and green – progressively further inside the city area) (from Clay and Guan 2019)

Figure 9 showed data for the transition between the urban area and parkland. We noted that, at times of low wind speed, the transition is rather sharp and that the cooled parkland temperatures did not extend into the urban area. On the other hand, the transition within the parkland is not a step function. The temperature reduces progressively with increasing distance into the parkland. The distance over which this transition occurs is some hundreds of metres (mean 300 m), which could well be limited by the finite width (typically 500 m) of the parklands. This distance is important in considerations of the use of parks for the mitigation of the UHI. Figure 13 shows data for a traverse through one of the five 'squares' within the central urban area. There is a small temperature reduction within the area of the square, as there are for other squares (data for four which were studied are shown in table 1).

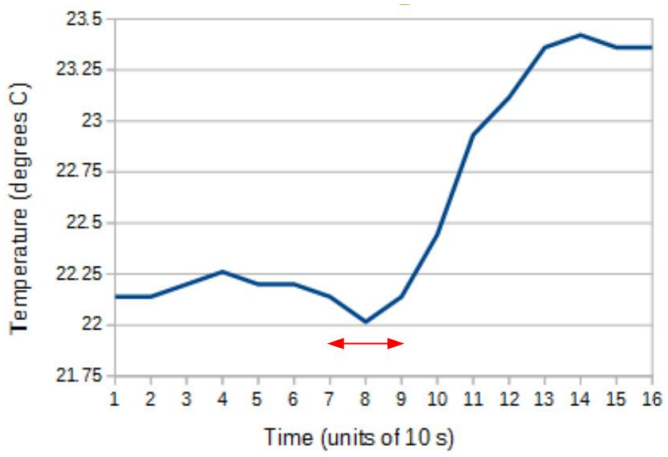


Fig. 13. Screen temperatures measured in a traverse through Hindmarsh Square (indicated by the red arrows, center at time mark 8). The route passes through an area with relatively low buildings (2 stories) before the Square and then enters a "canyon" region after the Square. (from Clay and Guan 2019)

Table 1. Temperature reductions on passing from the built area into City squares. The reduction to the lowest temperature in each square is shown as a fraction of the reduction found at the parkland boundary for that traverse.

	Dimensions	Fractional Temp. Drop	
Hindmarsh Square	145 x 230 m	0.19 +/-0.02	(8 entries)
Hurtle Square	145 x 230 m	0.10+/-0.005	(8 entries)
Light Square	120 x 220 m	0.1	(1 entry)
Victoria Square	100 x 240 m	0.056 +/-0.003	(7 entries)

Conclusions

Studies have been made of the UHI effect in the City of Adelaide and its surrounding parklands. The UHI shows substantial structure which reduces with increasing wind speed and changes its distribution under the influence of external winds. At low wind speeds, there is a sharp transition at the urban/park boundary which shows a progressive fall in temperature into the parkland but little temperature influence into the urban areas. At higher speeds, there is evidence of increasing effect inwards from the boundary. There is evidence that evapotranspiration, particularly outside the rather impervious urban area, is an appreciable influence on the UHI. this may be a factor determining the cooling effects of the city squares.

Acknowledgements

We thank our collaborators John Bennett, Cecilia Ewenz, Vinokumar, and Neville Wild, in particular, for their contributions to our recent studies of the Adelaide Urban Heat Island.

References

Clay, R.W. and Guan H. (2019). Night-time boundaries of an urban heat island, Urban Climate, submitted.

Clay, R.W., Guan, H., Wild, N., Bennett, J., Vinodkumar, Ewenz, C. (2016). Urban heat island traverses in the City of Adelaide, South Australia. Urban Climate, 17, 89-101.

Guan, H., Soebarto, V., Bennett, J., Clay, R., Andrew, R., Guo, Y., Gharib, S., Bellette, K. (2014). Response of office building energy consumption to urban weather in Adelaide, South Australia. Urban Climate, 10, 42-55.

Guan, H., McGrath, A., Clay, R., Ewenz, C., Benger, S., Bennett, J. (2015). Effective surface areas for optimum correlations between surface brightness and air temperatures in an urban environment. Journal of Applied Remote Sensing, 9, 096059-1 - 096059-16

Guan, H., Vinodkumar, Clay, R., Kent, C., Bennett, J., Ewenz, C., Hopkins, G., Simmons, C. (2016). Temporal,and spatial patterns of air temperature in a coastal city with a slope base setting. Journal of Geophysical research: Atmospheres, Research Article 10.1002/2016JD025139.

Nichol, J., Wong, M. (2008). Spatial variability of air temperature and appropriate resolution for satellite-derived air temperature estimation. Int. Journal of remote Sensing, 29, 7213-7223.

Yan, H., Wu, F., Dong, L. (2018). Influence of a large urban park on the local urban thermal environment. Science of the Total Environment, 622, 882-891.

Zhu, S., Guan, H., Bennett, J., Clay, R., Ewenz, C., Benger, S., Maghrabi, A., Millington, A. (2013). Influence of sky temperature distribution on sky view factor and its application in urban heat island. International Journal of Climatology, 33, 1837-1843.

Monitoring the urban heat island effect and the efficacy of future countermeasures in the Los Angeles Basin

Ronnen Levinson, Lawrence Berkeley National Laboratory (USA)
George Ban-Weiss, University of Southern California (USA)
Sharon Chen, Lawrence Berkeley National Laboratory (USA)
Haley Gilbert, Lawrence Berkeley National Laboratory (USA)
Howdy Goudey, Lawrence Berkeley National Laboratory (USA)
Joseph Ko, University of Southern California (USA)
Yun Li, University of Southern California (USA)
Arash Mohegh, University of Southern California (USA)
Angie Rodriguez, National Autonomous University of Mexico, Mexico City (Mexico)
Jonathan Slack, Lawrence Berkeley National Laboratory (USA)
Haider Taha, Altostatus Inc. (USA)
Tianbo Tang, University of Southern California (USA)
Jiachen Zhang, University of Southern California (USA)

ABSTRACT

To understand spatial air-temperature variations in local urban heat islands (UHIs) and urban cool islands (UCIs), and their relationship to land-use and land-cover (LULC) properties in the Los Angeles Basin, we sought to (a) use fine-resolution climate models to identify UHI / UCI areas, (b) relate observed intra-urban temperature variations (from mobile transects and stationary monitors) to LULC and surface physical properties, and (c) calibrate/validate the fine-resolution meso-urban climate models that were used in identifying the UHI / UCI. We conducted a multi-dimensional assessment of urban temperature variations based on numerical modeling and several types of observations, including mobile transects, dense networks of personal weather stations, and sparse but more accurate research-grade stationary weather monitors. To identify the causative factors of the UHI / UCI at the neighborhood scale, we collected detailed LULC datasets, such as 1-m resolution roof albedo and tree canopy cover, as inputs for the meteorological modeling and analysis. The fine-scale meteorological model was used to design mobile-transect routes and to site the stationary monitors based on the definition of UHI / UCI areas.

This study provides the first observational evidence from analysis of high spatial density weather stations that increases in roof albedo at neighborhood scale are associated with reductions in near-surface air temperature. This was corroborated with the analysis from mobile transect measurements and correlation of observed air temperature with neighborhood-scale albedo and vegetation canopy cover, which revealed a cooling effect from area-wide increase in albedo and/or canopy cover.

Introduction

Cities need to characterize urban heat and related causes to design and implement urban heat island countermeasures appropriate to current and future climates. This project set out to understand spatial variations in local heat and cool islands and the relationship to land-use and land-cover (LULC) properties, providing guidance for future mitigation via control measures such

as higher albedo (solar reflectance) and more vegetation. The objective was to establish the causative factors of the local heat and cool islands at the neighborhood scale in the study areas, based on site-specific and upwind micrometeorological dynamics (e.g., local generation of heat and transport of heat from upwind sources), LULC properties, and surface physical properties. We sought to use fine-resolution climate models to identify UHI/urban cool island (UCI) areas, relate observed intra-urban temperature variations (from mobile transects and fixed weather stations) to LULC and surface physical properties, and calibrate/validate the fine-resolution meso-urban climate models that were used in identifying the UHI/UCI. By understanding the variations in local heat and cool islands and the associated interaction with LULC properties, cities can implement policies to address UHIs now and build resiliency to future urban warming from climate change.

To characterize the meteorological variables in the study areas, we collected data from existing weather networks; conducted detailed, fine resolution meteorological modeling; installed research-grade stationary weather monitors; and performed mobile transects. We partnered with the City of Los Angeles, County of Los Angeles, and Los Angeles Unified School District (LAUSD) to help identify and host stationary monitors in two study areas that the research team identified: “SFV5”, an area that is part of the San Fernando Valley (SFV); and “LA1”, a region that includes and extends to the southeast of downtown Los Angeles. We installed three research-grade stationary monitors in the SFV5 study area, and another at the University of Southern California campus west of downtown Los Angeles. To supplement the data collected from these stationary monitors we designed and executed multiple mobile transects. To identify the causative factors of the local heat and cool islands at the neighborhood scale, we collected detailed LULC datasets for the L.A. Basin, such as 1-m. resolution roof albedo and tree canopy cover, as inputs for the meteorological modeling and analysis. The fine-scale meteorological model was used to design mobile-transect routes and site the stationary weather monitors based on the definition of UHI/UCI areas.

Identifying and Characterizing Study Regions in the Los Angeles Basin

Acquisition of External Weather Measurements

To inform placement of new stationary monitors and provide observations to compare to modeled temperatures, the research team created a database of accessible historical weather data from all sources that had at least 10 stations available for the L.A. Basin. These sources included the California Irrigation Management Information System (CIMIS), WeatherBug, and Weather Underground. However, for simplicity and to avoid temperature differences that might result from variations in measurement techniques between networks, the research team’s analysis of PWS data included only monitors from the Weather Underground network and focused on a single season (summer 2015). Data downloaded from the existing weather station sources were postprocessed to remove outliers. Acquisition and refinement of external weather measurement data are detailed by Mohegh et al. (2018) and in Appendix G of Levinson et al. (2019).

Study Area Characterization

LULC analysis was the first step in identifying urban areas with delineations or transitions of interest—i.e., changes in physical properties. This analysis, performed to derive surface inputs to the meteorological model and provide a basis for relating observed air temperature to LULC

properties at stationary monitor sites or along mobile-transect routes, is detailed in Appendix A of Levinson et al. (2019).

Study Area Selection

Error! Reference source not found. shows four study areas initially considered for meteorological modeling (LA1, LA2, LA3, and SFV5), along with the two areas used in analysis of personal weather station data (Central L.A. and SFV_R). The two most promising study areas identified—LA1, containing downtown Los Angeles in its northwestern tip, and SFV5, a portion of the San Fernando Valley—were modeled to assess the potential UHI or UCI signals or both that stationary monitors and mobile transects in this area would capture. This preparatory modeling is detailed in Appendix A of Levinson et al. (2019).

To quantitatively evaluate the model prediction of temperature tendency and spatial gradients in temperature in the modeled areas, we devised preliminary mobile-transect measurements of temperature for initial feedback and preparation for more rigorous model performance evaluation. The transect was conducted in Area LA1 during April 2016. Execution of the preliminary transect and design of the mobile monitor are detailed in Appendices B and C, respectively, of Levinson et al. (2019).

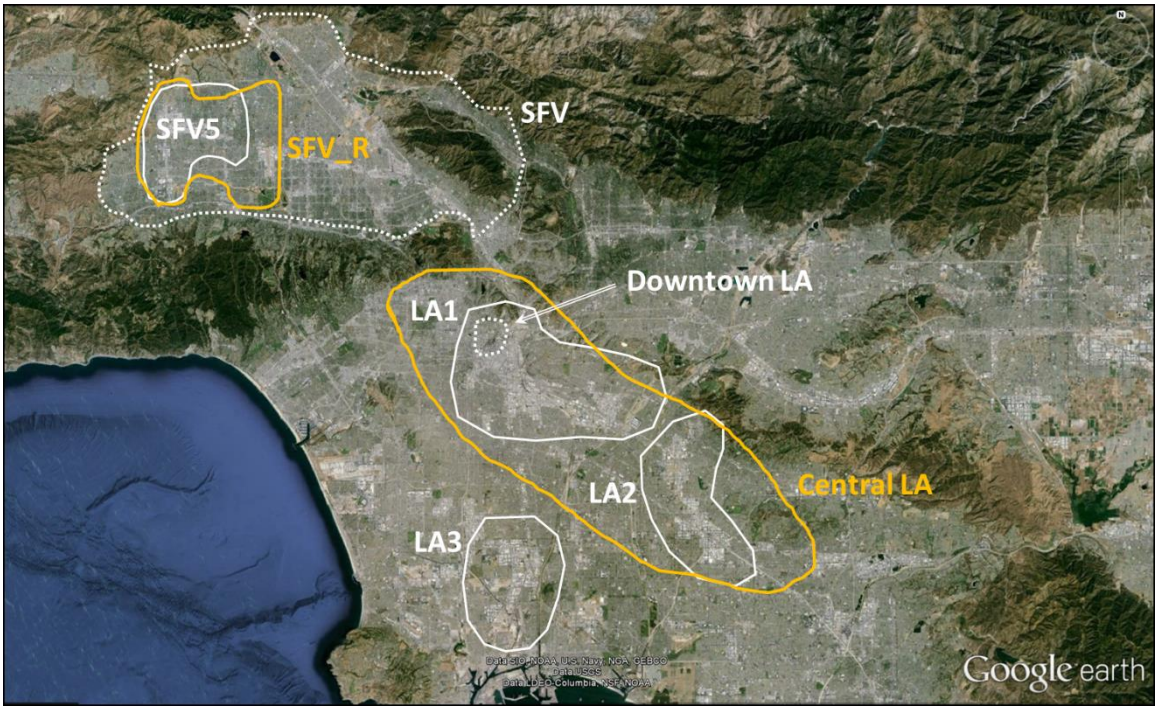


Figure 1. Boundaries of initial study areas LA1, LA2, LA3, and SFV5 (solid white lines) considered for meteorological modeling, installation of new stationary monitors, and mobile transects; LA1 and SFV5 were selected. Also shown are the boundaries of study areas Central L.A. and SFV_R (solid gold lines) used in analysis of personal weather station data, and the boundaries of the San Fernando Valley (SFV) and downtown L.A. (dotted white lines).

The transect observations confirmed the findings from the model, allowing the team to use the modeled results to select the study areas of interest. Therefore, the research team chose to install stationary monitors in areas SFV5 and LA1 to capture the interactions between LULC and microclimates in inland regions (the San Fernando Valley) and areas influenced by the sea breeze flow and climate archipelago[1] effects (the semi-coastal region that includes Area LA1). Monitoring two unlike areas helps the team understand the role of local surface properties and impacts on temperature in different climate regimes—here, inland valleys, and quasi-coastal areas.

Developing a Monitoring Plan, Designing Instrumentation, and Deploying a Sensor Network to Measure the Urban Heat Island Effect in the Selected Study Regions

Note that mobile monitor design and stationary monitor design, placement, installation, and placement are detailed in Appendix C of Levinson et al. (2019).

Mobile Monitor Design

Horizontal variations in air temperature near the ground—say, 2 m above ground level—can be mapped by attaching a thermometer to roof of a vehicle, such as a car, then logging temperature, position, and time during a transect. To ensure that the thermometer accurately measures air temperature, the sensor should be aspirated by the motion of the vehicle, shielded from the sun, and radiatively isolated (decoupled) from the shield. The sensor should also respond quickly to air temperature changes to minimize spatial inaccuracies, or blurring, in the air temperature map induced by the motion of the vehicle.

Our mobile monitor contains five elements: a shielded temperature sensor aspirated by vehicle motion; a quick-install mount to attach the shielded sensor to the roof of a vehicle (**Error! Reference source not found.**); a portable data logger to record the temperature time series; a global positioning system (GPS) to record the position time series; and a dash camera (dash cam) to record time-stamped video of the transect from the perspective of the driver.

Stationary Monitor Design

We sought the following performance characteristics for each stationary monitor:

- The monitor should accurately and continuously measure the primary signal, dry-bulb air temperature; secondary signals, including wind speed, wind direction, solar irradiance, and relative humidity, useful for interpreting variations in air temperature; and monitor diagnostics, such as radiation-shield fan speed, needed to verify that the sensors are operating as designed.
- To ease installation and subsequent maintenance, the monitor should be easy to assemble and program.
- The monitor should be readily installed on an elevated surface, such as that of a low-slope roof, to measure air temperature at some fixed height above ground.

[1] An archipelago is group of islands or a body of water containing a group of islands. The research team uses the term “climate archipelago” to refer to the complex climate effects of a very large, continuous urban area in which upwind portions can affect downwind portions.

- The monitor should communicate over the internet or by cellular modem for convenient data collection and (if necessary) reprogramming.
- The monitor should be durable, ideally with a service life approaching a decade.

Selecting Stationary Monitor Sites

Several points in the LA1 and SFV5 study areas were identified as localized UHI or UCI areas based on model and initial mobile-transect results. The research team shared these points and study areas with project partners—including the City of Los Angeles, County of Los Angeles, and LAUSD—and collectively developed a list of their facilities that could serve as potential sites for the stationary monitors. Upon further evaluation of these sites via examination of three-dimensional imagery (e.g., Google Earth Pro) and location visits, certain sites were assigned a lower priority because of such factors as unavailability of flat roofs (sloped roofs can be an issue for installing weather stations), lack of secure sites in open areas (at ground level), and physical characteristics of the site. These factors resulted in a top tier of 10 potential sites.

Installing and Calibrating Monitors

After extensive negotiation, we received partner approvals to install four monitors. The first monitor (Monitor 0, the reference monitor) was installed October 26, 2016, on the campus of the University of Southern California (USC) inside a gated area in a parking lot, 2 m above ground level (AGL). Monitor 1 was installed July 25, 2017, at the City of Los Angeles' Bureau of Street Services Facility Yard in Topanga Canyon, 2 m above the roof of a structure that shades a parking lot. Monitor 2 was installed January 11, 2018, at LAUSD's Sunny Brae Elementary School, 2 m above the roof of a school building. Monitor 3 was installed April 13, 2018, at LAUSD's Melvin Elementary School, also 2 m above the roof surface of a school building.



Figure 2. Mobile monitor on quick-install car-roof mount. System includes white PVC-pipe shield, gray PVC-pipe vertical risers, aluminum tube roof mounting on plastic and rubber feet, and white PVC-pipe crossbeams. Straps with hooks (not shown) secure the bars to the vehicle frame.

The temperature sensors in all four monitors were cross-calibrated at the USC (Monitor 0) site before Monitors 1, 2, and 3 were deployed.

Collecting and Analyzing Weather Data from Fixed and Mobile Monitors

To observationally quantify the UHIE and the relationship to LULC, establish a baseline for future UHI mitigation, and calibrate/validate a fine-resolution mesoscale climate model, our plan included:

- Collecting data from the new stationary monitors.
- Designing and conducting mobile measurements of near-ground air temperature.
- Using stationary and mobile measurements to update fine-resolution model simulations and parameterizations, such as those supported by the California Environmental Protection Agency for UHI Index development, and to calibrate/validate these models.
- Using hourly air temperature measurements and other meteorological variables from the existing weather stations to evaluate the UHIE, and to correlate spatial variations in air temperature and UHIE intensity with LULC and urban morphological characteristics.

Stationary Monitor Measurements

The research team has continuously collected data from Monitors 0–3 since installation. However, because of logistical delays in the installations of Monitors 2 and 3, the analysis in the current study is based instead on the team's mobile transect measurements

Mobile Transect Measurements

Mobile-observation transects were carried out to measure microclimate variations along the routes. Of particular interest was air temperature variation as the LULC and surface properties change along each route segment. The goal was to develop correlations that quantify the responses in temperature to changes in albedo and vegetation canopy.

In all, 15 transects were carried out in the summers of 2016 and 2017 in SFV5 and LA1, as detailed in Appendix E of Levinson et al. (2019).

Calibration of Climate Model to Mobile Observations

We evaluated the model performance against fine-scale observations from mobile transects. For transect-specific modeling (500-m resolution), modeled air temperature was compared to observations from transects at the coincident time (subhourly intervals). The goal was to ascertain that the model correctly captures the micrometeorological variations in the urban areas and to validate the modified WRF model against the mobile observations. We found good agreement between along-transect roadway observations and area-averaged model results. The calibration process is detailed by Taha et al. (2018a,b).

Relating Mobile Air Temperature Observations to LULC

Following model performance evaluation, the research team evaluated correlations between observed temperature and surface physical properties. In this case, two surface properties

of interest were examined: neighborhood-scale albedo and vegetation canopy cover (500-m scale). The research team examined these two properties because they have been shown in many studies to influence significantly the urban air temperature and they are easy to control and use as mitigation measures. The relationships between observed air temperature (predictand) and either albedo or canopy cover (predictors) or both were examined in three manners: (1) simple linear regression, (2) multiple regression, and (3) CART analysis for further detail. Examples of each analysis are given in this discussion. This work is detailed in Taha et al. (2018a,b).

Simple Linear Regression. In the downtown Los Angeles (LA1) domain, observed air temperature from mobile transects was correlated to grid-level albedo and canopy cover. For the San Fernando Valley study area, the observed temperature was correlated only with canopy cover (as predictor) since albedo has a smaller variability in this domain. All but two transects yielded statistically significant correlations (probability value < 0.05) of air temperature to albedo or canopy cover fraction, and correlations for all but two transects were negative (when albedo or canopy cover or both increase, temperature decreases).

Multiple Regression. Multiple regression was carried out for albedo and canopy cover as predictors to observed air temperature from the transects. This analysis applies only to the downtown area, LA1, since the SFV5 analysis involved only variations in one predictor (canopy cover) because the variability in albedo in SFV5 is small. The correlations were overwhelmingly negative—as albedo and canopy cover increase, temperature decreases—and statistically significant except in one transect, where the role of canopy cover was insignificant, and in two other transects, in which the role of albedo was insignificant.

Classification and Regression Tree. A classification and regression tree (CART) analysis was undertaken to assess the multiple interactions among predictors of mobile-observed air temperature. This analysis is an extension to the multiple regression analysis above and provides additional information. In the CART analysis, the roughness length parameter was introduced as an additional predictor to evaluate the role, if any, relative to that of albedo and canopy cover.

Detection of Intraurban Heat and Cool Islands

Because the Los Angeles region is one large urban climate archipelago (a built-up area stretching from the ocean to the mountains), there is no rural reference against which the urban temperature is compared as in a "conventional" urban heat island definition. As such, the task was to identify intraurban variations in heat or cool islands or both as a function of LULC (as an embedded signal) and correlate the temperature variations to changes in LULC and surface physical properties. As discussed above, the research team's LULC analysis coupled with the fine-scale meteorological modeling result allowed the team to identify such signals in the study areas.

The model performance evaluation in this study demonstrated that the WRF model and the modifications to the associated urban modules performed in this project can reproduce reasonably well the observations in the temperature, including the locations of UHI and UCI spots. As such, the model can be reliably applied to other urban areas and regions in California, as well as for other applications such as in designing community- or neighborhood-scale UHI mitigation strategies.

Neighborhood-Scale Interactions Between Air Temperature and Land Cover

The research team chose two study areas ("regions") of interest within the Los Angeles Basin that met two requirements: (1) the study area should be sufficiently small such that distance from the coast does not dominate temperature variations, and (2) there should be sufficient variation in land-cover properties of interest (e.g., roof albedo) to enable discerning effects of land cover on measured air temperatures. The first region encompasses an area of roughly 500 square kilometers (km^2) and includes downtown Los Angeles; the research team refers to this region as Central Los Angeles. (Central Los Angeles contains all of LA1.) The second region encompasses roughly 160 km^2 and is within the San Fernando Valley; the research team refers to this region as SFV_R.

The research team investigated the effects of LULC properties on observed air temperatures for different neighborhoods in each region, using Weather Underground near-ground air temperatures measurements recorded in July 2015. Here a "neighborhood" is an area of 500 m radius, centered on a weather station.

The research team focused on roof albedo (and solar power reflected from roofs) and tree cover, although further LULC parameters were analyzed. The research team found that the sensitivity of air temperatures to these LULC properties varied by region, likely due to the related different baseline land cover and meteorology. Increases in roof albedo were associated with observed air temperature reductions. Average daily sensitivities were 1.84 °C and 0.25 °C per 0.1 increase in roof albedo in neighborhoods in Central Los Angeles and SFV, respectively. Observed sensitivities in air temperature to albedo were substantially higher than reported by previous modeling studies.

In Central Los Angeles, variations in solar power reflected from roofs (and thus roof albedo) appear to dominate variations in observed air temperature relative to the effects of tree fractions. This observation is based on current neighborhood-to-neighborhood variability in tree fraction in this region and may not predict how adding more trees would affect temperatures. For SFV_R, observations suggest an overnight (00:00 – 07:00 local time) temperature reduction of up to about 1.5 °C per 0.1 increase in tree fraction at night. To the team's knowledge, this study is the first to report observational evidence that roof albedo increases are associated with neighborhood-scale temperature reductions.

Policy Implications

The research team found empirical evidence that there is intraurban temperature variability correlated to LULC properties. The albedo and vegetation coverage values in the analysis are existing conditions in Los Angeles neighborhoods where there has not been a concerted effort to address UHIs. This finding suggests that there are opportunities for community cooling using existing technologies and practices to increase urban albedo and canopy cover. Knowing that these are effective cooling measures, cities can also accelerate the implementation of these UHI countermeasures in heat-vulnerable neighborhoods. Addressing UHIs helps locally offset future warming in cities from climate change. This action helps the city build resiliency to future extreme heat events.

Local and state government policy makers can conduct similar modeling to identify local UHI areas to target policies to increase roof albedo and canopy cover. They can also review their city/community LULC datasets to identify areas where there is potential to increase roof albedo

and vegetation cover. This review will help them develop targeted strategies to implement UHI countermeasures. In turn, these strategies can conserve city resources, program budgets, and staff while improving climate resiliency in the most heat-vulnerable communities. For example, the City of Los Angeles' Department of Water and Power runs a residential cool roof rebate program. Department officials can direct communication efforts to residential areas identified as local UHIs following the method of modeling used for this study. The installation of cool roofs in these UHI areas provide the neighborhood cooling benefits and building energy savings, while conserving program funds from citywide outreach and implementation.

The California Natural Resources Agency also offers urban greening grants to cities, counties, and nonprofits. Local or state agencies can review LULC datasets to target areas of low canopy coverage within disadvantaged communities for project implementation. If planted appropriately, trees could achieve the program objectives as well as providing the cooling benefit in heat-vulnerable communities.

Conclusions

California's urban heat islands are exacerbated by climate change in a manner that can compromise electricity sector resilience and public health. It is important to understand the factors that contribute to UHI, as well as how UHI can be mitigated. In this study, the research team carried out a multidimensional assessment of urban temperature variations based on state-of-the-science numerical modeling and several types of observations, including mobile transects and personal weather stations. The research team sought to understand spatial air-temperature variations in local heat and cool islands and the relationship to land-use and land-cover properties in the Los Angeles Basin.

The research team collected detailed LULC datasets for the L.A. Basin that were used as inputs for the meteorological modeling and analysis. The research team also developed a database of historical micrometeorological information from existing weather station networks.

The research team collaborated with the City of Los Angeles, County of Los Angeles, and Los Angeles Unified School District to find sites and hosts for stationary monitors in two study areas that the research team identified, San Fernando Valley (SFV5) and downtown Los Angeles (LA1). The research team used fine-resolution climate models to assess the potential local UHI or UCI signals or both in these two areas. The results of the modeling informed the design of mobile-transect routes and siting of the stationary monitors. The research team designed a highly accurate and affordable stationary monitor that was installed in three locations in the SFV5 study area and at the University of Southern California campus west of downtown Los Angeles. To supplement the data collected from the stationary monitors, the research team completed 15 mobile transects. The research team designed and constructed an apparatus that is easily mounted on the roof of a car to measure air temperature along the transect routes.

The research team assessed data from personal weather stations in the Weather Underground network to relate observed intraurban temperature variations to LULC and surface physical properties. The research team also analyzed observational micrometeorological data from mobile transects and correlated them with neighborhood-scale albedo and vegetation canopy cover.

The research team found the first observational evidence from analysis of high-spatial-density weather stations that increases in roof albedo at neighborhood scale are associated with reductions in near-surface air temperature. This evidence was corroborated with the analysis from

mobile transect measurements, which revealed a cooling effect from areawide increase in albedo or canopy cover or both. The albedo and canopy cover values in this analysis are existing conditions in Los Angeles neighborhoods where there has not been a concerted effort to address UHIs. This finding suggests that there are opportunities for community cooling using existing technologies and practices to increase urban albedo and canopy cover. Knowing that these are effective cooling measures, cities can also accelerate implementation of these UHI countermeasures in heat-vulnerable neighborhoods.

In addition, the calibrated meteorological model accurately identified the localized urban heat islands and urban cool islands observed in this study. Therefore, the model can be applied by stakeholders, including city and state government, to characterize the intraurban microclimate variations elsewhere in California, and stakeholders can use the model to analyze the benefits from launching UHI countermeasures.

Acknowledgements

This research was supported by the California Energy Commission under contract EPC-14-073 and the National Science Foundation under grants CBET-1512429, 1752522, and CCF-1539608. The researchers from Lawrence Berkeley Laboratory were also supported by the Assistant Secretary for Energy Efficiency and Renewable Energy, Building Technologies Office of the U.S. Department of Energy under Contract No. DE-AC02-05CH11231. We thank Susan Fischer Wilhelm (California Energy Commission) for her support and guidance.

References

Mohegh, A., Levinson, R., Taha, H., Gilbert, H., Zhang, J., Li, Y., Tang, T., & Ban-Weiss, G. (2018). Observational evidence of neighborhood scale reductions in air temperature associated with increases in roof albedo. *Climate*, 6(4), 98. https://doi.org/10.3390/cli6040098

Levinson, R., Ban-Weiss, G., Chen, S., Gilbert, H., Goudey, H., Ko, J., L, Y., Mohegh, A., Rodriguez, A., Slack, J., Taha, H., Tang, T., & Zhang, J. (2019). Monitoring the urban heat island effect and the efficacy of future countermeasures. Publication CEC-500-2019-020, California Energy Commission, Sacramento, CA. https://www.energy.ca.gov/2019publications/CEC-500-2019-020

Taha, H., Ban-Weiss, G., Chen, S., Gilbert, H., Goudey, H., Ko, J., Mohegh, A., Rodriguez, A., Slack, J., Tang, T., & Levinson, R. (2018a). Modeling and observations to detect neighborhood-scale heat islands and inform effective countermeasures in Los Angeles. Publication CCCA4-CEC-2018-007, California's Fourth Climate Change Assessment, California Energy Commission, Sacramento, CA. https://www.energy.ca.gov/sites/default/files/2019-07/Energy_CCCA4-CEC-2018-007.pdf

Taha, H., Levinson, R., Mohegh, A., Gilbert, H., Ban-Weiss, G., & Chen, S. (2018b). Air-temperature response to neighborhood-scale variations in albedo and canopy cover in the real world: fine-resolution meteorological modeling and mobile temperature observations in the Los Angeles climate archipelago. *Climate*, 6(2), 53. https://doi.org/10.3390/cli6020053

Impact Analysis of Deep Static Bluespace on Urban Heat Island: Case of Chandigarh

Aditya Rahul[1]*, Indian Institute of Technology Roorkee (India)*
Mahua Mukherjee, Indian Institute of Technology Roorkee (India)

ABSTRACT

Urbanisation has picked up rapid pace since dawn of the industrial revolution. This unprecedented and unplanned urbanization is leading to Urban Heat Island effect. Urban Heat Island effect is a rise in temperature of the urban area in comparison to nearby rural areas, which in turn have a multidimensional impact on human health. Urban waterbody can act as a viable solution to attenuate this phenomenon. This research investigates the impact of Sukhna Lake (deep static waterbody) on heat stress in Chandigarh, India using remotely sensed data (LANDSAT-8 TIRS). It also examines the influence of urban form in the vicinity of the waterbody in propagating or reducing the impact. The results show that in Subtropical Humid climate of Chandigarh, waterbody provides a cooling effect in both summer and winter, with the cooling impact being greater in summer. Impact amplitude can go as high as 6.1 ℃ in summer in an area of sparsely built and low plant. The maximum impact range was observed to be 1080m in winter in the area of dense trees, whereas maximum impact gradient of 0.1383 ℃/m is achieved in the compactly built low-rise area during summer. This result will assist urban planners and designers to plan suitable built environment around waterbody and vice versa for better heat stress attenuation as well as optimal urban landscape designs for a more ecologically sound and pleasant living environment.

Introduction

Urban waterbody plays a multidimensional role in healthy well-being of the city by catering to its economical, ecological and socio-cultural needs. They were an integral feature of the urban landscape of most of the Indian cities but over the past few decades, unprecedented and unplanned urbanisation has led to a steady decline in urban waterbody area in India (Bindu & Mohamed, 2016). This decline in waterbody area is coinciding with rise in temperature of urban area. It has been established that urban areas have higher temperature than surrounding rural area (Oke, 1987). In regions with very hot summers, any reduction in temperature is a welcome relief. This study investigates the potential of waterbody to provide cooling in its surroundings.

Previous studies have shown that waterbody has the ability to influence thermal environment of its nearby surroundings (Hathway & Sharples, 2012; Y. Wang, Zhan, & Ouyang, 2019). It can provide cooling effect, sometimes referred as water cooling island (Coutts, Tapper, Beringer, Loughnan, & Demuzere, 2012; Gunawardena, Wells, & Kershaw, 2017; Sun & Chen, 2012) and in some cases it has also been observed that it can contribute to thermal stress by providing warmth in some climate zones (Moyer & Hawkins, 2017). Waterbodies can be

[1] Aditya Rahul: arahul@ar.iitr.ac.in, +91 8558069778.

classified in two categories i) Dynamic (rivers, streams) and ii) Static (lakes, ponds). Due to their difference in fluid flow characteristics, sensible thermal impact of these two differ from each other (Gunawardena et al., 2017). Where there has been substantial amount of work on the thermal impact of dynamic waterbodies (Hathway & Sharples, 2012; Moyer & Hawkins, 2017), impact of static waterbody is still comparatively less explored.

Traditionally thermal investigation was carried out through on site temperature measurement. This methodology is highly resource intensive. Recent developments in remote sensed imagery provides a viable alternative to study the thermal environment by providing the land surface temperature owing to its continuity in spatial resolution (Cristóbal et al., 2018; F. Wang et al., 2015).

This study aims to investigate the thermal impact of a deep static waterbody (Sukhna Lake) on its nearby surroundings in Subtropical Humid climate of Chandigarh, India. Land Surface Temperature (LST) derived from LANDSAT-8 TIRS data is employed to quantitatively assess i) thermal impact range, ii) maximum amplitude of impact and iii) thermal impact gradient of Sukhna Lake in city of Chandigarh, India. The surroundings of lake are classified in various local climate zones (LCZ) (Stewart & Oke, 2012a), to facilitate analysis of waterbody impact with respect to change in surrounding area. This study will help in establishing the role of waterbodies in controlling the microclimate of its nearby surroundings, thus motivating the concerned authorities to undertake steps for its conservation. It will also assist urban planners and designers in better planning of built environment around waterbody.

Materials and Method

Study Area

Chandigarh (30.74ºN, 76.79ºE) is a union territory and serves as the capital of two states namely Punjab and Haryana in India. It is located at an altitude of 321m and covers a total area of about 114 km^2. It is one of the most rapidly growing city in northern India with population of 1,055,450 in 2011 and an average population growth of 4% per annum.

Chandigarh lies on the foothills of Shivalik ranges of lesser Himalayas. According to Koppen climate classification, it has a humid subtropical climate characterized by very hot summers, mild winters, unreliable rainfall and great variation in temperature. Sukhna Lake is a man-made lake located in Chandigarh. Designed by Le Corbusier, it serves as a recreational and rejuvenation spot for residents and tourists. It has a total surface area of 3 km^2 and maximum depth of 4.9m with average depth being 2.4m. it is fed by Sukhna Choe, a seasonal stream.

Data

To conduct this study remotely sensed data from LANDSAT 8 OLI/TIRS is acquired. Two sets of imagery representative of two different seasons i.e. summer and winter are obtained, where summer is represented by imagery obtained from March 31st 2018 to June 19th 2018 and winter by imagery obtained from October 25th 2018 to December 28th 2018. The images used had 0% cloud cover.

Methodology

To analyse the thermal impact of waterbody on its nearby surroundings, the data obtained from LANDSAT 8 TIRS satellite is initially pre-processed in ERDAS Imagine 2018 software. The pre-processed data is then used to calculate Land Surface Temperature (LST), classify LCZ and extract the waterbody shape in ArcGIS 10.4. After the extraction, 100 buffers at a distance of 30m from waterbody edge was created covering a total of 3000 meters. Mean LST of each buffer situated in the particular LCZ was evaluated by overlay analysis of LST, buffer and LCZ. To identify the extent of the impact of waterbody, mean LST of the buffer with respect to the LCZ is plotted against the distance from waterbody edge. As proposed by *Sun et al.* (Sun & Chen, 2012) the first turning point of the curve represents the maximum amplitude of impact and the distance till first turning point is considered the impact range. The average slope of the curves over different surroundings is calculated to represent the impact gradient (Xue et al., 2019). This analysis was carried out for two different seasons i.e. summer and winter to identify the change in seasonal thermal impact of the waterbody. A methodology flow chart is presented in Figure 1.

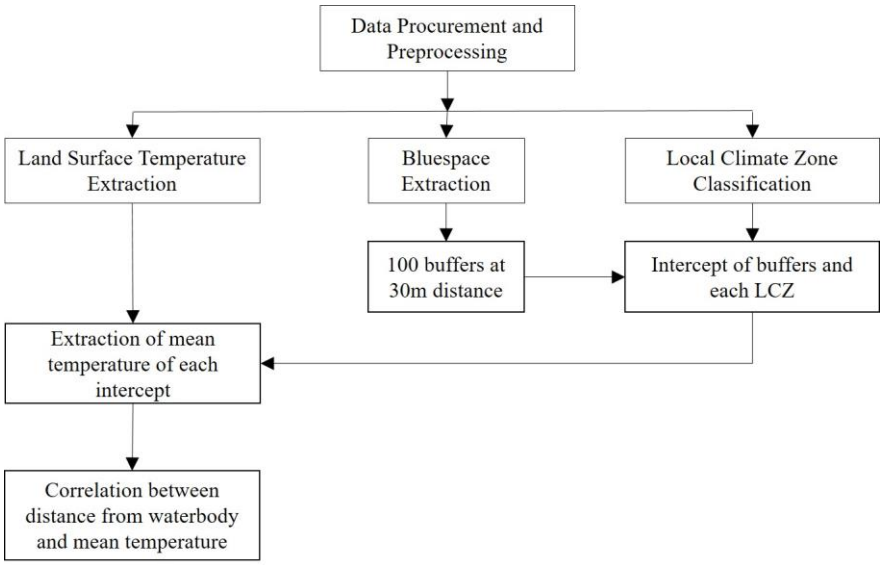


Figure 1: Flow chart of methodology used in this study

Land Surface Temperature retrieval:

There are three methods available for LST retrieval from LANDSAT imagery namely: a) Mono window algorithm, b) Single Channel Algorithm and c) Split window algorithm. The first two uses only a single thermal band (Band 10) whereas the third ie Split window algorithm uses 2 thermal bands (Band 10 and Band 11).

The mono-window algorithm proposed by *Wang et al.* (F. Wang et al., 2015) is used to retrieve Land Surface Temperature from the Landsat 8 TIRS Band 10 data. Following equation is employed for the same:

$$Ts = [a_{10}(1 - C_{10} - D_{10}) + (b_{10}(1 - C_{10} - D_{10}) + C_{10} + D_{10})T_{10} - D_{10}T_a]/C_{10}$$

equation (i)

Ts is the LST retrieved from Landsat 8 TIRS band 10; T_a stands for effective mean atmospheric temperature; T_{10} is the brightness temperature of band 10; a_{10} and b_{10} are the

constants of the algorithm with value of -70.1775 and 0.4581 respectively. C_{10} and D_{10} are the internal parameters derived by:

$$C_{10} = \tau_{10}\varepsilon_{10} \quad \text{equation (ii)}$$

$$D_{10} = (1 - \tau_{10})[1 + (1 - \varepsilon_{10})\tau_{10}] \quad \text{equation (iii)}$$

Where τ_{10} stands for atmospheric transmittance of Landsat 8 TIRS Band 10 and ε_{10} is ground emissivity.

Brightness Temperature (T_{10}):

Top of Atmosphere thermal radiance (L) is calculated using Digital numbers (Q_{10}) and Landsat 8 calibration coefficients. M_{10} is the multiplicative rescaling factor for Landsat 8 TIRS band 10 and A_{10} is the additive rescaling factor with values of 0.0003342 and 0.1 respectively.

$$L = M_{10}Q_{10} + A_{10} \quad \text{equation (iv)}$$

Planks radiance function was employed to convert thermal radiance (L) into brightness temperature (T_{10}) employing the following equation:

$$T_{10} = \frac{K_2}{\left\{\log_{10}\left(1+\frac{K_1}{L}\right)\right\}} - 273.15 \quad \text{equation (v)}$$

K_1 and K_2 are band specific thermal constants, which are 774.8853 and 1321.0789 respectively. T_{10} is the at sensor brightness temperature (°C).

Effective mean atmospheric temperature (T_a):

Linear relation proposed by *Qin et al.* (Qin, Karnieli, & Berliner, 2001) for the approximation of effective mean atmospheric temperature (T_a) from near surface air temperature (T_0) is used. For mid latitude summer T_a = 16.0110 + 0.9262T_0 . Temperature data from NOAA, (National Centers for Environmental Information) is used to obtain T_0 for each day.

Atmospheric Transmittance (τ_{10}):

Atmospheric transmittance is derived according to the linear relation mentioned by *Wang et al.* (F. Wang et al., 2015). For Mid-latitude summer with water vapour content of 1.6-4.4 g.cm^{-2} atmospheric transmittance is given by:

$$\tau_{10} = 1.0163 - 0.1330\, w \quad \text{equation (vi)}$$

Water vapour content (w) can be considered as 2.5 g.cm^{-2} for clear sky in mid latitude summer. Thus τ_{10} is 0.6838.

Ground emissivity (ε_{10}):

Ground emissivity is estimated through NDVI threshold method (Yu et al., 2014).

Ground Emissivity (ε_{10})	**NDVI**
$0.973 - 0.047\rho_4$	NDVI < 0.2
$0.9863p_v + 0.9668(1-p_v) + C_i$	0.2 ≤ NDVI ≤ 0.5
$0.9863 + C_i$	NDVI > 0.5

C_i is the surface roughness coefficient; p_v is the fractional vegetation cover derived from NDVI by:

$$p_v = \left[\frac{NDVI - NDVI_{min}}{NDVI_{max} - NDVI_{min}}\right]^2$$ equation (vii)

and

$$NDVI = \frac{\rho_5 - \rho_4}{\rho_5 + \rho_4}$$ equation (viii)

Where ρ_5 and ρ_4 are land surface reflectance of near infrared band and red band respectively.

Waterbody Extraction:

Remote sensed data provides a viable alternative to extract waterbody shape and area. Different approaches are available for waterbody extraction through both spectral analysis and image classification method. Waterbody indices such as NDWI, MNDWI and AWI based on spectral analysis method are sometimes unable to extract the waterbody area accurately from satellite imagery due to its inability to segregate various urban structures (eg. Roads, dark built-up areas, shadows etc.)(Huang, Xie, Fang, & Zhang, 2015). Techniques based on image classification method offers a better alternative for waterbody shape and area extraction (Huang et al., 2015). This investigation employs Support Vector Machine algorithm with RBF kernel for waterbody extraction.

Local Climate Zone Classification:

It has been observed that climatic behaviour in urban area changes with change in surroundings(Oke, 1987). Researchers for urban climate study have proposed various classification scheme of the urban area. From Chandler's classification of Greater London in four parts in 1965 to Oke's "Urban Climate Zones" in 2004, the classification schemes have evolved to incorporate parameters that are more just. This study adopts Local Climate Zone classification (Stewart & Oke, 2012b) to classify the designated urban area. This classification scheme has a total of 17 categories in which the area is classified. These categories are based on surface cover, structure, material and human activity (Stewart & Oke, 2012a).

In this study, Local Climate Zone classification is carried out through Satellite image based method (Bechtel, Alexander, Böhner, Ching, & Conrad, 2015). Training areas, representative of typical LCZ are identified using google earth. Random Forest classifier in SAGA-GIS is employed using the defined training area polygons for classification of different LCZ around the waterbody.

For further climatic analysis, the following four Local Climate Zones are identified around the waterbody in the city of Chandigarh Figure 2:

1. LCZ6 (Open Low rise)
2. LCZ3 (Compact Low rise)
3. LCZ A (Dense Trees)
4. LCZ 9D (Sparsely Built and Low plant)

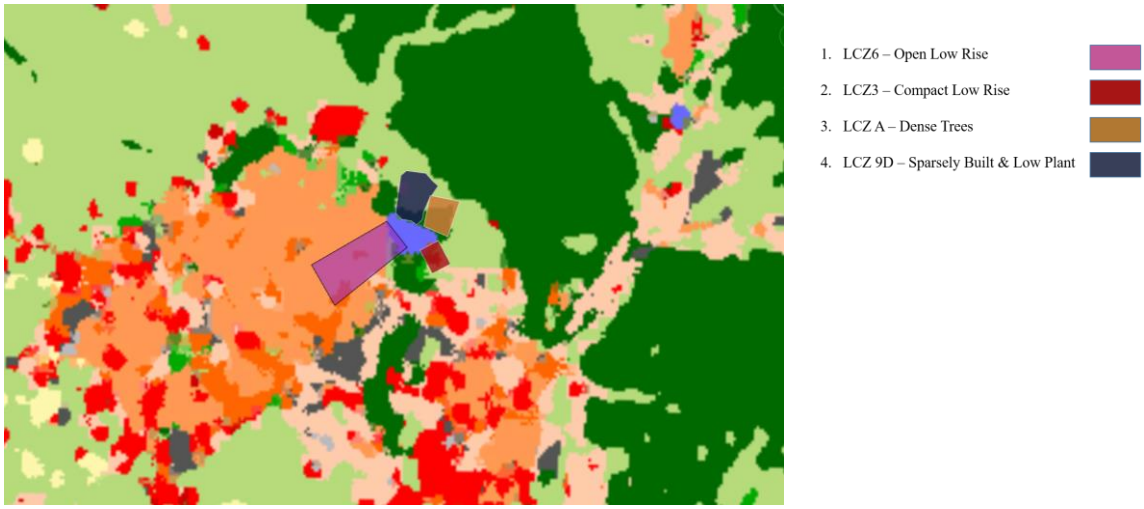


Figure 2: LCZ classification of Chandigarh, India with selected LCZ's for analysis

Results:

The four LCZ's have shown different trends in land surface temperate change while the distance from the waterbody edge varies. The summer and winter trends reveal that the change in season affects the LST differently for the same LCZ. In the city of Chandigarh which has a humid subtropical climate, presence of waterbody provides a cooling effect in both summer and winter months in the zones considered for the study (LCZ6, LCZ 3, LCZ A, LCZ 9D). However, the trends for each LCZ have different magnitudes which are discussed below in detail.

In summers, the distance and temperature difference of first inflection point in the curve of surface temperature with respect to edge of waterbody is; (i) 600m, and 4.86℃ for LCZ6; (ii) 420m, and 5.81℃ for LCZ3; (iii) 1020m, and 4.04℃ for LCZA; (iv) 450m, and 6.1℃ for LCZ 9D; respectively Figure 3.

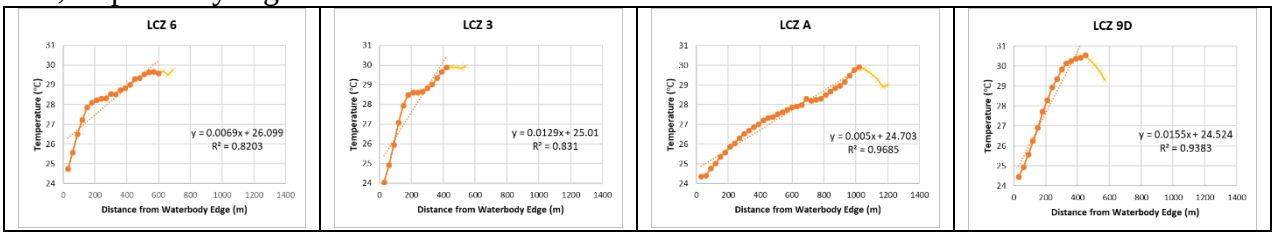


Figure 3: Graph representing LST with respect to distance from waterbody edge with inflection point in summer

In winters, the distance and temperature difference of first inflection point in the curve of surface temperature with respect to edge of waterbody is; (i) 400m, and 1.72℃ for LCZ6; (ii) 210m, and 1.56℃ for LCZ3; (iii) 1080m, and 3.36℃ for LCZA; (iv) 630m, and 3.16℃ for LCZ 9D; respectively Figure 4.

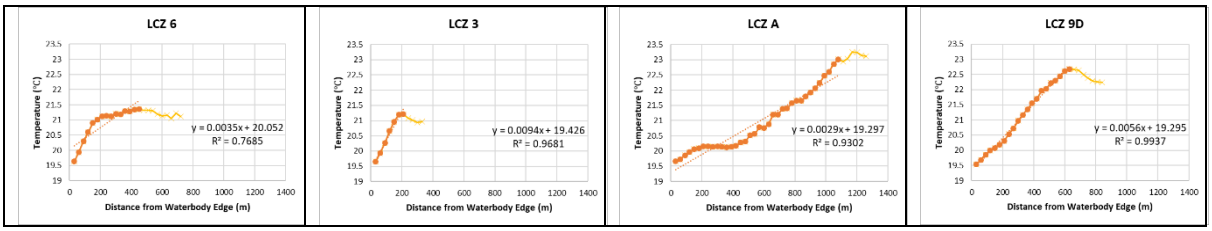


Figure 4: Graph representing LST with respect to distance from waterbody edge with inflection point in winter

All four cases have shown a good value of Pearson correlation Table 1.

Table 1: Waterbody cooling impact

Season	LCZ	Impact Amplitude (°C)	Impact Range (M)	Impact Gradient (°C/M)	Pearson Correlation between LST and distance from waterbody
In Summers	LCZ6	4.86	600	0.0081	0.90
	LCZ3	5.81	420	0.1383	0.91
	LCZ A	4.04	1020	0.0039	0.98
	LCZ 9D	6.1	450	0.0135	0.97
In Winters	LCZ6	1.72	450	0.0038	0.87
	LCZ3	1.56	210	0.0074	0.98
	LCZ A	3.36	1080	0.0031	0.96
	LCZ 9D	3.16	630	0.0050	0.99

Discussion:

Waterbody impact on heat stress:

Result of this investigation shows that waterbody has a cooling effect in a Humid Subtropical climate on its nearby surroundings. This can be a result of higher air humidity due to more evaporation (Gunawardena et al., 2017). A similar investigation carried out by Moyer & Hawkins (2017) in Harrisburg area which too has Humid and Subtropical climate found that river has a heating impact on its nearby surroundings (Moyer & Hawkins, 2017). This study indicates that waterbody has the lowest temperature when compared to its nearby surroundings and lake of 3km^2 surface area can have a cooling impact of up to 6.1 °C and can have impact distance of 1080m. It is also evident from the results that the cooling effect decreases with increase in distance from the waterbody, which is observed in various previous researches as well (Chen et al., 2009; Saaroni & Ziv, 2003).

Influence of LCZ on waterbody impact:

This study reflects that impact of waterbody on heat stress differs in different surroundings as stated by various researchers previously(Hathway & Sharples, 2012; Manteghi, 2015; Sun & Chen, 2012). Range of waterbody impact is maximum in LCZ A (dense trees), which can be owing to the fact that LCZ A in itself promotes cooling through evapotranspiration

and does offer comparatively fewer obstacles for air flow than other LCZ's considered here. Highest waterbody impact gradient of 0.1383 ℃/M is observed during summer in LCZ 3 (compact low rise), which can be attributed to the smaller building envelope and narrow streets. Smaller building envelope absorbs less radiation and narrow streets facilitate mutual shading thus keeping the surroundings cooler. Narrow streets also exhibit higher wind velocity (Blocken, Carmeliet, & Stathopoulos, 2007), thus allowing for greater cooling.

Seasonal Variation of waterbody impact:

Results of this investigation show a definitive trend that cooling impact of a waterbody is greater in summer than in winter. This phenomenon can be owing to the high heat capacity of water. During the daytime, in summer the land temperature rises rapidly creating a larger temperature difference between waterbody temperature and the land temperature, whereas during winter this temperature difference is comparatively lower due to less intense solar radiation, so, in turn, allowing for greater cooling amplitude during summer.

In case of impact range, it is higher during summer in LCZ 6 and LCZ 3 which can be attributed to larger amount of paved surface being present in these two LCZ's leading to greater atmospheric pressure difference between waterbody and surroundings thus stronger wind movement during summer. Whereas in LCZ A and LCZ 9_D the impact range is greater in winter.

Limitation and scope of future research:

This investigation has its own set of limitations. The spatial and temporal resolution of the remotely sensed data (LANDSAT-8 TIRS) is too coarse and can be further improved by the use of data having better temporal and spatial resolution. The satellite data employed here is captured at 5:20 am thus this result is unidimensional in time of study as it fails to capture the mid-day temperature or the night-time temperature. Thermal impact of waterbody can also be explored in various other LCZ's as this case provided the opportunity to explore just some of them.

This study analyses the impact from just a single waterbody, thus there is a need to explore this phenomenon with different waterbodies in different settings so that a relationship can be established between shape, size and depth of waterbody to its impact on heat stress. Future research should also investigate this relationship through the use of on-site measured data, as the LST generated from satellite imagery has some limitations.

Conclusion:

This study analysed the thermal impact of waterbody (Sukhna Lake) on its surrounding microclimate in the city of Chandigarh, India. Remote sensed data from LANDSAT-8 TIRS was used for this investigation. The results indicate that a deep static waterbody provides a cooling effect during summer as well as winter in Subtropical Humid climate of Chandigarh. The cooling impact can go as high as 6.1 ℃ in summer in an area of sparsely built and low plant and upto 3.36 ℃ in area of dense trees. The maximum impact range is observed to be 1080m in winter and 1020m in summer in the area of dense trees. Maximum impact gradient of 0.1383 ℃/M in summer and .0074 ℃/M in winter is achieved in an area that is compactly built low-rise structure.

These results are representative of a single case of Chandigarh and employ a single methodology. There is a need to evaluate this behaviour through various other methods in different cases so it can help urban designers and urban planners in taking a better-informed decision regarding planning built environment beside a waterbody or vice-versa for better heat stress attenuation.

Acknowledgement:

The author would like to sincerely thank Indian Institute of Technology Roorkee, India for supporting this research.

References:

Bechtel, B., Alexander, P. J., Böhner, J., Ching, J., & Conrad, O. (2015). Mapping Local Climate Zones for a Worldwide Database of the Form and Function of Cities. *ISPRS International Journal of Geo-Information*, *4*, 199–219. https://doi.org/10.3390/ijgi4010199

Bindu, C. A., & Mohamed, A. R. (2016). Water Bodies as a Catalyst to Growth and Development- The Case of Kodungallur Town, Kerala. *Procedia Technology*, *24*, 1790–1800. https://doi.org/10.1016/J.PROTCY.2016.05.222

Blocken, B., Carmeliet, J., & Stathopoulos, T. (2007). CFD evaluation of wind speed conditions in passages between parallel buildings—effect of wall-function roughness modifications for the atmospheric boundary layer flow. *Journal of Wind Engineering and Industrial Aerodynamics*, *95*(9–11), 941–962. https://doi.org/10.1016/J.JWEIA.2007.01.013

Chen, Z., Zhao, L., Meng, Q., Wang, C., Zhai, Y., & Wang, F. (2009). Field measurements on microclimate in residential community in Guangzhou, China. *Frontiers of Architecture and Civil Engineering in China*, *3*(4), 462–468. https://doi.org/10.1007/s11709-009-0066-6

Coutts, A. M., Tapper, N. J., Beringer, J., Loughnan, M., & Demuzere, M. (2012). Watering our cities: The capacity for Water Sensitive Urban Design to support urban cooling and improve human thermal comfort in the Australian context. *Progress in Physical Geography*, *37*(1), 2–28. https://doi.org/10.1177/0309133312461032

Cristóbal, J., Jiménez-Muñoz, J. C., Prakash, A., Mattar, C., Skoković, D., & Sobrino, J. A. (2018). An improved single-channel method to retrieve land surface temperature from the landsat-8 thermal band. *Remote Sensing*, *10*(3). https://doi.org/10.3390/rs10030431

Gunawardena, K. R., Wells, M. J., & Kershaw, T. (2017). Utilising green and bluespace to mitigate urban heat island intensity. *Science of the Total Environment*, *584–585*, 1040–1055. https://doi.org/10.1016/j.scitotenv.2017.01.158

Hathway, E. A., & Sharples, S. (2012). The interaction of rivers and urban form in mitigating the Urban Heat Island effect: A UK case study. *Building and Environment*, *58*, 14–22. https://doi.org/10.1016/j.buildenv.2012.06.013

Huang, X., Xie, C., Fang, X., & Zhang, L. (2015). Combining Pixel-and Object-Based Machine Learning for Identification of Water-Body Types from Urban High-Resolution Remote-Sensing Imagery. *IEEE Journal of Selected Topics in Applied Earth Observations and Remote Sensing*, *8*(5), 2097–2110. https://doi.org/10.1109/JSTARS.2015.2420713

Manteghi, G. (2015). Influence of Street Orientation and Distance To Water Body on Microclimate Temperature Distribution In Tropical Coastal City of Malacca. *International Journal of Applied Environmental Sciences ISSN*, *10*(2), 973–6077. Retrieved from http://www.ripublication.com

Moyer, A. N., & Hawkins, T. W. (2017). River effects on the heat island of a small urban area. *Urban Climate*, *21*, 262–277. https://doi.org/10.1016/j.uclim.2017.07.004

Oke, T. R. (1987). *Boundary Layer Climates*. *Earth-Science Reviews* (Vol. 27). https://doi.org/10.1016/0012-8252(90)90005-G

Qin, Z., Karnieli, A., & Berliner, P. (2001). A mono-window algorithm for retrieving land surface temperature from Landsat TM data and its application to the Israel-Egypt border region. *Int. j. Remote Sensing*, *22*(18), 3719–3746. https://doi.org/10.1080/01431160010006971

Saaroni, H., & Ziv, B. (2003). The impact of a small lake on heat stress in a Mediterranean urban park: the case of Tel Aviv, Israel. *International Journal of Biometeorology*, *47*(3), 156–165. https://doi.org/10.1007/s00484-003-0161-7

Stewart, I. D., & Oke, T. R. (2012a). Local climate zones for urban temperature studies. *Bulletin of the American Meteorological Society*, *93*(12), 1879–1900. https://doi.org/10.1175/BAMS-D-11-00019.1

Stewart, I. D., & Oke, T. R. (2012b). Supplement DATASHEETS FOR LOCAL CLIMATE ZONES. *Bulletin of the American Meteorological SocietyAmer. Meteor. Soc*, (December), 108–125. https://doi.org/10.1175/BAMS-D-11-00019.2

Sun, R., & Chen, L. (2012). How can urban water bodies be designed for climate adaptation? *Landscape and Urban Planning*, *105*(1–2), 27–33. https://doi.org/10.1016/j.landurbplan.2011.11.018

Wang, F., Qin, Z., Song, C., Tu, L., Karnieli, A., & Zhao, S. (2015). An Improved Mono-Window Algorithm for Land Surface Temperature Retrieval from Landsat 8 Thermal Infrared Sensor Data. *Remote Sensing*, *7*(4), 4268–4289. https://doi.org/10.3390/rs70404268

Wang, Y., Zhan, Q., & Ouyang, W. (2019). How to quantify the relationship between spatial distribution of urban waterbodies and land surface temperature? *Science of The Total Environment*, *671*, 1–9. https://doi.org/10.1016/J.SCITOTENV.2019.03.377

Xue, Z., Hou, G., Zhang, Z., Lyu, X., Jiang, M., Zou, Y., … Liu, X. (2019). Quantifying the cooling-effects of urban and peri-urban wetlands using remote sensing data: Case study of cities of Northeast China. *Landscape and Urban Planning*, *182*, 92–100. https://doi.org/10.1016/J.LANDURBPLAN.2018.10.015

Yu, X., Guo, X., Wu, Z., Yu, X., Guo, X., & Wu, Z. (2014). Land Surface Temperature Retrieval from Landsat 8 TIRS—Comparison between Radiative Transfer Equation-Based Method, Split Window Algorithm and Single Channel Method. *Remote Sensing*, *6*(10), 9829–9852. https://doi.org/10.3390/rs6109829

EVALUATING URBAN HEAT ISLAND DUE TO BUILT MORPHOLOGY IN PUNE CITY

Shruti Khandelwal[1]*, SavitriBai Phule Pune University (India)*
Namrata Dhamankar, SavitriBai Phule Pune University (India)
Sujata Karve, SavitriBai Phule Pune University (India)

ABSTRACT

Urban heat island describes built up areas that are hotter than nearby rural areas. The cities are becoming complex character consisting of different surface materials of low albedo and with lack of vegetative cover provides multiple surfaces for the reflection of solar radiation as well as absorption & storage of heat.

Urbanization is taking place at a faster rate in India. Population residing in urban areas in India, according to 1901 census, was 11.4%. This count increased to 30% according to 2011 census. According to a survey by UN State of the World Population report in 2007, by 2030, 40.76% of country's population is expected to reside in urban areas.

Pune is one of the fastest growing cities in India. It is the seventh largest metropolitan city of India and the second largest in Maharashtra. Urbanization has led the migration of people from rural to urban areas which increases the need of infrastructure. Between 1991 and 2001, the city grew by 40%, increasing from 1.6 million to 2.5 million and it's estimated that population will hit 5.6 million by 2031 if this trend continues. The Environment Status Report (ESR) for 2016 by the Pune Municipal Corporation (PMC) has categorically stated that “construction activities in the city and use of heat-absorbing construction materials has increased in the last few years, leading to UHI Effect. This effect has resulted in a difference of 4 to 5 degrees between the temperatures of the Pune city to that of surrounding rural areas”. The report states that there is a direct impact of the Urban Heat Island Effect on human health issues such as heat stroke, headache, and tiredness.

This project aims to study and analyze the impact of urban morphology on the formation of UHI in Pune city and also focuses on investigating mitigation strategies.

Objectives are:

- Generate thermal maps for Pune.
- To identify Local climatic zone (LCZ)
- To identify construction materials.

The study shows how the urban factors such as the vegetation cover, shadings, orientation and aspect ratio of canyon are important elements that urban planners may take into account, especially for new urban developments in Pune.

[1] Shruti Khandelwal: [shruti1621@gmail.com].

Introduction

In the first issue of the Journal City, David Harvey wrote: 'The 20th century has been the century of urbanization'. Urbanization in low- and middle-income countries is one of the most influential transformation processes, altering the climate on the local, regional and global level (Butsch, 2017). The cities or urban areas are warmer than their surrounding or rural areas, this phenomenon is known as Urban Heat Island (UHI) effect (Oke T. R.), the clearest example of unintended climate modification due to human activities. UHI was first noticed by Luke Howard in London in 1833. Today it is the most studied phenomenon of cities. (Filho, 2017)

This urbanization is contributing to the increase in surface temperature by replacement of vegetation with impervious and high albedo materials, minimizes the natural cooling effects of shading and evaporation of water from soil (https://scied.ucar.edu/longcontent/urban-heat-islands, n.d.). These materials absorb and store solar heat from sunrise to late afternoon. At night, the heat stored in structures is released to the environment in the form of long wave radiation. The quantity of heat release depends on controllable factors like the sky view factor and building material. (Hu Y., 2016)

The UHI intensity is measured as the difference between the temperature of urban area and rural area $\Delta Tu\text{-}r = Tu - Tr$, negative value shows UCI effect. Typically, the temperature difference between urban and rural ranges from 3 °C- 5 °C during the day. However, at night the temperature difference can reach up to 12 °C due to long wave radiation from the urban surfaces (Kumar R., 2017). This effect is more intense under calm and weak wind conditions with a cloudless sky at night in the summer (Aslam M. Y., 2017). UHI can also worsen the impact of heat waves, which are periods of abnormally hot weather. Heat wave has negative health impact on sensitive populations, such as children, older adults and those with existing health conditions.

Taslim S. et al. mentioned the causes of UHI on city level in their research (Aslam M. Y., 2017):

Surface: Land surface material is the main factor which affects UHI. Rasul A et al. studied that the outskirts of the city have more modern built-up with wide open areas, hence it experiences higher temperature than urban, as urban areas are densely packed and provide shadow.

Lack of plants: Trees provide local shade and evaporative cooling. Urban greenery increases to 30% can provide up to 2 °C cooler urban climate (Soltani A., 2017). Trees in open spaces can avoid extra radiation. Trees can also obstruct wind so it should be carefully planted on streets. (Yang X., 2016)

Human activities: Human activities affect the climate, such as air conditioning of buildings, motor traffic and Industrial production (Taslim S. P. D., 2015). Thermal emission from heated buildings, industries and transport can increase the temperature up to 12 °C than the surrounding area (Oke, 1973).

In India, fair amount of research has been conducted in the field of UHI effect. Rahul et al. investigated the dominant controls of UHI across 89 cities of India that area planned to be developed as smart cities. The study concluded that rapidly growing urban areas show UHI effect in night with intensity of 1-5 °C in the pre-monsoon and post monsoon seasons and during peak

summer months, the daytime surface temperature of urban- core regions is lower than their surrounding non-urban areas (UCI), this is due to changes and reduction in agricultural land on the outskirt of the cities due to urbanization. (Aslam M.Y. et al.) In their research performed analysis of air quality over Delhi and observed the UHI intensity of 2.2 °C and 5 °C in nighttime during May and December (Aslam M. Y., 2017). (Ram J et al) In their research. Patki and Alange, 2006 focused their study on finding out whether change in various land cover in Pune contributes to the change in land surface temperature over a period from 1999 to 2006 and as an outcome it was found that the built up area was increased 32.68% which lead to a decline of 10% in agriculture, 21.91% area in barren land and vegetation had been decreased by 10%. As a result, there had been a 1 °C to 4 °C rise in surface temperature in Pune (Nesarikar Patki P., 2012).

The Context of the Study

The research is based on Pune, India. It is situated in the western side of the Deccan plateau, surrounded by hills on the east and south side. It is elevated 560m above the sea level and has jurisdiction over an area of 243sq. km. About 63 lac people live in the city. To accommodate population, the city is growing in South-West, West and North-East direction due to availability of land and also IT companies around Pune gives future employment. The study is done in Kharadi located on the Eastern corridor of Pune. Due to some of the biggest IT parks and low residential cost, Kharadi is growing at a fast rate. Also, generated thermal maps of years 2001 and 2018 show that due to increasing built-up, hot pockets are developed in between built-up and leading to different microclimate. This study is carried out for Summer month where the maximum temperature ranging from 35 °C to 38 °C in the month of April and May.



Figure 1. Maharashtra Map showing Pune and Pune PMC area.

Methodology

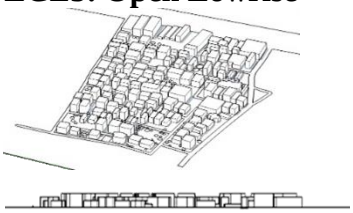
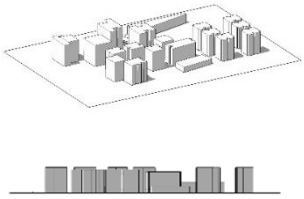
According to the Local Climate Zone scheme (Oke T.R.), two areas were selected by viewing satellite image, site visits and thermal maps. The sites were investigated for assessing the Urban Heat Island. These two areas are different in their location, buildings materials and height of buildings. Both the zones occupy the same area. The sites are 2 Km away and are located in Kharadi. Envimet simulations were done for existing condition of sites, analyzed the results and then mitigation strategies are provided for the area experiencing UHI and simulations were done after strategies as well. The day chosen for simulation is 28 April 2018 because it was the hottest day with maximum temperature 40 °C.



Figure 2. Kharadi with selected areas. Source: Google earth. And Thermal Maps of the year 2000 and 2018 of Kharadi. Source: Landsat.

Identification of Local Climate Zone

Table 1. Classification of Local climate zone of selected areas

Classification	Satellite image	Eye level photo	Properties of Site
LCZ5: Open Lowrise 	Area1 		Sky View Factor: 0.4 - 0.8 Aspect Ratio: 1 - 2 Mean Building Height: 3 - 20m Pervious Surface Fraction: 20 - 40% Impervious Surface Fraction: 20 - 40%
-  **LCZ4E: Open Highrise with paved surface**	Area2 		Sky View Factor: 0.4 - 0.8 Aspect Ratio: 1 - 2 Mean Building Height: 30 - 40m Pervious Surface Fraction: 20 - 40% Impervious Surface Fraction: 40 - 60%

Area1

Small residential building 1-3 stories tall attached in rows. Located on West side of Kharadi, suburbs of Pune. Construction material is burnt brick. Scattered trees and plant cover. Low traffic flow in internal streets but high traffic on highway located on north side of the area. Area comes under LCZ5, open low-rise.

Area2

Residential buildings 10-12 stories high, set in open arrangement. Located on East side of Kharadi, suburbs of Pune. Heavy building materials are used (concrete, steel) with flat roof. Land cover mostly paved with few trees. It has moderate traffic flow. Area comes under LCZ4E, open high-rise with paved surface.

The area of both the sites are 122500 sq.m.

Simulation for Urban Heat Island Effect

Table 2. Input data for simulation in Envimet

Main model parameters	
Simulation Date	28-Apr-18
Start & Duration of Simulation	11:00 15 Hrs
Climatic data	EPW File of Pune
Simulation Input Data	
Geographic Location (Latitude, Longitude)	18.52N 73.86E
Nesting grids	10
Method of vertical grid generation	Equidistant
Reference time zone	India Standard Time
Simulation Model size	120 X 120 X 80
Model Area	60 X 60 X 40
Size of grid	2 X 2 X 2

Table 3. Material types of base models

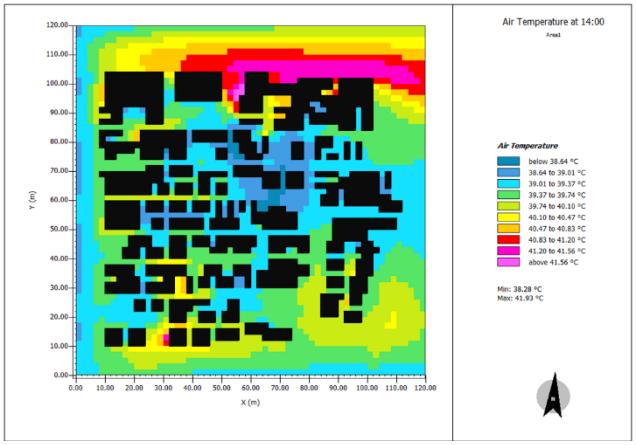
Material	Solar reflectance(α)	Thermal emittance(ε)	Heat Capacity(C) J/K
Asphalt (Road)	0.2	0.95	1.94
Soil	0.19	0.90	1.42
Concrete (Paved area)	0.45	0.75	2.11
Grass	0.1	0.95	

Air Temperature Results

The distribution of air temperatures for the two areas were plotted at daytime at 14:00 PM when the temperature is highest. The hour to represent the distribution of air temperature at night was picked according to Oke (1981,1987) who indicated that the effect of the Urban Heat Island is the strongest around 3-5 h after sunset. The sunset in Pune on 28 April started from 6:58 p.m. Hence, 22:00 p.m. was selected assuming that the Urban Heat Island phenomenon could occur.

The measurements are taken at 1.5 m height because traditionally described heat island is that which is measured at standard screen height (1–2 m above ground), below the city's mean roof height.

The figures below show that the maximum temperature at 14:00 p.m. in Area 1 is 41.93 °C and in area 2 is 40.80 °C. The minimum temperature in area 1 is 38.28 °C and in area 2 is 38.97 °C. The temperatures are higher above roads and low in-between buildings



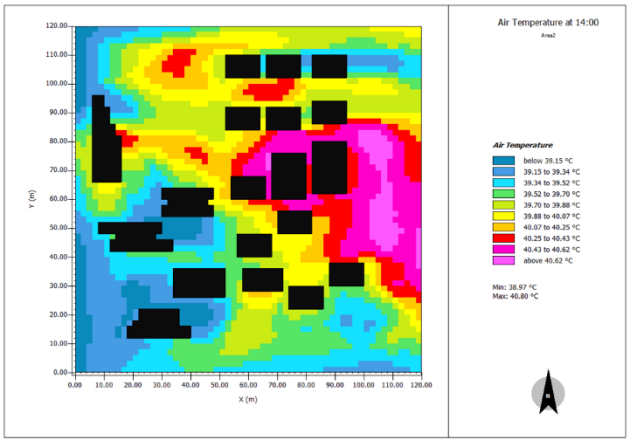
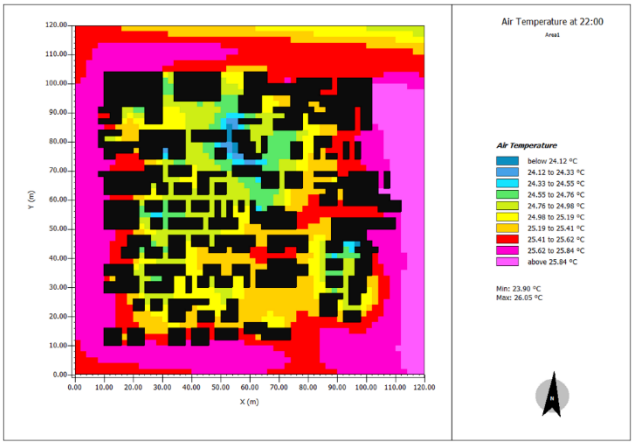


Figure 3. Air temperature distribution for area1 and area2 at 14:00 p.m., at 1.5 m above the ground.
Source: Generated from Envimet.



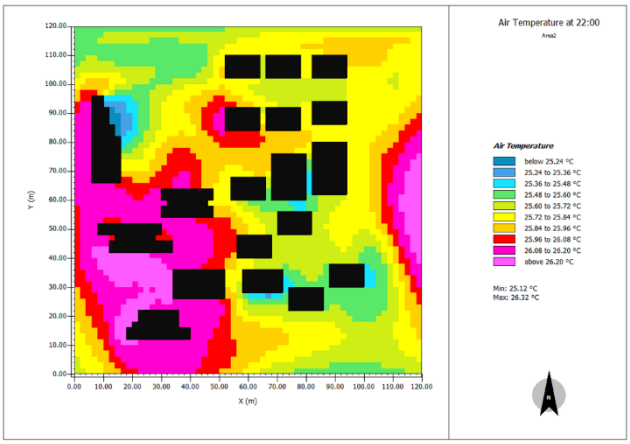


Figure 4. Air temperature distribution for area1 and area2 at 22:00 p.m., at 1.5 m above the ground.
Source: Generated from Envimet

The figures above show that the maximum temperature at 22:00 p.m. is 26.05 °C for area1 and 26.32 °C for area2 and the minimum temperature for area1 is 23.90 °C and for area2 it is 25.23 °C. At night 22:00p.m. the air temperature has decreased in area1 by 15.13 °C and in area2 by 14.165 compared with the air temperature at daytime (14:00 p.m.). Area2 has low cooling rate, this can imply that UHI could be present in area2.

To find UHI magnitude temperature difference of area2 and area1 is plotted. The graph shows that area 2 is experiencing higher temperature than area 1 except during daytime (14:00 and 16:00 p.m.). At 22:00 p.m. the magnitude of UHI is 0.745

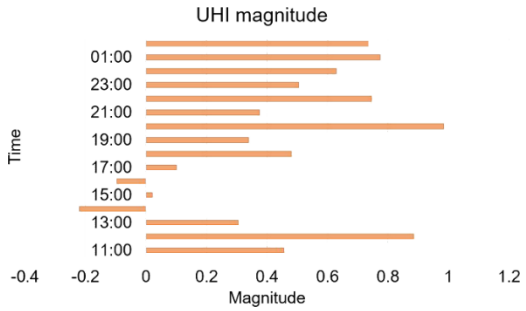


Figure 5. Magnitude of Urban Heat Island (Difference between area2 and area1)

Table 4. Percentage of Landcover

Land Cover	Area1(%)	Area2(%)
Road	52.11	12.44
Paved area	-	53.14
Bare Soil	47.89	32.16
Grass	-	2.26

Analysis

The percentage of road in area1 is 52.11% whereas in area 2 it is 12.44%. The material used for road is asphalt. Asphalt as a material has low solar reflectance than concrete, so it absorbs more of the solar radiation and heat up more than concrete. Therefore, area1 experiences higher temperature during daytime (14:00 p.m.). The emittance of asphalt is more than concrete hence it reaches its thermal equilibrium at lower temperature and gives off its heat more readily. Whereas the heat capacity of concrete is higher than asphalt and soil, so it stores more heat. Due to low thermal emittance and high heat capacity, concrete emits longwave radiation during night-time. Therefore, area2 experiences UHI at night (22:00 p.m.).

The Results of the outdoor thermal comfort index (Mean Radiant Temperature)

The mean radiant temperature is related to thermal comfort. The maximum mean radiant temperature for area1 is 73.00 °C and for area2 is 76.82 °C. And the minimum temperature for area1 is 42.60 °C and for area2 is 48.57 °C.

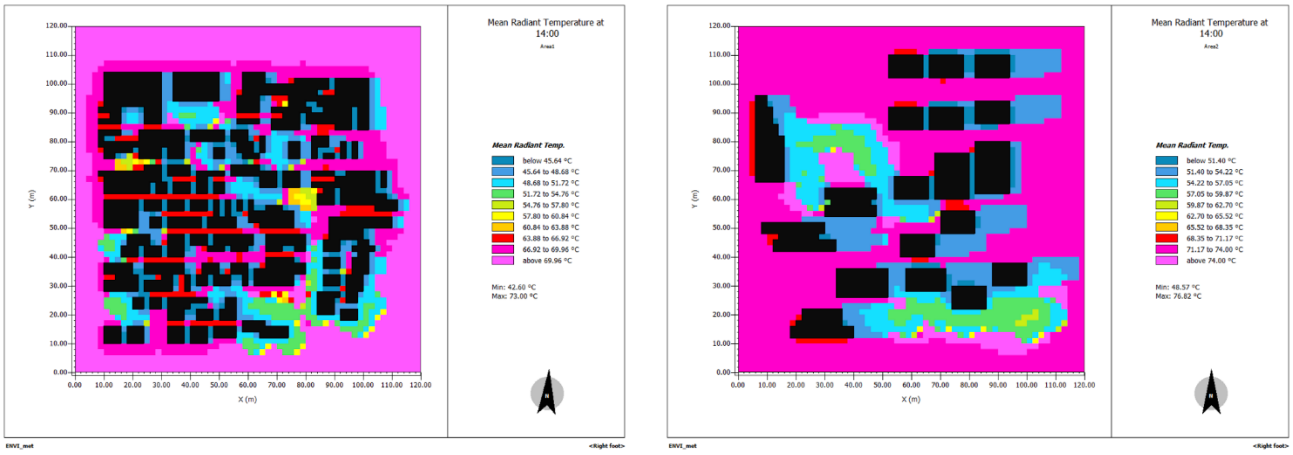


Figure 6. Mean Radiant temperature distribution for area1 and area2 at 14:00 p.m., at 1.5 m above the ground. *Source*: Generated from Envimet

Analysis

The mean radiant temperature (Tmrt) at 14:00 p.m. at daytime in area1 is less, as the area1 has narrow streets the shadows from building obstruct the solar radiation reaching the ground and reduces the mean radiant temperature. As the shadow fall on east direction at 14:00 p.m., North-South streets are in shade and experience lower Tmrt than east- west streets. Also, the open spaces in area1 has vegetation which provide shade and encourage evapotranspiration which helps in reducing temperature. Whereas in area2 due to lack of vegetation and the scarcity of shadow contribute to increase values of Tmrt.

Effect of the Shadings Pattern, Greenery Strategies and Pavement Material on the Urban Heat Island and Outdoor Thermal Comfort

As area2 is experiencing UHI at night, so mitigation strategies are provided in area2 to lower the air temperature.

The conventional urban surfaces have less solar reflectivity and emittance which leads to absorption of solar radiation and higher temperature of surface. As increase in surface temperature increases the air temperature above it through convection, the existing pavements can be resurfaced to avoid excessive heating and decrease emission of long-wave radiation at night. Resurfacing can increase the reflective properties and can also increase the durability of existing surface below.

As seen in previous simulation results, trees and shading helps to increase the thermal comfort. This strategy can be used to reduce mean radiant temperature during daytime. Trees should be placed according to sun's direction to get more shadow during daytime and also it should not obstruct longwave radiation at nighttime.

PVC sun shade is provided above parking and recreational area to cut off the harsh solar radiation after noon. White topping of white Portland concrete on the existing pavement to increase the reflectance. Trees are planted on west side of area and above garden for shading. The properties of selected materials area given below.

Table 4. Material Properties

Material	Albedo (α)	Thermal emittance (ε)	Heat Capacity(C)
PVC Shade	0.70	0.90	1.47
Concrete white topping	0.75	0.90	1.42

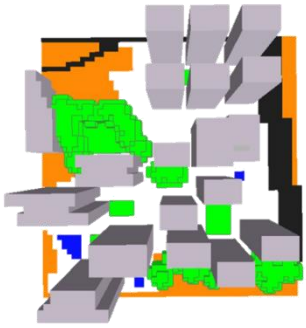


Figure 7. Base model of area2. *Source*: Generated from Envimet

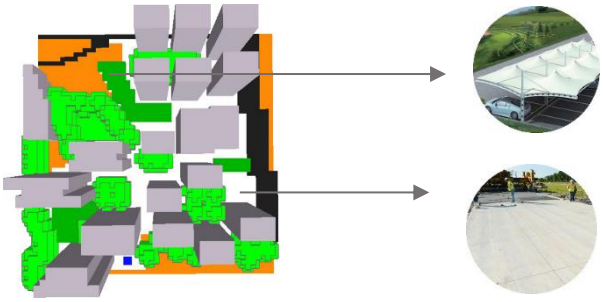


Figure 8. Shading, Trees and Pavement model of area2. *Source*: Generated from Envimet

Air Temperature Results

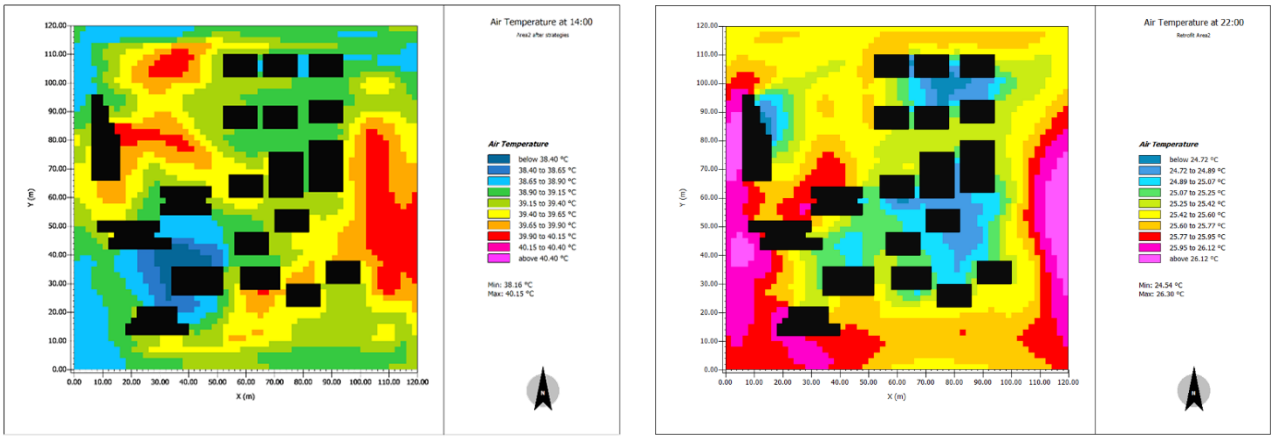


Figure 9. Air temperature distribution for area2 after strategies at 14:00 pm and 22:00 p.m., at 1.5 m above the ground. *Source*: Generated from Envimet

At 14:00 pm, the minimum temperature in area2 is 38.97 °C and after strategies the minimum temperature is 38.16 °C. and the maximum temperature of area2 is 40.80 °C and after strategies the temperature drops to 40.15 °C. At 22:00 pm, the maximum temperature in area2 is 26.32 °C and after strategies it is 26.30 °C. The minimum temperature of area2 is 25.12 °C and after strategies it is 24.54 °C. The areas with trees are cooler.

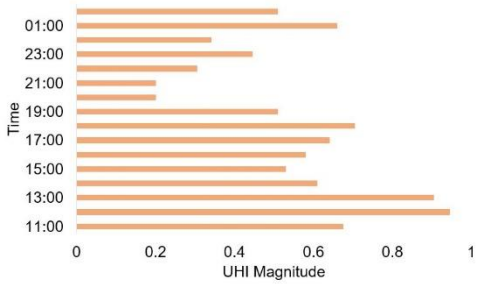


Figure 10. Magnitude of Urban Heat Island (Difference between area2 and area2 after strategies)

As shade above parking reduces the sky view factor and the effect of sun radiation. Also, trees obstruct the radiation reaching to the ground and thus reducing heating of concrete and emission of long wave radiation. After strategies area2 is experiencing lower temperature than before at all the time of the day.

Conclusions

For UHI results, simulation model was generated using a three-dimensional urban micro-climate simulation tool, ENVI-met 4.0. This model was used to simulate urban heat island conditions in two parts of the city of Pune.
The influence of three parameters including the greenery, reflectivity of pavements and shading was evaluated. The results suggested modifications within the reflectivity of pavement and increase in greenery were effective in influencing the temperature of area2. Also shading decreases the Mean radiant temperature and hence helps in increasing the thermal comfort outside during daytime.

The temperature difference is calculated for area2 before and after strategies. The difference is more during day time at 12:00 and 1:00 p.m. As at 12:00 due to sun's angle, the vertical structures like buildings has very less shadow to obstruct the radiation, providing horizontal shade and increasing the trees as strategies increases the shadow below them and hence reduces the temperature of the area. After providing strategies the area2 experience lesser temperature all time of the day as compared to before. At 12:00 the temperature difference is 0.945 °C and at 22:00 pm the difference is 0.305 °C. The spaces with trees are experiencing lower temperature at night with respect to PVC shade due to some amount of long wave radiation emission from the PVC shade, hence vegetation can be used in existing as well as developing areas of Pune to reduce Urban Heat Island effect.

References

http://worldpopulationreview.com/world-cities/pune-population/
https://en.wikipedia.org/wiki/Urbanisation_in_India

Butsch, C., Kumar, S., Wagner, P., Kroll, M., Kantakumar, L., Bharucha, E., . . . Kraas, F. (2017). Growing 'Smart'? Urbanization Processes in the Pune Urban Agglomeration. Sustainability, 9(12), 2335. doi:10.3390/su9122335

Oke, T. R., Mills, G., Christen, A., & Voogt, J. A. (n.d.). Urban Heat Island. Urban Climates, 197-237.

Filho, W. L., Icaza, L. E., Emanche, V., & Al-Amin, A. Q. (2017). An Evidence-Based Review of Impacts, Strategies and Tools to Mitigate Urban Heat Islands. International Journal of Environmental Research and Public Health,14(12), 1600. doi:10.3390/ijerph14121600

Urban Heat Islands. (n.d.). Retrieved from https://scied.ucar.edu/longcontent/urban-heat-islands

Hu, Y., White, M., & Ding, W. (2016). An Urban Form Experiment on Urban Heat Island Effect in High Density Area. Procedia Engineering, 169, 166-174. doi:10.1016/j.proeng.2016.10.020

Kumar, R., Mishra, V., Buzan, J., Kumar, R., Shindell, D., & Huber, M. (2017). Dominant control of agriculture and irrigation on urban heat island in India. Scientific Reports, 7(1). doi:10.1038/s41598-017-14213-2

Joshi, R., Raval, H., Pathak, M., Prajapati, S., Patel, A., Singh, V., & Kalubarme, M. H. (2015). Urban Heat Island Characterization and Isotherm Mapping Using Geo-Informatics Technology in Ahmedabad City, Gujarat State, India. International Journal of Geosciences, 06(03), 274-285. doi:10.4236/ijg.2015.63021

Aslam, M. Y., Krishna, K. R., Beig, G., Tinmaker, M. I., & Chate, D. M. (2017). Seasonal Variation of Urban Heat Island and Its Impact on Air-Quality Using SAFAR Observations at Delhi, India. American Journal of Climate Change, 06(02), 294-305. doi:10.4236/ajcc.2017.62015

Taslim, S., Parapari, D. M., & Shafaghat, A. (2015). Urban Design Guidelines to Mitigate Urban Heat Island (UHI) Effects In Hot-Dry Cities. Jurnal Teknologi, 74(4)

Soltani, A., & Sharifi, E. (2017). Daily variation of urban heat island effect and its correlations to urban greenery: A case study of Adelaide. Frontiers of Architectural Research, 6(4), 529-538

Oke, T. (1973). City size and the urban heat island. Atmospheric Environment (1967), 7(8), 769-779. doi:10.1016/0004-6981(73)90140-6

Rasul, A., Balzter, H., & Smith, C. (2015). Spatial variation of the daytime Surface Urban Cool Island during the dry season in Erbil, Iraqi Kurdistan, from Landsat 8. Urban Climate, 14, 176-186. doi:10.1016/j.uclim.2015.09.001

Nesarikar-Patki1, P. and Raykar-Alange, P. (2012) Study of Influence of Land Cover on Urban Heat Islands in Pune Using Remote. IOSR Journal of Mechanical and Civil Engineering (IOSR-JMCE), 3, 39-43.

REVISED CITY DEVELOPMENT PLAN FOR PUNE - 2041, MAHARASHTRA, UNDER JNNURM (Rep.). (n.d.).

Pune. (2019, February 11). Retrieved from https://en.wikipedia.org/wiki/Pune#Climate

Local Climate Zones for Urban Temperature Studies. (n.d.). Retrieved from https://journals.ametsoc.org/doi/pdf/10.1175/BAMS-D-11-00019.1

Heat Vulnerability Index for Urban Heat wave Risk Adaptation for Indian Cities: A Case Study of Akola

Rajashree Kotharkar[1]*, Professor, Visvesvaraya National Institute of Technology (India)*
Sahil Aneja, M.Tech Student, Visvesvaraya National Institute of Technology (India)
Aveek Ghosh, PhD Scholar, Visvesvaraya National Institute of Technology (India)

ABSTRACT

According to IPCC report 2012, the intensity, duration, and frequency of heat wave are going to increase in the upcoming future (IPCC 2012) and from past experience shows that heatwave has a strong relation to human health. (Meteorological Bulletins 2003)(NDMA 2016)(Climate Council 2016). However, in India to tackle heat wave, Heat Action Plan (HAP) was prepared involving do's and don'ts strategy in which spatial pattern of vulnerability have not been addressed and excludes the role of an urban planner (Anjali Jaiswal, 2013). A Heat Vulnerability Index (HVI) was proposed using the GIS-based spatial information system which presents an overall vulnerability considering three more indices based on sensitivity, exposure, and adaptive capacity. This study entails a comprehensive method for preparing HVI which is constructed based on data extracted from census tract and remote sensing data assessed via Principal Component Analysis (PCA). The study also describes the criteria for selecting the indicators for constructing three indices and overall HVI taking weightage factor by variance in the context of Indian cities. The objective of the study is to perform a comparative analysis of vulnerability considering the indices and their interrelationship study at a local scale in India. These indices will further help in resource distribution, urban planning measures and also for proposing the specific policies which can help in risk adaptation of heat hazards in the dynamic nature of urban areas in a more accurate way.

Introduction

Heat wave does not have a universally accepted definition but defined by different countries in a different manner. In India, National Disaster Management Authority (NDMA) defines heat wave as a *"condition where the maximum temperature at a grid point is 3˚C or more than the normal temperature, consecutively for three days or more"* (NDMA 2016). In European countries, heat wave is defined by a combination of three criteria that is a minimum duration of heat event, relative humidity and threshold based on maximum and minimum temperature (WHO Europe 2009). While Australia has succeeded in establishing location-specific criteria in defining heat wave as *"a period of at least three days where the combined effect of excess heat and heat stress is unusual on the local climate"*. Both maximum and minimum temperatures are used in this assessment (Nairn and Fawcett 2013). Heat Index (Mohan et al. 2014) was not constructed in this study but rather is adopted by Meteorological Department of India which defines threshold temperature at 45ºC for plain areas and 30ºC for hilly areas (NDMA 2016). However, in India, the maximum temperature was found alone for constructing Heat Index and

[1] Rajashree Kotharkar: [rskotharkar@gmail.com]

previous research have laid the importance of incorporating minimum temperature as a factor of accumulating heat load in defining heatwave (ARUP 2014)(Pattenden et al. 2003).

Heat wave is regarded as a silent killer where its intensity, duration and frequency is going to increase in future (Steffen et al. 2014). It's impact on mortality can be understood from past experiences like European heat wave, 2003 and Russian heat wave, 2010 which took 70,000 and 56,000 lives respectively (Climate Council 2016). The situation is similar in India where heat wave has taken more than 15,000 lives during the year 2000 to 2014 (NDMA 2016). Several pilot projects such as Climate Change and adaptation strategies for human health and Euro HEAT had established the heat-health relationship to understand and evaluate the impact of extreme heat and proposed the need for adaptation strategies to tackle heat wave implications (World Health Organization and World Meteorological Organization 2014).

For adaptation strategies, several countries including India have prepared Heat Action Plan. Reports suggests that rise in global average temperatures from 1.5 degrees Celsius to 2 degrees will lead to non-linear increases in mortality risks across Indian cities, according to a study by the Council on Energy, Environment and Water (CEEW), Indian Institute of Management Ahmedabad and Indian Institute of Technology Gandhinagar. Rising to the challenge of climate change, the Ahmedabad Municipal Corporation (AMC) prepared the 2013 Heat Action Plan, which was the first comprehensive early warning system and preparedness plan to tackle extreme heat events. Similarly, Heat Action Plan of Greater Manchester, UK and Australia have defined vulnerable population to heat hazard in terms of socio-economic profile, spatial distribution of facilities and past experience of heatwave impact (Kazmierczak 2012)(Met Office 2015)(The Office of Environment and Heritage 2016)(Trundle et al. 2015). While in India, identification of vulnerable population is based on health perspective only with laid emphasis on do's and don'ts strategies. Moreover in Indian scenario, vulnerability pattern is unequally distributed within the cities because of their composite character having socio-spatial segregation based on caste, religion, income and type of occupation (Dupont 2004)(Singh and Vithayathil 2012) linked to the availability of amenities like water supply (Sidhwani, 2015). Due to this socio-social segregation phenomenon like developing of slum and squatters took place in environmentally prone areas whose dwelling solution are not enough to cope with the growing climate impact (World Health Organization 2010).

Heat Vulnerability Index is the spatially explicit method which offers the solution to identify spatial pattern of vulnerability as done in the case of Santiago (Chile), London and various cities (Inostroza et al. 2016)(Wolf and Mcgregor 2013)(Bao et al. 2015)(Johnson and Wilson 2009). HVI can be quantified by three component indices that are sensitivity, exposure and adaptive capacity as defined by IPCC report (IPCC 2012) for a better understanding of vulnerability and deploying location-specific measures. There is a need to understand the spatial pattern of vulnerability in India which are not covered in heat action plan considering the following objective: 1) To explore the spatial pattern of heat vulnerability within the urban area. 2) To identify hotspot clusters of heat vulnerability formed spatially and understand their constituting factors.

Methods and Materials

Case Study Area

Akola (20.7059° N, 77.0219° E) is a city in the Vidarbha region of Maharashtra state in central India situated at 925 ft (300 m) above mean sea level. It has a municipal area of 27 sq. km. and a population of 4,25,817 as per census of India, 2011. Akola has extreme weather conditions with very cold winter & hot summer with annual temperatures ranging from 5.6 ºC to 45.9 ºC (Akola District Gazetteers 2016). The population density of the city varies from 86.362 to 1512 persons per hectares and average being 326 persons per hectares for the continuous urban area. There are total 194 slums of which 92 are notified consisting of about 32% of the total city population (Municipal Corporation, Akola).

As per the census of India, Akola consists of 71 wards which have been used as the spatial unit of exploration for an understanding pattern of vulnerability. The fringe areas of the city remain undeveloped though city limits are extended to open or agriculture land, thus affiliating household census data at the actual urban and peri-urban area. This un-continuous urban area can produce biases in results of pixel based indexes. To avoid such an error, the study focused on the spatial assessment of continuous urban area demarcated based on an evaluation of Google map image of Akola city.

Heat Vulnerability Index (HVI)

HVI is the approach for vulnerability characterization and its consequent mapping. The purpose of the index is to identify areas with increased vulnerability so that specific adaptation and mitigation tactics can be implemented to reduce the probability of severe heat related impacts such as illness, death, damage to infrastructure and property (Loughnan et al. 2013). The approach to developing vulnerability index was first introduced by Cutter, 2003 (Cutter et al. 2003). It was applied for the first time at a spatial level based on the best knowledge of the concern of heat hazard (Wolf and McGregor 2009) in UK and Reid (Reid et al. 2009) in the US country level.

In this study, a HVI is developed using an inductive approach (Tate, 2012) in which principal component analysis is used to identify the principal components representing the group of covariant of factors related to the heat risk. This method was adopted to reduce the complexity of the indicators defined and further reduce it to a smaller set of indicators representing most of the variance (Wolf and Mcgregor 2013)(Inostroza et al. 2016).

HVI was developed using the geographic information system platform and calculated as shown in equation (1). Vulnerability is defined as a function of exposure, sensitivity and adaptive capacity as per 12th IPCC assessment report (IPCC 2012) and is used for the classification of indicators. Each component of vulnerability was quantified to form individual indices which then combined to form overall HVI to understand the spatial pattern of vulnerability. Vulnerability indices are convenient tools for a better understanding of the underlying cause of vulnerability for suggesting appropriate measures to natural hazards for example heatwaves (Loughnan et al. 2013). HVI was calculated using the in the equation:

$$V_j = E_j + S_j + A_j \qquad (1)$$

Where V is a vulnerability, E is exposure, S is sensitivity, and A corresponds to the adaptive capacity calculated at census tract *j* (IPCC 2012).

Data collection and identification of indicators

Heat vulnerability can be measured by specific set of factors that have an impact on human health, and these factors can be determined through literature, referring relevant experts, and related research work. Multiple studies conducted in London (Wolf and Mcgregor 2013), Phildadelphia (Weber et al. 2016), Chile (Inostroza et al. 2016) and New York (Nayak et al. 2017) have assessed vulnerability of urban populations to deadly heat wave health impacts. At the same time several studies have used readily available data from census tract such as in case of developing HVI for London, Santiago (Chile) and USA (Inostroza et al. 2016)(Wolf and Mcgregor 2013)(Schmidtlein et al. 2008)(Bao et al. 2015). In this particular study, the criteria for defining indicators is based on data extracted from the Census of India, Municipal Corporation and remote sensing data that are considered as a determinant of risk before and after being impacted by the heat hazard. Indicators are reclassified in three domains of vulnerability that are sensitivity, exposure and adaptive capacity which are considered as a function of vulnerability in diverse research works (Inostroza et al. 2016)(Wolf and Mcgregor 2013)(Cutter et al. 2003). Further, in this study adaptive capacity is taken as a component to increase vulnerability as all of its indicators are defined regarding teh reduction in capacity with an incraese in values.

Exposure to climate phenomena is the degree to which the system or community comes in contact with that threat (Climate Proof Cities Consortium 2014). In this study, Land Surface Temperature (LST) was used to represent exposure. LST was extracted from the remote sensing data which stored thermal emissivity of the land surface. Landsat imagery band six was processed based on standard procedure mentioned by United States Geological Survey (USGS). The image was then clipped along the municipal boundary using GIS platform. (Refer Table 3 for quantification method).

While sensitivity to the outcome of climate threat concerns the degree to which a community is influenced by the changing climatic condition. Unlike exposure, sensitivity portrays the intrinsic features of a system (Climate Proof Cities Consortium 2014). There are total five indicators used to quantify sensitivity (Table 2). Intrinsic factors broadly refer to the physical condition of individuals (typically called susceptibility factors or sensitivity in public health literature) that make them more sensitive to heat hazard due to a different thermoregulatory system and also depends upon behavioural characteristics of the individual (Milan and Creutzig 2015).

The IPCC Fourth Assessment Report has defined adaptive capacity as "*the ability or potential of a system to respond successfully to climate variability and change and includes adjustments in both behaviour and in resources and technologies*" (Barker 2007). IPCC also laid stress on the unequal distribution of adaptive capacity within the urban area (Barker 2007). There are total fourteen indicators used to quantify adaptive capacity in this study. Many indicators are defined considering a situation having high level of vulnerability such as lack of water supply, electricity and galvanised iron roof material are taken as roof material as it accounts high thermal conductivity.

Selection of Indicators

Further for selection of indicator chosen at a broader level, fourteen case studies including research papers on heat and social vulnerability were analysed. Indicators used in more than four studies were selected for further analysis. This shows the availability of necessary data required for constructing HVI in which out of possible 44 indicators, 20 indicators are selected for further analysis (Table 1).

Table 1. Indicators selection validation through case studies

	Case studies																
No	Indicators	1	2	3	4	5	6	7	8	9	10	11	12	13	14	NO	SL
1	Old population	Y	Y	Y	Y	Y	Y	Y	Y	Y	Y			Y	Y	12	Y
2	South facing top flat	Y			Y		Y									3	
3	Pre-medical condition	Y		Y	Y	Y	Y			Y			Y			7	
4	Occupational group	Y		Y	Y									Y	Y	5	Y
5	Poverty	Y	Y		Y	Y			Y	Y	Y	Y		Y	Y	10	
6	Young population	Y	Y	Y	Y	Y		Y	Y	Y	Y			Y	Y	11	Y
7	Urban heat island		Y			Y										2	
8	Rented housing		Y			Y	Y			Y				Y	Y	6	Y
9	Social infrastructure		Y			Y		Y		Y				Y	Y	6	Y
10	Green space distribution		Y						Y							2	Y
11	Transient/Communal/ Slum communities		Y	Y			Y							Y		4	Y
12	Bus railway passengers			Y												1	
13	Pregnant or nursing mothers				Y											1	
14	Condition to regulate body temperature				Y											1	
15	Heat intolerant condition				Y											1	
16	Living alone				Y	Y	Y					Y	Y			5	Y
17	People with disability				Y	Y		Y								3	
18	People without air conditioning				Y								Y			2	
19	Homeless people				Y											1	
20	People with limited access to transport				Y									Y		2	Y
21	Not have access to health services because of culturally and linguistically diverse background				Y		Y									2	
22	Population density		Y			Y	Y		Y					Y	Y	6	Y
23	Single pensioner households						Y									1	
24	Land surface temperature					Y		Y				Y				3	Y
25	Education level							Y	Y		Y		Y	Y	Y	6	Y
26	Unemployment							Y					Y	Y	Y	4	Y
27	Access to communication technologies							Y								1	Y
28	Access to water supply							Y								1	Y
29	Material index							Y	Y							2	Y
30	NDVI							Y								1	Y
31	Roads km per sq. km							Y								1	

32	Land cover vegetation abundance								Y							1	Y
33	Mortality: Heat as primary cause of death									Y						1	
34	Mortality: Heat as one of the cause									Y						1	
35	Heat wave intensity and duration									Y						1	
36	Zoning and land use											Y				1	Y
37	Living units in building					Y							Y			2	Y
38	Ceiling Height												Y			1	
39	Outside wall material												Y			1	
40	People per housing unit							Y		Y				Y	Y	4	Y
41	Social Security recipients													Y		1	
42	Housing density					Y						Y		Y		3	
43	Recent immigrants													Y		1	
44	Ethnic group					Y	Y		Y	Y	Y	Y	Y	Y	Y	9	

Note-The pre-medical condition being necessary excluded from PCA because of data unavailability. Y, No and SL depict indicator, repetition and selection respectively.

Indicators Quantification

Most of the indicators selected are quantified in unit per hectares to avoid the biases in results produced due to variation in ward sizes of the census tract (Table 2). The values of indexes guide to determine the comparable level of vulnerability between the wards which could be wrongly interpreted due to the high variation in scale and density. Afterwards, due to the different unit, each indicator is converted into unit less quantity using standardisation method.

Table 2. Indicator quantification and classification method

Domain	Indicators	Method to quantify	Data Source and Year
Sensitivity	Population below 6 years (UNU-EHS 2014)	Wardwise population below six years of age per hectare.	Census of India Website: http://www.censusindia.gov.in/2011census/HLO/HL_PCA/Houselisting-housing-HLPCA.html. Year: 2011
	Single household size (M. Loughnan et al. 2012)	Inhabitants per hectares who live alone.	
	Education (UNU-EHS 2014)	Inhabitants per hectares who are illiterate.	
	Age above 60 years (Kenny, Yardley, Brown, Mph and Jay, 2010)	Inhabitants per hectares whose age are equal or greater than the age of 60.	
Exposure	LST (Inostroza et al. 2016)	It was computed by average temperature plus one standard deviation for each census tract to provide a conservative estimation of LST.	Landsat TM band 6. Source: https://www.usgs.gov/ Year: 2013
Exposure because of condition	Slum (Johnson and Wilson 2009)	Number of slums in each ward.	Data collected from MunicipalCorporation, Akola.Year: 2016
	Rented (Kazmierczak 2012)	Wardwise rented household per hectare.	Census of India Website: http://www.censusindia.gov.in/2011census/HLO/HL_PCA/Houselisting-housing-HLPCA.html Year: 2011
	Temporary structure (Johnson and Wilson 2009)	Wardwise household per hectare of a temporary structure.	
	Roof material (Kendrick 2009)	Wardwise household per hectares with GI/metal as a roof material.	

Adaptive capacity	Congestion (Tate 2012)	Single household X average household size ≥ 5 for each ward giving population per hectare living in congestion.	
	Infrastructure facilities- electricity & water supply (Mooventhan and Nivethitha 2014)	Wardwise household per hectare that are not covered with electricity. Wardwise household per hectare has water facility away premises.	
	No communication facilities	Wardwise household per hectare that has no landline and mobile phone.	
	No personnel vehicle (Wilhelmi et al. 2004)	Wardwise household per hectare having no personal vehicle.	
	No bank account, factor to predict poverty (Johnson and Wilson 2009)	Wardwise household per hectare availing no banking facilities.	
	Residual green space (Oliveira, Andrade and Vaz, 2011)(Upmanis, Eliasson and Lindqvist 1998)	Standard 9 sq.m. per person per person required as per WHO. Residual Green area per hectares = (area required– existing green area)/ward area.	Remote sensing and data gathered from MC. Year: 2016
	NDVI (Kendrick 2009)	NDVI was computed as the average NDVI value per census tract plus one standard déviation.	Landsat TM band 6. Source: https://www.usgs.gov/ Year: 2013
	Health facilities (M. Loughnan et al. 2012)	The distance of centroid of the continuous urban area in each ward to the nearest government hospitals.	Remote sensing and data gathered from MC. Year: 2016
	Social facilities- religious facilities & schools (Kazmierczak 2012)	The distance of centroid of the continuous urban area in each ward to the nearest social facilities.	

Statistical analysis:

Detail procedure for HVI calculation

Heat vulnerability pattern is not explained uniformly by selected indicators and prior assumptions related to their importance can produce biases. Also, there is a strong correlation between the indicators defining the socio-economic condition (Wolf and Mcgregor 2013). To avoid this co-linearity issue the complications of selected indicators have been further reduced to a smaller set of principal components (PCs) that describe most of the variance in the selected indicators. As PCA is highly sensitive to the input values, it is of paramount importance to standardise the data into the same magnitude. This criterion was achieved by converting the values in z-score using equation (2).

$$Z_i = (Xi - \eta)/SD \quad (2)$$

where Z_i is z-score for each ward of respective indicator, X_i is original value, η is mean of all the values of the individual indicator and SD is standard deviation of all the values of the individual indicator. Standardization of data also avoid biases that are produced by low and very high variance level. This will result in centering and scaling of dataset with mean 0 and standard deviation 1 on which PCA can be performed (Schmidtlein et al. 2008). Both tests are required to check the appropriateness of using PCA (Wolf and Mcgregor 2013). The number of components

to be retained in PCA is done using Kaiser criteria and scree test where only those components are selected whose eigenvalues are greater than one as they explained maximum of the variance.

For improving interpretation, varimax rotation developed by Kaiser was performed on eigenvectors in revealing the simple structure (Abdi and Williams 2010). Afterwards, PC scores were generated for n retained components, so that each 71 wards possessed the n-PC scores. These retained PCs are then weighted according to the variance explained and combined to get overall PC score for each ward results to form vulnerability index on which PCA was performed (Wolf and Mcgregor 2013). This method was applied to reduce any prior assumptions related to the importance of indicator which can produce biases in the results. While doing this, weight as well as a sign of each score were retained. XLSTAT an extension of Excel was used for performing PCA calculation. Partial results of each index that is sensitivity, exposure, and adaptive capacity were then normalised using equation (3) to get values in 0 to 1 range.

$$\alpha = \left\lfloor \frac{X - Xmin}{Xmax - Xmin} \right\rfloor \quad (3)$$

Where α is normalized value, X_{max} is maximum value and X_{min} is minimum value of the input dataset. Normalized values are then grouped in five categories based on equal interval to understand spatial pattern of vulnerability for each index. HVI is then calculated using eq. (1) and then normalized using eq. (3).

Cluster Analysis

Cluster analysis was performed using Hot Spot Analysis by Getis-Ord Gi tool within the ArcGIS 10.4 software from ESRI to understand the spatial pattern of vulnerability for all four indexes. This tool identifies whether low, or high values tend to form cluster using Getis-Ord Gi statistics (Ord and Getis 1995). The output of the operation gives the z-score for all 71 wards. In this method, the statistical significance of clustering was represented by the z-score at a specified distance where values less than -1.96 were classified as cold spots and greater than 1.96 formed hotspots at 0.05 level of significance. In this analysis, only the hot spot clusters were considered for further analysis.

Results and Analysis

Outlier identification and error correction

Ward 67 having density 1512 persons per hectare is much higher than the city average density and seemed to be behaving in an unexpectedly different manner with much higher values for all variables creating dominance in PCA. So to reduce error induced by Ward 67, it was excluded from PCA analysis. Based on results of PCA performed with its inclusion while the highest value was assigned on one to five scales for calculation of sensitivity and adaptive capacity index.

The spatial pattern of heat hazard exposure

Land surface temperature (LST) has an average temperature within the municipal limit of value 27.12ºC. LST has minimum value 23.68ºC found in the south-west of the city, and the maximum value is 31.23ºC located in the core or old area in the town with a standard deviation

of 1.011. The difference between the highest and lowest value of LST was found to be 7.55ºC. Analysing the spatial relationship between the values of LST and slum location shows the significant link between the socio-economic condition and exposure level.

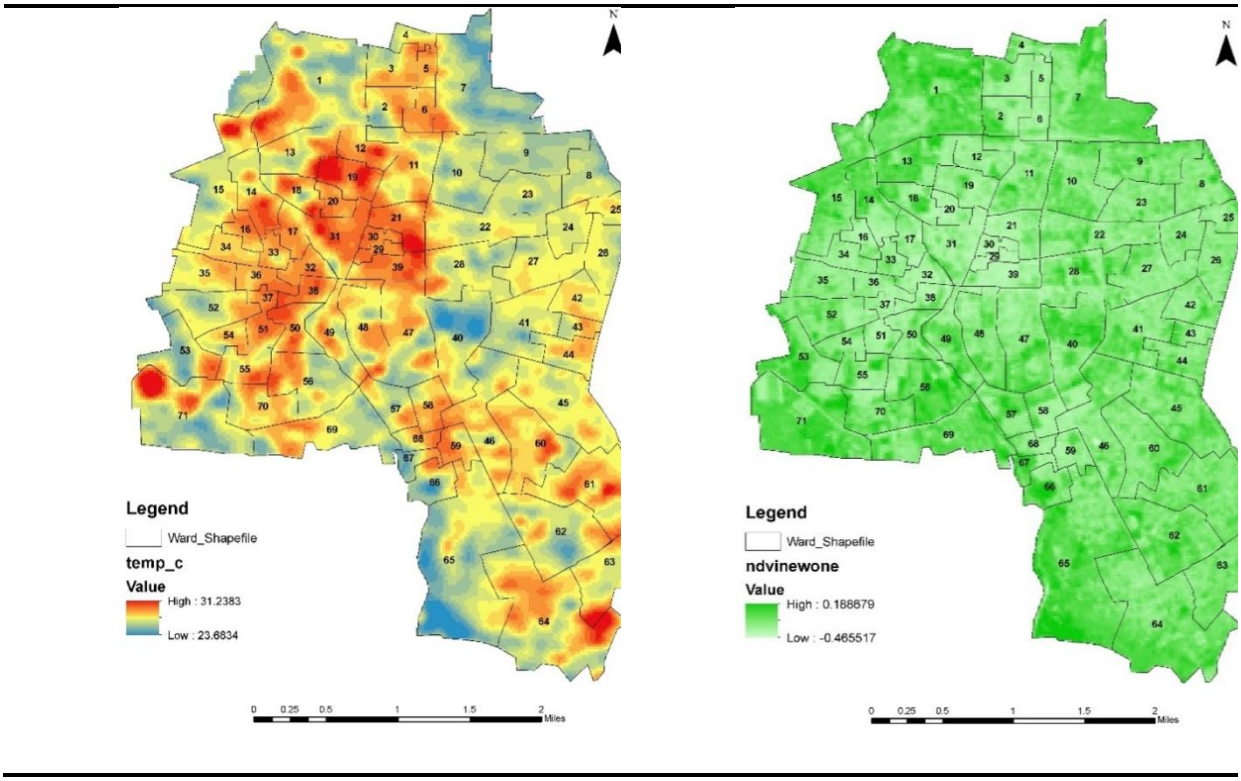


Figure 1. (i) Land surface temperature (LST) (ii) Both are calculated using the LANDSAT-TM image, 2009 band 6 acquired from the USGS

Also, the average ward value plus one standard deviation of LST is found highly correlated with the values of NDVI (r Pearson = -0.7434, $p < 0.05$). LST is found to have a negative correlation with NDVI values which tend to the significant positive correlation with the increase in open, green area and area with high vegetation. This result shows the influence of parks, open space, and areas with high vegetation on temperature. Analysing the results of the exposure shows the average city value of 0.472 at five level scales with a standard deviation of 0.23. The correlation of exposure with distance from the city centre is not significant (r Pearson = -0.0955, $p < 0.05$) but found be important with population density (r Pearson = 0.4505, $p < 0.05$). The weight of exposure with HVI is found to be 0.705.

Analysis and results for indicators of sensitivity

Bartlett's sphericity test result shows value less than 0.0001, so one should accept the alternative hypothesis depicting that atleast one of the correlations between the variables is significantly different from 0. Based on kaiser rule and scree test, two PC's were retained. The first PC has considerably large eigenvalue (3.492) and the second PC has eigenvalue very close to 1 (0.885) explaining the 69.85% and 17.71% of the total variance respectively. These two retained PCs explaining the 87.56% of total variance captured most of the data. The variables which dominate in PC 1 are illiteracy (0.51), children (0.516), living alone (0.385) and unemployment (0.518). PC 1 is interpreted as the "ability to respond" by considering the dominant variable while PC 2 having one variable elderly population (0.960) is interpreted as "dependency" (Table 3). The biplot axes depicting the z-score dispersion along with magnitude and correlation (sign) of eigenvectors after varimax rotation are shown in Fig 2.

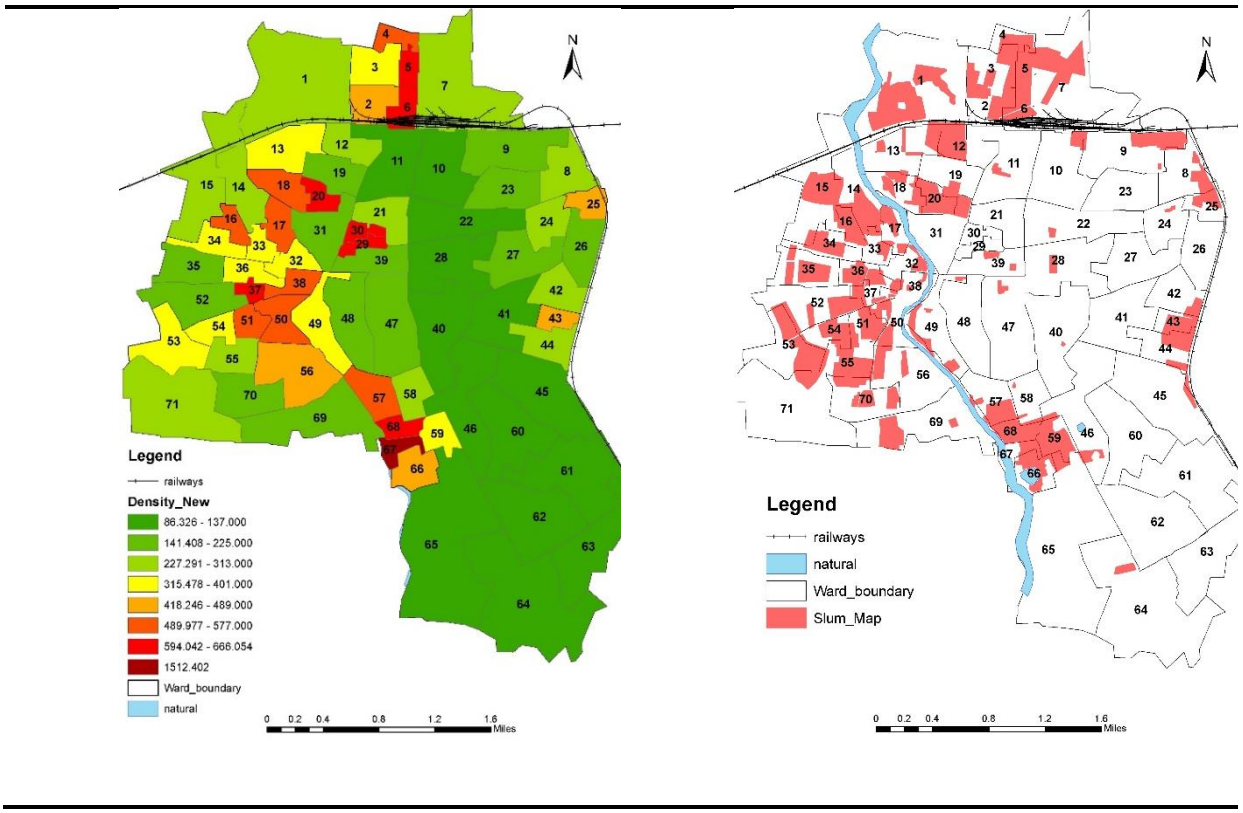


Figure 2. (i) Density map based on continuous urban area (Census 2011) (ii) Slum location map prepared using GIS 10.4 platform based on information acquired from Municipal Corporation, Akola

The asymmetric sensitivity profile was seen in ward number 65 while wards that are close to the centre have shared properties *(Note: Ward 67 was excluded from analysis).* The normalized sensitivity has a mean value of 0.34 (moderate according to scale from 0 to 1) and standard deviation (SD) of 0.264. The sensitivity found highly correlated with density (0.897) while showing a negative correlation with ward area (-0.485), means smaller wards are more sensitive than a larger one. Sensitivity show minimal and adverse relation (-0.11) with distance

from the city centre depicting the non-relevance of centrality issue. Moreover, the weight of sensitivity (0.944) with HVI is found to be very high than any other index.

Table 3. PC loading following Varimax rotation for sensitivity

	PC 1	PC 2	PC 3	PC 4
Population Illiterate	**0.966**	-0.105	-0.136	-0.189
Population below 6 years	**0.965**	-0.057	-0.250	0.009
Population living alone	**0.721**	-0.228	0.654	0.008
Non workers population	**0.970**	-0.050	-0.155	0.177
Population above 60 years	0.409	**0.904**	0.125	-0.010

Note: Bold depicts statistically significant values.

Analysis and results for indicators of adaptive capacity

Bartlett's sphericity test results shows value less than 0.0001. As the computed p-value is lower than the significance level alpha=0.05, one should accept the alternative hypothesis that at least one of the correlations between the variables is significantly different from 0. Based on kaiser Rule, four PC retained for adaptive capacity (Ward 67 excluded from the calculation). The four retained PC has eigenvalues 6.128, 1.657, 1.383 and 1.044 explaining 43.77%, 11.84%, 9.88% and 7.457% of the total variance respectively. Together all four PC explain 72.949% of the total variance is retaining much of the data structure. The left out PCs do not satisfy Kaiser rule and for the same reason not included for further analysis.

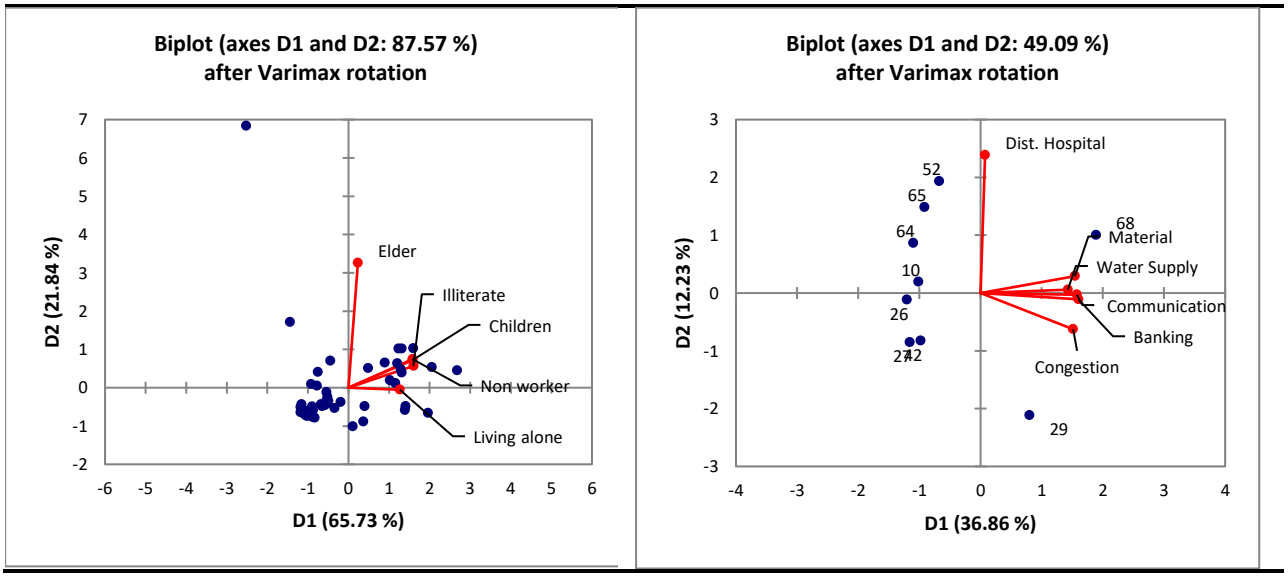


Figure 3. Scatter plot depicting the z values for sensitivity (left) and adaptive capacity (right). Principal components (PC) load are shown in red.

After varimax rotation, considering the values of squared cosines, a total of seven variables are dominant in PC 1. Variables dominant in the first PC are no banking facilities (0.879), no communication (0.853), roof material (0.817), congestion (0.787) and water supply

away premises (0.70) while two more variables that are rented household (0.40) and temporary structure (0.26) but having little dominance.

The dominant variables in the second PC are the distance from the hospital (0.529), school (0.216) and social facilities (0.454)and NDVI (0.371). The dominant variables in the third PC are a residual green area (0.684) and no personal vehicle (0.436). While there is only one variable no electricity (0.820) that is dominant in the fourth PC.

Table 4. PC loading after Varimax rotation for adaptive capacity

	PC1	PC2	PC3	PC4
Rented	**0.400**	0.061	0.311	0.040
Temporary structure	**0.260**	0.007	0.093	0.001
Roof material	**0.817**	0.008	0.035	0.014
No water supply	**0.700**	0.000	0.009	0.001
No electricity	0.022	0.010	0.000	**0.820**
No communication	**0.853**	0.000	0.054	0.004
No personal vehicle	0.258	0.007	**0.436**	0.000
No banking facilities	**0.879**	0.001	0.059	0.000
Congestion	**0.787**	0.036	0.065	0.005
Hospital distance	0.002	**0.529**	0.165	0.018
School distance	0.059	**0.216**	0.000	0.140
Religious facilities distance	0.021	**0.455**	0.012	0.001
Residual green area	0.015	0.010	**0.685**	0.005
NDVI	0.087	**0.372**	0.205	0.162

Bold depicts statistically significant values.

The first PC is interpreted as socio-economic condition, the second PC as natural and built environment. The biplot axes are depicting the z-score dispersion of eigenvectors after varimax rotation shows asymmetric profile while the ones which are present near the centre of the plane shows average values of adaptive capacity. The normalised index for adaptive capacity has an average city value of 0.453 with SD of 0.270. Adaptive capacity shows a negative and less necessary relation with distance from the centre (-0.139) and highly significant correlation with population density (0.782). The weight of adaptive capacity with HVI is found to be 0.890.

Though weight of adaptive capacity index is smaller than that of sensitivity index still it is the crucial index which includes socio-economic status in its principal component (Table 4).

The HVI for Akola, Maharashtra

Statistical analysis results show that the inner structure of HVI is uneven, where sensitivity (0.944), adaptive capacity (0.890) weight more than the exposure (0.705). HVI has a high correlation with population density (0.846) as expected (Table 5).

Table 5. List of 17 wards with HVI value greater than 0.6

Ward No	Adaptive index	Sensitivity index	Exposure index	HVI index
4	0.919795	0.67983	0.337833	0.708771
5	0.973635	1	0.625968	1
6	0.900615	0.865831	0.665359	0.926199
14	0.654587	0.371494	0.670937	0.603019
16	0.689653	0.596543	0.675348	0.719365
17	0.912177	0.682927	0.740431	0.883856
18	0.787476	0.679473	0.626719	0.777476
20	0.612946	0.72411	0.745456	0.77257
29	0.553146	0.7425	0.806767	0.781323
30	0.567687	0.739983	0.846876	0.804252
37	0.853287	0.809305	0.784825	0.933065
38	0.587209	0.608735	0.921257	0.787827
43	0.80192	0.591454	0.357371	0.62665
50	0.87568	0.782062	0.761853	0.920828
51	0.737515	0.59862	0.738352	0.769041
56	0.706011	0.614858	0.708745	0.749304
67	1	1	0.560972	0.983009
68	1	0.722023	0.496401	0.832347

The normalised Heat Vulnerability Index (HVI) has an average value of 0.416 and the standard deviation is 0.287 (moderate on a five-point scale). Among the 71 wards, 18 wards have HVI greater than 0.6 (Table 4). Out of them, five wards have very high HVI value greater than 0.9 namely ward number 5, 6, 37, 50 and 67. All these wards have high values for adaptive capacity index than sensitivity index. These 17 wards have a total area of 187.72 hectares which account 9.6% of the total continuous urban area. Lower HVI values are mainly in the eastern and southern part of the city.

Table 6. Pearson correlation matrix between four indexes at 0.05 level of significance

Variables	Centre Distance	Ward Area	Density, 2011	Adaptive index	Sensitivity index	Exposure index	HVI index
Centre Distance	**1**	0.224	-0.066	-0.140	-0.118	-0.096	-0.139
Ward Area	0.224	**1**	**-0.546**	**-0.414**	**-0.485**	**-0.457**	**-0.530**
Density, 2011	-0.066	**-0.546**	**1**	**0.782**	**0.898**	**0.451**	**0.846**
Adaptive index	-0.140	**-0.414**	**0.782**	**1**	**0.873**	**0.350**	**0.890**

Sensitivity index	-0.118	**-0.485**	**0.898**	**0.873**	**1**	**0.505**	**0.944**
Exposure index	-0.096	**-0.457**	**0.451**	**0.350**	**0.505**	**1**	**0.705**
HVI index	-0.139	**-0.530**	**0.846**	**0.890**	**0.944**	**0.705**	**1**

Note: Values in bold are different from 0 with a significance level alpha=0.05

Cluster analysis of heat vulnerability

Cluster analysis was performed using Getis-Ord Gi tool in Arc-GIS which shows that the wards with low adaptive capacity also tends to show high sensitivity. Cluster formation took place in core area and areas at the fringes. Analysing this pattern of clustering with the location of slums defined the relation of vulnerability with their socio-economic status of the city. It was also interpreted that the two barriers within the city limit are not only physically dividing the city but also affecting vulnerability. Total 19 wards are forming two hotspots clusters based on values of HVI. Cluster 1 in the north consists of 3 wards of 44.38 hectares of the continuous urban area while Cluster 2 in the core area in the west consists of 16 wards of 235.71 hectares of area. It was analysed that the density of all wards in cluster 1 and 14 out of 16 wards in cluster 2 are higher than the city average density (309.65 per/hectares, excluding Ward 67). Average density of cluster 1 is 496.35 per hectares and cluster 2 is 437.30 per hectares. The average HVI values are high in both clusters that are 0.721 and 0.678 for cluster 1 and 2 respectively (Table 5).

Spatial structure of four indexes

For the analysis of the spatial distribution of four indices namely exposure, sensitivity, adaptive capacity and HVI, correlation matrix test was performed between indices, the density of continuous urban area and distance from city centre (Table 6). It was found that centrality is not a major factor for analysing vulnerability which was unevenly distributed within the city. While the density which was not taken in the initial set of indicator, a significant correlation was found with all the indexes having sensitivity (0.86) and HVI (0.84) being the highest. High-population density areas mainly lie in the core area of the city having a greater number of slums with the low-income group as residents.

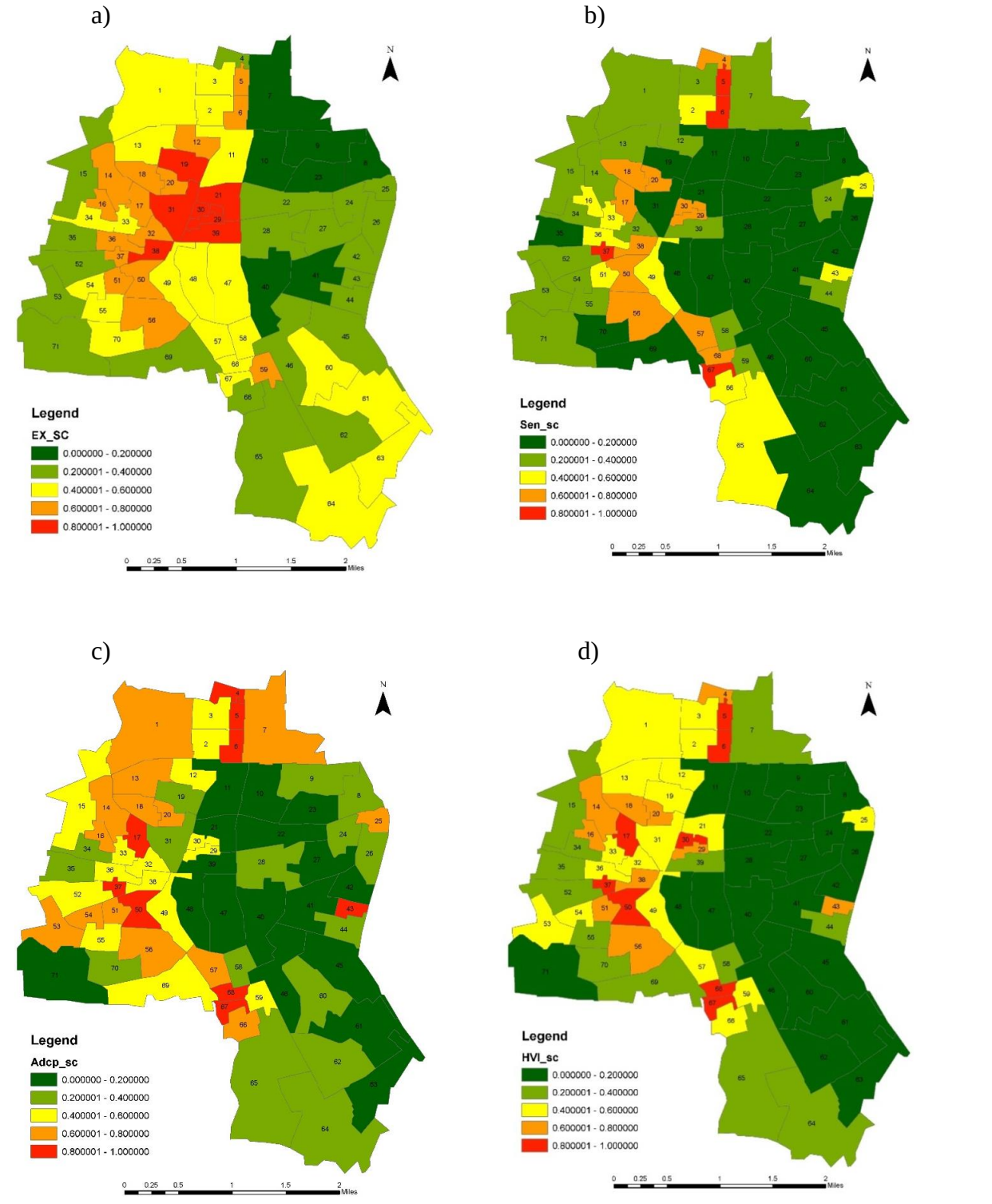


Figure 4. Results for a) Exposure index, b) Sensitivity Index, c) Adaptive capacity index and d)Heat vulnerability index for 71 wards, Akola

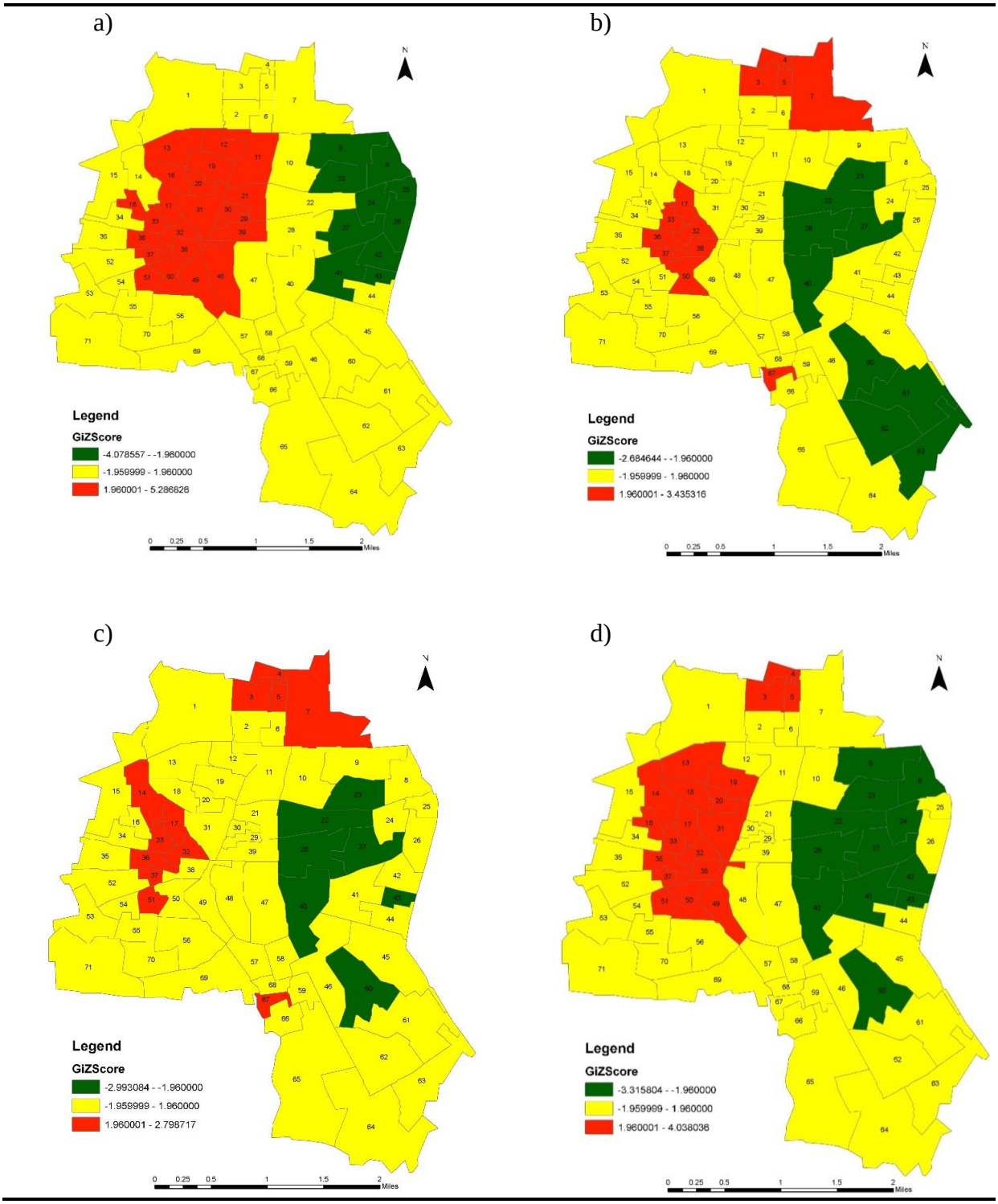


Figure 5. Cluster Analysis. Getis-Ord Gi for a) Exposure, b) Sensitivity, c) Adaptive capacity and d) HVI. Two clusters are statistically significant hotspots in HVI considering z value greater than 1.96 at 0.05 level of significance.

Overall, HVI is found to be highly correlated with all other indexes and are governed by the socio-economic pattern of the city (Table 7).

Table 7. List of 19 wards contained in the two identified hotspots cluster

Cluster	Ward No	Density	Adaptive	Sensitivity	Exposure	HVI
1	3	333.0292	0.57226	0.362727	0.426455	0.455424
	4	489.9771	0.919795	0.67983	0.337833	0.708771
	5	666.0543	0.973635	1	0.625968	1
2	13	315.4782	0.601559	0.329057	0.594368	0.527354
	14	312.6835	0.654587	0.371494	0.670937	0.603019
	16	511.4344	0.689653	0.596543	0.675348	0.719365
	17	535.6377	0.912177	0.682927	0.740431	0.883856
	18	529.3337	0.787476	0.679473	0.626719	0.777476
	19	211.2655*	0.241536	0.199961	1	0.490635
	20	614.9244	0.612946	0.72411	0.745456	0.77257
	31	179.2951*	0.384048	0.137058	0.82316	0.44787
	32	368.0168	0.53279	0.37029	0.743121	0.580669
	33	372.1265	0.549774	0.46348	0.598377	0.565464
	36	384.6699	0.437833	0.439285	0.696269	0.548643
	37	661.253	0.853287	0.809305	0.784825	0.933065
	38	532.1908	0.587209	0.608735	0.921257	0.787827
	49	385.7516	0.597613	0.482754	0.430269	0.521043
	50	544.828	0.87568	0.782062	0.761853	0.920828
	51	537.9299	0.737515	0.59862	0.738352	0.769041

**Wards' density which are lower than city average are marked with asterisk.*

Discussion and Conclusion

Major Findings

Prior identification of vulnerability to extreme heat events can guide public health efforts ahead of, during, or in the aftermath of the event. In this study, we created a fine-scale cumulative HVI for Akola city using census tract level information to identify communities that are most likely to be impacted during extreme heat events. In HVI results, 18 critical wards were identified having HVI value greater than 0.6. While results of HVI cluster analysis show 11 out of 18 critical wards tends to form cluster excluding ward numbers 6, 29, 30, 43, 56, 67, and 68. Average HVI values for these seven wards are quite high (0.8). Comparing these wards with the slum location reveals that more than 90% of the area of four wards namely 6, 43, 67 and 68 are under slum which consists of low income group and having very low average adaptive capacity (0.93) as compared to other two clusters. As these four wards have similar socio-economic character and adaptive capacity, they can form one different cluster with special need other than the clusters formed by spatial location. For all three clusters, urgent urban planning measures are required to deal with heat vulnerability.

Strength, Added Value and Limitations

Though cumulative HVI aids in swiftly recognizing susceptible communities with to extreme heat, it is of paramount importance in understanding underlying basis of vulnerability. This in turn is equally important for targeted and strategic public and community health efforts. Furthermore, interventions can then be structured for and disseminated to the appropriate target groups. A systematic group of indicators taken collectively provide a general assessment of the vulnerability of urban populations to extreme heat events. By understanding the distinct components of vulnerability (exposure, sensitivity, and adaptive capacity), policy makers can better understand what contributes to vulnerability and can decide how best to plan adaptation solutions. Decision makers can opt to consider the details of each component, or simply focus on high-level vulnerability results through longer-term responses such as urban tree planting, or identify short-term solutions such as social services for the most sensitive populations.

Specific indicators such as exposure and sensitivity are designed to provide decision makers a clear picture of immediate significance regarding historical and recent exposures to high temperatures. To look at longer term trends, adaptive capacity indicators can provide incremental and additive changes made to the urban environment targeted at urban greening and cooling. The use of indicators for monitoring and evaluation of adaptation programs can help to assess results, and will feature the most relevant policy interventions.

Implication on Practice and Research

Future research could test the satellite datasets at a much higher resolution to better capture the urban landscape and further enhance the resultant local vulnerability models. Studies could also undertake costs and benefits to evaluate the importance of urban greening and vegetation programmers while making the indicators more accountable. The spatial configuration of exposure, sensitivity, adaptive capacity and heat vulnerability indexes can be better used to inform urban planning and management and as a platform for public discussions for community awareness. Location of heavy heat intensive infrastructures such as urban parks, public facilities large commercial centres or parking lots, should take into account their impact in terms of HVI values. Results and findings can be used to improve urban planning and land policy regulations in coping with heat stress while reforming energy efficient building codes and regulations. Institutional, infrastructural, financial and social adaptation strategies must be homogenized to reduce heat stress.

Conclusion

India has worked in this direction to develop Heat Action Plan which was not enough as it does not include the understanding of the spatial pattern of heat vulnerability and also did not assign the role of urban planner. In this study, with the aim to spatially understand the pattern of heat risk factor, HVI was proposed which is a spatially explicit index composed of three indexes namely, exposure, sensitivity and adaptive capacity following the IPCC vulnerability method. Through HVI, one can explore the patterns of spatial distribution of vulnerability by identifying clusters of hotspots and determine their driving factors at ward level as the smallest spatial unit in India. The heat vulnerability index developed in this study observed geographical variability with heat vulnerability due to differences in land cover and local socio-demographic

characteristics. The study offers an inclusive approach in identifying, quantifying and mapping heat-related vulnerability for use by public health officials, policy makers, and data users as they prepare climate change adaptation plans for their communities. In the event of an extreme heat event, identification of these vulnerable areas can help streamline efforts toward mitigation of the effect of heat on health.

References

Abdi, H. and Williams, L. J. (2010). *Principal component analysis*. *Wiley Interdisciplinary Reviews: Computational Statistics*, *2*(4), 433–459. https://doi.org/10.1002/wics.101.

Akola District Gazetteers. (2016). The Gazetteers Department. Retrieved from https://cultural.maharashtra.gov.in/english/gazetteer/AKOLA/gen_climate.html.

ARUP. 2014. *Reducing urban heat risk*, (July). Retrieved from http://publications.arup.com/Publications/R/Reducing_urban_heat_risk.aspx.

Bao, J., Li, X., and Yu, C. 2015. *The Construction and Validation of the Heat Vulnerability Index*, a Review, 7220–7234. https://doi.org/10.3390/ijerph120707220.

Barker, T. 2007. *Climate Change 2007 : An Assessment of the Intergovernmental Panel on Climate Change*. *Change*, *446*(November), 12–17. https://doi.org/10.1256/004316502320517344.

Cavan, G. 2012. *Spatial modelling and web-GIS tools for climate change adaptation planning in urban areas*, (July), 3–5.

Chen, L., and Ng, E. 2011. Q*uantitative urban climate mapping based on a geographical database: A simulation approach using Hong Kong as a case study*. *International Journal of Applied Earth Observation and Geoinformation*, *13*(4), 586–594. https://doi.org/10.1016/j.jag.2011.03.003.

Chow, W. T. L., Chuang, W.C., and Gober, P. 2011. *Vulnerability to Extreme Heat in Metropolitan Phoenix : Spatial,Temporal, and Demographic Dimensions*, (November 2014), 37–41. https://doi.org/10.1080/00330124.2011.600225

Climate Council. 2016. *The silent killer : Climate change and the health impacts of extreme heat*. Climate Council of Australia Limited.

Climate Proof Cities Consortium. (2014). *Climate Proof Cities Final Report*.

Cutter, S. L., Boruff, B. J., and Shirley, W. L. 2003. *Social vulnerability to environmental hazards*. *Social Science Quarterly*, *84*(2), 242–261. https://doi.org/10.1111/1540-6237.8402002.

Dupont, V. 2004. *Socio-spatial differentiation and residential segregation in Delhi: A question of scale? Geoforum*, *35*(2), 157–175. https://doi.org/10.1016/j.geoforum.2003.08.003.

Fernandez Milan, B., and Creutzig, F. 2015. R*educing urban heat wave risk in the 21st century*. *Current Opinion in Environmental Sustainability*, *14*, 221–231. https://doi.org/10.1016/j.cosust.2015.08.002.

Hondula, D. M., Davis, R. E., Leisten, M. J., Saha, M. V, Veazey, L. M., and Wegner, C. R. 2012. *Fine-scale spatial variability of heat-related mortality in Philadelphia County,USA, from 1983-2008 : A case-series analysis*. 1–11.

Inostroza, L., Palme, M., and Barrera, F. De. 2016. *A Heat Vulnerability Index : Spatial Patterns of Exposure, Sensitivity and Adaptive Capacity for Santiago de Chile*. 1–26. https://doi.org/10.1371/journal.pone.0162464.

IPCC 2012. *Managing the risks of extreme events and disasters to advance climate change adaptation*. *IPCC*. https://doi.org/10.1596/978-0-8213-8845-7.

Jaiswal, A. 2013. *Ahmedabad Heat Action Plan : South Asia's First Climate Adaptation and Early Warning System for Extreme Heat*.

Johnson, D. P., and Wilson, J. S. 2009. T*he socio-spatial dynamics of extreme urban heat events : The case of heat-related deaths in Philadelphia*. *Applied Geography*, *29*(3), 419–434. https://doi.org/10.1016/j.apgeog.2008.11.004.

Kazmierczak, A. 2012. *Heat and social vulnerability in Greater Manchester : a risk-response case study*.

Kendrick, C. 2009. *Metal roofing on residential buildings in Europe : A dynamic thermal simulation study* (Vol. 44). Retrieved from http://www.brookes.ac.uk/schools/be/oisd/act/technology.

Kenny, G. P., Yardley, J., Brown, C., Mph, R. J. S., and Jay, O. 2010. *Heat stress in older individuals and patients with common chronic diseases*. *182*(10), 1053–1060. https://doi.org/10.1503/cmaj.081050.

Kilbourne, E. M., Choi, K., Jones, T. S., Thacker, S. B., Field, T., and Team, I. 2015. R*isk Factors for Heatstroke*, *30333*.

Kumar, K. 2007. Minimizing Urban Heat Island Effect and Imperviousness Factor in Bangalore. In D. E. V. S. K. Kumar (Ed.), *Minimizing Urban Heat Island Effect and Imperviousness Factor in Bangalore* (p. 38). Bangalore: The Energy and Resources Institute (TERI), India. Retrieved from http://www.teriin.org/projects/apn_capable/pdf/bang_present/Kiran_Kumar.pdf

Loughnan, M. E., Tapper, N. J., Phan, T., Lynch, K., and McInnes, J. A. 2013. A spatial vulnerability analysis of urban populations during extreme heat events in Australian capital cities.

Loughnan, M., Nicholls, N., and Tapper, N. J. 2012. M*apping Heat Health Risks in Urban Areas*. https://doi.org/10.1155/2012/518687

Met Office. 2015. *Heatwave plan for England*. England: Public health department.

Meteorological Bulletins. 2003. Impacts of Summer 2003, (September).

Mohan, M., Gupta, A., and Bhati, S. 2014. A *Modified Approach to Analyze Thermal Comfort Classification*. Atmospheric and Climate Sciences, 4(January), 7–19. https://doi.org/10.4236/acs.2014.41002

Mooventhan, A., and Nivethitha, L. (2014). Scientific Evidence-Based Effects of Hydrotherapy on Various Systems of the Body, *6*(5). https://doi.org/10.4103/1947-2714.132935

Nairn, J., & Fawcett, R. 2013. *Defining heatwaves*. Australia: CSIRO.

NDMA. 2016. *Guidelines for Preparation of Action Plan – Prevention and Management of Heat-Wave*.

Oliveira, S., Andrade, H., and Vaz, T. 2011. *The cooling effect of green spaces as a contribution to the mitigation of urban heat: A case study in Lisbon*. Building and Environment, 46(11), 2186–2194. https://doi.org/10.1016/j.buildenv.2011.04.034

Ord, J. K., and Getis, A. 1995. L*ocal Spatial Autocorrelation Statistics: Distributional Issues and an Application*. Geographical Analysis, 27(4), 286–306. https://doi.org/10.1111/j.1538-4632.1995.tb00912.x

Pattenden, S., Nikiforov, B., and Armstrong, B. G. 2003. M*ortality and temperature in Sofia and London*. J Epidemiol Community Health, 57(8), 628–633. https://doi.org/10.1136/jech.57.8.628

Reid, C. E., O'Neill, M. S., Gronlund, C. J., Brines, S. J., Brown, D. G., Diez-Roux, A. V., and Schwartz, J. 2009. *Mapping community determinants of heat vulnerability*. Environmental Health Perspectives, 117(11), 1730–1736. https://doi.org/10.1289/ehp.0900683

Schmidtlein, M. C., Deutsch, R. C., Piegorsch, W. W., and Cutter, S. L. 2008. *A Sensitivity Analysis of the Social Vulnerability Index.* 28(4). https://doi.org/10.1111/j.1539-6924.2008.01072.x

Sidhwani, P. 2015. *Spatial Inequalities in Big Indian Cities*. Economic & Political Weekly, 50(22), 55–62. Retrieved from http://www.epw.in/system/files/pdf/2015_50/22/Spatial_Inequalities_in_Big_Indian_Cities.pdf

Singh, G. and Vithayathil, T. 2012. S*paces of Discrimination*. Economic and Political Weekly, 47(37), 60–66. Retrieved from http://www.epw.in/special-articles/spaces-discrimination.html

Steffen, W., Hughes, L., and Perkins, S. 2014. *Heatwaves : Hotter, Longer, More Often.* Retrieved from http://www.climatecouncil.org.au/uploads/9901f6614a2cac7b2b888f55b4dff9cc.pdf

Wolf T., McGregor G. and Antonis A. 2009. *Assessing Vulnerability to Heat Stress in Urban Areas. The Example of Greater London.* EPIDEMIOLOGY, 20(6), 13–265. Retrieved from http://journals.lww.com/epidem/Citation/2009/11001/Assessing_Vulnerability_to_Heat_Stress_in_Urban.37.aspx

Tate, E. 2012. *Social vulnerability indices: a comparative assessment using uncertainty and sensitivity analysis*, 325–347. https://doi.org/10.1007/s11069-012-0152-2

The Office of Environment and Heritage. 2016. *Minimising the impacts of extreme heat : A guide for local government*. Office of Environment and Heritage. Retrieved from www.environment.nsw.gov.au

Trundle, A., Bosomworth, K., Mcevoy, D., Williams, N., Coutts, A., Norton, B., Harris R. and Livesley S. 2015. Urban Heat Reduction through Green Infrastructure (GI) : Polciy guidance for State Government, (February), 1–9.

United Nations Framework Convention on Climate Change. 2015. Paris Agreement. https://doi.org/FCCC/CP/2015/L.9

UNU-EHS. 2014. *Assessing Vulnerability to Heat Waves and Heavy Rainfall at a Community Level* (Vol. 11). Retrieved from www.bbk.bund.de

Upmanis, H., Eliasson, I., and Lindqvist, S. 1998. T*he influence of green areas on nocturnal temperatures in a high latitude city (Goteborg, Sweden)*. International Journal of Climatology, 18(6), 681–700. https://doi.org/10.1002/(SICI)1097-0088(199805)18:6<681::AID-JOC289>3.0.CO;2-L

USGS. (2011). Landsat 7 Science Data Users Handbook Landsat 7 Science Data Users Handbook. *National Aeronautics and Space Administration*, 186.

Victorian Government. 2009. *Heatwave planning guide: development of heatwave plans in local councils in Victoria*. 52. Retrieved from http://docs.health.vic.gov.au/docs/doc/18BA71008326BA63CA257A360018513D/$FILE/planning-guide.pdf

WHO Europe. 2009. *Health & Global environment change* (Series 2). Europe.

Wilhelmi, O. V, Purvis, K. L., and Harriss, R. C. 2004. *Designing a Geospatial Information Infrastructure for Mitigation of Heat Wave Hazards in Urban Area*s, (August), 147–158.

Wolf, T., and Mcgregor, G. 2013. *The development of a heat wave vulnerability index for London, United Kingdom*. Weather and Climate Extremes, 1(August 2003), 59–68. https://doi.org/10.1016/j.wace.2013.07.004.

World Health Organization. 2010. *Environment and health risks: a review of the influence and effects of social inequalities*. *WHO Regional Office for Europe*, 268. Retrieved from http://www.euro.who.int/__data/assets/pdf_file/0003/78069/E93670.pdf.

World Health Organization, & World Meteorological Organization. (2014). *Heatwaves and Health: Guidance on Warning-System Development*.

Extent vs. Impact: A modeling study of Targeted Heat Mitigation Strategies

David J. Sailor[1], Arizona State University (USA)
Peter J. Crank, Arizona State University (USA)
Jannik Heusinger, TU Braunschweig (GERMANY)
Masayuki Hara, Center for Environmental Science in Saitama (JAPAN)

ABSTRACT

The strength of any downwind cooling effect of high-albedo surface modifications on near-surface air temperature depends upon the location of the mitigation strategy (roof vs ground level), local turbulent mixing, and the spatial extents of the modified surface and the downwind region of interest. A vexing question in the urban climate community and local government decision-makers is: how far downwind are the effects of any mitigation strategy felt?

To address this question, we conduct an idealized modeling study to explore downwind effects of urban heat mitigation. The simulations, while idealized, are focused on the city of Phoenix Arizona, USA. We explore the question across scales by using both microscale and mesoscale atmospheric models—ENVI-met and WRF, respectively. Each model is centered on the same residential neighborhood near the center of a city comprising a uniform array of residential neighborhood blocks. A base case (control) simulation is conducted for each simulation set, followed by high albedo roof and high albedo ground cases. The hybrid modeling approach allows investigation of mitigation scales ranging from hundreds of meters to tens of kilometers.

We present results from these suites of simulations demonstrating the relationship between the spatial extent of the ground-level and roof-level mitigation action and the local and downwind footprint of the resulting air temperature perturbations.

Introduction

The urban-rural temperature difference, or urban heat island (UHI) has become the focal point of many recent efforts related to managing urban thermal environments. The UHI affects many aspects of the health, well-being, and prosperity of urban residents (Hajat et al., 2006; Tan et al., 2007; Kalkstein et al., 2013; Akbari and Konopacki, 2005). The UHI is caused by a number of factors whose relative importance differs depending upon local geography, seasonality, and time of day. The radiative properties of the surfaces that make up the urban built environment are key drivers of the UHI that can be readily modified. Specifically, many road and rooftop surfaces have low reflectivity to solar radiation (low albedo).

There is a large body of literature exploring the effect of highly-reflective surfaces as mitigation strategies for local, neighborhood, and city/regional scale urban climates (e.g., Botham-Myint et al., 2015; Ban-Weiss et al., 2015, Vahmani and Ban-Weiss, 2016; Santamouris, 2007; Akbari et al., 2009; Zhang et al., 2016). Such studies generally reveal that domain-wide application of mitigation (whether at the neighborhood or city scales) can cool urban air

[1] Corresponding Author: dsailor@asu.edu, +1 480-965-4082.

temperatures during hot summer weather by as much as a few degrees Celsius. However, very little work has addressed a key implementation question: what is the relation between the spatial extent of mitigative actions and the magnitude of the resultant local and downwind cooling benefits. This paper seeks to address this question by using microscale and regional scale atmospheric models to explore the effects of high-albedo road and roof modifications at multiple scales of spatial implementation.

To analyze the microscale effects, we elected to use ENVI-met, which is a Computational Fluid Dynamics (CFD) model that uses the Reynolds-Averaged Navier-Stokes equations to model fluid flow and heat transfer in neighborhoods. This software, developed by Bruse (Bruse and Fleer, 1998) is widely used in urban microclimate studies due to its ability to model complex 3D geometries of buildings, vegetation, and water features via a relatively user-friendly modeling interface. In the latest version (v.4), the software allows the import of shapefiles, full control over the thermal characteristics of urban materials, definition of atmospheric forcing, and the use of multi-core computation. This software is widely used for modelling the local environment, though at times is used with insufficient evaluation of model performance or applicability (Crank et al., 2018). Both Blocken et al., (2007) and Maggiotto et al., (2014) have discussed various concerns with the model's stability and limitations (Blocken et al., 2007). Nevertheless, ENVI-met can be a useful tool for evaluating the local effects of heat mitigation strategies such as high-albedo roof and road modifications.

At the mesoscale we use the Weather Research and Forecasting (WRF) model with a simple urban canopy layer parameterization (Chen et al., 2018). The WRF model is a mesoscale (regional) numerical weather prediction modeling system that is typically run with model grid cells as fine as 500 m to 1 km on a side, with finer-scale processes being parameterized. The model version used in the present work is v3.8. The WRF model can be forced with realistic boundary conditions that vary in time based on available atmospheric reanalysis data products and digital elevation maps of the simulation domain. While WRF allows for three options of varying sophistication for urban parameterization, we chose to use the relatively simple single layer canopy model, which allows for detailed specification of building geometries and material properties, but parameterizes the aggregate effect of neighborhood design at the scale of the smallest grid cell (typically ~ 1 km for urban applications).

Each of these models has its strengths and limitations. For the purposes of this study, a key common limitation is related to scale. Typically, due in large part to parameterization of subgrid scale turbulence, regional scale models such as WRF are considered to be of questionable accuracy at grid sizes below 500 m (with most researchers simulating urban areas at grid sizes of 1 km or larger). Microscale atmospheric models such as ENVI-met, on the other hand, resolve individual buildings with grid resolutions of 1-2 m. The main scale constraint of microscale models is due to the computational costs and data requirements of simulating large domains. An added constraint is that ENVI-met runs only in a Windows operating system environment, making simulations of domains much larger than 1 km^2, computationally challenging.

Given these spatial scale constraints of microscale and regional scale models, the most effective investigation strategy for our research question is to conduct simultaneous complementary investigations with both types of models, attempting to match results at the scale limits of each model. The results can then be used to assess how the spatial scale of mitigation

action affects the magnitude and extent of local and downwind cooling.

Methods

Given the scale limitation discussed above, we have selected three scales of mitigation to explore using each type of model. In each case, we model a city comprised of many identical neighborhoods. For a single representative summer period we model a control simulation as well as simulations in which the albedo of roads and/or roof surfaces is increased for a subset of neighborhoods. The microscale model is used first to explore how changes in albedo within an individual neighborhood comprising 14 homes (180 m by 60 m) affect the surface and air temperatures within that neighborhood and in neighborhoods downwind. With the same model, we then simulate the effects of modifying a 2 by 2 and then a 3 by 3 array of these 14-home neighborhood blocks. In these simulations, the long-side of the neighborhood array is aligned with the wind direction (wind from the west). Thus, the length of modified area simulated with the microscale model ranges from 180 m to 540 m. Then, using the regional scale model with grid cells of 500 m on an edge, we simulate the same set of control and mitigation cases using arrays of mitigated neighborhood grid cells: 4x4, and 8x8. Thus, while the microscale model explores the spatial effects of mitigated areas up to 540 m in length, the mesoscale model explores mitigated areas ranging from 2 km to 4 km in length.

Generic Neighborhood Element

For all simulations we created a generic neighborhood element that is replicated across the full extent of the model domain to represent a hypothetical residential region within the city of Phoenix AZ. This neighborhood includes Xeric landscaping (dirt, sand, decomposed granite) and a single block of 14 detached 1-story buildings (see Fig 1).

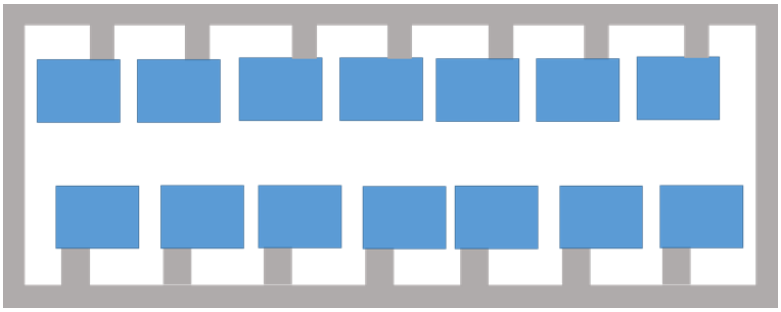


Figure 1. The generic neighborhood element for this study (not to scale).

The neighborhood element is 180 m by 60 m, terminating along the centerlines of roads oriented N-S and E-W. Each road half-width is 4 m. Driveways are 4 m wide by 6 m long. Each neighborhood element (block) consists of an array of 7 by 2 one-story homes that are 20 m long by 12 m deep and 4 m tall with flat roofs. Horizontal spacing between buildings is 4 m. Corner lots have 4 m between the building edge and the edge of the road. All space between buildings is xeric landscape. Backyards are 8 m deep (total of 16 m between back walls of homes). The detailed material thermal and radiative properties for the neighborhood element are provided in Table 1.

Table 1. Thermal and radiative characteristics of the generic neighborhood element*.

Material or Construction	Roughness Length (m)	Thickness (m)	Avg. Thermal Conductivity (W/mK)	Avg. Heat Capacity	Avg. Density (kg/m^3)	Avg. Spec. Heat (J/kgK)	Surface Albedo	Surface Emissivity	Interior /lower Temperature(°C)
Bldg Wall	0.001	0.160	0.002	$1.10*10^5$	400	1500	0.28	0.900	26.0
Bldg Roof - dark	0.001	0.298	0.172	$3.11*10^4$	1900	800	0.20	0.900	26.0
Bldg Roof - light	0.001	0.298	0.769	$7.15*10^4$	1900	800	0.65	0.910	26.0
Driveway	0.001	1.550	0.166	$6.66*10^5$	*	*	0.20	0.925	23.9
Road - dark	0.001	1.550	0.166	$6.66*10^5$	*	*	0.15	0.925	23.9
Road - light	0.001	1.550	0.166	$6.66*10^5$	*	*	0.40	0.925	23.9
Bare Soil	0.001	1.550	0.166	$1.28*10^6$	*	*	0.27	0.900	23.9

** Sources: Oke et al., (2018); Taha et al., (1992); Levinson et al., (2005); Crevier and Delage, (2001); Luca and Mrawira, (2005); Clark, (1983); Abbasi et al., (2003).*

Simulation Episode

The simulations are for an idealized situation that is based on an actual historical weather episode. The simulation episode is a 2-day period, intended to be representative of summer conditions in Phoenix Arizona (33.448 °N, 112.074 °W). As the goal was to explore the effects of high albedo surfaces during particularly adverse thermal conditions, the simulation period was selected such that it was cloud-free with relatively calm winds emanating from a relatively consistent direction.

The specific model episode selected was the period of June 14-15, 2017. Using a control simulation with WRF for this episode, we generated initial and boundary condition temperature and humidity conditions that were used to drive the ENVI-met simulations.

Simulation Cases

The modeling study includes three distinct land cover scenarios. First, is the base case in which the generic neighborhood is modeled with roof and road albedo of 0.20 and 0.15, respectively. In the high-albedo roof case, roof albedo is increased from 0.20 to 0.65. In the high albedo road case, the road albedo is increased from 0.15 to 0.40. Note, that in the high albedo road cases, the driveway albedo is not altered. A combined case simulates increases in both roof and road albedo.

These cases are modeled separately within ENVI-met and WRF. As noted above, in each model, each surface modification case is simulated at 3 scales (summarized in Table 2). In ENVI-met, one set of simulations focuses on modifications that are applied only over one neighborhood block (E1), then over an array of 2x2 blocks (E2), and then over an array of 3x3 blocks (E3). This

corresponds to modified areas of sizes 0.009 km2, 0.036 km2, and 0.081 km2. Within WRF, the two scales of modification (W2, and W3) were simulated: 4.0, and 16 km^2, respectively. A third, finer scale of modification (W1) yielded inconsistent results and is not presented.

Table 2. Summary of simulation scales investigated.

Case	Domain Size (m)	Spatial Resolution of grid cells (m)	Modified Length (m)
Control	600 x 300	2 x 2	0
E1	600 x 300	2 x 2	180
E2	600 x 300	2 x 2	360
E3	600 x 300	2 x 2	540
W2	74500 x 74500	500 x 500	2000
W3	74500 x 74500	500 x 500	4000

Implementation in WRF

The WRF model was used to represent mitigation strategies at scales greater than 1 x 1 km^2 in dimension. This was accomplished by simulating a single model domain centered in the Phoenix metropolitan area (latitude of 33.351 and longitude of -111.777). The model used a square array of 149 by 149 grid cells that are 0.5 km by 0.5 km in size. The NLCD 2011 40-category land use data base was used to initialize the WRF domain to facilitate use of the single layer urban canopy layer option. A "real" case simulation was conducted using the NCEP North American Regional Reanalysis (NARR) 3-hourly atmospheric data for initialization and boundary condition data, for all simulations. All simulations were initialized at 11 pm local time to allow model spin-up in the overnight hours. Simulations were conducted for 36 hours, with the analysis focus on the final 24-hour period. Consistent with WRF model guidance, model time steps were set to 3 s. Key model physics parameterization options are summarized in Table 3.

Table 3. Physics options and parameterizations used within WRF simulations.

Physics Parameterization Option	Scheme selected
Cloud Microphysics	None (clear sky simulation)
Long- and short-wave radiation	Rapid Radiative Transfer Model (RRTM) and Dudhia SW scheme
Surface Layer Option	Monin-Obukhov (Janjic Eta) similarity scheme
Land Surface Model	Noah LSM
Urban Physics	Single layer Urban Canopy Model (UCM)
Boundary Layer Physics	Mellor-Yamada-Janjic (Eta) TKE scheme
Cumulous Physics	None

The W2 and W3 scale modifications are for arrays of 4 by 4 (2km by 2km) and 8 by 8 (4km by 4km). In each case, the southwestern edge of the modification was located in the middle of the 75 km square domain. Modification of surface conditions in these mitigation regions was accomplished using in-house scripts to modify the input files to WRF. By using the single layer UCM, we were able to explicitly modify roof and/or road albedo values as needed.

For each mitigation scale (W2, W3), a control case and three mitigation cases were tested. The mitigation cases included one in which only road albedo values were increased from 0.15 to 0.40, one in which only roof albedo values were increased from 0.20 to 0.65, and a final simulation in which both road and roof albedo values were modified.

Implementation in ENVI-met

A regional scale model such as WRF is helpful for understanding the weather patterns at scales above 500 m; however, this scale does not allow analysis of impacts the urban form or materials have on the environment at finer scales (e.g. within neighborhoods). This scale is referred to as the microscale and a different suite of models must be used to explicitly model the wind flow and heat transfer among the various surfaces within the urban canopy layer. ENVI-met has become one of the primary microscale modeling tools in the fields of landscape architecture and urban climatology.

The simulation cases are represented in ENVI-met as a 2 m by 2 m spatial grid, with 1.6 m vertical resolution. The sub-cell resolution is 0.32 m, thus in the lowest 5 grid cells, this resolution was used to reach a minimum height of 1.6 m. This allows for each type of surface to be simulated with at least a 2x2 pixel grid for various surfaces and facades. The simulation is conducted with no cloud cover and using open lateral boundary conditions. The weather forcing for ENVI-met was created by the WRF model for each simulation case. Additionally, three scales—E1, E2, and E3—were used as illustrated in Figure 2. In total, 9 simulations were run in ENVI-met. To ensure quality of data, the neighborhood blocks with mitigation strategies implemented are located in the interior of the domain, leaving a minimum of one full neighborhood block on the periphery to avoid edge effects. Additionally, 10 grid cells were left empty on the periphery of the simulation domain to limit potential numerical instabilities related to the inflow boundary (Middel et al., 2014). Also, near-surface air temperature data are available for export from ENVI-met simulations at heights corresponding to the vertical structure of the model domain. Hence, in referring to near-surface air temperatures for ENVI-met simulations, we present results from the 1.44 m grid height.

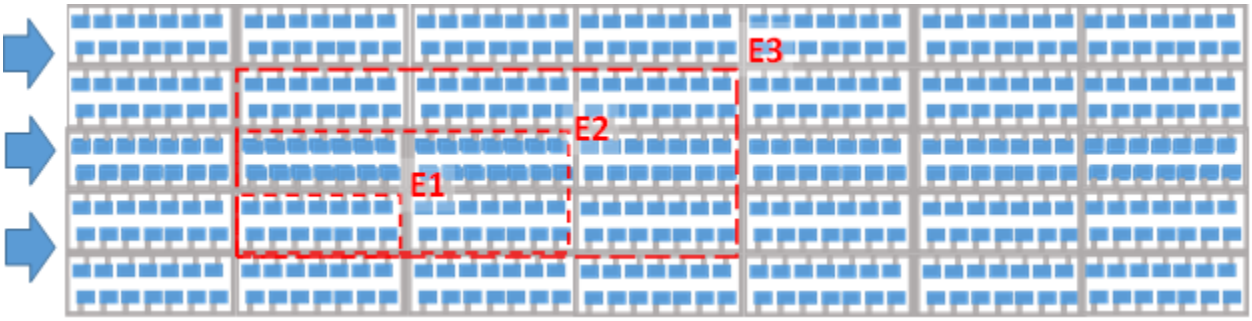


Figure 2. ENVI-met modeling domain showing the full model domain extent (an array of 7 by 5 generic neighborhoods as illustrated in Figure 1). The scales of mitigation range from a single generic neighborhood (E1) to an array of 4 neighborhoods (E2) and an array of 9 neighborhoods (E3).

Results

Fairly consistent with the results from Taleghani et al. (2016) and Botham-Myint et al. (2015) we found that roof-level albedo modification in the microscale modeling resulted in very little impact for the near-surface air temperature within the modeling domain. Larger effects of rooftop mitigation were evident within the mesoscale simulations. Nevertheless, for brevity, we share here the results for only the cases where the road surface albedo was modified. Figure 3 shows the ENVI-met predicted near-surface air temperature effects of the high albedo road treatment for scales of mitigation ranging from 1 neighborhood to an array of 9 neighborhoods. The top panel in this figure reveals that, for a modified area the size of a single neighborhood (approximately 180 m) there is a clear air temperature impact within the neighborhood and up to 80-90 m downwind. For the four-neighborhood array (approximately 360 m in length), the downwind effect is approximately 150 m downwind. And, for the nine-neighborhood array (approximately 540 m in length), the downwind effect is felt only about 200 m downwind. Hence, this figure shows qualitatively that the downwind effect of mitigation increases with the spatial scale of mitigation, but that this relationship is less than proportional to the size of the modified area.

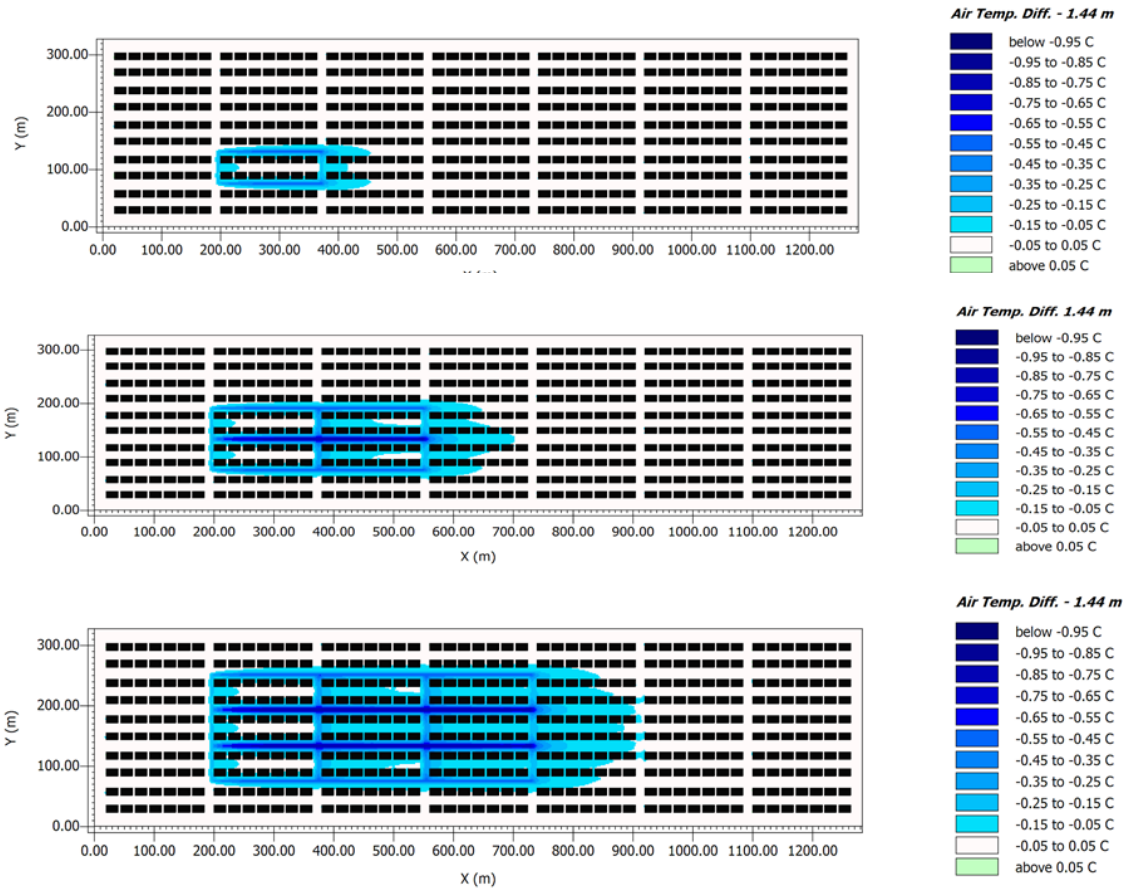


Figure 3. Near-surface (1.44 m) air temperature cooling effect of high albedo road surfaces for mitigation areas of (a) a single neighborhood, (b) four neighborhood blocks, and (c) 9 neighborhood blocks at 3pm.

To quantify the role of spatial scale of mitigation we define two metrics. First, we evaluate the average temperature perturbation (ΔT) within the mitigated area (positive values denote cooling). For example, in the case of the single neighborhood, the mitigated area is taken as the spatial extent of the neighborhood (180m by 60m). Second, we define a normalized mitigation parameter similar to that used by Botham-Myint et al. (2015). If A_{mod} is the area of the actual modified surface (e.g., 1,856 m^2 of road surface in the case of the single neighborhood), we identify all grid cells at a given height (1.44m) in ENVI-met simulations for which the temperature perturbation ΔT is above some threshold (0.1 K). The corresponding area for which a non-trivial air temperature perturbation is observed is notated as A_{dT_thresh}. This normalized mitigation area NMA is then defined by:

$$NMA = A_{dT_thresh} / A_{mod} \quad (1)$$

Using this definition, NMA can take on values larger than 1.0. For example, if modifying streets in a single neighborhood has a non-trivial air temperature cooling effect in two full neighborhoods, this situation would correspond to NMA=2.0. The values of these two metrics for the ENVI-met simulations are shown in Table 4. The length scale in this table is simply the length of the modified area from west to east.

Table 4. Impact metrics (average neighborhood ΔT and Normalized Mitigation Area, NMA) for simulations for the case of a scenario involving an increase in road albedo. The Length Scale in this table refers to the length of the modification area from west to east.

Case	**Modified Length (m)**	**ΔT at 9am**	**ΔT at 3pm**	**NMA at 9am**	**NMA at 3pm**
E1	180	0.05	0.09	2.29	4.01
E2	360	0.09	0.16	2.48	3.58
E3	540	0.10	0.18	2.52	3.54
W2	2000	0.54	0.40	--	--
W3	4000	0.63	0.59	--	--

Initially, we explored an even finer scale of modification in the WRF simulations (W1) in which the modified area corresponded to a single 500m square grid cell. However, the noise in the model response to such a small modification area was too large to yield consistent results (e.g. occasional apparent warming directly above the modified area). Furthermore, due to the complexities in extracting the NMA metric for WRF, only ΔT results for W2 and W3 are presented.

This table reveals two important aspects of how the spatial scale of mitigation efforts affects the magnitude of the cooling effect. First, as the size of the modified area is increased, the average cooling effect over the modified region increases substantially, at a rate of roughly 0.1 to 0.2 ^oC per km of surface mitigated (see Figure 4). It is expected that this effect will level off as the modified surface area increases further, but additional simulations would be required to identify an asymptotic limit. Second, based on the NMA values it appears that the spatial extent (downwind cooling) is not substantially affected by scale. At 9am, NMA increases slightly with larger modification areas, while at 3pm, the trend—while still small—is the opposite. Nevertheless, in the morning hours the area that benefits from heat mitigation strategies is roughly twice the size of the mitigation area, while in the afternoon, this ratio is closer to four.

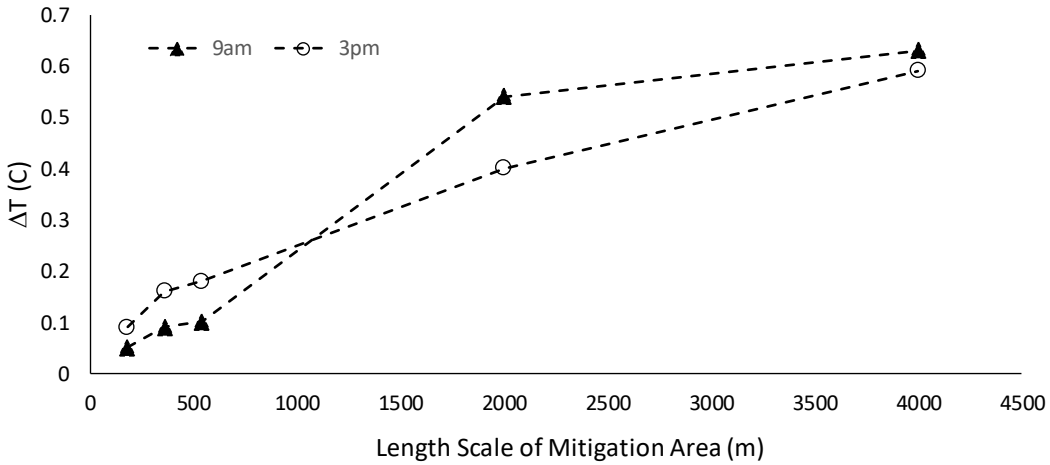


Figure 4. Average near-surface cooling effect as a function of the size of the mitigated area. Data from three scales of modification from the microscale model ENVI-met and two scales of modification from the mesoscale (WRF) simulations. Here, length scale refers to the east-west length of the modified zone.

Conclusions and Key Findings

Simulations from the microscale to the mesoscale have been used to assess the magnitude of heat mitigation impacts within and downwind of modified neighborhoods. The microscale simulations, in particular, found relatively little effect of rooftop implementation of high albedo surfaces on pedestrian-level thermal environments, while the mesoscale simulations suggest a modest cooling effect of large-scale implementation of high-albedo rooftops. In both cases, implementation of high-albedo surfaces at ground-level resulted in significant cooling within and downwind of modified neighborhoods.

The magnitude of the in-neighborhood cooling effect appears to scale with the size of the modified area (by 0.1 to 0.2 ^{o}C per km of surface mitigated). However, the limits of this scaling were not explored. Furthermore, the simulations suggest that the downwind footprint of cooling effects of mitigation strategies is largely unaffected by the size of the mitigated area.

These simulations represent a blueprint for further exploration of the underlying question addressed by the study. Future simulation efforts should explore more variations of scale within each category of model, seeking to increase the overlap region of the scales explored.

Acknowledgments

The authors wish to acknowledge support from the Urban Climate Research Center at Arizona State University. This research is also an outgrowth of, and supported in part by the National Science Foundation under grant 1623948.

References

Abbasi, F., Simunek, J., Feyen, J., van Genuchten, M. Th., Shouse, P. J. (2003). Simultaneous inverse estimation of soil hydraulic and solute transport parameters from transient field experiments: homogeneous soil. Transactions of the ASAE, 46(4), 1085-1095.

Akbari, H., S. Menon, A. Rosenfeld (2009). Global cooling: Increasing world-wide urban albedos to offset CO_2. Climatic Change. 94 (3-4), 275-286

Akbari, H. and S. Konopacki (2005). Calculating energy-saving potentials of heat-island reduction strategies. Energy Policy 33(6), 721-756.

Blocken, B., T. Stathopoulos, J. Carmeliet (2007). CFD simulation of the atmospheric boundary layer: wall function problems. Atmos. Environ. 41, 238–252.

Botham-Myint, D., G.W. Recktenwald, and D.J. Sailor (2015). "Thermal footprint effect of rooftop urban cooling strategies," Urban Climate, DOI 10.1016/j.uclim.2015.07.005.

Bruse, M., H. Fleer (1998). Simulating surface-plant-air interactions inside urban environments with a three dimensional numerical model. Environmental Modeling Software, 13, 373–384.

Crank, P.J., D.J. Sailor, G. Ban-Weiss, and M. Taleghani (2018). Evaluating the ENVI-met microscale model for suitability in analysis of targeted urban heat mitigation strategies", Urban Climate, 26, 188-197.

Chen, F. H. Kusaka, R. Bornstein, J. Ching, C.S.B. Grimmond, C., S. Grossman-Clarke, T. Loridan, K.W. Manning, A. Martilli, S. Miao, D. Sailor, F.P. Salamanca, H. Taha, M. Tewari, X. Wang, A.A. Wyszogrodzki, C. Zhang (2011) The integrated WRF/urban modeling system: development, evaluation, and applications to urban environmental problems, International Journal of Climatology, 31, 273-288.

Clark, A. J. (1983). Temperature and thermal properties of selected Arizona soils. Thesis, The University of Arizona, 94 p.

Crevier, L., Delage, Y. (2001). METRo: A New Model for Road-Condition Forecasting in Canada. Journal of Applied Meteorology, 40, 2026-2037.

Hajat, S., B. Armstrong, M. Baccini, A. Biggeri, L. Bisanti, A. Russo, and T. Kosatsky (2006). Impact of high temperatures on mortality: is there an added heat wave effect? Epidemiology, 17, 632–638.

Kalkstein, L.S., D.J. Sailor, K. Shickman, S. Sheridan, and Vanos, J. (2013). Assessing the Health Impacts of Urban Heat Island Reduction Strategies in the District of Columbia, in Global Cool Cities Alliance. 2013: Washington, D.C.

Levinson R., P. Berdahl, H. Akbari (2005). Solar spectral optical properties of pigments, part II: Survey of common colorants, Solar Energy Materials & Solar Cells 89, 351-389.

Luca, J., Mrawira, D. (2005). New Measurement of Thermal Properties of Superpave Asphalt Concrete. Journal of Materials in Civil Engineering, 17(1), 72-79.

Maggiotto, G., R. Buccolieri, M.A. Santo, L.S. Leo, S. Di Sabatino (2014). Validation of temperature-perturbation and CFD-based modelling for the prediction of the thermal urban environment: The Lecce (IT) case study. Environmental Modeling Software 60, 69–83.

Middel, A., K. Hab, A.J. Brazel, C.A. Martin, S. Guhathakurta (2014). Impact of urban form and design on mid-afternoon microclimate in Phoenix Local Climate Zones. Landscape and Urban Planning, 122, 16–28

Oke, T. R., Mills, G., Christen, A., Voogt, J. A. (2017). Urban Climates. Cambridge University Press, 546 p.

Santamouris, M. (2007). Heat island research in Europe: The state of the art. Advances in Building Energy Research, 1(1), 123-150.

Taleghani, M., D.J. Sailor, and G. Ban-Weiss (2016). Micrometeorological simulations to predict the impacts of heat mitigation strategies on pedestrian thermal comfort in a Los Angeles neighborhood, Environmental Research Letters, 11 (2)

Tan, J., Y. Zheng, G. Song, L. Kalkstein, A.J. Kalkstein, and X. Tang (2007). Heat wave impacts on mortality in Shanghai, 1998 and 2003. International Journal of Biometeorology, 51, 193–200.

Taha, H., Sailor, D., Akbari, H. (1992). High-Albedo Materials for Reducing Building Cooling Energy Use, Rep. No. LBL-31721. Lawrence Berkeley National Laboratory, Berkeley, 72 p.

Vahmani P. and G.A. Ban-Weiss (2016). Impact of remotely sensed albedo and vegetation fraction on simulation of urban climate in WRF-urban canopy model: A case study of the urban heat island in Los Angeles. Journal of Geophysical Research, 121(4), 1511-1531.

Zhang, J., K. Zhang, J. Liu, G. Ban-Weiss (2016). Revisiting the climate impacts of cool roofs around the globe using an Earth system model. Environmental Research Letters 11, 084014.

Conceptual Framework for Environmental City Planning Tool with an Intelligent System based on BIM and GIS Technology

Shinji Yamamura[1]*, Nikken Sekkei Research Institute (Japan)*
Liyang Fan, Nikken Sekkei Research Institute (Japan)
Yupwng Wang, Xi'an Jiaotong University (China)
Dian Zhou, Xi'an Jiaotong University (China)

ABSTRACT

Recently, the rising of the maximum temperature in summertime and air pollution in the winter time have been common issues in the cities of China, especially the large cities. The heat island phenomenon, triggered by urbanization based on the global warming, are caused by different factors. The high density of building development which change the urban typology, leading to the change of traffic volume, vegetation coverage and the urban micro-climate are considered as the important factors. Most of the existing studies to mitigate heat island phenomenon usually weight on introduction of low surface temperature material, reduction of the heat exhaust or vegetation from building-scale viewpoint, or strategies as instruction of large parks, shifting to public transportation systems from district-scale viewpoint.

However, the community-scale environmental friendly planning method are merely to be discussed, such as making effective network of cool spots and the wind path in the community. It is an optimal approach, with synergies among various elements and solutions interactively consider existing community structures, energy systems for different building types, traffic strategies, greenery renovation possibility and city typologies.

In this paper, we propose a system for environmental urban planning tool with Geographic information system (GIS) and Information and Communication Technology (ICT). We firstly introduce the concept and architecture of the tool. The applicability of the resulting model is then examined by applying it to the city of Xi'an, China. Finally, thermal environmental simulation are adopted to figure out the opportunities and challenges for environmental urban development in these target area.

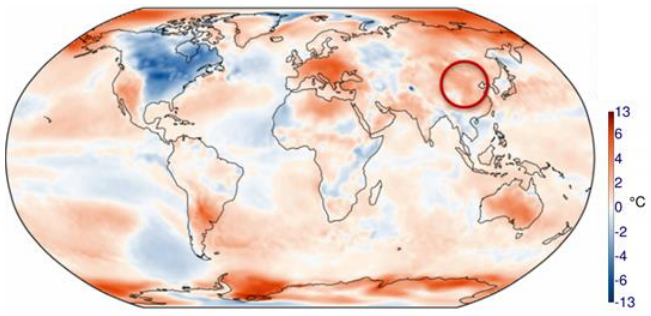
Introduction

Recently, the rising of the maximum temperature in summertime and air pollution in the winter time have been common issues in the cities of China, especially the large cities like Xi'an. From the view of non-industrial field, these environmental problems are mainly resulted from the increasing population, energy consumption and automobile utilization during the rapid urban development. As a solution for both considering the urban environment and construction cost, the researches and the design initiation for environment-friendly planning and its related methodologies that can manage different issues like buildings, greenery and transportation should be comprehensively proceeded from the early stage of construction projects.

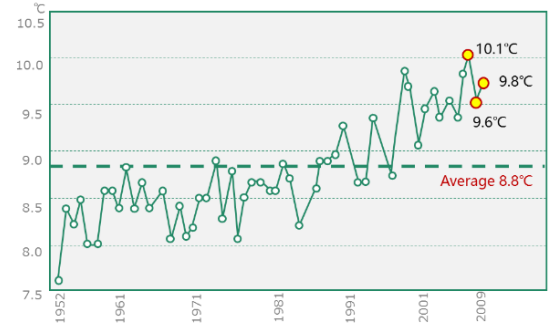
[1] Yamamura Shinji, +810352596080, yamamura@nikken.jp

Environmental issues with urbanization

The rapid urban development in the mega cities with urban population growth and land expansion significantly change the urban energy balance, increase energy consumption thereby causes the higher temperature compared to the surrounding area, which is known as a phenomenon of urban heat island effect (UHIE). In recent years, UHIE is widely observed in the worlds developed countries and also effect the inland in China (Figure1a). During the past 100 years, the global average air temperature increased around 0.68℃) while china increased around 2.0 ℃ (Figure1b), especially, during the recent 50 years as the nation level.



(a) Surface air tempreature anomaly for April 2018 relative to 1981 – 2010 (Source:World Meteological Organization HP)



(b)Average temperature increase from 1952 to 2009 in China (Annual report of Japan Meteorological Agency,2011)

Figure1 Global Warming and Urban Climate Change

Opportunities and challenges for environmental planning

Given these environmental issues, especially the UHIE and air pollution, sustainable urban development becomes an important task. Most of existing research for the heat island mitigation has weighed on building oriented issues and evaluate the effect of energy conservation, low surface temperature material and façade design (J,Fox et.al,2018). In addition, from the large-city scale viewpoint, the research about the effect of increasing the uniform greenery rate in whole cities, shifting to the public transportation system, reducing fossil fuel vehicles have been enough referred (X.Li et.al,2019). However, especially for in the central part of the cities, the urbanization patterns has a large impact on urban climate change (T. Hung, et.al, 2006). The spatial variability of urban pattern especially in community scale, includes urban block form, vegetation coverage and building density. Instead of single solution in/around buildings, environmental friendly city planning should be an optimal approach, with considering status of existing community structures and synergies among various elements and solutions that can develop the effective network of the cool spots and window path in community scale with considering both existing community structures and advanced low energy methodologies.

However, there are two main challenges for the offer the comprehensive solution on urban heat island mitigation methods. The first one is observational methodology. There are various methods for observe, analysis and understanding of the urban heat island, as the analysis of Landsat data, simulation and survey. The measurement data and the simulation in the limited scale are difficult to estimate and understand overall thermal condition in an urban area, while the Landsat data analysis is hard to figure out the effect of the factors in the community. The observational methodology that can figure out from the building scale to city scale are limited.

The other challenge is the lack of platform to unify and analyses the existing data from different standpoint of urban sector, such as transportation, city infrastructure and urban information as a base for comprehensive discussion.

As one of the important part of the comprehensive solution, we propose a smart city planning tool in the previous research (Yamamura, 2016), and developed the sub tool for district energy system planning in consideration of current energy consumption, built year, district energy plant and renewable energy introduction. This research, we focus on the urban climate change in the community scale and develop an urban environmental friendly planning tool based on the system we proposed.

Historical development and issues in Xi'an

Xi'an is one of the most representative historical and cultural cities as well as one of the most developed cities in China. It is suggested that until the year 2016, the urbanization rate (percentage of the total population living in urban areas) in Xi'an is around 73%, ranked as top three in China (Shanxi Provincial Bureau of Statistics,2016). It is one of the cities that with highest urbanization speed.

The city is developed during the different time in the different period that it has the different styles and residential building types. As a historical city, it have the characteristic common pattern that have preserved low rise high density buildings in the center of the city and high rise building in the suburban area. Furthermore, the additional large amount of greenery is difficult to be introduced in the historical areas. Therefore, compared with other cities, the environmental plan for Xi'an should pay more attention on the integration of urban typology, available green space and transportation that can creates detailed networks of the cool spots and small/mid -size wind path comprehensively in the community scale.

From the climate aspect, Xi'an is an inland city with averaged low wind speed that is not enough to diffuse the stagnated high temperature air, which is a more sever model for heat island mitigation case study.

To overcome these problems, and studies the special issues of Xi'an. In this paper, we propose a system for environmental urban planning tool based on Geographic information system (GIS), Information and Communication Technology (ICT) and Building Information Modeling (BIM). In the research reported herein, the data of building and community which supported by BIM are unified by a three-dimensional (3D) city model in a GIS which combine the urban information as urban infrastructure and structure. Further, the information of traffic, people flow, environment and energy consumption collected with sensors from various aspect are described in a geometric manner with detailed information.

We firstly introduce the concept and architecture of the tool. The applicability of the resulting model is then examined by applying it to the city of Xian, China. Based on the existing information analysis, one residential blocks with the green space are selected as case studies. Finally, environmental simulation are adopted to figure out the opportunities and challenges for environmental urban development pattern in the target area.

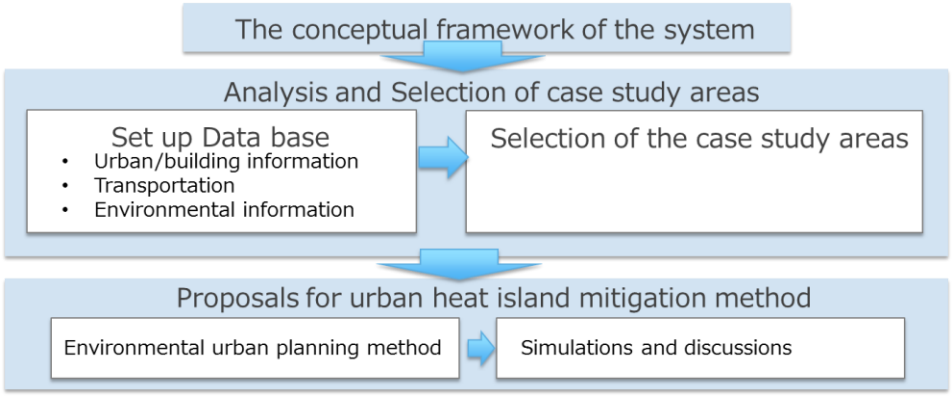


Figure1 Research flow

The conceptual framework of the system

System architecture

As a sub tool for the smart city planning tool that we proposed in the previous studies, it has the same architecture. Figure 2 shows the outline of the system. It constitute with three parts data base, layer integration and the optimal design parts. Database sector and layer integration sector interpret the city information by layered data, including the data related to urban planning, transportation and other various sectors. The two parts are the set based on cyber physical space that built with GIS and ICT technology. The city 3D model is built with the basic urban information from GIS data, while the transportation information, environmental information and energy information are collected with various sensors. These data are plot to the city 3D model built by GIS platform.

Optimal design sector is the simulation and assessment model for optimal thermal environment planning which come from urban heat island mitigation strategies based on the BIM. This tool can comprehensively evaluate the community greenery which are able to be implemented between buildings, energy conservation with building types and age, detailed transportation status in community level. . The result of the simulation is evaluated, feedback and readjust the urban plan until the optimal solution.

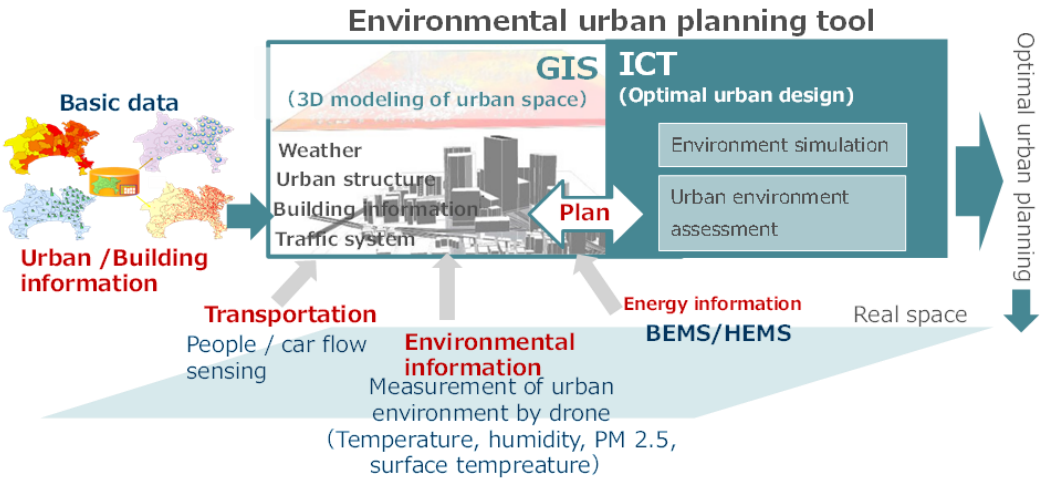


Figure2 Conceptual framework of the system (Environmental planning sub tool)

Datasets for analysis

For comprehensive analysis and planning, various data are adopted in the database. They are as below:

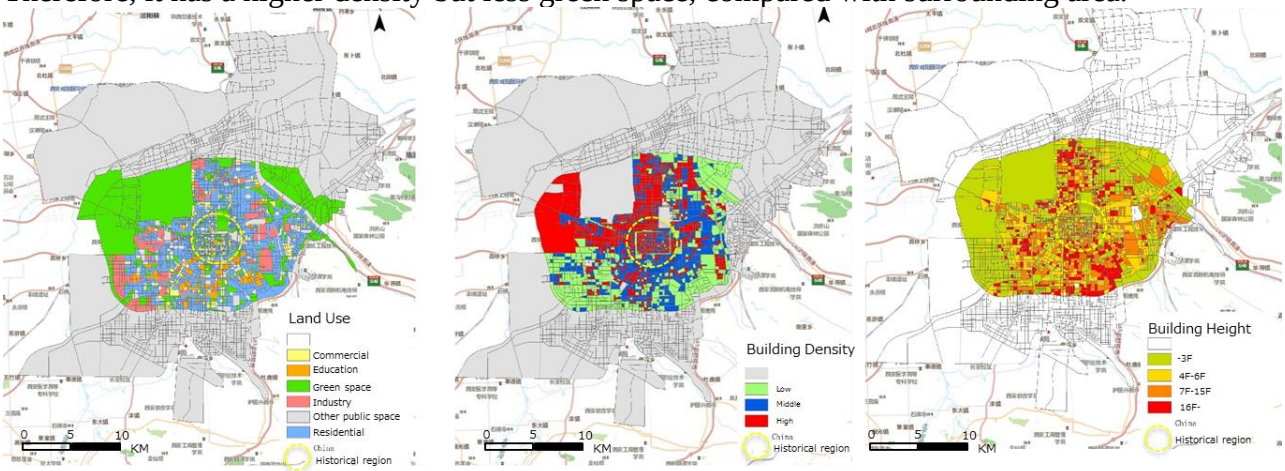
Table1 Datasets

Type	Data
Urban Planning	Land use Building density: Estimated by building area and height Building height
Environment condition	Land surface temperature: analysis data from Landsat (11:29 14th July, 2014) Air temperature data: measurement data from 11th June 2014 to 27th August 2014 Air quality: PM10
Transportation	The measurement on 10th June,2018

Analysis and Selection of case study areas

Urban structure analysis

Firgure3, the land use, building density and building height can figure out the features of urban structure. In the center of the city, the historical area is constitute of low rise residence. Therefore, it has a higher density but less green space, compared with surrounding area.

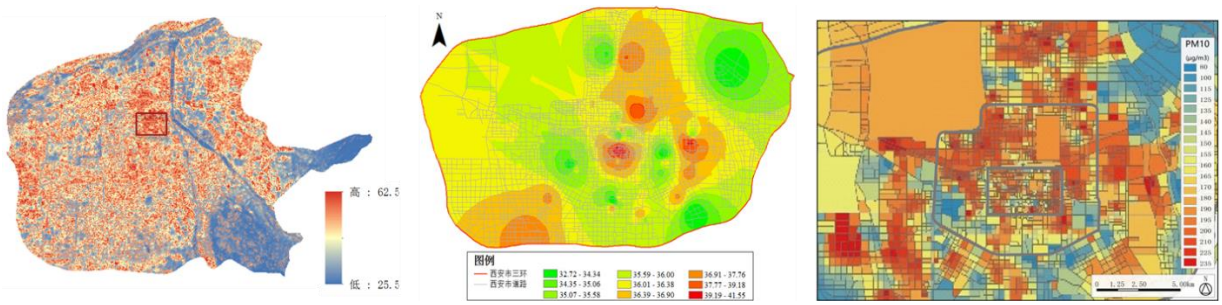


Land use Building density Building hight

Figure3 Analysis of urban structure

Environment condition analysis

Figure4 is the environment condition with land surface temperature, air temperature and air pollution (PM10.0). It suggested that, historical area in the center of the city has the highest surface temperature and air temperature than the surrounding area.



Land surface temperature　　Air temperature　　Air pollution

Figure4 Analysis of urban structure

Selection of the case study areas

As one of the most serious areas under UHIE. This study selects one of the low rise and high density area around a park, Xi'an Revolution Park as case study (Figure5).

Xi'an Revolution Park is located inside Xi'an Circumvallation. As an historical city, the building height in this area is limited no more than 36m and Floor Area Ratio is less than 300%.

By this case study, the research is aim to confirm the effect of the park in residential area and also its environmental effect with the urban typology.

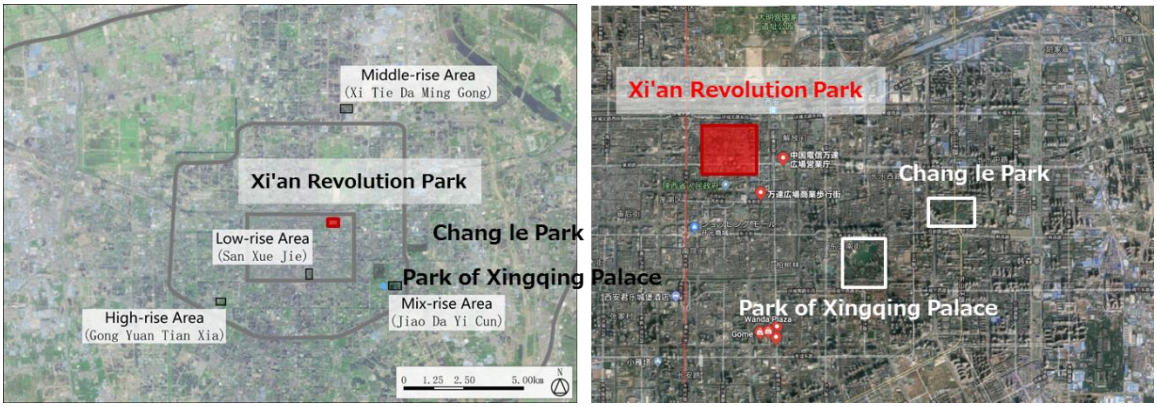


Figure5 Xi'an Revolution Park

Proposals for urban heat island mitigation method

Introduction of cool spots network and the wind path are the usual method for environmental planning. However, in the historical area, the reconstruction and the height of the building is limited, which made the environmental planning difficult.

In this research, we proposed the regeneration method by insert the small green space nearby "Living space" in the building block, the way for revitalize area with the traditional "Courtyard" pattern and introduction of roof greening during the reconstruction of the aged building (Figure6). At the same time, the existing part place is also revitalized by increasing tall trees.



Figure6 Proposed Courtyard pattern for environmental plan

Simulation model

Simulation method

We use 3D thermal radiational environment analysis tool "THERMORender" for simulate the 3D surface temperature and k-εturbulent model "STREAM®" for the average wind distribution and the air temperature distribution.

For the integrated planning, the simulation model we used in this research is a model that can combine the building energy consumption simulation and outdoor thermal environmental simulation (Figure 7). It includes three, modelling parts (input 3D model), solver and output. The modelling parts is the input for simulation, which consists of 3D model and database. Solver is the part of simulation, including thermal environment simulation module, building load simulation module and energy consumption simulation module (Yamamura 2009).

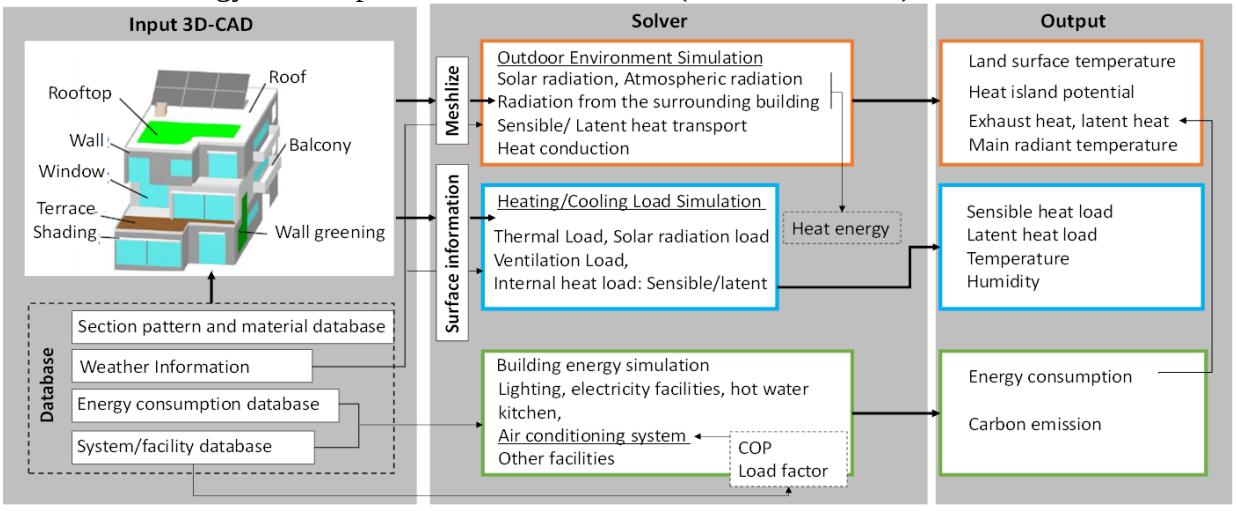


Figure7 Image of Simulation model (S.Yamamura, 2009)

Case setting

In order to find out the effect of the proposed environmental development pattern. Two cases are set for simulation, the existing pattern and the proposed patter (Figure8)

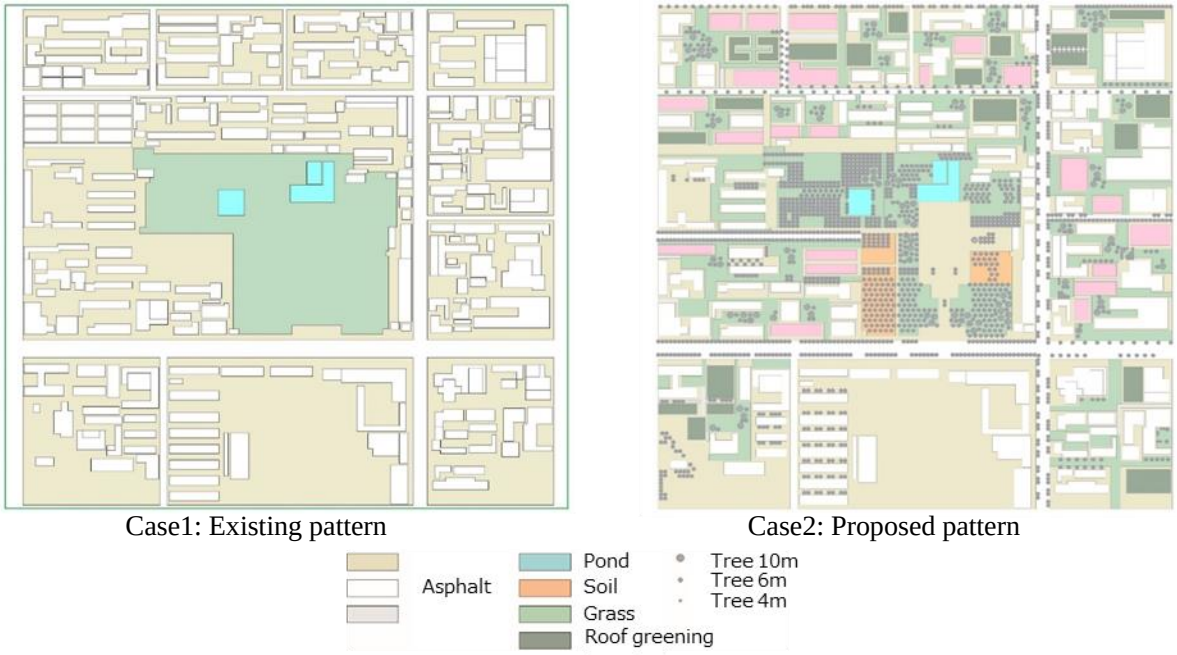


Figure8 Simulation case setting

The setting for simulation are as Table2

Table2 Detail input for simulation

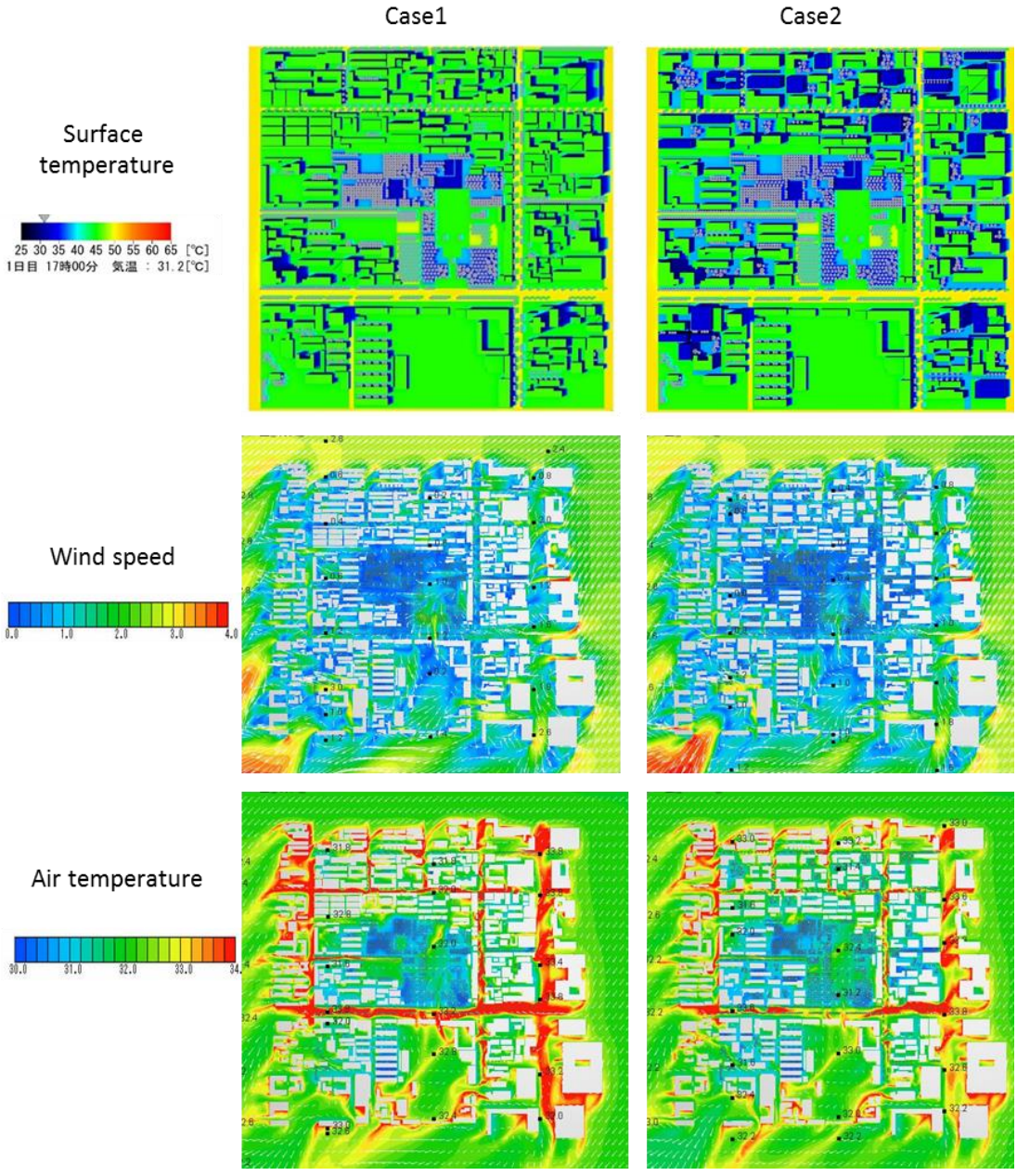
Category	Case1	Case2
Weather data	EnergyPlus™ weather data (August, Typical summer day)	
	Simulation time: 15:00 Wind Speed:2m/s, Northeast Solar radiation: 790 w/m^2 (2.844 MJ/m^2)	
Indoor temperature	Non-residential: 6:00~24:00 26℃ Residential: 19:00~24:00 26℃	
Transportation	Based on the existing survey	50% EV introduction
Energy consumption	Existing energy system	LED and high efficient Air conditioner for 30% energy consumption reduction

Result and Discussion

The surface temperature, Figure9 suggests that the surface temperature of the water remain pavement and the roof greening are 5 ℃ lower than case1. It contributes to spread the lower surface temperature area surrounding buildings in each building block. The wind speed of the two cases can suggest that the introduction of the additional trees in the public space slightly slow down the wind speed. In that case, the cool air that created by the greenery remain in the space and make

the air temperature lower. The air temperature of different building blocks, show in figure10, shows that the maximum temperature of the blocks distributes from around 0.2 to 2.0℃ and averagely decreased 0.63 ℃. The air temperature of the public space, the courtyard, averagely decreased 0.33 ℃. Although the cooling effect is affected by the specific structure in building blocks, it is clarified that introduction of cool spots in every building block and making a network between them leads to create wind paths across the street.

Figure9 Simulation result



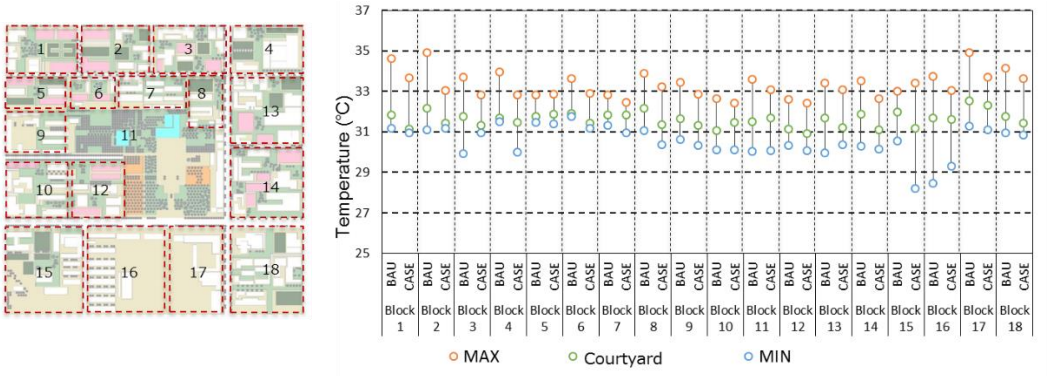


Figure10 Air temperature of different blocks

Conclusions

Based on the concept in the previous research (Yamamura, 2016), we developed a conceptual framework to support environmental friendly planning with integrating BIM and GIS technology in an intelligent system for environmental design. The effectiveness of our proposed system was illustrated by conducting case studies in Xi'an that is traditional and complex urban structure and more difficult to proceed extensive and drastic redevelopment. It is approved that the system can mainly achieve the following:

Combination, analysis, and visualization of the data from urban planning, transportation, and the building information from BIM;

Simulation, analysis, and comparison of the effects of different environmental design patterns, and presented the result through easily understood 3D models.

With the support of the simulation tool, it is proved that the planning method with introduction of small scale cool spot and network of wind path can be a practical urban heat island mitigation method in the historical city as Xi'an. This method considerate existing community structure, development phase, and the practically possibility for environment-friendly planning that can also be used in the similar cities in China and other countries. The tool can be effectively used to confirm various environment-friendly planning strategies and form an action guideline for urban heat island mitigation from community view, instead of building or city view.

Reference

T., Hung, D., Uchihama, S., Ochi, Y., Yoshifumi. Assessment with satellite data of the urban heat island effects in Asian mega cities. Int. J.Appl. Earth Obs. Geoinf. 2006, 8(1): 34–48.

S.Yamamura, Assessment of urban energy performance through integration of BIM and GIS for smart city planning, Procedia Engineering,2017

Shanxi Provincial Bureau of Statistics,2016

J.Fox, P.Osmond, A.Peters, The Effect of Building Facades on Outdoor Microclimate—Reflectance Recovery from Terrestrial Multispectral Images Using a Robust Empirical Line Method, http://dx.doi.org/10.3390/cli6030056

S.Yamamura, O.Nagase ; Study on Methodology about Environmentally Friendly Urban Development for Creating Cool Spots and Reducing CO2 Emissions in Urban Area, The seventh International Conference on Urban Climate, 29 June - 3 July 2009, Yokohama, Japan

29 June - 3 July 2009, Yokohama, Japan

X.Lia, W.Zhou, Spatial patterns and driving factors of surface urban heat island intensity: A comparative study for two agriculture-dominated regions in China and the USA, Sustainable Cities and Society 48 (2019) 101518

Characteristics of micro weather stations distributions for urban heat island monitoring and corresponding thermal mapping

Tzu-Ping Lin, Department of Architecture, National Cheng Kung University, Taiwan
Yu-Cheng Chen, Department of Architecture, National Cheng Kung University, Taiwan

ABSTRACT

Urbanization has been one of the most efficient factors for urban heat island. City planning from the government is a crucial role of the urbanization. Planning strategies are always based on the observation data collected by the weather bureau. However, the lack of integration environment assessment would be leading to an irreversible result to the land and nature. A small number of meteorological stations are insufficient for representing the atmospheric changes and understanding the microclimate, thermal conditions, and built environment in large complex urban areas. The urban heat island effect indicates that the temperature differences between various environments are affected not only by natural climatic conditions, but also by different built environments. Therefore, a suitable number of meteorological stations is required in urban areas to accurately understand how different land covers, land uses, and other factors such as impermeable surface area and total floor area affect thermal conditions. This study aims to compare the three meteorological data, a temperature observation network approaches which installed in three different cities including Chiayi (LATiC), Tainan (HiSAN) and Kaohsiung (STONK) to comprehend the air temperature distribution in different purpose of setting and different number of standard weather station, to realize the advantages and disadvantage of each method. and compare the land pattern differences with the local micro thermal condition.

Introduction

The "urban heat island effect" is an important research topic in the current development of global warming and urban intensification. Under the high-density development of the city, due to the factors of heat storage, artificial heat exhaustion and airflow obstruction, the problem of high temperature in the downtown area is higher than that in the suburbs (Baker et al., 2002; Kotharkar and Surawar, 2015; Lu et al., 2012). The urban heat island will cause indoor air conditioning energy consumption and outdoor heat stress problems, which is an important issue for the ankle joint to reduce carbon and comfort.

In order to understand the phenomenon of time and space distribution of urban heat islands, sufficient weather stations in urban and suburban areas are necessary (Chen et al., 2016a, 2016b; Honjo et al., 2015; Chang et al., 2010; Merbitz et al., 2012). However, the traditional use of officially built standard weather stations does not present the ideal urban heat island phenomenon. This is because the standard weather station has the characteristics of accurate instrument, good maintenance and reliable data. However, due to the high cost of equipment and maintenance, it cannot be intensively measured, and the weather station is mostly located in the suburbs or open space, which cannot reflect the thermal climatic characteristics due to high density of buildings and anthropogenic heat.

Therefore, there are also many cities at home and abroad that use small monitoring stations for temperature measurement. The Tokyo Metropolitan Area Project (METRO), which was

established on the alliance platform of several scholars including the first-ever Chiba University, is located in 90.4 km by 111.3 km, covering the entire Tokyo metropolitan area and the Tokyo Bay area. Established a total of 200 campus temperature and humidity stations (Mikami et al., 2011; Honjo et al., 2015; Honjo, 2012); Finland Turku (Turku) by Suomi et al. Established 50 different temperatures in different built environments such as residential and commercial areas in the city. The Turku Urban Climate Research Project (TURCLIM) explores the effects of coastal and surfacing features on urban hyperthermia in different seasons (Figure 1) (Hjort et al., 2016).

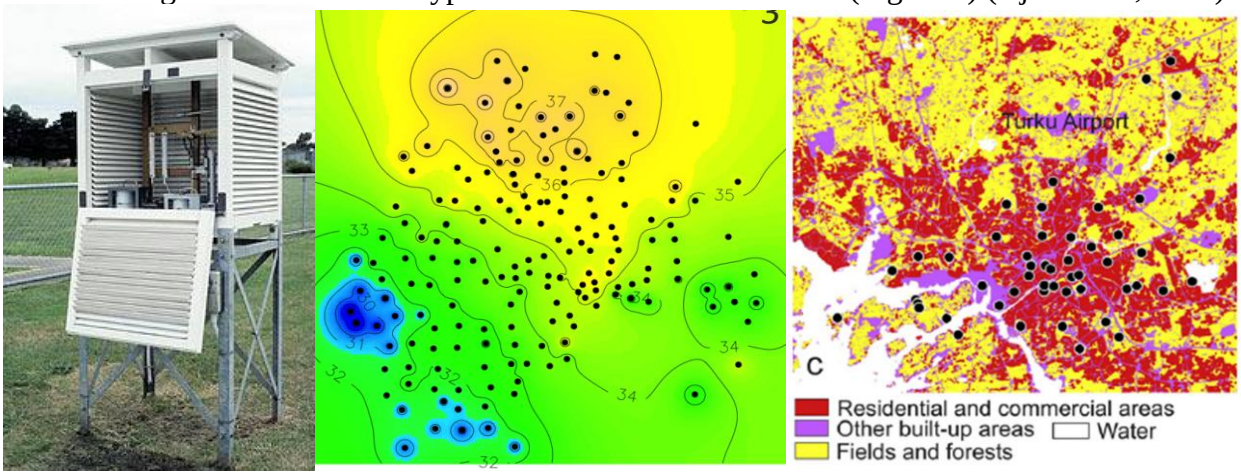


Figure 1 Intensive measuring point measurement plan in Tokyo, Japan (left is instrument, middle measuring point and distribution map and Finland Turku (right) (Honjo et al., 2015; Hjort et al., 2016)

And the Urban-Path project in Szeged, Hungary, with 24 temperature and humidity measurements (Figure 2). Although these plans are not instantaneous, they can produce a more accurate temperature distribution at different time periods for subsequent time-varying analysis and analysis associated with urban characteristics. (URBAN-PATH Project, 2014)

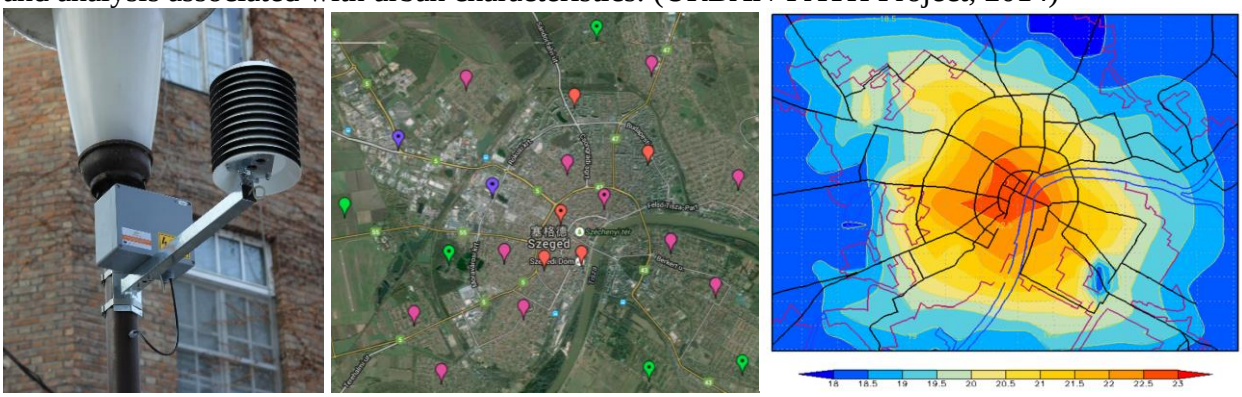


Figure 2 Urban-Path project of Szeged, Hungary, from left to right for instruments, measuring points, and instant distribution maps (URBAN-PATH Project, 2014) (http://en.urban-path.hu/)

Therefore, this study aims to compare the three approaches which installed in three different cities including Chiayi, Tainan and Kaohsiung to comprehend the air temperature distribution in different purpose of setting and different number of standard weather station, to realize the advantages and disadvantage of each method.

Method

Study area

Chiayi city is situated on the south of Taiwan, which includes various kinds of land features (Fig 3a). The urbanized area covers approximately 60 km2 and has a population estimated to 268 thousand by 2019. The population density is in second place in Taiwan. The climate in Chiayi region is humid tropical and influenced by monsoon. According to the Central Weather Bureau (CWB), the annual average air temperature from 1981 to 2010 in Chiayi City is 23.8 ℃. The warmest month is July (33.1 ℃) and the coolest month is January (12.5 ℃). (Chen et al., 2019)

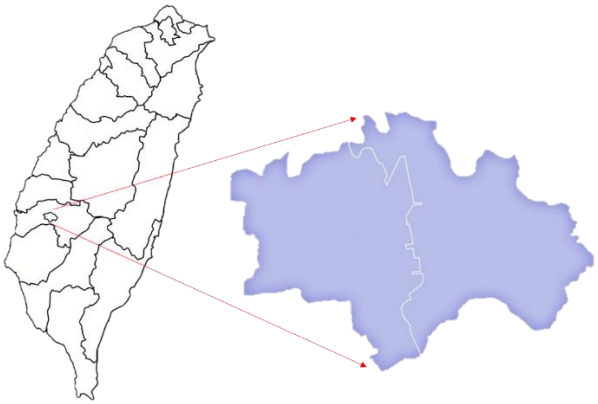


Figure 3a Study area of Chiayi city (Chen et al., 2019)

As a high development city (22˚59'N, 120˚11'E) in the south of Taiwan, Tainan is selected to be the study area (Figure 3b). The total area of Tainan is 175.6465 km^2, including 6 administrative districts. In 2010, Tainan city had been upgraded to a special municipality. However, this transformation results in the increase of population and land operations, make it urgently and necessary to consider of microclimate research in order to give local government assistance by making urban development policies. The Tainan city is in tropical areas, the annual mean temperature in this area is 24.6°C. July is the hottest month; the mean temperature is 30.4°C, January is the coldest month; the mean temperature is 17.6°C, and the annual mean relative humidity is 74.4% (Chen et al., 2018).

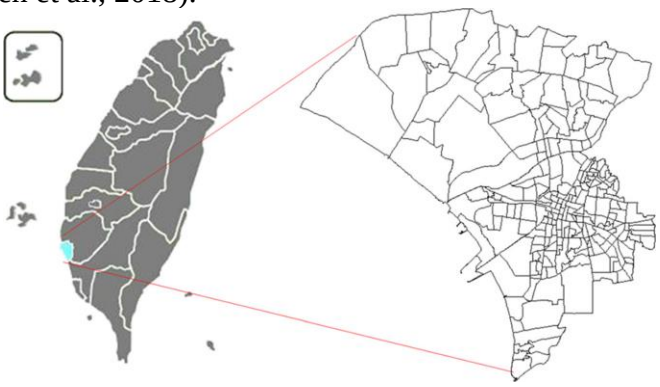


Figure 3b Study area of Tainan city (Chen et al., 2018)

The Kaohsiung City (latitude 22°38' east longitude 120°16'), and its administrative scope includes 11 districts with a total area of 153.5927 km2. The temperature is the lowest in February with an average of 18.6 degrees Celsius. In June, the average temperature was 28.7 degrees Celsius, the relative humidity was the lowest in March with an average of 60%, and the highest in August was 81%. It is a tropical monsoon climate zone. (Chen., 2018)

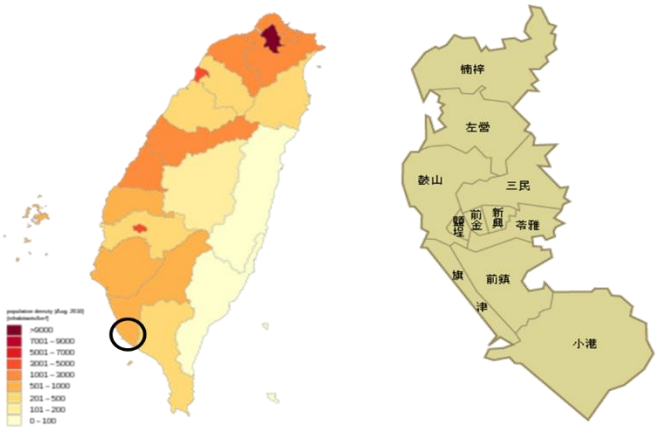


Figure 3c Study area of Kaohsiung city (Chen., 2018)

Configuration principle of observation network

LATiC in Chiayi

This study's meteorological data were measured from LATiC (Large Area network of Temperature in Chiayi) and from the central weather station. This method set 8 points in Chiayi city (Fig 4). Each point represents the local land feature. In order to increase the diversity of meteorological data in researching area, this study is applicate many kinds of index to choose those one hundred points, include land use and land cover.

This study applies the automatic measurement record instrument by Verigo which can record air temperature and relative humidity in certain time interval and download the data by Blue-tooth technology. In this study, the meteorology data was obtained in five-minute interval. In order to avoid solar radiation increasing recording temperature. Every automatic measurement instrument is put in the wing and rain cover and installed at 2.5m in street lamps and utility poles. This installing method is not only preventing solar radiation but also getting better ventilation environment. (Chen et al., 2019)

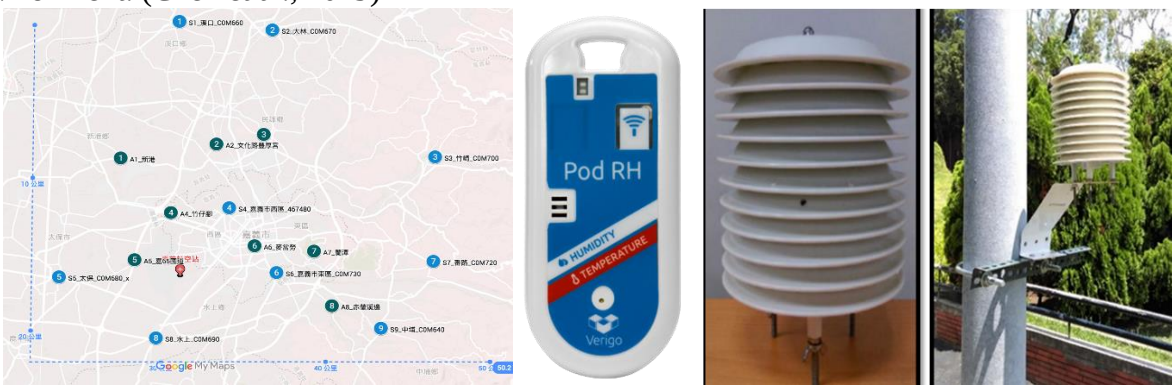


Figure 4 Verigo installed in the utility poles (Chen et al., 2019)

HiSAN in Tainan

For the high-density street-level air temperature observation network (HiSAN) One hundred automatic recording instruments (LOGPRO TR-32, Tecpel Co., Ltd.) were distributed in the study area to collect meteorological data. The LOGPRO (Fig. 5) was selected for the study because it is lightweight, energy efficient, and can store a large amount of data. The sensors in the LOGPROs were checked before installation to confirm accuracy. Air temperature (Ta) and RHwere recorded at 5-min intervals in the study area with an accuracy of ±0.5 °C and ±5% and a measurement resolution of 0.1 °C and 1%, respectively.

Radiation covers were used to protect the LOGPROs from the elements (rain, sun, and wind) and ensure that all data collected were accurate. The LOGPROs were installed on the utility poles of street lamps at a height of 2.5m. At this height, the LOGPROs were adequately ventilated and posed no safety concerns for pedestrians or motorists. Data were collected from the LOGPROs monthly to ensure that the batteries remained charged. At each inspection, the LOGPROs were synchronized with a standard LOGPRO that Tecpel Co. Ltd. calibrated monthly. This ensured that the field LOGPROs were accurate during the study period.

The measurement locations were selected according to the following three principles (Fig. 3a): First, to achieve an average distribution of measurement points, the study area was equally divided into 58 sections, each comprising a 3 km × 3 km grid (Fig. 5). The measurement points were scattered in each grid (each grid contained at least one measurement point). Second, the sections were then classified according to regional features, including land use, land cover, building density, and normalized difference vegetation index.

Doing this prevented the selection of sections with the same or similar urban patterns. Third, the comparison of homogeneity, the green areas were intentionally selected to investigate the influence of green spaces on thermal conditions in the study area. The final measurement points were selected because they represented the most significant attributes of Tainan's urban morphology. Overall, the selected measurement points accurately recorded the characteristics of UHI, including temporal temperature distribution and movement of the UHI over the study period,which revealed the impacts of urban development on the thermal conditions in the study area (Chen et al., 2018).

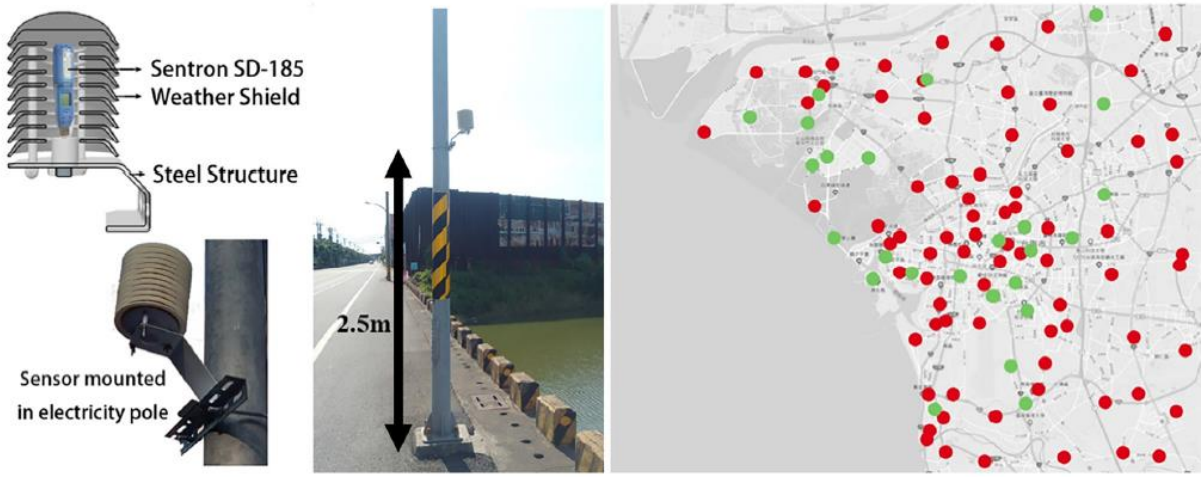


Figure 5. The instrument and points distribution of HiSAN, the red points mean the surrounding area of instrument is urban area, and green points mean the surrounding area of instrument is greenery (Chen et al., 2018).

STONK in Kaohsiung

The total research area was 7.5 km × 6 km, covering multiple types of land, including the mountainous area of Shoushan, populous residential areas, and river courses. To effectively obtain the temperature data in different areas, this study constructed temperature measurement sites by referring to the method proposed by Chen et al. (2017), who used 2.75-km2 grids to establish a temperature observation network in Tainan. To precisely investigate the status of urban temperature, this study used grids with an area of 1.5 km2 to segment the research area and constructed 16 measurement sites, as indicated in Figure 6, namely the smart temperature and environment observation network in Kaohsiung (STONK)

The measurement sites were not established in the center of the grids but rather in areas deemed most suitable after considering the difficulty of construction; for example, D13 was constructed in the mountainous area. In addition, measurement sites were constructed on a specific type of land or on the major road in a region, such as was the case for F13, H13, and E14. F13 and H13 were located at the train station and a major road, respectively, and E14 was at the estuary of Love River. E12 was constructed next to the Jhongdou Wetlands Park to investigate the temperature reduction caused by a large open green space (Chen, 2019).

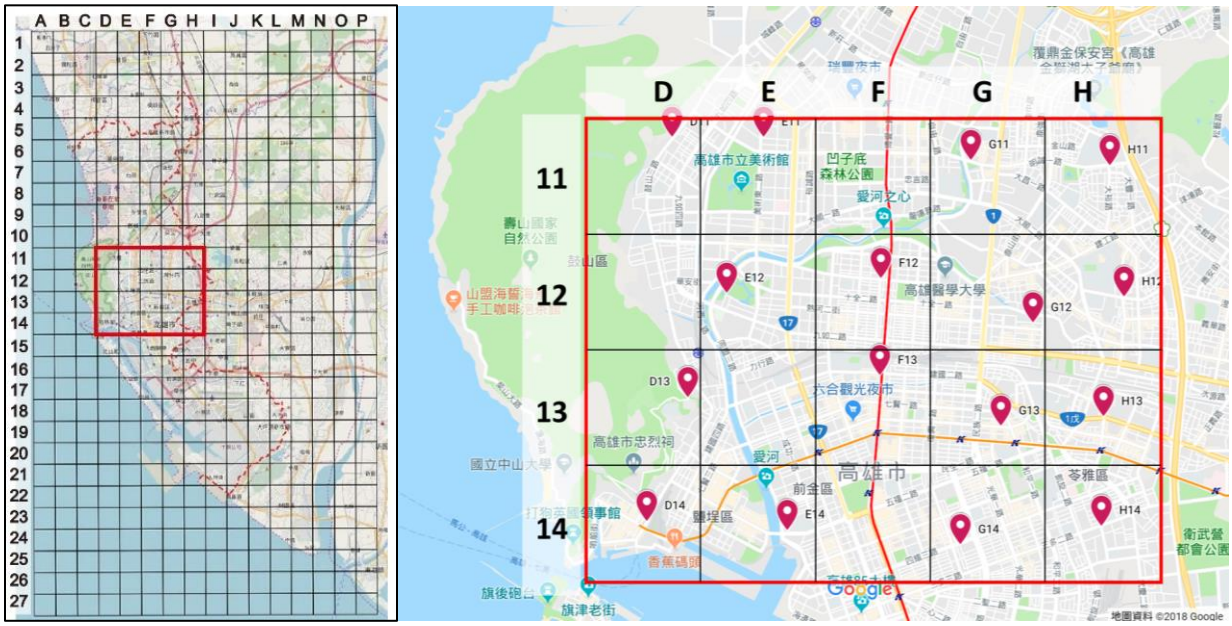


Figure 6. Distribution of measurement sites in the research area. (Chen, 2019)

Results

LATiC in Chiayi

By using the interpolation approach, the temperature data obtained from LATiC can be used to establish the air temperature distribution map in various time period for example in summer day time (Fig. 8a), the urban heat island in Chiayi city is reach to 2℃ highest temperature of 31℃ can be found in the downtown area where is surrounded by impermeable pavement and buildings.

And the lower thermal condition of 29℃ can be found in the rural area where more vegetation and water area located.

The air temperature distribution map of winter daytime (Fig. 7) shows that, the UHI is from 17℃-19℃. The downtown area significantly forms a higher thermal condition area, which mean the different land morphology and land surface pattern can affect the temperature change and cause the different microclimate condition (Chen et al., 2019).

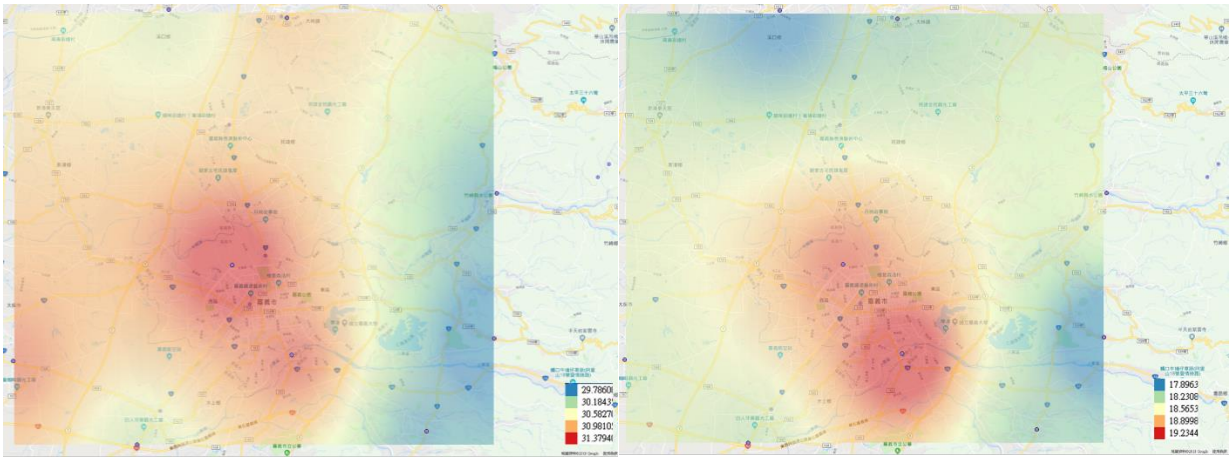


Figure 7. Air temperature distribution map in Chiayi (Chen et al., 2019)

HiSAN in Tainan

The air temperature distribution map shows there are different urban climate in different area. In the mid night, there are many hot spots in city center. This shows high density artificial land stores more hotly than others. In the midday, hot areas move to inland.

The hot spots are moving along with different time (Liao, 2018). This phenomenon is possibility from island climate. Not only artificial land affects the hot spot, but also effected by sea breeze and land breeze. Therefore, the hot spots are moving to different area in daytime and night time (Fig. 8).

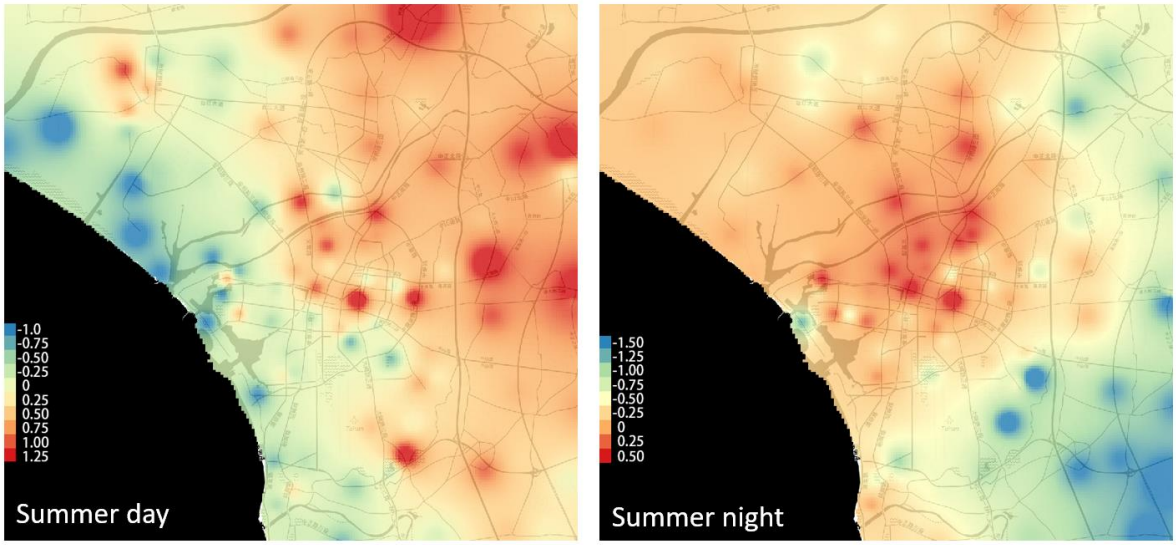


Figure 8. Air temperature distribution map in Tainan of summer day time (left) and night time (right) (Liao, 2018)

STONK in Kaohsiung

Figure 9 presents the interpolation results of the average temperature during the hot season, which clearly indicate the range of the heat island intensity and the high- and low-temperature areas. The Jhongdou Wetlands Park and the west bank of Love River can be regarded as the temperature boundaries. Kaohsiung Main Station (F13), Jianguo 2nd Road (H13), and Liuhe Road (G13), all of which are located in the city center, had average temperatures higher than 30°C and were therefore regarded as high-temperature area. By comparison, Shoushan (D11), the Jhongdou Wetlands Park (E12), and the Kaohsiung Museum of Fine Arts (E11) were regarded as the low-temperature area. The temperature difference between these two areas was 2°C (Chen, 2019).

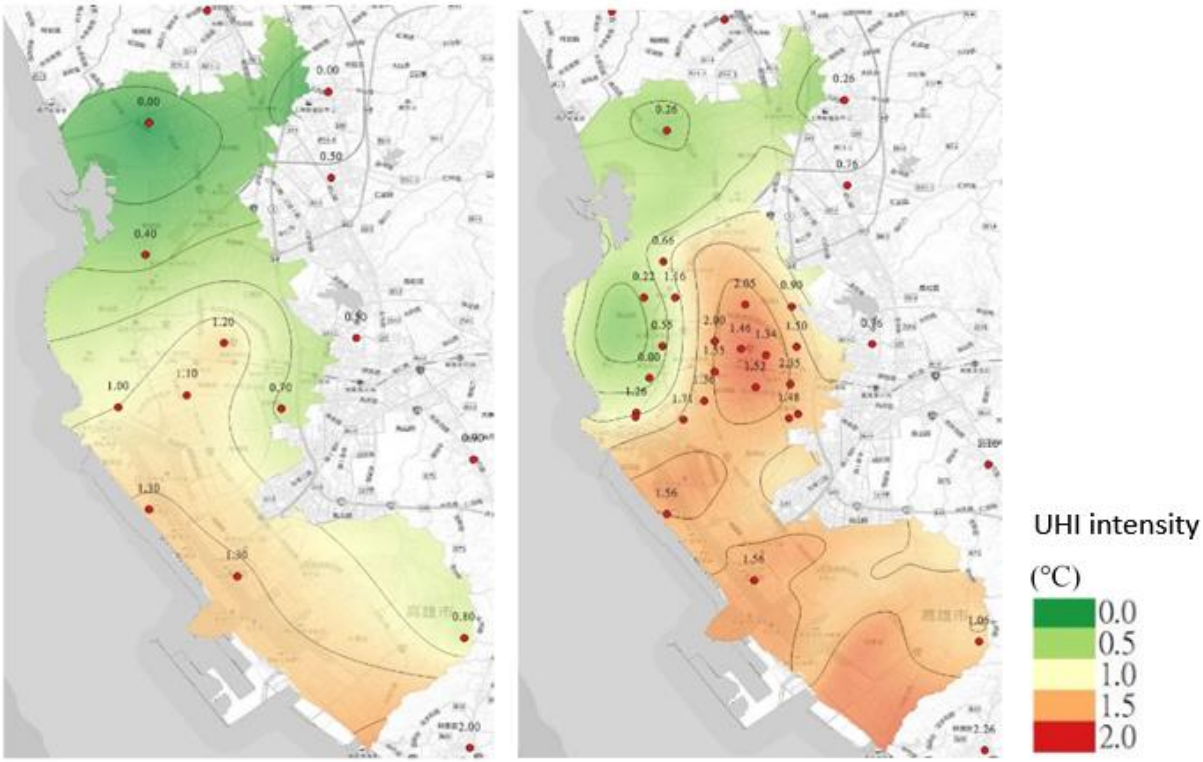


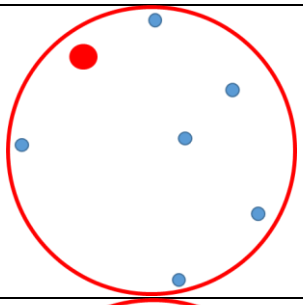
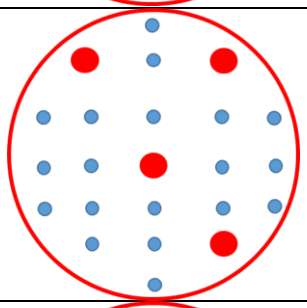
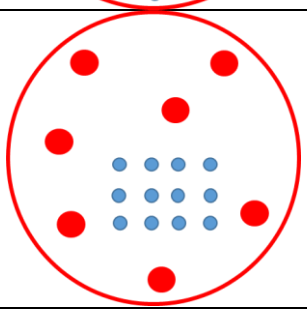
Figure 9. Air temperature distribution map in Kaohsiung by only CWD station (left) and STONK station added (right) (Chen, 2019)

Comparison of observation network

This study compares the three air temperature observation network in Chiayi city, Tainan city and Kaohsiung city, the purpose and aim are not same and have their own advantage of measurement survey. For LATiC in Chiayi city, the purpose is that, this study aims to understand the land features on thermal condition, therefore, to comprehend temperature differences caused by various land use is the priority. For HiSAN in Tainan city, the purpose is that, to complete and homogeneous temperature distribution in the study area, therefore, neat fish net was used to distribute the measurement points to have the clearly thermal condition. For STONK in Kaohsiung city, the purpose is to correct the regional deviation of temperature caused by the interpolation of

standard station, owing to only conduct interpolation by few standard weather stations will have mistaken in the areas between hot spots.

Table 1. Comparison of observation networks

Location	**Purpose**	**Number of Standard station**	**Illustration** (Red point refer to Standard station Blue to the measurement points)
Chiayi city (LATiC)	Comprehend temperature differences caused by various land use	1	
Tainan city (HiSAN)	Complete and homogeneous temperature distribution	4	
Kaohsiung city (STONK)	Correct the regional deviation of temperature caused by the interpolation of standard station	15	

Conclusion

During the rapid urbanization process in Taiwan, air temperature is higher than before. The urbanization process will consistently move forward. There is different phenomenon will occur due to various developing way UHI. However, the lack of integration environment assessment would be leading to an irreversible result to the land and nature. In order to find better urbanization process for environment, this study analyze and introduce three air temperature observation network including Chiayi (LATiC), Tainan (HiSAN) and Kaohsiung (STONK) and compare the result and install approach in different faces because of the urban heat island has become a severe and urgent issue in cities in Taiwan.

For LATiC in Chiayi city, the purpose is that, this study aim to understand the land features on thermal condition, therefore to comprehend temperature differences caused by various land use is the first priority.For HiSAN in Tainan city, the purpose is that, to complete and homogeneous temperature distribution in the study area, therefore, neat fish net were used to distribute the

measurement points to have the clearly thermal condition. For STONK in Kaohsiung city, the purpose is to correct the regional deviation of temperature caused by the interpolation of standard station, owing to only conduct interpolation by few standard weather stations will have mistaken in the areas between hot spots.

This study not only can present the thermal condition characteristics in urban areas but also can provide meteorological knowledge to urban planners and architects who should consider the urban climate. In the future, observations system or IOT meteorological instruments can also be applied to further explore the details and features of microclimate conditions, which will be helpful to comprehend the issues of mitigating the severe climatic problems, including high UHIs and climate changes, when conducting urban planning and building designs.

Acknowledge

This article is a review and comparison of micro weather stations distributions for urban heat island monitoring from previous or current studies of Building and Climate Lab (BCLab) in Taiwan. The introduction, research methods, and research results are based on the content of the master thesis of Chien-Ting Lin, Chih-Hsua Yang, Chun-Kuei Yao, Yu-Jie Liao, Kuo-An Hung, Yu-Cheng Chen in HISAN of Tainan, Cheien-Jung Huang in LATiC of Chiayi, and Szu-Yuan Chen in STONK of Kaohsiung. This article is also part of the author's research project and technical reports, journal papers, conference proceedings. The authors would like to thank the above people and other BCLab members for their assistance and contributions to this article.

References

Baker, L.A., Brazel, A.J., Selover, N., Martin, C., McIntyre, N., Steiner, F.R., Musacchio, L.,2002. Urbanization and warming of phoenix (Arizona, USA): impacts, feedbacks and mitigation. Urban Ecosyst 6 (3), 183–203.

Chang, B., Wang, H.Y., Peng, T.Y., Hsu, Y.S., 2010. Development and evaluation of a city-wide wireless weather sensor network. J. Educ. Technol. Soc. 13 (3), 270–280.

Chen, Y.C., Chen, C.Y., Matzarakis, A., Liu, J.K., Lin, T.P., 2016a. Modeling of mean radiant temperature based on comparison of airborne remote sensing datawith surfacemeasured data. Atmos. Res. 174, 151–159.

Chen, Y.C., Lin, T.P., Lin, C.T., 2016b. A simple approach for the development of urban climatic maps based on the urban characteristics in Tainan, Taiwan. Int. J. Biometeorol. 61 (6), 1029–1041.

Chen, Y.C, Liao, Y.J., Yao, C.K., Honjo, T., Wang, C.K., Lin, T.P (2019). The application of a high-density street-level air temperature observation network (HiSAN): The relationship between air temperature, urban development, and geographic features. Science of the Total Environment, 685, 710-722.

Chen, Y.C, Huang, C.J., Lin, T.P (2019). The relationship between urban morphology change and urban climate, a case study in southern.

Hjort, J., J. Suomi, and J. Kayhko, Extreme urban-rural temperatures in the coastal city of Turku, Finland: Quantification and visualization based on a generalized additive model. Science of the Total Environment, 2016. **569**: p. 507-517.

Honjo, T. Daily movement of heat island in Kanto area. in 6th Japanese-German Meeting on Urban Climatology. 2012. Hiroshima Institute of Technology, Japan.

Honjo, T., et al., Network optimization for enhanced resilience of urban heat island measurements. Sustainable Cities and Society, 2015. **19**: p. 319-330.

Kotharkar, R., Surawar, M., 2015. Land use, land cover, and population density impact on the formation of canopy urban heat islands through traverse survey in the Nagpur urban area. India. J Urban Plann Dev. 142 (1).

Lu, J., Li, C., Yu, C., Jin, M., Dong, S., 2012. Regression analysis of the relationship between urban heat island effect and urban canopy characteristics in a mountainous city, Chongqing. Indoor and Built Environ 21 (6), 821–836.

Merbitz, H., Buttstädt, M., Michael, S., Dott, W., Schneider, C., 2012. Gis based identification of spatial variables enhancing heat and poor air quality in urban areas. Appl. Geogr. 33, 94–106.

Mikami, T., H. Yamato, and M.R.G. Extended, High-resolution Temperature Observations Using Extended-METROS in the Tokyo Metropolitan Area and Their Urban Climatological Significance. Journal of Geography (Chigaku Zasshi), 2011. **120**(2): p. 317-324.

Assessment of variation in Intra Canopy Layer Urban Heat Island Intensity in Residential areas --- A case study of Nagpur City

Sujata Godbole[1] Smt. M.M.College of Architecture, Nagpur (India)
Dr. Ravikumar Bhargava[2] T.G.P.College Of Architecture, Nagpur (India)

ABSTRACT:

Urbanization of recent times has brought many climatological changes in cities around the world, a major one being rise in temperature. Central Indian city of Nagpur is no exception to this phenomenon. Outdoor thermal discomfort is a major outcome of Urban heat island effect. Present study focuses on urban canopy level heat island in city of Nagpur, and aims to understand the temperature distribution in urban canyons, as most of life occurs in this layer and is directly affected by the rise in temperature. This paper reports spatial and temporal variation of air temperature within selected residential areas of Nagpur. Field surveys were carried out, wherein actual physical measurements of outdoor air temperature & humidity were done using fixed station method. Data regarding Urban morphology such as H/W ratio, vegetation, building material & built-up density was recorded by visual observation and mapping. The study shows intra-urban variation in air temperature at canopy level in all seasons and existence of daytime as well as nocturnal urban heat island in city of Nagpur.

Key Words : canopy layer, urban heat island, Nagpur, intraurban, temperature variation, vegetation, Height-width ratio, materials

Introduction:

Cities and people residing therein, are major contributors to climate change. Microclimatic changes are often brought about by manmade alterations of the urban surfaces. The phenomenon, wherein air temperature in urban areas is found to be higher than surrounding open-spaces and rural areas is called urban heat island effect. The intensity of urban heat island effect is observed to be directly related to the degree of urbanization (Oke 1987, Santamoris 2001).

Heat islands are of two types - Surface UHI and Atmospheric UHI. Atmospheric UHI are further classified into Boundary Layer UHI and Canopy Layer UHI – i.e. UHI at micro scale. These UHIs are related to each other, but differ in their processes, observations and models.

The effect of rise in temperature is strongly felt in canopy layer where most of city life occurs. Micro-climate of urban canopy is the result of its immediate surroundings - such as land use / land cover pattern, building materials, geometry i.e. height-width ratio, percentage of vegetation etc. and any change in these parameters results in modification local climate. Thus, meteorological condition within urban canopy is much a localized phenomenon and varies significantly within cities. Hence, the urban canyon or street has been considered as a unit for investigation in the present urban heat island study.

In case of Nagpur city, most of previous UHI studies have investigated the influence of land-use, land cover on air temperature at spatial and temporal scale by using remote sensing data (LST), while only a few have used traverse surveys. These studies indicate presence of urban heat island in city.

Present study aims to investigate factors which are responsible for rise in temperature within the urban canyons. The urban factors that are important from urban designer's point of view (as they can be modified through planning) which include : Percentage of Vegetation,

Building material, Geometry of Canyons i.e. Height-width ratio, Colors of buildings, Percentage & density of built-up areas, and orientation of streets have been considered in the study. This paper focuses on analysis of air temperature variation between study areas for all the seasons in context of urban morphological factors.

STUDY AREA:

Nagpur, the second capital of Maharashtra, is in eastern part of the state. The city acquired historical importance from 18th century after its founder Gond King Bakht Buland Shah made it Capital of his kingdom. City of Nagpur originated in the eastern part known as Mahal and later spread to present south-central part of Sitabuldi and western parts. The present scenario of Nagpur city indicates that it is developing in all directions. The urban pattern of Nagpur reveals its transformation from an old congested city form to that of a planned development. The city does not show much of vertical growth but is undergoing rapid horizontal & radial growth. City has moderate industrial activity and is dominated by presence of residential areas. It also has major retail commercial areas at its center, while few commercial sub centers are spread all over the city. Wholesale markets are concentrated in Eastern part (Godbole S, 1999).

CLIMATE OF NAGPUR:

Nagpur witnesses a very hot and dry summer from March to May. Well-distributed rainfall occurs during the southwest monsoon from June to September, while period from October to November is the post monsoon season. Winter is cool and dry from December to February. During Summer, temperature ranges from minimum 29º C to maximum 47° c and in Winter it ranges from minimum of 10º C to maximum 30°C. Average rainfall is about 45inches (1150 mm). Relative Humidity is about 90% during monsoons and around 20% in the summer. Winds are generally light to moderate, with some increase in the speed in the later part of the Summer season and the Monsoons. Although Nagpur is in the composite zone, the climate is somewhat warmer than other northern cities, mainly because of the rocky terrain that surrounds the city *(Source: Indian Meteorological Department Regional Center at Nagpur Airport)*

RESEARCH METHODOLOGY:

Numerous earlier studies have indicated that the land use land cover (LULC) pattern has most significant influence on urban climate (Givoni,1989;L.W.A. Vanhove 2015;Eliasson, 2000,Roth 2013). Based on spatial organization of city, it was therefore decided to consider Land use Land cover as the main variable influencing the urban climate in city.

Literature study also reveals that Land Use/Land Cover pattern and geometry of urban areas are important factors for development of UHI (Borthakur et al., 2012; Eliasson et al., 2005; Li.Reuben Mingguang et al., 2009; Emmanuel, R, 1997; Mohan et al., 2012; Z.Bottyan et al., 2003). Hence following two land use classifications were selected for this research – i.e. Purely Residential zone (R1) and Residential zone with retail commercial areas (R2). In Nagpur too, the commercial activity mostly goes on along the main road like in any other Indian city, and it is surrounded by residential areas. Therefore, survey was carried out in selected residential areas which are representative of zones mentioned above, to understand its geometry i.e. Height/Width ratio of urban canyons, its density and type of buildings forming the canyon.

Data collected during different seasons was then statistically analyzed to understand contribution of different parameters in formation of UHI at Canopy layer.

MONITORING SITES:

Residential areas were further sub-classified based on urban structure i.e. built-up density into following categories: High density, Medium density and low density. Based on these, following 4 study areas were selected. To study urban heat island at canopy level, three street canyons were selected from each study area (Ref. Table 1). Out of these three, one street canyon was commercial while other two were residential. In order to monitor and record air temperatures within the canyons, fixed point measurement method was used. No. of monitoring points in each canyon varied as per the canyon length. Table-1 below shows details of Street Canyons where measurements were taken :

TABLE 1

Area	Street No.	Length of Road	Width of the Road	H/W	Orientation	Land use	Road Material
Mahal	1	90m	6m	2.25	NE_SW	Resi	Concrete
	2	486m	17.5m	1.06	E-W	Comm	Asphalt
	3	90m	9m	1.8	N-S	Resi	Asphalt
Dhan-toli	1	165	6m	2.5	N-S	Resi	Asphalt
	2	435m	10m	2.1	N-S	Mixed	Asphalt
	3	288 m	10m	1.35	NW-SE	Resi	Asphalt
Dhara-mpeth	1	285m	4.5m	2	E-W	Mixed	Asphalt
	2	968m	24m	0.75	NW-SE	Comm	Concrete
	3	478m	9m	1.66	N-S	Resi	Asphalt
Shankar Nagar	1	140m	7.5m	1.2	N-S	Resi	Asphalt
	2	118m	9m	1	N-S	Resid	Asphalt

Mahal:-

This oldest part of Nagpur is located on eastern sides and is considered as origin of city. It is a congested area with organic pattern of growth dominated by residential and commercial activities i.e. mixed land use. It can be classified as that having compact low-rise and midrise buildings with a few open spaces, narrow lanes of organic pattern and few trees. Land cover is mostly paved. Bricks, cement plasters, cement concrete are construction materials. Population density is 700-850 pph, while percentage of built-up area is around 76 percent.

Dhantoli:-

This is well planned area with open spaces and parks, having gridiron pattern of roads dominated by residential and commercial activities i.e. Mixed land use. Road widths are 6m, 9m and 12m. This area consists of an open arrangement detached midrise buildings (3-9stories),with few low-rise buildings. Percentage of Built up area is 50%. Percentage of pervious land is less with scattered trees (percentage of vegetation is 20%). Construction material mostly is Brick, cement plaster and concrete. Built up area mostly consists of residential buildings, hospitals and commercial.

Dharampeth:-

Situated in the Westside of Nagpur it has Medium dense built up area with a built up area of40%of total area. Built up area mostly consists of shopping centers, shops, vegetable markets, commercial areas etc. Area is dominated by residential and commercial activities i.e.mixed land-use (Figure.6). Land-cover is mixed i.e. pervious and impervious type, impervious area is more than pervious one.

This area is a combination of open arrangement of midrise buildings (3 to 9 stories) and compact low-rise buildings with few trees. Land cover is mostly paved.

Shankar Nagar:-
This is well planned colony with Parks, Playgrounds and Residences. It is a purely residential area (Figure 7) Built up area is 23% of total area. . This area can be termed as open low rise buildings (1-3stories) with 22 percent of vegetation. Percentage of pervious land-cover is more. Construction materials are mainly bricks, cement plasters and concrete.

INSTRUMENTATION:

Instruments for recording temperature and humidity were selected on basis of their accuracy, minimum error and easy in handling. Field measurements of Air temperature and relative humidity within the street canyons were recorded by instruments such as :HTC wireless data logger and Lutron hand held 4-in-one instruments, Hand held Kusam-meco infrared thermometer Model IRL-300 was used to measure the horizontal and vertical surface (street, pavements and adjacent facades) material temperatures. The temperature range is -30˚C to 550˚C.

All the instruments were calibrated before taking readings/observations. Air temperature measuring instruments were installed at a height of about 1.5 m to 2.0 m above ground level as per WMO guidelines. The Air temperature, relative humidity and temperature for surface material were recorded for all the four seasons such as summer, monsoon, post-monsoon, and winter so that seasonal variations along with the diurnal variations in temperature can be studied. Temperatures were recorded at all monitoring points in all study areas on the same day simultaneously at 3 hours intervals from 12 pm in the morning to 10 pm in night. These timings were considered for analysis because most human activities take place during these periods. During entire period of survey, sky was clear, and winds were calm. Wind speed was very low at 0.4 to 0.8 m/s, and therefore has not been considered for analysis in this study. To compliment continuous measurements by HTC data loggers, instantaneous measurements of air temperatures were also done manually at each station in these time slots with the help of Lutron LM-8000A temperature and humidity measuring instruments.
Effect of anthropogenic heat on air temperature in canyons was beyond the scope of this study.

CALCULATIONS FOR UHI INTENSITY :-

Urban heat island intensity is calculated as a difference between the maximum urban temperature and nearby rural area temperature. As rightly pointed out by Stewart and Oke (2012), the classification of field sites as conventionally “urban or rural” has become especially difficult in regions where both cities and country sides are now densely populated and land uses are intensely mixed. City of Nagpur is also expanding in all four directions with urban influence, and it is very difficult to find rural site very near to Nagpur. Therefore in the present research, UHI Intensity has been calculated as difference of the temperature at a given study area location and the temperature recorded by meteorological station at Nagpur Airport (baseline temperature) at the same time. The intra-urban UHI intensity has been calculated as difference between temperature at a given study area location and the lowermost temperature recorded at the same time amongst all stations within the same study area.

RESULT AND ANALYSIS:

As urban heat island intensity is not constant but shows fluctuations in strength during day and night, analysis of data is done considering study areas, seasons and temporal scale.Comparison

of average ambient air temperatures among study areas during various time slots is done. Since all values of average temperature are very close to the average street Measurement point temperature for Summer, Monsoon, Post-monsoon, winter obtained from Indian Meteorological Department (IMD)Regional Centre at Nagpur Airport, it can be said that period of observation was representative of the particular season. Comparative analysis of average temperature for particular season for each time slot of all the 4 study areas was carried out. In each study area, three canyons/ streets were selected for recording ambient air temperature, and temperature of horizontal and vertical surfaces. It was observed that in all areas, there was no significant difference in the average air temperature on different streets for all the 3-time slots. Therefore, we can consider average temperature of all streets of a study area as temperature of that area.

Analysis of air temperature at different locations within study areas shows that, all urban locations (study areas) show higher temperatures than that recorded at meteorological station at Nagpur Airport (baseline temperature) at the same time in all the seasons. This strongly indicates formation of Urban Heat Island over city of Nagpur during most of the time of year.(Refer Fig.1,2,3).Analysis of variance (ANOVA) a statistical method was carried out to test whether observed air temperature differences within different four study areas were statistically significant during three different time slots. Two-way analysis of variance (ANOVA) was performed to study (a) whether there is significant difference in average temperature of four study areas and (b) whether there is significant difference in average temperature in different time slots. The two null hypotheses tested were :H0: There is no significant difference between average air temperatures of study areas. Against alternative hypothesis - there is a significant difference between average air temperatures among study areas. H0: There is no significant difference between average air temperatures in three different time slots. Against alternative hypothesis - there is a significant difference between average air temperatures in three different time slots.

The results of analysis shows that p-value is less than 0.05. Thus we can reject null hypothesis at 5% level of significance, and we can conclude that there is a significant difference in the average summer temperatures of different localities (p-value 0.000147) as well as in various time slots (p-value0.000289).The same analysis was done for other 3 seasons viz, monsoon, post-monsoon, and winter. For Monsoon, p value is found to be 0.0005 for localities and 0.00 for various time slots. For Post-monsoon season, p value is found to be for localities 0.0002 for various time slots value of p is 0.00.

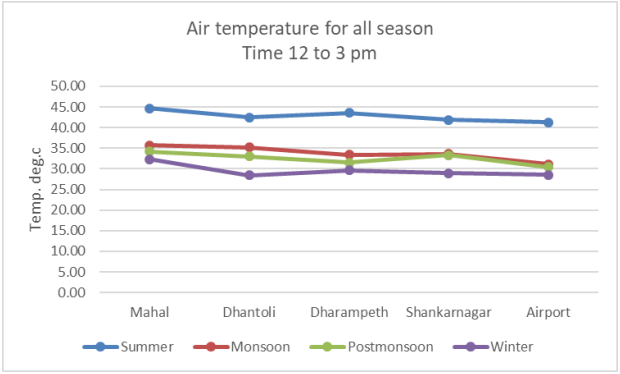


Fig.1 Air temperatures for all seasons (12 to 3 PM)

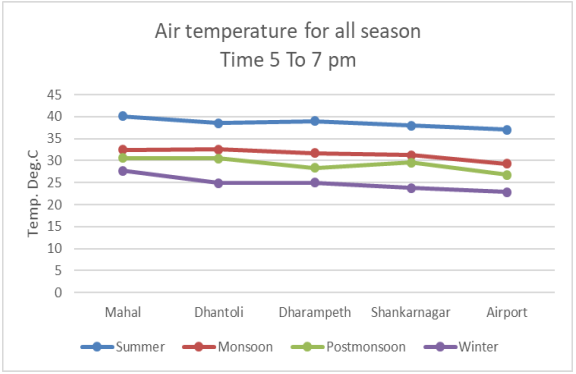


Fig.2 Air temperature of all Seasons (5 to 7 PM)

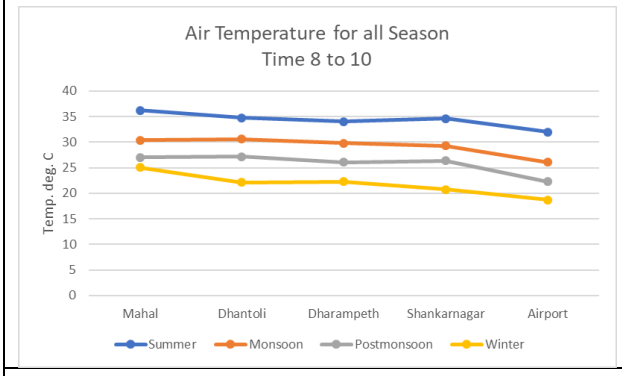


Fig.3 Graph Showing Air temperature of All Seasons (Time 8 to 10 PM)

For Winter, p value is found to be 0.0001 for localities and 0.00 for various time slots, indicating that there is a significant difference in the average temperatures of different localities as well as in various time slots.

Effect of this temperature variation on humans' outdoor comfort was also studied. Experience of outdoor thermal discomfort is a major impact of UHI phenomenon, that is strongly felt in canopy layer. Evaluation of outdoor thermal comfort was carried out by using random sample surveys during Summer, as it is the hottest season. A guided questionnaire was used for user survey which addressed user's experience of thermal condition - i.e. thermal sensation and feeling of comfort and with other information such as name, age, location (area), and address. The participants were asked to classify sensation of thermal comfort based on ASHRAE thermal comfort 7 point scale. The results of questionnaire survey were analyzed and following inferences were derived:

1) As regards experience in outdoor spaces in summer during different slots, 74% of respondents felt outdoor spaces are Hot in Summer during 12 to 3 pm , while 26% felt Warm. Responses for time slot 5 to 7 pm and 8 to 10 pm were more or less same with 67% respondents feeling Warm, 28% feeling Slightly warm and 5% choosing not to mention their rating.

2) 55% people strongly felt that they could experience temperature difference while moving from one locality to other, 30 % respondents agreed to having felt such a difference while 15% people said they didn't find any change in temperature.

COMPARISON OF AIR TEMPERATURE OF URBAN LOCATIONS WITH REFERENCE SITE I.E. IMD AIRPORT STATION NAGPUR:

All urban locations i.e. study areas show higher air temperature when compared to the IMD Airport station, Nagpur, for all seasons and various time slots. The intensity of UHI is a function of time during day i.e. it changes according to temporal scale. During a large part of the year, the day time UHI intensity i.e. difference between mean temperature of all residential areas and IMD is more than 2.5 deg. C expect for summer is 1.85º C. This is because the open land/borrow land in and around IMD Airport Nagpur has the heat holding capacity and it absorbs more solar radiation. But during the night in summer season, the difference of mean temperature of all residential areas is 2.88ºC and winter it is 3.86 deg. C more than reference site, as IMD observatory is in open area, whereas during night radiant heat loss is more. On the other hand, residential areas of Nagpur city consist of compact mix of midrise and low-rise built-up area with roads of Asphalt and concrete. Both daytime and Nocturnal Canopy level UHI exist in residential areas of Nagpur.

COMPARISON OF INTRA-URBAN HEAT ISLAND INTENSITY OF STUDY AREAS WITH BASELINE UHI :

The intra urban UHI intensity has been calculated as difference between higher temperature recorded at a given study area location and the lower most temperature recorded at the same time amongst all stations in all the study area.

Table No.2: - Intensity of Urban heat island (Intra-urban)

INTRAURBAN HEAT ISLAND INTENSITY			
Season/ Time slot	**12 to 3 pm**	**5 to 7 pm**	**8 to 10 pm**
Summer	2.84	2.08	1.61
Monsoon	2.04	2.08	1.11
Postmonsoon	1.0	1.06	1.0
Winter	3.38	3.85	4.26

The Intra urban UHI for Mahal area (which recorded highest temperature amongst all the 4 study area) varied substantially for all the seasons and three time slots.

It is observed that Mahal area (which is part of the old city) has high Intra urban UHI intensity during noon i.e. 12 to 3 PM for summer and monsoon. For post monsoon it is almost the same for all 3 timeslots. During winter it is highest in 8 to 10 pm time slot.-Earlier research on UHI has indicated that higher densities are likely to have higher temperature due to their physical structure (Givoni, 1998; Oke, 1988).

In an urban area large amount of reflected radiations hits walls of adjacent buildings and this initiates the process of radiation reflecting back and forth a number of times between the walls of different buildings. Due to this, in densely built urban areas, only a small part of solar radiation falling on wall is reflected upward to sky, while most is absorbed by walls of the buildings and slowly released back to atmosphere in the evening and night hours. Thus temperature in a built environment is influenced by its surfaces, as energy is transferred through convective process (Givoni, 1998). This explains higher temperature recorded in dense areas.

INTRA URBAN UHI INTENSITY: -

It is observed that there is substantial difference between mean air temperature within the residential study areas in all seasons and during all time slots. It is observed that Mahal area recorded highest ambient air temperature amongst the 4 residential areas and Shankar nagar lowest. The mean temperature difference between Mahal and Shankar-nagar during summer is almost 3ºC during 12 to 3 pm timeslot and during night it is 1.61(i.e. Temperature at Mahal is 1.61ºC higher than Shankar nagar). During daytime intensity is higher may be due to larger impact of radiant surface temperature during the day because of the solar heat. During night difference is less this may correspond to highest energy use for ACs and coolers due to which anthropogenic heat increases which further add to increase in air temperature.

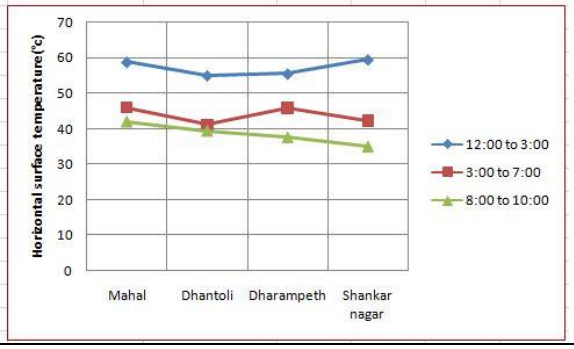
During Winter, the temperature difference between Mahal and Shankar nagar is 3.38ºC between 12 to 3 pm timeslot and during night (8 to 10 pm) it is 4.26ºC. This may be due to the fact that reradiation from canyon is fast as H/W ratio is less, percentage of vegetation is more as compared to other study areas and Also Shankar nagar is attached by a farmland on one side the cumulative effect of all this is responsible for drop in ambient air temperature. The surrounding area is also influencing temperature with in urban areas. The mutual difference between residential

areas is more in winter and summer as compared to monsoon and postmonsoon as in postmonsson days are comfortable and nights are cooler. The substantial difference in intra urban heat island intensity or temperature variation within the study areas of Nagpur city indicates that land-use, percentage of built-up area, vegetation, Materials of Surfaces and other urban characteristics has an influence on the urban heat island intensity.

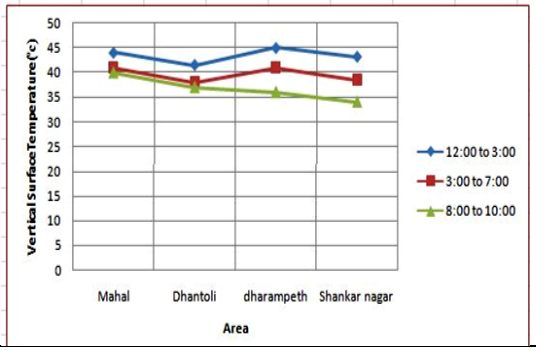
RELATIONSHIP OF UHI WITH VARIABLES OF CANYON:

RELATIONSHIP WITH BUILDING MATERIAL:

The surface temperature of facades (Vertical) and Streets (horizontal) varied considerably depending upon their exposure to solar radiation. In these study areas, streets were mainly of Asphalt & Concrete and facades were of brick with cement plaster and painted with color. It was found that horizontal surfaces of streets had a high temperature between 50 and 60 deg C in the afternoon during summer (Refer Fig.4). These materials are dense; dark in color (asphalt) with low albedo and therefore absorb more heat than material for facades. Temperatures of facades were found to be less than surface temperatures of horizontal surfaces during summer The difference was much more pronounced during noon, and gradually reduced during evening and night time. This was because of orientation of facade and light color of the facades (i.e. high albedo).The horizontal surfaces (streets) and vertical surfaces (facades) were always observed to be warmer than air temperature in canyon – both during daytime & night time almost in all season.



horizontal Surface temperature



Vertical Surface temperature

Fig.4 Graph showing temperature of horizontal and vertical surfaces in Summer season

B) RELATIONSHIP WITH PERCENTAGE VEGETATION :

Various forms of greenery which exists in study area are gardens, trees along the road sides, and trees, shrubs, lawns within individual house lots. Extent of Tree cover was computed using Arc-Gis software. Their percentage varied from 7 to 25% (Ref. Fig.5). Greenery was acting as sources of moisture for evapotranspiration, due to which absorbed solar radiation is dissipated as latent heat and thus helps in reducing urban temperature (Sharifi et al., 2015). In all four study areas, it was found that in summer air temperature increases when percentage of vegetation within the canyons is lower. For example, in case of Mahal where extent of vegetation within the canyon is less than 10 percent, the air temperature was higher when compared with the other study areas.

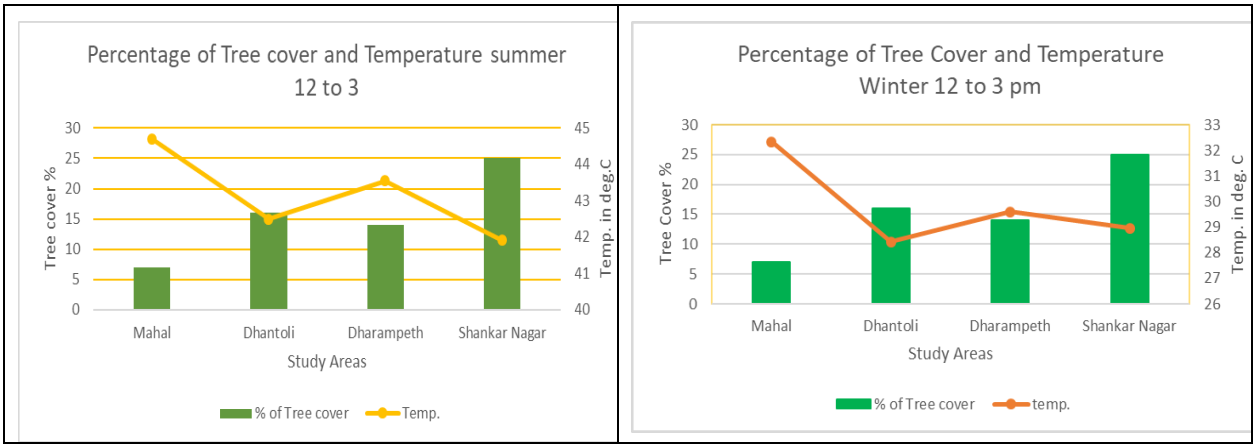


Fig.5 Observed summer air temperature in study areas against percentage of tree / vegetation cover in Canyons

C) RELATIONSHIP WITH H/W RATIO OF STREET CANYON:

The study found that in summer during 12 to 3 pm, area with lowest H/W ratio of street canyon (Shankar nagar) recorded lowest temperature (Ref. Fig.6). while Mahal which is having highest among the study areas shows more temperatures. Above table shows that temperature in Dharampeth is more than dhantoli though its H/W is less than dhantoli one of the reason may be percentage of vegetation as percentage of vegetation in dharampeth is less than Dhantoli. Seasonal variation is seen in temperature of summer and winter but highest H/W ratio shows more temperature as compared to lowest H/W.

At broader level above mentioned factors found to be playing role in formation of urban heat island. This matches with the results of earlier studies.

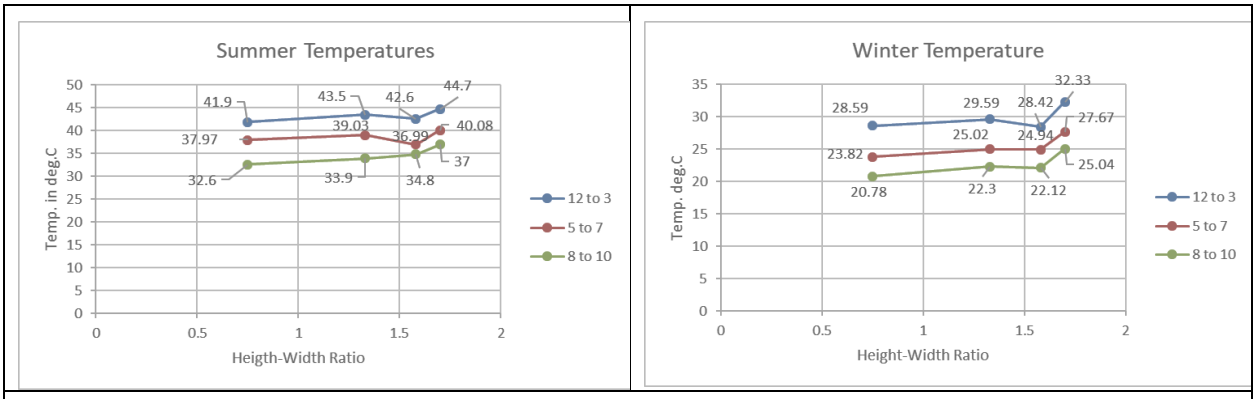


Fig.6 Graph Showing relationship between Mean H/W of Areas with Air Temperature

CORRELATIONAL ANALYSIS

To study the pattern of relationship between air temperature (as an indicator of UHI) and other variables commonly observed in the urban canyon (as an indicator of urban morphology), correlation analysis was carried out for all study areas as per season and 3 different time slots. Correlation is used to measure the strength of the association between numerical variables and is obtained by using Karl Pearson's correlation coefficient (r). In this analysis, temperature was taken as dependent variable and other variables such as extent of vegetation, (building)height / (road)width ratio of canyon, material of horizontal and vertical surfaces, density of built-up were

taken as independent variables. Correlational analysis shows that, there is a strong correlation between average air temperature in urban canyons and surface temperature of materials used for streets and facades. The main reason for this is thermo-physical properties of materials. However, it is also observed that in certain cases where percentage of vegetation is more and height / width ratio is lower, air temperature is slightly lower. These factors also have correlation with air temperature, but it is not that significant.

CONCLUSION:

The results show that there is existence of Day time as well as Nocturnal canopy level /canyon level Urban Heat Island in city of Nagpur, and intensity of said UHI varies with seasons. There is also a variation in Intra-urban heat island intensity at canopy level, due to local urban structure, urban characteristics and land use. The UHI seems to have considerable impact on outdoor thermal comfort as well as health of residents of Nagpur city.

This study indicates that urban factors like material used for horizontal and vertical surfaces, percentage of built area & land-use / land cover have influence over spatial air temperature at canopy level within study areas, resulting in day time as well as night time UHI.

REFRENCES:

Borthakur M , Nath B Kr (2012). A Study of Changing Urban Landscape and Heat Island Phenomenon in Guwahati Metropolitan Area. Int.J. of Scientific & Research Publication, vol 2, issue 11 pp 1-6.

Bottyan Z, Unger J (2003). A Multiple Linear Statistical Model for Estimating the Mean Maximum Urban Heat Island. J. Theoretical & Applied Climatology pp 233-243

Emmanuel, R (2005). An urban approach to climate sensitive Design (strategies for the Tropics),Published by Spon Press.

Emmanuel, R (1997) Summer Time Urban heat Island Mitigation: Propositions Based on an investigation of Intra Urban Air Temperature Variations. J. Architecture Science Review Vol.40 Issue 4 pp 135-149 .

Eliasson & Sevensson M.K. (2005) .Spatial air temperature variations and urban land use – a statistical approach. J.Meteorol Appl,10,pp 135-149

Eliasson I (2000), Use of Climate knowledge in urban planning. J Elsevir Landscape & Urban Planning 48- (2000) PP 31-44.

Givoni (1998) Climatic Considerations in Building and Urban Design, published by John Wiley & Sons, INC, Canada.

Godbole S (1999). Planning for the Improvement of the Old City Area of Mahal Nagpur. Thesis submitted for partial fulfillment of the requirement for the degree of M.tech in Urban Planning (1998-99), Department of Arcitecture & Planning, VNIT (VRCE) Nagpur. pp 13-26.

Mohan M1*, Yukihiro Kikegawa†, Gurjar B.R.**, Bhati S*, Kandya A, Ogawa K. (2012). Urban heat island assessment for a tropical Urban airshed in Delhi, J Atmospheric & climate Sciences,2012,127-138.

Oke T R (1976). The Distinction Between Canopy andBoundary-Layer Urban Heat IslandsThis article was downloaded by: [114.143.168.188]On: 09 April 2015, At: 07:18Publisher: Taylor & Francis.

Oke T R (1988). The Urban Energy Balance. Progress in Physical Geography, 12(4), 471-508, www.researchgate.net/profile/T_Oke/publication/275590257_The_urban_energy_ balance_Prog_Phys_Geogr/

Santamouris M (2001). Energy & Climate in the Urban Built Environment, London: Publisher James&James(science Publisher) Ltd.

Sharifi E , Lehmann S (2015). Correlation analysis of surface temperature of Roof tops, Street scapes & Urban Heat Island Effect : Case study of Central Sydney. J Of Urban & Environmental Engineering V-9,n-1, pp 3-11.

Stewart, I. D. and Oke,T.R. (2012). local climate zones for urban temperature studies, J American Meteorological Society 2012. Pp 1879-1899.

VanHove L W A, Jacobs C H J, Heusinkveld B G, Elbers J A , Van Driel B L, Holtslag A A M (2015). Temporal & Spatial Variability of urban Heat Island and Thermal comfort within the Rotterdam agglomeration. J Elsevir Building and Environment 83 (2015) pp 91-103.

Satellite based observations for Surface level Urban Heat Island over Bhubaneswar: A case study

Dudam Bharath Kumar*
Assistant Professor, School of Civil Engineering
KIIT-Deemed to be University KIIT-DU, Bhubaneswar-751024 (India)
**Correspondaning Contact: dudam.kumarfce@kiit.ac.in*

ABSTRACT

We present a case study on identification of surface level urban heat island (SUHI) based on a land surface temperature (LST) of satellite observational data. Further, relevance of air pollution on dynamics of the LST is explained. Ground based observation at KIIT-DU station for air pollution was carried out to assess the climatology of air pollution in Bhubaneswar. Results show that the LST over Khandagiri region exhibits SUHI compared to that over adjoining regions of the city. Analysis of present study suggests that heavy built-up area followed by land-use or land-cover change over Khandagiri made a region consisting of SUHI on its own region. On the other hand, the Chandaka a forest region shows contrasting results being a region full of vegetation. The normalized deviation of vegetative index (NDVI) from Moderate Resolution Imaging Spectrophotometer (MODIS) -Aqua algorithm based data also supports the vegetation information over study region. Efforts to relate pollution and other geographical information are required to infer heat island not only at surface level but also at canopy and at boundary layer level are essential.

Introduction

Rapid urbanization and consequent industrialization in cities pose a challenge to the scientific community to understand the urban environment and the consequent climatic changes. Recent studies on population growth and rapid urbanization suggest that about 55% of population lives in urban areas, which is further projected to be 68% by 2050 (UNDESAP, 2019). Based on the report, this increasing trend in population growth is significant in Asian and African countries with 90% of increase is constituted of these two continents. Urban population growth of state of odisha recorded as ~31%, which is almost equal to that of India (i.e 36%) as reported (BCDP, 2019). The city Bhubaneswar has grown its urban cover with 83% in fifteen years of time between 2000 to 2014 (Swain et al., 2017). On the other hand, there is a decreasing order of 89% and 83% of dense vegetation and crop field cover, respectively, according to their study. Considerable attention must be payed towards the effect of urbanization along with the land surface temperature. This led our study to focus on urban heat island identification, which is likely to act as one of the significant parameter to be taken into account for the urban development in terms of policy making for pollution mitigation and its consequent urban climatic changes.

Surface temperature levels are influenced by several factors such as land cover or land use change (Benjamin et al., 2012), surface albedo and emissivity of objects on land (Abdelmoneim et al., 2017) and green house effect. However, most of these factors and their influence perturb surface temperature in a long-run but not in short-run. Short-term living pollutants (i.e. aerosols) are identified as most challenging pollutants those change the atmospheric Earth's radiation balance, which survive in the atmosphere about a week. Aerosols are solid or liquid particles of size ranging between 0.01 to 100 μm in a air or gas medium. Aerosols play a significant role on temperature level changes in surface, canopy and boundary layer level.

Our study emphasizes much on role of air pollution on anomalies of surface urban heat island (SUHI) through analysing the interrelation between Land surface temperature (LST) and particulate matter pollution.

2. Methodology

2.1 Land surface temperature (LST)

Satellite observations of temperature over the surface of the land is obtained from Moderate Resolution Imaging Spectro-photometer (MODIS) satellite. Surface temperature in the atmosphere is considered as a salient property to analyse the urban heat island as it can be used as a proxy for the SUHI estimation. These observations for day and night time period were obtained from satellite measurements onset each day and captures the temperature at the surface at about 1km x 1 km resolution. Satellite retrieved temperature is evaluated using ground based observations of weather-underground research (airport based weather observation station) of Bhubaneswar city.

Winter episodic days included in this study: Julian day of 345 (11-12-2018) and 353 (19-12-2018) day in December; 1 (01-01-2019) and 17 (17-01-2019) day in January; 45 (14-02-2019) day in February. Whereas in spring the episodic days are as follows: Julian day of 73 (14-03-2019) in March and 105 (15-04-2019) day in April.

2.2 Surface concentration: Particulate matter (PM)

Continuous monitoring of particulate matter for the corresponding episodic days (as mentioned previously) was carried out at a geographical point in Kalinga institute of industrial technology Deemed to be university (KIIT-DU) during pollution episodes during winter and spring months. This was done using Envirotech made dust sampler measures the particulate matter of aerodynamic size less than or equal to 10 μm in an entire day at a height of 10 m above ground level (agl) for each sample collection.

3. Results and discussion

3.1 Surface urban heat lsland (SUHI)

Land surface temperature over the city or urban environment relative to the nearby rural locations are treated as surface urban heat island. It acts as a proxy for the SUHI estimations. Spatial distribution of LST exhibits a high gradient with a difference of 2-3 K in study domain [85.5-86E, 20-20.5N] as shown in Figure 2 (a) & 2 (b). On 11 December 2018, the LST over Khandagiri region depicts 300-307 K and 289-293 K for the day-time and night-time, respectively. Similar features were observed on 19 December 2018, 1 January 2019. These SUHI pattern is reasoned by accumulation of built-up area over the region followed by the low vegetation across the region. It is also supported by low emissivity (0.970) noticed over Khandagiri region compared to that of rest of the locations (0.98) with a difference of about 0.01 over Bhubaneswar. This shows the consistency with the normalized division of vegetation index (NDVI, which represents the amount of vegetation or green cover over the land) that obtained from MODIS-Aqua satellite estimates (refer Figure 3). The NDVI over city built-up environment shows 0.4-0.5 on each study day period.

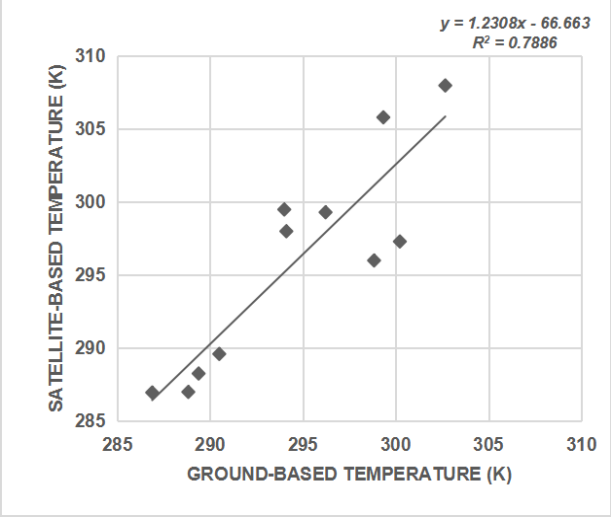


Figure 1. Correlation plot of land surface temperature (LST in Kelvin (K)) between satellite- and ground-based observations during study period (Winter and Spring) 2018-19 over Bhubaneswar.

3.2 Normalized deviation of vegetation index (NDVI)

Fractional difference of radiation between near infrared (NIR) and far infrared (FIR) can be defined as normalized deviation of vegetation index (NDVI).

$$NDVI = (NIR-FIR)/(NIR+FIR)$$

The NDVI over the forest areas of Chandaka region [85.6-87.85E, 20.2-20.25N] were noticed to be very high in all the seasons irrespective of spatio-temporal variation. Taking into account the spatial and temporal difference, relative difference of NDVI is considered to be an indicator of urban settlements. Many of urban-settlement regions study region are identified as built-up areas using land-use and land-cover change in Bhubaneswar. Relative difference of NDVI exhibits 0.2

to 0.4 between built-up area and forest green covered regions. This difference is lower in spring as compared to that in winter days as shown in figure 3. Reduction in green cover in city landscapes is likely to be the reason. However, the NDVI over water bodies and forest land regions are often less varying over the period of time.

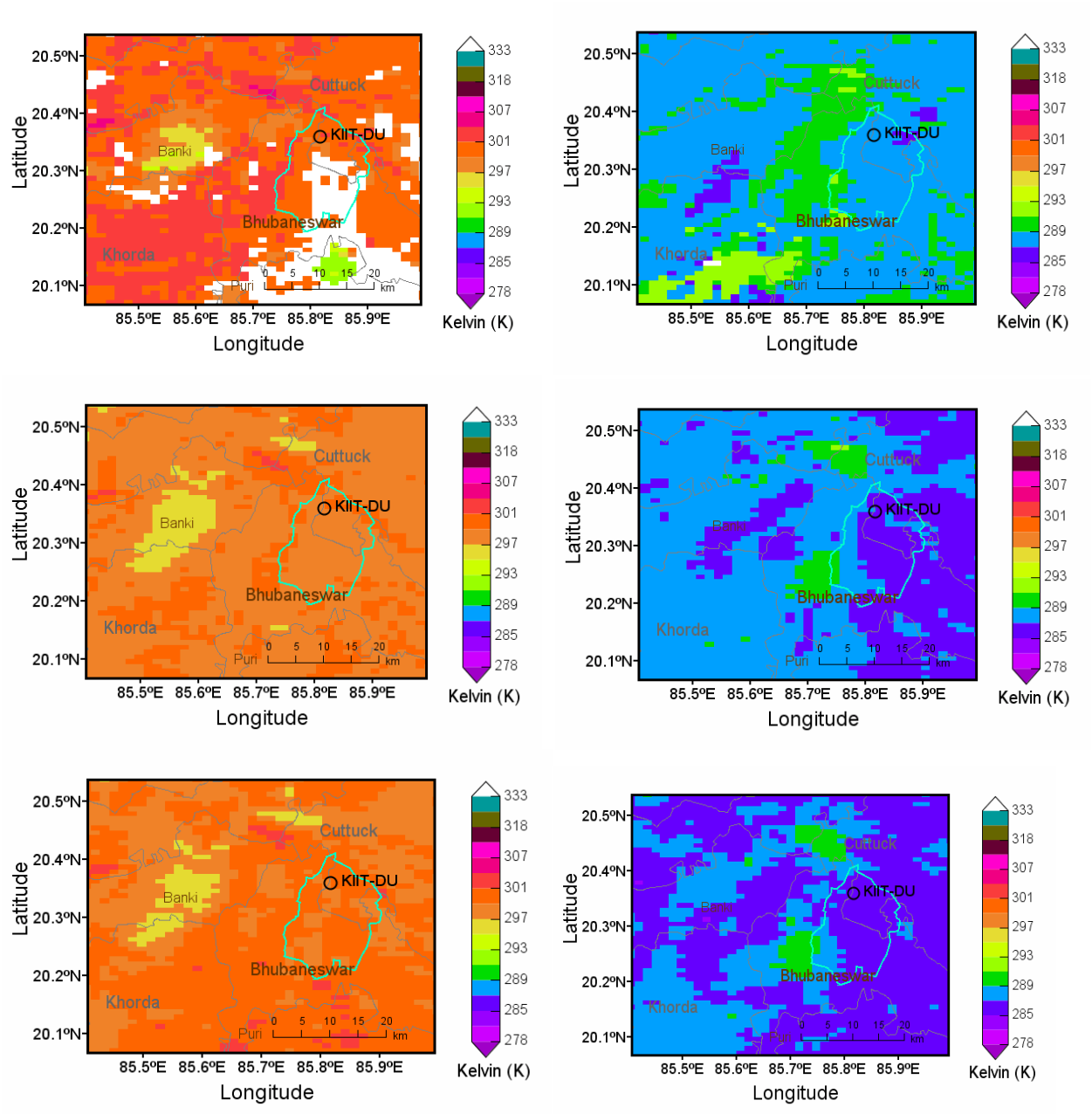
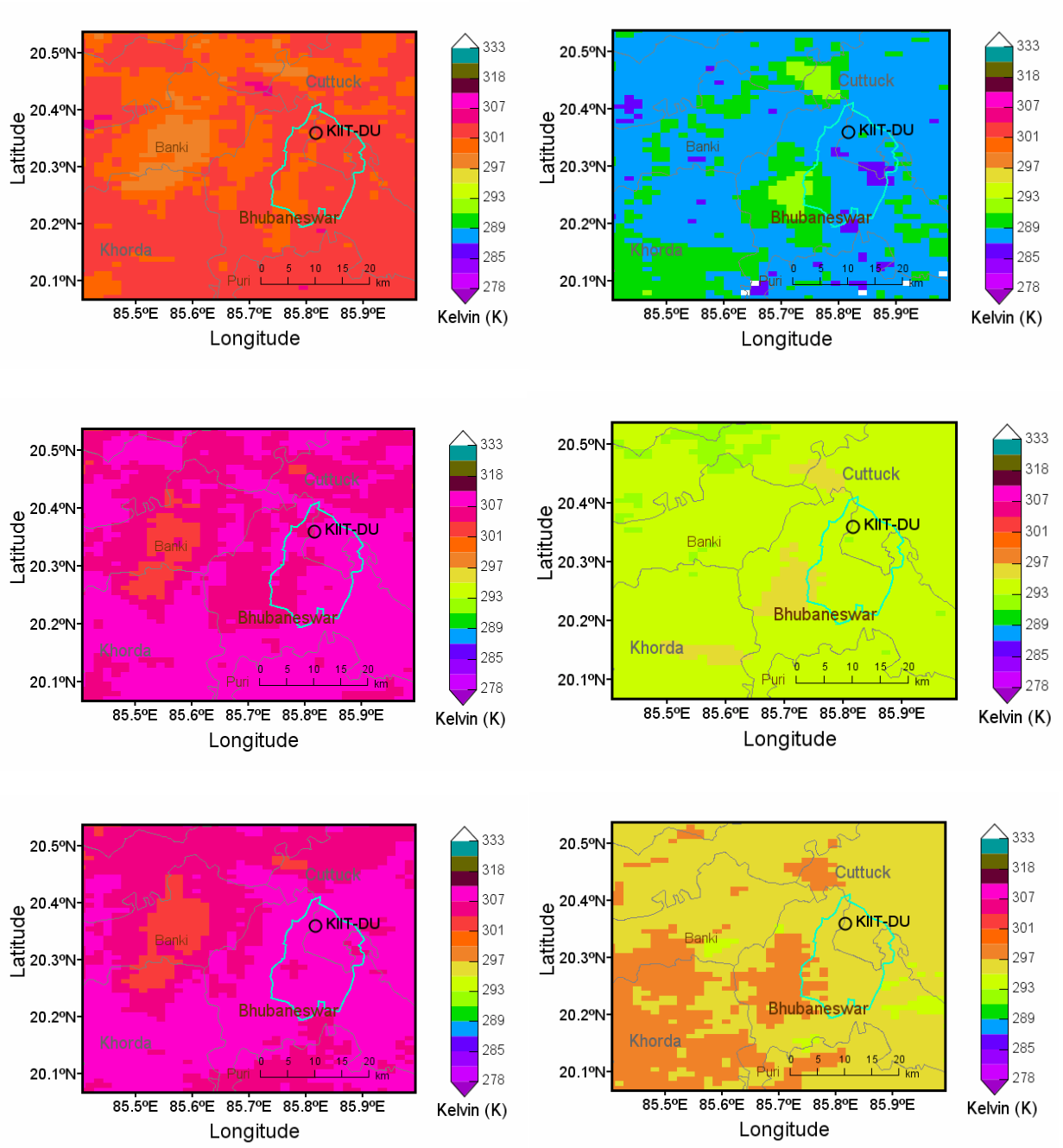


Figure 2(a). Ilustration of land surface temperature (LST, in Kelvin (K)) from MODIS satellite observations over Bhubaneswar Municipal corporation (BMC) as highlighted as a dotted hatch over the map approximately occupied area between 20.19-20.41˚N, 85.65-85.90˚E. Left panel depicts LST of daytime while right panel depicts nighttime LST for 345, 353 Julian day of 2018 and 001 Julian day of 2019.


Cuttuck
KIIT-DU
Banki
Bhubaneswar
Khorda
Puri
0 5 10 15 20 km
20.5ºN
20.4ºN
20.3ºN
20.2ºN
20.1ºN
Latitude
85.5ºE 85.6ºE 85.7ºE 85.8ºE 85.9ºE
Longitude
333
318
307
301
297
293
289
285
278
Kelvin (K)

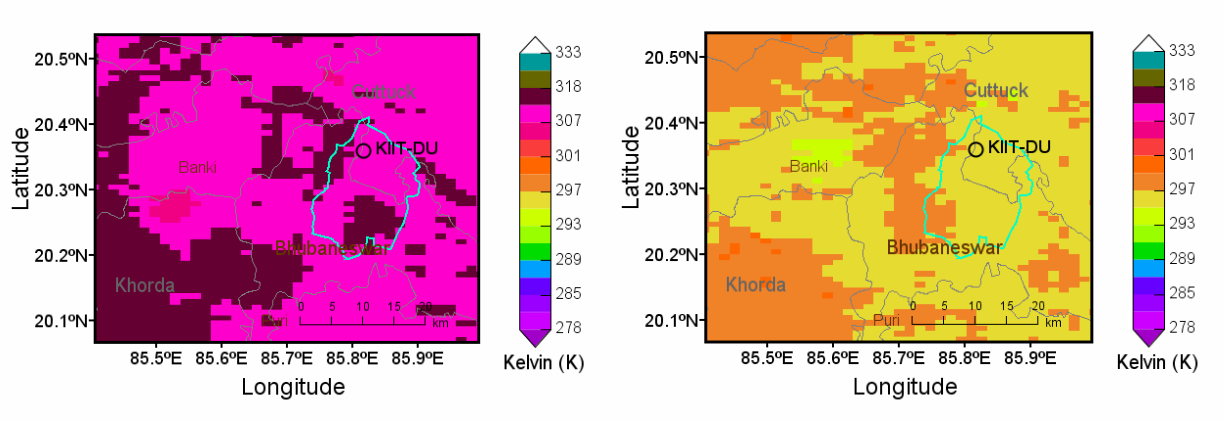


Figure 2(b). Same as figure 1(a), but for 017, 049, 073 and 107 Julian day of 2019.

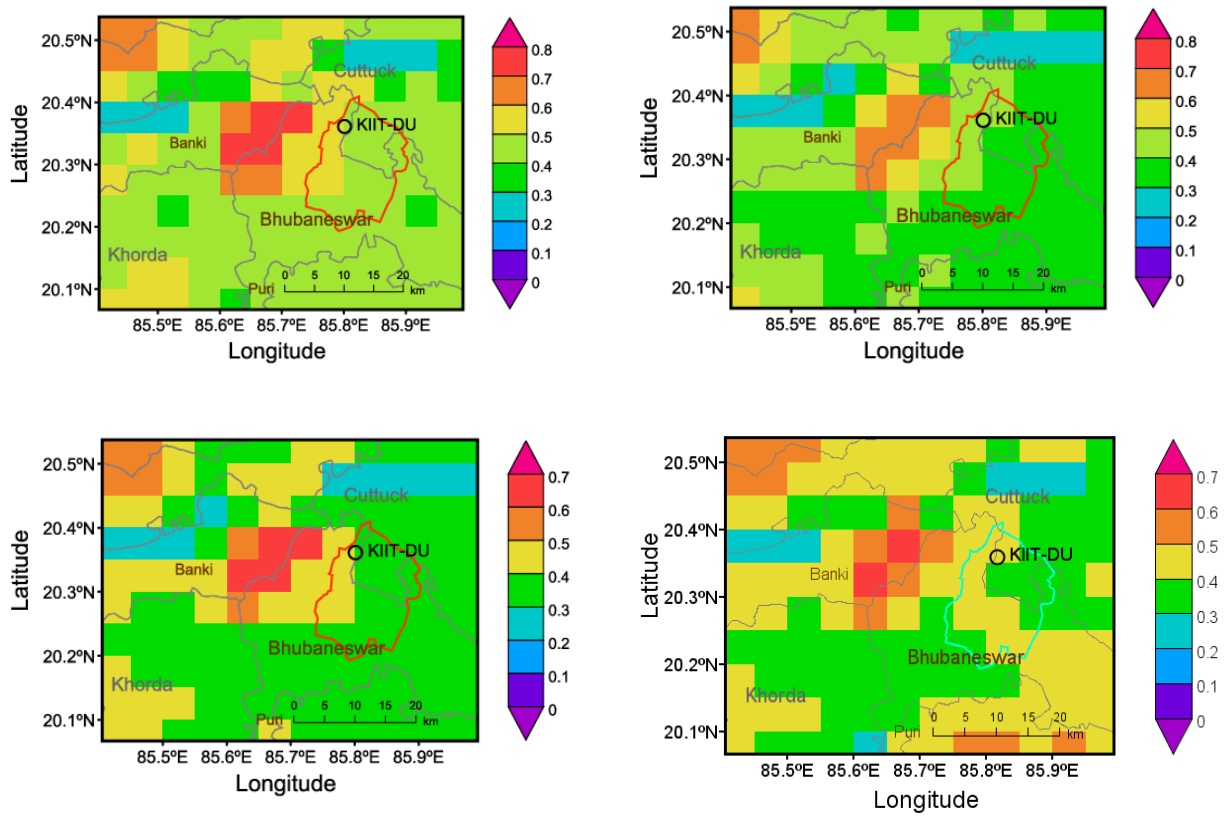


Figure 3. Normalized Deviation of Vegetation Index (NDVI, Unit less) for the corresponding months of winter monsoon season including November (Left-upper), December (Right-upper), January (Left-lower) and February (Right-lower) panels of the year 2018-19 over Bhubaneswar Municipal Corporation (BMC) (marker in red boundary).

3.3 Surface mass concentration

Seasonal variability of PM10 and total suspended particulate matter (TSP) in Bhubaneswar city during December 2018-April 2019 in terms of 24-hourly, daily and seasonal mean quantities are

as shown in Figure 4. Spring months (14 February, 14 March and 15 April, 2019)show high difference of concentration between TSP-PM_{10} compared to that of other months. It signifies the presence of dust in the atmosphere, though there is no prominent dust emission sources near the station. This is likely due to the inter-continental transport of dust from adjoining continental source regions.

Surface PM_{10} concentration exhibits relatively high during winter (11 and 19 December 2018, 1 and 17 January 2019) followed by spring season (Figure 4). Coarser size aerosols are predominantly present in the spring airmass, this was reasoned by the long range transport of dust (from desert or plain regions) originating from regional to continental region level. Fine aerosols dominates the airmass in winter due to the prevailing meteorology favors the emissions to accumulate in the lower boundary layer, particularly, at the surface level. In spring, slight increase of PM_{10} is observed as the biomass burning activities due to the action of crop-field burning emanating carbonaceous emissions escalates the pollution -burden and -transport in IGP and its adjoining outflow regions (e.g. Eastern India).

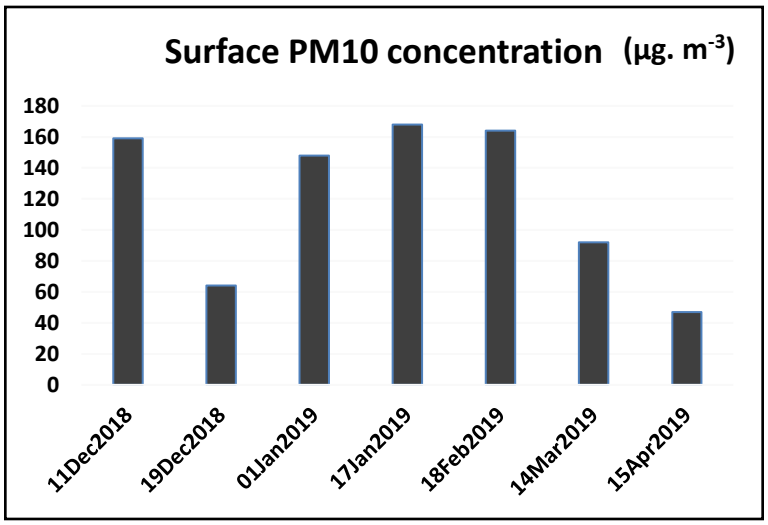


Figure 4. Bar plot of PM10 concentration (in µg. m^{-3}) for the days of ground-based observations over [85.81E, 20.35N] Kalinga Institute of Industrial Technology-Deemed to be University (KIIT-DU), Bhubaneswar in winter (December 2018-January 2019) and Spring (February-April 2019).

4. Conclusions

We conclude that difference of surface UHI (SUHI) between winter and spring days are well addressed by the land surface temperature of satellite data. The temperature data from satellite observations show consistent results as it exhibited a good correlation (R^2 =0.78) of land surface temperature (LST) and surface temperature over the surface level atmosphere over KIIT-DU station. The following conclusions were drawn from the present study are listed as below:

(i) The surface urban heat island (SUHI) was found over Khandagiri region as the LST over this region has 2-3 K higher than that from adjoining regions of Bhubaneswar. This was reasoned by high built-up area and low NDVI results.

(ii) Over the KIIT-DU region the SUHI shows low compared to that over Khandagiri region. Pollution measurements over KIIT-DU shows relatively high for the days of winter compared to that for spring days. Low boundary layer height followed by low convective transport of pollution air mass vertically in the atmosphere brings down temperature to lowest in winter at surface level. Though production of air pollution emissions from vehicular activities and resuspended dust in urban areas, high convective transport of pollution from surface to the elevated layers of atmosphere was noticed on the days of spring season (14 February and 14 March, 2019) results to have less cooling at the surface level. As a result, the LST in spring season is considerable compared to that in winter.

(iii) The normalized deviation of vegetation index (NDVI) analysis highlighted more on green cover, which represents the changes of land use and land cover over a landscape. Many of urban-settlements in Bhubaneswar were identified as built-up areas as per the land-use and land-cover change data. Relative difference of NDVI exhibits 0.2 to 0.4 between built-up area and forest green covered regions. However, the NDVI correlates well with the LST over Khandagiri and Chandaka region.

As a summary, present study highlighted about surface urban heat island (SUHI) identification on consistency of the LST, correlation of the NDVI with the LST and emissivity over two distinct land-scapes of Bhubaneswar region during winter and summer 2018-19. More studies on the UHI at canopy level, boundary layer level and surface level are needed to be carried out to evaluate significance of pollution, land-use and land-cover change and meteorolody on escalating heat over urban locations at local level and Earth's radiation budget at global level.

Acknowledgments

Dudam Bharath Kumar acknowledges Prof. Sukanya Das Gupta, School of Civil Engineering; Ms. Sushree Sashmita of School of Civil Engineering, Kalinga Institute of Industrial Technology-Deemed to be University (KIIT-DU), Bhubaneswar.

References

Abdelmoneim A. M., John O. and Onisimo M. (2017). Land surface temperature and emissivity estimation for Urban Heat Island assessment using medium- and low-resolution space-borne sensors: A review, Geocarto International, 32(2), 455-47. http://dx.doi.org/10.1080/10106049.2016.1155657

Benjamin B., Klemen Z. and Gholamali H. (2012). Downscaling Land Surface Temperature in an Urban Area: A Case Study for Hamburg, Germany, Remote Sensing, 4, 3184-3200. http://dx.doi.org/10.3390/rs4103184

Bhubaneswar City Developmet Plan (BCDP). (2019), City Development Plan, Bhubaneswar, Orissa, India, Final Report. 1-2. https://cdn.s3waas.gov.in/s35737034557ef5b8c02c0e46513b98f90/uploads/2018/05/2018050480.pdf

Swain D, Roberts GJ, Dash J, Lekshmi K, Vinoj V, Tripathy S (2017) Impact of rapid urbanization on the city of Bhubaneswar, India. Proc. Natl. Acad. Sci. India, Sect. A 87(4): 845-853. https://doi.org/10.1007/s40010-017-0453-7

United Nations, Department of Economic and Social Affairs, Population Division (UNDESAP) (2019). World Urbanization Prospects: The 2018 Revision (ST/ESA/SER.A/420). New York: United Nations

Land surface temperature variations: Case study Bhopal (MP)

Pallavi Tiwari
Architect | Urban Planner
School of Planning and Architecture, New Delhi
Arka Kanungo
Architect | Transport Planner
School of Planning and Architecture, New Delhi

Abstract
With the increasing urbanization the cities today are facing multiple urban risks. Rising temperatures within the city is one such risk that the city dwellers are exposed to. Not only is the temperature both air and surface an issue of concern, but also the varied distribution of this increase is a cause of many issues. The land surface temperature study is important to address and analyse the various impacts caused thereby. The land surface temperature is globally rising all across the world. The present study takes Bhopal in Madhya Pradesh as a case study to develop a framework for the estimation of land surface temperature. The temperatures have been compared for the month of June in year 2014 and 2019. Normalized vegetation index and land surface temperature data has been computed for the case study to analyse the area under various temperature ranges. Results have been drawn through a correlation of NDVI and LST and the impact of reduction in the area of upper lake.

Keywords: Urban Heat Island, Land surface temperature, LANDSAT 8, Microclimatic conditions, Climate Change, GIS, Global Warming

1. Introduction

The Earth's climate is changing, and it is evolving at a much rapid rate today with the advent of multiple urban risks that the cities are exposed to. The vulnerability of communities at large is globally increasing with every passing day. It is visibly affecting the environment with prominent changes and social issues pressed upon the society with the increased exposure.
The ice is melting, the sea is rising and the temperature is getting hotter day by day. To understand the global changes that occurring, one must realize the micro implication that are being faced by the population.
The cities are facing microclimatic changes which are more prominent than ever. Urban heat island which is defined as a metropolitan area being significantly warmer than its surrounding rural areas due to human activities. The phenomena is not limited to a boundary of "urban" and "rural" but has over the years and with the complicated intermix of activities and spaces in the urban centres, have transitioned to a more varied heat island distribution within an urban area itself.

Due to the ever-increasing pressure of built up areas encroaching over the liveable spaces within the cities, the microclimatic conditions have started to deteriorate at much higher rate than it did a decade ago, thereby creating urban heat island pockets inside the city boundaries making the harsh climate even more un-bearable.
In order to cope with the challenges of the changing climate, climate risk mitigation strategies and climate adaptation strategies should be incorporated in the urban centres at all levels (national,

state, city, community and individual) to prepare and adapt the urban development. This, however, is a challenge in itself considering the rigid nature of plans that are in place for cities today.

Land surface temperature is how hot the surface of the Earth would feel to the touch in a particular location. From a satellite's point of view, the surface is whatever it sees when it looks through the atmosphere to the ground. It could be snow and ice, the grass on a lawn, the roof of a building, or the leaves in the canopy of a forest.

Land surface temperature (LST) is defined by the International LST and Emissivity Working Group as a measure of how hot or cold the surface of the Earth would feel to the touch (*Comprehensive Remote Sensing, 2018*)

2. Research methodology

The methodology of research implementing the Technical paper broadly involves the following stages:

1. **Stage I:** This initial stage involves necessary background study associated with the literature analysis of the data available on the land surface temperature and the urban heat islands. Study of best practices were undertaken around the globe to foster the use of GIS based technology to calculate the land surface temperature using satellite data and establishing the relevance of the same in Indian context.
2. **Stage II:** This intermediate stage involves analysis of the data obtained from LANDSAT-8 for the case study area for various years. The stage involves the processing of the various bands of the image retrieved from USGS, while applying the various formulas for estimating first the land surface temperature and then the urban heat island intensity of the study area.
3. **Stage III:** This stage involves establishing the differences between the time frames and the percentages of the area under the urban heat island and analysing how the changes in the vegetation index impact the intensity of the urban heat island.
4. **Stage IV:** The final stage tries to establish the co relation between the vegetation index and the land surface temperature. A way forward is suggested in the paper to mitigate and offset the increasing land surface temperature.

3. Objectives of the Study

An attempt is made in the research paper to devise a generic methodology, which can be implemented in other urban areas to establish such relationship between the vegetation intensity of a city and the urban heat islands within the city. The Research also tries to establish the mitigating measures to be implemented at spatial planning stages of such urban areas to counter the increasing the temperature through suitable systems in place.

4. Approach for Estimation of land surface temperature

The calculation of the land surface temperature is done using the data from LANDSAT 8 retrieved from USGS earth explorer. The Land Surface Temperature can be estimated or calculated using the Landsat 8 thermal bands with the following formulas:

i. **TOA (Top of Atmospheric) spectral radiance**

$$\mathbf{TOA\ (L) = M_L * Q_{cal} + A_L}$$

where:
ML = Band-specific multiplicative rescaling factor from the metadata (Radiance_Mult_Band_x, where x is the band number).
Q_{cal} = corresponds to band 10.
AL = Band-specific additive rescaling factor from the metadata (Radiance_Add_Band_x, where x is the band number).

ii. **TOA to Brightness Temperature conversion**

$$\mathbf{BT = (K2 / (\ln (K1 / L) + 1)) - 273.15}$$

where:
K1 = Band-specific thermal conversion constant from the metadata (K1_Constant_Band_x, where x is the thermal band number).
K2 = Band-specific thermal conversion constant from the metadata (K2_Constant_Band_x, where x is the thermal band number).
L = TOA

iii. **Calculate the NDVI**

$$\mathbf{NDVI = (Band\ 5 - Band\ 4) / (Band\ 5 + Band\ 4)}$$

iv. **Calculate the proportion of vegetation Pv**

$$\mathbf{P_v = Square\ ((NDVI - NDVI_{min}) / (NDVI_{max} - NDVI_{min}))}$$

v. **Calculate Emissivity ε**

$$\mathbf{\varepsilon = 0.004 * P_v + 0.986}$$

vi. **Calculate the Land Surface Temperature**

$$\mathbf{LST = (BT / (1 + (0.00115 * BT / 1.4388) * Ln(\varepsilon)))}$$

vii. **Calculation of urban heat island intensity**

$$\mathbf{\mathit{UHI} = \mu + \sigma / 2}$$

in which μ is the mean LST value of the study area, and σ is the standard deviation of the LST.

5. Case study area

Bhopal is the capital of the central state of Madhya Pradesh and the administrative headquarters of Bhopal District. Bhopal is known as the City of Lakes for its various natural as well as artificial lakes. It is one of the greenest cities in India. It is the 17th largest city in the country and the 131st in the world. Bhopal has

been selected as one of the cities to be developed as a smart city under the Smart Cities Mission. It houses various institutions of national importance, including ISRO's Master Control Facility and BHEL.The city acts as a nodal center of trade and commerce of regional importance. Furthermore, the city being relatively well-provided with various services and facilities, acts as a major service center for the region.

Bhopal District has a population of 23.7 lakh with an area of 2772 $km^{2.}$ The district is divided into 2 parts, Berasia and Huzur subdistrict. Bhopal sub district (Huzur) has a population of 21.1 lakh with an area of 1345 km^2Out of the total Huzur tehsil the population of the Bhopal municipal corporation is 17.98 lakh with an area of 422 km^2. And the population of the rest of tehsil is around 3.09 lakh.



Figure 1 Location of Bhopal (Madhya Pradesh, India)

6. Results

NDVI or the normalized vegetative index of Bhopal was computed from the Band 5 and Band 4 of the Landsat 8 data retrieved from USGS Earth explorer for 2014 and 2019 for the month of June. In June 2014 NDVI values ranged from -0.049 to 0.48 whereas the range is -0.0445 to 0.428 in 2019. The NDVI value is an indication of the vegetation in the area. A higher value of the NDVI represents healthy dense vegetation whereas a low value of the NDVI value represents less to no vegetation in the area.

The comparison of both the NDVI value ranges and the area extent under each value suggests that the area under the healthy dense vegetation has decreased from 2014 to 2019 by 22%. Also the area under water body category has reduced by 24%. The changes in such land cover categories can be attributed to the significant increase in the built up area in the city. The development is observed to be significantly higher in the peri urban areas I.e area outside the city municipal corporation boundary thus a higher variation is observed in the reduction ofthe vegetation in this area. The map shows the highest change in the NDVI is near the upper lake of Bhopal, indicating reduction in water.

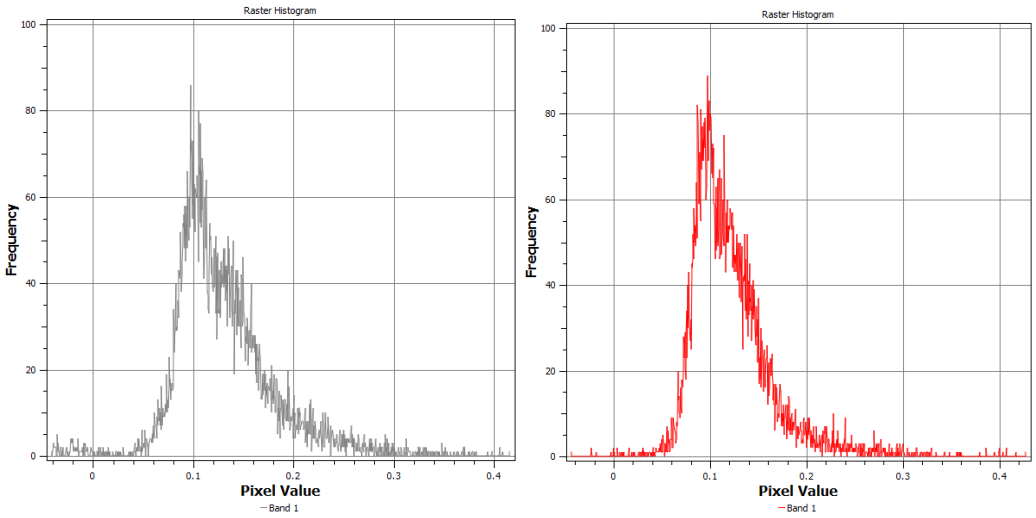


Figure 2 Left: NDVI distribution in 2014 Right: NDVI distribution in 2019
Source: Author

Subsequently the change in the land surface temperature were studied and a similar pattern of higher land surface temperatures was observed in the peri urban areas of the city. The Highest LST in Bhopal in June 2014 was of 39.81 deg C and in 2019 the highest lst increased to 46.62 deg c, a difference of 6.81 deg C in the highest LST. The lowest LST in june 2014 was 28.62 deg C whereas it increased in 2019 to 38.53 deg C indicating a difference of 9.91 deg C. Impact of the water body can be seen on the LST of Bhopal in both 2014 as well as 2019. The periphery of the planning area is having higher temperature due to sparse vegetation (indicated by the NDVI maps). The core city has a lower temperature due to the presence of upper lake.

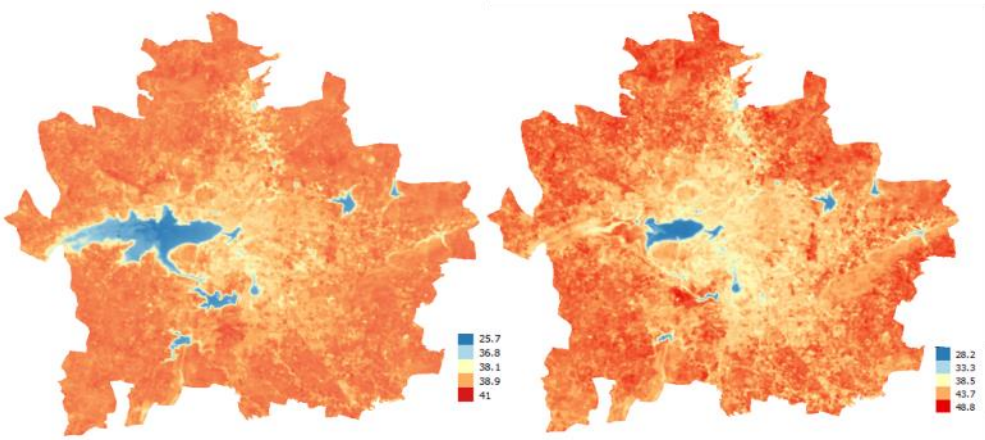


Figure 3 Left: LST in 2014 Right: LST in 2019
Source: Author



Figure 4 Land surface temperature variation across the city in 2014 (in blue) and 2019 (in red)
Source: Author

The cross section of the surface temperature profile of the city shows that the surface temperature is the lowest in the inner parts of the city due to the presence of water bodies. The temperature is highest in the barren lands.

Table 1 Area under each land surface temperature range (Source: Author)

Land surface temperature in ^{0}C (2014)	**Percentage of land (2014)**	**Land surface temperature in ^{0}C (2019)**	**Percentage of land (2019)**
28.62	10.22	29.5	3.7
31.42	1.1	34.2	1.08
34.21	7.8	38.9	16
37.01	27.3	43.6	76
39.81	53.5	48.3	2.7

The above table shows the range of land surface temperature in the city with the percentage of land having a specific temperature. It was observed that only 10.2% of the area in the municipal corporation boundary of bhopal has the lowest land surface temperature whereas 53.5% of the area has the maximum surface temperature in the city. Similar analyses was done for the year 2019 and it was found that only 3.7% area in the city has the lowest land surface temperature of 29.5 deg c whereas76% of the total area has a lst of 43.6 deg c and about 2.7% area has the highest temperature of 48.3 deg c. In 2019 55% of the land has the temperature range in the Urban Heat Island intensity range.

The variation around the upper lake was observed to be maximum in the month of June (peak summer season). The satellite imagery of the upper lake area was compared for the 10 june 2014 and 10 june 2019 in order to investigate the change in the extent and area of the water body. A reduction of 33% was observed during this period in the area of the lake.



Figure 5 Reduction in the upper lake area Left: June 2014 Right: June 2019
Source: Satellite Imagery

The land surface temperature was analysed at the cross sections of the upper lake. And it was observed that around the water body the surface temperatures were significantly lower than the surroundings. An average dip of 11.38 deg C in the land surface temperature was observed in 2014 whereas a dip of 13.68 deg c was observed in 2019.

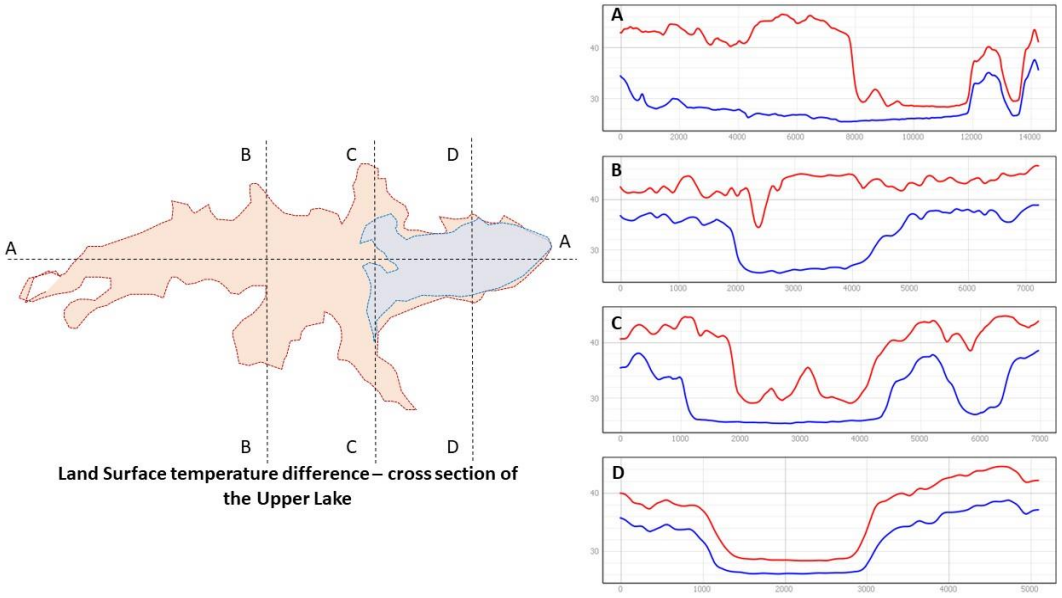


Figure 6 LST distribution across cross-sections
Source: Author

The cross-section study shows that as the distance from the water body increases, the land surface temperature increases. The water body reduction has a direct impact on the surface temperature of the surrounding areas. The temperature range has significantly risen due to reduction in the area of upper lake.

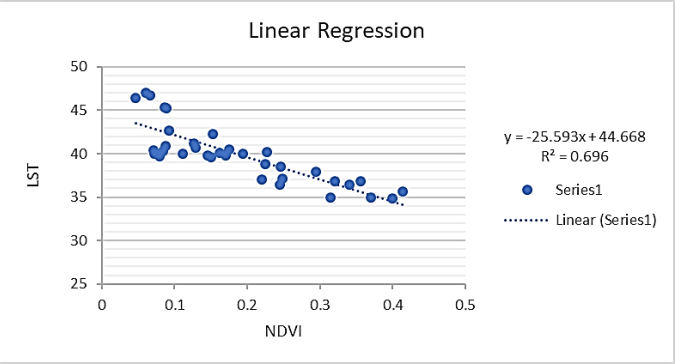
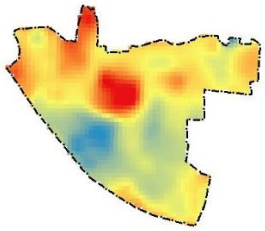
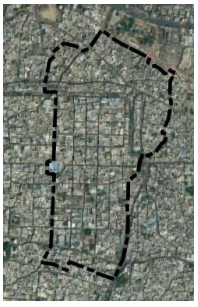
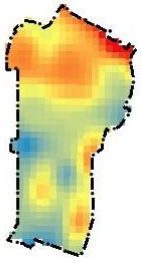
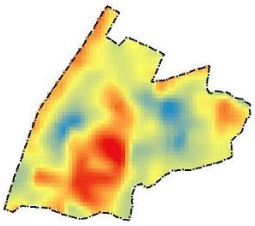
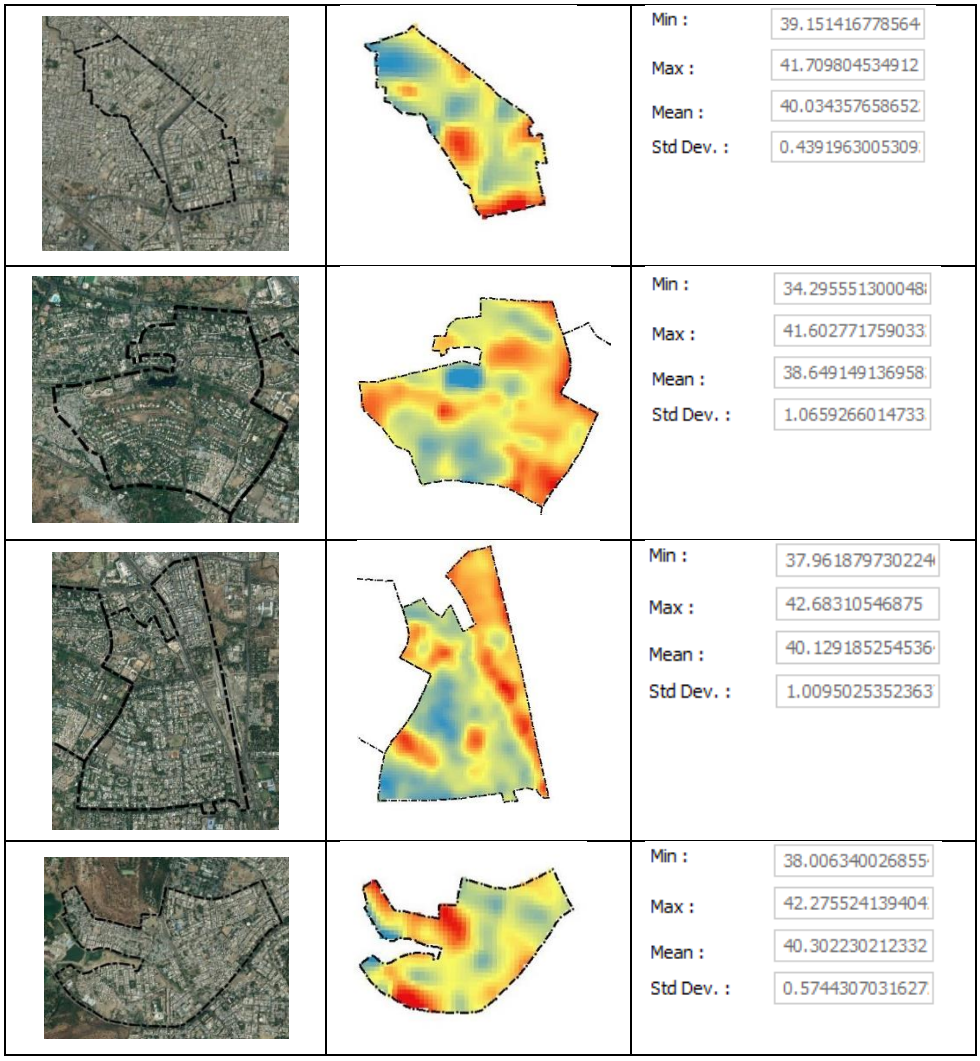


Figure 7 Linear regression of LST and NDVI (Bhopal 2019)
Source: Author

The above figure shows the strong negative correlation between the LST and the NDVI values. R square value of 0.696 is observed while establishing a linear regression between LST and NDVI which means the lower the NDVI value (apart from when the land cover is water) the higher the surface temperature and the higher the NDVI value or more the vegetation, the lower the land surface temperature in the area. Many areas with built-up area in the New Bhopal area show a lower surface temperature because of extensive roadside vegetations, neighborhood parks and green areas. Based on the above results, 7 wards land surface temperature data were extracted, to study the applicability of the procedure at ward level.

Table 2 Land surface temperature (Ward level)

Ward Google Imagery	Ward LST	Ward LST Details
		Min : 36.853515625 Max : 43.193862915039 Mean : 39.751423104643 Std Dev. : 1.0770747440295
		Min : 39.510990142822 Max : 41.574016571044 Mean : 40.272219041771 Std Dev. : 0.3540140703135
		Min : 37.185962677001 Max : 43.275787353515 Mean : 40.130275343481 Std Dev. : 1.1086464154171



Source: Author

7. Conclusion

The results of the study indicate that greens along the road and at local level are very crucial in reducing the land surface temperatures. The dense built-up areas in the old Bhopal lack green spaces both as parks as well as roadside plantation and thus experience higher land surface temperatures. The crop lands within the boundary also show higher temperatures, thus tree plantation in the boundaries of crop lands is suggested to lower the temperatures in the peri urban areas of the city. The difference in the temperatures in last five years are maximum in the hinterlands because of the extensive construction in the sprawling city and the increasing distance of the development from the water bodies. Water bodies can be planned in specific locations to maintain the microclimate of the city. Local level strategies specific to the land cover and land use of the local areas (wards) should be made to bring down the land surface temperatures and the subsequent urban heat island intensities in wards.

8. Way Forward

The findings of the research study establishes the importance of extraction of data at city level and at ward level. Presently there is a huge data gap. City level information is available only through published research work, state level information however is available at multiple portals. There is a requirement of city level data spatially understand the implications of human activities, physical conditions and the thermal conditions. The authors of the paper are working on a proposal to build a web portal and mobile app, which would have updated spatial information about cities urban heat islands. This application would show the cities microclimatic conditions and how it has been changing and by what rate or degree. The portal would also indicate remedial measures and their outcomes if implemented (i.e if tree plantation is done in an area how much would it affect the land surface temperature or if a water body is introduced what would be the impact).

References

Javed Mallick, Y. K. (2008). Estimation of land surface temperature over Delhi usingLandsat-7 ETM+. *J. Ind. Geophys. Union* , 131-140.

Jeevalakshmi. D, D. S. (2017). Land Surface Temperature Retrieval from LANDSAT data using Emissivity Estimation. *International Journal of Applied Engineering Research*, 9679-9687.

Ramachandra T. V., B. H. (2012). Land Surface Temperature Analysis in an Urbanising Landscape through MultiResolution Data. *Journal of Space Science & Technology*, 1-10.

S.B. Ali, S. P. (2017). Microclimate land surface temperatures across urban land use/land cover forms. *Global J. Environ. Sci. Manage*, 231-242.

Sun, Y. (n.d.). Retrieval and Application of Land Surface Temperature.

Ugur Avdan, G. J. (2016). Algorithm for Automated Mapping of Land Surface Temperature Using LANDSAT 8 Satellite Data. *Journal of Sensors*.

Patnaik, S; Ali, S.B., 2018. Parks and Gardens of Bhopal: Development and attributes of urban green space in the city, Urban India 37(2).

Ali, S.B.; Patnaik, S., 2017. Thermal comfort in urban open spaces: Objective assessment and subjective perception study in tropical city of Bhopal, India, Urban Climate.

Evaluation of sleep disorder caused by urban heat island based on the Pittsburgh Sleep Quality Index

Tomohiko Ihara[1]*, The University of Tokyo (Japan)*
Daisuke Narumi, Yokohama National University (Japan)
Sanae Fukuda, Kansai University of Welfare Sciences (Japan)
Hiroaki Kondo, Japan Weather Association (Japan)

ABSTRACT

Climate change directly affects the human body. When exposed to the heat, there is a possibility that sleep is disturbed. Several epidemiological studies have clarified the relationship between outdoor temperature and sleep disturbance. However, the damage of heat-related sleep disturbance has not been shown as numerical values comparable with other heat-related health outcomes. A self-administered questionnaire for daily sleep quality, the revised Sleep Quality Index for Daily Sleep (SQIDS2) was developed for assessing daily sleep disturbance by referring and simplifying Pittsburgh Sleep Quality Index (PSQI). The study conducted in Nagoya city in August of 2011 and 2012. The participants' sleep quality was measured by SQIDS2. The number of the respondents was 574 for 2011 survey and 710 for 2012 survey. Sleep disturbance prevalence calculated from SQIDS2 score was correlated to daily minimum temperature ($p=0.0067$) and increased when daily minimum temperature was above 24.8 °C. DALY loss due to heat-related sleep disturbance of Nagoya city (population: 2,266,851) was estimated to 97.4 years in 2012. This value was comparable to DALY loss due to heat stroke death there. Policymakers should recognize that the damage of sleep disturbance caused by nighttime high temperature is not small. Additionally, if they create a goal or regulation for nighttime temperature, daily minimum temperature of 25 °C would be a guide.

Introduction

Climate change directly affects the human body. When exposed to the heat, the human body increases the skin blood volume and perspiration volume to promote heat dissipation. If the heat dissipation is insufficient, the deep body temperature rises and becomes heat stroke. Both sleep and body temperature have a circadian rhythm, sleep tends to occur when the body temperature falls, sleep ends in the rising period. If the ambient temperature is not appropriate, sleep is disturbed. World Health Organization (WHO) (2014) suggests that the impact of future climate change on direct heat is greater than indirect influences such as dengue and malaria. However, sleep disturbance is not included in direct heat here.

Several epidemiological studies have clarified the relationship between outdoor temperature and sleep disturbance (Rifkin, Long, and Perry 2018). Nastos and Matzarakis (2008) found that the emergency cases of sleep disturbance correlated with daily minimum temperature. Obradovich et al (2017) quantified the relationship between insufficient sleep and daily minimum temperature and estimated increase in sleep disturbance by future climate change. van Loenhout et al (2016) found that sleep disturbance increased with 11% for an increase of 1 °C of

[1] Corresponding Author: ihara-t@k.u-tokyo.ac.jp, +81-4-7136-4722.

outdoor temperature. Näyhä et al (2014) found that 32.4% of the residents felt sleep disturbance for hot weather. Quante et al (2017) clarified the relationship between temperature and sleep duration from the measurement with accelerometers. However, the numerical values shown in these studies cannot be compared with deaths by direct heat shown in WHO. Therefore, the society does not understand importance of sleep disturbance by climate change.

In order to compare with other climate change-driven diseases, it is necessary to quantify damage of sleep disturbance caused by temperature rise with a general health metric, which is disability-adjusted life year (DALY). This study aims at quantifying loss of DALY by sleep disturbance caused by temperature rise. It also compares the loss of sleep disturbance with loss of heat stroke.

Methods

Study Design

One of methods to assess sleep disturbance with DALY is use of Pittsburgh Sleep Quality Index (PSQI) (Buysse et al 1988, Doi et al 1998). PSQI is a widely used standardized measure to assess subjective quality and generates a global score. The previous studies have showed that use of a cut-off point of 5.5 in the PSQI global score provides high estimation on whether or not sleep disorder (Buysse et al 1988, Doi et al 2000). We can calculate DALY of sleep disturbance by multiplying the prevalence of sleep disturbance by PSQI, disability weight of sleep disturbance (Fukuda et al 2013), and duration of sleep disturbance.

However, PSQI asks sleep quality for the past one month, which cannot be correlated to daily temperature. In order to correlate daily temperature for quantifying, we had already developed a self-administered questionnaire for daily sleep quality, Sleep Quality Index for Daily Sleep (SQIDS) (Okano, Ihara, and Genchi 2008) by referring and simplifying PSQI. The question items of original SQIDS did not coincide with PSQI in order to reduce the number of questions. In this study, SQIDS was revised to almost follow the question items of PSQI (hereafter, revised SQIDS is called SQIDS2) (see Appendix). By using SQIDS, we can assess the relationship between daily prevalence of sleep disturbance by SQIDS and daily temperature. Furthermore, we can quantify the impact on sleep disturbance by temperature increase with DALY for comparing other illnesses.

Participants

We set Nagoya city, the central city of the third metropolitan area in Japan, as our survey area. Nagoya city has been exposed to the heat due to global climate change and urban heat island. The outdoor temperature of Nagoya city raised by 2.9 ℃ in 100 years (Japan Meteorological Agency 2019). The number of days on which temperature is more than 35 ℃ of recent years has reached about 30 days.

We used the survey company (INTAGE Research Inc., Tokyo, Japan)’s panel to select a panel of individuals for our study, considering ensuring various participants living in the city and possibility to get the responses to our survey continuously for long period. Online survey in Nagoya city was considered to represent Nagoya citizens because average Internet personal penetration rate in Japan was 79.1% in 2011 and that of urban area including Nagoya city was higher than that of rural area (Ministry of Internal Affairs and Communications 2019). Each monitor is an adult and registers not via online ads, etc. but the company’s banner. They are for

survey only and not used for ad delivery, direct mail, etc. Recruitment from the company's panel was done by the following conditions; living in Nagoya city, not traveling during the survey period, and owing thermometer which can measure the room temperature. We aimed to extract more than 550 monitors. Additionally, the age and sex structure of the extracted monitors was set to be the same as those of the residents as possible.

Online questionnaire survey was done during August 2nd to 11th (10 consecutive days) of 2011 and July 31st to August 16th (9 days of Tuesday, Wednesday, and Thursday of 3 consecutive weeks) of 2012 in Nagoya city. We asked the respondent's attribute (age, sex, etc.) on the first survey day. Then, we asked SQIDS every survey day.

We used observed data of one Japan Meteorological Agency's observation site and four air pollution monitoring sites by the Ministry of the Environment of Japan for the outdoor temperature data. Nagoya city is divided to sixteen wards (Figure 1). The outdoor temperature around each respondent was assumed to be the temperature at the observation site closet to the center of population of the ward where they live.

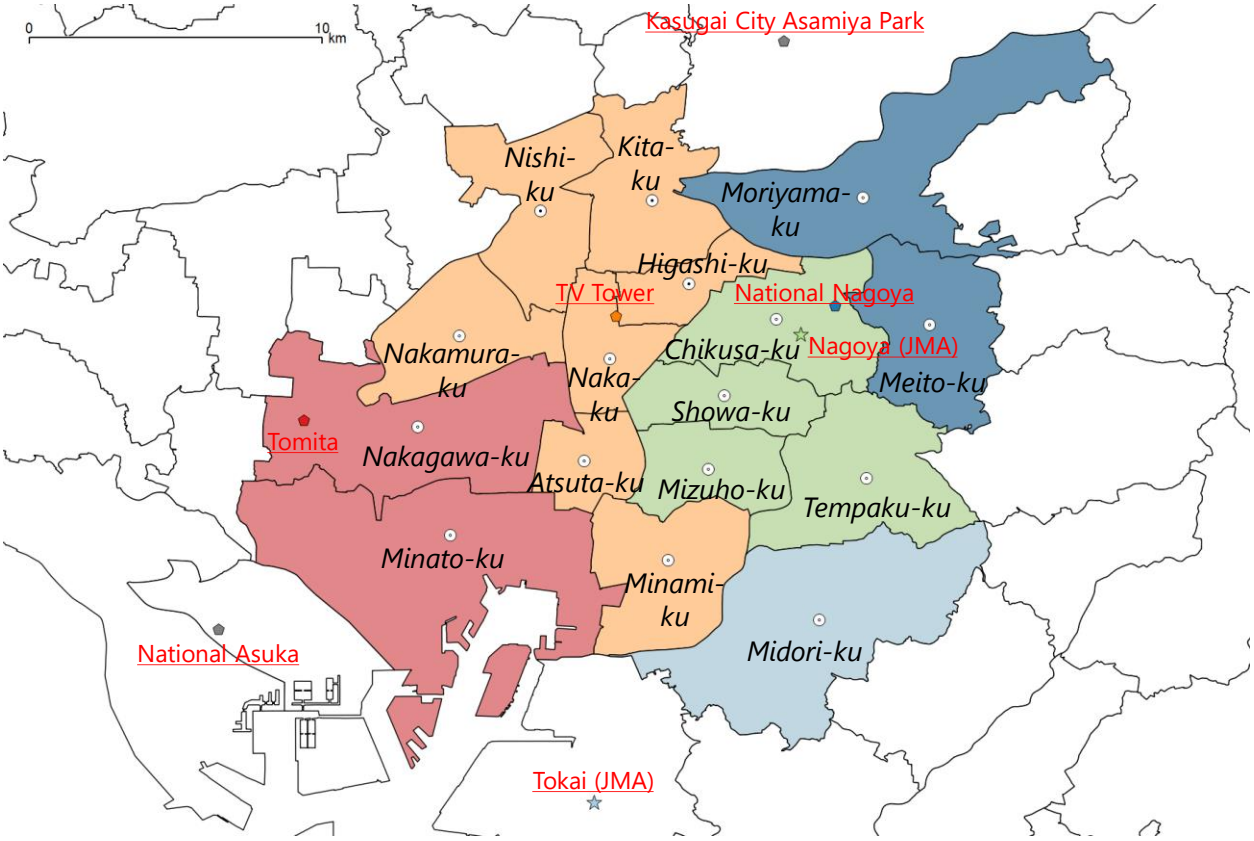


Figure 1. Nagoya city and temperature observation sites. The sites (JMA) are by Japan Meteorological Agency, and other sites are by the Ministry of the Environment. Temperature data for each resident refer to the temperature observation site colored with the same colored district where they live.

The ethics committee of National Institute of Advanced Industrial Science and Technology approved our survey (No. 2010-268).

Data analysis

SQIDS global scores for 19 days were calculated. The daily sleep disturbance prevalence was calculated by judging that the respondents who had global score of 5.5 or more suffered from sleep disturbance based on the cut-off point in the PSQI global score (Buysse et al 1988, Doi et al 2000).

Then, a generalized linear model was performed for showing the relationship between daily outdoor air temperature *temp* and sleep disturbance prevalence *sd* estimated by SQIDS using R version 3.5.3. The binomial distribution was assumed and the smoothed spline regression was applied.

$$sd \sim s(temp) \quad (1)$$

Then, we calculated DALY by using the disability weight of sleep disturbance.

Results

The number of the respondents was 574 for 2011 survey and 710 for 2012 survey. The age and sex structure of the respondents is shown in Table 1. The number of the respondents who is 70 or over is small. It is considered to be due to low Internet penetration of aged people. Except 70 or over, the age and sex structure of the respondents was close to that of the population in Nagoya city.

Table 1. Age and sex structure of the respondents

		20s	30s	40s	50s	60s	70 or more
2011 survey	M	42 (7.3%)	52 (9.1%)	69 (12.0%)	61 (10.6%)	46 (8.0%)	12 (2.1%)
	F	62 (10.8%)	63 (11.0%)	71 (12.4%)	56 (9.8%)	37 (6.4%)	3 (0.5%)
2012 survey	M	51 (7.2%)	86 (12.1%)	76 (10.7%)	72 (10.1%)	57 (8.0%)	15 (2.1%)
	F	65 (9.2%)	72 (10.1%)	69 (9.7%)	99 (13.9%)	37 (5.2%)	11 (1.5%)
2010 population census	M	- (7.6%)	- (9.5%)	- (8.8%)	- (7.3%)	- (8.1%)	- (7.4%)
	F	- (7.3%)	- (9.2%)	- (8.4%)	- (7.1%)	- (8.4%)	- (10.7%)

M indicates male and F indicates female. *Source*: Ministry of Internal Affairs and Communications (2011) for 2010 population census.

The valid response rate was 100% because they were from the online survey company's panel and the company asked to respond when they did not make any responses.

The relationship between daily minimum temperature and sleep disturbance prevalence calculated from SQIDS2 scores was analyzed (Figure 2). Sleep disturbance prevalence calculated from SQIDS2 was correlated to daily minimum temperature (p=0.0067) and increased when daily minimum temperature was above 24.8 °C. Hereafter, excess sleep disturbance prevalence of the day when daily minimum temperature is over the optimum temperature (24.8 °C) is defined as heat-related sleep disturbance prevalence.

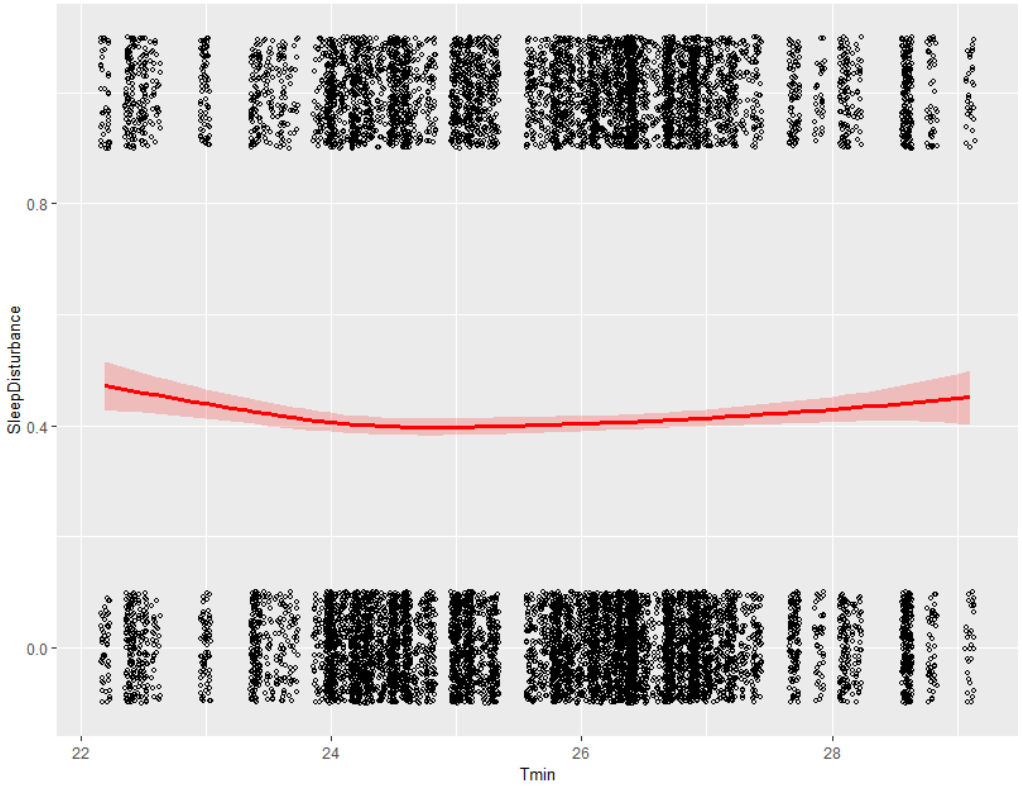


Figure 2. Relationship between daily minimum temperature (Tmin) [°C] and sleep disturbance prevalence (SleepDisturbance). The red line shows the smoothed-spline regression result by the generalized linear model based on binomial distribution. The light red region shows a 95% confidence interval.

The population of Nagoya city was 2,266,851 in 2012 (Nagoya City 2019). The annual total number of those who suffer from heat-related sleep disturbance based on SQIDS2 was estimated to 355,000 by using daily minimum temperature of each day in 2012 and the regression model. The disability weight of sleep disturbance is 0.1 (Fukuda et al 2013), and the duration of sleep disturbance can be set to 1 day (because those prevalence is counted every day). Therefore, DALY loss due to heat-related sleep disturbance of Nagoya city was estimated to 97.4 years in 2012.

Discussion

Heat stroke death is remarkable as heat-related health damage. Five people died due to heat stroke and their DALY is calculated to 63.54 years in Nagoya of 2012 when using the vital table of Nagoya city. In the five-year average from 2010 to 2014, there were seven deaths due to heat stroke and its DALY is 92.66 years. DALY loss due to heat-related sleep disturbance was calculated to 97.4 years in Nagoya of 2012. Sleep disturbance is not focused in the society. However, the damage of sleep disturbance is comparable to that of heat stroke death.

Policymakers should recognize that the damage of sleep disturbance caused by nighttime high temperature is not small. Additionally, if they create a goal or regulation for nighttime temperature, daily minimum temperature of 25 °C would be a guide.

Acknowledgments

This study was supported by JSPS KAKENHI Grant Number 23360437, Grant-in-Aid for Scientific Research (B), the Research Program on Climate Change Adaptation (Research representative: Satoru Iizuka) of the Ministry of Education, Culture, Sports, Science and Technology, and the Environment Research and Technology Development Fund (S-14) of the Environmental Restoration and Conservation Agency of Japan.

References

Buysse, D. J., Reynold III, C. F., Monk, T. H., Berman, S. R., Kupfer, D. J., (1988). The Pittsburgh Sleep Quality Index: a new instrument for psychiatric practice and research, Psychiatry Research, 28 (2), 193–213. https://doi.org/10.1016/0165-1781(89)90047-4

Doi, Y., Minowa, M., Okawa, M., Uchiyama, M. (1998). Development of the Japanese version of the Pittsburgh Sleep Quality Index. Japanese Journal of Psychiatry Treatment. 13 (6), 755–763.

Doi, Y., Minowa, M., Uchiyama, M., Okawa, M., Kim, K., Shibui, K., Kamei, Y. (2000). Psychometric assessment of subjective sleep quality using the Japanese version of the Pittsburgh Sleep Quality Index (PSQI-J) in psychiatric disordered and control subjects. Psychiatry Research, 97, 165–172. https://doi.org/10.1016/s0165-1781(00)00232-8

Fukuda, S., Ihara, T., Genchi, Y., Narumi, D. (2013). Japanese sleep disturbance and fatigue disability weights in evaluating the effects of increasing temperatures on health by a life cycle approach. International Journal of Life Cycle Assessment, 18 (5), 1089–1097. http://dx.doi.org/10.1007/s11367-013-0551-y

Japan Meteorological Agency. (2019). How much does temperature in cities raise? https://www.data.jma.go.jp/cpdinfo/himr_faq/04/qa.html

Ministry of Internal Affairs and Communications. (2011). 2010 National Census. https://www.stat.go.jp/data/kokusei/2010/

Ministry of Internal Affairs and Communications. (2019). Communications Usage Trend Survey. http://www.soumu.go.jp/johotsusintokei/statistics/statistics05.html

Nagoya City. (2019). Statistics Nagoya web edition. http://www.city.nagoya.jp/shisei/category/67-5-0-0-0-0-0-0-0-0.html

Nastos, P. T., Matzarakis, A. (2008). Human-biometeorological effects on sleep disturbances in Athens, Greece: A preliminary evaluation. Indoor Built Environment, 17 (6), 535–542. https://doi.org/10.1177/1420326X08097706

Näyhä, S., Rintamäki, H., Donaldson, G., Hassi, J., Laatikainen, P. J. T., Jaakkola, J. J. K., Ikäheimo, T. M. (2014). Heat-related thermal sensation, comfort and symptoms in a northern population: the National FINRISK 2007 study. European Journal of Public Health, 24 (4), 620–626. https://doi.org/10.1093/eurpub/ckt159

Obradovich, N., Migliorini, R., Mednick, S. C., Fowler, J. H. (2017). Nighttime temperature and human sleep loss in a changing climate. Science Advances, 3 (5), e1601555. https://doi.org/10.1126/sciadv.1601555

Okano, Y., Ihara, T., Genchi, Y. (2008). Evaluation of environmental impacts on disturbed sleep by nighttime urban heat island phenomena using surveys via the Internet. Journal of Heat Island Institute International, 3, 22–33. http://www.heat-island.jp/web_journal/download/08A003.pdf

Quante, M., Wang, R., Weng, J., Kaplan, E. R., Rueschman, M., Taveras, E. M., Rifas-Shiman, S. L., Gillman, M. W., Redline, S. (2017). Seasonal and weather variation of sleep and physical activity in 12–14-year-old children. Behavioral Sleep Medicine, 17 (4), 398–410. https://doi.org/10.1080/15402002.2017.1376206

Rifkin, D. I., Long, M. W., Perry, M. J. (2018). Climate change and sleep: A systematic review of the literature and conceptual framework. Sleep Medicine Reviews, 42, 3–9. https://doi.org/10.1016/j.smrv.2018.07.007

van Loenhout, J. A. F., le Grand, A., Duijm, F., Greven, F., Vink, N. M., Hoek, G., Zuurbier, M. (2016). The effect of high indoor temperatures on self-perceived health of elderly persons. Environmental Research, 146, 27–34. https://doi.org/10.1016/j.envres.2015.12.012

World Health Organization. (2014). Quantitative risk assessment of the effects of climate change on selected causes of death, 2030s and 2050s. https://www.who.int/globalchange/publications/quantitative-risk-assessment/en/

Appendix. Revised Sleep Quality Index for Daily Sleep (SQIDS2)

Instructions:

Please answer the following questions about your state of sleep yesterday (sleep where you got up this morning)

1. When did you go to bed last night?
   BEDTIME LAST NIGHT _____
2. How long (in minutes) did it take you to fall asleep last night?
   NUMBER OF MINUTES _____
3. When did you get up this morning?
   GETTING UP TIME THIS MORNING _____
4. How many hours of actual sleep did you get last night? (This may be different than the number of hours you spend in bed.)
   HOURS OF SLEEP PER NIGHT _____
5.
   a. Did you wake up in the middle of sleep?
      Yes. _____ No. _____
   b. How often did you wake up in the middle of sleep?
      Once _____ Twice _____ Three times _____ Four times and more _____
   c. Did you fall asleep within 30 minutes after you woke up?
      Please answer "I could every time." or "I could not every time." when you woke up once.
      I could every time. _____ I could sometimes and could not at other times. _____ I could not every time. _____
6. Could you sleep well?
   I could well. _____ I could. _____ I could not well. _____ I could not. _____
7. How was a feeling of waking when you got up?

Very good. _____ Fairly good. _____ Fairly bad. _____ Very bad. _____

8. Did you take medicine (prescribed or "over the counter") to help you sleep last night?
   Yes. _____ No. _____
9. Did you spend today without sleepiness clearly?
   I was feeling clearly. _____ I was feeling fairly clearly. _____ I was a little sleepy. _____ I was very sleepy. _____

Scoring Instructions for SQIDS2

Component 1: Subjective sleep quality

1. Examine question #6, and assign scores as follows:

Response	Score
I could well.	0
I could.	1
I could not well.	2
I could not.	3

   Question #6 score: _____
2. Examine question #7, and assign scores as follows:

Response	Score
Very good.	0
Fairly good.	1
Fairly bad.	2
Very bad.	3

   Question #7 score: _____
3. Add #6 score and #7 score
   Sum of #6 and #7: _____
4. Assign component 1 score as follows:

Sum of #6 and #7	Component 1 score
0	0
1–2	1
3–4	2
5–6	3

   Component 1 score: _____

Component 2: Sleep latency

Examine question #2, and assign scores as follows:

Response	Component 2 score
≤ 15 minutes	0
16–30 minutes	1
31–60 minutes	2
> 60 minutes	3

Component 2 score: _____

Component 3: Sleep duration

Examine question #4, and assign scores as follows:

Response	Component 3 score
> 7 hours	0
6–7 hours	1
5–6 hours	2
< 5 hours	3

Component 3 score: _____

Component 4: Habitual sleep efficiency

1. Write the number of hours slept (question #4) here: _____
2. Calculate the number of hours spent in bed:
   Getting up time (question #3): _____
   − Bedtime (question #1): _____
   Number of hours spent in bed: _____
3. Calculate habitual sleep efficiency as follows:
   (Number of hours slept / Number of hours spent in bed) × 100
   = Habitual sleep efficiency (%)
   (_____ / _____) × 100 = _____%
4. Assign component 4 score as follows:

Habitual sleep efficiency %	Component 4 score
> 85%	0
75–84%	1
65–74%	2
< 65%	3

Component 4 score: _____

Component 5: Sleep disturbances

1. Examine questions #5a–5c, and assign component 5 score as follows:

Response #5a	Response #5b	Response #5c	Component 5 score
Yes.			0
No.	Once	I could every time.	0
		I could not every time.	1
	Twice	I could every time.	1
		I could sometimes and could not at other times.	1
		I could not every time.	2
	Three times	I could every time.	2
		I could sometimes and could not at other times.	2
		I could not every time.	3
	Four times and more		3

Component 5 score: _____

Component 6: Use of sleeping medication

Examine question #8 and assign scores as follows:

Response	Component 6 score
No.	0
Yes.	2

Component 6 score: _____

Component 7: Daytime dysfuntion

Examine question #9 and assign scores as follows:

Response	Component 7 score
I was feeling clearly.	0
I was feeling fairly clearly.	1
I was a little sleepy.	2
I was very sleepy.	3

Component 7 score: _____

Global SQIDS2 Score

Add the seven component scores together:

Global SQIDS2 score: _____

Evaluation of the Daily Cycle of UHI using Multi-site Measurements in a Central European Capital City

Rita Pongrácz[1]*, Eötvös Loránd University (Hungary)*
Judit Bartholy, Eötvös Loránd University (Hungary)
Zsuzsanna Dezső, Eötvös Loránd University (Hungary)
Csenge Dian, Eötvös Loránd University (Hungary)
Dóra Incze, Eötvös Loránd University (Hungary)
Máté Kurcsics, Eötvös Loránd University (Hungary)

ABSTRACT

We aim to analyze the urban climatic effects in several districts of Budapest (the capital city of Hungary) relative to the synoptic station of Budapest that is located in the southeastern suburban district. Thus, we initiated a specific urban climate program with multi-site in-situ meteorological measurements (air temperature and humidity) in the spring of 2015. In order to calculate the urban heat island intensity, temperature measurements are compared to the hourly recorded data of the synoptic station of Budapest. The full daily cycle of air temperature is analyzed in this study from recorded continuous measurements in different seasons of 2016-2018. The resulting climatic conditions are evaluated along a pre-defined route, which consists of 24 measuring points within the studied area. The measuring sites are located in different characteristical points of the district, such as green parks, narrow streets, paved squares, and wider roads with busy city traffic. After the initial phase, the measuring program has been extended to other districts with continuous measurement at fixed measuring points.

Introduction

On the basis of several international research it is quite well-known that the concentrated presence of people and their anthropogenic activities substantially modify the natural environment including (i) atmospheric composition primarily due to air pollution (e.g. Sokhi 1998), (ii) radiation characteristics as a result of artificial covers (e.g. Oke 1982), and (iii) local circulation mainly because of the vertical extent and density of buildings (e.g. Eliasson and Holmer 1990). All these fundamentally influence the everyday lives of inhabitants resulting in several health issues and implying the necessity for complex urban planning (Eliasson 2000, Ichinose, Matsumoto, and Kataoka 2008). In order to address the possible raising issues, one of the useful approaches (Mirzaei and Haghighat 2010) focuses on the urban climatic influences with special emphasis on the urban heat island (UHI). The UHI intensity of an urban area is defined by the temperature difference between the particular urban area and its rural surroundings (Oke 1973). This study focuses on the thermal differences of urban and suburban area in Budapest (Hungary) using in-situ measurement campaigns.

[1] Corresponding Author: prita@nimbus.elte.hu, +3613722500/6609.

Data and methodology

Budapest (47.5°N, 19°E), the capital city of Hungary, is divided by the river Danube (at 96 m above sea level) into the hilly, greener Buda side on the west (with the highest point at 527 m), and the flat, more densely built-up Pest side on the east. The capital occupies 525 km^2 (HCSO 2019, 18) with an extension to the greater agglomeration area exceeding 7600 km^2. The target area of the current analysis has a spatial extent of about 1.6 km^2, and it is located near the river Danube (i.e. east from the river) in a very heterogeneous district (district IX with a total area of 12.5 km^2) of Budapest. More specifically, building blocks with 3-4 levels, block houses with 8 levels, brown industrial areas can be found in the district IX as well as large areas occupied by the railways system. The local government started a block rehabilitation program in the 1990s in order to improve the urban environment for their citizens. In the framework of this block rehabilitation program (targeting the northern part of the district and close to the city center) old houses have been replaced by new buildings with a special structure, namely, the inner parts of old house blocks were demolished completely, and common green areas have been created inside the blocks (LGF 2010). The population density of the entire district is 4766 inhabitants/km^2 as of 1st January 2019 (HCSO 2019, 22). The target area of this study is the most densely populated part of the district, namely, its population density is about four-fivefold of the district-average population density. The climate of Budapest is mainly continental with the average monthly mean temperature ranging between (–5)–(+5) °C (in January) and 19–24 °C (in July) on the basis of measurements during 1981–2010 at the synoptic station located in the southeastern suburb of the city. The wettest months are May and June (with ~60-65 mm precipitation on average each) associated to the frontal activity of midlatitude cyclones and convective processes, while the driest months are January and February (with ~25-30 mm precipitation on average each).



Figure 1. The locations of measurements along the route in the District IX of Budapest, Hungary. Green color indicates parks (measuring points: 103, 106, 202, 203, 212), red color indicates high artificial cover ratio (measuring points: 104, 107, 110, 113/213, 207, 206, 205), yellow color indicates other urban sites (measuring points: 101/201, 102, 105, 108, 111, 112, 204, 208, 209, 210, 211). *Map*: Google Earth.

Data for this study were collected during several measurement campaigns with multi-site in-situ measuring sites (Figure 1). The measuring sites are located in different characteristical points of the district, such as green parks (e.g. 106, 109, 212, etc.), narrow streets (e.g. 104, 205, 206, etc.), paved squares (e.g. 113/213, 207), and wider roads with busy city traffic (e.g.

101/201, 111, 112, 211, etc.). The entire route consists of 24 measuring sites within the southeastern and northwestern parts (indicated by 1-- and 2-- in the numbering of measuring sites, respectively). The two parts meet in measuring sites 101 (which is identical to 201), and 113 (which is identical to 213). The measuring protocol is defined as follows.

1. Start route at measuring site 101/201.
2. Turn on the measuring device TESTO-635 (Figure 2) and wait 2 minutes.
3. Make measurements at the height of 1.5 m in shades for 2 minutes (measurements are digitally stored in data logger, which is programmed to a sampling frequency of 10 s).
4. Turn off the measuring device TESTO-635 and walk to the next measuring site, 101+*i* in the southeastern part and 201+*i* in the northwestern part (this is why two measuring devices are needed).
5. Follow steps 2-4 with $i = 1, \ldots, 12$, i.e. until reaching the other meeting point (113/213). These series of measurements (from 101 to 113, and 201 to 213) are coded as 'A_k' in the *k*th series during a given measuring campaign (*k* is always odd).
6. Wait if necessary to make measurements simultaneously with the two measuring devices.
7. Continue route in the other part with steps 2-4 with passing the measuring sites in reverse order (i.e. from 213 to 201 and 113 to 101) until reaching the starting site (101/201). These series of measurements (from 111 to 101, and 213 to 201) are coded as 'B_{k+1}' in the *k*th series during a given measuring campaign (*k*+1 is always even).
8. Wait if necessary to make measurements simultaneously with the two measuring devices.
9. Continue this cycle (from step 2) until the measuring campaign is terminated (with $k = K$).



Figure 2. TESTO-635 temperature/humidity measuring instrument with data logger. (TESTO-635-2 set: 0563 6352 with probe 0636 9735)

Measurements along the entire route last for about 2-2.5 hours. In order to analyse the spatial structure of UHI, the following calculation procedure is defined. Measuring laps during a particular continuous measuring campaign are coded consecutively starting as A_1, B_2, A_3, B_4, etc. The measured air temperature values ($T(X_{i,j})$, where X is either A or B, $i = 1, \ldots, K$, K is the total number of measurement laps during a given campaign, j = 101, …, 113, 201, …, 213) are organized into paired-averages (i.e. $T_{i,j} = (T(X_{i,j}) + T(X_{i+1,j}))/2$, for each station j, both A and B).

In addition, similar paired-averages ($t_{i,j}$) are calculated from time $t(X_{i,j})$ and $t(X_{i+1,j})$ when measurements were recorded. The mapped spatial structures of temperature values are associated to the mean value of $t_{i,j}$ for each i (i.e. mt_i, $i = 1, \ldots, K$). This averaging procedure of consecutive measurements enables us to prepare maps representing a virtual time, and it assumes linear changes in temperature between two consecutive measurements at any particular site along the defined route. For calculating UHI intensity, temperature measurements from the target area were compared to the hourly recorded data of the Budapest synoptic station (ID number: 12843) located in the southeastern suburb district of the city.

A more detailed analysis of the temporal evolution of temperature difference between the district IX and the suburbs is included in this study for a selected measuring site, namely, site 105. This measuring site is located in a passage surrounded by buildings with six levels and a height of about 20 m. The vegetation cover of the local vicinity of this site is ~60% (Figure 3). The measuring device was operated here continuously with a recording frequency of 1 minute, thus enabling us to evaluate in details the daily cycle of temperature.



Figure 3. Measuring site 105 in summer: July 2017 (left), and autumn: October 2016 (right)

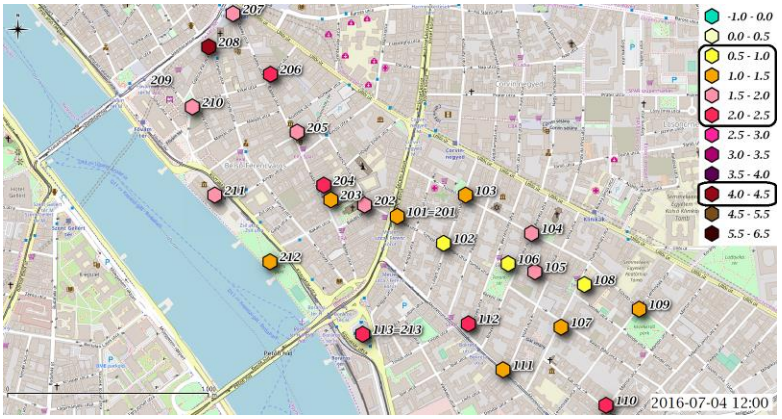
The urban climatological program was initiated in spring, 2015, and the main experiences of the first year were summarized and published (Pongrácz et al. 2016). The continuous, at least 24-hour-long measurement campaigns started in 2016. Altogether 126 days with more than 1400 hours of measurements are collected by now, from which 77 days with 853 hours were recorded in the district IX. The measurements were scheduled once a week during the spring and autumn semesters from 2 p.m. on Thursdays to 2 p.m. on Fridays. In addition, summer campaigns (in July 2016, 2017, 2018) covered at least 72 hours continuously.

Results and Discussion

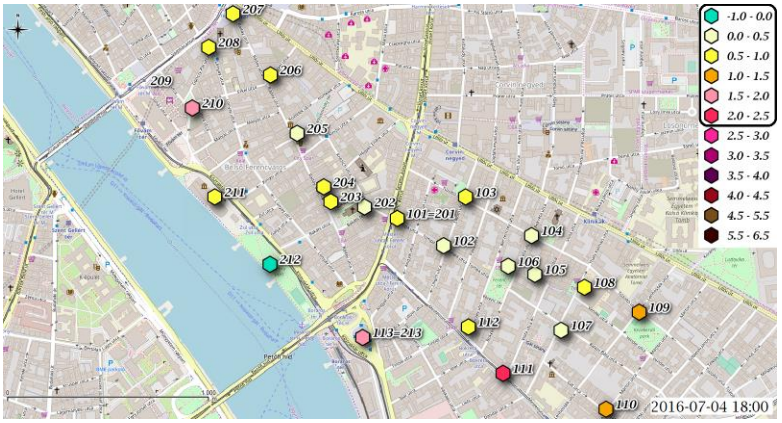
First, results from the summer measuring campaign in 2016 are shown in Figures 3–4, more specifically, the maps represent the daily cycle of the UHI intensity structure for 4-5 July when sunset and sunrise occurred at 8:43 p.m. and 4:53 a.m., respectively. The synoptic situation during this measuring campaign was ideal to detect the UHI effect, namely, we recorded anticyclonic weather over the Carpathian basin with high pressure (sea level pressure values exceeded 1020 hPa) and clear sky conditions with daily maximum temperature of 26–27 °C measured at the synoptic station of Budapest located in the southeastern suburb district. The target area was definitely warmer than the suburban area throughout the whole day (except late

afternoon in a park along the riverside). The maximum UHI intensity was detected after sunset, with slightly higher intensity values at 3 a.m. than at 11 p.m. The measuring sites were generally warmer by 3–4.5 °C before midnight and by 3.5–5.5 °C after midnight. On the one hand, lower UHI intensity values can be identified in the greener parts of the target area. On the other hand, higher UHI intensities occurred in narrow streets. These maps clearly show the roles of the building density and vegetation ratio in the UHI intensity during night.

12:00 CEST (4/7/2016)



18:00 CEST (4/7/2016)



23:00 CEST (4/7/2016)

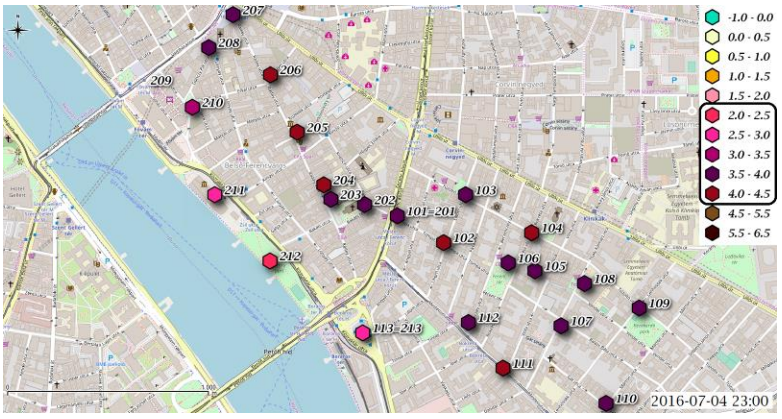


Figure 4. The first part of the daily cycle of the spatial patterns of UHI intensity before midnight, 4 July 2016

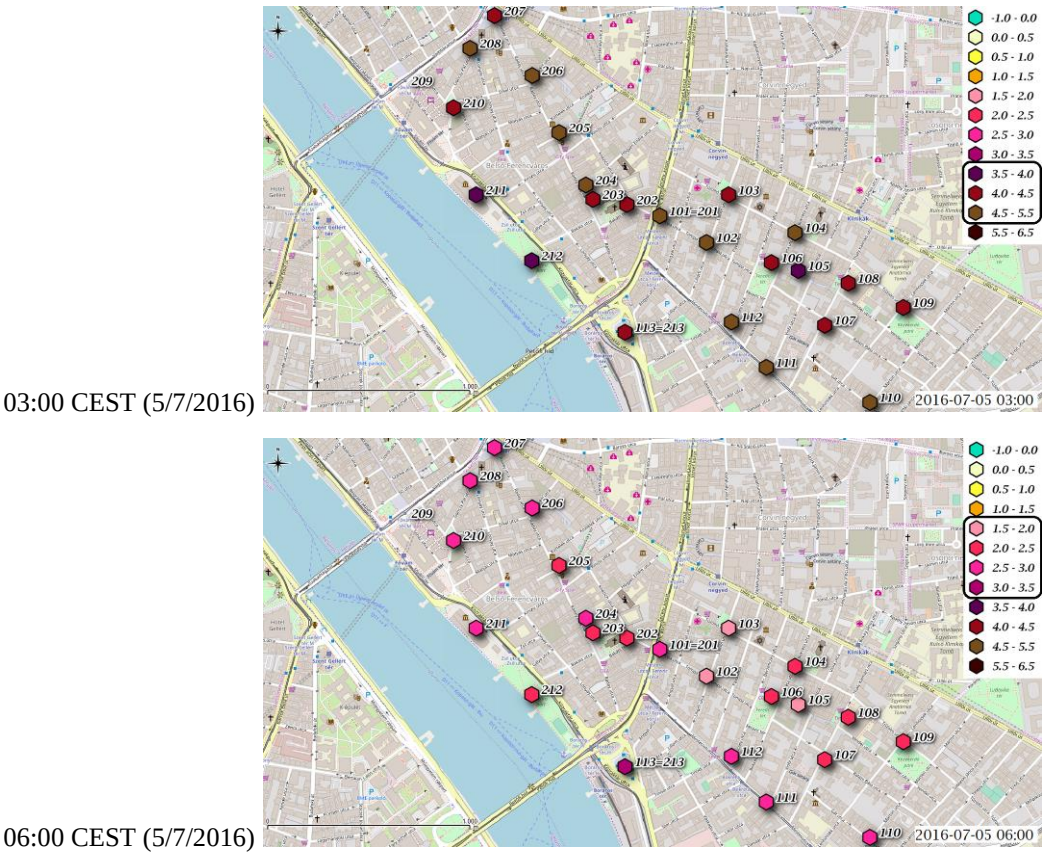


Figure 5. The second part of the daily cycle of the spatial patterns of UHI intensity after midnight, 5 July 2016

Then, the daily cycle of UHI intensity is analyzed on the basis of air temperature measurements in measuring site 105 compared to the temperature data of the suburban synoptic station. Figure 6 shows the results from the summer campaign in 2016. The measured temperature values clearly indicate that the measuring site 105 in the district IX is generally warmer than the southeastern suburbs of Budapest. The difference is the greatest after midnight, whereas the two time series are the closest to each other in the evenings.

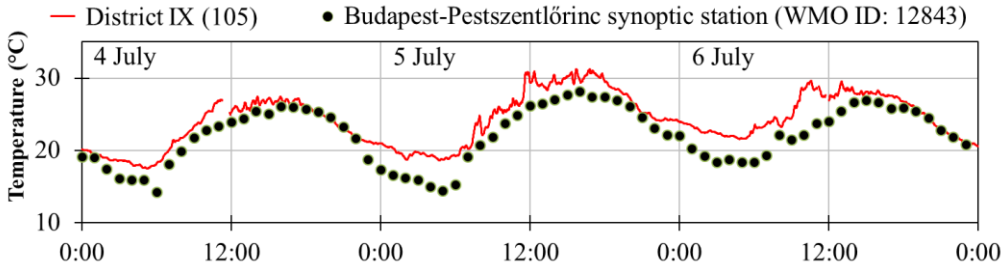


Figure 6. The daily cycle of continuous temperature measurements (at measuring site 105 with a recording frequency of 1 minute, compared to the synoptic station of Budapest, WMO ID: 12843 with hourly data available), 4–6 July 2016

We defined the UHI intensity in this study as the temperature difference between the two measuring sites (105 vs. synoptic station). Figure 7 compares the daily cycles of UHI intensity in 2016 and in 2017. We carried out measuring campaigns in both years, in early July when anticyclonic weather conditions dominated the region. The results are similar, overall, although some differences can also be found. The greatest UHI intensities (exceeding 4 °C in 2016, and 3 °C in 2017) were detected during night time, after midnight. The smallest temperature differences (around 0 °C) between the two sites occurred in the evening hours. The UHI clearly started to intensify after sunset and reached its maximum before sunrise.

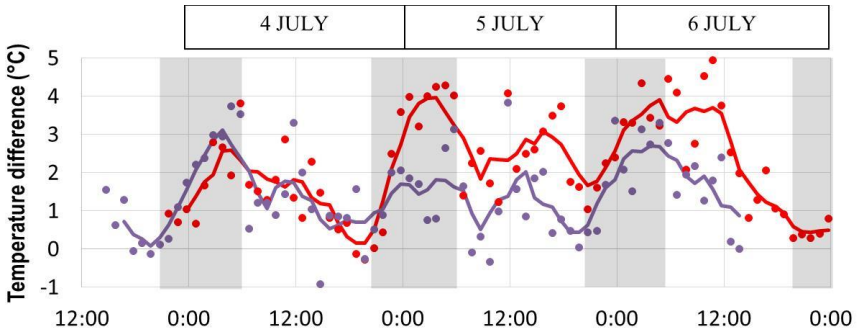


Figure 7. Comparison of UHI intensity in two consecutive years (2016 is indicated by red, whereas 2017 is indicated by purple) calculated for measuring site 105 compared to the synoptic station of Budapest (WMO ID: 12843). Night time between sunset and sunrise is indicated by the grey background of the diagram.

On the basis of the measurements in different seasons the relationships between the UHI intensity values and various weather conditions are also evaluated. The strongest relationships (with 0.54 R^2-value) were found between the maximum UHI intensity and the cloud cover (Figure 8), namely, intense UHI occurs in clear sky conditions, whereas the UHI effect becomes quite small when cloudy conditions occur. The equation for the fitted linear regression is indicated in the diagram.

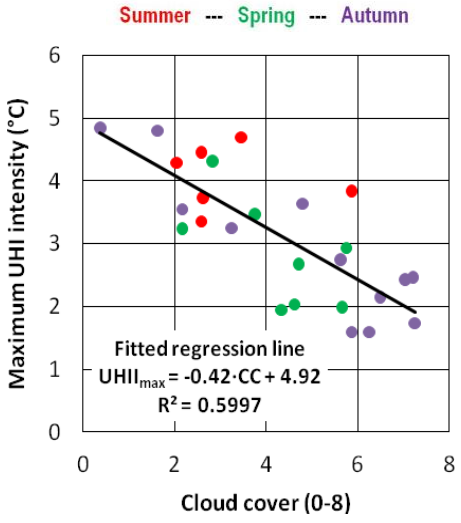


Figure 8. Relationship between the maximum UHI intensity ($UHII_{max}$) and cloud cover (CC) on the basis of data from the measuring site 105 and the synoptic station of Budapest (WMO ID: 12843), 2016-2018

Acknowledgments

Research leading to this paper has been supported by the following sources: the Hungarian National Research, Development and Innovation Fund under grants K-129162, K-120605 and K-109109, the Hungarian Ministry of Human Capacities under the ELTE Excellence Program (grant number: 783-3/2018/FEKUTSRAT), and the Széchenyi 2020 programme, the European Regional Development Fund and the Hungarian Government via the AgroMo project (GINOP-2.3.2-15-2016-0028). In-situ measurements were completed by BSc and MSc students of the Eötvös Loránd University.

References

Eliasson, I. (2000). The use of climate knowledge in urban planning. Landscape and Urban Planning 48(1-2) 31-44. https://doi.org/10.1016/S0169-2046(00)00034-7

Eliasson, I. & Holmer, B. (1990). Urban heat island circulation in Göteborg, Sweden. Theoretical and Applied Climatolology 42(3), 187-196. https://doi.org/10.1007/BF00866874

HCSO, Hungarian Central Statistical Office, (2019). Gazetteer of Hungary, 1 January 2019. Budapest (Hungary).

Ichinose, T., Matsumoto, F. & Kataoka, K. 2008. Urban thermal environment and its mitigation through urban planning process. Geographical Reports of Tokyo Metropolitan University 43: 33-40.

LGF, Local Government of Ferencváros (2010). Rehabilitation of Budapest Ferencváros. Budapest (Hungary).

Mirzaei, P. A. & Haghighat, F. (2010). Approaches to study urban heat island – abilities and limitations. Building and Environment 45(10), 2192-2201. https://doi.org/10.1016/j.buildenv.2010.04.001

Oke, T.R. (1973). City size and the urban heat island. Atmospheric Environment 7(8), 769–779. https://doi.org/10.1016/0004-6981(73)90140-6

Oke, T.R. (1982). The energetic basis of the urban heat island. Quarterly Journal of the Royal Meteorological Society 108(455), 1–24. https://doi.org/10.1002/qj.49710845502

Pongrácz, R., Bartholy, J., Dezső, Zs., & Dian, Cs. (2016). Analysis of the air temperature and relative humidity measurements in the Budapest Ferencváros district. Hungarian Geographical Bulletin, 65(2), 93–103. https://doi.org/10.15201/hungeobull.65.2.1

Sokhi, R.S., Ed. (1998). Urban air Quality: Monitoring and Modelling. Kluwer. Dordrecht (The Netherlands).

COOL MATERIAL DEVELOPMENT AND CHARACTERISTICS

Quantum Dots: A New Generation of Fluorescent Materials for UHI Mitigation

Samira Garshasbi, Faculty of Built Environment, University of New South Wales, Sydney, 2052 (Australia)
Shujuan Huang, School of Photovoltaic and Renewable Energy Engineering, University of New South Wales, Sydney 2052 (Australia)
Mat Santamouris[1]*, Faculty of Built Environment, University of New South Wales, Sydney, 2052 (Australia)*

ABSTRACT

Quantum dots (QDs) are novel nano-scale fluorescent materials with tunable optical properties offering the great opportunity to customize their properties based on the application. In this paper, we have developed a novel algorithm to identify the optimum optical properties of QDs to achieve the highest cooling/temperature reduction potential. Based on our model, surface temperature reduction potential through photoluminescence (PL) effect can be improved by modulating band gap energy/ PL peak wavelength, PL quantum yield (PLQY). Our results also show that QDs demonstrate their highest temperature reduction potential with PL peak at 1100 nm. Furthermore, there is a linear correlation between temperature reduction and PLQY, which means higher temperature reduction could be achieved with QDs having higher PLQY values.

Introduction

Urban overheating is a serious energy problem causing a severe increase of the energy consumption for cooling and have a negative impact on thermal comfort and heat related health issues. Since conventional heat-absorbing construction materials are one of the main contributors to the urban overheating effect, an effective strategy to mitigate the effect is to replace them with materials exhibiting highest potential to reject sunlight by reflection and/or fluorescence (photoluminescence) (Berdahl, Chen, Destaillats, Kirchstetter, Levinson, and Zalichb 2016; Levinson, Chena, Ferrari, Berdahla, and Slacka 2017; Garshasbi and Santamouris 2019). While there has been a large number of studies on highly reflective/cool materials (Synnefa, Santamouris, and Akbari 2007; Synnefa, Santamouris, and Apostolakis 2007; Santamouris 2013), application of the so-called fluorescent materials is still undeveloped and there are only a few studies on urban overheating mitigation with fluorescent materials. Berhadl et al., for instance, reported a surface temperature reduction of 6.5 °C by application of ruby crystals as conventional fluorescent materials with Photoluminescence (PL) peak at 694 nm and Photoluminescence quantum yield (PLQY) of 95% compared to the non-fluorescent reference sample. As indicated in the paper, the estimated effective solar reflection (ESR) is equal to 0.73 and solar reflection (SR) is 0.43, which means contribution of photoluminescence effect is around 0.3 (Berdahl, Chen, Destaillats, Kirchstetter, Levinson, and Zalichb 2016).

Considering the promising urban overheating potential of bulk fluorescent materials, this paper took one step further and studied UHI mitigation potential of quantum dots as Nano-scale

[1] Corresponding Author: [m.santamouris@unsw.edu.au].

fluorescent materials with tunable optical properties. According to Garshasbi and Santamouris, quantum dots are Nano-scale fluorescent materials with tunable optical properties, in contrast to their bulk counterparts (e.g. ruby) with specific optical properties/restricted cooling potential. In this paper, a novel algorithm to compute the cooling potential/temperature reduction and fluorescence contribution of QDs for the mitigation of urban heat island (UHI) effect has been developed. Since it's tricky to distinguish surface temperature reduction caused by reflection from cooling potential of photoluminescence effect, our proposed algorithm/model can be used as a solid method to have a precise estimation of the Photoluminescence (PL) effect contribution in urban overheating mitigation. More importantly, this algorithm could be used to determine the optimum optical properties of QDs to achieve the highest cooling potential.

MATERIALS AND METHODS

In this paper, we developed a theoretical model that effectively predicts the optical behavior of quantum dots under the sunlight and enables us to have an estimation of potential temperature reduction caused by the PL effect in quantum dots. The thermal model was developed in two steps: First, a dynamic thermal model for non-fluorescent materials was developed. For this purpose, the surface temperature, T_{Surf}, was modelled and computed by the following thermal balance equation using an in-house computer code in Lazarus 1.2.4 programming language (Akbari, Levinson, and Berdahl 1996):

$$\alpha_{SW} A I_{SW}\big|_t + \varepsilon\sigma\left(T_{Sky}^4 - T_{Surf}^4\right)\Big|_t - hA\left(T_{Surf} - T_{Ambient}\right)\Big|_t - Q_{PL}\big|_t = mc\frac{dT_{Surf}}{dt} = mc\frac{T_{Surf}\big|_{t+dt} - T_{Surf}\big|_t}{dt} \quad (1)$$

where m, c, and A are mass, specific heat capacity, and area, respectively. Also, α_{SW}, I_{SW}, and $\mathcal{E}$ stand for short wave solar absorbance, short wave irradiation, and infrared emittance, respectively. Furthermore, $T_{Ambient}$ and h are ambient temperature and convective coefficient, respectively. σ is Stephan Boltzman Constant (5.67×10^{-8} W/m^2.K^4). It is worth mentioning that Q_{PL} is the heat loss by PL effect, which is considered equal to zero for non-fluorescent materials. This term must be calculated for fluorescent materials.

By rearranging equation (1), a first-order ordinary differential equation is achieved:

$$\frac{dT_{Surf}}{dt} = \frac{\alpha_{SW} A I_{SW}}{mc} + \frac{\varepsilon\sigma}{mc}\left(T_{Sky}^4 - T_{Surf}^4\right) - \frac{hA}{mc}\left(T_{Surf} - T_{Ambient}\right) - \frac{Q_{PL}}{mc} \quad (2)$$

This first-order ordinary differential equation is solved using the fourth order Runge-Kutta method. Then, surface temperature and boundary conditions measurements were conducted for a non-fluorescent material in a mostly sunny day from 9 am to 4 pm every 15 seconds in Sydney, Australia. Following that, the thermal model was executed using measured boundary conditions, optical, and thermal properties as inputs and model results were compared against measured surface temperature.

After validation of thermal model for non-fluorescent materials, a method for calculation of heat loss by photoluminescence (Q_{PL}) is introduced. To calculate heat loss by PL effect, quantum yield and spectral Photoluminescence must be measured using the Fluorescence

Spectrophotometer. Quantum yield is defined as the ratio of photons re-emitted to the number of photons absorbed:

$$Quantum\,Yield = QY = \frac{Number\ of\ \ photons\ reemitted}{Number\ of\ \ photons\ absorbed\ (Capable\ of\ \ exciting,\ i.e.\ \lambda < \lambda_{AEW})} \quad (3)$$

It should be noted that only wavelengths shorter than Absorption Edge Wavelength, λ_{AEW}, can excite quantum dots. Absorption Edge is the wavelength where energy of the photon is equal to band gap energy. Number of photons absorbed can be calculated by the following equations:

$$Number\ of\ \ photons\ absorbed = \frac{Total\ absorbed\ energy}{Energy\ of\ \ each\ absorbed\ \ photon}$$
$$= \frac{E_A(300\,nm)}{E_P(300\,nm)} + \frac{E_A(301\,nm)}{E_P(301\,nm)} + \ldots + \frac{E_A(\lambda_{\max})}{E_P(\lambda_{\max})} = \sum_{\lambda=300}^{\lambda_{AEW}} \frac{E_A(\lambda)}{E_P(\lambda)} \quad (4)$$

Where $E_A(\lambda)$ is the total absorbed energy with a wavelength of λ and $E_P(\lambda)$ is the energy carried by a single photon having a wavelength of λ. $E_A(\lambda)$ can be calculated with the following equation:

$$E_A(\lambda) = \alpha_{SW} A I_{SW} \varphi(\lambda) \quad (5)$$

where $\varphi(\lambda)$ denotes relative spectral of global solar radiation based on the global standard spectrum (AM1.5g). It is obvious that the energy carried by a single photon having a wavelength of λ can be calculated as follows:

$$E_P(\lambda) = \frac{h_{Planck} C}{\lambda} \quad (6)$$

where h_{Planck} and C are the Planck constant (6.626 x 10^{-34} j.sec) and speed of light (3 x 10^8 m/sec), respectively. Finally, the Q_{PL} can be predicted as follows:

$$Q_{PL} = Total\ reemitted\ energy = Number\ of\ \ photons\ reemitted \times Band\ Gap\ Energy \quad (7)$$

As can be seen in the equations, quantum yield and PL peak wavelength are two determining factors affecting the cooling potential by PL effect in QDs. In this study, cooling potential of commercially available quantum dots is calculated and then, optimum optical properties to achieve quantum dots with highest surface temperature reduction are proposed.

RESULTS AND DISCUSSION

Thermal Model for Non-Fluorescent Materials

The thermal model was executed for a 10 cm by 10 cm roof membrane sample as a typical non-fluorescent material. The spectral reflectance was measured with Perkin Elmer

Lambda 950 spectrophotometer and broad band values were calculated from the spectral data according to ASTM E 903 (Anon., 2012). The thermal emittance was measured with the TIR 100-2 emissometer by Inglas, according to EN 15976 and specific heat capacity was measured with Hot Disk TPS 1500. The broadband reflection, emissivity, specific heat capacity, and mass of sample are displayed in Table 1.

Table 1. Definition of the sample

Properties	Values
Broadband Reflection	0.86
Thermal Emissivity	0.75
Specific Heat Capacity (J/kg.^{o}C)	1170
Mass (g)	23.93
Area (m^2)	0.01

Sample was exposed to sunlight in a mostly sunny day on 18th April 2019 from 9 am to 4 pm and surface temperature and all required boundary conditions were monitored every 15 seconds. Shortwave and Longwave solar irradiations were measured with Hukseflux NR01 net radiometer. Ambient temperature and wind speed were monitored using Gill Instrument MetPak Pro weather station. Surface temperature measurements were also conducted using the LSI Surface (Pt100) temperature sensors. The acquisition of the outputs was performed via Lontek datalogger dataTaker DT85.

Then, calculation of surface temperature was performed using the boundary conditions, optical, and thermal properties of the samples. As can be seen in Figures 1 and 2, the difference between calculated and measured surface temperature is negligible and our developed thermal model can be used as a reliable method for calculation of surface temperature. Statistical analyses also confirm that our model is capable of precisely anticipating the experimental data on surface temperature (See Table 2).

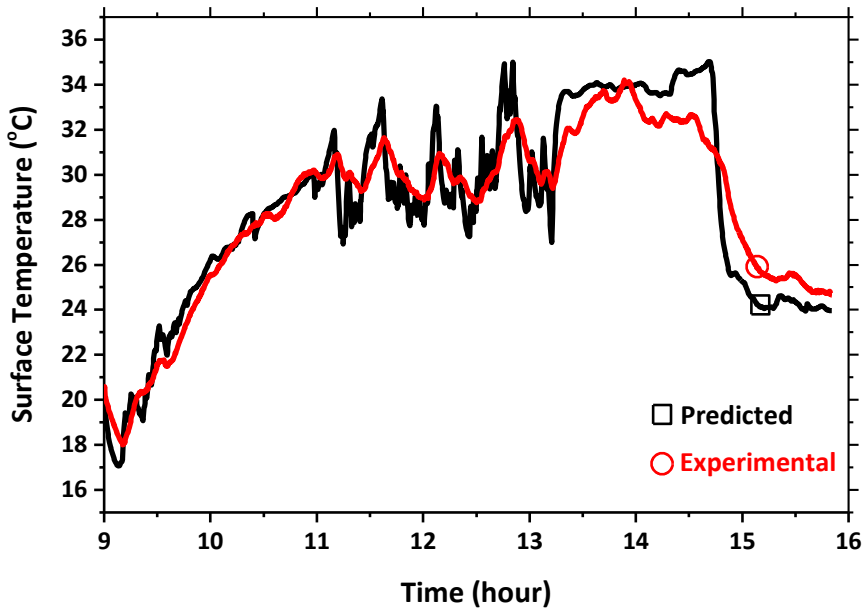


Figure 1. Predicted and experimental surface temperature trend by time.

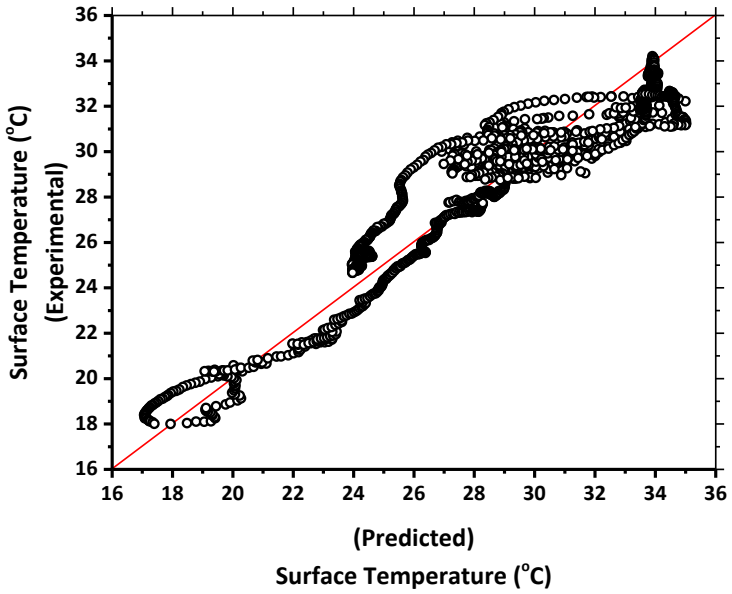


Figure 2. Predicted vs experimental surface temperature.

Table 2. Statistical Analysis

	Predicted	Experimental
Average	28.0	28.6
Variance	20.5	14.6
Standard Deviation	4.5	3.8
Covariance	16.9	
Correlation Coefficient	0.97	
R-Squared	0.94	
Coefficient of Efficiency	0.88	
Goodness of Fit (%)	65.56	
Coefficient of Determination	0.94	

Thermal Model for Fluorescent Materials/Calculation of Q_{PL}

The developed thermal model for fluorescent materials was executed for quantum dots with Solar absorption of 0.5, PLQY of 40% and PL peak of 1100 nm under same radiative properties and boundary conditions in step 1. Based on the results, quantum dots yielded average and maximum surface temperature reduction of around 4.6 and 7.4 °C. Results also suggest that maximum and average surface temperature were decreased up to 9.5 C and 15.1 °C for PLQY equal to 80%, and quantum dots with PLQY of 50%, 60%, and 70% decreased average surface temperature by 5.8°C, 7.1 °C, and 8.3 °C, respectively (See Figures 3 and 4).

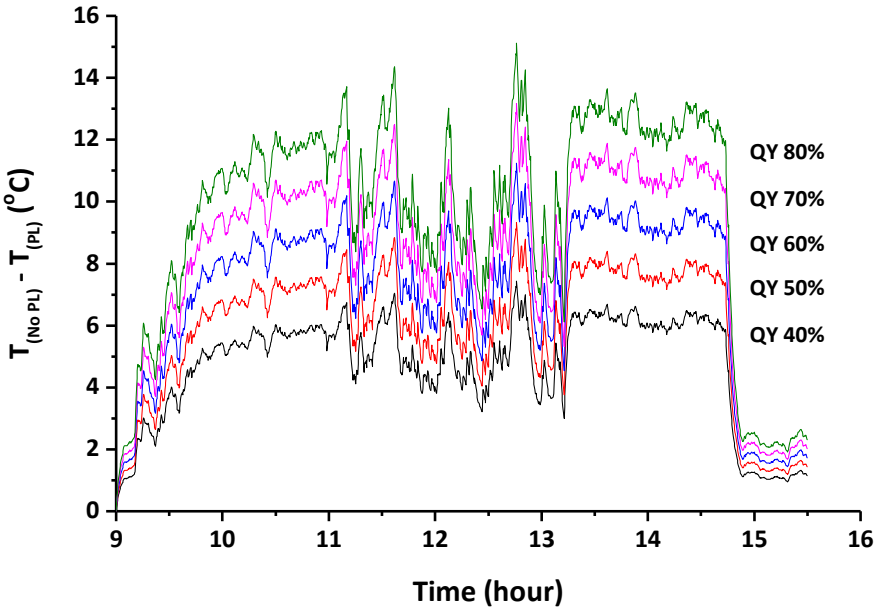


Figure 3. Surface temperature reduction (Surface temperature difference for quantum dots with PL effect and the corresponding quantum dots without PL (Q_{PL}= 0)) at PLQY and PL peak= 1100 nm.

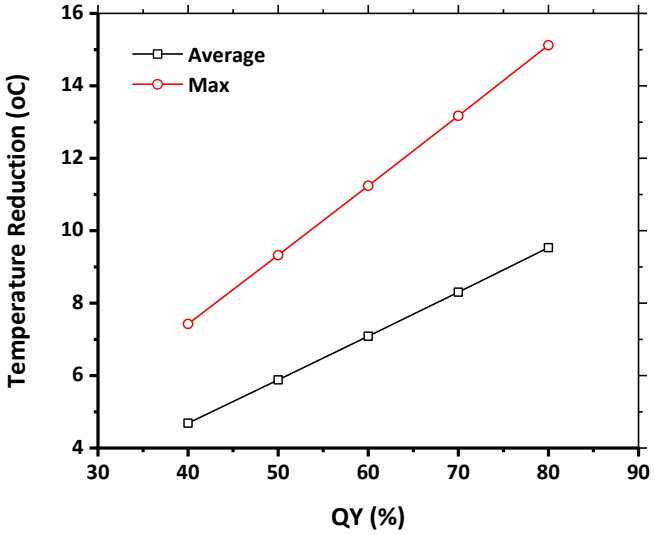


Figure 4. Average and maximum surface temperature reduction (Surface temperature difference for quantum dots with PL effect and the corresponding quantum dots without PL (Q_{PL}= 0)) at PLQY and PL peak= 1100 nm.

Similarly, PLQY was kept constant at 40% and PL peak wavelength was changed from 500 nm to 1700 nm. As indicted in Figures 5 and 6, maximum surface temperature reduction happens at PL peak wavelength of 1100 nm. The surface temperature reduction is significantly affected by PL peak as we enter visible range which can be justified since solar radiation contains a considerable amount of visible irradiation.

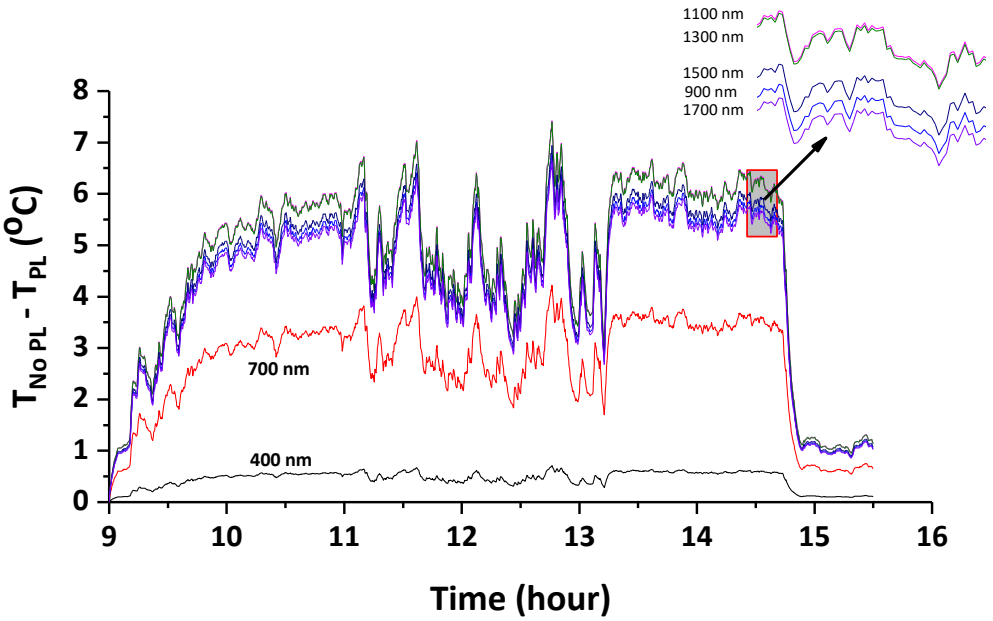


Figure 5. Surface temperature reduction (Surface temperature difference for quantum dots with PL effect and the corresponding quantum dots without PL (Q_{PL}= 0)) at different PL peaks and PLQY= 40%.

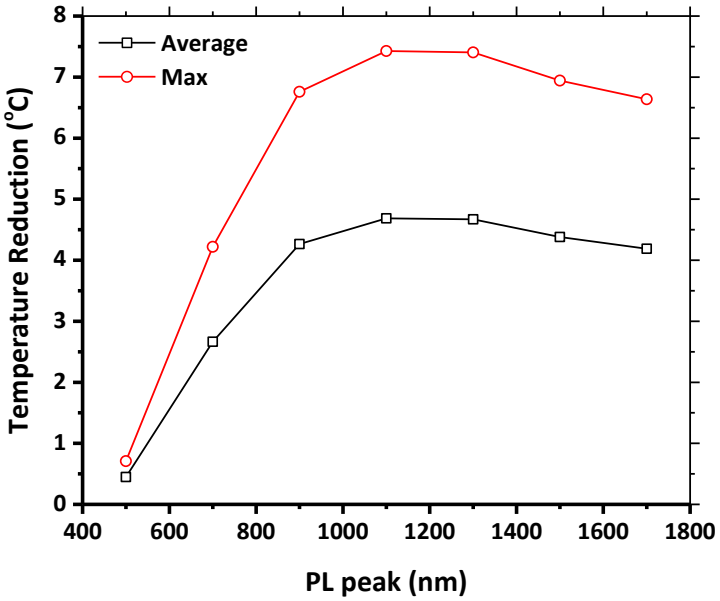


Figure 6. Average and maximum surface temperature reduction (Average surface temperature difference for quantum dots with PL effect and the corresponding quantum dots without PL (Q_{PL}= 0)) at different PL peaks and PLQY= 40%.

CONCLUSION

Fluorescent materials offer cooling effect through photoluminescence/fluorescent effect in contrast to non-fluorescent materials which rely solely on heat rejection via reflection. In this paper, we have developed a novel algorithm to compute the cooling potential/temperature reduction of QDs as novel fluorescent materials with tunable optical properties for the mitigation of urban heat island (UHI) effect. Our developed algorithm could be also employed to compute the fluorescence contribution of QDs to the urban overheating mitigation. More importantly, this algorithm could be used to determine the optimum optical properties of fluorescent materials which provide highest cooling potential.

Our results show that up to 15.1 ^{o}C temperature reduction via PL effect was achieved with application of quantum dots with solar absorption equal to 0.5, photoluminescence (PL) peak at 1100 nm and PLQY of 80% compared to corresponding non-fluorescent reference sample during a sunny autumn day in Sydney, Australia. Our model also shows that cooling effect through PL effect is affected by the following fluorescent properties (i) Band gap energy/PL peak wavelength, (ii) PL quantum yield. Based on our results, QDs show the highest temperature reduction at PL peak wavelength equal to 1100 nm, with significant drop in temperature reduction potential for PL peak wavelengths equal to/shorter than 700 nm. In addition, temperature reduction potential is directly proportional to PLQY, which means high QY value gives rise to temperature reduction potential.

References

Synnefa, A., Santamouris, M. & Apostolakis, K. (2007). On the development, optical properties and thermal performance of cool colored coatings for the urban environment. Solar Energy, 81(4), 488-497. https://doi.org/10.1016/j.solener.2006.08.005

American Society for Testing and Materials (2012). Standard Test Method for Solar Absorptance, Reflectance, and Transmittance of Materials Using Integrating Spheres (ASTM E 903-12). https://doi.org/10.1520/E0903-12

Akbari, H., Levinson, R. & Berdahl, P. (1996) ASTM Standards for Measuring Solar Reflectance and Infrared Emittance of Construction Materials and Comparing Their Steady-State Surface Temperatures. Proceedings from ACEEE Summer Study on Energy Efficiency in Buildings, United States, 1996. https://www.osti.gov/servlets/purl/432933

Berdahl, P., Chen, S., Destaillats, H., Kirchstetter, T., Levinson, R. & Zalichb, M. (2016). Fluorescent cooling of objects exposed to sunlight - The ruby example. Solar Energy Materials and Solar Cells, 157, 312-317. https://doi.org/10.1016/j.solmat.2016.05.058

Levinson, R., Chena, S., Ferrari, C., Berdahla, P. & Slacka, J. (2017). Methods and instrumentation to measure the effective solar reflectance of fluorescent cool surfaces. Energy and Buildings, 152, 752-765. https://doi.org/10.1016/j.enbuild.2016.11.007

Garshasbi, S. & Santamouris, M. (2019). Using advanced thermochromic technologies in the built environment: Recent development and potential to decrease the energy consumption and fight urban overheating. Solar Energy Materials and Solar Cells, 191, 21-32. https://doi.org/10.1016/j.solmat.2018.10.023

Santamouris, M. (2013). Using cool pavements as a mitigation strategy to fight urban heat island - A review of the actual developments. Renewable and Sustainable Energy Reviews, 26, 224-240. https://doi.org/10.1016/j.rser.2013.05.047

The evaporative cooling and its impact on the urban climate: study of the influence of road covering materials

Sophie Parison[1],
Paris City Hall, Water and Sanitation & Roads and Traffic Divisions (France)
Univ Paris Diderot, Sorbonne Paris Cité, LIED, UMR 8236, CNRS (France)
Martin Hendel,
Univ Paris Diderot, Sorbonne Paris Cité, LIED, UMR 8236, CNRS (France)
Université Paris-Est, ESIEE Paris, département SEN, (France)
Arnaud Grados,
Univ Paris Diderot, Sorbonne Paris Cité, MSC, UMR 7057 (France)
Laurent Royon,
Univ Paris Diderot, Sorbonne Paris Cité, LIED, UMR 8236 (France)

ABSTRACT

The thermal behavior of different pavement structures and their evaporative cooling has been tested in the laboratory under conditions similar to those observed during a heat wave in Paris. Different surface watering rates are thus tested in order to optimize the process according to the structure that will then be implemented on Parisian sites. Using a surface heat budget, it is possible to estimate the evaporative cooling flux depending on the chosen watering rate. Two linear cooling regimes are observed, allowing the maximizing the effects of watering while minimizing water consumption. The effects for each structure are quantified and compared.

Introduction

During heat waves, urban heat islands (UHIs) pose a serious threat to urban populations (Lemonsu et al. 2012). As a direct consequence of climate change, such events are likely to become both more frequent and intense in the upcoming years, particularly in Paris (Robine et al. 2008).

In order to mitigate UHIs, the City of Paris has been interested in the implementation of experimental pavement-watering campaigns since 2013 during heat waves. This method was found to reduce the UTCI-equivalent temperature at pedestrian height up to 2 to 3°C during the day (Hendel et al. 2016, Hendel et al. 2014, Parison et al. 2017). The study of these tests also highlighted the influence of pavement materials on the optimal watering strategy to be adopted in order to maximize cooling effects while minimizing the water consumption of the process (Hendel et al. 2014). Moreover, since urban materials strongly contribute to the formation of urban heat islands, their thermo-climatic study is relevant in order to propose cooler alternative pavements than the existing roads.

In the paper, we propose to study the thermo-climatic behaviour of different conventional Parisian road materials (asphalt road, asphalt and granite sidewalks and stabilized sand) and alternatives (concrete sidewalk and thermochromic and near-infrared reflective paints) undergoing heat-wave-like conditions inside a climate chamber, including a day phase with artificial insolation and a night phase (Hendel et al. 2018). A water sprinkler device also allows the control of the watering rate of the surfaces in order to determine the optimal rate and the maximum cooling

[1] Corresponding Author: sophie.parison@univ-paris-diderot.fr.

effects of this method. Temperatures as well as heat fluxes are monitored using sensors integrated into the samples.

More than ten tests at different watering rates are performed, ranging from 0.1 to 3 mm/h. The temperature differences between "dry" and "wet" tests are studied versus the chosen watering rate in order to optimize the process for each structure. By studying the heat budget of the different tests, it is also possible to estimate the cooling flux due to watering, as well as the radiative, convective and conductive contributions of the watering.

Methodology

Experimental setup

The structures were studied under climatic conditions similar to those observed during a Parisian heat wave (Hendel et al. 2018). Samples undergo a 24-hour cycle divided into an 8-hour daytime period with artificial sunlight provided by a halogen lamp, and a 16-hour night time period without insolation. Air temperature and relative humidity are set respectively to 35°C and 35% during the day and to 25°C and 70% during the night. Those set values were chosen to be representative of a Parisian heat-wave, as they are inherited from averaged daily field measurements conducted by the authors on *rue du Louvre*, Paris, France, over several summers during hot days (Hendel et al. 2016, Hendel et al. 2014,). Prior to the experiment, the samples were stabilized at night conditions. A diagram of the experimental set-up is shown in Figure 1.

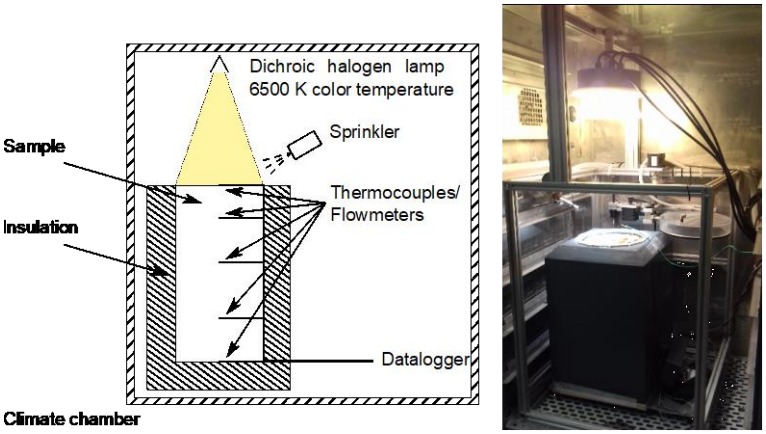


Figure 1. Experimental set-up diagram (left, (Hendel et al. 2018)) and photograph (right)

What is more, during the day phase, surface-watering can be programmed at fixed frequency using a sprinkler placed near the sample's surface. Thermocouples and flowmeters placed on the surface and at different depths monitor the thermal behavior of the sample. Table 1 sums up the characteristics of each phase. Radiation flow density is specified for both short (SW) and long wavelength (LW) radiation, i.e. for 0.3-3 μm and for 3-100 μm.

Table 1: Characteristics of the day and night phases

Parameter	Day phase	Night phase
Duration	8 h	16 h

Air temperature	35°C	25°C
Relative humidity	35%	70%
SW radiation (0.3-3 μm)	1200 W/m²	0 W/m²
LW radiation (3-100 μm)	180 W/m²	450 W/m²
Watering rates (*Q*)	0 - 0.1 - 0.25 - 0.4 - 0.5 - 0.6 - 0.75 - 1.0 - 1.25 - 1.5 - 2.0 - 2.5 - 3.0 mm/h	0 mm/h

Case study structures

Five Parisian pavement structures are studied in this paper: asphalt road, asphalt sidewalk, stabilized sand, granite sidewalk and concrete sidewalk. The composition of the samples, representative of the Parisian structures implemented is the streets, is shown in Figure 2. Each cylindrical specimen is 32 cm high with a 16 cm diameter.

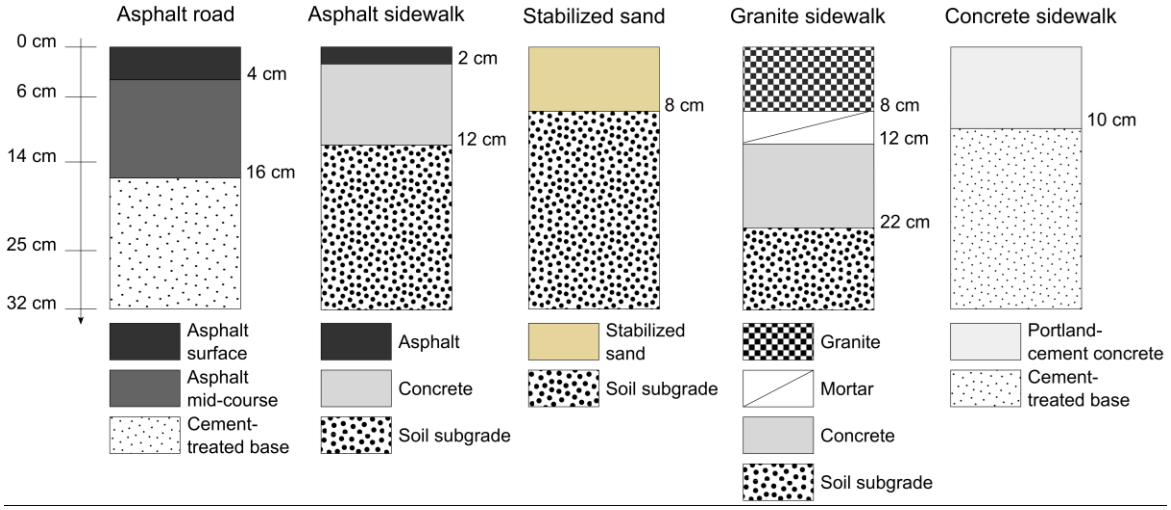


Figure 2. Studied structure samples (adapted from Hendel et al. (2018)).

In addition, two surface coatings were tested on the asphalt sidewalk structure: a thermochromic paint, which is dark-green at room temperature but become reflective above 29°C, and black paint in appearance but reflective in the near-infrared (NIR) band. An albedo measurement of the studied samples surface was conducted using a UV-Vis-NIR Cary 5000 spectrophotometer with a Spectralon integrating sphere following the ASTM E903 standard (ASTM 2012). To obtain a result representative of the entire surface of the heterogeneous samples, a minimum of five measurements were made. In each case, the relative measurement uncertainty is about 1% to 5% depending on the sample. The reflectivity measurements obtained were weighted by the spectrum of the halogen lamp (250-1700 nm) used in the chamber, shifted in the infrared band with respect to the solar spectrum, both shown in Figure 3.

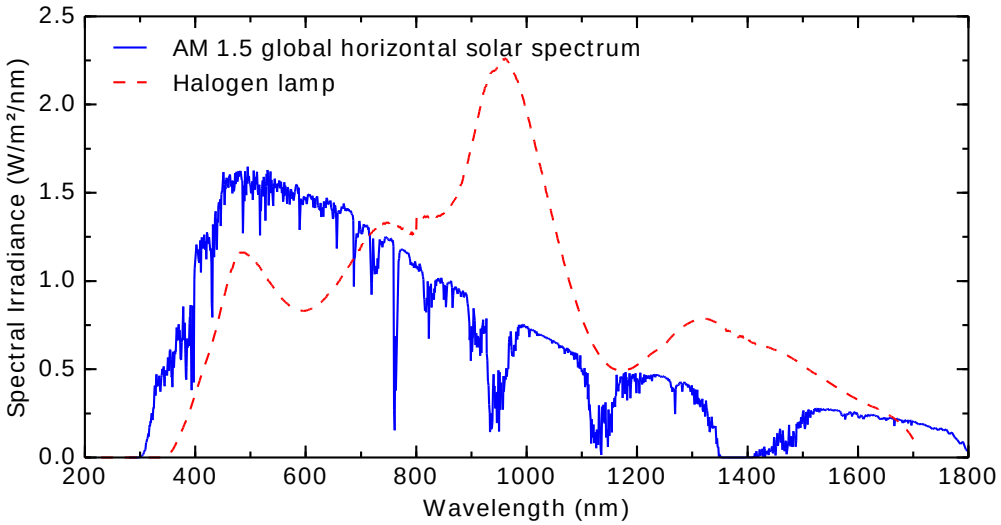


Figure 3. Irradiance of the halogen lamps (dashed) and of the AM1.5 global horizontal solar spectrum (solid) in the 200–1700 nm band (Hendel et al. 2018).

An emissivity measurement of the sample surfaces was also performed using an infrared camera. Albedo values of each structure, both dry and wet, as well as emissivity values, are summarized in Table 2.

Table 2. Emissivity and albedo values of the samples studied for both a dry and wet surface

Structure	Albedo (Halogen lamps, ASTM E903)		Emissivity (infrared camera)
	Dry	Wet	Dry
Asphalt road	0.066	0.048	0.98
Asphalt sidewalk	0.094	0.058	0.98
Stabilized sand	0.438	0.387	0.92
Granite sidewalk	0.264	0.221	0.99
PCC sidewalk	0.409	0.308	0.98
Thermochromic paint (>29°C)	0.308	0.266	0.97
NIR reflective paint	0.303	0.310	0.95

Surface heat budget

The methodology described hereafter is thoroughly presented in (Hendel et al. 2015, Parison et al. 2019). The surface heat budget of the sample surface is completely described by the following equation:

$$R_n^{dry} = H^{dry} + V_{0cm}^{dry} \quad (1)$$

with R_n the net downward radiation received by the surface, H the upward atmospheric convective heat flux and V_{0cm} the absorbed heat flux at the surface. In case the latter is watered, the budget is:

$$R_n^{wet} = H^{wet} + V_{0cm}^{wet} + \Phi \quad (2)$$

with Φ the total cooling flux due to watering. A scheme of the surface heat budget is illustrated in Figure 4.

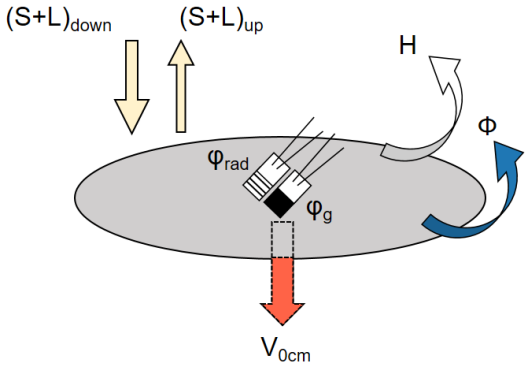


Figure 4. Schematic diagram of heat balance at the pavement surface (Parison et al., 2019). *S* is downward shortwave (SW) radiations, *L* longwave (LW) radiations, S_{ref} and L_{up}, respectively the reflected SW and upward LW radiations, *H* the upward atmospheric convective heat flux, V_{0cm} the absorbed heat flux at the surface, Φ the cooling flux due to watering. φ_{rad} is the radiative flux measured by a radiative heat flow sensor (ε=1, α=0) and φ_g the global heat flux measured by the fluxmeter (ε=0.95, α=0.05).

The parameter Φ is obtained by subtracting (1) and (2):

$$\Phi = \Delta H^{dry-wet} + \Delta V_{0cm}^{dry-wet} - \Delta R_n^{dry-wet} \quad (3)$$

Convective and radiative terms, $\Delta H^{dry\text{-}wet}$ and $\Delta R_n{}^{dry\text{-}wet}$ respectively, are determined using the following equations applied to dry and watered trials:

$$H = h(T_s - T_a) \quad (4)$$

$$R_n = (1-\alpha)S + \varepsilon\,(L - \sigma T_s^4) \quad (5)$$

Hence:

$$\Delta H^{dry-wet} = h(T_s^{dry} - T_s^{wet}) \quad (6)$$

$$\Delta R_n^{dry-wet} = \sigma\left(\varepsilon_{arr} T_s^{wet\,4} - \varepsilon_{dry} T_s^{dry\,4}\right) + \left(\varepsilon_{dry} - \varepsilon_{wet}\right)L + (\alpha_{wet} - \alpha_{dry})S \quad (7)$$

with h the convective heat transfer coefficient (hypothesising that the latter is constant between a dry and watered trial), T_s the surface temperature, T_a the air temperature, α the albedo, ε the emissivity, *S* and *L* respectively short and longwave radiations and σ the Stefan-Boltzmann constant. The conduction term, $\Delta V_0{}^{dry\text{-}wet}$, is obtained experimentally by using the difference between the fluxes measured by the sensors 6 cm deep, between a dry and watered test. This assumes that the thermal properties of the sample are not influenced by watering and that the flow absorbed by the first 6 centimetres is constant regardless of the test. This hypothesis is found to experimentally validated.

The estimation of these different parameters therefore allows us to calculate the maximum evaporative cooling flux for each watering rate and sample.

Results

Surface temperatures

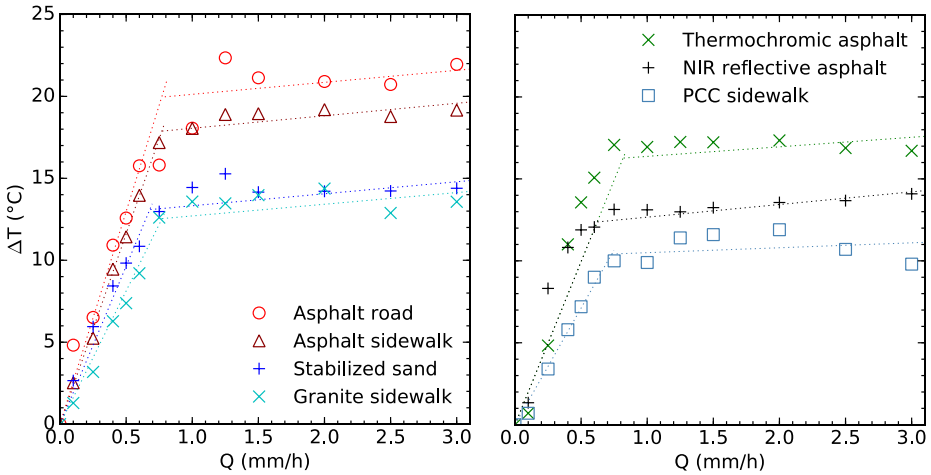


Figure 5. Maximum surface temperature differences between a dry and watered tests as a function of the watering rate *Q* for traditional structures (left) and alternative pavements (right). The double piecewise linear regression is represented with dashed lines (see Table 3 for regression statistics).

Figure 5 shows the difference in maximum surface temperatures (at the end of the day phase) of each sample as a function of the watering rate, denoted *Q*. The dry behaviour of these samples is thoroughly described in reference (Hendel et al. 2018), while the watered trials for the asphalt road sample are detailed in reference (Parison et al. 2019).

Two linear cooling regimes are observed, corresponding respectively to the increase in evaporation due to watering, then, after a certain watering rate, to the marginal increase of cooling once the maximum evaporation is reached. In order to identify the two cooling regimes visible in this figure, a double piecewise linear regression with a forced zero-intercept was conducted for each sample and is represented with dotted lines. In each case, an R^2 coefficient greater than 0.95 is found for the first regime, and greater than 0.98 for the second. The optimal watering rate, Q_{opti}, corresponds to the intersection of the two regimes and provides the adapted watering rate for each structure in order to maximize the cooling effects of the watering while minimizing the water consumption of the method. The results of this regression are summarized in Table 3.

Table 3: Best fitting equations for the first and second cooling regimes (y_2 and y_2 respectively) and optimal watering rate Q_{opti} for each structure

	y_1	y_2	Q_{opti} (mm/h)
Asphalt road	25.7 Q	0.73 Q + 19.4	0.80
Asphalt sidewalk	23.0 Q	0.76 Q + 17.3	0.78
Stabilized sand	19.1 Q	0.73 Q + 12.6	0.69
Granite sidewalk	16.1 Q	0.71 Q + 12.0	0.78
Thermochromic asphalt	19.7Q	0.58 Q + 15.8	0.83
NIR reflective asphalt	19.7Q	0.77 Q + 11.9	0.63
PCC sidewalk	14.1Q	0.30 Q + 10.2	0.74

For all pavement structures studied, strong reductions of surface temperatures are exhibited with watering, that is up to 10° to 22°C depending on the structure. Higher decreases are observed for dark structures (asphalt road and sidewalk).

For the asphalt sidewalk structure, the simple application of a thermochromic paint or a NIR reflective paint respectively lead to a reduction of 6° and 9°C for a dry test.

Conductive. convective and radiative terms

We now propose to use the surface heat budget to determine the terms $\Delta V_0^{dry\text{-}wet}$, $\Delta H^{dry\text{-}wet}$ and $\Delta R_n^{dry\text{-}wet}$, which represent the reductions in absorbed heat and convective flux respectively, as well as the increase in net radiation due to watering. These terms are illustrated in Figure 6 for the traditional and innovative structures.

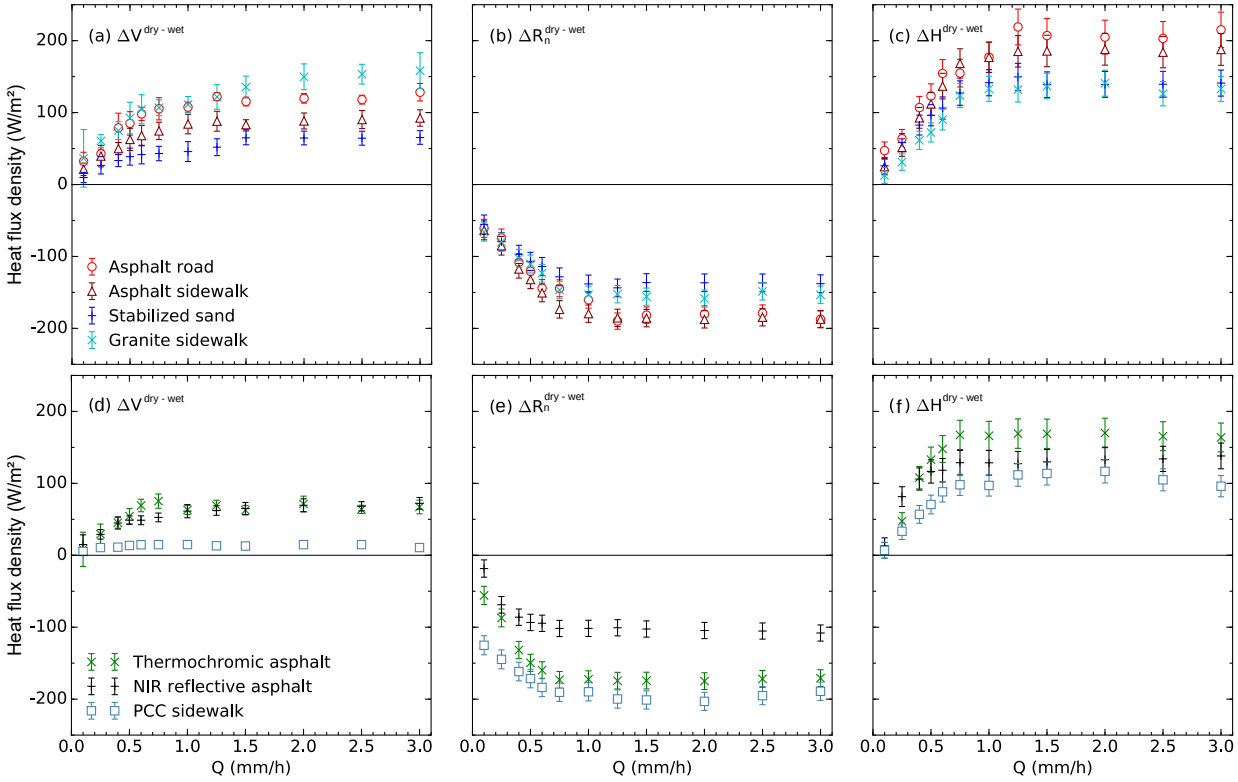


Figure 6. From left to right, respectively, dry-watered differences of absorbed heat flux $\Delta V_0^{dry\text{-}wet}$. net radiation $\Delta R_n^{dry\text{-}wet}$ and convective flux $\Delta H^{dry\text{-}wet}$ as a function of the watering rate Q, for traditional samples (a, b and c) and alternative structures (d, e and f).

For each structure, for a dry test, a convective exchange coefficient of about 10 W/(m².K) was found (Parison et al. 2019). For watered tests. the emissivity of the water (i.e. 0.98) is used for each sample.

In Figure 6 (a) and (d), we can see that heat storage is greatly reduced by watering, i.e. $\Delta V_0^{dry\text{-}wet}$ increases. The structure most impacted by watering in terms of heat storage appears to be the granite sidewalk, although the latter remains relatively "cool" on the surface due to its higher albedo. compared to the pavement and the asphalt sidewalk (daytime end-of-phase temperature of 52°C versus more than 60°C. respectively) (Hendel et al. 2018). This is due to the highly

conductive nature of granite. which. although reflective. transmits as much heat 6 cm deep as the asphalt road when tested without watering (Hendel et al. 2018). On the other hand, for the traditional structures, the stabilized sand seems to be the least affected by watering due to its low thermal conductivity. The same tendency is observed for the concrete sidewalk for alternative structures for the same reason.

In Figure 6 (b) and (e), we notice that $\Delta R_n^{dry\text{-}wet}$ decreases significantly with Q. i.e. the net radiation increases with watering in all cases. The dark structures. i.e. asphalt road and sidewalk. are the ones for which this decrease is strongest, mainly due to the large difference in surface temperature of these samples between their dry and watered behaviour. For the alternative structures (fig. 6 (e)), the concrete sidewalk is the sample exhibiting the lowest value of $\Delta R_n^{dry\text{-}wet}$ although the dry-wet surface temperature difference is the lowest between all samples. This is most likely because of the strong change in albedo between dry and wet tests (about 10% change), which offset weak temperature differences for this structure as a consequence.

Finally, in Figure 6 (c) and (f). we can see that convective exchanges between the surface and the ambient air decrease with Q, i. e. $\Delta H^{dry\text{-}wet}$ gradually increases with watering. This increase is directly proportional to the temperature difference between the dry and wet tests of each structure, as shown in equation (7). Since the convective exchange coefficient h is similar for each structure, tendencies follow that of the temperature differences visible in Figure 5. The hottest structures (asphalt road and sidewalk) are therefore more impacted by watering than the "cooler" structures (granite. stabilized sand).

Evaporative cooling flux

From equation (4), knowing $\Delta V_0^{dry\text{-}wet}$, $\Delta H^{dry\text{-}wet}$ and $\Delta R_n^{dry\text{-}wet}$, it is possible to calculate the evaporative cooling flux Φ for each watering rate and for each structure at the end of the day phase. This value is shown in Figure 7. Again. a double piecewise linear regression with forced zero intercept was performed for each sample and is represented with dashed lines. Results are summarized in Table 4.

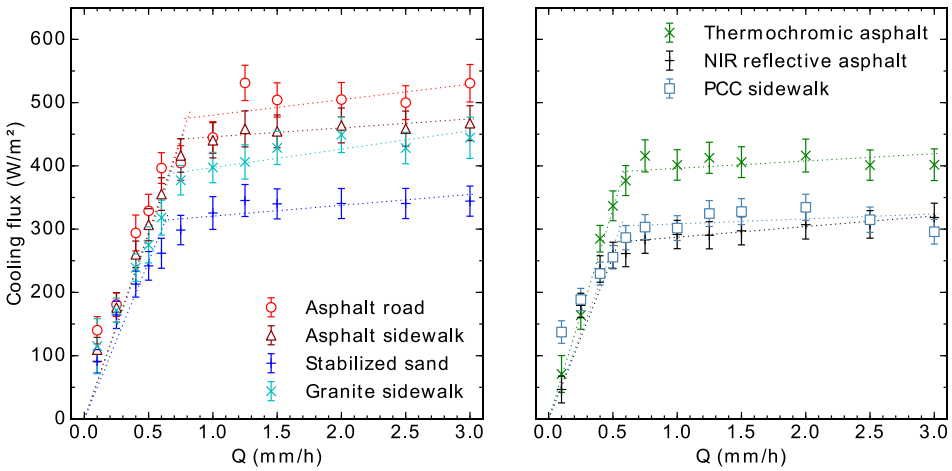


Figure 7. Total evaporative cooling flux as a function of the watering rate Q. The double piecewise linear regression is represented with dashed lines. (see Table 4 for regression statistics).

Table 4: Optimal values of Φ and best fitting equations for the two linear regimes (y_2 et y_2 respectively) and optimal watering rates Q_{opti} for each sample.

	y_1	y_2	Q_{opti} (mm/h)	Φ (W/m²)
Asphalt road	591 Q	24.5 Q + 455	0.80	475
Asphalt sidewalk	585 Q	14.2 Q + 432	0.76	440
Stabilized sand	497 Q	17.2 Q + 303	0.63	310
Granite sidewalk	575 Q	29.1 Q + 368	0.67	385
Thermochromic asphalt	663 Q	11.6 Q + 384	0.59	390
NIR reflective asphalt	513 Q	16.7 Q + 271	0.55	280
PCC sidewalk	542 Q	7.9 Q + 300	0.56	300

Globally, it can be seen that brighter and thus cooler structures have a lower optimal watering rate. Since the pavement structures presented here are impervious, the optimal watering rate should not be directly influenced by pervious subgrade materials. It is expected, however, that water absorption should play a role for pervious pavements.

Maximum cooling is obtained for the classic asphalt road structure and is around 500 W/m². This value, which corresponds approximately to twice what had been observed in the field (Hendel et al. 2018), seems to be interpreted because of the amount of energy received by the pavement inside the chamber. which also doubles (Parison et al. 2019).

In any case, tests on other structures, such as permeable pavements, would be interesting in order to complete and therefore explain these results in greater detail.

Conclusion

Various pavements used in Paris (asphalt road and sidewalk, granite sidewalk and stabilized sand) as well as alternatives (thermochromic and NIR reflective paint as well as concrete sidewalk) were tested in the lab inside a climate chamber reproducing conditions similar to those observed during a heat wave in Paris. A watering of their surface with more than ten different watering rates was also carried out, in order to optimize the process before deployment in the field.

Using a surface heat budget with and without watering, the evaporative cooling flux can be evaluated as well as the reductions in heat flow absorbed by the different structures, the reductions in convective exchange between the surface and the ambient air and the increase in net radiation due to watering. So far, the device has shown results consistent with the *in situ* watering experiment, taking into account the different conditions in both cases.

The reductions in convective exchange are directly driven by the surface temperature reductions due to watering, while the heat absorption reductions seem to be linked to the conducting properties of the structures. Finally, the increase in net radiation due to watering is influenced by different factors, such as temperature reduction and albedo variation between a dry and wet surface. Regardless, this needs to be better quantified to better understand the implication of each factor in the process of cooling.

Further tests will aim to analyse the thermo-climatic behaviour of other structures, including permeable concrete structures and compare them with existing structures. The energy partitioning for each of the structures and their behaviour in depth will also be characterized. Also, various indicators taking into account the radiative (albedo, emissivity) and thermal properties (such as the thermal conductivity) will be developed to predict and explain the cooling potential of each pavement structure under the normalized conditions of the chamber.

Acknowledgements

Funding for this study was provided by the Paris City Hall. Authors would like to acknowledge the technical support and expertise of the Paris City Hall Roads and Traffic and the Water and Sanitation Divisions.

References

ASTM. Standard test method for solar absorptance, reflectance, and transmittance of materials using integrating spheres. 2012.

HENDEL. Martin. GUTIERREZ. Pierre. COLOMBERT. Morgane. *et al*. Measuring the effects of urban heat island mitigation techniques in the field: Application to the case of pavement-watering in Paris. *Urban Climate*. 2016. vol. 16. p. 43-58.

HENDEL. Martin. COLOMBERT. Morgane. DIAB. Youssef. *et al.* Improving a pavement-watering method on the basis of pavement surface temperature measurements. *Urban Climate*. 2014. vol. 10. p. 189-200.

HENDEL. Martin. PARISON. Sophie. GRADOS. Arnaud. *et al.* Which pavement structures are best suited to limiting the UHI effect? A laboratory-scale study of Parisian pavement structures. *Building and Environment.* 2018. vol. 144. p. 216-229.

HENDEL. Martin. COLOMBERT. Morgane. DIAB. Youssef. *et al.* An analysis of pavement heat flux to optimize the water efficiency of a pavement-watering method. *Applied thermal engineering*. 2015. vol. 78. p. 658-669.

LEMONSU. Aude. KOUNKOU-ARNAUD. Raphaëlle. DESPLAT. Julien. *et al*. Evolution of the Parisian urban climate under a global changing climate. *Climatic change*. 2013. vol. 116. no 3-4. p. 679-692.

ROBINE. Jean-Marie. CHEUNG. Siu Lan K.. LE ROY. Sophie. *et al*. Death toll exceeded 70.000 in Europe during the summer of 2003. *Comptes rendus biologies*. 2008. vol. 331. no 2. p. 171-178.

PARISON. Sophie. HENDEL. Martin. JURSKI. Kristine. *et al.* The Impact of Different Watering Strategies on the Cooling Effects of Pavement-Watering during Heat-Waves. *in PLEA 2017 Proceedings - Design to Thrive*. 2017. pp.120-127

PARISON. Sophie. HENDEL. Martin. GRADOS. Arnaud. *et al.* A lab Experiment for Optimizing the Cooling Efficiency and the Watering Rate of Pavement-Watering. *Urban Climate.* 2019. *under review*

Development of heterogeneous directionally reflective materials for building facades and measurements of their reflective properties

Chiara Ferrari, Department of Engineering "Enzo Ferrari", University of Modena and Reggio Emilia (Italy)
Riccardo Paolini, Department of Built Environment, University of New South Wales, Sydney (Australia)
Alberto Muscio[1], Department of Engineering "Enzo Ferrari", University of Modena and Reggio Emilia (Italy)
Mat Santamouris, Department of Built Environment, University of New South Wales, Sydney (Australia)

ABSTRACT

Solar reflective materials are recognized as an effective countermeasure to UHI. They show high values of albedo, so they can easily reflect toward the sky most of solar radiation hitting the low-sloped surfaces to which they are applied. Nonetheless they are not equally effective when applied to vertical surfaces in densely-built areas due to the strong absorption of solar radiation that occurs in the so-called urban canyon, caused by multiple reflection-absorption effects. Such issue has been addressed by several researchers. Directionally reflective materials that rely upon a proper surface and color texture have ~~also~~ been investigated for sloped roofs, with reflective facets that face the sky, whereas facets with a desired but absorbing color are visible from the below. During summer they can reflect sunlight, which impinges onto the reflective facets, whereas in winter sunlight impinges onto the absorbing facets. Such materials can also be exploited for facades, which is the subject of this work. Combinations of reflective and absorbing coatings are applied on shaped prototypes of 3D printed façade elements. Their behavior is analyzed through field measurements aimed to evaluate the response to sun's height (comparing the measured performance with that predicted by theoretical models) and façade orientation, comparing the measured performance with that predicted by theoretical models and providing an accurate projection of such performance across the daytime and the season.

Introduction

The increase of temperatures of urban areas, with respect to the surrounding rural areas, that the whole world is experiencing in the last decades can be identified as the urban heat island (UHI) effect (Santamouris & Asimakopoulos, 2001). This leads to higher energy demand for air conditioning systems as well as a higher energy consumption and increased pollutants emission (Santamouris et al., 2001; Vallati et al., 2015), moreover it increases human health risks and mortality (Pantavou et al., 2013; Sakka et al., 2012; Santamouris & Kolokotsa, 2015). To reduce the UHI impact, several strategies were proposed such as the use of solar reflective materials (Zinzi, 2010), both white (Kolokotsa et al., 2012; Santamouris et al., 2008), to maximize the solar reflection, and colored (Ferrari et al., 2015; Ferrari et al., 2016; Levinsonet al., 2010; Pisello et al., 2014; Synnefa & Santamouris, 2013), to better meet architectonic requirements, green roofs (Castleton et al., 2010; M. Santamouris, 2014) and also advanced materials such as PCM (Ranade

[1] Corresponding Author: [alberto.muscio@unimore.it], [+390592056194].

et al., 2010), thermochromic (Karlessi & Santamouris, 2013; Perez et al., 2018) and fluorescent materials (Berdahl et al., 2016). Recently also a new approach to traditional roofing materials was proposed by (Akbari & Kolokotsa, 2016; Akbari & Touchaei, 2014) introducing new heterogeneous directional reflective materials (DRM): these are characterized by a series of right triangular prisms, with the hypotenuse of the cross section lying on the roof surface, the short reflective side of the cross section facing skywards, in order to reflect sunlight during summer (when the sun is high in the sky), and the long absorptive side facing streetward and absorbing sunlight during winter (when the sun is low). Due to this particular shape, DRM's look dark from the street and light from the sky.

The increasing density of population required dedicated urbanization strategies such as the vertical development of cities with the consequent creation of the urban canyons, the spaces between buildings characterized by an increased surface area for walls and facades at the expense of roof surface and by new microclimatic conditions (Morini, et al., 2018; Paolini et al., 2014). As a result, taking care of the building envelope does not mean only optimizing the roofs, but more attention must be paid to the reflective properties and energy efficiency potential of walls and facades (Gago et al., 2013; Georgakis et al., 2014; Rosenfeld et al., 1995), and, together with this, to all the radiative phenomena occurring in the canyon (Morini et al., 2017; Qin, 2015). Despite several solutions were proposed to improve the facades thermal performances such as cool walls, green walls, and PCM, canyon overheating issues remains significant. Recently some strategies such as retroreflective (RR) materials were proposed in order to remedy to canyon overheating (Rossi et al., 2015, 2014). These materials are characterized by reflecting backward the striking energy (Morini et al., 2018). Approaches to retro-reflective materials were made, by using films (Rossi et al., 2015), glass microspheres embedded in paints (Castellani et al., 2017; Han et al., 2015; Morini et al., 2018).

This study is aimed to investigate a new type of directional reflective materials, inspired by a similar solution proposed for sloped roofs (Akbari & Touchaei, 2014). More specifically, DRM's have been applied as facades elements, where the white reflective side is positioned skywards, while the colored absorbing side is positioned streetward. The behavior of different small scale prototypes, printed via Fused Deposition Modelling (FDM) and characterized by different colors, have been analyzed by means of radiometric measurements. The level of solar radiation reflected by the samples, placed in a model of a urban canyon, has been analyzed, and the performance of DRM's has been compared with that of flat surfaces characterized by the same colors.

Materials and methods

Five different 100 mm x 100 mm x 3 mm prototypes were printed via FDM in white filament. Each one is a plate characterized by the presence of 25 triangular prisms with cross section 3.5 mm x 1.1 mm x3.9 mm, where the longer side of the cross section is laying on the surface of the sample (Figure 1).

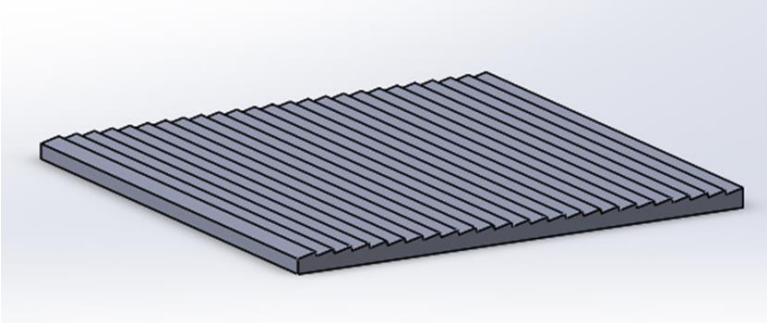


Figure 1 - Sample structure

The prototypes were characterized by different colors applied via airbrush: white, brick red, black, brick red/white (short exposed facet of the prism white, long exposed facet brick red), black/white (short exposed facet of the prism white, long exposed facet black) (Figure 2). Together with the profiled samples, three samples with flat surfaces were prepared. The three flat samples where coated with white, brick red and black paints.

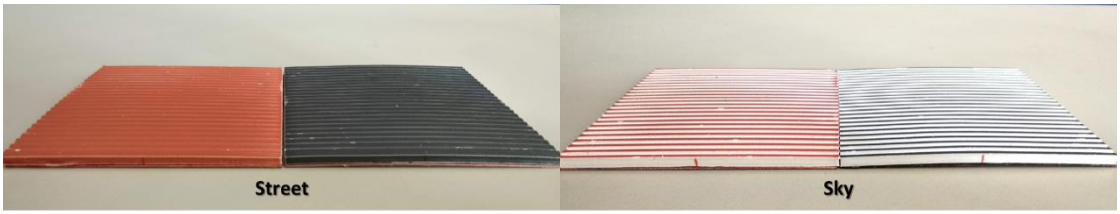


Figure 2 – brick red/white and black/white samples as seen from the street and from the sky

As shown in Figure 3 (left), the prototype samples have been placed in a model of a canyon with 3:1 height to width ratio (dimensions: 30 cm x 10 cm), made of 5 cm thick XPS panels and representative of an actual canyon with about 1:100 scale. The external surfaces of the canyon model have been painted with white paint having high solar reflectance (SR=0.842), whereas the internal surfaces of the canyons have been covered with a black coating (SR=0.045) in order to make reflection from the samples dominant on any other reflection phenomena in the canyon. Two small cavities for radiative measurement have been opened on the canyon as shown in Figure 3 (right): one on the bottom of the canyon in correspondence of the center of the sample and three on facing the sample, respectively at 1/4, 2/4 and 3/5 in height. To fill the opening not occupied by sensors in the wall facing the sample, a pice of insulating panel with the same black coating of other canyon surfaces (SR=0.045) was used.

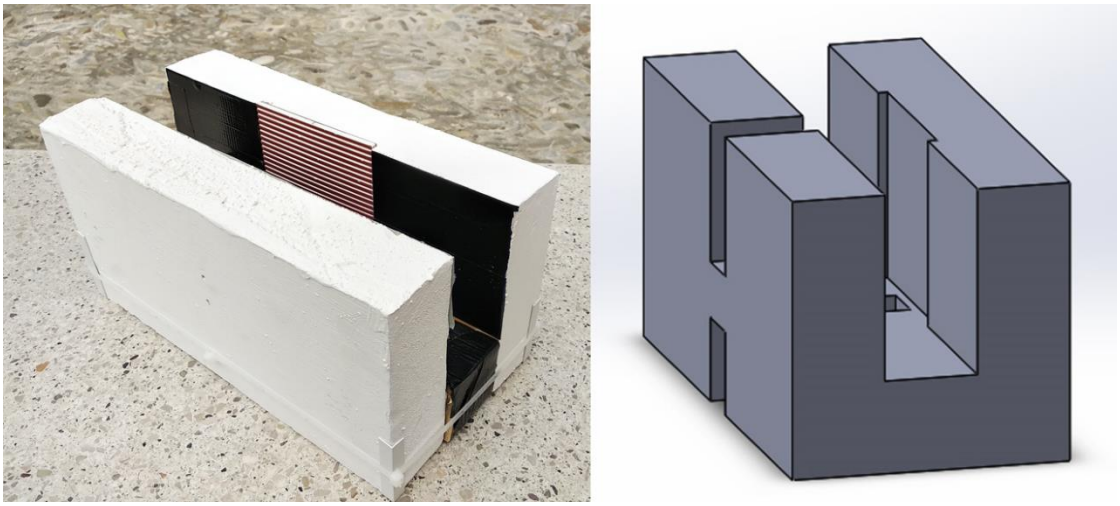


Figure 3 - Canyon small scale model in which the samples are placed (see left) and sketch of cavities for radiometric measurements (right)

The canyon has been oriented with samples facing SE, S and SW and has been inclined in order to obtain an angle between the façade plane and the sun radiation direction equal to 15° or 30°. The first angle represents the situation during summer at low latitude (i.e. North Africa) while the second angle represents the situation during summer for a higher Mediterranean latitude (i.e. Southern Europe). For each sample, canyon inclination and canyon orientation, the solar irradiance incident on the top of the canyon was measured. Moreover, white, brick red and black paints were characterized in the lab according to ASTM E903 (ASTM International, 1996) by a Jasco V-670 spectrophotometer with a 150mm integrating sphere. Together with solar reflectance, CIELAB parameters (L*a*b*) were calculated via ISO 11664-4 (ISO, 2004). The solar reflectance was calculated by integrating over the range from 300 nm to 2500 nm the measured spectral reflectivity weighted by the standard spectral irradiance of the sun at the earth surface. In this case, the AM1GH solar spectrum (air mass 1 global horizontal) was used for the spectral irradiance (Ferrari et al., 2013; Levinson et al., 2010). A portable radiometer (HD 9221, Delta ohm) equipped with a LP 9221/RAD sensor with spectral measurement range from 350 nm to 950 nm was used to perform irradiance measurements.

Results

In Figure 4 the spectral reflectivity and the values of solar reflectance calculated with the AM1GH irradiance spectrum have been reported. In addition to solar reflectance, L*a*b* parameters calculated accordint to ISO 11664-4 are reported in . The spectral reflectivity of the three samples presents relatively high values in the NIR region (above 700 nm), demonstrating a marked ability to reflect solar radiation without affecting the visual response. This is a result of the white basecoat onto which the paint was applied. Regarding color parameters, both white and black coatings presents small values for a* and b*: this indicate a color without chromatic influences brought by red-green (a* parameter) and yellow-blue (b*parameter).

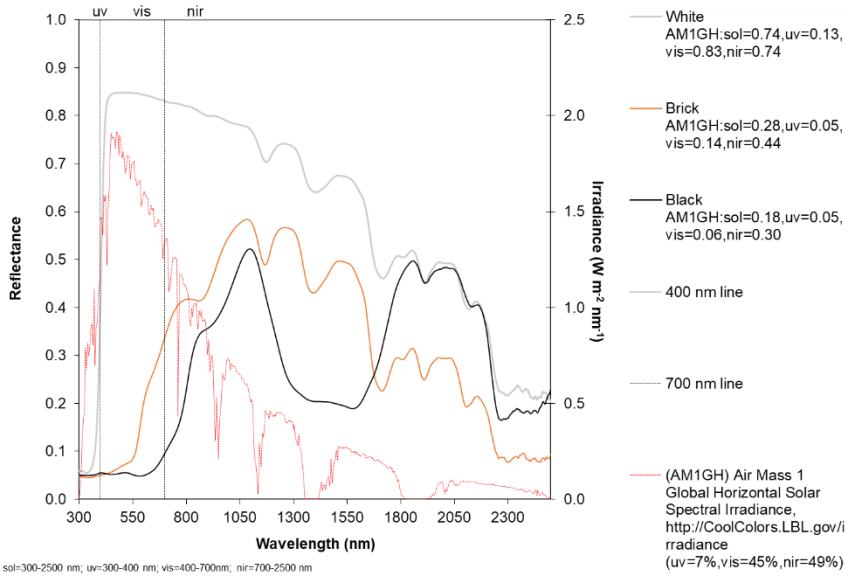


Figure 4 - Spectral reflectivity of coatings applied on directional reflective materials

*Table 1. L*a*b* parameters for analyzed coatings*

Coating	L*	a*	b*
White	93.13	0.47	-0.27
Brick red	40.51	22.51	20.01
Black	27.18	0.26	-0.62

Below, the two analyzed scenario are reported, considering that the average incident irradiance for the canyon with facades forming an angle of 15° with the incident solar radiation is equal to 623 W/m^2, while the irradiance for the canyon with facades forming an angle of 30° with the incident solar radiation is equal to 564W/m^2. The values of irradiance reported for each sample and each orientation are normalized to the incident solar radiation measured during each test.

Table 1 – Values of normalized radiation for flat samples with canyons inclined 15° with respect to solar radiation

		I (W/m^2)	Horizontal	Vertical low	Vertical mid	Vertical high	Vertical avg
Black planar	SE	607.5	0.184	0.041	0.049	0.044	0.045
	S	630	0.160	0.040	0.037	0.035	0.037
	SW	612.5	0.212	0.038	0.042	0.065	0.048
Brick red planar	SE	595	0.190	0.067	0.064	0.067	0.066
	S	626.5	0.171	0.064	0.073	0.085	0.074
	SW	581	0.177	0.043	0.046	0.055	0.048
White planar	SE	626.5	0.184	0.158	0.176	0.172	0.169
	S	657.5	0.195	0.114	0.119	0.111	0.115
	SW	607.5	0.173	0.099	0.099	0.102	0.100

Table 2 - Values of normalized radiation for flat samples with canyons inclined 30° with respect to solar radiation

		I (W/m^2)	Horizontal	Vertical low	Vertical mid	Vertical high	Vertical avg
Black planar	SE	550	0.164	0.062	0.055	0.064	0.060
	S	567.5	0.070	0.049	0.051	0.048	0.049

	SW	550	0.091	0.047	0.036	0.045	0.043
Brick red planar	SE	550	0.136	0.069	0.091	0.091	0.084
	S	550	0.067	0.045	0.082	0.104	0.077
	SW	560	0.068	0.059	0.080	0.086	0.075
White planar	SE	560	0.125	0.164	0.182	0.182	0.176
	S	557.5	0.081	0.145	0.197	0.233	0.192
	SW	562.5	0.098	0.121	0.133	0.192	0.149

Table 3 - Values of normalized radiation for profiled samples with canyons inclined 15° with respect to solar radiation

		I(W/m^2)	Horizontal	Vertical low	Vertical mid	Vertical high	Vertical avg
Black	SE	560	0.080	0.052	0.075	0.100	0.076
	S	552.5	0.054	0.029	0.058	0.081	0.056
	SW	542.5	0.065	0.037	0.052	0.074	0.054
Black/ White	SE	585	0.077	0.044	0.079	0.140	0.088
	S	575	0.061	0.035	0.083	0.130	0.083
	SW	580	0.066	0.041	0.098	0.122	0.087
White	SE	570	0.084	0.137	0.193	0.184	0.171
	S	565	0.064	0.099	0.142	0.204	0.148
	SW	575	0.061	0.143	0.200	0.209	0.184
Brick red/ White	SE	580	0.069	0.074	0.121	0.138	0.111
	S	577.5	0.057	0.050	0.071	0.139	0.087
	SW	582.5	0.062	0.062	0.108	0.129	0.100
Brick red	SE	566	0.097	0.046	0.069	0.076	0.064
	S	550	0.045	0.036	0.060	0.109	0.068
	SW	572.5	0.065	0.044	0.070	0.096	0.070

Table 4 - Values of normalized radiation for profiled samples with canyons inclined 30° with respect to solar radiation

		I(W/m^2)	Horizontal	Vertical low	Vertical mid	Vertical high	Vertical avg
Black	SE	641	0.140	0.041	0.050	0.070	0.054
	S	649.5	0.065	0.046	0.057	0.072	0.059
	SW	642.5	0.062	0.039	0.050	0.075	0.054
Black/ White	SE	620	0.066	0.060	0.077	0.084	0.074
	S	625	0.064	0.074	0.088	0.096	0.086
	SW	640	0.063	0.066	0.094	0.094	0.084
White	SE	611.5	0.303	0.106	0.131	0.131	0.123
	S	634	0.091	0.142	0.166	0.189	0.166
	SW	622.5	0.093	0.161	0.169	0.180	0.170
Brick red/ White	SE	622.5	0.085	0.080	0.088	0.112	0.094
	S	637.5	0.083	0.094	0.097	0.125	0.106
	SW	617.5	0.083	0.086	0.102	0.113	0.100
Brick red	SE	615	0.075	0.062	0.065	0.073	0.067
	S	622.5	0.071	0.064	0.077	0.077	0.073
	SW	616	0.084	0.065	0.073	0.081	0.073

Due to the amount of data, a graphical approach may facilitate the comprehension of what observed during the measurements campaign (Fig. 5).

As expected, the canyons containing white samples present higher irradiance reaching both the bottom of the canyon and the façade facing the canyon. Moreover, analyzing the black and brick red samples, both DRM and flat surfaces, the flat samples present slightly lower values of solar irradiance on the façade facing the analyzed sample. On the same facing façade, as expected, increasing the distance from the bottom of the canyon, the irradiance increases. Drawing general observations, it can be noticed how samples with the same layout (i.e. flat samples or DRM's) present analogous behavior. Samples characterized by the same color, even though characterized by different morphology, present similar trend with the variation of the orientation and inclination of the canyon.

From the plots it emerged that for 15° for canyons with sample facade inclined 30° with respect to the incident solar radiation, the normalized radiation measured on the bottom of the canyon, that is on the horizontal bottom surface, is significantly higher than the normalized radiation measured in vertical positions on the faced facing the samples, and this trend is more evident for black and brick red flat samples with respect to the white samples.

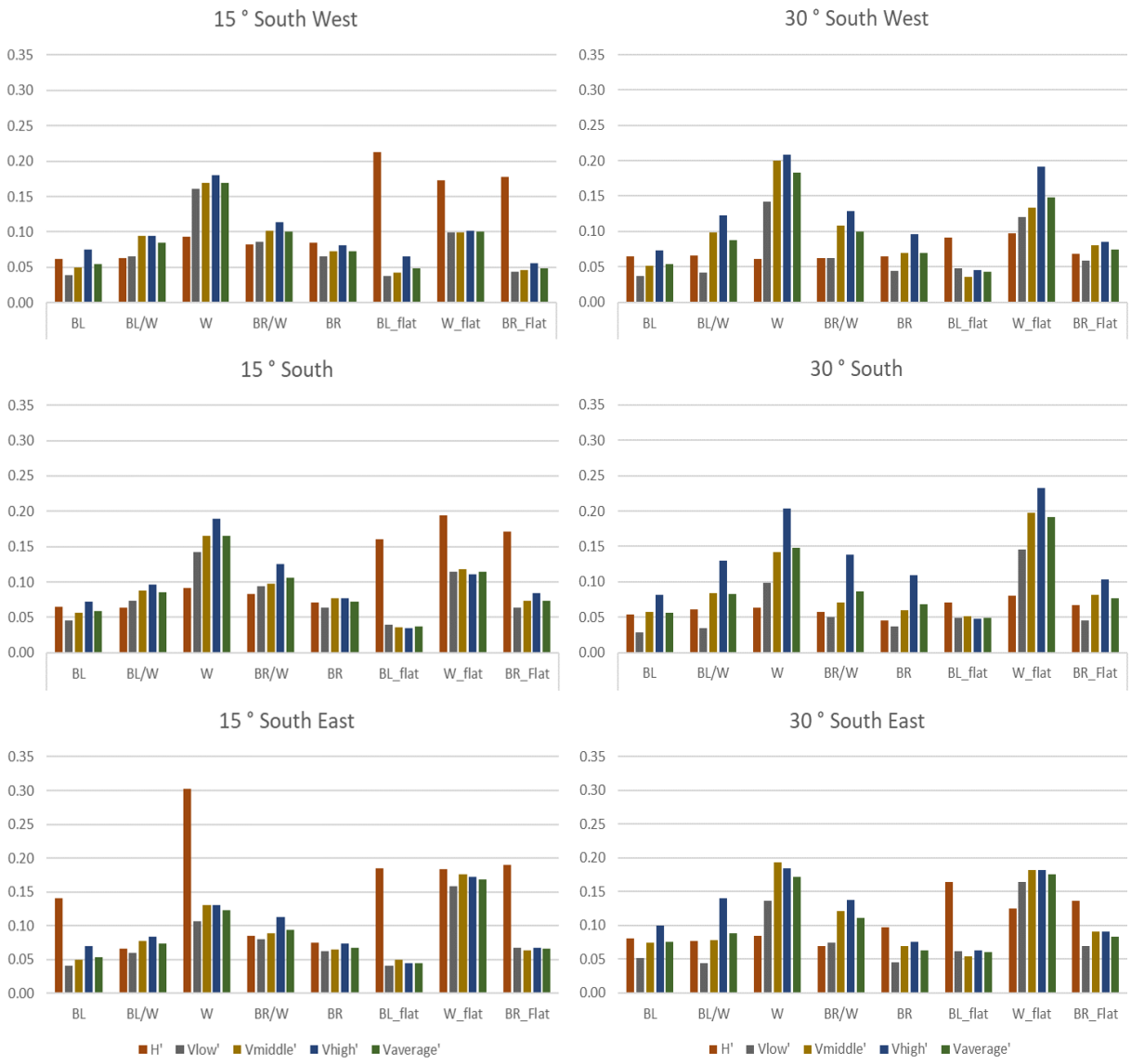


Figure 5 - Plot summarizing normalized radiation values. In the left column, data are reported for solar radiation forming a 15° angle with the irradiated facade, in the right column data are reported for solar radiation forming a 30° angle with the irradiated facade. In the first row data are reported for canyon with samples facing south-west, in the second row for canyon with samples facing south and, in the third row for canyon with samples facing south-east. The bars represent, from left to right, horizontal normalized radiation, vertical normalized radiation on the facing faced in the lower position, in the mid-height position, in the high position, and on average for all position.

This trend highlights the non-Lambertian behavior of flat samples placed in canyons at low latitude. The same trend, however, cannot be found for canyons with sample facade inclined 30° with respect to the incident solar radiation as it is visible on the right column in Figure 5.

Analyzing the data, it emerges how, with respect to the flat surface, in sub-Mediterranean contexts (15° angle) the profiled solutions allow the reduction of radiation reaching the canyon pavement without a steep increase of reflection on the façade facing the sample.

Conclusions

Urban summer overheating is one of the main features of urban heat island effect. In particular, due to the demographical increase within urban areas, the development of urban canyons occurs more frequently. Together with the traditional passive cooling techniques suitable for the building envelope, concerning urban canyons, a particular attention should be paid to the overheating of the canyon itself: the reflective surfaces covering the building envelope, generally characterized by a Lambertian behavior, spread a significant amount of the solar radiation not just back to the sky but also down to the bottom of the canyon. This workis aimed to suggest an adaptation of an approach, already proposed for roofing solutions (Akbari & Touchaei, 2014), to canyon façades. Several prototypes, characterized by three different coatings (black, white and brick red) applied with different combinations have been prepared, as well as three flat reference samples characterized by the same black, white and brick red colors. All the samples have been placed inside a 3:1 small scale model of a urban canyon and the irradiance in four different spots inside the canyon has been measured (one on the bottom of the canyon, in correspondence of the sample, and in three positions on the façade facing the sample) by means of a solar radiometer. During the campaign, both 15° and 30° inclinations toward solar radiation (that is the angles between the irradiated façade and the direct solar radiation direction) have been investigated, as well as solutions with DRM samples facing south-east, south and south-west. All the results have been normalized to the average of solar radiation measured on the top of the canyon before and after each measurement.

In view of the measurement results, the proposed solution based on DRM can be successful since, in particular in sub-Mediterranean areas, as it allows reducing significantly solar radiation reaching the bottom of the canyon, with just a slight increase of the solar reflectiong toward the façade facing the samples. This study, however, is still a preliminary investigation. Further work will be aimed to produce larger samples and, consequently, a more realistic canyon model, also instrumented in order to make thermal measurements possible.

References

Akbari, H., & Kolokotsa, D. (2016). Three decades of urban heat islands and mitigation technologies. *Energy & Buildings*, 133, 834–842.

Akbari, H., & Touchaei, A. G. (2014). Modeling and labeling heterogeneous directional reflective roofing materials. *Solar Energy Materials and Solar Cells*, 124, 192–210.

ASTM International (1996). *ASTM E903 − 12 Standard Test Method for Solar Absorptance, Reflectance, and Transmittance of Materials Using Integrating Spheres*, 1–9.

Berdahl, P., Chen, S. S., Destaillats, H., Kirchstetter, T. W., Levinson, R. M., & Zalich, M. A. (2016). Fluorescent cooling of objects exposed to sunlight – The ruby example. *Solar Energy Materials and Solar Cells*, 157, 312–317.

Castellani, B., Morini, E., Anderini, E., Filipponi, M., & Rossi, F. (2017). Development and characterization of retro-reflective colored tiles for advanced building skins. *Energy and Buildings*, 154, 513–522.

Castleton, H. F., Stovin, V., Beck, S. B. M., & Davison, J. B. (2010). Green roofs; Building energy savings and the potential for retrofit. *Energy and Buildings*, 42(10), 1582–1591.

Ferrari, C., Muscio, A., Siligardi, C., & Manfredini, T. (2015). Design of a cool color glaze for solar reflective tile application. *Ceramics International*, 41(9), 11106–11116.

Ferrari, Chiara, Libbra, A., Muscio, A., & Siligardi, C. (2013). Influence of the irradiance spectrum on solar reflectance measurements. *Advances in Building Energy Research*, 7(2), 244–253.

Ferrari, Chiara, Muscio, A., & Siligardi, C. (2016). Development of a Solar-reflective Ceramic Tile Ready for Industrialization. *Procedia Engineering*, 169, 400–407.

Gago, E. J., Roldan, J., Pacheco-Torres, R., & Ordóñez, J. (2013). The city and urban heat islands: A review of strategies to mitigate adverse effects. *Renewable and Sustainable Energy Reviews*, 25, 749–758.

Georgakis, C., Zoras, S., & Santamouris, M. (2014). Studying the effect of "cool" coatings in street urban canyons and its potential as a heat island mitigation technique. *Sustainable Cities and Society*, 13, 20–31.

Han, Y., Taylor, J. E., Pisello, A. L., Laura, A., & Pisello, A. L. (2015). Toward mitigating urban heat island effects: Investigating the thermal-energy impact of bio-inspired retro-reflective building envelopes in dense urban settings. *Energy and Buildings*, 102, 380–389.

ISO 2004. *ISO 11664-4 Colorimetry — Part 4: CIE 1976 L*a*b* Colour space*, 2004.

Karlessi, T., & Santamouris, M. (2013). *Research on thermochromic and pcm doped infrared reflective coatings*. Bentham Science Publishers Ltd., pp. 83–103.

Kolokotsa, D., Maravelaki-Kalaitzaki, P., Papantoniou, S., Vangeloglou, E., Saliari, M., Karlessi, T., & Santamouris, M. (2012). Development and analysis of mineral based coatings for buildings and urban structures. *Solar Energy*, 86(5), 1648–1659.

Levinson, R., Akbari, H., & Berdahl, P. (2010). Measuring solar reflectance-Part I: Defining a metric that accurately predicts solar heat gain. *Solar Energy*, 84(9), 1717–1744.

Levinson, R., Akbari, H., Berdahl, P., Wood, K., Skilton, W., & Petersheim, J. (2010). A novel technique for the production of cool colored concrete tile and asphalt shingle roofing products. *Solar Energy Materials and Solar Cells*, 94(6), 946–954.

Morini, E., Castellani, B., De Ciantis, S., Anderini, E., & Rossi, F. (2018). Planning for cooler urban canyons: Comparative analysis of the influence of façades reflective properties on urban canyon thermal behavior. *Solar Energy*, 162, 14–27.

Morini, E., Castellani, B., Nicolini, A., Rossi, F., & Berardi, U. (2018). Effects of aging on retro-reflective materials for building applications. *Energy and Buildings*, 179, 121–132.

Morini, E., Castellani, B., Presciutti, A., Anderini, E., Filipponi, M., Nicolini, A., & Rossi, F. (2017). Experimental analysis of the effect of geometry and façade materials on urban district's equivalent albedo. *Sustainability*, 9(7), 1245.

Pantavou, K., Theoharatos, G., Santamouris, M., & Asimakopoulos, D. (2013). Outdoor thermal sensation of pedestrians in a Mediterranean climate and a comparison with UTCI. *Building and Environment*, 66, 82–95.

Paolini, R., Mainini, A. G., Poli, T., & Vercesi, L. (2014). Assessment of thermal stress in a street canyon in pedestrian area with or without canopy shading. *Energy Procedia*, 48, 1570–1575.

Perez, G., Allegro, V. R., Corroto, M., Pons, A., & Guerrero, A. (2018). Smart reversible thermochromic mortar for improvement of energy efficiency in buildings. *Construction and Building Materials*, 186, 884–891.

Pisello, A. L., Cotana, F., & Brinchi, L. (2014). On a cool coating for roof clay tiles: Development of the prototype and thermal-energy assessment. *Energy Procedia*, 45, 453–462.

Qin, Y. (2015). Urban canyon albedo and its implication on the use of reflective cool pavements.

Energy and Buildings, 96, 86–94.

Ranade, A. N., Fulton, C., Seebergh, J. E., Nichols, M., Remillard, J., Graham, M., & Chung, Y. W. (2010). Synthesis, structure, and optical properties of Au-TiO_2 composite thin films. *Thin Solid Films*, 519(5), 1490–1494.

Rosenfeld, A. H., Akbari, H., Bretz, S., Fishman, B. L., Kurn, D. M., Sailor, D., & Taha, H. (1995). Mitigation of urban heat islands: materials, utility programs, updates. *Energy and Buildings*, 22(3), 255–265.

Rossi, F., Morini, E., Castellani, B., Nicolini, A., Bonamente, E., Anderini, E., & Cotana, F. (2015). Beneficial effects of retroreflective materials in urban canyons: Results from seasonal monitoring campaign. *Journal of Physics: Conference Series*, 655, 012012.

Rossi, Federico, Castellani, B., Presciutti, A., Morini, E., Filipponi, M., Nicolini, A., & Santamouris, M. (2015). Retroreflective façades for urban heat island mitigation: Experimental investigation and energy evaluations. *Applied Energy*, 145, 8–20.

Rossi, Federico, Pisello, A. L., Nicolini, A., Filipponi, M., & Palombo, M. (2014). Analysis of retro-reflective surfaces for urban heat island mitigation: A new analytical model. *Applied Energy*, 114, 621–631.

Sakka, A., Santamouris, M., Livada, I., Nicol, F., & Wilson, M. (2012). On the thermal performance of low income housing during heat waves. *Energy and Buildings*, 49, 69–77.

Santamouris, M. (2014). Cooling the cities - A review of reflective and green roof mitigation technologies to fight heat island and improve comfort in urban environments1. Santamouris M. Cooling the cities – A review of reflective and green roof mitigation technologies to fight. *Solar Energy*, 103, 682–703.

Santamouris, M., Synnefa, A., Kolokotsa, D., Dimitriou, V., & Apostolakis, K. (2008). Passive cooling of the built environment - use of innovative reflective materials to fight heat islands and decrease cooling needs. *International Journal of Low-Carbon Technologies*, 3(2), 71–82.

Santamouris, M, & Asimakopoulos, D. N. (2001). *Energy and Climate in the Urban Built Environment*, vol.1. James & James.

Santamouris, M, Papanikolaou, N., Livada, I., Koronakis, I., Georgakis, C., Argiriou, A., & Assimakopoulos, D. N. (2001). On the impact of urban climate on the energy consuption of building. *Solar Energy*, 70(3), 201–216.

Santamouris, Mattheos, & Kolokotsa, D. (2015). On the impact of urban overheating and extreme climatic conditions on housing, energy, comfort and environmental quality of vulnerable population in Europe. *Energy and Buildings*, 98, 125–133.

Synnefa, A., & Santamouris, M. (2013). White or light colored cool roofing materials, in Kolokotsa, D., Santamouris, M. & Akbari, H., *Advances in the development of cool materials for the built environment*, Bentham Science Publishers Ltd, pp. 33–71.

Synnefa, A., Santamouris, M., & Apostolakis, K. (2007). On the development, optical properties and thermal performance of cool colored coatings for the urban environment. *Solar Energy*, 81(4), 488–497.

Vallati, A., De Lieto Vollaro, A., Golasi, I., Barchiesi, E., & Caranese, C. (2015). On the impact of urban micro climate on the energy consumption of buildings. *Energy Procedia*, 82, 506–511.

Zinzi, M. (2010). Cool materials and cool roofs: Potentialities in Mediterranean buildings. *Advances in Building Energy Research*, 4(1), 201–266.

Potential of switching cool materials to optimize the thermal response of residential buildings in the Mediterranean region

Michele Zinzi, ENEA (Italy)
Stefano Agnoli, ENEA (Italy)
Giulia Ulpiani, The University of Sydney (Australia)
Benedetta Mattoni, University of Rome La Sapienza (Italy)

ABSTRACT

Cool materials are a well-established solution to mitigate urban overheating. Notwithstanding, their net energy and cost impact might turn negative in year-round assessments, owing to space heating penalties. Thermochromic materials, that are able to switch from a prevalent absorbing to a prevalent reflective behaviour, may overcome this problem. Several studies at the material level show advantages and limits of the technology, however no marketable solution exists yet. This study aims at quantifying the energy saving potential of switching cool roofs to optimize the thermal response of residential buildings in the Mediterranean Basin. The task is performed by simulation in transient regime, drawing on different material modelling approaches. The analysis is carried out in three cities: Barcelona, Palermo and Cairo, representative of different areas of the Basin. Several scenarios are considered, different in terms of building insulation, transition temperature and switching magnitude. Thermochromic materials exhibit potential annual energy savings up to 8.5% and 19% with respect to cool and conventional roofs, respectively, when the solar reflectance switches from 0.15 to 0.75. Smaller annual energy savings are achieved as the switching magnitude is decreased. Due to several factors, thermochromic cool roof can also lead to annual energy penalties compared to static roofs. Further modelling and experimental efforts are needed to better predict the response of the material during the transition phase and refine the optimization process.

Special Issue Journal	:	Energy and Buildings
DoI	:	https://doi.org/10.1016/j.enbuild.2020.110698
Citation	:	Zinzi, Michele et al. "On The Potential of Switching Cool Roofs to Optimize the Thermal Response Of Residential Buildings In The Mediterranean Region". Energy And Buildings, vol 233, 2021, p. 110698.

Black Titanium Dioxide: An Innovative Material to minimize the Urban Heat Island Effects in Walled city of Jaipur

Prasanna Bhangdia[1]*, PG Student, Dept. of Architecture & Planning, MNIT Jaipur (India)*
Dr. Tarush Chandra, Professor, Dept. of Architecture & Planning, MNIT Jaipur
Dr. Pooja Nigam, Assistant Professor, Dept. of Architecture & Planning, MNIT Jaipur

ABSTRACT

The walled city of Jaipur is one of the notable examples of medieval Indian Town planning and architecture. The city rich in its cultural and heritage value is now urbanizing exponentially, facing the problems of population growth, lack of space, minimal green area, traffic congestion and so on. This results in an increase of Urban Heat Island effect leading to several secondary issues. Time has come to address this issue in a way that does not disturb existing settlement and at the same time generate the desired output. Technology has widened the canvas of our future by contributing in the form of various innovations. One of them is Black Titanium Dioxide- a photocatalyst having a property to remove the polluting agents from the air which contributes to UHI. This research attempts to use Black Titanium Dioxide nameplates, already existing feature of architecture in the walled city of Jaipur to reduce the number of pollutants emitted by vehicles and other activities. Based on the traffic survey of this area approximate quantity of pollutants emitted in the area and the colour coating area available is figured out, and the relationship between both of them has been established. This study will help to understand that the effects of UHI can be minimized by the application of innovative material within the strong historical context of the walled city.

INTRODUCTION

With the increase in population and vast spread of urbanization, today we are facing many problems that are the direct cause of what we did to elevate our standard and quality of life. Many innovations from the last century have reduced our efforts but at the same time have damaged our nature to a great extent. The consequences of which are immeasurable and one of them is the Urban Heat Island effect. In urban areas, especially around the central business district (CBD) of the city, built-up density is higher than the suburban and rural areas and this causes higher surface and air temperatures at and around the CBD of the city. The difference in surface and air temperatures of urban and rural areas are designated as surface UHI (SUHI) and atmospheric UHI (AUHI), respectively (Mathew, 2018). Urbanization leads to loss of vegetation around the urban fringe area. Increasing urban sprawl also contribute to unplanned growth and haphazard development increasing surface temperature (Khandelwal, 2010). Increase in population of urban areas and related economic growth are the main reasons for the expansion of urban sprawl and have increased UHI over most cities of the world. The resulting rise in temperatures in urban zones is causing an increase in demand for air conditioning, higher pollution levels and may alter precipitation patterns. Studies have shown that the UHI effect results in higher energy and water consumption. UHI during the summer season has a major effect of the increase in energy demand and reduction in outdoor air quality levels. The peak urban electrical demand rises by about 2–4% for each 1°C rise in the daily maximum temperature above a threshold of 15–20°C (Akbari, 1996).

[1] Prasanna Bhangdia: [prasanna.bhangdia@gmail.com], [91-9405043132].

Urban sprawl has resulted in urban spatial expansion, which is associated with a number of environmental and social issues (Xueqin, 2015). There are many factors affecting the phenomena of Urban Heat Island. Some of them are greenhouse gas emission, loss of urban forest cover, impermeability of building material, urban morphology and an excessive amount of anthropogenic heat. But as we can see most of them are induced due to human interventions. This lead to deterioration of air quality, increase in energy consumption and ill impact on the natural sources existing in that area and thus affecting the health of people. Hence as a planner, it is our job to incorporate this issue in our planning and design the cities that can resist the negative impact of such phenomena.

As the entire world is facing the problem of climate change, UHI studies are important in understanding the phenomenon and its widespread growth. This knowledge will help in developing strategies for mitigating effects of UHI in urban areas and ultimately at the National level. Urbanization has accelerated the rate of economic prosperity in India. Rapid urban transitions have affected the lives of urban inhabitants significantly as well as it has worsened the urban environment and urban climate. Therefore, in view of the expected urbanization and its associated effects, it seems that there is an urgent need to address the problems of the UHI effect of cities.

JAIPUR CITY PROFILE

Jaipur is the first planned city of India and is the capital of the state of Rajasthan. Figure 1 shows the location of city. It is located 260 km from New Delhi, capital of India, and forms a part of a popular Tourist Golden Triangle along with Agra (240 km). Jaipur also serves as a gateway to other tourist destinations in Rajasthan such as Jodhpur (348 km), Jaisalmer (571 km), Udaipur (421 km) and Mount Abu (520 km). The Jaipur Municipal Corporation is responsible for maintaining the city's civic infrastructure and carrying out associated administrative duties. The Jaipur Development Authority (JDA) is the nodal government agency responsible for the planning and development of Jaipur. In addition to its role as the provincial capital, educational, and administrative centre, the economy of Jaipur is fuelled by tourism, gemstone cutting, the manufacture of jewellery and luxury textiles, and information technology.

As per data of Census 2011 the population of the city is about 3.15 million. The city is situated on flat plain and is surrounded by Aravalli hill ranges on the North, North-East and East sides. The city broadly encounters three seasons in a year viz. winter, summer and monsoon season. Generally, winters range from November to February with average air temperature dropping up to 3 degree C, summer season range from March to June with an extremely hot temperature rising up to 48 degree C and monsoon season from July to October with extensive variations in daily average air temperature due to atmospheric conditions. The region is water scarce with an annual average precipitation of about 55 cm, as per data of IMD, concentrated mostly during monsoon season. Cultivation in the various parts of the region is mainly dependent on precipitation during monsoon season. Vegetation cover and agriculture in the city and its surroundings are dependent on precipitation during the monsoon season, and it decreases considerably during the summer season (Mathew, 2018). The walled city of Jaipur (CBD Area) has got its significant importance due to its planning style, building design, and beautiful stone carving. Besides this, the area of the walled city is still in use and contribute to the major economy of the state. But the area designed to cater pedestrian movement is now facing the problem of heavy traffic congestion due to minimum right of way and nearly inaccessible areas with high population density. The entire area of the walled city is now facing the problem of air pollution due to increased vehicular movement, creating a problem in breathing and living in so dense and compact area. Time has arrived to address this problem but we cannot alter the existing settlement pattern and can't even spoil the beauty of this area. It is very difficult to add some secondary element in the existing scenario since it will disturb the existing skyline of the city. Thus it becomes important to consciously attempt this problem that too at minimal cost and maintenance cycles.

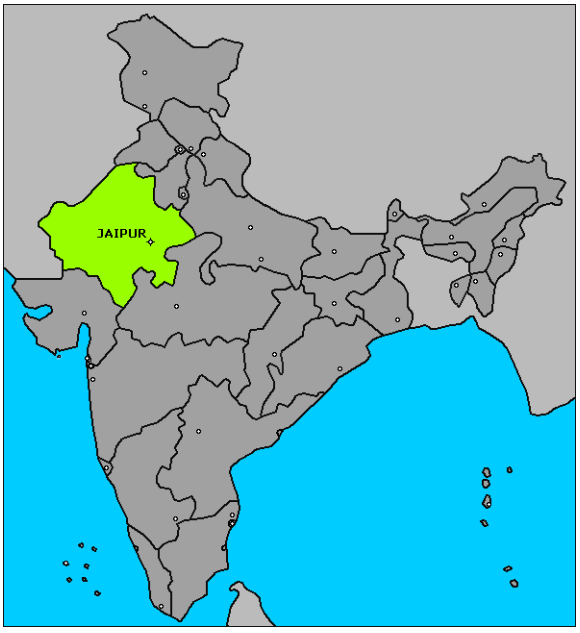


Figure 1 Map of India Showing Jaipur, Rajasthan

PAST RESEARCH WORKS

Studies on Jaipur's land surface temperatures indicate that the most urbanized areas are the hottest. The coolest are those with the largest amount of preserved vegetation. A study by Rupesh Gupta (2013) to understand the zones that have the potential to be urban heat islands shows that 13.12% of Jaipur's area is under moderate urban heat island potential zone and 0.97% is under high urban heat island potential zone. The latter is located close to the walled city in the core region. Another study by Seema Jalan and Kavita Sharma (2014) on the urban heat island phenomenon in Jaipur city, states that over a period from 2000 to 2011, Jaipur has witnessed considerable growth in the built-up area at the cost of greener patches. This has had a clear impact on the variation in land surface temperature. There has been an average rise of 2.99 degree Celsius in overall summer temperature. New suburbs of the city record two to four degree Celsius increase in land surface temperature. This is inversely related to a change in vegetation cover and positively related to the

extent of the built-up area. The study concludes that urban heat islands of Jaipur city have intensified and extended over new areas.

Centre for Science and Environment (CSE) released a citizens survey and study of air pollution in Jaipur in 2012. The perception among citizens that air pollution has increased is validated by data that shows that the levels of PM10 were almost 3 times the prescribed standard. The increase in private vehicular traffic is responsible for much of this according to the report. Jaipur has about 18 lakh vehicles and adds nearly 400 vehicles a day to its existing fleet. Vehicles are growing at a rate of about 10 percent per annum with cars increasing at a faster rate than two-wheelers. A point of note is that Jaipur has 551 vehicles per 1,000 people compared to Delhi at 332 vehicles. Another telling statistic that illustrates the level of traffic congestion in Jaipur is that 60 percent of the cities roads are used for parking – the highest in any city in India (Sarath K. Guttikunda, 2019).

POLLUTANT EMISSION SCENARIO IN JAIPUR

Below is a summary of the ambient monitoring data available under the National Ambient Monitoring Program (NAMP), operated and maintained by the Central Pollution Control Board (CPCB, New Delhi, India). In Jaipur, there are 2 continuous air monitoring stations (CAMS) reporting data for all the criteria pollutants and 6 manual stations reporting data on PM, SO2, and NO2. For urban Jaipur, average PM2.5 concentration was 99.6 ± 19.4 micro g/m3. Figure 2 shows the variation of annual PM2.5 concentration in micro-gram per m3 for city of Jaipur from 1998 to 2014. This is more than 2 times the national standard and almost 10 times the WHO guideline.

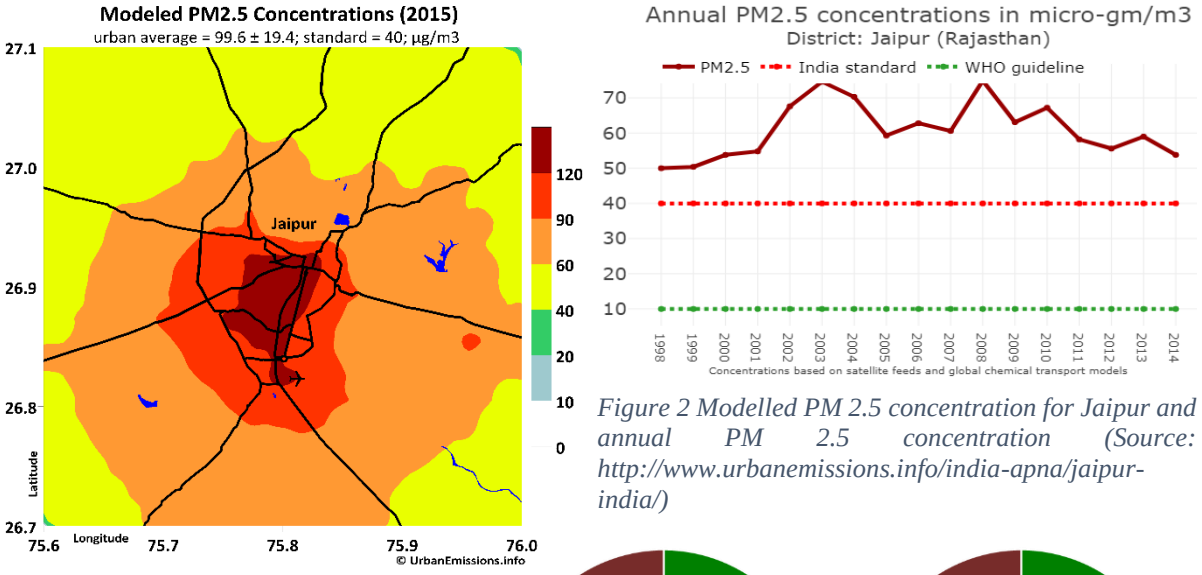


Figure 2 Modelled PM 2.5 concentration for Jaipur and annual PM 2.5 concentration (Source: http://www.urbanemissions.info/india-apna/jaipur-india/)

Figure 3 on the side shows the share of various sectors in PM 2.5 emission as on 2015 and as estimated for 2030 as per the report. The share of Transport and outside is much more as compared to the rest of the factors within the city limits. Hence it is necessary to

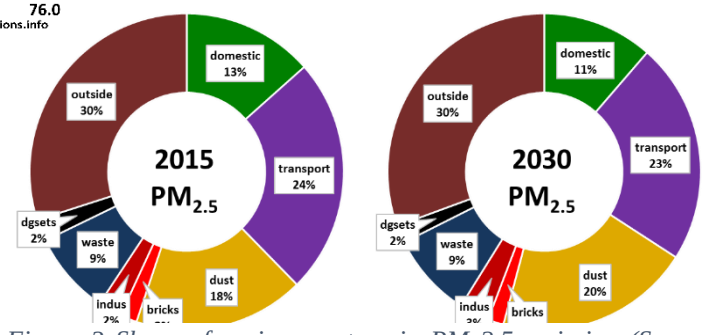


Figure 3 Share of various sectors in PM 2.5 emission (Source: http://www.urbanemissions.info/india-apna/jaipur-india/)

control the pollution generating from vehicles.

Figure 4 below shows the changing concentration of NO2 and SO2 for Jaipur for the last two decades. If compared with annual national standards it can be seen that emission of NO2 is much more than the standards while that of SO2 is within the limits.

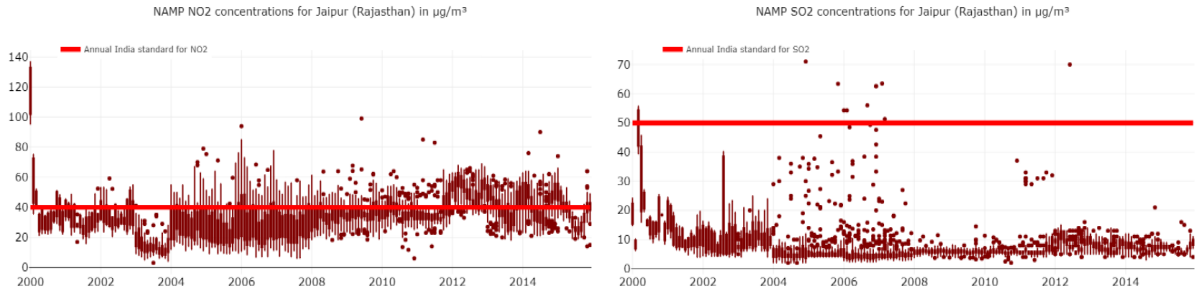


Figure 4 Changing concentration of NO2 & SO2 for Jaipur; Red line indicates the annual Indian standard for NO2 and SO2 respectively (Source: http://www.urbanemissions.info/india-apna/jaipur-india/)

USE OF INNOVATIVE MATERIAL TO TACKLE THE PROBLEM

As seen earlier, the walled city of Jaipur has its own rigid context and need very careful decision while planning to control the UHI, mainly arising due to the emission of pollutants from the vehicles. Use of some innovative technology or material will surely help to minimize effects of urban heat island within a short time and that too at a relatively lower cost. In this regard, many new materials were innovated and tested for their suitability, but very few of them were used at ground zero just because of their infeasible workability. One of such materials invented in previous research works is Titanium Dioxide- a photocatalytic semiconductor, and is claimed to have property to trap and absorb various organic and inorganic particle in air and hence purify the air by removing various harmful pollutants by converting them into harmless inorganic compounds in presence of sunlight (Dijy Davis, 2015). Research says that these properties are the result of its nuclear structure, which helps the material to convert water in the air into a form that further converts pollutant into a neutral substance (Dijy Davis, 2015) (Stephen O. Hay, 2015). Besides this, it is available in abundant quantity in various natural forms in India and also is used in various day to day products such as sunscreen lotions, various cosmetic products, and industry related manufacturing and that too at an economical price. But Research by Indiana University environmental scientists shows that air-pollution-removal technology used in "self-cleaning" paints and building surfaces may actually cause more problems than they solve. There are some debate and uncertainty over whether these air purifiers could pose a greater risk to human health than the pollutants they are designed to remove (University, 2013). Thus to overcome this situation scientists have discovered an advanced version of this material by the process of hydration, and is known as ‘Black Titanium Dioxide'. This material overcomes all the disadvantages of Titanium Dioxide and thus draws attention owing to its application as energy harvesting, pollutant removal and many biomedicine applications (Xiaobo Chen, 2017). Further, the researcher says that the process of conversion of Titanium Dioxide to Black Titanium Dioxide is neither complicated nor costly, which itself is a great success of this system. Thus the use of this hydrated Titanium dioxide as air purifier near the heavy traffic areas can control the emission of pollutant into the atmosphere, further improving the deteriorating condition of air in the city (Xiaobo Chen, 2017). Figure 5 shows white and black Titanium Dioxide nano particles.

Photocatalytic air cleaning has the potential for removing nitrogen oxides (NOx) and volatile organic compounds (VOCs) from polluted urban air and consequently for reducing concentrations of toxic gaseous. Black Titanium dioxide (TiO_2) nanoparticles absorb the ultraviolet component of sunlight, acting as a catalyst to form reactive hydroxyl (OH) radicals in the presence of atmospheric moisture. These radicals can oxidize and destroy most pollutant molecules (Xiaobo Chen, 2017) (Laboratory, 2008). This property of the material is used in this research to remove the polluting agents emitted from vehicles. One of the research by Lawrence Berkeley National Laboratory clarified the technology potential by focusing on measured values of catalytic activity, that is, the rate at which air can be cleaned by a given area of photocatalyst (if 1 m^2 of catalytic film or plate can clean 100 m^3 of air per day, it has an activity of 100 m/day). Laboratory data show that a high-quality black TiO_2 catalyst has an activity of about 200 m/day for NOx, about 60 m/day for typical VOCs, and approximately 0 m/day (not useful) for carbon monoxide (Laboratory, 2008). This data will help to quantify the required amount of black TiO2 particle within the city that can nullify the effect of pollutants.



Figure 5 White & Black TiO2 nano particles (Source: https://www.acsmaterial.com/blog/index/view/id/31/)

APPLICATION IN THE STUDY AREA

Area for application of this material is ‘Traditional Nameplates' of the shops along all major roads throughout the walled city of Jaipur. This is a historic character of the old city having the typical design of Black signage over white background. As we have discussed earlier, the character of the old settlement is very strong and rigid, and changing or altering this is not possible at all. As a planner, it is our responsibility to maintain the existing character of the city and try to best fit the existing situation with technological intervention, in order to achieve sustainable development.

Thus this research target the unique feature of settlement and collaborate it with the use of innovative material, Black Titanium Dioxide.

METHODOLOGY



Figure 6 Photographs showing traditional nameplates in Walled city of Jaipur (Source: Author)

Onsite traffic count survey was done for a single stretch (Chandpol bazaar road) within the study area and based on that the tentative emission factor was calculated. While the complete analysis for the pollutant will be beyond the scope of this paper, the peak hour variations of pollutant emission were carried out on the fixed location for different days and average data of all (per Hour) is considered for study purpose. Emissions from the vehicle depend mainly on the type of transport and fuel apart from the type of combustion engine, emission mitigation techniques, maintenance procedures and vehicle age (Ramachandra, 2009). Thus only the type of vehicle is considered to project the value of emitted pollutants. Once this value is obtained then the area available for application of Black Titanium Dioxide will be calculated. Data will be compared from these two values and relative output will be discussed.

RESULTS AND DISCUSSION

Total Emission

In order to study the total emission from vehicles in study area, first on site vehicle survey was conducted during peak hours of morning, afternoon and evening at fixed points for several days (working day, weekends and holidays). Once the vehicle count was complete then based on the research by S. Baidya & J. Borken-Kleefeld (2009), emission value of pollutant's in ppm was calculated. These value per day were then converted into µg/m3 using conversion factor as mentioned into UK Air Quality Archive European Commission. Table 1 shows final emission of pollutants calculated from this survey work.

Table 1: Per day emission of pollutants along Chandpol bazaar road area (in ppm)

Pollutant's	CO	HC	NO	PM	CO2	SO2
2 Wheeler	24180	32643	967.2	2176.2	531960	169.26
3 Wheeler	9479.6	6489.88	291.68	838.58	142194	47.39
4 Wheeler	17514.08	1094.63	6439	1223.41	1526043	959.411
LDT	3812.58	344.64	915.45	183.09	329562	206.78
HDT	234	80.6	460.72	52.48	36712	22.88
Total ppm	55220.26	40652.75	9074.05	4473.76	2566471	1405.721
µg/m3	64.0552	16.2611	68.2611	447.376	10.265884	37.373

We can see that the emission of PM, NO & CO is beyond the Indian standards of emission. Whereas for HC, CO2 & SO2 total emission is within the given standard limits.

Total Available Area for Black TiO2 Application

Along the Chandpol bazar road (study area), there are nearly 48 shops on each side of the road. Each shop has its own nameplate of area 2.6 sq.m., on average, on which we will apply Paint of black TiO2. Although the material used is Black Titanium Dioxide, but this material is available in various colours and of which white colour is adopted for this research proposal. Thus for a single shop, the aggregate area of black TiO2 will be 2.6 sq.m. and the total area covered along the entire stretch of this material will be 249.6 sq.m. Thus significant area is available for this material. Following image shows the section of Chandpol bazar road and area of application of this paint.



Figure 7 Section of Chandpol bazar road showing traffic movement and location of nameplates (Source: Author)

Discussion

If compared the data from Table 1 to the research output by Lawrence Berkeley National Laboratory, the effective available catalytic film (considering the efficiency of 70%) can easily clean the air containing pollutants such as HC, NO, PM & SO2 from the surrounding area. Thus improving the quality of air and reducing the Urban Heat Island effect produced due to greenhouse gases.

ADVANTAGES

This research shows that use of black Titanium Dioxide paint can remove the pollutants emitted from vehicles and can clean the air in that area. Nameplate made of black TiO2 requires less maintenance and is not a complicated job. Availability and use of material is convenient and hence can be adopted at local level. There is no special requirement for installation of the catalyst paint coat, since it can simply be applied over existing structure. There is no hamper to the historical character of city and hence itself is a great achievement. This air purifying material, synthesised from its previous version, has no side effects on health of human beings (Xiaobo Chen, 2017).

LIMITATIONS

Due to the restriction of time and resources, no actual experiment was done on site to check the feasibility of the proposal. This research model is based on secondary data set and earlier research work reports done in this field. Further, there can be many solutions to address the problem of UHI effect but this research addresses very few out of it.

CONCLUSION

Urban heat island effect is a very complicated phenomena caused due to uncontrolled and haphazard urbanization; loss of green cover and vegetation further adds to undesirable effects. It's effects are long lasting and as a planner it becomes very important to design for our climate. Adaptation for environmental planning consists of various site and problem specific solutions, which need careful analysis. Technology intervention may upgrade the existing situation and hence need to be incorporated within the planning. This research focus on removing pollutant emitted from vehicles which contributes in Urban Heat Island effect. The walled city of Jaipur has its unique character and is an important location in State of Rajasthan. The proposed model best suited to the existing situation of the walled city of Jaipur, without disturbing the character of old settlement. The historic value of the city can be preserved and at the same time, the problem of UHI can be minimized. Based on the traffic survey of Chandpol bazar road and available area for installation of black Titanium Dioxide paint it was observed theoretically that even with the efficiency of 80% this material can remove the pollutants within the surrounding area. If this material is further applied throughout the walled city of Jaipur then we can entirely control the pollution and hence UHI. Use of black Titanium Dioxide is much easier and need no special assistance. Process can be adopted by local workers. Maximum benefits can be achieved from this simple change that too at relatively lower cost and within short time period.

FUTURE SCOPE

Since black TiO2 is available in various colour shades it can be even applied to other building parts promoting the existing architectural style, and additionally catalysing the speed of removal of pollutants in its surroundings. Further, this paint can be used to colour the light poles along the main roads within the city, Median of the road, pedestrian side paver blocks and sometimes on roads along zebra-crossings. The application of paint on such additional locations will surely help to minimize the urban heat island effects in city.

REFERENCES

- ADB, A., 2008. Vehicle Emissions Reduction/Country Data of India. Asian Development Bank, Manila, Philippines; http://www.adb.org/ vehicle-emissions/IND/fuel.asp#dsl
- Akbari, H. P. M. T. H., 1996. Policies to reduce Heat Islands: Magnitudes of benefits and incentives to achieve them. s.l., ACEEE Summer Study on Energy Efficiency in Buildings.
- Baidya, S., Borken-Kleefeld, J., Atmospheric emissions from road transportation in India. Energy Policy (2009), doi:10.1016/j.enpol.2009.07.010
- Dijy Davis, D. C. R., 2015. REDUCTION OF AIR POLLUTION FROM VEHICLES USING TITANIUM DIOXIDE. International Research Journal of Engineering and Technology, 02(05), pp. 1308-1314.
- IPCC (Inter-Governmental Panel on Climate Change), 1996. IPCC Good Practice Guidance and Uncertainty Management in National Greenhouse Gas Inventories. Cambridge University Press, New York
- Khandelwal, S. G. R., 2010. Effect of Vegetation and Urbanization over Land. Remote Sensing for Science Education Natural and Cultural Heritage.
- Laboratory, L. B. N., 2008. EVALUATION OF TITANIUM DIOXIDE AS A PHOTOCATALYST FOR REMOVING AIR POLLUTANTS, Berkeley : Lawrence Berkeley National Laboratory .

- Mathew, A. K. S. &. K. N., 2018. Investigating spatio-temporal surface urban heat island growth over Jaipur city using geospatial techniques. Sustainable Cities and Society.
- Padam, S., Singh, S.K., 2001. Urbanization and Urban Transport in India: the sketch for a policy. Transport Asia Project Workshop, Pune, India
- Patankar, P., 1991. Urban Transport in India in Distress. Central Institute of Road Transport, Pune, India
- Gupta, R. (2012). Temporal and Spatial Variations of Urban Heat Island Effect in Jaipur City Using Satellite Data. *Environment and Urbanization ASIA*, *3*(2), 359–374. https://doi.org/10.1177/0975425312473232
- Ramachandra, T.V., Shwetmala, Emissions from India's transport sector: Statewise synthesis, Atmospheric Environment (2009), doi:10.1016/j.atmosenv.2009.07.015
- Sarath K. Guttikunda, N. K. P. J., 2019. Air pollution knowledge assessments (APnA) for 20 Indian cities. Urban Climate, Volume 27, pp. 124-141.
- Seema Jalan, Kavita Sharma, 2014, Spatio-temporal assessment of land use/ land cover dynamics and urban heat island of Jaipur city using satellite data. The International Archives of the Photogrammetry, Remote Sensing and Spatial Information Sciences, Volume XL-8.
- Stephen O. Hay, T. O. Z. L. T. J. Y. M. J. H., 2015. The Viability of Photocatalysis for Air Purification. Molecules , Volume 20, pp. 1319-1356.
- University, I., 2013. ScienceDaily. [Online] Available at: https://www.sciencedaily.com/releases/2013/06/130613092346.htm.
- Xiaobo Chen, Y. C., 2017. Black TiO2 Nanomaterials for Energy Applications. 1st ed. Singapore : World Scientific Publishing Europe Ltd. .
- Xueqin, L. D. W. X. L., 2015. Eco-environment response to urban spatial expansion and its driving forces in Beijing. Journal of Ecology and Environmental Sciences , Volume 7, pp. 1159-1165.
- http://www.urbanemissions.info/india-apna/jaipur-india/
- http://www.mapaplan.com/travel-map/jaipur-city-top-tourist-attractions-download-printable-street-guide/high-resolution/jaipur-top-tourist-attractions-map-09-old-pink-city-detailed-oajmer-ghat-sanganeri-gate-albert-hall-hawa-mahal-palace-winds-high-resolution.htm
- https://uk-air.defra.gov.uk/assets/documents/reports/cat06/0502160851_Conversion_Factors_Between_ppb_and.pdf
- https://www.acsmaterial.com/blog/index/view/id/31
- http://tarunbharatsangh.in/location-grass-root-level/
- https://www.sciencedaily.com/releases/2013/06/130613092346.htm

Analysis of the heat budget of standard, cool and watered pavements under lab heat-wave conditions

Sophie Parison, Univ Paris Diderot, CNRS, LIED, UMR 8236, Paris, France
Martin Hendel, Université Paris-Est, ESIEE Paris, département SEN, France
Arnaud Grados, Université Gustave Eiffel, ESIEE Paris, département SEN, France
Laurent Royon, Univ Paris Diderot, CNRS, LIED, UMR 8236, Paris, France

ABSTRACT

The thermal behavior of 12 standard and cool pavement structures (asphalt, granite, stabilized sand, cobblestones, reflective paints, pervious concretes, dry grass, etc.) coupled with pavement-watering is studied in the lab under heat-wave-like conditions. Watering is fine-tuned for each structure to maximize cooling and minimize water consumption using two linear cooling regimes, before deployment in the field. The surface heat budget is closely studied and the partitioning of irradiance and net radiation into conductive, convective, radiative and cooling flux at surface is analyzed for each structure. Energy partitioning, surface temperature increase and optimal watering rates all exhibit good correlation with overall surface absorptivity. The transmitted flux at varying depths is also characterized using a transmission index that includes surface absorptivity and apparent conductivity of the traversed layers. Results of this study intend to improve our understanding of the energy balance of cool pavements compared to traditional ones under given weather conditions, as well as that of processes involved in the optimization of their evaporative cooling versus watering rate. Benefits of each pavement, efficiency of the method, limitations of the protocol and its potential transposition to the field are all discussed in this contribution.

Special Issue Journal	:	Energy and Buildings
DoI	:	https://doi.org/10.1016/j.enbuild.2020.110455
Citation	:	Parison, S., Hendel, M., Grados, A., & Royon, L. (2020). Analysis of the heat budget of standard, cool and watered pavements under lab heat-wave conditions. Energy And Buildings, 228, 110455.

Numerical Analysis of Human Thermal Load Affected by Solar Reflection Characteristics of Vertical Wall in Street Space

Shinichi Kinoshita[1]*, Osaka Prefecture University (Japan)*
Atsumasa Yoshida, Osaka Prefecture University (Japan)

ABSTRACT

Recently, heat island phenomenon becomes remarkable with expansion of the urban area. So far it is refrained because the adaptation to the wall surface of highly reflective materials leads to aggravation of the thermal comfort of the street space. In order to decrease the heat load from a wall surface to the atmosphere and mitigate the effect of solar reflection to street space, it is necessary not only to raise the reflectance on the wall surface but also to apply the materials with retro-reflection property that can reflect the sunlight in the incidence direction. In this study, it is assumed that retroreflective wall materials is constructed for a wall surface, and the thermal influence to human body near the wall surface affected by solar reflection characteristics, especially reflection directivity is numerically evaluated.

Introduction

Recently, urban heat island is getting worse with expansion of urban area. As one of the mitigation, it is recommended to cover the horizontal surfaces with higher solar absorptance by highly solar reflective materials such as paint or membrane, which are called ‘cool materials’. The effect of higher solar reflective materials applied to the roof and road surfaces are evaluated, and the certification system for the techniques comes to be performed in some area. On the other hand, application of this technique to the wall surface has been restricted because that leads to deterioration human thermal comfort along the street space and increase of thermal load of other building wall surfaces.

In order to mitigate the influence of reflected solar radiation from the building wall to street space as well as to reduce the thermal load to the atmosphere, it is necessary not only to increase the reflectance of wall surface but also to apply the materials with retroreflection, such that the major part of the reflected direction is same as the incidence, to the vertical surface. So far, retroreflective materials with sphere beads or polyhedral shape have been developed, and the performances have been evaluated experimentally (Sakai et al. 2008 and 2011) or numerically (Nishioka et al. 2008). Rossi et al. (Rossi et al. 2015) has been developed the retroreflective façades, and has experimentally evaluated the directional reflection performance of the material samples, and has analytically predicted the cooling potential of the materials in urban canyon applications. In addition, the countermeasures for the window which considerably occupies the range of the wall surface are examined. Near-infrared upward reflective solar control window film has been developed and the optical performance about directional and spectral reflectivity has been evaluated with the measurement instrument including an integrating sphere which can measure the directional-hemispherical spectral reflectivity (Harima and Nagahama 2017a and 2017b).

[1] Corresponding Author: kinosita@me.osakafu-u.ac.jp

In this study, the retroreflective materials assumed to be constructed for a vertical wall surface, and the thermal influence of solar reflectance of exterior wall materials, particularly directional reflectivity, on the human body staying near the wall is numerically evaluated.

Solar reflective properties of wall surface and numerical model

Definition of upward and downward solar reflectances

Reflective properties in ordinary outer wall materials and coating films are diffusive, and in the case of an opaque wall material, half of the reflection solar radiation on the vertical wall surface faces downward and becomes a load to the ground surface and the lower wall surface. As a countermeasure against this, a retroreflective material whose reflection directivity is controlled so that more radiation reflects in the incident direction has been considered. The directional reflectance is a function in both directions of the incident direction and the reflection direction in addition to the wavelength of the incident light. In evaluating it as a heat island countermeasure technique, it is desirable that the performance can be expressed with simpler parameters. Therefore, as shown in fig. 1, the ratio of the energy reflected upward from the horizontal plane to the solar radiation energy incident on the vertical plane from the sky is defined as the upward solar reflectance, and the ratio of the energy reflected downward is defined as the downward solar reflectance. When both of these two reflectances are simply added, the value corresponds to the hemispherical solar reflectance. These reflectances, for example, can be evaluated by the method developed by Harima et al 2017a.

Figure 2 shows the numerical model of street space near vertical wall, which is considered for the purpose of simply evaluating the heat balance on the surfaces of building and

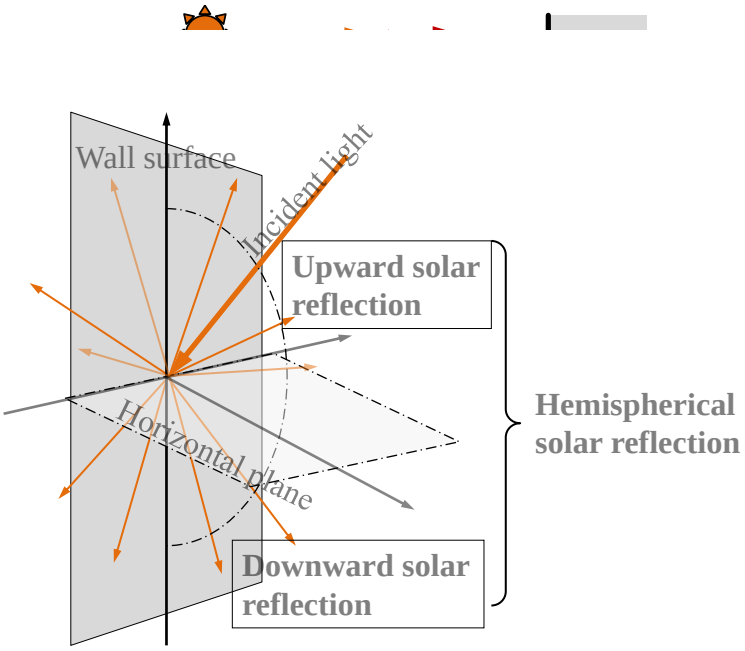


Figure 1. Definition of upward and downward solar reflectance.

Table 1 Numerical conditions

Solar height	°	71.48 (Osaka 8 Aug.)
Solar direction	°	0 (culmination)
Wind speed	m/s	1.5
Air temperature	°C	30
Room temperature	°C	28
Underground temperature	°C	15
Reflectance of wall	-	0.2, 0.4, 0.7
Offset from wall surface	m	1.0, 5.0, 10.0

ground and the heat balance around the human body. The building surface and the ground surface have a uniform structure in the direction along the street and the wall surface extends in the height direction and the ground surface extends to infinity in the width direction. As shown in the figure, it is assumed that a person is standing by x [m] from the wall. The human body is represented by a cuboid model, with a height of 1.2 [m], a width of 0.4 [m], a thickness of 0.2 [m], and a center of gravity height of 1.0 [m]. As meteorological elements, azimuth and zenith angles of solar position ϕ and θ, normal direct solar radiation S_C [W/m^2], diffuse solar radiation S_D [W/m^2], infrared atmospheric radiation L [W/m^2], wind speed U [m/s] and air temperature T_a [°C] are given. On the wall surface, upward and downward solar reflectances ρ_{wu} and ρ_{wd} , infrared emissivity ε_w =0.97, thermal conductivity λ_w =1.4 [W/(m·K)], wall thickness d =0.2 [m], outer wall and the inner wall heat transfer coefficient α_a and α_r [W/(m^2·K)] and the room temperature T_r =28 [°C] are given. On the ground surface, solar reflectance ρ_g =0.15, infrared emissivity ε_g =0.97, thermal conductivity λ_g =1.05 [W/(m·K)], ground thickness d_g =2.0 [m], heat transfer coefficient on the ground α_g [W/(m^2·K)] and underground temperature T_{g0} =15 [°C] are given. External wall and surface heat transfer coefficient are given by Jürges equation as a function of wind speed. The outer wall temperature and the ground surface temperature are decided such that the heat balance on each surface is satisfied. Solar radiation and infrared radiation from each component surface can be calculated from the radiation environment from the sky and the outer wall, the temperature of the ground surface, solar reflectance and infrared emissivity. The calculation of the net radiation of the human body R_{net} is evaluated taking into consideration solar reflectance of clothes ρ_h =0.1, infrared emissivity ε_h =0.95 and skin surface temperature T_{skin} =35[°C].

$$R_{\mathrm{net}} = (1-\rho_h)R_S + \varepsilon_h(R_L - \sigma T_{\mathrm{skin}}^4) \tag{1}$$

$$R_S = \frac{\sum_i A_i S_i}{\sum_i A_i} \quad R_L = \frac{\sum_i A_i L_i}{\sum_i A_i} \tag{2}$$

$$S_i = \sum_j F_{ij} S_{wj} \quad L_i = \sum_j F_{ij} L_{wj} \tag{3}$$

where S_i and L_i are solar and infrared radiations to the i-th surface constituting cuboid model , respectively. A_i is area of i-th surface, S_{wj}, L_{wj}: insolation and reflected solar radiation and

infrared radiation emitted from *j*-th surface which is surface element of sky, walls and ground surrounding human body model, F_{ij}: view factor of *i*-th surface to *j*-th surface.

Numerical conditions

Table 1 shows the numerical conditions. Solar position was supposed to be in south at central time on August 8, Osaka, the vertical wall faced the south, and the human body model was located at 1m, 5m, 10m offset from the wall. The hemispherical solar reflectance of the wall surface is changed in the three conditions of 0.2, 0.4, 0.7. Retroreflection is represented by changing the content of the upward and downward solar reflectance under the condition that the hemispherical solar reflectance is 0.7. Human body thermal load is represented by net radiation of human body which is evaluated by Eq. (1).

Results and discussions

Figure 3 shows the effect of offset from wall surface to human body location on the human thermal load. In the figure, the wall is perfect diffuse reflective surface, and the hemispherical solar reflectance is 0.4, that is ρ_{wu} and ρ_{wd} = 0.2. As shown in the figure, human thermal load tends to become larger with increase of the offset, but the value asymptotically approaches in constant, and the amount of change is approximately 10W/m^2.

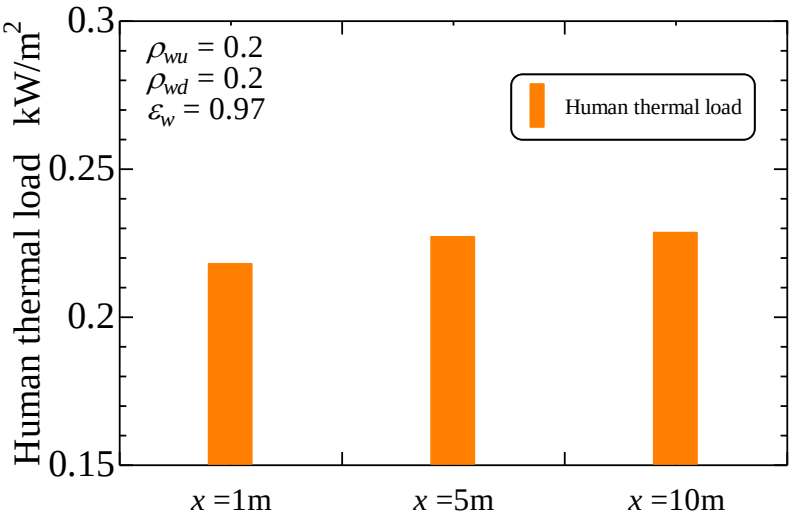


Figure 3. Effect of offset from wall surface on human thermal load. Solar reflectance of wall is fixed to 0.4, and the directivity is uniform.

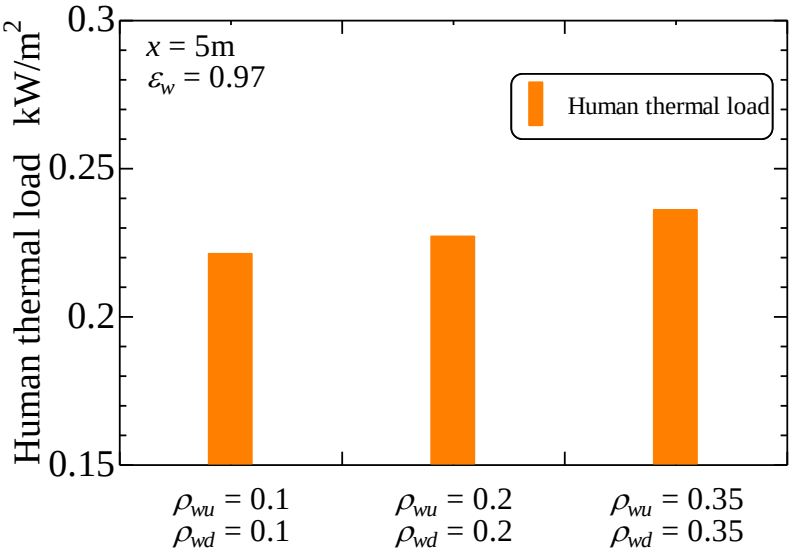


Figure 4. Effect of hemispherical reflectance in the case of perfect diffuse reflection.

Figure 4 shows the effect of hemispherical solar reflectance on human thermal load. In the figure, the wall is also perfect diffuse reflective surface. As shown in the figure, human thermal load tends to become larger with increase of the solar reflectance of wall surface.

Figure 5 shows the results in the case when upward solar reflectance is changed with a fixed hemispherical reflectance 0.7. As shown in the figure, it is considered that thermal load of the human body becomes smaller as the ratio of upward solar reflection becomes larger. It is confirmed that the large part of the human thermal load is due to the direct insolation from the sky and the loads on the top and back surfaces are significant in this case. On the other hand,

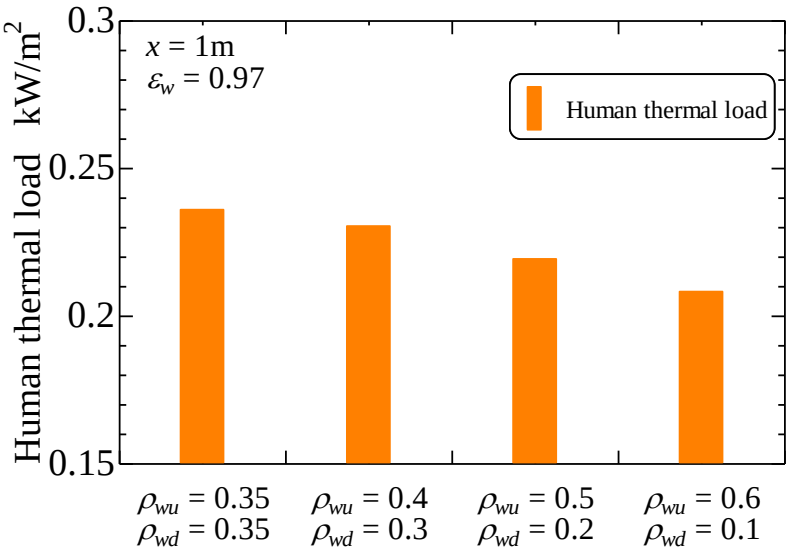


Figure 5. Effect of upward reflectance in the constant condition of hemispherical reflectance.

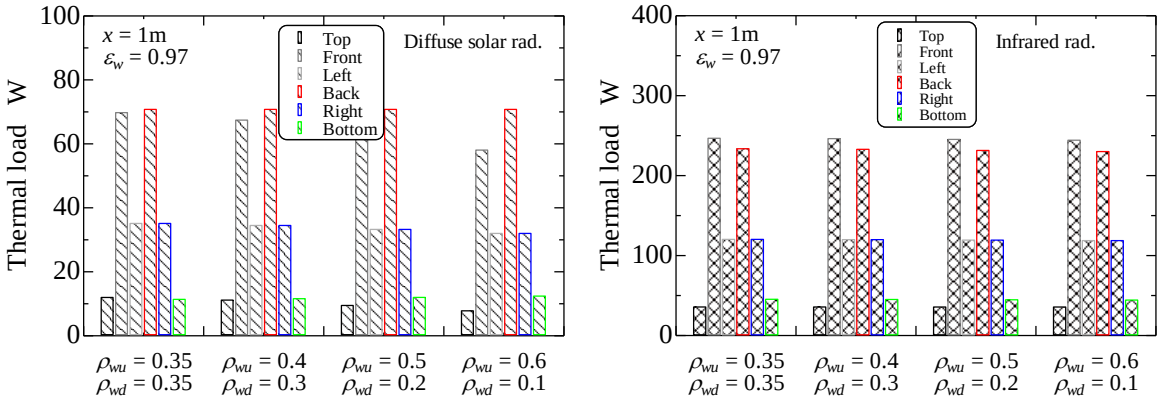


Figure 6.Details of diffuse solar and infrared radiations to each surface of human body model. Left and right figures correspond to diffuse solar and infrared radiations, respectively.

Figure 6 shows the absorbed energy on each surface of human body model associated with diffuse solar radiation and infrared radiation including the solar reflection and infrared emission from the wall surface. It is considered that the thermal loads on 4 surfaces except back and bottom surfaces are reduced and the load on the front surface toward the wall is especially reduced. The reduction effect associated with infrared radiation is hardly confirmed.

Conclusions

The results obtained are as follows. (1) The position of the human body model from the wall hardly affects the net radiation of the human body. (2) When the wall surface is a perfectly diffuse reflection surface, as the solar radiation reflectance increases, the load due to diffuse reflection increases and the net radiation of the human body tends to become large. (3) As the lower solar reflectance of the wall surface decreases, the load due to diffusion solar radiation

decreases and the net radiation of the human body tends to be smaller. (4) Infrared radiation from the wall tends to decrease as the wall surface temperature decreases when the solar reflectance condition of the wall surface is changed, but overall there is little change in the infrared radiation from the surroundings.

References

Harima, T. and Nagahama, T. (2017a). Evaluation method for retroreflectors and quantitative analysis of near-infrared upward reflective solar control window film – Part I: Theory and evaluation methods. Solar Energy 148, 177-192.

Harima, T. and Nagahama, T. (2017b). Evaluation method for retroreflectors and quantitative analysis of near-infrared upward reflective solar control window film – Part II: Optical properties evaluation and verification results. Solar Energy 148, 164-176.

Nishioka, M., Inoue, S., Sakai, K., Nakao, M. and Nabeshima, M. (2008), Numerical simulation on basic properties of retroreflectors – Performance evaluation of solar retroreflectors. J. Environ. Eng., AIJ, 73, 630, 1013-1019.

Rossi, F., Castellani, B., Presciutti, A., Morini, E., Filipponi, M., Nicolini, A. and Santamouris, M. (2015). Retroreflective façades for urban heat island mitigation: Experimental investigation and energy evaluation. Applied Energy, 145, 8-20.

Sakai, H., Emura, K. and Igawa, N. (2008). Reduction of reflected heat by retroreflective materials. J. Struct. Constr. Eng., AIJ, 73, 630, 1239-1244.

Sakai, H., Iyota, H., Emura., K., and Igawa, N. (2011). Development and evaluation of directional retroreflective materials – Directional retroreflective materials as a heat island countermeasure Part 1. J. Struct. Constr. Eng., AIJ, 76, 665, 1229-1234.

Harnessing Benefits of Pervious Concrete Pavements: A Novel UHI Mitigation Strategy

Poornachandra Vaddy, Postgraduate Student, Indian Institute of Technology Tirupati (India)
Avishreshth Singh, Doctoral Research Scholar, Indian Institute of Technology Tirupati (India)
Prasanna Venkatesh Sampath, Asst. Professor, Indian Institute of Technology Tirupati (India)
Krishna Prapoorna Biligiri[1], Assoc. Professor, Indian Institute of Technology Tirupati (India)

ABSTRACT

With growing urbanization and associated development of infrastructure, urban heat islands (UHI) have emerged as major challenges, which needs to be addressed, in order to endure sustainable urban conglomerates. In this study, pervious concrete pavement (PCP) sections were constructed to assess their suitability in mitigating UHI through actual field implementation and testing. Temperature profiles of PCP and Portland cement concrete pavement (PCCP) were measured, recorded and compared under both dry and wet conditions by embedding thermocouples across their depth. The pavement temperature was recorded at 15-minute intervals under dry conditions, while under wet conditions the pavement temperature was examined after every three hours. Wet conditions were simulated by pouring water over the pavements, which was quantified when the pavement temperature decreased by 1 °C across its depth. Under dry conditions, it was found that PCP system was warmer compared to PCCP, irrespective of the time in one day. The quantity of water required was about 0.54 L/m^2 to reduce the surface temperature of PCP by 1 °C. Further, in order to achieve similar reduction in temperature throughout the thickness of PCP, the quantity of water required ranged from 37.07-89.83 L/m^2. Owing to its impervious nature, no change in temperature was observed in PCCP system even with inundation of water, except at the surface that exhibited very minute reduction. The experimental findings showed that negative impacts of UHI can be countered by using PCP systems as a potential for harnessing evaporative cooling effects that is remarkably higher than conventional pavements.

Introduction

The augmented rate of urban expansion and wide infrastructure development has resulted in a phenomenon called Urban Heat Island (UHI), where urban dwellers experience increased temperatures in their jurisdiction than rural areas, especially during night hours. Additionally, due to lack of proper mitigation strategies and ever-expanding rates of construction of impervious civil infrastructures such as buildings, pavements, and airports, the impact of UHI has intensified manifold eventually leading to elevated temperatures and increased energy consumption for cooling purposes (EPA 2005). In the domain of transportation infrastructure, pavement systems comprise of expressways, highways, elevated corridors, streets, and parking lots, etc., which contribute to about one-third of the impervious area in an urban conglomerate (Gui et al 2007; Qin and Hiller 2014). Hence, environmental agencies across the world are focusing on developing

[1]Corresponding Author: Associate Professor, Department of Civil & Environmental Engineering, Indian Institute of Technology Tirupati, AP 517506, India; E-mail: bkp@iittp.ac.in

engineered materials and technologies that can curb the high impacts of escalated temperatures in urban setups, and contribute to the development of sustainable roadway systems. One such technology is cool pavement systems, which encompasses a broad set of established and emerging materials (EPA 2008). Cool pavement technology refers to those materials that lower the pavement temperature by reflecting the incident solar radiation, or in other words by storing and releasing less heat back to the atmosphere. With increasing acceptance of pervious pavements as green and stormwater management tools (EPA 2004; Abdel-Aziz, Al-Maani, and Al-Azhari 2015), some researchers have expanded the concept of cool pavements to pervious concrete pavements (PCPs) as well (Kevern, Shaefer, and Wang 2009; Li et al 2013). PCP systems tend to lower the pavement surface temperatures through evaporative cooling mechanism, in a broader context.

Pervious concrete (PC) has gained acceptance as a sustainable stormwater management system because of its ability to allow stormwater to pass through its interconnected porous structure that is developed by elimination of fine aggregates from concrete mixture design (Tennis, Leming, and Akers 2004). The functional characteristic of PC is its porosity (minimum 15%) unlike traditional concrete pavements, where compressive and flexural strengths are the criteria to govern the quality of pavement material. Traditional pavement systems store a portion of incoming solar radiations within them, and transfer the heat to underlying layers through conduction, which leads to elevated air temperatures during daytime (Haselbach et al 2011). During night hours, the heat stored within the pavement systems is released back to the atmosphere, thus altering the natural evaporative-cooling cycle, and requiring additional energy for cooling units such as air conditioners and refrigerators.

The Leadership in Energy and Environmental Design (LEED) rating system of the US Green Building Council utilizes the concept of solar reflectance index (SRI) to classify the coolness of pavements (Marceau and Geem 2007). An investigation concluded that though the SRI of PCP was much lower than conventional pavement systems, it still has UHI mitigation capabilities attributed to its higher insulation capacity than asphalt and concrete pavement systems, and evaporative cooling mechanism similar to that of porous natural ground (Haselbach et al 2011; Lorenzi, Haselbach, and Filho 2015). A comparative field study performed over a five-day period suggested that the surface temperature of PCP was higher than conventional Portland cement concrete pavement (PCCP) during daytime, whereas during night and early mornings, the surface temperatures were almost similar (Kevern, Haselbach, and Schaefer 2012). After five-day heating cycle, it was further observed that the heat stored within PCP was about 12% lower than PCCP. This was attributed to the open pore structure of PCP, which allows the expulsion of heat at a predominantly faster rate than PCCP.

A recent field investigation suggested that the thermal conductivity and albedo of PCP systems were lower by about 8.5-14.3% and 17.7-29.1%, respectively in comparison with PCCP (Hu et al 2017). Another recent investigation examined that the near surface air temperatures of PCCP were between 22 and 30% higher than PC mixtures, thus more likely to cause higher thermal discomfort to urban dwellers (Wu et al 2017). Moreover, the thermal energy released by PCCP during nights was higher than PC, thus intensifying the temperature profiles during nighttime and causing higher thermal discomfort. Past studies have shown that rainwater also has a direct cooling impact on PCP systems, as it not only reduces the surface temperatures but also flows through the tortuous pore structure of PC. Later, this entrapped water within the pores of PC material and porous granular sub-base (GSB) is evaporated back to the atmosphere, thus maintaining a cooling system, as also mitigating UHI in a substantive manner.

Based on the abovementioned studies, it can be inferred that pavements significantly contribute to UHI as they cover the natural ground, and interfere with natural hydrologic cycle. Though investigation of a wide variety of novel materials and innovative technologies such as PCPs are underway, there is still limited research available pertaining to the benefits that can be harnessed from PCP systems. More research is needed to characterize the behavior of PCPs under rainwater, windy situations, and regions subjected to extreme climatic conditions to develop strategies that can augment the multitude of benefits offered by PCP systems, and further help in mitigation of UHI effects. The current study tries to evaluate the effectiveness of one such strategy, which has been discussed in subsequent sections.

Research Objective and Scope

The objective of this research study was to quantify the amount of water required for per degree decrement of temperature across different depths in the pavement slabs. In order to monitor the change in temperature profile, thermal probes were embedded in PCP and PCCP slabs, while the surface temperatures were recorded with the help of a thermal gun. The scope of the effort included:

- Preparation of PC and PCC field pavement test sections
- Embedment of thermal probes across the pavement slabs at different depths
- Assessment of temperature profiles under dry and wet pavement conditions
- Quantification of water required for per degree decrement of temperature across pavement depths at different hours during day and nighttime
- Performance evaluation of two pavement systems in mitigating UHI

It is envisioned that the current study will contribute to the development of a generic approach that counters the UHI effect, and proliferates the potential benefits offered by PCP for wider applicability. Further, it will advance the current state-of-the-knowledge pertinent to contribution of PCP and PCCP systems to climate of urban dwellings.

Materials and Methodology

In order to accomplish the proposed research objective, a PCP parking lot covering an area of 50 m x 5 m was constructed using a single mixture at transit campus of Indian Institute of Technology Tirupati, State of Andhra Pradesh, India. The parking lot encompassed over thirty-four PC slabs each having dimensions: 3 m × 2.5 m × 0.15 m overlaid on 0.20 m thick GSB. PCCP slabs of width 0.5 m were constructed on either side of PCP, which served as shoulders. The cross-sectional view of PCP is depicted in Figure 1.

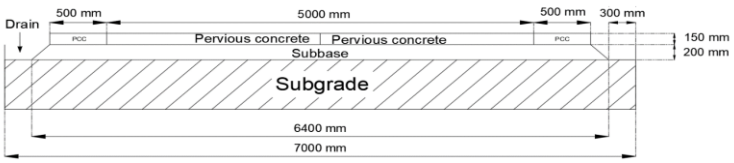


Figure 1: Cross-sectional view of pervious concrete pavement

Materials

Crushed aggregates were procured from a local crusher plant and indexed as 12.5 mm and finer size. Ordinary Portland cement 53-grade conforming to IS: 12269 (IS:12269 - 2013) was used in this study. The water-to-cement ratio was 0.30 and the aggregate-to-cement proportion was 1:3.75. A polycarboxylic ether based superplasticizer conforming to ASTM C494 Type F (ASTM C494/C494M-17) was added to the PC mixture at a dosage of 0.5% by dry mass of cement to enhance workability and strength. PCCP shoulders were prepared using M20 grade concrete.

The GSB layer was categorized as a two-layered system: coarse GSB 170 mm thick, underlying a fine GSB layer of 30 mm thickness. The coarse GSB layer had more than 70% aggregates falling in the size range of 19-6.3 mm. The fine GSB layer, which was a mixture of 75% quarry dust and 25% 4.75 mm retained chips was overlaid after compacting the coarse GSB layer.

Experimental Plan

In the parking lot, one slab each of PC and PCCP were dedicated as test sections for investigating UHI phenomenon. Seven Type K thermocouples with a standard accuracy of ±2.2 °C or 0.75% (whichever was greater) were embedded each into PCP and PCCP systems to monitor the temperature profiles across the full depth of pavement. A wooden thermocouple assembly unit was prepared, and thermocouple sensors were attached to it at 30, 60, 90, 120, 150, and 290 mm depths, as shown in Figure 2a. The thermocouple sensors were attached to a data logger to collect the temperature profiles across different depths of pavements, as shown in Figure 2b.

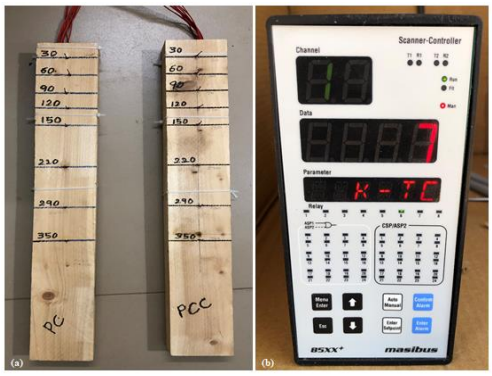


Figure 2: Test setup to monitor temperature profiles across different depths of pavement slabs: (a) Thermocouple sensors installed on assembly unit; (b) Data logger to collect and record temperature profiles

Field Monitoring Scheme

The installation of thermocouple sensors within PCP and PCCP slabs began with the excavation of soil from natural subgrade. The thermocouple assembly unit was embedded into pavement system such that 350 mm mark was exactly at the interface of subgrade and GSB layer. The next stage involved placement of GSB material over the subgrade such that the thermocouple sensor installed at 150 mm depth was positioned at the interface of GSB and pavement surface course. Finally, fresh concrete material was laid and the top surface of thermocouple assembly was flushed with the existing roadway level to provide a smooth and finished wearing course. The

thermocouples were extended to the side of pavement through a 25-mm diameter polyvinyl chloride (PVC) pipe and connected to the data logger. PVC pipes served as a protective medium to prevent the thermocouples from being damaged during the construction program. The steps involved during the placement of thermocouples in the pilot test sections are presented in Figure 3.

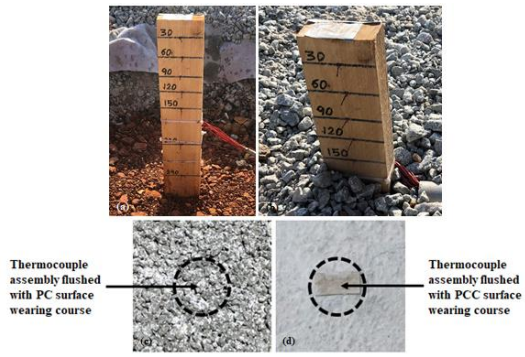


Figure 3: Steps involved in field monitoring program: (a) Thermocouple assembly resting over natural soil subgrade; (b) Thermocouple assembly extending over GSB layer; (c) Thermocouple assembly flushed with existing pervious concrete roadway level; (d) Thermocouple assembly flushed with existing Portland cement concrete roadway level

Test Methodology

Initially, the temperature profile of the pavement was examined under dry conditions during summer season (May 2019). Note that the maximum day-time temperature was about 44 °C. The temperature data under dry conditions was collected from 17:30 hours on 25 May 2019 for 24 hours at an interval of every fifteen minutes set in the data logger. The pavement surface temperature was recorded with the help of a thermal gun at similar time intervals. The wet condition test was conducted from 18:00 hours on 26 May 2019 to 15:00 hours on 27 May 2019 at three-hour intervals. The quantity of water required for per degree decrease of temperature within PCP and PCCP systems was recorded, and comparisons were made for future recommendations. To ensure that the water poured on to the pavement slabs did not spread out laterally, glass putty was applied all around the thermocouple assembly, as shown in Figure 4.

Results and Discussion

Higher surface temperature was observed for PCP, as in Figure 5a, with a peak temperature difference of almost 11 °C at around 13:45 hours. It was further observed that the temperature of PCP system was higher throughout the 24-hour period, with late night and early morning temperatures being lower and similar to PCCP, as shown in Figures 5b through 5g. Such high temperatures of PCP may be attributed to the presence of large sized porous channels within its matrix that capture the incident solar radiations. The findings of this study corroborated the literature that even though PCP had higher temperatures than PCCP, it still had less heat energy stored within its system (Kevern, Haselbach, and Scahefer 2012). Such behavior was ascribed to the high porosity of the PCP system. More so, another investigation suggested that low albedo of PC material did not allow the incoming solar radiations to reflect from its surface, thus resulting

in higher temperatures than conventional PCCP (Hu et al 2017), as also found in this research investigation.



Figure 4. Glass putty surrounding thermocouple over pervious concrete pavement

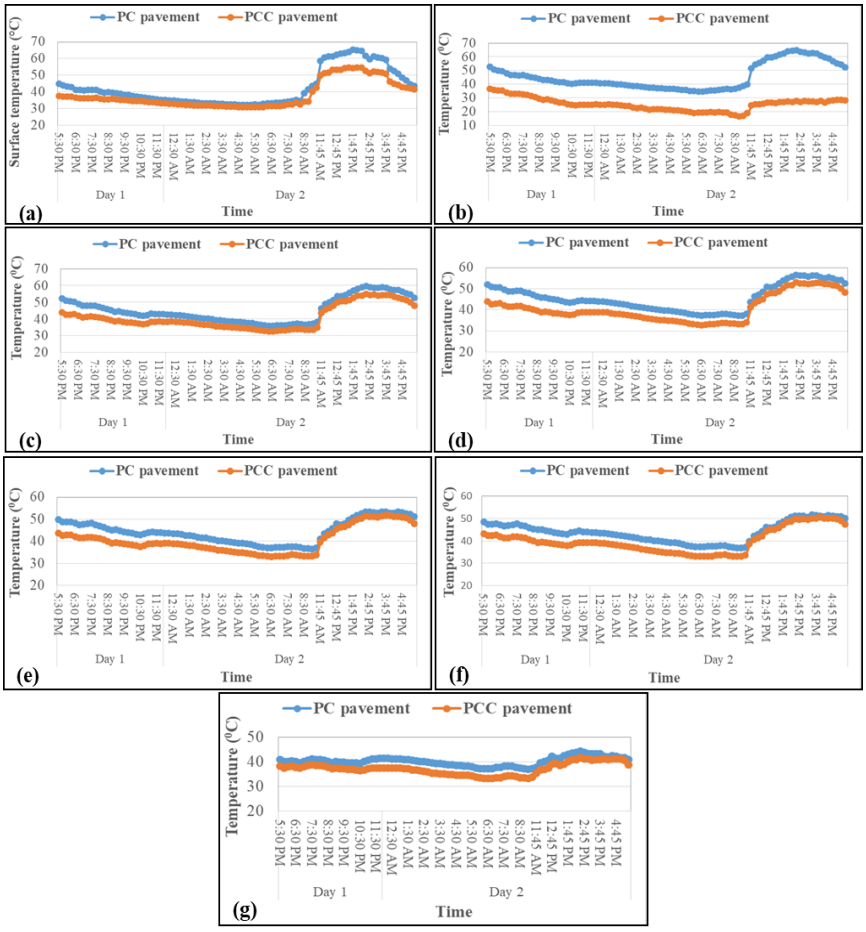


Figure 5. Temperature profiles of pervious concrete and Portland cement concrete pavement systems under dry conditions: (a) at surface; (b) at 30 mm depth; (c) at 60 mm depth; (d) at 90 mm depth; (e) at 120 mm depth; (f) at 150 mm depth; (g) at 290 mm depth

For wet pavement conditions, the temperature of water used for testing was about 34 °C. It was observed that small quantities of water were sufficient to reduce the pavement surface temperatures during different time intervals. The average quantity of water required for per degree decrease in the surface temperature for PCP was about 0.54 L/m^2. Further, the average quantity of

water poured (required) over an area of 0.07 m^2 on PCP system for reducing the temperature across the pavement slab during different time spans is depicted in Figure 6. Note that the thermocouple sensor stopped responding at 90 mm depth on the second day of wet condition test, thus it was ignored from final computation.

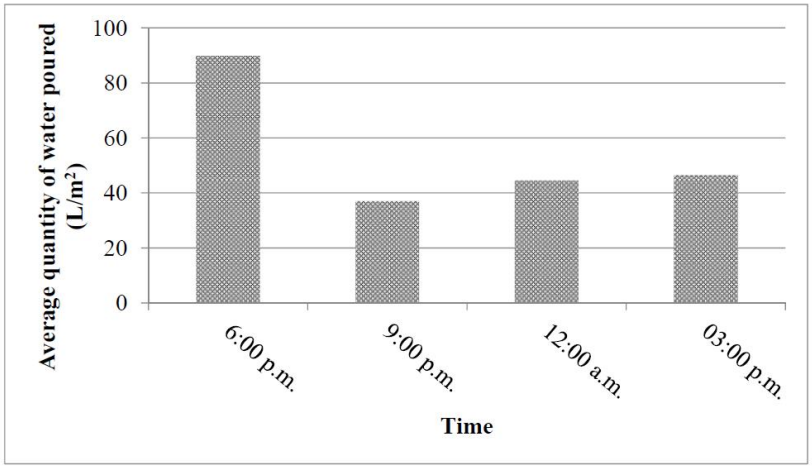


Figure 6: Average quantity of water poured over PCP system

Note that results from 9:00 and 12:00 hours on 27 May 2019 have not been shown in Figure 6, as it was observed that the temperature of the pavement increased, rather than decreased, when water was poured. Although the pavement surface temperature decreased as expected, there was a rise in temperature ranging from 0.8 to 3.9 °C within the pavement. This may be attributed to the rapid heating of water as it came in contact with the PCP surface such that by the time it reached the full depth of the slab, water was warmer than the pavement.

In case of PCCP systems, it was observed that the surface temperature reduced by 1 °C by pouring around 0.28 L/m^2 of water, which was about 50% less compared to PCPs. This can be attributed to the fact that PCCP has rather a smooth surface wearing course, and pouring of designated quantity of water over its surface would have higher cooling effect immediately, which would eventually diminish as soon as water evaporated. Figure 7 shows that the effect of pouring of water is more sustained in the case of PCP compared to PCCP system.

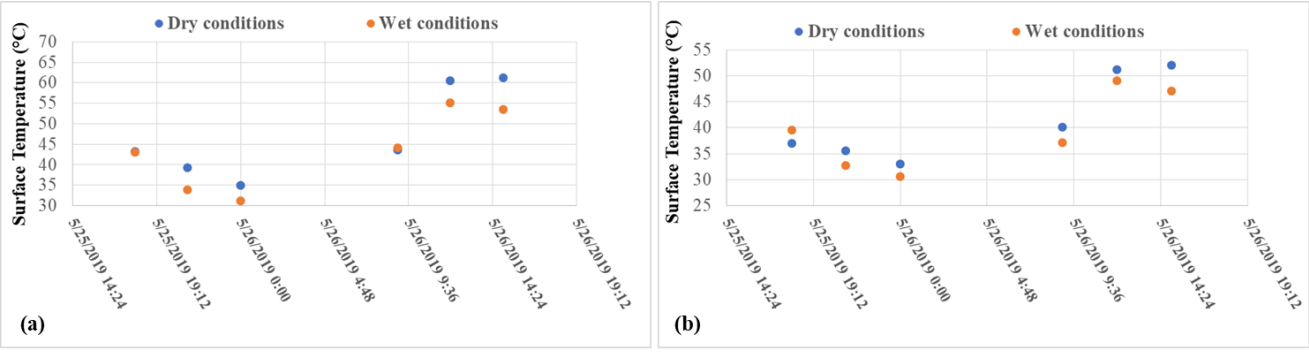


Figure 7. Effect of pouring of water on pavement surface temperatures: (a) pervious concrete pavement; (b) Portland cement concrete pavement

In particular, three hours after pouring water, the surface temperature of PCP showed a reduction of as much as 7.8 °C compared to dry conditions, while the corresponding reduction for PCCP was 5 °C. This can be attributed to the evaporative cooling effect that PCP offers due to the percolation of water to the underlying layers that remains captured within the porous matrix, thus allowing for more sustained (or endured) cooling. Obviously, PCCP being impervious in nature does not allow the percolation of water into its underlying layers, thus heat energy stored within PCCP would dissipate gradually, and cause prolonged thermal discomfort.

Conclusions and Recommendations

The findings from this research study imply that applying water over PCP can be an effective strategy to mitigate UHI. Though the temperature of PCP is generally higher than PCCP, its higher porosity allows capturing of water into its voids, and providing endured evaporative cooling effect for prolonged durations, unlike PCCP.

The ability of PCPs to mitigate UHI is a function of its material characteristics such as aggregate type, porosity and pore connectivity. More research is needed by comprehensive examination of PCP under field conditions during different seasons and time intervals. Such an approach would not only provide additional information on the benefits offered by PCP over conventional pavement systems, but will also aid in designing most conducive PCP systems for UHI mitigation.

References

Abdel-Aziz, D. M., Al-Maani, D. O., & Al-Azhar, W. (2015). Using Pervious Concrete for Managing Storm Water Run-off in Urban Neighborhoods: Case of Amman. American International Journal of Contemporary Research, 5(2), 78-86.

American Society of Testing and Materials (2017). Standard specification for Chemical Admixtures for Concrete (ASTM C494/C494M)

Gui, J., Phelan, P. E., Kaloush, K. E., & Golden, J. S. (2007). Impact of pavement thermophysical properties on surface temperatures. Journal of Materials in Civil Engineering, 8, 683–690. https://doi.org/10.1061/(ASCE)0899-1561(2007)19:8(683)

Haselbach, L., Boyer, M., Kevern, J. T., & Schaefer, V. R. (2011). Cyclic Heat Island Impacts on Traditional Versus Pervious Concrete Pavement Systems. Transportation Research Record: Journal of the Transportation Research Board, 2240, 107–115. https://doi.org/10.3141/2240-14.

Hu L., Li Y., Zou X., Du S., Liu Z., & Huang H. (2017). Temperature characteristics of porous Portland cement concrete during the hot summer session. Advances in Materials Science and Engineering, 2017, 1-10. https://doi.org/10.1155/2017/2058034

Kevern, J. T., Schaefer, V. R., & Wang, K. (2009). Temperature Behavior of Pervious Concrete Systems. Transportation Research Record: Journal of the Transportation Research Board, 2098, 94–101. https://doi.org/10.3141%2F2098-10

Kevern, J. T., Haselbach, L., & Schaefer V. R. (2012). Hot weather comparative heat balances in pervious concrete and impervious concrete pavement systems. Journal of Heat Island Institute International, 7, 231–237.

Li, H., Harvey, J. T., Holland, T. J., & Kayhanian, M. (2013). Corrigendum: The use of reflective and permeable pavements as a potential practice for heat island mitigation and stormwater management. Environmental Research Letters, 8 (4). https://doi.org/10.1088/1748-9326/8/4/049501

Lorenzi, A., Haselbach, L., & Filho, L. C. P. S. (2015). Field data for heat island mitigation by pervious concrete in Porto Alegre. Proceedings from 3rd International Conference on Best Practices for Concrete Pavements. Zardim (Brazil), 28-30 October 2015.

Marceau, M., & Geem, M. V. (2007). Solar Reflectance of Concretes for LEED Sustainable Site Credit: Heat Island Effect. Publication SN2982. Portland Cement Association, Skokie, Illinoise.

Qin Y., & Hiller J. E. (2014). Understanding pavement surface energy balance and its implications on cool pavement development. Energy and Buildings, 85, 389-399. https://doi.org/10.1016/j.enbuild.2014.09.076

Tennis P. D., Leming M. L., & Akers D. J. (2004). Pervious concrete pavements. Portland Cement Association, Skokie, Illinois.

United States Environmental Protection Agency (2004). National Menu for Best Management Practices, Post-construction Stormwater Management.

United States Environmental Protection Agency (2005). Reducing urban heat islands: compendium of strategies, EPA's heat island reduction initiative.

United States Environmental Protection Agency (2008). Reducing urban heat islands: Compendium of strategies, Cool Pavements.

United States Green Building Council (2009). LEED-Leadership in Energy and Environmental Design for New Construction and Major Renovations Rating System.

Wu H., Sun B., Liu Z., & Yin J. (2017). Laboratory-simulated investigation on thermal behaviours of permeable concrete pavements. Road Materials and Pavement Design, 18 (3), 97-108. https://doi.org/10.1080/14680629.2017.1329865.

Cool Roof initiatives in India: An evaluation of the existing conditions and lessons to be learnt from global best practices.

Hema Sree Rallapalli[1]*, PhD Student, School of Planning and Architecture, Vijayawada (India)*
Assistant Professor, GITAM (Deemed to be University), Hyderabad (India)
Janmejoy Gupta, Associate Professor, School of Planning and Architecture, Vijayawada (India)

ABSTRACT

Cool roof is a simple yet powerful technology used for temperature control of buildings and urban areas. To understand the effectiveness of cool roof application in Indian cities and to understand the existing policies, codes and practices being carried out in India, a review of the existing conditions is done. This paper also studies various best practices from around the world and suggests the lessons India can learn from these global examples. There have been several studies done to prove the applicability and effectiveness of cool roofs in Indian conditions. In line with the country's National Cooling Policy, there are a few state and city level initiatives for the wider application of cool roof technology. Several green rating systems in India highlight cool roof as an energy saving strategy. There is a code specific to energy conservation in buildings with cool roofs requirement. However, at this point this code is not mandatory for majority of the Indian states. As learnt from the global examples, mandatory codes, policies, incentives, tax credits, and other such similar measures have a higher outreach for this technology adoption. India would benefit greatly from updating the existing policy framework to include cool roof related interventions, supporting focused research in the area and maximizing ground implementation through short and long term strategies. A consortium of scientific partners, industry partners, policy makers, along with the NGOs and volunteers working towards a common goal will make wider adoption and visible reduction in Urban Heat Island a reality.

Keywords: Cool roof, High reflective surfaces, UHI mitigation, India, Global learning

Introduction

Human activities are estimated to have caused approximately 1.0°C of global warming above pre-industrial levels, with a likely range of 0.8°C to 1.2°C. Global warming is likely to reach 1.5°C between 2030 and 2052 if it continues to increase at the current rate (IPCC, 2018). The effects of global warming include severe weather conditions such as high temperatures, change in the amount and pattern of precipitation and related extreme events such as flooding, droughts, glacier retreat, landslides, sea level rise which we are already experiencing.

Added to the effect of global warming, cities, due to high built-up areas and high concentrations of anthropogenic activities, have led to the development of higher temperatures in urban microclimates. This phenomenon, which is widely known as the Urban Heat Island (UHI), is regarded as the best documented proof of climate modification in times of intensifying

[1] Corresponding Author: hemasree.gsa@gmail.com, Phone:+91 9908874594

urbanization. The causes for higher temperatures in urbanized environments are anthropogenic heat, excess of heat stored by buildings, roads, and other constructions materials that absorb heat during the day and re-emit after sunset, decreased long-wave radiation losses from urban areas, lack of vegetation and reduced evaporate-transpiration processes, reduction of wind speed and consequent reduction of convective heat removal from urban surfaces to the atmosphere. In some cases, it causes an average urban daytime air temperatures of typically 5.6°C higher than the surrounding rural areas in summer (Akbari, Menon & Rosenfeld 2009).

As major cities globally are experiencing increasing urban heat island effect and more extreme heat events due to global warming and changing weather patterns, addressing these hazards through cooling techniques and strategies is a key way to undertake urban climate change adaptation while reducing greenhouse gas emissions and offsetting global temperature increase.

Role of Cool Roofs in Urban Heat Island Mitigation

Sustainable solutions to improve resiliency against UHI effects, both short and long-term, have received attention in recent years in the context of creating and maintaining livable cities. In light of this, cool roofing is one of the main strategies used to mitigate the effects of heat island effects. Cool roof is a simple yet powerful technology used for temperature control of buildings and urban areas. A cool roof made of a highly reflective type of paint, a sheet covering, or highly reflective tiles or shingles prevents heat absorption by reflecting the sun's heat and then emitting its radiation back into the atmosphere. By doing this, cool roofs allow for a more comfortable and controlled indoor environment.

Quoting Dr.Steven Chu, US Energy Secretary "Cool roofs are one of the quickest and lowest cost ways we can reduce our global carbon emissions and begin the hard work of slowing climate change." There are several direct and indirect benefits of cool roofs, out of which as few key benefits are: (i) mitigation of global warming by reflecting the component of short wave radiation coming from the Sun, out of the atmosphere, (ii) energy saving by reducing cooling requirements of buildings and increasing comfort, (iii) mitigating the urban heat island phenomenon. There are several studies that prove these benefits.

A cool roof on an air-conditioned building can save energy and reduce power-plant emissions of CO_2, SO_2, and NO_x (Akbari et al., 1999; Levinson and Akbari, 2010), while a cool roof on an unconditioned building can lower indoor air temperature and improve indoor comfort (Synnefa et al., 2007). Widespread adoption of cool roofs is thought to be an effective strategy for mitigating UHI. A study by Oleson et al (2010) estimate that adopting cool roofs in cities around the globe could decrease the difference between urban and rural air temperature by 0.4 K on an average. Taha et al (1998) and Taha (2008a, 2008b) show that large-scale increase in urban albedo can reduce summertime 2 pm air temperatures in various cities in the United States, and also decrease building energy use and mitigate photochemical air pollution.

One of the studies based in Hyderabad, India in year 2011 mentions that, with the projected annual increase of 100,000 square meters of new roof construction for the next 10 years, the annual cooling energy savings due to whitening of concrete roof would be 13 -14 GWh of electricity and cumulative cooling energy savings of 73 – 79 GWh for the region

(Akbari et al., 2011). The reduced energy demands leads to reduced energy generation which further leads to less use of fossil fuels and hence reduces harmful air pollutants like NO_x, CO_2, etc. One of the studies in Houston and Baton Rouge estimated that there is a possibility of CO_2 reduction by 6-7% from reduced energy use in the buildings (Konopacki and Akbari, 2002). There are also studies that suggest that implementing cool roofs in cities around the globe would lead to global cooling (Akbari et al 2009, 2012).

Though it is clear from these studies that cool roofs have many direct and indirect benefits almost everywhere, the exact benefits and costs of cool surfaces will depend on a variety of locally specific conditions. To understand the effectiveness of cool roof application in Indian cities and to understand the policies, codes and practices being carried out in India at present with respect to cool roofs, a review is done. This study tries to understand the aspects that lead to success of the existing cool roof programs in the country and to identify the areas for improvement. This paper further studies various best practices from around the world and suggests the lessons India can learn from these global examples.

Cool Roof Initiatives in India

India's increasing cooling energy demand has an increased environmental and social impact such as requirement for significant additional power generation, peak load impacts, and an enormous greenhouse gas (GHG) footprint. Managing India's cooling energy needs is one of the key contributors to meeting India's sustainable development goals and its international climate change commitments under the Paris Agreement (2015) and the Kigali Amendment (2016) to the Montreal Protocol. The following are the list of initiatives taken by Indian Government and various state and city governments for reducing their cooling needs and their contribution to UHI.

National Cooling Action Plan, India

The Ministry of Environment, Forest and Climate Change (MoEFCC), Government of India, is in the process of developing a National Cooling Action Plan (NCAP, 2019) that provides a 20-year outlook on how cooling demand in India evolves and grows, and outline strategies and actions that promote sustainable and smart cooling practices across the nation while mitigating adverse impacts. MoEFCC's approach to formulate a powerful narrative that will resonate with multiple stakeholders in the government, private sector, and non-profit and research organizations in India, and help position India as a leader in using sustainable and smart cooling strategies, linking Montreal Protocol to both mitigate climate change and support India's sustainable development goals. The India Cooling Action seeks to

(i) reduce cooling demand across sectors by 20% to 25% by 2037-38,
(ii) reduce refrigerant demand by 25% to 30% by 2037-38,
(iii) reduce cooling energy requirements by 25% to 40% by 2037-38,
(iv) recognize "cooling and related areas" as a thrust area of research under national Science and Technology programme,
(v) training and certification of 100,000 servicing sector technicians by 2022-23, synergizing with Skill India Mission.

These actions will have significant benefits to society and the environment such as provision for cooling for Economically Weaker Section (EWS) and Low Income Group (LIG) housing, sustainable way of cooling - lowering GHG emissions related to cooling, Robust R&D on alternative cooling technologies – to provide push to innovation in cooling sector etc. This national level policy is hoped to influence many city and state level policies and initiatives to promote cool roofs as a measure to reduce the cooling needs of Indian cities.

The Telangana Cool Roofs Program

The Telangana Cool Roofs Program (Telangana Cool Roof Policy, 2019) aims to meet the following specific objectives:

1. Drive rapid state-wide adoption of cool roofs to save energy, strengthen heat resilience and increase thermal comfort.
2. Support inter-agency coordination to implement the city-wide cool roof program.
3. Identify financing frameworks, outreach and awareness building tools for implementing cool roofs
4. Support workforce development and training programs for cool roof application

Three main program areas that will help achieve these objectives:

1. Mandatory Program (government and commercial): Mandatory cool roofing for all municipal, government-owned, and commercial buildings covered under the state building efficiency codes, for new and major upgrades.
2. Voluntary Program (residential): Voluntary cool roofing for residential and smaller buildings for new and major upgrades.
3. Vulnerable Communities Program: Cool roofing for all low-income housing related to the city's Heat Action Plan.

This program has recently been launched and yet to see to the results.

City-level cool roof initiatives by Indore and Surat

The city governments of Indore and Surat, with the support of TARU Leading Edge and the Rockefeller Foundation, in 2011 initiated a project to address the potential of cool roofs in the two cities (NRDC Report, 2019). Covering over 100 households and 40,000 square feet in Indore and Surat, the Cool Roof Project used simple products such as lime concrete, China mosaic tiles, and broken earthen pots, helping to reduce temperatures and the associated costs of electricity and water. Cost benefit analysis of the implemented locations showed the city government, real estate developers, and technology providers the impact of cool roofs on thermal comfort for vulnerable populations in these cities and ways to incorporate cool roofs into future building projects. The program worked to leverage these local success stories into a compelling case for a cool roof policy development process in the cities of Surat and Indore.

Ahmedabad cool roofs initiative: Addressing cool roofs as a response to extreme heat, 2017 and 2018

A devastating heat wave hit Ahmedabad city in 2010, that heat contributed to more than 1,300 deaths. City leadership in Ahmedabad in order to protect local communities from rising temperatures and the deadly threat of extreme heat, unveiled a cool roofs initiative as a part of

the updated Heat Action Plan (Ahmedabad Heat Action Plan, 2017). The Ahmedabad Municipal Corporation initiated a cool roofs pilot for the city of Ahmedabad with a target to convert 3000 homes to cool roofs. This pilot was carried out in collaboration with the private sector and their corporate social responsibility activities in the city, coupled with a volunteer program.

Mahila Housing SEWA Trust (MHT), a non-profit organization, has installed over 250 cool roofs in low income communities in Ahmedabad, using a material called ModRoof – roofs made of coconut husk and paper waste – as an alternative to concrete roofs. According to MHT, these modular roofs provide greater cool roof benefits than regular roof materials and data collected from installed sites showed indoor air temperature being lower by 7-8°C, as compared to conventional concrete roofs. Building on the findings of the pilot, the Ahmedabad Cool City Program, if implemented city-wide, will go a long way in making the city cooler and protecting the most vulnerable from deadly impacts of heatwaves (NRDC Report, 2019).

Cool roofs initiatives in Delhi

In January 2011, the Chief Minister of the City of Delhi announced a pilot project to install cool roofs on the government buildings in the city. It was done with the intention that the visibility of these demonstration projects to the public will help raise awareness of the energy saving and thermal comfort benefits of cool roofs. In the same year Bureau of Energy Efficiency commissioned Environmental Design Solutions to develop a design manual (Cool Roofs for Cool Delhi, 2011) design manual that describes different elements of a cool roof initiative, from materials to case studies of energy savings in buildings. The manual is structured to be a source of information for key stakeholders – decision makers, citizens and industry on the benefits of adopting cool roofs in buildings in Delhi.

Research on Cool Roofs in India

There have been several studies using both field measurements and computer simulations that document the energy savings from increasing the solar reflectance properties of buildings in India. One such study is the Cool Roof Pilot on Affordable Houses in Ahmedabad by CEPT University, where of the thermal comfort benefits of applying cool coatings to a metal roofs on a traditional affordable houses were recognized. A cool roof monitoring experiment was done at Satyam Learning Centre in Hyderabad (Akbari, 2011), in which installing a white roof coating reduced the average summertime daily maximum roof-surface temperature of a two-storey office building in Hyderabad, India from 52°C to 32°C. The total airconditioning energy use was reduced by 30 kWh/day (5% on hot days and 8% on average days). At Rs.5 per kWh, the coating on this 700 m^2 building is estimated to save about Rs 450,000 over the 10 year life of the roof.

To assess this impact of cool roofs on buildings in rural and peri-urban areas of India, a study (Garg, 2016) was performed on two un-conditioned school buildings in Hyderabad (ZPH School) and Nagpur (VNHM School). Two classrooms of same size, function, and occupancy from both the school buildings were monitored for a period of ten weeks starting from March 2014 till May 2014. The average reduction and peak reduction in indoor air, roof underdeck and roof overdeck surface temperatures are 2.1°C, 5.0°C and 12.3°C and 4.3°C, 10.0°C and 26.3°C respectively for the room with white roof as opposed to grey roof in ZPH School and 1.5°C, 4.0°C and 9.5°C, and 3.3°C, 4.2°C, and 25.2°C respectively in VNHM School.

A field monitoring experiments (Rallapalli, 2016) for MSEDCL Building in Nagpur demonstrate the impact of cool roofs in reducing energy use and improving thermal comfort. The results were observed that daily cooling energy savings per unit roof area is maximum in April with average saving of 0.15 kWh/m^2/day (40% cooling energy savings) and minimum in December with average saving of 0.07 kWh/m^2/day (15% cooling energy savings). An online cool roof calculator was developed by IIIT Hyderabad which works on EnergyPlus engine, to estimate the energy saving potential of cool roofs in various Indian cities. In another study, a controlled field experiment (Arumugam, 2014) was done to demonstrate the energy saving potential of high albedo roofs using an apparatus consisting of two nearly identical test chambers has been built in four Indian climates: Chennai (hot & humid), Bangalore (temperate), Jhagadia (hot & dry) and Delhi (composite). The results shows that savings from high albedo roof ranges from 0.04 kWh/m^2/day in temperate climates, to 0.08 kWh/m^2/day in hot & dry climate. In another simulation based study (Arumugam, 2015), to identify suitable roof insulation thickness for a roof with high albedo and radiant barrier combination, it was found that incremental benefits decline after 25mm thickness of insulation (1.02 m^2K/W).

There is some very important ongoing research such as the natural exposure of cool roofing products in India to study the weathering and aging process. This research would lead to the development a protocol for accelerated weathering and aging in laboratory that would aid the development and testing of new cool roof products. Another controlled experiment is being carried out for estimating the energy saving potential and indoor thermal comfort improvement by the use of high-albedo surfaces on a pitched concrete roofs funded by Indo-French Centre for the Promotion of Advanced Research (IFCPAR). All these studies are a proof that cool roofs are an effective energy saving and UHI mitigation strategy for Indian conditions. Research and development are crucial in understanding potential of a technology and to constantly be upgrading with the changing conditions. It provides empirical data on how cool roof can help in UHI mitigation for various city contexts that would act as a driver for policy change. Therefore, government should make it a priority to fund R&D in this field for evaluating, testing and aiding the development of new products.

Codes and Rating Systems

Cool roof programs have been gaining momentum in Indian cities in the past decade. Green building rating systems such as Leadership in Energy and Environmental Design (LEED), Green Rating for Integrated Habitat Assessment (GRIHA) and the Indian Green Buildings Council (IGBC) rating systems highlight cool roofs as a key strategy in reducing the energy consumption in buildings. These rating systems require mandatory Energy Conservation Building Code (ECBC) norms compliance as a prerequisite for buildings applying for rating.

The Energy Conservation Building Code (ECBC, 2017) requires commercial building roofs with a minimum solar reflectance of 0.6, either through the prescriptive method or whole building simulation method to prove a minimum expected reflectance of 0.6. While the ECBC does not specify cool roof requirements for different climate regions, it does state: “Roofs with slopes less than 20 degrees shall have an initial solar reflectance of no less than 0.6 and an initial emittance no less than 0.9. Where solar reflectance shall be determined in accordance with ASTM E903-96 and emittance in accordance with ASTM E408-71 (RA1996).

Apart from these codes, City governments are in a position to effect change on cool roof strategies, since they often exercise control over local development control regulations and building codes. However, different sections of Indian cities are controlled and managed by different city, state and regional agencies. Therefore, for collective impact to reduce the urban heat island effect coordination among various groups is critical.

Global Best Practices & Policies Related to Cool Roofs – Lessons to be Learnt

Cool roof initiatives have been implemented in the past two decades in leading cities around the world as an effective strategy to counter the urban heat island effect and reduce cooling loads in buildings. While the cool roof movement began to take shape in the late 1990s as a policy program, the nature of its inclusion in policies has evolved over time. While initially building owners were provided credits and rebates to incentivize the inclusion of a cool roof strategy in their building, it has gradually evolved into a requirement as part of the building code in many cities around the world.

The EU Cool Roofs Council (EU-CRC) was founded on February 2009, within the framework of the Cool Roofs Project, aiming to merge all the driving forces for the promotion and adoption of Cool Roofs in Europe (Synnefa, 2011). The EU-CRC's aim is to accelerate the transfer of knowledge, to remove market barriers, to help manufacturers to develop Cool Roofs products, to educate the public and policy makers and to develop incentive programs. Four countries (Greece, UK, Germany, and Italy) in Europe have adopted initiatives to promote cool materials and Greece particularly has adopted cool roof standards. Apart from this, under a program called "Building the future" European government offered incentives for the application of 20,000 cool roofs on residential buildings as a means to improve their energy performance.

Italy is developing a national declaration that promote cool materials as a part of EPBD that focuses on regulating the cooling issues of buildings: residential, public and industrial. In the UK, BREEAM Communities is a voluntary certification standard that includes cool materials as a heat island mitigation strategy. The German Sustainable Building Certificate [2009], which is effectively a standard of the German Sustainable Building Council, on the topic of ecological quality includes the Criterion 9: Microclimate, that specifies that the choice of appropriate materials can contribute to the heat island mitigation and requires the documentation of the albedo values of roofs and facades.

New York City's (NYC) cool roofs program has done an exemplary job of securing the participation of volunteers to help speed the City's transition to cool roofs. The NYC CoolRoofs program is run as a joint effort between NYC Department of Buildings and NYC Service, the agency responsible for coordinating city-wide volunteer efforts. In 2010, NYC CoolRoofs coated 1,168,369 square feet (108,545 m^2) of rooftops across 135 buildings. Sixteen-hundred volunteers participated in these coating efforts. So far the city has coated over 5.7 million ft^2 (around 530,000 m^2) of rooftop (626 buildings) with a white, reflective coating, offsetting the urban heat island effect and thereby cooling the city (Practical guide to cool roofs and cool pavements, 2012). The programme provides benefits and savings directly to the building owner by reducing cooling costs by 10-30% and has proved to be an effective way to help tackle the urban heat island effect and reduce GHG emissions. This type of solution works well when a city does not

have a budget earmarked for cooling but has other resources to contribute – such as a volunteer force or training programmes that can be mobilized and matched with building owners etc.

Some cities have undertaken comprehensive evaluation of the urban heat island effect impact on their communities through satellite imagery to identify the hotspots in the cities that need urgent attention (Eg. Dallas, Houston). In 2005, California prescribed white surfaces for low-sloped commercial roofs as part of its Title 24 energy efficiency codes. In 2008, the state prescribed cool colored surfaces on steep roofed residential buildings in its five hottest climate zones. It was one of the first US states to enact a robust cool roof standard. Japan Ministry of Environment announced "Cool Roof Project" in 2006 that provided subsidies for buildings that covered at least 50 square meters of their rooftops with a green roof or highly reflective paint.

The City of Toronto launched the Eco-Roof Incentive Programme in 2009 to encourage the uptake of eco-roofs by building owners, make buildings more sustainable and promote the creation of green jobs. The Programme provided grant funding for building owners to install new roofing materials – green roofs with living plants and cool roofs that reflect solar heat – that provide environmental benefits and build resilience. Since its introduction, the programme has avoided 106 tonnes of GHG emissions and established 233,000 m^2 of eco-roof space (cool + green). The "One Degree Less" movement pioneered in Brazil, has adopted cool roofs and heat island mitigation as its first practical program to combat global warming (ODL 2009).

Market penetration of cool materials across the US, Singapore and Canada were driven to a large extent by the creation of supportive policies backed by long term financial support (example: utility rebates, federal tax deductions and incentives) based on voluntary systems. In US, the federal government set up and heavily promoted the Energy Star for Cool Roofs. (Kolokotsa, 2015). Sharing information and knowledge among cities across the globe concerning their achievements and the evaluation of their experiences is important. Recognizing that cities can learn from each other, global networks working to promote cool cities have been formed, such as the Global Cool Cities Alliance and the Cool Cities Network.

Conclusion

Cool roofs are an affordable and smart solution that helps manage cooling demand and mitigate the impact of urban heat island effect. Solutions, such as the heat action plan and new cool roofs initiative, are critical to saving lives and addressing skyrocketing cooling demand in cities across India, as climate change continues to drive towards extreme temperatures. Interdisciplinary applied research can help policy makers to gather intelligence and to monitor and evaluate the efficacy of their approaches.

Policy makers at all levels should be able to draft policies, incentives and regulations matching economic, social and environmental factors. A market study for understanding the current status of cool roofs among market key players in India is necessary. The more the demand, the more would be chances to get the materials at a cheaper cost in the local market. Quality certification in-line with the technical standards will increase the credibility of these products among the stakeholders. The database thus developed can be made public through a

web portal for the benefit of architects, engineers, policy makers, building owners and other stakeholders.

Building relationships with local and international experts will prove to be extremely valuable to develop national and state level cool roof programs. These experts, researchers, academicians, manufacturers, consultants, and more—have a wealth of knowledge and experience. One needs to identify the potential for cool roofs in their region and connect with these experts to get their guidance to adopt cool roofs, identify suitable materials and means of increasing the life of cool roofs. Consistent partnership between different stakeholders such as the policy makers, academicians, industry partners, and environmental monitoring agencies is crucial for the implementation of cool roofs on a wider scale.

References

V. Masson-Delmotte, P. Zhai, H. O. Pörtner, D. Roberts, J. Skea, P.R. Shukla, A. Pirani, W. Moufouma-Okia, C. Péan, R. Pidcock, S. Connors, Y. Chen, X. Zhou, M. I. Gomis, E. Lonnoy, T. Maycock, M. Tignor, T. Waterfield, (IPCC, 2018): Global Warming of 1.5°C. An IPCC Special Report on the impacts of global warming of 1.5°C above pre-industrial levels.

Akbari, H. Menon & Rosenfeld (2009) Global Cooling: increasing world-wide albedos to offset CO2 Climate Change 94:275 – 286

Akbari,H.,Konopacki,S.,Pomerantz,M.,(1999).Cooling energy savings of reflective roofs for residential and commercial buildings in the United States. Energy 24, 391–407.

Levinson, R., Akbari, H., (2010). Potential benefits of cool roofs on commercial buildings: conserving energy, saving money, and reducing emission of greenhouse gases and air pollutants. Energy Effic. 3 (1), 53–109.

Synnefa, A., Santamouris, M., Akbari, H., (2007). Estimating the effect of using cool coatings on energy loads and thermal comfort in residential buildings in various climatic conditions. Energy Build. 39, 1167–1174.

Oleson KW, Bonan G B and Feddema J (2010). Effects of white roofs on urban temperature in a global climate modelGeophys. Res. Lett. 37 2119–26

Taha H, Konopacki S and Gabersek S (1998). Impacts of large-scale surface modifications on meteorological conditions and energy use: a 10-region modeling study Theory and Application of Climatology. 62 175–85

Taha H (2008a). Meso-urban meteorological and photochemical modeling of heat island mitigation Atmos. Environ. 42 8795–809

Taha H (2008b). Urban surface modification as a potential ozone airquality improvement strategy in California: a mesoscale modelling study Bound.-Layer Meteorol. 127 219–39

Akbari, H., Tengfang X., Haider T., Craig W., Jayant S., Vishal G., Surekha T., M. Hari Babu, and Reddy, K. N. (2011). Using Cool Roofs to Reduce Energy Use, Greenhouse Gas Emissions, and Urban Heat-¬island Effects: Findings from an India Experiment. Lawrence Berkeley National Laboratory Report.

Konopacki, S., and H. Akbari (2002). Energy Savings for Heat Island Reduction Strategies in Chicago and Houston (Including Updates for Baton Rouge, Sacramento, and Salt Lake City). Paper LBNL-49638. Lawrence Berkeley National Laboratory, Berkeley, CA.

Akbari H, Menon S and Rosenfeld A (2009). Global cooling: increasing world-wide urban albedos to offset CO_2Clim. Change 94 275–86

Akbari H and Matthews H D (2012). Global cooling updates: reflective roofs and pavements Energy Build. 55 2–6

Synnefa and M. Santamouris, (2011) "Advances on technical, policy and market aspects of cool roof technology in Europe: The Cool Roofs project," Energy and Buildings.

National Cooling Action Plan (NCAP) (2019) Alliance for an Energy Efficient Economy. Retrieved 28 August 2019, from https://www.aeee.in/national-cooling-action-plan/

Telangana Cool Roof Policy (2019). Retrieved 28 August 2019, from https://tsredco.telangana.gov.in/PDFs/Telangana_Cool_Roofs_Policy_for_Public_Comments.pdf

NRDC Report, (2018). Issue Brief - Cool Roofs: Protecting Local Communities and Saving Energy. (May, 2018).

Ahmedabad Municipal Corporation, "Ahmedabad Heat Action Plan 2017", (2017), https://www.nrdc.org/sites/default/files/ahmedabadheat-action-plan-2017.pdf (accessed on 25 August 2019)

Cool Roofs for Cool Delhi. (2011). Retrieved 28 August 2019, from https://shaktifoundation.in/report/cool-roofs-cool-delhi/

Garg, V., Kotharkar, R., Sathaye, J., Rallapalli, H., Kulkarni, N., Reddy, N., Sarkar, A. (2016). Assessment of the impact of cool roofs in rural buildings in India. Energy and Buildings, 114, 156–163. https://doi.org/10.1016/j.enbuild.2015.06.043

Rallapalli, H., Reddy, N., Rao, P., Garg, V., Sathaye, J., & Levinson, R. (2016). Cool Roof Monitoring Experiment in a Real Building in Nagpur , India. 4th International Conference on Countermeasures to Urban Heat Island, 1–13.

Arumugam, R., Garg, V., Mathur, J., Reddy, N., Gandhi, J., & Fischer, M. L. (2014). Experimental determination of comfort benefits from cool-roof application to an un-conditioned building in India. Advances in Building Energy Research, 8(1), 14–27. https://doi.org/10.1080/17512549.2014.890540

Arumugam, R. S., Garg, V., Ram, V. V., & Bhatia, A. (2015). Optimizing roof insulation for roofs with high albedo coating and radiant barriers in India. *Journal of Building Engineering*, *2*, 52–58. https://doi.org/10.1016/j.jobe.2015.04.004

Bureau of Energy Efficiency, "Energy Conservation Building Code 2017", (2017), Ministry of Power, Government of India,https://beeindia.gov.in/sites/default/files/BEE_ECBC%202017.pdf

GERMAN SUSTAINABLE BUILDING COUNCIL (2009) German Sustainable Building Certificate. Structure – Application – Criteria. Second English Edition March 2009, http://www.dgnb.de/fileadmin/downloads/DGNB_system_en_44S_20091217_ohneblatt.pdf

A Practical Guide to Cool Roofs and Cool Pavements. (2012). Retrieved 28 August 2019, from https://www.coolrooftoolkit.org/wp-content/pdfs/CoolRoofToolkit_Full.pdf

ODL. 2009. One Degree Less. http://www.onedegreeless.org (accessed on 27 Aug 2019)

Kolokotsa, D. (2015). Advances in the development of cool materials for the built environment. Sharjah, U.A.E: Bentham Science Publ.

Development of an online calculator for cool roof and green roof

Shanmukh Dontu[1], International Institute of Information Technology, India
Vishal Garg, International Institute of Information Technology, India

Abstract

Cool and green roofing strategies are proven to reduce the cooling load in air-conditioned spaces and improve thermal comfort in unconditioned spaces. Calculators that use simulated models to estimate cost savings are used to evaluate various roof configurations. Currently available online calculators that estimate savings provide limited possibilities for locations and roofing options. In this paper, we present a unified online calculator which can simulate both cool as well as a green roof over flat and sloped roofs for all locations for which weather data is available on the EnergyPlus website. It provides an option to simulate an unconditioned building which helps the user to know monthly Fanger Predicted Mean Vote and Indoor Air Temperature. This calculator includes various cool roofing options with different Solar Reflectance Index values and green roofs with different plant and soil properties. It also supports parametric simulations and provides a graphical view of roof insulation thickness v/s energy savings, for different insulation thickness values where multiple simulations are needed to run. We use distributed tasks queues to handle requests at peak calculator usage.

Introduction

With an increase in the growth of construction of buildings, urban heat island effect is a major point of concern. Unconventional roofs known as high albedo roofs and green roofs can provide a solution to this. (Garg et al. 2016) Experimental studies in the past show a significant reduction in energy consumption for conditioned buildings and increased comfort levels in unconditioned buildings with the use of cool roofs. For performing simulations, various parameters such as building location, building type, roof type, HVAC systems are considered. The US Department of Energy and Oak Ridge National Laboratory have developed several cool roof calculators for the United States and surrounding locations which either use DOE 2.1E or uses a lookup table based on the data resulted in experimental facilities in the US. Efforts to make green roof calculator (David J Sailor and Bass 2014) for the US and few locations of Canada has also been made in the past. In this context, Online tool for analyzing benefits of a cool roof over conventional roofs in India using EnergyPlus has been developed by ("IIIT Hyderabad Publications" n.d.; Garg et al. 2016). This calculator is an update to this work which brings everything at the same place. The calculator uses (Garg et al. 2016) simulation model of cool roof and provides an additional feature of a sloped roof and a vegetated roof.
In Table 1, we made a comparison of various calculators available online.

1

[1] Shanmukh Dontu: [shanmukh.dontu@research.iiit.ac.in], [+91-8555096748]
[2] Vishal Garg: [vishal@iiit.ac.in]

Key features added in this version of the calculator are:

- Online distributed EnergyPlus simulation tool
- Simulation monitoring tool for administrator
- Performs simulations for green roof and sloped roof
- Updated system design, framework and user interface
- Applicable for all climate zones across the globe

Background

Cool roof

A roof that reflects and emits solar radiation back to the sky rather than transferring it into the building even under high solar loads is termed as a cool roof. ("Cool Roof Rating Council" n.d.) It helps in reducing the cooling load in a conditioned building and maintains thermal comfort in an unconditioned building. A study(Konopacki and Akbari 2001) shows the energy savings achieved in a building depends on various parameters such as the location, orientation, shading, roof type, wall type, ventilation, equipment load, occupancy, and operational schedules. The use of cool roof rather than a dark or high albedo roof is highly advantageous. In a study (Akbari, Menon, and Rosenfeld 2009), it is estimated that increasing the use of cool roofs will induce a negative climate forcing on the earth which is equivalent to 44 Gt of CO2. There are already a few internet-based calculators developed for understanding the use of cool roofs. Roof savings calculator developed by Oak Ridge National Laboratory(ORNL)("Roof Savings Calculator | ORNL" n.d.) uses DOE-2.1E and AtticSim simulations tools and ("Cool Roof Calculator" n.d.) uses a lookup table based on data from experimental facilities in the US. ("Roof Savings Calculator | ORNL" n.d.) is no longer available online for free and requires a license to use it.

Green roof

A green roof is a technique in which vegetation is grown on rooftops and is widely used as a method to reduce storm-water runoff. This is not modern technology, Romans used trees on top of buildings, such as the mausoleum of Augustus and Hadrian. In (Peck 2002) efforts have been made to study different types of green roofs consisting of many vegetation types each require different depths for growing medium. Usually, there are three types of green roofs: intensive, semi-intensive and extensive and different types of vegetation known as Moss-Sedum, Sedum-moss-herbaceous plants, Sedum-herbaceous-grass plants, and grass-herbaceous plants; these types of vegetations require 2–20 cm depth of medium for growing and are used in Extensive green roofs. (Banting et al. 2005) The extensive roof is the cheapest among all in terms of setup and maintenance, as it can be self-retained. A study (Li and Yeung 2014) conducted in a residential building of Cairo and Egypt between a green roof and a normal roof system demonstrated an annual energy savings of 15%–32% depending on the soil thickness and the thermal conductivity of the soil. The energy savings depends upon various properties such as building type, roof type, leaf area density, plant height, irrigation rate and maintenance (Kamel Basil et al., n.d.). To justify any installation, we need to survey whether it is worth investing.

An online green roof calculator ("Green Roof Energy Calculator - Urban Climate Research Center" n.d.) for the US and few locations of Canada has been developed by (David J Sailor and Bass 2014) to provide a solution to the market with an easy-to-use web-based tool.

Tool Comparison

Calculator	Weather Data	Simulation Engine	Roof	Building type	HVAC	Output
Cool roof IIIT	World ("Weather Data | EnergyPlus " n.d.)	EnergyPlus v8.9 ("EnergyPlus | EnergyPlus" n.d.)	• Green • Cool • Sloped	• Office • Institute • Retail • Residential (24 hr , night only)	• PTHP • PSZHP • Aircooled • Watercooled	• Tabular • Graphical
Cool roof ORNL("Cool Roof Calculator")	US, Pacific Territories, Puerto Rico, Canada	DOE-2.1E	• Cool	• Facilities (small,medium)	• PTHP • Fuel	• Numerical
Roof Savings("Roof Savings Calculator | ORNL")	US	DOE-2.1E+ AtticSim	• Cool • Sloped	• Residential • Commercial	• PTHP • Natural Gas Furnace	• Tabular
Green roof energy calculator("Green Roof Energy Calculator)	US, Canada	EnergyPlus v3 and v6	• Green	• New, Old Office • New, Old Residential	• Undefined	• Tabular

Table 1. Online calculator comparison

Methodology

The methodology used in the development of the online tool is mainly divided into three parts: 1) Web Client, interface to get simulation parameters from users and display results. 2) Django app, a backend program which interfaces with Task queues, database, and Web client. 3) Task manager, it schedules and executes the tasks in a distributed manner. The system design of the tool is shown in Figure 1. In this section, we give a detailed description of each part of the system.

Web Client

The web client is a collection of webpages that act as an interface to run simulations and display results. We use HTML and CSS to build webpages and forms. We provide 3 different types of simulation panel: Simple, Detailed and Parametric. Simple simulation form takes minimal inputs to create simulation, Detailed simulation form provides users with deeper control over simulation

parameters, whereas Parametric simulation provides the same control as Detailed form, apart from that it allows users to pass additional variable known as k-value of insulation which performs simulation on multiple thickness values and the user can pick a suitable insulation thickness corresponding to the energy savings. We do form validation using JQuery(js.foundation n.d.) and notify the user if any field is incorrectly filled. If all fields are valid, then we send the valid form data to Django App using POST API request which it exposes. Figure 3 shows a screenshot of the input form. After successfully submitting simulation information, we redirect to a page that prompts the user to wait for the simulation. Meanwhile, we use AJAX request to check the status of the simulation with Django App every 10 seconds. If and when the simulations are finished we automatically redirect to a results page. For Simple and Detailed simulation, we display annual energy comparison of end uses (interior lighting, fans, pumps, equipment) tabular comparison for both the roofs and show heating, cooling savings/month graphically for better analysis (example figure 5 and 6). For Parametric simulation, we show Thickness vs Energy savings graph. All the graphs are generated using Google Charts("Charts" n.d.). A user can pick an option of email results, where we send them the results upon the completion of simulations.

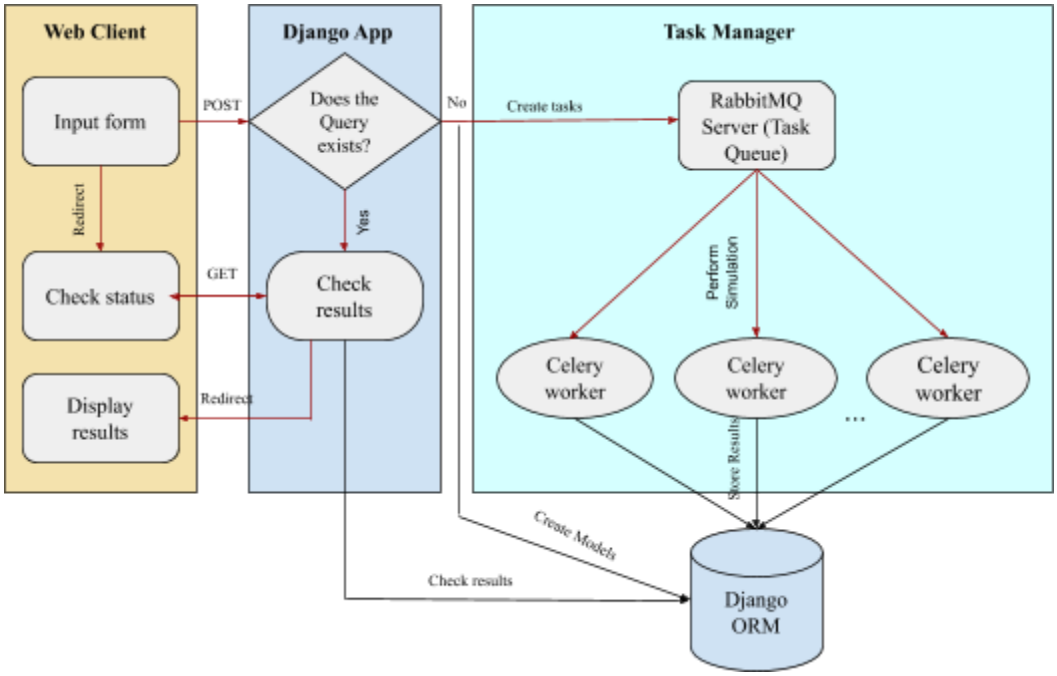


Figure 1. System Design

Django App

Django ("The Web Framework for Perfectionists with Deadlines | Django" n.d.) is a Python orientated high-level web framework which follows Model-View-Controller (MVC) architecture and provides an ORM to interface with Database. Additionally, we use Rest framework ("Home

- Django REST Framework" n.d.) to expose CRUD (Create - Read - Update - Delete) RestAPIs. It is these APIs that are used by Web Client to create a simulation and check the status of the simulation. Both Django App and Web Client are hosted on the same server which we call Master. In other words, Django MVC is used to serve pages for the Web Client. After receiving the simulation request, we check if any of the requested simulations have already been performed. If the simulation has already been performed then we directly redirect to the results page, we call this Caching, this helps us reduce the load on the distributed system. If the simulation is not already performed, we dispatch request for these simulation using Celery ("Homepage | Celery: Distributed Task Queue" n.d.), to be computed in Slave or Worker servers. Whenever the Web client request for the status of a simulation, it checks of results for all simulations are populated in the database, if all results are available then we redirect to Results webpage.

Task Manager

Celery is an open-source asynchronous (background) task queue which uses a distributed system for passing messages to the machines. It also supports scheduling and focuses on real-time operations. It is an easy to use API for building distributed python apps. It is compatible with major messaging queues (RabbitMQ, Redis), databases (Django ORM, MongoDB, MySQL) and monitoring interfaces (Flower, Clearly). We use Celery to create our distributed framework. Multiple Django servers which are enabled with Celery are running on Slaves or Workers servers. We use RabbitMQ ("Messaging That Just Works — RabbitMQ" n.d.) message queues to connect all the celery workers, and they are all connected to the same database as well. Whenever a free worker encounters a task on the message queue (Task queue), it dequeues that task and retrieves the simulation parameters from the common database (Simulation parameters are populated in the DB by Django App). Upon completion of the task, it populates the Database with results, which are later accessed by the Django App. We use EnergyPlus v8.9 to simulate energy consumption. The ease of deploying new Celery workers makes the framework highly scalable. A new worker can be added easily by just installing the requirements and connecting to the message queue and task manager. We also use Flower ("Flower - Celery Monitoring Tool" n.d.) to provide the administrator with detailed statistics about the task queue usage.

Framework

The supervisor("Supervisor: A Process Control System" n.d.) is a client/server that provides a platform for users to monitor and control numerous processes in Linux based operating systems. Administrator is given the privilege of controlling django, flower and celery app in any system/computer using this tool. This can be configured in a way which can start any program at boot time, it makes the system persistent. Supervisor is used to control Django and Flower app at the master node and Celery worker in the slave node (figure 2).

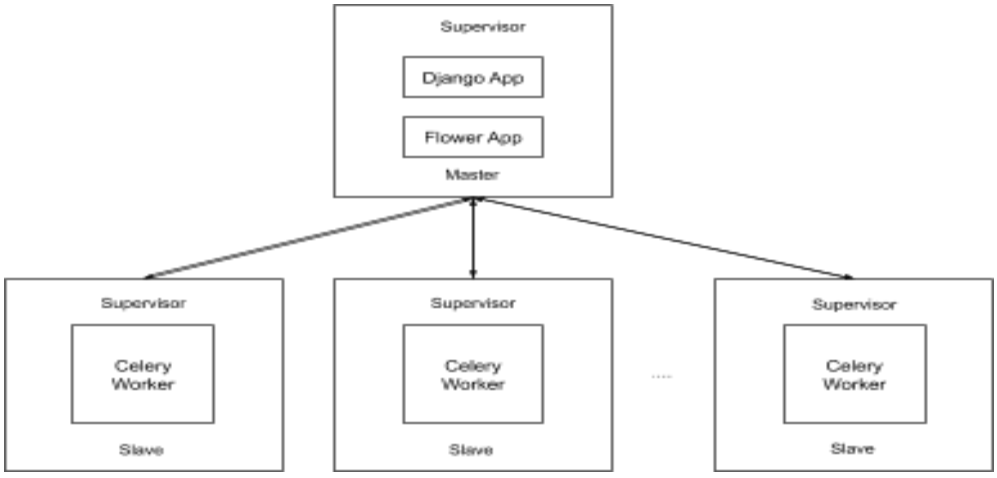


Figure 2. Framework

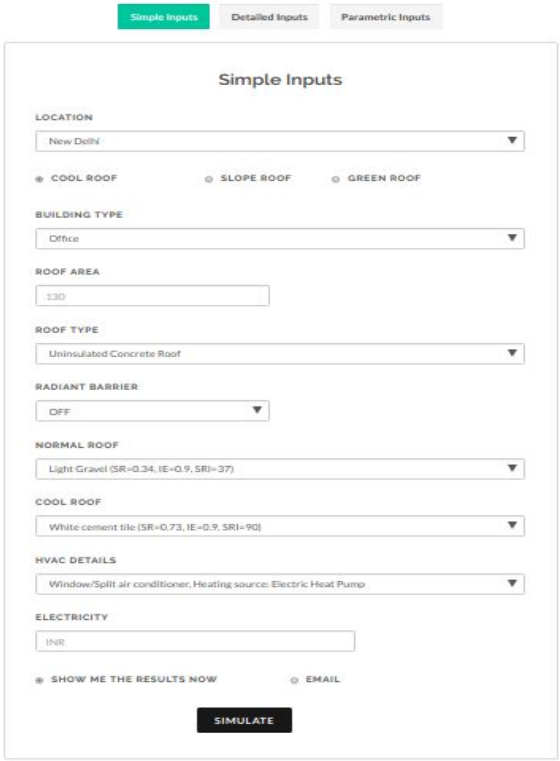


Figure 3. Application Interface

Model setup

The model used by (Garg et al. 2016) has been used for cool roofs. Occupancy schedule for different types of buildings is also described. All the models are square having 5 zones in total which includes 4 perimeters and 1 core zone (figure 4). This new version of the calculator has

added support for green roof model (Sailor 2008) on a five-zone building and sloped roof calculator on a one-zone building. EnergyPlus v7.2 simulation models have been updated to v8.9.

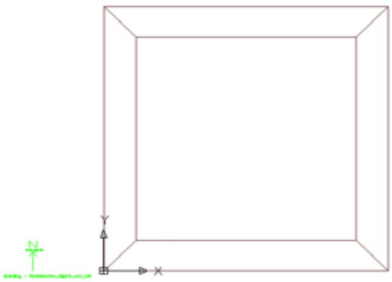


Figure 4. Top view of the Cool roof and Green roof model. Source : (Garg et al. 2016)

Results

Benefits of the cool roof have been shown in (Garg et al. 2016). A comparison of normal, cool and green roof is analysed globally and few results are shown in Table 3. Input parameters for cool and green roof is provided in table 1 and 2. We observed heating penalties in cool roofs for most of the regions and cooling penalties in green roofs for cold climatic conditions.

Cool roof	Building type	Office
	Roof area	2000 meter^2
	Roof type	Uninsulated concrete roof
	Radiant Barrier	Off
	Normal roof	SR-0.34 , IE=0.9,SRI=37
	Cool roof	SR-0.8 , IE=0.91,SRI=100
	HVAC	Window/Split AC, Heating Source: Electric Heat Pump

Table 1. Input Parameters for cool roof simulation

Green roof	Building type	Office
	Roof area	2000 meter^2
	Roof type	Uninsulated concrete roof
	Radiant Barrier	Off
	Normal roof	SR-0.34 , IE=0.9,SRI=37
	Height of Plant	0.8 meters
	Leaf Area Index (LAI)	1 (Dimensionless)
	Soil Thickness	0.6 meters
	The Conductivity of Dry Soil	0.3
	HVAC	Window/Split AC, Heating Source: Electric Heat Pump

Table 2. Input Parameters for green roof simulation

Energy savings v/s normal roof (in kWh/m^2 per annum)						
City	Cool Roof			Green Roof		
	Heating	Cooling	Total	Heating	Cooling	Total
Phoenix	-3.16	31.37	28.21	2.96	20.6	23.56
Cairo	-1.62	27.39	25.77	0.85	15.46	16.31
Kuwait City	-1.54	28.3	26.76	0.83	25.3	26.13
Delhi	-1.86	33.23	31.37	0.49	24.89	25.38
Kuala Lumpur	0	24.38	24.38	0	17.48	17.48
Singapore	0	22.91	22.91	0	12.75	12.75
Dublin	-5.39	3.41	-1.98	26.86	-7.26	19.6
London	-5.96	6.02	0.06	25.7	-5.7	20
San Francisco	-5.51	11.68	6.17	5.57	-4.06	1.51
Adelaide	-3.43	16.29	12.86	3.18	-0.31	2.87

Table 3. Energy Savings in different climatic conditions

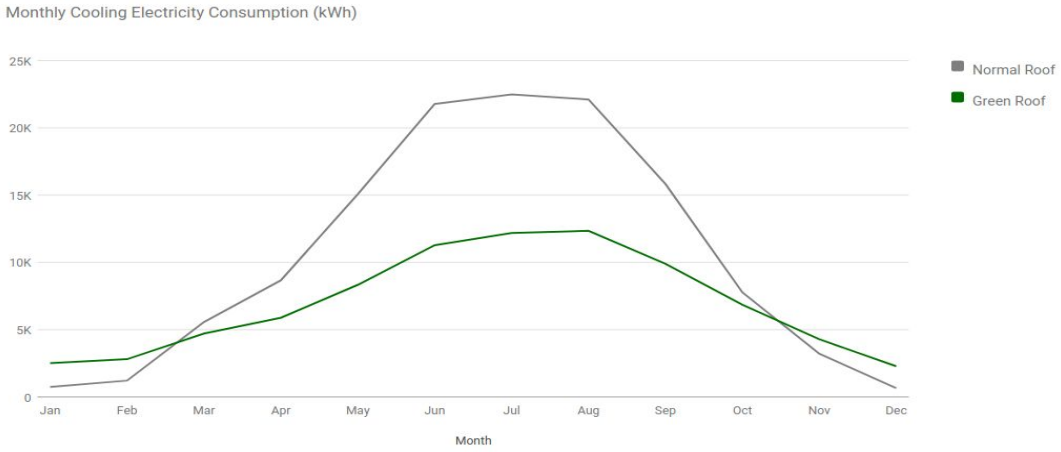


Figure 5. Annual cooling loads(kWh) of green roof v/s normal roof (Phoenix, Arizona)

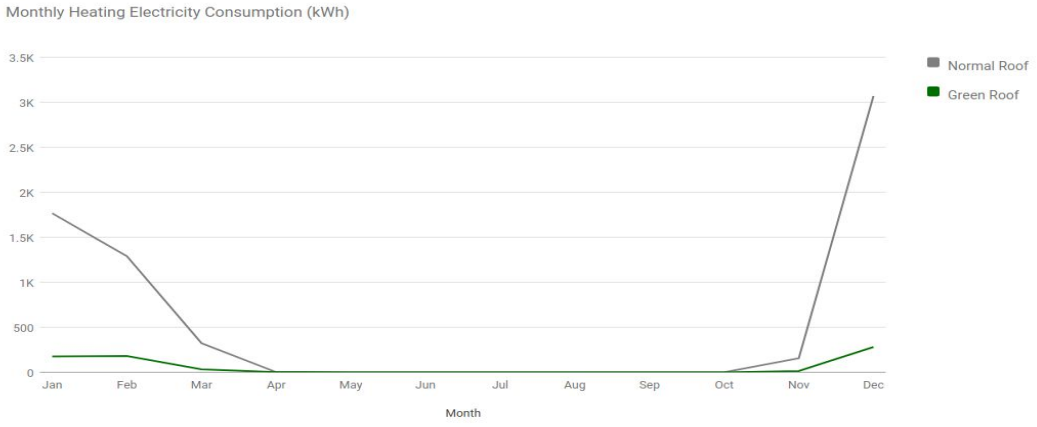


Figure 6. Annual heating loads(kWh) of green roof v/s normal roof (Phoenix, Arizona)

Conclusion

We have developed a simple and easy-to-use online application which analyses energy savings and comfort analysis of unconventional roofs over normal roofs. This application can be used to study the performance of a building considering various roofs, HVAC systems and works for all locations provided in EnergyPlus weather data. It has been designed in a way that multiple users with multiple requests can operate the tool at the same time. We also provide registered user, an interface to view/edit completed simulations which can further help in analyzing various queries at the same place in less time. Hence, We provide a platform for architects, developers, researchers, students, house owners or any organization to see the impact of cool roofs and green roofs across the globe.

References

Akbari, Hashem, Surabi Menon, and Arthur Rosenfeld. 2009. "Global Cooling: Increasing World-Wide Urban Albedos to Offset CO2." *Climatic Change* 94 (3): 275–86. https://doi.org/10.1007/s10584-008-9515-9.

Banting, Doug, Hitesh Doshi, James Li, Paul Missios, Angela Au, Beth Anne Currie, and Michael Verrati. 2005. "Report on the Environmental Benefits and Costs of Green Roof Technology for the City of Toronto." *City of Toronto and Ontario Centres of Excellence—Earth and Environmental Technologies*.

"Cool Roof Calculator." n.d. Accessed August 14, 2019. https://web.ornl.gov/sci/buildings/tools/cool-roof/.

"Cool Roof Rating Council." n.d. Accessed August 14, 2019. https://coolroofs.org/.

"EnergyPlus | EnergyPlus." n.d. Accessed August 29, 2019. https://energyplus.net/.

Garg, Vishal, Shikher Somal, Rathish Arumugam, and Aviruch Bhatia. 2016. "Development for Cool Roof Calculator for India." *Energy and Buildings*, SI: Countermeasures to Urban Heat Island, 114 (February): 136–42. https://doi.org/10.1016/j.enbuild.2015.06.022.

"Green Roof Energy Calculator - Urban Climate Research Center." n.d. Accessed August 27, 2019. https://sustainability.asu.edu/urban-climate/green-roof-calculator/.

"Home - Django REST Framework." n.d. Accessed August 30, 2019. https://www.django-rest-framework.org/.

"Homepage | Celery: Distributed Task Queue." n.d. Accessed August 14, 2019. http://www.celeryproject.org/.

"IIIT Hyderabad Publications." n.d. Accessed August 29, 2019. http://web2py.iiit.ac.in/research_centres/publications/view_publication/inproceedings/677.

Kamel Basil, Wahba Sherine, Nassar Khaled, and Abdelsalam Ahmed. n.d. "Effectiveness of Green-Roof on Reducing Energy Consumption through Simulation Program for a Residential Building: Cairo, Egypt." *Construction Research Congress 2012*, Proceedings, , 1740–49. https://doi.org/10.1061/9780784412329.175.

Konopacki, Steven J., and Hashem Akbari. 2001. "Measured Energy Savings and Demand Reduction from a Reflective Roof Membrane on a Large Retail Store in Austin," June. https://escholarship.org/uc/item/7gw9f9sc.

Li, W. C., and K. K. A. Yeung. 2014. "A Comprehensive Study of Green Roof Performance from Environmental Perspective." *International Journal of Sustainable Built Environment* 3 (1): 127–34. https://doi.org/10.1016/j.ijsbe.2014.05.001.

"Messaging That Just Works — RabbitMQ." n.d. Accessed August 14, 2019. https://www.rabbitmq.com/.

Peck, Steven W. 2002. "Green Roofs: Infrastructure for the 21st Century." *Clean Air Partnership and Presented at the 1st Annual Urban Heat Island Summit, May 2*–3.

"Roof Savings Calculator | ORNL." n.d. Accessed August 27, 2019. https://www.ornl.gov/content/roof-savings-calculator.

Sailor, David J, and Brad Bass. 2014. "Development and Features of the Green Roof Energy Calculator (GREC)," 23.

Sailor, D.J. 2008. "A Green Roof Model for Building Energy Simulation Programs." *Energy and Buildings* 40 (8): 1466–78. https://doi.org/10.1016/j.enbuild.2008.02.001.

"Supervisor: A Process Control System — Supervisor 4.0.4 Documentation." n.d. Accessed August 14, 2019. http://supervisord.org/.

"The Web Framework for Perfectionists with Deadlines | Django." n.d. Accessed August 14, 2019. https://www.djangoproject.com/.

"Weather Data | EnergyPlus." n.d. Accessed August 29, 2019. https://energyplus.net/weather.

IMPLEMENTATION ON URBAN HEAT MITIGATION STRATEGIES

Increasing urban albedo to reduce heat-related mortality in Toronto and Montreal, Canada

Zahra Jandaghian, Research Assistant at Ryerson University
Hashem Akbari, Professor at Concordia University, Canada

ABSTRACT

Heat-related mortality (HRM) is increasing because of the climate change and urbanization leading to extreme heat events. This paper summarizes the results of the excess mortality attributed to excessive heat events in two largest cities in Canada, Toronto and Montreal, during three heat wave periods. We present an application of a fine-resolution, urban-mesoscale model to assess the impacts of heat and heat mitigation strategy on heat death. The Weather Research and Forecasting model (WRF) is coupled with a multi-layer of the Urban Canopy Model (ML-UCM) to assess the impacts of heat and heat mitigation strategy on heat - related death. The background albedo of 0.2 for urban surfaces are respectively increased to 0.65, 0.60, and 0.45 for roofs, walls, and grounds. The changes of the air mass category, ambient and apparent temperatures interpret the impacts of extreme heat and the potential of increasing surface albedo (ISA) on HRM. Here, the calculations and estimations of HRM is based on the data obtained from Canadian Environmental Health Atlas (CEHA) indicating an average of 120 heat-induced deaths in Toronto and Montreal. ISA affords a reduction in air temperature (1–2 °C), a decrease in dew point temperature (0.2–0.5 °C), and a slight increase in near-surface wind speed (−0.01 to −0.4 m/s). Increase in albedo shifts days into more benign conditions by nearly 60%. The HRM will lessen by 3–7%, pointing that seven to eighteen lives could be saved. Cooling the urban climate will improve discomfort index, lessen the impacts of elevated temperature, enhance human thermal comfort, and decrease HRM to some significant extent.

Special Issue Journal	:	Energy and Buildings
DoI	:	https://doi.org/10.1016/j.enbuild.2020.110697
Citation	:	Jandaghian, Z., & Akbari, H. (2021). Increasing urban albedo to reduce heat-related mortality in Toronto and Montreal, Canada. Energy And Buildings, 237, 110697.

Potential of switching cool materials to optimize the thermal response of residential buildings in the Mediterranean region

Michele Zinzi, ENEA (Italy)
Stefano Agnoli, ENEA (Italy)
Giulia Ulpiani, The University of Sydney (Australia)
Benedetta Mattoni, University of Rome La Sapienza (Italy)

ABSTRACT

Goiânia is a city in the late 1930s, and one of the two cities constructed in the Brazilian savannah. In 2018, it had 1.4 million inhabitants and 2,05217 inhabitants per km2. With less than 100 years of age, the urbanization model associated with the effects of global climate change has led the city to live, in recent periods, with moments of water scarcity and flooding. In view of this, the urban municipal policy seeks to point out actions that aim to control land use and occupation from an environmental sustainability perspective. Urban and peri-urban agriculture (UPA) is one strategy and will be the main objective of this article. The urban municipal policy will indicate areas for the practice of UPA as a strategy for adapting cities in the context of climate change. As a secondary objective, the potential for carbon sequestration by this activity was analyzed. The methodology was based on the analysis of urban land use in a Geographic information system (GIS) environment. The database of the Municipality of Goiânia was used. The results indicated three levels of priorities, with a total of 10,650 hectares. In terms of carbon sequestration, this area would result in the capture of 5.536.764,60 tons of CO2 from the atmosphere in 20 years.

Special Issue Journal	:	Urban Climate
DoI	:	https://doi.org/10.1016/j.uclim.2020.100732
Citation	:	Marçal, D., Mesquita, G., Kallas, L., & Hora, K. (2021). Urban and peri-urban agriculture in Goiânia: The search for solutions to adapt cities in the context of global climate change. Urban Climate, 35, 100732.

A pavement-watering thermal model validation for SOLENE-microclimat: application to the Buire street

Marie-Hélène Azam, Univ. Nantes, CNRS UMR 6183, GeM, Nantes, France
Auline Rodler[1]*, Cerema, Equipe-Projet BPE, F-44000, Nantes, France*
Marjorie Musy, Cerema, Equipe-Projet BPE, F-44000, Nantes, France
Benjamin Morille, Soleneos, France
Sihem Guernouti, Cerema, Equipe-Projet BPE, F-44000, Nantes, France

ABSTRACT

Pavement watering is considered as a solution to mitigate the Urban Heat Island, particularly for compact urban areas. This technique has been mainly studied through experimental works and its impact on urban energy balance at the microscale has rarely been addressed by modeling. A thermal soil model dedicated to pavement watering has been developed within the urban climate model SOLENE-Microclimat. Watering events are modeled through a runoff convective heat flux and a latent heat flux. This watering model is presented here and applied to the Buire street, in the city center of Lyon (France). The model performances are assessed on two hot, clear and sunny days. Simulated and measured *in-situ* surface temperatures as well as radiation measurements are compared. A RMSE of 2.99°C is observed. Modeling such a complex environment requires multiple input data which are not always available. The influence of using non-local data and thus neglecting the UHI effect on the soil temperature is studied. It leads to an underestimation of the surface temperature by 0.93°C. Finally, the effect of pavement watering on soil temperature is evaluated. Evening watering scenario (17h to 22h GMT) decreases the surface temperature by 4.09 °C.

Introduction

Reducing the urban heat island (UHI) effect has become a challenge for the technical and scientific community. For that purpose, several countermeasures are investigated for various regions and climates. In dense urban areas, one of the solutions to mitigate the UHI consists in spreading water over paved areas. Several techniques can be used: cleaning trucks, spray nozzles in the pavement. Under warm conditions, they provide a quick answer to high ground surface temperatures, first contributing to cool the surface temperatures and then the air temperature.

Watering has been mainly studied through experimental works (Hendel and Royon 2015). Its efficiency has been proven under warm conditions. Takahashi et al. (2010) have shown that it can reduce the air temperature by 4°C in the afternoon.

However, this solution has rarely been modeled. To the best of our knowledge only Town Energy Balance (TEB) model is able to simulate pavement watering events at mesoscale (Broadbent et al. 2017). In previous works, a pavement watering model has been developed in the micro-scale simulation tool SOLENE-Microclimat (Azam, Bernard, et al. 2018). Watering events are modeled through a runoff convective heat flux and a latent heat flux.

[1] Corresponding Author: [auline.rodler@cerema.fr], [+332 40 12 83 19].

This pavement watering model has been evaluated on an open-space area, a parking-lot. It is now applied to a complex urban scene to evaluate it under these conditions.

For that purpose, the Buire street, in the city center of Lyon (France), is modeled with SOLENE-Microclimat. It has been equipped by Veolia 2EI with a watering device, consisting of sprinklers located in the curbside (Fig. 2). An experimental campaign has been carried out by Veolia 2EI to evaluate the impact of those waterings, including different scenarios. In this paper, we aim to evaluate the model behavior by comparing the *in-situ* measured pavement temperatures to the results of the simulations.

Modeling such a complex environment needs multiple data, in particular the materials properties and local meteorological data. They are usually not accessible for the user of the model. Local meteorological data are important to take into account local phenomenon as the UHI. We will assess the error on the pavement temperature due to the use of reference meteorological data instead of local data. Finally, the influence of the watering practice is quantified in the Buire street by comparing simulations with and without waterings.

Materials and method

SOLENE-microclimat pavement watering model is briefly presented here. Then, the considered case study and the different hypothesis made are detailed. SOLENE-microclimat improved soil model is used described in (Azam, Morille, et al. 2018). The watering events affecting the surface energy balance of the soil model are described below.

Surface energy balance

Usually, the surface energy balance of a dry surface is composed of three heat fluxes: the net radiative heat flux (R_{net}), the conductive heat flux (Q_{cond}) and the sensible heat flux. In order to model a watering event, several additional heat fluxes are considered. The water spread over a surface can either infiltrate in the soil, runoff, or evaporate. For each of those paths, the surface energy budget should be adapted.

The soil model used here has been designed for impervious surface. The portion of water that infiltrates in the soil is supposed negligible compared to the one that runs-off and evaporates. Only runoff and evaporation are thus considered and two additional heat fluxes are taken into account. While the water runoff over the surface, a convective heat flux density ($Q_{wat-pav}$) is exchanged between the soil surface and the water spread. Meanwhile, a part of the water evaporates, leading to a latent heat flux (LE). Eq. (1) describes the resulting surface energy balance. The method and equations used to calculate each heat flux are described hereafter.

$$R_{net} = Q_{cond} + h_c\,(T_{surf} - T_{air}) + Q_{wat-pav} + LE \quad (1)$$

Net radiative heat flux. It is calculated using Eq. (2), considering the short-wave incident radiation R_{sun}, long-wave radiative budget of the soil surface with the surrounding ones noted $R_{IR,Urb}$ and with the net sky noted R_{sky}(Bouyer 2009). The albedo of the urban surfaces is denoted α.

$$R_{net} = (1-\alpha)\,R_{sun} + R_{IR,Urb\downarrow} + R_{IR,Urb\uparrow} + R_{sky\downarrow} + R_{sky\uparrow} \quad (2)$$

The sky total heat flux is defined as the total net flux exchanged between the sky and the ground's surface. The flux incoming from the sky can either be measured or estimated through correlation involving the outside bulb temperature and/or the air water steam (sky nebulosity) (Martin and Berdahl 1984). The used correlation is described by Eq. (3). It considers that the sky temperature is equal to the outside bulb temperature minus ten degree Celsius (Clus 2007).

$$R_{sky\downarrow} = \sigma\,(T_{air} - 10 + 273.15)^4 \tag{3}$$

Sensible heat flux. It is calculated by multiplying the convective heat transfer coefficient (CHTC) denoted h_c by the difference between the surface (T_{surf}) and the air (T_{air}) temperatures. The evaluation of the CHTC is a tricky point. It can either be deduced by a coupled thermo-aeraulic simulations or estimated through empirical correlations. The first method being expensive in terms of computational cost, correlations are usually used in building energy simulation tools. Those correlations evaluate the CHTC from the wind speed (v_{air}) monitored at the studied surface (Palyvos 2008). Jayamaha, Wijeysundera, and Chou (1996) correlation is used here (Eq. 4).

$$h_c = 5{,}85 + 1{,}7\,v_{air} \tag{4}$$

Runoff sensible heat flux. It is exchanged between the water and the soil surface and estimated by means of the energy absorbed by the water layer as shown in Eq. (5) with ρ the density (kg/m³) and $C_p$the specific heat (J/Kg/K). At the time step t, a water height $h_{w,spr}$ is evenly sprinkled over the surface. The water is assumed at the network temperature (T_w).

$$\boldsymbol{Q_{wat-pav} = \frac{\rho_w C_{p,w} h_{w,spr}(t)}{\Delta t}\,(T_{surf} - T_w)} \tag{5}$$

Latent heat flux. It is emitted when a part of the water runoff evaporates. It depends on the amount of water available at the surface and the potential latent heat flux. The latter represents the *evaporative power* of the air (LE_{th}). It can be calculated by the Dalton Equation using the mass-transfer method (Eq. 6) with L the latent heat of the vaporization of water (J/kg). The vapor pressures ($P_{sat}$and P_v) are calculated using the Magnus-Tetens formulas.

$$\boldsymbol{LE_{th} = \frac{h_c L}{C_{p,air}}\,.\,[P_{sat}(T_{surf}) - P_v(T_{air})]} \tag{6}$$

From the potential latent heat flux, a potential evaporation water height ($h_{evap,th}$) can be calculated as described by Eq. (7).

$$\boldsymbol{h_{evap,th} = \frac{LE_{th}\,\Delta t}{L.\rho_w}} \tag{7}$$

The latent heat flux can then be calculated from the available water height at the surface. If the potential evaporation water height is higher than the available water height, all the water present at the surface evaporates. Otherwise, only a part of the water layer evaporates.

Water height monitoring. At each time step, a water layer can be spread over the surface. The amount of water spreads over the surface is added to the previous one. Part of this water layer can then runoff and part of it can be stored at the surface until it evaporates. The surface water-holding capacity defines which proportion of the water height is stored in the pavement porosity. If the resulting water layer is higher than the pavement water holding capacity, part of the water layer runoffs directly to the sewage. The resulting water layer is then set at the pavement water holding capacity. Three cases are distinguished to calculate the surface energy balance and monitor the water height. Details on the flowchart and the heat fluxes can be found in Azam, Bernard, et al. (2018).

Description of the case study

The model is applied to the Part-Dieu district at Lyon in France (see Fig. 2). The system spreads a thin layer of water over the road pavement surface thanks to sprinklers located in the curbside (see Fig. 2a). It has been tested during three consecutive summer periods from 2012 to 2014, with various watering scenarios. Data from the last and most complete measurement campaign are used here. The soil model is evaluated on two days : the 26th and the 27th of July 2014. Data from the 25th of July are used to initialize the model.



Fig a. Pavement watering device included in the curbside of the Buire street.

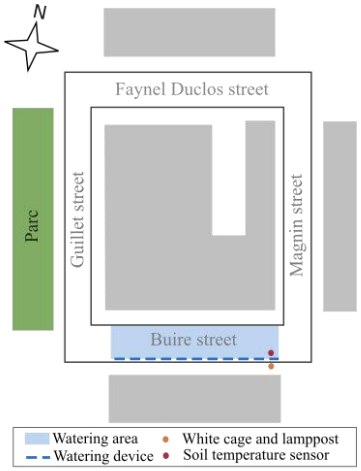


Fig b. Part Dieu district



Fig c. Lamppost

Figure 2. Experimental case study presentation. Wind speed and global horizontal irradiance are measured on the lamppost at a height of 4 m, the air temperature in the white cage at a height of 1.5 m, the soil temperature sensor is located at a depth of 1 cm (Source Veolia 2EI).

Several parameters of the street have been monitored to evaluate the efficiency of the watering events. We focus on the soil temperature, the wind speed, the global horizontal irradiance and the air temperature. The data were collected with a time step of one minute and averaged over 15 minutes.

Data on the events intensity and duration were collected from the *info-climat.fr* website. Six watering events occurred during the 26th and the 27th of July. Events from the 26th of July are natural rain events. At midnight, 5.9 mm water height during 90 minutes is measured. The same day at 13h, 3 mm and at 18h 0.2 mm are measured. On the 27th of July, the watering device was tested from 17:00 to 22:00 (GMT). A thin layer of 0.063 mm on average was spread every 20 minutes on the road surface.

Model setup

The simulations are run from the 25th of July 2014, 00:00 to the 27th of July 2014, 23:45 with a time step of 15 minutes. The surface characteristics of the urban scene have not been measured. Surface composition, layer thickness and thermal characteristics are assumed. Theoretical composition of the road and sidewalk of the Buire street are known, but the thermal properties have not been measured. We defined them using data measured on similar materials (Pilate, O. 2006). They are presented in table 2. The albedo of the buildings walls, roofs and urban soils have been set respectively to 0.54, 0.40, 0.17 and the emissivity to 0.90, 0.90, 0.95. The road water-holding capacity have not been measured either. It has been set to 0.8 mm using data from a parking lot with similar pavement characteristics (Azam, Bernard, et al. 2018).

Table 2. Soil thermal characteristics defined from Pilate, O. (2006)

Surface	Layer	layer thickness (m)	conductivity (W/mK)	specific heat (J/kgK)	density (kg/m3)
Buire Road	very thin asphalt concrete	0.03	2.0	869	2350
	thick solution system	0.07	2.0	869	2142
	"as dug" gravel	0.08	0.52	838	1703
	Asphalt	0.08	2.0	869	2350
	"as dug" gravel (GNT031)	0.10	0.52	838	1703
	"as dug" gravel (GNT080)	0.50	0.89	837	1750
Buire Sidewalks	Very thin asphalt concrete	0.02	0.7	920	2120
	Concrete	0.10	1.51	880	2200
	"as dug" gravel (GNT031)	0.08	0.52	838	1703
	"as dug" gravel (GNT080)	0.50	0.89	837	1750
Building	Concrete	0.20	1.75	1000	2300
	Insulation	0.15	0.04	1030	30

Methodology and assessment procedure

The ability of the model to reproduce the physical phenomena involved is first evaluated using data measured locally by Veolia 2EI for the air temperature and wind speed. This first scenario will be defined as the reference one.

As designers usually do not have access to local weather data but use data from meteorological site, the results of the reference scenario will be compared to various scenario using data from Vaulx-en-Velin meteorological site for the air temperature and the wind speed. One input parameter is modified at a time for simulation 2 and 3. Simulation 4 studies the combined effect. Table 3 sums up the origin of the input data used for each simulation scenario. The root-mean-square error between the soil temperatures at a depth of 1 cm (where a sensor has been put by Veolia 2EI) is used to compare the simulation results.

Finally, in order to quantify the impact of watering on the surface temperature. The surface temperature with and without watering are compared for the Buire street.

Table 3. Simulation scenarios definition

Scenario	Simulation 1	Simulation 2	Simulation 3	Simulation 4
Air temperature	Buire	Buire	Vaulx-en-Velin	Vaulx-en-Velin
Wind speed	Buire	Vaulx-en-Velin	Buire	Vaulx-en-Velin

Results and discussions

Comparison between simulations and measurements

First, the model ability to reproduce the physical phenomenas evaluated using local data. Fig. (3) presents the evolution of the temperature measured and calculated at a depth of 1 cm in the soil. The model mainly under-estimates the surface temperature for the 26th and the 27th of July during the night. During the 27th of July afternoon (14:00-16:00), the surface temperature is overestimated. The RMSE error between the two curves is of 2.99 °C. Each source of uncertainty that could explain this error is discussed hereafter. The first point investigated is the global horizontal irradiance. Fig. 4 compares the global irradiance measured by Veolia 2EI and the one calculated by SOLENE. Results of the simulation are given for a triangle located on the soil as close as possible to the temperature sensor. The global horizontal irradiance has been measured at a height of 4 m. Despite the altimeter difference, the dynamic of the radiation is respected. The street is lighted at the beginning of the day (5h-6h30) and during the afternoon (14:00-16:00). For both curves, sunrise and sunset occurred simultaneously. During the day, the heat flux measured is higher than the one calculated, on the contrary, during the afternoon, the simulation overestimates this heat flux. An error of 72.79 W/m² (RMSE) has been calculated between the two curves. Those differences could explain part of the surface temperature underestimation during the day from 5h to 14h and overestimation at the end of the afternoon between 14h and 16h. Another point could be the sky total heat flux. Meteorological data were not available to estimate it precisely at the meteorological station. Among the correlations found to model the sky radiative heat flux, large differences are observed (Clus 2007). Therefore, the sky heat flux has an important uncertainty, as sky temperature has an uncertainty of ±10 °C.

As cited before, the soil composition is not known with accuracy. It will definitely have a large impact on the conductive heat flux. The number of layers and the few measurements made it impossible to calibrate the soil properties.

The runoff sensible heat flux depends on the pavement water holding capacity and the spread water temperature. This last parameter has not been monitored. An hypothesis is then made on the network temperature.The surface state (dry or wet) has not been monitored neither the sewage heat flow. As a consequence, the water holding capacity of the pavement can not be calibrated. Finally, the sensible heat flux depends on the CHTC, which depends on the correlation used. Here, the choice was made to use a linear equation lying on the local wind speed. In order to improve the estimation of the sensible heat flux, a coupled simulation could be done to obtain local wind velocities.

Two others parameters affect the sensible heat fluxes calculation, the air temperature and wind speed. Here local data are used. Yet, they are not always available.

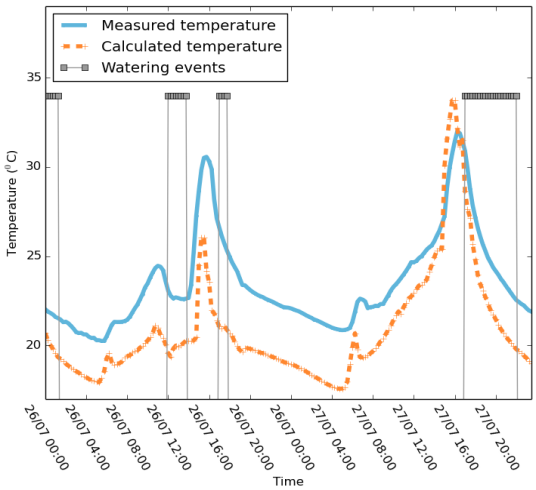


Figure 3. Comparison of the measured temperature at a depth of 1 cm and the one simulated using scenario 1.

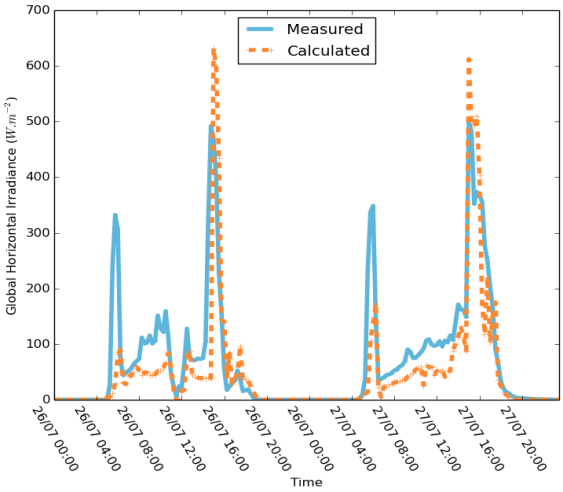


Figure 4. Comparison of the global horizontal irradiance calculated and measured in the street.

Sensitivity analyses: impact of using non-local data

In this second part, we aim at quantifying the impact of using non-local data for the air temperature and the wind speed. First, the input data are compared, then their effect on the soil temperature is studied. Results of the four simulations are compared.

Input data comparison. Usually the air temperature comes from an operational measure station (at an airport for example) which can be far away from the studied district.Fig. (5) shows the local data measured in the studied street by Veolia 2EI and the one from Vaulx-en-Velin operational weather station (7 km distant). During the night, the meteorological station temperature are lower than the air temperature measured in the street, what clearly denotes a UHI effect. A RMSE of 1.89 °C can be observed between the two curves.

Similarly, wind velocity measured from the meteorological station is not representative of the one observed in the street. For the calculation CHTC, the local wind speed is needed. In order to estimate precisely this wind speed using the given meteorological wind speed and direction, a coupled thermo-aeraulic simulation can be done. As it has a very large computation cost, this option is not considered here but we will assess the impact it would have.

Meteorological data from the Vaulx-en-velin site has been analysed to defined the site principal wind direction and intensity. For the 26th of July, three main directions can be observed: West, North-North-East, West-South-West. For the 27th of July, the main direction is North. Consequently, aeraulic simulations have been launched for three directions: North (10°), East (67.5°), West (280°) and 7 intensities from 0.1 to 5.5 m/s. Results from the North (10°) direction are used when the wind direction is included in the segments (0°,45°) and (320°, 360°),the East direction for the segment (45°, 180°) and the West direction for the segment (180°, 320°).

Three wind speed curves are compared in Fig. (6) : the measurement in the Buire street by Veolia 2EI, the measurement at Vaulx-en-velin station and the estimation from the aeraulic simulation (Saturne model). During the nights, the local wind speed was below the anemometer release speed. At the Vaulx-en-Velin station, the wind intensity is also higher during the daytime than during the night. However, the intensity is generally above the one measured locally. For the 27th of July, the estimated wind speed is close to the measurement during the daytime. Indeed, the

direction selected to execute the aeraulic simulations are in good agreement with the wind rose principal direction. However, for the 26th of July, more directions would have been necessary to represent the direction in the segment (90, 270). The calculation overestimates the local wind speed.

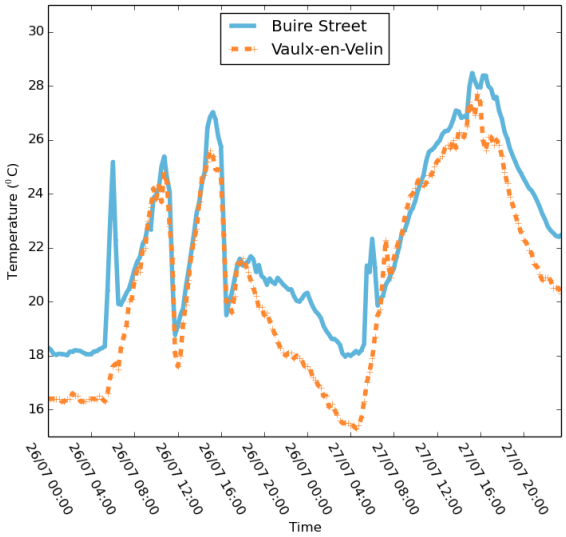


Figure 5. Comparison of the air temperature measured in the street and at the meteorological station Vaulx-en-Velin.

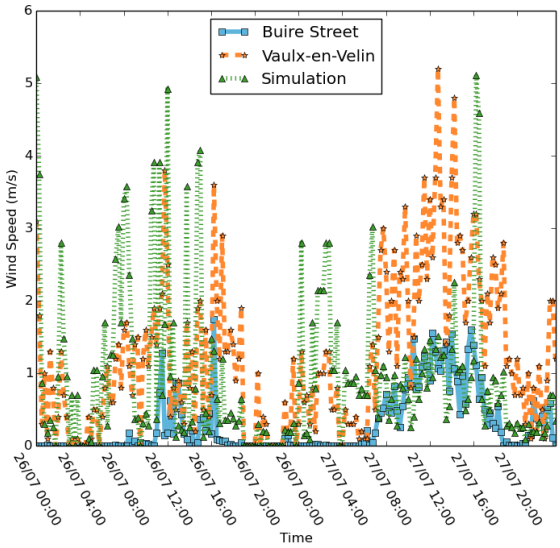


Figure 6. Comparison of the wind speed measured in the street, the one measured at the Vaulx-en-Velin site and the one estimated from the aeraulic simulations

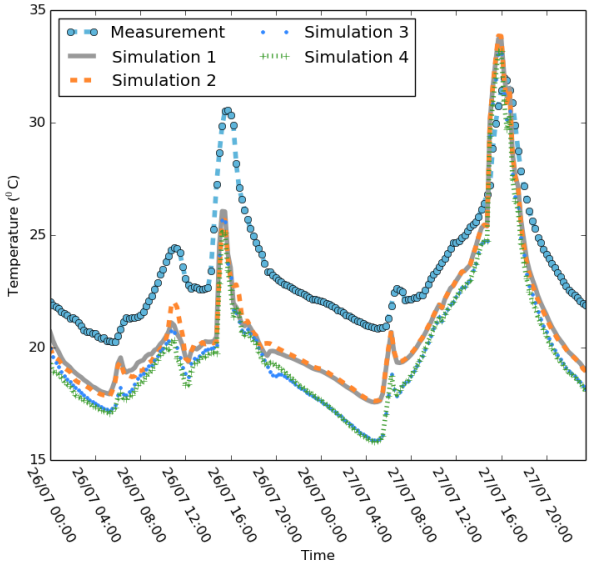


Figure 9. Comparison of the soil temperature calculated for the four scenarios and the measured one.

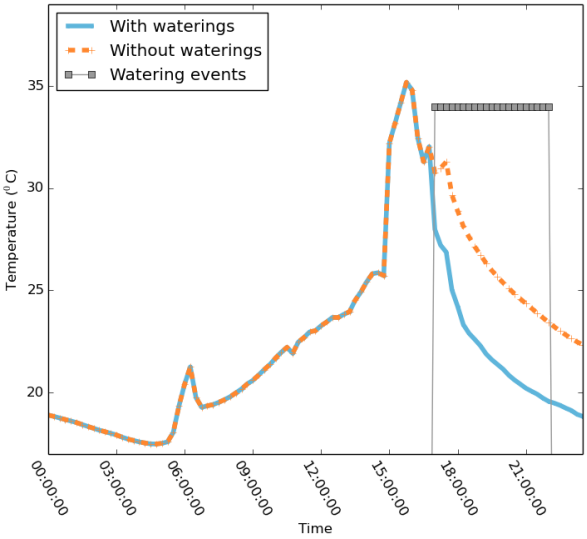


Figure 10. Comparison of the soil surface temperature calculated with and without watering for the 27th of July.

Influence on the soil temperature. The impact of using non-local data on the soil temperature calculation is studied. Fig. (9) shows the results of the four simulated scenarios (see table 3). Errors between the several curves are summarized in table 4.

Table 4. RMSE using local and non-local data (temperature at a depth of 1cm).

	Simulation 1	Simulation 2	Simulation 3	Simulation 4
Measurements	2.99	2.99	3.75	3.75
Simulation 1	-	0.27	0.93	0.87

Simulation 3 uses non-local air temperature and local wind speed. Using non-local air temperature has a high impact on the soil temperature. The error calculated between this simulation and the reference simulation reaches 0.93 °C. However, if we consider using non-local wind speed (Simulation 2), the error with the reference simulation reaches only 0.27 °C. Considering the local air temperature (UHI effect), the street surface temperature is more accurate.

Simulation 4 considers the combined effects of taking into account non-local data for both the air temperature and the wind speed. During the nighttime, the resulting errors cancel out. Curve of simulation 4 exceeds curve of simulation 3.

Influence of the watering scenario on the surface temperature

The influence of the watering on the pavement temperature is now assessed. Results of simulation 1 are compared to the results of a simulation with the same input conditions but without evening watering. As soon as water has been spread over the surface, the temperature drops (Fig. (10)). The surface cooling persists during the whole event. It decreases the surface temperature by 4.09 °C (RMSE calculated from 17:00 to 00:00), with a maximal difference of 4.81 °C.

Due to the East-West orientation of the street, the impact of the watering from 17:00 to 22:00 is limited. It would have been higher if the watering scenario was synchronized with the street irradiance.

Conclusion

The pavement watering model has been applied under urban conditions. The RMSE of 2.99 °C between the soil temperature measurements and the calculation highlights the difficulties to reproduce such conditions. A coupled heat and mass transfer soil model could have improved the results dynamics. However, whatever the level of detail of the soil model used, we face up the reality of lacking information: thermal materials characteristics, pavement water holding capacity, sky total heat flux...

In a second part, the influence of using non-local climate input data has been investigated. The air temperature had more influence on the soil temperature than the wind speed. These results show the impact of the UHI on the surface temperature. Having the local air temperature is an important challenge to improve the simulation results.

Finally, the impact of an evening watering scenario has been quantified. Results of the simulation show that the surface temperature can be reduced by 4.09 °C with such a watering scenario and bring to light the fact that this model can be used to assess the cooling effect of waterings at micro-scale.

The efficiency of this mitigation technique is constrained by the potential evaporation of the surface. It depends mainly on two parameters, the surface energy balance and the surface characteristics. For the first parameters, a watering scenario could be optimized based on the global horizontal irradiance and CHTC. For the second parameters, the characterization of the water

holding capacity of the surface would permit to optimize the water layer spread over the surface to maximized evaporation and minimize water use.

Acknowledgments

The first part and this work was conducted within the framework of the EVA project funded by the ADEME under contract 1216C0037. We acknowledge Veolia 2EI that in the frame of this contract shared their measurement data.

References

Azam, Marie-Hélène, Jérémy Bernard, Benjamin Morille, Marjorie Musy, and Hervé Andrieu. 2018. « A pavement-watering thermal model for SOLENE-microclimat: Development and evaluation ». *Urban Climate* 25: 22-36. https://doi.org/10.1016/j.uclim.2018.04.005.

Azam, Marie-Hélène, Benjamin Morille, Jérémy Bernard, Marjorie Musy, and Fabrice Rodriguez. 2018. « A new urban soil model for SOLENE-microclimat: Review, sensitivity analysis and validation on a car park ». *Urban Climate* 24 (juin): 728-46. https://doi.org/10.1016/j.uclim.2017.08.010.

Bouyer, Julien. 2009. « Modélisation et simulation des microclimats urbains-Étude de l'impact de l'aménagement urbain sur les consommations énergétiques des bâtiments ». Université de Nantes.

Broadbent, Ashley M., Andrew M. Coutts, Nigel J. Tapper, and Matthias Demuzere. 2017. « The cooling effect of irrigation on urban microclimate during heatwave conditions ». *Urban Climate*, mai. https://doi.org/10.1016/j.uclim.2017.05.002.

Clus, Owen. 2007. « Condenseurs radiatifs de la vapeur d'eau atmosphérique (rosée) comme source alternative d'eau douce ». Phdthesis, Université Pascal Paoli. https://tel.archives-ouvertes.fr/tel-00320450/document.

Hendel, Martin, and Laurent Royon. 2015. « The Effect of Pavement-Watering on Subsurface Pavement Temperatures ». *Urban Climate* 14 (décembre): 650-54. https://doi.org/10.1016/j.uclim.2015.10.006.

Jayamaha, S. E. G., N. E. Wijeysundera, and S. K. Chou. 1996. « Measurement of the heat transfer coefficient for walls ». *Building and Environment* 31 (5): 399-407. https://doi.org/10.1016/0360-1323(96)00014-5.

Martin, Marlo, and Paul Berdahl. 1984. « Characteristics of infrared sky radiation in the United States ». *Solar Energy* 33 (3): 321-36. https://doi.org/10.1016/0038-092X(84)90162-2.

Palyvos, J.A. 2008. « A Survey of Wind Convection Coefficient Correlations for Building Envelope Energy Systems' Modeling ». *Applied Thermal Engineering* 28 (8-9): 801-8. https://doi.org/10.1016/j.applthermaleng.2007.12.005.

Pilate, O. (2006). Evolution de la température d'une... - Google Scholar ». s. d. Consulté le 10 avril 2019. https://scholar.google.fr/scholar?hl=fr&as_sdt=0%2C5&q=Pilate%2C+O.+%282006%29.+Evolution+de+la+temp%C3%A9rature+d%27une+couche+d%27enrob%C3%A9+bitumineux+nouvellement+pos%C3%A9e.+Compte+rendu+de+recherche+C.+R.+R.&btnG

Takahashi, R., A. Asakura, K. Koike, S. Himeno, and S. Fujita. 2010. « Using snow melting pipes to verify the water sprinkling's effect over a wide area. Sustainable techniques and strategies in urban water management ». In *7th International Conference. Lyon, France, Novatech*.

The Oasis Project: UHI mitigation strategies applied to Parisian schoolyards

Ghid Karam[1]
Univ Paris Diderot, Sorbonne Paris Cité, LIED, UMR 8236, CNRS, F-75013, Paris, (France)
Université Paris-Est, ESIEE Paris, département SEN, F-93162, Noisy-le-Grand, France

Martin Hendel
Univ Paris Diderot, Sorbonne Paris Cité, LIED, UMR 8236, CNRS, F-75013, Paris, (France)
Université Paris-Est, ESIEE Paris, département SEN, F-93162, Noisy-le-Grand, France

Cécilia Bobée
Univ Paris Diderot, Sorbonne Paris Cité, LIED, UMR 8236, CNRS, F-75013, Paris, (France)

Alexandre Berthe
Univ Paris Diderot, Sorbonne Paris Cité, LIED, UMR 8236, CNRS, F-75013, Paris, (France)

Patricia Bordin
Univ Paris Diderot, Sorbonne Paris Cité, LIED, UMR 8236, CNRS, F-75013, Paris, (France)

Laurent Royon
Univ Paris Diderot, Sorbonne Paris Cité, LIED, UMR 8236, CNRS, F-75013, Paris, (France)

ABSTRACT

Paris is experimenting and implementing strategies to increase the capital's resilience and promote climate change adaptation. Major heatwaves have been hitting the French Capital lately (Bador et al., 2017) and have thus focused attention on UHI countermeasures, such as pavement-watering solutions and urban greening. The Oasis Project is one such strategy aiming to transform schoolyards into urban cool islands that would benefit surrounding neighborhoods and their inhabitants during heatwaves.

The work presented here focuses on identifying high-priority schoolyards among the 670 city-owned schools. This is conducted using a GIS tool used to identify areas with high cooling potential, which would benefit most from UHI countermeasures. After extracting bare schoolyard from the facilities, we built a cooling indicator based on the ratio of high solar irradiance surface to the whole schoolyard area. We were thus able to identify 38 schoolyards with high cooling potential, 157 with medium cooling potential and 286 facilities with moderate cooling potential, out of the 670 facilities.

The methodology can be applied to other cities, and therefore helps set up GIS tools that can provide municipalities with meaningful insight into their urban cooling strategy.

[1] Ghid Karam: ghid.karam@esiee.fr.

Introduction

Climate change is expected to result in an overall increase in annual temperatures in France: 1 to 4°C compared to the current reference (12.4°C) (Bador et al., 2017) as well as a multiplication of heat waves, with frequencies of up to 25 heat-wave days per year compared to 1 day at present (Lemonsu, Kounkou-Arnaud, Desplat, Salagnac, & Masson, 2013). These heat waves are amplified by the urban heat island (UHI) phenomena rooted in several different city parameters: urban morphology, permeability, as well as human activity (Oke, 1982)

The 2003 heat wave caused 70,000 deaths in Western Europe, and particularly affected Paris where its impacts were aggravated by the UHI effect (Robine et al., 2008).

The school network managed by the Paris City Hall is a dense network of 656 kindergarten and elementary schools and 115 middle schools. These areas cover nearly 73 hectares, which tallies to nearly 14% of the actual areas of parks and gardens within the City[2], and are evenly distributed throughout the capital, located within a 200 m radius of each inhabitant. For the time being, schoolyards are paved with asphalt concrete, with low albedo and permeability, and thus contribute to the UHI effect. The transformation of these schools into cooling islands open to the public outside of school time would therefore make up for the lack of green space in the capital (5.8 m^2/capita[3]) and help limit urban heat in Paris, while providing climate refuges for nearby inhabitants. Paris City Hall, via its Oasis Schoolyard program, hopes to renovate all its schoolyards within the next 20 years into cool islands.

Among the first schools to undergo this kind of renovation, 10 schoolyards scheduled for works in 2020 and will be subject to scientific evaluation under the European ERDF UIA "OASIS" project, aiming among other things to quantify the microclimatic impact of the transformations. The targeted schoolyards will be equipped with meteorological station that will monitor microclimatic parameters such as temperature, heat flux, relative humidity and wind speed. The meteorological monitoring of the schoolyards before and after transformation will allow a concrete and experimental evaluation of the microclimatic impact of this initiative.

This paper will present the GIS tool used to prioritize the schoolyards under municipal management according to their cooling potential, i.e. their ability to benefit from UHI countermeasures. The indicator builds on previous work by M. Hendel et al. (Hendel et al., 2018) for urban watering in extreme heat. The indicator for cooling potential, based on morphological data, vegetative cover, and computed solar irradiance is adapted to the case of long-term, permanent UHI countermeasures.

[2] In 2010, out of the 553 hectares of green spaces within the city of Paris, 39 hectares were with restricted access
[3] This ratio does not take into account the Bois de Vincennes and Bois de Boulogne

Methodology

Identifying schoolyards using GIS

Beforehand, it is necessary to identify and map the 770+ Parisian schoolyards. In order to do so, we extracted schoolyards from the geo-referenced datasets provided by Paris City Hall: built areas, land registry[4], vegetation.

Subtracting the Built areas (listed buildings in the city) from the cadastral parcel dataset (listing the city-owned land) provides a first approximation of the schoolyards (Figure 1). A visual analysis of aerial photographs coupled with a comparison with the attributes of the other data sets as well as the layout plans provided by Paris City Hall enables us to isolate schoolyards from decorative gardens, car parks and sports grounds.



Figure 1. From left to right: after identifying the school in the land register, then the built areas, we isolate the schoolyard by subtracting the second from the first.

Cooling Potential Indicator

In order to estimate the cooling potential indicator, we cross-reference solar irradiance data with the schoolyards that we obtained, excluding vegetation cover.

Using a vegetation canopy model, we can identify trees and low-lying vegetation and single out bare, unshaded schoolyard areas.

Solar Irradiance

Direct sunlight is the predominant energy source; we determine the cooling potential by evaluating the cumulative solar irradiation level of the surface of the courtyards that is not sheltered.

Solar Irradiance is calculated to be representative of a Parisian summer in clear, cloudless sky conditions. It is simulated from a digital elevation model (DEM) with a resolution of 0.5 m obtained from LIDAR measurements made in 2012.

The daily solar irradiance of an unmasked flat surface is calculated with a 30-minute time step during the heatwave-prone period that stretches from June 15 to September 15 (Figure 2).

[4] The cadastral parcel is the unitary element of land ownership. It is formed by any portion of land in a single block belonging to a single owner (or to the same joint ownership). The DGFiP manages the cadastral parcel. The latter is a territorial division, and is an entity contained in the same commune, and the same section. Not all the space is fragmented by the land registry (public road, river...).
The cadastral plan that we used was updated in July 2015

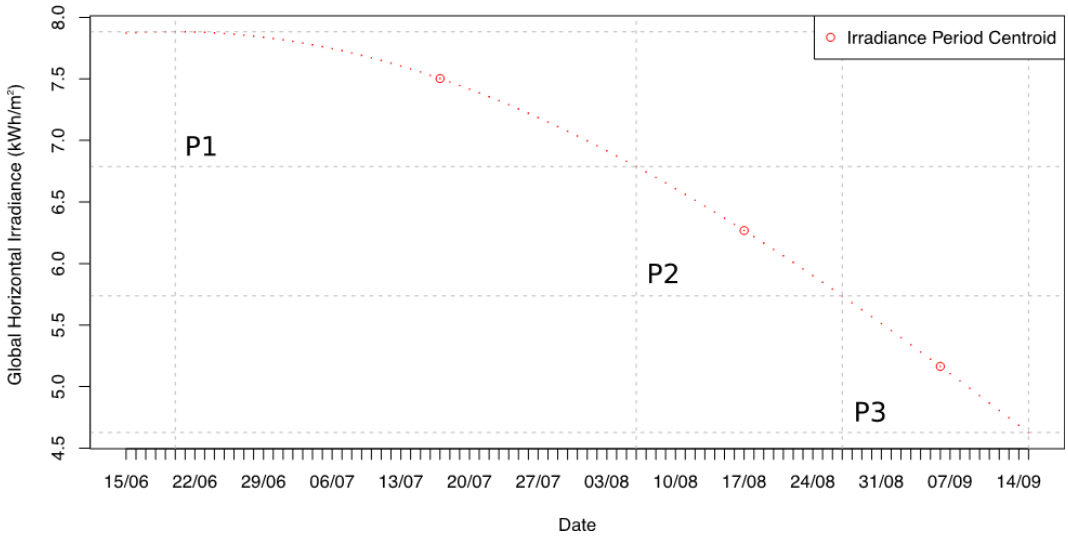


Figure 2. Global daily horizontal solar irradiance from June 15 to September 15

In order to optimize calculation time, the surface irradiance, also computed with a 30-minute time step, we select three representative days by dividing the daily overall horizontal sunshine into three energy bands: P1, P2 and P3 as defined in Table 1. The centroids of the bands correspond to the three representative dates. We thus restrict the calculations to these 3 days.

Table 1. Solar Irradiance energy intervals and representative dates

Solar irradiance (kWh/m²)	Min	Max	Date
P1	7.9	6.8	July 17th
P2	6.8	5.7	August 17th
P3	4.6	5.7	September 6th

The cooling potential analysis is based on a precise time range, a target period. In the case of the schoolyards, this period extends from 6 am to 6 pm UTC (solar time), i.e. half a day. In addition, we set a critical solar irradiance threshold, above which we consider the cooling potential to be high and low below. The threshold value corresponds to half of the total energy that the surface received over the target period. Within the framework of the OASIS project, the transformations are sustainable over time and must therefore be adapted to the entire summer period. We therefore calculate the average sunshine representative of summer, derived from the three standard days.

A weighted average of the sunshine thresholds corresponding to the 3 typical days, makes it possible to obtain an overall critical threshold above which the sunny surface is declared to have a high cooling potential (see Table 2)

Table 2. Solar irradiance threshold computed for each standard day, and global irradiance threshold

Energy band	Number of days	Solar irradiance Threshold (kWh/m²)
P1	52	3.6791
P2	21	3.1206
P3	19	2.5996
Total Number of days	92	
Global Threshold		3.3287

Existing paving materials

Schoolyards are paved with asphalt concrete. However, they also have vegetation covers, i.e. trees, low-rise vegetation that we must take into account while evaluating the cooling potential. In order to do so, we use the raster image provided by the APUR, which is obtained by processing aerial imaging of land cover: each pixel value represents the height of the vegetation cover. We proceeded to vectorising the raster image in order to ease data handling.

The Schoolyards' cooling potential

Once we have identified the schoolyards, it is possible to calculate their cooling potential. At the scale of the School building, we calculate the ratio of high cooling potential areas over the total schoolyard area. This allows us to rank schoolyards accordingly and categorizing into priority levels.

Figure 3 shows the process that is undergone in order to compute the schoolyard's cooling potential. The left image shows the mean solar irradiance raster image of a schoolyard. Using the vegetation vector layer, we create a clipping mask in order to remove vegetalized areas from the mean solar irradiance raster. The center image shows in green, the vegetation mask. The raster obtained is the mean solar irradiance raster image of the bare, unshaded surface of the schoolyard. We then apply our critical threshold to the newly obtained raster, thus spotting the high cooling potential areas, i.e. the areas that would benefit the most from cooling strategies (right image).

We compute the areas of the high cooling potential surface previously obtained, and then calculate the ratio of these areas over the total area of the schoolyard. We obtain a percentage that will help us determine the priority level of the schoolyard. If less than a quarter of the schoolyard's ratio is of high cooling potential, our schoolyard has a low overall cooling potential. The overall cooling potential of the schoolyard rises according to the percentage of high cooling potential areas in the schoolyard. The level is moderate when less than half of the schoolyard's surface is of high cooling potential, medium when it rises to more than the half, and high when more than three quarters of the surface have a high cooling potential.

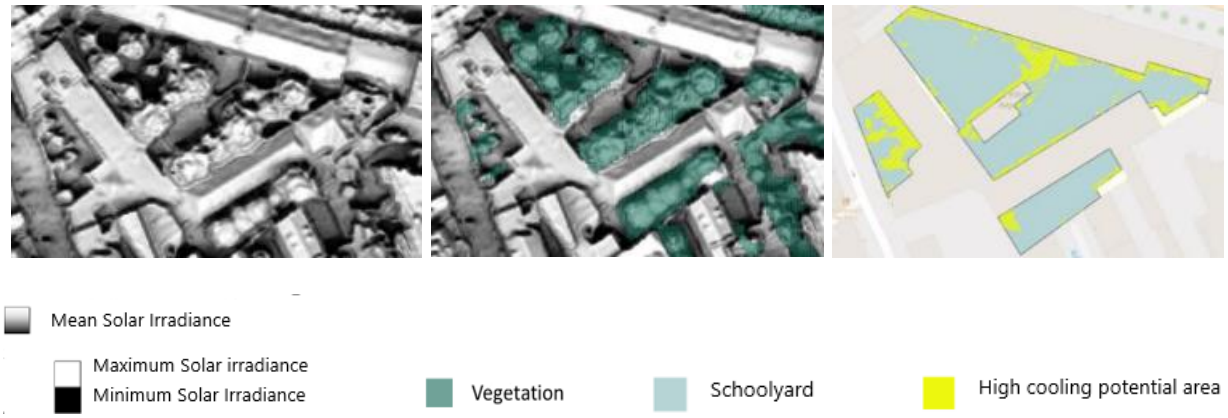
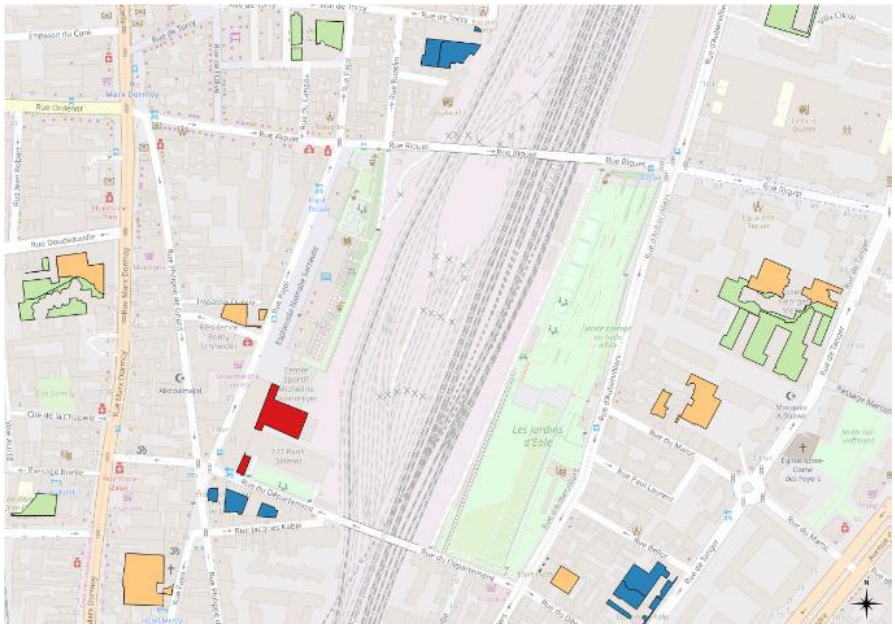


Figure 3. Method for calculating the surface ratio with high cooling potential. We apply the critical threshold to the mean solar irradiance map, while removing vegetalized areas.

Results and discussions

Initial calculations helped create the schoolyard dataset and build a cooling potential indicator based on the proportion of schoolyards' areas with high cooling potential (Figure 4). Out of the 670 establishments managed by the City of Paris, the suggested methodology identifies 38 facilities with high cooling potential, 157 with medium potential and 286 with moderate potential.



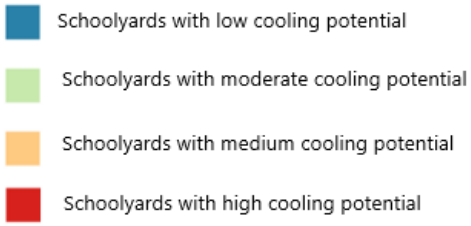


Figure 4. Mapping of the cooling potential of schoolyards around the Paris Diderot IUT in Paris. The cooling potential is proportional to the percentage of the yard's surface area receiving surface energy above the previously defined sunlight threshold. Respectively, the scale represents schoolyards having at least 1%, 24%, 47% or 71% of surface area with high cooling potential.

In our case, we applied this selection criterion to schoolyards, but we could easily transpose it to other facilities (terraces, gardens, public and private spaces, etc.). The indicator is indeed intrinsic to the geometric and physical characteristics of the apprehended area. It takes into account vegetation and sunshine.

The method can be refined insofar as the cooling potential indicator currently concerns an average over the entire schoolyard attached to an establishment, without taking into account the connectedness of the spaces. We can indeed take as an example a multiple courtyard, formed by two lots, one of which is very shaded, and the other very exposed (Figure 5).

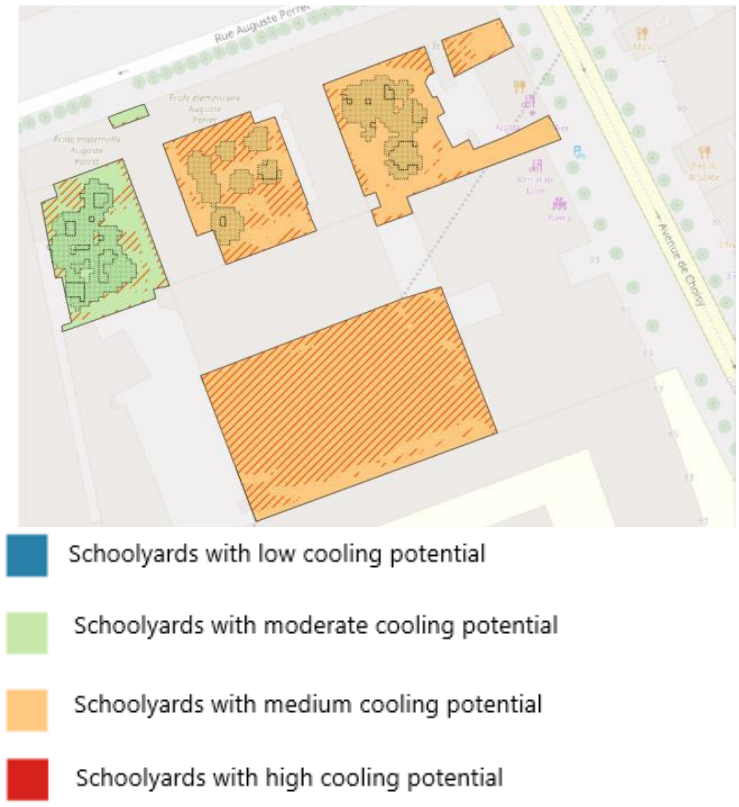


Figure 5. Example of a multiple-entity schoolyard in the Choisy neighborhood. Red lines represent high potential, while vegetation is represented as a green cloud.

Conclusion

This preliminary work aimed to identify schoolyards with a high cooling potential by setting up an indicator. This enables us to target schoolyards where improvement of thermal stress is expect to improve drastically following the renovation work: Out of 670 facilities, we identified 38 with a high cooling potential.

Other future analyses will focus on cross-referencing this information with a heat wave risk assessment, the latter being broken down into several factors. Among the heat wave risk factors, a spatial assessment of microclimatic hazard will determine areas with record temperatures during heat wave episodes. Similarly, we will define the exposure factor to estimate the number of people affected by the heat wave, for instance, children attending the facility or the population density around the facility. Finally, an assessment of the vulnerability of populations will be integrated, quantifying their ability or not to protect themselves during a heat wave.

Future analysis will consist in cross-referencing meteorological data (including air temperature simulations from the EPICEA[5] project), with the influence of nearby parks, vegetation and water points, and then to integrate socio-economic criteria (REP, INSEE socio-economic data, etc.). The schoolyards thus selected for the OASIS project will undergo microclimatic monitoring before and after the retrofitting. The targeted schoolyards will then be equipped with meteorological station that will monitor microclimatic parameters such as temperature, heat flux, relative humidity and wind speed. These stations will help us observe the evolution of the schoolyards condition prior to the transformation and after the renovation. Other data sets include meteorological information gathered by private individuals. These datasets are interesting, as they directly involve Paris inhabitants and promote citizen participation, in addition to helping us cover larger areas for our investigation, even if the data is less precise.

The construction of this indicator is part of the process of developing a GIS tool to support decision-making, and could be applied to other city facilities, or even transposed to other cities and territories. Provided that we have, for a given city, an equivalent to land registry, (such as aerial imaging of buildings and constructions) vegetation and solar irradiance data, we can apply our methodology to diverse surfaces, such as courtyards, sidewalks, roads, rooftops… and compute the high cooling potential surface areas, thus enabling us to apply our indicator.

Acknowledgement

This study is funded by the European ERDF project UIA03-344-OASIS. The authors would also like to thank the APUR for the solar irradiance datasets.

[5] Epicea: Multidisciplinary study of the impacts of climate change on the scale of the Paris urban area, Project jointly conducted by Météo-France, the Centre Scientifique et Technique du Bâtiment (CSTB) and the City of Paris

References

Robine J.-M. Et Al., (2008) Death Toll Exceeded 70,000 In Europe during The Summer Of 2003 C. R. Biologies 331

Lemonsu A., R Kounkou-Arnaud., J., Desplat J.L Salagnac, And V Masson., (Jul. 2013) Evolution Of The Parisian Urban Climate Under A Global Changing Climate, Clim. Change, Vol. 116, No. 3–4, Pp. 679–692,

Hendel M. Et Al, Developing a Gis Tool For Emergency Urban Cooling In Case Of Heat-Waves

Oke, T. R., (1982) the Energetic Basis of The Urban Heat Island. Q.J.R. Meteorol. Soc., 108: 1-24. Doi:10.1002/Qj.49710845502,

Hendel, M., Colombert , Y. Diab, And L. Royon (2015a, March). An Analysis of Pavement Heat Flux to Optimize the Water Efficiency of a Pavement-Watering Method. Applied Thermal Engineering 78, 658–669.

Saneinejad S., P. Moonen, J.Carmeliet (2014) Comparative Assessment of Various Heat Island Mitigation Measures. Building and Environment, Volume 73, Pages 162-170, Issn 0360-1323

O'malley C., P. Piroozfar, Eric R.P. Farr, F.Pomponi,(2015) Urban Heat Island (Uhi) Mitigating Strategies: A Case-Based Comparative Analysis, Sustainable Cities And Society, Volume 19, Pages 222-235, Issn 2210-6707

Bador, M., Terray, L., Boé, J., Somot, S., Alias, A., Gibelin, A. L., & Dubuisson, B. (2017). Future summer mega-heatwave and record-breaking temperatures in a warmer France climate. *Environmental Research Letters*, *12*(7). https://doi.org/10.1088/1748-9326/aa751c

Hendel, M., Bobée, C., Berthe, A., Parison, S., Bordin, P., & Royon, L. (2018). *Developing a GIS Tool for Emergency Urban Cooling in Case of Heat-Waves | Request PDF*. Retrieved from https://www.researchgate.net/publication/328020206_Developing_a_GIS_Tool_for_Emergency_Urban_Cooling_in_Case_of_Heat-Waves

Lemonsu, A., Kounkou-Arnaud, R., Desplat, J., Salagnac, J. L., & Masson, V. (2013). Evolution of the Parisian urban climate under a global changing climate. *Climatic Change*, *116*(3–4), 679–692. https://doi.org/10.1007/s10584-012-0521-6

Oke, T. R. (1982). The energetic basis of the urban heat island. *Quarterly Journal of the Royal Meteorological Society*, *108*(455), 1–24. https://doi.org/10.1002/qj.49710845502

Robine, J. M., Cheung, S. L. K., Le Roy, S., Van Oyen, H., Griffiths, C., Michel, J. P., & Herrmann, F. R. (2008). Death toll exceeded 70,000 in Europe during the summer of 2003. *Comptes Rendus - Biologies*. https://doi.org/10.1016/j.crvi.2007.12.001

Impact of Urban Heat Island formation on electricity consumption over Delhi region

Priyanka Kumari[1]*, School of Environmental Sciences, Jawaharlal Nehru University, New Delhi, India*

Vishal Garg, International Institute of Information Technology, Hyderabad, India

Krishan Kumar, School of Environmental Sciences, Jawaharlal Nehru University, New Delhi, India

ABSTRACT

Urban heat island (UHI) effect is a common phenomenon found in urban areas which is associated with the increased ambient temperature resulting from man-made alteration of the land. Urban structures with complex geometry, increased concretized surfaces and reduced natural land cover cause reduction in the rate of heat loss leading to increased temperature over urban areas and creating urban heat island (UHI). This study explores the temporal and spatial pattern of urban heat island (UHI) formation over Delhi. It is observed that the night-time surface temperature of central Delhi is higher in all months as compared to its surrounding rural areas. Thus, a nocturnal heat island forms over Delhi in all the seasons. The dense built-up area and impervious surfaces of Delhi are responsible for trapping heat which causes discomfort to humans, resulting in increased use of cooling devices with higher electricity consumption. Polynomial regression model based calculations show cooling load may be reduced up to 21-23% in summer months, 10 to 14 % in monsoon season, and 8 to 17 % in post-monsoon season if urban heat island effect is removed.

Introduction

Industrialization and economic growth lead to the process of urbanization. This involves the movement of people from the rural areas to the cities/towns in search of employment and is accompanied by significant modification in the land use and land cover of a local region. These modifications include the replacement of vast areas with soil and vegetation cover by impervious surfaces that inhibit the percolation of water into the soil. In the process, small rural structures and predominantly agriculture land in rural areas are replaced by densely packed high rise urban structures with complex geometry. These changes bring about reduction in soil moisture content over urban surfaces and a decrease in evapotranspiration (Priyadarsini 2012.). Further, the high rise buildings with complex geometry in the urban areas reduce the sky view factor, thereby reducing the efficiency of radiation loss in the long wave region (Oke 1981). This significantly decreases the rate of cooling of urban surfaces as compared to their rural counterparts. The extensive commercial, industrial, transportation activities over the urban region also lead to the emission of a large amount of waste heat and pollutants in urban atmosphere. All these changes alter the energy budget, leading to increased temperatures over urban areas as compared to the surrounding rural areas and create the so-called urban heat island (UHI).

[1] Priyanka Kumari: [jnu13priyanka@gmail.com]

Gallo et al. (1993) reported the UHI effect over thirty-seven cities of the United States. Their results revealed that the difference in NDVI (normalized difference vegetation index) between urban and rural regions was the most important factor responsible for urban heat island formation. Similarly, Gaffin et al. (2008) also confirmed the formation of urban heat island over New York. Buyantuyev and Wu (2010) also revealed that during the nighttime, urban core was generally found to be warmer than its surrounding rural areas over Phoenix metropolitan region of Arizona, USA. Their results showed the important role of vegetation (day time) and pavements (night time) in explaining spatio-temporal variations of surface temperatures.

Besides their important role in regional climate and air quality, urban heat islands are known to cause thermal discomfort to humans. Urban communities respond to this increased thermal discomfort by employing energy devices (HVAC, Heating Ventilation and Air Condition) to make their indoor climate more comfortable. Thus, urban heat island formation in a city is expected to have a significant bearing on its energy demands (Priyadarsini 2012). Kolokotroni et al. (2007) used a building simulation program to study the cooling and heating load of air conditioning in office buildings located in different locations within London. It was observed that the effect of the UHI formation over the city on the energy used for heating and cooling depends on the degree of urbanization at a particular location, radial distance from the city center. Delhi, the capital city of India has witnessed rapid urbanization over the last few decades (Rahman et al 2011). Earlier studies (Pandey et al. 2012, Pandey et al. 2014) have shown the formation of nocturnal UHI over Delhi during most part of the year. Notable efforts to examine the relationship of electricity consumption of Delhi with weather parameters were made by Ramesh et al (1988) and Gupta (2012). However, there has not been any comprehensive effort till date to examine the impact of UHI on the electricity consumption in Delhi. The present study attempts to evaluate this impact with respect to the central district of Delhi.

Data Description

Study Area

India is expected to overtake China as the world's most populous country by 2050 (UN, 2017). Most of this growth in population will be absorbed in cities, resulting in an increased urbanization rate. Delhi is situated on the banks of river Yamuna (a tributary of the river Ganga) at a latitude of 28.38° N and the longitude of 77.17°E. It is spread over 1,483 sq Km and its population is 1.68 Crores with a density of 11,320 persons per sq km (Census 2011). More than half a million population resides in the Central district of Delhi (Census 2011). It includes the five sub-districts of Paharganj, Shankar Road, Patel Nagar, Darya Ganj, and Chandani Chowk. These sub-districts are highly populated and totally built-up areas.

Paharganj and Chandani Chowk are highly concentrated with both residential and commercial buildings like hotels, lodges, restaurants, dhabas and a wide variety of shops that sell books, clothing, electronics, consumer goods, shoes, and leather goods. Thus people come here from all over India for trading. Daryaganj is also a residential cum commercial area which is known for its books shops. Shankar road and Patel Nagar are totally residential areas. Population data of central Delhi given in the census data is actually an underestimate of the real population density of this area as most of the people throng this area during the day for commercial reasons. These people are not the residents of this area and include shopkeepers, street vendors, drivers of

autorikshaws & e-rikshaws and visitors from other states as well. Thus, most of this area is highly congested in terms of vehicular and population density.

MODIS data

MODIS is a sensor mounted on the Terra and Aqua Satellites of NASA's EOS (Earth Observing System) Mission having 36 spectral channels in the range 0.405 and 14.385 μm, which provide information about the Earth Atmosphere, Ocean and Land Condition. Terra and Aqua are sun-synchronous, near-polar satellites having different equator crossing times i.e. 10.30am/pm and 1.30pm/am respectively, covering the whole earth's surface every 1-2 days (http://modis.gsfc.nasa.gov/data). MODIS has a swath resolution approximately 2330 km wide. In the present study, we have used the MODIS Aqua satellite product MYD11A2 Version 6, which provides an average 8-day per-pixel Land Surface Temperature with a 1 kilometer (km) spatial resolution in a 1200 x1200 km grid. The Land Surface Temperature (LST) data of MODIS are retrieved at 1 km pixels by the generalized split-window algorithm (Wan and Li 1997).

Maps of night-time Land Surface Temperature (LST) were created for the Delhi region for all seasons summer (April, May & June), winter (January & December), spring (February and March), post monsoon/autumn (September, October & November) and monsoon season (July and August) from Level 3 global data product (MYD11A2) acquired from MODIS Aqua satellite.

Estimation of Urban Heat Island Intensity (UHII)

The existence of an urban heat island is determined by calculating the urban heat island intensity, defined below:

$$\text{UHI Intensity} = \text{Temperature}_{\text{urban}} - \text{Temperature}_{\text{rural}}$$

For urban heat island intensity (UHII) estimation, the monthly average of nighttime land surface temperatures over the rectangular strips outside Delhi and over the central Delhi (Figure 1) was extracted for the period January 2017-December 2017 from the MODIS-AQUA monthly land surface temperature product (1 km resolution) MYD11A2. To estimate the UHII, the average temperature in the strip outside Delhi where mostly agriculture land use is predominant, was subtracted from the average temperature of the strip located over the central Delhi that is mainly comprised of dense built-up areas.

Electricity Consumption Data

Electricity is distributed in Delhi by three distribution companies, viz. BSES Rajdhani Power Limited, BSES Yamuna Power Limited, and Tata Power Delhi Distribution Limited. BSES Rajdhani distributes electricity in 19 sub-districts of South and South-West Delhi, BSES Yamuna distributes 14 sub-districts of the east and central Delhi, while NDPL distributes electricity in 13 sub-districts of North Delhi. For the present study, we used electricity consumption monthly data of 2017 for the Central Circle distributed by BSES Yamuna Power Limited which covers five areas viz. Pahar Ganj, Shankar Road, Patel Nagar, Darya Ganj, and

Chandani Chowk. The data comprised of the electricity consumption in all economic sectors (industrial, residential, and commercial) at the sub-district level of Delhi, because sectoral wise data was not available.

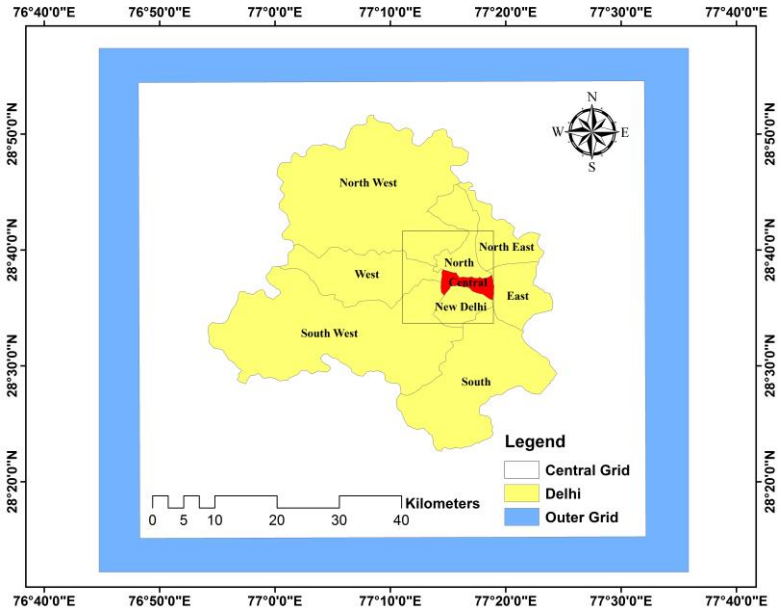


Figure1. Schematic diagram showing central part of Delhi (Central Grid) and outside (Outer Grid) for the estimation of urban heat island intensity (UHII).

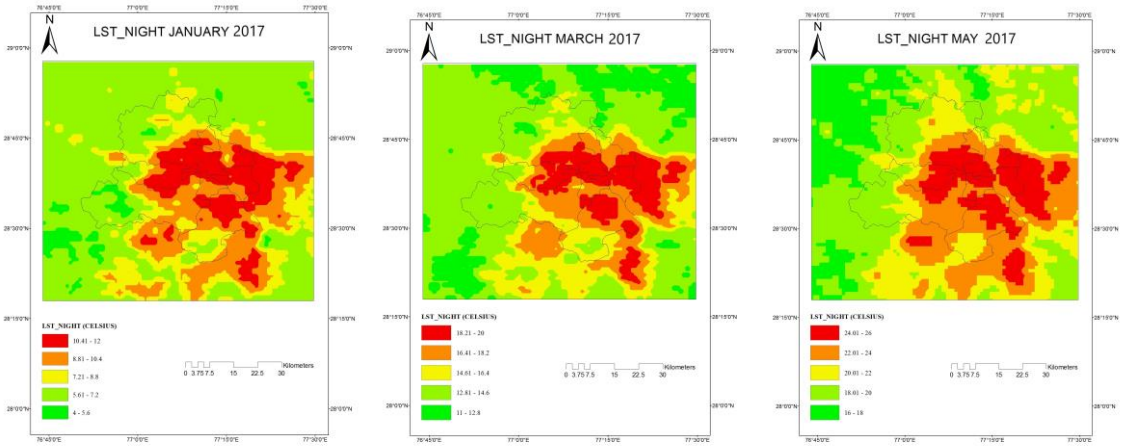
Results and Discussion

Night time land surface temperature variation

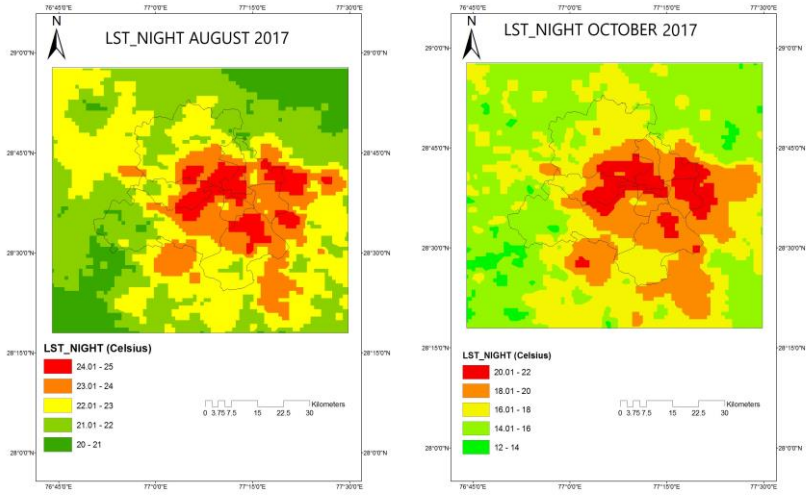
Spatial variation in night-time land surface temperature over central Delhi and its surrounding regions, for the different seasons, is shown in Figure 2 (a - e). It may be observed that in the month of January (figure 2 a), night-time surface temperatures over central Delhi were higher (10°C - 12 °C) as compared to those of the surrounding rural regions that ranged from 4°C to 7°C. The minimum night-time surface temperature (11°C -12°C) in the month of March (figure 2 b) was observed in the region lying North-East and South West of Delhi while in the central part of Delhi, the land surface temperature was observed to be in the range of 18°C to 20°C. This kind of temperature differential sustained till the month of May (figure 2 c). Maximum temperatures (24°C-26°C) occurred over central Delhi and minimum temperatures (16°C-20°C) were observed in some parts lying north-west and south-west of Delhi's surroundings.

In the month of August (figure 2 d), it was observed that the range of night-time temperatures over most parts of the study region reduced significantly. Maximum temperatures (~23°C - 25 °C) were observed over the central district of Delhi. In other parts of Delhi's surroundings, temperatures were found to lie in the range of 20 °C to 23°C. Night-time surface temperature variations during the month of October (figure 2 e) also depicted the clear existence of nocturnal heat island over central Delhi. Maximum temperatures over central Delhi ranged from 20 °C to 22 °C while minimum temperatures existed in Delhi's surroundings in the range of

12°C to 18 °C. So, it was observed that Delhi always has higher temperatures in the night as compared to the surrounding areas, which confirms the formation of a 'nocturnal heat island' in almost all the seasons. Badarinath et al. (2005) reported similar trends for the city of Hyderabad and found that heat island formations can be seen in the night time with core urban regions showing high temperatures. Pandey et al. (2012) also reported similar results and confirmed the formation of nocturnal heat island over Delhi which was found to be warmer by 4–7°C than the surrounding rural regions.



(a) (b) (c)



(d) (e)

Figure 2. MODIS night time land surface temperature over Delhi and it's surrounding for the month of (a) January (winter season); (b) March (spring season); (c) May (summer season); (d) August (monsoon season) and (e) October (Post monsoon season).

Variations of Urban heat island intensity

The monthly variations in night-time Urban Heat Island Intensity over Delhi and its surrounding regions, retrieved from MODIS AQUA satellite product MYD11A2 for different months for the year 2017 are shown in Figure 3. It is seen that temperatures over central Delhi were higher than the surrounding rural areas almost throughout the year during night-time. The plot reveals that the nocturnal UHII was the maximum (~ 4-5 °C) during the months of April and November. The nocturnal UHII was minimum (~ 1.5- 2°C) during the month of July.

The seasonal variations in the nocturnal UHI in this study were found to be similar to those for Mexico City by Cui and Foy (2012), who reported maximum values of night-time UHII for the dry season and minimum values for the wet season. Alonso et al. 2003 also revealed similar trends and found that during night-time the UHII values remained positive throughout the period. Their study reported nocturnal UHII to be highest during autumn and winter.

.

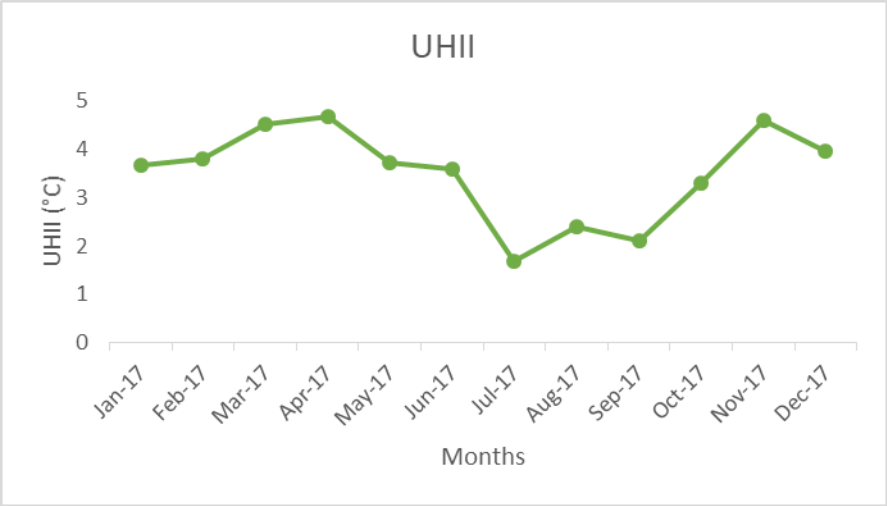


Figure 3. Monthly night time urban heat island Intensity for the year 2017.

Monthly electricity consumption pattern

Figure 4 shows the average monthly consumption of electricity in central Delhi for the year 2017. The graph shows a distinct pattern of electricity consumption rising up to 250 MU (1 MU = 1000 MWh) in summer season which is the result of increased use of cooling devices for thermal comfort. During monsoon season also consumption was observed to be high. This is because air temperature is not the only factor affecting thermal. There are other parameters like relative humidity, wind and precipitation which are equally important. Minimal electricity consumption can be seen in the months of January, February, November, and December, as in these months UHI plays a positive role and people don't require intensive usage of heating appliances. Similar monthly consumption pattern over Delhi has been reported by Gaur (2016).

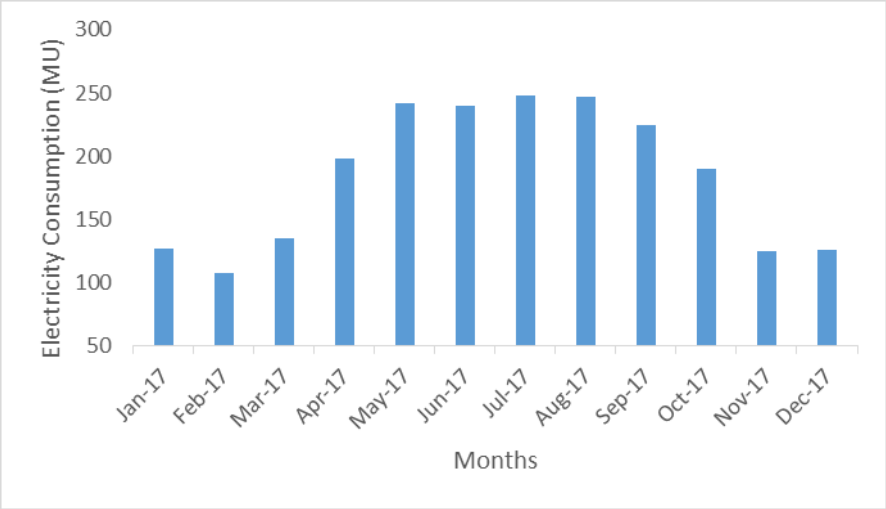


Figure 4. Monthly electricity consumption of central Delhi for the year 2017.

The relation between land surface temperature and electricity consumption

Many studies approached various methodologies to estimate the impact of UHI on energy consumption. The bottom-up and top-down approaches have been developed to estimate the energy consumption at multiple spatial scales from the building level to the city level and state level (Li et al. 2019). The bottom-up approaches include physical based and statistical models. In the present study, we have used a statistical model for the estimation of relationship between energy consumption and LST.

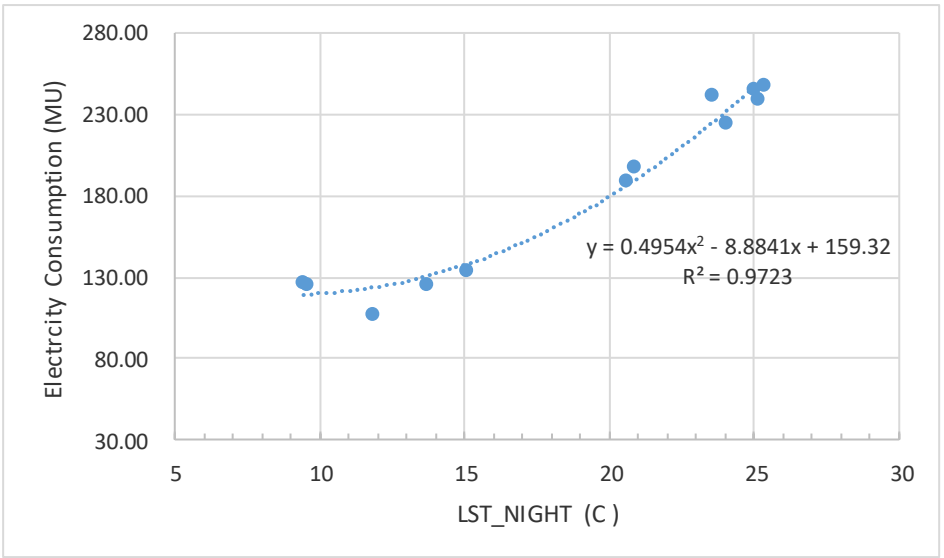


Figure 5. Scatter plot of monthly electricity consumption and night time land surface temperature.

Figure 5 shows the scatter plot between the electricity consumption and nighttime land surface temperature for central Delhi. It is seen that their relationship is well explained by the polynomial regression equation with $R^2 \sim 0.97$.

$$E = 0.495\ (T)^2 - 8.8841\ (T) + 159.32 \quad (1)$$

Where, T is the temperature in Celsius and E is electricity consumption in Million Units. We have calculated the monthly electricity consumption with and without UHI effect by putting monthly LST value of the rural area and urban area for each month in the above Eq (1). The Net Energy saving potential for each month was computed from the equation given below.

Net saving potential = Energy consumption $_{\text{with UHI effect}}$ – Energy consumption $_{\text{without UHI effect}}$

Table 1. Monthly electricity consumption under with and without UHI effect and monthly net saving potential.

Months	UHII (°C)	Electricity Consumption under UHI impact (MU)	Electricity Consumption without UHI impact (MU)	Net Saving Potential (%)
January	3.7	119.6	124.6	-4%
February	3.8	123.4	120.0	3%
March	4.5	138.0	120.7	12%
April	4.7	189.0	145.0	23%
May	3.7	224.3	177.5	21%
June	3.6	248.9	197.6	21%
July	1.7	252.4	226.3	10%
August	2.4	246.2	211.1	14%
September	2.1	231.9	202.5	13%
October	3.3	186.3	153.7	17%
November	4.6	130.5	119.5	8%
December	4.0	119.6	125.2	-5%

Table 1 explains electricity consumption under UHI impact, non-UHI impact, and net saving potential for each month. Monthly electricity consumption for the summer months was observed to be between 189.0 –248.8 MU with UHI effect while removing the UHI effect, the consumption was calculated to be around 145–197.5 MU. When we reduce UHI effect from urban area by 3-4 $^{\circ}$C, we found net saving potential on consumption or in other words consumption during these months was reduced by 21-23 %. Whereas during the monsoon months of July & August, the calculated consumption without UHI effect was observed to be 226 - 221 MU, however, higher consumption of 245 & 252 MU was observed under the UHI effect. Net saving potential on electricity consumption is observed to be 10 to 14 % in the monsoon season after removing the difference of 1^{-}2 $^{\circ}$C UHII from central Delhi.

During the post-monsoon season, 8 to 17 % net saving potential on consumption was seen over central Delhi without the UHI effect. Similarly, saving potential is positive during the spring season and it is observed to lie between 3-12 % when we remove the UHI effect from the

urban region. UHI plays a positive role in the urban areas in terms of impact over the electricity consumption during the winter season as it reduces heating load on houses. Thus, more consumption (124-125 MU) can be seen without UHI impact rather than consumption (~119 MU) under the UHI impact during the winter season. Thus, a negative net saving potential (-4 % to -5%) was seen in these months. Many studies have reported similar results of UHI impact on building consumption. Radhi and Sharples (2013) reported that domestic energy consumption increased up to 10% in urban sites as compared to the rural sites in Bahrain due to UHI effect. Santamouris et al. (2001) also evaluated urban heat intensity impact on building cooling energy load. They reported that due to an increase in 10% mean urban heat intensity, the cooling load almost doubled in central Athens.

Conclusion

This study shows that central parts of Delhi experience increased night-time temperature as compared to the surrounding rural areas. A 'nocturnal heat island' is observed over Delhi in almost all the seasons though its intensity is seen to be the minimum during the monsoon months. Higher temperatures in the Delhi's center affect the cooling load of urban buildings as well. Polynomial regression model based calculations show that higher electricity consumption was under UHI effect rather than without UHI effect except for the winter months. Saving potential or cooling load may be reduced by up to 21-23% in summer months, 10 to 14 % in monsoon season, and 8 to 17 % in the post-monsoon season if UHII intensity reduces by ~3-4°C in summer, 1-2 °C in monsoon, and 2-4°C in the post-monsoon season. However, in the winter season UHI plays a positive role and reduces load on heating appliances. It may be possible to reduce energy consumption by applying UHI mitigation measures and energy conservation policies. The results of this study will provide valuable information for developing appropriate strategies to for energy conservation in megacities like Delhi.

Acknowledgments

The authors are thankful to acknowledge the Moderate Resolution Imaging Spectroradiometer (MODIS) scientific and data support teams, developed and maintained by the NASA GES DISC for making the data available. Further, the authors would like to thank the Bureau of Energy Efficiency (BEE) for providing data. Priyanka Kumari acknowledges the University Grant Commission (UGC), MHRD, and Government of India for financial support to this work.

References

Alonso, M. S., J. L. Labajo, and M. R. Fidalgo. Characteristics of the urban heat island in the city of Salamanca, Spain. Atmósfera 16.3 (2003): 137-148.

Badarinath, K.V.S., Kiran, Chand.T.R., Madhavi, Latha.K., Raghavaswamy, V., 2005. Studies on urban heat islands using ENVISAT AATSR data. J. Indian Soc. Remote Sens. 33 (4), 495–501.

Buyantuyev, A., Wu, J., 2010. Urban heat islands and landscape heterogeneity: linking spatiotemporal variations in surface temperatures to land-cover and socioeconomic patterns. Landscape Ecol. 25, 17–33.

Cui, Y. Y., & De Foy, B. (2012). Seasonal variations of the urban heat island at the surface and the near-surface and reductions due to urban vegetation in Mexico City. Journal of Applied Meteorology and Climatology, 51(5), 855-868.

Gaffin, S.R., Rosenzweig, C., Khanbilvardi, R., Parshall, L., Mahani, S., Glickman, H., Goldberg, R., Blake, R., Slosberg, R.B., Hillel, D., 2008. Variations in New York City's urban heat island strength over time and space. Theoret. Appl. Climatol. 94, 1–11.

Gallo, K.P., McNab, A.L., Karl, T.R., Brown, J.F., Hood, J.J., Tarpley, J.D., 1993. The use of NOAA AVHRR data for assessment of the urban heat island effect. J. Appl. Meteorol. 32, 899–908.

Gupta, E. (2012). Global warming and electricity demand in the rapidly growing city of Delhi: a semi-parametric variable coefficient approach. Energy Economics, 34(5), 1407-1421.

INDIA, P. O. M. P. I. (2011). Census of India 2011 Provisional Population Totals.

K. Gaur, H. Kumar, R. P. K. Agarwal, K. V. S. Baba and S. K. Soonee, "Analysing the electricity demand pattern," 2016 National Power Systems Conference (NPSC), Bhubaneswar, 2016, pp. 1-6.

doi: 10.1109/NPSC.2016.7858969.

Kolokotroni, M., Zhang, Y., & Watkins, R. (2007). The London heat island and building cooling design. Solar Energy, 81(1), 102-110.

Li, X., Zhou, Y., Yu, S., Jia, G., Li, H., & Li, W. (2019). Urban heat island impacts on building energy consumption: A review of approaches and findings. Energy.

Mao Kebiao, Q. (2005). The research of split-window algorithm on the MODIS. Geomatics and Information Science of Wuhan University, 30(8), 703r707.

Oke, T.R., 1981. Canyon geometry and the nocturnal Urban Heat Island: comparison of scale model and field observations. J. Climatol. 1, 237–254.

Pandey, P., Kumar, D., Prakash, A., Masih, J., Singh, M., Kumar, S., & Kumar, K. (2012). A study of urban heat island and its association with particulate matter during winter months over Delhi. Science of the Total Environment, 414, 494-507.

Pandey, A. K., Singh, S., Berwal, S., Kumar, D., Pandey, P., Prakash, A. & Kumar, K. (2014). Spatio–temporal variations of urban heat island over Delhi. Urban Climate, 10, 119-133.

Priyadarsini, R. (2012). Urban heat island and its impact on building energy consumption. In Advances in building energy research (pp. 267-276). Routledge.

Rahman, A., Kumar, Y., Fazal, S., & Bhaskaran, S. (2011). Urbanization and Quality of Urban Environment Using Remote Sensing and GIS Techniques in East Delhi-India. J. Geographic Information System, 3(1), 62-84.

Ramesh, S., Natarajan, B., & Bhagat, G. (1988). Peak load prediction using weather variables. Energy, 13(8), 671-679.

Radhi, H., & Sharples, S. (2013). Quantifying the domestic electricity consumption for air-conditioning due to urban heat islands in hot arid regions. Applied energy, 112, 371-380.

Santamouris, M., Papanikolaou, N., Livada, I., Koronakis, I., Georgakis, C., Argiriou, A., & Assimakopoulos, D. N. (2001). On the impact of urban climate on the energy consumption of buildings. Solar energy, 70(3), 201-216.

United Nations, Department of Economic and Social Affairs, Population Division (2017). World Population Prospects: The 2017 Revision, World Population 2017 Wallchart. ST/ESA/SER.A/398.

Wan, Z., & Li, Z. L. (1997). A physics-based algorithm for retrieving land-surface emissivity and temperature from EOS/MODIS data. IEEE Transactions on Geoscience and Remote Sensing, 35(4), 980-996.

Outdoor thermal comfort improvements due to innovative solar awning solutions: An experimental campaign

Federico Rossi, University of Perugia, Perugia, Italy
Marta Cardinali, University of Perugia, Perugia, Italy
Alberto Maria Gambelli, University of Perugia, Perugia, Italy
Mirko Filipponi, University of Perugia, Perugia, Italy
Beatrice Castellani, University of Perugia, Perugia, Italy
Andrea Nicolini, University of Perugia, Perugia, Italy

ABSTRACT

Urban areas are increasingly affected by the Urban Heat Island (UHI) phenomenon, which is mainly due to highly dense urban environments and to solar and radiative properties of outdoor surfaces. UHI has a strong impact on urban microclimate, significantly contributing to the deterioration of outdoor human thermal comfort. Solutions based on high reflective materials in outdoor applications, e.g. solar awnings, could represent an important issue for mitigating UHI and improving pedestrians' thermal comfort. For this purpose, the present research aims to investigate the effect of different radiative properties of solar awning textiles on microclimate and outdoor thermal comfort below them. High reflective materials are usually used for awning textile, but they are often characterized by high emissivity properties downward that may affect the pedestrians' thermal comfort. The proposed solution consists in an awning textile with highly-reflective, highly-emissive properties upward and highly-reflective but low-emissive properties downward. Different solar awning configurations were tested by a microclimate experimental campaign on summer 2019. Outdoor thermal comfort under each awning was assessed by evaluating Physiological Equivalent Temperature (PET). Results show that a daily average PET reduction up to 2.5 °C is achieved thanks to the proposed solutions, proving benefits to pedestrians' thermal comfort.

Special Issue Journal	:	Energy and Buildings
DoI	:	https://doi.org/10.1016/j.enbuild.2020.110341
Citation	:	Rossi, F., Cardinali, M., Gambelli, A., Filipponi, M., Castellani, B., & Nicolini, A. (2020). Outdoor thermal comfort improvements due to innovative solar awning solutions: An experimental campaign. Energy And Buildings, 225, 110341.

Physical and geographic analysis of the urban cooling potential

Martin Hendel[1],
Univ Paris Diderot, Sorbonne Paris Cité, LIED, UMR 8236, CNRS (France)
Université Paris-Est, ESIEE Paris, département SEN, (France)
Sophie Parison,
Paris City Hall, Water and Sanitation & Roads and Traffic Divisions (France)
Univ Paris Diderot, Sorbonne Paris Cité, LIED, UMR 8236, CNRS (France)
Laurent Royon,
Univ Paris Diderot, Sorbonne Paris Cité, LIED, UMR 8236 (France)

ABSTRACT

The performance of a number of urban cooling techniques has been thoroughly studied by the scientific community. However, decision-makers lack the tools to spatialize their deployment as part of their urban cooling and climate change adaptation strategies. Among other indicators, a spatial assessment of the cooling potential for a technique in a given area is lacking. To this end, we analyze the physical mechanisms on which these techniques are based and identify corresponding geographical indicators that influence their cooling performance. Solar irradiance, existing material properties and underground infrastructure stand out as essential indicators for this purpose.

Nomenclature

Symbol	*Quantity*	*[SI unit]*
α	albedo	[-]
ϵ	emissivity	[-]
E	evaporation rate	[$kg.s^{-1}$]
H	sensible (convective) heat flux density	[$W.m^{-2}$]
l	latent heat of vaporization of water	[$kJ.kg^{-1}$]
L	LW radiation	[$W.m^{-2}$]
R_n	net radiation	[$W.m^{-2}$]
σ	Boltzmann constant	[$W.\ m^{-2}.K^{-4}$]
S	SW radiation	[$W.m^{-2}$]
T	surface temperature	[°C]

Abbreviation	*Description*
GIS	geographic information system
LW	longwave (3-100 μm)
PCM	phase-change materials
SW	shortwave (0,3-3 μm)
UHI	urban heat island
up	upwards

[1] Corresponding Author: martin.hendel@univ-paris-diderot.fr.

Introduction

The goal of countering the effects of heat waves and urban heat islands (UHI) has been adopted by many cities around the world. This awareness is accelerated by climate change forecasts, which predict an increase in these phenomena. Depending on the considered greenhouse gas emission scenario, some cities are even facing the risk of becoming uninhabitable all or part of the year (Kang & Eltahir, 2018; Mora et al., 2017; Pal & Eltahir, 2015). The interest of urban decision-makers in cooling techniques is therefore growing and has stimulated research.

Many efforts have been made to study the performance of various cooling techniques. This includes, for example, cool materials, which include reflective, emissive, permeable or PCM materials (Santamouris, 2015; Taha, 1997). Urban greening has also been widely studied with numerous studies focusing on the benefits of planting trees, developing green facades or roofs, planters, and greening tree bases or creating parks (Bowler, Buyung-Ali, Knight, & Pullin, 2010; Taha, 1997). Energy efficiency measures are also important, particularly those that seek to limit the impact of air conditioning (Oke, 1982; Taha, 1997; Tremeac et al., 2012). Finally, less common techniques such as urban watering have also been studied (Hendel, Gutierrez, Colombert, Diab, & Royon, 2016; Kinouchi & Kanda, 1997; Takahashi, Asakura, Koike, Himeno, & Fujita, 2010; Yamagata, Nasu, Yoshizawa, Miyamoto, & Minamiyama, 2008).

These techniques are nowadays generally categorized by their place of application, i.e. roof, façade or pavement. This work is useful in making solutions available to urban decision-makers, however they lack the tools to build an urban cooling strategy over their jurisdiction. Specifically, it is difficult to integrate these solutions into spatial analyses without the need for generally slow, cumbersome and delicate simulations, often outside the technical capabilities of these actors. On the other hand, geographic information system (GIS) tools are very common in urban studies, but there is little work to bridge the gap between known physics and this type of tool.

To this end, this contribution aims to identify readily-available geographical indicators that can be used in GIS tools to assess the cooling potential of a given area for hot weather conditions. First, the urban energy balance is analyzed to discriminate techniques according to the physical phenomena on which they rely rather than on their place of application. From this, the urban geographical parameters best able to transcribe them are identified. These geographical parameters can then be used to calculate an indicator of urban cooling potential for a given area for various techniques using standard GIS tools.

Methodology

The cooling potential indicator aims to identify areas with favorable conditions suited to obtaining the highest performance from cooling techniques. It is therefore necessary to identify these conditions and the urban parameters that make it possible to evaluate them. Several parameters may be necessary and they are dependent on the cooling technique considered. We begin by analyzing the energy balance of an urban facet and an urban volume to identify the physical phenomena on which cooling techniques are based and classifying them accordingly.

Urban facet energy balance

The urban energy balance can be analyzed at the scale of an urban facet, i.e. a roof, facade or pavement, as shown in Figure 1.

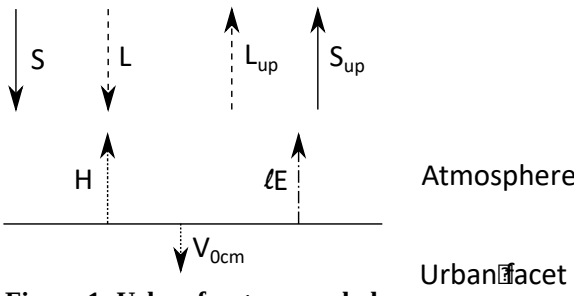


Figure 1: Urban facet energy balance

The term *H* represents the convective exchange between the ground and the atmosphere; *V* is surface conduction into the ground; *lE* is the latent heat flow due to the (possible) evaporation of water present at the surface. The latter is the product of the latent heat of water vaporization *l* and the evaporation rate *E*. Incident radiative fluxes are noted *S* and *L* for short and long wavelengths respectively (SW and LW) and S_{up} and L_{up} for SW and LW radiosity, respectively.

We note R_n the net radiation, i.e. the radiative balance of incident radiation and radiosity:

$$R_n = S + L - L_{up} - S_{up} \quad (1)$$

Furthermore, the energy conservation principle gives us:

$$R_n = H + lE + V \quad (2)$$

In other words:

$$S + L = \alpha S + (1 - \epsilon)L + \epsilon\sigma T^4 + H + lE + V \quad (3)$$

In this last equation, the term on the left is incident radiation, i.e. the inbound flows, while the terms on the right represent the outbound flows. The latter depend on the surface's radiative properties (albedo α and emissivity ϵ) and surface temperature for the radiative portion, while the other terms depend on convective and conductive exchange coefficients and temperature or vapor pressure gradients, which itself is dependent on surface temperature. Albedo and emissivity are fixed parameters, resulting from the choice of material or paint, therefore the remaining (non-reflective) radiative, convective and conductive heat flows change during the day to balance out incident radiation.

Urban volume energy balance

Figure 2 illustrates the energy balance of an urban volume whose upper limit is above the urban canopy layer and whose depth is such that the conductive heat flux is negligible over the time scale considered. Q_F refers to the release of anthropogenic atmospheric heat; ΔQ is the heat storage term within the urban materials present in the volume. We note Q_A the term for heat advection outside the volume. This exchange can be horizontal, for example due to wind or river transportation, but can also be vertical, e.g. in the case of geothermal energy.

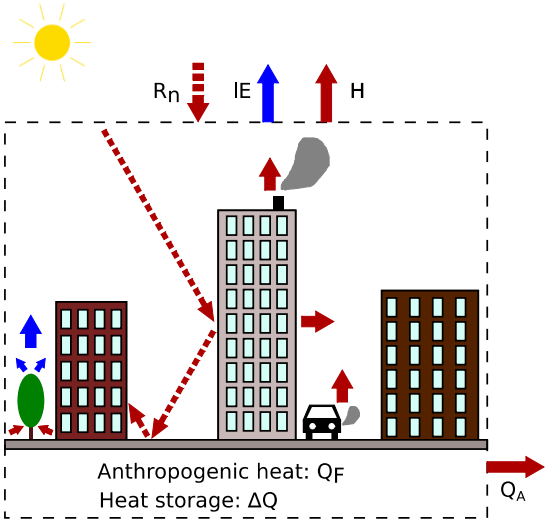


Figure 2: Urban volume energy balance

The energy conservation equation for the urban volume is:

$$R_n + Q_F = H + lE + \Delta Q + Q_A \quad (4)$$

By expliciting the contents of R_n, a similar form to equation (3) with incident flows on the left and outbound flows on the right can be obtained for an urban volume:

$$S + L + Q_F = \alpha S + (1 - \epsilon)L + \epsilon\sigma T_s^4 + H + lE + \Delta Q + Q_A \quad (5)$$

Incident radiation partitioning

The analysis of the partition of net radiation (i.e. absorbed radiation) between convective, latent and conductive flux (*H*, *E* and *V*) was initiated for an agricultural area by Camuffo and Bernardi (1982) and subsequently adapted to the study of urban materials (Anandakumar, 1999; Asaeda, Ca, & Wake, 1996; Qin & Hiller, 2014).

We adopt this approach and extend it to analyze the partitioning of the inbound flows, i.e. incident radiation (S+L) and anthropogenic releases (Q_F), for an urban volume. This allows us to make clear the physical role of urban radiative properties (albedo α and emissivity ϵ).

Table 1 and Table 2 illustrate the relative importance of the heat flow and radiative terms found in equation (5) for a mid-latitude city under clear skies in summer.

Table 1: Clear sky summertime heatflows for a mid-latitude city in W/m² (Oke, 1988, 1997)**.**

	R_n	Q_F	lE	H	ΔQ
Day	516	30	158	240	148
Night	-80	20	13	7	-80

Table 2: Clear sky summertime radiative balance for a mid-latitude city in W/m² (Oke, 1988, 1997)**.**

	S	L	S_{up}	L_{up}
Day	760	365	106	503
Night	0	335	0	415

Clearly, the most important incoming flux is net radiation R_n, more specifically solar irradiance S.

Urban cooling mechanisms

Regardless of the scale considered, it is the sensitive heat exchanges (H) that are responsible for the increase in air temperature observed in cites. UHI countermeasures therefore aim to reduce them by acting on the other terms of the energy balance (Christen & Vogt, 2004), either by reducing inbound energy flows or increasing outbound flows other than H.

On this basis, the following classification of cooling mechanisms can be proposed according to the terms of the energy balance that are modified:

- **Reduce inbound flows**
  1. Improve the urban radiative balance (reduction of R_n)
     a. via shading (reduction of S)
     b. via higher reflectivity (increase S_{up})
     c. via higher emissivity (increase L_{up})
     d. via lower LW radiation (decrease L)
  2. Decrease in atmospheric anthropogenic heat release
     a. energy efficiency (decrease Q_F)
     b. heat sink transfer (from Q_F to Q_A)
- **Increase outbound flows**
  3. Increase latent flows (lE)
  4. Increase heat storage (V and/or ΔQ)
     a. via heat harvesting
     b. via modified thermal properties (e.g. thermal conductivity and inertia)
     c. other methods

Mechanisms 1 and 2 seek to reduce the incoming flows R_n and Q_F. As described above, it does not matter which of the terms of the radiation balance is affected: (a) reduction of solar irradiance S, (b) increase of SW radiosity S_{ref} or (c) increase of LW radiosity (L_{up}) or (d) decrease of LW incident radiation (L). This last lever is not generally mentioned in the literature separately from shading. Indeed, shading devices do not necessarily contribute to reducing L, especially when the temperature of the shading device rises due to solar heating. However, there are devices that address both simultaneously (S Sakai et al., 2012; Satoshi Sakai, Sugawara, Misaka, Narita, & Honjo, 2018). Nevertheless, we leave this mechanism aside here.

Mechanism 2 aims to reduce the source term Q_F, either by improving energy efficiency or by transferring atmospheric emissions to other sinks, for example via geothermal air conditioning, which results in a decrease of Q_F in exchange for an increase in Q_A.

Mechanisms 3 and 4 aim to increase outflows, i.e. provide an alternative outbound heat flow to sensible heat. In essence, they seek to absorb source heat (solar or anthropogenic) to evaporate water (Mechanism 3) or for energy use or storage (Mechanism 4). Mechanism 3 focuses on increasing latent flows. Mechanism 4, on the other hand, includes changes in heat conduction or storage. These may include (a) the harvesting of solar energy, for example absorbed by heat exchangers integrated into a pavement or by thermal or photovoltaic solar collectors. Finally, it includes (b) techniques to increase the thermal inertia of materials, with or without the incorporation of phase change materials. While this does not modify the energy balance, it serves to smooth out the intensity of heat flows by lowering urban facet surface temperatures.

It should be noted that in reality most cooling techniques involve a combination of these mechanisms. This is the case, for example, for trees that provide shade during the day, but also limit LW radiosity at night by changing the sky view factor in addition to increasing latent flows by evapotranspiration.

Table 3 provides a classification of the most common cooling techniques by their principal mechanism.

Table 3: Classification of standard approaches to urban cooling by mechanism

Mechanism	*Techniques*
1	Reflective and/or emissive materials
2	Energy efficiency, aqua- or geothermal energy
3	Urban vegetation (additional parks or trees), green materials (facades or roofs), permeable materials
4	Solar panels, heat exchangers incorporated in coatings, urban materials incorporating MCP or other meta-materials

Results

From the previous classification of the physical mechanisms on which cooling techniques are based, we now identify the GIS information or data that may correspond to them.

Solar irradiance (mechanisms 1a, 1b, 3 and 4)

As shown in Table 2, this is the most important inbound flow and affects the most cooling mechanisms. Indeed, mechanisms 1a, 1b, 3 and 4 are concerned since they aim to reduce solar gains, i.e. avoid the absorption of solar energy in the form of sensible heat or change its form. This is true of shading devices (1a), cool materials (1b), or evaporative cooling via permeable materials or by greening (3) whose performance is highest under direct sunlight. The same applies to harvesting solar energy or its storage in phase change materials (4). In other words, only techniques which rely on mechanisms 1c or 2 are not directly affected by the intensity of solar irradiance. This makes the solar irradiance of a targeted area an essential parameter to evaluate the cooling potential of cooling techniques based on mechanisms 1a, 1b, 3 and 4.

Clear-sky surface irradiance in a neighborhood or city can be simulated via ray-tracing from a digital elevation model (DEM) of the study area, i.e. a 3D map, for any time of the year, specifically in summer. This type of simulation is already available in some popular GIS tools (e.g. SAGA). In the field, the more recent the DEM is and the higher its spatial resolution is, the more reliable the simulation will be. Figure 3 illustrates the surface irradiance of the Alesia district in

Paris on August 16th between 10am and 2pm (solar time) as simulated from a 2012 DEM with a spatial resolution of 0.5 m.

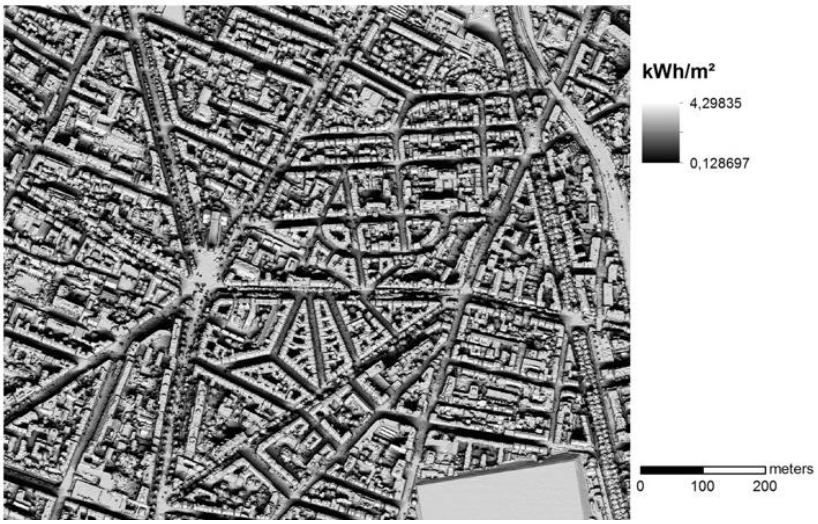


Figure 3: Cumulative solar irradiance between 10 am and 2 pm (local solar time) simulated on the 16th of August

By setting an appropriate threshold, for example 50% of global horizontal irradiance during the considered period, it is thus possible to immediately identify areas with high cooling potential from this type of information.

Existing material properties (mechanisms 1, 3 and 4)

The orders of magnitude cited in Table 1 and Table 2 are valid for the average thermal (thermal conductivity and capacity) and radiative (albedo and emissivity) properties of materials encountered in cities. Of course, they depend on the materials and morphology actually present at a finer scale. In other words, the gains to be expected from techniques under mechanisms 1, 3 and 4 depend on the materials already present that will be replaced or treated. Obviously, reducing solar gains from low albedo materials will be more effective than from high albedo materials. This also applies to permeable materials that will more advantageously replace impermeable materials.

This type of information is not widely available for many urban areas, Paris being no exception. Nevertheless, when available, this information is useful in assessing the cooling potential.

Underground infrastructure (mechanisms 1b, 1c, 3 and 4)

The presence of underground infrastructure can locally affect the heat balance in a positive or negative way by adding a source term that affects the term *V*. This mainly concerns shallow infrastructure (a few meters deep at most) such as district heating (negative local impact) or cooling (positive local impact) networks or shallow high-traffic metro stations for which the daily average of *V* is not equal to zero.

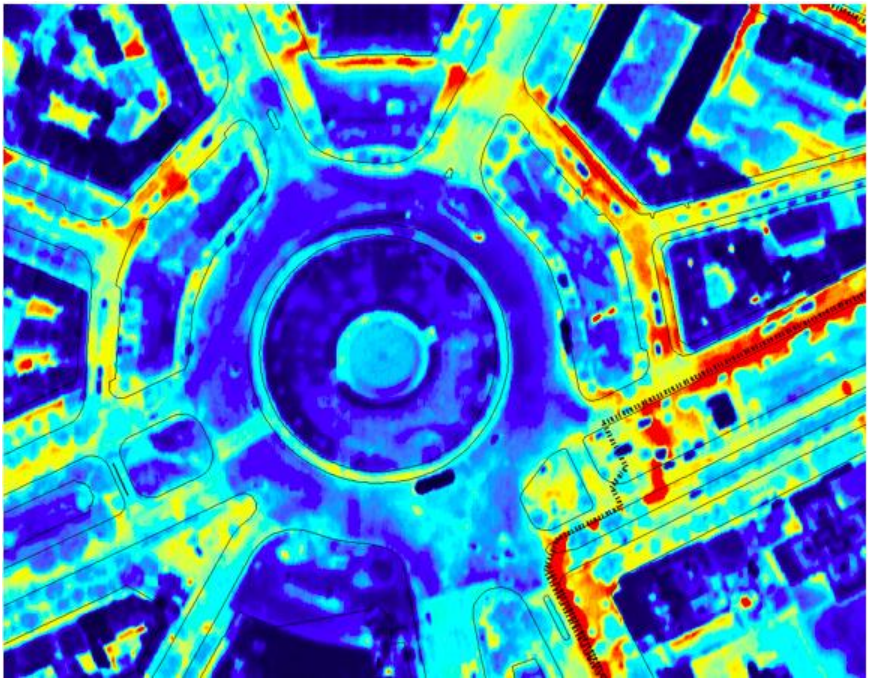


Figure 4: Airborne infrared photograph of Place d'Italie in Paris taken on the night of August 18th, 2015 under clear sky conditions.

The infrared thermography of Place d'Italie in Paris presented in Figure 4 provides some concrete examples of this. In the East, the impact of the heating network (dotted black line) has a visible impact on surface temperatures. On the northern half of the outer circumference of the Place, it is the thermal impact of metro Line 5 that is visible.

Urban decision-makers generally have maps of heating or cooling networks or metro stations, which facilitates their integration into this type of approach, even if their impact is very localized.

Other parameters

Several other parameters can be taken into account though their importance may be specific to certain cooling techniques.

- **Sky view factor (mechanisms 1b and 1c)**

Radiative cooling techniques (mechanisms 1b and 1c) reflect or re-emit the solar energy received back towards the sky, outside the urban volume. Their effectiveness therefore depends on the sky view factor of the treated surfaces, whether they are horizontal (roofs or pavements) or vertical (facades). As a result, it is clear that roofs are the surfaces most likely to benefit from these techniques, benefiting from both high solar irradiance (for 1b only) and high sky view factor.

As with solar irradiance, this parameter can be calculated on the basis of a DEM.

- **Relative humidity (mechanism 3)**

Techniques based on water evaporation (mechanism 3) will depend on the level of moisture saturation in the air and the ventilation rate of the target area. In other words, cities located in humid climates will benefit less from these techniques than those in dry ones. Similarly, poorly ventilated and confined urban areas are likely to saturate the vapor pressure deficit and will therefore also benefit less from evaporative cooling than more open and highly ventilated areas such as rooftops.

Accurate knowledge of this parameter requires a numerical simulation and is a priori out of reach for simple GIS tools.

- **Building typology (mechanism 2)**

Even though energy efficiency measures can be applied blindly, information on the building stock and its energy performance is useful to target the least efficient buildings first.

More and more cities already have such databases at the building level. However, more detailed knowledge may be required to better model anthropogenic heat release to the atmosphere at the pedestrian or street level (e.g. position and type of air conditioners).

Conclusion

The physical mechanisms on which cooling techniques rely were analyzed on the basis of the energy balance of an urban surface and volume. This made it possible to classify the techniques according to these mechanism(s).

On this basis, the most influential parameters for each technique were identified and their correspondence with geographical data established where available. Three parameters appear to be of primary importance and affect a large number of cooling techniques: solar irradiance, existing materials and underground infrastructure. Solar irradiance is the most important of these, especially because it is the strongest inbound flux during the day. Knowledge of existing materials and underground infrastructure is also very useful, although both provide information relevant more locally. Other parameters, relevant for a narrower spectrum of cooling techniques, have also been identified.

Among the data identified, it appears in particular that access to a DEM of the city studied is very important, since it is key to gaining access to solar irradiance and sky view factor in particular.

Acknowledgments

The authors acknowledge the Parisian Urban Planning Agency (APUR) and Paris City Hall for the solar irradiance data and infrared photograph. This research was funded by the Urban Materials for Cool Cities (UMat4CC) project (ANR-18-CE22-015-01).

References

Anandakumar, K. (1999). A study on the partition of net radiation into heat fluxes on a dry asphalt surface. *Atmospheric Environment*, *33*(24–25), 3911–3918. https://doi.org/10.1016/S1352-2310(99)00133-8

Asaeda, T., Ca, V. T., & Wake, A. (1996). Heat storage of pavement and its effect on the lower atmosphere. *Atmospheric Environment*, *30*(3), 413–427. https://doi.org/10.1016/1352-2310(94)00140-5

Bowler, D. E., Buyung-Ali, L., Knight, T. M., & Pullin, A. S. (2010). Urban greening to cool towns and cities: A systematic review of the empirical evidence. *Landscape and Urban Planning*, *97*(3), 147–155. https://doi.org/10.1016/j.landurbplan.2010.05.006

Camuffo, D., & Bernardi, A. (1982). An observational study of heat fluxes and their relationships with net radiation. *Boundary-Layer Meteorology*, *23*(3), 359–368. https://doi.org/10.1007/BF00121121

Christen, A., & Vogt, R. (2004). Energy and radiation balance of a central European City.

International Journal of Climatology, *24*(11), 1395–1421. https://doi.org/10.1002/joc.1074

Hendel, M., Gutierrez, P., Colombert, M., Diab, Y., & Royon, L. (2016). Measuring the effects of urban heat island mitigation techniques in the field: Application to the case of pavement-watering in Paris. *Urban Climate*, *16*, 43–58. https://doi.org/10.1016/j.uclim.2016.02.003

Kang, S., & Eltahir, E. A. B. (2018). North China Plain threatened by deadly heatwaves due to climate change and irrigation. *Nature Communications*, *9*(1), 1–9. https://doi.org/10.1038/s41467-018-05252-y

Kinouchi, T., & Kanda, M. (1997). An Observation on the Climatic Effect of Watering on Paved Roads. *Journal of Hydroscience and Hydraulic Engineering*, *15*(1), 55–64.

Mora, C., Dousset, B., Caldwell, I. R., Powell, F. E., Geronimo, R. C., Bielecki, C. R., … Trauernicht, C. (2017). Global risk of deadly heat. *Nature Climate Change*, *7*(7), 501–506. https://doi.org/10.1038/nclimate3322

Oke, T. R. (1982). The energetic basis of the urban heat island. *Quarterly Journal of the Royal Meteorological Society*, *108*(455), 1–24. https://doi.org/10.1002/qj.49710845502

Oke, T. R. (1988). The urban energy balance. *Progress in Physical Geography: Earth and Environment*, *12*(4), 471–508. https://doi.org/10.1177/030913338801200401

Oke, T. R. (1997). Urban environments. In W. G. Bailey, T. R. Oke, & W. R. Rouse (Eds.), *The Surface Climates of Canada* (pp. 303–327). Montreal: McGill-Queen's University Press.

Pal, J. S., & Eltahir, E. A. B. (2015). Future temperature in southwest Asia projected to exceed a threshold for human adaptability. *Nature Climate Change*, *6*, 197. Retrieved from https://doi.org/10.1038/nclimate2833

Qin, Y., & Hiller, J. E. (2014). Understanding pavement-surface energy balance and its implications on cool pavement development. *Energy and Buildings*, *85*, 389–399. https://doi.org/10.1016/j.enbuild.2014.09.076

Sakai, S, Nakamura, M., Furuya, K., Amemura, N., Onishi, M., Iizawa, I., … Yamaji, K. (2012). Sierpinski ' s forest : New technology of cool roof with fractal shapes. *Energy & Buildings*, *55*, 28–34. https://doi.org/10.1016/j.enbuild.2011.11.052

Sakai, Satoshi, Sugawara, H., Misaka, I., Narita, K., & Honjo, T. (2018). Mitigation of Urban Heat Island using Fractal Sunshade. In *ICUC10 & 14th Symposium on Urban Environment*. August 6-10, New York, NY.

Santamouris, M. (2015). Regulating the damaged thermostat of the cities - Status, impacts and mitigation challenges. *Energy and Buildings*, *91*, 43–56. https://doi.org/10.1016/j.enbuild.2015.01.027

Taha, H. (1997). Urban climates and heat islands: albedo, evapotranspiration, and anthropogenic heat. *Energy and Buildings*, *25*(2), 99–103. https://doi.org/10.1016/S0378-7788(96)00999-1

Takahashi, R., Asakura, A., Koike, K., Himeno, S., & Fujita, S. (2010). Using Snow Melting Pipes to Verify the Water Sprinkling's Effect over a Wide Area. In *NOVATECH 2010* (p. 10).

Tremeac, B., Bousquet, P., de Munck, C., Pigeon, G., Masson, V., Marchadier, C., … Meunier, F. (2012). Influence of air conditioning management on heat island in Paris air street temperatures. *Applied Energy*, *95*, 102–110. https://doi.org/10.1016/j.apenergy.2012.02.015

Yamagata, H., Nasu, M., Yoshizawa, M., Miyamoto, A., & Minamiyama, M. (2008). Heat island mitigation using water retentive pavement sprinkled with reclaimed wastewater. *Water Science and Technology: A Journal of the International Association on Water Pollution Research*, *57*(5), 763–771. https://doi.org/10.2166/wst.2008.187

Effect of surface treatment and built form on thermal profile of open spaces: A case of Mumbai, India

Surabhi Mehrotra[a,b], Divya Subramanian[b], Ronita Bardhan[b,c], Arnab Jana[b]
[a] Maulana Azad National Insitute of Technology, Bhopal, India
[b]Indian Institue of Technology, Mumbai, India
[c]University of Cambridge, United Kingdom

ABSTRACT

The thermal environment in Recreational Open Spaces (ROS) is primarily a result of the surrounding built form which includes buildings, trees, and surface treatment materials. To study the impact of land surface treatment choice and urban form on the thermal characteristics of open spaces, a case study assessment was undertaken in the dense urban context of Mumbai, India. To study ROS and its thermal profile, we selected three open spaces adjoining a school in Mumbai exhibiting different surface material treatments and built form. A comparative analysis was done using ENVI-met model. The model outcomes were validated using field measurements. The results highlighted the significant impact of the land surface choice and vegetation on the ambient air temperature and surface temperature of ROS. Open spaces with concrete paving and open mud surface showed the air temperature about 3 °C and 1.5 °C higher than the surfaces covered with tree litter. During the evening, concrete surfaces showed that maximum surface temperature (Ts) was comparatively higher (4 °C), as compared to others. The inferences from this study would assist in appropriate policy formation and design guidelines that could favourably impact the thermal profile of ROS and aid in mitigating the urban heat island effect.

Special Issue Journal	:	Urban Climate
DoI	:	https://doi.org/10.1016/j.uclim.2020.100736
Citation	:	Mehrotra, S., Subramanian, D., Bardhan, R., & Jana, A. (2021). Effect of surface treatment and built form on thermal profile of open spaces: A case of Mumbai, India. Urban Climate, 35, 100736.

Effect of UHI and Building Geometry on Pollution Dispersion in an Urban Street Canyon

Udayraj[1], Department of Mechanical Engineering, Indian Institute of Technology Bhilai, Raipur, Chhattisgarh, India

ABSTRACT

Air pollution caused by vehicle traffic inside a street canyon is one of the major source of pollution and air quality degradation. It represents a significant health risk to the inhabitants in urban areas. Migration from rural to urban areas and growing economic activities are leading to many high rise buildings in the urban areas to accommodate large population. Rapid urbanization and urban heat island (UHI) effect are also cause of concern apart from rising urban pollution level. In the present work, a numerical model is developed to analyze and understand effect of UHI and building geometry on pollutant dispersion behavior in a typical urban street canyon scenario. Detailed validation study is carried out to ensure reliability of the developed numerical model. Higher pollution dispersion in vertical direction was observed at higher temperatures, especially on the leeward side. It is observed that building geometry plays an important role on pollutant dispersion. Pollution level for gable roof buildings is found to be significantly lower compared to similar buildings with mono-pitched roof and flat roof.

Introduction

Street canyon, also known as an urban canyon, is a place where buildings are flanked on both sides of the street creating a canyon-like environment. Street canyon is an outcome of vertical habitation due to the prevalence of high-rise, high-density residential and commercial buildings in the congested metropolitan cities. Build environment causes hindrance to the airflow and deep valley like structures in urban street canyon result in recirculation of trapped air in the region (Li, Liu, and Leung 2008). High pollution levels have been often observed in urban street canyons because of reduced natural ventilation. Air pollution caused by vehicle traffic inside a street canyon is one of the major source of pollution and air quality degradation and discomfort of city inhabitants. It represents a significant health risk to the inhabitants in urban areas (Zhong 2016). Street canyon is an important platform to understand local atmospheric flow and other related processes in the built environment.

Microclimate of the urban street canyon which generally includes wind flow, temperature, noise and pollution affects both outdoor and indoor air quality in the nearby area and buildings. Flow in an urban street canyon depends on the local urban morphology such as the aspect ratio (AR), building structure and wind patterns (Jicha and Pospisil 2017). Most of the previous studies (Ai and Mak 2017; Chew, Glicksman, and Norford 2017; Yang et al. 2016) focused on the rectangular buildings. However, building geometry has a profound impact on the pollution dispersion inside a street canyon (Sabatino et al. 2008). Nazarian and Kleissl (2016) showed that solar insolation affects the ventilation process in a street canyon at different times of a day. Present

[1] Corresponding Author: udayraj@iitbhilai.ac.in, +91 771 2551300-6134

study is conducted to analyze and understand fluid flow and pollutant dispersion inside an urban street canyon by conducting a detailed numerical study. Effect of building geometry and urban heat island is analyzed on fluid flow and pollutant dispersion in a typical urban street canyon.

Problem Description

For better understanding of the pollutant dispersion inside an urban street canyon, Computational Fluid Dynamics (CFD) is used as a tool in the present study. The present numerical study is focused on an idealized urban street canyon, which consist of eight rows of buildings forming seven rows of street canyon as shown in Figure 1. It has been observed that pollutant dispersion is difficult when wind is blowing in a perpendicular direction to the buildings (Ai and Mak 2017). Hence, in this study a perpendicular wind flow direction is simulated. Three building geometries including buildings with flat roof (building type B1), mono-pitched roof (building type B2) and gable roof (building type B3) are considered in the present study. These building geometries with the key dimensions are depicted in Figure 2.

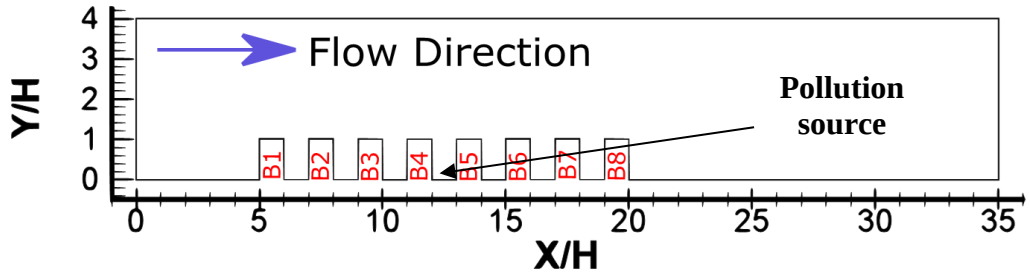


Figure 1. Typical computational domain with rectangular buildings.

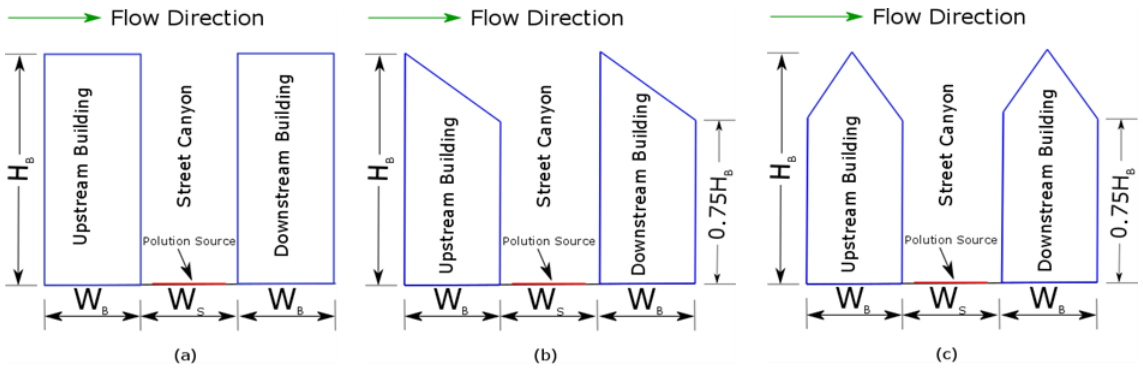


Figure 2. Schematic representation of investigated building geometries (a) flat roof (B1), (b) mono-pitched roof (B2), and (c) gable roof (B3).

In this study, width of street (W_S) and width of buildings (W_B) are kept equal whereas height of building (H_B) is twice of the width of building (W_B). Thus, aspect ratio (H_B/W_B) investigated in this study is two for all the three building geometries. Bulk Richardson number (R_b) is varied from 0.0 to 0.26 so that the effect of different time of a day on the pollution dispersion can be analyzed. The pollutants emitted from the local traffic are considered as passive scalars i.e. no chemical reactions are taken into account following the work of Gao et al. (2018).

Numerical Modeling

A two-dimensional numerical model is developed to analyze fluid flow, heat transfer and pollutant dispersion associated with the urban street canyon. Time-averaged continuity, momentum, species concentration and energy equations are solved considering steady, incompressible and turbulent flow. The governing equations are as follow:

$$\frac{\partial u_i}{\partial x_i} = 0 \tag{1}$$

$$\rho u_j \frac{\partial u_i}{\partial x_j} = -\frac{\partial P}{\partial x_j} + \frac{\partial}{\partial x_j}\left[\mu\left(\frac{\partial u_i}{\partial x_j} + \frac{\partial u_j}{\partial x_i}\right) - \rho\overline{u_i' u_j'}\right] + (\rho - \rho_0)g_i \tag{2}$$

$$u_j \frac{\partial C^\alpha}{\partial x_j} = \frac{\partial}{\partial x_j}\left[\left(D_m{}^\alpha + \frac{\nu_t}{Sc_t}\right)\frac{\partial C^\alpha}{\partial x_j}\right] \tag{3}$$

$$\rho u_j \frac{\partial T}{\partial x_j} = \frac{\partial}{\partial x_j}\left[\frac{\mu}{\mathrm{Pr}}\left(\frac{\partial T}{\partial x_j}\right) - \rho\overline{T' u_j'}\right] \tag{4}$$

where, u, P, C and T are mean velocity, pressure, concentration and temperature components, respectively. u' and T' are the fluctuating components of velocity and temperature, respectively. g is gravitational acceleration. $-\rho\overline{u_\iota' u_J'}$ and $c_p\overline{T' u_J'}$ are the Reynolds stress tensor and specific turbulent heat fluxes which are calculated based on the Boussinesq hypothesis and the simple eddy diffusivity model.

$$-\rho\overline{u_i' u_j'} = \mu_t\left(\frac{\partial u_i}{\partial x_j} + \frac{\partial u_j}{\partial x_i}\right) - \frac{2}{3}\rho k\delta_{ij} \tag{5}$$

$$\rho\overline{T' u_j'} = -\frac{\mu_t}{\mathrm{Pr}_t}\left(\frac{\partial T}{\partial x_j}\right) \tag{6}$$

where, k, μ_t and Pr_t are turbulent kinetic energy, turbulent viscosity and turbulent Prandtl number, respectively. Two-equation Realizable k-ε turbulence model with standard wall function is used in the present work to deal with turbulent flow. These turbulent models are not discussed in detail here considering brevity and more details related to the turbulence model can be found in Fluent theory manual (Ansys 2014).

Boundary Conditions and Solution Procedure

Air enters into the computational domain from the left hand side at a velocity (U_{ref}) 5 m/s, temperature 300 K and turbulent intensity 5 %. Pressure outlet boundary condition is assigned at the outlet with gauge pressure zero. Pollutant (carbon monoxide, CO) source is defined in the fourth street (line source in between fourth and fifth buildings) as shown in Figure 1 and Figure 2. Street vehicles are considered to be pollution source and pollution data is taken from Delhi Pollution Board. 750 vehicles per day are considered on the street and accordingly pollutant flow rate (Q_e) of 2.1812×10^{-04} m^3/s is assigned at the source. Pollutant temperature at the entry is taken as 345 K. All the building walls are considered to be maintained at a same constant temperature.

In order to consider effect of solar heating and urban heat island (UHI), building walls are considered to be at different temperatures. Three different building wall temperatures (300 K, 310 K and 320 K) are considered. All the remaining walls of the computational domain are considered to be adiabatic with no-slip boundary conditions.

The governing time-averaged continuity, momentum and energy equations along with species concentration equations (Eq. (1)-Eq. (4)) and turbulence equations are solved using the finite volume method (FVM) based commercial CFD solver FLUENT. All the governing equations are discretized using a second-order upwind interpolation scheme. Pressure-velocity coupling is ensured with the help of SIMPLE algorithm (Patankar 1990). The solutions are considered to be converged if the residual becomes lower than 10^{-08} for energy equation and 10^{-05} for all the remaining equations.

Model Validation

Detailed validation studies are performed first to check reliability of the developed numerical model in terms of prediction of flow field, temperature distribution and concentration dispersion. Figure 3 and Figure 4 shows the comparison of predicted horizontal and vertical velocities along building heights with experimental results of Li, Liu and Leung (2008) and numerical results of Ai and Mak (2017). The validation study is conducted on eight rows of rectangular shaped (flat roof, B1 type) buildings of unit aspect ratio. The mainstream Reynolds number defined based on the channel height ($4\times H_B$) and air properties was 12,000. Horizontal and vertical wind velocities inside a street canyon formed by 4th and 5th rows of buildings are shown in the figures. It can be observed from Figure 3 and Figure 4 that the developed model can predict the complex flow field in the urban street canyon satisfactorily.

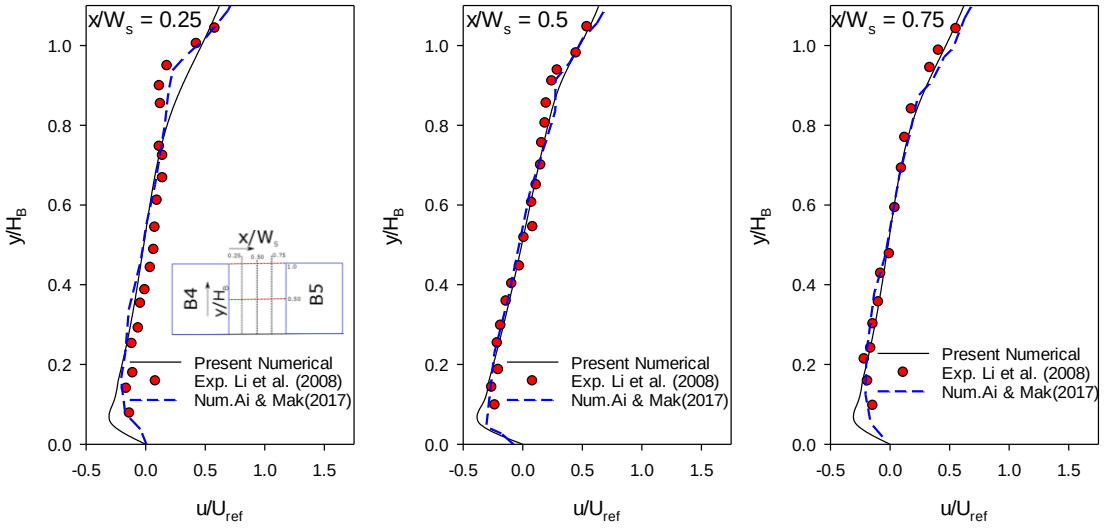


Figure 3. Comparison of horizontal velocity profile along the building height obtained from the present model with the experimental (Li, Liu and Leung 2008) and numerical (Ai and Mak 2017) results available in the literature for a flat roof building of aspect ratio, AR = 1 (a) at $x/W_s = 0.25$ (b) at mid-span of street i.e. $x/W_s = 0.5$ (c) at $x/W_s = 0.75$.

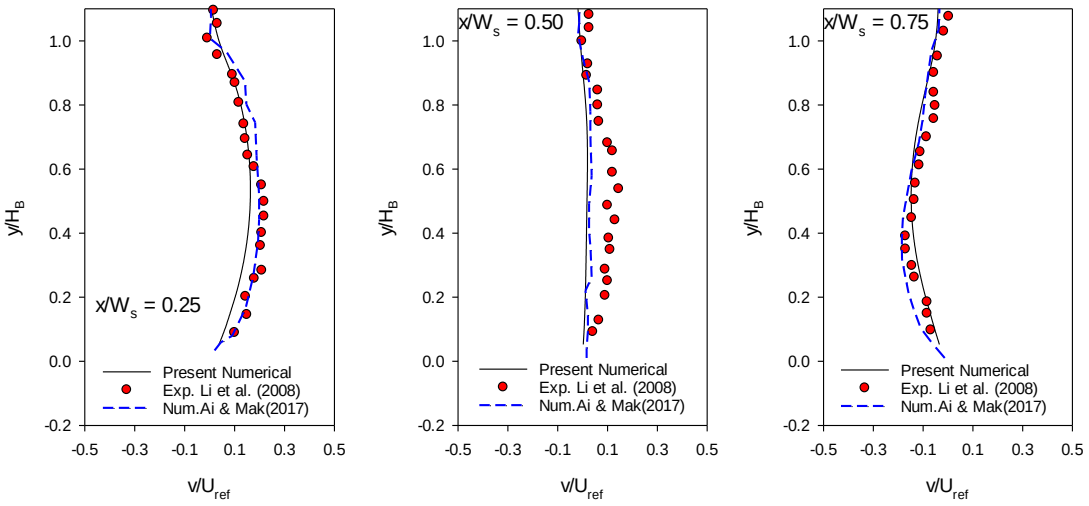


Figure 4. Comparison of vertical velocity profile along the building height obtained from the present model with the experimental (Li, Liu and Leung 2008) and numerical (Ai and Mak 2017) results available in the literature for a flat roof building of aspect ratio, AR = 1 (a) at x/W_s = 0.25 (b) at mid-span of street i.e. x/W_s = 0.5 (c) at x/W_s = 0.75.

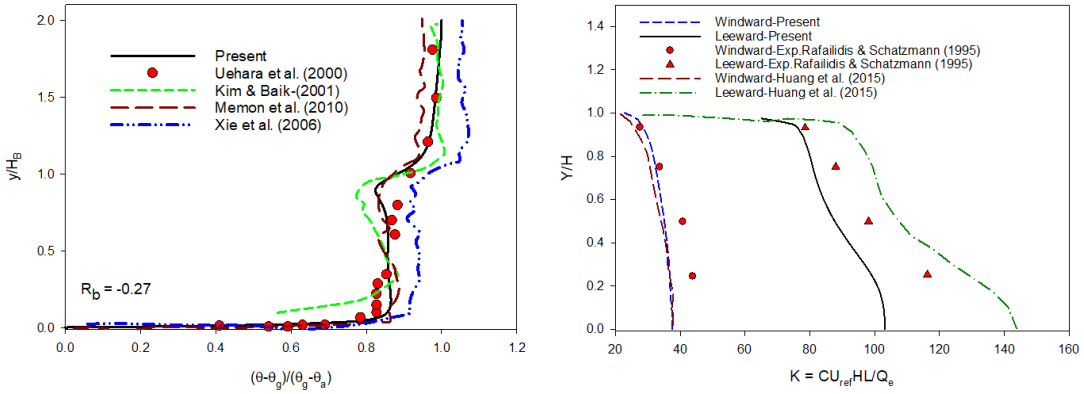


Figure 5. Comparison of the predicted (a) non-dimensional temperature variation along the building height at mid-span of street with the previous experimental (Uehara et al. 2000) and numerical (Kim and Baik 2001; Memon, Leung and Liu 2010; Xie et al., 2006) results, and (b) non-dimensional pollutant concentration along height at leeward and windward sides with previous experimental (Rafailidis and Schatzmann 1995) and numerical (Huang et al. 2015) results.

In order to validate the model performance in predicting the heating effect caused due to solar insolation and urban heat island (UHI), experimental study of Uehara et al. (2000) and other numerical studies (Kim and Baik 2001; Memon, Leung and Liu 2010; Xie et al. 2006) are referred. The simulations studies were performed based on the experimental conditions of Uehara et al. (2000). Comparison of the predicted non-dimensional temperature variation along the building height at mid-span of street with the previous experimental and numerical results are shown in Figure 5(a). Further, in order to validate the performance and reliability of the developed numerical model to predict pollutant dispersion, predicted non-dimensional pollutant concentration

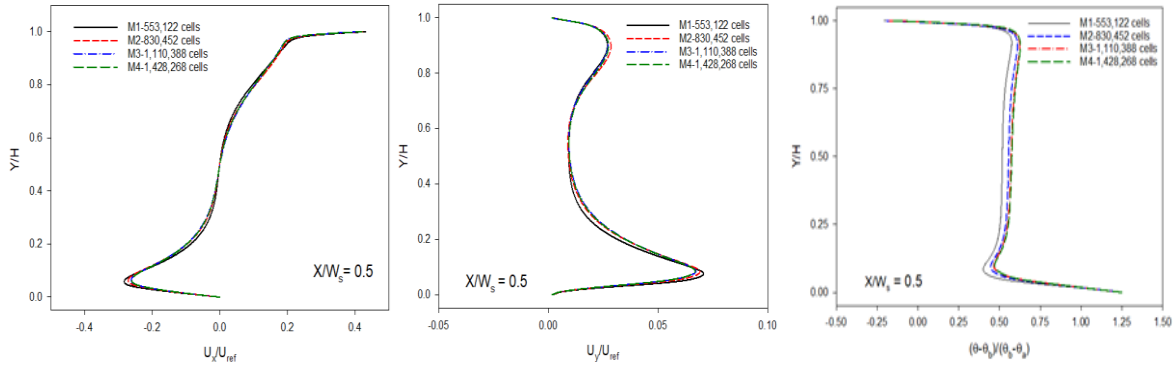
$K = \frac{CU_{ref} H_B L}{Q_e}$ along building height were compared with experimental measurement of Rafailidis and Schatzmann (1995) and numerical results of Huang et al. (2015) as shown in Figure 5(b). It can be observed from Figure 5(a) and Figure 5(b) that the current model can predict the temperature distribution appropriately. Based on the good agreement of the present numerical results with the available experimental results obtained in Figure 3-Figure 5, it can be inferred that the present computational methodology can be utilized satisfactorily for flow, heat transfer and pollutant dispersion predictions inside urban street canyons.

Results and Discussion

Effect of heating and building geometry on flow field, temperature distribution and pollutant dispersion in a typical urban street canyon are studied in the present work based on the validated two-dimensional numerical model.

Grid Independence Study

Detailed grid independence study is performed to ensure results are not affected by the grid size. Structured hexahedral meshing is performed in the computational domain with non-uniform grid size. Finer mesh is adopted near the building walls and floor to capture the gradient near the walls properly. Four mesh sizes with 553,122 cells, 830,452 cells, 1,110,388 cells and 1,428,268 cells are considered for the grid independence study. It can be observed from Figure 6 that horizontal velocity, vertical velocity and temperature does not vary much with mesh refinement beyond mesh size with 1,110,388 cells. So, mesh size with 1,110,388 cells is used throughout the study.



(a) (b) (c)

Figure 6. (a) Non-dimensional horizontal velocity, (b) non-dimensional vertical velocity and (c) non-dimensional temperature profiles for various cases with different grid size.

Effect of Urban Heat Island (UHI)

In order to simulate heating caused by solar radiation and urban heat island (UHI) effect, uniform surface (building walls and street floor) heating is considered with ΔT_{s-a} (difference between surface/wall temperature and ambient air temperature) values 0 K, 10 K and 20 K. It is well-known the UHI effect can lead to 5-7 °C higher temperature in the urban areas compared to

neighboring regions. Considering this, the range of ΔT_{s-a} (Minimum and maximum wall temperatures 27 °C and 47 °C, respectively) is selected in such a way that it covers the entire range of daily temperature in a typical summer day in the composite climate of India. ΔT_{s-a}=0 K denotes case of isothermal condition (no solar heating or no UHI effect) where building walls/ground are at the same temperature as that of the ambient air (i.e., 300 K). ΔT_{s-a}=20 K denotes upper limit of the heating of walls and ground caused during diurnal cycle. Figure 7-Figure 9 shows the variation of vertical velocity, pollutant concentration profiles along vertical direction, and pollutant concentration contour and velocity vectors in case of flat roof building (B1) for different temperatures, respectively.

It can be observed from the results that the upward motion of the air increases as building temperature increases due to buoyancy induced flow. This is leading to significant rise in pollutant dispersion in the vertically upward direction, especially toward the leeward side. The urban street canyon effect lead to recirculation in the streets and cause pollutants entrapment within the street which is a health hazard for people in the streets. The present results suggest that the pollutant dispersion is more in case of higher building temperatures. This suggests that UHI can make the street environment even more challenging as far as pollution and health is concerned.

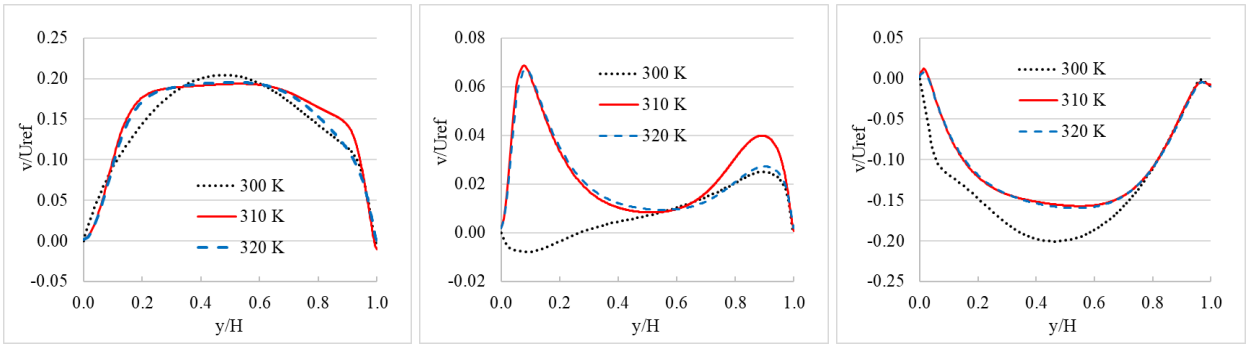


Figure 7. Variation of non-dimensional vertical velocity along building height at (a) x/H=0.25, (b) x/H=0.50, and (c) x/H=0.75 distance between building 4 and building 5 for different wall temperatures.

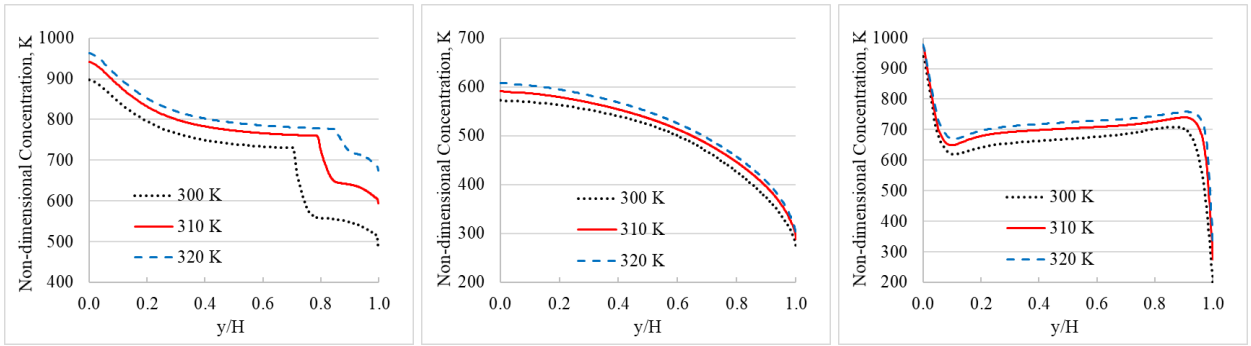


Figure 8. Non-dimensional pollutant concentration variation along building height on (a) leeward side, (b) windward side, and (c) at mid-section of the street for different wall temperatures.

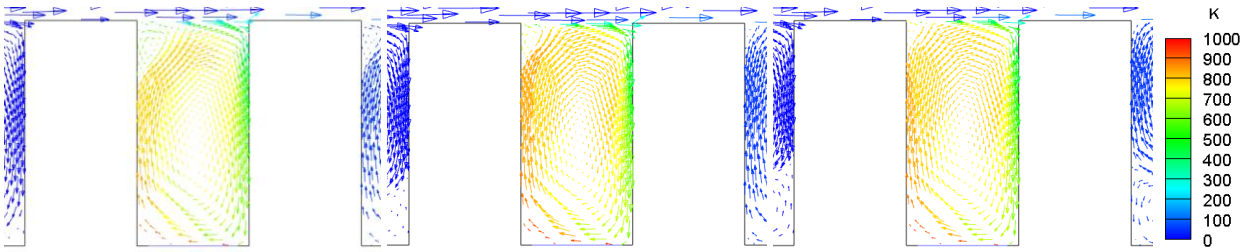


Figure 9. Velocity vectors along with non-dimensional pollutant concentration between building 4 and building 5 at building temperatures (a) 300 K, (b) 310 K and (c) 320 K.

Effect of Building Type

Effect of building design on fluid flow and pollutant dispersion is studied in this section. Three building types (B1, B2 and B3 as shown in Figure 2) with different roof designs are considered. Figure 10-Figure 12 shows the variation of temperature, pollutant concentration profiles along vertical direction, and pollutant contour with velocity vectors at 310 K building temperature for different building types, respectively. It can be observed that the building type and roof design affects the fluid flow, temperature and pollutant dispersion significantly within the street canyon. Pollutant level can be reduced significantly within streets by adopting gable or mono-pitched roofs in buildings in the urban streets compared to flat roofs.

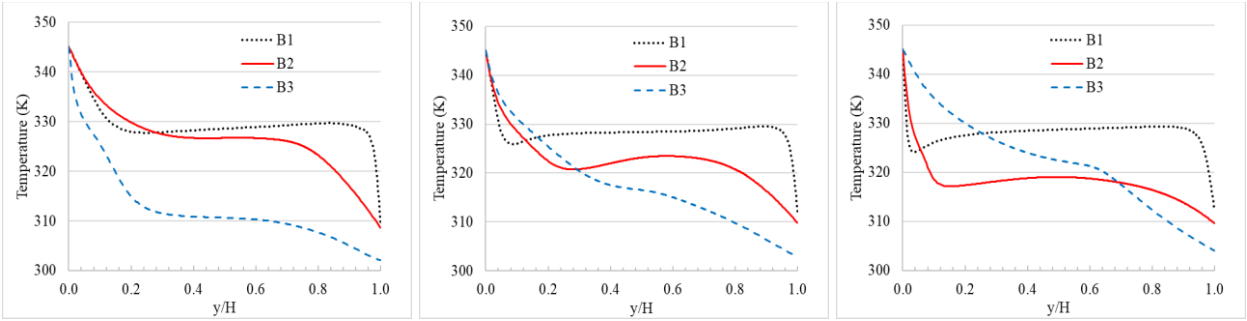


Figure 10. Variation of temperature along building height at (a) x/H=0.25, (b) x/H=0.50, and (c) x/H=0.75 distance between building 4 and building 5 for different types of building.

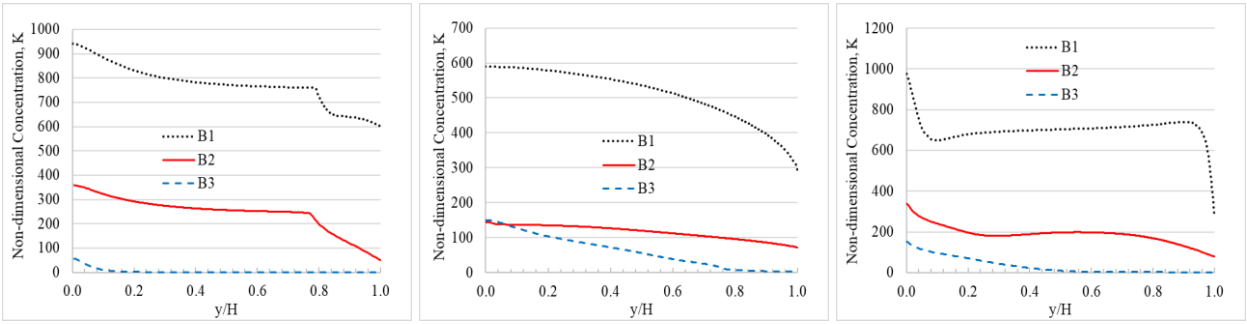
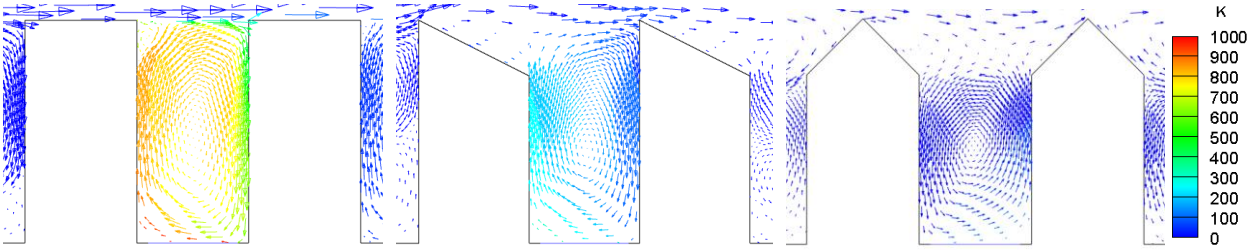


Figure 11. Non-dimensional pollutant concentration variation along building height on (a) leeward side, (b) windward side, and (c) at mid-section of the street for different types of building.



(a) (b) (c)

Figure 12. Velocity vectors along with non-dimensional pollutant concentration between building 4 and building 5 at 310 K temperature for building type (a) B1, (b) B2 and (c) B3.

Conclusions

A numerical model is developed in the present study to analyze fluid flow, heat transfer and pollutant dispersion in a typical urban street canyon. Reliability of the developed numerical model is ensured by conducting detailed validation study. It is found that the numerically predicted velocity, temperature and pollutant dispersion profiles agree well with the previous experimental results. Effect of urban heat island in terms of building wall temperature is studied and pollutant concentration is found higher in case of higher building temperature. The effect of temperature is found to be higher on leeward side compared to other places within the street canyon. This indicates that the consequences of vehicular pollution in urban street canyon can be even more severe due to UHI effects. Results of the study also indicate that the building roof design plays a critical role in pollutant dispersion within street canyons. Pollution level is found to be lowest in case of the gable roof design followed by mono-pitched and flat roof designs. The pollution level and thus health hazard can be reduced significantly by adopting appropriate building or roof designs.

Acknowledgments

Author would like to thank Dr. Kuldeep Singh, Senior CFD Research Fellow, Faculty of Engineering, The University of Nottingham (UK) for his generous technical helps during problem formulation, numerical modeling and detailed technical discussions.

Nomenclature

Symbol	*Quantity*	*[SI unit]*
A	Surface area	[m^2]
C	Mole fraction of pollutant	[-]
L	Length of the pollution source	[m]
Q_e	Source strength of pollutant	[m^3/s]
U_{ref}	Reference (wind) velocity	[m/s]
ρ	Density	[kg/m^3]

References

Ai, Z.T., & Mak, C.M. (2017). CFD simulation of flow in a long street canyon under a perpendicular wind direction: Evaluation of three computational settings. Building and Environment 114, 293–306.

Ansys Fluent 14.5 (2014). User's and theory guide. Canonsburg, Pennsylvania, USA: ANSYS, Inc.

Chew, L.W., Glicksman, L.R., & Norford, L.K. (2018). Buoyant flows in street canyons: Comparison of RANS and LES at reduced and full scales. Building and Environment 146, 77-87.

Gao, Z., Bresson, R., Qu, Y., Milliez, M., Munck, C., & Carissimo, B. (2018). High resolution unsteady RANS simulation of wind, thermal effects and pollution dispersion for studying urban renewal scenarios in a neighborhood of Toulouse. Urban Climate 23, 114-130.

Huang, Y.D., Xu, X., Liu, Z.Y., & Kim, C.N. (2015). Effects of strength and position of pollutant source on pollutant dispersion within an urban street canyon. Environmental Forensics 16(2), 163-172.

Jicha, M. & Pospisil, J. (2017). Influence of vehicle-induced turbulence on pollutant dispersion in street canyon and adjacent urban area. International Journal of Environment and Pollution 62(2-4), 89-101.

Kim, J., & Baik, J. (2001). Urban street-canyon flows with bottom heating. Atmospheric Environment 35(20), 3395-3404.

Li, X. X., Liu, C.H., & Leung D.Y.C. (2008). Large-eddy simulation of flow and pollutant dispersion in high-aspect-ratio urban street canyons with wall model. Boundary-Layer Meteorology, 129, 249-268.

Memon, R.A., Leung, D.Y.C., & Liu, C.H. (2010). Effects of building aspect ratio and wind speed on air temperatures in urban-like street canyons. Building Environment 45, 176-188.

Nazarian, N., & Kleissl, J. (2016). Realistic solar heating in urban areas: Air exchange and street-canyon ventilation. Building and Environment 95, 75-93.

Patankar, S.V. (1990). Numerical Heat Transfer and Fluid Flow. Hemisphere. Washington, DC (USA).

Rafailidis, S., & Schatzmann, M. (1995). Concentration measurements with different roof patterns in street canyons with aspect ratios B/H=1/2 and B/H=1. Report, Meteorology Institute, University of Hamburg, Hamburg, Germany.

Sabatino, S.D., Buccolieri, R., Pulvirenti, B., & Britter, R.E. (2008). Flow and pollutant dispersion in street canyons using FLUENT and ADMS-Urban. Environmental Modeling & Assessment 13(3), 369-381.

Uehara, K., Murakami, S., Oikawa, S., Wakamatsu, S. (2000). Wind tunnel experiments on how thermal stratification affects flow in and above urban street canyons. Atmospheric Environment 34(10), 1553-1562.

Xie, X., Liu, C., Leung, D.Y.C., & Leung, M.K.H. (2006). Characteristics of air exchange in a street canyon with ground heating. Atmospheric Environment 40, 6396-6409.

Yang, F., Gao, Y., Zhong, K., & Kang, Y. (2016). Impacts of cross-ventilation on the air quality in street canyons with different building arrangements. Building and Environment 104, 1-12.

Zhong, J. (2016). Modelling air pollution within a street canyon. PhD Thesis, University of Birmingham.

Controlled experiment for estimating the energy-saving potential and indoor thermal comfort improvement by the use of high albedo surfaces on pitched concrete roofs

Vishal Garg[1], Sraavani Gundepudi[1], Aviruch Bhatia[1], Rathish Arumugum[2], Sasank Bethapudi[2]
[1] International Institute of Information Technology, Hyderabad (India)
[2] Saint-Gobain Research India (India)

ABSTRACT

Reflecting the solar radiation incident on the roof surface helps in reducing the surface temperatures. Cool roof help in reducing the cooling energy requirement of a building. There have been many studies conducted to estimate the potential of energy savings and comfort improvement using cool roof on a flat surface. However, results from these studies are not directly applicable for a sloped surface. This paper presents an experiment that was performed to identify the energy-saving potential and thermal comfort improvement for pitched/sloped cool roofs in India. Four test rooms in two locations Chennai (Warm and Humid) and Bhiwadi (Composite) were installed with Shingle-1 (initial albedo of 0.15) and Shingle-2 (initial albedo of 0.30). The difference in roof albedo between both the shingles is 0.15. The Chennai site was used for comfort monitoring and the Bhiwadi site was used for energy studies.
To assess the indoor comfort, a frequency graph has been plotted with the occurrence of indoor air temperatures. The histogram plot of temperatures recorded for Chennai displays a shift in the peak temperatures towards the comfort range in case of high albedo roof compared to roof with low albedo. There was 26% increase in overall thermal comfort by using cool roof.
The experimental results for Bhiwadi show that minimum and maximum electrical energy savings from the air conditioners are 27.1 Wh/m^2-day and 60.8 Wh/m^2-day respectively.

Introduction

The roof of a building receives the maximum direct solar radiation compared to the other envelope components (Takebayashi and Moriyama 2007). A roof that reflects and emits the solar radiation back to the sky rather than transferring it into the building is termed as a cool roof (Cool Roof Rating Council n.d.). The cool roof helps in reducing air conditioning energy consumption in a conditioned building and improves thermal comfort in an un-conditioned building. The percentage energy savings achieved in a building from cool roofs is dependent on various parameters like the location, orientation of the building, local shading by trees or other buildings, construction type, insulation type, plenum ventilation, equipment load, occupancy and operational schedules (Konopacki and Akbari 2001). With the increase in the electricity consumption in the building sector and as the urban landscape is becoming more and more compared to the rural areas surrounding it, high albedo surfaces are employed as a geoengineering technique to delay the global carbon emissions, reduce the temperature of cities and to achieve energy savings in the buildings.
By installing high albedo roof, one can expect energy savings in the HVAC systems in conditioned buildings and increased thermal comfort in un-conditioned buildings. Early experiments to verify these results have been performed in the United States, and slowly and steadily, many countries have rigorously tested and adopted them. It is notable that the maximum

benefits of high albedo roofs can be seen in the hot and humid climatic zones. Florida Solar Energy Centre has conducted an early investigation to identify the savings that can be achieved from high albedo roofs (Parker et al. 1996). One such experiment was conducted in a commercial building in Coca Beach, Florida, for a period of two years. An annual savings of 13,000 kWh was observed from the chiller. An experiment was performed to understand the energy-saving benefits from high albedo roofs in developing countries (Akbari et al. 2011). The metropolitan area of Hyderabad was chosen for this study in which a commercial building was monitored for a period of one year. The measured annual energy savings from white roofs over black roofs ranged from 20 -22 kWh/m^2 of roof area and the corresponding energy use reduction of 26 % was observed. This study also concluded that over a concrete roof in commercial buildings of Hyderabad a savings of 13-14 kWh/m^2 of roof area which transcribes to 10% -19% of annual energy can be achieved. A study performed in rural and peri-urban areas of India shows improvement in thermal comfort with the application of cool roof (Garg et al. 2014). Study performed in Greece shows 17% reduction in annual cooling demand with the application of cool roof (Kolokotsa et al. 2018). A study (Rosado et al. 2014) performed in central California shows annual energy cost savings were \$0.886/m^2 (20%) with the use of high albedo roof. Another study was conducted to find the impact of high albedo roofs, and green roofs in a Mediterranean climate (Zinzi and Agnoli 2012) found that there is an improvement of indoor thermal comfort in summer using cool roofs.

In India, there is an increase in trend of having steep-sloped roofs, particularly in places with high precipitation and coastal regions. Using cool roofing solution can help in bringing down the air conditioning energy consumption and increase thermal comfort conditions. In this paper, an experimental study performed in two locations of India is demonstrated.

Methodology

The methodology for identifying the energy-saving potential and comfort improvements involve experiment design and measurements at the site.

Monitoring parameters

Cool roof reflects the incident solar radiation at the roof surface, thereby reducing the over deck surface temperature and heat ingress into the house. To quantify the energy-saving potential and comfort improvements due to cool roofs, it is necessary to understand the heat ingress through the roof surface. In case of a conditioned home, cool roof helps in reducing the air conditioning energy. A cool roof also reduces the mean radiant temperature inside a house, which helps in increasing the thermal comfort conditions. In the experiment outdoor roof surface temperatures, ceiling temperatures, indoor air temperatures were measured. Apart from these indoor parameters, the outdoor weather conditions such as the Global Horizontal radiation, dry bulb temperature, outdoor relative humidity, wind velocity and direction, and precipitation were measured. These parameters were logged continuously using a data logger. The sampling rate of the sensors was one data point per second, and the data has been averaged and logged for every five minutes.

Experimental design

The study was performed on two near-identical test rooms in two cities of India - Chennai, and Bhiwadi. The experiment was performed for a roof with a slope of 30 degrees to the horizontal. The roof of one of the test rooms was coated with a dark conventional roof and another one coated with a cool roof. The test rooms in Bhiwadi were set up to run in a conditioned mode to measure the energy savings potential through high albedo shingles. The test rooms in Chennai were set up to run in an unconditioned mode to test the improvement in thermal comfort. The test rooms have been built of a brick wall and concrete roof. A schematic of the test rooms is shown in Figure 1. The test rooms were designed for two person occupancy with a carpet area of 24 m^2. During the day time on weekdays, only one person is considered to occupy the test hut. During weekends the house is considered to be fully occupied. The heat generation from the internal loads is considered to be 120 W.

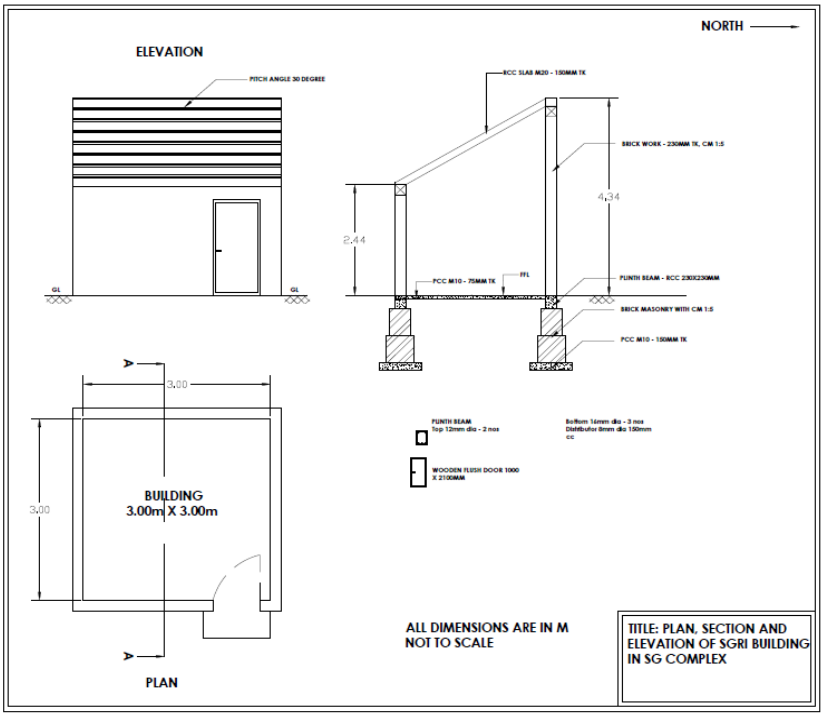


Figure 1 Schematic of test rooms

Monitoring Phases

The test apparatus was monitored in two phases.

a) The first phase was when both the buildings were near identical.

b) In the second phase, the roof of one of the test apparatus (Room A) was changed to a high albedo surface and Room B was changed to a low albedo roof.

First phase

During this phase all the monitoring parameters were matched between the two test apparatus. This phase was to ensure that both test apparatus behave in the same way before the start of the experiment.

Chennai (Warm and Humid)

Measurements were performed in the calibration phase when roofs of both the rooms were identical. Data for outdoor roof surface temperatures, ceiling temperatures, indoor air temperatures were measured and analysed. It was observed that in unconditioned mode, the test rooms were performing identically. The Outside Roof Surface Temperature (ORST) was plotted as shown in Figure 2. Data were nearly identical for both roofs indicating the roof albedo were similar in both.

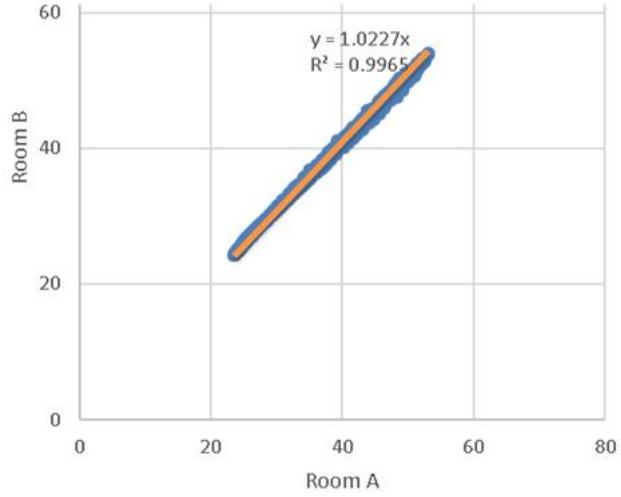


Figure 2 Scattered Plot ORST (°C) for Room A and Room B

Bhiwadi (Composite)

Measurements were performed in the calibration phase when roofs of both the test rooms were identical for the Bhiwadi location. Sensor locations are shown in Figure 3. It was observed that in conditioned mode, the test rooms were performing identically as seen in Figure 4.

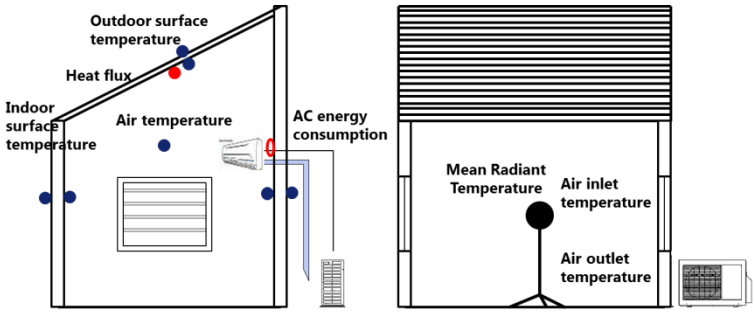


Figure 3: Instrumentation for the test rooms

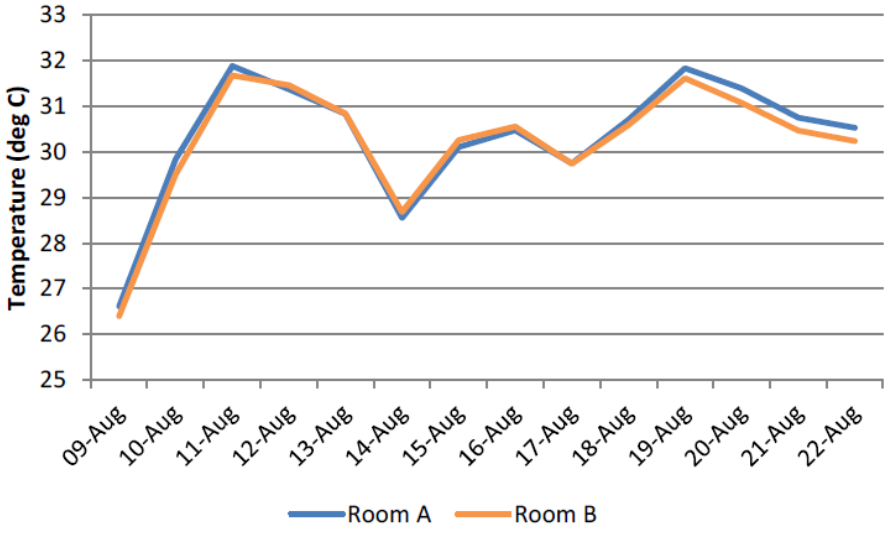


Figure 4 Daily ORST (deg C)

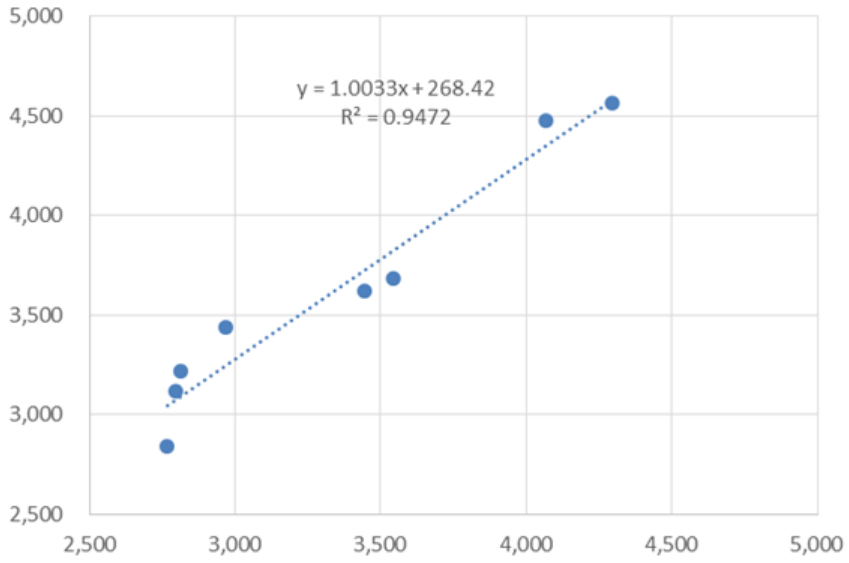


Figure 5 Calibration phase - Daily AC electrical energy consumption (kWh) for Bhiwadi

From Figure 5, the relation between Room A daily energy consumption E_A and Room B daily energy consumption E_B is as follows:

$$E_B = (E_A \times d) + c \quad (1)$$

To correct the daily cooling energy use in Room B to match that of Room A, the following correction factor is applied to the daily cooling energy of Room B:

$$E'_B = (E_B - c)/d \quad (2)$$

where
E_A = daily cooling energy use of Room A
E_B = daily cooling energy use of Room B
E'_B = corrected daily cooling energy use of Room B
c = fitted coefficient (268.4)
d = fitted coefficient (1.003)

Table 1 Measured daily cooling energy consumption for Rooms A and Room B, and corrected daily cooling energy consumption for Calibration phase

Date	E_A (kWh)	E_B (kWh)	$(E_B - E_A) / E_A$ (%)	E'_B (kWh)	$(E_{B'} - E_A) / E_A$ (%)
15-08-17	3,445	3,617	5.0%	3337.6	-3.1%
16-08-17	2,797	3,115	11.4%	2837.2	1.4%
17-08-17	2,814	3,214	14.2%	2935.9	4.3%
18-08-17	2,972	3,436	15.6%	3157.2	6.2%
19-08-17	4,071	4,477	10.0%	4194.7	3.0%
20-08-17	4,296	4,565	6.3%	4282.4	-0.3%
21-08-17	3,547	3,683	3.8%	3403.3	-4.0%
22-08-17	2,769	2,839	2.5%	2562.1	-7.5%

From Table 1 it can be observed that the corrected daily cooling energy use of Room B is much closer to the daily cooling energy use of Room A after the correction is applied, with a maximum difference of -7.5%. Therefore, this correction can be applied to the daily cooling energy data monitored during Phase II as well.

Second Phase

In the second phase, the roof of one of the test apparatus (Room A) was changed to a high albedo surface and Room B was changed to a low albedo roof.

Results and Analysis

Post calibration, Chennai site was chosen for comfort analysis. The test rooms were run in unconditioned mode and the temperature inside the rooms was used as a parameter to measure comfort.

Temperatures

The reduction on temperatures such as the over deck surface temperatures and the under deck surface temperatures were analyzed on an hourly basis to understand the effectiveness of cool roof over the dark roof. Indoor air temperatures were measured to ensure both the test huts are conditioned to the same temperature. The histogram plot of temperatures (deg C) for Chennai Figure 6 and Figure 7 show a shift in the peak temperatures towards the comfort range in case of high albedo roof compared to roof with low albedo.

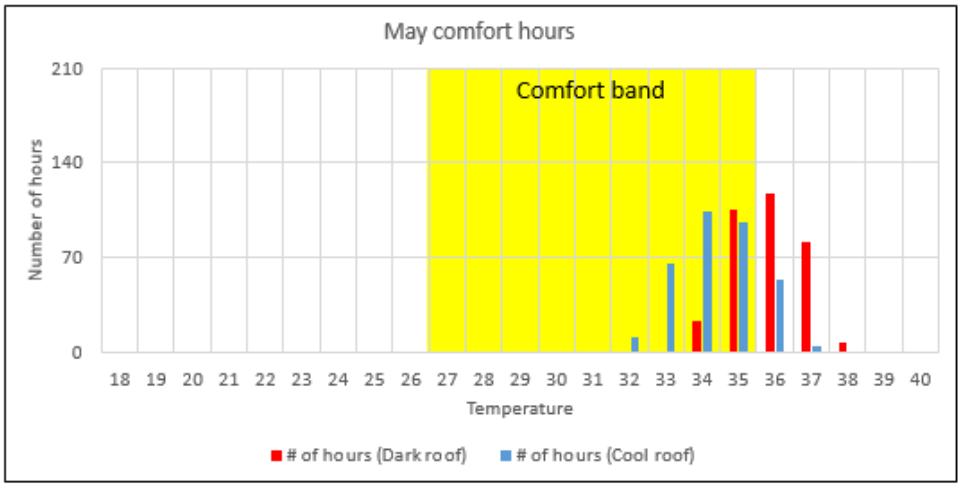


Figure 6 Comfort analysis May

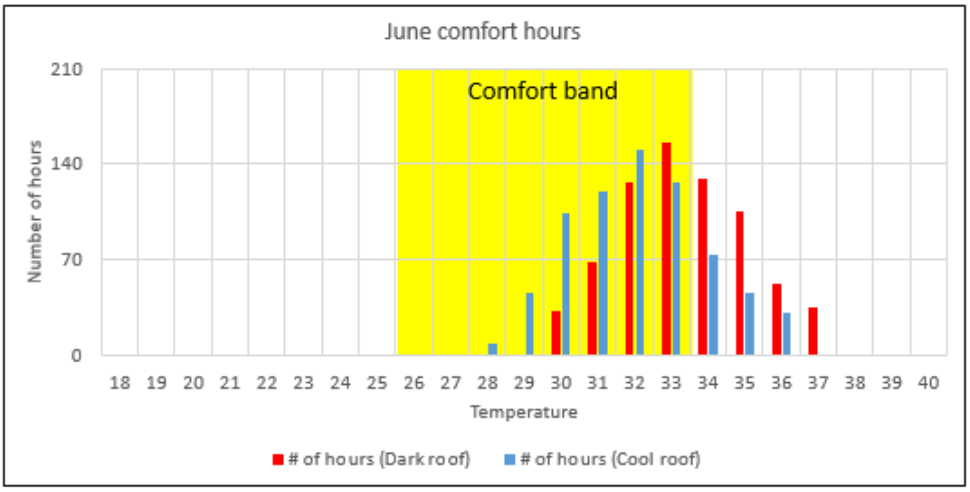


Figure 7 Comfort analysis June

Energy-saving potential

After the calibration and roofing installation monitoring was started for AC electrical energy in Bhiwadi. Using the electrical power meter sensors the air conditioning energy savings achieved by using cool roofs as compared to the dark roof were calculated and normalized to the roof area. To measure the outdoor conditions, a weather station was also installed.

On examining the roof surface temperature, the difference of ORST between Rooms A & B is 3.8°C during the monitoring period with the maximum difference of 14.8°C which occurs during the peak hours. A scatter plot between the ORST of the test Rooms shown in Figure 8. The slope of the plot is less than 45 degrees, indicating the roof surface temperatures of Room B is higher than that of Room A.

The electrical AC energy savings from the experiment is shown in Figure 9, the maximum electrical AC energy savings from high albedo roof (Room A) is 397 Wh/day which accounts to 21% of the energy consumption of low albedo roof (Room B) and the minimum energy savings

is 110 Wh/day which accounts to 8% of the energy consumption of Room B. These results are before applying correction from first (calibration) phase. After applying the correction, the slope of the graph has shifted from 0.82 to 0.75. In both cases, the R-square value is close to 0.98 which implies a very good fit of the model with the real data as seen in Figure 10.

Both Room A & B electrical energy consumption after the correction has been plotted in Figure 11 and the savings have been plotted in Figure 12. It was observed that minimum and maximum energy savings are 27.1 Wh/Sqm-day and 60.8 Wh/sqm-day respectively.

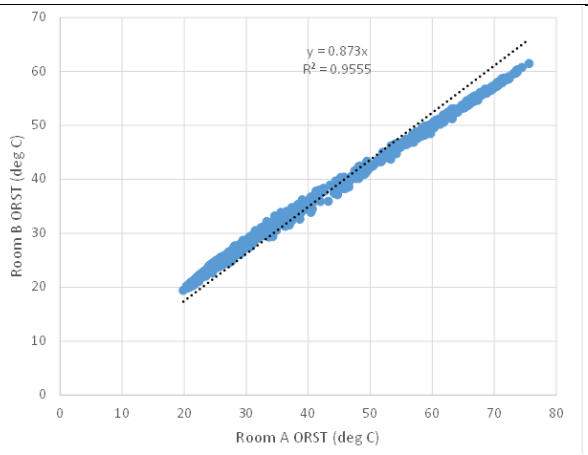


Figure 8 Scatter plot hourly ORST for test Rooms (Bhiwadi)



Figure 9 Daily average AC electrical energy consumption of test Rooms (Bhiwadi)

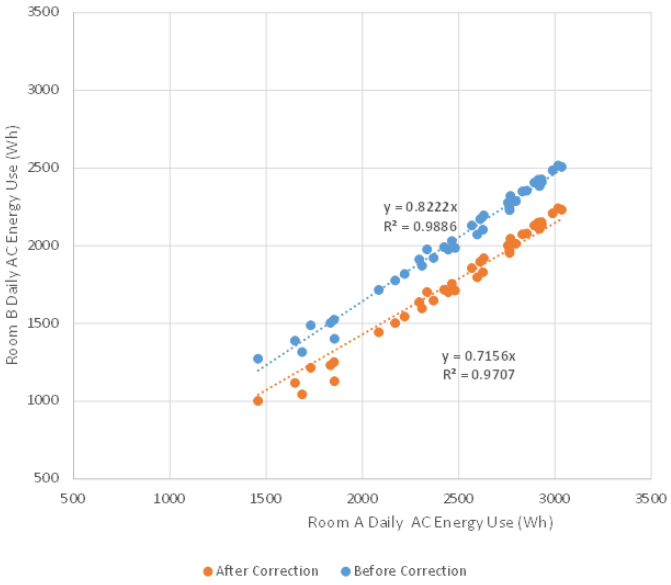


Figure 10 Scatter plot of daily AC consumption before & after applying correction- phase II

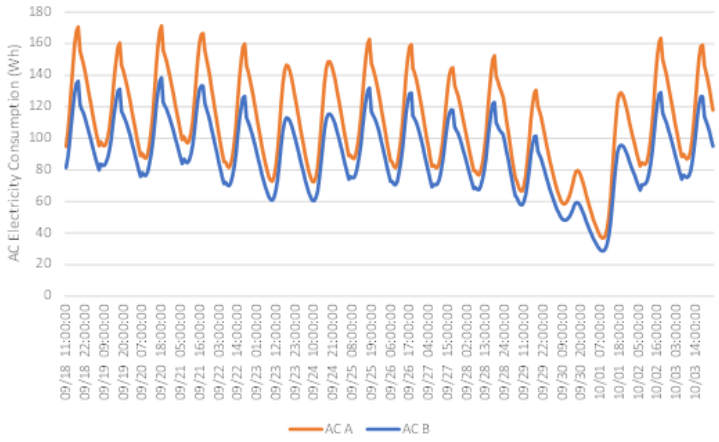


Figure 11 Hourly AC electrical energy consumption of test Rooms (Bhiwadi)

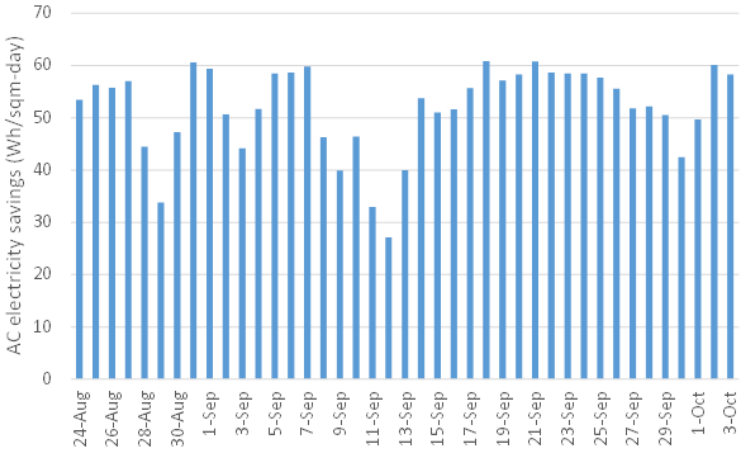


Figure 12 AC electricity savings Bhiwadi

Conclusions

To assess the benefits of albedo on a sloping roof, an experiment was performed in two Indian cities situated in different climate zones. In this experiment, two experimental near identical test rooms were constructed in each city. Each test room roof is installed with shingles having different albedos. The Shingle 1 (albedo 0.15) was compared against Shingle 2 (albedo 0.30). The experimental results show that minimum and maximum electrical energy savings from the air conditioners are 27.1 Wh/m^2-day and 60.8 Wh/m^2-day respectively and the over deck roof temperatures for the rooms with Shingle 2 is 3.8°C lower on average and the maximum reduction of 14.8 deg C can be observed. The reduction in indoor temperature, which corresponds to an improvement in thermal comfort is about 1.5-2°C, which translates to 26% improvement in thermal comfort.

Acknowledgments

The authors acknowledge the Indo-French Research Consortium (CEFIPRA) for funding this study. The authors also acknowledge the efforts of Saint-Gobain India Private Limited (Glass division) for providing the space for the experiments, support in civil construction and providing security to the test rooms.

Abbreviations

ORST	Outside Roof Surface Temperature
RCST	Room Ceiling Surface Temperature
AC	Air Conditioner
OAT	Outdoor Air Temperature

References

Akbari, Hashem et al. 2011. *Using Cool Roofs to Reduce Energy Use, Greenhouse Gas Emissions, and Urban Heat-Island Effects: Findings from an India Experiment*. http://escholarship.org/uc/item/5c5929hg.

"Cool Roof Rating Council." http://coolroofs.org/.

Garg, Vishal et al. 2014. "Assessment of the Impact of Cool Roofs in Rural Buildings in India." In *Third Int. Conf. on Countermeasures to Urban Heat Island*, Venice, Italy, 1–11.

Kolokotsa, Dionysia Denia et al. 2018. "Cool Roofs and Cool Pavements Application in Acharnes, Greece." *Sustainable Cities and Society* 37(November 2017): 466–74. https://doi.org/10.1016/j.scs.2017.11.035.

Konopacki, Steven J., and Hashem Akbari. 2001. 2 *Measured Energy Savings and Demand Reduction from a Reflective Roof Membrane on a Large Retail Store in Austin*. http://eetd.lbl.gov/sites/all/files/lbnl-47149.pdf.

Parker, Danny S, J ohn R Sherwin, J K Sonne, and Barkaszi Jr. 1996. Florida Solar Energy Center *Demonstration of Cooling Savings of Light Colored Roof Surfacing in Florida Commercial Buildings: Our Savior's School*. http://azcoolroof.com/downloads/Resources/Article Cooling Savings of Light Colored Roof Surfacing.pdf.

Rosado, Pablo J., David Faulkner, Douglas P. Sullivan, and Ronnen Levinson. 2014. "Measured Temperature Reductions and Energy Savings from a Cool Tile Roof on a Central California Home." *Energy and Buildings* 80: 57–71. http://dx.doi.org/10.1016/j.enbuild.2014.04.024.

Takebayashi, Hideki, and Masakazu Moriyama. 2007. "Surface Heat Budget on Green Roof and High Reflection Roof for Mitigation of Urban Heat Island." *Building and Environment* 42(8): 2971–79. https://linkinghub.elsevier.com/retrieve/pii/S0360132306001752.

Zinzi, M., and S. Agnoli. 2012. "Cool and Green Roofs. An Energy and Comfort Comparison between Passive Cooling and Mitigation Urban Heat Island Techniques for Residential Buildings in the Mediterranean Region." *Energy and Buildings* 55: 66–76. https://linkinghub.elsevier.com/retrieve/pii/S0378778811004129.

MEASUREMENT TECHNIQUES AND STANDARDS

Impact Zonation and Mitigation of UHI (….through remote sensing & development of Blue-Green Infrastructure Network)

Atul Kumar[1], Indian Institute of Technology Roorkee (India)
Jagrati Sehgal[2], MIT School of Architecture Loni Pune (India)
Mahua Mukherjee[3], Indian Institute of Technology Roorkee (India)
Ajanta Goswami[4], Indian Institute of Technology Roorkee (India)

ABSTRACT

The world is moving towards urban transition–rural areas losing their identity and amalgamate into near urban sectors forming huge urban centers. The paper is concerned about the notorious effect of urbanization, where rapid and unplanned urbanization of cities and concomitant reduction in vegetation result in raised temperature compared to non-urban areas, creating a phenomenon known as the 'Urban Heat Island' (UHI).

The study focused on the surface UHI (SUHI), SUHI is the effect generated by heating of infrastructure and land surface. SUHI thermal trend can be identified in daytime as well as in nighttime. An image analysis procedure based on a two-dimensional Gaussian fitting to describe the surface urban heat island (SUHI) is developed using MODIS LST night-time data. This fitting provides a spatial extent, critical location, and magnitude of SUHI. SUHI parameters extracted for the Area of Interest (AOI) by exploring Temperature difference of the cells of the LST night band of MODIS. Landsat data used to extract LULC change pattern, the data processed in ArcGIS using maximum likelihood classification techniques. The study result shows that urban-rural temperature differences between the urban center and its surrounding areas show a maximum of 5℃ for the year 2016 at night whereas it was 4℃ for the year 2000 and 2008. This implies increase in heat island intensity. Ultimately, blue-green infrastructure is proposed for the critical zone of UHI.

Keywords: - SUHI (surface urban heat island), LST (Land surface temperature), Spatio-temporal, Blue-Green infrastructure

Introduction

An urban heat island (UHI) is defined as rise in temperature over an urban area with respect to surrounding area. A town or city has an ability to generate urban heat island (Oke, 1972). The boundary of the urban heat island is defined by a sharp change in magnitude of the skin temperature or land surface temperature (LST) over the area. The concept of urban heat island can be well understood by studying the urban area and the thermal characteristics with its surrounding area (Howard 1833, Shuzhen 1994). Surface modification due to urbanization leads to increases the imperviousness of the urban surface and thereby making the urban submission of climate warmer as compared to surrounding non-urbanized areas (Oke et.al. 1967). A recent survey reports reveal that 60% of the global population is concentrated in Asian countries among which India is the second most populated with 1.3 billion people (World Population Prospects, 2015). In recent times,

[1] Atul Kumar: [akumar5@ar.iitr.ac.in]

urban areas are growing population hubs with about 54% of the total world population living in urban areas. India is one of the fastest-growing countries in terms of population and economy, has an urban population of 410 million in 2014 (World Migration Report, 2015). This remarkable population can be stated responsible for the formation and expansion of UHI. According to the statistics of the World migration report, 2015, the urban growth in India is showing steady growth with an urban population of 410 million in 2014 and the estimated urban population by 2050 is 814 million. The tremendous growth in the number of cities with an average population of 1 million is from three in 1951 to fifty-three in 2014 respectively (World Migration Report, 2015).

Urban heat island can be studied by ground-based observation that involves collection of data from fix automatic weather station or by collecting the data along a transverse with thermometers mounted on a vehicle (Voogt and Oke, 2003). Several statistical methods have been developed to understand the change in growth of the city or urban area (Weng et al., 2004). The concept of remote sensing, to highlight the heat signature of an area, with respect to the surrounding was implemented from early 1970s (Rao et al., 1972). The size of the city plays an important role in determining the magnitude of the urban heat island (Oke, 1972). The study of urban heat island using thermal remote sensing becomes possible only because of advancement of sensor technology and the use of satellite, airborne and aircraft platforms. The surface temperature calculated using thermal data contains the effects of surface radiative and thermodynamic properties that include surface emissivity, moisture, and surface albedo, and contain the effect of the near-surface atmosphere.

Urban climates are influenced by a combination of process occurring at a variety of scales, which intern effects by the biophysical nature of cities and the structure of the urban atmosphere. The scale is considered as one of the important parameters while characterization urban heat island and modeling its different forms. Scale helps us to determine the size of the source area from where thermal influence originates and how it slowly changes the urban climate. A small-scale study of the UHI found inside the roughness layer (RSL) is known as microscale, where we study individual buildings, trees and the intervening spaces between the buildings. The mesoscale study involves plumes from individual local scale system, which extends vertically above and produce urban boundary layer (UBL) over the entire city. The growth of UHI has been monitor and study by numerous methods, of which we exploit MODIS thermal remote sensing data to measure the land surface temperature. The prime objective of the research is to assess the UHI pattern in the city of Gurugram and suggesting blue-green infrastructure measure to mitigate its effect.

Study area

Gurgaon or Guru-gram, the city is a glaring example of urban growth and emerges as a millennium city of the country. Witnessing modern reincarnation, the city has developed in both forms spatially and demographically. The state of Haryana was formulated in 1966 and Gurugram was one of its districts. Earlier most of the landmass was devoted to agriculture; the district has an agro-based economy. After 1990s Gurugram become hub for numerous job options this leads to the moving of a huge population to the city. Right now the city has become a financial and industrial center and contributing third highest per capita income. Gurgaon District is in the southernmost region of Haryana. Latitudinal and longitudinal expansion for the city is 27° 27’ 20” and 28° 32’25’’ latitude, and 76° 39’ 39’’ and 77° 20’ 50’’ longitude. The spatial expansion of the city is the part of National Capital Region, which is situated to the north of the district. The district has 1254 sq. km area. It has 1,514,432 population with a population density 1,241 people per square kilometer as per census 2011.

The AOI is selected in such a way that it covers urban pockets as well as an underdeveloped pocket to measure the temperature difference and to characterize UHI magnitude. Gurugram urban center is considered for the interested area for study. A shapefile is generated and with the layer of MODIS data for LST, a rectangle of dimension 30x30 is set for extraction of AOI. An extent of buffer zone is set under 30x30 tile, keeping center point at urban center of city. The rectangle for the area of interest has geographical dimension of 30 km x 30 km. It covers urban area as well as some part of Delhi and rural extent of Gurugram as buffer zone.

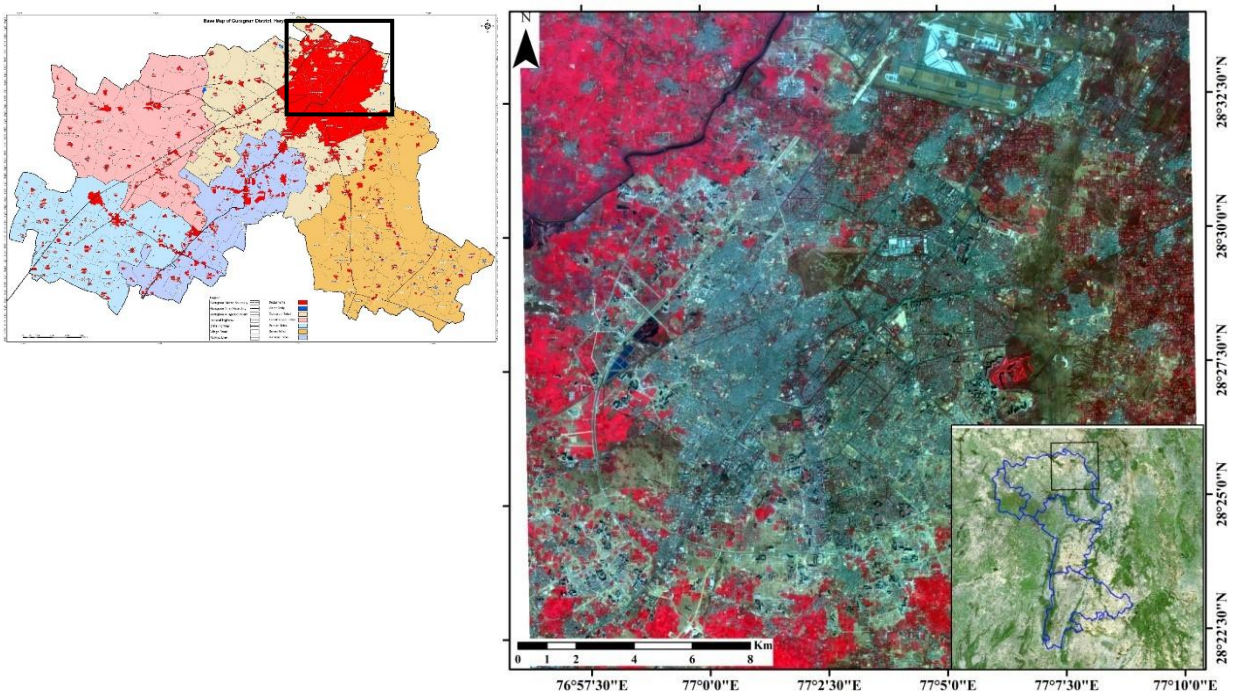


Figure 1. Area of interest for the study 30x30 km square marked on the Gurugram district map. *Source*: https://gurugram.gov.in/about-district/map-of-district/.

Methodology

The study methodology stars with the problem identification and literature study (case study) about the UHI effect. Objectives for the study is set under three separate work process, first is to analyze UHI change pattern, second is to analyze LULC change pattern and further relation is established with the LULC pattern and UHI intensity to get the result. Tools and techniques are set with the reference of literature review of the research paper that has worked on the UHI and LULC. For UHI change pattern MODIS data of spatial resolution 1km is used as the UHI effect can be identified at least over a city region, UHI characterization is done by estimating six parameters of UHI such as spatial extent, central location, orientation, and UHI intensity. LULC map is prepared for the area of interest considering 30km x 30km region of urban patch along with the buffer zone. Each extracted data has been plot on graph and relation has been set to get the result.

Mapping of the UHI zone

The land surface temperature depicts the radiative heat of the body or surface. In this

research study, MOD11A2 product of MODIS data is used to extract LST day time and LST night time, over the AOI for the year 2000, 2008 and 2016. Gaussian fitting algorithm is applied to analysis the temporal assessment of LST for interested years. The study follows the same method to quantify the UHI intensity for the Gurugram city as described by Streutker 2002 in the research paper titled 'Satellite-measured growth of the urban heat island of Houston, Texas' (Streutker 2003). Streutker used least square fit method to developed Gaussian surface for the UHI magnitude over the area of interest and calculation of all variables such as (x,y) represents the location of a pixel, T (x,y) is the LST of a pixel at (x,y), T0 is the mean rural surface temperature, a_1 and a_2 are the coefficients determining spatial gradient of rural temperature and UHI (x,y) is the pixel-based heat island intensity. The method used to determine the UHI magnitude is designated as a0 along with spatial extent (a_x and a_y), orientation (ϕ) and the central location (x_0 and y_0) of the heat island. The version v005 of MOD11A2 of 8 day product from band 31 (10780 – 11.280 µm) and band 32 (11.770 – 12.270 µm) of terra satellite is used for the UHI change pattern study, out of 12 layers the layer number 4 is used for processing to extract LST as this layer provide LST night data. Accuracy of MODIS LST product is better than 1K in most of the cases. 39 out of the 47 scenes give an accuracy of land surface temperature better than 1K (D. Zhou et al. 2014). The data set acquired from the MODIS has sinusoidal projection system and it needs to be changed into Lambert Conformal Conic (LCC) projection of datum WGS_1984. MODIS provides raw dataset in HDF (hierarchical data format), the raw data set in HDF format is processed to extract SDSs scientific datasets and store as raster imagine file with the spatial reference system information. The SDSs acquired from the extraction of raw dataset provide LST 1_km in raster imagine file which is further processed for mosaicking and LST map is extracted for the AOI (Gurugram city), using input shapefile of Gurugram city and its neighboring area.

In order to perform the fit, each rural temperature image is fit to a planar surface and the rural temperature image is subtracted from LST image which enhanced the urban temperature signature. Mathematically this step is expressed as $T\ (x,y) = T_0 + a_1x + a_2y$; where T_0 is the mean temperature in degrees centigrade, a_1 and a_2 are the longitudinal and latitudinal measure in ºC / km. The enhanced urban temperature signature provides the SUHI signature. The process of linear fitting is executed in Matlab, 2012a.

Finally, a 2D Gaussian surface is developed in Matlab along with 12 parameters. Major advantage of this method is that it provides the difference in temperature between the urban and the surrounding rural area. The expression used to determine SUHI intensity on least square technique is as:

$$SUHI(x,y) = a_0 \times \exp\left[-\frac{\{(x-x_0)\cos\phi+(y-y_0)\sin\phi\}^2}{0.5a_x^2} - \frac{\{(y-y_0)\cos\phi+(x-x_0)\sin\phi\}^2}{0.5a_y^2}\right] \quad (1)$$

Equation 1 Equation for SUHI intensity Source: A Stable Gaussian Fitting Procedure for the Parameterization of Remote Sensed Thermal Images

In this expression (x, y) represents the location of a pixel, a_0 is the magnitude of the UHI, spatial extent (a_x and a_y), orientation (ϕ), and the central location (x_0 and y_0) of the heat island. Spatial extent provides the extent of SUHI horizontally. The AOI has been plot in the form of ellipse with a_x and a_y as major and minor axis and the angle ϕ is the angle made by major axis with x-axis and the central location (x_0 and y_0) gives the critical location with respect to SUHI intensity, it also provides the shifting of critical UHI point with respect to map central location. The central location

(x_0 and y_0) is the center of the ellipse and tells the point of highest SUHI intensity, further spatial extent is represented with concentric ellipse in which the inner ellipse represents the spatial extent up to which SUHI magnitude has 61% of its maximum values it marked as A_61% the outer ellipse defines the region having SUHI magnitude greater than the 1.0 k and marked as A_1K.

Initial UHI parameter estimation: a least-square fit is performed. Equation 1 can be exactly transformed into a linear equation with the use of the logarithm and can be expressed as a linear equation with six unknown variables:

$$\ln\big(SUHI(x,y)\big) = a_1x^2 + a_2xy + a_3y^2 + a_4x + a_5y + a_6 \quad (2)$$

Equation 2 logarithmic SUHI intensity (source: A Stable Gaussian Fitting Procedure for the Parameterization of Remote Sensed Thermal Images)

For equation 2 the variables a_i is directly calculated by using linear regression. Gaussian fitting: starting from the initial guess parameters, a nonlinear data-fitting in a least-squares sense is executed. It is an iterative fitting procedure implemented with the function lsqcurvefit.m (Matlab Optimization Toolbox) that finds the coefficients that best fit the Gaussian function to the data (Anniballe and Bonafoni 2015). All the parameters directly computed with equation 1 and equation 2 as well as the spatial extent. The correlation coefficient and R square between the Gaussian model and the SUHI is also evaluated. The graphical representation also developed for the SUHI, it provides better understanding of the shape and orientation of urban heat island. 2D Gaussian surface and 1D plot of Gaussian surface along major and minor axis.

Mapping Land Use Land Cover (LULC)

The LULC for the Gurugram city considering some spatial extent as a buffer zone is prepared using LANDSAT data. For the year 2000 the data of LANDSAT -5 is used whereas for the year 2008 and 2016 LANDSAT-7 and 8 are used respectively. LULC map is prepared using supervised classification in ArcGIS, the layers like build-up, water, vegetation (dense and sparse), barren land, etc. are classified.

Blue-Green Infrastructure

Green Infrastructure provides ecosystem services and maintains thermal balance by regulating the fresh air supply, reduced surface runoff and thus modify the local microclimate through the production of oxygen. They help in capturing carbon and reducing the level of smog, which are the reasons for rising temperature.

The use of vegetation is the most effective measure to reduce the UHI effect (Wilmers F 1988). Grass over open land helps in providing low resistance to airflow, which might enhance cooling by convection (Bowler, 2010). Based on studies conducted, it has been found out that urban parks could reduce the air temperature of the surrounding area by 4°C (Oke 1998; Jonsson 2004; Zoulia Santamouris and Dimoudi 2009). Dense tree shade on the street with minimal traffic has the cooling effect of 2.2°C (Tsiros 2010). 21% to 26% of the surface area in cities is comprised of roof surface (Wong 2005) therefore, few green roofs over some buildings would not be enough to provide large effect on a local scale in spite in some special cases. Green roofs absorb heat and filter the air and keep the air temperature low (Getter 2006).

In spite of green vegetation other high albedo materials also help in controlling temperature. By the use of permeable pavement air temperature can be reduced up to some extent. Thus, repaving streets with cool paving materials is expected to lower urban air temperatures (Taha 1997). An increased amount of water bodies may reduce temperature due to their evaporative action and enhanced wind speed (Robitu et al. 2006).

Vegetation lower surface and air temperature through evapotranspiration. Through the process of evaporation, energy gets transferred from the atmosphere and hence, links the energy balance of the hydrological cycle and if there is less amount of vegetation in the environment the remaining energy would be responsible for the formation of extra heat which is responsible for the formation of UHI. Therefore, the provision to design network of these green interventions is the most effective and efficient measure to control the intensity of UHI.

Result and discussion

The SUHI island is characterized for the year 2000, 2008 and 2016 for the densest urban patch of 30km x 30km area in Gurugram with remotely sensed data of MODIS images and plotted, it provides not only monthly UHI magnitude variation (a0) but also the spatial extent (a_x and a_y) along with the orientation (ϕ) central point (x_c, y_c). Data is retrieved using Matlab 2012 and after analyzing the result and collected in a tabular form as shown in table below. It is noticed that the month of MAY and JUNE fall under the highest UHI intensity for the year 2000 and 2008 respectively were as for the year 2016 it's shifted to month of FEBRUARY. For temporal variations of the UHI magnitude graph of months vs. average UHI magnitude has been plot. For spatial extent of UHI effects over the city LST map has been prepared as well as variation of monthly spatial extent graph is plotted. LULC map is prepared considering four classes (build-up, vegetation, water, and barren land) with specific color code.

The urban-rural temperature differences between the urban center and its surrounding areas show a maximum of 5℃ for the year 2016 at night whereas it was 4℃ for the year 2000 and 2008 this implies increase in heat island intensity. The aerial extent A-61 defines the area's spatial extent up to which SUHI intensity lower down to 61% were as A-1K defines the area SUHI intensity is considerable or greater than threshold value that is 1.0 k. monthly variation graph for the spatial extent depicts that for the year 2016 maximum value of the A-61 is 87 km^2, for the year 2008 and 2000 the maximum aerial extent is 73 km^2 and 74 km^2. The area of A-61 for inner ellipse and area A-1k for outer ellipse is increasing continuously during last years as shown in the plotted excel sheet. LST map developed for the area also show the increasing spatial extent of heat island effect along with the change of geographical landscape or urban sprawl, map with blue colour code show the extent of UHI effects for the year 2000 and 2008 it was concentrated near national capital region of Delhi over the time period of urban sprawl its extent increase.

Table 1 Average monthly UHI magnitude and spatial extent for the year 2000, 2008 and 2016

Months	2000		2008		2016	
	UHI	SPATIAL	UHI	SPATIAL	UHI	SPATIAL
Jan			3.65	33	2.63	42
Feb	3.64	31	3.46	40	5.13	54
March	3.41	35	1.40	42	3.38	46
April	3.17	34	3.04	41	2.97	50
May	4.54	45	1.96	34	2.19	45

June	3.09	27	3.89	27	1.85	44
July	1.06	74	2.26	33	1.82	44
Aug	2.12	47	2.41	25	1.65	52
Sept	2.33	37	1.80	48	1.76	56
Oct	2.84	29	1.99	26		
Nov	3.50	30	2.70	34		
Dec	3.58	27	3.18	36		

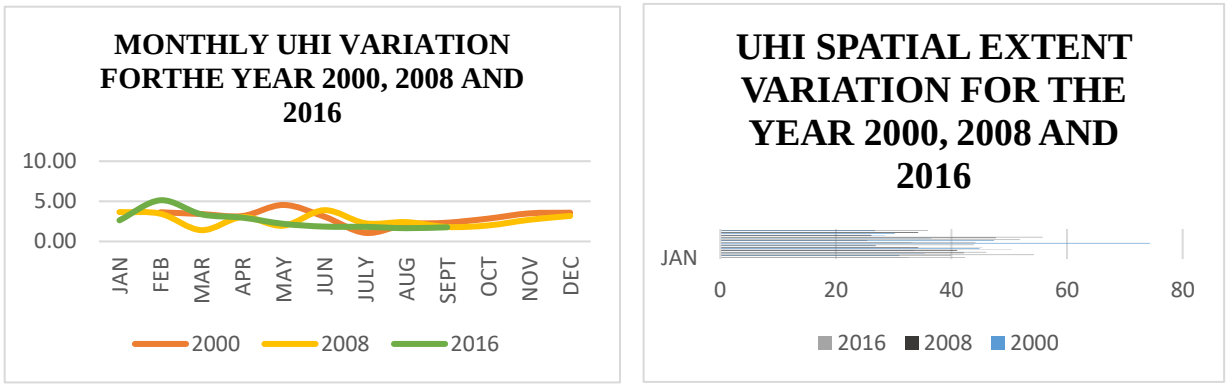


Figure 2 (a) graph between UHI magnitudes vs months (b) graph between spatial extent vs months

LULC map of the area depicts drastic changes in urban patches from the year 2000 to 2016. In the year 2000 and 2008 the area allocated for the urban or build-up was 95 square km and 242 square km respectively whereas for the year 2016 it increases to 287 square km. During the 16 years of period Gurugram experienced about 200% hike in urban regions. Waterbody shows constant trend. Vegetative land patches are kept on depleting from 188-kilometer square to 52-kilometer square in 2016.

Table 2 LULC classification and area for the year 2016 / 2008 / 2000

LULC			
Class	**2016**	**2008**	**2000**
Build Up	287.6526	242.7192	95.3343
Vegetation	52.4349	66.5217	187.7085
Barren land	247.5504	279.2241	305.1171
Water body	1.6434	0.8145	1.1214
Total	**589.28**	**589.28**	**589.28**

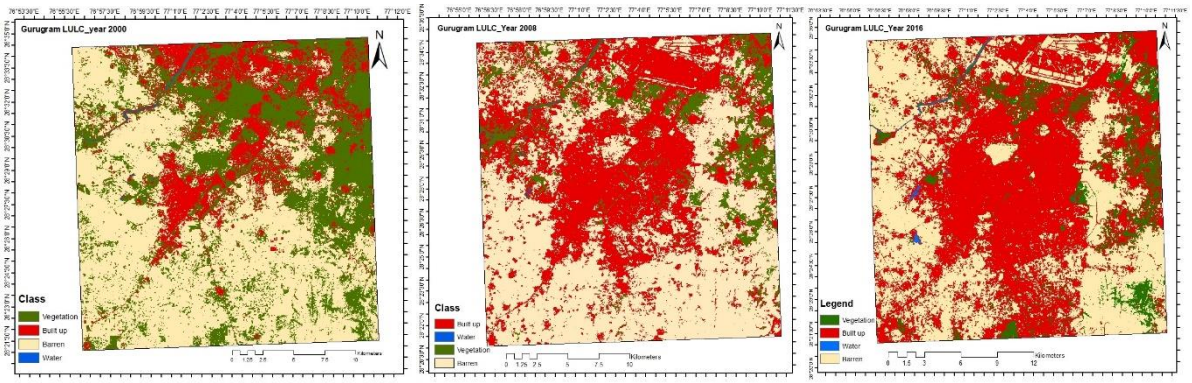
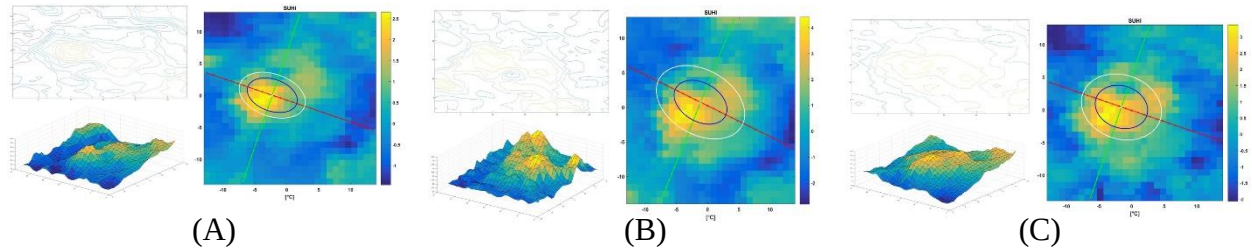


Figure 3 LULC for year (a) 2000/ (b) 2008/ (c) 2016

Conclusion

The study quantifies the present status of urban heat island in the Gurugram city area, it also identifies the heat island spatial pattern and its temporal variation for the area of interest. The result implies that due to urban growth the city is feeling more heat as change in its local climatic condition and the city is experiencing less cold in winter season as well as intense hot in summer season. Although heat island effect is also present in day time with intense magnitude the study focus on night time as to get good signature of SUHI. For analyzing the UHI Gaussian surface method used which was developed by Streutker in 2002, this method has been used for various cities throughout the globe. For Indian city this method is new; the main purpose of this study is to understand the heat island effect in terms of magnitude and spatial extent along with the land use land cover change of the city.



(A) (B) (C)

Figure 4 Gaussian surface developed for AOI (A) 2000, (B) 2008, (C) 2016

In this study urban heat island is quantify for the three years considering an interval of 8 years that is 2000, 2008 and 2016 as well as land use land cover map is also developed to set the relation between heat island critical point and urban setting. The UHI signature is studied for the night LST which shows the radiant temperature of the materials. UHI magnitude for all the months for the year 2000, 2008 and 2016 is estimated and graph of monthly variation of average UHI magnitude is plotted for the three marked years. It is found that for the year 2000 and 2008 UHI intensity was maximum for the month of May and June respectively whereas for the year 2016 it is shifted to the month of January. Land use land cover map also shows increasing trend as the urban patch increase from 95 km^2 in the year 2000 to 287 km^2 in the year 2016. With the increase of urban area the spatial extent of UHI is also increased. The critical point of UHI is found at the urban center of the city with variable spatial extent. Here, regional study is carried out to quantify

UHI intensity as MODIS provides data of 1 km spatial resolution as the phenomenon of UHI can be identified at city or municipality region level. LULC map is prepared with the processing of Landsat data as it provides 30m spatial resolution. The plot and all other intermediate result show the present status of UHI effect in Gurugram city.

REFERENCE

Anniballe, Roberta, and Stefania Bonafoni. (2015). "A Stable Gaussian Fitting Procedure for the Parameterization of Remote Sensed Thermal Images." *Algorithms* 8 (2): 82–91. https://doi.org/10.3390/a8020082.

Bowler, D. E. et. al. (2010), Urban greening to cool towns and cities: A systematic review of the empirical evidence, Landscape and Urban Planning, 97:147–155.

"Chapter 2 THE GROWTH JOURNEY OF GURGAON TO THE MILLENNIUM CITY 2.1 Introduction 2.2 Gurgaon from the Mahabharata Days to Its Modern Avtaar: The Millennium City of India 2.3 The Growth Dynamics of Gurgaon 2.4 Conclusion." n.d.

Getter, K. L., & Rowe, D. B. (2006), The role of extensive green roofs in sustainable development, HortScience, 41(5): 1276-1285.

"Government of Haryana DISTRICT DISASTER MANAGEMENT PLAN GURGAON 2013 Sh. Shekhar Vidyarthi, IAS Deputy Commissioner-Cum-Chairperson District Disaster Management Authority District Gurgaon, Haryana." n.d.

Jiahua, ZHANG, and YAO Fengmei. 2009. "The Characteristics of Urban Heat Island Variation in Beijing Urban Area and Its Impact Factors." *2009 Joint Urban Remote Sensing Event*, 1–6. http://ieeexplore.ieee.org/xpls/abs_all.jsp?arnumber=5137502.

Kaushik, Rajesh, District Town Planner, and Country Planning. n.d. "NEED FOR TRANSIT ORIENTED."

Kumar, Atul, and Dhanu Singh. 2017. "Built Environment Issues in India and an Approach to Mitigation" 8 (1): 156–58.

Mirzaei, Parham A., and Fariborz Haghighat. 2010. "Approaches to Study Urban Heat Island - Abilities and Limitations." *Building and Environment* 45 (10). Elsevier Ltd: 2192–2201. https://doi.org/10.1016/j.buildenv.2010.04.001.

Mohan, Manju, Anurag Kandya, and Arunachalam Battiprolu. 2011. "Urban Heat Island Effect over National Capital Region of India: A Study Using the Temperature Trends." *Journal of Environmental Protection*. https://doi.org/10.4236/jep.2011.24054.

Mohan, Manju, Yukihiro Kikegawa, B.R. Gurjar, Shweta Bhati, Anurag Kandya, and Koichi Ogawa. 2009. "Assessment of Urban Heat Islands Intensities over Delhi." *The Seventh International Conference on Urban Climate* 3 (July): 3–6.

Nunez, M., and T. R. Oke. 1977. "The Energy Balance of an Urban Canyon." *Journal of Applied Meteorology*. https://doi.org/10.1175/1520-0450(1977)016<0011:TEBOAU>2.0.CO;2.

Nuruzzaman, Md. 2015. "Urban Heat Island: Causes, Effects and Mitigation Measures - A Review." *International Journal of Environmental Monitoring and Analysis* 3 (2): 67. https://doi.org/10.11648/j.ijema.20150302.15.

Oke, T. R. (1988). "The urban energy balance", Prog. Phys. Geogr. 12: 471–508.

RIZWAN, Ahmed Memon, Leung Y.C. DENNIS, and Chunho LIU. 2008. "A Review on the Generation, Determination and Mitigation of Urban Heat Island." *Journal of Environmental Sciences*. https://doi.org/10.1016/S1001-0742(08)60019-4.

Robitu, M., Musy, M., Inard, C., & Groleau, D. (2006), Modeling the influence of vegetation and water pond on urban microclimate, Solar energy, 80 (4): 435-447.

Roth, Matthias, and Winston T.L. Chow. 2012. "A Historical Review and Assessment of Urban Heat Island Research in Singapore." *Singapore Journal of Tropical Geography*. https://doi.org/10.1111/sjtg.12003.

Sadashivam, T, and Shahla Tabassu. 2016. "Trends of Urbanization in India: Issues and Challenges in the 21 St Century" 3: 2375–84.

Santamouris, M. 2014. "On the Energy Impact of Urban Heat Island and Global Warming on Buildings." *Energy and Buildings*. https://doi.org/10.1016/j.enbuild.2014.07.022.

Streutker, David R. 2003. "Satellite-Measured Growth of the Urban Heat Island of Houston, Texas." *Remote Sensing of Environment* 85 (3): 282–89. https://doi.org/10.1016/S0034-4257(03)00007-5.

Taha, H. (1997), Urban climates and heat islands: albedo, evapotranspiration, and anthropogenic heat, Energy and buildings, 25(2): 99-103.

Taha, H. (1997), Modeling the impacts of large-scale albedo changes on ozone air quality in the south coast air basin, Atmospheric Environment, 31:1667–1676.

Tsiros, I. X. (2010), Assessment and energy implications of street air temperature cooling by shade trees in Athens (Greece) under extremely hot weather conditions, Renewable Energy, 35:1866–1869.

Tzavali, A., J. Paravantis, G. Mihalakakou, A. Fotiadi, and E. Stigka. 2015. "Urban Heat Island Intensity: A Literature Review." *Fresenius Environmental Bulletin* 24 (December 2016): 4535–54.

Wilmers, F. (1988), Green for melioration of urban climate, Energy and buildings, 3: 660-666.

Yamamoto, Y. (2006), Measures to mitigate urban heat islands, Science and Technology Trends Quarterly Review, 18 (1): 65- 83.

Zhou, Decheng, Shuqing Zhao, Shuguang Liu, Liangxia Zhang, and Chao Zhu. 2014. "Surface Urban Heat Island in China's 32 Major Cities: Spatial Patterns and Drivers." *Remote Sensing of Environment* 152. Elsevier Inc.: 51–61. https://doi.org/10.1016/j.rse.2014.05.017.

Zhou, Ji, Ji Zhou, Yunhao Chen, Jinfei Wang, Wenfeng Zhan, and Jinfei Wang. 2011. "Maximum Nighttime Urban Heat Island (UHI) Intensity Simulation by Integrating Remotely Sensed Data and Meteorological Observations." *IEEE Journal of Selected Topics in Applied Earth Observations and Remote Sensing* 4 (1): 138–46. https://doi.org/10.1109/JSTARS.2010.2070871.

Zoulia, I., Santamouris, M., & Dimoudi, A. (2009), Monitoring the effect of urban green areas on the heat island in Athens, Environmental Monitoring and Assessment, 156: 275-292.

Green Infrastructure Strategies as Countermeasures to Urban Heat Islands with particular reference to the Bangalore Metropolitan Region

Reshmi Manikoth Kollarath[1], *BMS College of Architecture (India)*
Vasseem Anjum Sheriff [2], *BMS College of Architecture (India)*

ABSTRACT

Bangalore the capital of the state of Karnataka is one of the fastest growing metropolises in India. Traditionally it enjoyed a salubrious climate and was referred to as Garden city for its numerous private gardens and parks and Pensioners paradise for its lifestyle. More recently it has emerged as the IT capital and has witnessed a sudden surge in the population seeking economic opportunity. Bangalore, in recent times, is experiencing unprecedented urbanisation and sprawl due to concentrated developmental activities with impetus on industrialization and development of grey infrastructure for the economic development of the region. This concentrated growth and increase in population and consequent pressure on infrastructure, natural resources and ultimately giving rise to a plethora of serious challenges such as climate change, enhanced green-house gas emissions, lack of appropriate infrastructure, traffic congestion, and lack of basic amenities, in many localities leading to change in different land use types. Recent research indicates that Greater Bangalore is an emerging Urban Heat Island. Factors contributing to the Urban Heat Island Effect include Urban Structure, Urban Surface Cover, Urban fabric, Urban Metabolism and distinct lacunae in urban planning. The alarming decline in the vegetation cover and water bodies has contributed significantly to discomforting rise in temperature. This paper seeks to examine green infrastructure strategies at varying urban scales in order to mitigate the impact of the Urban Heat Island Effect.

Keywords: Bangalore, Urbanization, Grey Infrastructure, Urban Heat Island Effect, Mitigation Measures, Green Infrastructure

Introduction

Bangalore with its salubrious climate and many parks was famous as the ‘Garden City’ of India till recent times. The city got the name from 1927 onwards when many parks were constructed along with other public works which were undertaken as part of silver jubilee celebrations of the rule of Krishna Raja Wodeyar IV. Urbanization in Bangalore has been steadily increasing since independence of India when it was declared as the capital of the state of Karnataka. It has accelerated considerably in the past couple of decades as the ‘garden city’ solely transformed into the ‘silicon city’ of India. The population in Bangalore has doubled from 4,301,326 in 2001 to 8,443,675 in 2011 over just one decade. This shows the rapid rate of urbanization in the city. Today Bangalore is a Megacity and ranked third in India in terms of population and has managed to surpass both Kolkata and Chennai over a period of 10 years. The population density of the city is a staggering 12,000 per sq km.

[1] Reshmi Manikoth Kollarath: [reshmimk@gmail.com].

Urbanization and consequent urban sprawl causes loss of agricultural land and ecological habitats. It also impacts urban infrastructure such as healthcare, transportation, energy, water supply etc (Sudhira 2008). There has been an increase of 632% of built up area and decrease of 72% of water bodies in Bangalore between 1972 and 2009. Vegetation has also decreased by 62% between 2002 to 2009 alone (Ramachandra & Kumar 2010). The decrease in vegetation and loss of waterbodies along with increase of impermeable surfaces has had a profound impact on the phenomenon of Urban Heat Island in Bangalore.

Urban Heat Island Effect

Urban Heat Island (UHI) is a phenomenon of higher temperatures experienced in an urban area when compared to its surrounding rural area. Urbanization is an important cause for UHI. Anthropogenic activities and increase in built up areas are the main contributors to UHI. Pavements and rooftops contribute significantly to UHI (Mohajerani et al 2017). Urban Heat Island has a huge impact on the urban climate, hydrology, ecosystems, environment and energy flows. It also has a negative impact on the health of the residents. Concrete, asphalt and other manmade materials trap the solar energy. This is aided by the loss of vegetation and natural surfaces in an urban area.

For every 0.6°C rise in temperature, there is an increase in electricity consumption of about 2%. (Voogt 2004). Increase in temperatures increases the use of air conditioning appliances, resulting in increased emission of harmful greenhouse gasses which has led to global climate change. The harmful gases released from power plants due to increased energy consumptions lead to air pollution. UHI also affects the water quality in urban areas. The surface runoff gets heated due to the increased surface temperatures. This water when it mixes with the water bodies will impact the aquatic eco systems.

Urban Heat Island impact on climate change

Climate change refers to changes in the global climate system which causes changes to weather patterns. Climate change phenomenon is increasingly being experienced across the world with changes in precipitation patterns and an overall increase in global temperatures. The impact of Urban Heat Island on the other hand is localized and limited to specific area. But as the global temperatures increase as a result of climate change it augments the heat island effect. This will expose urban dwellers to extreme heat events which in turn will adversely impact the health of the residents. This will highly impact the economically and socially vulnerable groups who don’t have adequate housing and are more exposed to working outdoors.

Urban Heat Island does have an impact on the local climate as well. Urban Heat Island influences the wind pattern in the urban area. It can change the rate of precipitation and aid in the causing fog and clouds. UHI can induce additional rain as well as thunderstorms. Urban Heat Island causes low pressure areas which are conducive to cloud formation.Urban Heat Island can increase precipitation rate in urban areas by as much as 51%.

Urban Heat Island and Urban Flooding

Urban Floods are a result of both natural and manmade activities. Some of the reasons for urban floods are

i. **Planning issues:** Increasing population, habitations coming up in low-lying areas and encroachment of catchment and drainage areas.
ii. **Technical issues:** Increased imperviousness leading to increased runoff. Lack of proper waste disposal resulting in clogged drains, high intensity – high load of runoff.
iii. **Meteorological issues:** Climate Change, resulting in extreme events, Urban Heat Islands.
iv. **Policy issues:** Absence of integrated flood control and implementing agency

Increased rate of precipitation combined with increased surface runoff due to increase in impervious surfaces can result in urban flooding in many urban areas and Urban Heat Islands are one of the main contributors to urban flooding.

Urban Heat Island Effect in Bangalore Metropolitan Region

The Impact of Urban Heat Island

In a remote sensing based study carried out by Shrinidhi Ambinakudige in 2011, the effects of UHI in Bangalore have been analysed with respect to the relationship betweeen vegetation cover and temperature in context of BangaloreThe study showed that temperatures varied by 1 ^{o}C to 7 ^{o}C within different land cover classes in the urban core. The study also showed that the core area of the city also had lesser mean temperatures than the suburbs and outgrowths. This was because of the presence of water bodies and vegetation in the core city while the uncontrolled urban sprawl towards the outskirts had very less green cover.

Most of the water bodies have been encroached or have dried up. This has led to increased temperatures in the outgrowth areas.

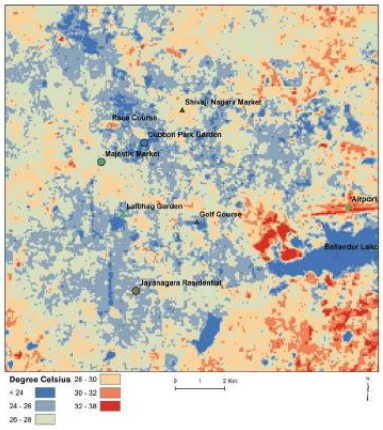


Figure 1. Land Surface temperatures in Bangalore. *Source*: Ambinakudige, Shrinidhi (2011)

The Tank system in Bangalore

The Garden city image of Bangalore was enhanced by its many lakes which also made it known as "The City of Lakes". Kempegowda, the founder of Bangalore was a visionary who by constructing the many reservoirs and lakes along the natural terrain of Bangalore ensured that the city had its own supply of potable water as well as water for cultivation. This was especially important in the context of Bangalore in the absence of any other source of water or a reliable river system. Ulsoor lake was one of the earliest lakes constructed by Kempegowda in the 16th century. This was later maintained bt the British. Sankey Tank, Miller's tank are other lakes used for water needs by the people of Bangalore.

Bangalore's has an average rainfall of 850 mm. This rainwater was traditionally captured by the cascading system of lakes. The outlets connecting these lakes to each other were called Raja Kaluves . The water moves from from one lake to the other till it is finally emptied into one the three main valley systems of Bangalore.

With the contamination of sewage into the lake water it soon became prohibited for consumption.In 1960 there were 262 lakes in Bangalore which have come down to 81 now of which only 34 are identified as live lakes. Lakes also form an important ecological system supporting many forms of life in Bangalore.

Traditionally the kere system in Bangalore has functioned as an efficient water management system in Bangalore by collecting the rainwater through a series of interconnected lake system. In the present time most of them have gone dry, or have been filled in and the remaining lakes have become waste and sewage dumps. The traditional linkages in the water systems have been disrupted due to urbanization. Adding to this are the effects of climate change which leads to higher intensity of rain in lesser number of rainy days which causes urban flooding in many areas in Bangalore.

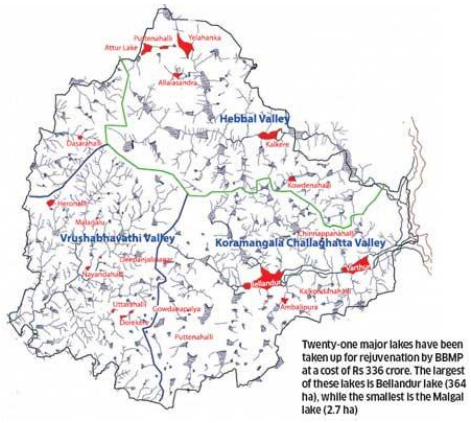


Figure 2. Tank System in Bangalore. *Source*:Kollarath (2013)

Impact of water bodies on Urban Heat Island Effect

The study of Land Surface Temperatures show a remarkable drop in temperatures near heavily vegetated areas and water bodies. The following studies undertaken by Ramachandra T V and Uttam Kumar (2010) show the significance of the tanks in Bangalore in reducing the Urban Heat Island effect.

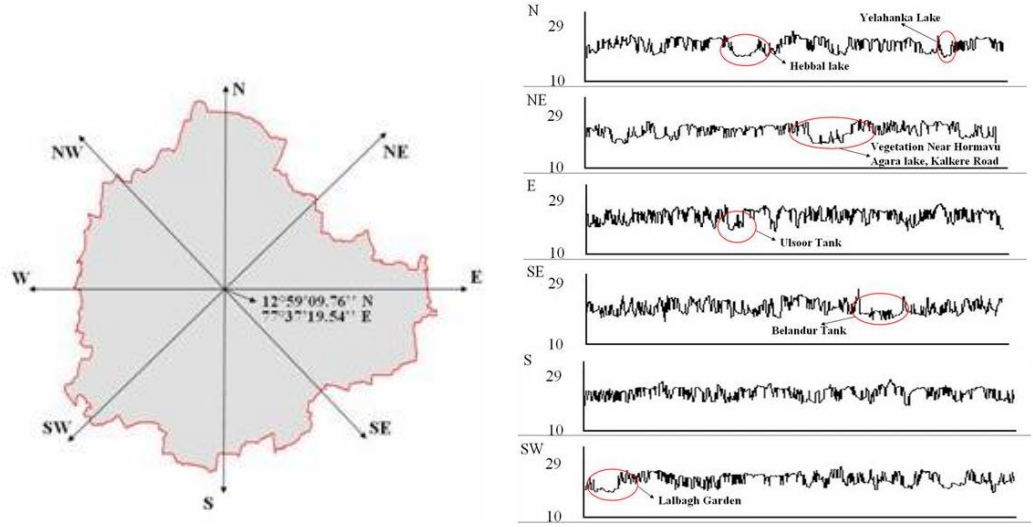


Figure 3. LST Studies in Bangalore Metropolitan Area. *Source*:Ramachandran & Kumar (2010)

Case of flooding in Bangalore

Urban Flooding has been becoming an increasing phenomenon in Bangalore in the recent years Unplanned and rampant urbanization has had a major impact on the existing natural systems. Infiltration capacity reduces with the expansion of impermeable surfaces. With installation of piped sewage systems the quality of natural retention in the catchment areas are reduced.

With increasing urbanization there are changes in the floodplain elevations which is a cause for urban floods. Infiltration capacity of the ground is reduced during summer time. In urban areas sudden rains are common in summer which is a result of the Urban Heat Island effect.

Bangalore city has in recent times been facing the problem of urban floods with many low lying areas flooding in a matter of few hours which have been mainly due to short bursts of rainfall with high rate of precipitation.

Koramangala Valley	**Hebbal Valley**	**Challaghatta Valley**	**Vrushabhavathi**
City Market Area	Brindavananagar below Matthikere Tank Market	Millers Tank, Chinnappa Garden	Gubbanna Layout
Sulthan Palya Main Road	KEB Compound Maththikere	Shivajinagar, Munireddy Palya	Shankarappa Garden Gopalapura
Jayanagar 3rd Block LIC Colony	Tannerana Halli	Saraswathipuram - Jogu Palya	Cholurpalya
Krishnapa Garden	Anandanagara	K R Garden	Bapujinagar
Arekempannahalli	Ring Road	Millers Tank, Chinnappa Garden	Minerva Mill
Jurist Colony	New - Bangalore Layout		Dhovi Colony
Marehalli Tank	Brindavananagar below Matthikere Tank Market		Tank Slum Area
Bismillanagar - Agencies			Binny Mill Tank Area
Pillappa Garden			Markandayyanagar
Arekempannahalli Area			Sanjaya Gandhi Slum Area
Jurist Colony			Rudrapa Garden
Marehalli Tank			Gubbana Layout

Table 1: Low lying and Floodprone areas in Bangalore.

Urban Heat Island Mitigation Strategies

Strategies for reducing Urban Heat Island effects include

- Vegetation
- Urban Geometry
- Water bodies & Features
- Materials & Surfaces
- Shading

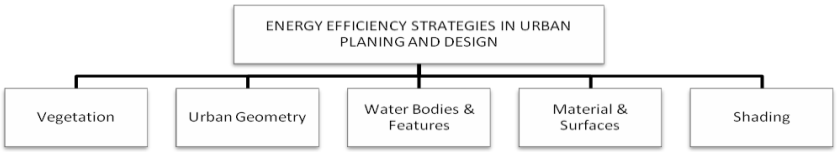


Figure 4. Energy Efficiency Strategies in Urban Planning and Design

Vegetation

As a mitigation strategy of 'urban heat island'(UHI) effect, Vegetation has extensively been used worldwide. High albedo and low heat admittance that have the effect of reducing accumulation of incoming solar energy in the urban area are the properties of vegetation. Additionally, to improve thermal comfort certain types of vegetation such as trees which can provide shade may be incorporated to reduce the heat gain from solar radiation. Also, the energy consumption for indoor cooling purpose can be reduced by the ambient air temperature reduction and building shading by vegetation.

Vegetation can be divided into three categories such as

i) Planting greeneries
ii) Parks and Open Spaces
iii) Green Corridors

Urban Geometry

The arrangement of various elements such as the building layout, the location of urban elements, the building height and geometry are variables that condition the thermal performance of the urban area and affects the spatial coverage of the shadowed areas as well as the wind environment

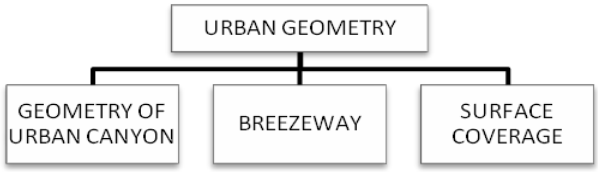


Figure 5. Types of Urban Geometry

Water bodies & Features

To improve the overheating of building environments to some extent Water bodies and features may be incorporated as countermeasures. The effect of water is related to its surface

temperature, which does not increase as much asthe rest of the urban area. Thus, it can be considered as a cool sink. Ponds are an accumulation of water that prevent the overheating of urban surfaces. They can be located on ground floor areas or on building roofs.

Water bodies are essentially of two types

i) Natural
ii) Manmade

Materials & Surfaces

The Urban climate and thermal balance of a city may be affected by the change in urban surface and materials. Cool pavements could be obtained by implementing lighter coloured asphalt on streets and roads and also by the use of cool tiles or special coatings on urban pavements. Materials and Surfaces in an urban environment mainly includes those of

i) Streets
ii) Open Spaces
iii) Buildings

Shading

Shading leads to the reduction of air and surface temperature and can therefore result in cooling. It is relevant during daytime, especially around noon when the sun angles are at the highest.

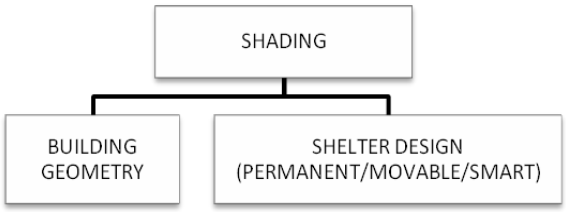


Figure 6 :Methods of Shading

Green Infrastructure Strategies to counter Urban Heat Island Effect

Green infrastructure is an important aspect of planning along with grey infrastructure, social infrastructure and other physical infrastructure. It refers to planned network of green spaces according to the Countryside Agency which can help to combat climate change as well as act as important components for disaster mitigation. It can also significantly reduce the Urban Heat Island Effect.

Countries like Singapore have been successful in creating efficient green infrastructure which helps to reduce urban heat island, cater to water requirements of the population and also prevent instances of flooding through a well defined system of collection, storage , conveyance and reuse of rain water.

Green infrastructure also serves other purposes including promotion of biodiversity, provide important lung spaces in the city and improve quality of life of its inhabitants. They also act as important places for recreation in the city and improve well being of the residents.

It consists of 'hubs and links' and should connect the whole city together. They can also become important economy generators. Green infrastructure planning if done properly can act similar to natural drainage system and help in recharge of groundwater as well as rejuvenation of existing water bodies.

Green Infrastructure strategies can also include

i) Urban Afforestation
ii) Increasing Pedestrianisation and enouraging bicycling

Green Infrastructure Strategies uses the combination of two main UHI mitigation measures – the use of vegetation and water bodies. In the Bangalore context, the existing kere system can be developed into an efficient blue green infrastructure combining both these features which will also help to preserve the remaining water bodies. The existing kere system of Bangalore can be effectively utilized to reduce UHI and create a green infrastructure network in the city. This in turn can become pedestrian and bicycling networks effectively reducing the carbon footprint in the city.

Current Scenario in Bangalore

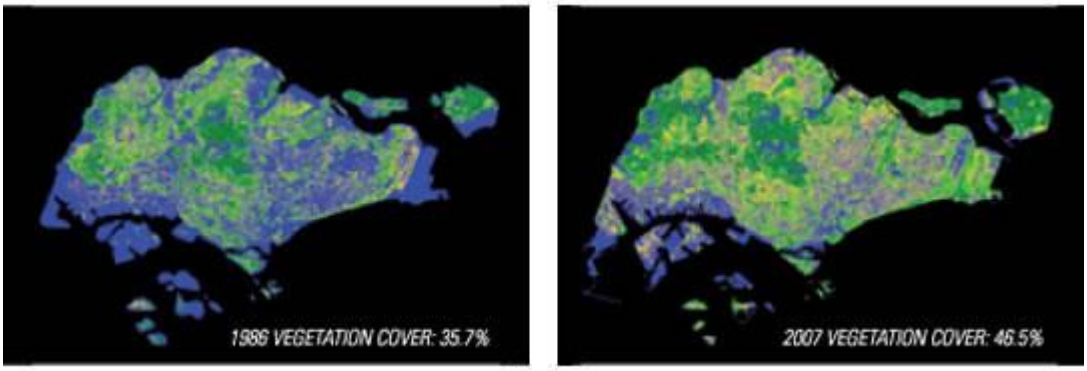
Bruhut Bangalore Mahangara Palike (BBMP) is set to receive 250 crores for rejuvenation of lakes within the city limits. The Bangalore Development Authority (BDA) and BBMP has mainly been involved in desilting the lakes along with fencing and making jogging tracks around the lakes. But the work has been slow and there is a need for spending money on maintenance of these cleaned up lakes along with the money spend on developing lakes. Lot of times sewage continues to be discharged in the rejuvenated lake thus interfering with all the work that has been done. In many cases the sewage is diverted to the lake downstream as the lake is getting rejuvenated which results in more pollution in the downstream lakes such as Bellandur and Varthur lakes.

There have been several citizen groups which have been involved in lake rejuvenation works in Bangalore such as The Lake Revivers Collective and The Better India. It is easier to clean up and revive lakes in the suburbs with lesser inflow of sewage compared to lakes inside the city which have more discharges polluting them. There is a need for a collective effort in the lake rejuvenation efforts and it is necessary to see each lake as a part of the larger watershed area. It is not enough to rejuvenate lakes separately without giving consideration to the overall network of *keres*.

The tree plantation drives organized by citizen groups in the city have done little with the green cover in the city coming down from 68% in 1973 to a mere 6% in 2017 according to a recent study conducted by IISC. Much has to be done to increase the green cover in the city.

Case Study of Singapore

Singapore is a densely populated country with an area of 722.5 sq kms is almost the same size of Bangalore. The population in Singapore has grown by 68% between 1986 and 2007. At the same time the green cover in the city has increased from 35.7% to 47.5%.



Source: NParks

Singapore has achieved this through a visionary approach to increase green cover which has also been incorporated in the Master plan of 2003 which envisioned a 15 year strategy. Singapore has implemented the park connector network by connecting the smaller and larger parks and providing recreational corridors for its citizens, this has also helped to expand the green cover in the city. Currently the city has 0.8 hectares of park space for every 1000 population.

Singapore is a very good example in the implementation of green infrastructure strategies which include increasing the green cover as well as the area of water bodies for reducing the urban heat island effects. Unlike Bangalore Singapore didn't have a system of water bodies and lakes. Singapore which was largely dependent on Malaysia for its water supply has gradually increased the water resources in the country by tapping rain water and increasing its reservoirs.

Singapore has also made huge strides in green building technologies and use of alternative energies. And they have managed to go forward in this direction in spite of various problems of urbanization and population pressures due to the political will of the administration and effective urban planning.

Conclusion

Urban Heat Island mitigation strategies are important in order to reduce greenhouse gas emissions and reduce energy consumption in urban areas. Green Infrastructure Strategies which involve increasing the vegetation cover and creating continuous linkages of green spaces can significantly contribute towards Urban Heat Island mitigation.

Bangalore has an existing natural flood control mechanism in the form of its tank system which needs to be recognized, protected and developed. In addition to flood control and disaster mitigation this system when developed into a blue green infrastructure will also enhance the quality of life in the city in addition to providing various economical, ecological and social

benefits. Most importantly conservation of these large water bodies and the green cover around them can significantly cool the localities around them.

It is important to recognize the relevance of the already existing green infrastructure and augment it as required so that it can become an effective method to cooling Bangalore Metropolitan area. The lakes and the sloping terrain of the city create a natural drainage mechanism in the city and it is necessary to implement efficient green infrastructure strategies in accordance to reduce the temperatures in Bangalore and once again transform it into a 'Garden City'. This can only be achieved through policies and legal mechanisms to increase the green cover and protect the water bodies in the city with a strong partnership between the civic authorities and the local community.

References

Ambinakudige, Shrinidhi (2011),Remote sensing of land cover's effect on surface temperatures:a case study of the urban heat island in Bangalore, India.. 1, Mississipi State : Applied GIS, 2011, Vol. 7.

Mohajerani et al(2017), The urban heat island effect, its causes, and mitigation, with reference to the thermal properties of asphalt concrete, Journal of Environmental Management, Volume 197, 15 July 2017, Pages 522-53(https://doi.org/10.1016/j.jenvman.2017.03.095)

Ramachandra T V & Uttam Kumar (2010), Greater Bangalore: Emerging Urban Heat, Island, GIS Development, Volume 14, Issue 01, Jan 2010. (http://www.gisdevelopment.net/application/urban/sprawl/Greater-Bangalore-Emerging-Urban-Heat-Island.htm).

Sudhira (2008). Studies on Urban Sprawl and Spatial Planning Support System for Bangalore, India, 12, May 2008.

T V Ramachandara and P P Mujumdar,(2009) 'Urban floods'

Voogt, James A.(2004), Urban Heat Islands: Hotter Cities. *Actionbioscience.* [Online] 2004. http://www.actionbioscience.org/.

Microclimate analysis of UHI affected areas through wearable monitoring systems: the case study of New York City

Benedetta Pioppi, CIRIAF, Interuniversity Research Center on Pollution and Environment Mauro Felli (Italy)
Ilaria Pigliautile, CIRIAF, Interuniversity Research Center on Pollution and Environment Mauro Felli (Italy)
Anna Laura Pisello, University of Perugia (Italy)

ABSTRACT

Urban heat island (UHI) is the best acknowledged climate-change related phenomenon also because it affects population health conditions in dense urban areas, even exacerbated during heat waves. While most of field studies are performed by means of permanent weather stations, this paper presents an intra-urban microclimate analysis through wearable sensing techniques for monitoring and characterizing granular peculiarities as perceived by urban pedestrians. The study is implemented in four areas of New York City presenting already mitigation techniques. These strategies are specifically analyzed from the pedestrians' perspective, who may walk along parks and sidewalks, to better study real boundary conditions responsible for thermal perception, even in those areas where vehicles are not allowed. A novel cluster analysis procedure is then carried out to perform data-driven identification of urban microclimate peculiarities in relation to its morphology (e.g. urban canyons etc.). Results show a non-negligible dependency from urban configuration both in winter and in summer. Measurements in the high-packed district winter daytime show a drop off of 0.6 °C in air temperature close to small parks. The packed low-rise district presents highest values of CO2, with respect to the other monitored areas both in winter and in summer. The same areas are automatically recognized through the data-driven clustering process. The data-driven approach may be therefore successfully integrated into classic measurements to investigate UHI and heat stress in dense anthropized areas.

Special Issue Journal	:	Urban Climate
DoI	:	https://doi.org/10.1016/j.uclim.2020.100716
Citation	:	Pioppi, B., Pigliautile, I., & Pisello, A. (2020). Human-centric microclimate analysis of Urban Heat Island: Wearable sensing and data-driven techniques for identifying mitigation strategies in New York City. Urban Climate, 34, 100716.

Local Climate Zone Classification and Seasonal Variation by using Land Surface Temperature: A case of National Capital Territory, Delhi, India

Manoj Panwar[1]*, D.C.R University of Science and Technology Murthal (India)*
Avlokita Agrawal, Indian Institute of Technology Roorkee, Roorkee (India)
Varuvel Devadas, Indian Institute of Technology Roorkee, Roorkee (India)

ABSTRACT

Local Climate Zones (LCZ) are a well-established concept in cities of the developed world and is beneficial for quantification of both spread and backwash effects in the system, forecasting the future under different scenarios and simulating the mitigation strategies for climate change adaptation. Temperature differentiation in LCZ classification (ΔT_{LCZ}) is considered a more appropriate, reliable and robust measure to analyze the magnitude of spatial temperature variations than temperature differentiation of urban and rural (ΔT_{u-r}). The seasonal behaviour of ΔT_{LCZ} is still to be established. Urban morphology of Indian cities is quite different from European and American cities due to non-uniform geometric and surface cover properties. The present work investigates the ΔT_{LCZ} based on the LCZ classification system and the seasonal behaviour of Land surface temperature (LST) for the National Capital Territory (NCT) Delhi, India. The Landsat 8 imageries of NCT Delhi are analyzed for the year 2016 and 2017, downloaded from USGS earth explorer, for the purpose of LST retrieval by using well-established single-window LST algorithm. A sample of 91 subsets, nearly uniform shape and size of 1 km^2 are classified by considering built-up, vegetation, water, and other classes, and are further categorized based on land-cover, built-up density, average building height and their closely matching LCZ. The spatial distribution of sample subsets is kept uniform for all classes to represent the entire study area. Variations of ΔT_{LCZ} and LST in the same LCZs ($\Delta T_{LCZ-LST}$) for all the subsets are quantified and comparative analysis is done a season-wise comparison between ΔT_{LCZ} and $\Delta T_{LCZ-LST}$ for all present climates in the study area. A seasonal variation of intensity ranging from 1.15^oC (airport site) to 4.78^oC (agricultural sample sites) with an average variation of 2.14^oC is observed in $\Delta T_{LCZ-LST}$. The paper concludes with the significance of seasonal $\Delta T_{LCZ-LST}$ in urban planning.

Keywords: *Local Climate Zone (LCZ) classification; Land Surface Temperature (LST); Seasonal Temperature Differentiation; Delhi*

INTRODUCTION

The temperature of a specific location is a function of energy exchanges over that space. Land-use land-cover, morphology and anthropogenic activity of that location affect the intensity

[1] Corresponding Author: [ar.manojpanwar@gmail.com]

of the energy exchanges. Urban Heat Island (UHI) is being measured as a temperature (energy exchange) difference between urban and rural settings (Tim R. Oke, 1987). Urbanization is a dynamic process over space. These urban and rural spaces have different degrees of dynamism associated with them both in space and time. The boundaries and intensity of land-uses land-covers and anthropogenic activities change over a period. The process of urbanization engulfs spaces, which were rural at one point in time. In addition, there remains high variability in urban and rural sites of reference. So, the temperature differentiation, among different land-use land-covers, and different compositions within a single type, across the world, has yielded better results in a dynamic situation of urbanism as compared to temperature differentiation of urban and rural ($\Delta T_{u\text{-}r}$). There have been regular attempts to classify local climates in different zones (Cahndler, 1965) (T. R. Oke, 2004); (Bechtel, 2011); (Bechtel & Daneke, 2012); (Stewart & Oke, 2012); (Perera, Emmanuel, & Mahanama, 2012) (Quan, Dutt, Woodworth, Yamagata, & Yang, 2017); (Kotharkar & Bagade, 2017); (Perera & Emmanuel, 2018) . The LCZ classification proposed by Stewart & Oke (2012) is widely accepted latest and has been very well adopted by different researchers across the world including World Urban Database and Access Portal Tools (WUDAPT) project, which is further used in numerous studies for LCZ classification. Classification of the urban morphology of urban areas in developing and underdeveloped countries is not very clear, so, Kotharkar & Bagade (2017); Perera & Emmanuel (2018) have suggested the development of detailed separate LCZ classification scheme. The UHI intensity varies with the change in the season due to variations in wind speed and water content available in different surfaces and atmosphere (Panwar, Agarwal, & Devadas, 2018). The authors have not come across any study on temperature differentiation behaviour of LCZ classes over different seasons. Therefore, the present investigation presents spatial and seasonal Inter & Infra-LCZ temperature variability as per LCZ and LST derived from Landsat 8.

BRIEF ABOUT STUDY AREA

The National Capital Territory (NCT) of Delhi, one of the seven Union Territories of India, has been selected for the study. Delhi, the capital city of India, is part of the study area. The study area under consideration is located at 28.7041° N 77.1025° E (Fig. 1 a & b). It has a geographical area of 1484 sq. km, surrounded by the States of Haryana and Uttar Pradesh. Delhi attracts in-migration from the entire nation for employment opportunities, as it is the political centre and major economic hub of India. Delhi is growing in almost all aspects because of the aforementioned reason.

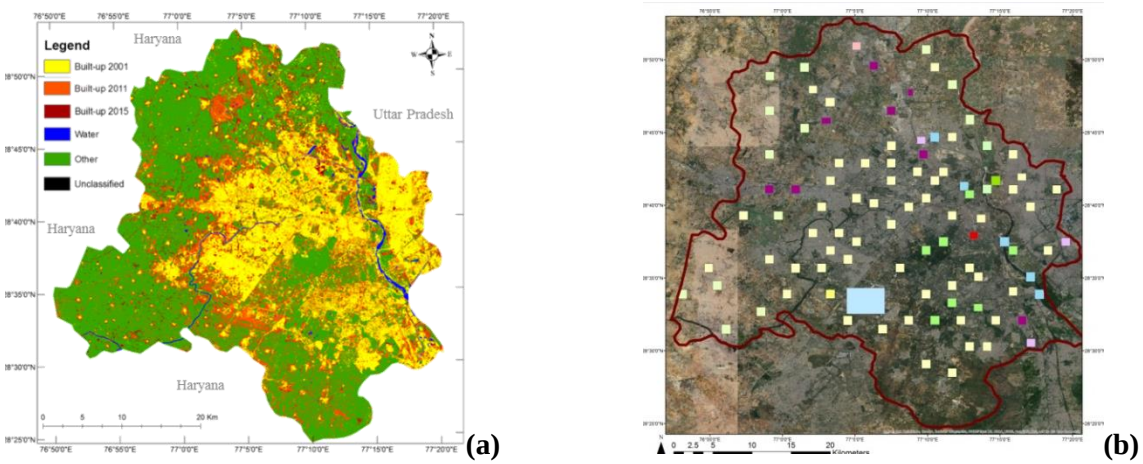


Fig. 1: (a) Spatial growth of urbanization in the NCT of Delhi. (b) Study area showing all the subsets used in the present investigation.

The built-up area & density, and energy consumed by different sectors are increasing at an exponential rate, and haphazard growth is adding to a vicious cycle. In accordance with Köppen climate classification, Delhi has climate overlapping humid subtropical (Cwa) and Semi-arid (BSh) climates. The study area is blessed with summer, monsoon, autumn, winter and spring seasons. The spatial sprawl and type of sprawl make Delhi the ideal case for analyzing the $\Delta T_{LCZ\text{-}LST}$.

CURRENT INVESTIGATION

Landsat 8 Imagery downloaded from https://earthexplorer.usgs.gov/ provide by NASA are used for this present study. Since, the objective of the research is to analyze the seasonal variations over LCZ, two year time period i.e. two years (2016 and 2017) kept is very short (so that the development within this period remains very little) and enough to capture all the seasons. Less than one per cent cloud cover criterion is used for selection of imagery for path 146 row 40 scene of Landsat 8 encompassing the study is for the previously mentioned period. Weather data, matching overpass time of Landsat 8, has been obtained from NCDC of NASA website https://www.ncdc.noaa.gov/ for weather station no. 421810 for Safdarjung Airport, New Delhi. The details of the data used for this research is presented in table 1. The methodology adopted for the present investigation is presented in Fig. 2. Authors are well versed with the study area. Land-use Map for the period 2011-12 is available in BHUVAN portal. However, the preliminary earmarking of the subsets has been done on Google earth (Fig. 1b) using the author's knowledge representing different land-cover land-use and morphology within single land-use representing entire Delhi. The 3D maps of the sub-sets are prepared to analyze rise and compactness (the generated data will be further used as training data set for LCZ mapping of entire NCT Delhi in near future). Google earth data is used for preparing the base map for the physical survey to analyze the LCZ of different subsets.

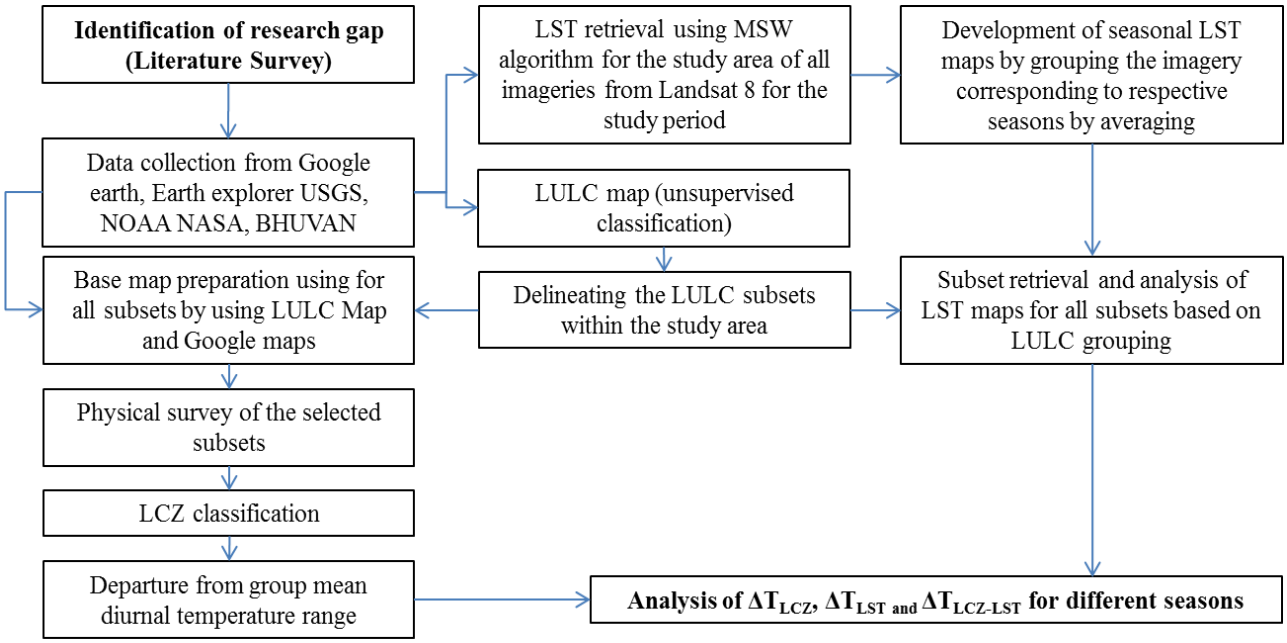


Fig. 2: Methodology used in the present investigation

Table 1. Data used for the study

Sl. No.	Landsat 8 Imagery Acquisition Date *	Seasonal classification for calculation of LST@	Actual classification #	Temperature (°K) at 11:00 AM $	Humidity (RH) $
1	30.01.2016	Winter	Winter	299.3	40.4
2	21.05.2016	Summer	Summer	315.4	16.1
3	12.10.2016	Winter	Autumn	307.0	27.5
4	28.10.2016	Winter	Autumn	304.8	18.5
5	13.11.2016	Winter	Autumn	302.0	28.2
6	21.03.2017	Summer	Spring	306.5	20.5
7	06.04.2017	Summer	Summer	310.9	17.9
8	24.05.2017	Summer	Summer	314.3	23.1
9	25.06.2017	Summer	Summer	313.2	35.0
10	29.09.2017	Summer	Monsoon	309.3	43.1
11	15.10.2017	Winter	Autumn	309.3	27.7
12	02.12.2017	Winter	Winter	297.6	28.6

Source: *USGS Earth Explorer; @ Classification used for various calculations in IMW algorithm; # (Delhi Tourism Department, 2018); $NCDC NASA

LST retrieval

Improved Mono Window (IMW) algorithm (Eq. 1 – Eq. 11) is proposed by Wang et al. (2015). Authors have adopted this algorithm for retrieval of LST for the NCT of Delhi. The study area has been considered as a flat surface for the calculation of LST. The atmosphere for the study area is considered as the mid-latitude atmosphere. All imagery has been classified in summer and winter seasons for applying respective effective mean atmospheric temperature equation for the mid-latitude atmosphere of the study area. Air density and saturation of water vapour to air is

calculated by using the respective air temperature given in Table 1. The values of constants and rescaling factors to be used for the analysis of LST from Landsat8 imagery by using the IMW algorithm as given by USGS, and are presented in table 2.

Table 2: Values of constants, rescaling factors used in IMW algorithm

Temperature Range	constants to an approximate derivative of the Planck radiance function for the TIRS Band 10		Multiplicative rescaling factor for TIRS Band 10	Additive rescaling factor for TIRS Band 10	Thermal conversion constants for Band 10	
	a_{10}	b_{10}	M_{10}	A_{10}	K_1	K_2
0°C - 50°C	-62.7182	0.4339	3.342×10^{-4}	0.1	774.89	1321.08

Source: https://earthexplorer.usgs.gov/ metadata file

Improved Mono Window (IMW) algorithm

$$T_s = [a_{10}(1 - C_{10} - D_{10}) + (b_{10}(1 - C_{10} - D_{10}) + C_{10} + D_{10})T_{10} - D_{10}T_a]/C_{10} \quad (1)$$

T_s is LST in degree Kelvin from Landsat 8 band 10; T_a is effective mean atmospheric temperature; T_{10} is brightness temperature band 10 of Landsat 8; C_{10} and D_{10} are internal parameters based on atmospheric parameters and ground emissivity;

$$C_{10} = \tau_{10}\varepsilon_{10} \quad (2)$$

$$D_{10} = (1 - \tau_{10})[1 + (1 - \varepsilon_{10})\tau_{10}] \quad (3)$$

τ_{10} and ε_{10} are atmospheric transmittance and ground emissivity

$$R_{10} = M_{10}Q_{10} + A_{10} \quad (4)$$

R_{10} is the spectral radiance of band 10 for Landsat 8 and Q_{10} is the DN value for pixels of band 10

$$T_{10} = \frac{K_2}{\ln(1+(K_1/R_{10})} \quad (5)$$

$$E = 3.7096\, e^{0.0663\, T_o} \qquad \{-20C^o \le T_o \le 45C^o\} \quad (6)$$

$$A = -0.0042\,T_o + 1.2936 \quad \{-20C^o \leq T_o \leq 45C^o\}$$
(7)

$$w(0) = E * A * H/1000$$
(8)

w is total water vapour content; E is the saturation mix ratio of water vapour and air at a specific temperature; A is air density at specific air temperature and H is the air humidity at the ground.

$$w = \frac{w(0)}{Rw(0)} \; (The\ value\ of\ Rw(0)\ considered\ for\ mid\ latitude\ winter\ is\ 0.6365)$$
(9)

$$\tau_{10} = 0.9228 - 0.0735\,w$$
(10)

The effective mean atmospheric temperature is calculated using Eq. 11.

$$T_a = 19.2704 + 0.9112\,T_o$$
(11)

Global values for Normalized Difference Vegetation Index (NDVI) for soil and vegetation ($NDVI_s$=0.2 and $NDVI_v$= 0.5) are used for emissivity calculation.

Deviation in LST for different land-uses and LCZ

The $\Delta T_{LCZ\text{-}LST}$ has been derived by analyzing the mean ΔT_{LST} for individual subsets and then aggregating the $\Delta T_{LCZ\text{-}LST}$ for subsets belonging to same LCZ class within a particular land-use (Eq. 12 & Eq. 13). The iterations have been done for all imageries used for summer, monsoon, autumn, winter and spring seasons.

$$\Delta_{LST} = LST_i - LST_{Min}$$
(12)

$$\Delta_{LCZ-LST_{ijk}} = \sum_{i=0}^{n} \frac{\frac{\sum_{j=0}^{m} \Delta_{LCZ-LST}}{m}}{n} - \sum_{i=0}^{n} \frac{\Delta_{LCZ-LST}}{n}$$
(13)

i - *No. of same LCZ classes belonging to k^{th} land-use*
j - *No. of images used for LST analysis*
k - *Land-uses considered in different subsets*

RESULTS AND DISCUSSION

The authors have done an extensive literature survey, reviewed the literature and observed the findings. However, the findings observed in the present investigation are very different from the findings, which were earlier observed. The findings of the present investigation revealed an additional component to the existing research, which was not investigated earlier. The major findings observed are presented below:

The variations in intensities of LST are clearly visible both with the change in land use land cover and with the change in season. The surfaces with lower moisture content show a higher temperature. Highest intensities are observed in built-up land cover followed by subsets having a mix of soft and hard land covers and then finally in unbuilt land covers. The land covers those show lower variations in ephemeral properties with seasonal changes observed fewer ΔT_{LST} variations with the change in season. The evapotranspiration from atmospheric moisture comes into play after the surface moisture. The availability of vegetation, which has the capability of shading the surfaces, i.e. high moisture content atmospheric zones shows lower temperature both surface and atmosphere. The order of intensity of LST in built-up, mix and unbuilt land covers are governed by land use. The planned urban residential subsets show lower LST due to the presence of higher tree and forest cover in those subsets. Subsets with water and dense vegetation, i.e., LCZ B and LCZ G (both urban forest and urban green) show the lowest temperature during all seasons. The observed LST (^oC) intensities and standard deviation for different land use land covers in winter, spring, summer, autumn and monsoon are presented in table 3.

The subsets having landfill sites, airport and industries observed consistently higher LST intensities in comparison with the average LST intensity. The LST intensities for landfill sites are 32.31 ^oC, 31.74 ^oC, 35.54 ^oC, 22.56 ^oC, and 30.16 ^oC for Autumn, Monsoon, Summer, Winter, and Spring season respectively. The observed LST for landfill sites is contributed by the burning of solid waste and availability of methane below the top surface of landfill. The LST intensities for airport are 32.50 ^oC, 32.32 ^oC, 36.73 ^oC, 23.56 ^oC, and 30.03 ^oC for Autumn, Monsoon, Summer, Winter, and Spring season respectively. The large hard paved surfaces contribute to the consistent high LST intensity at airport. The LST intensities at industrial sites are due to anthropogenic activities and high energy consumption leading to heat, and the mean intensities of LST in industrial sites are 31.84 ^oC, 31.95 ^oC, 35.35 ^oC, 22.65 ^oC, and 29.23 ^oC for Autumn, Monsoon, Summer, Winter, and Spring season respectively. The LST intensities for roads in the study area has also been observed consistently higher than the average LST intensity. The intensity of anthropogenic activities contributes to higher intensity of LST on roads.

The subsets with agriculture, water, a mix of agriculture and water, forest greens, urban greens, and institutional campus observed intensities of LST consistently lower than the average LST intensities in all seasons except subsets with agriculture land use. The mean intensities of LST in

subsets with agriculture land use are 32.12 ^{o}C, 29.13 ^{o}C, 35.32 ^{o}C, 21.51 ^{o}C, and 23.73 ^{o}C for Autumn, Monsoon, Summer, Winter, and Spring season respectively. The variations in the intensity of LST in agriculture land use is due to the variation in surface moisture content. The mean intensities of LST in subsets with water land cover are 27.79 ^{o}C, 26.68 ^{o}C, 29.34 ^{o}C, 19.95 ^{o}C, and 25.09 ^{o}C for Autumn, Monsoon, Summer, Winter, and Spring season respectively. The mean intensities of LST in subsets with mix of water and green land cover are 28.72 ^{o}C, 26.92 ^{o}C, 30.92 ^{o}C, 20.77 ^{o}C, and 23.70 ^{o}C for Autumn, Monsoon, Summer, Winter, and Spring season respectively. The observed lower intensities of LST in land covers as water, agriculture and green, and mix of these, are due to availability of moisture content for evapotranspiration during all seasons.

The detailed analysis of residential land use provides information about intensity of LST as a function of built-up density and availability of greens. The intensity of LST in rural and urban residential land use remain fluctuating in different seasons but intensity of LST in rural subsets always remain lower than urban counterparts. The mean intensities of LST in subsets with rural settlements are 29.58 ^{o}C, 30.15 ^{o}C, 34.06 ^{o}C, 21.18 ^{o}C, and 26.12 ^{o}C for Autumn, Monsoon, Summer, Winter, and Spring season respectively, however, the mean intensities of LST in subsets with residential land use in towns are 30.51 ^{o}C, 31.58 ^{o}C, 34.93 ^{o}C, 21.05 ^{o}C, and 27.69 ^{o}C for Autumn, Monsoon, Summer, Winter, and Spring season respectively. Within residential land use the LST intensities for farmhouses are always lower, however, high-rise apartments have been observed closer to the average intensities of LST for entire study area. The intensities of LST for farmhouses are 29.06 ^{o}C, 28.55 ^{o}C, 32.40 ^{o}C, 19.62 ^{o}C, and 26.37 ^{o}C for Autumn, Monsoon, Summer, Winter, and Spring season respectively.

Table 3. Season-wise Mean LST (^{o}C) and Standard Deviation for all subsets grouped for different LULC

Land use Land cover	Residential (Rural)	Residential (Town)	Residential (Urban - Unplanned)	Residential (Urban Planned) Midrise	Residential (Urban Planned) High-rise	Residential (Urban Planned) Farmhouses	Industrial	Comm-ercial
	1	2	3	4	5	6	7	8
No. of Sites	3	2	10	28	2	4	9	1
Season	LST (SD) Mean	LST (SD) Mean	LST (SD) Mean	LST LST Mean	LST (SD) Mean	LST (SD) Mean	LST (SD) Mean	LST
Autumn	29.58 (0.33)	30.51 (0.30)	30.12 (0.45)	29.37 29.87	29.73 (0.12)	29.06 (0.19)	31.84 (0.43)	29.87
Monsoon	30.15 (0.69)	31.58 (0.86)	30.96 (0.63)	29.64 30.52	29.60 (0.33)	28.55 (0.42)	31.95 (0.53)	30.52
Summer	34.06 (1.22)	34.93 (0.25)	34.55 (0.64)	33.12 33.34	34.26 (0.03)	32.40 (0.38)	35.35 (0.65)	33.34
Winter	21.18 (0.48)	21.05 (0.05)	20.77 (0.41)	20.43 20.52	21.44 (0.11)	19.62 (0.91)	22.65 (0.72)	20.52
Spring	26.12 (0.57)	27.69 (0.17)	27.47 (0.64)	26.85 27.30	27.87 (0.11)	26.37 (0.43)	29.23 (0.91)	27.30

Land use Land cover	Institutional	Air-port	Agriculture	Agriculture + Water	Water	Forest Green	Urban Green	Landfill Sites
	9	10	11	12	13	14	15	16

No. of Sites	1	1	2	10	28	2	4	9
Season	LST	LST	LST (SD) Mean	LST (SD) Mean	LST (SD) Mean	LST (SD) Mean	LST (SD) Mean	LST (SD) Mean
Autumn	28.89	32.50	32.12 (3.28)	28.72 (0.77)	27.79 (0.32)	27.56 (0.67)	27.68 (0.49)	32.31 (0.47)
Monsoon	28.56	32.32	29.13 (2.83)	26.92 (0.16)	26.68 (0.72)	25.97 (0.86)	26.81 (0.54)	31.74 (0.41)
Summer	32.78	36.73	35.32 (1.96)	30.92 (0.39)	29.34 (1.03)	32.25 (1.73)	31.07 (1.27)	35.54 (0.22)
Winter	20.09	23.56	21.51 (0.94)	20.77 (0.45)	19.95 (0.60)	21.07 (0.73)	20.30 (1.01)	22.56 (0.14)
Spring	26.80	30.03	23.73 (1.63)	23.70 (2.11)	25.09 (0.84)	26.75 (1.26)	25.91 (2.07)	30.16 (0.56)

The results of $\Delta T_{LCZ\text{-}LST}$ after averaging the subsets pertaining to different LCZ classes and in comparison with the ΔUHI_{LCZ} recorded by Stewart & Oke (2012) and Perera & Emmanuel (2018) in Table 4. The seasonal variation of intensity 1.58ºC and 3.07ºC are observed in ΔT_{LST} over built-up and counterparts area in the study area. A seasonal variation of intensity ranging from 1.15ºC (over fully paved airport site) to 4.78ºC (average over agricultural sample sites) with an average variation of 2.14ºC is observed in temperature differentiation over different land-cover land-uses. This difference is due to continuous burning on landfill sites, use of concrete surfaces without shade at airport and use of high albedo CGI sheets in industrial areas but the variation in the intensity of ΔT_{LCZ} is low due to very little changes in the ephemeral properties of the surface. The subsets over agricultural land have high variability, which is because of the variations in vegetation cover and soil moisture content. Subsets showing LST over institutional and commercial land-uses show lower LST values. The institutional subsets have good tree cover, whereas the commercial has a central grass surface. The numbers of subsets analyzed are less in number, so further investigation is required.

Table 4: Season-wise ΔTLCZ-LST in the present investigation and UHILCZ presented in the literature

				Departure from Average (ºC)					Departure using LCZ classification (ºC)	
Sr. No.	LCZ Classification	LULC	No. of Samples	Autumn	Monsoon	Summer	Winter	Spring	(Stewart & Oke, 2012)	(Perera & Emmanuel , 2018)
1a	LCZ 7C	Residential (Rural)	3	-0.86	0.70	-0.02	-0.06	-0.70	1.50	0.31
1b	LCZ 3F	Residential (Town)	2	0.06	2.13	0.85	-0.20	0.87	0	3.19
1c	LCZ 3E	Residential	10	-0.32	1.51	0.47	-0.48	0.65	-	3.19
1d	LCZ 5	Residential	28	-1.07	0.19	-0.96	-0.82	0.03	4.00	3.71
1e	LCZ4	Residential	2	-0.72	0.15	0.18	0.19	1.05	-	4.35
1f	LCZ9	Residential	4	-1.39	-0.90	-1.68	-1.63	-0.46	0.30	-
2	LCZ10	Industrial	9	1.40	2.50	1.27	1.40	2.41	5.50	-
3	LCZ 8	Commercial	1	-0.57	1.07	-0.74	-0.73	0.48	1.80	1.10
4	LCZ 5	Institutional	1	-1.55	-0.89	-1.30	-1.16	-0.02	4.00	3.71

5	LCZ 8E	Public & semi-public (Airport)	1	2.06	2.87	2.65	2.31	3.21	-	1.04
6	LCZ F	Agriculture	12	1.68	-0.32	1.24	0.26	-3.10	-9.50	-0.90
7	LCZ FG	Agriculture + Water	2	-1.73	-2.53	-3.17	-0.48	-3.13	<-9.5	NA
8	LCZ G	Water	4	-2.65	-2.77	-4.74	-1.30	-1.73	-	0.62
9	LCZ A	Forest Green	5	-2.88	-3.48	-1.83	-0.17	-0.07	-7.20	-0.12
10	LCZ B	Urban Green	4	-2.76	-2.65	-3.02	-0.95	-0.91	-7.20	-0.09
11	LCZ 10	Landfill site	3	1.87	2.29	1.46	1.31	3.33	-	NA

The morphological characteristics of the study area are entirely different from the existing classes of LCZ proposed by Stewart & Oke (2012) or any other scholar due to differences in nature of the economic and spatial development of the settlement. LCZ classification a very good concept for doing the prima-facie analysis for a lot of users need but further development especially for unplanned urban areas as they don't have classes even near matching to existing classes of LCZ proposed by Stewart & Oke (2012) or any other scholar. Furthermore, the LST based temperature departure differentiation is used for the first time in the LCZ study. The relationship between $\Delta T_{LCZ\text{-}LST}$ and ΔT_{LCZ} couldn't be established due to the non-matching of LCZ classes and lack of $\Delta T_{LCZ\text{-}LST}$ data of the existing published research. The observed seasonal variation in $\Delta T_{LCZ\text{-}LST}$ offered research question for the scholars in this field of study and need for addressing such issue. Season wise ΔT_{LST} for studied land use land covers are presented in Fig. 3.

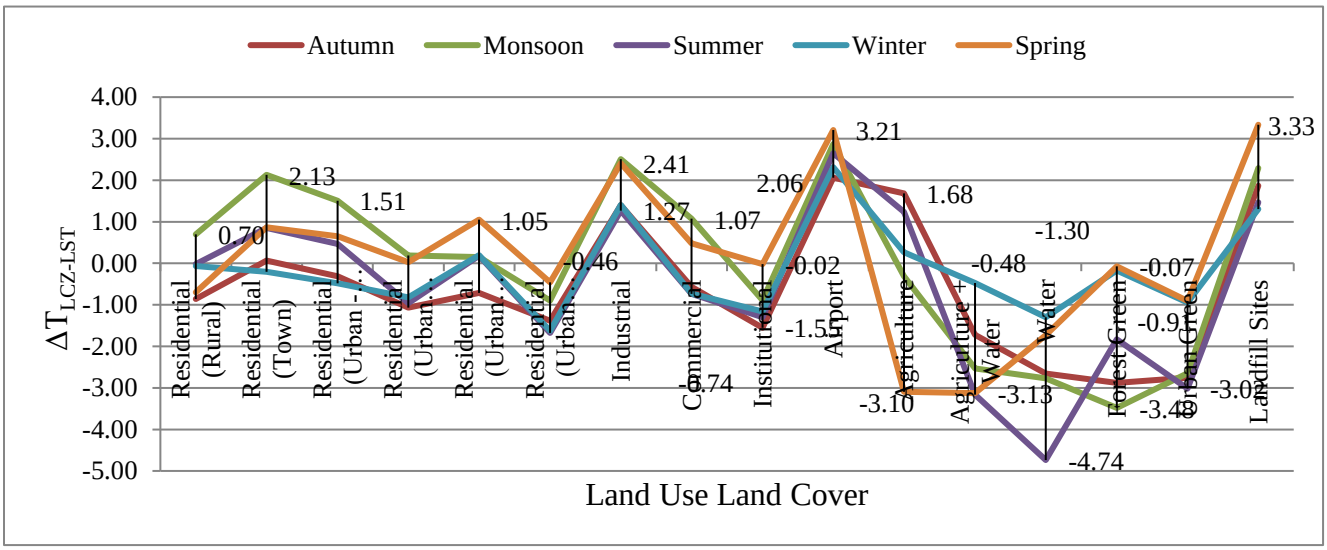


Figure 3. Season-wise LST departure from average LST for different Land Use Land Covers

Generally, planning for the development of the urban system the authors used to consider physical subsystem, social sub-system to some extent and infrastructure sub-system. The Brundtland Commission published the sustainable development concept in the year 1987, since then environmental sub-system is considered as a pillar of sustainable development along with social and economic. To quantify the environment sub-system and its functions in the urban system, the present research, which is an attempt by the authors, is very much essential. The present research focuses on the quantifying the variations in the LST in different seasons along

with land-use land-cover and its comparison to LCZ based temperature differentiation. The land-use in the urban system varies based on the functional character of the urban system. It may be observed that the functional character of the urban system will differ from one urban system to another urban system, even within a state, region or country. The LST varies from one area to another area in urban system, which alters the functions of the urban system and impacts the entities of the urban system. The variation in LST differentiation over different seasons will provide boundary conditions for doing sensitivity analysis in seasonal and spatial dimensions in urban planning.

CONCLUSION

The present investigation uses LST retrieved by using IMW algorithm as a tool for the analysis of seasonal temperature differential for the 91 subsets covering different land-use land-cover spread across the study area of NCT Delhi. The temperature differentiation obtained by using the retrieved LST in different LULC is compared with the LCZ based temperature differentiations. The papers conclude that the classification of the urban morphology of unplanned urban areas in developing and underdeveloped countries is not very clear. Different LCZ classes are showing variations in LST differentiation but the quantification of the relationship between LCZ based temperature differentiation and LST temperature differentiation could not be established due to non-matching of LCZ classes and lack of LCZ based temperature differentiation data. LCZ based UHI provides Canopy Layer UHI whereas LST is a surface phenomenon, the development of LCZ for entire NCT Delhi and installation of AWS for analysis of air temperature will unfold relationship between $\Delta UHI_{LCZ,}$ field measurements and $\Delta UHI_{LCZ\text{-}LST}$. The depiction of ΔUHI_{LCZ} in range format is a better option for generalization of the results to be applicable to a larger number of settlements, and also for capturing the season-wise variations in same settlement. Further, a detailed investigation in this field of research is proposed for future work.

ACKNOWLEDGEMENT

Authors are thankful to D.C.R. University of Science & Technology, Murthal (India), Indian Institute of Technology Roorkee (India) and All India Council of Technical Education, Ministry of Human Resource and Development, India for allowing this research under Quality Improvement Programme Scheme. Authors are also thankful for the reviewers for their worthy comments on the manuscript, which help in the improvement of the presentation and content.

REFERENCES

Bechtel, B. (2011). Multitemporal Landsat data for urban heat island assessment and classification of local climate zones. In *Joint Urban Remote Sensing Event 2011* (pp. 129–132). Munich, Germany. https://doi.org/10.1109/JURSE.2011.5764736

Bechtel, B., & Daneke, C. (2012). Classification of local climate zones based on multiple earth observation data. *IEEE Journal of Selected Topics in Applied Earth Observations and Remote Sensing*, *5*(4), 1191–1202. https://doi.org/10.1109/JSTARS.2012.2189873

Chandler, T. J. (1965). *The Climate of London* (1st ed.). London: Hutchinson & Co Ltd.

Delhi Tourism Department. (2018). :: Seasons of Delhi :: Retrieved May 5, 2018, from http://www.delhitourism.gov.in/delhitourism/aboutus/seasons_of_delhi.jsp

Kotharkar, R., & Bagade, A. (2017). Local Climate Zone classification for Indian cities: A case

study of Nagpur. *Urban Climate*, *UCLIM-0028*, 24. https://doi.org/10.1016/j.uclim.2017.03.003

Oke, T. R. (1987). *Boundary-Layer Climates* (2nd.). Routledge.

Oke, T. R. (2004). Initial guidance to obtain representative meteorological observations at urban sites. *World Meteorological Organization*, (81), 51. https://doi.org/Reporte

Panwar, M., Agarwal, A., & Devadas, V. (2018). Analyzing land surface temperature trends using the non-parametric approach: A case of Delhi, India. *Urban Climate*, *24*, 19–25. https://doi.org/10.1016/j.uclim.2018.01.003

Perera, N. G. R., Emmanuel, M. P. R., & Mahanama, P. K. S. (2012). Mapping "Local Climate Zones" and relative Warming Effects in Colombo, Sri Lanka. *ICUC8–8th International Conference on Urban Climates. Dublin, Ireland (6-10 August)*, (Fig 1), 2010–2013.

Perera, N. G. R., & Emmanuel, R. (2018). A "Local Climate Zone" based approach to urban planning in Colombo, Sri Lanka. *Urban Climate*, *23*, 188–203. https://doi.org/10.1016/j.uclim.2016.11.006

Quan, S. J., Dutt, F., Woodworth, E., Yamagata, Y., & Yang, P. P. J. (2017). Local Climate Zone Mapping for Energy Resilience: A Fine-grained and 3D Approach. *Energy Procedia*, *105*, 3777–3783. https://doi.org/10.1016/j.egypro.2017.03.883

Stewart, I. D., & Oke, T. R. (2012). Local climate zones for urban temperature studies. *Bulletin of the American Meteorological Society*, *93*(12), 1879–1900. https://doi.org/10.1175/BAMS-D-11-00019.1

Wang, F., Qin, Z., Song, C., Tu, L., Karnieli, A., & Zhao, S. (2015). An Improved Mono-Window Algorithm for Land Surface Temperature Retrieval from Landsat 8 Thermal Infrared Sensor Data. *Remote Sensing*, *7*(4), 4268–4289. https://doi.org/10.3390/rs70404268

"Inverted" Surface UHI: An artefact of relying solely on Satellite Remote Sensing data for measuring the Urban Heat Island Phenomenon

Prasad Pathak*, *Centre for Earth and Environment, FLAME University, Lavale, Pune, India*
Raja Sengupta, Dept. of Geogrpahy, McGill University, Montreal, CA
Bakul Budhiraja, Dept. of Civil Engineering, Shiv Nadar Univeresity, Greater Noida, India

Abstract:

Traditional definitions of the Urban Heat Island (UHI) effect focus on the observed increase in night time canopy layer air temperatures in an urban core (as measured by ground based weather stations), in comparison to a surrounding rural (usually agricultural or forest) reference. The maximum difference in temperature between rural and urban areas (usually measured in degrees Celsius) is also referred to as the "UHI Intensity". Remotely sensed measurements of "skin" or Land Surface Temperatures (LST) from satellite-borne thermal sensors such as MODIS Terra, MODIS Aqua and Landsat 8, can be used to derive Surface UHI (SUHI). However, solely relying on SUHI for UHI measurements have recently led to observations of "Inverted" UHI phenomenon in Deserts and Semi-Arid conditions (in countries such as UAE and India), where the rural reference is seen to be warmer than the urban core. Such claims of "observing" inverted surface UHI in remotely sensed data should be treated with caution, as they are predominantly the artefact of satellite sensor readings taking during certain periods of the day at specific seasons.

Introduction

The "Urban Heat Island (UHI)" effect is the observed increase in nighttime canopy layer air temperatures of urban built-up areas, in comparison to a surrounding rural reference, as measured by ground-based weather stations (Struetker, 2003). Moreover, the greatest difference in temperatures between the urban and rural air temperature values, known as the Urban Heat Island Intensity (UHI Intensity), tends to occur just after sunset (Oke and East 1971). And this value of UHI Intensity has been correlated with both population (Oke 1973) as well as areal expansion of built up areas (Struetker, 2003). Oke (1973; 1976) showed that during nights with clear skies, an empirical relationship can be defined that relates the value of UHI intensity for a city to the log of its population. Struetker (2003) indicated that this relationship may also be a function of the city's built up area, and showed that the growth of Houston, Texas, over a period of 12 years increased the mean UHI Intensity of the city by 0.8K, or 35% (as measured using nighttime satellite images collected by the Advanced Very High Resolution Radiometer (AVHRR)). Akbari et al. (2001) demonstrated the use of "cool surfaces" and "shade trees" to reduce the effect of UHI in Urban areas.

Over the last three decades, Airborne or Satellite based sensors have become promising approaches to give an integrated value of the urban `skin' temperature, also called the Land Surface Temperature (LST), which in turn can be used to measure urban-rural difference (Voogt and Oke (1998). Commonly used thermal sensors for LST include those on board AVHRR, MODIS (Terra and Aqua), and Landsat satellites (Ayanlade & Jegede, 2015). While there are known and well documented issues with respect to these measurements (mostly related to biases generated as a consequence of the urban

surface structure in combination with Sun-sensor-surface geometry, particularly when measuring off-nadir surfaces), these methods are nevertheless useful. However, there are discrepancies that arise when comparing remotely sensed urban heat islands (UHIs), also referred to as Surface UHI or SUHI (Clinton & Gong, 2013; Voogt & Oke, 2003), to those derived from more conventional means (Roth et al., 1989). In fact, the correlation between remotely sensed UHIs and temperature measured at the Urban Canopy layer via temperature sensors can be weak, and even inverted. In this regard, Roth (1989) suggests that there are different types of UHIs that can and should be defined, and these can be differentiated by: medium sensed (air, surface, sub-surface); location (surface nature and height); and sensing technique.

To date, the major use of remote sensing has been for estimating land use land cover (particularly the abundance and spatial pattern of impervious surface and green space), and the associated Normalized Difference Vegetation Index (NDVI) as a contributing factor to SUHI (Estoque et al., 2017). Additionally, fusion of Landsat and MODIS data can be used estimate LST with higher spatial accuracy than with MODIS alone (Weng et al., 2014). A more recent trend has been to study the SUHI exclusively through remote sensing, for example, a study of 419 global cities showed positive SUHI with diurnal variations (Peng et al., 2012). The satellite sensors used most frequently for SUHI studies are Landsat series (53%) and MODIS (25%), as presented in Table 1 (Zhou et al., 2019).

Sensor	Landsat Series	MODIS	ASTER	Multiple Sensors	AVHRR	Others [1]
Proportion	53%	25%	7%	6%	4%	5%

[1] SEVIRI, GOES, HCMM, HJ-1B, AATSR, ITOS-1, COMS, FY-2F, AMSR-E, AMSR2.

Table 1: Satellite Sensors used for SUHI studies (from Zhou et al., 2019)

The growth of studies relying exclusively on satellite derived estimations of SUHI have also led to recent papers identifying the occurrence of "Surface Urban Cool Islands" or SUCI (also referred to as Inverted SUHI) in Arid and Semi-Arid conditions (Lazzarini et al., 2013; Shastri et al., 2017) where the surrounding rural reference is cooler than the center of an urban area, particularly at daytime. Lazzarini et al. (2013) identified SUCI during the daytime for the Abu Dhabi Metropolitan area over a 10-year period, when the surrounding rural reference are desert sands. Shastri et al. (2017) similarly observed inverted SUCI for 84 Indian cities during the pre-monsoon months, when the croplands surrounding the cities remain dry and barren (and behave similar to arid regions with minimum vegetation).

We contend that observations of UHI from satellite remote sensing (i.e., SUHI or UHI_{Surf}) alone can results in observations of the SUCI effect, whereas canopy level air temperature sensors (i.e., traditional method of measuring UHI, abbreviated UHI_{UCL} and CLUHI) still show normal UHI. To elucidate our point, we compare measurements of air temperatures from agricultural and rural weather stations to estimate the UHI intensity at Canopy level (CLUHI/UHI_{UCL} intensity) across the diurnal range at different seasons for 2018. We then compare images of Surface Urban Heat Island (UHI_{Surf}) from two different satellites (MODIS Terra and MODIS Aqua) to see if similar temperature differentials are observed across land covers through the diurnal cycle.

Study Areas:

We selected three cities, one in Canada and two in India, that belong to different climatic zones to look at the variations in UHI effect over seasons, and at different times of the day and night. According to the Koppen Climate Classification system (Figure 1 and Table 2), Montreal, Canada, lies in the Humid Continental, Delhi, India lies in Humid Subtropical, and Pune, India, lies in Tropical Savanna climate zones. Land use and UHI (both UHI_{UCL} and UHI_{Surf}) were calculated within a 50km buffer of the center of the city, which was identified as the centroid of urban boundaries obtained from the respective censuses of Canada (Ville Marie for Montreal) and India (Figure 2).

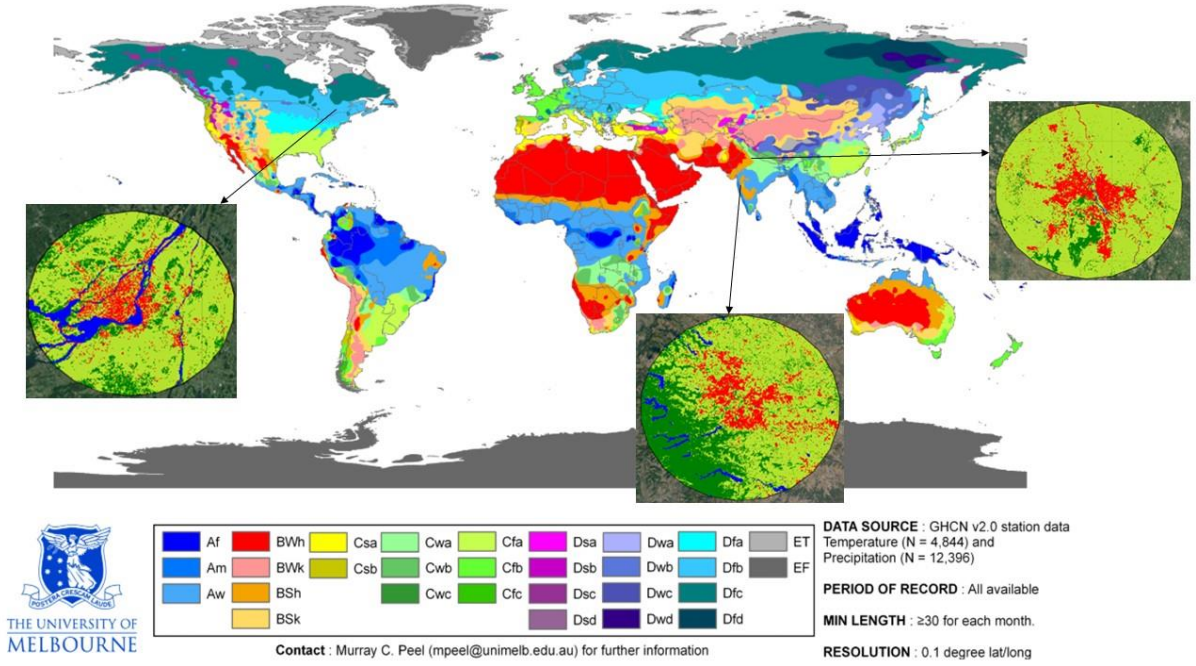


Figure 1: Study area a) Delhi b) Pune c) Montreal overlaid on the Köppen climate classification map of the world (Peel et al., 2007).

City	Köppen climate classification	Seasons	Latitude, Longitude	Population
Montreal	Warm summer continental (Dfb)	Autumn, Winter, Spring, and Summer	45.50^0 N and 73.35^0 W	3 million
Delhi	Subtropical (Cwa) and Semi-arid (BSh)	Spring, Summer, Monsoon, Autumn and Winter	26.61^0N and 77.23^0E	28.5 million
Pune	Tropical savanna (Aw)	Spring, Summer, Monsoon, and Autumn	18.53^0 N and 73.85^0 E	6.2 million

Table 2: Attributes of the three cities

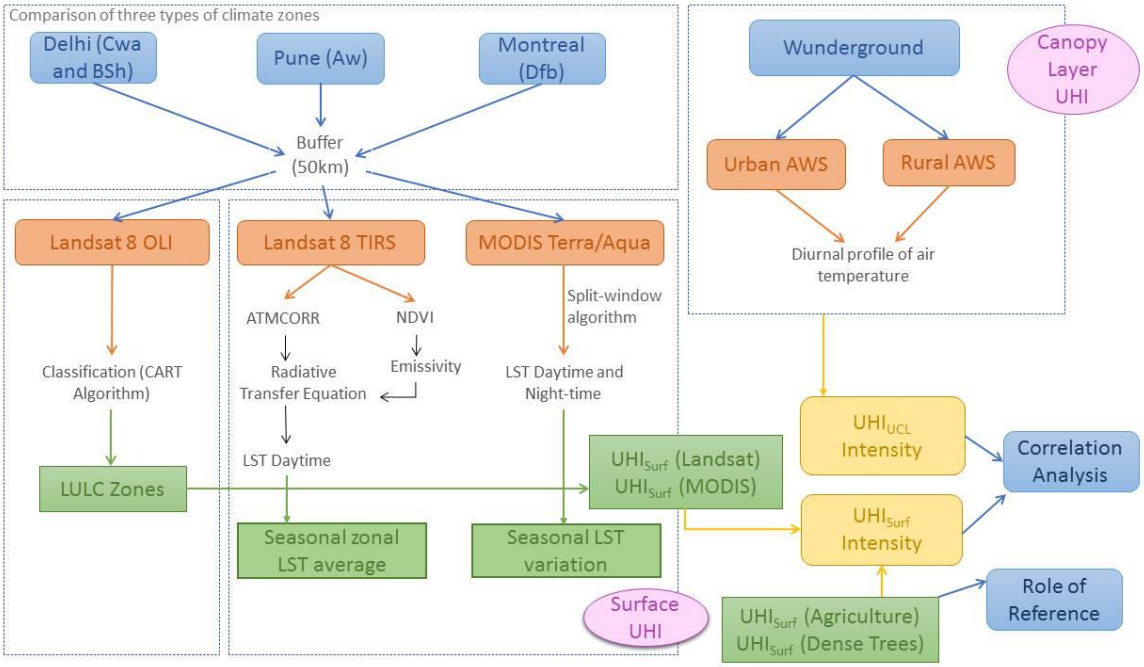


Figure 2. Methodology flow chart

Methods:

CLUHI intensity: To estimate CLUHI intensity, air temperature data was obtained from official government sources whenever possible. For Montreal, the weather station data were obtained from Environment Canada (http://climate.weather.gc.ca); and for Delhi, the Central Pollution Control Board (CBCP) data was used. For Pune, continuous data was not available from government data sources; therefore, data was obtained from Personal Weather Stations (PWS) from Wunderground (https://www.wunderground.com/). For all three cities, data was retrieved for an urban station in the city and a respective rural reference within the 50 km buffer zone. The stations used are shown in Table 3. The UHI_{UCL} Intensity was calculated based on these air temperature data, i.e. the difference of air temperature between rural reference and urban reference. This intensity was also calculated across seasons and between day and night. The definition of seasons and their duration were derived from Indian Meterological Department (IMD) for India, and Environment Canada for Canada.

City	**Montreal (Urban)**	**Montreal (Rural)**	**Delhi (Urban)**	**Delhi (Rural)**	**Pune (Urban)**	**Pune (Rural)**
Name of Station	McTavish	Ste-Clotilde	Dwarka	Najafgarh	Waterbay, Kalyani Nagar (IPUNE8)	Kanchan Farms, Daund (IDAUND3)
Source of	Environ-	Environ-	Central	Central	Wunder-	Wunder-

Data	ment Canada	ment Canada	Pollution Control Board	Pollution Control Board	ground	ground

Table 3: Source of weather station data for measuring CLUHI intensity (Refer to Annexure 1 for location details)

Surface Urban Heat Island (SUHI): The Surface Urban Heat Island (SUHI or UHI_{Surf}) intensity (SUHII) is estimated as the difference between rural and urban areas with respect to LST. To obtain these estimates, thermal images from two satellites, MODIS Aqua and MODIS Terra were analyzed within Google Earth Engine (Yu and Gong, 2012) for 2018. All images with cloud cover less than 10% were utilized for the analysis. As mentioned above, Land Surface Temperatures (LST) was estimated for 50 km radius around 3 central points of the cities. The buffer distance was carefully selected to encompass the complete urban expanse and the nearby rural background with at least one rural weather station. Composite images were created for the seasons for the three cities (see Table 1 for seasons).

The land use land cover is based on the seasonal Landsat 8 OLI (T1) with a spatial resolution of 30m is accessed through GEE cloud engine. The image composite was classified in the four land use land cover categories, namely, dense vegetation, agriculture, urban and water. The CART (classification and regression trees) algorithm was used on the cloud free Landsat composites. The accuracy assessment of the classified images, have been performed using 30% of the training data. Overall accuracy for the classified images ranged from 86% to 92% (Table 4).

	Delhi	Pune	Montreal
Overall accuracy	86.58%	88.39%	92.73%
Kappa coefficient	0.80	0.80	0.83

Table 4: Accuracy Assessment

Daily daytime and nighttime land surface temperature products from MODIS Terra/Aqua with a spatial resolution of 1km (MOD11A1 and MYD11A1) were retrieved for 2018 using GEE cloud database. The LST was retrieved from clear-sky thermal images acquired at ~ 11:00, 13:00, 22:00 and 02:00 (Quan et al.,2014a) local solar time using the split window algorithm (Wan and Dozier, 1996). The LST products report an accuracy within 2K over homogeneous surfaces (Wan, 2014).

The Landsat based LULC obtained from GEE was converted into shapefile and zonal analysis of MODIS derived LST on daily basis were arranged with respect to their land use class for each season considered. Using LST estimated from MODIS data, subsequent seasonal SUHIIs were calculated for the three cities. To understand the role of rural reference, UHI_{Surf} intensity were calculated in two ways using vegetated rural reference vs. agricultural rural reference. They were plotted together to understand the impact of

vegetated rural background over UHI intensity vs impact of agricultural rural background over UHI intensity.

Results:

Distributions of canopy level air temperatures by time of day and season (in 2018), obtained from weather stations located in urban areas and the rural reference within 50 kms, are shown in Figure 3. The times shown (2:30 am, 11:30 am, 2:30 pm and 11:30 pm correspond approximately with the time that the MODIS satellites (Terra and Aqua) overfly these locations. For Delhi (Figure 3a), maximum CLUHI intensity is observed at 11:30 pm in the winter months and is almost absent during the monsoons. In Pune (Figure 3b), the maximum CLUHI intensity occurs at 11:30 pm, and is almost equal for Spring, Summer and Autumn months. As with Delhi, CLUHI intensity for Pune is highly attenuated during the monsoon season. Montreal (Figure 3c) shows the greatest CLUHI intensity in the summer at 10:30 pm, and is highly attenuated during the winter months.

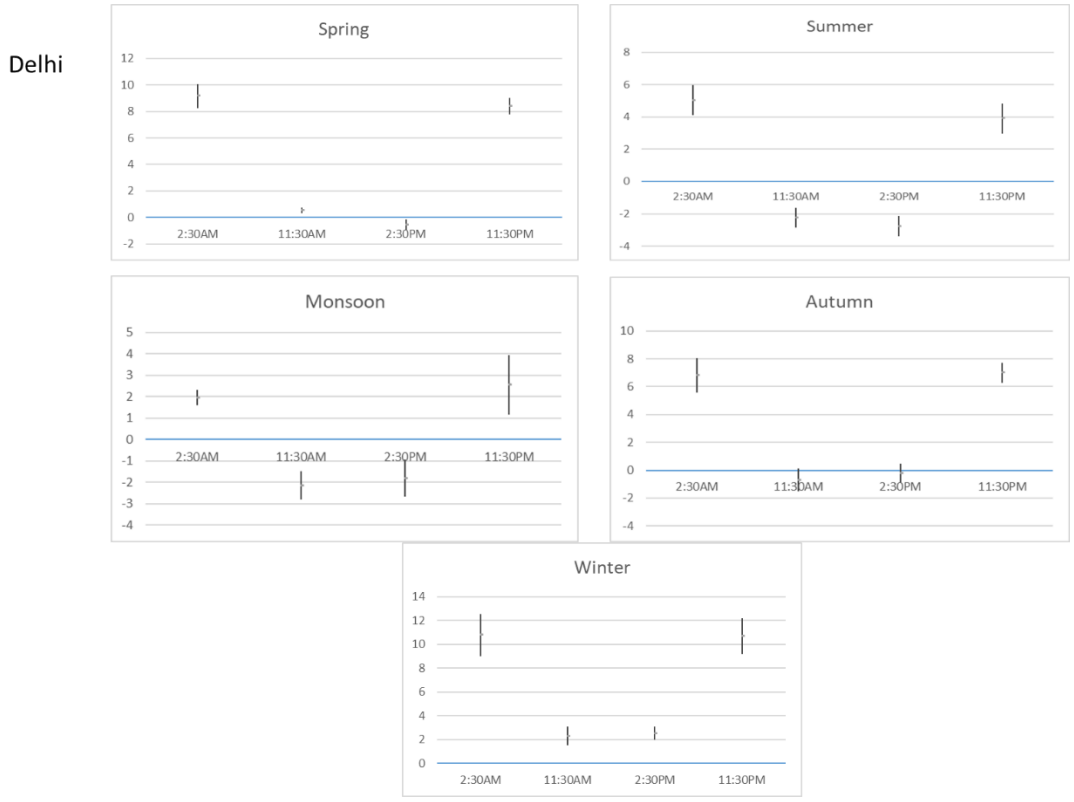


Figure 3a: CLUHI Intensity: air temperatures for Delhi at various times of the day and by seasons.

Pune

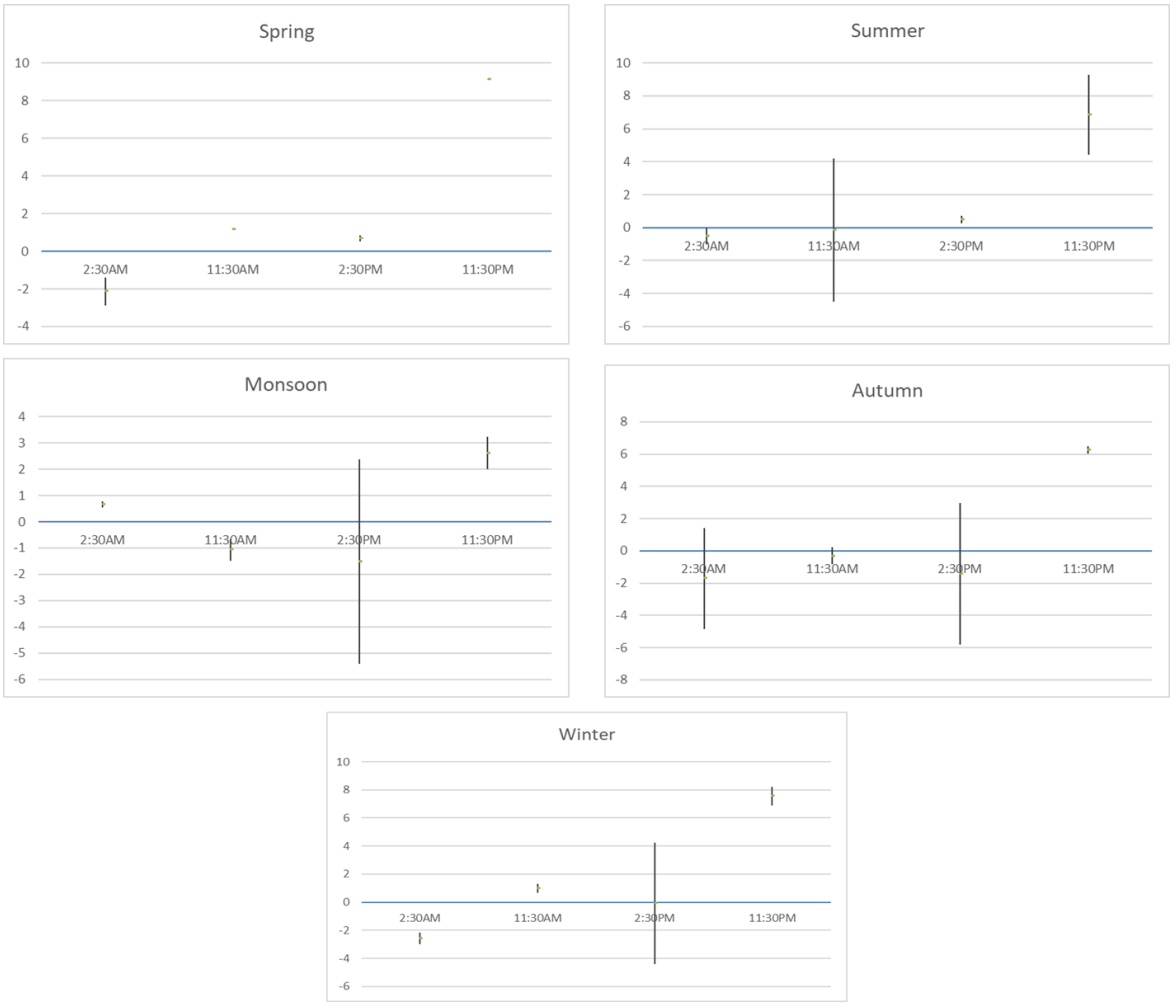


Figure 3b: CLUHI Intensity: air temperatures for Pune at various times of the day and by seasons.

Montreal

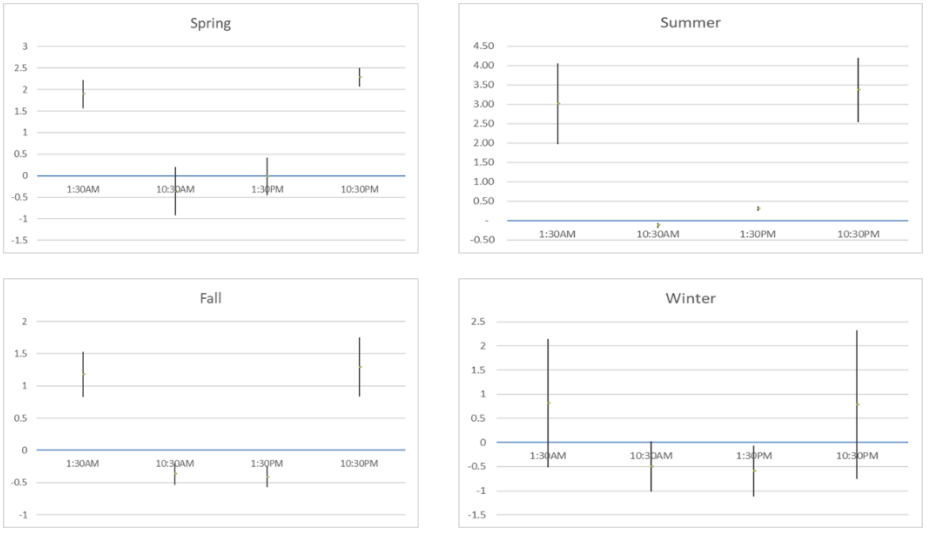


Figure 3c: CLUHI Intensity: air temperatures for Montreal at various times of the day and by seasons.

To compare against the CLUHI intensities, the SUHII composite images obtained from MODIS Terra and Aqua for 2018 are shown in Figure 4 for Delhi, Pune and Montreal. Visually, the SUHII effect for Delhi is clearly visible at 1:30 am (Figure 4). Additionally, "inverted" SUHI is visible at 10:30 am with the urban areas being cooler than a surrounding rural reference. For Pune, the SUHII effect, although visible at 11:30 pm, is less clear and mixed in with the rural agricultural reference. "Inverted" SUHI, corresponding to agricultural fields, can be seen in the daytime images (10:30 am and 1:30 pm). Montreal does not show any clear SUHII effect at night, but the urban core has higher LST during the day at 11:30 am.

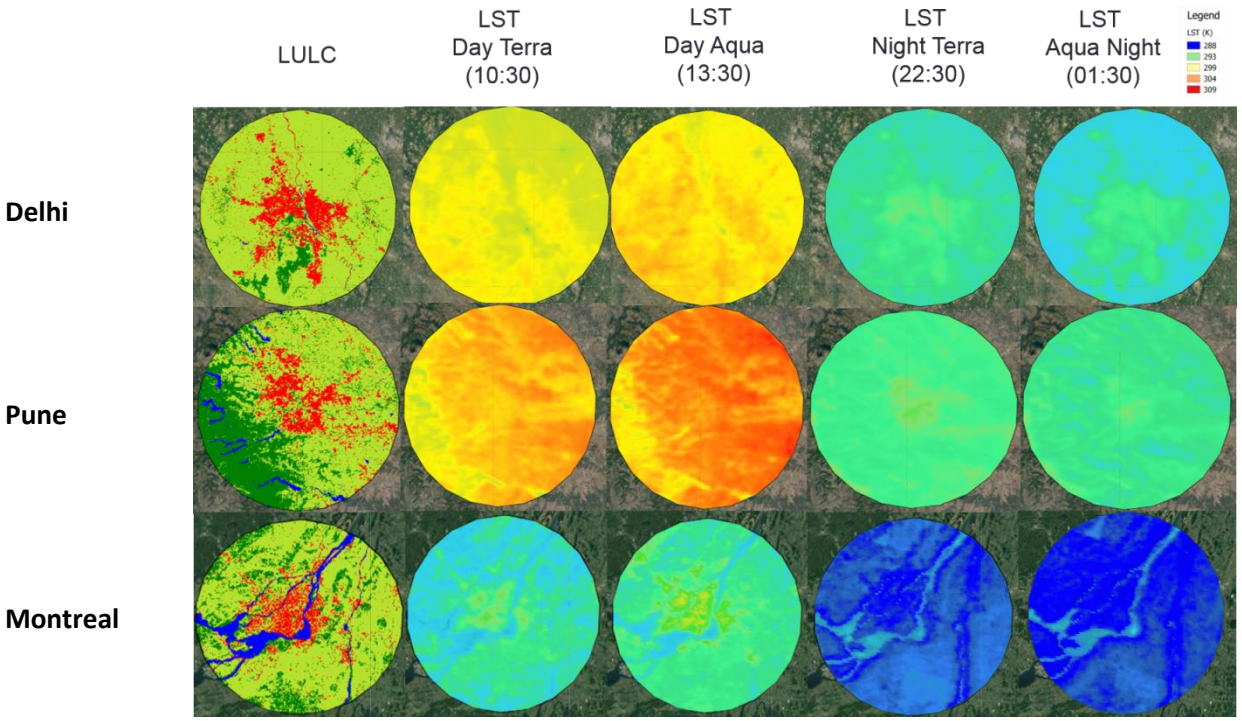


Figure 4: SUHII obtained from MODIS Terra and Aqua

Discussions:

Clearly, inverted UHI is present when observing SUHII in Indian cities, particularly during the daytime (10:30 am). Interestingly, the inverted UHI presented in the literature is from using Landsat 8 data, which has a sun synchronous orbit and therefore also presents data daytime imagery (approximately around 11 am) (Lazzarini et al., 2013; Shastri et al., 2017). However, the inverted UHI does not show up in the canopy level measurements of air temperature, thus leading us to believe that the observations of "inverted" SUHI are an artefact of relying on satellite measurements alone, and may be a result of these readings being biased by the moisture content of the rural reference (explaining its occurrence for Indian cities, but not in Montreal). We therefore emphasize caution when using UHI_{Surf} by itself. It does not substitute for proper ground-based measurements of traditional UHI, which uses air temperature measurements from standard weather stations.

Reference

Akbari, H., Pomerantz, M. and Taha, H., 2001. Cool surfaces and shade trees to reduce energy use and improve air quality in urban areas. *Solar energy*, 70(3), pp.295-310.

Ayanlade, A. and Jegede, O.O., 2015. Evaluation of the intensity of the daytime surface urban heat island: how can remote sensing help? *International Journal of Image and Data Fusion*, 6(4), pp.348-365.

Clinton, N. and Gong, P., 2013. MODIS detected surface urban heat islands and sinks: Global locations and controls. *Remote Sensing of Environment*, 134, pp.294-304.

Estoque, R.C. and Murayama, Y., 2017. Monitoring surface urban heat island formation in a tropical mountain city using Landsat data (1987–2015). *ISPRS journal of photogrammetry and remote sensing*, 133, pp.18-29.

Peng, S., Piao, S., Ciais, P., Friedlingstein, P., Ottle, C., Bréon, F.M., Nan, H., Zhou, L. and Myneni, R.B., 2012. Surface urban heat island across 419 global big cities. *Environmental science & technology*, 46(2):.696-703.

Lazzarini, M., Marpu, P.R. and Ghedira, H., 2013. Temperature-land cover interactions: The inversion of urban heat island phenomenon in desert city areas. *Remote Sensing of Environment*, 130, pp.136-152.

Peel MC, Finlayson BL & McMahon TA, 2007. Updated world map of the Köppen-Geiger climate classification, *Hydrology & Earth System Science*, 11: 1633-1644.

Shastri, H., Barik, B., Ghosh, S., Venkataraman, C. and Sadavarte, P., 2017. Flip flop of day-night and summer-winter surface urban heat island intensity in India. *Scientific reports*, 7, p.40178.

Streutker, D.R., 2003. Satellite-measured growth of the urban heat island of Houston, Texas. *Remote Sensing of Environment*, 85(3), pp.282-289.

Oke, T.R., 1973. City size and the urban heat island. *Atmospheric Environment* (1967), 7(8), pp.769-779.

Oke, T.R., 1976. The distinction between canopy and boundary-layer urban heat islands. *Atmosphere*, 14(4), pp.268-277.

Oke, T.R. and East, C., 1971. The urban boundary layer in Montreal. *Boundary-Layer Meteorology*, 1(4), pp.411-437.

Roth, M., Oke, T.R. and Emery, W.J., 1989. Satellite-derived urban heat islands from three coastal cities and the utilization of such data in urban climatology. *International Journal of Remote Sensing*, 10(11), pp.1699-1720.

Voogt, J.A. and Oke, T.R., 1998. Radiometric temperatures of urban canyon walls obtained from vehicle traverses. *Theoretical and Applied Climatology*, 60(1-4), pp.199-217.

Voogt, J.A. and Oke, T.R., 2003. Thermal remote sensing of urban climates. *Remote sensing of environment*, 86(3), pp.370-384.

Wan, Z. and Dozier, J., 1996. A generalized split-window algorithm for retrieving land-surface temperature from space. *IEEE Transactions on geoscience and remote sensing*, 34(4), pp.892-905.

Wan, Z., 2014. New refinements and validation of the collection-6 MODIS land-surface temperature/emissivity product. *Remote sensing of Environment*, 140, pp.36-45.

Weng, Q., Fu, P. and Gao, F., 2014. Generating daily land surface temperature at Landsat resolution by fusing Landsat and MODIS data. *Remote sensing of environment*, 145, pp.55-67.

Yu, L., & Gong, P. 2012. Google Earth as a virtual globe tool for Earth science applications at the global scale: progress and perspectives. International Journal of Remote Sensing, 33(12), 3966-3986.

Zhou, D., Xiao, J., Bonafoni, S., Berger, C., Deilami, K., Zhou, Y., Frolking, S., Yao, R., Qiao, Z. and Sobrino, J., 2019. Satellite remote sensing of surface urban heat islands: progress, challenges, and perspectives. *Remote Sensing*, 11(1), p.48.

Annexure 1



Urban and rural weather station locations in the study cities

MODELLING AND FORECASTING URBAN CLIMATE AND WEATHER

Improving the Accuracy of Simplified Urban Models Using Actual Radiation Parameters

Afshin Afshari[1], Fraunhofer Institute of Building Physics (Germany)
Nicolas Ramirez, Smart4Power (United Arab Emirates)

ABSTRACT

While detailed modeling of urban momentum/energy exchanges can be attempted via Computational Fluid Dynamics (CFD), developing and simulating a comprehensive CFD model of a realistic urban domain is a monumental task. In fact, a comprehensive model implementing the dynamic coupling of urban microclimate to building heat transfer is currently out of reach. Not to mention that an overly complex model would not be of much practical use in a decision support setting where multiple parametric simulations are often necessary. Simplified Urban Canopy Models (SUCM) are mainly contingent on the assumption of an idealized form for the urban roughness elements. They are often a component of larger mesoscale climate models, but could also be used in stand-alone mode—provided that certain boundary condition simplifications are made. Some of the most notable SUCMs are: Town Energy Balance (TEB), Square Prism Urban Canopy (SPUC), Urban Weather Generator (UWG) and variants. The complexity and computational speed of these models is significantly reduced thanks to the implementation a simplified representation of momentum transfers. Concurrently, the spatial organization of the surfaces (slopes, orientations, shape factors), and their physical characteristics (albedo, emissivity, thermal conductivity) need to be simplified as well. In particular, the models often rely on very rough estimations of short-wave (solar) and long-wave (infrared) radiation heat transfer. In this study, we assess the comparative validity of the radiation heat transfer approximations proposed by the different simplified modelling approaches in comparison to exact solutions calculated for an actual urban district. The main contribution is the assessment of the impact of the improvement of an existing SUCM by replacing the default radiation transfer calculations with much more accurate ones determined in consideration of the detailed geometry of a real urban district. We show that the implementation of a more accurate radiation estimation can result in significantly different results in some cases. In particular, under a Cool Surfaces scenario, the average urban heat island intensity can be underestimated by TEB, by as much as 13%.

1. Introduction

Urbanization results in larger cities' and denser urban tissue. The temperature of the air in densely built areas is generally higher than in the surrounding rural hinterland, a phenomenon known as the "Urban Heat Island" (UHI) [1]. The UHI creates demand for more indoor cooling in hot climate and increases the mortality rate during heat waves [2]. The temperature differential can reach a maximum 12°C [3]. Many researchers have worked on modelling UHI and the most accurate way of doing so is via Computational Fluid Dynamics (CFD). However, the construction, simulation and validation of such models present significant challenges [4]. To address this difficulty, researchers have proposed Simplified Urban Canopy Models (SUCM) which reduce the computational time at the expense of accuracy. The SUCM usually replace the real urban geometry

[1] Corresponding author: afshin.afshari@ibp.fraunhofer.de

with an idealized regular geometry (infinite rows of buildings, regular array of cuboid building, etc.). The complexity of these models is significantly reduced thanks to the implementation a simplified representation of momentum transfers. Concurrently, the spatial organization of the surfaces (slopes, orientations, shape factors), and their physical characteristics (albedo, emissivity, thermal conductivity) need to be simplified as well. In particular, the models often rely on very rough estimations of short-wave (solar) and long-wave (infrared) radiation heat transfer. Two categories of SUCM are described in the literature, single layered and multilayer. Single-layer schemes can be as simple as modifications to the surface characteristics of the urban landscape (Liu et al [5], Grossman-Clarke et al [6]) or more sophisticated urban models such as the Town Energy Balance (TEB) by Masson [7], the Square Prism Urban Canopy (SPUC) by Aoyagi and Seino [8], the Urban Weather Generator (UWG) by Bueno et al [9] or the sensible/latent thermal network model of Afshari [10]. Numerous UHI case studies have shown that these schemes are able to compute sufficiently accurate predictions of surface fluxes, temperatures, and net radiation. Instances of multilayer schemes are described by Brown and Williams [11], Vu et al. [12], and Martilli et al. [13]. Multilayer SUCM can be as simple as basic modifications of the predictive equations to simulate urban effects (i.e., Brown and Williams [11]) while more advanced implementations include predictive equations for roof and wall, incorporating complex radiative effects such as shadowing and reflection at multiple levels within the urban canopy (i.e., Kusaka et al [14]; Martilli et al. [13]).

Radiation heat transfer is comprised of shortwave and longwave components. Shortwave radiation can be direct or diffuse, while longwave radiation is diffuse. Most of the energy of solar radiation is within the short wavelength range (hereafter referred to as “shortwave radiation”). Once in the Earth’s atmosphere, clouds and the surface absorb some of the energy of solar radiation. The remainder contributes to heating the ground and other urban surfaces. In turn, these surfaces re-emit in the long wavelength range (hereafter “longwave radiation”) onto other urban surfaces or the sky. Longwave radiation is dependent on surface temperature, emissivity and view factors. The view factors are purely mathematical constructs that characterize how much a given surface can see the other surfaces. In particular the Sky View Factor (SVF) of a surface is the portion of the sky seen by the surface. In this study, we assess the comparative validity of the radiation heat transfer parameters (net incident global irradiance on urban surfaces, and surface view factors) approximated by the different simplified modelling approaches in comparison to exact solutions that we calculate for an actual urban district. The impact of these approximation on the accuracy of the model is evaluated by taking, as an example, the SUCM described in [10]. This evaluation is done by replacing the default TEB approximations with more accurate ones determined for the detailed geometry of a real urban district in downtown Abu Dhabi. In the next section, we describe the case study and derive the average geometric and thermophysical parameters to be fed to the SUCM. In the subsequent section, the methodology for the accurate determination of radiation parameters for the actual geometry (GIS data) is described and applied to the case study. Section 4 contains a brief description of the sensible-latent thermal network model used to simulate the thermal state of the urban canopy. Thereafter, the simulation results are discussed, with a special emphasis on the UHI. It is shown that the usual approximate characterization of the radiation parameters prevalent in existing SUCM schemes can have a significant detrimental impact on the accuracy of the estimation of the UHI intensity while the impact on cooling energy is moderate (albeit not negligible). In the last section, we present the main conclusions of the study and suggest tracks for future research.

2. Case Study

We evaluate the impact of the proposed improved radiation scheme using, as case study, a district in Abu Dhabi, UAE referred to as district E3-02 which includes 60 buildings. The simplest representation of the urban canopy relies on 3 parameters: average building height h, plan area index λ_p and frontal area index λ_f. h is the area-weighted average height of all buildings in the studied region. λ_p is the ratio of the plan area of buildings over the total area of the site. Finally, λ_f is the ratio of average vertical area of roughness elements (buildings) opposing the urban wind flow over the total site area. The latter parameter is, in the general case, is dependent on the actual wind flow direction. However, in most studies it is approximated as 1/4th of the vertical façade area divided by the site area. Instead of attempting to model the full geometric complexity of the actual site, we examine, as is customary in SUCM, an equivalent regularized arrangement of buildings and streets that is based on the morphological parameters h, λ_p and λ_f of the actual domain. For instance, we assume a regular array of identical buildings with a square footprint $l \times l$ interlaced by streets having the same width w (see Figure 1). Then, from the primary parameters, secondary parameters l and w can be derived. Thereafter, using the symmetry properties of the simplified regular geometric representation, the urban domain model is reduced to a single regularized building surrounded by half the width of the regularized street. From this, we can derive A_t the total area of the domain to be modeled. The values of these parameters for district E3-02 of Abu Dhabi, as computed from GIS data, are listed in Table 1.

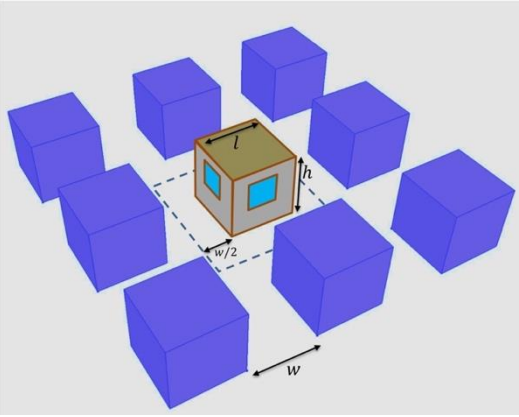


Figure 1: Schematic representation of the simplified geometry

Table 1: Main morphological parameters for the island of Abu Dhabi (determined from GIS data)

$\boldsymbol{h}$	$\boldsymbol{36.7\ m}$
$\boldsymbol{\lambda_p}$	0.239
$\boldsymbol{\lambda_f}$	0.282
$\boldsymbol{l = h\lambda_p/\lambda_f}$	$31.1\ m$
$\boldsymbol{w = l\left(1/\sqrt{\lambda_p} - 1\right)}$	$32.5\ m$
$\boldsymbol{A_t = (l + w)^2}$	$4045\ m^2$

The properties of the prototypical building and paved street in the downtown district are displayed in Table 2.

Table 2: Specifications for the building and the road

Urban Domain Properties	**Value**
Building height (m)	20.3
Building length (m)	28.8
Paved street width (m)	41.1
Floor to ceiling height (m)	2.85
Floor/roof thickness (m)	0.35
Paved street thickness (m)	1.00
Roof U-value (W/m^2K)	1.29
Wall U-value (W/m^2K)	2.25
Window U-value including films (W/m^2K)	3.88
Paved street U-value (W/m^2K)	1.20
Glazing Ratio	33%
Solar Heat Gain Coefficient (SHGC)	0.75
Roof solar reflectance (albedo)	0.26
Wall solar reflectance (albedo)	0.30
Glazing solar reflectance (albedo)	0.15
Paved street solar reflectance (albedo)	0.10
Roof emissivity	0.90
Wall emissivity	0.90
Glazing emissivity	0.84
Paved street emissivity	0.95
Roof mass heat capacity (kJ/ m^3K)	$1.2*10^3$
Wall mass heat capacity (kJ/ m^3K)	$1.2*10^3$
Paved street mass heat capacity (kJ/ m^3K)	$1.6*10^3$
Indoor CHTC* (W/m^2K)	5
Roof-air CHTC (W/m^2K)	5.6+4V
Wall-air CHTC (W/m^2K)	5.6+4V
Street-air CHTC (W/m^2K)	7.8+4.27V
People heat gains (W/m^2)	Max 5 (daily schedule)
Equipment/lighting heat gains (W/m^2)	Max 5 (daily schedule)
Latent portion of internal heat gains (W/m^2)	20%
Vehicular anthropogenic heat gains (W/m^2)	Max 21.6 (daily schedule)
Latent portion of anthropogenic gains (W/m^2)	9%
COP**	2.5
Infiltration	0.5
Fraction of chiller waste heat rejected into	100%

* CHTC: Convective Heat Transfer Coefficient
** COP: Coefficient of Performance of the chiller

3. Methodology

Our SUCM (described in the next section) uses TEB's radiation formulae by default. The goal of this study is to assess the accuracy of the TEB formulae for shortwave and longwave radiation and evaluate the impact on the SUCM of improving upon the default (TEB) formulae. A first level of improvement would consist in replacing some of the TEB radiation formulae by the corresponding SPUC ones. A more substantial improvement would result from the incorporation of hourly shortwave radiation (diffuse + direct) and longwave view factors determined for the *Actual* geometry.

As a reminder, the TEB model assumes infinitely long rows of identical buildings separated by infinitely long identical urban canyons. Therefore, the domain of study can be reduced to a 2D cross-section. Furthermore, using symmetry properties, it is possible to reduce the model to a single road and two opposing walls. The SPUC scheme, on the other hand, is 3-dimensional. It considers regularly positioned cuboid buildings. The cuboid buildings are identical and positioned in a regular grid-like array (i.e., same street width). It should be noted that in their description of the SPUC idealized geometry [8], the authors only set forth formulae for view factors as well as shortwave beam radiation and its first specular reflection (i.e., diffuse radiation not considered). We have

improved the scheme to include diffuse radiation as well as diffuse reflection of beam radiation beyond the first bounce. Said improvements were inspired by the TEB formulas.

The calculation of *Actual* view factors and hourly global irradiance on all surfaces was conducted using DIVA [15] running on the Grasshopper plugin of Rhino 3D. Ecotect [16] was also used as an alternative method for the estimation of the view factors.

3.1. Shortwave radiation

A ray tracing simulation was executed on DIVA/Grasshopper for the *Actual* urban case. A $5m \; x \; 5m$ grid was found to provide optimal accuracy. Figure 2 shows the net incident global irradiance on each urban surface.

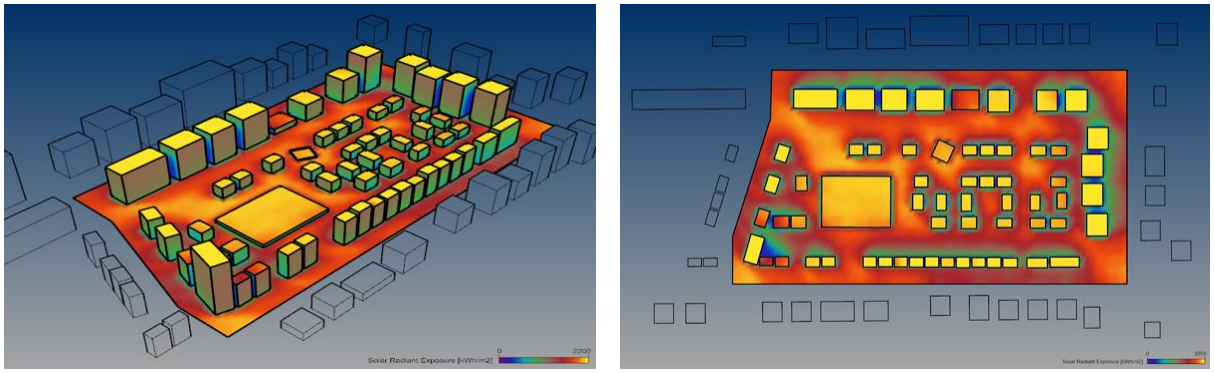


Figure 2: Global irradiance on all surfaces for the Actual urban case

Figure 3 displays average global irradiance on roof/façade/pavement for the rural and urban cases. The area-weighted average results per surface type (roof/façade/pavement) are shown: hourly values for the whole year and average daily profiles for summer and winter. The urban TEB and SPUC irradiance values are presented in Figure 4. It should be noted that the rural global irradiance on vertical façades is based on a cylindrical assumption for a stand-alone building (no shading from neighboring buildings). Its direct component is derived from the DNI (Direct Normal Irradiance) and the zenith angle while its diffuse component is a function of DHI (Diffuse Horizontal Irradiance) and GHI (Global Horizontal Irradiance) as described in standard solar radiation textbooks. The rural global irradiance on horizontal surfaces (roof, paved surfaces) is assumed to be identical with the GHI.

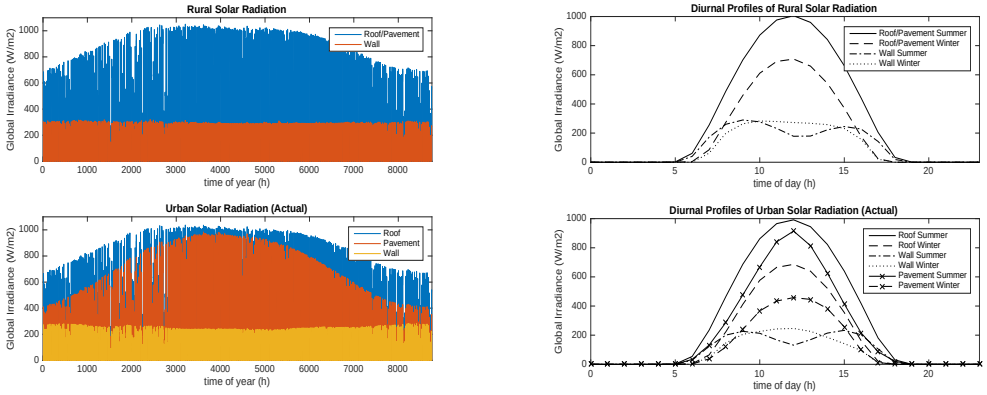


Figure 3: Annual and diurnal global irradiance per surface type for the rural and Actual urban cases

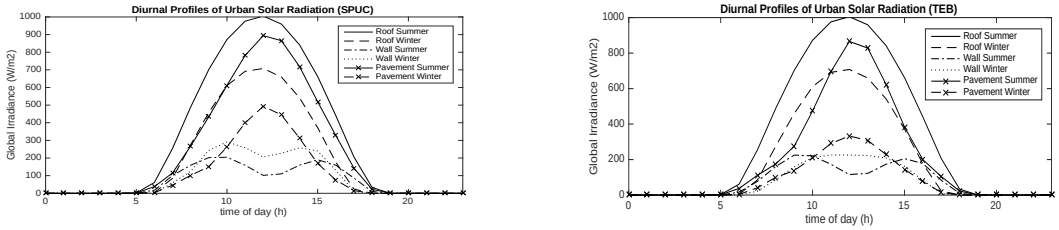


Figure 4: Global irradiance per surface type for the TEB and SPUC schemes

For paved surfaces, the SPUC solar scheme results in markedly higher mean global irradiance values, especially in winter with day-time average peaks of about 500 W/m2 instead of 300 W/m2 for TEB. When it comes to the mean global irradiance on the walls, SPUC predicts lower values in the summer, whereas TEB does not predict a significant difference between summer and winter. Furthermore, we can observe a more distinct double-peak profile for the mean wall irradiance calculated by SPUC for the wall in winter. When it comes to the pavement, in comparison to the TEB scheme, the modified SPUC solar radiation is higher, especially in winter. And the results for the roof are of course the same for both schemes because of the regularity of the buildings. In comparison to the *Actual* data, the TEB results seem to be globally more accurate—although SPUC is slightly better for the pavement. We will only retain the TEB irradiance estimates in the remainder of our analysis.

3.2. Longwave radiation

The view factors among urban surfaces and between urban surfaces and the sky are displayed in Table 3 for different models. The *Actual* view factors are area-weighted averages per surface type. The last column corresponds to the empirical model of Leung & Steemers [17].

Table 3: View Factors

	Actual	**TEB**	**SPUC**	**L&S [17]**
Ground to sky F_{ps}	**0.60**	0.38	0.67	0.63
Facade to sky F_{fs}	**0.30**	0.27	0.22	0.37
Roof to sky F_{rs}	**0.94**	1	1	1
Ground to facade F_{pf} (derived: $F_{pf} = 1 - F_{ps}$)	**0.40**	0.62	0.33	0.38
Facade to ground F_{fp} (derived: $F_{fp} = F_{fs}$)	**0.30**	0.27	0.22	0.37
Facade to facade F_{ff} (derived: $F_{ff} = 1 - 2F_{fs}$)	**0.40**	0.44	0.56	0.26

When it comes to sky view factor SPUC shows better accuracy than TEB for the ground-to-sky value in comparison to the *Actual* value estimated by DIVA/Grasshopper and Ecotect. For the walls, on the other hand, TEB is slightly more accurate. L&S is most accurate for the ground but not for walls. The other sky view factors are derived using the usual relationships.

4. Urban canopy model

We use a dynamic thermal network lumped-parameter model to represent the dynamic thermal interactions between buildings and the urban environment. As shown on Figure 2, these interactions are mainly mediated by the urban canyon air, itself in contact with the paved surfaces as well as the free atmosphere above the canopy.

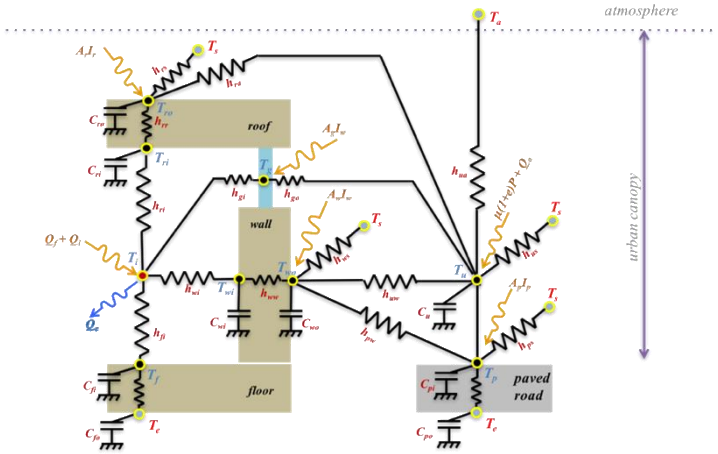


Figure 2: The urban canopy model

In addition to sensible heat network shown in Figure 2, the SUCM computes, in a coupled manner, a latent heat network model for latent heat (not shown here). In this parallel thermal network, using the MATLAB/SIMSCAPE terminology, humidity ratio replaces temperature as 'potential variable' of the network and latent flux replaces sensible flux as 'flow variable'. That latent component of the SUCM model is dynamically coupled with the sensible component's evapotranspiration flux and infiltration latent heat flux on one hand and the ambient humidity level (prescribed by the weather file) on the other. Soil moisture is not considered given the target domain's arid climate and urban setting. The sensible-latent thermal network model is fully specified using a combination of coding and graphical representation. The energy exchanges are iteratively resolved by SIMSCAPE/MATLAB. This SUCM has many parameters, in particular sophisticated aerodynamic and evapotranspiration schemes are implemented. A more detailed exposition can be found in [10]. The simulation runs for every hour of a standard year (8760 hours) and is driven by standard hourly weather data for Abu Dhabi airport. The main outcomes are cooling electricity and Urban Heat Island (UHI) intensity. The latter defines the urban-rural air temperature differential.

5. SUCM Simulation Results & Discussion

5.1. Baseline Simulation

If we use the *Actual* radiation parameters in the SUCM, we obtain after an annual hourly simulation (8760), average cooling electricity consumption per floor area of 147 kWh/m^2 with a peak cooling electricity demand of 52.1 W/ m^2. The average annual UHI intensity is 1.95 °C. If we use the TEB radiation parameters in the SUCM, we obtain average cooling electricity consumption per floor area of 143.9 kWh/m^2 with a peak cooling electricity demand of 49.5 W/ m^2. The average

annual UHI intensity is 1.94 °C. The TEB results are generally lower but the error is small (Table 4).

Table 4: Baseline simulation results

	Actual	TEB	Error
Cooling electricity use (kWh/m^2)	**147**	143.9	-2%
Cooling peak demand (W/m^2)	**52.1**	49.5	-5%
Average annual UHI intensity (°C)	**1.95**	1.94	negligible

The average daily profiles of UHI intensity, for *Actual* and TEB, are shown in Figure 3. The differences are small and not immediately noticeable.

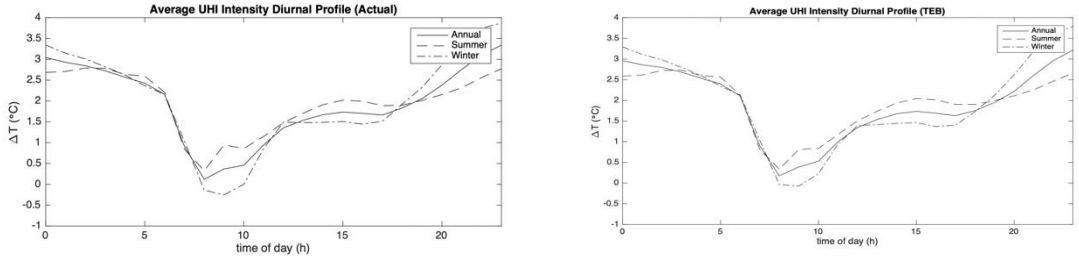


Figure 3: Average Daily profile of the Urban Heat Island intensity in the Baseline scenario: Actual radiation parameters (left) versus TEB radiation parameters (right)

5.2. Cool Surfaces Simulation

In the Cool Surfaces scenario, we assume that all urban surfaces (roof/façade/pavement) are treated with 'cool coating'. The coating is assumed to have some thermal insulation benefit with an R-value that is typical for 1000-micron coating with ceramic particles. In addition, the glazing has improved Solar Heat Gain Coefficient (SHGC). The modified urban properties, compared to the baseline case, are reported in Table 4.

Table 4: Cool Surfaces scenario summary

Building Design Specifications	**Value**	**Comment**
Solar Heat Gain Coefficient (SHGC)	0.28	Single clear with LLumar R20 SR CDF Film
Roof solar reflectance (albedo)	0.75	Cool coating
Wall solar reflectance (albedo)	0.75	Cool coating
Paved street solar reflectance (albedo)	0.50	Extreme cool scenario in [28]
Roof U-value (W/m^{2}K)	0.83	Added R-value of 0.422 m^{2}K/W (=1000 μ of cool coating)
Wall U-value (W/m^{2}K)	1.15	Added R-value of 0.422 m^{2}K/W (=1000 μ of cool coating)
Paved street U-value (W/m^{2}K)	0.80	Added R-value of 0.422 m^{2}K/W (=1000 μ of cool coating)

If we use the *Actual* radiation parameters in the SUCM, we obtain after an annual hourly simulation (8760), average cooling electricity consumption per floor area of 131 kWh/m^2 with a peak cooling electricity demand of 46.2 W/ m^2. The average annual UHI intensity is 1.59 °C. If we use the TEB radiation parameters in the SUCM, we obtain average cooling electricity consumption per floor area of 127 kWh/m^2 with a peak cooling electricity demand of 45.4 W/ m^2. The average annual UHI intensity is 1.39 °C. The difference in cooling electricity estimates is now larger, standing at –4%. However, the most significant error is committed when using the TEB radiation parameters (instead of *Actual*) for the estimation of the average annual UHI intensity: -13%. See Table 5.

Table 5: Cool Surfaces simulation results

	Actual	**TEB**	**Error**
Cooling electricity use (kWh/m^2)	**132**	127	-4%
Cooling peak demand (W/m^2)	**46.8**	45.4	-3%
Average annual UHI intensity (°C)	**1.59**	1.39	-13%

The average daily profiles of UHI intensity, for *Actual* and TEB, are shown in Figure 4. Clearly the error is largest towards the end of the morning, when the UHI intensity is typically at its lowest level. TEB seems to exaggerate the 'cool island' effect during this period. This error is even more pronounced in winter.

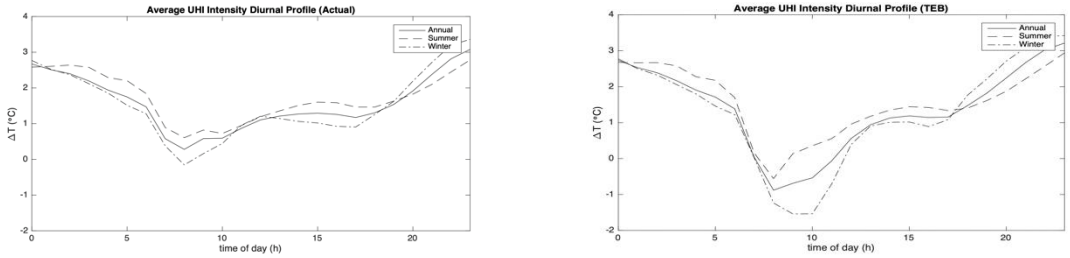


Figure 4: Average Daily profile of the Urban Heat Island intensity in the Cool Surfaces scenario: Actual radiation parameters (left) versus TEB radiation parameters (right)

6. Conclusion

The main contribution of this study is the assessment of the impact of the improvement of an existing simplified urban canopy model by replacing the default radiation transfer calculations with much more accurate ones determined in consideration of the detailed geometry of a real urban district. We show that the implementation of a more accurate radiation estimation can result in significantly different results in some cases.

Specifically, we evaluate the benefits of using the *Actual* radiation parameters instead of those provided by TEB or SPUC in a SUCM model (the latter is described in detail and validated in [10]). The comparisons are conducted for a real district in downtown Abu Dhabi for which GIS data is available. The SPUC scheme has been improved to include diffuse radiation as well as diffuse reflection of beam radiation beyond the first bounce.

Initially, we validate TEB and SPUC Sky View Factor (SVF) estimates by comparing to *Actual* values. SPUC is more accurate. SPUC is more accurate for the ground SVF while TEB is better for the façade SVF. For the roof SVF, it is acceptable to use 1 in most usual cases. The empirical model of Leung & Steemers is generally superior to both TEB and SPUC.

Further, we looked at shortwave radiation and its impact on urban canopy model accuracy. While it can be presumed that, here too, SPUC should be closer to *Actual* given that the cuboid geometry is closer to the real geometry than TEB's infinite urban canyons, the differences between TEB and SPUC are small. The modified SPUC solar radiation is generally higher for the ground in winter and lower for the walls in summer. We decided to retain only the TEB in our subsequent assessment of UCM accuracy. The radiation parameters do not have a significant impact on SUCM simulation results in a business-as-usual case. However, in a Cool Surfaces scenario where all urban surfaces are coated with a cool coating, the differences become noticeable with a 4% underestimation of the cooling electricity when using TEB radiation parameters. In the case of the

UHI intensity, the discrepancy reaches 13%. This is far from negligible and shows that TEB radiation assumption may result in a significant underestimation of the UHI intensity.

A promising future research track consists in applying the same principle to urban wind flow profile. Accurate flow data, produced by urban weather stations or mechanical-only CFD simulations, can replace the usual aerodynamic formulate typically used in SUCM schemes in order to further enhance the accuracy of the models.

References

[1] H. E. Landsberg, The Urban Climate, New York: Academic Press, 1981.

[2] K. M. Gabriel and W. R. Endlicher, "Urban and rural mortality rates during heat waves in Berlin and Brandenburg, Germany," Environmental Pollution, p. 2044–2050, 2011.

[3] T. R. Oke, "City Size and Urban Heat Island," Atmospheric Environment Pergamon Pres, pp. 769-779, 1973.

[4] P. A. Mirzaei, "Recent challenges in modeling of urban heat island," Sustainable Cities and Society, pp. 200-206, 2015.

[5] Y. Liu, F. Chen, T. Warner and J. Basara, "Verification of a mesoscale data-assimilation and forecasting system for the Oklahoma City area during the Joint Urban 2003 field project," Journal of Applied Meteorology, pp. 912-929, 2006.

[6] S. Grossman-Clarke, J. A. Zehnder, W. L. Stefnov, Y. Liu and M. A. Zoldak, "Urban Modifications in a Mesoscale Meteorological Model and the Effects on Near-Surface Variables in an Arid Metropolitan Region," Journal of Applied Meteorology, pp. 1281-1297, 2005.

[7] V. Masson, "A Physically-Based Scheme For The Urban Energy Budget In Atmospheric Models," Boundary-Layer Meteorology, p. 357–397, 2000.

[8] T. Aoyagi and N. Seino, "A Square Prism Urban Canopy Scheme for the NHM and Its Evaluation on Summer Conditions in the Tokyo Metropolitan Area, Japan," Journal of Applied Meteorology and Climatology, pp. 1476-1496, 2011.

[9] B. Bueno, L. Norford, J. Hidalgo and et al., "The urban weather generator," J. Build. Perform. Simul., vol. 6, no. 4, pp. 269-281., 2013.

[10] A. Afshari, "A new model of urban cooling demand and heat island—application to vertical greenery systems," Energy and Buildings, pp. 204-217, 2017.

[11] M. Brown and M. Williams, "An urban canopy parameterization for mesoscale meteorological models," in Second Symp. on the Urban Environment, Albuquerque, NM, 1998.

[12] V. T. Ca, T. Asaeda and Y. Ashie, "Development of a numerical model for the evaluation of the urban thermal environment," Journal of Wind Engineering and Industrial Aerodynamics, pp. 181-191, 1999.

[13] A. Martilli, A. Clappier and M. W. Rochta, "An urban surface exchange parameterization for mesoscale models," Boundary Layer Meteorology, pp. 261-304, 2002.

[14] H. Kusaka, H. Kondo, Y. Kikegawa and F. Kimura, "A simple single-layer urban canopy model for atmospheric models: Comparison with multi-layer and slab models.," Boundary Layer Meteorology, pp. 329-358, 2001.

[15] J. A. Jakubiec and C. F. Reinhart, "Diva 2.0: integrating daylight and thermal simulations using Rhinoceros 3D, Daysim and EnergyPlus," in 12th Conference of International Building Performance Simulation Association, Sydney, 2011.

[16] "autodesk Ecotect Analysis," 22 april 2017. [Online]. Available: https://knowledge.autodesk.com/support/ecotect-analysis?sort=score.

[17] K. S. Leung and K. Steemers, "Estimating Average Sky View Factors of Urban Surfaces with Simple Geometric Parameters," in PLEA, Dublin, 2008.

[18] Z. Bottyan and J. Unger, " A multiple linear statistical model for estimating the mean maximum urban heat," Theoretical and Applied Climatology, pp. 233-243, 2003.

[19] C. S. Grimmond, S. K. Potter, H. N. Zutter and C. Souch, " Rapid methods to estimate sky-view factors," International Journal of Climatology, p. 903–913, 2001.

[20] L. Chapman, J. E. Thornes and A. V. Bradley, "Sky-view factor approximation using GPS receivers," International Journal of Climatology, p. 615–621, 2002.

[21] L. Chapman, J. E. Thornes, J.-P. Muller and S. McMuldroch, "Potential Applications of Thermal Fisheye Imagery in Urban Environments," IEEE Geoscience and Remote Sensing Letters, pp. 56-59, 2007.

[22] T. Gal, M. Rzepa, B. Gromek and J. Unger, "Comparison between Sky View Factor Values computed by two different methods in an urban environment," Acta Climatologica et Chorologica, pp. 17-26, 2007.

[23] U. D. o. E. Energy, "EnergyPlus™ Version 8.5 Documentation,Engineering Reference," Energy, U.S. Department of Energy, 2016.

[24] J. Noilhan and S. Planton, " A simple parameterization of land surface processes for meteorological models," Monthly Weather Review, pp. 536-549, 1989.

[25] E. S. Krayenhoff and J. A. Voogt, "A microscale three-dimensional urban energy balance," Boundary-Layer Meteorology, p. 433–461, 2007.

[26] D. Bachman, Grasshopper: Visual Scripting for Rhinoceros 3D, Industrial Press, 2017.

[27] E. Sparrow and R. Cess, Radiation Heat Transfer, CRC Press, 1978.

[28] N. Yaghoobian and J. Kleissl, "Effect of reflective pavements on building energy use," Urban Climate, p. 25-42, 2012.

Urban Heat Island Minimisation, Local Climate Zones and Parametric Optimisation: A "Grasshopper" Based Model

Madhuranga K.K.K.D.R..[1]*, Department of Architecture, University of Moratuwa (Sri Lanka)*
Perera, N. G. R., Department of Architecture, University of Moratuwa (Sri Lanka)

ABSTRACT

Many cities have undergone severe transformation, creating unliveable environments, polluted and stagnant air and effected by Urban Heat Island (UHI). With the prevailing rapid development in Sri Lanka in general, and Colombo in particular, the impact of the phenomena is evident. Thus, it needs to become a key consideration in the urban design process to optimise building morphology for minimum UHI impact, especially in the Tropics. The main objective of the study is to build a parametric model to analyse the behaviour of the Urban Heat Island (UHI) effect with the changing land cover and geometric properties, based on the Local Climatic Zone (LCZ) classification. A parametric model is developed using Grasshopper VPL to match the corresponding geometric and land cover properties and thereafter, used with a derivative free optimisation algorithm to find the respective forms that generate maximum and minimum UHI values. Findings show a direct association of the building height to the UHI intensity. Higher impervious land cover percentages contribute to the increase of the UHI value. As an outcome of the research, a protocol model process is presented, which allows the input of multiple variables and generates real-time adaptive results, dramatically reducing the time of the optimising process, for UHI minimisation. Thus, allowing planners and urban designers to explore different morphologies through real-time analysis.

Keywords: urban heat island, Local Climate Zone, Parametric Optimisation, Grasshopper, Urban Weather Generator

Introduction

As indoor overheating is directly associated with energy demand and thus has significant impact on the microclimatic context as waste heat, it has to become a key consideration in the urban design process to optimise building morphology for minimum UHI impact. However, the widely used orthodox method for reducing the UHI is to use heuristic data with trial and error methods based on the previous known experiences and protocols; this practice often uses a base case to compare between variations and their combinations, by selecting the best-generated options based on the stochastic data. However, this would be a very time consuming and inefficient method that may not provide a sufficiently good solution to an optimisation problem. Further, the practice does not generate sufficient data to analyse and it cannot predict or create a functional dependence for the behaviour of variables considered.

Alternatively, it is convenient to have a parametric platform that allows multiple variables and gives real-time adaptive results, as it would dramatically reduce the time and cost of the optimising process.

[1] Corresponding Author: [dilushanr@gmail.com].

The main objective of the study is to build a parametric model to analyse the behaviour of the Urban Heat Island (UHI) effect with the changing land cover and geometric properties of the Local Climatic Zone (LCZ) classification framework. In this particular research, only the LCZ1 (compact high-rise) is selected for modelling and analysis due to its high impact on UHI (Perera et al. 2012 and 2018; Perera, 2015) and as a limitation of research scope.

A research workflow using Grasshopper VPL as a parametric modelling platform is adopted, with Rhino 3D® platform to create a parametric model for LCZ1 in real-time. The Dragonfly plugin for Grasshopper, is utilised to set up the Urban Weather Generator (UWG) and calculate the average and maximum UHI. An evolutionary solver is applied to find optimum values and according to systematic inputs. The process is recorded, by setting up a recorder -Colibri plugin - to save the data. Next, the results are mapped to present the outdoor thermal comfort levels using the Ladybug tool.

The research outcome is focused on the behaviour of UHI against the defined parameters of LCZ1 of the LCZ classification system, to ascertain the maximum and minimum values possible in a given range. The analysed results seek to determine and communicate the best geometric and surface cover values for outdoor thermal comfort.

Background

As defined by (Rizwan, Dennis, & Liu, 2008), there are three major factors for urban warming; anthropogenic heat, land cover and ventilation. UHI manifestation and intensity is seen as the most representative form to communicate urban warming, especially in research. The simplest definition of the UHI is the atmospheric warmness of a city or an urban quarter compared to its countryside.

According to the description of (Stewart & Oke, 2012), This singularity occurs in cities despite its size, traditionally measured at 1-2 meters above ground level known as the urban canopy layer, just below the mean city roof height. When related with a rural area, the temperature in an urban setting at the same height is higher, in comparison to the rural areas and defined as the urban heat island effect.

Luke Howard in 1833 described the UHI in London in his studies. The magnitude of the UHI was communicated as per the following equation;

UHI Magnitude = T_a in city centre – T_a in rural areas. (T_a - Ambient temperature)

Building Morphology and UHI

Various changes in the built form of the context modify the thermal environment around it, especially in relation to high-rise clusters - where the impacts are generally significant. Local climatic elements such as relative humidity, external air temperature and prevailing wind speed and directions also cause alteration of the microclimate around a particular urban plot. Solar access to urban canyons, incoming solar radiation effects in urban areas occur due to the qualities of the incident surfaces such as albedo effect, are also identified as causes for the variations of the climatic effects in urban areas. Due to these changes, classification of the urban zone is very important in understanding the climatic effects on urban spaces in particular.

Classification between urban and rural usually correspond with population magnitude and density of built structures. This can be interpreted as rural landscapes to be less populated than urban areas, with lesser-built structures and more natural space with vegetation, open soil, whereas urban landscapes have significantly more built structures with larger population. Stewart & Oke,

2012, states that the term urban evokes an eclectic mix of local settings from which its observations have originated, which means, the different characteristics of diverse urban scenarios.

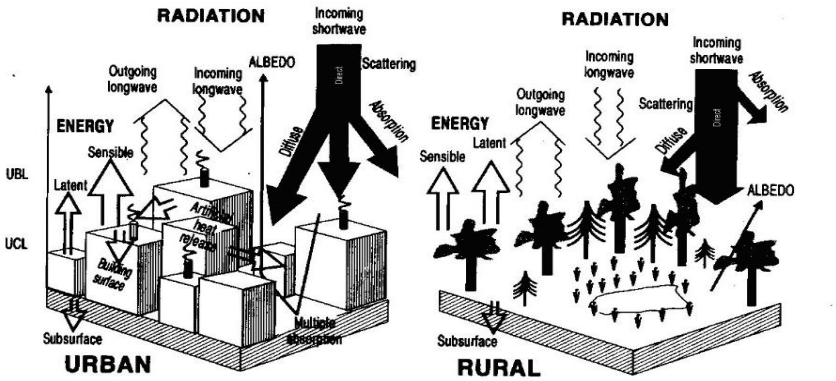


Figure 1: Difference between urban - rural energy exchanges. *Source*: http://urbanez.blogspot.com

Adopting the Local Climatic Zone (LCZ) classification for the study

The logical structure of the LCZ system is supported by observational and numerical modelling data (Stewart & Oke 2010; Stewart, 2011). There are seventeen standard types of LCZs, of which two are defined by construction materials and anthropogenic heat emissions. while the rest are defined by the surface cover and structure. Although there are seventeen different groups, it is still a generic system and thus, cannot capture all the various peculiarities of a city. Its view of the landscape universe is highly reductionist, and, like all classifications, its descriptive and explanatory powers are limited (Stewart & Oke, 2012). However, this classification can be easily applicable to most cities in the World.

The divided classes are “local in scale, climatic in nature, and zonal in representation”. This allows to formally define local climate zones as regions of uniform value quantities. It also delivers a research framework for UHI studies with temperature observations in an urban level with a more standard format, which can correspond, with worldwide level. (Stewart & Oke, 2012). Defined, “local climate zones” as regions of uniform surface cover, structure, material, and human activity that span hundreds of meters (10^2) to several kilometres (10^4) in horizontal scale.

Approach to the study

With regard to calculating the optimum values of UHI effect in a selected area, a separate parametric model is created for optimisation in each design domain. This model is used to determine the optimum form of buildings within defined geometric properties limited to the LCZ1 parameter range. To measure these UHI values depending on different climates, certain data should be included into this aforementioned parametric model. Among the various input data needed in this calculating process, the anthropogenic heat value and the albedo effect values are considered as constant, thus a limitation in this process. Here, anthropogenic heat is a default value extracted from previous research.

Method

LCZ classification system is identified as standard protocol for urban temperature studies. The LCZ1 - compact high-rise of the LCZ classification signifies increased human activities and higher density. The scope of the study is limited to LCZ1.

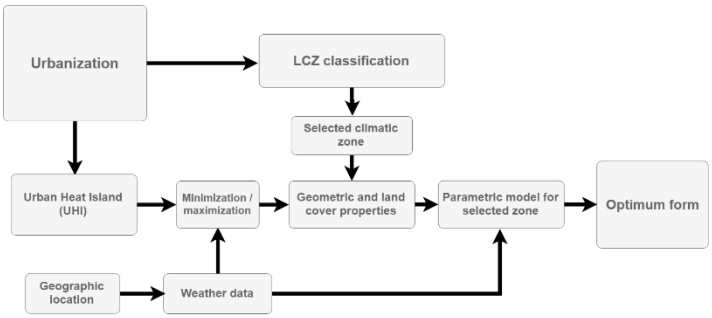


Figure 2: Research workflow. *Source*: Author.

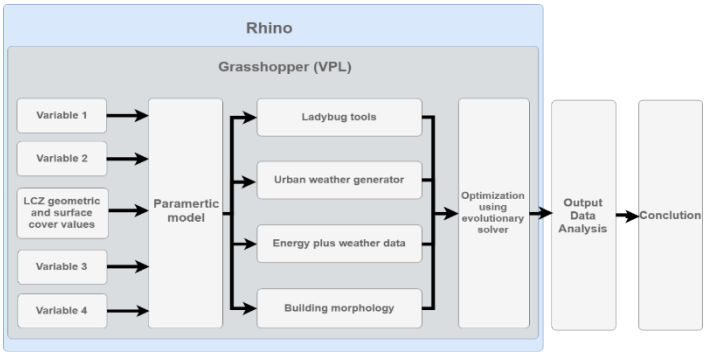


Figure 3: Methodology workflow. *Source*: Author.

Generating a block model for LCZ1

Rhino 3D was used as the primary modelling software with the Grasshopper VPL for the generation of the parametric model for LCZ1. As the first step, a square of 250m by 250m was created as the city block. The values of geometric land cover values for LCZ1 were used to subdivide the city blocks. Assumptions were made to have roads at the perimeter of the city block and 10m offset line was created so the 20m width of roads are created when the city blocks placed together in a grid. This surface area of the road falls under impervious land cover. Thereafter, another offset line was created, but the offset value is a variable defining the impervious land cover area, which is varied between 0-10% of the total area. Within the perimeter of a block, 49 dynamic points were generated in a 7x7m grid as the base points for the buildings (however this can be easily changed using a slider - mode of modification in VPL platform - and use any number of buildings for a particular study). Next, the area of the calculated building surface fraction (see Table1) is divided by the number of buildings, to correspond with the area from the last step. In height control, the slider will be connected to extrude the buildings surface squares according to the height range of the LCZ1. The value for height roughness elements (see Table1) for LCZ1 is >25, but a height limit maximum of 350m is adopted as a limitation for this study. The remaining infill areas between the buildings and road surface areas are considered as the impervious land cover.

Table 1. Values of geometric and surface cover properties of LCZ1 (Stewart & Oke, 2012)

Factor	Property	Value	Description
a)	Sky view factor	0.2-0.4	*Ratio of the amount of sky hemisphere visible from ground level to that of an unobstructed hemisphere*
b)	Aspect ratio	> 2	*Mean height-to-width ratio of street canyons (LCZs 1–7), building spacing (LCZs 8–10), and tree spacing (LCZs A–G)*
c)	Building surface fraction	40-60	*Ratio of building plan area to total plan area (%)*
d)	Impervious surface fraction	40-60	*Ratio of impervious plan area (paved, rock) to total plan area (%)*
e)	Pervious surface fraction	<10	*Ratio of pervious plan area (bare soil, vegetation, water) to total plan area (%)*
f)	Height of roughness elements	>25	*Geometric average of building heights (LCZs 1–10) and tree heights (LCZs A–F) (m)*
g)	Terrain roughness class	8	*Davenport et al.'s (2000) classification of effective terrain roughness (z0) for city and country landscapes.*

From the data above, only c), d), e), and f) were taken as the direct inputs for the parametric variables. a) sky view factor is a dependant of the above selected inputs and b) aspect ratio – is satisfied by the setting up of the road around the city block perimeter. g). Terrain roughness class – is a representation of the character of the category and not considered as an input (*All the above properties are unitless except height of roughness elements are in meters.)*

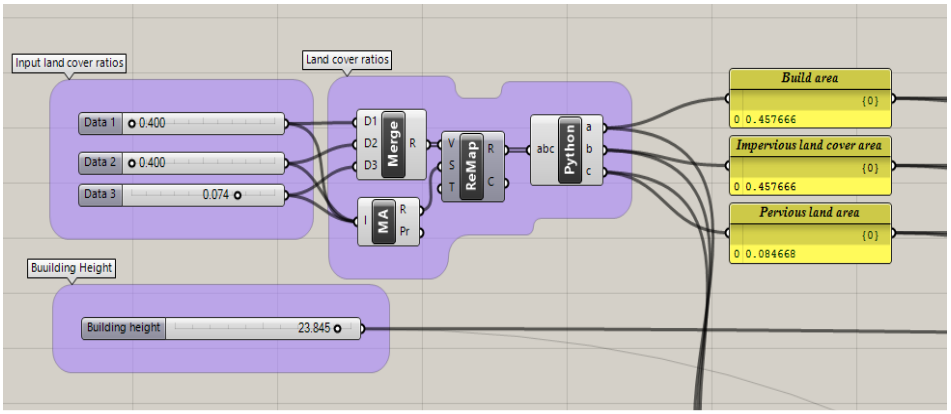


Figure 4: Input of geometric and surface cover properties for LCZ 1 as parameters. Source-Author

The Dragonfly tool (one of main components of Ladybug tools for Grasshopper) is utilised to run the Urban Weather Generator (UWG). UWG is a commonly used UHI modelling software.

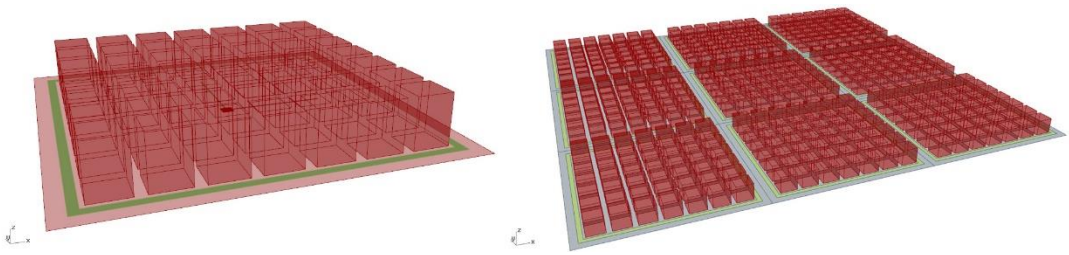


Figure 5: Left image -Completed block model for LCZ1 and Right image - Array of city blocks. Source-Author

The hourly values are calculated by UWG using the input weather data file and the created model. These output results can be easily transferred to other performance simulation processes as well.

UWG consists of four coupled modules,

1. The rural station model
2. The vertical diffusion model
3. The urban boundary layer model
4. The urban canopy + building energy model

After connecting the city geometries and other relevant parameters as inputs for Dragonfly workflow, the UWG is run to test the particular UHI values for that particular input values. Figure 6 shows the hourly data from the modified weather file and the original weather data file. Thereafter, a simple custom Grasshopper code filters out the maximum, minimum and average UHI values. The output data can be used for mapping outdoor comfort.

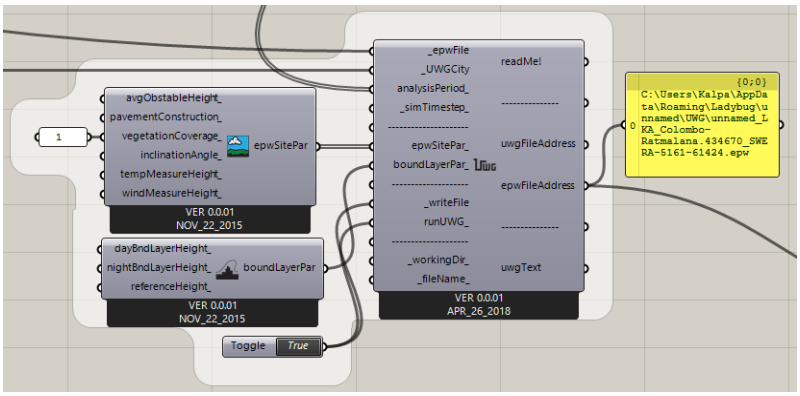


Figure 6: Urban Weather Generator component of Dragonfly. *Source*: Author.

The entire workflow is attached to an Optimisation solver for Grasshopper called Opossum, to find the maximum and minimum of UHI from the model iterations and their respective geometric land cover and building input values relative to LCZ1. Opossum is suitable for time intensive multi objective performance simulations like building energy demand calculation with daylighting and solar radiation optimisations. (Wortmann, 2017)

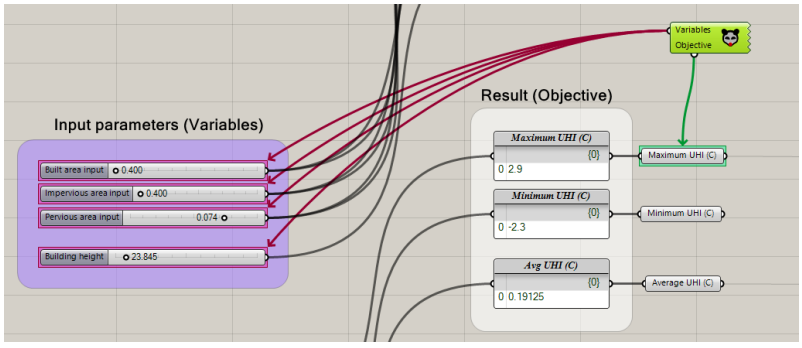


Figure 7: Opossum solver attached to input variables and one of the outputs. *Source*: Author.

Results and discussion

Results from the simulations compare the effect of UHI intensity with the varying LCZ1 parameters. The parametric models generated for LCZ1 is connected to the rest of the workflow to generate a series of iterative simulations to find the best form for each given optimisation, either

minimum or maximum UHI value. Mean Radiant Temperature (MRT) is used as the means to communicate outdoor thermal comfort and comparative urban warming.

Recorded Minimum and Maximum Changes in the UHI Values

Case1 - Search for the maximum magnitude warmer UHI values recorded (in hourly data) and its corresponding geometric values

Build %	43.7729
Built area	27358.0625
Impervious %	54.9451
Impervious land cover area	34340.6875
Pervious %	1.2821
Pervious land area	801.3125
Building height	75
No. of Buildings	49
Block(Length)	250
Block (Width)	250
Total area	62500
% Sum	1
Area per building	558.327806
Max UHI (C)	2.5
Min UHI (C)	-3.1
Avg UHI (C)	-0.14375

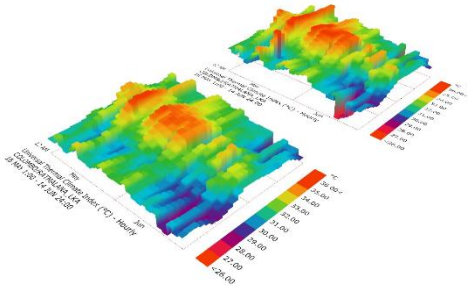


Figure 8: Input values and 3D chart for Case 1. The chart shows the changes of hourly MRT against rural temperature. *Source*: Author.

The hourly MRT values in the chart above (Figure 8.) show a significant increment in both lower and higher MRT values compared to the rural weather data chart. However, the magnitude of increments in the higher MRT values are consequently lower than the increment in lower temperature values. The maximum UHI possible (2.5^{o} C) for this particular zone is caused where, building height reaches its minimum, pervious land cover percentage reaches its minimum and built percentage reaches a below average value (43.7%). However, the average UHI recorded for this form is still a minus value, albeit with a small magnitude (-0.14375).

Case2 - Search for the minimum magnitude of warmer UHI values recorded (in hourly data) and its corresponding geometric values

The minimum magnitude of minimum UHI possible for this particular zone is caused where, the building height reaches its minimum, both building surface cover and impervious cover percentages are in similar value. The results show a similar scenario as the maximum magnitude discussed under Case1. In addition, the magnitude of decrements in the higher temperatures are consequently lower than the increment in lower temperature values.

Case3 - Search for the minimum magnitude of cooler UHI values recorded (in hourly data) and its corresponding geometric values

The hourly MRT values of the chart show a significant decrement in both lower and higher MRT values compared to the rural weather data chart. However, the magnitude of decrements in the lower MRT values are consequently lower than the decrements in higher temperature values. The minimum magnitude possible for maximum UHI is caused where building height reaches above average, both built and impervious land cover percentages are same and pervious land cover percentage reaches an upper limit value.

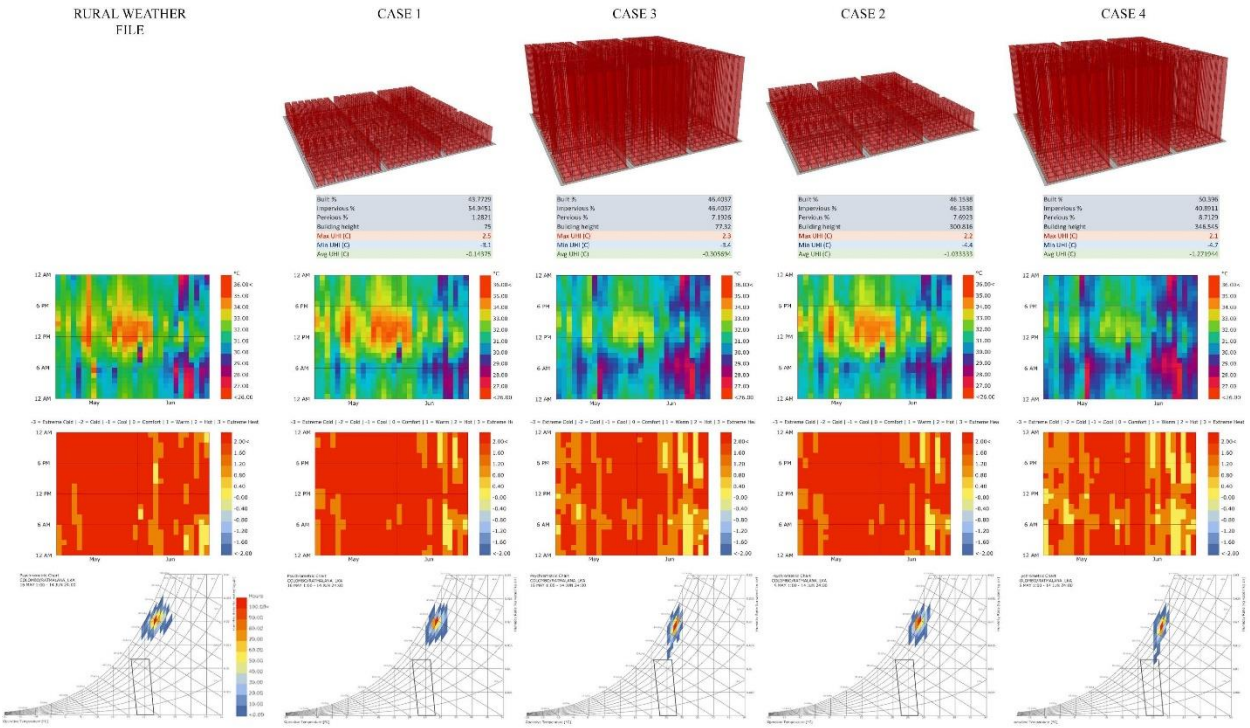


Figure 9: Comparison of results (case1 case2 case3 and case 4). *Source*: Author.

Case4 - Search for the maximum magnitude of cooler UHI values recorded (in hourly data) and its corresponding geometric values.

The hourly temperature values show a significant decrement in both lower and higher MRT values compared to the rural hourly MRT chart. However, the magnitude of the decrement in the higher MRT values are significantly higher than the decrement in lower MRT values. The minimum UHI compared to the original weather file is caused where, building Height reaches its maximum, impervious land cover reaches its minimum and pervious land cover gets an above average value. Average UHI shows a minus value and it shows the highest magnitude among all the LCZ1 optimisation results (-1.271944).

Conclusion

The study is aimed at exploring the relationship between Urban Heat Island effect and the city form, using the existing Local Climatic Zone classifications as a base protocol. The initial inception turned toward the parametric modelling considering its potential of finding an optimal solution for the problem using the derivative free optimisation techniques.

Out of the 17 LCZ categories in the existing framework, LCZ1 was selected to analyse the UHI effect due to the density and high-energy consumption associated with it. Four optimisation runs were tested, focusing on the maximum and minimum boundaries of the warmer UHI values, maximum and minimum boundaries of the cooler UHI values of calculated hourly data of each optimisation.

- Findings clearly show the direct association of the building morphology to UHI as results depict particular parts of an urban block can create areas of reduced UHI intensity.

- The morphology optimisation for a LCZ1 block fails to create thermally comfortable areas within the zones (see Figure 9). Although, morphology changes drive comparably cooler areas. Thus, compact high-rise areas of a city are not conducive for UHI mitigation, primarily due to factors that research show are the main causes for UHI are heightened in this particular form.
- Building surface cover for the optimised forms showed lower percentages. Therefore, it is evident that a block form that is classified as LCZ1 needs a lower threshold of built space for UHI minimisation. The implication of which is that compact high-rise areas of a city should be avoided. If high-rise developments are needed the LCZ classification should be more towards LCZ4 or open-set high-rise, where the building surface fraction upper limit is 40%.
- It was found that higher impervious land cover percentages contribute to the increase of the UHI value.
- Optimised forms from LCZ1 suggest forms of higher UHI values consists of minimum pervious land cover percentages and forms of lower UHI values consists of higher percentages of pervious land cover values.

.

According to the above observations, it is possible to generally suggest the possibility to minimise the UHI by raising the building heights, reducing the impervious land cover and maximising the pervious land cover in zoning stages. However, the input percentage variables are interdependent of each other and this rule of thumb could possibly be valid only inside the parameter value range of LCZ1 and cannot suggest a globally valid answer for different forms outside the parameter value range. Further, the minimisation occurs at specific parts of an urban block, not as an overall phenomenon. As the study explores, building a custom parametric model to correspond with the context and then running the optimisation is recommended to gain more accurate and finite results.

The search for optimum block form for UHI minimisation is crucial in today's warming city contexts in particular and the world in general. Evaluation protocols that can be developed from this platform signifies the way forward, where overall planning and building regulation thresholds are insufficient to deal with specific parts of the city, with differing orientations and exposures to natural boundaries. The ultimate step could be an approval system that evaluates UHI impacts, albeit over-the-counter, encouraging climate sensitive intervention into everyday urban design.

Limitations of Methodology and Study

- The parametric model is developed only as a block model and does not explore the possible forms of complex building shapes.
- Anthropogenic heat input value added during the calculation is a default value based on the city characteristics and does not use a proper calculated method for the selected city.
- City block is considered to have no vegetation; which research shows as a significant means for UHI mitigation.

Future Research

This initial research limits its scope to a context to consider the parametric model-based analysis to cater to a design process of built morphology in urban planning viewpoint. This could

be further developed by increasing the scope of the study where much specific details and characteristics can be included to increase the precision of the results. In addition, this parametric model only explores the behaviour of UHI with a block model of a cuboid shaped buildings and further developed for testing of different types of cities with different building languages.

Additional parameters also could be considered in calculations as anthropogenic heat, albedo and vegetation. In addition, it is possible to integrate the advanced material properties into the workflow as well, where the inclusion of these properties will also improve the precision of the results. These implementations can be done in future researches as to improve the realistic nature of the calculations and simulations to gain much more precise results to work on productive building technologies and architecture to cater for the sustainability of urban contexts.

References

Perera, N. G. R., Emmanuel, M. P. R., & Mahanama, P. K. S. (2012). 576: Mapping "Local Climate Zones" and relative Warming Effects in Colombo, Sri Lanka. In ICUC8 – 8th International Conference on Urban Climates, Dublin, Ireland.

Perera, N.G.R. (2015). Climate-Sensitive Urban Public Space: A Sustainable Approach to Urban Heat Island Mitigation in Colombo, Sri Lanka. PhD Thesis. University of Moratuwa, Sri Lanka

Perera N.G.R., Emmanuel. R. (2018). A "Local Climate Zone" based approach to urban planning in Colombo, Sri Lanka. URBAN CLIMATE, Vol.23, Pages 188-203 http://dx.doi.org/10.1016/j.uclim.2016.11.00621.

Rizwan, A. M., Dennis, L. Y. C., & Liu, C. (2008). A review on the generation, determination and mitigation of Urban Heat Island. Journal of Environmental Sciences, 20(1), 120–128. https://doi.org/10.1016/S1001-0742 (08)60019-4

Stewart, I. D., (2011). Redefining the urban heat island. Ph.D. dissertation, Department of Geography, University of British Columbia, 352 pp. [Available online at https://circle.ubc.ca/handle/2429/38069.]

Stewart, I. D., & Oke, T. R. (2010). Thermal differentiation of local climate zones using temperature observations from urban and rural field sites. Extended Abstracts, Ninth Symp. on Urban Environment, Keystone, CO, Amer. Meteor. Soc., 1.1. [Available online at http://ams.confex.com/ams/19Ag19BLT9Urban/webprogram /Paper173127.html.]

Stewart, I. D., & Oke, T. R. (2012). Local Climate Zones for Urban Temperature Studies. Bulletin of the American Meteorological Society, 93(12), 1879–1900. https://doi.org/10.1175/BAMS-D-11-00019.1

Wortmann, T. (2017). Model-based Optimisation for Architectural Design—Optimizing Daylight and Glare in Grasshopper (Vol. 1). https://doi.org/10.1080/24751448.2017.1354615

Modeling potential air temperature reductions yielded by cool roofs and urban irrigation in the Kansas City Metropolitan Area

Seongeun Jeong, Lawrence Berkeley National Laboratory (USA)
Dev Millstein, Lawrence Berkeley National Laboratory (USA)
Ronnen Levinson, Lawrence Berkeley National Laboratory (USA)

ABSTRACT

We evaluate two mitigation strategies for urban heat island (UHI) in the Kansas City Metropolitan Area (KCMA). Using the Weather Research and Forecasting (WRF) model, we assess the potential benefits of reflective "cool" roofs and urban irrigation on air temperature in typical summer conditions between 2011 and 2015, and during six of the strongest historical heat waves from 2005 to 2016. Under the typical summer conditions, we simulate 2-m air temperature for 10 summer weeks, finding average daytime (07:00–19:00 local time) temperature reductions of 0.08 and 0.28 °C for cool roofs and urban irrigation, respectively. During the six heat-wave episodes, we find daytime temperature reductions of 0.02 and 0.26 °C for the two scenarios, similar to those under typical summer conditions. Our results suggest that urban irrigation can be more efficient than cool roofs in mitigating UHI in metropolitan regions where the majority of the land cover is comprised of areas with low urban (i.e., non-vegetated) fractions. Finally, we find the alteration of surface conditions due to enhanced roof albedos influences precipitation within the WRF simulation, in particular during the heat waves. Further research would be necessary to determine the robustness of this last finding.

Special Issue Journal	:	Urban Climate
DoI	:	https://doi.org/10.1016/j.uclim.2021.100833
Citation	:	Jeong, S., Millstein, D., & Levinson, R. (2021). Modeling potential air temperature reductions yielded by cool roofs and urban irrigation in the Kansas City Metropolitan Area. Urban Climate, 37, 100833.

Envelope heat load characteristics of the building cluster considering radiate heat exchange process in an urban district

Yasunobu Ashie[1]*, Building Research Institute (Japan)*

ABSTRACT

We developed a numerical model to calculate the annual envelope thermal load of several buildings in the urban area taking a radiative impact of neighboring buildings into consideration. We conducted benchmark tests on air-conditioning thermal load simulation targeting single building to verify this development model and confirmed that we can obtain results appropriate compared to those obtained with existing air-conditioning thermal load calculation tools. Moreover, we conducted case studies targeting building clusters. Their results proved for the first time that a change in the aspect ratio between building height and pitch significantly affects envelope thermal load and quantitatively proved an effect of higher reflection of the urban surface on cooling and heating load.

Introduction

Energy saving of buildings is one of important factors in order to address the issue of global warming (IPCC, 2018). In the past, a number of the latest technologies were conducted to the buildings for the reduction of thermal load and improvement of energy performance of equipment and facilities of buildings (SHASE 2017). The simulation technology to predict thermal load of buildings is, in particular, the basis of the designers' direction of energy minimum. In general, the response factor method based on the Laplace transformation theory was applied to the thermal load predictive model so that the heat-transfer process of multi-layer walls can be calculated efficiently (Mitalas and Stephenson 1967).

On the other hand, if we extend the target of analysis to the city level, there are a variety of possibilities of energy-saving design such as radiate interactions in multi buildings, cooling effects of greenery or water and optimal placement of DHC system all of which cannot be achieved by only one building. As part of these possibilities, it is necessary to handle complex geometric forms and diversified physical phenomena to predict an outdoor thermal environment. Therefore, it is difficult for the traditional method on the basis of the linear theory to be extended to the non-linear problem and to respond to the problem of coordinating several buildings. This study applies the finite difference method and intends to establish a thermal load prediction method targeting several buildings in the urban area taking into account a neighboring radiative impact which has not been considered sufficiently in the past such as shades formed by buildings.

Method

We assume that each building consists of one room in the thermal load prediction targeting several buildings in the urban area. We predicted thermal load integrated the envelope as a whole and it is noted that we did not handle the problem of realistic buildings with several rooms.

[1] Corresponding Author: [ashie@kenken.go.jp].

A similar assumption is made in the urban canopy model (Taha *et al.* 1991). However, this study is more precious in that the thermal load characteristics of each building in the urban area can be considered individually. Figure 1 shows the heat balance of the urban surface and the heat balance in buildings. We can see that this model has a coupled structure of those heat balances. The finite difference method applies as an analytical method, since it has high non-linearity and targets diversified physical phenomena.

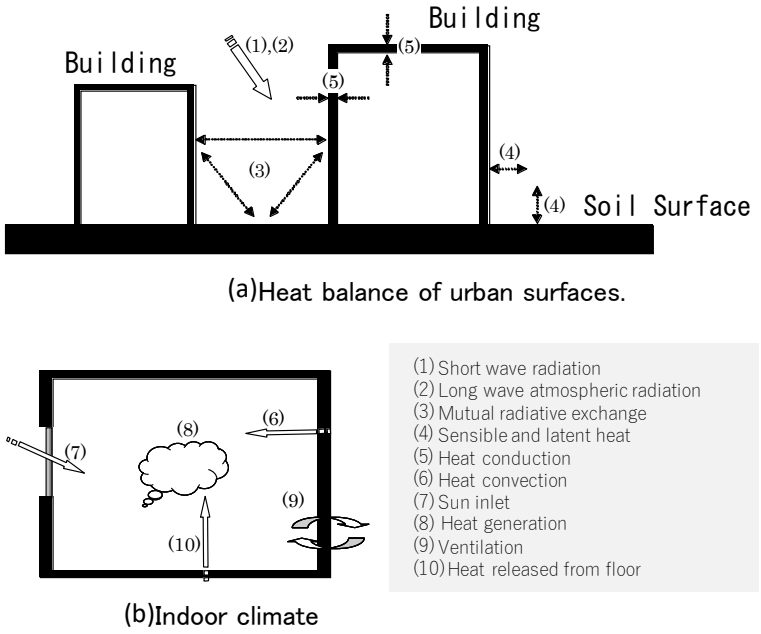
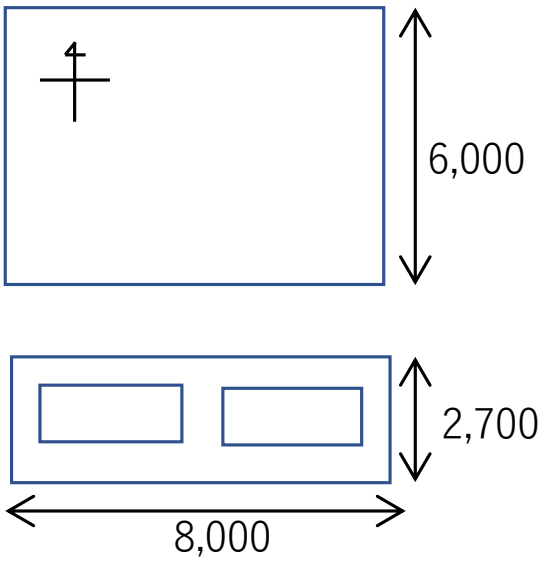


Figure 1 Heat balance model of urban surfaces coupling Indoor climate.

Verification of model by benchmark tests

BESTEST (Judkoff and Neymark 1995) approved by IEA is a highly reliable benchmark test, because it records results of calculations of thermal load of single building on the basis of detailed calculation conditions and main tools. As the outcomes by our development tool can be applicable to analysis of single building, we compared NO.600 which incorporates various conditions such as openings and intermittent air conditioning in BESTEST. The outline of NO.600 is shown in Figure 2. Figure 3 compares our tool with calculation tools used by other countries to calculate the annual cooling thermal load and heating load. The cooling load falls within the range of the results obtained with traditional tools. On the other hand, the heating load is undervalued compared to the results obtained using traditional tools, but the values are similar.



Item	Setting
Weather data	Typical meteorological year Weather data
Location	39.8°N, 104.9°W, Alt: 1 609 [m]
Building size	6 000 × 8 000 × 2 700
Heat mass	Low
Air exchange rate	0.5 [-]
Heating start temperature	20 [°C]
Cooling start temperature	27 [°C]
Short wave radiation absorption of opaque external surface	0.6 [-]
Short wave radiation absorption of opaque internal surface	0.6 [-]
Glass area and orient	12 [m^2], south

Figure 2 Building form and settings in BESTEST NO. 600.

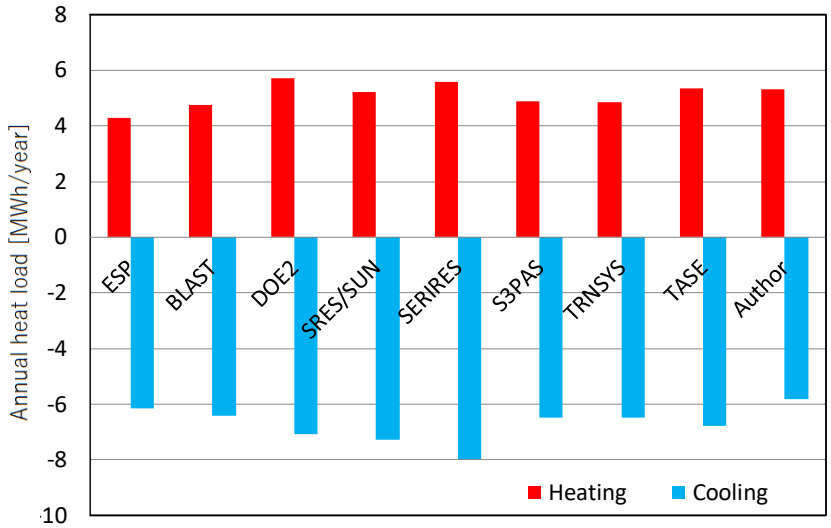


Figure 3 Simulated results of NO. 600.
In the figure, heating load is displayed to the positive side, cooling load to the negative side.

Case studies

We conducted 12 case studies shown in Table 1 by changing the aspect ratio of the layout of buildings and the solar reflectance of the urban surface. The meteorological conditions and other conditions of buildings are set to be the same as those used in BESTEST. Figure 4 shows the surface temperature distribution at 2:00 p.m., August. Here, it is noted each hourly simulated surface temperature is monthly averaged from 1 August to 31 August. The surface temperature of windows facing south is low. We can understand that shades created depending on the distance from neighboring buildings affect the surface temperature. Figure 5 shows the surface temperature distribution in medium located cases where the solar reflectance of the roof, wall and ground increased. A highly reflective roof decreased the roof surface temperature by around 15 degrees, but no change is found in other areas. A highly reflective wall decreased the wall surface temperature by around 10 degrees, and the window surface temperature increases by 2-3 degrees due to reflection from the wall surface. A highly reflective ground decreases the ground temperature by around 10 degrees and more, and the wall surface/window surface temperatures increase by 2-3 degrees due to reflection from the ground.

Figure 6 shows the relationship between the annual envelope thermal load and the aspect ratio. Moreover, Figure 7 indicates relative changes in a similar manner on the basis of the cases before the roof, wall and window were replaced to highly reflective ones. Consequently, relative change can be shown by next equation.

$$\text{Relative change} = (\text{annual load with measures minus without measures}) / (\text{annual load without measures}) \times 100 \big|_{\text{aspect ratio}}. \quad (1)$$

These results proved that the change in the aspect ratio, that is, the change in the distance from neighboring buildings dominantly affects the envelope thermal load. If a highly reflective roof is adopted, the cooling load shown by dotted line may drop by 6~12%, but the heating load shown by solid line increases by 1~2%. It was also proven that relative changes become notable in cases where the aspect ratio is smaller. A highly reflective wall surface result in the reduced cooling load by 1~4%, and it was proven that relative changes become notable in cases where the aspect ratio is larger. The changes by high albedo wall are not clear in heating load. In the case of a highly reflective ground, the cooling load increases by 2~5%, while the heating load increases by 0~1%. It was proven that relative changes become notable in cases where the aspect ratio is larger.

Conclusion

We created a model of the heat transfer process of several buildings in the urban area and developed a method of calculating the envelope thermal load by building. We conducted benchmark tests on single building on the basis of BESTEST. It indicated that the major air-conditioning thermal load calculation tools and the development tools we used in this study produce similar results. We also conducted case studies on several buildings, and it was proven for the first time that a change in the distance from the next building significantly affects the envelope thermal load. Moreover, it was proven quantitatively that the highly reflective surface of buildings contributes to the reduced cooling load, while the highly reflective ground increases the

cooling load. In addition, further consideration will be required for the verification of numerical modeling.

References

IPCC 2018. "Global Warming 1.5°C: An IPCC Special Report on the impacts of global warming of 1.5°C above pre-industrial levels and related global greenhouse gas emission pathways, in the context of strengthening the global response to the threat of climate change, sustainable development, and efforts to eradicate poverty", *IPCC Special Report*.

SHASE 2017. "Expansion and Advanced Rationalization of the Building Equipment Field Through Collaboration in New Technology - Aiming to Build an Ultra-Low Carbon Society", *The SHASE 21st Century Vision Plus*.

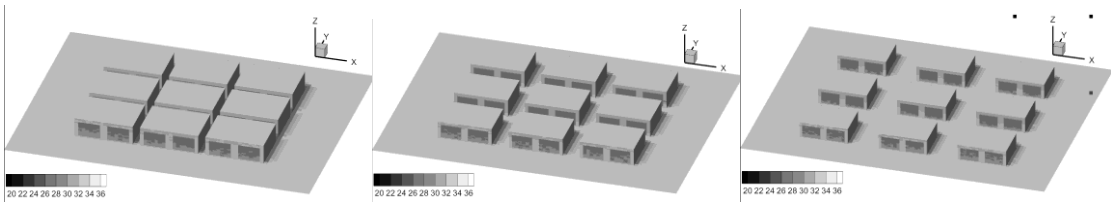
Mitalas, G.P. and D. G. Stephenson 1967. "Room Thermal Response Factors", *ASHRAE Transactions*, 73.

Taha, H, H. Akbari, A. Rosenfeld 1991. "Heat island and oasis effects of vegetative canopies: Micro-meteorological field-measurements", Theoretical and Applied Climatology, 44-2: 123-138.

Judkoff, R., J. Neymark 1995 "International Energy Agency Building Energy Simulation Test (BESTEST) and Diagnostic Method", NREL/TP-472-6231.

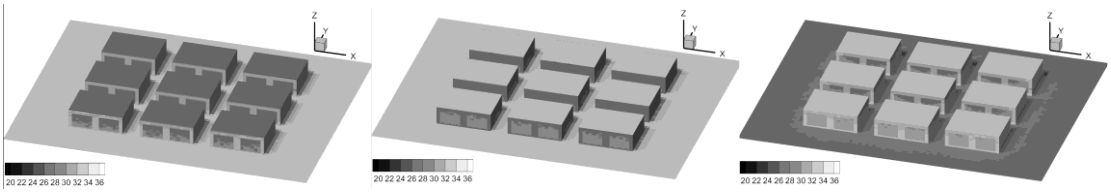
Table 1 Case study changing the aspect ratio of the layout of buildings and the solar reflectance. Aspect ratios (building pitch L/ building height H/) for low, medium, high layout are 0.37, 0.93, 1.85. Building surface albedo is 0.4 for default, 0.8 for countermeasure, and soil surface albedo 0.2 for default, 0.6 for countermeasure.

Name	Aspect Ratio	High Albedo
Case_ ℓ	low	None
Case_m	medium	None
Case_h	high	None
Case_ ℓ R	low	Roof
Case_mR	medium	Roof
Case_hR	high	Roof
Case_ ℓ W	low	Wall
Case_mW	medium	Wall
Case_hW	high	Wall
Case_ ℓ S	low	Soil
Case_mS	medium	Soil
Case_hS	high	Soil



(a) Case_ ℓ (b) Case_m (c) Case_h

Figure 4 Simulated surface temperatures at 14:00, August.
Panel (a) shows the case of aspect ratio low, panel (b) medium and panel (c) high.



(a) Case_mR (b) Case_mW (c) Case_mS

Figure 5 Simulated surface temperatures at 14:00, August.
Panel (a)-(c) shows the cases of aspect ratio medium, panel (a) high albedo roof, panel (b) high albedo wall and panel (c) high albedo soil, respectively.

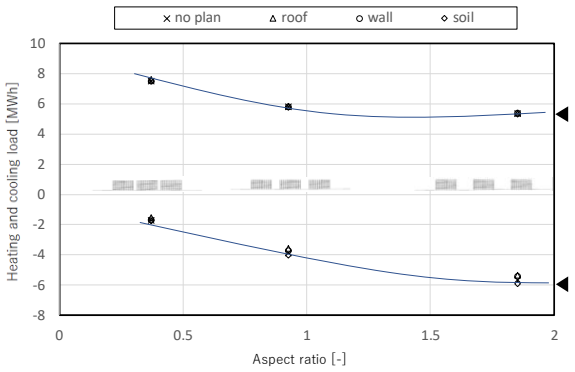


Figure 6 Relation between aspect ratio and annual load.
The arrow heads shown in the right side of the figure show the numerical result of case_m.

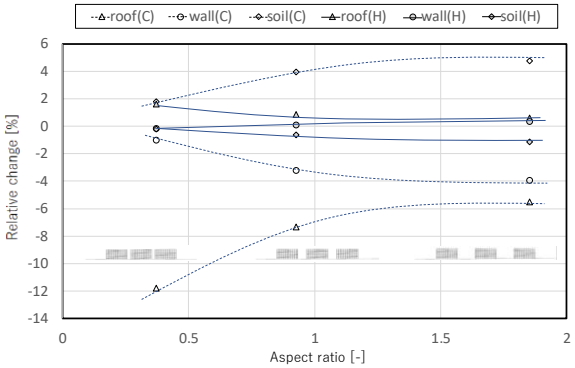


Figure 7 Relation between aspect ratio and relative change of annual load.
If relative change is displayed to the negative side, the loads decrease by measures. On the contrary, the loads increase by measures in the positive side.

Minimizing the inconsistencies of urban building energy simulations through strong microclimate coupling

Georgios – Evrystheas Kyriakodis[1]*, University of La Rochelle / CSTB (France)*
Emmanuel Bozonnet, University of La Rochelle (France)
Peter Riederer, CSTB (France)

ABSTRACT

The impact of microclimate conditions on energy demand is investigated through various coupling schemes between a zonal microclimatic tool and an urban building energy simulation software for a canyon settlement. Additionally, the impact of split air condition units on ambient air temperatures is examined for an annual period. The numerical calculations for a mild oceanic climate confirm the necessity of integrating the microclimate conditions in building energy performance simulations. Air conditioning units, have a significant impact on air temperature both for cooling and heating period. Furthermore, discrepancies emerging from online and offline coupling schemes are highlighted.

Introduction

The increased urbanization of the past decades combined with energy harvesting constructions and huge alterations in land use constitute the base of the local climate change, known as urban heat island (UHI) effect. It deals with the development of higher air temperatures in city centers compare to the rural environment. UHI is experimentally documented for hundreds of cities around the world (Santamouris 2015). Local characteristics and their respective heat sources contribute to the amplitude of the effect (Santamouris et al. 2015). In parallel, energy demand for cooling is the fastest growing end-use in buildings. According to IEA's Tracking Clean Energy Progress 10 air conditioners will be sold every second over the next 30 years.

To this end, particular attention has been paid to the feedback of AC systems on outdoor air temperatures. De Munck (De Munck et al. 2013) demonstrate a coupling scheme between a meso-meteorological model and a single layer-module to account for the built environment, in order to estimate Paris air temperature increase due to air conditioning units. The 6 days' simulation period was chosen for anticyclonic conditions of the 2003's heatwave. The outcomes revealed a maximum of 2°C for the future doubling of air conditioning waste heat released to air. Similarly, Salamanca et al. (2011) integrated a meso-scale with a multilayer urban canopy and a simplified building energy model for the city of Houston (nested area of 110km). The results obtained from a 2-day simulation period, found an increase in night temperatures of up to 2°C. Concerning district scale, a coupled "ping-pong" scheme was developed from Hsieh et al. (2007) based on a BES and a computational fluid dynamics (CFD) code. In this study only five simulation hours where realized during a hot night in Taipei city in Taiwan, although the authors indicated that the maximum measured heat island intensity was depicted at 2pm with a value of 4.9°C. He estimated that the maximum air temperature increase was found to be 1.89°C for a fixed COP value of a window type AC unit. Finally, Wen and Lian (Wen and Lian 2009) developed a

[1] Corresponding Author: gkyria01@univ-lr.fr, gkuriakodis@phys.uoa.gr

mathematical nested urban box model, to correlate the atmospheric stability with the possible air temperature increase due to the fluxes of the AC units injected in the lower level of the atmosphere. In their method building parameterizations were not taken into account. They estimated that air temperature increase could reach 2.56°C and 0.2°C under inversion and normal conditions respectively. These studies could give an estimation about the amplitude of the UHI combined with systems feedback in air temperatures, however they are either temporally limited (from hours to days) either the representation of buildings as cells of coverage ratio do not allow to correlate individual building thermal footprint with the local ambient environment.

The dependency of rising energy demand and local climatic phenomena is demonstrated in various studies. Considerable attention has been concentrated to cooling dominated period, since the phenomenon is much more intense during it. To this end, various numerical approaches and studies arise with the scope of estimating the potential energy loss capture due to the local phenomena. Usually, a Building Energy Simulation (BES) model coupled with a microclimate code is preferred. Martin (Martin et al. 2017), performed a one-way coupling of a lumped thermal parameter model with a BES. The outcomes of this study showed that the divergence between estimates of the cooling demand varies whether detailed and simplified BEMs are run under isolated or non-isolated conditions. Gobakis (Gobakis and Kolokotsa 2017) followed a similar coupling approach between a BES and a microclimate model to study the impact of different convective heat transfer coefficients to a building settlement in the University campus of Chania. In their study showed that cooling demand could vary up to 25%. Another effort to minimize the uncertainties of building energy simulation has been conducted by Allegrini (Allegrini, Dorer, and Carmeliet 2012). In their approach, they examined the variations on energy demand between a stand-alone building and buildings integrated in a street canyon by coupling a 2D CFD code and a BES tool for a moderate climate in Basel, Switzerland. He showed that space cooling demand is higher while space heating demand lower for the street-canyon configuration. He suggested that neglecting UHI effect leads to an important underestimation of the cooling demand. This type of approaches seem capable to serve the concept of Net zero energy buildings (NZEB) however, they are also temporally limited due to the time expensive microclimate simulations (CFD), and also spatially restrained, as they account just for the building scale. Moreover, the offline coupling schemes, could give a general estimation about the actual environmental conditions but crucial information is lost. Considering a district, the site-specific air temperature could significantly vary.

In order to extend the boundaries of the simulation domain, a novel series of coupled models have emerged. Mauree (Mauree et al. 2017), applied a one-way coupling scheme between an UBEM and a 1D meteorological model to study the impact on energy demand when urban climate is taken into account for the EPFL campus. They demonstrated that the wind speed and air temperature deviations compared to a typical dataset, could lead to a reduction of the simulating heating demand error by a factor of 2.

In this framework, we propose a new methodology of a coupling scheme between an UBEM and a coupled microclimate model aiming in a twofold study: minimizing the inconsistencies of the UBEM model by considering local microclimate phenomena and testing the impact of energy systems to microclimate and vice versa. The developed coupled model allows to take into account a variety of phenomena, such as detailed radiative and convective transfers for the buildings and the outdoor environment, building thermal transfers, and a diversity of detailed representation of energy systems.

In the present study, three coupling schemes are tested for a street canyon settlement. Annual simulation results of energy loads are examined, while the feedback of air conditioning

systems to ambient air is also evaluated. Furthermore, the discrepancies between online and offline coupling schemes are estimated.

Methodology

Overview

Considering the existing challenges in energy assessment simulations, a strong coupling scheme (Kyriakodis, 2019) is implemented to enhance the meteorological boundary conditions of the urban building energy model. The proposed combination could offer also the possibility to address the objective of systems feedback to air temperatures, subtracting them from the sensible heat ejected from the buildings. Thus, a research developed tool, (1) EnviBatE (Gros, Bozonnet, and Inard 2014), representing a coupled scheme between a simplified BES tool, a solar radiation model and an urban airflow simulation code and a dynamic simulation platform based on the bottom-up approach for district and territory energy assessment, (2) Dimosim (Riederer et al. 2015) have been selected to fulfill the assessment. EnviBatE initially aim to assess building energy demand, including microclimate interactions on buildings. It was further used to study the impact of cool materials in various rehabilitation projects. Dimosim developed with the aim to simulate any possible combination of systems, models and buildings at any scale, at a high execution time and in a modular and flexible way in order to respond to any demand and type of project. Both tools are developed in object-oriented programming language, Python.

Workflow

Import layouts. The geometrical data of Dimosim are characterized by an open structure to enable multiple data sources like databases, standardized information models, or self-defined file formats. More in detail, the structural geometrical file corresponds to a cityGML or json file format. The data are obtained by 2D or 3D vector databases. EnviBatE uses a design software of 3D modeling to process the geometrical layouts. A module capable to transform data between the referenced formats, has been implemented in the coupled model. It allows to index the studied elements (building, surfaces) while in parallel, ensures that the building footprints are identically imported to both tools.

Meshes generation. The generation of various different meshes is a necessary action in order to perform the microclimate simulations. Each of them corresponds to a different calculation domain. At the end, all of them are integrated in a unique final zonal mesh that accounts for buildings, outdoor surfaces and outdoor air cells. More in detail, EnviBatE tool, is using a fine triangulated mesh (**Figure 1**b) for the calculation of solar radiation, a hexahedral structure grid for the airflow calculation (**Figure 1**a) and an unstructured zonal outdoor mesh (**Figure 1**c). Indexation and generation of the meshes are automatically performed by the core code of the tool. In the actual case study, we choose a characteristic length of the outdoor cells equal to the length of each thermal zone. This option ensures that the heat injected from buildings and the respective system flux is equally diffused in the adjacent air volumes.

Solar calculation. Solar radiation is pre-processed for both tools. In this case study, we choose to integrate in the coupled model the solar radiation calculation module of EnviBatE. It corresponds to Solene (Groleau, Fragnaud, and Rosant 2003) radiation model and it is based in the radiosity

method. This option allows to evaluate the: 1) direct solar irradiance, 2) sky luminance, 3) solar reflections and longwave interchanges in the urban environment. The spatial resolution of the solar mesh corresponds to maximum 2m, discretizing each building surface to at least 44 sub-surfaces (**Figure 1**b). At the end, the incident radiation corresponds to the sum of its respective triangles. Sky vault generation is required and it is also discretized to 256 patches.

In order to perform fast calculations in a detailed meshed geometry, the calculation is performed in a daily basis with standard conditions of a clear sky. Thus, solar irradiance from the meteorological file was used to weight it as a function of real conditions. For the diffuse component, daily average Perez coefficients were used.

Airflow calculation. For the airflow calculation, the three components (u, v, w) of air velocity are required for each outdoor cell. They are provided to the model by the use of the urban airflow model QUIC (Pardyjak and Brown 2003). This model is based on empirical laws and a zonal approach developed by Rockle (1990) to provide airflows consistent with the continuity equation. This approach was selected in order to avoid time consuming CFD calculations, as our purpose is to compute the coupled effects of buildings and microclimate over an annual period. The computational domain of this case study consists of 86 x 86 x 24 computational cells, discretized to 1(dx) x 1(dy) x 3(dz) m for each axis respectively (**Figure 1**a).

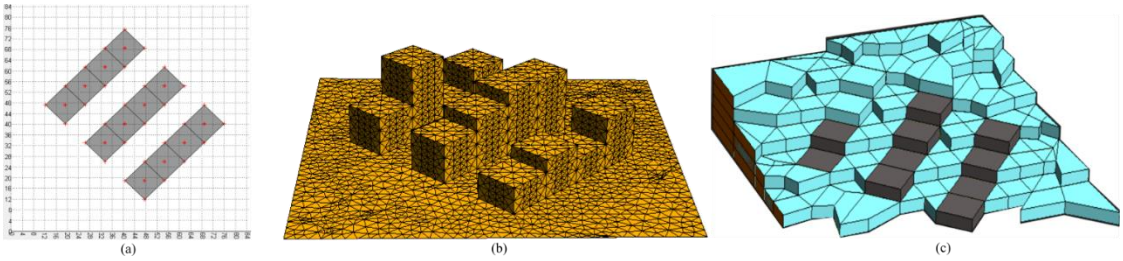


Figure 1. The fine airflow grid (a), triangulated solar mesh (b) and the integrated zonal mesh (c).

Building models. Both models perform building energy simulations for energy consumption (heating, cooling, ventilation and lighting) in buildings. Notably, the building model of EnviBatE is established with the Weighting Factors method (Rousseau 1978). The surface temperature, calculation is strongly coupled to the respective outdoor air temperature, allowing to take into account convective exchanges. Ventilation and occupancy schedules are also included in the model, according to French national regulations or user defined data. In parallel, the building model of Dimosim, corresponds to RC structure taking into consideration the necessary features to perform the thermal calculations. Windows, wall/roof and floor external envelopes, thermal bridges and internal mass, ventilation/infiltration and internal gains from occupants and appliances are included to perform the thermal model computation. In the current version of Dimosim, heat exchange between zones is neglected and only thermal inertia is considered. This is currently being updated and multizone calculations could be achieved in a future version of the tool.

Case study Implementation

The case study is based in an urban canyon settlement composed of 16 buildings of various heights randomly selected. The orientation of the domain is 45° (from N counter clockwise). Each thermal zone is 3m height and the floor surface is 100m². Window to wall ratio is assumed to be 0.2. The thermal transmittance is 0.34, 0.78 and 2.5 [W/m²K] and the solar reflectance is 0.3, 0.2

and 0.08 for zone envelopes and floors, roofs and windows respectively. Interior insulation of polystyrene has been added, as it is the most common application in French building stock. Constant infiltration rate of 0.7 [ACH] is selected. The set point temperatures are forced to be 28 and 19 [°C] for the cooling and heating season. The selection is established to represent buildings constructed after 2000s. Indeed, the thermal characteristics are strongly affecting the performance of the buildings and thus their respective impact to the microclimate. For comparison purposes, we followed this general application.

The urban geometry has a maximum aspect ratio of 1.8 [H/W] formation, depicting a discontinuous row of mid-rise high density urban canyon, following the urban typologies classification of (Stewart and Oke, 2012). The outdoor space is formed by concrete pavements presenting a thermal transmittance of 3.2 [W/m²K] and 0.5 albedo. This morphology is representative of many European cities.

Split air conditioning units amount to the energy system providing the necessary loads. This type of systems are commonly used and preferred as an instant and low-cost solution for individual usage. The efficiency is set to 1 and the mode is reversible to account both for heating and cooling period. The fuel type is set to electricity. In this case study, we assume that in every thermal zone a local AC unit is operating. The meteorological file corresponds to typical meteorological year data (TMY2) and it is interpolated with CCWorldWeatherGen (Jentsch et al., 2013) to 2030 according to the A1B future scenario of forcing agents given in the IPCC Special Report.

Coupling Procedures

Coupling surface temperature (Cpl_Ts). In the microclimate model, surface temperature is strongly coupled with the outdoor air temperature. Thus, we can assume that the impact of microclimate (present wind speed and air temperature conditions) is embedded in the calculation. We choose, as a first step, to impose this parameter combined with the pre-calculated shortwave solar radiation to all building surfaces of the UBEM (Figure 2). Simultaneously, the estimated heat flux of the AC unit is injected to the adjacent outdoor air cell. The concurrent exchange is established through a co-simulation platform based on sockets for every time step of the annual simulation.

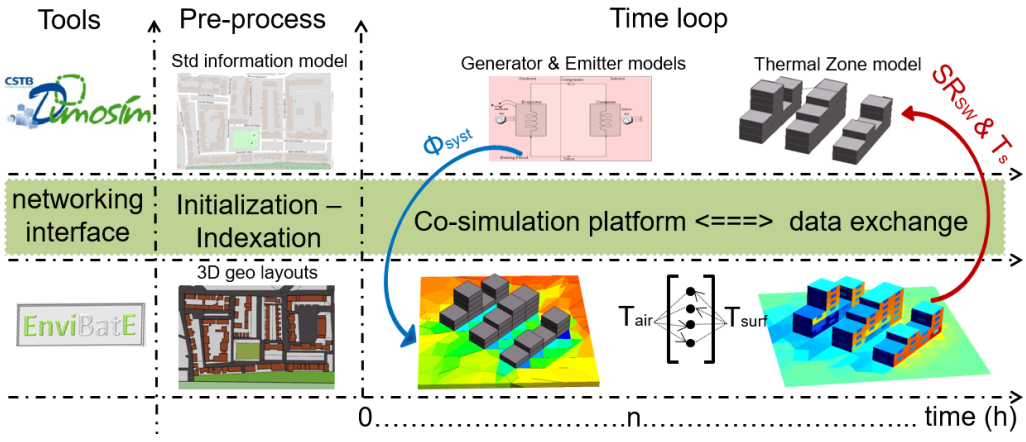


Figure 2. The initial coupling scheme (CPL_Ts) where the surface temperature is provided to the UBEM.

Coupling air temperature (Cpl_Inter). A second coupling scheme (Figure 3) is established following the same exchange approach. At this step, we choose to "integrate" the zonal model to the UBEM. In order to perform the concurrent exchange, we set the calculated outdoor air temperature of the microclimate model as a boundary condition to the UBEM. In parallel, building and system thermal fluxes are injected to the zonal cells. Notably, the building model is simulated only once (UBEM calculation) reducing the execution time in half. Solar radiation has remained intact.

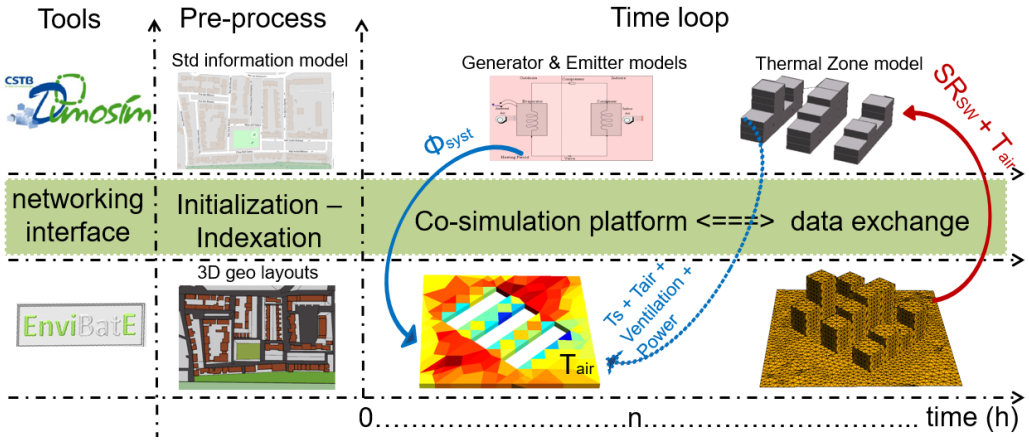


Figure 3: The integrated coupling scheme (CPL_Integ) where the air temperature is used as boundary to the UBEM.

Offline coupling of air temperature. The last years the most commonly used methodology to account microclimate in BES has increasingly become the one-way coupling of specific climate parameters. Based on the simulation results of the last coupling scheme two modified annual meteorological files were generated and imported to the UBEM as boundary conditions. We scope to evaluate the discrepancies between these two coupling approaches. Thus, the average air temperature of the entire district is considered in the first offline scenario (EB_int) while the average air temperature of the canyon cells forms the second (EB_int_can). Solar radiation still remains intact. Annual simulations of the UBEM (standalone) were performed with the modified boundary conditions.

Results

Impact on Energy loads

In order to estimate the impact of microclimate to building energy demand, a comparison between the standalone (UBEM) and the coupled model (Cpl_Inter) has been realised. Cooling loads and the respective relative difference between the two scenarios is plotted for each building (Figure 4). The average increase of the cooling loads is 20%, while the peak is reaching 35% (B_5). In terms of absolute values the maximum increase is reaching 0.5MWh. The 2-storey buildings are mainly affected and exhibit the maximum differences, prooving the capability of the coupled model to account the SUHI and the CUHI effects. Moreover, the coupled model can efficiently capture the feedback caused by the ejected system fluxes. During the cooling period, the flux injected to the ambient environment (evaporator) is warmer than the respective air. This

is causing a further increase on energy loads for cooling, presenting a maximum difference of 2.1%.

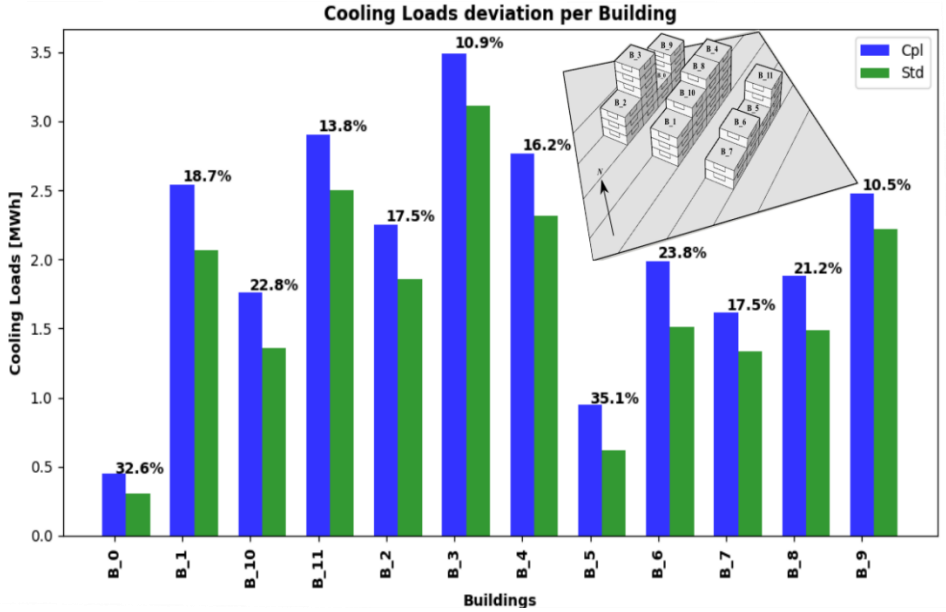


Figure 4. Cooling loads comparison between standalone and coupled simulations.

Heating loads are also presenting the same trend especially when system fluxes are taken into account. In general, the increase is less intense but still significant. The average increase of heating loads is 7%, while the peak is way much smoother, reaching 7.8% (B_5). Systems feedback is captured and presents a further slight increase of heating loads with a maximum value of 1.2%.

A straight comparison between the standalone (UBEM) and the coupled model (Cpl_Ts) is not possible to be conducted, mainly due to the fact that the surface temperature parameter is not converging between the two models. Although, the maximum absolute difference of the surface temperature between the two models is 1,2^{o}C, it is sufficient to underestimate the effect of local climate conditions to the ambient environment.

The average increase of the cooling loads is 20%, while the peak is reaching 35%. The 2-storey buildings are mainly affected due to the interference with the outdoor space. Generally for the entire cooling period the difference between S3 and S4 is almost neglectible reaching maximum the value of 0.02%. Further studies (hourly load differences, different climatic zones, etc.) have to be examined in order to correlate more accurately the temperature increase with the increase of cooling loads. Refering to bilbiography this is in aggreement with (Santamouris, 2015) for a mild climate.

Impact on Air Temperature

The impact of systems flux to ambient air is captured on both coupling procedures. During the summer period, the air temperature of the canyon derived from the coupled simulations is increasing and most of the canyon cells present a 0.2 - 0.5^{o}C increase of air temperature. At the same time the average air temperature of the canyon is slightly higher compared to the standalone simulation. The absolute difference varies from 0.1 ^{o}C to 1.4 ^{o}C (Figure 1Figure 5a). The same trend is observed also for the heating period. The range of difference is higher, since the heating

loads and the respective ejected flux of a heating dominated city (La Rochelle) are higher. The maximum air difference is observed inside the canyon with an absolute value of 1.94 (Figure 5b).

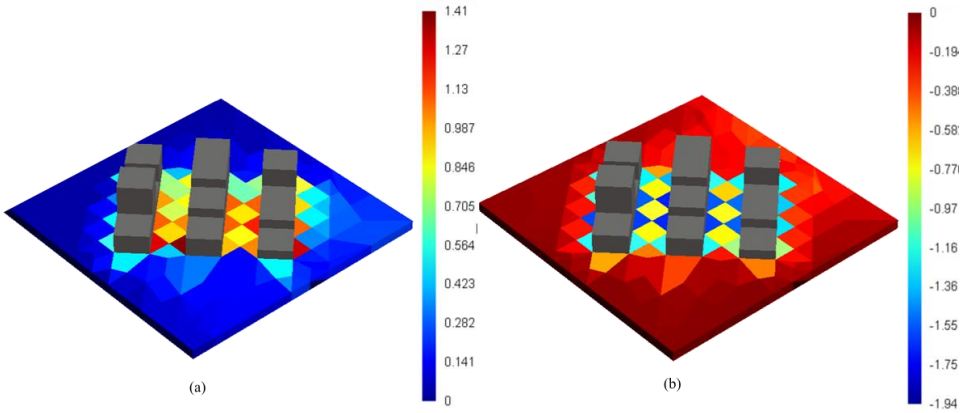


Figure 5: Maximum absolute difference of the air temperature distribution in the canyon during cooling (a) and heating (b) periods when system fluxes are injected.

Coupling Schemes Comparison (Online Vs Offline)

In this section we present the discrepancies between the online coupling scheme (Cpl_Inter) and the commonly used approach of offline coupling. As shown in Figure 6. Online Vs offline comparative results. the average relative difference on cooling loads between online and offline coupling scenarios is reaching 8%. The maximum difference is approximately 22%. Moreover, the cooling loads of two buildings (B_3 and B_9) are overestimated in the offline coupling scenario, while in the rest of them, we can observe an underestimation.

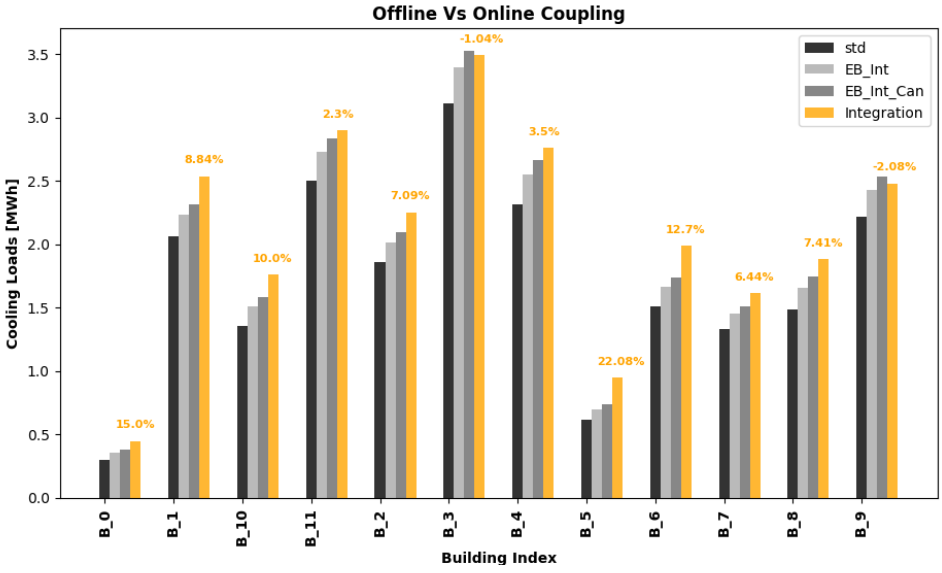


Figure 6. Online Vs offline comparative results.

Discussion & future perspectives

A monitoring campaign for a district in La Rochelle (smart meters and local meteorological stations) is actually ongoing. The onsite measurements could allow validating the new developed model. Comparative analysis for different climate zones, building thermal characteristics and system types is also ongoing.

References

Allegrini, J., Dorer, V., Carmeliet, J., 2012. Influence of the urban microclimate in street canyons on the energy demand for space cooling and heating of buildings. Energy and Buildings 55, 823–832. https://doi.org/10.1016/j.enbuild.2012.10.013

Bozonnet, E., Belarbi, R., Allard, F., 2005. Modelling solar effects on the heat and mass transfer in a street canyon, a simplified approach. Solar Energy 79, 10–24. https://doi.org/10.1016/J.SOLENER.2004.10.007

De Munck, C., Pigeon, G., Masson, V., Meunier, F., Bousquet, P., Tréméac, B., Merchat, M., Poeuf, P., Marchadier, C., 2013. How much can air conditioning increase air temperatures for a city like Paris, France? - de Munck - 2012 - International Journal of Climatology - Wiley Online Library. Wiley Online Library International Journal of Climatology, 210–227. https://doi.org/10/fxn3np

Gobakis, K., Kolokotsa, D., 2017. Coupling building energy simulation software with microclimatic simulation for the evaluation of the impact of urban outdoor conditions on the energy consumption and indoor environmental quality. Energy and Buildings 157, 101–115. https://doi.org/10.1016/j.enbuild.2017.02.020

Groleau, D., Fragnaud, F., Rosant, J.-M., 2003. Simulation of the radiative behavior of an urban quarter of Marseille with the Solene model, in: Fifth International Conference on Urban Climate. Lodz.

Gros, A., Bozonnet, E., Inard, C., 2014. Cool materials impact at district scale—Coupling building energy and microclimate models. Sustainable Cities and Society 13, 254–266. https://doi.org/10/gcv7kx

Hsieh, C.-M., Aramaki, T., Hanaki, K., 2007. Estimation of heat rejection based on the air conditioner use time and its mitigation from buildings in Taipei City. Building and Environment 42, 3125–3137. https://doi.org/10.1016/j.buildenv.2006.07.029

Kyriakodis, G-E, Bozonnet, E., Riederer, P., 2019. Quantifying the impact of microclimate in detailed urban building energy simulations, IBPSA Conference 2019

Martin, M., Wong, N., Hii, D., Ignatius, M., 2017. Comparison between simplified and detailed EnergyPlus models coupled with an urban canopy model. Energy and Buildings 157, 116–125. https://doi.org/10.1016/j.enbuild.2017.01.078

Mauree, D., Coccolo, S., Kaempf, J., Scartezzini, J.-L., 2017. Multi-scale modelling to evaluate building energy consumption at the neighbourhood scale. PLOS ONE 12, e0183437. https://doi.org/10.1371/journal.pone.0183437

Pardyjak, E., Brown, M., 2003. QUIC-URB v1.1 - Theory and User's Guide (Software Users Guide No. LA-UR-07-3181). Los Alamos National Laboratory, University of California, US.

Riederer, P., Partenay, V., Perez, N., Nocito, C., Trigance, R., Guiot, T., 2015. Development of a simulation platform for the evaluation of district energy system performances. Presented at the Fourteenth International IBPSA Conference, pp. 2499–2506.

Rockle, R., 1990. Bestimmung der Stomungsverhaltnisse im Bereich komplexer Bebauungsstrukturen. (Ph.D. thesis, Vom Fachbereich Mechanik, der Technischen Hochschule Darmstadt). Germany.

Rousseau, S., 1978. Simulation numérique du comportement thermique des locaux d'habitation: évaluation de l'influence de la radiation solaire, des conditions climatiques et des paramètres caractéristiques du bâtiment (Thèse de docteur-ingénieur). Université Claude Bernard, Lyon, France.

Salamanca, F., Martilli, A., Tewari, M., Chen, F., 2010. A Study of the Urban Boundary Layer Using Different Urban Parameterizations and High-Resolution Urban Canopy Parameters with WRF. J. Appl. Meteor. Climatol. 50, 1107–1128. https://doi.org/10/bs5w69

Santamouris, M., 2015. Analyzing the heat island magnitude and characteristics in one hundred Asian and Australian cities and regions. Science of The Total Environment 512–513, 582–598. https://doi.org/10.1016/j.scitotenv.2015.01.060

Santamouris, M., Cartalis, C., Synnefa, A., Kolokotsa, D., 2015. On the impact of urban heat island and global warming on the power demand and electricity consumption of buildings—A review. Energy and Buildings 98, 119–124. https://doi.org/10.1016/j.enbuild.2014.09.052

Stewart, I.D., Oke, T.R., 2012. Local Climate Zones for Urban Temperature Studies. American Meteorological Society 93. https://doi.org/10 .1175/BAMS-D-11-00019. 2

Wen, Y., Lian, Z., 2009. Influence of air conditioners utilization on urban thermal environment. Applied Thermal Engineering 29, 670–675. https://doi.org/10.1016/j.applthermaleng.2008.03.039

OUTDOOR COMFORT AND HEALTH IN THE URBAN ENVIRONMENT

Effect and Development of Cool Roofs: A Review

Meng ZHEN, Department of Architecture, School of Human Settlements and Civil Engineering, Xi'an Jiaotong University, China
Ru JIA[1]*, Department of Architecture, School of Human Settlements and Civil Engineering, Xi'an Jiaotong University, China*
Qishu ZOU, Department of Architecture, School of Human Settlements and Civil Engineering, Xi'an Jiaotong University, China
Wei DING, Department of Architecture, School of Human Settlements and Civil Engineering, Xi'an Jiaotong University, China
Weihan ZOU, Department of Architecture, School of Human Settlements and Civil Engineering, Xi'an Jiaotong University, China
Ling WANG, Department of Architecture, School of Human Settlements and Civil Engineering, Xi'an Jiaotong University, China

ABSTRACT

This article reviews a large number of existing studies and discusses the working principle and characteristics of cool roofs, such as utilisation of radiation reflectivity, high infrared radiation emissivity and excellent thermal insulation properties. This mechanism enables the release of additional energy back into the sky such that less heat remains in the ground or passes into rooms. The following three main functions of cool roofs are discussed: (1) saving cooling energy and extending the roof life; (2) alleviating urban heat island effect and improving urban thermal environments; (3) decelerating global warming and prot`ecting the ozone layer. The history of the cool roof development, including the three important cool roof standards (i.e. ASHRAE 90.1, EPA Energy Star label and LEED 2.0) since the 1990s and the advancement of materials used in the five generations of cool roofs, is presented. This article also introduces three shortcomings of cool roofs, namely, higher cost than ordinary roofs, light pollution and additional heating load in winter.
KEYWORDS: Cool roof; Energy saving; Heat island effect; Global warming

Introduction

In recent years, the ambient temperature has increased due to global climate change, especially climate warming and ozone holes. Simultaneously, a large amount of greenhouse gases emitted from cities, as well as black asphalt pavement and roofs, have led to the development of the urban heat island effect. According to existing studies, the heat island effect may cause an average temperature increase of 2 °C to 6 °C (Santamouris 2013; Taha 2000). Rising temperatures in the urban environment have resulted in an increasing number of studies focusing on improving urban thermal environments.

The commonly used active building technology can quickly and effectively change the indoor thermal environment but will considerably increase building energy consumption, which is the most important factor of urban energy consumption. For example, in building energy consumption accounts for approximately 40% of the total final energy consumption and 36% of carbon dioxide emissions in Europe (Library WP 2010).

[1] Corresponding Author: [2336921652@qq.com].

The continually high temperature of urban environments will lead to an increase in the cooling load of active buildings. Therefore, adopting green energy-saving passive building technology has gradually become a research hotspot. Controlling solar radiation is the core of the passive strategy research, and the roof system is an envelope opaque component that is mainly involved in controlling solar radiation. Thus, the improvement of roof systems is the focus of passive building technology research.

The roof system can change the rate of energy passing through the roof such that energy does not directly enter the building. According to existing research, three properties of the roof surface affect this energy throughput, namely, solar radiation reflection, infrared radiation emission and insulation properties.

Solar radiation reflection means that the roof reflects back a part of the received solar radiation into the sky. Increasing the reflectivity of the outer surface can reduce the energy absorbed by the roof and allow the passage of less heat into buildings. Solar radiation reflectance can be frequently adjusted by changing the colour of the roof surface or using highly reflective materials (Levinson and Akbari 2010). Amongst these materials, white coatings are the commonly used; studies have shown that the high solar radiation reflectance of white coatings can even cool metal roofs with low emissivity and high thermal conductivity (Synnefa, Santamouris and Livada 2006).

Infrared radiation emission pertains to the conversion of heat during solar radiation absorption of roofs. Heat is reflected in the form of infrared radiation according to the infrared radiation characteristics of the roof. This method reduces the heat in incoming rooms to facilitate timely dissipation of heat in the building. In hot or mild climates, roofs with high infrared radiation emissivity can emit energy back into the sky without passing the heat indoors, thereby allowing rapid cooling. By contrast, cold climates, roofs with high infrared radiation emissivity may negatively affect indoor insulation.

Insulation is the characteristic that determines the energy entering or leaving buildings through the roof. Given that the temperature difference between the roof and the environment after solar radiation absorption is up to 30 °C, excellent thermophysical properties can effectively reduce the heat conduction caused by the temperature difference to reduce the indoor temperature. The use of insulation materials is the most effective measure to save building energy. The heat transfer and heat capacity of materials depend on the physical construction, which is usually expensive.

Therefore, roofs with high solar radiation reflectivity, high infrared radiation emissivity and excellent thermal insulation will absorb less energy and are easier to cool down than ordinary roofs. This technology is frequently referred to as cool roof. It mainly has the coating or film composition of the aforementioned characteristics and is usually applied to flat roofs of buildings mainly located in hot and mild climates. This technology can reduce the cooling load of buildings and effectively improve the urban thermal environment and the thermal comfort of residents.

This article reviews a large number of studies on cool roofs and discusses the main effects, development and existing problems of cool roofs.

Functions and Effects

According to past research, there are three main effects of cool roofs including saving building cooling energy, alleviating urban heat island effect and decelerating global warming (Pisello, Piselli and Cotana 2015).

Save Cooling Energy

The most significant effect of cool roof is to save cooling energy of buildings, especially in the peak electricity consumption of summer.

When the weather is hot and requires artificial cooling to improve the indoor thermal environment, cool roofs can reduce indoor temperatures by reducing solar radiation absorption, increasing infrared radiation release and diminishing heat transfer to lessen the need for cooling power in buildings. Studies have shown that cool roofs absorb less solar energy during the day; thus, temperature changes are smaller in cool roofs than those in ordinary roofs. Reduced thermal stress causes roofing materials to age very slowly, which extends roof life and reduces maintenance costs (Akbari et al. 2001).

The United States firstly focused on the energy-saving effect of cool roofs and conducted numerous experiments and studies. For example, Konopacki et al. (1997) performed a simulation in 11 metropolitan areas in the United States and inferred that using light-coloured roofs can reduce the peak power demand by 5.2 GW to 6.2 GW, which is equivalent to 12 to 14 power plants. Hildebrandt et al. (1998) measured the daily cooling energy consumption of an office, a museum and a hospice care centre in Sacramento City in the summer. They found that with the cool roof, the energy consumption of these three locations were respectively reduced by 23, 44 and 25 Wh/m^2, accounting for 17%, 26% and 39% of the original energy consumption respectively. Parker et al. (1998) measured the energy consumption of a school building in Florida and found that the daily cooling energy saving was 25% and the peak power demand was reduced by 30%.

In recent years, a considerable amount of research has also been conducted in European countries to demonstrate the effectiveness of cool roofs under different climatic conditions and various types of buildings. Synnefa et al. (2007) studied the effects of cold storage on the cooling load of residential buildings in various climates (i.e. the Mediterranean, humid continental, subtropical drought and desert climates). The simulation results show that increased roof reflectance coating leads to minimum and maximum reductions of 18% and 93%, respectively, in terms of cooling load across regions. Kolokotsa et al. (2012) calculated the performance of the cold roof on a laboratory in Crete, Greece. Their results show that the annual energy saving rate of the coating is 19.8% and that in summer is 27%. The above results show that the cool roof has higher energy saving efficiency than the traditional modification.

Although high infrared emissivity is advantageous in hot and mild climates, if cool roofs with high infrared emissivity are chosen without considering the climate, then the heat in the room may be rapidly dissipated during the winter, causing additional electrical load. Synnefa et al. (2012) evaluated the effect of applying a cool roof coating on a flat roof of a school building in Athens and obtained the following results: the indoor air temperature in summer was reduced by 1.5 °C to 2.2 °C and the summer cooling energy load was decreased by 40%. However, the indoor air temperature in winter was reduced by approximately 0.5 °C and winter heating energy demand increased by 10%. Therefore, materials with low infrared emissivity or green roofs should be chosen in cold winters to prevent heat loss in the house.

Alleviate Urban Heat Island Effect

Another important role of cool roofs is to alleviate the urban heat island effect and improve the urban thermal environment.

The roof accounts for a large proportion of the urban area, and changing the roof will have a huge impact on the environment. Akbari et al. (2009) using four large American cities as an

example, estimated that roofs account for 20% to 25% of the total urban areas, and the roof area of the world's cities is close to 3.8×10^{11} m^2 (accounting for 2% of the entire land). Compared with ordinary roofs, cool roofs reflect back additional solar radiation to the sky, and excess heat is emitted in the form of infrared radiation. This phenomenon effectively balanced the excess heat of urban surfaces, improved the urban thermal environment and outdoor thermal comfort of the human body. From the perspective of cities, the popularization of cold roofs can increase the average albedo of the city, which can effectively alleviate the impact of the urban heat island effect and reduce the outdoor temperature of the city. From a global perspective, reducing the absorption of solar radiation on the earth's surface can lessen the effects of climate change and benefit the ecological environment.

Numerous studies have been conducted in various countries to verify the effects of cool roofs on improving urban thermal environment and mitigating the benefits of urban heat islands for different albedos and regions. For example, Sharma et al. (2016) studied a core dense urban area in Chicago and found that the ambient peak temperature drops by 7 °C to 8 °C when the roof albedo is 0.85. Campra et al. (2008) demonstrated their observations on the Almeria region in Spain for 10 years. They found that the temperature in the region has been reduced by 0.3 K through large-scale constructions of cool roofs over the past decade. Salamanca et al. (2016) illustrated that cool roofs can cool an average urban area by 0.8 °C during an ordinary day in Tucson. Based on data from existing studies, Santamouris (2014) found a linear relationship between albedo and reductions in urban ambient temperatures and peak temperatures. The results show that for every 0.1 increase in albedo in urban areas, the average urban ambient temperature is reduced by 0.3 K, and the urban peak temperature is reduced by 0.9 K.

Other studies have shown that the cooling capacity of cool roofs at night is weaker than that of green roofs. However, when roof albedo is higher than 0.68, the average cooling effect is much better than that of green roofs (Liu et al. 2018).

Decelerate Global Warming

In addition, cool roofs can decelerate global warming by mitigating the greenhouse effects and ozone holes.

Cold roofs reflect most of the heat back into the sky and reduce the amount of greenhouse gases that can be kept warm, which reduces the amount of heat that remains on the ground. Such an approach can effectively alleviate the effects of the greenhouse effect, thereby delaying global warming. Georgescu et al. (2014) proposed that using cool roof technology in the process of urban expansion in the United States has minimised climate warming by reducing greenhouse gases. Moreover, the scope of technology has not only affected individual cities but also large areas in the US. Akbari et al. (2012) found that the increase in urban albedo may significantly reduce greenhouse gas emissions in the atmosphere, which alleviates the greenhouse effect. A cool roof per 1 m^2 is equivalent to a long-term global cooling effect of 3×10^{-15} K. In addition, a 0.01 increase in albedo is equal to a CO_2 reduction of approximately 7 kg. According to Van Curen (2011), the average radiation was reduced by 1.38 W/m^2 for every 0.01 albedo increase after using cool roofs in California and this phenomenon may result in a reduction of 1.76 million tons of CO_2 emissions in the state.

At the same time, studies have shown that cool roofs can also reduce the formation of ozone by reducing the ambient temperature of the city, thus protecting the ozone layer. Taha (2001) simulated the impact of temperature drop in Los Angeles on ozone concentration. The results show that when the temperature is lowered, ozone concentration is reduced by 10%–20%, which is

equivalent to the amount of ozone generated by replacing fuel cars with electric cars in Los Angeles. In addition, reducing atmospheric ozone levels can also help improve residents' comfort and health.

Development and Problems

Standards

Since the United States implemented the ‘Cool Roof’ project in the 1990s, the current cool roof technology has become a major technical measure for the energy efficiency of buildings and reduction of urban heat island effects and has been widely applied. This article summarizes three authoritative standards that are still in force and will continue to influence the application and development of cool roofs.

ASHRAE pioneered the US energy-saving design standard ASHRAE 90.1 for federal government adoption and is still being updated today. The standard sets the minimum requirements for energy-efficient building designs and requires a minimum roof reflectance and emissivity of 70% and 75%, respectively.

In 1998, the Cool Roof Rating Committee was established as a non-profit organisation that aims to implement and promote a fair and accurate assessment of solar reflectance and radiance on roof surfaces. In addition, CRRC incorporates cool roofs into the United States EPA ‘Energy Star’ certification. The roof product outline of the Energy Star label sets a minimum standard for cool roofs. This standard requires initial and three-year ageing reflectivities for low-slope roofs to be at least 0.65 and 0.50, respectively, and initial and three-year ageing reflectivities for steep-sloping roofs of at least 0.25 and 0.15, respectively.

In 2001, the US Green Building Council introduced the LEED 2.0 standard, which sets new requirements for the roof reflection index. The standard requires at least 75% surface coverage of cooling roofs, and the material should have an initial reflectance of at least 0.65, approximately no less than 0.5 after three years of use and emissivity of at least 0.90.

Materials

Previous studies have reviewed the research progress of materials used in cool roofs (Santamouris 2014; Santamouris et al. 2011). This paper has organized and divided them into the following five stages.

The first generation used mostly natural white materials such as white marble and white mosaic. It is characterized by a relatively low price and an albedo rarely above 0.75 (Bretz et al. 1992). Most of the research at this stage focused on expanding the spectrum of the reflection by changing the colour of the roof based on the traditional building materials, thereby reflecting more energy back into the sky.

The second generation is usually an artificially developed white material designed to provide an albedo value of 0.85 and above. Its low price and considerable effect make it widely used. Synnefa et al. (2006) measured 14 common materials in the international market.

The third generation of cool roofs has chosen coloured high-reflective materials, which have much higher reflectivity than traditional materials of the same colour, and are often referred to as cool coloured materials. Its most important role is to enhance the aesthetic appeal (Synnefa et al. 2007).

The fourth generation of cool roof is a reflective material with nano-materials presenting high sensible or latent heat storage capacity, and its colour richness and cooling capacity are greatly improved, but the price may be higher than ordinary materials. It mainly includes PCM doped cool materials (Tyagi and Buddhi 2007) and thermochromic materials (Karlessi et al. 2009).

The fifth generation of cool roof is a material with dynamic optical characteristics under development. In addition to excellent cooling capacity during the hot summer, this material can also dynamically adjust itself to the ambient temperature and solar radiation intensity, making it possible to exhibit excellent insulation or heating in cold winters.

Problems

Based on a large number of existing studies, this paper summarizes the following three problems that exist in the current cold roof:

1) Higher cost of cool roofs than ordinary roofs. Although cool roofs have become popular due to their low cost and high efficiency and the development of cool roof technology is constantly improving, the manufacturing cost of this technology is also increasing. Moreover, cool roof coatings are exposed to solar radiation for a long time, thus requiring regular repairs and replacements, which result in additional costs.
2) Light pollution due to this technology. High-reflection materials may cause unnecessary light pollution and the visual disturbance of the public has resulted in increased city accident rates due to reflections.
3) Additional heating load problem. In the cold winter climate, if the material with suitable infrared radiation rate cannot be selected to prevent rapid heat loss, cool roofs may increase the heating load.

Conclusions

Cool roof technology, which can effectively improve indoor and outdoor thermal environments, has gradually become popular to alleviate the effects of global warming and urban heat island. This technology uses high solar radiation reflectivity, high infrared radiation emissivity and excellent thermal insulation to release additional energy back into the sky, leaving less heat on the ground or into the room.

This paper reviews a large number of existing studies and mainly discusses the following three functions of cool roofs. 1) Cool roofs reduce building cooling energy and the energy-saving effect is more evident at the peak of power consumption. Cool roofs can also extend roof life and reduce roof maintenance costs. 2) Cool roofs alleviate urban heat island effects by increasing albedo, which effectively reduces solar radiation in cities and improves the urban thermal environment and thermal comfort of the human body. 3) Cool roofs decelerate global warming and protect the ozone layer by decreasing environment temperature and reducing greenhouse gas and ozone emissions.

The history of cool roof developments, which includes three important standards (i.e. ASHRAE 90.1, EPA Energy Star label and LEED 2.0) since the 1990s and the development of materials used in the five generations of cool roofs, is discussed. Moreover, the three shortcomings of cool roofs, namely, higher cost than that of ordinary roof, increased light pollution resulting in increased accident rates and additional heating load in winter, are presented.

Overall, the cool roof technology has gradually matured and effectively improved the indoor and outdoor thermal environment and the thermal comfort of urban residents at a relatively low cost. The extensive use of this technology is also of considerable importance for building energy efficiency during the summer peaks of urban use and will considerably alleviate the problems caused by global warming and urban heat island effect.

Acknowledgements

The paper was supported by the Fundamental Research Funds for the Central Universities (grant number: xjj2017191), the Scientific Research Support of New Teacher of Xi'an Jiaotong University (grant number: JZ1K004), the China Postdoctoral Science Foundation (grant number: 2018M633514), the National Natural Science Foundation of China (grant number: 51808440) and the Shaanxi Province Natural Science Basic Research Programme – General Project (Youth) (grant number: 2019JQ-595).

References

Akbari, H., M. Pomerantz and H. Taha. 2001. 'Cool surfaces and shade trees to reduce energy use and improve air quality in urban areas', *Solar Energy*, vol 70, no 3, pp295–310 https://www.sciencedirect.com/science/article/pii/S0038092X0000089X

Akbari, H., Menon, S., and Rosenfeld, A. (2009). "Global cooling: increasing world-wide urban albedos to offset CO_2." *Climatic change* 94.3-4 (2009): 275-286. https://link.springer.com/article/10.1007/s10584-008-9515-9

Akbari, H., Matthews, H. D., and Seto, D. 2012. "The long-term effect of increasing the albedo of urban areas." *Environmental Research Letters* 7(2): 024004.

Bozonnet, E., Doya, M., and Allard, F. 2011. "Cool roofs impact on building thermal response: A French case study." *Energy and Buildings* 43(11): 3006-3012. https://www.sciencedirect.com/science/article/pii/S0378778811003227

Bretz, S., Akbari, H., Rosenfeld, A., Taha, H. 1992. "Implementation of Solar Reflective Surfaces: Materials and Utility Programs." LBL Report–32467, University of California. https://escholarship.org/content/qt8cc7d67k/qt8cc7d67k.pdf

Buratti, C., Moretti, E., Belloni, E., and Cotana, F. 2013. "Unsteady simulation of energy performance and thermal comfort in non-residential buildings." *Building and Environment* 59: 482-491. https://www.sciencedirect.com/science/article/abs/pii/S0360132312002570

Campra, P., Garcia, M., Canton, Y., Palacios-Orueta, A., 2008. "Surface temperature cooling trends and negative radiative forcing due to land use change toward greenhouse farming in southeastern Spain." *Journal of Geophysical Reseach* 113 (18), D18109. https://agupubs.onlinelibrary.wiley.com/doi/full/10.1029/2008JD009912

Hildebrandt, E., W. Bos and R. Moore .1998. 'Assessing the impacts of white roofs on building energy loads', *ASHRAE Technical Data Bulletin*, American Society of Heating, Refrigerating

and Air-Conditioning Engineers, Atlanta, GA, vol 14,no 2, pp28–36 https://search.proquest.com/docview/192534420?pq-origsite=gscholar

Georgescu, M., Morefield, P. E., Bierwagen, B. G., and Weaver, C. P. 2014. "Urban adaptation can roll back warming of emerging megapolitan regions." *Proceedings of the National Academy of Sciences* 111(8): 2909-2914. https://www.pnas.org/content/111/8/2909/

Karlessi, T., Santamouris, M., Apostolakis, K., Synnefa, A., and Livada, I. 2009. "Development and testing of thermochromic coatings for buildings and urban structures." *Solar Energy* 83(4): 538-551.

Karlessi, T., Santamouris, M., Synnefa, A., Assimakopoulos, D., Didaskalopoulos, P., Apostolakis, K., 2011. "Development and testing of PCM doped cool colored coatings to mitigate urban heat island and cool buildings. " *Building and Environment* 46 (3), 570–576. https://www.sciencedirect.com/science/article/pii/S0360132310002738

Kolokotsa, D., Diakaki, C., Papantoniou, S., and Vlissidis, A. 2012. "Numerical and experimental analysis of cool roofs application on a laboratory building in Iraklion, Crete, Greece." *Energy and Buildings* 55: 85-93. https://www.sciencedirect.com/science/article/pii/S0378778811003999

Konopacki, S., Akbari, H., and Gartland, L. 1997. "Cooling energy savings potential of light-colored roofs for residential and commercial buildings in 11 US metropolitan areas." No. LBNL-39433-Exec. Summ. Lawrence Berkeley Lab., CA (United States). https://www.osti.gov/biblio/508151

Konopacki, S. and H. Akbari. 2001. "Measured Energy Savings and Demand Reduction from a Reflective Roof Membrane on a Large Retail Store in Austin", LBNL-47149, Lawrence Berkeley National Laboratory, Berkeley, CA https://escholarship.org/uc/item/7gw9f9sc

Levinson, R. and Akbari, H. 2010. "Potential benefits of cool roofs on commercial buildings: conserving energy, saving money, and reducing emission of greenhouse gases and air pollutants." *Energy Efficiency* 3(1): 53. https://search.proquest.com/openview/781a4a827d2b25aef5c615db5a1f0f44/1?pq-origsite=gscholar&cbl=54357

Library, W. P. 2010. "Directive on the energy performance of buildings."2002/91/EC

Liu, X., Tian, G., Feng, J., Wang, J., and Kong, L. 2018. "Assessing summertime urban warming and the cooling efficacy of adaptation strategy in the Chengdu-Chongqing metropolitan region of China." *Science of the Total Environment* 610: 1092-1102. https://www.sciencedirect.com/science/article/pii/S0048969717320806

Parker, D., J. Huang, S. Konopacki, L. Gartland, J. Sherwin, and L. Gu.1998. 'Measured and simulated performance of reflective roofing systems in residential buildings', *ASHRAE Transactions*, vol 104, no 1, Atlanta, GA https://search.proquest.com/docview/192625246/fulltext/BF8D011DD5C74DD2PQ/1?accountid=16294

Pisello, A. L., Piselli, C., and Cotana, F. 2015. "Influence of human behavior on cool roof effect for summer cooling." *Building and Environment* 88: 116-128. https://www.sciencedirect.com/science/article/pii/S0360132314003175

Ray, S. D. 2010. "Energy saving potential of various roof technologies." https://dspace.mit.edu/bitstream/handle/1721.1/57790/650086010-MIT.pdf

Salamanca, F., Georgescu, M., Mahalov, A., Moustaoui, M., and Martilli, A. 2016. "Citywide impacts of cool roof and rooftop solar photovoltaic deployment on near-surface air temperature and cooling energy demand." *Boundary-layer meteorology* 161(1): 203-221. https://link.springer.com/article/10.1007/s10546-016-0160-y

Santamouris, A., Synnefa, and T.Karlessi., 2011. "Using advanced cool materials in the urban built environment to mitigate heat islands and improve thermal comfort conditions. " *Solar Energy* 85 (12), 3085–3102. https://www.sciencedirect.com/science/article/pii/S0038092X10004020

Santamouris, M. 2013. "Heat island research in Europe: the state of the art." *Advances in building energy research*. Routledge, 2013: 137-164.

Santamouris, M. 2014. "Cooling the cities–a review of reflective and green roof mitigation technologies to fight heat island and improve comfort in urban environments." *Solar energy* 103: 682-703. https://www.sciencedirect.com/science/article/pii/S0038092X12002447

Sharma, A., Conry, P., Fernando, H. J. S., Hamlet, A. F., Hellmann, J. J., and Chen, F. 2016. "Green and cool roofs to mitigate urban heat island effects in the Chicago metropolitan area: Evaluation with a regional climate model." *Environmental Research Letters* 11(6): 064004. https://iopscience.iop.org/article/10.1088/1748-9326/11/6/064004/meta

Synnefa, A., Saliari, M., and Santamouris, M. 2012. "Experimental and numerical assessment of the impact of increased roof reflectance on a school building in Athens." *Energy and Buildings* 55: 7-15. https://www.sciencedirect.com/science/article/pii/S0378778812001028

Synnefa, A., Santamouris, M., and Akbari, H. 2007. "Estimating the effect of using cool coatings on energy loads and thermal comfort in residential buildings in various climatic conditions." *Energy and Buildings* 39(11): 1167-1174. https://www.sciencedirect.com/science/article/pii/S0378778807000126

Synnefa, A., Santamouris, M. and Livada, I. 2006. "A study of the thermal performance of reflective coatings for the urban environment." *Solar Energy* 80(8): 968-981. https://www.sciencedirect.com/science/article/pii/S0038092X05002975

Synnefa, A., Santamouris, M., Apostolakis, K., 2007a. "On the development, optical properties and thermal performance of cool colored coatings for the urban environment. " *Solar Energy* 81 (4):488–497. https://www.sciencedirect.com/science/article/pii/S0038092X06002039

Taha, H. 2000. "Meteorological and air quality impacts of heat island mitigation measures in three US Cities." https://escholarship.org/content/qt9bh7t157/qt9bh7t157.pdf?t=p2asdr

Taha, H. 2001. "Potential impacts of climate change on tropospheric ozone in California: a preliminary episodic modeling assessment of the Los Angeles Basin and the Sacramento Valley. " No. LBNL-46695. Lawrence Berkeley National Lab., CA (US), 2001. https://www.osti.gov/biblio/781837

Tyagi, V. V., and Buddhi, D. 2007. "PCM thermal storage in buildings: a state of art. " *Renewable and Sustainable Energy Reviews* 11, 1146–1166. https://www.sciencedirect.com/science/article/pii/S1364032105000973

Van Curen, R., 2011. "The radiative forcing benefits of "cool roof" construction in California: quantifying the climate impacts of building albedo modification." *Climatic Change* 1–13. http://dx.doi.org/10.1007/s10584-011-0250-2

Xu, X., Taylor, J. E., and Pisello, A. L. 2014. "Network synergy effect: Establishing a synergy between building network and peer network energy conservation effects." *Energy and Buildings* 68 (2014): 312-320. https://www.sciencedirect.com/science/article/pii/S0378778813005938

Outdoor Thermal Sensation and Thermal Comfort in Xi'an

Meng ZHEN[1]*, Department of Architecture, School of Human Settlements and Civil Engineering, Xi'an Jiaotong University (China)*
Ru JIA, Department of Architecture, School of Human Settlements and Civil Engineering, Xi'an Jiaotong University (China)
Weihan ZOU, Department of Architecture, School of Human Settlements and Civil Engineering, Xi'an Jiaotong University (China)
Wei DING, Department of Architecture, School of Human Settlements and Civil Engineering, Xi'an Jiaotong University (China)
Ling WANG, Department of Architecture, School of Human Settlements and Civil Engineering, Xi'an Jiaotong University (China)

ABSTRACT

To study the current situation of outdoor thermal comfort in Xi'an, this research conducted a questionnaire survey from April to May 2019. The questionnaire included basic information, thermal sensation, thermal comfort and thermal expectations of the respondents. A total of 248 valid questionnaires were returned. Survey results indicated that the thermal comfort characteristics across gender, age, educational background, height and weight were analysed and climate differences in typical cities in five climate zones were compared and evaluated. Results showed that women are more sensitive to thermal sensation and thermal comfort than men. The respondents aged 31–35 have the lowest and highest sensitivities to thermal sensation and thermal comfort, respectively. Below undergraduate respondents have the highest and highest sensitivities to thermal sensation and thermal comfort, respectively. Body mass index is positively correlated with thermal sensation. When thermal sensation increases, the respondents expect that the temperature and solar radiation are decreased but wind speed and relative humidity are increased. Xi'an has large geographical differences with cities in other climate zones, thereby indicating that outdoor thermal comfort has significant regional differences.
Keywords: Outdoor thermal environment; Questionnaire survey; Thermal comfort; Thermal sensation; Cold area

Introduction

The improvement in the standard of living of people has resulted in an increase in their requirements for the environment. Apart from suitable facilities and landscape, a comfortable outdoor thermal environment can improve the efficiency of urban space use. Therefore, thermal comfort has gradually become an important factor in optimising architectural design and urban planning.

Human thermal comfort represents a state of mind that expresses satisfaction with the thermal environment (ASHRAE 1992). The traditional thermal comfort theory is based on the balance between human body heat production and loss (Nikolopoulou and Lykoudis 2006). Hence, designing effective standards and models can effectively deepen the understanding of the thermal environment. Over the past few decades, over 100 indicators have been developed to assess human thermal comfort (Blazejczyk et al. 2012). Different meteorological, geographical,

[1] Corresponding Author: [zhenmeng@xjtu.edu.cn].

psychological and socio-cultural factors have led to varied understanding of thermal comfort across regions (Kovács et al. 2016). Therefore, a single index cannot accurately describe the thermal environment characteristics of all regions. Most of them are only applicable to the place of development (Europe or the US). Accordingly, accurately grasping the local thermal environment will help improve environmental comfort and building energy consumption. Moreover, numerous studies have focused on the local thermal environment. A few of these studies have calibrated the existing thermal comfort indices (Lin and Matzarakis 2008; Cohen, Potchter and Matzarakis 2013), whereas others have discussed the characteristics of the local thermal environment and how to improve comfort (Ridha, Ginestet and Lorente 2018; Spangenberg et al. 2019).

The existing research has the following characteristics and limitations. (1) The research on indoor thermal environment outnumbers those on outdoor thermal environment because many people spend more time indoors than outdoors; the indoor thermal environment is likewise easy to control (Höppe 2002; De Dear and Brager 1998). (2) The majority of the related studies have focused on temperate and subtropical climates (Lin et al. 2013; Ng and Cheng 2012), whereas only a few studies on cold climates have been conducted. On the basis of the national standard Thermal Design Code for Civil Buildings (GB50176-51993 1993), China is divided into five climatic zones (i.e. severe cold, cold, hot summer and cold winter, hot summer and warm winter, and temperate zones). The majority of the studies on Chinese cities have concentrated on the hot summer and cold winter or hot summer and warm winter zones (Yin et al. 2012; Zeng and Dong 2015). Only a few studies on the cold zone, mainly in economically developed regions in Northern China, such as Tianjin (Lai et al. 2014), have investigate the Northwest Territories. (3) In the majority of the related studies, establishing and calibrating thermal comfort models are based on the use of the thermal sensation vote (TSV) as a ruler (Lin 2009). Thus, thermal comfort is a subjective concept, which differs in the understanding of different regions, cultures and crowds. That is, the relationship amongst thermal sensation, thermal comfort and respondent information should be identified.

Xi'an is a typical city in China's cold zone and an important central city in the country's northwestern region. This study used a questionnaire survey to analyse the current status of outdoor thermal environment in Xi'an from April to May 2019. This research aims to investigate and compare the thermal comfort characteristics of different people in the cold zone and compare these characteristics with typical urban meteorological parameters in other climate zones.

Methods

Research Site and Personal Information Survey

A questionnaire survey was conducted in the Qujiang campus of Xi'an Jiaotong University from April to May 2019. The total area of the campus is approximately 12,000 m^2 and the university's function is mainly based on scientific research.

The total number of survey respondents was 264 and were mainly school teachers and students. The respondents were composed of 162 men and 102 women with the age range concentrated below 35 years old (approximately 85%).

The background survey of the respondents indicated that they generally achieved higher education and over 93% of the respondents obtained a bachelor's degree or above. The highest proportion is 40.9% for bachelor's degree and 37.5% for doctoral degrees or above.

Additionally, we investigated the physical condition of the respondents. Over 95% of the respondents were in good health and above and the questionnaires of the uncomfortable respondents were excluded in the statistical process. The respondents' physical condition showed that those with height of above 170 cm accounted for 57.1% and those with weight of over 60 kg accounted for 60.2%.

Questionnaire Design

The questionnaire used in this study consisted of Part A, which is a survey on respondent information; and Part B, which is an evaluation of thermal comfort. Part B includes the following parameters:

(1) TSV uses the seven-point scale recommended by ASHRAE-55 2013 (ASHRAE 2013): cold (−3), cool (−2), slightly cool (−1), neutral (0), slightly warm (+1), warm (+2) and hot (+3). The respondents were asked to vote separately for the thermal sensation of the Xi'an outdoors.

(2) Thermal comfort vote (TCV) uses a seven-point scale as follows: very uncomfortable (−3), uncomfortable (−2), slightly uncomfortable (−1), neutral (0), slightly comfortable (+1), comfortable (+2), and very comfortable (+3).

(3) Thermal expectation vote uses four meteorological parameters by designing a three-level ruler, namely, increase (+1), no change (0), and decrease (−1), and requiring the respondents to vote on how the four meteorological parameters are expected to change.

Survey Campaign

Information from the returned questionnaires was initially processed and statistical results were analysed using SPSS17.0.

We considered at least one of the following methods in discussing the effects of a single element on thermal sensation and thermal comfort.

(1) We took the average of the votes corresponding to different options and used image or regression analysis to determine the relationship. For example, each option for age was counted as a set of mean thermal sensation vote (MTSV) and an image was drawn on the bases of the data to visually display the impact of each element.

(2) We used a different set of options to draw a scatter plot of all the respondents with TSV and TCV as the independent and dependent variables, respectively, and fit the straight line to intuitively compare the influences of each option.

To further analyse the meteorological characteristics of Xi'an, we selected typical cities from four other climate zones in China and compared their climate data with those of Xi'an in the cold area (climate data were derived from Climate Consultant 6.0 and DeST 2.0).

Discussion and Results

Thermal Comfort Characteristics of Different Groups of People

We analysed different personal factors (i.e. gender, age, educational background, height and weight) to study the thermal comfort characteristics of different groups of people.

Gender. Figure 1 depicts the distribution of MTSV and MTCV across gender. In terms of MTSV, men and women reached 0.71 and 1.23, respectively, with a difference of 0.52. This result indicates that women are more sensitive to thermal sensation than men. In terms of MTCV, men and women are −0.27 and −0.02, respectively, with a difference of 0.25, thereby indicating that men have higher requirements for thermal comfort than women.

Figure 2 illustrates the relationship between TSV and TCV across gender. The slope indicates that women's thermal comfort is higher than that of men under different thermal sensation. That is, thermal comfort for women generally changes with a change in thermal sensation, thereby indicating that women are more sensitive to thermal comfort than men.

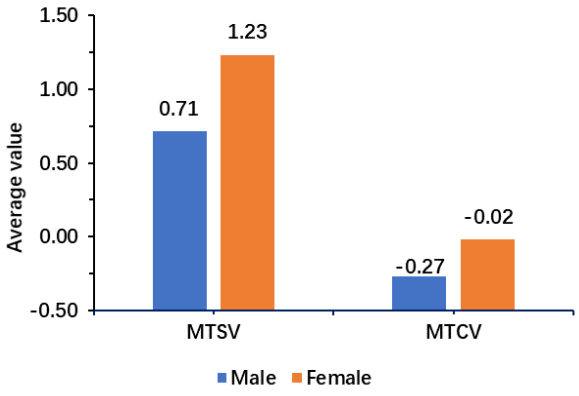


Figure 1. MTSV and MTCV across genders

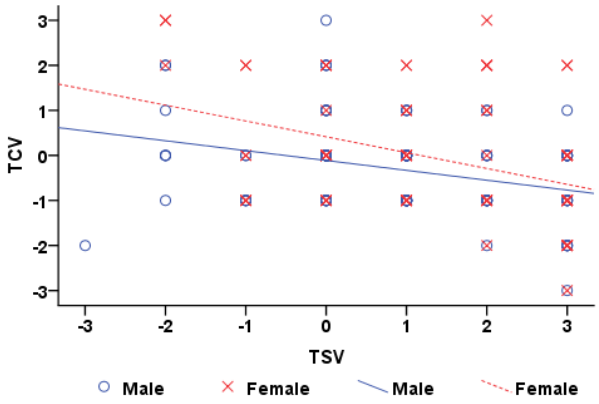


Figure 2. Relationship between TSV and TCV across genders

Age. Figure 3 indicates that MTSV shows a trend of 'initial drop and increase'. The valley value (0.59) and peak value (1.57) of MTSV pertain to the respondents aged 31–35 years and 41–50 years, respectively, with a difference of 0.98. This finding shows that people aged 41–50 years and 31–35 years have the highest and lowest sensitivities, respectively, to thermal sensation.

Figure 4 depicts the relationship between TSV and TCV across age groups. The thermal comfort of the three age groups, namely, 35 to 50 years, under 25 years and over 50 years is arranged from high to low. The overall trend is similar, thereby indicating that the three age groups have similarities in the perception of thermal sensation and thermal comfort. When thermal sensation changes, the 25–35 year respondents experience the most changes in thermal comfort. Additionally, the slope for this group differs from those of the other age groups, thereby indicating that this age group is considerably sensitive to thermal comfort.

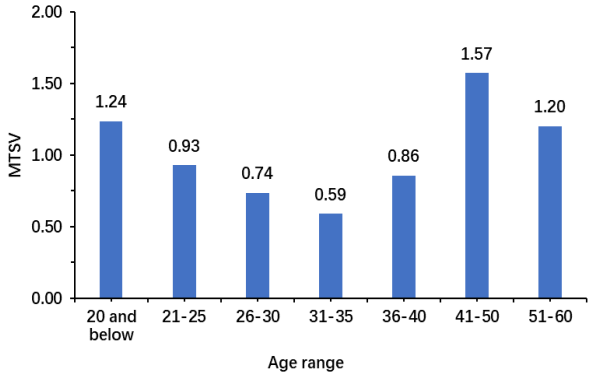


Figure 3. MTSV across age groups

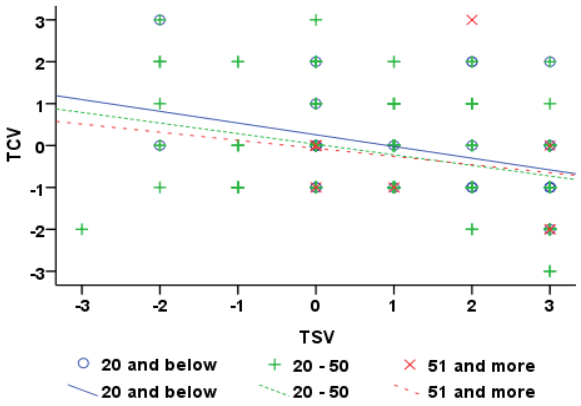


Figure 4. Relationship between TSV and TCV across age groups

Educational background. Figure 5 shows that MTSV is highest (1.40) and lowest (0.58) for the respondents who are below undergraduate and with master's degrees, respectively, with a difference of 0.82. The MTSV values are 1.08 and 0.78 for the respondents with bachelor's degrees and PhDs and above, respectively. This result indicates that the former is considerably sensitive to thermal sensation.

Figure 6 depicts the relationship between TSV and TCV of the respondents with different educational backgrounds. Those with bachelor's and master's degrees and PhDs have similar thermal comfort trends (that are decreasing). The trend of the below undergraduate respondents differs. That is, when thermal sensation changes, their thermal comfort changes decreases.

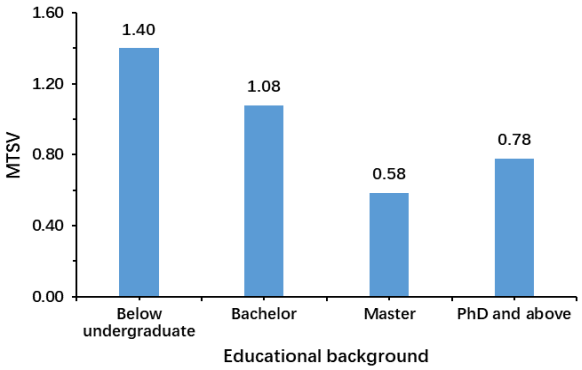


Figure 5. MTSV across educational backgrounds

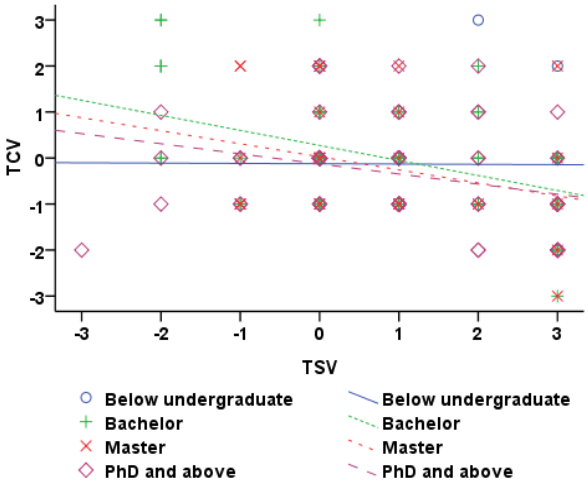


Figure 6. Relationship between TSV and TCV across educational backgrounds

Body mass index. This study uses body mass index (BMI), which is weight divided by the square of height, to measure the physique of the respondents. We referred to the China Standard

BMI (see Table 1) to divide the respondents into groups of 18.5 and below, 18 to 19.5, 19.5 to 21, 21 to 22.5, 22.5 to 24 and 24 and above. Their MTSV values were obtained.

Table 1. China Standard BMI

BMI	Evaluation	BMI	Evaluation
Below 18.5	Underweight	18.5 to 23.9	Normal weight
23.9 to 28	Overweight	Above 28	Obesity

Figure 7 shows that BMI is positively correlated with MTSV, with R^2 and slope values of 0.36 and 0.05, respectively. That is, the higher the BMI value, the higher the respondents' thermal sensation.

Figure 8 shows that thermal comfort decreases with an increase in thermal sensation for the underweight (BMI < 18.5) respondents, although the variation is minimal. For the normal weight respondents (18.5 < BMI < 23.9), thermal comfort decreases with an increase in thermal sensation, although the variation range is large. For the overweight respondents (BMI > 23.9), thermal comfort value remains nearly constant with an increase in thermal sensation.

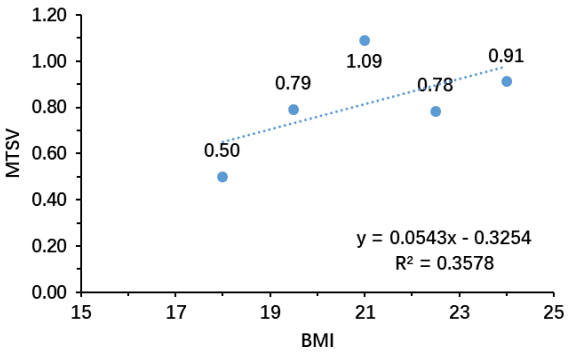


Figure 7. MTSV across BMI values

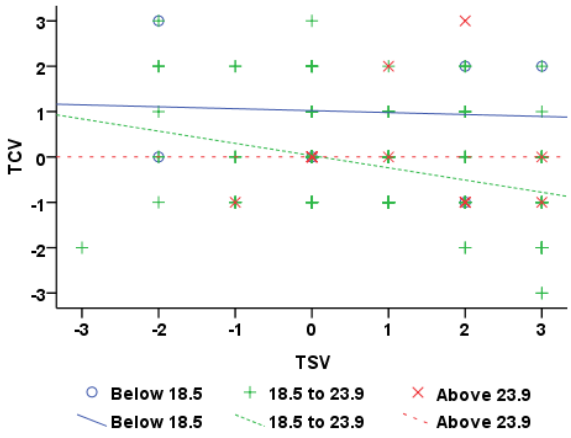


Figure 8. Relationship between TCV and TSV across BMI values

Impact of Meteorological Parameters on Thermal Comfort

Studies have shown that meteorological parameters affecting thermal comfort include temperature, relative humidity, wind speed and solar radiation (Mayer 1993). Therefore, the present study uses thermal expectation to analyse the impact of the four parameters on thermal sensation.

Temperature. Figure 9 shows that TSV is negatively correlated with thermal expectation (temperature) with R^2 and slope values of 0.66 and −0.14, respectively. This result indicates that the larger the TSV, the more the temperature is expected to decrease.

Solar radiation. Figure 10 shows that TSV is negatively correlated with thermal expectation (solar radiation) with R^2 and slope values of 0.86 and −0.13, respectively. This result indicates that the larger the TSV, the more the solar radiation is expected to decrease.

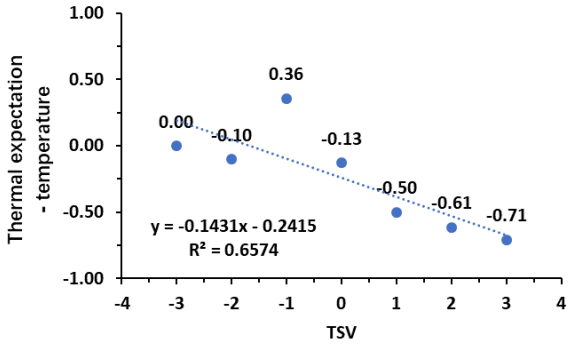


Figure 9. The relationship between thermal expectation (temperature) and TSV

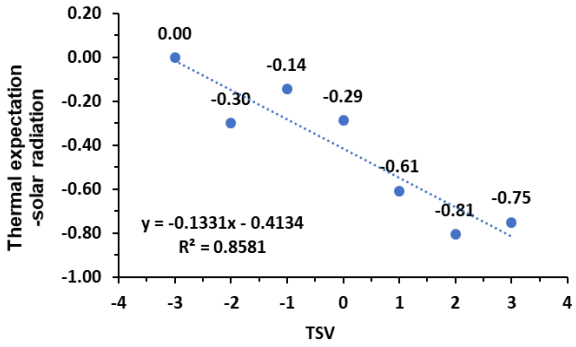


Figure 10. The relationship between thermal expectation (solar radiation) and TSV

Wind speed. Figure 11 illustrates that TSV is positively correlated with thermal expectation (wind speed) with R^2 and slope values of 0.71 and 0.21. This result implies that the larger the TSV, the more the wind speed is expected to increase.

Relative humidity. Figure 12 shows that TSV is positively correlated with thermal expectation (relative humidity) with R^2 and slope values of 0.71 and 0.21, respectively. This result indicates that the larger the TSV, the more the relative humidity is expected to increase.

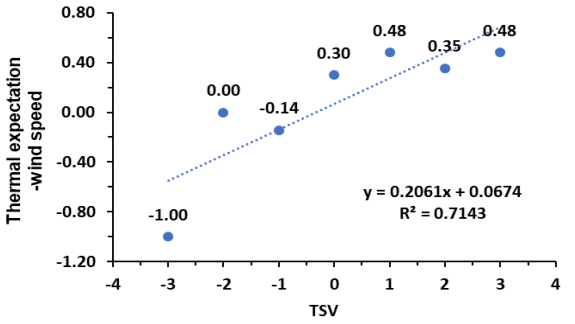


Figure 11. Thermal expectation (wind speed) and TSV

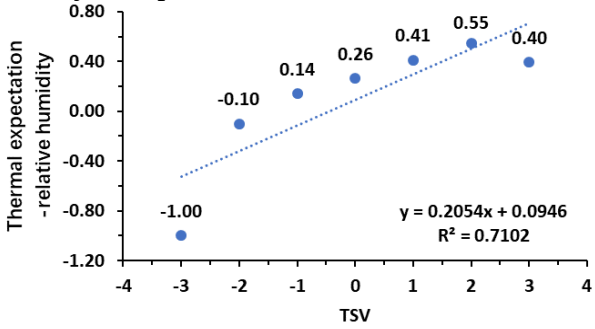


Figure 12. Thermal expectation (RH) and TSV

The fitting line of temperature and solar radiation are below 0. This outcome indicates that the respondents perceive Xi'an as having high temperature and strong solar radiation from April to May and expect them to decrease.

Regional Differences in Thermal Comfort

The team listed the climate data in Xi'an (cold) during the survey period and typical cities in the other four climate zones, namely, Harbin (severely cold), Shanghai (hot summer and cold winter), Guangzhou (hot summer and warm winter) and Kunming (temperate) and compare their climate data.

Temperature. Figure 13 shows that the average temperature in Xi'an is 18.13 °C, which is 6.12 °C lower than that in Guangzhou with the highest average temperature (24.25 °C) and is 7.11 °C higher than that in Harbin (11.02 °C) with the lowest average temperature.

Solar radiation. Figure 14 shows that Xi'an has an average solar radiation of 185 W/m^2, which is 130.5 W/m^2 lower than that in Harbin with the strongest solar radiation (315.5 W/m^2) and is 104.5 W/m^2 higher than that for Guangzhou with the weakest solar radiation (80.5 W/m^2).

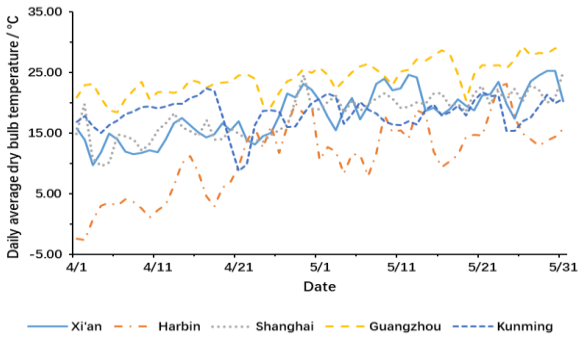


Figure 13. Average dry bulb temperature in five cities

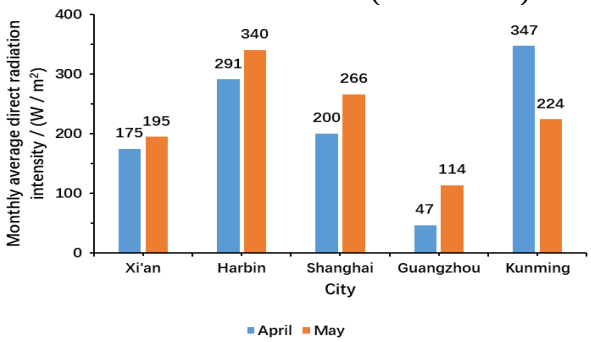


Figure 14. Average direct solar radiation in the five cities

Wind speeds. Figure 15 shows that the average wind speed in Xi'an is 1.5 m/s, which is 1.5 m/s lower than those in Harbin and Shanghai with the highest wind speed (3 m/s) and is 0.5 m/s higher than that for Guangzhou with the lowest wind speed (1 m/s).

Moisture content. Figure 16 shows that Xi'an has an average moisture content of 8.80 g/kg, which is 7.05 g/kg lower than that in Guangzhou with the highest moisture content (15.85 g/kg) and is 4.40 g/kg higher than that in Harbin with the lowest moisture content (4.40 g/kg).

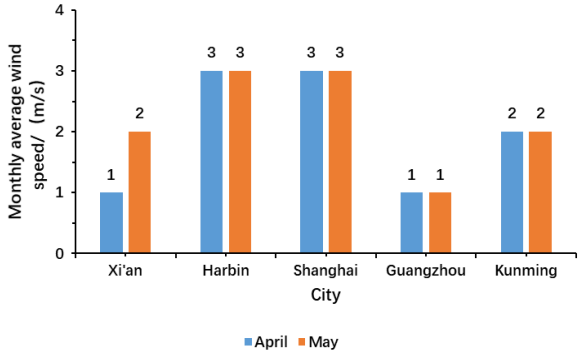


Figure 15. Monthly average wind speed in five cities

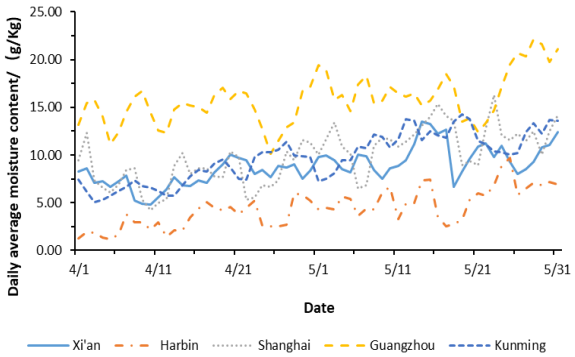


Figure 16. Daily average relative humidity in five cities

The climate data analysis indicates that Xi'an has high temperature, strong solar radiation and low wind speed and moisture content from April to May. Significant differences exist in the meteorological characteristics of typical cities with the other four climate zones, thereby indicating that a regional difference exists in terms of thermal comfort.

The existing research has indicated that increasing urban green plants has a significant effect on improving such thermal environments and thermal comfort in urban areas (Vanos et al. 2019). This method is called green cooling island.

Conclusions

This study conducted a questionnaire survey from April to May 2019 and aimed to understand the outdoor thermal comfort characteristics across groups of people in the cold zone of China. The following conclusions are based on the analysis of the survey results and comparison with other typical cities.

In the comparison of thermal comfort amongst groups of people in terms of gender, women are more sensitive to thermal sensation and thermal comfort than men. In terms of age, the respondents aged 31–35 have the lowest and highest sensitivities to thermal sensation and thermal comfort, respectively. In terms of educational background, the below undergraduate respondents have the highest and lowest sensitivities to thermal sensation and thermal comfort, respectively. BMI was positively correlated with thermal sensation. The respondents with normal body weight are most sensitive to thermal comfort.

In the research on thermal expectation, the findings show that the respondents expect decreases in temperature and solar radiation and increases in wind speed and relative humidity with the increase in thermal sensation. Respondents perceive that Xi'an has a higher temperature and stronger solar radiation in April and May and expect them to decrease.

In the comparison with typical cities in the five climate zones, Xi’an in the cold zone has large geographical differences compared with the other cities, thereby indicating significant regional differences in outdoor thermal comfort. Compared with the other cities, Xi’an has high temperature, strong solar radiation and low wind speed and moisture content from April to May.

Acknowledgements

This study was supported by the Fundamental Research Funds for the Central Universities (Grant Number: xjj2017191), Scientific Research Support of New Teacher of Xi’an Jiaotong University (Grant Number: JZ1K004), China Postdoctoral Science Foundation (Grant Number: 2018M633514), National Natural Science Foundation of China (Grant Number: 51808440) and Shaanxi Province Natural Science Basic Research Program — General Project (Youth) (Grant Number: 2019JQ-595).

References

Blazejczyk, K., Epstein, Y., Jendritzky, G., Staiger, H. and Tinz, B. 2012. "Comparison of UTCI to selected thermal indices." *International journal of biometeorology* 56(3):515-535.

Cohen, P., Potchter, O. and Matzarakis, A.2013 "Human thermal perception of Coastal Mediterranean outdoor urban environments." *Applied Geography* 37: 1-10. https://www.sciencedirect.com/science/article/pii/S0143622812001142/pdfft?md5=59923c09ef6d38ae2ef1b82fe7881beb&pid=1-s2.0-S0143622812001142-main.pdf

De Dear, R. and Brager, G. S. 1998. "Developing an adaptive model of thermal comfort and preference." https://escholarship.org/content/qt4qq2p9c6/qt4qq2p9c6.pdf?t=lpz1vq

Höppe, P. 2002. "Different aspects of assessing indoor and outdoor thermal comfort." *Energy and buildings* 34(6): 661-665.

Kovács, A., Unger, J., Gál, C. V. and Kántor, N. 2016. "Adjustment of the thermal component of two tourism climatological assessment tools using thermal perception and preference surveys from Hungary." *Theoretical and Applied Climatology* 125(1-2): 113-130. https://link.springer.com/content/pdf/10.1007%2Fs00704-015-1488-9.pdf

Lai, D., Guo, D., Hou, Y., Lin, C. and Chen, Q. 2014. "Studies of outdoor thermal comfort in northern China." Building and Environment 77: 110-118. https://www.sciencedirect.com/science/article/pii/S0360132314000869/pdfft?md5=b818a964bcb7668605592e3d2e6ade34&pid=1-s2.0-S0360132314000869-main.pdf

Lin, T. P. 2009. "Thermal perception, adaptation and attendance in a public square in hot and humid regions." *Building and environment* 44(10)2009: 2017-2026.

Lin, T. P. and Matzarakis, A. 2008. "Tourism climate and thermal comfort in Sun Moon Lake, Taiwan." *International Journal of Biometeorology* 52(4): 281-290.

Lin, T. P., Tsai, K. T., Liao, C. C. and Huang, Y. C. 2013. "Effects of thermal comfort and adaptation on park attendance regarding different shading levels and activity types." *Building and Environment* 59: 599-611. Mayer, H. 1993. "Urban bioclimatology." *Experientia* 49(11): 957-963. https://link.springer.com/content/pdf/10.1007%2FBF02125642.pdf

Mayer, H. 1993. "Urban bioclimatology." Experientia 49(11): 957-963. https://link.springer.com/content/pdf/10.1007%2FBF02125642.pdf

Ng, E. and Cheng, V. 2012. "Urban human thermal comfort in hot and humid Hong Kong." *Energy and Buildings* 55: 51-65. https://www.sciencedirect.com/science/article/pii/S0378778811004130/pdfft?md5=6d1322585bc9d700a9cef12cfbd5f235&pid=1-s2.0-S0378778811004130-main.pdf

Nikolopoulou, M., and Lykoudis, S. 2006. "Thermal comfort in outdoor urban spaces: analysis across different European countries." *Building and environment* 41(11): 1455-1470. https://www.sciencedirect.com/science/article/pii/S0360132305002039/pdfft?md5=c300639eace5bde43f37cd2ad6a8ebdf&pid=1-s2.0-S0360132305002039-main.pdf

Ridha, S., Ginestet, S. and Lorente, S. 2018. "Effect of the Shadings Pattern and Greenery Strategies on the Outdoor Thermal Comfort." *International Journal of Engineering and Technology* 10(2).

Spangenberg, J., Shinzato, P., Johansson, E. and Duarte, D. 2019. "Simulation of the influence of vegetation on microclimate and thermal comfort in the city of São Paulo." *Revista da Sociedade Brasileira de Arborização Urbana* 3(2): 1-19. https://revistas.ufpr.br/revsbau/article/view/66265/38139

Standard, A. S. H. R. A. E. 1992. "Standard 55-1992, Thermal environmental conditions for human occupancy." *American Society of heating, Refrigerating and Air conditioning Engineer*.

Standard, A. S. H. R. A. E. 2013. "Standard 55-2013, Thermal environmental conditions for human occupancy." *American Society of heating, Refrigerating and Air conditioning Engineer*.

Thermal Design Code for Civil Buildings. 1993. GB 50176–51993. Ministry of Housingand Urban-rural Development of the People's Republic of China. Beijing. China,

Vanos, J. K., Kosaka, E., Iida, A., Yokohari, M., Middel, A., Scott-Fleming, I. and Brown, R. D. 2019. "Planning for spectator thermal comfort and health in the face of extreme heat: The Tokyo 2020 Olympic marathons." *Science of The Total Environment* 657: 904-917. https://www.sciencedirect.com/science/article/pii/S0048969718348022/pdfft?md5=9e49a04806efe4d1c465069d31f0257d&pid=1-s2.0-S0048969718348022-main.pdf

Yin, J., Zheng, Y., Wu, R., Tan, J., Ye, D. and Wang, W. 2012. "An analysis of influential factors on outdoor thermal comfort in summer." *International journal of biometeorology* 56(5): 941-948. https://link.springer.com/content/pdf/10.1007%2Fs00484-011-0503-9.pdf

Zeng, Y. and Dong, L. 2015. "Thermal human biometeorological conditions and subjective thermal sensation in pedestrian streets in Chengdu, China." *International journal of biometeorology* 59(1): 99-108. https://link.springer.com/content/pdf/10.1007%2Fs00484-014-0883-8.pdf

Heat Health Warning System in Germany – Implementation of city issues

Andreas Matzarakis[1], *Research Centre Human Biometeorology, German Meteorological Service (Germany)*
Stefan Muthers, Research Centre Human Biometeorology, German Meteorological Service (Germany)

ABSTRACT

After the heat waves in the year 2003 and the statements of IPCC about the increase and the related consequences several countries in Europe decided to develop or implement a Heat Health Warning System (HHWS) and provide information for general public and public health. In Germany, weather Forecast is used to predict heat episodes, which are associated with negative health impacts. Therefore, a heat balance model of the human body and an extracted equivalent temperature (Perceived Temperature) is applied. Thresholds for strong and extreme heat stress based on thermal perception classification are used and build the first approach of the HHWS. Furthermore, the threshold of strong heat stress includes a short term adaptation component and considers the previous thermal stress conditions of the last 30 days. The second step includes nocturnal conditions, based on forecasted minimum air temperature or a simulated maximum indoor temperature for typical houses. Both criteria are important for the decision about warnings for the present and next days. Warnings are generated by daily weather forecast automatically and are additionally confirmed or adjusted by a biometeorological forecaster. The warning is valid on county level considering several elevation classes. The heat warning is available as a map on the internet and registered users can receive information by a daily newsletter. A specific smartphone app is also available for general use. The main target groups are the public, nursing homes and ministries of the federal states and other authorities.

Introduction

There is evidence that heat has a big influence on human health especially on mortality and morbidity. The 2003 heat waves led to a significant increase in the number of fatal casualties (IPCC 2007; Matzarakis et al. 2011; Larsen 2006). Due to the climate change in the future both the frequency and intensity of heat waves is expected to increase, which will lead to a rise in heat-related mortality (Matzarakis et al. 2011; Muthers et al. 2010), with the main risk for the elderly, chronically ill, very young children and socially isolated people (Koppe 2009).

In Germany the HHWS is based on a thermal index (Perceived Temperature) and the impact analysis is based on the quantification how the different thermal stress categories impact on human health, and when it is necessary to issue a warning, and analysis of mortality data from various European regions (Koppe 2005; Koppe and Matzarakis 2016; Matzarakis, 2017). As the morbidity data available is often inadequate, unfortunately, total mortality can be selected as the indicator of health impacts. It was found that in all the regions investigated, heat loads classified as "heavy" and “extreme” were associated with a clear deviation of actual mortality from the

[1] Corresponding Author: andreas.matzarakis@dwd.de, +49 69 8062 9610, Research Centre Human Biometeorology, German Biometeorological Service, Stefan-Meier-Str. 4, D-79104 Freiburg, Germany.

expectation value (Koppe 2005). On average days with a heavy heat load result in a mortality rate that is about 13% higher than the expected. (Koppe 2005, 2009). Even a moderate heat load is linked to a significant increased mortality.

As a consequence of the 2003 heat waves, many European weather services have set up HHWS. The HHWS can utilize weather forecast to predict specific periods of heat, which can have negative implications and impacts on human health (Koppe 2009). For protection of population appropriate communication strategies and a well-structured preparedness plan to trigger intervention measures need to be provided and established (Koppe 2009; Straff et al. 2017; Zielo and Matzarakis 2017; Matzarakis and Zielo 2017).

Methodology

The HHWS of the German Meteorological Service (DWD) consists of several components and includes both automatically generated information from the numerical weather forecasts and human consideration and decisions by biometeorologists. The HHWS includes also ways of communication and preventive actions to be taken. In the following, the processes included and involved are explained.

Perceived Temperature

There is knowledge and evidence that a single meteorological factor like air temperature is not appropriate to describe the entire effect extraordinary heat might have on the human body (Matzarakis 2013). Therefore the energy exchange between the human body and its environment, which takes place via short- and long wave radiation, the turbulent flows of sensible and latent heat including breathing, sweating and other energy fluxes, is applied. For the calculations of the energy balance of the human body, there are four basic meteorological variables: air temperature, mean radiant temperature (which considers short- and long wave radiation fluxes), air humidity, and wind speed at a human related height (Matzarakis 2007; Parsons 2003). Together with thermo-physiological factors like the metabolic rate and the clothing, these meteorological elements provide the six fundamental factors which define the conditions for energy/heat exchange between the human body and its environment (Matzarakis 2007; VDI 1998).

The method used by the German Meteorological Service for the health-relevant assessment of the thermal environment is Perceived Temperature (PT) (Jendritzky 1990; VDI 1998; Staiger et al. 2012). This is based on a complete energy budget model of the human body and takes into account all relevant mechanisms of heat exchange with the atmospheric environment. The computation of Perceived Temperature is based on a standard male, known as "Klima-Michel". This standard male chooses his clothing in order to remain in thermal comfort as far as possible, with a clothing value (clo) from 0.5 to 1.75. The Perceived Temperature (PT) is given in the dimension °C and can be summarized in terms of a scale of physiological stress or strain (Table 1).

Table 1. Perceived Temperature, thermal perception and physiological stress (after VDI 1998; Staiger et al. 2012)

Perceived Temperature (°C)	Thermal perception	Thermo-physiological strain
< -39	Very cold	-4: Extreme cold stress
-39 to -26	Cold	-3: Heavy cold stress
-26 to -13	Cool	-2: Moderate cold stress
-13 to 0	Slightly cool	-1: Less cold stress
0 to 20	Comfortable	0: No thermal stress
20 to 26	Slightly warm	1: Less heat load
26 to 32	Warm	2: Moderate heat load
32 to 38	Hot	3: Heavy heat load
≥ 38	Very hot	4: Extreme heat load

The calculation of Perceived Temperature is performed based on hourly data of the weather forecast of the German Meteorological Service and for heat warning the value of PT at 12 UTC is used with the warning criteria of classes of the heavy heat load (3) and extreme heat load (4) (Table 1). However, because days with at least a moderate heat load occur relatively frequently – between 30 and 40 times a year – "moderate heat load" is not suitable for use as a warning criterion; excessively frequent warnings may result in "warning fatigue", with people failing to take them seriously (Koppe 2009).

Short Time Acclimatization and Nocturnal Conditions

During summer, humans gradually become more acclimatized to high temperature conditions. Heat loss becomes more efficient, e.g. through an increase in the sweating rate. In order to account for this acclimatization, a procedure has been developed which allows the threshold value of the comfort range (Table 1) to be adjusted according to the thermal conditions of the last 30 days (Koppe 2005). The classification bands are maintained, however, and the threshold values for moderate, heavy and extreme stress shift accordingly (Koppe 2009). The thresholds for individual stress categories vary, in addition, from region to region: for example, they are generally higher in southwestern than in northern Germany in summer (Koppe 2009).

Implementation of Elderly Population

The adaptation possibility of elderly people is much lower than for healthy people, therefore the effect of heat stress is different. From thermos physiological perspective there is a reduction of the seat rate, reduction of elasticity of the blood vessel, lower skin and core temperature of the human body and limitations in blood circulation in general. In addition mobility is lower and therefore the walking speed is from 4 km/h much lower and about 1 km/h.

Nocturnal Conditions

For the night situation, the minimum temperature is considered, if it falls below a specific threshold (16–18 °C, depending on the region), as night-time cooling guarantees a recovery period (Koppe 2009). During long-lasting heat waves, acclimatization adjustment of the threshold values to weather conditions over recent weeks could well produce too high threshold value for "heavy heat load". Therefore, in order to ensure that warnings continue to be issued during this type of scenario, the warning threshold value is fixed at a maximum of 34 °C Perceived Temperature.

In addition, for a more appropriate description of the conditions indoors, information from a building simulation model that provides data about thermal conditions in the indoor environment is considered in issuing of the heat warning (Pfafferott and Becker 2008).

The building simulation model estimates the thermal indoor conditions. The year of construction and the material of the building give information about physical properties of the building (Rosenfelder et al. 2016). But also the quality of windows and shading, the user profile (presence of the person) and the user behaviour (opening and closing of windows and shading) are considered for the simulation of the indoor climate (Rosenfelder et al. 2016). Due to these possible combinations of user behaviour and building type, different heat stress situations can occur indoors during a hot period (Pfafferott and Becker 2008).

We defined a standard building in order to control the physical properties of the building structure. This standard building refers to a typical nursing facility. It describes a building constructed in the 1990s or later. The standard building is characterized by an air-proof facade and very little cross-ventilation. The natural ventilation is simulated as a system with an air flow network. This system is represented by a collection of nodes distributed in the modelled room. Inter-nodal connections represent the distributed flow paths associated with cracks, doors, windows etc. Because of the pressure difference between the nodes and the conservation of mass, a set of non-linear equations can be solved for each time step to characterize the flow throughout the network (Clarke and Hensen 1991).

The geometric model consists of two standard rooms in a nursing facility with the same base area of 14.25 m^2 and a height of 2.8 m connected by a corridor. The windows' opening section is 1.3 m^2 and describes two large windows positioned side by side that can either be totally opened or just tilted. Additionally, the window has double heat protection glass and external shading. Generally, this model accords to a good modern building standard in Germany.

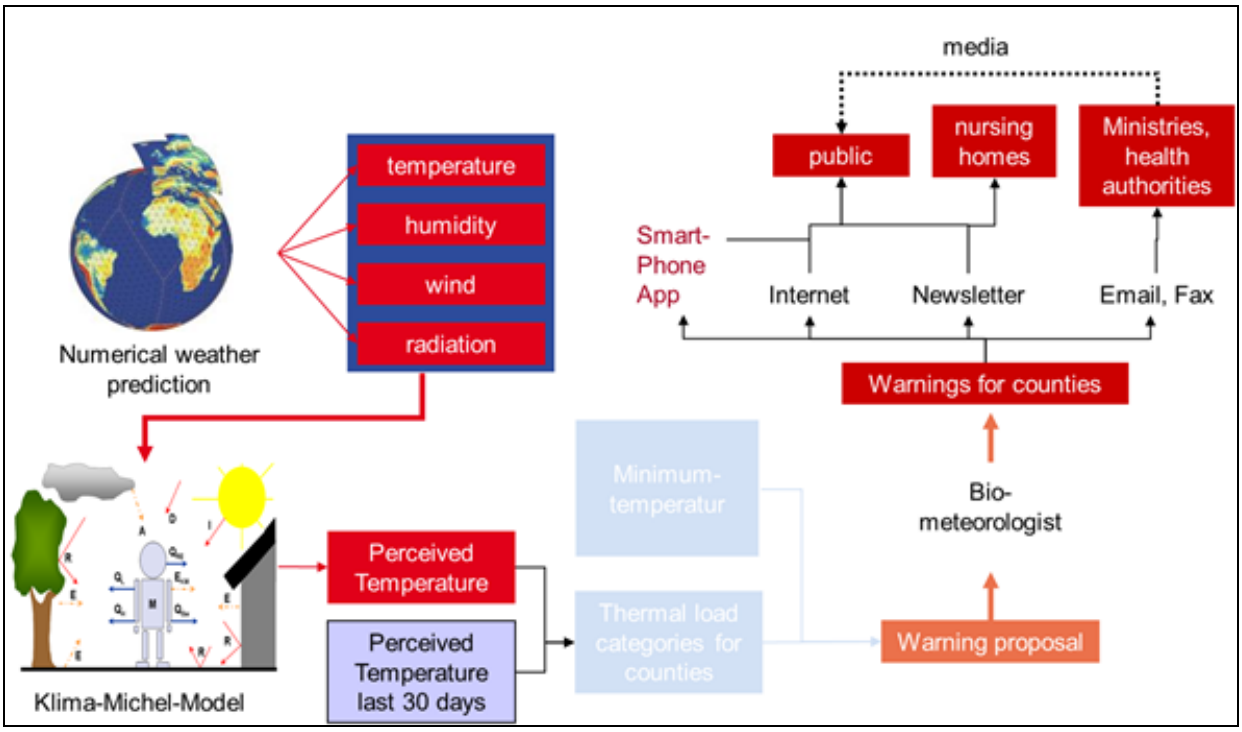


Figure 1. Workflow of HHWS and ways of communication

Implementation of Urban Heat Island

For a more comprehensive implementation of the night conditions in urban areas for cities over a population of 100.000 urban heat island, which are especially during heat waves more worse are considered. For the development of the urban heat island a number of impacts have to be considered such as the degree of sealed surface, built-up density, physical properties of building material, anthropogenic heat production. In addition the intensity of the urban heat island depends on different weather conditions, like cloudless and warm weather and wind speed and this not only for one specific day (Wienert et al. 2013). Based on the Wienert et al. (2013) approach, which is valid for cities with a population over 100.000, the heat health warning system is able to deliver specific conditions during the night are now expanded with this information, which is helpful for the decision about the indoor conditions. This means that the weather forecast is modified for cities with an additional rate of the urban heat island, which can have an effect on the indoor conditions.

Warning Criteria

Based on the above automated factors, the biometeorologist considers the preliminary warning proposal, adjusts and modifies it, if needed, and – most importantly – decides about issuing the warning. On each day that the Perceived Temperature at 12.00 Universal Time Coordinated (UTC) exceeds the warning threshold, a warning is issued by the DWD at around 10 a.m. The warning covers a two day period. The information pathways are followed when the

"heavy heat load" threshold is exceeded. Based on numerical weather prediction for the next 48 hours, the model calculates whether the "heavy heat load" warning threshold will be exceeded in the individual counties across Germany, and up to which altitudes. This generates a warning recommendation which is then reviewed by bio-meteorologists. They have the option to accept the recommendation to issue a warning, and they can also add warnings of their own if, in their view, a critical situation could arise (Koppe 2009). The warning is valid on county level including several elevation classes.

Communication and Application of Warnings

The warnings generated in this way are published on the DWD website (http://www.dwd.de/gesundheit). The heat warning is available as maps and registered users can receive information by daily newsletter. A specific smartphone application is also available for general use. The main target groups are the public, nursing homes and ministries of the federal states and other authorities. The relevant health and supervisory authorities are also notified; they are responsible for drawing up a list of intervention measures and monitoring their implementation. There is also the option of broadcasting the warning more widely to the public on radio and television. In addition to the heat warning for the next 48 hours, the DWD provides heat load information for the next 2–7 days. In addition the warning includes information about the number of days of heat warning.

Discussion and Conclusion

Nowadays it is important, to, not only issue warnings about high air temperatures but also to consider other meteorological parameters that influence the energy balance of the human body (Matzarakis 2007, Koppe 2009). The DWD applies the Perceived Temperature for this purpose. When issuing heat warnings, the threshold values that must be exceeded in order to trigger a warning are adjusted to local weather conditions over the past 30 days. This adjustment is necessary to take account of the fact that the human body adapts to its thermal environment (acclimatisation). For a southern European, for example, a Perceived Temperature of 30 °C is a common condition, whereas for people in northern Germany, such temperatures may result in considerable physical stress.

Evaluations of the HHWS in the Federal State of Hessen show that the system is working effectively, especially in the area of residential elderly care. There is a clear signal that the number of admissions has fallen significantly (Koppe 2009). This shows that the measures taken in Hessen in response to heat warnings have successfully reduced the number of heat-related health complaints. Additionally a high awareness and acceptance of the HHWS has been lately confirmed by a project of the Federal Environmental Agency, where the current warning systems in Germany were assessed (Capellaro and Sturm 2015).

In view of the climate change and the prospect of more frequent and intensive heat waves, it is important to develop such intervention measures further and extend them to other areas outside residential care. Although the elderly are classed as particularly vulnerable, other groups of person can suffer during heat waves, as well.

References

Capellaro M, Sturm D (2015) Evaluation of Information Systems Relevant to Climate Change and Health. Volume 1: Adaption to Climate Change: Evaluation of Existing National Information Systems (UV-Index, Heat Warning System, Airborne Pollen, Ozone Forecasts) from a Public Health Perspective – How to Reach Vulnerable Populations. Umwelt und Gesundheit 03/2015.

Clarke JA, Hensen JLM (1991) An approach to the simulation of coupled heat and mass flows in buildings. Indoor Air 3: 283–296.

IPCC (2007) Climate Change 2007: Impacts, Adaptation and Vulnerability. Contribution of Working Group II to the Fourth Assessment Report of the Intergovernmental Panel on Climate Change. Eds.: Parry ML, Canziani OF, Palutikof JP, van der Linden PJ, Hanson CE. Cambridge University Press. Cambridge, UK.

Jendritzky G (1990) Methodik zur räumlichen Bewertung der thermischen Komponente im Bioklima des Menschen – Fortgeschriebenes Klima-Michel-Modell. Beitr. Akademie f. Raumforschung u. Landesplanung 114:7-69.

Koppe C (2005) Gesundheitsrelevante Bewertung von thermischer Belastung unter Berücksichtigung der kurzfristigen Anpassung der Bevölkerung and die lokalen Witterungsverhältnisse. Berichte des Deutschen Wetterdienstes 226. Offenbach am Main.

Koppe C (2009) The Heat Health Warning System of the German Meteorological Service. In: UMID Special Issue: Climate Change and Health 3: 39-43.

Larsen J (2006) Setting the Record Straight: More than 52,000 Europeans Died from Heat in Summer 2003. Earth Policy Institute, http://www.earth-policy.org/plan_b_updates/2006/update56 (last access at 01.10.2014).

Matzarakis A (2007) Climate, human comfort and tourism. In: Amelung B, Blazejczyk K, Matzarakis A (eds.) Climate Change and Tourism: Assessment and Coping Strategies. 139-154.

Matzarakis A (2013) Stadtklima vor dem Hintergrund des Klimawandels. Gefahrstoffe – Reinhaltung der Luft 73, 115-118.

Matzarakis A (2016) Das Hitzewarnsystem des Deutschen Wetterdienstes (DWD) und seine Relevanz für die menschliche Gesundheit. Gefahrstoffe – Reinhaltung der Luft 76, 457-460.

Matzarakis A (2017) The Heat Health Warning System of DWD – Concept and Lessons learned. In: Karacostas et al., (Eds) Perspectives in Atmospheric Sciences. Springer Atmospheric Sciences, 191-196.

Matzarakis A, Koppe C (2016) Hitzewellen – eine zunehmende Gesundheitsgefahr. Internistische Praxis 56, 585-592.

Matzarakis A, Zielo B (2017) Maßnahmen zur Reduzierung von Hitzebelastungen für Menschen – Bedeutung von Hitzeaktionsplänen. Gefahrstoffe – Reinhaltung der Luft 77, 316-320.

Matzarakis A, Muthers S, Koch E (2011) Human-biometeorological evaluation of summer mortality in Vienna. Theoretical and Applied Climatology 105: 1-10.

Muthers S, Matzarakis A, Koch E (2010) Climate Change and Mortality in Vienna—A Human Biometeorological Analysis Based on Regional Climate Modeling. Int. J. Environ. Res. Public Health 7: 2965-2977.

Muthers S, Laschewski G, Matzarakis A (2017) The Summers 2003 and 2015 in South-West Germany: Heat Waves and Heat-Related Mortality in the Context of Climate Change. Atmosphere (11), 224, 1-13.

Parsons KC (2003): Human thermal environments: the effects of hot, moderate, and cold environments on human health, comfort and performance. 2nd edition. Taylor & Francis. London.

Pfafferott J, Becker P (2008) Erweiterung des Hitzewarnsystems um die Vorhersage der Wärmebelastung in Innenräumen. Bauphysik 30: 237-243.

Rosenfelder M., Koppe C., Pfafferoth J, Matzarakis A (2016) Effects of ventilation behavior on indoor heat load based on test reference years. International Journal of Biometeorology 60: 277-287.

Staiger H, Laschewski G, Grätz A (2012) The Perceived Temperature – A versatile index for the assessment of the human thermal environment Part A: Scientific Basics. International Journal of Biometeorology 56: 165–176.

Straff W, Mücke H-G, Baeker R, Baldermann C, Braubach A, Litvinovitch J, Matzarakis A, Rexroth U (2017) Handlungsempfehlungen für die Erstellung von Hitzeaktionsplänen zum Schutz der menschlichen Gesundheit. Bundesgesundheitsblatt-Gesundheitsforschung-Gesundheitsschutz 60, 662-672.

VDI (1998) Methods for the human biometeorological evaluation for climate and air quality for the urban and regional planning. Part I: climate. VDI guideline 3787. Part 2. Berlin, Beuth

Wienert U, Kreienkamp, F, Spekat A, Enke W (2013) A simple method to estimate the urban heat island intensity in data sets used for the simulation of the thermal behavior of buildings. Meteorologische Zeitschrift 22, 179-185.

Zielo B, Matzarakis A (2017) Bedeutung von Hitzeaktionsplänen für den präventiven Gesundheitsschutz in Deutschland. Gesundheitswesen 79, 1-10.

Thermal Sensation and Thermal Load of Human Body in Irradiated Hot Environment

Atsumasa Yoshida, Osaka Prefecture University (Japan)
Takuma Naka, Osaka Prefecture University (Japan)
Narihisa Chigusa, Osaka Prefecture University (Japan)
Shinichi Kinoshita, Osaka Prefecture University (Japan)

ABSTRACT

Subject experiment and numerical calculation were carried out to study the thermal sensation under awning and heat stress reduction effect to the human body outdoors in summer. The thermal sensation was reduced in the awning space, and the thermal load reduction effect was confirmed. There was a correlation between the change in thermal sensation and the change in mean skin temperature due to entering and leaving the awning space. The influence of weather conditions such as air temperature on the behavior of mean skin temperature and human thermal load was clarified. The relationship between the solar radiation characteristics of the awning material, the infrared radiation characteristics and the reduction of the human thermal load was clarified. The effect of ambient weather conditions on the relationship was discussed.

Special Issue Journal	:	Urban Climate
DoI	:	https://doi.org/10.1016/j.uclim.2020.100765
Citation	:	Yoshida, A., Naka, T., Chigusa, N., & Kinoshita, S. (2021). Thermal sensation and thermal load of human body in irradiated hot environment. Urban Climate, 36, 100765.

Comprehensive evaluation of the influence of outdoor temperature change on health around the urban area

Daisuke Narumi[1]*, Yokohama National University (Japan)*
Tomohiko Ihara, The University of Tokyo (Japan)
Sanae Fukuda, Kansai University of Welfare Sciences (Japan)
Yoshiyuki Shimoda, Osaka University (Japan)

ABSTRACT

This paper aims to comprehensively and quantitatively evaluate the impact of urban outdoor temperature change on human health in Osaka Prefecture, based on the data accumulated by the authors and some other researches, conducted an annual evaluation from fatal severe to relatively mild impact. Specifically, based on the concept of endpoint-type life cycle impact assessment method, human health impact due to various diseases was integrally evaluated using DALY (disability-adjusted life year). The evaluated diseases were heat / cold stress and heatstroke (death) as fatal severe effect, infections such as Herpangina, sleep disturbance, fatigue and mild heatstroke (not death) as an effect that do not lead to death. The time range of the evaluation was from 1967 to 1977 (1970s) as the base period, from 1987 to 1997 (1990s), further from 2007 to 2017 (2010s) over the past 40 years.

As a result, the largest increase of DALY was seen in August, especially deterioration in sleep disturbance, fatigue, death by heat stress and death by heatstroke showed large impact. On the other hands, the largest decrease was seen in February, mitigation in fatigue and cold stress showed large impact. The annual total value of DALY increased by 2,854 [DALY]. The influence of sleep disturbance and fatigue had a large impact on the change in DALY. Although the disability weight and the disease period are small for these diseases, these influences are indispensable to evaluate the entire of human health from the macro viewpoint of urban area.

Introduction

Recently, increasing urban temperatures due to urban heat islands (UHI) and global warming (GW) have become remarkably around the world. Especially in Japan, during the last century, annual average air temperature has increased about 1 K all over Japan, and this is seen as the influence of GW (JMA 2016). In addition to the influence of GW, high temperatures in the summer have increased about 1 K to 2 K, and low temperatures in the winter have increased about 3 K to 6 K in some large cities (JMA 2016). In these cities, the rate of temperature rise remained unchanged even before entering the twenty-first century. Based on past trends, it is easy to imagine that the temperature rise will continue for some time into the future.

UHI and GW not only cause temperatures to rise, they also have diverse impacts on urban dwellers. In this regard, the authors (Shimoda, Narumi, and Mizuno 2005) showed a cause-effect chain between air temperature changes around urban area and their effects and the impact has been assessed as quantitatively as possible (Narumi et al. 2007) (Narumi, Shimoda, and Kondo 2009). Following these examinations, in this paper we try to examine as comprehensively as possible the impact on the health of urban dwellers.

[1] Corresponding Author: [narumi-daisuke-rs@ynu.ac.jp], [+81-45-339-3719].

With regard to the relationship between outdoor temperature change and human health, the media or government have paid attention to prevent urban dwellers from heatstroke, but they seem to make nothing of the other health effects. Under these circumstances, the authors have evaluated the influence of temperature changes in urban areas on infections (Kadobayashi et al. 2007) and sleep disturbance (Okano, Ihara, and Genchi 2008) (Narumi, Ihara, and Fukuda 2016) and fatigue (Narumi, Ihara, and Fukuda 2017). In this paper, based on the data accumulated by authors and the results of previous research, we conducted the comprehensive annual evaluation from serious effects leading to death to relatively mild effects.

Framework for health impact assessment

Evaluation procedure

In this paper, following the author's method (Ihara and Genchi 2008) based on LIME (Life-cycle Impact Assessment Method based on Endpoint Modeling) (Itsubo and Inaba 2005), the human health impact of various diseases caused by urban temperature change are evaluated by using DALY (disability-adjusted life year).

The concrete evaluation procedure of this research is described below. Firstly, regarding the relationship between outdoor temperature change and human health, we determine the framework to be evaluated based on the results of previous research. Next, we evaluate the temperature sensitivity of various disease to be evaluated based on the data accumulated by the authors and some other researches. Next, based on parameters such as disability weight and duration, we evaluate the amount of damage caused by each disease with DALY used as an evaluation index. Finally, by multiplying the obtained temperature sensitivity by the temperature deviation from the past to the present, the human health effects associated with temperature changes are compared among various diseases.

Target disease for evaluation

The temperature change in urban area affects various levels from death to mild without hospitalization. Here, because different procedures are required to calculate the value of DALY, the impact evaluation targets were determined by dividing into two levels, "death (level 1)" and "not death (level 2)". Table 1 shows the diseases evaluated in this paper according to each level. By evaluating these diseases, we considered that it is possible to comprehensively evaluate the effects of temperature changes in urban area on human health. The spatial range to be evaluated is the whole of Osaka Prefecture where temperature sensitivity data on health effects are easily available and the effects of UHI are remarkable.

As for level 1, in addition to the change in mortality risk associated with cardiovascular and respiratory disease caused by heat and cold stress, heatstroke leading to death was set to the target disease. Level 1 evaluates the value of DALY by YLL (years of life lost). As for level 2, various infections, sleep disturbance, fatigue, and heatstroke not leading to death were set to the target diseases. Level 2 evaluates the value of DALY by YLD (years lived with a disability). Please refer to Ihara et al. (Ihara and Genchi 2008) for the detail of how to calculate YLL and YLD.

Table 1. Evaluated disease or disturbance and its disability level

Level	Disease, Disturbance		Disability weight	Ill period (day)
Death (Level1)	Heat/Cold stress (65 and over)		1.000	-
	Death by Heatstroke (under 65)		1.000	
Not death (Level2)	Infections	Herpangina	0.160	8
		Hand, foot and mouth disease	0.170	10
		Pharyngo-conjunctival fever	0.120	6
		Escherichia coli	0.220	7
		Gastroenteritis	0.110	2
		Keratoconjunctivitis	0.090	14
		Exanthema subitum	0.130	5
	Sleep disturbance		0.069	1
	Fatigue		0.050	1
	Heatstroke (Not death)		0.140	4

Impact analysis

Here, according to the evaluation framework described in the above chapter, the impact analysis for each disease shown in Table 1 was carried out based on the data accumulated by the authors and some other researches. Specifically, the relationship between outdoor temperature and DALY was evaluated for the entire Osaka prefecture as a target area.

Death (level 1)

a) Death due to heat and cold stress

Honda et al. (Honda et al. 1998) has analyzed Japanese demographic statistical data and clarified the relationship between the daily maximum outdoor temperature and the mortality rate over the age of 65 years. In this paper, based on these data, the temperature sensitivity was quantified from the relationship between the daily maximum outdoor temperature and the number of deaths due to heat and cold stress in Osaka Prefecture. Here, Kunst et al. (Kunst et al. 1993) pointed out that half of the cold side effects are due to an increase in respiratory disease and are not affected by temperature change, so that the amount of cold side effect was multiplied by 0.5. The YLL for this section is two years, as it is expected that the harvesting effect will be exerted on death caused by such vulnerability to heat or cold stress. The relationship between the daily maximum outdoor temperature and DALY estimated by using the above parameters is shown in Figure 1.

b) Death due to heatstroke

As for death due to heatstroke, using death statistics data cause by heatstroke by Ono (Ono 2009), temperature sensitivity was quantified from the relationship between the daily maximum outdoor temperature and the number of deaths due to heatstroke younger than 65 years. YLL for death due to heatstroke was estimated by the weighted average life expectancy based on the average life expectancy and the mortality rate by age in Osaka by Ono (Ono 2009). As a result,

YLL was evaluated as 27.4 years. The relationship between the daily maximum outdoor temperature and DALY estimated by using the above parameters is shown in Figure 2.

Not death (Level2)

a) Infections

The authors (Kadobayashi et al. 2007) analyzed the relationship between the number of outbreaks of various infectious diseases and the outdoor temperature based on the infectious disease trend survey data provided by the Osaka City Public Health Center. As the first step, 16 items considered to be related to temperature were selected which have seasonal variation from the number of weekly reports. And the next step, for these 16 items, regression equations were calculated using a linear or an exponential function from the correlation between the weekly average temperature. As a result, only 7 items (Herpangina, Hand-foot-and-mouth disease, Pharyngo-conjunctival fever, Escherichia coli, Gastroenteritis, Keratoconjunctivitis, Exanthema subitum) were evaluated as having significant temperature sensitivity. In this paper, we quantified temperature sensitivity for these infections. The disability weight and ill period were set as shown in Table 1 referring to the description of GBD. Figure 3 shows the relationship between the average weekly temperature and DALY estimated by using the above parameters.

b) Sleep disturbance

Narumi et al. (Narumi, Ihara, and Fukuda 2016) clarified the influence of changes in outdoor temperature on sleep disturbance in different seasons of summer and winter by questionnaire survey. The subjects of this survey were approximately 600 men and women aged 20 and over who live in Osaka Prefecture. Please refer to Narumi et al. (Narumi, Ihara, and Fukuda 2016) for details of survey method and results. As a result, the prevalence rate by sleep disturbance based on the SQIDS score from the survey results, it was estimated that 0.84% of patients per 1 ℃ increased when the outdoor temperature at 12 midnight was 18.1 ℃ or higher. In this paper, we used this data to quantify the temperature sensitivity for sleep disturbance from the relationship between the outdoor temperature at 12 midnight and the estimated prevalence rate. As for the disability weight caused by sleep disturbance, 0.069 was set based on the results of interviews with the 6 experts (4 sleeping medicines and 2 psychiatry) conducted by the authors (Fukuda et al. 2013). The ill period was set to 1 day. Figure 4 shows the relationship between the outdoor temperature at 12 midnight and DALY estimated by using the above parameters.

c) Fatigue

In the above survey on sleep disturbance, a survey on fatigue was also conducted. Please refer to Narumi et al. (Narumi, Ihara, and Fukuda 2017) for details. As a result, the prevalence rate by fatigue based on the DCF score from the survey results, it was estimated that 0.76% of patients per 1 ℃ increased when the daily maximum outdoor temperature was 24.2 ℃ or higher in summer season and 0.70% of patients per 1 ℃ increased when the daily maximum outdoor temperature was 12.0 ℃ or lower in winter season. In this paper, we used this data to quantify the temperature sensitivity for fatigue from the relationship between the daily maximum outdoor temperature and the estimated prevalence rate. As for the disability weight caused by fatigue, 0.05 was set based on the results of interviews with the 7 experts (5 fatigue medicines and 2 psychiatry) conducted by the authors (Fukuda et al. 2013). The ill period was set to 1 day. Figure 5 shows the relationship between the daily maximum outdoor temperature and DALY estimated by using the above parameters.

d) Heatstroke (Not death)

In Japan, while the average number of heatstroke fatalities from 2011 to 2016 was 942, but the emergency transportation (not death) was 49,384, the number of emergency transportation was by far the larger than fatalities. Therefore, in this paper, by using the data of emergency transfer due to heatstroke from the National Institute for Environmental Studies (NIES 2018) in Osaka City from 2004 to 2009, we quantified the temperature sensitivity for heat stroke (not death) relationship between the daily maximum outdoor temperature and the number of emergency transportation. As a result, by calculating weighted average of the disability weight and the ill period from the ratio of severity patient, the former was set to 0.14 and the latter was 4.03 days. Figure 6 shows the relationship between the daily maximum outdoor temperature and DALY estimated by using the above parameters.

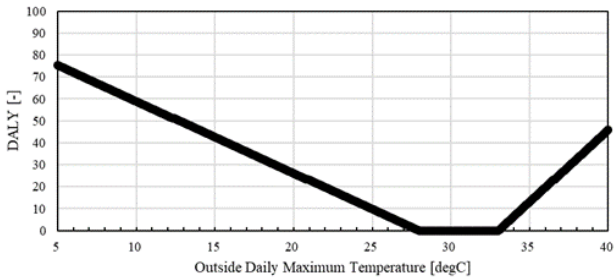


Figure 1. Relationship between daily max. outdoor temperature and DALY (death by heat / cold stress over 65s, Osaka Pref.)

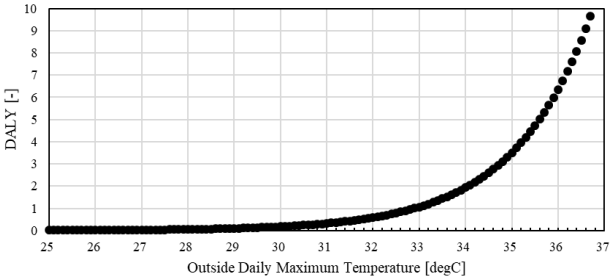


Figure 2. Relationship between daily max. outdoor temperature and DALY (death by heatstroke under 65s, Osaka Pref.)

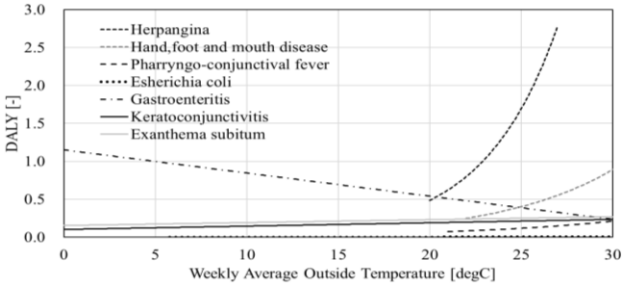


Figure 3. Relationship between daily max. outdoor temperature and DALY (infections, Osaka Pref.)

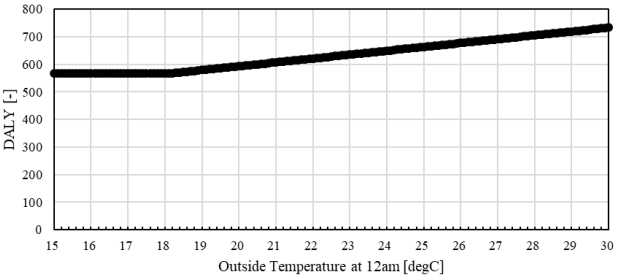


Figure 4. Relationship between outdoor temperature at 12 midnight and DALY (sleep disturbance, Osaka Pref.)

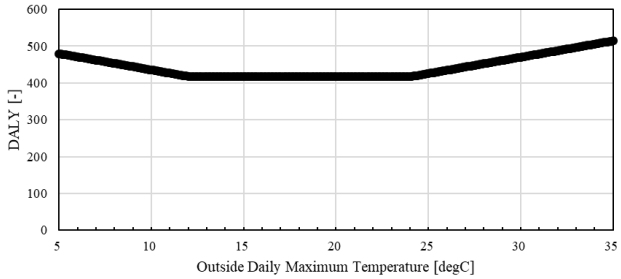


Figure 5. Relationship between daily max. outdoor temperature and DALY (fatigue, Osaka Pref.)

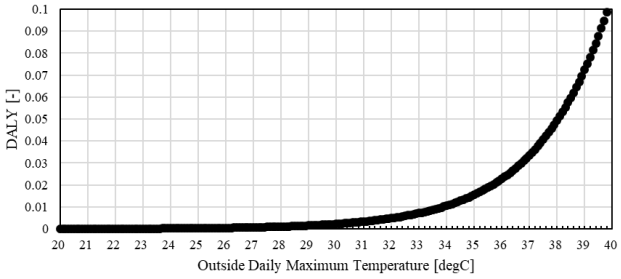


Figure 6. Relationship between daily max. outdoor temperature and DALY (heatstroke (not death), Osaka Pref.)

Damage analysis

Analysis conditions

Based on the relationship between outdoor temperature and DALY obtained in the previous chapter, we comprehensively evaluate the influence of outdoor temperature that has changed from the past to present because of UHI and GW on DALY of each disease. Regarding the time range to be evaluated, 1967 to 1977 (central year: 1972, hereinafter referred to as 1970s) was set as a reference period, and 1987 to 1997 (central year: 1992, hereinafter referred to as 1990s), 2007 to 2017 (central year: 2012, hereinafter referred to as 2010s). As for the temperature change of 40 years, the comparison result of the daily maximum outdoor temperature in Figure 7 and the outdoor temperature at 12 midnight is shown in Figure 8, respectively. The line shows the average value over 11 years for each age, and the bar shows the difference. The increase of outdoor temperature at 12 midnight showed a large value compared to the daily maximum outdoor temperature. As for the outdoor temperature at 12 midnight, the reversal was seen in January, but the temperature had generally risen over the years. On the other hand, regarding the daily maximum outdoor temperature, the trend was that the temperature declines in April and May in the 1990s, and the temperature in the 1990s was the highest in the early winter (November to January).

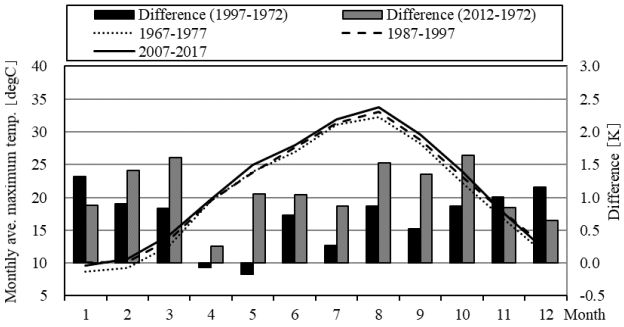


Figure 7. Secular change in monthly average of daily max. outdoor temperature (Osaka Pref.)

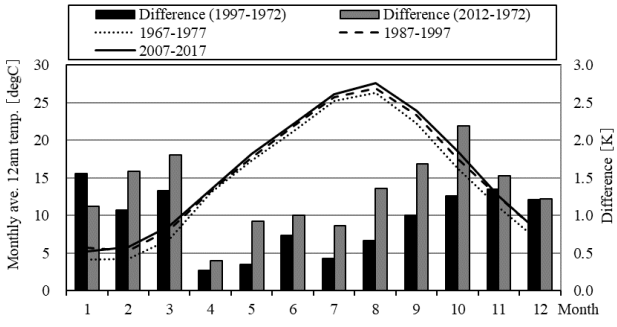


Figure 8. Secular change in monthly average of outdoor temperature at 12 midnight (Osaka Pref.)

Evaluation results

Table 2 shows the evaluation results of DALY for each disease in each period. For each disease, the average value, maximum value, minimum value for each period (11 years), and the change rates for the 1990s and 2010s compare to the 1970s are described in the lower part of each table. The following outlines the results for each level.

a) Death (level 1)

Regarding heat stress, DALY increased almost linearly in the average value, while the maximum increased approximately double compare to the 1970s in both of the 1990s and 2010s. The maximum throughout the years was 1994, when it was hit by a record-breaking heat wave, not necessarily consistent with the secular change trend. Regarding cold stress, the average value of the yearly evaluation tended to decrease, and the decrease especially in the 1990s was remarkable. Although the rate of decrease was small because the absolute amount is very large, the difference had a large effect, about twice that of heat stress. The maximum and minimum value

of the yearly evaluation showed almost the same change as the average value. Regarding heatstroke (death), the average value showed the same tendency as heat stress, and the absolute amount was also the same value. The maximum annual value was recorded in 1994 and was about 2.5 times compared to the 1970s.

b) Not death (level 2)

Regarding infections, the absolute quantity was small throughout the evaluation period, and the effects of period change and temperature change were unremarkable. Here, Table 2 summarizes all target infectious diseases and evaluates them as “infections”. As for sleep disturbance, DALY increased almost linearly. The increase rate was not so large at around 14% among the period, but the absolute amount was large as well as the cold stress, and the difference was significantly large compared with the cold stress. The maximum value for each period was recorded in 1995, which is different from heat stress and heatstroke (death) which use the daily maximum outdoor temperature as a variable. The minimum value of the yearly evaluation had increased significantly in the 2010s, and this result showed the night temperature is rising steadily in recent years. As for fatigue, the yearly evaluation showed a smaller rate of change in all indicators. This is because, in addition to the large absolute amount, it decreases in winter as the temperature rises and is offset by increase in summer. The absolute amount was as large as sleep disturbance and cold stress. As for heatstroke (not death), the absolute amount was overwhelmingly small compared to the infection, and the effect was minimal.

c) Comprehensive assessment of health effects

By combining the above, the impact on overall health caused by the temperature change in the past 40 years was evaluated by the total DALY value of all diseases. The average comprehensive value of DALY for annual evaluation was particularly remarkable increase in the period from the 1990s to the 2010s, it was about four times as much as the change from the 1970s to the 1990s. The maximum comprehensive value of DALY throughout each period was recorded in 1994, this indicate slightly different from secular trend of average value and the influence of sudden and intense heat was strong. The minimum comprehensive value in the 2010s was almost the same as the average value of the 1970s, this showed that DALY increased steadily and extremely low situation did not occur.

Figure 9 shows the results of monthly evaluation of the DALY difference between the 2010s and the 1970s. As described above, DALY of heatstroke (not death) and infections was very small and difficult to distinguish. According to the results, the comprehensive value of DALY increased from May to October due to the temperature change of 40 years but decreased from November to April. In other words, urban temperature change had a negative impact on health from the early summer to the early autumn, while a positive impact from late autumn to spring. However, the effects in April and November were very small. Although cold stress would be expected to be reduced from May to October, it was offset by adverse effects. The largest increase of DALY was seen in August, especially deterioration in sleep disturbance, fatigue, death by heat stress and death by heatstroke showed large impact. On the other hands, the largest decrease was seen in February, mitigation in fatigue and cold stress showed large impact. The annual total value of DALY increased by 2,854 [DALY]. The influence of sleep disturbance and fatigue had a large impact on the change in DALY. Although the disability weight and the disease period are small for these diseases, these influences are indispensable to evaluate the entire of human health from the macro viewpoint of urban area.

Table 2 Evaluation results of DALY for each disease or disturbance in each period

Disease	index	1967 to 1977	1987 to 1997	2007 to 2017	Disease	index	1967 to 1977	1987 to 1997	2007 to 2017
Heat stress (death)	Avg.	191.1	309.6	443.7	Sleep disturbance	Avg.	10311.6	11749.2	12946.5
			0%	0%				0%	0%
	Max.	401.1	797.5	745.2		Max.	11870.2	15139.5	14376.4
			0%	0%				0%	0%
	Min.	63.5	62.2	182.5		Min.	8599.5	9151.2	11482.4
			0%	0%				0%	0%
Cold stress (death)	Avg.	10216.5	9567.0	9272.0	Fatigue	Avg.	9223.7	8986.8	9976.6
			0%	0%				0%	0%
	Max.	10706.0	10208.5	10022.0		Max.	11192.3	11366.9	11631.8
			0%	0%				0%	0%
	Min.	9461.6	8941.8	8565.6		Min.	7397.7	6857.2	8756.2
			0%	0%				0%	0%
Heatstroke (death)	Avg.	141.9	222.0	299.5	Heatstroke (mild)	Avg.	0.6	0.7	0.9
			0%	0%				28%	60%
	Max.	255.2	621.0	487.1		Max.	0.7	1.3	1.1
			0%	0%				66%	43%
	Min.	74.6	63.5	151.2		Min.	0.4	0.4	0.6
			0%	0%				-9%	65%
Infections	Avg.	68.5	68.9	68.7	Total	Avg.	30154.2	30904.8	33008.5
			0%	0%				2%	9%
	Max.	73.7	72.9	72.7		Max.	33029.2	36938.9	36553.9
			0%	0%				12%	11%
	Min.	65.7	65.6	65.4		Min.	26700.5	26100.5	29777.7
			0%	0%				-2%	12%

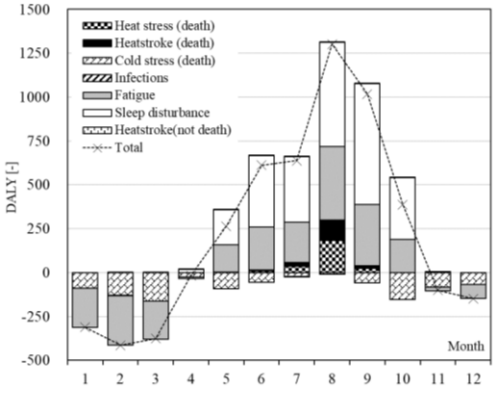


Figure 9. Secular change in monthly average of daily max. temperature (Osaka Pref.)

Summery

This paper aims to comprehensively and quantitatively evaluate the impact of urban outdoor temperature change on human health in Osaka Prefecture, based on the data accumulated

by the authors and the results of past researches, conducted an annual evaluation from fatal severe to relatively mild impact. Specifically, based on the concept of endpoint-type life cycle impact assessment method, human health impact due to various diseases was integrally evaluated using DALY (disability-adjusted life year). The evaluated diseases were heat / cold stress and heatstroke (death) as fatal severe effect, infections such as Herpangina, sleep disturbance, fatigue and mild heatstroke (not death) as an effect that do not lead to death. The time range of the evaluation was from 1967 to 1977 (1970s) as the base period, from 1987 to 1997 (1990s), further from 2007 to 2017 (2010s) over the past 40 years.The results of this research are described below.

1) The average comprehensive value of DALY for annual evaluation was particularly remarkable increase in the period from the 1990s to the 2010s, it was about four times as much as the change from the 1970s to the 1990s.

2) The maximum comprehensive value of DALY throughout each period was recorded in 1994, this indicate slightly different from secular trend of average value and the influence of sudden and intense heat was strong.

3) The minimum comprehensive value in the 2010s was almost the same as the average value of the 1970s, this showed that DALY increased steadily and extremely low situation did not occur.

4) The comprehensive value of DALY increased from May to October due to the temperature change of 40 years but decreased from November to April. In other words, urban temperature change had a negative impact on health from the early summer to the early autumn, while a positive impact from late autumn to spring.

5) The largest increase of DALY was seen in August, especially deterioration in sleep disturbance, fatigue, death by heat stress and death by heatstroke showed large impact. On the other hands, the largest decrease was seen in February, mitigation in fatigue and cold stress showed large impact. The annual total value of DALY increased by 2,854 [DALY].

6) The influence of sleep disturbance and fatigue had a large impact on the change in DALY. Although the disability weight and the disease period are small for these diseases, these influences are indispensable to evaluate the entire of human health from the macro viewpoint of urban area.

Acknowledgments

This work was supported by JSPS KAKENHI Grant Numbers JP23360437, JP18KK0123.

References

Fukuda S., Ihara T., Genchi Y., Narumi D. (2013). Japanese Sleep Disturbance and Fatigue Disability Weights in Evaluating the Effects of Increasing Temperatures on Health by a Life Cycle Approach. International Journal of Life Cycle Assessment No.18, 1089-1097

Honda Y., Ono M., Sasaki A., Uchiyama I. (1998). Shift of the Short-term Temperature-mortality Relationship by a Climate Factor - Some Evidence Necessary to Take Account in Estimating the Health Effect of the Global Warming. Journal of Risk Research Vol.1 No.3, 209-220

Ihara T., Genchi Y. (2008). Environmental Impact Assessment of Urban Heat Island Phenomena Based on Endpoint-type Life Cycle Impact Assessment Methodology. Journal of Environmental Engineering (Transactions of AIJ) No.634, 1407-1415 (in Japanese)

Itsubo N., Inaba A. (Editor) (2005). Life Cycle Environmental Impact Assessment Method, Japan Environmental Management Association for Industry (in Japanese)

JMA (The Japan Meteorological Agency) (2017). Climate Change Monitoring Report 2016 Chap.2 Climate Change, 37-57 (in Japanese)

Kadobayashi A., Niurao Y., Narumi D., Shimoda Y., Mizuno M. (2007). How the Air Temperature Change in Urban Region Influences Human Health. Technical Papers of Kinki-chapter Meeting the Society of Heating, Air-conditioning and Sanitary Engineers of Japan, 25-28 (in Japanese)

Kunst A. E., Looman C. W., Mackenbach J. P. (1993). Outdoor Air Temperature and Mortality in the Netherlands: A Time-series Analysis. Am J Epidemiol. Vol.37(3), 331-41

Narumi D., Niurao Y., Shimoda Y., Mizuno M. (2007). Effects of Increasing Temperature on the Regional Energy Consumption in Osaka Pref.. Journal of Environmental Engineering (Transactions of AIJ) No.613, 71-78 (in Japanese)

Narumi D., Ihara T., Fukuda S. (2016). Study on the Impact for Sleep Disturbance Due to Changing Urban Outdoor Temperature. AIJ Journal of Technology and Design No.52, 1045-1048 (in Japanese)

Narumi D., Ihara T., Fukuda S. (2017). Study on the Impact for Fatigue Due to Changing Urban Outdoor Temperature. AIJ Journal of Technology and Design No.54, 563-566 (in Japanese)

Narumi D., Shimoda Y., Kondo A. (2009). The Effect of the Increase in Urban Temperature on the Concentration of Photochemical Oxidants. Atmospheric Environment Vol.43 Issue14, 2348-2359

NIES (National Institute of Environmental Studies, Japan) (2018). Information on Heat Stroke Patients. available from <http://www.nies.go.jp/gaiyo/archiv/risk8/index.html>, (accessed 2018-02-15) (in Japanese)

Okano Y., Ihara T., Genchi Y. (2008). Evaluation of Environmental Impacts on Disturbed Sleep by Nighttime Urban Heat Island Phenomena Using Surveys via the Internet. Journal of Heat Island Institute International Vol.3, 22-33 (in Japanese)

Ono M. (2009). Risk of Health Emerging Due to Climate Change Citizen's Role and Response. IGES-WHO International Symposium on climate change and health (in Japanese)

Shimoda Y., Narumi D., Mizuno M. (2005). Environmental Impact of Urban Heat Island Phenomena - Cause-effect Chain and Evaluation in Osaka City -. Journal of Life Cycle Assessment, Japan, 44-148

The effects of commuter travel behavior on transportation heat and pollution emissions

Man Li, Xi 'an Jiaotong University (China)
Yupeng Wang[1]*, Xi 'an Jiaotong University (China)*
Jun Zhou, Shenzhen Urban Planning and Land Resource Research Center (China)

ABSTRACT

Transportation systems have been identified as significant component of the gross anthropogenic heat emission, which was investigated in cities of America and Australia. Existing empirical studies, however, lack to answer whether individual commute travel behavior influence the UHI effect through affecting anthropogenic heat from transportation. Using Shenzhen as a case, this paper answers this question by: a) estimating how the heat and pollution from transportation changes in different behavioral models; b) identifying factors affecting individual commute travel behavior change; c) finding methods contributing to reducing anthropogenic heat from transportation. Results show that individual commute travel behavior do have a great influence on urban thermal environment and some effective measure can be applied to achieve a lower anthropogenic heat from transportation.

Introduction

Urban heat island (UHI) is becoming one of the biggest environment issues in the 21-century. Anthropogenic heat is one of the three main causes of UHI, which causes higher air temperature in the city central areas of up to 2-3°C at nighttime in winters (Fan & Sailor, 2005). Transportation systems has the dominant effect on the gross anthropogenic heat emission, which was investigated in cities of America and Australia (Khan & Simpson, 2001; Sailor & Lu, 2004).

Generally, anthropogenic heat emission from transportation is calculated as a significant component of anthropogenic heat rather than independently (Sailor & Lu, 2004; Lee et al., 2009; Quah & Roth, 2012). Since the objective of this research are to estimate the total anthropogenic heat of the study area and heat from other transport means is small, heat emission of transportation is usually assumed to equal to heat from vehicular traffic. Furthermore, due to data availability, heat from vehicles is considered an equation of the number of vehicles, energy used by vehicles, and distance travelled by vehicles within the study area. In this research, we focus on the effects of commute travel behavior on urban thermal environment. The detailed commute travel behavior from “Residents’ travel survey of Shenzhen” was used for analyzing the current situation in Shenzhen city. A new method is proposed in this paper to estimate the anthropogenic heat emission from transportation.

Individual commute travel in rush hours is potentially affecting the urban heat island phenomenon though influencing transportation heat emissions. However, the relationship between travel behavior and anthropogenic heat of a city has not been proved yet, researchers has proved that reducing the level of urban vehicular passenger travel is one of the efficient approaches for urban energy savings (Kwan & Hashim, 2016; Moriarty, 2016). Meanwhile, some researchers proved that the increase of public transport proportion locally would be helpful in pursuing energy

[1] Yupeng Wang: [wang-yupeng@mail.xjtu.edu.cn]

savings in Beijing, China (Liu et al., 2015). Hence, it's needed to figure out the effects of commute travel behavior on urban thermal environment.

The analysis of travel mode choice is useful to understand and predict travel demands and considered to be an important tool in transportation planning and policy making (Hagenauer & Helbich, 2017). In this paper, in order to explore factors influencing residents' commute travel mode choice, multinomial logit model (MNL) for mode choice are used. The multinomial logit (MNL) model and its variations, based on random utility theory, with efficient enclosed mathematical structure and explainable model estimation results, become the dominating and most-used travel mode choice model for decades (Wang & Ross, 2018). Some researchers examined whether the construction of flyover infrastructure induces travel mode switch behavior of individuals using a multinomial logistic regression model and found that flyovers have a significant impact on induced travel mode switch behavior of individuals (Rahman & Baker, 2018).

The objective of this paper is to figure out the effects of commute travel behavior on urban thermal environment and the quantitative relationship. Based on resident' commute travel behavior, we proposed a new function to calculate anthropogenic heat emission from transportation. Then we investigated how anthropogenic heat emission from transportation changed within different commute modes using scenario analysis. Furthermore, we analyze factors influencing individual commute travel behavior and hints for future urban island heat effect mitigation will be given to policy makers.

Data and modeling framework

Database

The database used in this research is "Residents' travel survey of Shenzhen" which was funded by Urban Planning, Land & Resources Commission of Shenzhen Municipality, and conducted in November 2016 to January 2017. This database is based on the household travel survey which includes 68,000 families (2% of the total) from the whole household in Shenzhen. In this survey, Shenzhen was divided into 1,114 traffic analysis zones (TAZs). The area of a TAZ is around 1 km^2 in urban areas and around 10 km^2 in green spaces. The survey consists of individual characteristics, household characteristics and all travels of each people in a day.

Another database used in this research is the 2016 Shenzhen building survey which was undertaken by Shenzhen Urban Planning and Land Resource Research Center. This survey obtained information of all 587,843 buildings in Shenzhen, which includes a building's location (longitude and latitude), height, usage, floor area, ownership and structure category.

Modeling framework

Heat and pollution from transportation. Heat from transportation is notoriously difficult to calculate and often evades systematic treatment (Afshari et al., 2018). Usually, a top-down method and a bottom-up method are used to estimate the traffic related anthropogenic heat. The former makes an estimation from large scales to a small scale and requires aggregate data of a large scale to be scaled down to smaller scales of interest (Lee et al., 2009). To the contrary, the latter makes an estimation from small scales to a larger scale (Sailor et al., 2007).

Generally, using a bottom-up method, detailed hourly fractional traffic profiles, hourly

population density, energy release per vehicle per meter of travel and per capita daily vehicle distance are needed to estimate heat released from transportation. Specifically, the most challenging aspect is the derivation of a typical daily profile of the anthropogenic heat release rate (Afshari et al., 2018). One of the most challenging data is the hourly distribution of vehicle classes, and to obtain this specific data, some assumptions are needed (Quah & Roth, 2012) and the accuracy of the result greatly reduced.

In this paper, the database from "Residents' travel survey of Shenzhen" will be used. All travels of each people in a day are listed in this survey. As this paper focuses on the heat and pollution emission from commute transportation, we take advantage of these traffic behavior data, a new function is proposed for deriving normalized daily profile(s) of traffic related heat release rates using this detailed travel behavior data as follows:

$$Q_{TR}(h) = [\sum_{ij}(RF_{ij} \cdot N_{ij} \cdot D_{ij} \cdot HE_j)/T_{ij}/3600]/A \quad (1)$$

Where $Q_{TR}(h)$ is the total anthropogenic heat release in any hour from transportation, RF_{ij} is the per capita energy consumption of residents taking class i vehicles consuming fuel type j of a day(*L/km/Person*), N_{ij} is the total number of residents taking vehicle i using fuel j, D_{ij} is the mean commuting distance of residents taking vehicle i using fuel j(k*m/Person*), HE_j is the net heat combustion of fuel type j (*J/ kg*),which is assumed to be 29307.T_{ij} is the mean travel time of residents taking vehicle i using fuel j(h), A is the size of the study area (m^2).

In the above function, the per capita energy consumption of residents taking class i vehicles consuming fuel type j in peak time of a day (RF_{ij}) is used empirical data from Beijing city (Table 1). As this empirical data is from Beijing city rather than Shenzhen city, which has a certain impact on the accuracy of the results. In addition, though electric bus is advocated by the local government, in this research, the number of electric bus is not available. Thus, we assume all buses are diesel ones with 40 seats. This method will greatly simplify the calculation, however may reduce overall accuracy of the results at same time. The total number of residents taking vehicle i using fuel j can be calculated using the total number of employees multiplied by the proportion of a class vehicle used.

Table 1. Energy consumptions of different urban transport modes

Energy consumption	Private cars	Taxi	Diesel buses	Metro
kgce/ km/v[1]	0.012	0.098	0.26	3.416
Occupancy rate	1.5	1.28	40	1440
kgce/ km/p[2]	7.87	8.52	0.85	0.242

1: kilogram standard coal consumption of per vehicle driving one kilometer; 2: kilogram standard coal consumption of per commuter driving one kilometer

Air pollution from transportation is an important research sector of transportation. Generally, CO, NOx and PM_x three main air pollutants in existing studies (Lozhkina & Lozhkin, 2015; Kishimoto et al., 2017). Since metro is powered by electricity that is considered as clean energy, air pollution from metro is not calculated. The occupancy rate of taxi, small passenger vehicles and public bus are 1.28, 1.5 and 40, respectively. They the total emissions of road vehicles can be calculated as follows:

$$E = \sum_i P_i \cdot EF_i \cdot D_i \times 10^{-6} \quad (2)$$

Where E is the total emissions of road vehicles *(t)*, EF_i is the pollution emission factor of vehicle i (*g/km*), P_i is the number of vehicle i, D_i is the average travelled distance of vehicle *i (km)*.

Table 2. Pollution emission factors of different vehicles

(Ministry of environmental protection of the People's Republic of China, 2015)

Vehicle types	Pollution emission factors (g/km)		
	CO	NO_x	$PM_{2.5}$
Small passenger vehicles	0.68	0.032	0.003
Public buses[1]	3.25	9.892	0.252
Taxi	2.45	0.135	0.003

1: As using electricity as power, metro can be regard as a kind of sustainable transportation mode.

Scenario analysis. Generally, the use of technology, infrastructure expansion, and behavioral change by modal shift are three common transport mitigation scenarios analyzed in existing research (Kwan & Hashim, 2016). For behavioral change, behavioral change was the decreased usage of personal car and increased usage of public transportation. The percentage of modal shift to public transportation ranged from 30% to 70%. Besides, two extreme scenarios are also compared. One scenario is 100% usage of public transportation. The proportion of public bus and metro are identified according to the actual research data. The other is 100% usage of private car. Therefore, there are five scenarios assumed as below:

- Scenario 1：100% usage of personal car
- Scenario 2：30% usage of public transportation and 70% usage of personal car
- Scenario 3：50% usage of public transportation and 50% usage of personal car
- Scenario 4：70% usage of public transportation and 30% usage of personal car
- Scenario 5：100% usage of public transportation

Multivariate logit analysis. In order to analysis factors influencing commuters' choice between car, metro and bus, a multinomial logit model (MNL) is proposed. Based on the independence of irrelevant alternatives (IIA) hypothesis, the MNL model assumes that the ratio of the choice probabilities of any two alternatives is independent to the attributes and the choice set (Hess, 2005). The utility of each traffic mode is a linear parameter function of the variable we chose. The proposed models were estimated by R (version 3.5.1) with package mlogit (Croissant, 2012) where the reference alternative is car.

$$U_i = \sum_j \beta_{ij} \cdot X_{ij} + \varepsilon_i \quad (3)$$

Where U_i is the travel utility of traffic mode i, X_{ij} is the jth variable of traffic mode i, β_{ij} is the coefficient of X_{ij}, and ε_i is the mode specific constant.

Built environment variables, travelers' socio-demographic attributes as well as traffic mode characteristics go into the model as independent variables. As special institutional population registration system, census register is included.

The Baidu map is used to estimate the in-vehicle travel and access times of metro, bus and car according to trip origin and destination (OD) locations. Since the object of this study is commuter's travel which happened at peak time, commuting trip data is extracted at peak hours in the afternoon when commuters go home from work. The variables contained in the dataset are shown in Table 3.

Table 3. Variables used in the model

	Variables	**Definition**
Mode related variables (3)	TTime	Travel time (h)
	TDistance	Travel distance (km)
	TCost	Travel cost (Yuan)
Individual related variables (2)	Age	-
	Gender	-
Household related variables (5)	HhSize	Household Size
	PCRegister	1= Traveler has Shenzhen census register 2= Other
	HhIncome	1= Household income⩽200,000 ¥ /a 2= 200,000 ¥ /a < Household income⩽500,000 ¥ /a 3= Household income > 500,000 ¥ /a
	Htype	1= Rental an apartment 2= Owning an apartment
	Owning a car or not	1=yes; 0=no
Land use variables (8)	FZ_PR	Plot ratio of origin TAZ
	FZ_ABH	Average building height of workplace TAZ
	FZ_BSN	Bus stations number of workplace TAZ
	FZ_MSN	Metro stations number of workplace TAZ
	TZ_PR	Plot ratio of home TAZ
	TZ_ABH	Average building height of home TAZ
	TZ_BSN	Bus stations number of home TAZ
	TZ_MSN	Metro stations number of home TAZ

Results

Heat and pollution from transportation in Shenzhen at 2016

Using data from "Residents' travel survey of Shenzhen", we found that car, bus and metro are three most used vehicles for residents to commute in Shenzhen, which is about 46.96%. The car sector can divide into taxi and small passenger vehicles. The mean commuting distance are 8.79 km and 8.07 km, respectively. The mean commuting distance via bus differs little from that

with cars. The commuting distance of residents using metro is 14.14 km, which is the longest in all of the transportation types, about 2.61 times of the average commuting distance.

In 2016, the number of employed population in Shenzhen is 9.26 million, which is used to calculate the number of commuters taking different transportation modes by multiplying the occupancy rate of different vehicles with the total number of employed persons.

As illustrated in table 4, heat from transportation system of Shenzhen in 2016 is 2.57 W/m^2. Heat from cars accounts 87% of the total, which means the usage of car largely influences transportation heat emission in Shenzhen. Heat from bus and metro is small. Especially, heat from metro is only 1%, which means usage of metro should be encouraged.

Table 4. Heat emission from transportation in Shenzhen at 2016

Commuting mode	Heat emission(w/m^2)	Percentage
Bus	0.07	6%
Metro	0.02	1%
Car	1.12	87%
Taxi	0.08	6%
Total	1.29	100%

As illustrated in table 5, pollution from transportation of Shenzhen in 2016 is 28.29t. CO, NO_X and $PM_{2.5}$ are 21.23t, 6.84t and 0.22t, respectively. CO emission from cars dominates the total CO emission while NO_X and $PM_{2.5}$ emission from buses are the most. What should be point out is that as using electricity as power, metro can be regard as a kind of sustainable transportation mode.

Table 5. Pollution from transportation in Shenzhen at 2016

Vehicle types	CO	NO_X	$PM_{2.5}$
Bus	1.94	5.90	0.15
Car	15.17	0.71	0.07
Taxi	4.12	0.23	0.01
Total	21.23	6.84	0.22

Heat and pollution from transportation under different scenarios

Five scenarios are assumed in this paper. The percentage of modal shift to public transport in scenarios ranged from 0% to 100%. The ratio between the usage of bus and metro is 2:1 which is identified according to the actual research data.

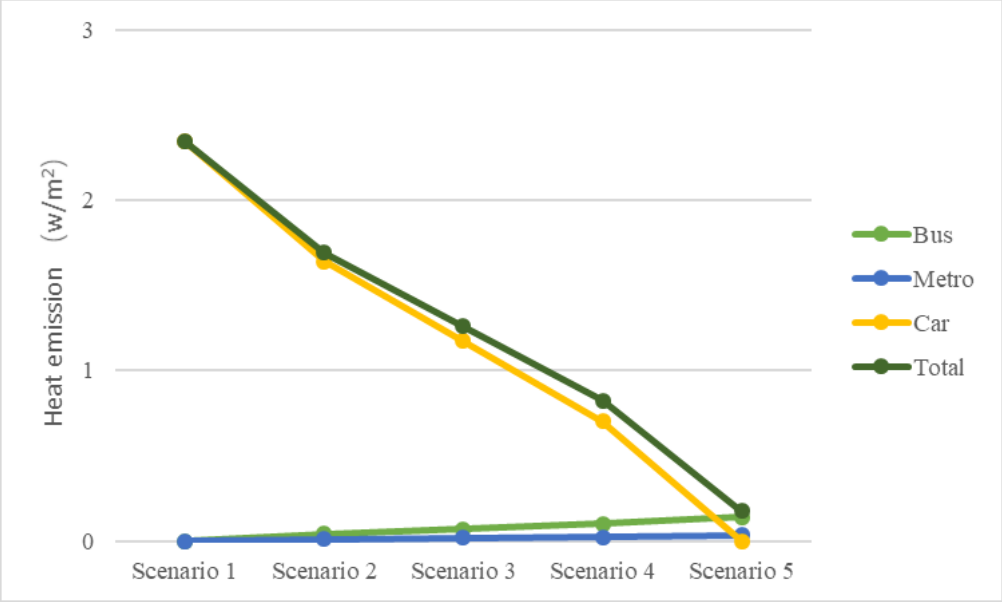


Fig.1 Heat emission of transportation at different scenarios

Heat emission at five different scenarios is showed in figure 1, with the decrease (from 100% to 0) of car usage and the increase (from 0 to 100%) of public transportation, the overall heat emission is decreasing sharply from 2.35 W/m^2 to 0.17 W/m^2. The decrease of heat from car is most significant, which shows a steep descent from 2.35 W/m^2 to 0. Oppositely, increase of heat from bus and metro is slowly. Heat from bus increases from 0 to 0.14 W/m^2 while heat from metro from 0 to 0.03W/m^2, which are much smaller than the reduction of heat from car. In conclusion, the most heat from transportation comes from car and as a result, the improvement of traffic structure contributes to the reduction of heat emission.

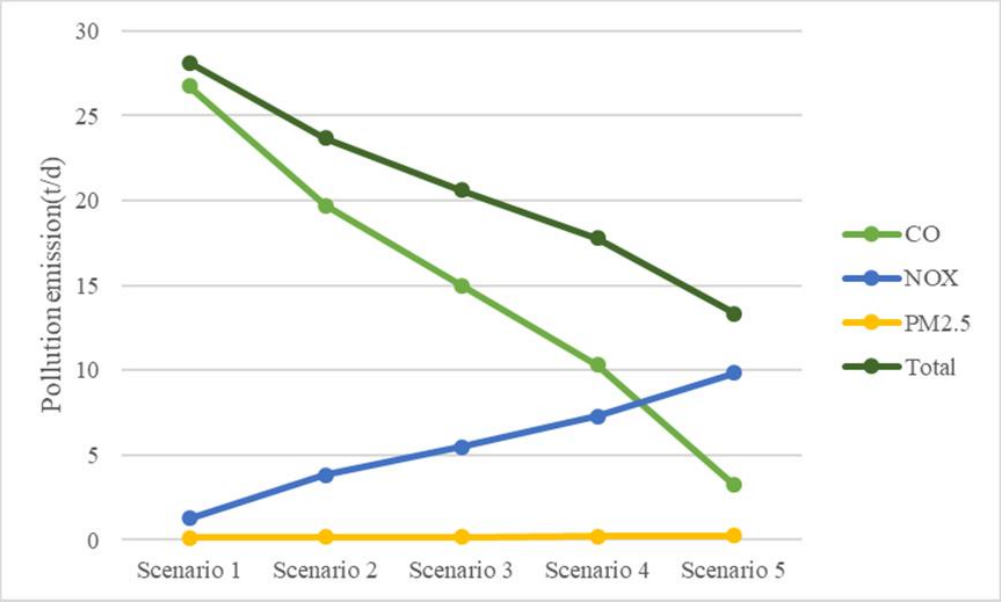


Fig.2 Pollution emission of transportation at different scenarios

Pollution emission at five different scenarios is showed in figure 2, with the decrease (from 100% to 0) of car usage and the increase (from 0 to 100%) of public transportation, the overall heat emission is decreasing from 28.13t/d to 13.32t/d. For different pollutants, the changing situation is different. The CO emission decreases greatly while the NO_X emission increases slightly. The emission of PM2.5 doesn't change much. In a long term, the pollution emission reduction will be more noticeable. If the usage of public transportation adds up from 30% to 70%, the total pollution emission will reduce as much as 2,148t in a year. That is to say, the improvement of traffic structure also contributes to the reduction of pollution emission.

Factors influencing residents' commuting mode choice

The impacts of individual related variables on mode choice. Both age and gender are significant variables (Table 6). The younger the commuter, the more metro and bus trips. The relationship between gender and the probability of choosing public transit is negative, which means female has more car trips comparing with male. From the perspective of operation, improving the carriage environment is useful measures.

The impacts of household related variables on mode choice. Three of five household related variables are statistically significant (Table 6). On the whole, the impacts of household related variables on mode choice is internal consistent. Commuters who have Shenzhen census register, commodity housing purchased and cars are more likely to choose car rather than bus and metro.

Statistically, the coefficients of census register and housing type variables are significant. This can be explained by the fact that these two variables are important aspects of economic capability. The ownership of car significantly impacts the commuters' mode choice. As expected, a commuter owning a car has considerably more car trips than a carless commuter. It suggests that increasing the cost of using cars, such as raising the fuel price and parking fee, are useful to the reduction of car usage.

The impacts of land use variables on mode choice. Six variables of eight land use variables are significant ones and five of them are significant the usage of metro (Table 6). This can be explain that the usage of metro are more impacted by building environment as the number of metro stations are much less than bus stations. Besides, four of the six significant variables are building environment of home. This suggests that the impacts of home area land use on mode choice are more significant than the impacts of workplace land use. As the number of stations influencing the choice of public transit, improving the coverage of public transport and operating extra public transport at rush hours are effective methods to the reduction of car usage.

Table 6. Parameter estimation results for multinomial logit (MNL) model

Variable	Traffic mode	Coeff.	Z-value	
Mode related variables				
Bus (intercept)		3.009	-3.039	***
Individual related variables				
Age	bus	-0.0192	-2.6732	**
	metro	-0.0291	-3.7737	***
Gender	bus	-0.7042	-7.4373	***
	metro	-0.4888	-4.7739	***
Household related variables				

PCRegister_1	bus	-0.4256	-3.7692	***
	metro	-0.3570	-2.8843	**
HType_1	bus	0.2477	2.0148	*
	metro	0.3728	2.7420	**
Hcarornot	bus	-3.524	-29.8894	***
	metro	-3.271	-25.1537	***
Land use variables				
FZ_ABH	metro	0.0117	2.6857	**
FZ_MSN	metro	0.1712	2.9635	**
TZ_PR	bus	-0.446	-5.6953	***
TZ_ABH	metro	0.0567	4.2914	***
TZ_BSN	bus	0.0129	2.8210	**
	metro	0.0082	1.6534	.
TZ_MSN	metro	0.7238	8.9321	***
Signif. codes: 0 '***' 0.001 '**' 0.01 '*' 0.05 '.' 0.1 1				
Log-Likelihood		-3841.8		
McFadden R^2		0.29247		
Likelihood ratio test		chisq = 3176.1 (p.value = < 2.22e-16)		

Conclusion

Commuter behavior influences heat and pollution from transportation. We found that the dominant factor is the usage of car. With the decrease of car usage and the increase of public transportation, the overall heat and pollution emissions decrease greatly. Thus, less use of cars and more use of public transportation, especially metro help to create a cleaner and more comfortable urban environment. In addition, as electrification of buses and cars (both taxi and private car) are useful method to reduce heat and pollution from transportation, commuters should choose greener means of transport.

Then factors influencing residents' commuting mode choice have been analyzed. Results showed that less travel time and travel cost increase the probability of choosing public transit. Younger male commuters who earn low household income, rent an apartment, have large household size and do not have Shenzhen household registration as well as cars are more likely to choose public transit. In addition, dense and diverse development of workplace help to enhance the ratio of public transit.

Therefore, some effective methods both from planning and operation aspect are given for policy makers to reducing heat and pollution from transportation. Improving the carriage environment increasing the cost of using cars, such as raising the fuel price and parking fee and improving the coverage of public transport and operating extra public transport at rush hours are all effective methods to the reduction of car usage.

References

Afshari, A., Schuch, F., & Marpu, P. (2018). Estimation of the traffic related anthropogenic heat release using BTEX measurements–A case study in Abu Dhabi. Urban climate, 24, 311-325.

Fan, H., & Sailor, D. J. (2005). Modeling the impacts of anthropogenic heating on the urban climate of Philadelphia: a comparison of implementations in two PBL schemes. Atmospheric environment, 39(1), 73-84.

Guidelines for the compilation of emission lists of road motor vehicle atmospheric pollutants (trial). Beijing: Ministry of environmental protection of the People's Republic of China, 2015.

Hagenauer, J., & Helbich, M. (2017). A comparative study of machine learning classifiers for modeling travel mode choice. Expert Systems with Applications, 78, 273-282.

Khan, S. M., & Simpson, R. W. (2001). Effect of a heat island on the meteorology of a complex urban airshed. Boundary-Layer Meteorology, 100(3), 487-506.

Kishimoto, P. N., Karplus, V. J., Zhong, M., Saikawa, E., Zhang, X., & Zhang, X. (2017). The impact of coordinated policies on air pollution emissions from road transportation in China. Transportation Research Part D: Transport and Environment, 54, 30-49.

Kwan, S. C., & Hashim, J. H. (2016). A review on co-benefits of mass public transportation in climate change mitigation. Sustainable Cities and Society, 22, 11-18.

Lee, S. H., Song, C. K., Baik, J. J., & Park, S. U. (2009). Estimation of anthropogenic heat emission in the Gyeong-In region of Korea. Theoretical and Applied Climatology, 96(3-4), 291-303.

Liu, X., Ma, S., Tian, J., Jia, N., & Li, G. (2015). A system dynamics approach to scenario analysis for urban passenger transport energy consumption and CO2 emissions: A case study of Beijing. Energy Policy, 85, 253-270.

Lozhkina, O. V., & Lozhkin, V. N. (2015). Estimation of road transport related air pollution in Saint Petersburg using European and Russian calculation models. Transportation Research Part D: Transport and Environment, 36, 178-189.

Moriarty, P. (2016). Reducing levels of urban passenger travel. International journal of sustainable transportation, 10(8), 712-719.

Quah, A. K., & Roth, M. (2012). Diurnal and weekly variation of anthropogenic heat emissions in a tropical city, Singapore. Atmospheric Environment, 46, 92-103.

Rahman, M. L., & Baker, D. (2018). Modelling induced mode switch behaviour in Bangladesh: A multinomial logistic regression approach. Transport Policy, 71, 81-91.

Sailor, D. J., & Lu, L. (2004). A top–down methodology for developing diurnal and seasonal anthropogenic heating profiles for urban areas. Atmospheric environment, 38(17), 2737-2748.

Sheng, Y. A. N. G., & Ling-Yun, H. E. (2016). Fuel demand, road transport pollution emissions and residents' health losses in the transitional China. Transportation Research Part D: Transport and Environment, 42, 45-59.

Wang, F., & Ross, C. L. (2018). Machine learning travel mode choices: Comparing the performance of an extreme gradient boosting model with a multinomial logit model. Transportation Research Record, 0361198118773556.

Quantitative outdoor thermal comfort assessment of street: A case in a warm and humid climate of India

Brinda Deevi[1], *Faiz Ahmed Chundeli*[2]
[1]Vaishanavi school of architecture and planning, Vijayawada, India
[2]*School of architecture and planning, Vijayawada, India*

ABSTRACT

Increasing air temperature in urban areas has been a global concern and is mostly attributed to the urban environment's physical changes. As a result, increased urban heat island phenomenon is often observed in cities impacting outdoor spaces' quality of life. This study investigates the factors influencing a street canyon's outdoor thermal comfort. User-perception surveys and empirical measurements using Testo 480 and Testo 870 thermal imager were carried out at selected six grid-points along 600 m long and 12 m wide Besant road, a semi-motorized commercial street in Vijayawada, Andhra Pradesh, India. Based on the thermal sensation questionnaire survey, Physiologically Equivalent Temperature (PET) for all the observation points were computed using RayMan pro. The correlation between the design control parameters identified and observed PET shows that the sky view factor (SVF) and mean radiant temperature (MRT) are major influencing factors determining the street's thermal conditions. Unlike aspect ratio, SVF showed a strong correlation with PET. The results indicate that by modifying physical parameters, significant improvement in overall outdoor comfort can be attained. Further, it was observed that the respondents' comfort sensitivity is higher in range than that of comfort standards, as the respondents showed increased tolerance to high temperatures.

Special Issue Journal	:	Urban Climate
DoI	:	https://doi.org/10.1016/j.uclim.2020.100718
Citation	:	Deevi, B., & Chundeli, F. (2020). Quantitative outdoor thermal comfort assessment of street: A case in a warm and humid climate of India. Urban Climate, 34, 100718.

Outdoor Thermal Comfort Implications of Planning and Building Regulation Induced Canyon Geometry

Hepsheba, J. J.[1], *Department of Architecture, University of Moratuwa (Sri Lanka)*
Perera, N. G. R., Department of Architecture, University of Moratuwa (Sri Lanka)
Emmanuel, R., Glasgow Caledonian University (United Kingdom)

ABSTRACT

The Planning and Building Regulations developed by the Urban Development Authority (UDA) of Sri Lanka are deemed to be inadequately equipped to deal with the major urban challenges of a rapidly developing Colombo, Sri Lanka - especially in terms of the climate sensitive aspects, within the overall sustainability of the City. The UDA regulations are applied for a specific plot of land. Therefore, the microclimatic impact of the regulations upon a city precinct or neighbourhood are not known. In order to understand the quality of the policy framework manifested in the Planning and Building regulations that define land use zoning and allowable building morphology imposed, we critically evaluate the outdoor thermal comfort impacts of the spaces around buildings in a typical street canyon form.

The simulation based study primarily focuses on assessing the impacts of urban geometries induced by regulations. We explore low-rise, intermediate-rise and mid-rise iterations as base cases. The simulations are generated by utilising the software ENVI-met, with the Mean Radiant Temperature (MRT) as the primary variable for outdoor thermal comfort. As an initiative to improve the climate sensitive aspects of the current regulations, we model a projected, staggered street edge option and a shaded street edge option. Results and analyses map the impacts of the base canyon morphologies and the projected. Results show that, the staggered and shaded cases reduced MRT, when compared with the base case morphology. Conclusions discuss directions for the optimum street canyon geometry by regulating the spaces around buildings.

Keywords: Outdoor thermal comfort; Canyon geometry; ENVI-met; Planning and Building Regulations; Colombo; Sri Lanka

Introduction

Ensuring outdoor comfort is an important part of the design agenda where urban heat island phenomenon plays a significant role. Space around the buildings are essential components of urban design in the Tropics, where increasing built density result in inadvertent microclimatic modifications. Colombo is the commercial capital of Sri Lanka and is located on the western coastline (6.92^{o} N, 79.86^{o} E). Today, it is the Country's most developed city. 60% of the total energy demand is consumed by the populace of the Western Province, and of this the highest percentage share is consumed within the City of Colombo.

Urban design interventions are crucial to facilitate thermal comfort in the urban outdoors. Modern development initiatives have failed in general to encompass the tenants of climate sensitive planning and building regulations into policy, especially in the warm humid tropics.

[1] Corresponding Author: [jenyhepsheba@gmail.com].

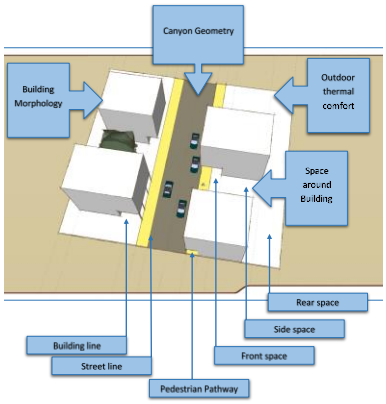


Figure 1. Area of concern. Source: Author

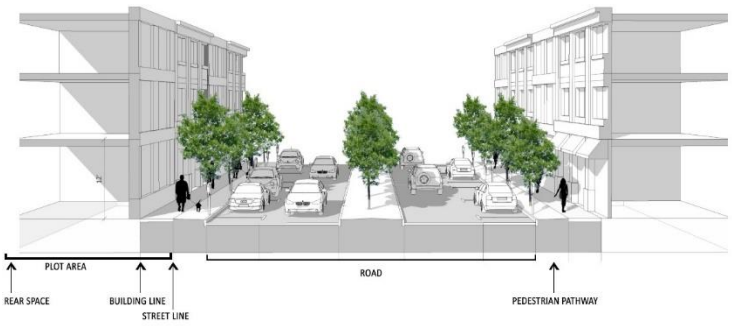


Figure 2. Street section. Source: Author

A thorough understanding of the impact of planning and building regulations is needed to create a microclimate conducive for naturally lit and ventilated building stock, which has been the core focus in its formulation, in Sri Lanka. The aim of the study is to systematically explore the impact of the building morphology and open spaces generated by the planning and building regulations. The open spaces take the form of front space (created by a defined building line or street reservation), rear space (a space created in relation to the height of the building on the plot, envisioned primarily as a fire gap), and side space (for light and ventilation). (see Figure1 and 2) These spaces around building create a distinct canyon geometry for the selected building typologies - low-rise, intermediate-rise and mi-rise. These typologies constitute the most predominant in the urban context of Colombo, thus utilised as a limitation in the scope of the study.

Based on the UDA regulation induced building morphology, we explore options for enhancements by simulating scenarios that introduce a variation to the otherwise linear canyon edge. The options take the form of arcades and a staggering of the street edge.

Background

Researchers (Oke & Cleugh, 1987, and Givoni, 1998) have pointed out that mitigating the effects of Urban Heat Island (UHI) should be considered as a fundamental element in urban design. Emmanuel (2005) has grouped three major themes of UHI mitigation strategies. Manipulating the urban geometry is one of the key factors among the three themes. “The urban geometry and profile-shape, height, and size of the buildings, orientation of streets and buildings, and nature of the surface of the urban open areas all these factors have an impact on the urban climate. On the other hand, the building itself, and especially group of buildings, modifies the climatic conditions surrounding it” (Givoni, 1998). Urban geometry or a build block can be arranged in a favourable manner to produce shaded outdoor spaces by itself. The concept, urban massing that can shade the immediate surrounding is what we known as “shadow umbrella” was first introduced by (Emmanuel, 1993).

The urban street canyon, which is a simplified rectangular vertical profile of infinite length, has been widely adopted in urban climatology as the basic structural unit for describing a typical urban open space (Ali-Toudert & Mayer, 2006). Simplifying it into a typical profile gives opportunities to quickly assess and also to enhance design explorations.

Method

The focus of the study is to explore the impact of the regulated 'open spaces' around a selected typology of buildings as categorised by the UDA, in a representative location in Colombo, Sri Lanka. The research objective of the simulation study is to understand the correlation between buildings, the regulated open spaces around the buildings and outdoor thermal comfort, in a microclimate created by such a morphology.

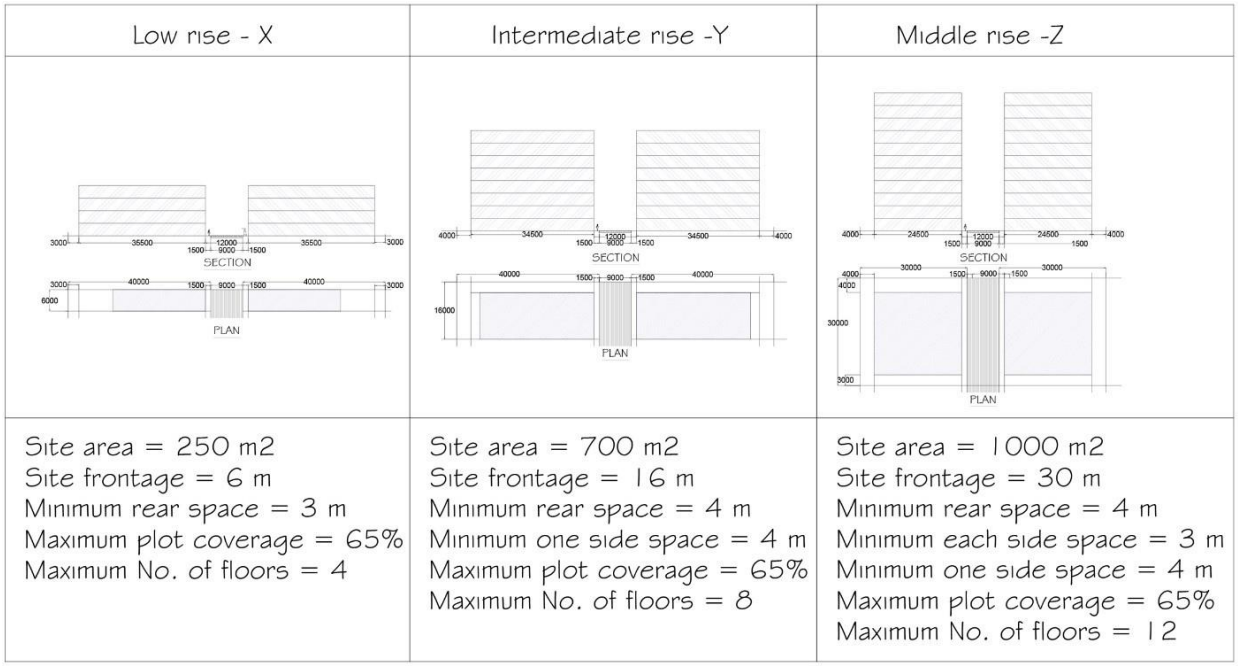


Figure 3. Base Case, Source: Author

The holistic three dimensional, non-hydrostatic model ENVI-met V4 to generate values of mean radiant temperature (MRT) and Air temperature is utilised for the simulations. The simulations are run for a day in April (2018), a hottest month, of a typical year in Sri Lanka and therefore the worst-case scenario to be designed for. The single day simulation is also a limitation of the software.

The allowable building height on a plot is directly proportional to the plot area. Typical building geometry has been categorised into three cases such as Low-rise, Intermediate-rise and Mid-rise in compliance to Specifications for Development - Form C1 and C2 of the City of Colombo Development Plan (Amendment) -2008 (prepared under Section 8H and approved under Section 8F of the Urban Development Authority (UDA) Law No. 41 of 1978).

Figure 3 details the minimum regulated street width and building line (front space), rear space and side space, together with maximum plot coverage and number of floors. These depict the base cases (Case 1). The suggested modification options encompass a staggered street edge scenario (Case 2) and modification for shading as opposed to building line (Case 3). (see Table 1, 3 and 5). The simulation study adopts a typical North/South street canyon configuration.

The data is generated from Receptor points placed on the centre of the street, street sidewalks, side space and rear space. (Receptor point, a term generic to ENVI-met, denotes a

measurement point in the simulation model. The simulation software generates specific data for each receptor point that is defined). The objective is to determine the impact on MRT and Air-temperature in relation to where the measurement point occurs. All data generated is measured at a screen height of 1.8m.

The analysis protocol utilises comparative graphs depicting a 24 hour day for both MRT and air temperature. Multiple linear regression analysis was employed - utilising STATA version 13.0 - taking MRT as the dependent variable with building type, case, time etc. as independent variables, to ascertain adjusted effect from each exposure on MRT. Multiple linear regression provides the risk adjusted pure effect from each independent variable and eliminate potential bias which can arise when variables are considered individually to calculate effects on MRT.

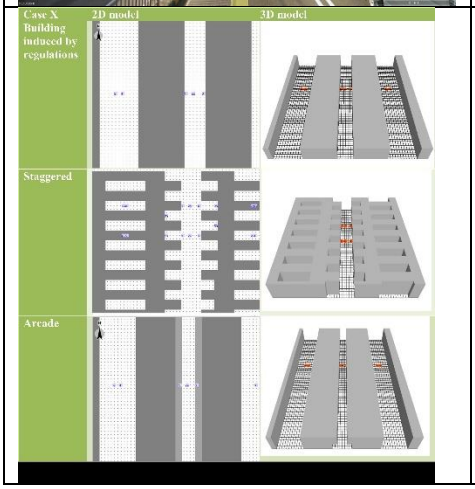
Results and Discussion

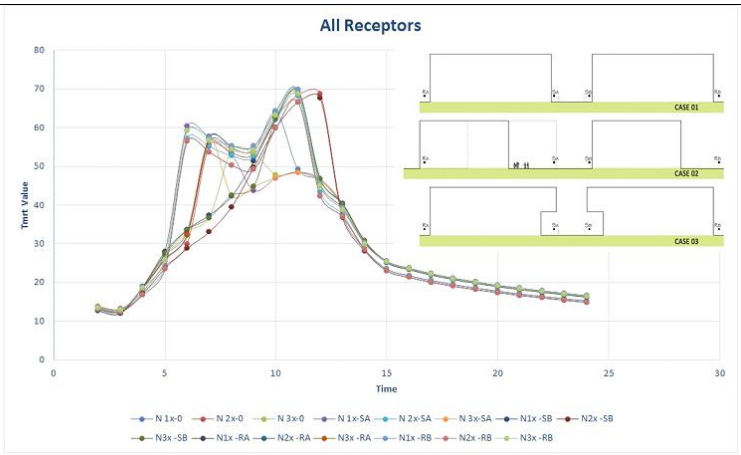
Low-rise Building

Table 1.Low-rise Building district (Case X).



Case	Receptor points				
	Center	Side A	Side B	Rear A	Rear B
Case 01	1x-0	1x-SA	1x-SB	1x-RA	1x-RB
Case 02	2x-0	2x-SA	2x-SB	2x-RA	2x-RB
Case 03	3x-0	3x-SA	3x-SB	3x-RA	3x-RB





The low-rise iteration depicts a typical commercial / residential street canyon, with limited road frontage, resulting in narrow building forms. (See Table 1). The superimposed MRT plot of the receptor point data show that overall, the staggered form (Case 2) offers the best option for MRT reduction in the spaces around the building, especially in relation to the night-time values. This is deemed to be caused by the mutual shading a staggered form offers. The arcade options is best for the values in the centre of the street. Yet, is warmer for the night-time. The analysis of the air-temperature values, depict a similar scenario, where the modified street edges offers the better option of reduced air temperature.

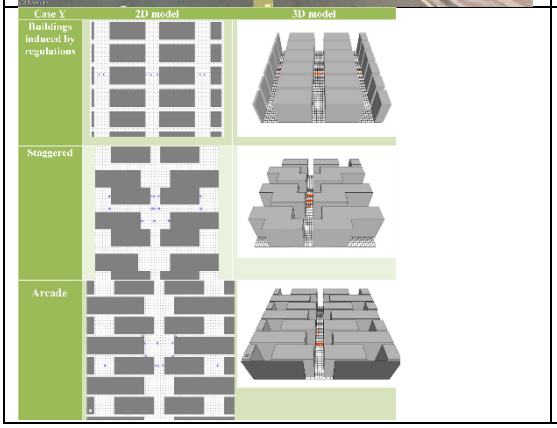
Therefore, for a low-rise street canyon, flexibility to modify the street edge by either staggering or introducing arcades is advantageous.

Intermediate-rise Building

Table 2. Intermediate-rise Building district (Case Y).



Case	Receptor points				
	Center	Side A	Side B	Rear A	Rear B
Case 01	1y-0	1y-SA	1y-SB	1y-RA	1y-RB
Case 02	2y1-0	2y1-SA	2y1-SB	2y1-RA	2y1-RB
		2y1-1xSA	2y1-1xSB		
	2y2-0	2y2-SA	2y2-SB	2y2-RA	2y2-RB
		2y2-1xSA	2y2-1xSB		
Case 03	3y-0	3y-SA	3y-SB	3y-RA	3y-RB



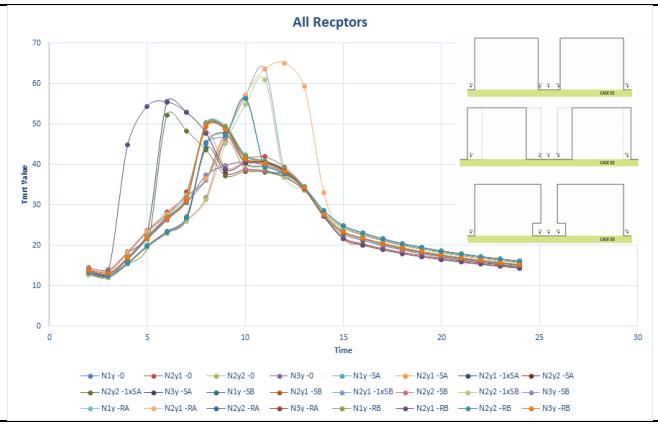
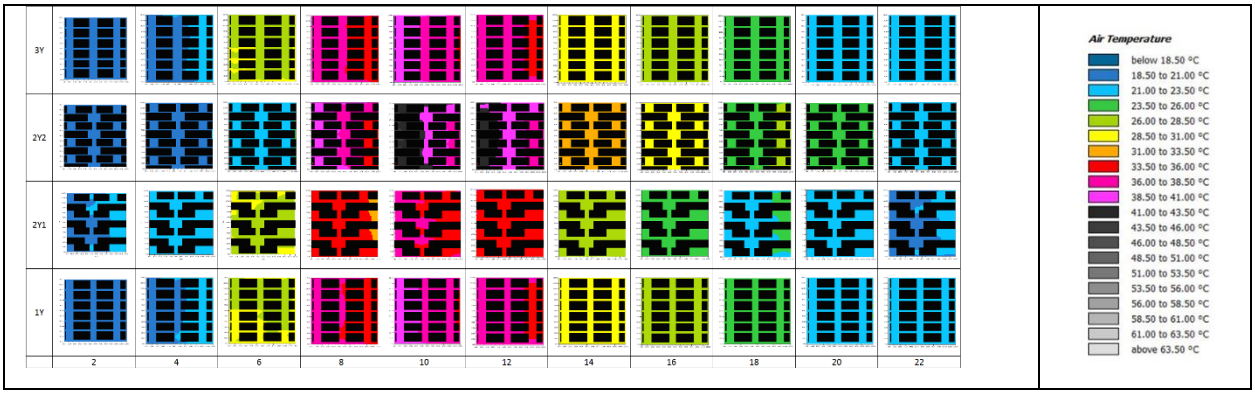


Table 3. Effect of the design forms on Air temperature



Intermediate-rise (Case Y) constitute buildings that range from 5 to 8 storeys high. The model projects the maximum development of 8 storeys. The increased width of the plots in this typology offers alternate options for a maximum plot coverage. Therefore, the simulation options explore the same. As shown in Table 2, the staggered street option encompasses two iterations, of which the second introduces spaces within blocks on the same plot.

Analyses show that there is little or no difference in MRT at the centre of the street. Unlike in the low-rise building, the MRT values generated for the staggered option does not show an improvement, but rather a marked increase in relation to the direction of the stagger, in the morning and afternoon hours alternatively. Yet, similar to the low-rise case, the staggered option offers the best scenario for night-time thermal comfort. The increased aspect ratio in an intermediate-rise street canyon aids reduction in MRT, by shading. This aspect is exaggerated by the introduction

of arcades, improving the MRT on the street fronts. The arcade case does not aid MRT reduction in other spaces. As seen in Table 3, the air-temperature variation paints a similar picture, where the solar direction has distinct effect on the staggered options, as opposed to that what is seen in the linear street edge options.

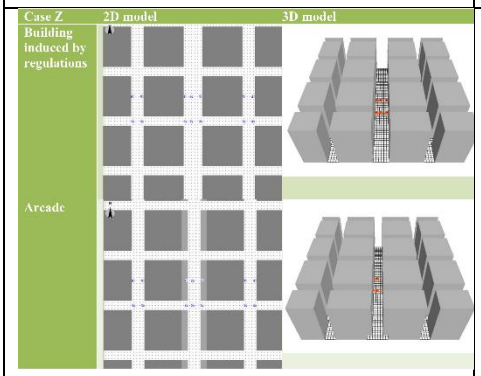
Therefore, a canyon geometry that adopts a linear street edge, with modifications such as arcades are seen to be the most advantageous for the intermediate-rise building option.

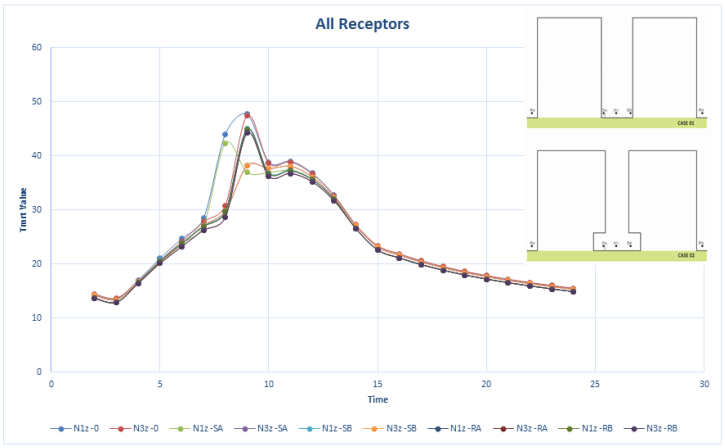
Mid-rise Building

Table 4. Mid-rise Building district (Case Z).



Case	Receptor points				
	Center	Side A	Side B	Rear A	Rear B
Case 01	1z-0	1z-SA	1z-SB	1z-RA	1z-RB
Case 03	3z-0	3z-SA	3z-SB	3z-RA	3z-RB





The mid-rise building typology allows a denser quantum of development, according to the UDA planning and building regulations. The effect of such is seen in the lack of possibility to stagger the street edge, as seen in the low-rise and intermediate-rise options. Therefore, the simulation evaluates only the base case and the arcade case in its analyses. The MRT graph in Table 4, depicts side A, side B and Rear, Rear B follow the similar MRT pattern as it is a symmetrical geometry. Overall centre receptor records the highest MRT value and Rear B perceive the lowest MRT for both cases. The arcade option shows a slight reduction in MRT. The air-temperature comparison within cases show a similar scenario, where there is little or no variation.

The cases show that the morphology of the built fabric, especially in relation to density is key to generate a microclimate conducive for a building stock with a focus on natural light and ventilation. Results show that:

- An increased density and therefore a higher aspect ratio results in a reduced MRT value in the spaces around the buildings.
- The staggered and arcade options depict a distinct advantage in all cases.
- In comparison of the receptor point positions between cases, it is seen that the centre of the street is most adversely effected.

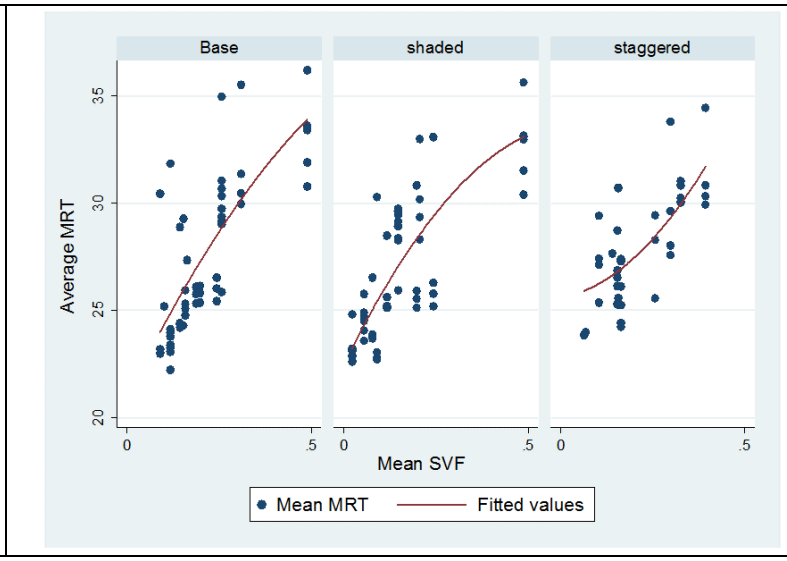
- The receptor points on the rear space and immediately adjacent to the street show a distinct improvement, in relation to the centre of the street.

Regression Analysis

The simulation data were analysed using STATA version 13.0 software employing the multiple linear regression analysis. A multiple linear regression model was fitted to identify influence of exposure variable on MRT. Relative humidity, building type, direction, proposed case, time and orientation were found as significant factors that influence MRT.

Table 7. Regression model

tmrt	Coef.	Std. Err.	t	P>|t|	[95% Conf.	Interval]
qrel	-.1748021	.0206967	-8.45	0.000	-.2153799	-.1342243
build_num						
2	-3.893882	.2506262	-15.54	0.000	-4.385257	-3.402507
3	-5.163881	.3169788	-16.29	0.000	-5.785346	-4.542416
direc_num						
minus	-4.609063	.4172755	-11.05	0.000	-5.427168	-3.790958
north	-2.117709	.2921568	-7.25	0.000	-2.690508	-1.54491
plus	-4.402681	.3878495	-11.35	0.000	-5.163094	-3.642268
case_num						
2	-1.089353	.2739856	-3.98	0.000	-1.626526	-.55218
3	-.4263011	.2346812	-1.81	0.070	-.8868063	.034204
time_new						
02:00:01	-.3859636	.7011457	-0.55	0.582	-1.760521	.988594
03:00:01	6.797474	.7017472	9.69	0.000	5.421637	8.173311
04:00:01	13.085	.7030483	18.61	0.000	11.70661	14.46338
05:00:01	21.19165	.7044625	30.08	0.000	19.81049	22.57281
06:00:01	25.33211	.7057494	35.74	0.000	23.94255	26.72166
07:00:01	27.28991	.7230482	37.74	0.000	25.87231	28.70751
08:00:01	28.41268	.761449	37.31	0.000	26.91979	29.90556
09:00:01	29.54347	.7989746	36.98	0.000	27.97701	31.10993
10:00:01	28.53694	.8501541	33.57	0.000	26.87014	30.20374
11:00:01	23.45517	.9016315	26.01	0.000	21.68744	25.2229
12:00:01	16.57834	.9118186	18.18	0.000	14.79064	18.36604
13:00:01	8.866147	.8209414	10.80	0.000	7.256619	10.47567
14:00:01	5.080857	.736808	6.90	0.000	3.63628	6.525434
15:00:01	4.049412	.7271694	5.57	0.000	2.623733	5.475092
16:00:01	3.19194	.7245241	4.41	0.000	1.771447	4.612433
17:00:01	2.483693	.7230111	3.44	0.001	1.066166	3.90122
18:00:01	1.87641	.7222709	2.60	0.009	.460335	3.292486
19:00:01	1.341296	.722073	1.86	0.063	-.0743911	2.756984
20:00:01	.8593871	.7223108	1.19	0.234	-.5567667	2.275541
21:00:01	.416329	.7229528	0.58	0.565	-1.001084	1.833741
22:00:01	.0044272	.7239458	0.01	0.995	-1.414932	1.423786
23:00:01	-.3828372	.7252167	-0.53	0.598	-1.804688	1.039014
23:59:59	-.696573	.7267101	-0.96	0.339	-2.120352	.7292061
ori_num						
rear A	.1059225	.3200129	0.33	0.741	-.5214908	.7333358
rear B	.0463242	.3200125	0.21	0.836	-.5610884	.6937368
side A	-1.370083	.3199965	-4.28	0.000	-1.997464	-.7427016
side B	-.8001706	.3200115	-2.50	0.012	-1.427581	-.1727599
_cons	38.56871	2.132444	18.09	0.000	34.38787	42.74956



The regression model explains 79% of variability of MRT, as correlated to the parameters considered.

Influence of Sky View Factor (SVF) (see Table 7) on MRT- The behaviour in correlation to SVF differs in comparison between cases, although all confirm established knowledge where MRT intensity increases with increased SVF. The staggered case is significant where the variations fall within a lower range. Thus, the impact of the morphology is deemed less effective in more open or less dense iterations.

Influence of building type- When compared to the Low-rise buildings, Intermediate-rise and Mid-rise buildings reduce MRT by 3.89 and 5.16 average units respectively, when other exposures are at constant levels and this relationship is significant at 5% significance level.

Influence of orientation on MRT- Orientation has significant effect on MRT when other variables are at constant levels. Average MRT change in minus, north, and plus are lower than the east receptor point data. This association is significant at 5% significance level.

Influence of proposed case on MRT- Staggered and Arcade shaded cases reduce MRT when compared with the base cases. The staggered case shows lower MRT than shaded. However, effect of the staggered case increases correlation between the form and average MRT, compared with the base case and this effect significant at 5% significance level when other variables are at rest. Similarly the correlation between the shaded case and average MRT also increases, compared to

the base case and this effect is significant at 1% significance level, reveals staggered and shaded facilitate better comfort possibilities than the base case.

Influence of time on MRT- As compared with 1AM, 3AM-6PM shows significant positive associations with MRT after adjusting other variables. MRT significantly rise from 3AM to 10AM and reduce monotonically thereafter, but is still higher than 1AM. MRT across time demonstrates higher effect sizes in the late morning and afternoon than counterparts after adjusting other variables.

Influence of receptor position on MRT- Receptors were placed in centre, side A, side B, rear A and rear B. When compared to the centre position, significant differences exist in side A and side B positions but not in rear A or rear B positions. Both side A and side B experience reduced MRT when compared with centre when other variables are at constant values.

Implications for Design, Planning and Building regulations

Open spaces in the staggered case and arcade case show distinct positive bearing on thermal comfort. The planning and building regulations induce continuous and linear open spaces taking the form of the front and rear space. The research findings show that that a heterogeneous edge is conducive for MRT reduction in spaces around buildings. Established knowledge dictates that a heterogeneous built fabric creates opportunities for mutual shading and encourages wind movement.

Low-rise and Intermediate-rise building -

- With a low built density the regulations should encourage flexibility of the built mass to be placed on the plot, while maintaining the overall 65% maximum plot coverage and minimum space for light and ventilation into the habitable spaces of the building.
- Large rear space or large front space can be a primary decision making step, where we now adhere to a standard width for the two spaces. The staggered case (see Table 1) offers opportunities for varied patterns of influence on MRT during the day. This allows design to zone outdoor functions according to time, as a strategy to create thermal comfort in the adjacent spaces. This can also be a method of avoiding radiation trapping with the control of materials in these defined zones.
- Overhangs and arcades should be encouraged in more commercial / public applications. The application of such private property for public use to include a system of incentives, encouraging the same. In this regard, a complete omission of the front space can be explored, given that the overall open space of 35% is maintained elsewhere on the plot.
- Street orientation is key. Although not presented as a part of this paper, differing protocols for differently oriented streets can optimise the canyon geometry for space around building and outdoor thermal comfort.

Mid-rise building-

With high built density the regulations define a reduced possibility for a heterogeneous built fabric and canyon geometry in relation to the lower density buildings.

- The 65% open space is an advantage, where it was a modification in the regulations from the previous regulations (1999), where residential was 65% and commercial was 80%. The

introduction of a side space is seen as a positive element that encourages air movement and mutual shading.

- As with the lower density options, detailed above, the introduction of arcade space is shown to be a positive option. (see Table 2)
- With limited options for differing placement within the plot, overhangs and orientation of the street, thus facades are key. Flexibility to extend such arcades and overhangs along street edges, purely for climate sensitive and pedestrian comfort based applications to be encouraged. The need for protocols for incentives and social justice in their application is highlighted.

Overall -

The inability to adequately affect the centre of the street by the built fabric is highlighted by the results of the simulation study.

- Measures to shade the centre of the streets / urban canyons for increased thermal comfort is needed.
- These measures can be in the form of vegetation and / or other shade structures in the urban context.
- Orientation of streets is a significant consideration. The research needs to extend to encompass such iterations and thereby generate appropriate options to increase thermal comfort in the urban outdoors.

Conclusion

The research was an exploration of the urban canyon form induced by the application of the Sri Lanka Urban Development Authority, Planning and Building Regulations. The focus was on the correlation between the built form and the open spaces around the building. The scope of the study was limited to low-rise, intermediate-rise and mid-rise building categories, in a typical north south street in Colombo. Further, the study limited its scope to a single day for its comparative morphology simulations.

The research showed that possibilities for modification of the built form, specifically and staggered street edges and arcades have a positive impact on the overall outdoor thermal comfort. Thus, planning building regulations that encourage heterogeneity in the urban context by generating options for positioning of spaces around buildings, yet maintaining overall open space on a precinct scale is important.

Directions for future study -

The UDA regulations define a wider range of building typologies than that the scope of this study encompassed. Therefore an extension of the typologies explored is needed for a thorough evaluation of the regulations. Similarly, street orientation is a crucial concern. An enhancement in scope is encouraged, to generate specific interventions for these specific iterations.

References

Ali-Toudert, F., & Mayer, H. (2006). Effects of Street Design on Outdoor Thermal Comfort.

Emmanuel, R. (1993). A Hypothetical 'Shadow Umbrella' for Thermal Comfort Enhancement in the Equatorial Urban Outdoors (Vol. 36). https://doi.org/10.1080/00038628.1993.9696759

Emmanuel, R. (2005). An Urban Approach to Climate-sensitive Design: Strategies for the Tropics (First Edit., p. 172). Taylor & Francis.

Givoni, B. (1998) Climate Considerations in Building and Urban Design. Van Nostrand Reinhold, the USA.

Oke, T. R., & Cleugh, H. A. (1987). Urban heat storage derived as energy balance residuals.

The Urban Development Authority. Retrieved May 14, 2019, from http://www.uda.gov.lk/acts-regulations.html, www.uda.gov.lk/

Study on the Microclimate Effect of Water Body Form in Urban Square

Ziyu Tong[1], *Nanjing University (China)*
Cong Zhang, Beijing Zhonghuan Century Engineering Design Co., Ltd. (China)
Juelun Zhou, Nanjing University (China)

ABSTRACT

In urban areas, water bodies have a positive effect on the microclimate of the surroundings. However, there is less information on the relationship between artificial water body forms and the microclimate, especially the artificial water bodies in urban squares. The study of the microclimate effect of the water body form and layout in the city square can provide the necessary reference for the design of a city square. This study first summarized the basic shape and area of the city square in Nanjing. Through the investigation of the water body form of the city square, two quantitative indicators of the water body were summarized: the water body area ratio and the water body shape index. According to these indicators, a series of different water body models were generated in the basic square model, which was used as the object of microclimate simulation. Using ENVI-met, simulations of city square models with different water forms were performed for a typical day of summer and winter, and their effects on thermal comfort were recorded. Through the statistical analysis of the simulation results, it was found that there is a clear correlation between the water body form indicators and the microclimate effects, although the microclimate effect intensity of different morphological indicators is different. The analysis results can provide a valuable reference for the design of city squares.

Introduction

In urban areas, water bodies have a positive effect on the surrounding microclimate (Manteghi et al. 2015). A number of studies have demonstrated the cooling effect of water on the surroundings through evaporation and convection, including large areas of lakes, rivers, or small ponds (Gupta et al. 2019, Masiero and Desouza 2012). However, most of the research aims at natural water bodies such as large lakes, rivers, or wetlands, with little attention to the smaller water bodies (Huang et al. 2008, Sun et al. 2012). Moreover, there is less information on the relationship between artificial water body form and microclimate (Jin et al. 2017). The natural water resources in cities are limited and fixed. In comparison, artificial water bodies, especially those in urban squares, are more common and can be controlled by urban design.

As an important part of public spaces, the city square has a very important influence on the life activities of the citizens (Chiesura 2004). Compared with other types of public spaces, such as parks or green spaces, the city square has its own characteristics. First, the city square is generally hard-paved to provide spaces for civic activities. Green spaces and water bodies, as part of the square, provide a richer visual landscape and effectively improve the microclimate, although this improvement is often not the main driver of the design but is merely a side effect. Second, the area of the city square is limited. The sum of the area of the hard paving, the green space and the water body is fixed. The area of green space and water should not be expanded indefinitely solely for microclimate effects. The proportion of water area in the square cannot be too high. Third, the

[1] Corresponding Author: [tzy@nju.edu.cn], [+86-25-83593020].

evaluation of microclimate cannot be limited to the temperature, nor to the surrounding or downwind direction of the water body. We need to think more about human thermal comfort in the activity area of the square. Finally, unlike natural water bodies, water in city squares can be controlled by design. Therefore, through the study of the microclimate effect of the water body form and layout in the city square, it can provide the necessary reference for the design of the city square and is used to maximize the microclimatic improvement effect of these artificial water bodies.

Methodology

Urban Square Prototype

This study uses Nanjing, China as a study case. The city has a hot summer and cold winter. The citizens have many outdoor activities and are very sensitive to the outdoor microclimate environment. The microclimate effect of water bodies is also very significant for their activities. Based on the Baidu Map open data, we obtained data of all the squares in the main city of Nanjing. Through the investigation of the area, shape, surrounding road grades and construction conditions of these squares, we established the basic prototype of the urban square (Figure 1). The prototype measures 144 by 144 meters and is surrounded by 24 meter-wide urban roads. The surrounding blocks are uniformly distributed in 18 meter high, 36 or 42 meter long and 12 meter wide residential buildings. The buildings are set back from the road 6 meters. The buildings are 24 meters apart from north to south and 12 meters from east to west.

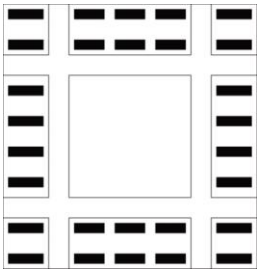


Figure 1. The prototype model of the square.

Water Body Prototype Models

The water in the urban square is mainly static. Therefore, the geometric form and spatial layout are the most important features of the water body and are affected by factors including water scale, dispersion, shape, and location. This study focuses on the analysis of the scale and shape of static water bodies.

The scale of the water body is the primary factor in the layout of water features. Different areas of water will give people a different sense of space. A small-scale water body is a space embellishment that enhances the quality of the space and creates a variety of spaces. A large-scale water body can become the center of the square. For the quantitative representation of the water body scale, we used the water area ratio, which is the ratio of the water area to the square area.

$$R = \frac{A_w}{A_s} \tag{1}$$

Where R is the proportion of water body area, A_w is the area of water body, and A_s is the total area of the square.

Figure 2 presents three cases with different R values. The left one is a water body of approximately 2,000 m^2, accounting for 10% of the total area of the square. The middle one is a water body of approximately 6,000 m^2, accounting for 30% of the square. Finally, the right one is a water body of Approximately 10,000 m^2, accounting for 50% of the square. These three were set as the study cases.

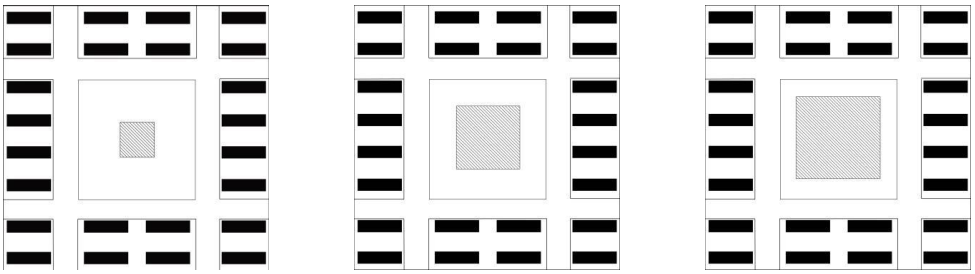


Figure 2. Different water body scale.

Water shape is also an important factor in waterscape design. The compact water body has a large water surface and plays a role as a focal point in the space. When the shape is relatively dispersed, the waterscape is generally directional, and can divide the square space. By comparing the length and area of the shape, the most compact geometry is a circle or a square, so they are usually used as the basis to measure the complexity of the shape of the patch. This paper uses squares as the benchmark for quantitative indicators of form.

$$S = \frac{0.25\mathrm{P}}{\sqrt{\mathrm{A}_w}} \tag{2}$$

Where S is the water body shape index, P is the circumference of the water body and A_w is the area of the water body. When the shape of the water body is square, the value of S is 1. The more complex or narrow the shape, the greater the value of S.

Figure 3 presents four cases with the same area and different S values for the water bodies. From left to right, the shape of the water body with the same area becomes much narrower from the squarest shape, and the value of S increases.

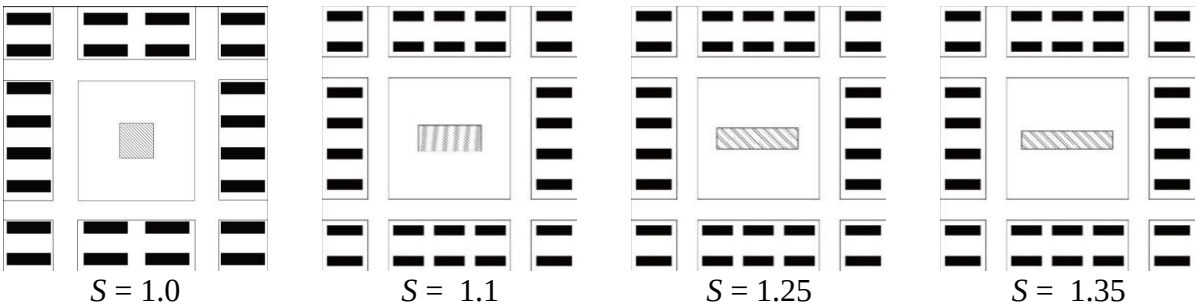


Figure 3. Different water body shape.

Based on Figure 3 and Figure 4, we have a total of 6 urban square models with different sizes and shapes of water bodies. These models will be used for microclimate simulations. Taking the case with *R=10%, S=1.0* as the control case, we will compare the differences in microclimate effects for these cases.

Microclimate Simulation with ENVI-met

We used the ENVI-met 4.0 beta version to perform microclimate simulations on all set square models. In the software, we choose the size of the model is 100m×104m×90m.The grid unit size is *dx* = 3 m, *dy* = 3 m, *dz* = 3 m. To eliminate the influence of the boundary on the simulation area, 30 nested grids are set to be similar to the shape of the simulation center area. Table 1 shows the relevant parameters.

Table 1. Parameter settings of ENVI-met

	Parameter settings	
Location	Nanjing	E118, N32
	Near ground roughness	0.01
Date	Summer	Jun. 22, 2016
	Winter	Dec. 22, 2016
Meteorological parameters	Wind speed at 10 m height	Summer 2.4 m/s
		Winter 1.1 m/s
	Wind direction	Summer 135
		Winter 45
	Air temperature	Summer 295 K
		Winter 275.15 K
	Relative humidity at 2 m height	Summer 77%
		Winter 69%
	Moisture content at 2500 m height	7 g/kg

To provide a more comprehensive analysis of the microclimate effects of water bodies, the simulation outputs include air temperature (AT), relative humidity (RH), wind speed (WS), and predicted mean vote (PMV) for typical climate days in summer and winter. PMV is an index that predicts the average of the thermal comfort of most people (ISO 2005).

Result Analysis

Simulation results

All 6 urban square models were imported into ENVI-met. With the parameter settings described before, microclimate results of the models for a typical day in summer and winter were simulated. Here, we show the simulation results of 1.5 m height at 12:00 as a typical value of microclimate effects. Figure 4 shows the simulated results for a square with different water body area and shape in the summer. From left to right are air temperature, relative humidity, wind speed, and PMV. Similarly, Figure 5 shows the simulated results of the square in the winter.

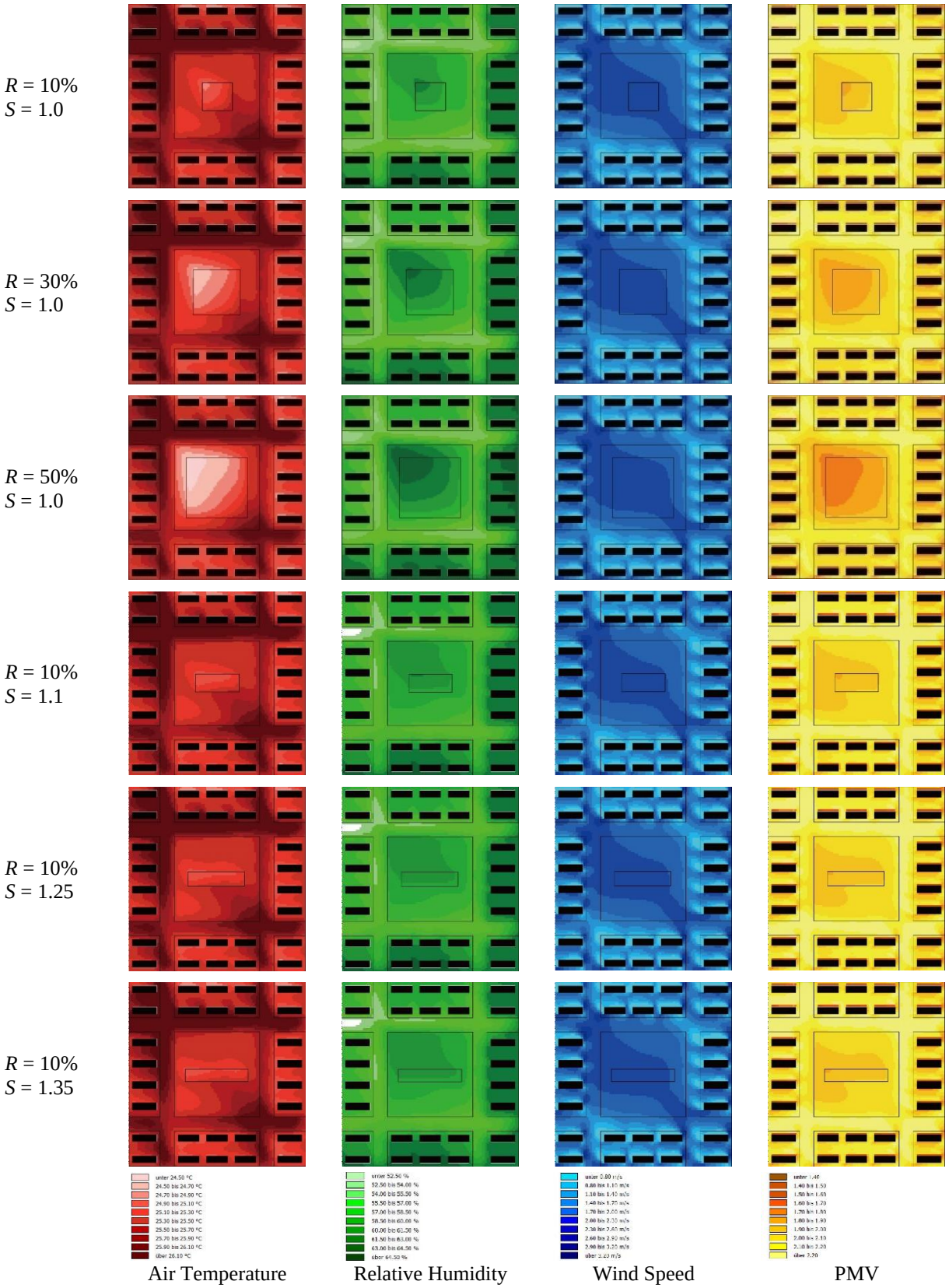


Figure 4. Simulated results in the summer.

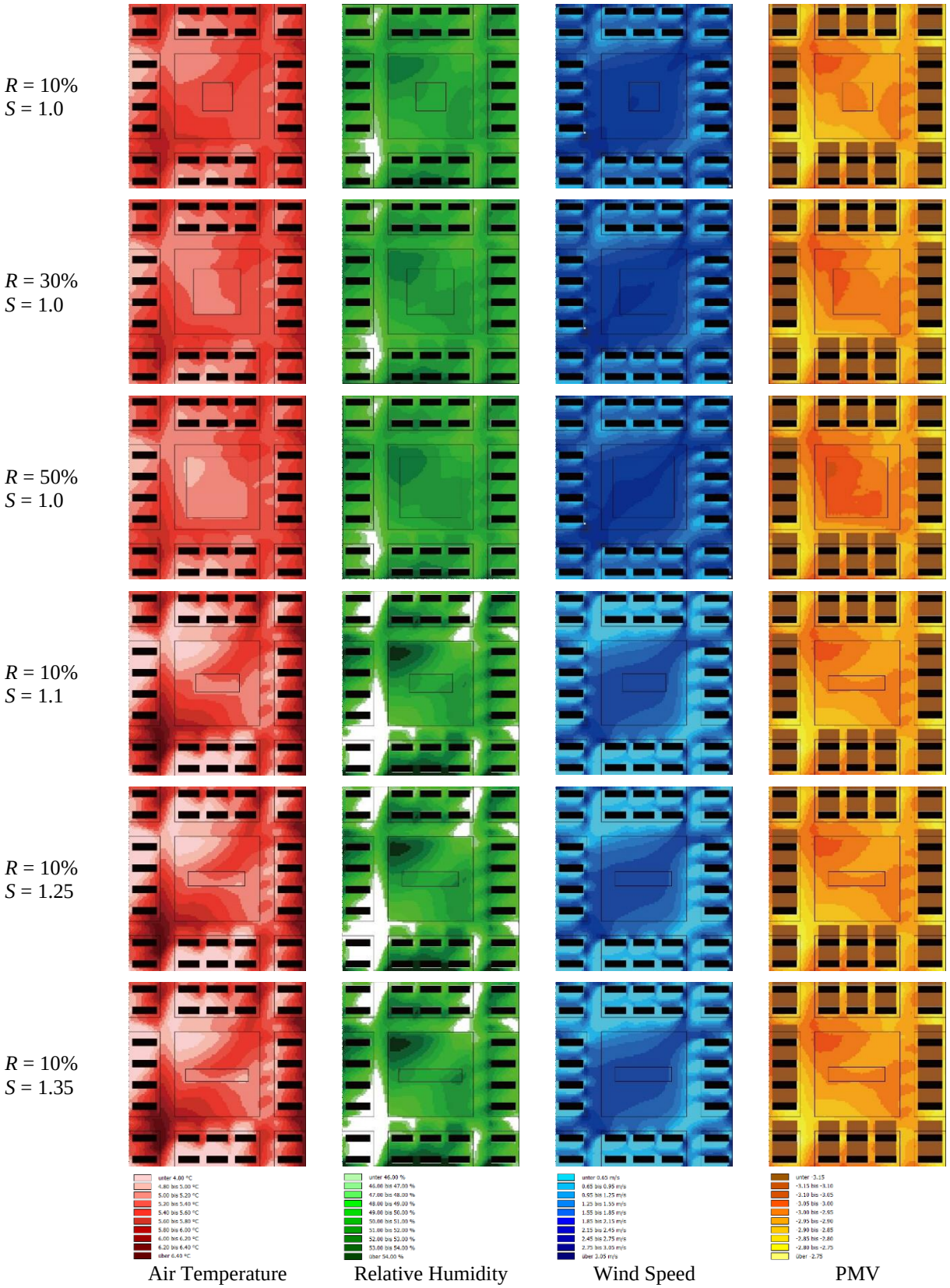


Figure 5. Simulated results in the winter.

It can be seen in the figures that the water body scale has a greater influence on the microclimate effect. Especially in the summer, with the increase in the water body scale, the low temperature zone and the high humidity zone are obviously enlarged, and both appear in the downwind direction of the water body. In addition, there is a significant improvement in the thermal comfort of the human body, and an area similar to the wind shadow area is formed. This shows that the influence of water body on the downwind area is much larger than that of other areas. However, even in the downwind area, the range of influence of the water body is still limited. Furthermore, for different water body shapes, the figures do not present an obvious difference.

Statistics of the microclimate effect of water bodies

Table 2 presents the average value of the different microclimate effects of all 6 models in summer and winter. Based on the simulation results, the impact on the microclimate effect is very weak, both in terms of water scale and water shape. In all 6 models, the difference between the maximum and minimum values of the average air temperature is 0.42 degrees in summer and only 0.16 degrees in winter. The difference in relative humidity is 0.0157 in summer and only 0.0036 in winter. The difference in wind speed is 0.017 m/s in summer and 0.021 m/s in winter. The difference in PMV is 0.14 in summer and 0.044 in winter. In comparison, the influence of water body scale difference on all microclimate effects is much greater, and the influence of water body difference in summer is greater than that in winter.

Table 2. Average value of microclimate effects of different models in summer and winter

Cases	Summer				Winter			
	AT (°C)	RH	WS (m/s)	PMV	AT (°C)	RH	WS (m/s)	PMV
R = 10% S = 1.0	25.44	59.13%	1.946	2.027	5.32	57.84%	2.127	-2.946
R = 30% S = 1.0	25.24	59.88%	1.954	1.961	5.25	58.01%	2.137	-2.967
R = 50% S = 1.0	25.03	60.67%	1.963	1.889	5.17	58.19%	2.147	-2.989
R = 10% S = 1.1	25.44	59.11%	1.946	2.029	5.33	57.84%	2.127	-2.945
R = 10% S = 1.25	25.44	59.12%	1.946	2.028	5.33	57.84%	2.127	-2.945
R = 10% S = 1.35	25.45	59.10%	1.946	2.029	5.33	57.83%	2.126	-2.945

For air temperature, both in summer and winter, the increase in water body scale has a significant cooling effect (Figure 6), and the impact in summer is greater than in winter. However, the change in shape of the water body has little effect on the average air temperature of the square.

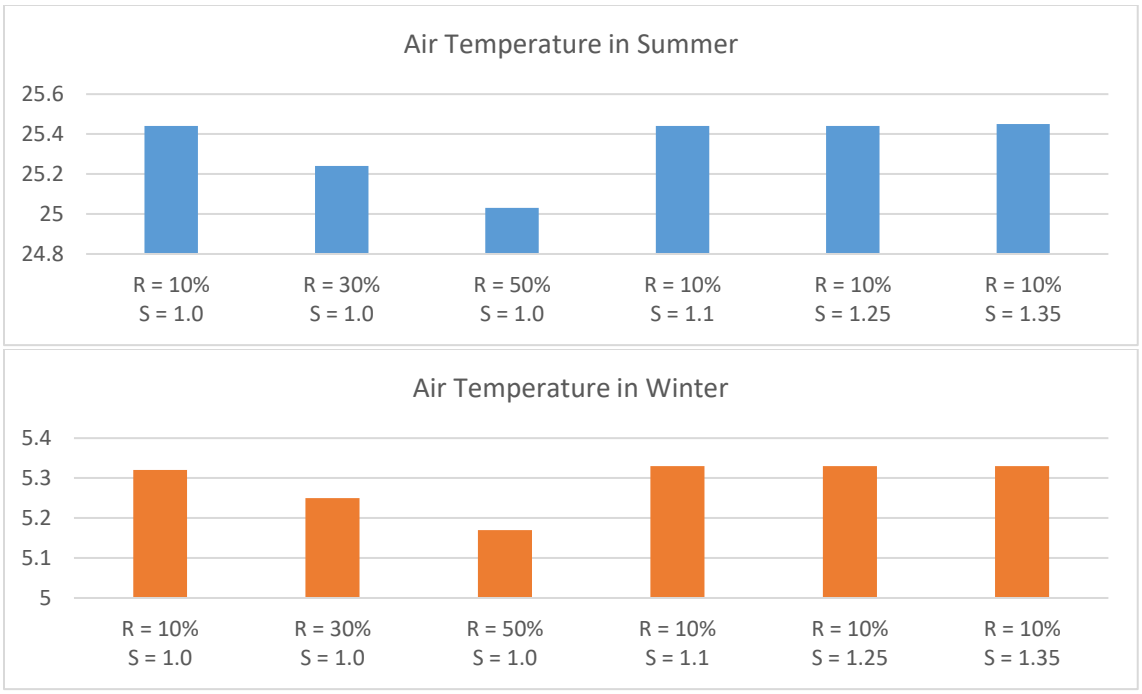


Figure 6. Comparison of air temperature of the models in summer and winter.

For relative humidity, the increase in water body scale has a significant humidification effect (Figure 7). The impact of these in summer is much greater than in winter. Similar to the air temperature, the change in shape of the water body has little effect on the average relative humidity of the square.

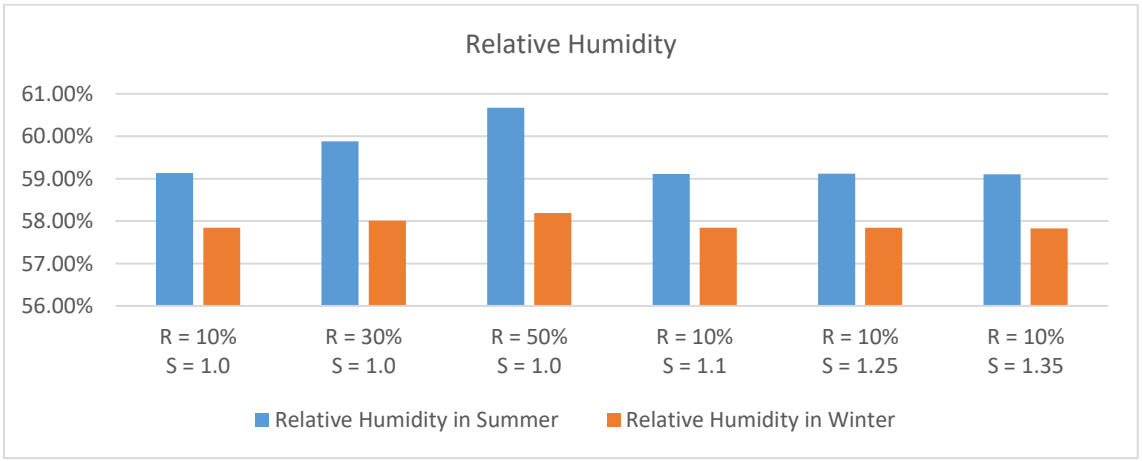


Figure 7. Comparison of relative humidity of the models in summer and winter.

For wind speed, whether in summer or winter, water body scale or shape, the impact on wind speed is minimal (Figure 8). This is because there is no vertical occlusion on the surface of the water.

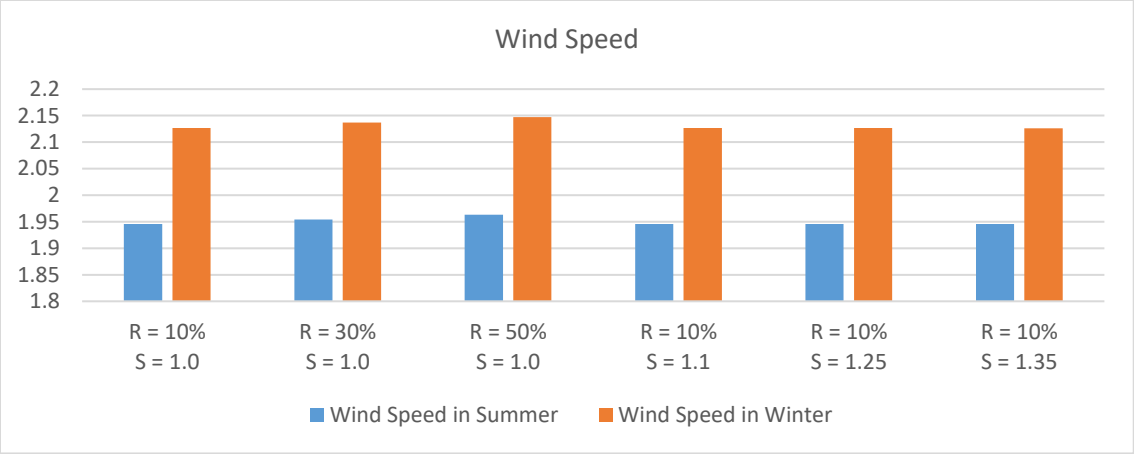


Figure 8. Comparison of wind speed of the models in summer and winter.

For PMV, in summer, an increase in water body scale will improve it, while in winter, an increase in water body scale will worsen it (Figure 9). Similarly, the change in the shape of the water body has little effect on the average PMV value of the square.

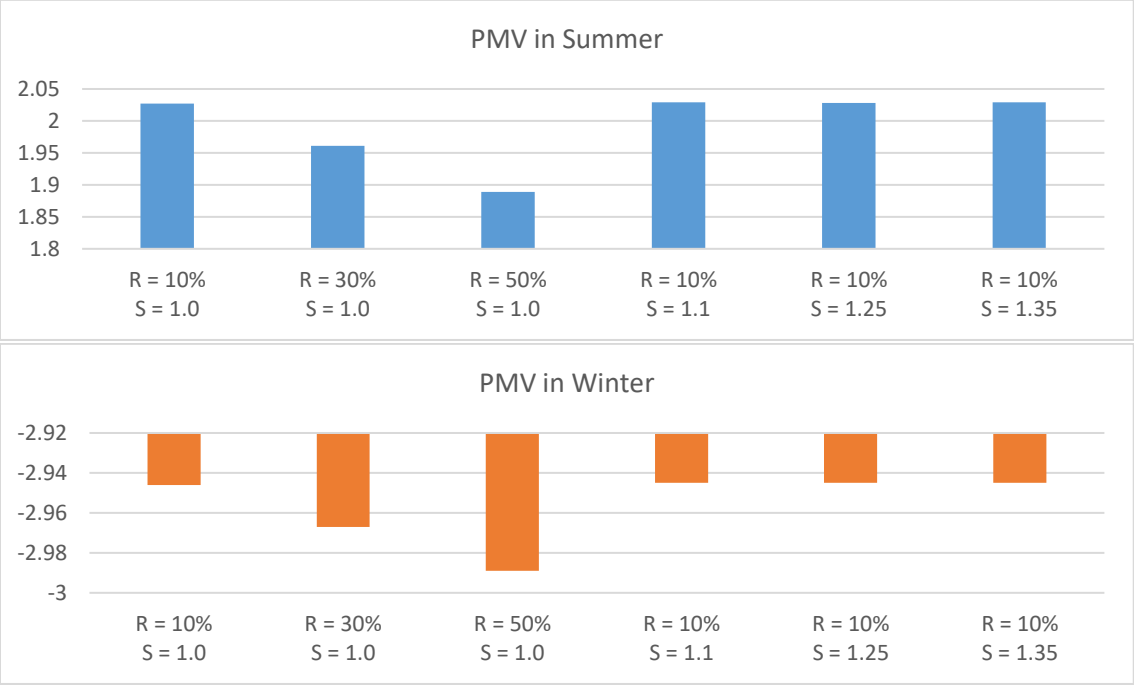


Figure 9. Comparison of PMV of the models in summer and winter.

Conclusion

Based on a survey of a large number of urban squares in Nanjing, China, this paper proposed a prototype square, including area, shape, surrounding roads and buildings. At the same time, the paper quantified the water body form with the scale and shape, and it constructed 6 basic urban square models for microclimate research. Using the ENVI-met software, we obtained

microclimate simulation results for all models in summer and winter, and the data collected included air temperature, relative humidity, wind speed, and PMV.

Through the analysis of simulation results and data statistics, we believe that there is a direct correlation between water form and microclimate effect. Among the factors analyzed, the water body scale has the greatest impact on the microclimate effect. With the increase in water scale, the low temperature zone and the high humidity zone are enlarged, and the PMV is changed. The change in shape of the water has little effect on the microclimate. In addition, the influence of water body differences in summer is greater than it is in winter.

The paper's discussion of the form of the water body is limited to scale and shape, and the position and dispersion of water distribution are also important parameters of water form. We will continue to explore these two parameters further in a follow-up study.

Acknowledgments

This research was supported by National Natural Science Foundation of China (51578277) and Major Program of National Natural Science Foundation of China (51538005).

References

Chiesura, A. 2004. The role of urban parks for the sustainable city. *Landscape and urban planning*, 68(1): 129-138.

Gupta, N., A. Mathew, and S. Khandelwal, 2019. Analysis of cooling effect of water bodies on land surface temperature in nearby region: A case study of Ahmedabad and Chandigarh cities in India. *The Egyptian Journal of Remote Sensing and Space Science*, 22(1): 81-93.

Huang, L., J. Li, D. Zhao, and J. Zhu, 2008. A fieldwork study on the diurnal changes of urban microclimate in four types of ground cover and urban heat island of Nanjing, China. *Building and environment*, 43(1): 7-17.

ISO, A. 2005. Determination and interpretation of thermal comfort using calculation of the PMV and PPD indices and local thermal comfort criteria. Ergonomics of the thermal environment, International Organization for Standards, Geneva, 52.

Jin, H., T. Shao, and R. Zhang. 2017. Effect of water body forms on microclimate of residential district. *Energy Procedia*, 134: 256-265.

Manteghi, G., H. bin Limit, and D. Remaz, 2015. Water bodies an urban microclimate: A review. *Modern Applied Science*, 9(6): 1.

Masiero, E., and L. C. L. Desouza. 2012. Influence of a Waterbody in the Urban Microclimate. In *28th Conference, Opportunities, Limits & Needs Towards an environmentally responsible architecture*, 7-9. Lima, Perú.

Sun, R., A. Chen, L. Chen, and Y. Lv, 2012. Cooling effects of wetlands in an urban region: the case of Beijing. *Ecological Indicators*, 20: 57-64.

Urban Micro-climate and Spatial Promotion for Creating the Historical Streets Sustainability

Zheyang Fei [1], *Xi'an Jiaotong University (China)*
Yupeng Wang[2], *Xi'an Jiaotong University (China)*
Man Li [3], *Xi'an Jiaotong University (China)*

ABSTRACT

Historic districts are important parts of a city's material, cultural and economic forms, which have become an important place to undertake the characteristic urban culture, show the charm of the city and inherit the traditional culture. This paper is based on the basic principles of space syntax and related practices of the internal morphological quantification of historic districts, and the related research on microclimate environment simulation of public space systems in historical blocks. From the deficiencies of the research areas of the public system space quantification and environmental simulation, the two research perspectives are combined to quantitatively evaluate the street and square space of the public space system in Xi'an Beilin historical district to explore the best location and the best form of the streets network and squares. Starting from the point of perspective of renewal and optimization of block space and microclimate, this paper puts forward specific suggestions.

1. Introduction

The updated design of public space within historical and cultural districts has been affected by various factors, and the historical block as the inheritance of the urban context, its spatial form characteristics, environmental quality. Meanwhile, as a residential and commercial mixed district, the design optimization of its internal public space system is more urgent and important.

On the one hand, relying on the rapid development of computer science, space syntax software can explore the internal laws of the spatial organization of the block and the activities of people by modeling and computing the spatial structure at the block scale (Hillier B & Hanson J, 1984). The analysis of the accessibility of the public space can obtain more accurate quantitative analysis results through software simulation results (Jiang B & Claramunt C, 2002). On the other hand, some studies on community renovation combined with environmental behaviour point out that people's perception of public space is affected by microclimate, and the vitality of public space can be improved to a large extent by optimizing the physical environment (Bin Li, 2008). Therefore, in recent years, some studies believe that natural vitality should be included in public space evaluation. Natural vitality means that the public space has the ability to attract people to carry out high-frequency, long-term activities in space. Its microclimatic environment makes people feel comfortable. The study contains a lot of considerations for temperature and sunshine (Cunyan Jiang & Hong Leng, 2017; Fei Chen et al, 2017). In addition, the improvement of

[1] Yupeng Wang: [wang-yupeng@mail.xjtu.edu.cn]

computer science has also enabled the micro-climate on the street scale to be simulated and evaluated by software. The ENVI-met software is suitable for mid-scale street microclimate simulation. A large number of previous studies have proved that its simulation calculation has certain accuracy (Dario A et al, 2014).

Many researches on the influencing factors of public space vitality has been studied. The influence range of these influencing factors includes space's comfort, attraction and accessibility. Due to historic blocks have the characteristics of high building density, sparse greening and broken road network, the transformation and improvement of public space vitality should be carried out on the basis of comprehensive quantification. In order to propose comprehensive and refined optimization suggestions, this paper selects three main influencing factors, combined with the field investigation results, and finally quantitatively evaluates the physical system quality of the physical environment and space environment of Xi'an Beilin Historic District.

2. Data and Method

2.1 Study Area



Figure 1. The scope of the research area Source: Based on Google Maps

Xi'an Beilin historical district is selected for study, and the image is shown in Figure 1. This district is located in the old town of Xi'an. It retains splendid historical and cultural heritages. After several renovations, the business gathering area of the Academy Gate was formed in the south of the Academy Gate Street and the north of Shuncheng Lane. After several renovations, the south side of Shuyuanmen street and the north side of Shuncheng Lane formed a commercial agglomeration area by self-organization. However, the residential environment has gradually decreased. In recent years, a large number of residential buildings have been rebuilt and added, increasing the building density and affecting ventilation and sunshine conditions. Meanwhile, the traditional spaces were changed in the reconstruction process, and the internal activity areas are compressed. Internal squares' distribution is scattered and insufficient, and doesn't meet the

demands from both tourists and residents.

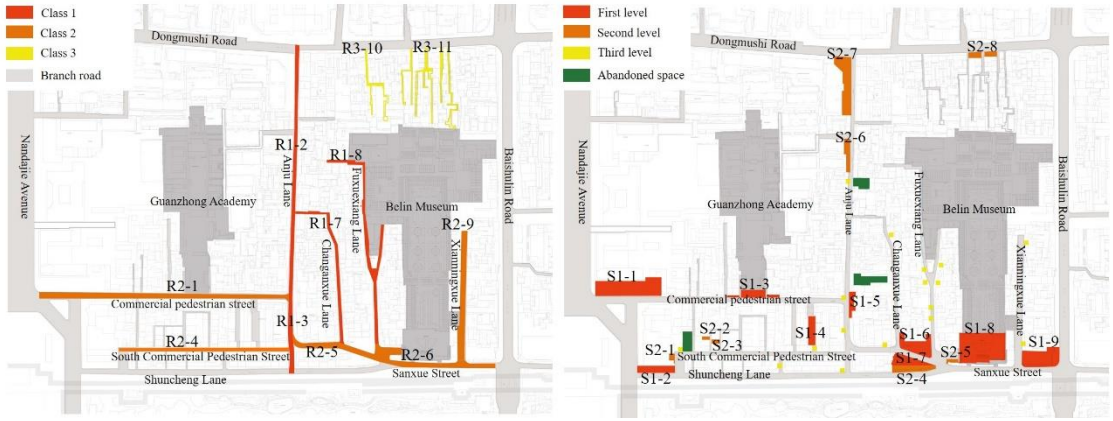


Figure 2. Classification of roads and squares

Based on the observation results, 11 main roads, 17 squares and some self-organized gathering sites were selected for study as show in Figure 2. For ease of statistics and analysis, the streets are divided into three categories according to the following two indicators, using crowd and the business along the street. Typical representative streets are selected for each category, and the numbers are shown in Table 1. According to the two indicators of service crowd and square formation, the open activity space is divided into three levels as show in Table 2. The first level is the space which used by residents and tourists. This level of space mainly includes the square in front of some public building scenic spots and the square at the entrance of streets and lanes. The second -level square is set up for residents, including some spaces connected by streets or intersections, and some courtyard spaces enclosed by the buildings, and the third-level square is a place where residents gather spontaneously.

Table 1. Classification of streets space

Classification	User	Commercial	Time	typical case
Class 1	Residents & Tourists	Mixed	15:00-18:00 19:00-21:00	R1-7, R1-8
Class 2	Tourists	Cultural product	15:00-18:00	R2-1,R2-4, R2-5, R2-6
Class 3	Residents	No	19:00-21:00	R3-10,R3-11

Table 2. Classification of square space

Classification	User	Formation	Time	typical case
First level	Residents & Tourists	Designed	15:00-18:00 19:00-21:00	S1-3,S1-8, S1-4
Second level	Residents	Designed	19:00-21:00	S2-4,S2-7 S2-8
Third level	Tourists	Not designed	19:00-21:00	No

This paper determines the research time of various public spaces according to the activity time of different people in the block. Usually, working hours are from 9:00 to 17:00, and their

spontaneous activities in the streets and squares are concentrated between 19:00 and 21:00. During 8:00 to 9:00 and 17:00 to 18:00, residents' commuting behavior takes place in the street space, the environmental quality has little impact on it, so the data during these times is not considered. For tourists, although they spend all day in the block, it takes time for visitors to arrive at the attractions, and the temperature is hot at noon in summer, so most of them choose to visit in the afternoon. Therefore, the time period from 15:00 to 18:00 was selected to evaluate the public space for tourists.

2.2 Research Method

Spatial Quantization Method

"Axis analysis method" is mainly used to extract the spatial morphological variables of historic streets. Based on the principle of drawing spatial syntactic axes, that is, keeping the spatial relationship of streets and lanes unchanged, the spatial structure is transformed into an axes map by covering the space system studied with the least and longest straight lines. The topological relationship between axes is quantified by a series of morphological variables through a mathematical model to form targets. Among them, the global integration degree (HH) represents the possibility of each space reaching all other spaces in the space system. The value quantifies the degree of concentration or dispersion of a street and other spaces in the system, also the accessibility of the space in the system and the possibility of being selected as a travel destination (Hillier B & Stutz C, 2005). Convex space analysis method is based on the principle of convex space segmentation, which translates street space into convex space, and then establishes the graphic relationship between them to quantify the open area (Jingwen Wang, 2010). In this paper, the software "convex polygon analysis method" is used to quantify the square space. Quantitative indicators also select the global integration value, which is also used to explain the daily activities of residents and the spatial exploration behavior of tourists at the topological level.

Microclimate simulation method

Table 3. ENVI-met model parameter settings

Model parameter	Numerical setting	Model parameter	Numerical setting
Category	23nd July, 2018	Wind direction	North east
Start time	23:00	Wind speed	1.5 m/s
Duration	23h	Building interior temperature	26.97°C

The ENVI-met microclimate numerical simulation software (Simulated Software Version: V4.4 Winter1819) was used to simulate and analyze the two microclimate indexes of air temperature and wind speed on pedestrian height in different types of public space. Usually, the microclimate environment of a block includes factors such as wind speed, wind direction, air temperature, air humidity, solar radiation and so on. These factors affect people's behavior and feelings through microclimate comfort to varying degrees, and then affect the vitality of the block (Yupeng Wang & Zacharias Jhn, 2015). The climatic characteristics of Xi'an are: the four seasons

are obvious and the summer is very hot, so the temperature and wind speed are two factors that have greater impact on the comfort of people in the summer block. Therefore, this paper chooses these two parameters for quantitative evaluation. The grid size for simulation modeling is 3m × 3m × 3m, and detailed simulation parameters are shown in Table 3. This paper chooses the typical numerical simulation results of the horizontal section at 1.5 meters of streets and squares in various classifications for analysis, in which the air temperature and wind speed are both average values. The computational method is counting all the grids contained in the boundary of the street or square area, summing the simulated values and then taking the average value.

Quantitative analysis of space and environment

Table 4. Space system quantitative evaluation standard table

Research object	Quantitative indicators	Scoring standard
Street space	Street aspect ratio (D/H)	(D/H) ≥ 1: 3 points; 1 > (D/H) > 0.5: 2 points; (D/H) ≤ 0.5: 1 point (LuyuanYixin, 2006)
	Spatial accessibility (HH)	HH ≥ 1.5: 3 points; 1.5 > HH > 1.3: 2 points; HH ≤ 1.3: 1 point (Karimi Hillier et al, 2018)
	Air temperature(T)	T≤27.5°C: 3 points; 27.5° C<T<29.0°C: 2 points; T≥29°C: 1 point (Junsheng Rao,2015)
	Regional wind speed(W)	W≥0.6 m/s: 3 points; 0.6m/s>W>0.5 counts: points; W≤0.5m/s: 1 point (Junsheng Rao,2015)
Square space	Open space area (S)	|S-625|≤100m^2: 3 points; 100m^2<|S-625|<500m^2: 2 points; |S-625|≥ 500m^2: 1 point (Leiqing Xu, 2012)
	Spatial accessibility (HH)	HH≥1.4: 3 points; 1.4 > HH>1.2: 2 points; HH≤1.2: 1 point
	Air temperature(T)	T ≤ 27.5°C: 3 points; 27.5 ° C < T < 29°C: 2 points; T ≥ 29°C: 1 point
	Regional wind speed (W)	W≥0.8 m/s: 3 points; 0.8 m/s>W>0.5: 2 points; W≤0.5m/s: 1 point

This study aims to promote the vitality of the public space system in historical blocks, and divides the overall goal into two sub-goals: promoting the vitality of streets in historical districts and promoting the vitality of public open spaces in historical blocks. More than ten years ago, Gale summarized 43 factors affecting the vitality of public systems in terms of safety, comfort and pleasure, including interface, noise, vision, street facilities, and spatial scale, etc (Gail, 2002). This article focuses on the main influencing factors in terms of comfort and pleasure, through the establishment of the physical environment (mean air temperature (T), mean wind speed (W)) quantitative model of the Xi'an Beilin historical block, the spatial environment (Global Integration （HH）)quantitative model, combined with the field investigate results, spatial form quantitative results (area(S), aspect ratio-(Street width D /Height of the exterior walls of buildings on both sides

of the street H)), quantitative evaluation of the quality of public systems. The quantitative index scoring standards are shown in Table 4.

3. Results

3.1 Integration analysis of typical street

Fig. 3 shows that Nandajie Street has the highest degree of integration (Maximum Integration [HH] = 2.47) and the smallest degree of integration appears in the Dongmutoushi Road (Minimum Integration [HH] = 0.83). As the main commercial pedestrian streets, the overall integration of the commercial pedestrian streets (R2-1) and part of the streets (R2-5 and R2-6) is only from 1.43 to 2.10, which indicates that the entrance has high accessibility. But inside of the block, the accessibility gradually decreases due to the lack of branches. The integration degree of the branches connected with Road 2-4 is low. The axis with low integration degree represents the space with low accessibility for consumers and also shows the relationship between streets and lanes in this area is not close enough. The area inside the block, especially the residential street, such as R3-10, R3-11, has a low degree of integration. This is because the long-term self-construction behavior of local residents has resulted in the break of the connectivity between streets and lanes. The public space that was originally available has been privately transformed into private space, and a large number of broken branches have been added.

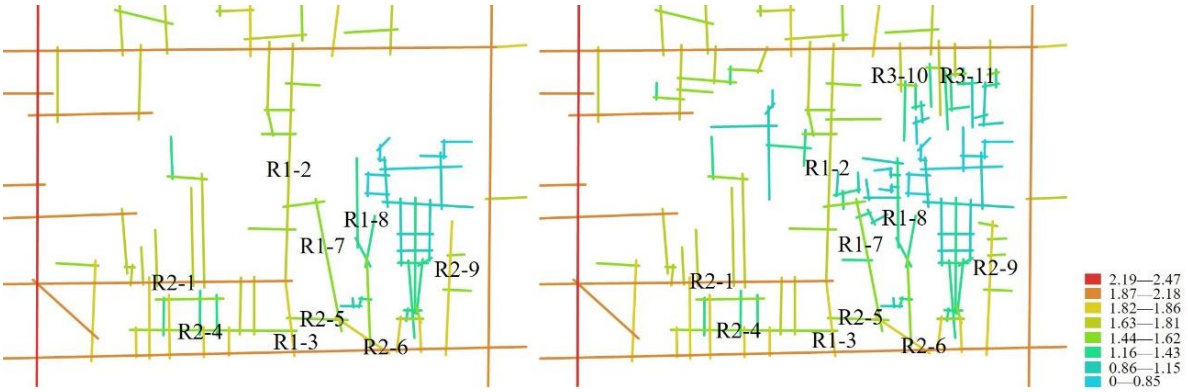


Figure 3. Overall Integration Value of Street Space (the left figure does not include the third type of street, the right figure is the whole road system)

3.2 Integration analysis of typical squares

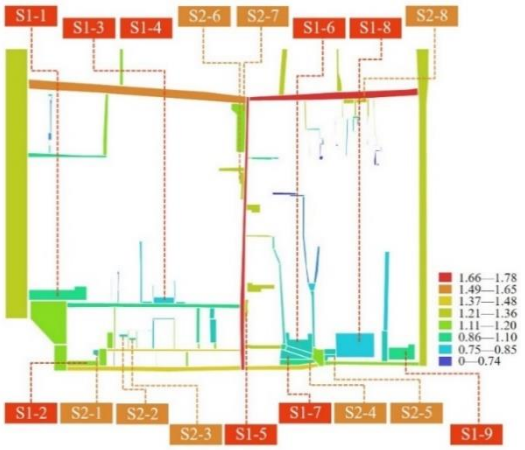


Figure 4. Overall Integration Value of Square Space

The entrance squares of Shuyuanmen Academy and Beilin Museum are 1-3 and 1-8 and their global integration values are 0.82 and 0.84. Even though the accessibility is low, still a lot of tourists coming into this area because of the scenic spots. The degree of integration is slightly higher than the entrance of scenic spots. The accessibility of 2-7 and 2-8 is relatively higher, and their position in the spatial pattern of the area also has a relatively higher control and influence, so it can be proved that it has the potential to become a good residential activity site.

3.3 Microclimate simulation of typical street

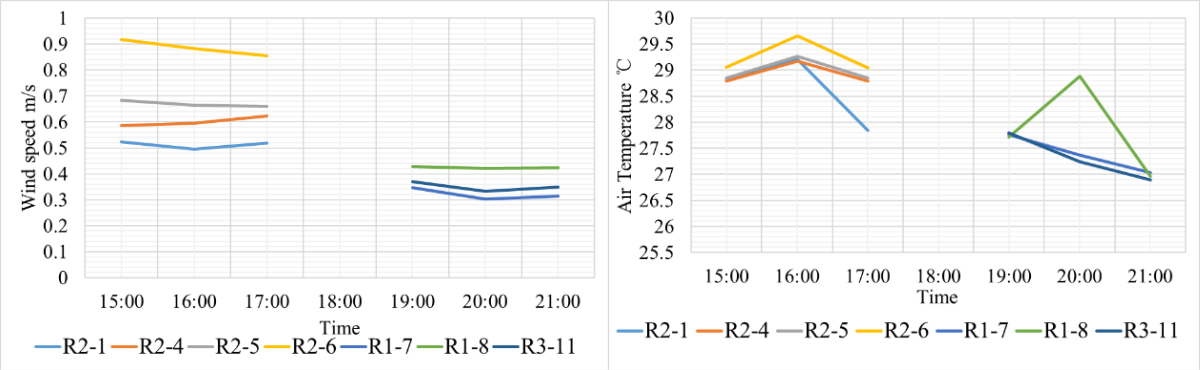


Figure 5. Representative street wind speed map and temperature map

The simulation results of wind speed are shown in Figure 5 (left). During the period of 15:00-18:00 and 19:00-21:00, the wind speed in most areas of commercial pedestrian streets and residential streets is below 0.6m/s. The maximum wind speed is 0.92m/s at 15:00. The wind speed in the R2-1 square is large, and the difference from the lowest average wind speed at that time is 0.6 m/s. The overall wind speed in the residential block is very low. This is because the north side of the R3-11 is mostly a high-rise building with a large volume of buildings.

The simulation results of air temperature are shown in Figure 5 (right). During the period of 15:00-18:00, the temperature of the commercial block slowly rises and then falls, reaching a peak of 29.7℃ at 16:00. During the period of 19:00-21:00, the temperature of R1-8 increased at 20:00, the temperature on the street was significantly higher than other spaces, and the maximum temperature was 28.88℃.

3.4 Microclimate simulation of typical squares

Through the environmental simulation of four typical squares in the object area, it was found that the wind speed of the four squares changed slightly all day. The wind speed of square 1-3 was lower than that of the other squares. The average wind speed at 21:00 was 0.41 m/s, which was the smallest wind speed in the whole day. It can also be seen from the temperature map that the temperature of the square at night decreases slowly with time, this is because the square is small in size and is located in the center of a densely built block with dense trees inside and around, which prevents the heat accumulated during the day from releasing faster at night. In the four squares, the temperature of Plaza 2-8 began to rise gradually from 13:00, and reached the highest peak at 16:00 (29.5℃), then dropped rapidly, reaching the lowest temperature (26.9℃) at 21:00. By contrast, there is a significant temperature difference in the square all day, the difference is 2.6℃. The large temperature difference between day and night is observed in the square with large area, low greening rate, and high degree of openness.

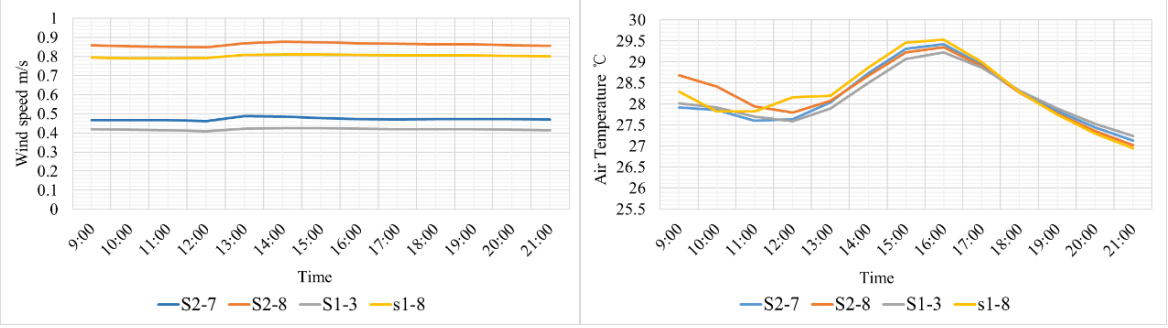


Figure 6. Representative square wind speed map and temperature map

3.5 Spatial and environmental quantitative analysis

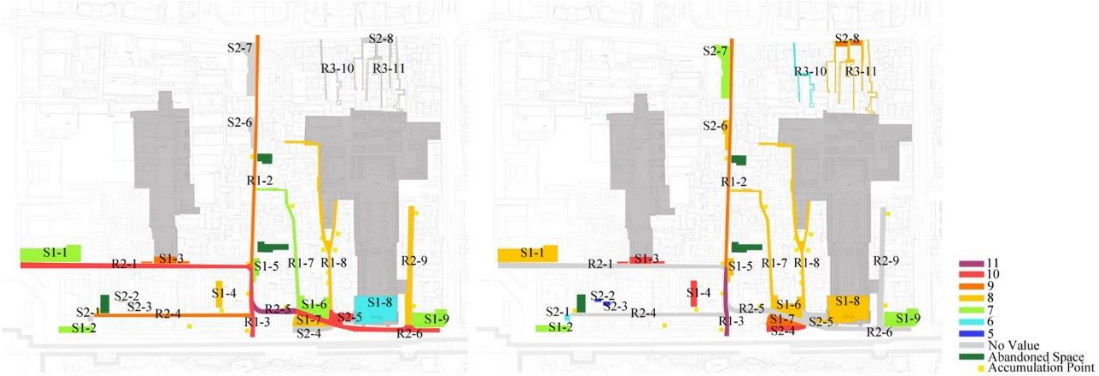


Figure 7. Public space integrated quantitative value (left: 15:00-18:00, right: 19:00-21:00)

The overall scores of the main streets and squares in the object area are evaluated, and the evaluation results are shown in Figure 7. The street with the highest comprehensive quantified value from 15:00-18:00 is R2-5 (11 points), followed by R2-1 (10 points) and R2-6 (10 points), covering the main part of the Commercial Street. It has high space quality, high population density, and full of commercial facilities. It can be combined with semi-outdoor space to set up diverse street activities to attract people to stay. R2-4 is also a main commercial street of Beilin historical district, but the comprehensive score is 9 points. The main problems here are the high local temperature and the low H/W ratio. The street space is high and narrow, the user's sight is constrained, bringing a sense of depression to tourists. It is suggested that the higher buildings at the intersection of R2-4 and R1-3 be properly demolished for open entrance space to guide tourists into the streets. R1-7 is a street shared by tourists and residents. It has the lowest comprehensive quantified value (7 points) due to the high density and irregular layout of the streets, the street is in a static wind zone (averagely 0.3 m/s). The building density of the block should be adjusted and reduced. During the field research, it was found that in the evening, some residents gathered spontaneously to play chess on the sidewalk of the block, which proved the high space quality. It was suggested that some recreational facilities should be added on both sides of the street for residential use.

According to the comprehensive quantitative score of the small open space in the block from 15:00 to 18:00, the S1-3 score is the highest (9 points) and the S1-8 score is the lowest (6 points). Comparing the scores of various indicators, it can be concluded that although the two squares are located at the entrance of the tourist attraction, the convenience of the S1-8 square is poor in the whole system, so the tourists are not easy to perceive. And the scale of the square is too large, far exceeding 25m×25m optimal base scale, which led to a higher average temperature (29 ℃) during the period from 15:00 to 18:00, making there uncomfortable to stay. Therefore, planting vegetation should be considered in the area to reduce the air temperature and enrich the spatial level, or use the transitional gray space such as the shade canopy to create a semi-outdoor space, to separate the large space and provide suitable environment for staying. As a point where crowds and activities are concentrated, the semi-outdoor space can “grow the surface” to drive the spatial vitality of the entire square. S2-4 has the highest comprehensive score in the period from 19:00 to 21:00 with higher wind speed and lower air temperature. However, because of the car and non-motor vehicle encroachment on the event venue and the break-up of public entertainment facilities, the public space is not well used. It is recommended to regulate the placement of non-motor vehicles to increase the utilization of the space.

4. Discussion

In this paper, numerical simulation was used for analyzing the public space system, which is lack of actual measurement correction. From the perspective of quantitative indicators, this paper does not cover the analysis of public facilities factors in public systems. On the one hand, there are fewer public facilities in the selected study area. On the other hand, this paper aims to provide reference for facility optimization through quantitative results. In addition, for the comprehensive

quantitative analysis of the Xi'an Beilin Historic District, only simulated the environment in summer, and the microclimate environment of other seasons will be simulated and analyzed in the future studies. The quantitative research of historical blocks under various factors is complex and versatile, and closely related to crowd activities. Fine quantification and transformation can improve the livability index of historical blocks.

5.Conclusion

1) This paper provides multi-dimensional quantitative analysis about public space from two aspects of spatial morphology: Features and outdoor climate. As a necessary supplement to traditional research methods and qualitative research results, it synthetically analyses block and public open space, and achieves the coupling analysis attempt of multiple quantitative analysis techniques.

2) Through the comprehensive quantitative map of Xi'an Beilin historical district, it is possible to visually measure the advantages and disadvantages of various public spaces in the area, and to analyze some indicators of various public spaces. From the perspective of space update and microclimate environment optimization, an accurate and detailed historical street protection and renewal strategy is proposed to improve the public system of the block and achieve the goal of improving the dynamic of the block.

References

Hillier B, Hanson J. 1984. *The social logic of space.* Cam Bridge, UK: Cam Bridge University Press.

Jiang B, Claramunt C. 2002. "Integration of space syntax into GIS: New perspectives for urban morphology."6(03):295-309.

Bin Li. 2008. "Environmental behavior theory of environmental behavior and its expansion." *Journal of Architecture* (2): 30-33

Cunyan Jiang, Hong Leng. 2017. "Climate comfortable condition analysis and planning implications of residential district public spaces in transition season of cities in severe cold region: taking harbin as an example." *Urbanism and Architecture*

Fei Chen, Jianqun Lin, Xun Zhu. 2017. "Factor analysis on public space activity evaluation of winter cities." *Journal Of Harbin Institute Of Technology* 49(4):179-188.

Dario A, Giorgio G, Biagio M. "Evaluating Mitigation Effects of Urban Heat Islands in a Historical Small Center with the ENVI-Met. Climate Model." *Sustainability* 6(10):7013-7029.

Gail. 2002. *Communication and Space*. Beijing: China Construction Industry Press.

Hillier B, Stutz C. 2005. " A New Method of Spatial Syntax. " *World Architecture* (1):54-55.

Jingwen Wang. 2010. "Research Status and Development Trend of Spatial Syntax. " *Huazhong Architecture* 28(6): 5.7.

Yupeng Wang, Zacharias Jhn. Landscape modification for ambient environmental improvement in central business districts – A case from Beijing [J]. Urban Forestry & Urban Greening,2015,14:8-18

LuyuanYixin. 2006. *Street Aesthetics*. Tianjin: Baihua Literature and Art Publishing House.

Karimi, Kayvan. 2018. "Space syntax: consolidation and transformation of an urban research field." *Journal of Urban Design* 23(1):1-4.

Junsheng Rao. 2015. "Evaluation of thermal environment snd thermal comfort on block scale in Guang zhou." *Harbin Institute of Technology* 4-6

Leiqing Xu. 2012. "Square Scale and Space Quality—A Virtual Study of the Relationship between Square Area, Aspect Ratio and Spatial Preference and Imagery." *Architectural Journal* (2):74-78.

Modelling the influence of high-rise urban geometry on outdoor thermal comfort in Singapore

Juan Angel Acero, CENSAM-SMART (Singapore)
Elliot J.Y. Koh, CENSAM-SMART (Singapore)
Lea A. Ruefenacht, Singapore-ETH Centre (Singapore)
Leslie K. Norford, Dept. Architecture (MIT) (EE. UU.)

ABSTRACT

Tropical cities are exposed to high air temperature and relative humidity throughout the year, causing pedestrian thermal discomfort. In this work, we present an evaluation of the impact of urban geometry on the outdoor thermal comfort (OTC) in Singapore, focusing on a new mixed-use high-rise development. Different urban design strategies/scenarios have been analyzed: two block forms, four street orientations (N-S, E-W, NE-SW, NW-SE), four street aspect ratios (from 1.5 to 3.5) and three building height profiles (arrangement of buildings based on height). The study is based on modelling techniques. Each scenario was analyzed for seven representative weather conditions during the year. The results are analyzed with specific metrics that take into account the spatial and temporal OTC variations. The results are conditioned by prevailing low winds and high frequency of cloudy days. The best OTC levels are observed on high street aspect ratios (2.5–3) and on N-S oriented streets. Although, on a yearly perspective the streets oriented NE-SW show the worst OTC performance, deviation from the acceptable range is not high. Higher differences between street orientations are encountered for specific weather types. The outcomes provide adequate urban parameters for high-rise developments to improve OTC in hot and humid tropical regions.

Special Issue Journal	:	Urban Climate
DoI	:	https://doi.org/10.1016/j.uclim.2021.100775
Citation	:	Acero, J., Koh, E., Ruefenacht, L., & Norford, L. (2021). Modelling the influence of high-rise urban geometry on outdoor thermal comfort in Singapore. Urban Climate, 36, 100775.

Experimental evaluation of thermal comfort improvement due to innovative solutions for tensile structures

Federico Rossi, Mirko Filipponi, Beatrice Castellani, Andrea Nicolini[1]*, University of Perugia, Perugia (Italy)*
Marta Cardinali, Alberto Maria Gambelli, CIRIAF Interuniversity Centre, Perugia (Italy)

ABSTRACT

In urban areas characterized by strongly prevailing cooling climate, an effective reduction of urban overheating might be pursued by using modular, adaptable structures as curtains, tensile structures or temporary coverings. Such solutions could contribute to reduce outdoor discomfort conditions, but a careful design phase has to be conducted, coupling with the appropriate choice of suitable materials for outdoor applications. The aim of the present research is to assess possible outdoor thermal comfort improvements under the coverings, due to the adoption of a textile with a low infrared emissivity layer downward. For that purpose, two tensile structure facilities were installed at University of Perugia in order to test and compare materials for awnings and curtains. Thus, two different textiles, a traditional and a low emissivity downward one, have been selected and tested. Both textiles are characterized by high solar reflectance towards the external environment. The experimental campaign was conducted in August 2019 and it consisted in the monitoring of thermo-hygrometric microclimate under the coverings. Therefore, outdoor human thermal comfort parameters have been calculated for both awning solutions. Results allowed to determine the benefits in terms of outdoor thermal comfort conditions given by the low infrared emissivity awning with respect to the standard textile material; furthermore, the experimental campaign allows to establish the suitability of the proposal for contributing to the improvement of urban microclimate and the mitigation of urban heat island and climate change phenomena.

Introduction

Urban Heat Island (UHI) is becoming an increasingly relevant phenomenon in cities due to the continue urbanization: as a result of highly dense urban environments, temperatures in cities are higher than in surrounding rural areas (Oke 1995). The most significant consequences of UHI are related to the increase of cooling energy demand for buildings and outdoor pedestrians' discomfort, especially in summer conditions. This could lead to serious risks for human health, due to the exposure to thermal stress and heat waves.

As stated by Nikolopoulou and Steemers (2003), microclimate parameters and psychological adaptation have a strong influence on human thermal sensation and therefore the correct design of urban spaces could positively affect the liveability of cities: urban density, buildings' height and orientation, materials for external surfaces and greenery rate are the most important aspects which could determine the optimal use of outdoor urban spaces (Nikolopoulou and Steemers 2003). Therefore, microclimate mitigation strategies, such as cool roofs and pavements, green roofs and the increase of vegetation, could positively affect outdoor human

[1] Corresponding Author: [andrea.nicolini@unipg.it], [+390755853714].

thermal comfort (Pisello et al 2018). However, there is a lack of studies on the assessing of outdoor thermal comfort, as stated by (Givoni et al 2003; Nikolopoulou, Baker and Steemers 2001; Spagnolo and de Dear 2003; Swaid, Bar-El and Hoffman 1993): outdoor environment is in fact more complex with respect to indoor ones, because of the greater variability of weather conditions depending on the period of the year, the time of the day and the specific location in space. Furthermore, the environment under the outdoor awnings is even less studied and peculiar. its microclimatic characteristics are different from both the indoor and the outdoor conditions. Solar and radiative capabilities of urban surfaces could affect outdoor human comfort sensation; for that reason, the choice of suitable materials for external urban surfaces play an important role for enhancing human thermal comfort in outdoor environments: in Rossi et al. (2015a) an integrated approach for occupants' thermal, visual and acoustic comfort during outdoor events is presented, involving the application of suspended modular tensile structures during temporary events. Moreover, recent studies on retro-reflectivity demonstrate the potential of retro-reflective (RR) materials for building applications (Morini et al 2017; Castellani et al. 2017; Rossi et al. 2015b), in terms of UHI mitigation and thermal comfort improvements.

Motivation

In this context, the need of taking into account pedestrians' thermo-hygrometric comfort in urban environments represents an important issue, as urban temperatures are becoming increasingly extreme in summer season, due to the Urban Heat Island effect. Materials for outdoor applications play a substantial role in the quality and liveability of urban areas, as well as in contributing to the mitigation of UHI. This is mainly due to solar and radiative properties of materials for outdoors, i.e. solar reflectance (α) and infrared emissivity (ξ), which could affect air temperature (T_a) and mean radiant temperature (MRT) and therefore thermal comfort sensation. This concept is summarized in Figure 1: various materials for outdoor awning applications could have a different impact on human thermal comfort, depending on the external solar reflectance and infrared emissivity of the surface downwards, as shown in Figure 1a, 1b and 1c.

In this framework, the aim of the present research is to investigate occupants' outdoor thermal comfort under different awning solutions in summer, focusing on the potential benefits achievable by adding a low infrared emissivity layer on the downward side of the awning. For this purpose, two textile materials with different solar and radiative capabilities have been selected for microclimate monitoring and comfort evaluation under the coverings: a traditional high-reflectance textile and an optimized solution, characterized by high solar reflectance upwards and low infrared emissivity downwards. The final purpose of the study is to propose suitable materials for outdoor applications for enhancing occupants' thermal comfort conditions in summer and contributing to the mitigation of Urban Heat Island phenomenon.

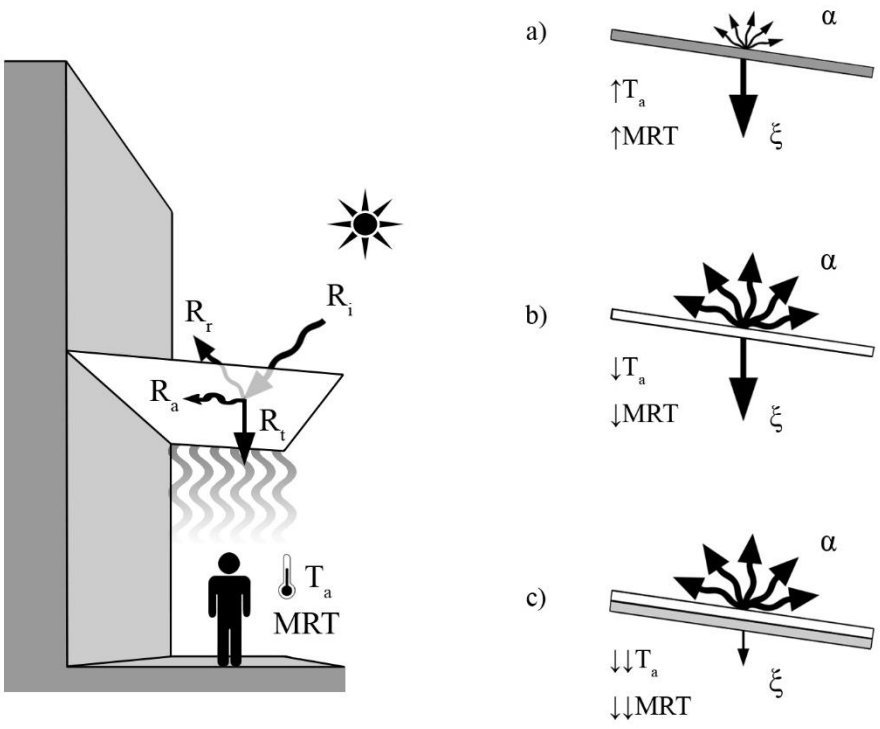


Figure 1: (left) *Concept of the research:* outdoor awning application and possible effects on human thermal comfort; a) *Traditional awning material*: low external solar reflectance and high infrared emissivity downwards; b) *Highly-reflective awning material*: high external solar reflectance; c) *Low-emissivity awning material:* high external solar reflectance and low infrared emissivity downwards.

Methodology

Two different textile materials for outdoor awnings (i.e. a traditional textile and a low infrared emissivity downward solution) have been selected for microclimate monitoring and occupants' thermal comfort evaluation: an optimized awning solution, characterized by a high reflectivity layer on the upper side, coupling with low infrared emissivity downwards, was compared to a traditional awning configuration in terms of thermo-hygrometric comfort conditions of occupants under the coverings. The experimental campaign has been conducted during the summer season, as it represents the worse condition for thermal comfort evaluation, due to the maximum solar irradiance conditions. For this purpose, two tensile structure facilities have been installed at the University of Perugia, in order to test materials for outdoor awnings. The tested awnings are characterized by the same solar reflectance and infrared emissivity on the upper side, but they have different infrared emissivity downward, in order to assess possible benefits on human thermal comfort under the low emissivity awning. A conceptual framework of such methodology is shown in Figure 2: during the experimental campaign, both microclimate monitoring and thermal comfort evaluation have been performed, in order to correlate local microclimate parameters and human outdoor comfort conditions under the coverings.

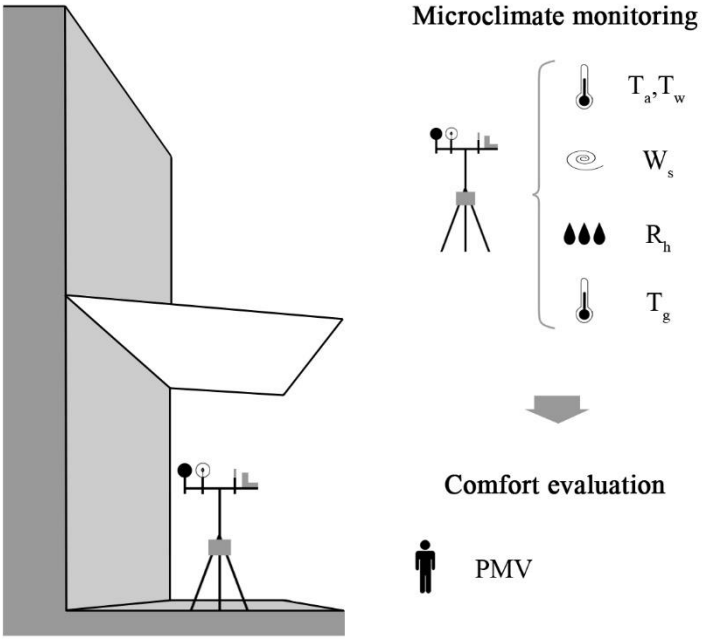


Figure 2: Conceptual framework for the experimental evaluation of occupants' thermo-hygrometric comfort under the coverings. Both microclimate monitoring and comfort evaluation have been assessed.

Description of samples

Two different awning materials for outdoor solar protection have been selected for the creation of two samples to be used for the experimental campaign: the former is a *Standard white (S_w)* textile, consisting of a white, composite polyester membrane with a PVC coating with high solar reflectance and high infrared emissivity; the latter is a *Low emissivity (L_e)* textile, consisting of a composite polyester membrane with a PVC coating with high solar reflectance on the upper side and low infrared emissivity downward.

The combination of the abovementioned textiles provided the creation of two double-layer samples for the experimental campaign, as described below:

- *Reference* sample: it is composed by two layers of *Standard white (S_w)* textile, as shown in Fig. 3a;
- *Low Emissivity* sample: it is composed by one layer of *Standard white (S_w)* textile on the upper side (i.e. facing the sun) and one layer of *Low emissivity (L_e)* textile towards the covered area (Fig.3b).

Both the *Reference* and the *Low Emissivity* samples are characterised by a solar reflectance of 76%, which is provided by the *Standard white* upper layer, the same for both configurations. Infrared emissivity downward is 0.87 for the *Reference* sample and it is 0.35 for the *Low Emissivity* sample downward, as depicted in Table 1.

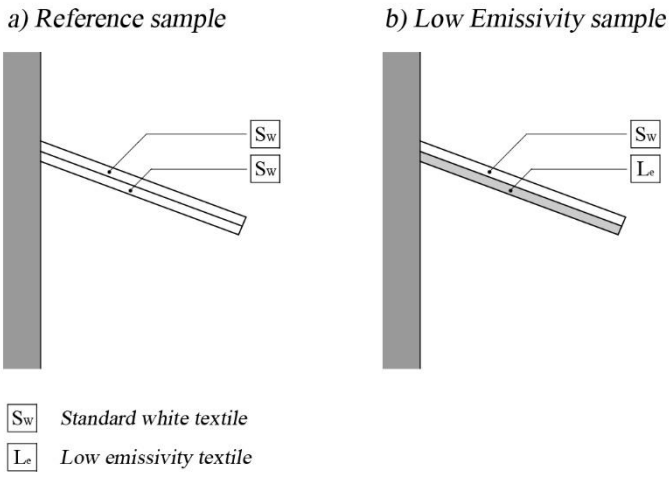


Figure 3: Composition of the tested awning samples: a) *Reference* sample; b) *Low Emissivity* sample.

Table 1: Solar and radiative features of the tested samples

Awning sample	Solar reflection [%]	Emissivity
Reference	76 *	0.87 **
Low Emissivity	76 *	0.87 ** (upward)
		0.35 * (downward)

Sources: * Data from textile materials' specification sheets; ** Emissivity measured by AE1 RD1 Emissometer D&S with Scaling Digital Voltmeter.

Experimental campaign

The experimental campaign was carried out in summer season, in August 2019, during the maximum solar irradiance conditions. It is widely known that in cooling dominated zones, in fact, summer is becoming increasingly critical for human thermal comfort conditions. Two tensile structure facilities have been installed at the University of Perugia (Italy). The site is located at 43°07'07"N, 12°21'20"E, at 300 m of elevation and the tested awnings were wall-mounted, with a southern exposure in order to avoid shading on the awnings. This allows to analyse the worse outdoor comfort conditions for pedestrians in summer.

Measures have been carried out on 9th, 10th, 12th, 13th, 14th of August 2019, from approximately 10 a.m. to 5 p.m., when the solar radiation was more intense. Both microclimate parameters and outdoor comfort conditions have been assessed, through a continuous microclimate monitoring. For this purpose, two identical thermal microclimate monitoring stations have been positioned under the two tensile structures and they are equipped with the following sensors: an omni-directional hot-wire probe, a temperature and relative humidity probe, a natural ventilation wet bulb probe and a globe thermometer, as shown in Fig. 4a and Fig. 4b. The globe thermometer probe was always shielded from direct solar radiation by the awning structure during all the microclimate monitoring, in order to avoid unreliable measured data.



Figure 4: a) Overview of the two tensile structures with thermal microclimate monitoring stations during the experimental campaign; b) Picture of one microclimate monitoring station, equipped with a temperature and relative humidity probe, a globe thermometer probe, an omni-directional hot-wire probe and a natural ventilation wet bulb probe.

As previously described, the following microclimate parameters which could affect thermal comfort have been monitored during the experimental campaign: wind speed [m/s], air temperature [°C], relative humidity [%], natural wet bulb temperature [°C], black globe temperature [°C], as depicted in Table 2. Therefore, Mean Radiant Temperature (MRT) and the Predicted Mean Vote (PMV) may be calculated. For the calculation of PMV comfort index, a clothing value of 0.5 and an activity level of a standing person sitting on a chair have been considered.

Table 2: Microclimate monitored parameters

Microclimate parameter	Probe	Measure unit
Wind speed	Omni-directional hot-wire probe	[m/s]
Air temperature	Temperature and relative humidity probe	[°C]
Relative humidity	Temperature and relative humidity probe	[%]
Natural wet bulb temperature	Natural ventilation wet bulb probe	[°C]
Black globe temperature	Globe thermometer probe	[°C]

Results and Discussion

Results of the experimental campaign are reported in graphs of Fig.5 and Fig.6, respectively in terms of Mean Radiant Temperature (MRT) and Predicted Mean Vote (PMV) for the 10th of August (similar results were obtained for the other measurement days). The red continuous line represents measurements collected under the *Reference* awning sample, while the blue one accounts for the *Low Emissivity* sample. The dotted lines are representative of the measurements' trend. For the 10th of August, the monitored microclimate parameters range of variation are reported in Table 3 and Table 4, for the *Reference* and *Low Emissivity* sample, respectively.

Table 3: Microclimate monitored parameters' ranges of variation for the *Reference* sample

Microclimate parameter	Range of variation	Measure unit
Wind speed	0.09 ÷ 4.45	[m/s]
Air temperature	32.4 ÷ 40.1	[°C]
Relative humidity	22.1 ÷ 44.8	[%]
Black globe temperature	36.9 ÷ 46.9	[°C]

Table 4: Microclimate monitored parameters' ranges of variation for the *Low Emissivity* sample

Microclimate parameter	Range of variation	Measure unit
Wind speed	0.03 ÷ 4.46	[m/s]
Air temperature	33.0 ÷ 40.6	[°C]
Relative humidity	21.3 ÷ 44.1	[%]
Black globe temperature	35.9 ÷ 45.5	[°C]

As shown in Fig.5, an average Mean Radiant Temperature reduction of 5.3 °C is achieved under the *Low Emissivity* awning sample with respect to the *Reference* one, with a maximum reduction of MRT of about 19.7 °C at 12:45 p.m. For what concerns PMV value (see Fig.6), the *Low Emissivity* sample provides for an average reduction of 0.4; furthermore, a maximum PMV difference of about 1.4 at 12:45 p.m. occurs.

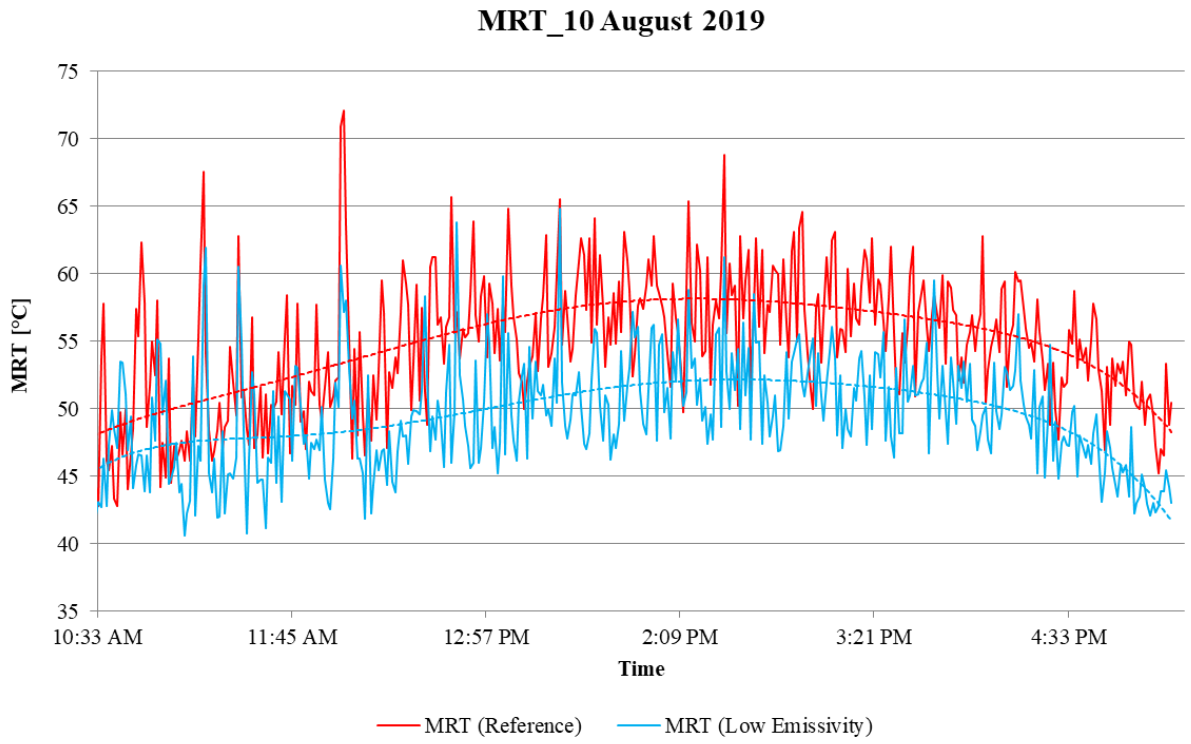


Figure 5: Mean radiant temperature (MRT) on 10th of August 2019 under the *Reference* sample and the *Low Emissivity* sample.

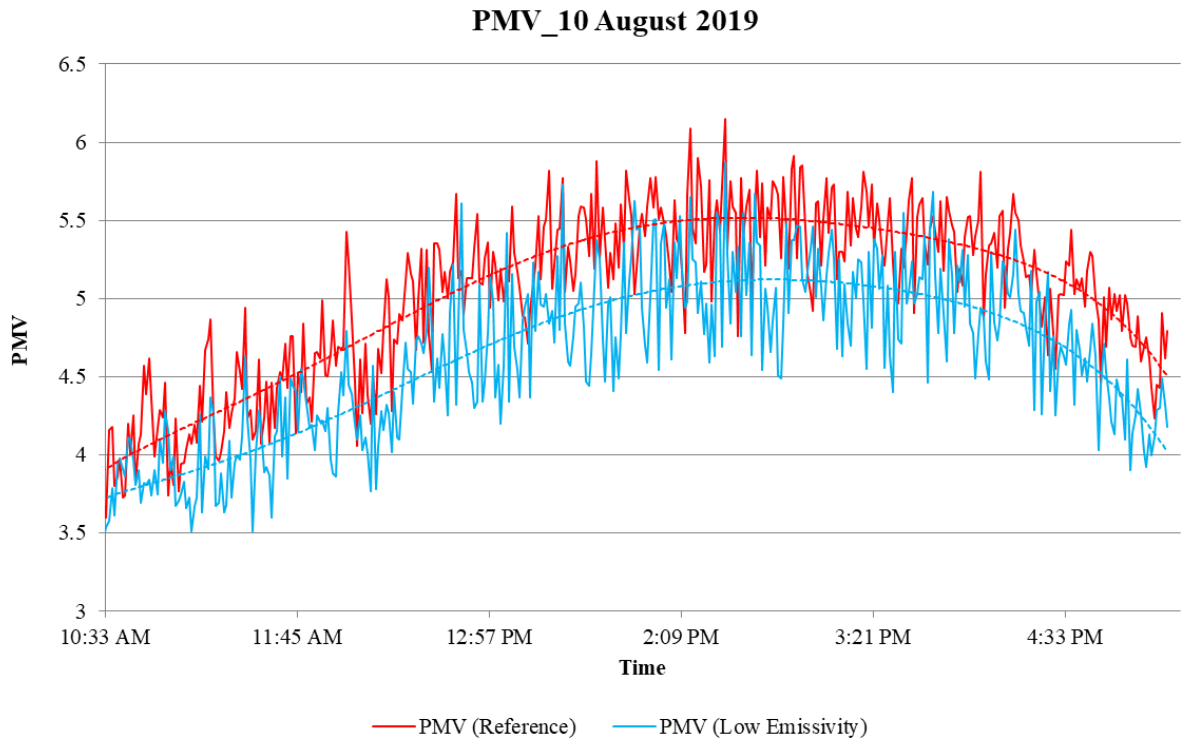


Figure 6: Predicted Mean Vote (PMV) on 10th of August 2019 under the *Reference* sample and the *Low Emissivity* sample.

Conclusions and Further Developments

In this work, a methodological approach for the evaluation of thermo-hygrometric comfort conditions of occupants under different awning typologies is presented. Possible comfort improvements due to the application of different materials for outdoor awnings have been assessed. Two textiles with different solar and radiative capabilities have been selected and tested: firstly, a traditional awning, with high albedo upwards and high emissivity downwards; then, an optimized solution, with high reflectivity upwards and low infrared emissivity downwards. Occupants' thermal comfort under the two different textiles has been assessed, in order to define suitable materials for outdoor awning applications. Experimental results verified that an awning solution characterized by low emissivity downward could highly improve the thermal comfort under the covering: maximum reductions of about 20°C in terms of mean radiant temperature and 1.4 in terms of PMV were determined. This study could positively contribute to reduce pedestrians' thermal discomfort in dense urban environments, also leading to the mitigation of urban microclimate and Urban Heat Island phenomenon. Future developments will concern the correlation of the monitored microclimate parameters with climate data collected by a nearby weather station, e.g. direct and global solar radiation, wind speed and wind direction. It might be also interesting to analyse different comfort indexes, such as Wet Bulb Globe Temperature when solar radiation occurs (WBGT outdoor). Finally, further research efforts could also involve the application of retro-reflective materials for outdoor awnings, in order to evaluate possible achievable benefits in terms of outdoor thermal comfort improvement under the coverings.

Acknowledgments

The authors would like to thank Solaris Tende srl company, which provided the awning samples for the experimental campaign.

References

Castellani, B., E. Morini, E. Anderini, M. Filipponi, F. Rossi. 2017. "Development and characterization of retro-reflective colored tiles for advanced building skins". *Energy and Buildings* 154: 513-522.

Givoni, B., M. Noguchi, H. Saaroni, O. Pochter, Y. Yaacov, N. Feller, S. Becker. 2003. "Outdoor comfort research issues". *Energy and Buildings* 35: 77-86.

Morini, E., B. Castellani, A. Presciutti, M. Filipponi, A. Nicolini, F. Rossi. 2017. "Optic-energy performance improvement of exterior paints for buildings". *Energy and Buildings* 139: 690-701.

Nikolopoulou, M., N. Baker, K. Steemers. 2001. "Thermal comfort in outdoor urban spaces: understanding the human parameter". Solar Energy, 70: 227-235.

Nikolopoulou, M., K. Steemers. 2003. "Thermal comfort and psychological adaptation as a guide for designing urban spaces". *Energy Building* 35: 95–101.

Oke, T.R. 1995. "The Heat Island of the Urban Boundary Layer: Characteristics, Causes and Effects". In: Cermak J.E., Davenport A.G., Plate E.J., Viegas D.X. (eds) Wind Climate in Cities. NATO ASI Series (Series E: Applied Sciences), vol 277. Springer, Dordrecht

Pisello, A.L., M. Saliari, K. Vasilakopoulou, S. Hadad, M. Santamouris. 2018. "Facing the urban overheating: Recent developments. Mitigation potential and sensitivity of the main technologies." *WIREs Energy and Environment* 7: e294. https://doi.org/10.1002/wene.294

Rossi, F., E. Anderini, B. Castellani, A. Nicolini, E. Morini. 2015a. "Integrated improvement of occupants' comfort in urban areas during outdoor events". *Building and Environment* 93: 285-292.

Rossi, F., B. Castellani, A. Presciutti, E. Morini, M. Filipponi, A. Nicolini, M. Santamouris. 2015b. "Retroreflective façades for urban heat island mitigation: Experimental investigation and energy evaluations". *Applied Energy* 145: 8-20.

Spagnolo, J., R. de Dear. 2003. "A field study of thermal comfort in outdoor and semi-outdoor environments in subtropical Sydney Australia". Building and Environment 38: 721-738.

Swaid, H., M. Bar-El, M.E. Hoffman. 1993. "A bioclimatic design methodology for urban outdoor spaces". Theoretical and Applied Climatology 48: 49-61.

Local scale climate change assessment for preservation of cultural heritage sites and their resilience, the case study of Gubbio medieval city in Italy

Benedetta Pioppi, CIRIAF Interuniversity research centre on pollution and environment Mauro Felli, (Italy)
Ilaria Pigliautile, CIRIAF Interuniversity research centre on pollution and environment Mauro Felli, (Italy)
Cristina Piselli, University of Perugia, (Italy)
Anna Laura Pisello[1], University of Perugia, (Italy)
Franco Cotana, University of Perugia (Italy)

ABSTRACT

Climate change related events have demonstrated to massively compromise citizens' wellbeing in urban environments but, at the same time, they may represent too severe boundary conditions affecting cultural heritage (CH) preservation and their attractiveness for tourists. These aspects may be considered when assessing CH resilience to climate change because local overheating phenomena are responsible for CH damaging, conservation issues and, at the same time, their appeal for tourists. In this study, an extensive experimental field monitoring and CFD modelling is carried out in the area of the historical site of Gubbio (Italy), which is affected by massive overheated summer days, exacerbated by climate change related forcing. Field monitoring is carried out by means of wearable microclimate stations in order to better describe the boundary conditions of pedestrian citizens. All these data were specifically analyzed aimed at characterizing local microclimate peculiarities, CH preservation issues and to calibrate CFD models. Finally, the analysis of both experimental and simulated results was carried out demonstrating the serious threat compromising CH resilience in terms of its suitability to host tourists during summer time, as typically happens for social-cultural purpose and economic sustainability of the sites.

Introduction

Extreme weather events such as heat waves, droughts, floods, landslides, cyclones and heavy precipitations are foreseen to be more frequent and more intense in the next future because of the on-going process of climate change. At the same time, the continuous growth of urban population, predicted to rise till 68% of the world population by 2050, and the consequent high rate of urbanization produces a progressively land cover and usage modification(UN DESA, 2018). These changes lead to an increase of air temperature in urban areas with respect to rural surroundings defined as the Urban Heat Island (UHI) phenomenon. Moreover, recent studies demonstrated the existing synergy between Urban Heat Island and heat waves frequency and duration (Li & Bou-Zeid, 2013). This urban overheating has multiple impacts on buildings' energy consumption (Huang & Gurney, 2017), urban air quality (Castaldo, Pisello, Pigliautile, Piselli, &

[1]Corresponding Author: [anna.pisello@unipg.it].

Cotana, 2017), human health (Liu et al., 2019), and more in general citizens' well-being and life quality (Chen & Ng, 2012). Furthermore, tourism, recreation and outdoor activities are strongly influenced by climate condition and hence strongly deterred by urban overheating and climate change related events. Human well-being is considered fundamental in order to manage tourist flows and dwellers activities. For example, Abed et al. demonstrated the role of thermal well-being on potential tourism in Algeria (Abed & Matzarakis, 2018). As matter of fact outdoor thermal comfort is tackled by researchers for decades (Rashidi, Stadelmann, & Patt, 2019), most of them focusing on the definition of practical indexes to evaluate outdoor thermal perception (Potchter, Cohen, Lin, & Matzarakis, 2018). A huge effort has been done by the scientific community also to identify and implement Urban Heat Island mitigation strategies and climate change adaptation techniques. Innovative materials characterized by high solar reflectance and thermal emittance reveal to be very effective to mitigate Urban Heat Island as well as the implementation of materials able to store and release thermal energy shifted in time, i.e. phase change materials. Moreover, the combination of such strategies with greenery implementation improve the mitigation potential and decrease air temperature up to 3.5 °C with a consequent improvement of human outdoor thermal comfort (Shahidan, Jones, Gwilliam, & Salleh, 2012). However, historical urban context presents several constraints, i.e. architectural modification, related to its cultural value presentation that prevent the application of the such mitigation strategies (Castaldo, Rosso, et al., 2017). Nevertheless, historic cities' structures depend on demographic and climatic conditions which are no more representative of the existing ones; therefore, climate change effects are more exacerbated in historical contexts and it is of primary importance to develop climate resilient plan to preserve the cultural heritage and city centers livability.

Built upon the outlined research background, the current work presents an innovative methodology coupling (i) experimental monitoring and (ii) numerical modeling to assess site-specific microclimatic conditions potentially critical for heritage site resilience and dwellers/tourists' wellbeing in actual and future scenarios according to climate change predictions. The experimental campaign integrates a novel wearable monitoring system focused on the pedestrian perspective with more classical monitoring set-up, i.e. fixed weather station and stand-alone thermo-hygrometer probes. This approach allows to investigate urban microclimate at different scales. Moreover, data collected by fix systems are used to calibrate and validate the developed microclimate numerical model. The proposed method is applied to the case study of Gubbio historic center (Italy). The Medieval hilly town is representative of dense historical cities where the implementation of common Urban Heat Island mitigation techniques is compromised.

Methodology

Field monitoring

Microclimate variability is analyzed by means of different techniques in order to investigate the phenomenon at different scales. In particular, the monitoring set-up includes: (i) a fixed weather station, (ii) two stand-alone thermohygrometer probes, and (iii) an innovative wearable environmental monitoring system specifically developed by the authors (Pigliautile & Pisello, 2018). Figure 1 shows spatial distribution of the presented set-up within the case study of this work. The fixed weather station is in a green open field area at the bottom of the town historic center and it provides air temperature and relative humidity long term profiles.

Two thermo-hygrometers are installed close to the main touristic areas: one is placed in the main square of the city center, while the other one is located just outside the ancient town wall,

along a popular footpath. They are adopted to get more punctual and site-specific values of air temperature and relative humidity.

Finally, the main environmental parameters, i.e. air temperature, relative humidity, wind speed and direction, solar irradiance and CO_2 concentration, are investigated along the dashed line in Figure 1 during a single monitoring day by means of an innovative wearable miniaturized system (Pigliautile & Pisello, 2018). The chosen day is selected during a heat wave to be representative of extreme weather conditions in summer, i.e. August 2nd. The monitoring pathway is planned taking into account specific characteristics of the case study in terms of (i) urban geometry, (ii) canyons orientation, (iii) anthropogenic sources, and (iv) greenery. It is repeated three times to get also the temporal variation of the monitored environmental parameters. On the other hand, each single pathway is covered in less than one hour to assume no time dependency for the environmental parameters' fluctuations observed in a single route.

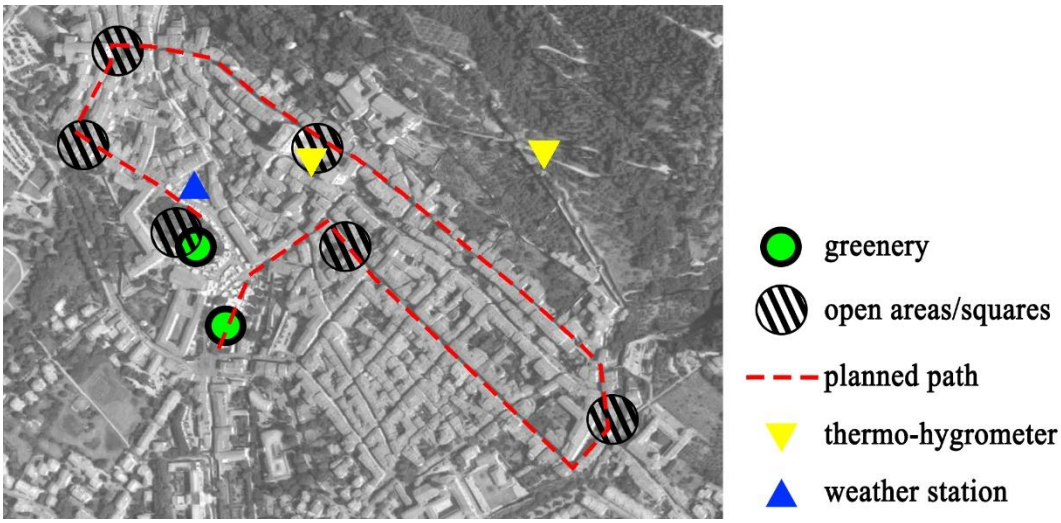


Figure 1. Site location of the fixed weather station, the two thermos-hygrometers and route covered by the wearable system

Numerical microclimate modeling and future scenarios predictions

The numerical analysis moves from the experimental campaign in order to extend in time the microclimate mapping of the analyzed area. The numerical simulations are performed by means of ENVI-met tool, a three-dimensional non-hydrostatic engine particularly suitable to simulate microclimatic and physical behavior of urban and rural spaces (Salata, Golasi, de Lieto Vollaro, & de Lieto Vollaro, 2016) due to a combination of high spatial and temporal resolutions. The spatial resolution adopted in the present study is 2 m units for both horizontal and vertical grids, and to reproduce the ground slope of the modeled area a specific digital elevation model is necessarily developed. Finally, to faithfully reproduce the case study area, tailored materials are created. The model is than calibrated setting data collected by the fixed weather station, i.e. air temperature and relative humidity hourly profiles and daily wind speed and prevalent direction, as input weather forces for the numerical simulation of a single day. The simulation starts at night-time, when turbulence conditions are weaker, and lasts 48 hours with a time step of 1 s to avoid turbulence issues and increase model outputs accuracy (Salata et al., 2016). The air temperature simulation outcomes and the air temperature values gathered by a single small probe are compared

to calculate calibration indexes, i.e. the Mean Bias Error (MBE) and the Root Mean Square Error (RMSE). Once validated, the microclimate model is tested under four weather forces generated for the specific location of the case study according to the worst IPCC scenario, i.e. A2 scenario, by means of Meteonorm tool. Such a tool consists of a meteorological and climatological database able to (i) generate representative typical year for any places on the Earth and (ii) simulate future climate change scenarios according to IPCC forecasts (Remund, Müller, Schilter, & Rihm, 2010).

In particular, the four weather forces adopted to investigate the impact of climate change on the next future include:

- a past reference scenario, which considers two distinctive periods for irradiance and air temperature profile definitions, i.e. from 1991 to 2010 and from 2000 to 2009 respectively;
- three projected years, i.e. 2020, 2050, and 2100.

A typical summer day is selected and simulated for each analysed year since summer is the most critical season in terms of human comfort and overheating impacts on tourism. The outcomes are then computed to evaluate the human thermal perception through two recognized thermal indexes, i.e. Physiological Equivalent Temperature (PET) and Apparent Temperature (AT). The PET is based on the Munich energy balance model for individuals (MEMI) (PR, 1999), which considers all the basic thermoregulatory processes of the human body. It is calculated by means of Rayman model (Matzarakis, Rutz, & Mayer, 2006)for a standard man of 35 years old, 1.75 m height and 75 kg weight, wearing clothing of 0.5 clo and walking, i.e. 2.5 met. The computed apparent temperature is calculated as combination of detected air temperature (°C), relative humidity (%) and wind speed (m/s).

Description of the case study

The proposed methodology is applied to the historic city of Gubbio, which is an ancient hilly town in the central Italy. Its urban configuration is characterized by narrow urban canyons, i.e. aspect ratio varying between 1.0 and 0.3, and the main building materials are stones and bricks. According to the Koppen and Geiger classification (Kottek, Grieser, Beck, Rudolf, & Rubel, 2006), its climate is classified as *Cfb*, which means mild temperate, fully humid with warm summer.

The current research work focuses the attention on the main touristic area of the city, i.e. Palazzo dei Consoli area, in order to assess cultural heritage resilience in terms of managing tourists flow and recreational activities, strongly influenced by the outdoor thermal comfort condition.

Results

Microclimate field analysis

According to the described method, in Figure 2 the air temperature and relative humidity trends collected during a summer heat wave by the fixed weather station, the two small probes and the wearable dynamic monitoring system are reported. In detail, the recorded data of the two small-probes show similar relative humidity profiles, i.e. maximum differences of 9.9% with an average daily fluctuation of 40.1%, while a significant deviation is shown between daily maximum detected air temperature, i.e. 3.7°C of maximum difference between air temperature profile of the

ancient town walls with respect to the profile got in the historic center. This is mainly imputable to the relationship between site specific urban morphology and microclimate conditions, which are deeply investigated through the tailored monitoring campaign by means the wearable system. The results of the performed dynamic monitoring campaigns are summarized in Figure 2 through the route averages and standard deviations of air temperature and relative humidity observations. Data collected at pedestrian level follow the daily trend continuously monitored by the fix probes. Moreover, data collected through the wearable system allow to deeply investigate the microclimate spatial variability just presented only for two areas of the monitored case study through the analysis of the two fix thermo-hygrometer collected profiles.

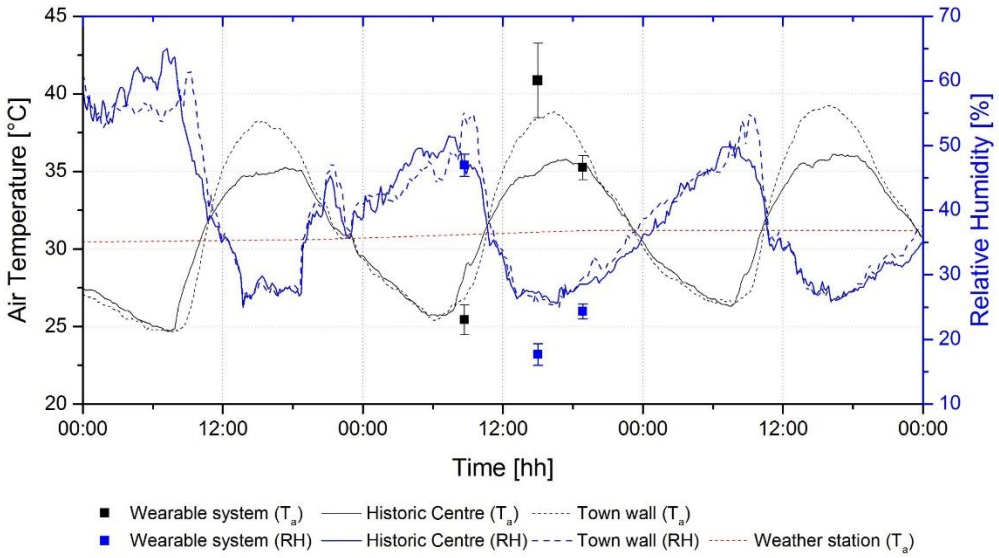


Figure 2. Data collected by different systems adopted for the monitoring campaign from August 1st to August 4th.

Switching from the canopy layer to pedestrian height, it is possible to investigate the influence of the morphological characteristics of an historical hilly town, i.e. different orientation and aspect ratio of canyons, presence or absence of greenery, and direct solar availability, on the microclimate variation and pedestrian thermal perception. Therefore, the collected data are used to evaluate the human thermal comfort in outdoors by computing the apparent temperature in order to manage tourism and outdoor recreation activities. More specific analysis on human comfort mapping is given in the following subsection.

Human outdoor comfort, actual spatial analysis. To effectively investigate the human thermal comfort, the apparent temperature is computed from air temperature, relative humidity, and wind speed data collected by means of the wearable system during the monitoring campaign. Solar irradiance is not taken into account for the air temperature correction into the perceived temperature. Nevertheless, radiative exchanges occurring between the pedestrian and the environment highly impact human comfort perception. Therefore, both the computed apparent temperature and the detected solar irradiance are analysed to assess actual thermal comfort condition for the pedestrian.

Figure 3 shows the apparent temperature obtained during the three representative moments of the day, i.e.8.00 am, 12.00 pm, 4.00 pm, and the solar irradiance gathered at the same instant.

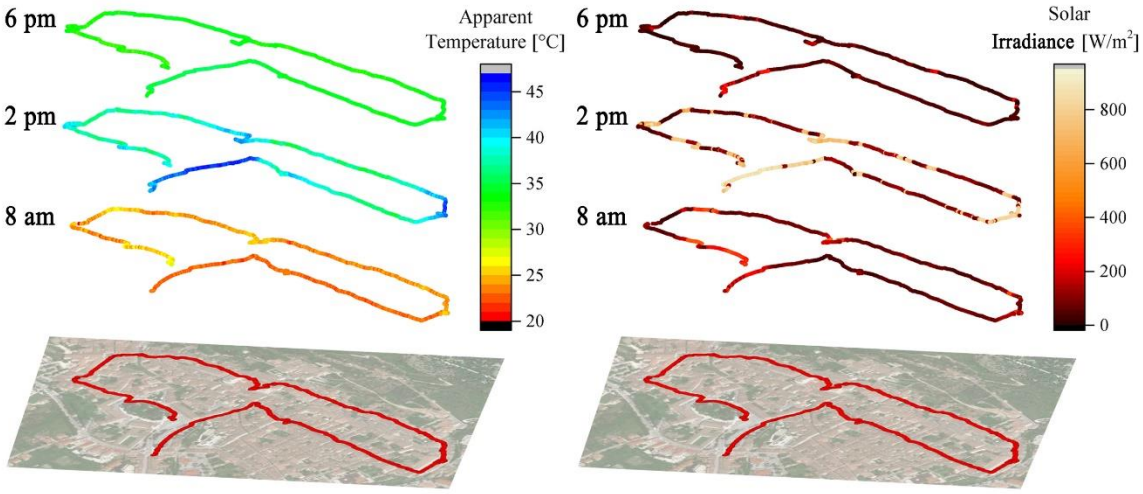


Figure 3. Apparent temperature and solar irradiance maps obtained by means experimental wearable campaign at 8.00 a.m., 2.00 p.m. and 6 p.m.

The apparent temperature values increase during the day according to the detected solar irradiance trends. The influence of the intra-urban morphology is clearly detectable in the apparent temperature map at 8 a.m., when it fluctuates between 20.1 and 26.8°C. The highest values of both apparent temperature and solar irradiance are gained crossing the most open areas on the route, i.e. areas with the greatest sky view factor. 2 p.m. is the worst moment of the day for tourist and/or dwellers and in general for outdoors activities. This is tangible especially along the North-East and South-West oriented canyons where the apparent temperature reaches value up to 46.7°C, and the measured solar irradiance is around 800 W/m^2. On the other hand, at 6 p.m. the apparent temperature distribution seems to be more homogeneous in line with the solar irradiance trend, which presents a general decrease at 6 p.m.

Numerical microclimate model, validation and simulation of future scenarios

After a preliminary phase of model calibration, the model is considered validated once obtained values of MBE and RMSE equal to 0.8°C and 0.7°C respectively, which are acceptable according to the last decade literature (Salata et al., 2016).
Weather forces of a typical summer day for each year of interest, i.e. reference past, 2020, 2050, and 2100, are used as input for the model simulation. The outcomes are analysed in terms (ii) environmental parameters distribution and time-trend and (ii) human thermal comfort. Therefore, the main environmental parameters considered are air temperature and relative humidity and they are analysed in terms of difference between the forecasted future scenarios, i.e. 2020, 2050, and 2100, and the reference one at three time of the day, i.e. 8 a.m., 12 p.m., 4 p.m. In terms of air temperature, a linear overheating trend is depicted from the reference scenario to the 2100; on the contrary a nonlinear trend is expected from the reference scenario to the furthest future one in relative humidity. More in detail, the maximum increase in air temperature average is expected in summer 2100, i.e. 3.6°C at 12.00 p.m. As well as the maximum relative humidity deviation is expected in the same year, i.e. 2100, equal to 15% at 8.00 a.m. This singular behavior highlights the tropical-like increasing climate trend of the case study area, which makes this analysis even

more urgent with the purpose to identify the cultural heritage resilience to climate change related events.

Human outdoor comfort, future spatial analysis. Figure 4 shows plots of the calculated physiological equivalent temperature (PET) and apparent temperature (AT) for all the simulated summer days dealing with a space varying representation. The reported outcomes are referred to 4 p.m. which is the most critical moment of the day.

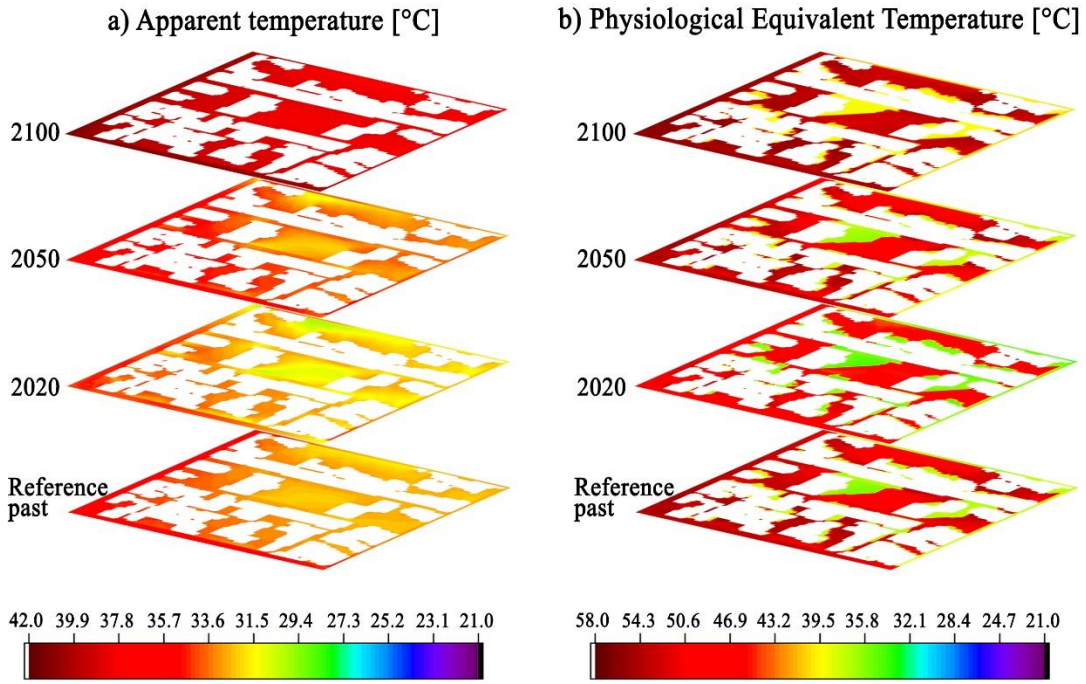


Figure 4. Spatial distribution of apparent temperature (a) and physiological equivalent temperature (b) for all the simulated summer days, i.e. reference past, 2020,2050,2100 at 4.00 p.m.

From the past to the future 2100 a linear increasing trend of both the AT and PET is depicted. Therefore, 2100 is expected to be the most hazardous year in terms of overheating risk for tourists/dwellers approaching urban outdoors. The apparent temperature outcomes show a spatially no-uniform distribution. Focusing the attention on the main square of the case study area, it seems to be the least risky area in terms of human thermal comfort. Even thought, an increase in apparent temperature values of 15.0°C is clearly visible from 2020 and 2100 scenario. In detail the values of apparent temperature expected in 2020 are around 32.5°C, while in 2100 values of 42.0°C are foreseen. This means a high thermal stress that heavy influences the city attractiveness for tourists. However, the formula used to compute the apparent temperature neglects the direct global radiation contribution; hence to have more realist thermal sensation forecast the PET index is also analyzed. In fact, PET considers all the thermoregulatory processes of the human body energy balance and it can be considered more faithful to the human perception. As matter of fact, the obtained PET is generally higher than the apparent temperature and clearly identifies comfort benefits due to shadowing effect.

Conclusions

Climate change related events hugely impact environment, cities and society, especially in terms of human well-being and in cultural heritage resilience. In this view, the scientific community has deeply investigated climate change related phenomena, i.e. UHI and overheating risk, and human thermal perception in outdoors by means of direct and rational thermal indexes, e.g. apparent temperature and Physiologically Equivalent Temperature (PET), to identify promising mitigation strategies. Even though, most of them are revealed to be effective, but often inapplicable in historical sites, due to the historical preservation constraints.

The current work presents an innovative methodology aiming to evaluate and forecast historical urban outdoor condition, that are fundamental to identify outdoor thermal criticalities strongly influencing the economic sustainability and the urban city cultural heritage resilience.

In detail the outlined methods couples (i) multi-scale experimental monitoring and (ii) microclimate modelling to characterize complex heterogeneous urban environment. The main novelty of such methodology consists of the integration of an innovative monitoring technique able to detect the pedestrian perspective, which is fundamental to assess human outdoor condition in overheated summer days, with classic monitoring tools used to calibrate microclimate model. In order to simulate future climate change, a tailored microclimate model is realized faithfully to the reality and calibrated though the small probe data. Moreover, four climate change forecast scenario, i.e. reference past, 2020, 2050, and 2100, are created according to the A2 scenario depicted by the IPCC and used as weather forcing to run the microclimate simulation of the modeled area. Since summer is considered the most problematic season in terms of human well-being, the outcomes are referred to selected summer days for each scenario. Current human thermal perception is given by apparent temperature computation from environmental data directly collected through the wearable innovative system, while the numerical simulations' outputs are used to foreseen the future values of both apparent temperature and PET. The proposed methodology is applied to Gubbio historical city center, in central Italy. The field monitoring results show the microclimate variation in accordance with site-specific peculiarities. Moreover, future weather forecast scenarios show, from the past to the future 2100, a linear overheating trend in terms of air temperature and a non-linear trend of relative humidity, i.e. foreseen tropicalization of the case study area. In addition, a linear increment of human thermal discomfort expressed by both computed indexes is depicted from the past to the future 2100, which is expected to be the most hazardous year.

The described methodology has a wide replicability in historical sites and could help local policymakers in managing the site considering tourist flows and local citizens' well-being enhancement.

Acknowledgements

Acknowledgements are due to the European Union's Horizon 2020 program under grant agreement No 678407 (ZERO-PLUS). This work has received funding from the European Union Horizon 2020 Programme in the framework of the "HERACLES" project under grant agreement n° 700395. Additionally, the first author is supported by Ministry funding and university funding of the PhD school in Energy and Sustainable Development.

References

Abed, S. S., & Matzarakis, A. (2018). Quantification of the Tourism Climate of Algeria based on the climate-tourism-information-scheme. *Atmosphere*, *9*(7). https://doi.org/10.3390/atmos9070250

Castaldo, V. L., Pisello, A. L., Pigliautile, I., Piselli, C., & Cotana, F. (2017). Microclimate and air quality investigation in historic hilly urban areas: Experimental and numerical investigation in central Italy. *Sustainable Cities and Society*, *33*. https://doi.org/10.1016/j.scs.2017.05.017

Castaldo, V. L., Rosso, F., Golasi, I., Piselli, C., Salata, F., Pisello, A. L., … De Lieto Vollaro, A. (2017). Thermal comfort in the historical urban canyon: The effect of innovative materials. In *Energy Procedia* (Vol. 134, pp. 151–160). https://doi.org/10.1016/j.egypro.2017.09.553

Chen, L., & Ng, E. (2012). Outdoor thermal comfort and outdoor activities: A review of research in the past decade. *Cities*, *29*(2), 118–125. https://doi.org/10.1016/j.cities.2011.08.006

Huang, J., & Gurney, K. R. (2017). Impact of climate change on U.S. building energy demand: Financial implications for consumers and energy suppliers. *Energy and Buildings*, *139*, 747–754. https://doi.org/10.1016/j.enbuild.2017.01.077

Kottek, M., Grieser, J., Beck, C., Rudolf, B., & Rubel, F. (2006). World map of the Köppen-Geiger climate classification updated. *Meteorologische Zeitschrift*, *15*(3), 259–263. https://doi.org/10.1127/0941-2948/2006/0130

Li, D., & Bou-Zeid, E. (2013). Synergistic interactions between urban heat islands and heat waves: The impact in cities is larger than the sum of its parts. *Journal of Applied Meteorology and Climatology*, *52*(9), 2051–2064. https://doi.org/10.1175/JAMC-D-13-02.1

Liu, T., Ren, Z., Zhang, Y., Feng, B., Lin, H., Xiao, J., … Ma, W. (2019). Modification effects of population expansion, ageing, and adaptation on heat-related mortality risks under different climate change scenarios in Guangzhou, China. *International Journal of Environmental Research and Public Health*, *16*(3). https://doi.org/10.3390/ijerph16030376

Matzarakis, A., Rutz, F., & Mayer, H. (2006). Modelling the thermal bioclimate in urban areas with the RayMan Model. *Energy*, *6–8*.

Pigliautile, I., & Pisello, A. L. (2018). A new wearable monitoring system for investigating pedestrians' environmental conditions: Development of the experimental tool and start-up findings. *Science of the Total Environment*, *630*. https://doi.org/10.1016/j.scitotenv.2018.02.208

Potchter, O., Cohen, P., Lin, T.-P., & Matzarakis, A. (2018). Outdoor human thermal perception in various climates: A comprehensive review of approaches, methods and quantification. *Science of the Total Environment*, *631–632*, 390–406. https://doi.org/10.1016/j.scitotenv.2018.02.276

PR, H. (1999). The physiological equivalent temperature - A universal index for the biometeorological assessment of the thermal environment. *International Journal of Biometeorology*, *43*(2), 71–75. https://doi.org/10.1007/s004840050118

Rashidi, K., Stadelmann, M., & Patt, A. (2019). Creditworthiness and climate: Identifying a hidden financial co-benefit of municipal climate adaptation and mitigation policies. *Energy Research and Social Science*, *48*(October 2018), 131–138. https://doi.org/10.1016/j.erss.2018.09.021

Remund, J., Müller, S. C., Schilter, C., & Rihm, B. (2010). The use of Meteonorm weather generator for climate change studies. *10th EMS Annual Meeting, 10th European Conference on Applications of Meteorology (ECAM) Abstracts, Held Sept. 13-17, 2010 in Zürich,*

Switzerland. Http://Meetings.Copernicus.Org/Ems2010/, Id.EMS2010-417. Retrieved from http://adsabs.harvard.edu/abs/2010ems..confE.417R

Salata, F., Golasi, I., de Lieto Vollaro, R., & de Lieto Vollaro, A. (2016). Urban microclimate and outdoor thermal comfort. A proper procedure to fit ENVI-met simulation outputs to experimental data. *Sustainable Cities and Society*, *26*, 318–343. https://doi.org/10.1016/j.scs.2016.07.005

Shahidan, M. F., Jones, P. J., Gwilliam, J., & Salleh, E. (2012). An evaluation of outdoor and building environment cooling achieved through combination modification of trees with ground materials. *Building and Environment*, *58*, 245–257. https://doi.org/10.1016/j.buildenv.2012.07.012

UN DESA. (2018). *2018 Revision of World Urbanization Prospects*. Retrieved from https://esa.un.org/unpd/wup/

Effectiveness of UHI mitigation strategies for outdoor thermal comfort enhancement

Ilaria Pigliautile, University of Perugia (Italy)
Anna Laura Pisello[1], University of Perugia (Italy)
Elie Bou-Zeid, Princeton University (NJ, USA)

ABSTRACT

Cities morphology and urban fabric characteristics modify energy balances in urban areas leading to the well-known phenomenon of the Urban Heat Island. This characteristic of the urban microclimate has several negative consequences including a worsening of citizens' well-being and life quality. Thermal comfort in outdoors is one aspect of citizens' life that is degraded by the UHI. The current work approaches thermal comfort investigation through numerical simulations. A parametrized human physiology is introduced in the Princeton Urban Canopy Model (PUCM), which captures the effect of greenery and different materials on the urban environment. Human comfort is given in terms of computed skin temperature and six different scenarios are simulated to assess the effect of common UHI mitigation techniques, i.e. application of cool materials and introduction of trees, on pedestrians' thermal perception during a hot summer week in Princeton. Results are critically analyzed and an accurate investigation of mitigation strategies' impact on each term of the simplified human energy budget is given.

Introduction

The current century has witnessed a rapid growth of the urban environment, and the urban population is predicted to be the 60% of the entire world population in 2030 (UN DESA, 2018). Cities' structure and materials impact the energy balance of the atmosphere in their proximity, producing the well-known phenomenon of the Urban Heat Island (UHI). The UHI mainly consists of higher air temperatures observed in urban areas with respect to air temperature monitored in rural surroundings. The phenomenon has several negative consequences affecting (i) buildings' energy consumption (Santamouris, 2014), (ii) urban air quality (Harlan & Ruddell, 2011), and (iii) citizens' health and life quality (Chen & Ng, 2012). Moreover, the on-going process of global climate change causes more frequent and more intense extreme weather events, such as heat waves, that act in synergy with the UHI to compromise human health even more (Zhao et al., 2018). Therefore, a huge effort of the scientific community has been devoted to find countermeasures to the UHI phenomenon in the last decades (Akbari & Kolokotsa, 2016). Nowadays, the most common UHI mitigation strategies concern the implementation of cool materials and the introduction of greenery in the urban environment. In the first case, treated urban surfaces reflect a large amount of the incoming shortwave radiation keeping urban surfaces "cooler". Potential of cool roofs in reducing heat-related mortality due to UHI during heatwaves up to a 25% is demonstrated in (Macintyre & Heaviside, 2019). Rosso at al. also proposed innovative "cool" materials suitable for historical contexts where aesthetical constrains could limit the applicability of this mitigation technique (Rosso et al., 2018).

[1] Corresponding Author: [anna.pisello@unipg.it].

On the other hand, implementation of greenery or permeable surfaces contributes to reduce UHI by means of evapotranspiration and the increase of latent exchanges in the urban energy balance (Dai, Guldmann, & Hu, 2019).

The effectiveness of UHI mitigation strategies has been investigated both experimentally and through numerical simulations. In particular, Urban Canopy Models (UCM) are numerical schemes that solve the energy balance of a geometrically simplified urban canyon assumed as representative of the local urban environment (e.g. at neighborhood scale). UCMs are mainly coupled with mesoscale atmospheric models such as the Weather Research Forecasting model (WRF), where the surface properties can be varied at the same resolution as the atmospheric component (Li & Bou-Zeid, 2014). Such up-scaling procedure allows to investigate the UHI phenomenon, and how it is coupled to weather extremes and global climate change. These analyses could be used by policymakers in order to propose effective strategies able to reduce negative effects of the UHI in a long-time perspective. Nevertheless, UCMs do not generally include the pedestrian perspective. Few studies adopt UCM to provide information concerning human outdoor thermal comfort even if it is a key issue to guarantee good life quality for citizens. For example, Morris et al. analyze outdoor thermal discomfort in outdoors in relation to urban parameters coupling WRF 3.5.1 and a UCM (Morris et al., 2017). In particular, they quantify thermal discomfort by means of direct comfort indexes without consider human physiology or human energy balance (Coccolo, Kämpf, Scartezzini, & Pearlmutter, 2016).

The current work implements a simplified human body physiology within the Princeton UCM (Wang, Bou-Zeid, & Smith, 2013) with the final aim to present a more complete tool able to show the effect of possible alternative scenarios not only in terms of air temperature variation, but also in terms of pedestrians' well-being. In particular, the implemented model is a single-mass model with constant core temperature and a thin outer skin shell with no thermal inertia. The computed skin temperature is assumed as thermal stress indicator within the parameterized urban context. The model is therefore tested in six different configurations of a defined urban canyon, i.e. fix canyon location, orientation, and geometrical characteristics. The designed configurations include the application of cool finishing on canyon walls and/or ground and the introduction of trees in the canyon section. Some of the most common UHI mitigations techniques are therefore numerically tested in terms of human comfort and a critical analysis of the produced alterations of each human energy balance component is given.

Methodology

Human body parametrization

The human comfort is assessed by introducing a simplified human body model in the Princeton UCM (PUCM). The developed code takes into account human body position within the urban canyon and computes the outer skin temperature of the pedestrian modelled as a single-mass with a constant core temperature and a skin shell with insignificant thermal inertia. The latest assumption can be considered accurate if the outer skin is conceptualized as a very thin interfacial layer. Under this thin layer, there exists a layer of constant thickness of 2 cm where the temperature varies linearly between the core value and the outer skin value. The 2 cm thickness is selected since the authors find that it yields a reliable fluctuation of the thermal comfort indicator, i.e. skin temperature, during a first phase of model robustness check.

The simplified energy balance of the human outer skin is given by the sum of the energy fluxes exchanged between the pedestrian and the surrounding urban environment (all in W/m^2) as shown by the following equation:

$$R + C + K + E_{sk} = 0 \quad (1)$$

Where each single term of Eq.(1) represent a component of the balance as follows:

- *R* is the radiative exchange; it comprises the balance between incoming and outgoing longwave, shortwave direct, and shortwave diffuse radiation with respect to the pedestrian. The incoming solar radiation is weighted by the exposed human body fraction to get the incoming shortwave component. The exposed body fraction is geometrically computed assuming the human body as a cylinder of 1.8 m height with a total surface of 2 m^2 according to the method already proposed by Ryu et al. in (Ryu, Bou-Zeid, Wang, & Smith, 2016). The incoming diffuse shortwave is computed considering multiple Labertian reflections of the sunrays off the canyon's walls and ground up to two times. The longwave budget comprises both the radiation emitted by surrounding surfaces and the measured radiation incoming from the sky while the re-emitted longwave component is function of the fourth power of the polynomial unknown, i.e. skin temperature (T_{sk}). Computed fraction of radiation reaching the human body are thus multiplied for human skin absorption coefficient settled equal to 0.7 and 0.9 for the short- and long-wave radiation respectively (Kenny, Warland, Brown, & Gillespie, 2008).
- *C* is the convective exchange; it depends on wind speed and temperature difference between the air and the outer skin surface.
- *K* is the conductive exchange; it is the energy flux occurring through the 2 cm outer layer due to temperature differentials between the outer skin surface and the body core which is set as constant and equal to 36.6°C.
- *E* is the evaporative exchange; it is an always negative component of the human budget and it sums up the latent heat lost through the skin by diffusion and the latent heat lost due to regulatory sweating. The evaporative exchange due to diffusion depends on environmental conditions and skin temperature while sweat production is function of skin temperature divergence from its value in comfortable condition settled equal to 34.1°C.

The human energy balance is solved as a 4th order polynomial for T_{sk}, i.e. skin temperature, every 1 s to capture the fast response of the human body to external stimuli. As to be pointed out that the simplified code presented in this work accounts impact of clothing on human energy balance only in the convective and evaporative terms while it does not consider clothing in radiative exchanges.

Simulated scenarios

In order to assess potential benefits of common UHI mitigation strategies in terms of human comfort, six different scenarios are modelled. The human body is positioned at the center of the modelled canyon, which is North-East/South-West oriented and has an aspect ratio of 1.3, i.e. uniform street canyon (Shishegar, 2013). The reference scenario has no greenery and its facets present low value of albedo, i.e. 0.25 and 0.15 for walls and ground respectively. Moving from the presented reference configuration, the optical characteristics of the urban facets are progressively modified, and trees are included in the section of the urban canyon. The proposed combinations

are summarized in Figure 1 where dark and light colors for walls and ground represent dark and cool finishing materials implied on each specific surface. Albedo for cool materials is set to 0.65 and 0.45 for walls and ground respectively according to literature (Castaldo et al., 2017).

The simulated trees are the ones already implemented in the PUCM and presented by Ryu at al. in (Ryu et al., 2016). The tree fraction in the along-canyon axis is set to 0.2, i.e. a tree every 5 m. Trees impact the simulated environment since the PUCM computes all the physical processes related to radiative exchanges, including mutual shading and multiple reflections, and sensible and latent exchanges, the latest occurring through transpiration. Nevertheless, this work aims to show only the indirect impact of trees on human comfort without considering the provided shade in the human body energy balance if the pedestrian is under the tree.

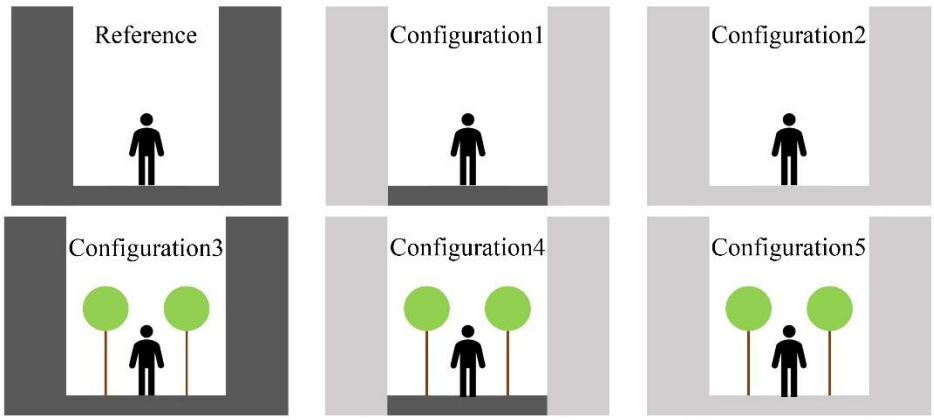


Figure 1. Scheme of the six analyzed configurations characterized by different albedo of the urban facets and presence or absence of trees.

All the realized configurations are simulated under the same weather forcing recorded during the hottest week of summer 2012 in Princeton (NJ, USA) by a dedicated station collecting data every 30 minutes. The selected period ranges from July 3rd to July 7th when monitored air temperature always exceeds 30 °C during day-time up to an absolute maximum of 39 °C.

Results

Hourly air and skin temperature differentials with respect to the reference scenario are shown in Figure 2 for the hottest simulated day. Air temperature variations depict the UHI mitigation effect of the implemented strategies during both day-time and night-time. The lower absorbed shortwave radiation produces up to 1.6 °C of air temperature reduction, i.e. configuration 1 with implemented cool walls, and the shadowing effect coupled with transpiration due to trees causes a further decrease, i.e. −0.6 °C in configuration 3 with dark canyon surfaces. Nevertheless, human comfort seems to be worsened by the implementation of cool materials within the urban canyon. Higher material reflection increases the amount of diffuse shortwave reaching the human body during day-time while the minor contribution of longwave re-emitted by surrounding surfaces, kept to lower temperatures due to the cool finishing, does not produce comparable benefits in the computed energy budget. Moreover, the indirect effect of trees, clearly shown from observed air temperature drops, is not effective leading to negligible variations of skin temperature in all the simulated scenarios.

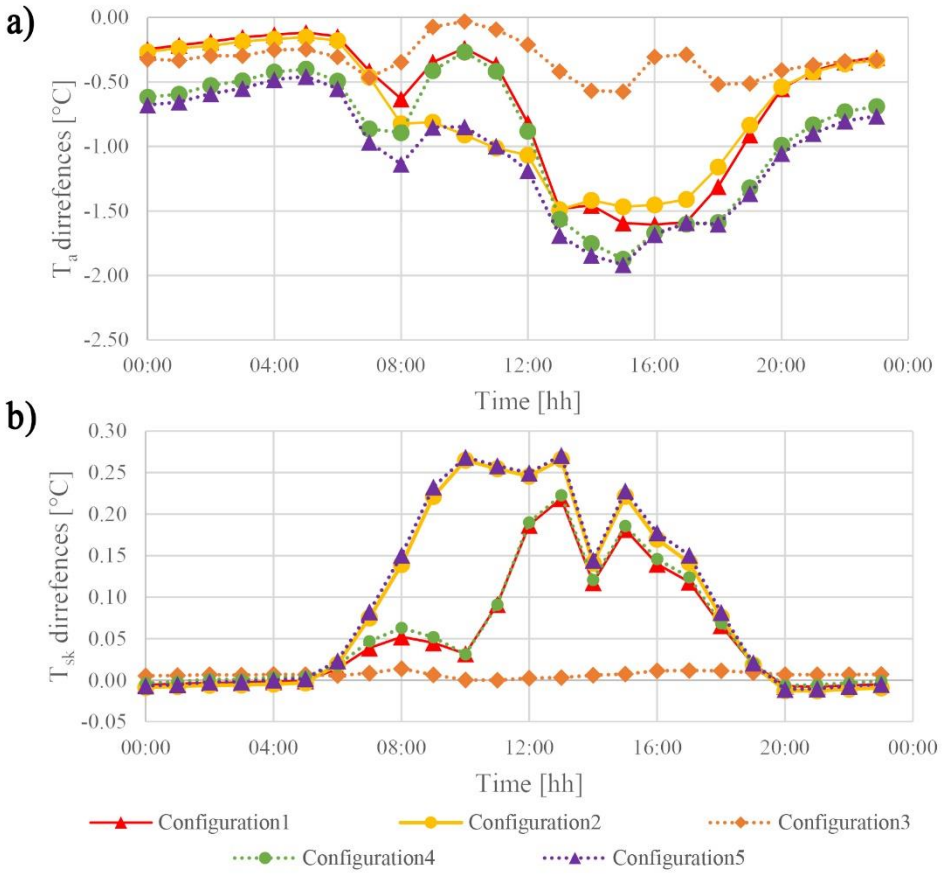


Figure 2. (a) air temperature and (b) skin temperature variations with respect to reference scenario

Figure 3 shows hourly values of each single component of the human energy balance for all the six simulated configurations. Once more, the outlined results confirm the negative impact associated with the implementation of cool surfaces within the urban canyon mainly imputable to higher contribution of the radiative component of the energy balance. Indeed, the convective exchanges between human body and the environment decrease in "cool scenarios", but the magnitude of this beneficial effect, i.e. maximum observed reduction of −6 W/m^2 in configuration 5, is negligible compared to the radiative increase, i.e. maximum gain of +79 W/m^2 in configuration 5. Significant changes are not highlighted in terms of evaporative exchange while the conduction term varies in accordance with the realized human body model showing particularly uncomfortable conditions during day-time. More in detail, the conductive flux from 10 a.m. to 4 p.m. is always negative for scenarios with both cool walls and ground. This means that the body core is gaining heat and the pedestrian health therefore deteriorates.

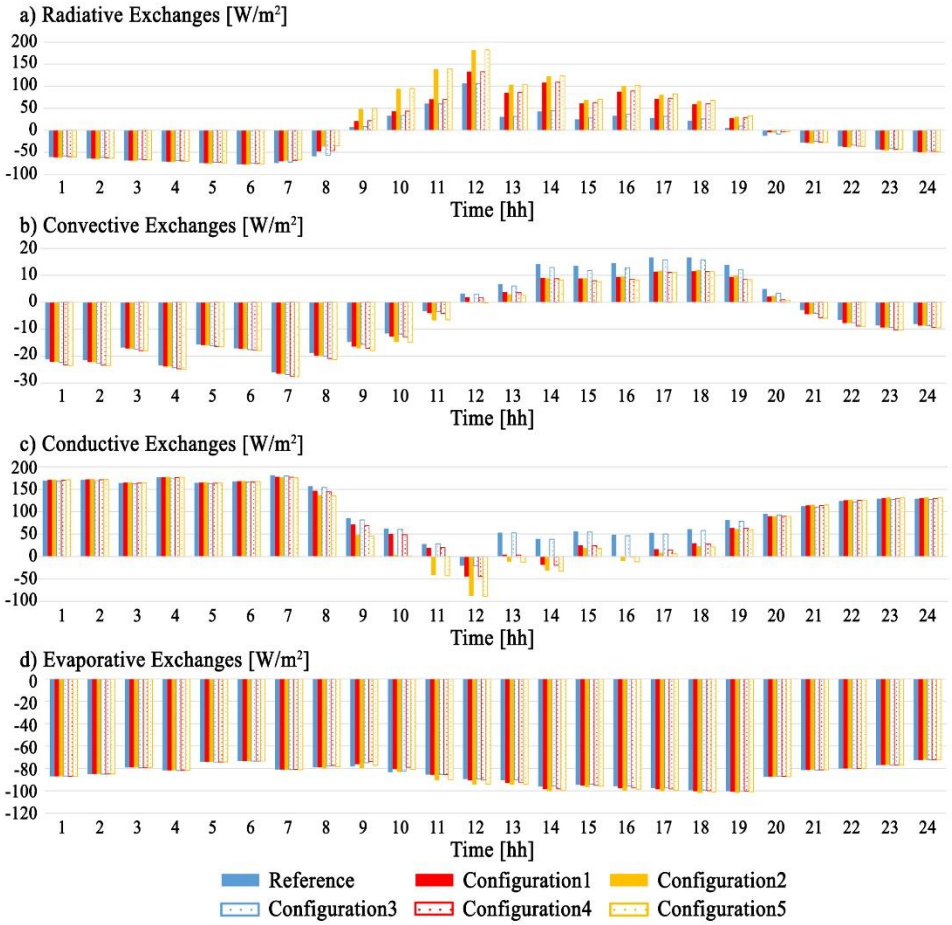


Figure 3. Hourly contribution of each component of the human energy balance, i.e. (a) radiation, (b) convection, (c) conduction, and (d) evaporation, for all the six simulated configurations.

Conclusions and Future Developments

The current work proposes the implementation of a simplified human body physiology within the Princeton UCM as an effective method to check pedestrians' thermal comfort in urban canyon. In particular, the developed model is a single-mass model with a constant core temperature and a skin shell with negligible thermal inertia. The computed outer skin temperature is adopted as comfort indicator and its variations due to different canyon characteristics is critically analyzed to assess potential benefits or disadvantages achievable with the implementation of common UHI mitigation strategies. In particular, six different configurations of the same urban canyon, i.e. defined canyon location, orientation, and aspect ratio, are tested varying facets albedo and introducing trees. The obtained results highlight the achieved benefits in terms of air temperature reduction and therefore the effectiveness of such strategies as countermeasures to the UHI phenomenon. Nevertheless, pedestrian comfort is compromised during day-time by the higher amount of radiative exchanges due to the higher reflection of cool materials implemented on walls and ground, which are surfaces in close proximity of the human body. The indirect effect of trees is also negligible compared to radiation impact. As further development of the presented work,

direct contribution of trees in human comfort enhancement will be tested including shadowing effect on the pedestrian. Moreover, alternative finishing materials of canyon surfaces will be tested with the final aim to find out a good compromise between UHI mitigation and outdoor spaces livability. In particular, the introduction of materials with dynamic properties, such as phase change materials, may be considered to achieve the proposed goal.

Acknowledgments

This work has received funding from the European Union Horizon 2020 Programme in the framework of the "HERACLES" project under grant agreement n° 700395. Additionally, the first author wish also to thank H2CU for the great international cooperation opportunities and the research staying in New York City for the purpose of this investigation. Elie Bou-Zeid is supported by the NOAA-Princeton Cooperative Institute for Climate Science and by the US-NSF under Grant 1664091.

References

Akbari, H., & Kolokotsa, D. (2016). Three decades of urban heat islands and mitigation technologies research. *Energy and Buildings*, *133*, 834–852. https://doi.org/10.1016/j.enbuild.2016.09.067

Castaldo, V. L., Rosso, F., Golasi, I., Piselli, C., Salata, F., Pisello, A. L., … De Lieto Vollaro, A. (2017). Thermal comfort in the historical urban canyon: The effect of innovative materials. In *Energy Procedia* (Vol. 134, pp. 151–160). https://doi.org/10.1016/j.egypro.2017.09.553

Chen, L., & Ng, E. (2012). Outdoor thermal comfort and outdoor activities: A review of research in the past decade. *Cities*, *29*(2), 118–125. https://doi.org/10.1016/j.cities.2011.08.006

Coccolo, S., Kämpf, J., Scartezzini, J.-L., & Pearlmutter, D. (2016). Outdoor human comfort and thermal stress: A comprehensive review on models and standards. *Urban Climate*, *18*, 33–57. https://doi.org/10.1016/J.UCLIM.2016.08.004

Dai, Z., Guldmann, J.-M., & Hu, Y. (2019). Thermal impacts of greenery, water, and impervious structures in Beijing's Olympic area: A spatial regression approach. *Ecological Indicators*, *97*, 77–88. https://doi.org/10.1016/J.ECOLIND.2018.09.041

Harlan, S. L., & Ruddell, D. M. (2011). Climate change and health in cities: impacts of heat and air pollution and potential co-benefits from mitigation and adaptation. *Current Opinion in Environmental Sustainability*, *3*(3), 126–134. https://doi.org/10.1016/J.COSUST.2011.01.001

Kenny, N. A., Warland, J. S., Brown, R. D., & Gillespie, T. G. (2008). Estimating the radiation absorbed by a human. *International Journal of Biometeorology*, *52*(6), 491–503. https://doi.org/10.1007/s00484-008-0145-8

Li, D., & Bou-Zeid, E. (2014). Quality and sensitivity of high-resolution numerical simulation of urban heat islands. *Environmental Research Letters*, *9*(5). https://doi.org/10.1088/1748-9326/9/5/055001

Macintyre, H. L., & Heaviside, C. (2019). Potential benefits of cool roofs in reducing heat-related mortality during heatwaves in a European city. *Environment International*, *127*, 430–441. https://doi.org/10.1016/J.ENVINT.2019.02.065

Morris, K. I., Chan, A., Morris, K. J. K., Ooi, M. C. G., Oozeer, M. Y., Abakr, Y. A., … Al-Qrimli, H. F. (2017). Impact of urbanization level on the interactions of urban area, the urban climate, and human thermal comfort. *Applied Geography*, *79*, 50–72.

https://doi.org/10.1016/J.APGEOG.2016.12.007

Rosso, F., Golasi, I., Castaldo, V. L., Piselli, C., Pisello, A. L., Salata, F., … de Lieto Vollaro, A. (2018). On the impact of innovative materials on outdoor thermal comfort of pedestrians in historical urban canyons. *Renewable Energy*, *118*. https://doi.org/10.1016/j.renene.2017.11.074

Ryu, Y. H., Bou-Zeid, E., Wang, Z. H., & Smith, J. A. (2016). Realistic Representation of Trees in an Urban Canopy Model. *Boundary-Layer Meteorology*, *159*(2), 193–220. https://doi.org/10.1007/s10546-015-0120-y

Santamouris, M. (2014). On the energy impact of urban heat island and global warming on buildings. *Energy and Buildings*, *82*, 100–113. https://doi.org/10.1016/j.enbuild.2014.07.022

Shishegar, N. (2013). Street Design and Urban Microclimate: Analyzing the Effects of Street Geometry and Orientation on Airflowand Solar Access in Urban Canyons. *Journal of Clean Energy Technologies*, *1*(1), 52–56. https://doi.org/10.7763/jocet.2013.v1.13

UN DESA. (2018). *2018 Revision of World Urbanization Prospects*. Retrieved from https://esa.un.org/unpd/wup/

Wang, Z. H., Bou-Zeid, E., & Smith, J. A. (2013). A coupled energy transport and hydrological model for urban canopies evaluated using a wireless sensor network. *Quarterly Journal of the Royal Meteorological Society*, *139*(675), 1643–1657. https://doi.org/10.1002/qj.2032

Zhao, L., Oppenheimer, M., Zhu, Q., Baldwin, J. W., Ebi, K. L., Bou-Zeid, E., … Liu, X. (2018). Interactions between urban heat islands and heat waves. *Environmental Research Letters*, *13*(3).

Effects of the Green Façade on Thermal Comfort in the Transitional Spaces: Field Measurements in Munich, Germany

Hankun Lin, School of Architecture, South China University of Technology (China)
Ata Chokhachian, Faculty of Architecture, Technische Universität München (Germany)
Florian Musso, Faculty of Architecture, Technische Universität München (Germany)
Yiqiang Xiao[1]*, School of Architecture, South China University of Technology (China)*

ABSTRACT

As a countermeasure to the high-density urbanization and urban heat island, urban green infrastructure has been promoted as an approach to improving human health and adapting to climate change. However, after rapid development in recent years, some high-density areas even lack green space in neighborhoods. In response to the limitation of green land and soil condition in some extreme urban space, planting the climbing plants strategically in both urban and building environment reveals a potential for increasing canopies and optimizing the pedestrian thermal comfort. This paper attempts to test the climbing plants façades', which are defined as green façades, effects on human thermal comfort in a dormitory building in Munich, Germany. Field measurements were set up with a toolkit to record the indices of micro-climate on the different floors of the test building alternately in order to compare the thermal environment of the shaded and unshaded area. Results reveal that the green façades reduced global solar irradiation, globe temperature, and air temperature significantly in typical summer days due to the shading effect. However, as a result of the dragging effect, the green façades also reduced wind flow velocity and influenced on the optimization of thermal comfort in the shaded area. This paper reveals the potential of improvement for thermal comfort in a transitional space via applications of green façades. Further studies would be taken in the urban environment in the future as well.

KEYWORDS

Green façade, Climbing plants, Transitional space, Human thermal comfort, UTCI

Introduction

Rapid urbanization in recent years has caused a sequence of problems such as urban heat island (UHI), urban noise, and air pollution and increased harms to human health. As one of the countermeasures, urban green infrastructure (UGI) including natural areas, farmland, and green space has been promoted as an approach to reducing the ecological footprint, improving human health and well-being, and adapting to climate change (Pauleit et al. 2017). However, some high-density urban neighborhoods even lack space for green and open space. In the urban canyon level, some extreme conditions such as harden pavements, power or water supply pipes, and soil containers also limit the environment for tree growing.

[1] Corresponding Author: yqxiao@scut.edu.cn, TEL: 86-020-22236588.

In response to the limitation of green land and soil condition, planting climbing plants strategically in landscape and building design reveals a potential for increasing canopies and optimizing the pedestrian thermal comfort in the high-density area (Figure 1). On the perspective of building design, strategies of training and guiding the climbing plants on building façade are defined as green facades (GFs). GFs and living wall system (LWS) are two technologies of the green wall (GW) (Perini 2011). Compare to the LWS, which normally constitute with a structure system, soil and plant containers or a substrate layer, and an irrigation and drainage system, the GFs are much more simple and low-cost technologies constituting with a training or guiding structure, a soil container (or planting on ground directly), and an irrigation and drainage system (Coma et al. 2017; Perini and Rosasco 2013).

In application, the GFs are applied not only on the external walls but also on the edge of some transitional spaces such as corridors, arcades, and balconies. In-between the outdoor and indoor space, the transitional space provides a better thermal comfort environment for human beings due to the solar irradiation shielding (Chun, Kwok, and Tamura 2004). On this aspect, there is a potential to provide a better outdoor thermal comfort environment via the combination with the GFs and the transitional space.

Thus, in order to obtain a better understanding on the effects of GFs and the optimization on human thermal comfort, field measurements were set up with a toolkit to record the indices of micro-climate in a test building in summer.



a. Climbing plants guiding by steel structure in MFO park, Zurich, Switzerland

b. Climbing plant forms a canopy with guiding structure

c. Climbing plants shade a street, Guangzhou, China

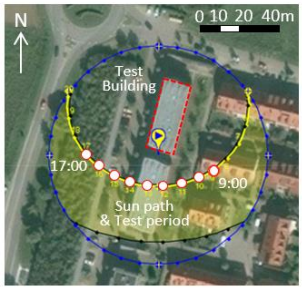
d. GFs with stainless steel rope (case study building in this paper), Munich, Germany

Figure 1. Scenarios of applications with climbing plants in landscape, urban, and building design. *Source*: a. Burckhardt+Partner 2019; b. Zimmermann 2011; c, d. Photographed by author.

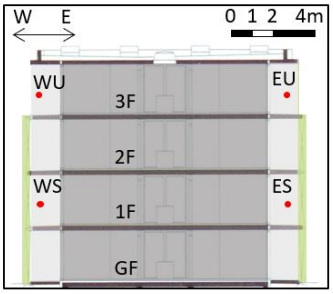
Methodology

The field measurements of this study were taken in a student dormitory at Garching of Munich, Germany (humid continental climate, Köppen classification: Dfb) (Köppen 1884). The building locates at the boundary of a residential neighborhood and the long façades are orientated to east-west. There are some 2 floors residential buildings in distance of 14m on the east side and farmlands on the west-north side. The test building is 4 floors in height. Rooms lie on the inner side with around of external corridors, which are enclosed by stainless steel wire ropes. Climbing plants of ivies were planted directly in the earth around the building facades and trained to grow along with the wire ropes. Canopies of the climbing plants have already formed a screen from the ground floor to the 2nd floor on all the orientations in recent years (the building was constructed in 2005, Figure 2).

The field measurements were separated into two typical summer days for both global solar irradiation (Ga) and thermal comfort indices measuring. A moveable toolkit with sensors was set alternately in the middle of the corridors with the distance of 0.7 m to the facades and the height of 1.1 m on the 1st floor (shaded with the GFs) and the 3rd floor (unshaded). On 10th July. 2018 the toolkit was just set on the west façade, then on 11th July. 2018 it was shifted from the east façade to the west façade after 13:00 and collected two groups of data to compare (Table 1).



a. Sun path overlapping on a GoogleEarth satellite photo for the test building



b. Section of the building an d the positions of test points



c. Corridor on 1st floor which was shaded by the GFs



d. Corridor on 3rd floor which was unshaded

Figure 2. Layout of the case study building, positions of test points, and photos of the corridors (ES, east and shaded; EU, east and unshaded; WS, west and shaded; WU, west and unshaded). *Source*: a. Sun Earth Tools 2019; b. Author's diagram based on the section of the building, which was collected from FJGAS 2019; c, d. Photographed by author.

Table 1. Instruments of the moveable toolkit

Instrument	Range	Accuracy	Freq	Duration	Position
LI-1500 Light Sensor Logger with LI-200R Sensor	Ga: Max. 3000 W/m^2	Ga: ±3% (within ±60 ° of incidence)	30 s	8:45-16:30, 10th July. 2018	West facade
Testo-480 with probes:			30 s	9:00-17:00, 11th July. 2018	9:00-13:00, East façade; 13:00-17:00 West facade
a. Humidity and temperature probe	Ta: -20 to +70℃	Ta: ±0.2°C (+15 to +30°C) ±0.5°C (remaining range)			
	RH: 0 to +100%	RH: ±(1.0% + 0.7% of m.v.) (0 to 90 %) ±(1.4% + 0.7% of m.v.) (90 to 100 %)			
b. Comfort probe	Va: 0 to +5 m/s	Va: ±(0.03 m/s + 4% of m.v.)			
c. Globe probe Ø 150mm	Tg: 0 to +120°C	Tg: Class 1			

* m.v., measurement value; Ga, Global Solar Irradiation; Ta, Ambient temperature; RH, Relative humidity; Va, Wind flow velocity; Tg, Black globe temperature.

Based on the indices of black globe temperature (Tg), ambient temperature (Ta), relative humidity (RH), and wind flow velocity (Va), which were recorded by the instruments, mean radiation temperature (MRT) and universal thermal climate index (UTCI) were calculated later. According to ISO 7726 Standard (ISO 1998), the equation that is used most frequently (forced convection) is the following, which for the standard globe (D = 0.15 m, diameter of the globe; μ= 0.95, the emissivity of the globe without dimension):

$$\mathrm{MRT} = \left[\left(\mathrm{T_g} + 273\right)^4 + 2.5 \cdot 10^8 \cdot {V_a}^{0.6}(\mathrm{T_g} - \mathrm{T_a})\right]^{\frac{1}{4}} - 273 \quad (1)$$

The UTCI aimed for a one-dimensional quantity adequately reflecting the human physiological reaction to the multi-dimensionally defined actual outdoor thermal environment (Fiala et al. 2001). The UTCI values were calculated in a software of BioKlima 2.6 with the input parameters of Ta, RH, Va, and MRT. The base human activities parameters were set as default in the software (Błażejczyk and Błażejczyk 2010).

Results and discussion

Results of global irradiation

Results of Ga data presented a significant change at the time of 14:30. The Ave. Ga of the unshaded area of 14:30-16:30 (Phase.2) was almost 4.5 times to which of 8:30-14:30 (Phase.1). Comparing two measured areas, the Ave. Ga of the shading area was reduced by 70.2% (Phase.1) and 88.4% (Phase.2). As the test points were only set on the west façade on 1st and 3rd floors, the Ga was increased after 14:30 due to the changing sun angle. The sky cloud condition was also collected from online weather data. Data of the hourly sky cloud cover ratio (CCR) and Ave. Ga reflected that before 14:00 even the CCR was at a high level, the Ga value still raised slowly because the sun angle was from south-east and the solar irradiation was blocked by the building itself, respectively, after 14:00 the Ga value increased obviously (Figure 3). The orientation of the building (east-west) influenced the results of the Ga values in the morning.

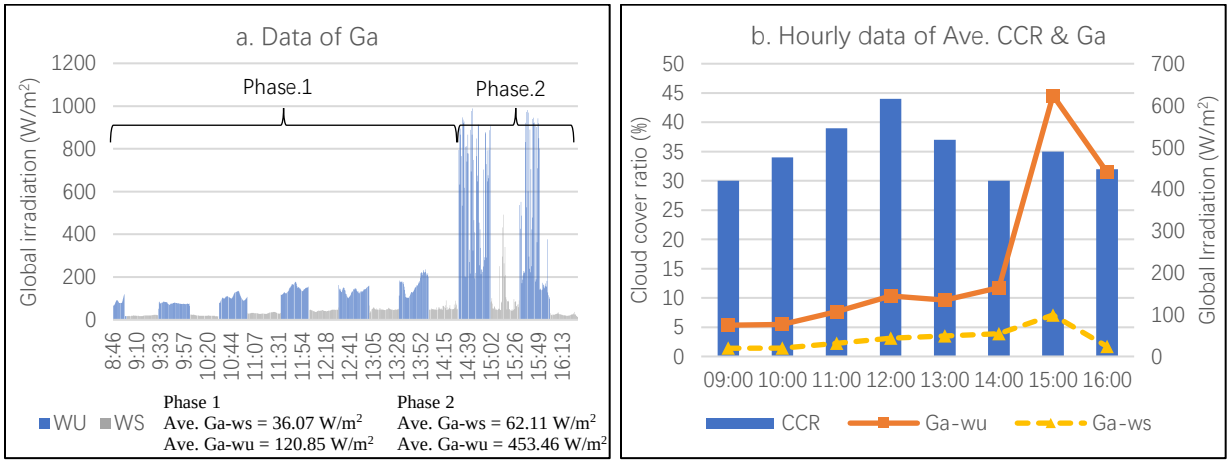


Figure 3. Data of Ga and CCR (Duration: 8:45-16:30, 10th July. 2018; WS, west and shaded; WU, west and unshaded). *Source*: a. Author's field measurement; b. CCR data collected from WWO 2019.

Results of thermal comfort indices

Outdoor environmental weather data was collected and show that the air temperature was stable (Ave. Ta = 17.5℃), the CCR increased after 12:00, and the main wind direction was north-west during the measurement period (Figure 4).

As the test points variated periodically between the shaded and unshaded positions, the trends of the measured results also changed in every half hour. The test points were also set to follow the sun angle and shifted from east to west façade at 13:00 so that the results presented some differences between two orientations (Figure 5). The main results are as follows.

- Comparison on measurements results and the weather data:

The Ga, Ta, and UTCI values were at a higher level, while the Va values were at a lower level before 13:00. It could be explained that the indices followed the variation of the weather data, which show that the CCR was lower and the solar irradiation was higher in the morning, respectively, the measured Va increased in the afternoon when the test points were set on the orientation facing to the main wind direction of north-west.

- Optimization of the human thermal comfort:

Ave. Tg, Ta, MRT, and UTCI of shaded area reduced by 0.8℃, 0.9℃, 1.4℃, and 0.9℃ on the east façade from 9:00 to 13:00, relatively, which increased by 2.2℃, 0℃, 2.7℃, and 0.8℃ on the west façade from 13:00 to 17:00. Ave. Va of shaded area reduced by 0.1 m/s (east) and 0.7 m/s (west) (Table 2). Results reveal that the GFs present potential of optimizing the human thermal comfort indices in the transitional spaces during the higher Ta and lower Va period. As the MRT was calculated basing on Tg, Ta, and Va, the calculation ignored the direct Ga so that it may underestimate the MRT values at where expose to the solar radiation directly, such as the unshaded areas. With the wind flow became stronger in the afternoon, the UTCI was lower in the unshaded than the shaded area. However, some of the Va values in the unshaded area were over 5 m/s in the afternoon, which is over the threshold of wind comfort for human beings (Stathopoulos 2009).

- Comparison on the shaded and unshaded scenarios:

Considering the values variated slowly when the test position changed periodically, the average values of different indices may not reflect the trend of the variation sufficiently. Thus, a further comparison of the haft hour data is added (Figure 5.f). Every half hour's average value is compared to the last value of the last measured position. Result reveals that the indices including Tg, Ta, MRT, and UTCI followed the decreasing trend during the shaded period. The average reduction of thermal comfort indices in the shaded period is 11.4℃ (MRT) and 2.0℃ (UTCI), respectively, the maximum reduction is 32.7℃ (MRT) and 7.9℃(UTCI). Through shifting the test positions between the shaded and unshaded area and following the sun path, the measurements reflected the shading effect significantly.

- Thermal comfort in the transitional space:

Comparing to the UTCI category (Broede 2013), results presented that 52.4% of the UTCI values were at the "no thermal stress level (+9 to +26℃)" and 39.4% of which were at the "moderate thermal stress level (+26 to +32℃)". All the transitional space in the test project presented a thermal comfort condition during the measurement period.

Regression and correlation analysis

Regression and correlation analysis for UTCI with other parameters reveal that Tg and MRT have higher correlations with UTCI, while Ta and Va present lower R^2 and correlation values (Figure 6 and Table 3). Results also show that the R^2 for Tg and MRT with UTCI are higher in the morning when Ave. Va is lower. Correlation for Va and UTCI is higher in the shaded area and implies that the GFs reduced the Va on both façades and influenced on the UTCI. In this case, even the Ta has been decreased by the shading effect of the GFs, the UTCI values variated much slower so that the correlation for Ta and UTCI was still at a lower level. Thus, in order to improve the wind flow in the corridors, it may need to keep some blanks or voids when forming GFs.

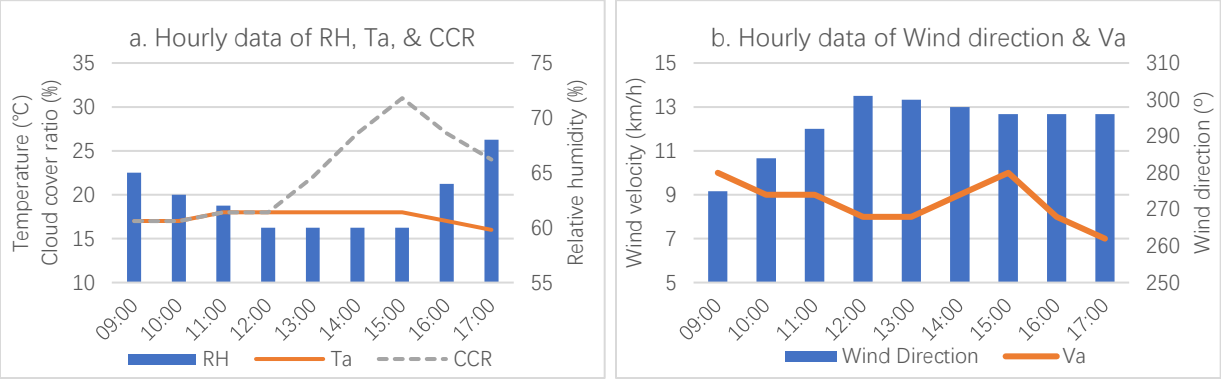


Figure 4. Data of weather station (Duration: 9:00-17:00, 11th July. 2018). *Source*: WWO 2019.

Table 2. Ave., Max., and Min. values of difference indices

Indices		Test points			
		ES	EU	WS	WU
Tg (℃)	Ave.	32.9	33.7	28.9	26.7
	Max.	44.8	45.2	35.4	30.1
	Min.	18.2	17.3	25.6	21.2
Ta (℃)	Ave.	19.4	21.3	18.2	18.2
	Max.	22.8	26.6	20.7	20.9
	Min.	15.2	17.1	16.5	16.8
RH (%)	Ave.	56.3	46.8	56.3	55.9
	Max.	74.3	63.7	66.7	64.9
	Min.	45.9	30.1	45.3	43.2
Va (m/s)	Ave.	0.4	0.5	0.4	1.1
	Max.	1.1	3.1	2.8	5.4
	Min.	0.1	0.1	0.1	0.1
MRT (℃)	Ave.	47.3	48.7	41.4	44.1
	Max.	83.4	93.9	75.1	85.4
	Min.	18.9	14.0	30.2	24.2
UTCI (℃)	Ave.	27.8	28.7	25.5	24.7
	Max.	37.7	39.1	30.6	27.7
	Min.	18.6	18.1	22.3	18.6

* EU, east and unshaded; ES, east and shaded; WU, west and unshaded; WS, west and shaded.

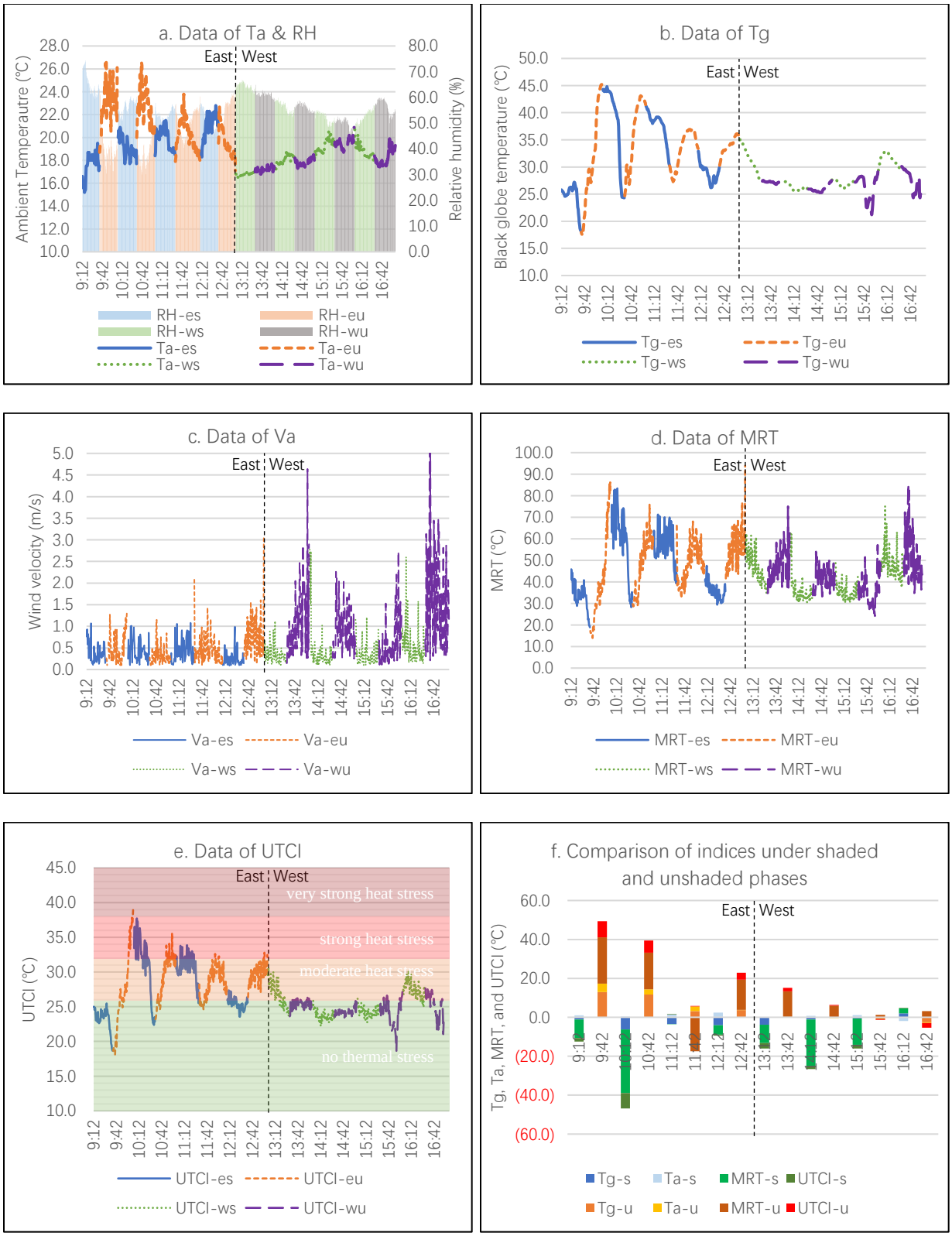
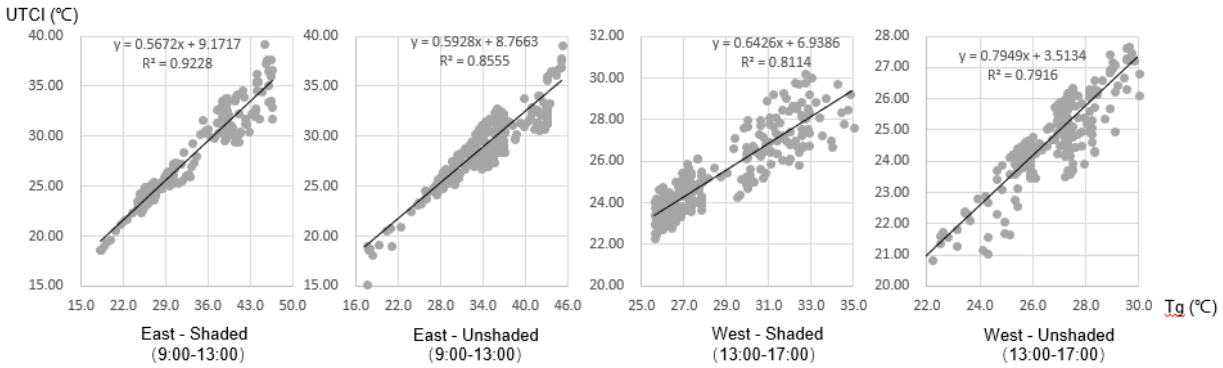
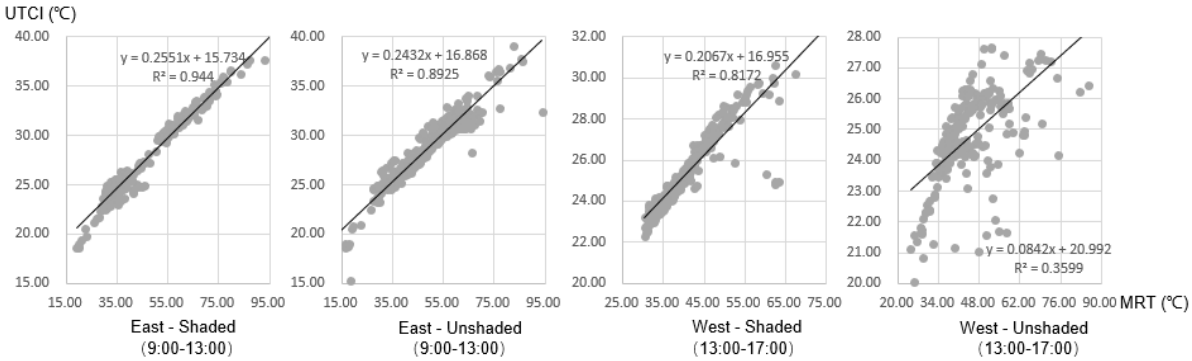


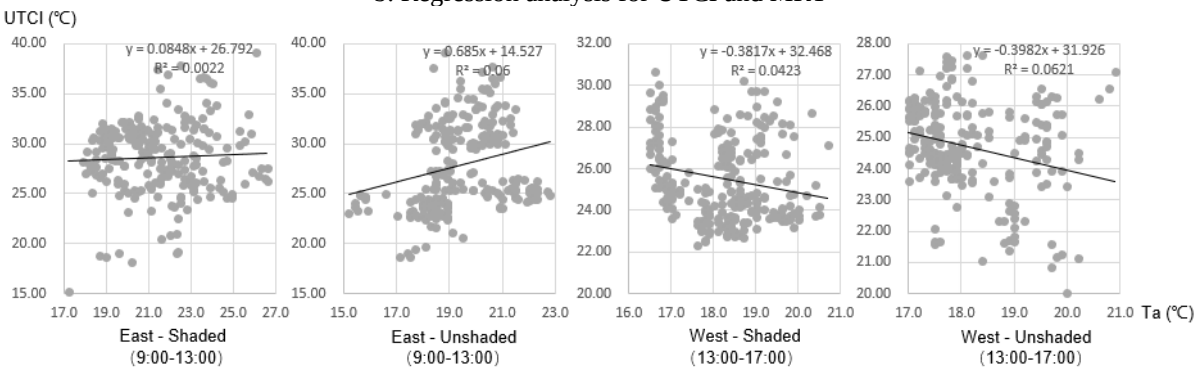
Figure 5. Data of different indices (Duration: 9:00-17:00, 11th July. 2018; Test points were shifted from east to west façade after 13:00 following the sun path; ES, east and shaded; EU, east and unshaded; WS, west and shaded; WU, west and unshaded). *Source*: Author's field measurement.



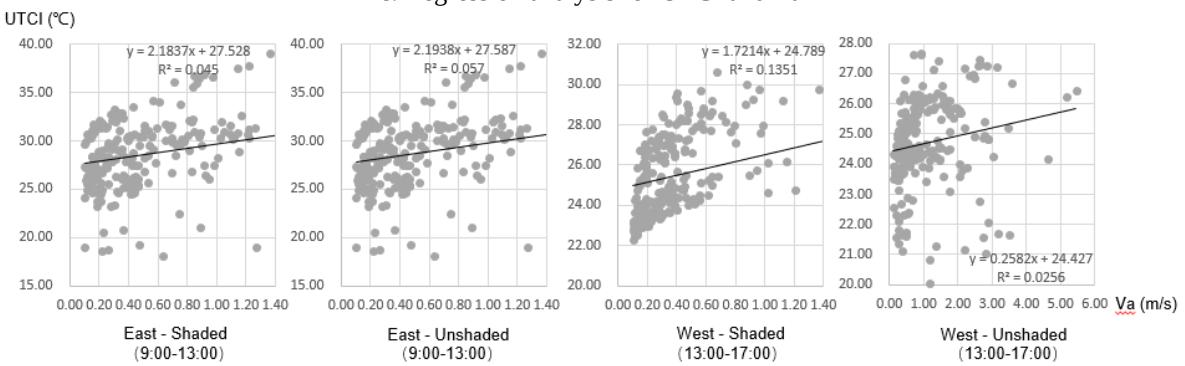
a, Regression analysis for UTCI and Tg



b. Regression analysis for UTCI and MRT



c. Regression analysis for UTCI and Ta



d. Regression analysis for UTCI and Va

Figure 6. Regression analysis for UTCI and different indices. *Source*: Author's field measurement.

Table 3. Correlation analysis for UTCI with different indices

Indices	Test points			
	ES	EU	WS	WU
Tg	0.961	0.926	0.905	0.890
MRT	0.972	0.953	0.903	0.600
Ta	0.245	0.024	-0.205	-0.249
Va	0.436	0.231	0.361	0.160

* EU, east and unshaded; ES, east and shaded; WU, west and unshaded; WS, west and shaded.

Conclusion

Through taking field measurements in the building with external corridors in Munich, Germany in typical summer days, the results reveal that the GFs reduced Ga, Tg, and Ta significantly due to the shading effect. However, as a result of the dragging effect, the GFs also reduced Va and influenced on the optimization of UTCI in the shaded area. This paper reveals the potential for improvement for human thermal comfort in the transitional spaces via the applications of GFs. The average reduction of thermal comfort indices in the shaded period are up to 11.4℃ (MRT) and 2.0℃ (UTCI). As the GFs reduced Ga up to 70-88%, on one side, they could reduce the internal gains for solar irradiation, on the other side, they could decrease the daylight availability of indoor environment in summer as well.

Some limitations of the settings in the field measurements may influence on the results. As the toolkit was only set on different floors in the building, the outdoor environmental data and boundary conditions were not measured but collected from open source weather data. The different height of the test points, which of the shaded and unshaded area is 5.2 m (2 floors), may also influence the results. The evaporation effect of the climbing plants was not discussed in the field measurements because a precise measurement for the canopy was lacked. The leaf area index (LAI) is also lacked to measure and discuss. Thus, some aspects of the study could be improved in future research. Further studies would be taken in the urban environment in the future as well.

Acknowledgments

This research is supported by the State Scholarship Fund of China (No. 201606150060), the National Natural Science Foundation of China (No. B51478188), and the Science and Technology Planning Project of Guangzhou, China (No. B3160760). The toolkit for the field measurements is supported by the Chair of Building Technology and Climate Responsive Design in the Faculty of Architecture, Technical University of Munich (TUM).

References

Błażejczyk, K. and Błażejczyk, M. 2010. BioKlima© 2.6. http://www.igipz.pan.pl/Bioklima-zgik.html

Broede, P., Blazejczyk, K., Fiala, D., Havenith, G., Holmer, I., Jendritzky, G., ... & Kampmann, B. (2013). The Universal Thermal Climate Index UTCI compared to ergonomics standards for assessing the thermal environment. *Industrial health, 51*(1), 16-24. https://doi.org/10.2486/indhealth.2012-0098

Burckhardt+Partner. 2019. https://www.burckhardtpartner.com/en/projects/detail/projekte/show/Projekte/new-mfo-park-zurich/#gallery-5

Chun, C., Kwok, A., & Tamura, A. (2004). Thermal comfort in transitional spaces—basic concepts: literature review and trial measurement. *Building and environment, 39*(10), 1187-1192. https://doi.org/10.1016/j.buildenv.2004.02.003

Coma, J., Pérez, G., de Gracia, A., Burés, S., Urrestarazu, M., & Cabeza, L. F. (2017). Vertical greenery systems for energy savings in buildings: A comparative study between green walls and green facades. *Building and environment, 111*, 228-237. https://doi.org/10.1016/j.buildenv.2016.11.014

Fiala, D., Lomas, K. J., & Stohrer, M. (2001). Computer prediction of human thermoregulatory and temperature responses to a wide range of environmental conditions. *International journal of biometeorology, 45*(3), 143-159. https://doi.org/10.1007/s004840100099

FJGAS (Fink+Jocher Gesellschaft von Architekten und Stadtplanern mbH). 2019. https://fink-jocher.de/projekte/studentenwohnheim-tum-garching

ISO, E. (1998). 7726. Ergonomics of the thermal environment-Instruments for measuring physical quantities (ISO 7726: 1998).

Köppen, W. (1884). Die Wärmezonen der Erde, nach der Dauer der heissen, gemässigten und kalten Zeit und nach der Wirkung der Wärme auf die organische Welt betrachtet. *Meteorologische Zeitschrift, 1*(21), 5-226.

Pauleit, S., Hansen, R., Rall, E. L., Zölch, T., Andersson, E., Luz, A. C., ... & Vierikko, K. (2017). Urban landscapes and green infrastructure. In *Oxford Research Encyclopedia of Environmental Science*. DOI: 10.1093/acrefore/9780199389414.013.23

Perini, K., Ottelé, M., Haas, E. M., & Raiteri, R. (2011). Greening the building envelope, façade greening and living wall systems. *Open Journal of Ecology, 1*(01), 1. http://dx.doi.org/10.4236/oje.2011.11001

Perini, K., & Rosasco, P. (2013). Cost–benefit analysis for green façades and living wall systems. *Building and Environment, 70*, 110-121. https://doi.org/10.1016/j.buildenv.2013.08.012

Stathopoulos, T. (2009). Wind and comfort. In *EUROPEAN & AFRICAN CONFERENCES ON WIND ENGINEERING (EACWE) 5th*.

Sun Earth Tools. 2019. https://www.sunearthtools.com/dp/tools/pos_sun.php

WWO (World Weather Online). 2019. https://www.worldweatheronline.com/

Zimmermann, A. (2011). *Constructing landscape: materials, techniques, structural components.* Birkhäuser.

Summertime Thermal Comfort Assessment for Compact Local Climate Zone

Dr. Rajashree Kotharkar[1], Professor at Department of Architecture & Planning, Visvesvaraya National Institute of Technology, Nagpur-440010, Nagpur (India)
Shweta Deshmukh, M. Tech student at Department of Architecture & Planning Visvesvaraya National Institute of Technology, Nagpur-440010, Nagpur (India)

ABSTRACT

Thermal comfort studies are under research since last decade. Outdoor spaces contribute to urban livability and vitality. People in the outside environment are directly exposed to urban climate, which cannot be totally controlled. The study of outdoor thermal comfort is critical in areas experiencing temperature and climate extremities and affecting human sustenance.

Central India is identified as the critical zone due to its growth patterns and heat related vulnerabilities. Urban climate studies in central region shows varying heat intensities. Previous studies have used different approaches and techniques to analyze the physical and geometrical attributes of city however they have not considered its effect on urban population.

This study evaluates social aspect (outdoor thermal comfort) by developing a systematic frame work. Physical, physiological and psychological level of assessment with the help of different parameters like building density, sky view factor aspect ratio, vegetation, micro metrological variables and thermal sensation vote (TSV) are studied.

The study focuses on Compact Local Climate Zone and uses Physiological Equivalent Temperature (PET) index for outdoor thermal comfort (OTC) assessment. The study shows strong correlation with sky view factor (SVF) and building density. Different mitigation scenarios are simulated and PET index is calculated with the help of computational tool Ray-man. Vegetation shows the maximum effect followed by combination of cool roof and cool pavement. However, the findings show that cool roof is the most feasible mitigation measures for dense urban pockets with respect to the surface treated and percentage reduction in temperature

The study develops a strategy for improving outdoor thermal comfort in urban areas, which could help in developing practices and policy interventions for future sustainable cities.

Introduction

Tropical countries have experienced temperature and climatic extremes affecting 70 % of the world population. Past studies have shown that increase in temperature affects the performance and efficiency at work in human beings and is fatal if it exceeds the body core temperature of 37 °C (Hugh and McMichael 2011). Urban heat island (UHI) studies have shown the existence of heat island and heat sinks within the city and have analyzed their relationship with environmental aspect (Frazer 2005) & economic aspects in terms of development of region. The social aspects of heat related vulnerability i.e. health of population is less studied.

Developing nations like India are transforming the land use and land cover drastically, influencing the urban climate. India has different climate zone and different development pattern. The absence of any standards or policies for planning of comfortable outdoor surroundings necessitates the study of outdoor thermal comfort and its effect on urban population in Indian context. The study aims to prepare a strategic plan for improving outdoor thermal comfort in

[1] Rajashree Kotharkar: [rskotharkar@gmail.com]

urban areas. It understands the effects of morphological elements on urban climate and evaluates the objective and subjective parameters of outdoor thermal comfort by developing a systematic frame work for assessment. Study uses different approaches like observation measurement, calculation and questionnaire survey (Field Survey) to highlight the critical areas. Different mitigation measures (Urban cooling measures) are simulated to suggest the most feasible and viable mitigation measures.

Study Region

Nagpur is located at an altitude of 310m with a latitude of 21° 8'47"N and longitude of 79° 5'19" E. It has an administrative area of 217sqm with a population of 25 lakhs (Census2011). The city is mono-centric with 62.5% of built up area and population density of 111pph. (Kotharkar, Bahadure and Sarda 2014).

Nagpur is situated at geographical center of India. According to Koppen climate classification system, Nagpur experiences Composite climate. Temperature reaches its maximum of 45°C in month of May and minimum temperature of 13°C in month of December. City reaches its highest relative humidity of 84% in the month of June.

Heat wave data by NDMA, have identified central India as heat vulnerable region. Due to the extremes of temperature and their direct and indirect effect on health of individual study is focused on summer season. Outdoor thermal comfort study is evaluated during heat wave period of March to May on a typical summer day.

Literature study

Outdoor thermal comfort studies (OTC) around the world are reviewed for understanding the different urban components and parameters affecting them. A review of OTC studies in the past five years show different approach for evaluating thermal comfort depending upon the scale of study. The selection of research paper was from SCI indexed, Scopus indexed and conference papers all peer review and open access source.

From the reviewed papers 90% of researches are conducted in single city at different scales. All the studies use either of the two approaches- survey based (field study) and Model based (simulation study). Maximum number of studies are researched in temperate climate zone with minimum share in Continental climate zone. Combined share of Tropical Climate zone and Dry climate zone constitute to 47% of studies, where temperature extremes are basic concern for thermal stress.

Studies majorly use three thermal indices namely Predicted Mean Vote (PMV), Physiological Equivalent Temperature (PET) and Universal Thermal Climate Index ((UTCI). PET index is used 57% of studies due to its relevance in in extreme climatic condition and availability of computational tools for its measurements.

Studies from different climate zone were identified, which have used PET index and subjective assessment for study. The identified studies are as follows; two studies in 2011 in Cairo (Mahmoud 2011), Lisbon (Andrade, Alcoforado and Oliveira 2011), two studies in 2012 in Hong Kong (Ng & Cheng 2012), Malaysia (Makaremi et.al 2012), five studies in 2013 in Changsha and Singapore (Yang, Wong and Zhang 2013), Chiayi city, Taiwan(Lin et.al. 2013), Glasgow(Krüger et.al. 2013), Tel Aviv (Cohen, Potchter and Matzarakis 2013), one studies in 2014 in Wuhan (Lai et.al. 2014), four studies in 2016 in Rome(Salata et al. 2016), Guangzhou(Li, Zang and Zhao 2016), Cairo (Elnabawi, Hamza and Dudek, 2016), Changsha

(Liu, Zhang, & Deng 2016) and one study in 2017 in Isfahan, Iran (Nasrollahi, Hatami and Taleghani 2017).
All studies show varying comfort range making it evident that European standard of comfort range of 18℃ - 21℃ is not valid for other cities. Two studies in Cairo in year 2011 and 2016 show same comfort range though the composition and number of respondents varied highlighting that comfort range average is not affected by the quantity and composition of respondents. Two studies in Changsha in 2013 and 2016 show varied though overlapping comfort range as the studies are evaluating single or multiple seasons highlighting the temporal and seasonal impact on outdoor comfort range. The difference in comfort range of the identified studies can also be attributed to psychological factor- people's acceptability and adaptability in different climate zones. Therefore each location requires a systematic evaluation and exclusive planning intervention for mitigation.

Investigation Area

LCZ map of Nagpur (Kotharkar and Bagade 2017) is adopted for outdoor thermal comfort study. The LCZ map of city shows LCZ3 (Compact low rise) and its sub-classes (LCZ32, 3F and 37) as the most prominent built up class comprising of 40% of the built up area of city (Refer fig1). The overlap of LCZ3 and its sub classes on ward density map of Nagpur shows 47% of the citizens residing in investigation area, justifying the selection. (Refer fig2)

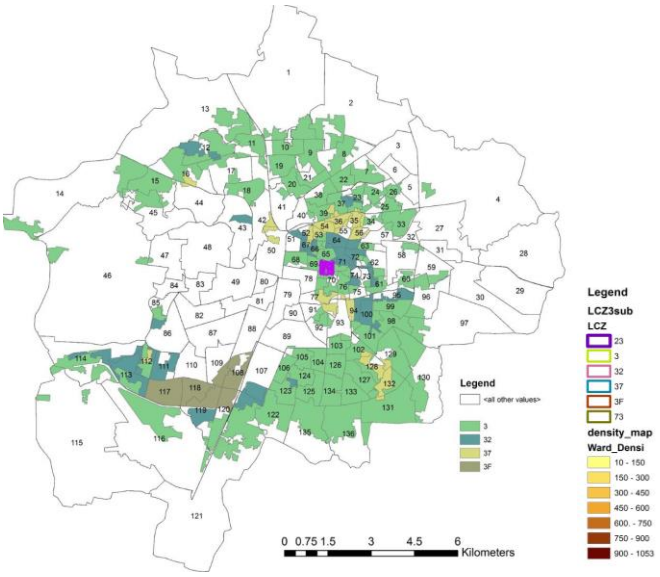


Figure 1 LCZ Map showing LCZ 3 and sub-classes

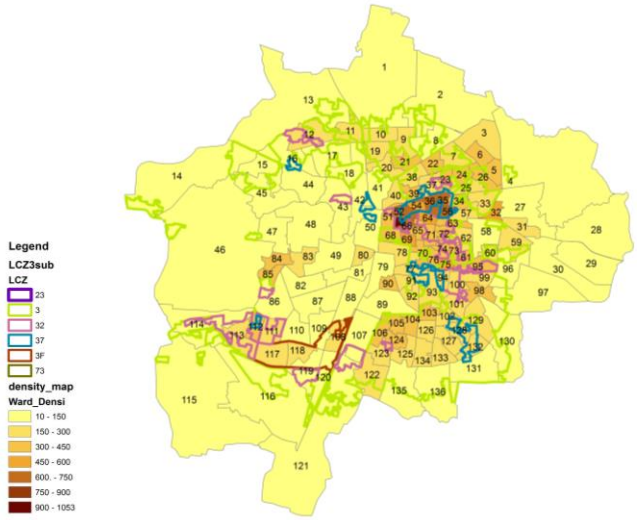


Figure 2 Map showing expanse of LCZ3 and affected population

Research methodology

Framework for OTC assessment

Outdoor thermal comfort is the product of urban structure pattern, urban climate and people's perception and requires three levels of assessment namely physical, physiological and psychological. These level of assessment depends upon influencing factors which are objective or subjective in nature and requires specific technique for measurement and documentation. (Ref

Table1). Thermal comfort assessment framework is developed, based on the literature review of outdoor thermal comfort studies.

The study is conducted at local scale. Neighborhood typical to the selected LCZ's are selected for physical assessment. Urban canyons which represent 80%- 90% of the area are selected for micro scale study and characteristics of the area are studied by parameters like building densities, sky view factor and aspect ratio

Table 1: Assessment Framework for Outdoor Thermal Comfort study

Level of Assessment	Approach	Influencing factors		Parameters studied	Scale
		Objective	Subjective		
Physical assessment	Observation	Urban form attributes	-	Building density, vegetation, sky view factor and aspect ratio	City scale and local scale
Physiological assessment	Measurement/ calculation	Measurement of micro meteorological variables and calculation of heat index	-	Temperature, relative humidity wind flow, wind direction and cloud cover	Local scale
Psychological assessment	Questionnaire survey/ Interview	-	Expectation, past experience, personal parameters	Thermal sensation vote, feeling of comfort, personal-activity, clothing, age gender	Micro scale

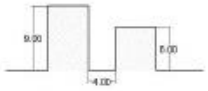
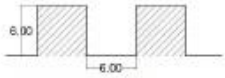
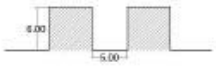
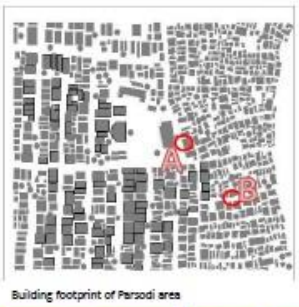
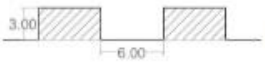
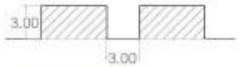
Objective parameter for physiological assessment involves measurement of micro meteorological data. It is done with the help of instrument- Weather station of Spectrum 2000 series. The instrument is calibrated and certified according to international standards. Physiological Equivalent Temperature (PET) index is used for outdoor thermal comfort assessment. PET index is used for study and calculations are done with the help of computational tool- Ray Man Pro. Subjective parameter for psychological assessment is documented with the help of questionnaire survey. It records thermal sensation vote on a 7-point scale and feeling of comfort and other thermal references on 5 point scale.

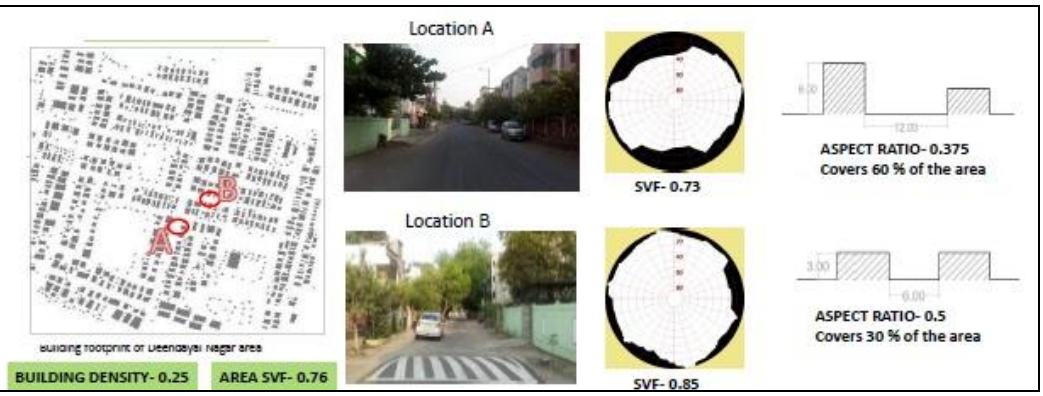
The finding of all the level of assessment are then statistically analyzed to understand the interrelation of parameters and their effect on outdoor thermal comfort.

Spaces studied

Urban morphology studies physical and geometrical aspect of study area. Two locations are selected for averaging the attributes of area. Attributes of the spaces studied are described in table 2; LCZ 3 shares the maximum proportion of built class and therefore two localities are selected for LCZ3 – one in core area and one in peripheral area. LCZ 3 subclasses have one locality each typical to the LCZ classification selected for study.

Table 2 : Attributes of study areas

LCZ	Localities	Locations	SVF	Aspect ratio
LCZ3 (core area Mahal	 Building footprint of Mahal area BUILDING DENSITY- 0.38 AREA SVF- 0.7	Location A  Location B 	 SVF- 0.556  SVF- 0.350	 ASPECT RATIO- 1.5 Covers 30 % of the area  ASPECT RATIO- 1.875 Covers 60% of the area
LCZ3 (Peripheral area) Manewada	 Building footprint of Manewada area BUILDING DENSITY- 0.29 AREA SVF- 0.76	Location A  Location B 	 SVF- 0.64  SVF- 0.54	 ASPECT RATIO- 0.5 Covers 30 % of the area  ASPECT RATIO- 1 Covers 50 % of the area
LCZ 32 Gopal nagar	 Building footprint of Gopal Nagar area BUILDING DENSITY- 0.37 AREA SVF- 0.65	Location A  Location B 	 SVF- 0.56  SVF- 0.699	 ASPECT RATIO- 0.5 Covers 50 % of the area  ASPECT RATIO- 1.20 Covers 30 % of the area
LCZ 37 Kamgar colony, Parsodi	 Building footprint of Parsodi area BUILDING DENSITY- 0.50 AREA SVF- 0.66	Location A  Location B 	 SVF- 0.67  SVF- 0.3	 ASPECT RATIO- 0.5 Covers 40 % of the area  ASPECT RATIO- 1 Covers 50 % of the area

LCZ 3F Deendayal nagar	

Subjective assessment is done with the help of questionnaire survey consisting of two sub parts- first part documents the physiological factors like clothing, activity level, gender, age etc. and the second part records the psychological parameters like thermal sensation, comfort level and preferred change in elements like wind movement, shade, vegetation.

Survey is done on a typical summer day for summertime OTC assessment. Sample size of N=384, is derived by calculating the affected population (residents of compact low rise zone) with 95% confidence level.

PET index is calculated with help of computational tool Ray Man Pro software developed by Martazarkis et.al in 2000. This tool is further used in study for assessing the feasible mitigation measure through simulation.

Results

PET statistical findings

The output of questionnaire survey and PET index is analyzed through regression analysis. The equations generated through linear regression analysis is used to calculate neutral PET and total PET range.

The regression analysis graph and equations are as shown in fig3. The findings of questionnaire survey show varying thermal sensation vote in all the surveyed areas. Respondents showed more percentage of feeling of comfort even when the thermal sensation is not neutral showing more adaptability to surrounding environment. Survey statistics show varying threshold limits of thermal comfort highlighting the effect of urban morphology on outdoor thermal comfort. R-square of all the areas is weak showing approx. 50% to 60 % of correlation of Thermal sensation vote (TSV) and PET. Neutral PET is therefore considered threshold limit above which more than half of the respondents are uncomfortable. The neutral PET derived by this equation by equating comfortable TSV value to equation. Similarly, acceptable PET and PET max is calculated to measure the recorded range of PET. (Refer table 3)

PET range is maximum in LCZ37- Kamgar colony, Parsodi and minimum in LCZ3F Deendayal nagar, which is attributed to the difference in land cover and construction material of building which affect the thermal reflectance and emissivity of area affecting albedo of area.

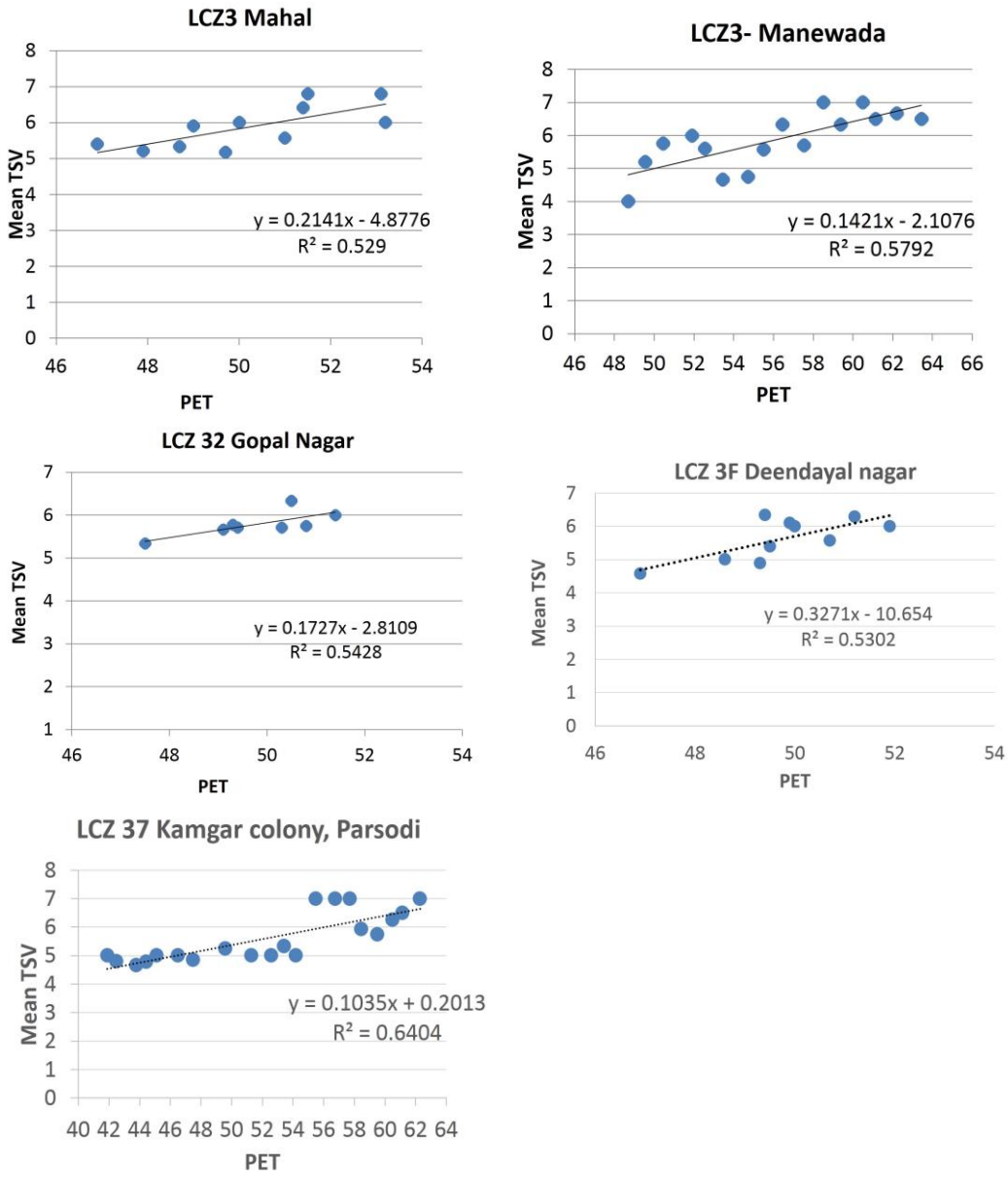


Figure 3 Regression analysis graph and equation of study areas.

Table 3 PET range and R-square of study areas

Localities	R-Square	NPET	PET acceptable	PET max
Mahal	0.53	41.46	46.1	55.48
Manewada	0.58	42.98	50	64.1
Gopal nagar	0.54	39.44	45.2	56.81
Kamgar colony, Parsodi	0.64	36.7	46.4	65.69
Deendayal Nagar	0.53	43.8	47.2	53.88

The neutral PET in Kamgar colony is lowest with highest in Deendayal nagar. The relation of neutral PET is reverse in case of PET max; where Kamgar colony is highest and Deendayal nagar is lowest. This shows that in early hours the Kamgar colony is more comfortable than Deendayal nagar but along with time Kamgar colony gets more heated than Deendayal nagar.

Hence more discomfort and heat stress is experienced in built class 37 (compact low rise with light weight low rise). Kamgar colony has a compact planning with high building density and impervious surface whereas Deendayal Nagar has less building density and approx. 25% of impervious land surface.

Effect of urban morphology on outdoor thermal comfort

Effect of urban morphology on outdoor thermal comfort is evaluated by correlating neutral PET to the physical and geometrical features of surveyed locations.

Sky view factor for area is calculated by Sky Helios software ((Matzarakis and Matuschek 2011). Sky view factor shows a strong positive correlation to neutral PET (Refer fig.4a). This depicts that the neutral PET can be reduced by decreasing the sky view factor, which can increase the percentage of feeling of comfort in an area. Sky view factor of an area could be reduced by increasing artificial shade, greenery.

Building density shows a negative effect on neutral PET i.e. value of neutral PET increase with decrease in building density (refer fig 4b). This shows that the areas with higher densities show more comfort than the areas with less density because they remain shaded for maximum hours of day but the building mass gains heat and radiates it to increase the temperature of the surrounding in later hours. Thus, areas with higher density show comfort in the early hours of a typical summer day, but the areas experience discomfort in later hours. Optimum building density can be calculated by equation generated by regression analysis for both night time and daytime data. Guidelines regarding building densities of new developed areas can assure thermally comfortable outdoor environment.

Aspect ratio shows weak correlation with neutral PET and need further assessment to understand its effect on outdoor thermal comfort (refer 4c).

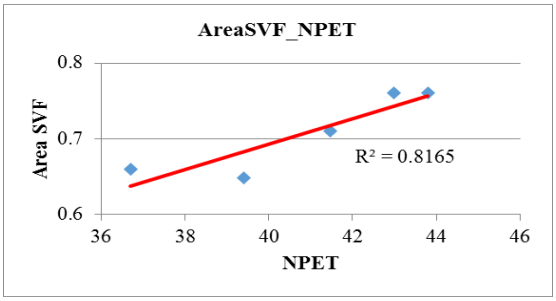
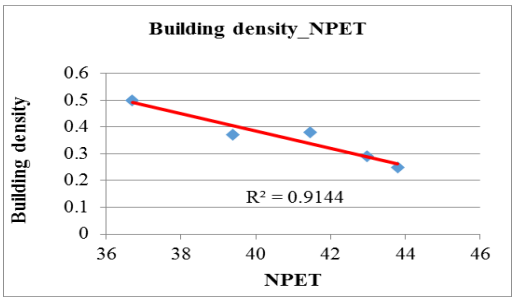
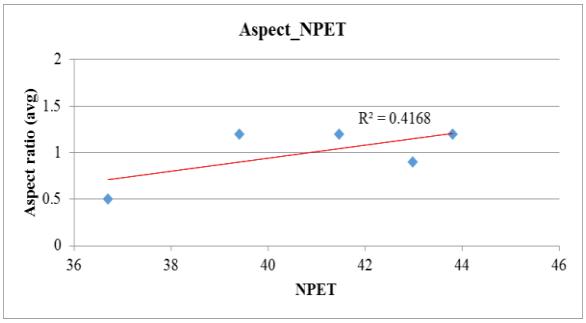


Figure 4 (a) Correlation of SVF with neutral PET Figure



4 (b) Correlation of Building density to neutral PET



4 (c) correlation of Aspect ratio to neutral PET.

Mitigation measures

Urban morphology affects natural energy budget of an area affecting health of individuals. The incident solar energy is absorbed by the urban surfaces and the energy is trapped for longer duration raising the temperature of an urban area. Mitigation measures help in minimizing the adverse effect and discomfort of city inhabitants. Mitigation measures require good thermal emissivity and reflectivity for changing the albedo of area.

Suitable mitigation measure depending upon the character of surveyed area is simulated with PET max. existing as base case and PET is recalculated in Ray man for evaluating feasible mitigation measure. Four scenarios are simulated namely, cool roof, cool pavements, combination of cool roof and cool pavement and vegetation. Areas lacking open spaces or having narrow roads are not simulated for vegetation scenario.

Results show maximum effect of vegetation followed by combination of cool roof and cool pavements, resulting in decrease of 1°C to 4°C (refer table 4). Percentage calculation of surface treated and the effect in reduction of PET is maximum in scenario I- cool roofs, it reduces approximately 3°C and therefore this mitigation measure is considered more suitable than other mitigation measures followed by scenario IV- vegetation.

Simulation study for selection of feasible mitigation measure help in formulating guidelines, development of regulation and policy framework for thermally comfortable outdoor surroundings.

Table 3: Calculated PET base case and four simulated scenarios

Location	Calculated PET (°C)				
	Existing (Base case)	Cool Roof (I)	Cool Pavement (II)	Cool Roof + Cool Pavement (III)	Vegetation (IV)
Mahal	59.7	56.9	56.0	54.4	X
Manewada	60.1	58.0	57.1	56.1	56.3
Gopal nagar	56.4	54.9	54.3	53.4	53.5
Parsodi	60.1	57.0	57.2	55.6	X
Deendayal nagar	52.5	52.0	51.7	51.4	51.5

Discussion and Conclusion

Changing environment and long exposure to this harsh climatic conditions change people's expectation and improve their adaptability which can be seen through the neutral PET

calculations which are close to 40º C and still comfortable for approximately 50% of the people. The questionnaire survey shows more percentage of feeling of comfort than neutral thermal sensation vote showing acclimatization.

The study methodology develops a framework for assessing the urban structure and development of intervention to improver outdoor thermal comfort of an area. The results show varying comfort level not only in different climate zone but also within an urban area. Optimum mitigation measure can be tested for feasibility with the help of simulation study and can be customized depending upon the character of the area. Following conclusions can be drawn;

- Areas show high neutral PET, proving that the European standards are not valid in Indian context, and so cannot be used as threshold limits for planning thermally comfortable urban areas in India.
- Study evaluated comfort within an urban area in the most prominent built class and subclasses, the difference in the PET comfort range shows that impact of urban morphology on outdoor thermal comfort.
- Some areas like Manewada, Gopal Nagar and Deendayal Nagar have more percentage of 'feeling of comfort' than the percentage of 'neutral thermal sensation' showing peoples adaptability to the surroundings.
- Areas with more PET range like Kamgar colony and Manewada show high tolerance level of the respondents towards thermal stress.
- Simulation results of different designed scenarios change the albedo value of the area, showing varying effect of mitigation measures. Therefore, whole city cannot have single mitigation proposal but is to be customized depending upon urban structure (area wise)
- The possible mitigation measures involve improving vegetation, reducing impervious layer and encouraging use of high albedo materials, but the optimum mitigation measure needs to be evaluated for feasibility.
- Aspect ratio does not show direct correlation and needs further study.
- Deendayal Nagar needs further assessment to understand other drivers and impacts influencing outdoor thermal comfort as area show the minimum PET variation.

Future scope

The study evaluates comfort for summer season further evaluation of different seasons will give a yearly average comfort range which could be analyzed for mitigating strategies. The study is done on a local scale on a prominent built class, the expanse of the study can be extended to other built classes to attain a thermally comfortable urban area.

Acknowledgement

We thank Department of Architecture and Planning, Visvesvaraya National Institute of Technology, Nagpur for providing necessary infrastructure for research work. We thank Andreas Matzarakis and team for providing free online computational tool RayMan Pro and SkyHelios which helped in calculating Sky view factor and thermal index. We are grateful for the team of students and Aparna. R, Aveek Ghosh for their help in questionnaire surveys.

References

Hughes, L., McMichael, T., (2011). The critical decade: climate change and health. Retrieved from http://climatecommission.gov.au./wp-content/uploads/111129_FINAL- FOR- WEB.pdf

Frazer, L., (2005). Paving paradise. Environ. Health Perspect. 113, 457–462.

Kotharkar, R., Bahadure, P., & Sarda, N. (2014). Measuring compact urban form: A case of Nagpur City, India. Sustainability, 6(7), 4246–4272.

Mahmoud, A.H.A., (2011). Analysis of the microclimatic and human conditions in an urban park in hot and arid regions. Building and Environment. 46, 2641- 2656.

Andrade, H., Alcoforado, M.J., & Oliveira, S. (2011). Perception of temperature and wind by users of public outdoor spaces: relationships with weather parameters and personal characteristics. International Journal of Biometeorology. 55, 665-680

Ng, E. & Cheng V. (2012). Urban human thermal comfort in hot and humid Hong Kong. Energy and Buildings. 55, 51-65.

Makaremi, N. et.al (2012). Thermal comfort conditions of shaded outdoor spaces in hot and humid climate of Malaysia. Building and Environment. 48, 7-14.

Yang, W., Wong, N.H., & Zhang, G., (2013). A comparative analysis of human thermal conditions in outdoor urban spaces in the summer season in Singapore and Changsha, China. International Journal of Biometeorology. 57, 895-907.

Lin, T.P. et.al. (2013). Effects of thermal comfort and adaptation on park attendance regarding different shading levels and activity types. Building and Environment. 59, 599-611.

Krüger, E. et.al. (2013). Urban heat island and differences in outdoor comfort levels in Glasgow, UK. Theory of Applied Climatology. 112, 127 – 141.

Cohen, P., Potchter, O., & Matzarakis, A. (2013). Human thermal perception of Coastal Mediterranean outdoor urban environments. Applied Geography. 37, 1-10.

Lai, D et.al. (2014). Outdoor space quality: A field study in an urban residential community in central China. Energy and Buildings. 68, 713-720.

Salata, F., et al. (2016). Outdoor thermal comfort in the Mediterranean area. A transversal study in Rome, Italy. Building and Environment. 96,46-61.

Li, K., Zang, Y., & Zhao, L.,(2016). Outdoor thermal comfort and activities in the urban residential community in humid subtropical area of China. Energy and Buildings.113, 498-511.

Elnabawi, M.H., Hamza. N. & Dudek, S. (2016). Thermal perception of outdoor urban spaces in the hot arid region of Cairo, Egypt. Sustainable cities and Society. 22, 136-145.

Liu, W., Zhang, Y., & Deng, Q. (2016). The effect of urban microclimate on outdoor thermal sensation and neutral temperature in hot-summer and cold-winter climate. Energy and Buildings. 128, 190-197.

Nasrollahi, N., Hatami, Z. & Taleghani, M. (2017). Development of outdoor thermal comfort model for tourist in urban historical areas, A case study of Isfahan. Building and Environment. 125, 356- 372.

Kotharkar, R., & Bagade, A. (2017). Local Climate Zone classification for Indian cities: A case study of Nagpur. Urban Climate. http://dx.doi.org/10.1016/j.uclim.2017.03.003

Matzarakis, A., & Matuschek, O., (2011) Sky View Factor as a parameter in applied climatology – Rapid estimation by the SkyHelios Model. Meteorol. Z. 20, 39-45.

Effect of urban morphology on urban microclimate: A case of Vijayawada

Ar.Madhavan Rajan, Department of Architecture, NIT Trichy, India
Dr.D.Kannamma, Assistant Professor, Department of Architecture, NIT Trichy, India

ABSTRACT

Changes that happen in the urban surface tend to change the local climate of the particular settlement through the land surface process that influences the surface energy balance and boundary layer (Andrew M. Coutts, 2007). This study is a quantitative analysis of the urban morphology concerning the microclimate of the Vijayawada. The microclimate is simulated by using Ladybug tools. Many variables were used to accesses the microclimate of an urban area for this study chosen variables are Green Plot Ratio (GPR) and Open area (OA). These two parameters were analyzed using UTCI (Universal thermal climate index) as the thermal index for selected urban morphology in Vijayawada. This study aims to compare the High-density settlement with the low-density settlement in terms of its performance of Outdoor thermal comfort (OTC) and to accesses the microclimate respect to vegetation cover in Vijayawada

Keywords: Microclimate, UTCI, OA, GPR and Outdoor thermal comfort (OTC).

INTRODUCTION

Urban microclimate can be defined as the local climate observed in urban areas, which can be significantly different from the climate of surrounding rural areas (AMS, 2017). The urban microclimate is a major phenomenon that describes the outdoor comfort of the particular morphology such phenomenon acts in a better way only if the morphology is precisely designed. After the growth of huge cities with organic settlements, The morphologies unintentionally created a microclimate called urban heat island that causes problems and starts to give more outdoor discomfort in the cities. IEQ (indoor air quality) of the naturally ventilated buildings depends on the outdoor microclimate (Ghiaus C, 2005). Various factors play a major role in increasing the UHI of the cities one of it is the morphology of the built environment so it has a direct effect on the surrounding outdoor spaces (Davies M, 2008). So more research on context-based planning is needed for the cities. In the past, several adaptation measures have been investigated for the potential to influence urban microclimate, mostly to reduce elevated temperatures (Davies M, 2008) (Gago EJ, 2103) (Ghiaus C, 2005) (Revi A, 2014) (Rizwan AM, 2008) (Rosenfeld AH, 1995). As a need for the thermal index in this study UTCI is chosen as it proves to be better performance in evaluating the Outdoor thermal comfort (Mahant, 2014). Variable that taken into consideration to calculate UTCI are Air temperature(Tair), Relative Humidity, Mean radiant temperature(MRT) and windspeed at 10m height. It takes into account the thermo-regulations of a human body.

[1] Corresponding Author: madhavangr2@gmail.com, +91-9123512719

SITE AREA DESCRIPTION

The case area of the present study is in Vijayawada with Latitude of 16.50 deg N and Longitude of 80.64 deg E(figure 1). It comprises of all types of settlements like typical cities. Since the study is about comparing high density with low density two types of morphologies are chosen they are

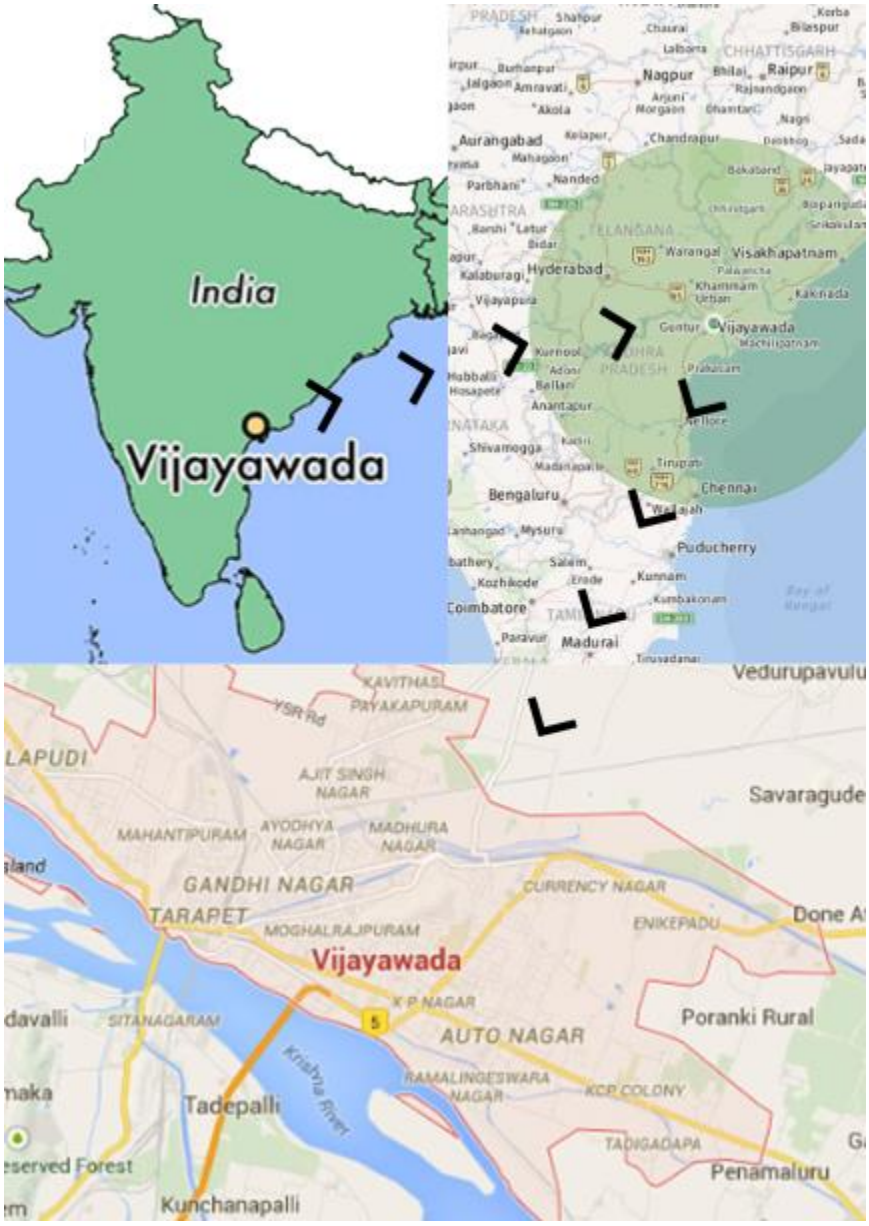
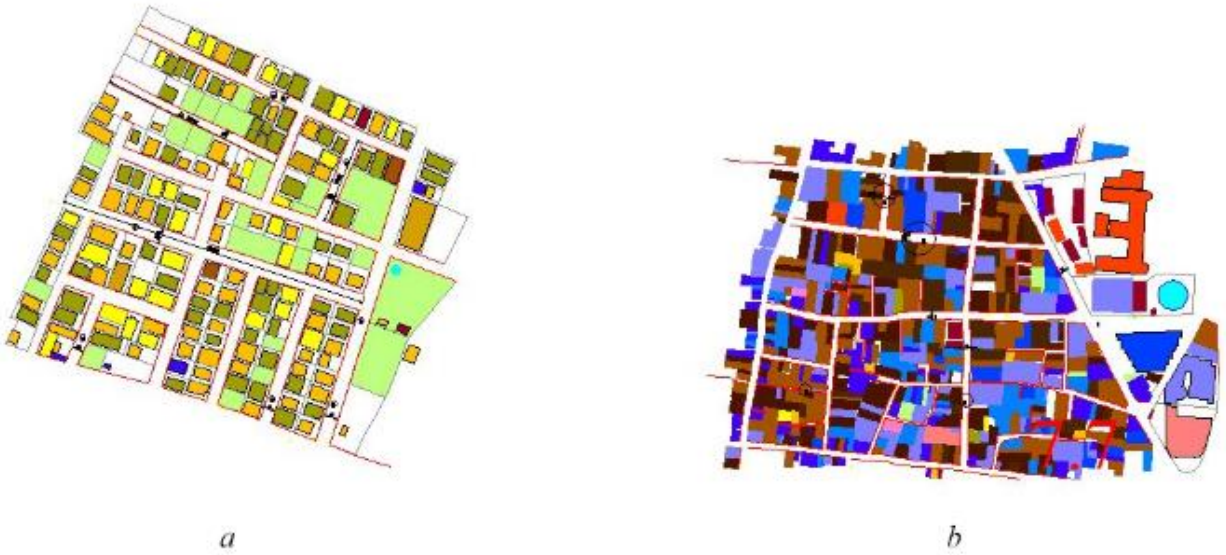


Figure 1- Vijayawada location Map *Source*: www.worldatlas.com

- Type1-Tarapet - High density (mixed-use with Ground floors as shops) Figure 2
- Type 2-Prashant Nagar- Low density (Residential use) Figure 2

Among these two morphology type 1 is in the Central Business District of Vijayawada and Type 2 is in the middle of the Residential sector. So the Anthropogenic Heat (heat released to the atmosphere as a result of human activities, often involving combustion of fuels) is more on Type 1 comparing with Type 2.



a *b*

Figure 2: a-Type 2 and b-Type 1 *source:* Author

Comfortable hours calculation

Comfortable hours are a Number of hours when there is absence cold or heat stress for a given region. Several thermal indices adopt each own method to accesses it. Since we use UTCI here the comfortable hours for the Vijayawada are obtained by the Epw file and plotted in a bar graph for the whole year in Figure 3.

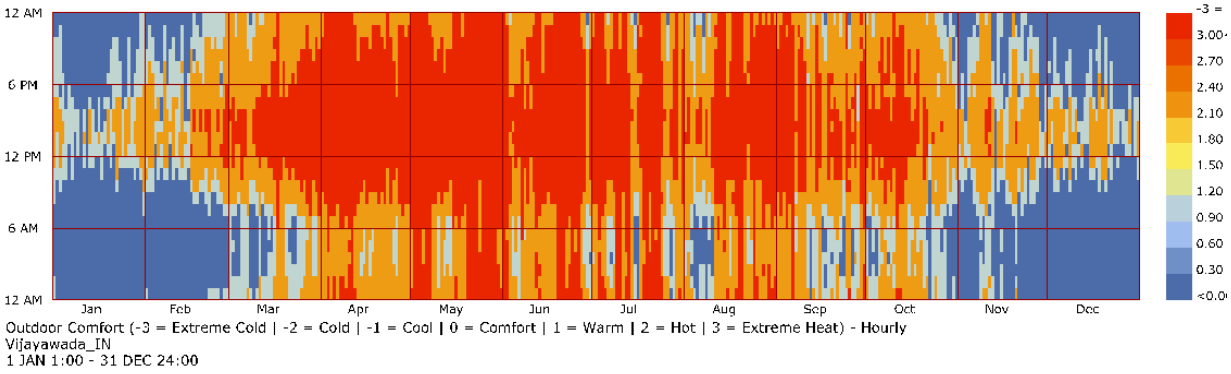


Figure 3 : 0 indicate the comfortable hours where it is mostly falls on colder months of the year *Source*: Author

Since there is no cold stress for Vijayawada the same bar graph is plotted in Boolean expression in Figure 4 where the uncomfortable hours fall on maximum hours (blue color) and comfortable hours fall mostly on night times (Red color). This indicates the Vijayawada has only 21.6% of comfortable hours and not especially in the summer months. As most of the warm and humid regions above the equator, the sun movement determines the hottest month as April, May, June and July. where the northern sun gives more discomfort and an average hourly temperature above 30 degrees in the daytime.

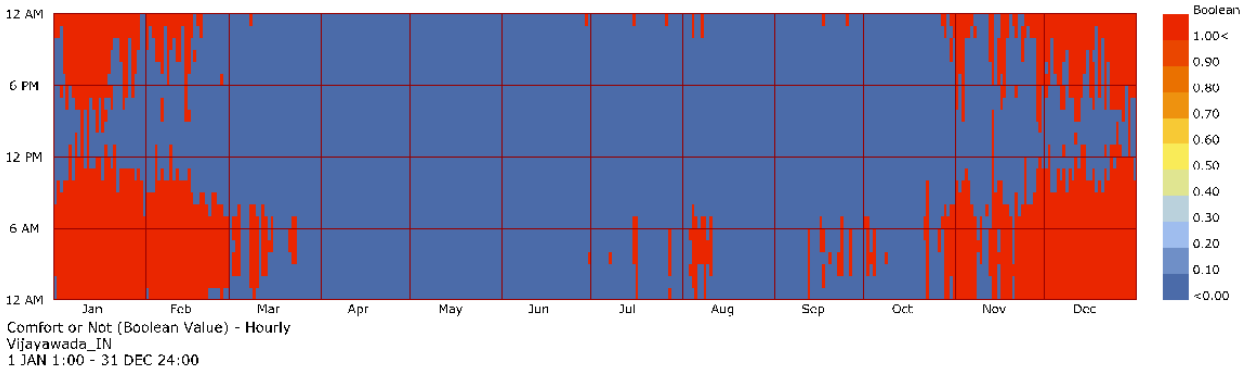


Figure 4 comfortable hours of vijayawada-21.6% of total hours *Source*: Author

SELECTION OF VARIABLES

The reason for choosing variables (OA and GPR) is to accesses the microclimate with a minimum data requirement. These two variable needs only two maps one is Figure-ground map and Area that under the green cover. This helps us to understand the role of Urban porosity concerning the microclimate of the city Vijayawada. Thus by getting the idea of how porus should an urban area must be to have an OTC. The values were given in table 1

Table 1: Variables data for morphologies

Morphologies	G P R	OA
Type 1	0%	10%
Type 2	15%	30%

The Green plot ratio is simply the average LAI of the greenery on-site and is presented as a ratio that is similar to the building plot ratio (Ong, 2003). Vegetation is the most effective landscape element in surface and air temperature modification (DUCHHART, 2011). Trees, shrubs, groundcovers, vines, and turf provide solar control by effectively reducing direct and reflected radiation and absorbing heat (DUCHHART, 2011).

RESULTS AND DISCUSSIONS

The Total percentage of comfortable hours is calculated for the two types of morphologies and presented as a bar graph for a year in figure (6-7) clearly shows that the Tarapet patch is performing well compared to the Prasanth Nagar with the increase in 8.4% of total comfortable

hours in a year. The impact of 10% GPR present in the Prashant Nagar does not give any impact on the outdoor thermal comfort. This is because the urban vegetation, on the other hand, performs well with increase in 50% or more GPR when it comes lesser than that is seems to be the temperature difference is less than 2 degree in Air temperature which is clearly seen in the figure 5 where the Prashant Nagar is simulated by increasing the GPR of the 66,398Sq.m-30.4% (Table 2) of the Open area up to 50% of the total Open area.

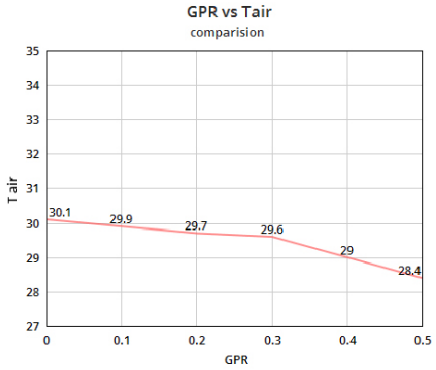


Figure 5 Relationship between Green plot ratio and Air temperature *source*: Author

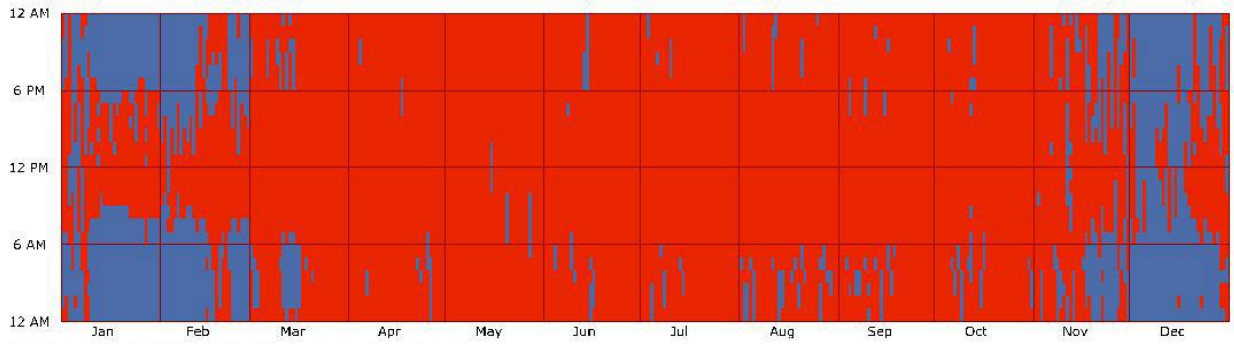


Figure 6 Total comfortable hours of a year-24.6% in Prashant Nagar source: Author

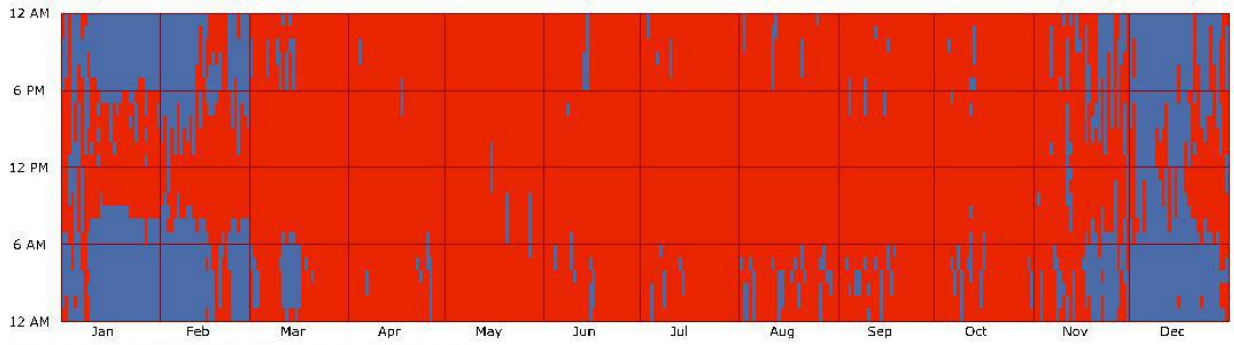


Figure 7 Total comfortable hours of a year-30% in Tarapet source: Author

The study clearly shows that the microclimate of the Vijayawada is enhanced by the following factors

- Reducing the porosity in the urban morphology
- Increasing the GPR above 50% of the total OA gives nominal effect in Temperature

The limitations in the implementation on this strategies were too utopia because the urban planning principle is dependant on the economy and the socio-cultural aspect so the guidelines and regulations were carefully formulated by keeping those two factors in mind by avoiding the outdoor thermal comfort phenomenon which is not much essential in terms of economic growth. Even growing new capitals like Amaravati planning concepts were devoid of ideas on outdoor thermal comfort.

Acknowledgments

This paper is a part of my thesis in my Master's program at the School of Architecture and Planning, Vijayawada. I thank my Thesis Guide Ar. Nagaraju Kaja Faculty of architecture for supporting me through my thesis process and Govt of Andhra Pradesh for providing the necessary information on websites that helped me in the research purpose.

REFERENCES

Ali-Toudert F, M. H. (2006). Numerical study on the effects of aspect ratio and orientation of an urban street canyon on outdoor thermal comfort in hot and dry climate. *Build. Environ*, 94-108.

AMS. (2017). *Meteorological glossary.* America: Meteorological glossary.

Andrew M. Coutts, J. B. (2007). Impact of Increasing Urban Density on Local Climate: Spatial and Temporal Variations in the Surface Energy Balance in Melbourne, Australia. *Journal of Applied Meteorology and Climatology*, 17.

Davies M, S. P. (2008). Strategies for the modification of the urban climate and the consequent impact on building energy use. *Energy Policy*, 4548-4551.

DUCHHART, S. A. (2011). Bioclimatic landscape design in extremely hot and. *Passive and Low Energy Architecture confrence* (p. 8). Louvain La Neuve: PLEA.

Gago EJ, R. J.-T. (2103). The city and urban heat islands: a review of strategies to mitigate adverse effects. *Renew. Sustain. Energy*, 749-758.

Ghiaus C, A. F. (2005). Natural ventilation in the urban environment: Assessment and design. *London: James and James science publishers*.

Khaled A. Al-Sallal, L. A.-R. (2012). Outdoor airflow analysis and potential for passive cooling in the modern urban. *Renewable Energy*, 10.

Mahant, M. M. (2014, April 17). OUTDOOR THERMAL COMFORT. *ARCHITECTURE-TIME SPACE & PEOPLE*, pp. 16-22.

Ong, B. L. (2003). Green plot ratio: an ecological measure for architecture and urban planning. *Landscape and Urban Planning*, 15.

Revi A, S. D.-D.-M. (2014). Urban Areas. Climate Change 2014: Impacts, Adaptation, and Vulnerability. *Cambridge University Press: Cambridge*, 535-612.

Rizwan AM, D. Y. (2008). A review on the generation, determination, and mitigation of urban heat island. *J. Environ. Sci.* , 120-128.

Rosenfeld AH, A. H. (1995). Mitigation of urban heat islands: materials, utility programs, updates. *Energy Build*, 255– 265.`

POLICIES, RATING & LABELLING PROGRAMS WITH UHI MITIGATION STRATEGIES

Solar-reflective "cool" walls: benefits, technologies, and implementation

Ronnen Levinson, Lawrence Berkeley National Laboratory (USA)
George Ban-Weiss, University of Southern California (USA)
Paul Berdahl, Lawrence Berkeley National Laboratory (USA)
Sharon Chen, Lawrence Berkeley National Laboratory (USA)
Hugo Destaillats, Lawrence Berkeley National Laboratory (USA)
Nathalie Dumas, University of California, San Diego (USA)
Haley Gilbert, Lawrence Berkeley National Laboratory (USA)
Howdy Goudey, Lawrence Berkeley National Laboratory (USA)
Sébastien Houzé de l'Aulnoit, Lawrence Berkeley National Laboratory (USA)
Jan Kleissl, University of California, San Diego (USA)
Benjamin Kurtz, University of California, San Diego (USA)
Yun Li, University of Southern California (USA)
Yan Long, University of California, San Diego (USA)
Arash Mohegh, University of Southern California (USA)
Negin Nazarian, University of California, San Diego (USA)
Matteo Pizzicotti, University of California, San Diego (USA)
Pablo Rosado, Lawrence Berkeley National Laboratory (USA)
Marion Russell, Lawrence Berkeley National Laboratory (USA)
Jonathan Slack, Lawrence Berkeley National Laboratory (USA)
Xiaochen Tang, Lawrence Berkeley National Laboratory (USA)
Jiachen Zhang, University of Southern California (USA)
Weilong Zhang, University of California, San Diego (USA)

ABSTRACT

Raising the albedo of a building's walls reduces unwanted solar heat gain in the cooling season. This saves electricity and lowers peak power demand by decreasing the need for air conditioning. It can also cool the outside air, which can mitigate the urban heat island effect and also improve air quality by slowing the reactions that produce smog. We quantified the energy savings, peak demand reduction, urban cooling, and air quality improvements attainable from solar-reflective "cool" walls in California; collaborated with industry to assess the performance of existing cool wall technologies, and to develop innovative cool wall solutions; and worked with government agencies, utilities, and industry to create a cool-wall infrastructure, including application guidelines, a product rating program, incentives, and building code credits.

Simulations indicate that cool walls provide annual energy savings, peak demand reduction, annual emission reduction, and summer heat island mitigation benefits comparable to those yielded by cool roofs, and are helpful across California and in United States climate zones 1 – 4. Natural exposure trials conducted at three sites in California and another three across the United States indicate that cool wall materials tend to stay clean and reflective. Significant advances were made in novel cool wall technologies, such as fluorescent cool pigments that expand the color palette for cool wall products. We prepared guidelines for the climate- and

building-appropriate use of cool walls. Ongoing efforts seek to introduce or expand cool wall provisions in building energy standards/programs and develop a cool-wall product rating system.

Introduction

The Lawrence Berkeley National Laboratory Heat Island Group has collaborated with the roofing industry and California regulators for two decades to advance the development and climate-appropriate use of solar-reflective "cool" roofs. There is now a large body of cool-roof science; a well-established cool roof rating system; cool roof requirements in building energy standards as well as voluntary incentive programs like Leadership in Energy and Environmental Design; and thousands of cool roofing products sold in the United States and abroad (Akbari and Levinson 2008; CRRC 2019).

Cool *walls* are also promising. Although the solar energy per unit area striking an east or west wall in summer is about half of what hits a horizontal roof, homes typically have about half as much wall insulation as roof insulation. For example, in a Fresno, California home with wood-framed walls, 2013 Title 24 requires R-38 (38 h·°F·ft²/BTU) ceiling insulation, but only R-19 wall insulation. Similarly, in a Fresno nonresidential building with light mass, heavy mass, or wood-framed walls, 2013 Title 24 requires R-26 roof insulation, but only R-6 to R-17 wall insulation. This suggests that the benefit of raising wall albedo (solar reflectance)—that is, the extent to which it reduces unwanted heat conducted into the interior space—is comparable to the benefit of increasing roof albedo.

A reflective coating or cladding can increase wall albedo. Cool-wall products available today include (1) light-colored paints that reflect 60 percent to 90 percent of sunlight when new, but which may also lose reflectance as they get dirty; and (2) darker "cool-colored" paints that come in a wide palette, but typically reflect less than 50 percent of sunlight when new.

In this study, our goals were to:

- Quantify the energy savings, peak demand reduction, urban cooling, and air quality improvements attainable from cool walls in California and the U.S., through modeling.
- Collaborate with industry to assess the performance of existing cool-wall technologies, and to develop innovative cool-wall solutions.
- Work with state and federal government agencies, utilities, and industry to create a cool-wall infrastructure, including application guidelines, a product rating program, incentives, and building code credits.

Lawrence Berkeley National Laboratory, the University of Southern California, and the University of California at San Diego collaborated with 10 partners from the wall product industry to advance the science and technology of cool walls. The study had five elements:

1. **Energy and Emission Savings Analysis**. We used building-energy simulations to quantify how increasing wall albedo affects the cooling, heating, and lighting energy uses of a building and its neighbors.
2. **Environmental Analysis**. We used building-, neighborhood-, and city-scale energy simulation models to assess pedestrian comfort, evaluate outdoor air temperature reductions, and assess changes to outdoor air quality.

3. **Technology Assessment**. We evaluated the performance of available and prototype cool-wall technologies, primarily the ability to reflect sunlight. We measured how solar reflectance changed when products were exposed outdoors at sites across California and the United States, with special attention paid to the performance of self-cleaning and de-polluting photocatalytic materials.
4. **Technology Development**. We explored innovative cool-wall technologies, including fluorescent cool pigments and retroreflective materials.
5. **Infrastructure Advancement**. We promoted the infrastructure needed to advance the climate- and building-appropriate use of cool walls, including application guidelines, a product rating program, incentives, and building code credits.

Energy and Emission Savings Analysis

Savings in an Isolated Building

Cool-wall changes to annual heating, ventilation, and air conditioning (HVAC) energy use depend on climate, wall construction, wall orientation, building geometry, HVAC efficiency, and operating schedule, while changes to annual energy cost and energy-related emissions further vary with local energy prices and emission factors. We used EnergyPlus to perform more than 100,000 building energy simulations spanning 10 different building categories, three building vintages, 16 California climate zones, and 15 United States climate zones. The simulations varied parameters such as wall albedo, roof albedo, combination of walls modified, and building orientation. Cool walls yielded annual savings in source energy and energy cost, as well as reductions in emissions (carbon dioxide, carbon dioxide equivalent, nitrogen oxide, and sulfur dioxide) in all California climate zones and in warm United States (ASHRAE) climate zones. Cool walls also yielded HVAC peak power demand reduction in all California and United States climate zones.

In California, cool walls reduced whole-building annual HVAC energy use 3.0 percent to 25 percent in single-family homes, 0.5 percent to 3.7 percent in medium offices, and 0.0 percent to 9.0 percent in stand-alone retail stores. In warm United States climates – zones 1A (Miami, Florida through 4B (Albuquerque, New Mexico) – cool walls reduced whole-building annual HVAC energy use 2.0 percent to 8.5 percent in single-family homes, 0.0 percent to 4.2 percent in medium offices, and -0.5 percent to 5 percent in stand-alone retail stores. Cool walls also yielded small annual HVAC source energy savings in some cold United States climates – zones 4C (San Francisco, California) through 7 (Duluth, Minnesota) – for certain building categories and vintages. Figure 1 shows annual whole-building HVAC fractional savings across the United States for two-story single-family homes of different vintages upon raising the albedo of all walls by 0.35 or upon increasing roof albedo by 0.30.

Annual HVAC source energy savings intensities (savings per unit of surface area modified) from east, south, and west walls were similar, and always larger than those from north walls. While walls often receive less incident solar energy per unit area than roofs, they are also less insulated than roofs. Therefore, savings intensities from modifying the four walls (albedo increase 0.35) were often comparable to those from modifying the roof (albedo increase 0.30 in residential and 0.40 in commercial).

This work is detailed by Rosado and Levinson (2019) and in Appendix A of Levinson et al. (2019b).

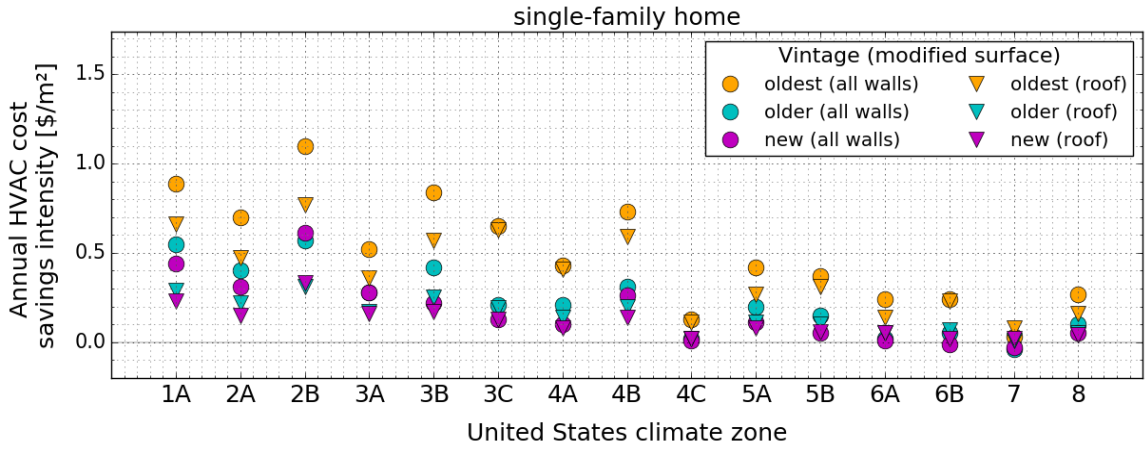


Figure 1. EnergyPlus simulations of annual whole-building source energy fractional HVAC savings in U.S. two-story single-family homes by climate zone and vintage.

Savings in a Building with Neighbors

The solar availability (incident solar radiation) of a central (modeled) building can be reduced by shadows cast by neighboring buildings and increased by sunlight reflected from neighboring buildings. We define the solar availability factor of a central building wall as the ratio of sunlight incident on the central building wall in the presence of the neighboring wall to that incident in the absence of the neighboring wall. One can scale cool-wall cooling savings, heating penalties, or HVAC savings simulated for an isolated central building (no neighbors) by the solar availability factor to account for interaction with the neighboring wall. One can also assess the effect of raising neighboring wall albedo on the solar availability of the central building wall. This analysis emphasizes simplicity, so that its results can be applied knowing only the canyon aspect ratio (ratio of building height to building separation), city, and month. It does not consider shading or reflection by surfaces other than neighboring walls, such as trees.

Monthly values of solar availability factor were evaluated in 17 climates across the United States, including three in California, for north, east, south, and west central walls, over a wide range of canyon aspect ratio (height/width). For example, solar availability factors for the walls of a single-family home in a residential neighborhood in Fresno, California range from about 0.5 to 0.9, depending on whether the wall faces a side, back, or front neighbor.

This work is detailed by Levinson (2019) and in Appendix C of Levinson et al. (2019b).

Environmental Analysis

Pedestrian Thermal Comfort

Cool walls affect the thermal environment of pedestrians by (a) increasing shortwave (solar) radiation striking the pedestrian; (b) decreasing longwave (thermal infrared) radiation incident on the pedestrian; and (c) lowering the outside air temperature. The magnitudes of these sometimes-opposing effects on pedestrians are quantified through human comfort models. Human comfort models attempt to emulate the typical human perception of environmental conditions through thermal comfort indices.

We analyzed thermal comfort for homogeneous neighborhoods. One year of typical weather data was input to a neighborhood microclimate model in three different California climate zones to understand the comfort effects of raising wall albedo on a pedestrian walking parallel to a wall 1.5 m away from the central building in a neighborhood. The latest version of the Pierce two-node model was used to compute pedestrian thermal comfort considering radiation from the sun, sky, and surrounding surfaces (for example, walls); wind speed; air temperature; humidity; metabolic activity (walking); and clothing. The principal model output is the Standard Equivalent Temperature, SET*. A higher SET* indicates that a human feels warmer, and a lower SET* indicates feeling cooler.

Near a multi-family residence in Fullerton, California (Orange County) with conventional walls of albedo 0.25, the annual average hourly SET* is about 18 °C at night and up to 30 °C during the day. During the day, cool walls raise SET* by up to 0.5 °C on average over the year. At night, cool walls lower SET* by up to 0.3 °C on average over the year. The smallest SET* rise occurs for a pedestrian near the north wall. The largest SET* rise occurs for the pedestrian near the south wall at noon in winter since winter solar irradiation on the south wall is the most of any wall orientation during any season. The absolute SET* difference induced by making walls more reflective is benign at less or equal to 0.2 °C over half of the time over the year. While SET* increases over 0.5 °C are occasionally observed, they occur exclusively during clear winter days when the pedestrian is more likely to experience a cold sensation. In that situation the SET* increase is beneficial to pedestrian thermal comfort. SET* differences by building type and climate zone were negligible. Results are sensitive to the pedestrian solar absorptance; on average over the year, a pedestrian with very light-colored clothing and light-colored skin (average solar absorptance 0.40) may even feel colder near a cool wall than near a conventional wall.

This work is detailed in Appendix D of Levinson et al. (2019b).

Urban Climate Effects of Cool Walls

The climate effects of increasing wall albedo are expected to differ from those for cool roofs and pavements for several reasons. First, the diurnal cycle and daily average values of solar irradiance (incident radiative power per unit area) on vertical walls differs from that on nearly horizontal roofs and pavements. Second, walls make up a different fraction of urban areas than do roofs and pavements. Third, air temperature affects per unit of grid cell albedo increase may differ for walls relative to roofs and pavements. We used the Weather Research and Forecasting model (WRF) version 3.7, coupled to an urban canopy model, to investigate how adopting cool walls and roofs influence albedos and near-surface canyon air temperatures in the Los Angeles basin.

To simulate the climate effects of cool walls, the researchers conducted three cases: CONTROL, in which roof, ground, and wall albedos are each set to 0.10; COOL_WALL_LOW, where wall albedo is raised to 0.50; and COOL_WALL_HIGH, where wall albedo is raised to 0.90. To compare the effect of increasing wall albedo to that of raising roof albedo, the team conducted two additional cases: COOL_ROOF_LOW, where roof albedo is raised to 0.50; and COOL_ROOF_HIGH, where roof albedo is raised to 0.90. Simulations were performed for 14 days (28 June 2012 to 12 July 2012).

Figure 2 shows the diurnal cycle of canyon air temperatures for each simulation, and changes in temperatures upon raising wall or roof albedo, spatially averaged over the urban regions of Los Angeles County. Peak temperature reductions for cool walls (that is, 0.64 K for COOL_WALL_HIGH – CONTROL and 0.28 K for COOL_WALL_LOW – CONTROL) occur

at 09:00 local standard time (LST). A local minimum in temperature difference (i.e., maximum in temperature reduction) is also observed around 18:00 LST.

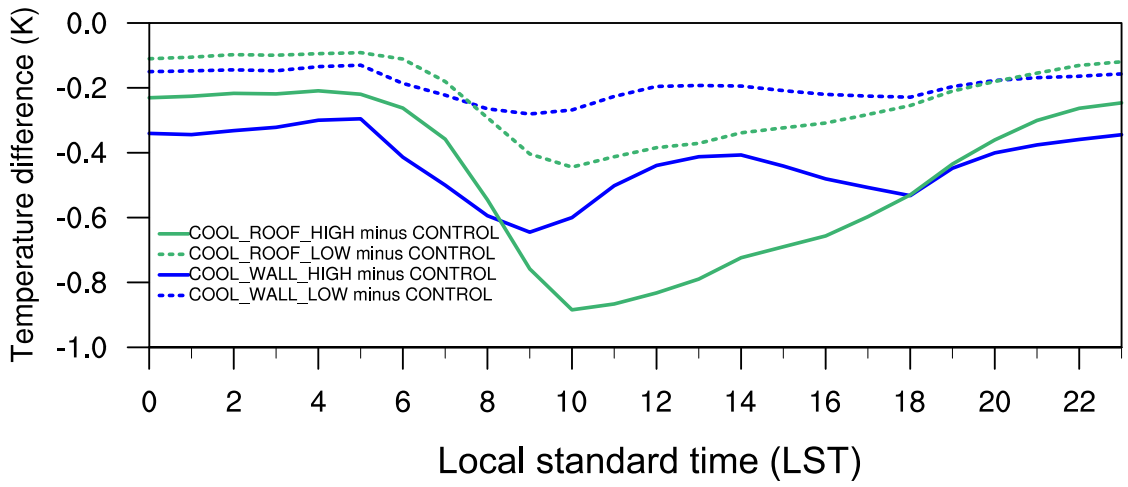


Figure 2. Canyon Air Temperature Change Upon Raising Wall or Roof Albedo. The diurnal cycle of differences in canyon air temperatures for COOL_WALL_LOW – CONTROL, COOL_WALL_HIGH – CONTROL, COOL_ROOF_LOW – CONTROL, and COOL_ROOF_HIGH – CONTROL. Values represent spatial averages in Los Angeles County for urban grid cells between July 3 and 12.

The average temperature reduction induced by cool walls (roofs) is approximately proportional to increases in wall (roof) albedo. Per 0.10 wall (roof) albedo increase, cool walls (roofs) can reduce summertime daily average canyon air temperature by 0.048–0.054 K (0.058–0.060 K). The ratio of the daily average air temperature reduction induced by cool walls to that yielded by cool roofs is about 86 percent, making their benefits comparable.

This work is detailed by Zhang et al. (2018) and in Appendix E of Levinson et al. (2019b).

Air Quality Effects of Cool Walls

We also investigated the influence of widespread deployment of cool walls on urban air pollutant concentrations, and systematically compared cool wall to cool roof effects. Simulations using a coupled meteorology-chemistry model (WRF-Chem) show that cool walls and roofs can reduce urban air temperatures, wind speeds, and planetary boundary heights in the Los Angeles Basin. Consequently, increasing wall (roof) albedo by 0.80, an upper bound scenario, leads to summertime maximum daily 8-hour average ozone concentration reductions of 0.35 (0.83) ppbv in Los Angeles County. However, cool walls (roofs) increase summertime daily average $PM_{2.5}$ concentrations by 0.62 (0.85) μg m^{-3}. We investigated the competing processes driving changes in concentrations of speciated $PM_{2.5}$. Increases in primary PM (elemental carbon and primary organic aerosols) concentrations can be attributed to reductions in ventilation of the Los Angeles Basin. Increases in concentrations of semi-volatile species (e.g., nitrate) are mainly driven by increases in gas-to-particle conversion due to reduced atmospheric temperatures.

This work is detailed by Zhang et al. (2019).

Technology Assessment

Natural Exposure of Wall Products

The solar reflectance of wall products can change over time as they soil and weather. The research team selected 69 materials from industry partners to expose in California and 55 to expose across the United States. The exposed set included factory-applied coatings, aluminum-plastic composite cladding, vinyl siding, architectural fabrics, retroreflecting materials, and different types of field-applied coatings. The latter included paint formulations with different surface finishes, some containing cool pigments and/or dirt-resistant formulations. Partners prepared paint samples on different substrates – metal, wood, concrete, and fiber cement – and provided many specimens of each product for use in natural exposure trials and additional lab testing.

The project team exposed specimens vertically, facing west, over two years at three sites in California representing different climate zones and pollution levels: the LBNL campus in Berkeley, an industrial partner facility in Fresno, and the USC campus in Los Angeles. The team similarly exposed specimens at three United States sites used by the Cool Roof Rating Council over a five-year period: New River, Arizona; Miami, Florida; and Medina, Ohio. In the California exposure program, the team deployed specimens in March/April 2016 that were retrieved quarterly for analysis at LBNL. Specimens used in the United States exposure program were deployed in August 2016 and are being collected annually.

Factory-applied coatings have shown excellent performance in all locations used for California and United States exposure, with negligible changes in solar reflectance. Composite metal cladding also exhibited great retention of initial solar reflectance values. In both cases, the use of fluorinated polymers in their formulation may explain the high performance. Factory-applied coatings with textured surfaces (for example, embossed or crinkled) behaved similarly to those with smooth surfaces (Figure 3).

In the case of field-applied coatings, the retention of initial solar reflectance values varied with coating formulation, surface finish, and substrate. Field-applied coatings colored with cool pigments were significantly more reflective than similarly colored products incorporating conventional pigments.

This work is detailed in Appendix J of Levinson et al. (2019b).

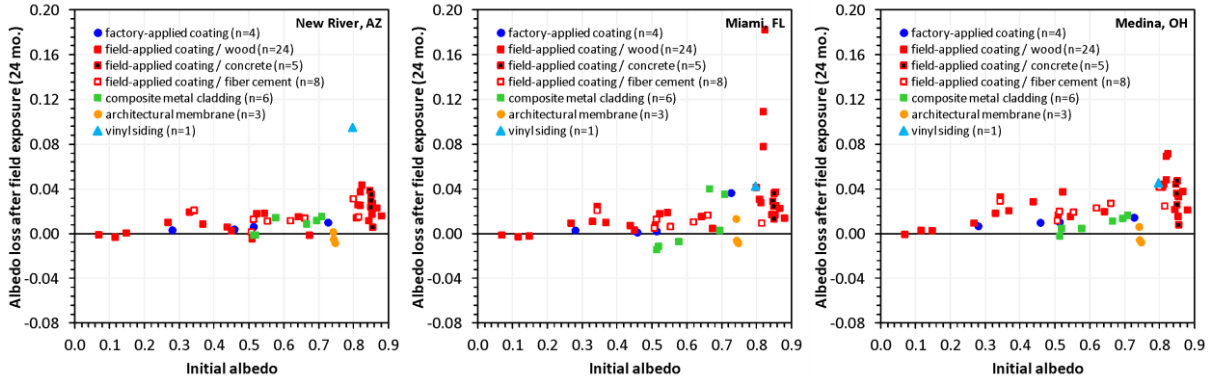


Figure 3. Most wall materials tested experienced minimal to modest albedo losses after 2 years of natural exposure at three sites across the United States in Arizona (hot/dry), Florida (hot/humid), and Ohio (temperate/polluted).

Self-cleaning and De-polluting Photocatalytic Materials

Two of the products evaluated in the natural exposure California and United States trials were architectural fabrics coated with photocatalytic titanium dioxide particles. A third material was an uncoated fabric of identical characteristics, used as a control. The project team evaluated specimens in the field and the laboratory.

The researchers exposed the photocatalytic specimens and their control vertically facing west in three sites in California representing different climate zones and pollution levels (Berkeley, Fresno, and Los Angeles) and in the three United States sites used by the Cool Roof Rating Council (CRRC): New River, Arizona (dry and hot weather); Miami, Florida (humid and hot weather); and Medina, Ohio (temperate weather with more pollution).

Photocatalytic materials exposed at the California sites showed negligible changes in solar reflectance over the course of two years. During the same period, the solar reflectance of the non-photocatalytic control decreased by 0.01—0.08. These changes reflected seasonal rainfall patterns, with soiling buildup during the dry season (April–November), and partial recovery of the initial solar reflectance value during the rainy season (December–March). These effects were more marked in Los Angeles and Fresno where ambient particulate matter levels are higher. The research team evaluated the de-polluting capacity of each photocatalytic product in the lab by measuring removal of nitrogen oxides (NO_x) from an airstream enriched in nitric oxide (NO). Tested samples included unexposed specimens and those retrieved from the field. The test conditions closely followed ISO Standard 22197-1: Test method for air-purification performance of semiconducting photocatalytic materials — Part 1: Removal of nitric oxide. Unexposed samples showed a higher NO_x-removal capacity, on the order of 0.7 micromoles of NO per hour (µmol NO h^{-1}), which was diminished by field exposure to values as low as 0.2 µmol NO h^{-1} for one of the products and 0.1 µmol NO h^{-1} for the other. During the rainy season the research team observed a recovery of the activity associated with a more effective cleaning of the catalyst surface.

This work is detailed in Appendix K of Levinson et al. (2019b).

Technology Development

Fluorescent Cool Pigments

Various pigments are used to formulate desired non-white colors that stay cooler in the sun than alternatives. These cool pigments provide a high near-infrared (NIR) reflectance in the solar infrared range of 700 nanometers (nm) to 2500 nm, and also a color specified by a reflectance spectrum in the 400 nm to 700 nm visible range. Still cooler materials can be formulated by also using fluorescence (photoluminescence) to re-emit some absorbed visible light as invisible NIR radiation.

Only a few pigments have demonstrated the potential for efficient fluorescence and also appear to have adequate (low) cost and durability. The first such pigment was ruby, which is composed of aluminum oxide doped with chromium. It can be used to produce red and pink colored materials. The second important class of materials includes the ancient pigment Egyptian blue. Egyptian blue has the chemical composition of $CaCuSi_4O_{10}$ – that is, calcium copper tetra-silicate. The most important other members of this class, the Egyptian blue family, have the same formula but with barium (Ba) or strontium (Sr) replacing calcium. The best performance to date with the Egyptian blue family has been achieved with the calcium and strontium compounds.

These blue pigments can also be blended with yellow pigment to achieve a green color, or with an orange pigment to obtain a blue-shade black.

Coatings incorporating either the ruby pigment or the Egyptian blue pigment can reject up to about 15% of incident sunlight via NIR-infrared fluorescence.

This work is detailed by Berdahl et al. (2016), Levinson et al. (2017), and Berdahl et al. (2018), and in Appendix N of Levinson et al. (2019b).

Retroreflectors

Raising a city's albedo (solar reflectance) increases the amount of incident sunlight returned to outer space, which cools cities and their buildings. Retroreflective cool walls could improve on diffusely reflecting cool walls by reflecting incoming beam radiation to the sun (if the retroreflection is three dimensional and ideal) or at least upwards (if the retroreflection is two dimensional and/or imperfect). For example, a retroreflective wall with albedo 0.60 would reflect 55 percent of incident light out of the city, while a Lambertian (perfectly diffuse) wall with the same albedo would only reflect 36 percent of incident light out of the city.

The greatest challenge in retroreflective wall design appears to be the need to operate at large incidence angles to reflect a substantial portion of incident sunlight. For example, on a summer day in Fresno, California, less than 37 percent of the beam radiation striking an east or west wall, and essentially none of that striking a south wall, will do so at an incidence angle less than or equal to 30°.

We explored wall retroreflector design using first-principle physics, ray tracing simulations, and goniometer measurements. Physics and simulations suggest that it will be difficult to achieve retroreflection at large incidence angle with surfaces that rely on total internal reflection, such as conventional safety films. This was confirmed with a simple goniometer that permits comparison of retroreflection to first-surface specular (mirrorlike) reflection, and with an advanced goniometer that measures solar spectral bi-directional reflectance intensity.

The most promising design was a two-surface retroreflector with orthogonal metal mirror faces. Attempts to fabricate this system by cutting and polishing grooves in an aluminum block indicate that residual surface roughness impedes retroreflection. Ongoing efforts focus on shaping aluminized Mylar film, a material with very high specular reflectance across the solar spectrum. This work is detailed by Levinson et al. (2019a) and in Appendix O of Levinson et al. (2019b).

Infrastructure Advancement

Cool-wall Application Guidelines

We created guidelines for the building- and climate-appropriate use of cool walls to conserve energy and reduce emissions of greenhouse gases and criteria pollutants across California and the United States. First, they explore the nature of cool walls by answering some fundamental questions such as "what is a cool wall?" and "why choose a cool wall?". Second, they provide a simple guide detailing the energy cost savings (or penalties) that arise from increasing wall reflectance in three common building categories—single-family home, medium office, and retail stand-alone. Third, they describe the operation and application of the Cool Surface Savings Explorer, a database tool that can report the cool-wall and cool-roof energy, energy cost, peak power demand, and emission savings simulated for many building categories. Fourth, they discuss

how to adjust cool walls savings and penalties to account for shading and reflection by neighboring buildings by applying a "solar availability factor".

These guidelines are presented in Appendix P of Levinson et al. (2019b).

Building Standards and Incentive Programs

Cool roofs can be found on buildings across the United States and are included in many city, state, and federal building codes/standards. To advance the adoption of cool walls, one can follow and learn from the cool-roof adoption model. Cool roofs were first incorporated in many codes/standards as credits and later became prescribed. The process was aided by the establishment of the Cool Roof Rating Council (CRRC). The CRRC is an independent organization that has developed methods for evaluating and labeling roofing products for reference by codes, standards, and rebates. It has also propagated the cool roof concept and its rating program.

ASHRAE 90.1 (2016), ASHRAE 189.1 (2014), California Green Building Standards Code; and Hawaii's State Energy Conservation Code already reference cool walls.

We are exploring the feasibility of expanding the scope of the CRRC to include wall products. We also seek to collaborate with California utilities to develop cool-wall incentives, and to sponsor an assessment of how cool walls could be included in California's Title 24 Building Energy Efficiency Standards.

This work is detailed in Appendix R of Levinson et al. (2019b).

Summary

Simulations indicate that cool walls save energy and reduce emissions in buildings across California and about half of the United States (climate zones 1 – 4). Thermal comfort changes for pedestrians walking next to a cool wall are small and will go unnoticed by most people. In Los Angeles, cool walls provided similar urban air temperature reductions as cool roofs per unit albedo in wall or roof albedo; cool walls and cool roofs each also reduce ozone concentration while increasing the concentration of $PM_{2.5}$.

After 24 months of natural exposure at three sites across California and another three sites across the U.S., cool-wall materials exhibited little to no loss in solar reflectance. Factory-applied coatings showed excellent performance in all locations, while the reflectance retention of field-applied coatings varied with coating formulation, surface finish, and substrate. Fluorescence (re-emission at longer wavelengths of light absorbed at shorter wavelengths) can expand the palette of colors for cool-wall products, while retroreflection (reflection of incident radiation toward its source) can increase the fraction of wall-reflected light that escapes the city.

We developed cool-wall guidelines to identify their building- and climate-appropriate use to conserve energy and reduce emissions of greenhouse gases and criteria pollutants across California and the United States. We identified existing cool-wall measures in building codes/standards and initiated contact with key stakeholders to develop new cool-wall measures, pilot credits, certification, and rebates. We also collaborated with the Cool Roof Rating Council to explore expansion of its program to include wall products.

Acknowledgements

This research was supported by the California Energy Commission under contract EPC-14-010, and by the Assistant Secretary for Energy Efficiency and Renewable Energy, Building Technologies Office of the U.S. Department of Energy under Contract No. DE-AC02-05CH11231. We thank David Hungerford (California Energy Commission) for his support and guidance.

References

Akbari, H., & Levinson, R. (2008). Evolution of cool-roof standards in the us. *Advances in Building Energy Research*, 2(1), 1–32. https://doi.org/10.3763/aber.2008.0201

Berdahl, P., Boocock, S. K., Chan, G. C.-Y., Chen, S. S., Levinson, R. M., & Zalich, M. A. (2018). High quantum yield of the Egyptian blue family of infrared phosphors ($MCuSi_4O_{10}$, M = Ca, Sr, Ba). *Journal of Applied Physics*, 123(19), 193103. https://doi.org/10.1063/1.5019808

Berdahl, P., Chen, S. S., Destaillats, H., Kirchstetter, T. W., Levinson, R. M., & Zalich, M. A. (2016). Fluorescent cooling of objects exposed to sunlight – The ruby example. *Solar Energy Materials and Solar Cells*, 157, 312–317. https://doi.org/10.1016/j.solmat.2016.05.058

CRRC (2019). Rated Products Directory, Cool Roof Rating Council. https://coolroofs.org

Levinson, R. (2019). Using solar availability factors to adjust cool-wall energy savings for shading and reflection by neighboring buildings. *Solar Energy*, 180, 717–734. https://doi.org/10.1016/j.solener.2019.01.023

Levinson, R., Chen, S., Ferrari, C., Berdahl, P., & Slack, J. (2017). Methods and instrumentation to measure the effective solar reflectance of fluorescent cool surfaces. *Energy and Buildings*, 152, 752–765. https://doi.org/10.1016/j.enbuild.2016.11.007

Levinson, R., Chen, S., Slack, J., Goudey, H., Harima, T., & Berdahl, P. (2019a). Design, characterization, and fabrication of solar-retroreflective cool-wall materials. *Solar Energy Materials & Solar Cells*, in press. https://doi.org/10.1016/j.solmat.2019.110117

Levinson, R., Gilbert, H., Zhang, J., Ban-Weiss, G., Kleissl, J., Pizzicotti, M., Zhang, W., Dumas, N., Kurtz, B., Long, Y., Nazarian, N., Mohegh, A., Li, Y., Tang, X., Chen, S., Russell, M., Houzé de l'Aulnoit, S., Berdahl, P., Rosado, P., Slack, J., Goudey, H., & Destaillats, H. (2019b). Solar-Reflective "Cool" Walls: Benefits, Technologies, and Implementation. Publication CEC-500-2019-040, California Energy Commission, Sacramento, CA. https://www.energy.ca.gov/2019publications/CEC-500-2019-040

Rosado, P. J., & Levinson, R. (2019). Potential benefits of cool walls on residential and commercial buildings across California and the United States: conserving energy, saving money, and reducing emission of greenhouse gases and air pollutants. *Energy and Buildings*, 199, 588-607. https://doi.org/10.1016/j.enbuild.2019.02.028

Zhang, J., Li, Y., Tao, W., Liu, J., Levinson, R., Mohegh, A., Ban-Weiss, G. (2019). Investigating the urban air quality effects of cool walls and cool roofs in Southern California. *Environmental Science & Technology*, 53(13), 7532–7542. https://doi.org/10.1021/acs.est.9b00626

Zhang, J., Mohegh, A., Li, Y., Levinson, R., & Ban-Weiss, G. (2018). Systematic comparison of the influence of cool wall versus cool roof adoption on urban climate in the Los Angeles Basin. *Environmental Science & Technology*, 52(19), 11188–11197. https://doi.org/10.1021/acs.est.8b00732

Review of heat wave studies and related urban policies in South Asia

Rajashree Kotharkar, Professor, Visvesvaraya National Institute of Technology (India)
Aveek Ghosh, PhD Scholar, Visvesvaraya National Institute of Technology (India)

ABSTRACT

The Intergovernmental Panel on Climate Change (IPCC) projects that the frequency of heat waves (HWs) is likely to increase over most land areas in the twenty-first century. Recurrent HWs are an emerging environmental and health concern and already distress in rapidly growing and fast urbanizing South Asia. A review of original research publications of the past five decades from peer-reviewed journals and conference proceedings, covering South Asia, revealed that the region is constantly experiencing the warmest temperatures. The review attempts to comprehend HWs in different contexts, geographic locations, and on previous studies. The paper presents a comprehensive review of existing plans/policies/guidelines in South Asia at the national/regional/city level to counter extreme heat risk. The study is extended to identify the issues and gaps in the current policies and frameworks in the larger setting of urban planning measures for adaptation and mitigation efforts. A specific set of long-term actions and vulnerability assessment concentrated on cities must be developed and integrated into a defined heat action plan coupled with improvements in urban and regional planning. Policies and actions must address the issues of the built environment in land use/planning and address the existing institutional and implementation gaps.

Special Issue Journal	:	Urban Climate
DoI	:	https://doi.org/10.1016/j.uclim.2021.100777
Citation	:	Kotharkar, R., & Ghosh, A. (2021). Review of heat wave studies and related urban policies in South Asia. Urban Climate, 36, 100777.

A big picture of urban heat island mitigation strategies and recommendation for India

Vaibhav Rai Khare, Environmental Design Solutions (India)
Akash Vajpai, PwC India (India)
Durva Gupta, Indian Institute of Technology Delhi (India)

ABSTRACT

Climate change poses a great threat to humans and the ecosystem of the planet. There are many factors that trigger climate change, and there are many aftereffects. One of the after-effects is Urban Heat Island (UHI), recognized as the most evident characteristic of urban climate which occurs due to dark, non-reflective surfaces. These surfaces absorb the warmth of the Sun, radiate heat; Thus, increase the land surface temperature. Additionally, heat islands increase cooling loads in the summer, which tends to increase energy consumption and produce more greenhouse gases. There are numerous strategies to mitigate the UHI effect. This study reviews various UHI mitigation strategies and their effectiveness in cooling the urban environment and propose a set of recommendation based on research and analysis. Broadly, the mitigation strategies have been divided into (i) Roof strategies, (ii) non-roof strategies, and (iii) covered parking strategies. It has been found out that the simultaneous use of several UHI mitigation measures has a more significant impact on lowering the urban temperature and could be mitigated. The study highlights the importance of each mitigation strategy and presents a set of recommendations for India that can be directed at the government level to policies to mitigate the UHI effect.

Special Issue Journal	:	Urban Climate
DoI	:	https://doi.org/10.1016/j.uclim.2021.100845
Citation	:	Khare, V., Vajpai, A., & Gupta, D. (2021). A big picture of urban heat island mitigation strategies and recommendation for India. Urban Climate, 37, 100845.

REMOTE SENSING OF CITIES AND URBAN CLIMATES

Assessment of urban cooling effect based on downscaled land surface temperature: A case study for Fukuoka, Japan

Wangchongyu Peng, Southeast University, Nanjing, China
Xin Yuan, Qingdao University of Technology, Qingdao, China
Weijun Gao, The University of Kitakyushu, Japan
Rui Wang, The University of Kitakyushu, Japan
Wei Chen, Yuncheng and Technical University, Yuncheng, China

ABSTRACT

The phenomenon of urban areas becoming warmer than surrounding rural areas, known as urban heat island, is one of the biggest urban issues due to human activities. The study adopted random forests (RF) based downscaling land surface temperature (LST) to assess the surface urban heat island (SUHI) of Fukuoka, Japan. The LST images were first downscaled to 250 m spatial resolution, and then the seasonal and diurnal SUHI was identified. The results implied that the SUHI in summer daytime is the most significant while in winter nighttime is the least significant in the area. Through the bivariate Moran's I test and zonal statistics, the cooling effect of the green-blue spaces were evaluated. The forest has the most substantial urban cooling effect with the average LST change occurs at a distance of about 1 km (maximum 6.32 K). The cooling effect of the sea is significant during daytime, whilst that of the lake/river and the cropland/grassland is not obvious. We concluded the urban population and land use and land cover (LULC) are significantly spatial correlated to UHI, and are important factors of considering the urban heat island (UHI) mitigation strategies.

Special Issue Journal	:	Urban Climate
DoI	:	https://doi.org/10.1016/j.uclim.2021.100790
Citation	:	Peng, W., Yuan, X., Gao, W., Wang, R., & Chen, W. (2021). Assessment of urban cooling effect based on downscaled land surface temperature: A case study for Fukuoka, Japan. Urban Climate, 36, 100790.

Urban surfaces analysis with remote sensing data for the evaluation of UHI mitigation scenarios

Francesca Despini, Department of Engineering Enzo Ferrari, University of Modena and Reggio Emilia (Italy)
Chiara Ferrari, Department of Engineering Enzo Ferrari, University of Modena and Reggio Emilia (Italy)
Giulia Santunione, Department of Engineering Enzo Ferrari, University of Modena and Reggio Emilia (Italy)
Stefano Tommasone, Department of Engineering Enzo Ferrari, University of Modena and Reggio Emilia (Italy)
Alberto Muscio, Department of Engineering Enzo Ferrari, University of Modena and Reggio Emilia (Italy)
Sergio Teggi, Department of Engineering Enzo Ferrari, University of Modena and Reggio Emilia (Italy)

ABSTRACT

Considering the new IPCC report and its recent suggestions, it is important to pay serious attention to the Urban Heat Island issue. In this study, satellite images acquired by the Worldview3 sensor (WV3) were processed to classify the different kinds of urban surface and to compute the albedo value for each surface. Then several UHI mitigation scenarios were analyzed, varying selectively the surface albedo by choosing solar reflective materials. Clay tile pitched roofs, dark roofs and parking areas were considered as “modifiable surfaces” and their albedo values were increased on the basis of the literature and of data made available by product manufacturers. For each proposed scenario, the reduction of intensity of the Urban Heat Island effect (ATD), the energy saving brought by lower absorption of air conditioning systems (ΔE) and the consequent cost savings were calculated. All the scenarios proved to be convenient and with a relatively fast return on investment. In particular, two scenarios involving the modification of several surfaces at the same time proved to be the most promising ones from the perspective of a public administration, with significant benefits on the well-being of the population, as well as with similar and relatively short payback periods.

Special Issue Journal	:	Urban Climate
DoI	:	https://doi.org/10.1016/j.uclim.2020.100761
Citation	:	Despini, F., Ferrari, C., Santunione, G., Tommasone, S., Muscio, A., & Teggi, S. (2021). Urban surfaces analysis with remote sensing data for the evaluation of UHI mitigation scenarios. Urban Climate, 35, 100761.

Relationship Between Urban Land Use Dynamics and Land Surface Temperature: Current and Future Scenario Modeling

Nimish G., Chandan M. C., Bharath H. A.
Ranbir and Chitra Gupta School of Infrastructure Design and Management
Indian Institute of Technology Kharagpur, West Bengal – 721302, India

Abstract

Anthropogenic activities have ominously transformed landscape (unplanned urbanization) over past few decades affecting the atmospheric processes and the most perilous amongst it is heat stress and thermal discomfort. Mitigation techniques for plummeting the surface temperature as suggested by the scientific community across the world include dedicating a part of land in every locality for plantation, construction of green roof, terrace gardens, etc. This study analyses the effect of Land use changes on Land Surface Temperature and its variability with features on the surface contribute to the absorption and reflection of heat influx for Indian city of Kolkata. The historical city of Kolkata has experienced extravagant development residentially, commercially, industrially and culturally that has led to modification in its microclimate. The study examined temporal land use changes for Kolkata Metropolitan Area using supervised classification algorithm to understand the urban footprint and it was observed that the study area has experienced a growth of 203% in urban area over three decades. Also, quantification of land surface temperature using single window method was performed to assess thermal comfortability and a rise of 7˚C was observed in the mean land surface temperature. A buffer was considered to understand the sprawl, and urban heat island. The study also tries to relate various land cover types with LST, estimates the urban heat island and further includes modeling future land use changes. Result of the developed model based on business as usual scenario shows an increasing trend of concretization that would lead to a rise in surface temperatures. The outcome of the study will assist the decision makers, government officials, higher authorities, etc. in developing a sustainable plan and modify policies that would help in creating a balance between environment and hominids.

Keywords*: Urban growth, Land use analysis, SLEUTH, Land Surface Temperature, Climate Change, Spatial Indices, Urban Heat Island*

1. Introduction

Since the emergence of history, hominids have had the ability to be superior than all other living forms and to abuse the resources for their immediate advantages. Previously, this was altering the climate only at local level that increased to regional, but over past few decades, due to the increased demographic pressure as a result of migration for better living standards, medical facilities and job opportunities, humans have significantly altered climate globally (Keeling, 1997; Karoly et al., 2003; Scott et al., 2006). Urbanization can be defined as a comprehensive phenomenon that can be inferred as an increment in paved surface in a town or a city due to increased population influx

or unification of sub-urban areas into nearby urban area (Ramachandra et al., 2012). As per various scientific literature, unplanned urbanization is the one that creates glitches (Chandan et al., 2017). Over few decades, urban growth is not only horizontal but vertical as well and the tall structures modify the wind turbulence causing reduced displacement of pollutants. This rise in concentration of GHGs and PMs changes the atmospheric reactions causing global warming (Ramachandra et al., 2015). As per scientific agencies such as NASA and NOAA, 10 warmest year have all occurred since 1998, 2016 being the warmest.

Studies have found that this rapid change in urbanization can be understood by LULC alterations and is referred as a vital cause of changing climate. It involves conversion of vegetation, agricultural fields, shrubby areas and barren areas into urban pockets (Ramachandra et al., 2016) that affects the rate of evaporation, surface albedo, storage of heat and moisture content of the soil, increased pollution levels, solar radiation and surface temperature LULC, LST and climate change are closely related and the relationship has been developed in numerous ways across the globe. One of the several primary parameters to comprehend climate change is Land Surface Temperature (LST) as it is responsible for upward thermal radiation of surface and defines the thermal comfortability of the region (Bento et al., 2017). LST is the radiative skin temperature of surface of landmass on earth (Ministry of Statistic and Programme Implementation, 2015). LST is the main parameter that affects earth's natural cycles (biogeochemical cycle, water cycle, Nitrogen cycle, Carbon cycle, Phosphorous cycle, etc.), rainfall pattern, regional biodiversity and contributes to climate change at micro-meso-macro level (Bharath et al., 2013; Nimish et al., 2018). LST serves as a vital parameter for diverse applications such as vegetation health monitoring, hydrological modeling, urban climatic studies, environmental parameter changes, Greenhouse gases estimation, Urban Heat Islands (UHI), etc. (Anderson et al., 2008; Li et al., 2013; Ramachandra et al., 2017).

Increase in LST causes heat waves that are considered a serious threat to all the living beings globally. Urban areas are more vulnerable to these heat waves due to UHI effect and high demographic pressure. As a result of increased cases of UHI, heat waves in current scenario has become a common phenomenon and is getting stronger for longer time durations, thus, exacerbating the problem of thermal risk for the local residents (Founda & Santamouris, 2017). Paved surfaces in cities have higher albedo when compared to any naturally occurring surface (vegetation, water body, wet soil) and construction materials used in rural areas. Paved surfaces in cities also is impervious in nature and increases surface runoff when compared to rural areas, thus, decreased vegetation and water reduces the rate of evapotranspiration causing increased heat entering the air in urban area.

Advancement in remote sensing data and with the launch of various satellites, sensor based analysis for investigating the climatic parameters, urbanization, surface temperature measurement has become easier for the policy makers and stakeholders (Jasim et al., 2016; Bharath et al., 2017). Assessment of LULC and prediction of likely changes, its relationship with LST will help the policy makers to improve the existing policies and formulating the newer ones for sustainable

development of future in terms of infrastructure, basic amenities, food, availability of fresh water, decorous solid waste management and health (Nimish et al., 2018). In this regard, one of the well-established urban growth models SLEUTH has been adopted in this study to foresee changes in urban land use by the year 2025 and therefore relate increase in growth to surface temperature variations. This communication explores the detailed linkage between Land Use, LST, future urban growth through modelling and spatial indices for Kolkata Metropolitan Area (KMA).

2. Study Area

Kolkata Metropolitan Area (KMA) also known as Greater Kolkata with 10 km buffer was considered, covers an area of 1850 km^2. As per census, 2011, it serves as a home for 14.11 million people, making it third most populous city in India and eighth largest urban agglomeration globally. Figure 1 depicts the study area and the basic geographic details is as shown in table 1.

Table 1: Geographic profile of Kolkata Metropolitan Area

Area	1886.67km^2
Latitude	22˚ 34’ 21” N
Longitude	88˚ 21’ 31” E
Altitude	1.5 – 9m above mean sea level (1% drainage gradient)

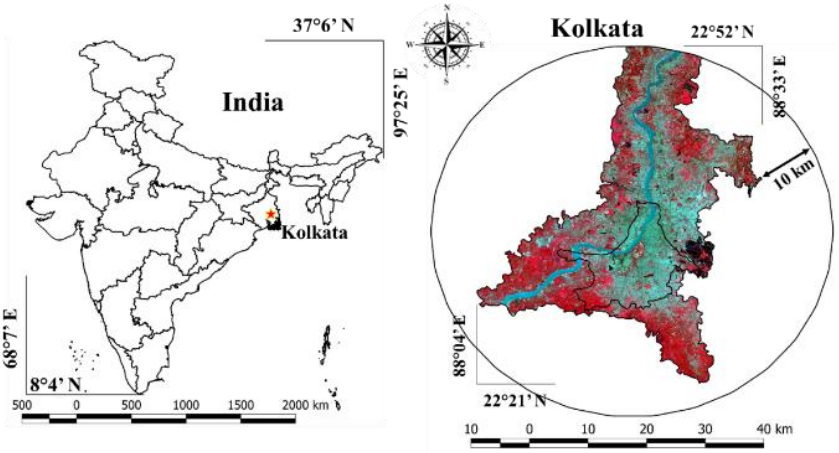


Figure 1: Study area depicting India and Kolkata Metropolitan Area with 10 km buffer and location details

3. Data and Method

A six phase process was involved in the communication as exemplified in figure 2. It includes – a) Data acquisition, b) Extraction and pre-processing, c) Landuse analysis, d) Quantification of Land Surface Temperature and NUHII (Normalized Urban Heat Island Index), e) Relationship between various Land cover and LST, and f) Landscape modeling and prediction

a) Data acquisition: Landsat and ASTER data was obtained from USGS earth explorer and were used for performing landuse classification, calculating LST and generating DEM. City development plan was downloaded from Government of Kolkata website and toposheets were acquired from Survey of India website. Road network was obtained by open street maps (OSM). Google earth, CDP and SOI toposheets were used as ancillary data.

b) Extraction and pre-processing: CDP was geo-registered using Ground Control Points (GCPs) and Google earth. Toposheets, CDP and other auxiliary datasets were used to identify Kolkata metropolitan boundary and was digitized. A 10 km buffer ring was considered around the city for understanding sprawl and urban heat islands. Road network

downloaded from OSM had few missing roads in the study area, they were identified using Google earth and were manually digitized. Slope and hillshade map was generated using DEM and exclusion layer were derived from CDP that includes water bodies and protected areas. Remotely sensed data was then preprocessed for geometric errors (if any) and was resampled using ancillary data. All the maps were then cropped pertaining to study area.

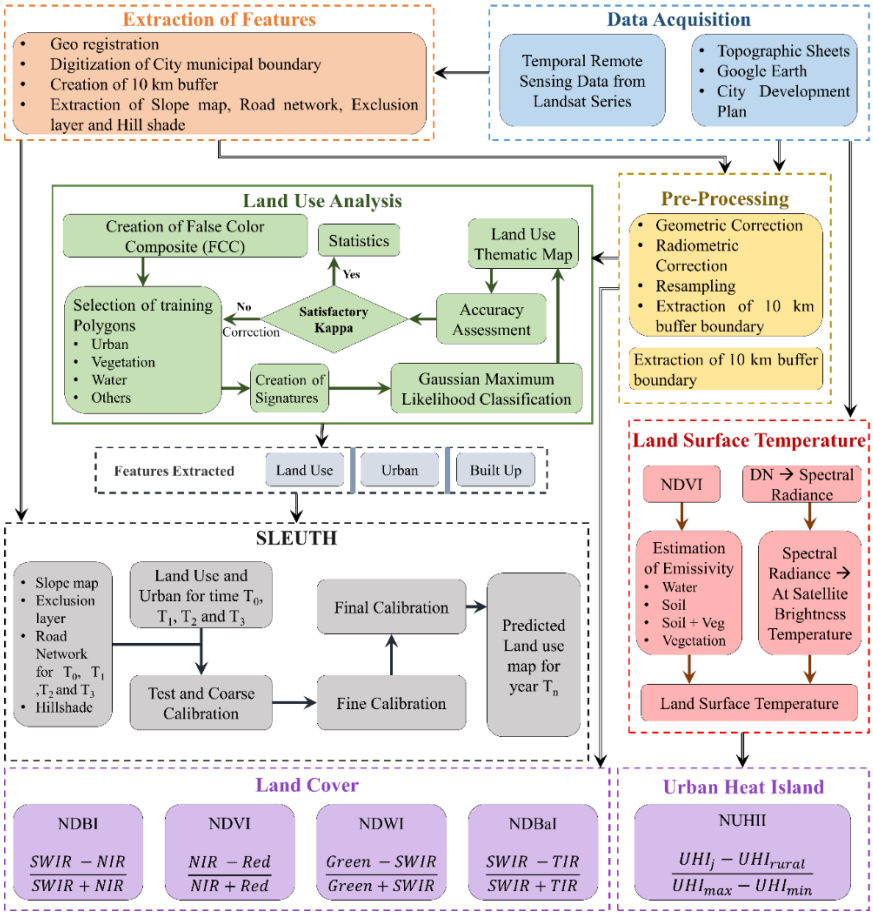


Figure 2: Method

c) Landuse Analysis: Landuse analysis is a four step process: (i) **Generation of FCC:** This involves assigning blue color to green band, green color to red band and red color to NIR band (ii) **Creation of signatures:** Training polygons are digitized based on heterogeneous and diverse features of each class from FCC. (iii) **Classification:** A supervised classification technique – Gaussian Maximum Likelihood Classification (GMLC) was performed to divide the study area into 4 classes (Urban, Vegetation, Water, Others). (iv) **Accuracy Assessment:** Google earth and ground truth data were incorporated to create a validation map. Using error matrix overall accuracy and kappa coefficient was estimated.

d) Quantification of LST and NUHII

LST: In acquired remote sensing data, thermal band ranges from 10.4 to 12.5 µm and each pixel is assigned with a DN (digital number) value equivalent to the reflectance/emitted values by the feature under consideration. For obtaining information, these values are converted into spectral radiance and top-of-atmosphere temperature. Single window algorithm was used to perform calculations and obtain at-satellite brightness temperature. Due to the presence of atmosphere between the feature and sensor, few distortions occur and they can be corrected by calculating surface emissivity. At-satellite brightness temperature and surface emissivity then serves as input to estimate LST. This method was followed as established in Nimish et al., 2018. Further to understand the intra-class variability COV was estimated using eq. 1. COV is a statistical parameter that defines how distributed and deviated the observations are from mean of that particular class.

$$COV = \frac{\sigma}{\mu} X100 \quad (1)$$

here, COV = Coefficient of Variation (%), σ = Standard deviation, µ = mean

Normalized Urban Heat Island Index (NUHII): To understand the difference in temperature of urban area and rural area, UHI was estimated. This was then further divided into six categories to understand and prioritize areas facing higher UHI. Normalized UHI was estimated using eq. 2.

$$NUHII = \frac{LST_j - LST_{rural}}{LST_{max} - LST_{rural}} \quad (2)$$

here, LST_j is Land surface temperature of the pixel under analysis; LST_{Rural} is surface temperature of rural area.

e) Relationship between Land cover and LST: Land cover can be defined as the natural features present on the surface of earth. Since, the study area was divided into four classes and thus, land cover corresponding to each class: NDBI, NDVI, NDWI and NDBaI were quantified. All these ranges from -1 to +1.

i. NDBI: NDBI (Normalized Difference Builtup Index) can be used to extract paved surface as it gives higher value for feature that are impervious and lower for all other features. It plays an important role in extracting urban builtup and can be computed using eq. 3.

$$NDBI = \frac{SWIR - NIR}{SWIR + NIR} \quad (3)$$

ii. NDVI: NDVI (Normalized Difference Vegetation Index) is an important index that describes the proportion of vegetation by measuring the difference between NIR band (strong reflectance for vegetation) and Red band (strong absorbance for vegetation) of electromagnetic spectrum. It can be expressed as shown in eq. 4.

$$NDVI = \frac{NIR - Red}{NIR + Red} \quad (4)$$

iii. NDWI: NDWI (Normalized Difference Water Index) is an indicator that can be used to extract water bodies in the remotely acquired data and can be equated from eq. 5.

$$NDWI = \frac{Green - SWIR}{Green + SWIR} \quad (5)$$

iv. NDBaI: NDBaI is an index that uses SWIR and TIR range of electromagnetic spectrum to differentiate barren area from any other features present. It can be estimated as shown in eq. 6.

$$NDBaI = \frac{SWIR - TIR}{SWIR + TIR} \quad (6)$$

f) Urban growth modeling and prediction: SLEUTH model involves various steps to arrive at future urban growth map. (i) Preparation of input layers. As the acronym suggests model stands for slope, land use, excluded, urban, transportation and hillshade, are used as input layers. (ii) Model has to be tested, calibrated in three phases viz. course, fine and final with spatial resolution of input images as 120m, 60m and 30m respectively. (iii) Five growth coefficients, governing the model, on a range of 0-100 are narrowed down to a single value used in prediction. (iv) Accuracy and validation of the model are tested with respect to goodness of fit statistics.

4. Analysis and Results

a) Landuse: Temporal land use analysis was performed for 1991, 2000, 2009 and 2017 for the study area using GMLC (supervised classification). Figure 3a illustrates landuse analysis for the study period and figure 3b depicts the area and percentage cover of each class. It was observed that urban area has increased three folds during the study period. Infill type of growth was observed, wherein the core area was densified in all the directions. Sprawling was witnessed in the eastern part wherein New town area is developing at an increased rate. Vegetation has not changed much during the study period but an increased percentage of water class was observed and that can be inferred to the increased wetlands in the eastern part of buffer area. The others category has shown a decline as the open areas within the city is utilized for construction of buildings and roads. Accuracy assessment was performed for all the years using google earth and ground truth data and the kappa coefficient was found to more than 0.85 (figure 3a).

b) *Land Surface Temperature:* LST for KMA region with 10km buffer was quantified as shown in figure 4 and it was observed that the mean surface temperature of KMA region ranges from 31-33˚C while with buffer region considered the mean temperature drops down by 1˚C. Table 4 shows the statistical description of the study area. The minimum temperature of the city has shown a rising trend and became 26.50˚C from 18˚C and the maximum temperature has increased from 35.40˚C to 43.50˚C. Post this, LST was analyzed class-wise and apparently the mean surface temperature of all the classes have increased during the study period. As a result of increment in impervious surface across the city and buffer, the mean surface temperature of urban category has increased from 27.70˚C to 34.96˚C. The mean surface temperature of vegetation has increased by 5.75˚C

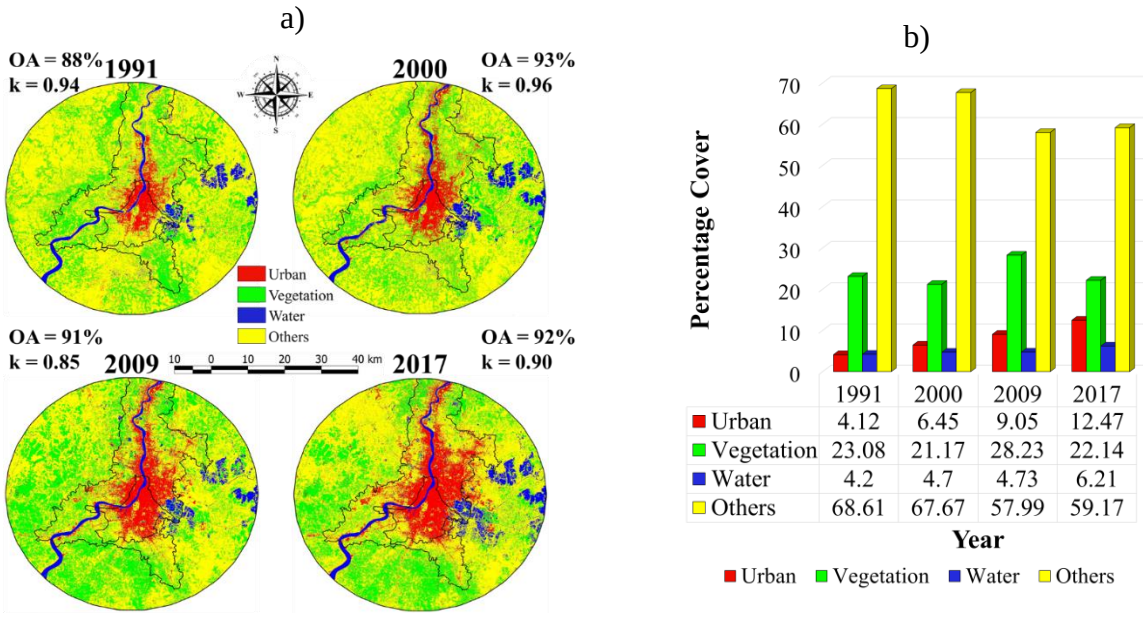


Figure 3:a) Landuse analysis for KMA with 10km buffer from 1991-2017, b) Percentage cover for each landuse class

c) ***Normalized Urban Heat Island Index (NUHII):*** NUHII for 2017 was quantified (figure 5) from eq. 2 and was further divided into 6 categories for better analysis as shown in table 5. It can be observed that only one sixth of the whole region that is close to river Hooghly and has low urban density has negative heat island. Thus, it can be inferred that presence of waterbody or a breathing green or open space nearby an urban area reduces the effect of urban heat islands. Majority of urban area shows low to moderate urban heat islands, while core region of Kolkata city along with Netaji Subhas Chandra Bose International Airport in the east, few small pockets in North and Tikiapara and Alipore region in south experiences high to extreme urban heat island.

Relationship between land cover and LST: Various land cover (LC) as shown in figure 6 were estimated using eq. 11-14. To obtain relationship a scatterplot was created between LST and various LC types as shown in figure 7. Figure 7, A) shows that as the value of NDBI increases (NDBI is high for urban area), LST increases; B) shows for higher values of NDVI (vegetation sparse to dense) LST reduces, for few lower values LST is low as values close to zero corresponds to water category (NDVI of water is close to zero), C) shows lower values of LST for higher NDWI values (NDWI is high for water) and D) shows higher LST values for higher NDBaI. It can be inferred that LST was positively correlated with NDBI (high) and NDBaI (low) while negatively correlated with NDVI and NDWI. Positive correlation signifies that as the value of NDBI and NDBaI increases, surface temperature of the region increases while a negative correlation as observed for LST and NDVI and NDWI implies that as the value of NDVI and NDWI increases the temperature reduces. This determines that paved surfaces including buildings, roads, etc. and barren areas such as open fields, unsowed agricultural land, mining areas, etc. contributes to high temperature and increases overall temperature of the region while presence of water body and

breathing space in terms of vegetation (mini-forest, parks and gardens) helps in regulating the microclimate of the region by reducing the thermal heat wave and UHI.

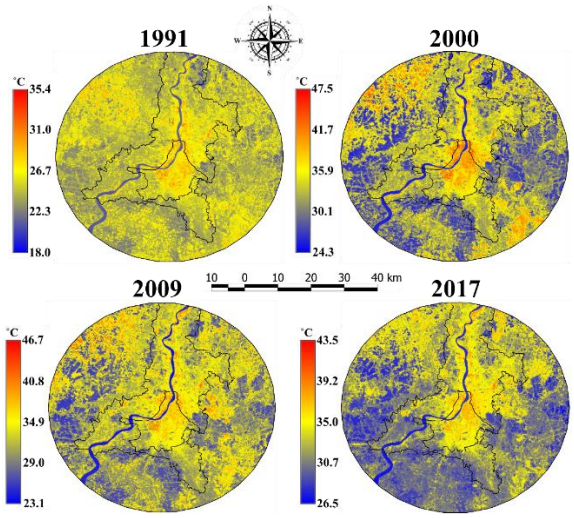


Figure 4: LST for KMA with 10km buffer from 1991-2017

Table 2: Statistical description of LST over KMA with 10km buffer region

Year	Landuse class	Min. Temp. (˚C)	Max. Temp. (˚C)	Mean Temp. (˚C)	Standard Deviation	Coefficient of Variation
1991	Urban	18.61	35.38	27.70	1.47	5.31
	Vegetation	18.00	31.66	24.31	1.04	4.29
	Water	18.00	31.66	22.80	1.59	6.96
	Others	18.00	33.74	25.11	1.54	6.12
2000	Urban	24.69	47.47	37.31	3.16	8.47
	Vegetation	24.69	44.83	31.70	2.72	8.56
	Water	24.78	45.21	28.70	2.44	8.50
	Others	24.26	46.72	32.49	3.52	10.85
2009	Urban	23.49	46.72	35.42	2.50	7.07
	Vegetation	24.69	41.35	29.12	1.90	6.52
	Water	23.05	44.06	27.86	2.94	10.56
	Others	24.35	44.44	32.99	2.55	7.73
2017	Urban	27.24	43.49	34.96	1.74	4.96
	Vegetation	27.30	40.04	30.06	1.49	4.95
	Water	26.49	39.58	29.68	1.81	6.08
	Others	26.74	42.12	32.23	1.89	5.85

d) Modelling and Prediction:

Model showed successful test results suggesting input layers were fit enough to conduct calibration and prediction. By the end of three phase calibration, optimum five growth coefficients of diffusion, spread, breed, slope resistance and road gravity were chosen as 1, 1, 27, 8 and 52 respectively. Since Kolkata is located on Indo-Gangetic plains, lower coefficient of slope is justified. Spreading and road gravity-oriented growth type dominates future land use change as it is evident from major roads passing across the region (figure 8). As far as the validation of the

model is considered, regressed population, urban edges, cluster and cluster size also showed acceptable values of greater than 0.7 in all phases of calibration suggesting high agreement between modeled urban areas versus actual urban area. Predicted urban growth, 2025 (urban area 757.91 km2) in comparison with 2017 (494.73 km2) are depicted in figure 6.

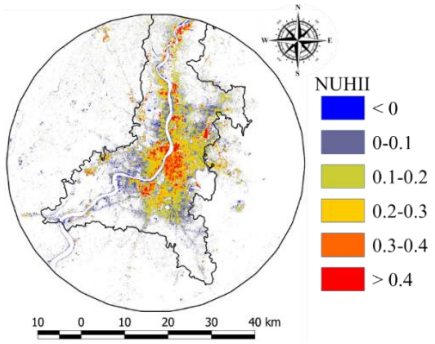


Figure 5: NUHII for KMA region with 10km buffer for 2017

Table 3: UHI types and percentage area covered

Category	Range	UHI type	Percentage area
1	< 0	Negative	16.58
2	0 - 0.1	Weakest	18.70
3	0.1 - 0.2	Low	29.49
4	0.2 – 0.3	Moderate	20.26
5	0.3 – 0.4	High	10.31
6	> 0.4	Extreme	4.65

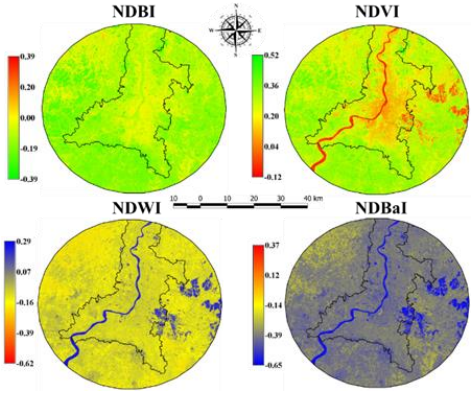


Figure 6: Land Cover types for KMA with 10km buffer for 2017

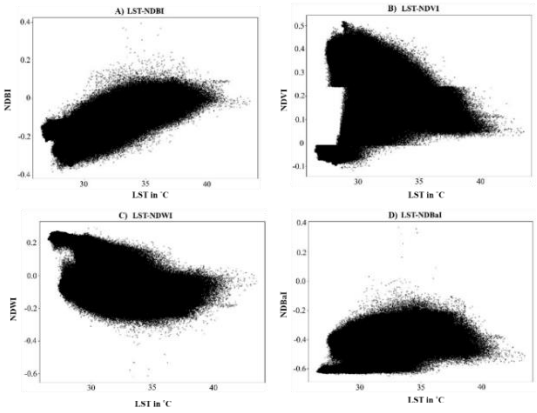


Figure 6: Relationship between LST and various Land cover types

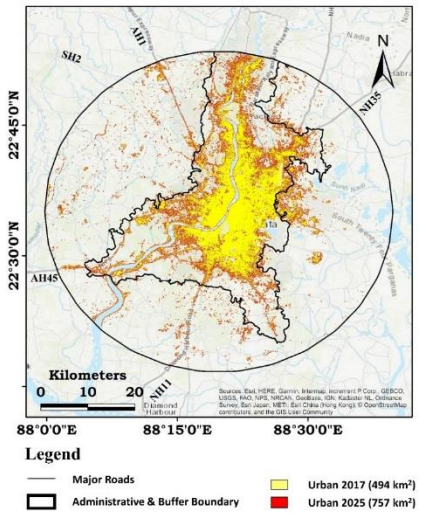


Figure 7: Simulated urban growth for the year 2025

5. Discussion and Conclusion

Over past few decades, Indian cities have undergone dynamic and inadvertent urban growth. It is one of the developed countries that is emerging as a key player in terms of global market with the support of government in the form of various schemes. Indian cities have grown at a remarkable pace but failed to meet the minimum criteria of the residents in terms of basic amenities of water, air and sufficient natural resources. As in the case of Kolkata, urban agglomeration is not very intensive due to diversified approach of development, but it would be an archetypal example of city development and probably would face unplanned urbanization in near future as predicted. As a result of these, the heat waves and surface temperature of the cities have shooted to high values (35-45˚C). The city is facing serious issues in terms of environmental deprivation, air pollution, unavailability of clean water, indecorous waste management, shortage of resources and comfortable thermal environment. This has further increased the problem of warming and altering the microclimate of the metropolitan area. There has been increased cases of casualties due to heat waves. Results of this communication shows a rise of 7˚C in mean surface temperature over a period of 26 years causing heat related issues (heat stress, pulmonary diseases, lethargic). All this can be related to the growing concretization of metropolitan and it can be understood by future prediction that the situation will only be worsening and will result in augmented urban hazards along with increased climate complexity. Future scope of this work can be forecasting LST for various scenarios to identify the vulnerable regions. The findings of this communication in collaboration with other research work and inputs on various environmental variables and climatic parameters will help in yielding better policies and will assist in developing the mitigation measures against climate change to fulfill 11th goal of UN Sustainable development that involve making cities inclusive, resilient and sustainable.

Acknowledgement

We are grateful to SERB, India, GOI, Sponsored research in Consultancy cell, IITKGP and West Bengal Department of Higher Education for the financial and infrastructure support.

References

Anderson, M. C., Norman, J. M., Kustas, W. P., Houborg, R., Starks, P. J., & Agam, N. (2008). A thermal-based remote sensing technique for routine mapping of land-surface carbon, water and energy fluxes from field to regional scales. *Remote Sensing of Environment*, *112*(12), 4227-4241. https://doi.org/10.1016/j.rse.2008.07.009

Bento, V. A., DaCamara, C. C., Trigo, I. F., Martins, J. P. A., & Duguay-Tetzlaff, A. (2017). Improving land surface temperature retrievals over mountainous regions. *Remote Sensing*, *9*(1), 38-50. https://doi.org/10.3390/rs9010038

Bharath, H. A., Chandan, M. C., Vinay, S., & Ramachandra, T. V. (2017). Intra and Inter Spatio-Temporal Patterns of Urbanisation in Indian Megacities. *International Journal of Imaging and Robotics™*, *17*(2), 68-86.

Bharath, S., Rajan, K. S., & Ramachandra, T. V. (2013). Land surface temperature responses to land use land cover dynamics. *Geoinformatics Geostatistics: An Overview, 1*(4), 1-10.

Chandan, M. C., Aishwarya, N., Nimish, G., & Bharath, H. A. (2017, October 23-27). *Multi temporal urban growth characterization using Geospatial technologies*. Paper presented at 38th Asian Conference of Remote Sensing. New Delhi, India.

Founda, D., & Santamouris, M. (2017). Synergies between Urban Heat Island and Heat Waves in Athens (Greece), during an extremely hot summer (2012). *Scientific reports*, *7*(1)

Jasim, M. A., Shafri, H. Z. M., Hamedianfar, A., & Sameen, M. I. (2016). Land transformation assessment using the integration of remote sensing and GIS techniques: a case study of Al-Anbar Province, Iraq. *Arabian Journal of Geosciences, 9*(15), 667.

Jin, M., Li, J., Wang, C., & Shang, R. (2015). A practical split-window algorithm for retrieving land surface temperature from Landsat-8 data and a case study of an urban area in China. *Remote sensing*, *7*(4), pp. 4371-4390. https://doi.org/10.3390/rs70404371

Karoly, D. J., Braganza, K., Stott, P. A., Arblaster, J. M., Meehl, G. A., Broccoli, A. J., & Dixon, K. W. (2003). Detection of a human influence on North American climate. *Science*, *302*(5648), 1200-1203. http://doi.org/10.1126/science.1089159

Keeling, C. D. (1997). Climate change and carbon dioxide: An introduction. *Proceedings of the National Academy of Sciences*, *94*(16), 8273-8274. https://doi.org/10.1073/pnas.94.16.8273

Li, Z. L., Tang, B. H., Wu, H., Ren, H., Yan, G., Wan, Z., Trigo, I. F., & Sobrino, J. A. (2013). Satellite-derived land surface temperature: Current status and perspectives. *Remote Sensing of Environment*, 131, 14-37. https://doi.org/10.1016/j.rse.2012.12.008

Nimish, G., Chandan, M. C., & Bharath, H. A. (2018). Understanding current and future landuse dynamics with land surface temperature alterations: A case study of Chandigarh. *ISPRS Annals of Photogrammetry, Remote Sensing & Spatial Information Sciences*, *4*(5), 79-86.

Ramachandra, T. V., Aithal, B. H., & Sreejith, K. (2015). GHG footprint of major cities in India. *Renewable and Sustainable Energy Reviews*, *44*, 473-495.

Ramachandra, T. V., Bajpai, V., Kulkarni, G., Aithal, B. H., & Han, S. S. (2017). Economic disparity and CO2 emissions: The domestic energy sector in Greater Bangalore, India. *Renewable and Sustainable Energy Reviews*, *67*, 1331-1344. https://doi.org/10.1016/j.rser.2016.09.038

Ramachandra, T. V., Bharath, H. A., & Sanna, D. D. (2012). Insights to urban dynamics through landscape spatial pattern analysis. *International Journal of Applied Earth Observation and Geoinformation*, *18*, 329-343. https://doi.org/10.1016/j.jag.2012.03.005

Ramachandra, T. V., Bharath, H. A., Vinay, S., Kumar, U., Venugopal, K. R., & Joshi, N. V. (2016). *Modelling and Visualization of Urban Trajectory in 4 cities of India.* Paper presented at IISc-ISRO STC, Bangalore, India. Retrieved from https://www.researchgate.net/publication/

Stott, P. A., Mitchell, J. F., Allen, M. R., Delworth, T. L., Gregory, J. M., Meehl, G. A., & Santer, B. D. (2006). Observational constraints on past attributable warming and predictions of future global warming. *Journal of Climate*, *19*(13), 3055-3069.

Land surface temperature responses to land use dynamics across the agro-climatic zones of Karnataka

Ramachandra TV[1]*, Bharath Setturu, Madhumita Dey,*
Energy & Wetlands Research Group, Centre for Ecological Sciences, Indian Institute of Science, Bangalore, Karnataka, 560012, India.

ABSTRACT

Landscape dynamics has a crucial role in the ecological processes and sustainability of natural resources. Understanding of landscape dynamics aids in planning and prudent management of natural resources. However, unplanned rapid urbanization during the post 1990's consequent to the globalization has driven anthropogenic activities leading to the alterations in the landscape structure, impacting the ecological process evident from the increase in land surface temperatures, alterations in the hydrologic regime, etc. Thus, land surface temperature being sensitive to land use dynamics, has become a vital factor in the regional climate change studies. The current study explores the relationship between biophysical parameters of earth to sub pixel thermal variations based on agro climatic zones of Karnataka. The general trend of temperature of the region with different land use class was established which indicates rise in temperature in the recent period. The study identifies the hotspot zones of higher temperature with the insights of land uses across the agro climatic zones of Karnataka.

Keywords: Landscape dynamics; Land use land cover; Land Surface Temperature; Remote sensing; GIS

Introduction

Landscape patterns plays an important role in ecological processes and the structure of a landscape, shape and configuration are responsible for its functional aspects such as bio-geo chemical cycling and hydrologic regimes (Chen et al. 2014; Ramachandra et al. 2016). The landscape transition can be natural or anthropogenic. The several studies across the globe have proved the anthropogenic activities are altering the global climate (Peng et al. 2011; Newbold et al. 2015; Grizzetti et al. 2017; Szymura et al. 2018). The abrupt environmental changes at local, regional and global scales are threatening the survival of humans and other biota. Land use land cover (LULC) are the important parameters of landscape which reflects its change characteristics (Ganasri et al. 2010). LC refers to the observed physical cover on the earth's surface whereas LU expresses arrangements, activities and inputs people undertake in a certain LC. LULC change is governed by the crucial drivers such as population, urban expansion, agricultural production and land management policies, which alters a landscape into heterogeneous mosaic of patches (Ramachandra et al. 2012). LULC alterations will affect the range of functionalities of landscape such as nutrient cycling, bio-geochemical cycle, hydrologic cycling, carbon sequestration potential, water retention capability, etc. (Ramachandra et al. 2018; Ramachandra and Bharath 2019). The rampant LULC changes of a region will affect the exchanges of energy that take place between the biophysical properties of the Earth with the atmosphere. The comprehensive

[1] Corresponding Author: [Email: tvr@iisc.ac.in]

understanding of these changes are necessary to evaluate critical drivers of changes and frame polies for sustainable development (Ramachandra et al. 2017). Land surface temperature (LST) is a prime climate variable to account climate change across the local and global scales and it is also an indicator of the energy balance of the land surface processes (James and Mundia 2014). Changes in LST can be directly linked with associate LULC changes to account adverse effect on environment, energy balance and biogeochemical interactions.

Global warming and consequent changes in the climate has given momentum to the research to understand the causes of LULC. LST is sensitive to vegetation, canopy layer and soil moisture, hence it can be used to detect LULC changes and link to climate alterations (Mallick et al. 2008). The unplanned developmental activities will intensify the environmental degradation, induce disasters, disrupting the sustainable economic growth (Ramachandra et al. 2019). LST changes play an important role in most of the environmental processes and effect microclimate through associated biophysical changes. Increase in surface temperature has been observed due to conversions of pervious or vegetation surfaces to impervious surfaces. These changes in turn affect the absorption of solar radiation, surface temperature, evaporation rates and wind turbulence and alters the conditions of the near-surface atmosphere (Aithal et al. 2014). Thus, understanding linkages between LST and landscape dynamics help in evaluating human-environment interactions, aids in the planning and management of natural resources with persistent knowledge of landscape at temporal scale (Bharath et al. 2013). The advancement of spatial technologies has aided in understanding LULC changes, precise evaluation of LST and its environmental consequences. The temporal satellite remote sensing data of thermal band can capture the variation in energy across various features of landscape. The abundant studies have tried to capture LST using split-window algorithms in Landsat 8 using band 10 and 11 (Li et al. 2013; Bunai et al. 2018). Moderate Resolution Imaging Spectral radiometer (MODIS) data has more advantageous in LST estimation due to its global coverage, high radiometric resolution and dynamic ranges makes it efficient for monitoring and estimation of land surface temperature over a large area (Wan et al. 2002). The satellite derived LST of a larger region will provide information of different types of Earth surface processes, surface-atmosphere interactions and evapotranspiration (Anderson et al. 2011). The Karnataka state of India is experiencing the LULC changes due to increase in anthropogenic pressure from post 1990's. In this regard, the current research tries to understand the LULC changes at a temporal scale from 1985-2018 and tries to explore correlation between biophysical parameters of earth to sub pixel thermal variations based on agro climatic zones of Karnataka. Evaluation of temperature variations across forest and non-forest cover regions.

Materials and Method

Study Area

Karnataka is the eighth largest state in India with varied agro climatic zones (Figure 1) and population density of 319 persons per sq.km as per 2011 census. It lies between 11.5° and 18.50° N and 74° and 78.30° E in the southern plateau with a geographic area of 1,91,791 km^2. It is bordered by Arabian Sea to the west, Goa to the northwest, Maharashtra to the north, Andhra Pradesh to the east, Tamil Nadu to the east and southeast, and Kerala to the southwest. The state comprises of diverse topographical features of high mountains, plateaus, residual hills and coastal plains and is enclosed by chains of mountains to its west, east and south. The region is endowed with the most magnificent forests in the country, from the rich evergreen forests of the Western Ghats to the scrub jungles of the plains, a wide variety of habitats exist and some of them endemic

to the region. The weather is very dynamic, changes from place to place owing to its altitude, topography and its distance from the sea. It experiences climatic variations from arid to semi-arid in the plateau region, sub-humid to humid tropical in the Western Ghats and humid tropical monsoon in the coastal plains. The mean rainfall varies from 400 mm in the Eastern parts to more than 4000 mm in the Western Ghats and coastal beach of the State.

Method

The method adopted for the analysis is illustrated in Figure 2. LU analysis involved (i) generation of False Color Composite (FCC) of remote sensing data (bands–green, red and NIR). This composite image helps in locating heterogeneous patches in the landscape, (ii) selection of training polygons by covering 15% of the study area (polygons are uniformly distributed over the entire study area) (iii) 60% of the training data has been used for classification, while the balance is used for validation or accuracy assessment. (iv) LU analysis was done using supervised classification technique based on Gaussian maximum likelihood algorithm through GRASS GIS (Geographical Resources Analysis Support System) a free and open source software accessible at http.//wgbis.ces.iisc.ernet.in/grass/index.php. MODIS Land surface temperature (LST) and emissivity data has retrieved from Land Processes Distributed Active Archive Center (LPDAAC), which has been re-projected from sinusoidal projection to UTM Zone 43 projection with WGS 84 datum using MODIS Re-Projection Tools. To investigate temporal patterns of temperature across the study region 2005, 2012 and 2018 of May month data were used. LST was computed by multiplying DN (Digital numbers) with a scale factor of 0.02 and then converted into degree Celsius. Validation of land surface temperature was done using ground data of 0.5 degree downloaded from Princeton University which gives air temperature above 2m ground level. Finally, statistical analysis has performed to understand the relationship among various LU classes and LST.

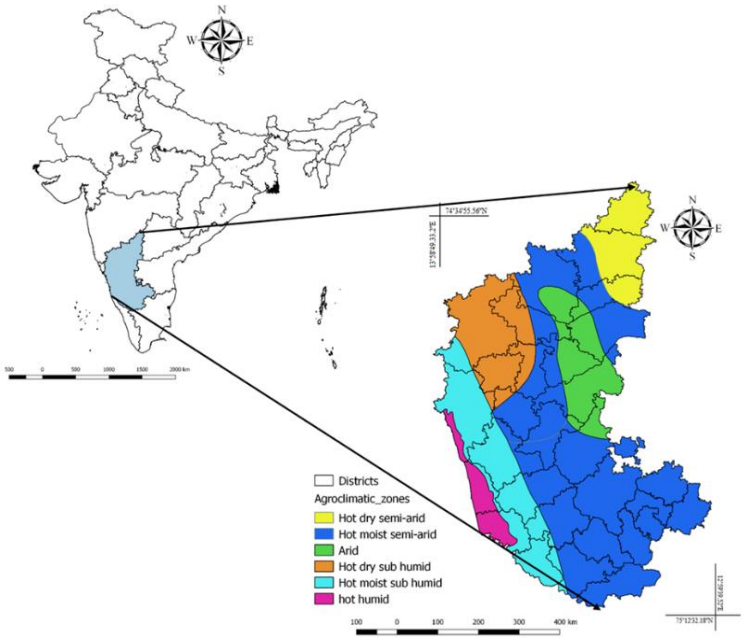


Figure1. Geographic location of the study area.

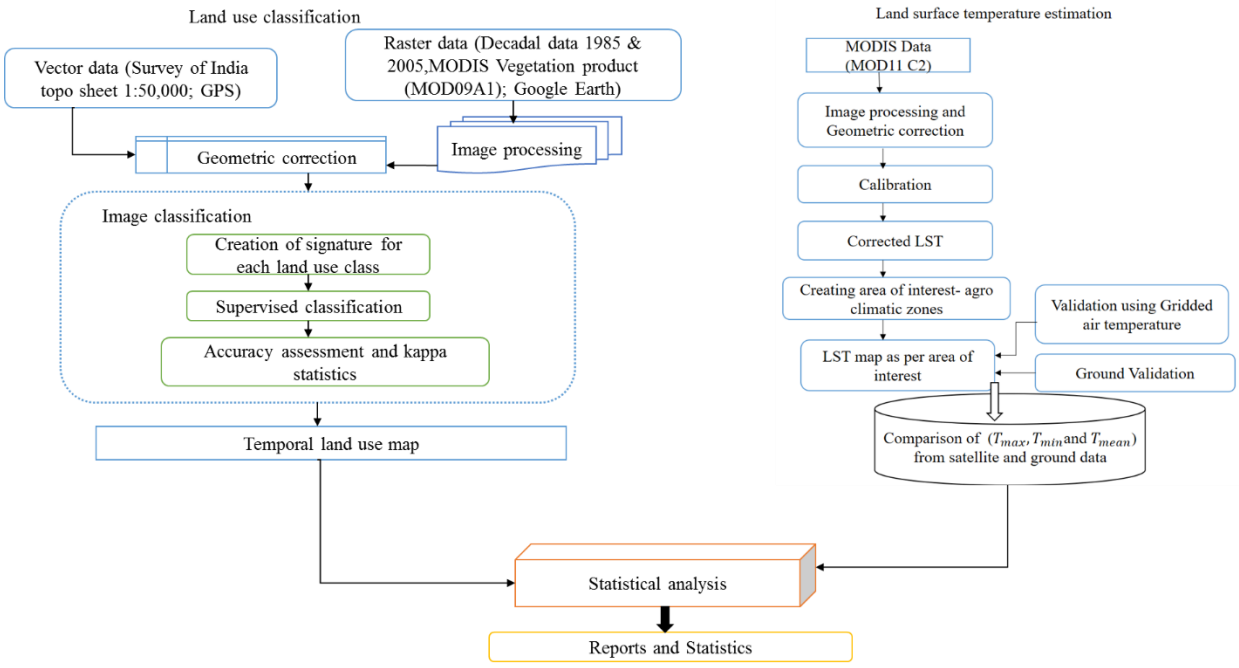


Figure 2. Method adopted

Results and Discussions

Analyses of spatio temporal LU changes for Karnataka highlights the loss of forest cover and conversion of agriculture to other use due to anthropogenic pressures. The evergreen forest cover has reduced from 4.2% (1985) to 3% (2018) with the increase in plantations, built-up areas. The new urban agglomerations were noticed across the cities and major towns such as Bengaluru, Mangalore, Hubli, Hassan, Mysore etc. The total forest cover loss was accounted to be 6.2%, where as non-forest over has increased by 5.7%. The major tracts of deciduous forests were replaced by anthropogenic as evident from 1985 to 2018. Due to large scale plantations of Eucalyptus, Rubber, Acacia, teak and Arecanut have increased from 1985 to 2018 covering 19.45% of the state. Due to increase in horticulture plantations and increase in paved surfaces croplands have decreased from 68% (1985) to 64.09% (2018). These changes are abrupt and resulting in imbalance of ecosystem services, hydrology, and natural resources availability. The temporal LST results further highlights the loss of forest cover has resulted in increase in temperature gradient across the state. The higher temperature can be seen especially in non-forest areas due to intensified built-up activities. The rise in temperature can be attributed to high deforestation with unplanned urbanisation and industrialisation. Table 1 illustrates temperature gradient across the agro climatic zones. Urban areas show increase in temperature (maximum) as population explosion exerts pressure on the local resources such as open lands and forest cover. Temporal analysis of LST indicates rise in mean temperature over the periods. The highest temperature of 48.46˚C was found in the hot dry semi-arid region and the lowest was found in hot humid of 32.46 ˚C.

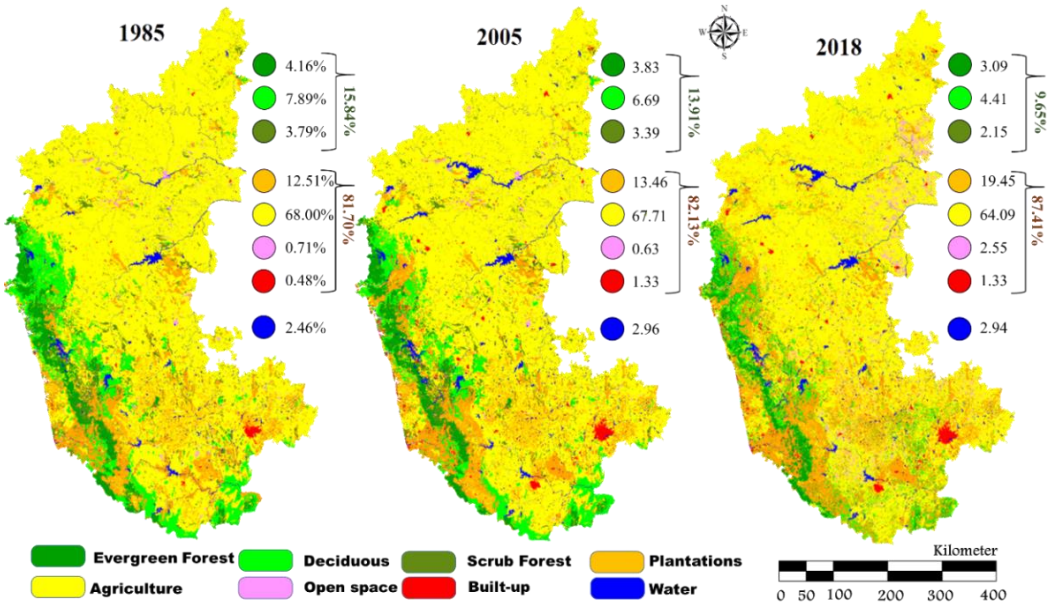


Figure 3. LU analysis of Karnataka from 1985 to 2018

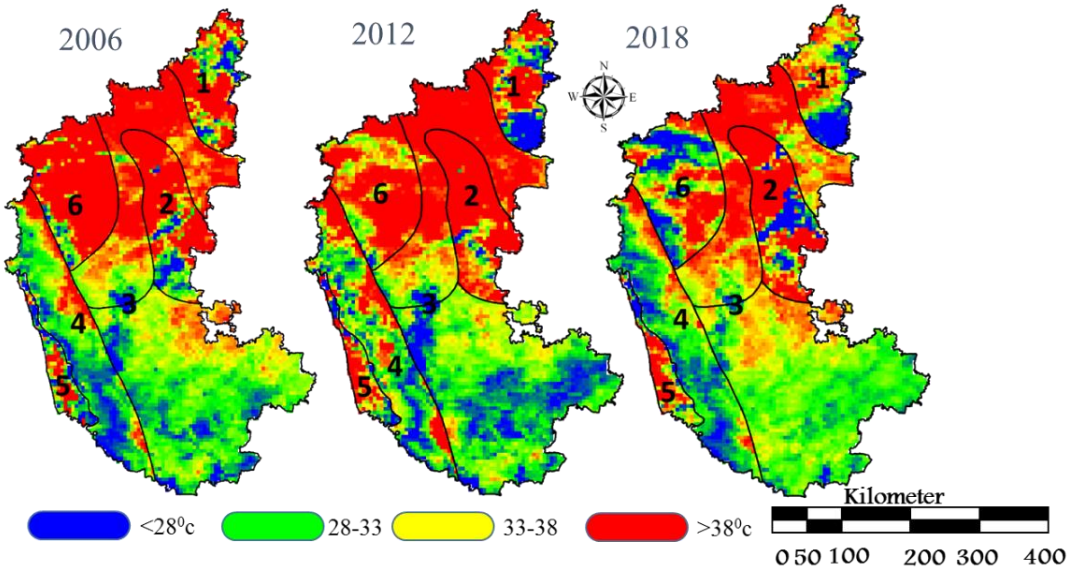
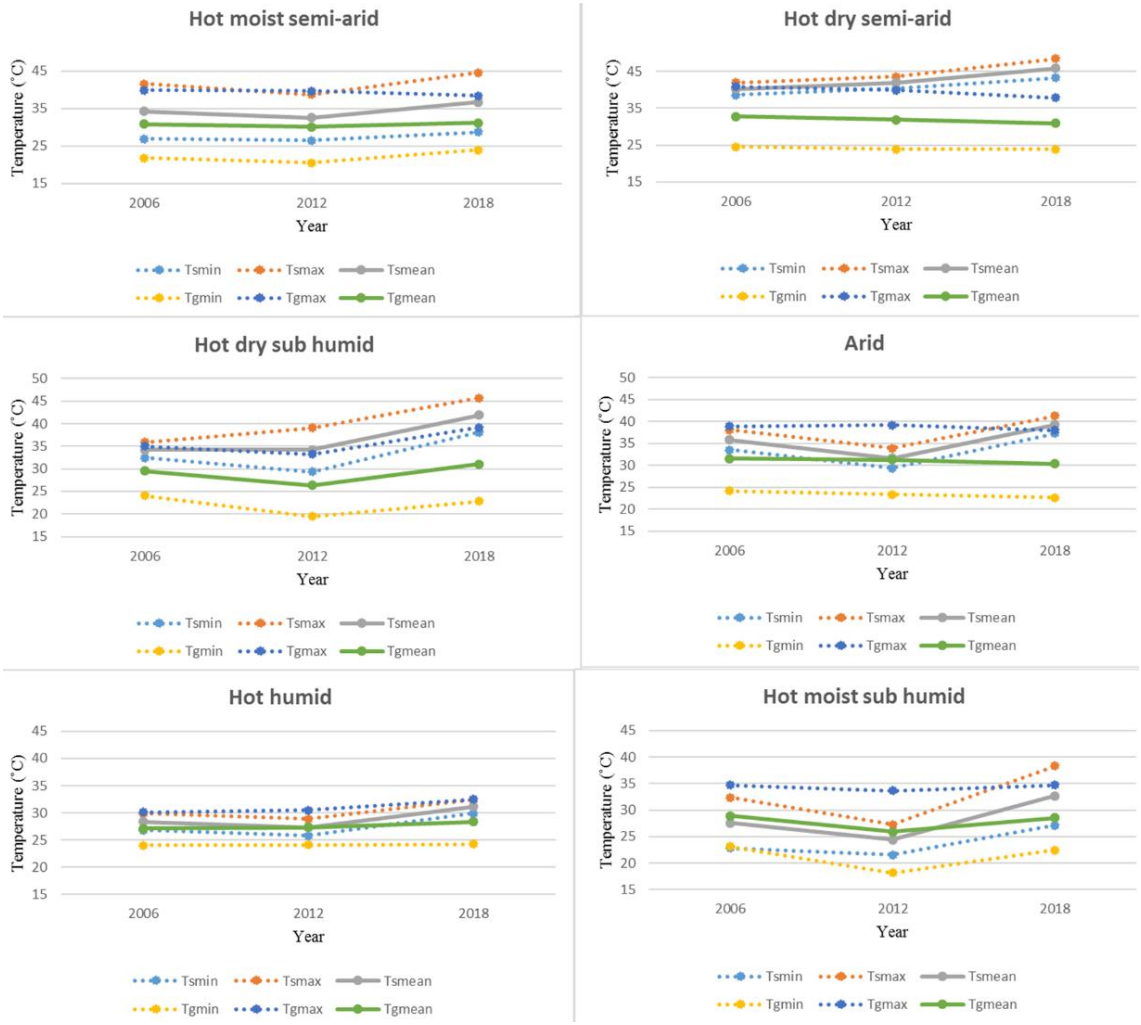


Figure 4. LST dynamics of Karnataka from 2006 to 2018

Table 1. LST across the agro climatic zones

Regions	2006		2012		2018	
	Min (˚C)	Max (˚C)	Min (˚C)	Max (˚C)	Min (˚C)	Max (˚C)
Hot dry semi-arid (1)	38.55	41.92	40.35	43.5	43.27	48.46
Arid (2)	33.57	38.08	29.39	33.88	37.21	41.25

Hot moist semi-arid (3)	26.91	41.58	26.49	38.7	28.78	44.57
Hot moist sub humid (4)	22.85	32.38	21.53	27.3	27.11	38.31
Hot humid (5)	26.83	29.9	25.77	28.9	29.89	32.46
Hot dry sub humid (6)	32.49	35.92	29.33	39.08	38.11	45.68



Where Tsmin = Satellite minimum temperature, Tsmax = Satellite maximum temperature, Tsmean = Satellite mean temperature, Tgmin = Ground minimum temperature, Tgmax = Ground maximum temperature Tgmean = Ground mean temperature

Figure 5. LST across agro climatic zones from 2006-2018.

Figure 5 confirms that LST (satellite temperature) are comparable to ground measurement across the agro climatic zones. Ground air temperature was measured at a distance of 2 m above ground while satellite gives temperature of land surface which may be 2-3 ˚C higher. The 1km gradient has been used for sampling across the agro climatic zones from forest and non-forest categories to assess the temperature variations across the LU. The two samples were taken for each agro climatic zone except Hot Moist semi-arid (4 samples) due to larger coverage. The correlation

analysis shows (Figure 6) forest decreases on increase in temperature indicating indirect relationship. This indicates forest holds strong co-relationship of 0.8 (r=0.94) with temperature. Whereas, it was observed that on increase built-up areas, temperature goes up which shows direct relationship. Also, non-forest cover holds a strong co-relationship of 0.5 (r=0.74) with temperature. The gradients depict as non-forest cover has increased in the region depicted rise in temperature. The results highlight the role of bio-physical variables in maintaining regional climate. The increase in temperature can induce higher loss of species, imbalance in ecosystem, vegetation die-off. It is suggested to curb the unplanned developments and increase in forest cover with native species through stakeholder's active involvement would help in the conservation and prevent further degradation of landscape. The effective forest management with forest regeneration activities would help in reducing LST and its ill effects.

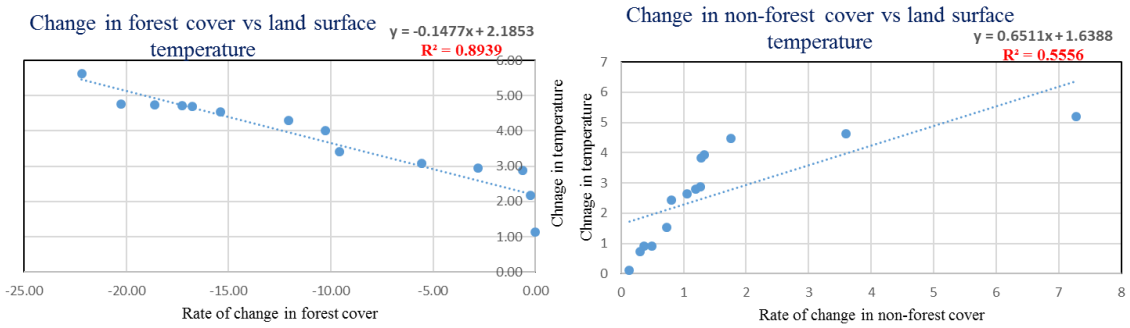


Figure 6. Correlation among forest, non-forest LU with LST

Conclusion

Spatial temporal LU analysis reveals increase in built-up area at the cost of forest cover, signifies anthropogenic pressure. The temporal analysis of forest and non-forest cover with temperature indicates a strong relationship among LU and bio-physical variables. The results revealed forest cover has reduced from 15.84% (1985) to 9.65% (2018) whereas non-forest cover has increased from 81.70% (1985) to 87.41% (2018). However, the temporal analysis of land surface temperature shows increase in temperature over the periods. Therefore, it can be understood that large scale deforestation will lead to increase in temperature. The investigation across agro-climatic zones of Karnataka, depicts increase in temperature in hot dry semi-arid regions which are devoid of forest cover. However, there is not much increase in hot humid region as the region has healthy vegetation. However, escalations in anthropogenic activities leading to degradation of forests. Will enhance the regional temperature. Statistical analysis of LST and LU indicates a negative correlation between vegetation with an increase in LST. The general trend in the ambient temperature of Karnataka further clarifies that there was a fundamental drift of temperature rise in recent years, especially during the last decade. Therefore, there is an urgent need to mitigate these issues and possible drought conditions. Proper land use planning and restoration of degraded land through the afforestation with native species would help in mitigating the increase in temperature.

Acknowledgement

We are grateful to (i) the ENVIS division, The Ministry of Environment, Forests and Climate Change, Government of India and (ii) Indian Institute of Science for the financial and infrastructure support.

References

1. Aithal, B. H., Vinay, S., & Ramachandra, T. V. (2014). Landscape dynamics modeling through integrated Markov, Fuzzy-AHP and cellular automata. 2014 IEEE Geoscience and Remote Sensing Symposium. https://doi.org/10.1109/igarss.2014.6947148
2. Anderson, M. C., Kustas, W. P., Norman, J. M., Hain, C. R., Mecikalski, J. R., Schultz, L., ... & Gao, F. (2011). Mapping daily evapotranspiration at field to continental scales using geostationary and polar orbiting satellite imagery. *Hydrology and Earth System Sciences*, *15*(1), 223-239. https://doi.org/10.5194/hess-15-223-2011
3. Bharath, S., Rajan, K.S. & Ramachandra, T.V. (2013). Land Surface Temperature Responses to Land Use Land

   Cover Dynamics. (2013). Geoinformatics & Geostatistics: An Overview, 01(04). https://doi.org/10.4172/23274581.1000112
4. Bunai, T., Rokhmatuloh, & Wibowo, A. (2018). Comparison Spatial Pattern of Land Surface Temperature with Mono Window Algorithm and Split Window Algorithm: A Case Study in South Tangerang, Indonesia. IOP

   Conference Series: Earth and Environmental Science, 149, 012066. https://doi.org/10.1088/17551315/149/1/012066
5. Chen, Z., Xu, B., & Devereux, B. (2014). Urban landscape pattern analysis based on 3D landscape models.

   Applied Geography, 55, 82–91. https://doi.org/10.1016/j.apgeog.2014.09.006
6. Ganasri, B. P., & Dwarakish, G. S. (2015). Study of Land use/land Cover Dynamics through Classification Algorithms for Harangi Catchment Area, Karnataka State, INDIA. Aquatic Procedia, 4, 1413–1420. https://doi.org/10.1016/j.aqpro.2015.02.183
7. Grizzetti, B., Pistocchi, A., Liquete, C., Udias, A., Bouraoui, F., & van de Bund, W. (2017). Human pressures and ecological status of European rivers. Scientific Reports, 7(1). https://doi.org/10.1038/s41598-017-00324-3
8. James, M.M. & Mundia, C.N. (2014). Dynamism of land use changes on surface temperature in Kenya: a case study of Nairobi City. International Journal of Science and Research, 3(4), 38–41.
9. Li, X., Zhou, W., & Ouyang, Z. (2013). Relationship between land surface temperature and spatial pattern of greenspace: What are the effects of spatial resolution? Landscape and Urban Planning, 114, 1–8. https://doi.org/10.1016/j.landurbplan.2013.02.005

10. Mallick, J., Kant, Y. & Bharath, B.D. (2008). Estimation of land surface temperature over Delhi using Landsat7 ETM+. Journal of Indian Geophysical Union, 12 (3), 131-140.
11. Newbold, T., Hudson, L. N., Hill, S. L. L., Contu, S., Lysenko, I., Senior, R. A., … Purvis, A. (2015). Global effects of land use on local terrestrial biodiversity. Nature, 520(7545), 45–50. https://doi.org/10.1038/nature14324
12. Peng, J., Xu, Y., Cai, Y., & Xiao, H. (2011). Climatic and anthropogenic drivers of land use/cover change in fragile karst areas of southwest China since the early 1970s: a case study on the Maotiaohe watershed. Environmental Earth Sciences, 64(8), 2107–2118. https://doi.org/10.1007/s12665-011-1037-5
13. Ramachandra, T.V., Bharath, S., & Chandran, S. (2016). Geospatial analysis of forest fragmentation in Uttara Kannada District, India. Forest Ecosystems, 3(1). https://doi.org/10.1186/s40663-016-0069-4
14. Ramachandra, T.V., Setturu, B., Rajan, K. S., & Subash Chandran, M. D. (2017). Modelling the forest transition in Central Western Ghats, India. Spatial Information Research, 25(1), 117–130. https://doi.org/10.1007/s41324-017-0084-8
15. Ramachandra, T.V., Vinay, S., Bharath, S., & Shashishankar, A. (2018). Focus: Ecology and Evolution: EcoHydrological Footprint of a River Basin in Western Ghats. The Yale journal of biology and medicine, 91(4), 431-444.
16. Ramachandra, T. V., & Bharath, S. (2019). Global Warming Mitigation Through Carbon Sequestrations in the Central Western Ghats. Remote Sensing in Earth Systems Sciences, 2(1), 39-63. https://doi.org/10.1007/s41976-019-0010-z
17. Ramachandra, T. V., Bharath, S., & Vinay, S. (2019). Visualisation of impacts due to the proposed developmental projects in the ecologically fragile regions-Kodagu district, Karnataka. *Progress in Disaster Science*, 100038.
18. Szymura, T. H., Szymura, M., Zając, M., & Zając, A. (2018). Effect of anthropogenic factors, landscape structure, land relief, soil and climate on risk of alien plant invasion at regional scale. Science of The Total Environment, 626, 1373–1381. https://doi.org/10.1016/j.scitotenv.2018.01.131
19. Wan, Z., Zhang, Y., Zhang, Q., & Li, Z. (2002). Validation of the land-surface temperature products retrieved from Terra Moderate Resolution Imaging Spectroradiometer data. Remote Sensing of Environment, 83(1-2), 163–180. https://doi.org/10.1016/s0034-4257(02)00093-7

Spatial and Temporal Nature of Urban Heat Island in Roorkee

Siva Ram Edupuganti[1]*, Research Scholar, IIT Roorkee (India)*
Arjun Satheesh, Research Scholar, IIT Roorkee (India)
Dr. Mahua Mukherjee, Professor, IIT Roorkee (India)

ABSTRACT

Urban areas occupy less than two per cent of the Earth's land surface but house 50 per cent of the world's population. By 2030, Urban areas will hold 60% of the world's population (United Nations, 2014)Cities are point sources of pollution and are responsible for 50-70% of Greenhouse gas emissions (Oke *et al.*, 2017) Urbanization has led to a phenomenon called Urban Heat Island(UHI) resulting in microclimatic variations in the city; characterized by higher temperatures when compared to the surrounding landscape. This can have an adverse impact on the health and comfort of the people and energy efficiency of the city. It is imperative to understand the phenomena of Urban Heat Island at different scales and come up with mitigation measures to make our cities more sustainable.

According to 2011 census of India, there are 468 cities with population exceeding 1 lakh. For this study, the categorization of cities done by Indian Government for House Rent allowance is adopted. As per this, cities are classified into 3 different categories ;

- Category X - Cities with population exceeding 50 lakhs,
- Category Y - Cities with population between 5 lakh and 50 lakh,
- Category Z- Cities with population between 1 lakh and 5 lakh.

Based on 2011 Census data, there are 8 category X, 88 category Y and 372 category Z cities in India. Currently, the UHI research is only focused at the scale of category X and Y cities like Nagpur, New Delhi, Kochi, Chandigarh, Noida etc. (Kotharkar and Bagade, 2018) (Thomas *et al.*, 2014) (Mathew, Khandelwal and Kaul, 2016). There are 372 cities which are at a nascent urbanization stage compared to the Category X and Y cities.There is a big gap in understanding of UHI in these smaller scale cities. By better understanding, there is great opportunity to intervene and mould these cities at this nascent urbanization stage. This paper intends to understand the Urban Heat Island phenomena in a Category Z city like Roorkee with population of 2,38,422. R

[1] Siva Ram Edupuganti: sivaedupu@gmail.com, [+91 9663023123]

The methodology involves generating LCZ maps for multiple cities using WUDAPT process in India to understand the composition of morphology in Category Z cities. This will throw light into the evolution their morphology. Further, CUHI (Canopy layer Urban heat island) will also be investigated spatially through mobile traversing techniques using Roorkee as a case study. Through this process, the phenomena and trends of UHI will be established in smaller scale cities.

Introduction

Urbanization in India

Over the last couple of decades urbanization trends in India have accelerated to increase the total urban population of India. Certain estimates put the Indian urban population to be at 460 million people which is 33.6% of the total urban population (Census of India, 2011). It has also been shown that more than 2/3rd of the national GDP is being contributed by urban areas in India (Bhagat, 2014). As such the construction boom in the country has been astronomical along with associated energy consumption. It has been shown that the annual growth rate of energy consumption in India is above 8% (Ministry of Urban Development Government of India, 2010). It suffices to say that the urban development in India has been exponentially growing and the impacts are being felt not only nationally but also internationally. This has led to a few studies covering Urban Heat Island impacts in the country. This paper looks in to the urban morphologies surrounding heat islands.

City categories in India

For any discussion about cities in India, the categorization and classification of cities need to be addressed. While various methods of categorizing cities exist, this paper utilizes the classification of cities as recommended by the sixth pay commission under the department of expenditure in the government of India (Ministry of Finance, 2008). This classification depends upon the cost of living expected in the cities mentioned and the average cost of living in India depends on multiple factors, including but not limited to income level, population, availability of buildable land and existing infrastructure within the city limits (Government of India, 2008). The cities considered to have the highest cost of living were classified as category X with the highest percentage, 30% of the basic pay granted as Home Rent Allowance (HRA) to the government employees in these cities. The next category was declared to be the category Y with 20% of the basic pay given as HRA and the last was category Z with 10% of the basic pay granted as HRA. Of particular interest is the fact that the urban agglomerations that come under category Z seem to be the areas where urbanization seems to have taken hold and the initial symptoms of growth have appeared but the general cost of living in these regions are still quite low.

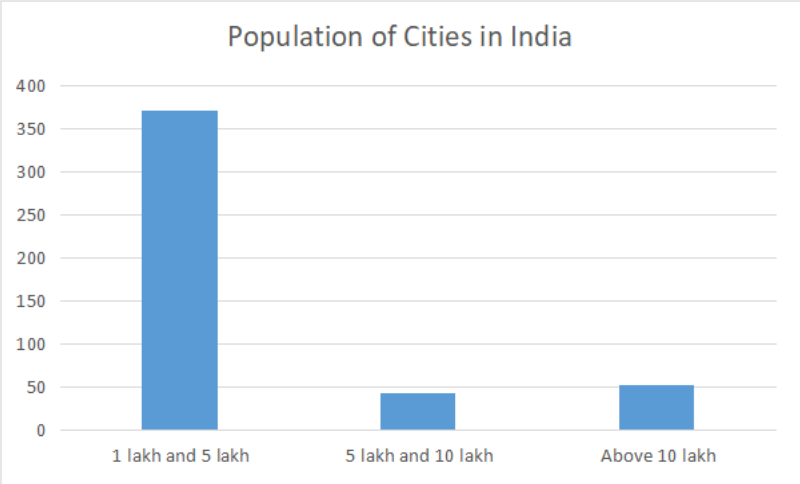


Figure 1- Population of Indian cities, there are 372 cities in India with population 1 lakh to 5 lakh.

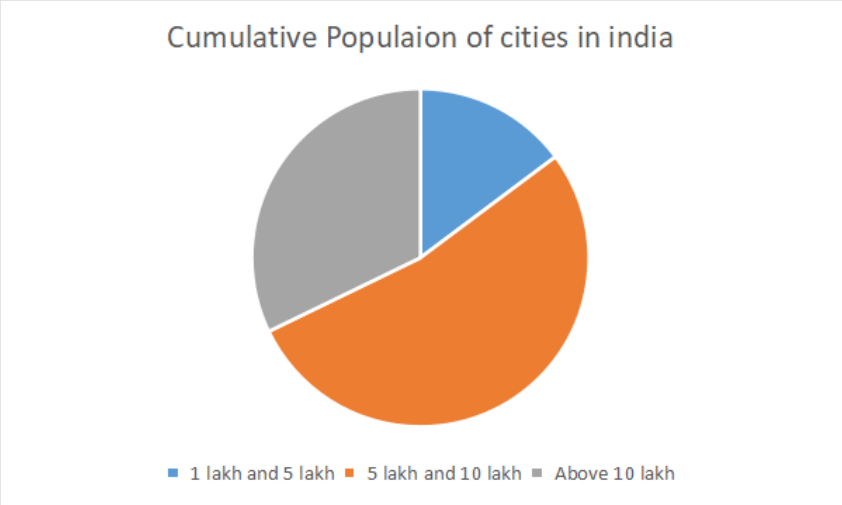


Figure 2 - Cumulative population of Indian cities shows that even though there are 372 cities with a population under 5lakh, the larger cities especially the one with 5 lakh to 10 lakh population make up the bulk of the Indian urban population.

Nature of urban heat island in India

The Urban Heat Island phenomenon has been explored and documented sufficiently in India. It has been noted that the urban heat island effects in certain areas of the National Capital Region (NCR) have ranged from 4 deg. Celsius to 12 deg. Celsius (Mohan *et al.*, 2009). Parts of Bhubaneshwar have recorded UHI intensities of 1.5 deg. Celsius or above and the cities of Mumbai, Kolkata and Bangalore have recorded UHI intensities of 2 deg. Celsius at the very least (Govindarajulu, 2014). The UHI effect in India is much more pronounced in the night time as has been observed world over and rapid urbanization has led to documented conversion of blue and green spaces in to urban built-up (The Hindu - Special Correspondent, 2017). It is worth noting at this point that a highly populated and fast urbanizing nation such as India could very

easily create urban hot pockets that could become a slow onset disaster through unregulated propagation of Urban Heat Islands. Based on 2011 Census data, there are 8 category X, 88 category Y and 372 category Z cities in India. Currently, the UHI research is only focused at the scale of category X and Y cities like Nagpur, New Delhi, Kochi, Chandigarh, Noida etc. (Kotharkar and Bagade, 2018) (Pandey *et al.*, 2014) (Thomas *et al.*, 2014) (Mathew, Khandelwal and Kaul, 2016). There are 372 cities which are at a nascent urbanization stage compared to the Category X and Y cities. There is a big gap in understanding of UHI in these smaller scale cities. The low cost of living in the category Z cities has seemingly led to a situation where a certain kind of construction seems to be favoured by the residents of such cities which in turn has led to Urban Heat Island effect being prevalent in the centres of such urban regions. This is precisely the effect that is to be explored by the research described.

LCZ & WUDAPT

LCZ and evolution of a city

The concept of Local Climate Zones as a basis for temperature studies in the urban context was first proposed by I. D. Stewart and T. R. Oke in their seminal paper titled Local Climate Zones for urban temperature studies (Stewart *et al.*, 2012). The paper proposes 17 standard classes defined by land cover and structural properties. The urban and rural areas of the world may be classified under these types and then studied for their climatic behaviour. Specifically, these climate zones are instrumental in affecting the air temperature of the area at screen height. The authors of the paper validated their proposal through a follow-up study which showed that there are measurable and sharp contrasts between the air temperature ranges among the identified classes (Stewart, Oke and Krayenhoff, 2014). The validation process also proved that the air temperature at screen height are determined by factors such as building height and spacing, pervious surface fraction, tree density and soil wetness. The use of a function called inter-zone temperature difference to quantify the magnitude of heat island intensity was also justified by the same publication. As a result of their efforts in creating a Local Climate Zone classification, a universal approach in the characterization of physical nature of cities became available to the urban climatologist. This eventually gave rise to the World Urban Database Access Portal Tools or (WUDAPT).

WUDAPT methodology

World Urban Database Access Portal Tools or (WUDAPT) is an international community based initiative to collect and disseminate relevant climatic data for analysis purposes (Ching *et al.*, 2018). The methodology for creating a Level 0 urban information map is available on the WUDAPT website (www.wudapt.org). The LCZ mapping of a city forms the primary basis for the Level 0 WUDAPT. As part of this paper, the LCZ map preparation method as suggested by the WUDAPT methodology was followed.

LCZ and UHI study

Building on the LCZ classification types and the WUDAPT methodology, the Urban Heat Island (UHI) scenario in Roorkee is being studied in this paper. The LCZ mapping for the city of Roorkee and two other category Z cities are done along with an on-ground traverse survey of Roorkee city to validate the observations from remote-sensed data.

Methodology of the study

Process of selection of the cities

All cities selected were category Z cities with a population of less than 5 lakh. The city of Roorkee was selected as the researchers involved are very familiar with the urban morphology of the city which is an important criterion for validation of LCZ maps created as per the WUDAPT methodology. Additionally, Sonipat and Kadapa are two cities selected are category Z cities which the researchers are familiar with. These cities also have a fairly long history and are close to industrial areas or contain major industrial complexes within their peripheries. Additionally, all of them have urbanized within the last two decades.



Figure 3- The location of the selected category Z cities in India. From the North they are, Roorkee in the state of Uttarakhand, Sonipat in the state of Haryana and Kadapa in the state of Andhra Pradesh.

Methodology for remote sensing study

The remote sensing data was collected from Landsat 8 as available on the Earth Explorer platform of the USGS portal (https://earthexplorer.usgs.gov). The data collected was classified

on the basis of training areas defined within the Google Earth software as per the WUDAPT methodology mentioned earlier. The work was carried out using SAGA GIS and later using QGIS.

Methodology for UHI study

The local traverse survey of Roorkee was done in the month of March 2019 which is the end of spring or the cooler season. The skies mostly remain clear during this period and therefore the readings are considered highly reliable. The traverse survey was done on three separate days using two separate two-wheelers and two air temperature sensors (Onset HOBO MX2301A Outdoor Bluetooth Humidity Data Logger) during the night time from 10:00 pm to 1:00 am period. Two separate tracks were traversed, one of 20km and another of 18km distance. The average time taken for each traversal was 1 hour 15 minutes as the traversal speed was kept in between 20 to 30 km/hr. Wherever the road or traffic conditions dictated a slowing down or speeding up of the traversing vehicles, the values recorded were eliminated to reduce outliers and inconsistencies. Data collected from highways and arterial roads was not considered. Further, the data from transition areas between different Local Climatic zones was purged. Only remote sensing studies were conducted over the other cities selected.

The identification of the temperature profile within as LCZ can be used to understand the inter-zone temperature difference. Temperatures in the urban fringes can be considered as the standard temperature of an area undisturbed by urbanization while other areas can be expected to have increased temperatures. This inter-zone temperature difference observed between the various LCZ classes of Roorkee will show the Urban Heat Island characteristics of Roorkee. As the traverse survey was conducted with GPS, the data is geo-referenced and as such can be directly used to validate the temperature profile based on the boundaries of the LCZs.Further to understand the strength and the weakness of the LCZ classification system few segments under the same LCZ were identified so that the temperatures readings in these segments can be analyzed

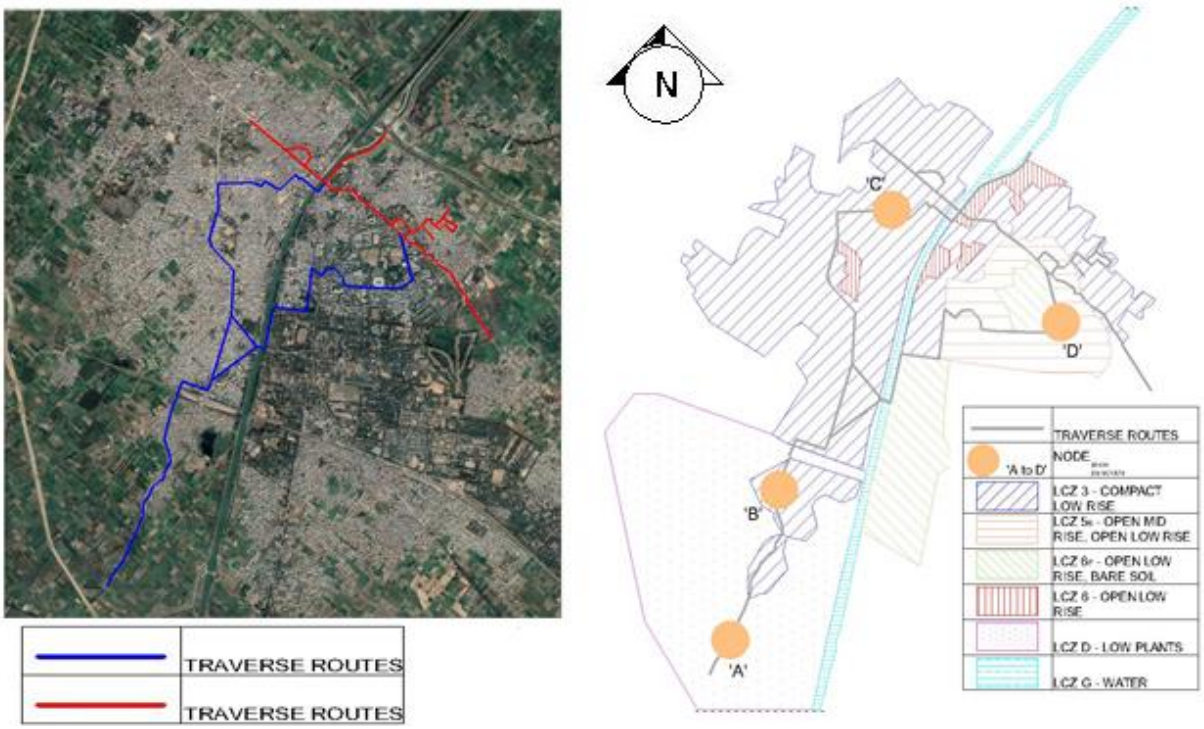


Figure 4- The traverse routes taken across Roorkee are indicated on the satellite imagery to the left and the nodes within the respective local climate zones are marked out on the drawing to the right.

Analysis

Data filtering process

The first step of analyzing the data is the filtering process as mentioned earlier. The filtering is to avoid any outliers in the temperature data and to create a geo-referenced temperature record for the same points along the traverse survey for the three days on which the survey was conducted. Further, data pertaining to highways, arterial roads, transition areas between different LCZ's was purged to get data representative of the morphological structure.

Mapping

Maps have been generated for the three cities based on the remote sensing data obtained from the earlier mentioned sources after following the process as provided by the WUDAPT platform. Table 1 shown below lists the 17 major built and land cover types as proposed in the LCZ classification system by Stewart and Oke (Stewart *et al.*, 2012).

Table 1 - The built and land cover types as per the Local Climate Zone classification system proposed by Stewart and Oke in 2012 which forms the basis of WUDAPT classification

Local Climate Zone Classification identifier	**Built types / Land cover types**
G	Water
F	Bare Soil or Sand
E	Bare Rock or Paved
D	Low plants
C	Bush, scrub
B	Scattered Trees
A	Dense Tress
10	Heavy Industry
9	Sparsely Built
8	Large low-rise
7	Lightweight low-rise
6	Open low-rise
5	Open mid-rise
4	Open high-rise
3	Compact low-rise
2	Compact mid-rise
1	Compact high-rise

The generated maps for three cities along with the associated colour coding as recommended by the WUDAPT platform are provided in Figures 5, 6 and 7. These images show a high prevalence of Compact low-rise and open low-rise built up structures or LCZ classifier 3 which is in fact consistent with the lower income profile of Category Z cities of India. Low income profile cities tend to spread out and occupy cheaper land areas as the population in the city increases. The high-rises are yet to appear in these cities. The built types as a percentage are expressed in the bar graphs shown in Figures 4, 5 and 6.

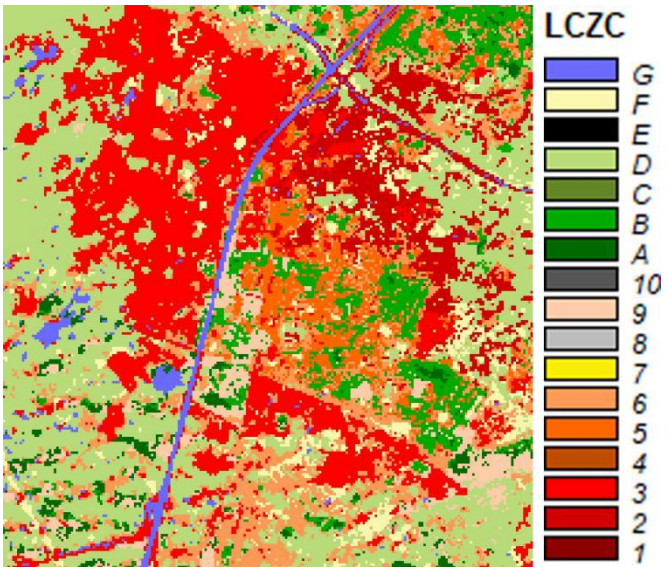


Figure 5 - Local climate zone classification for Roorkee

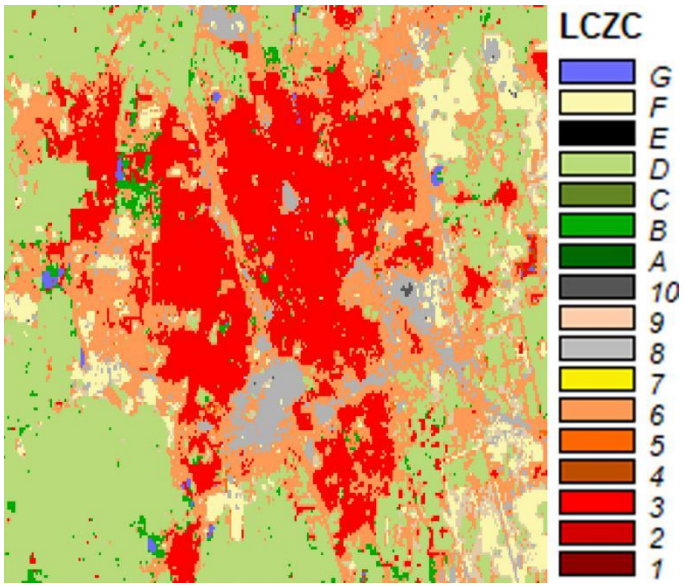


Figure 6 - Local climate zone classification for Sonipat

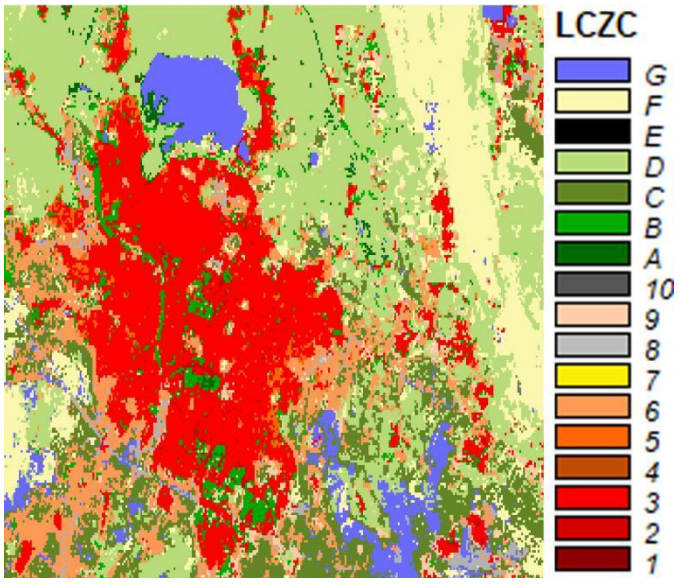


Figure 7 - Local climate zone classification for Kadapa

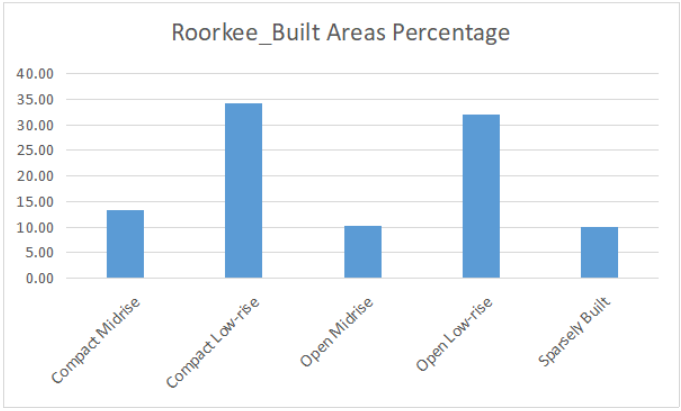


Figure 8 - Built type percentage asper LCZC for Roorkee

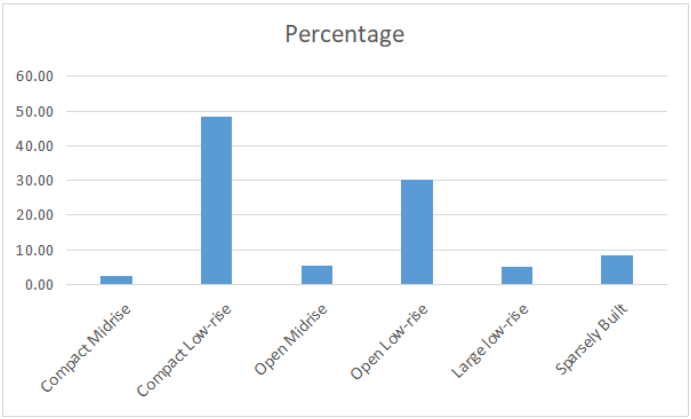


Figure 9 - Built type percentage asper LCZC for Kadapa

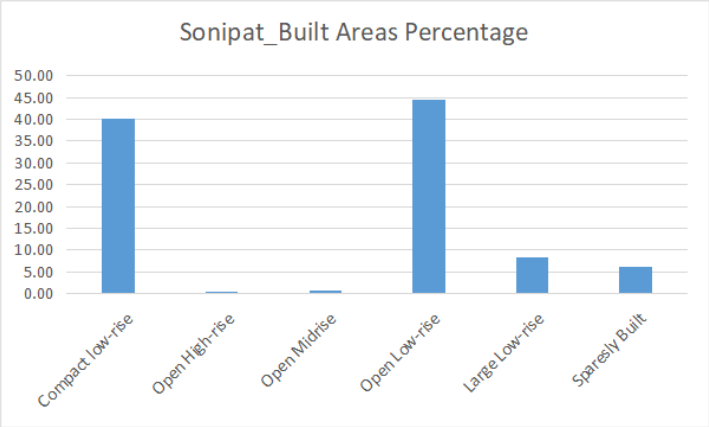


Figure 10 - Built type percentage asper LCZC for Sonipat

Immediate observations show us that

- Roorkee has 34% Compact low-rise and 32% Open low-rise making a total of 66% low-rise construction in the city.
- Kadapa has 48% Compact low-rise and 30% Open low-rise making a total of 78% low-rise construction in the city.
- Sonipat has 40% Compact low-rise and 44% Open low-rise making a total of 74% low-rise construction in the city.

Results & Discussion

In terms of LCZ classification, It is imperative for the researcher to be mindful of arterial road network even if it is in the same LCZ zone as it has significant impact on the temperature readings. In our case, a difference of about 1-0.5 deg, Celcius (Segment 1 and Segment 4) was observed.

The survey results show us that the areas with low-rise profile in a category Z city have about 2 deg. Celsius increase in temperature over the fringes. Further, from the LCZ mapping of the cities we have observed a homogeneity in the building morphology. Morphology is predominantly low rise. And over period of time open low rise is transforming into compact low rise or compact mid rise. This homogeneity is not ideal and research has pointed towards mixing of morphological types. In the short term, the Urban Heat Island effect within the areas with open low-rise profile can be reduced provided there are enough open spaces where blue-green infrastructure interventions can be introduced. The compact low-rise profile areas may require certain policy interventions apart from direct physical blue-green infrastructure interventions wherever possible to be achieve heterogeneous nature over time. The policy interventions may be used to either create more open spaces where blue-green infrastructure can be introduced and development plans should also promote mixed use. Further developmental bye-laws have to be analyzed as some of the homogeneity is driven by them

Table 2- Results of the traverse survey in Roorkee

Representative Temperature at 11:30pm - March 28th, March 29th, April 1st			
Node	LCZ Zone	Ta - Air Temperature (Celsius)	Inter LCZ Air difference (reference Node A)
Node A	Low Plants LCZ D	20.93	0
Node B	Compact Low-rise surrounded with Low Plants LCZ 3d	21.38	0.45
Node C	Compact Low-rise LCZ 3	23.86	2.93
Node D	Open Midrise and Open Low-rise LCZ 56	22.43	1.5

Table 3- Results of the traverse survey in LCZ3 zone in Roorkee

Representative Temperature at 11:30pm - March 28th, March 29th, April 1st		
Segment	Ta - Air Temperature (Celsius)	Air temperature Difference (reference Segment 4)
Segment 1	23.4	0.5
Segment 2	23.97	1.07
Segment 3	23.86	0.96
Segment 4	22.9	0

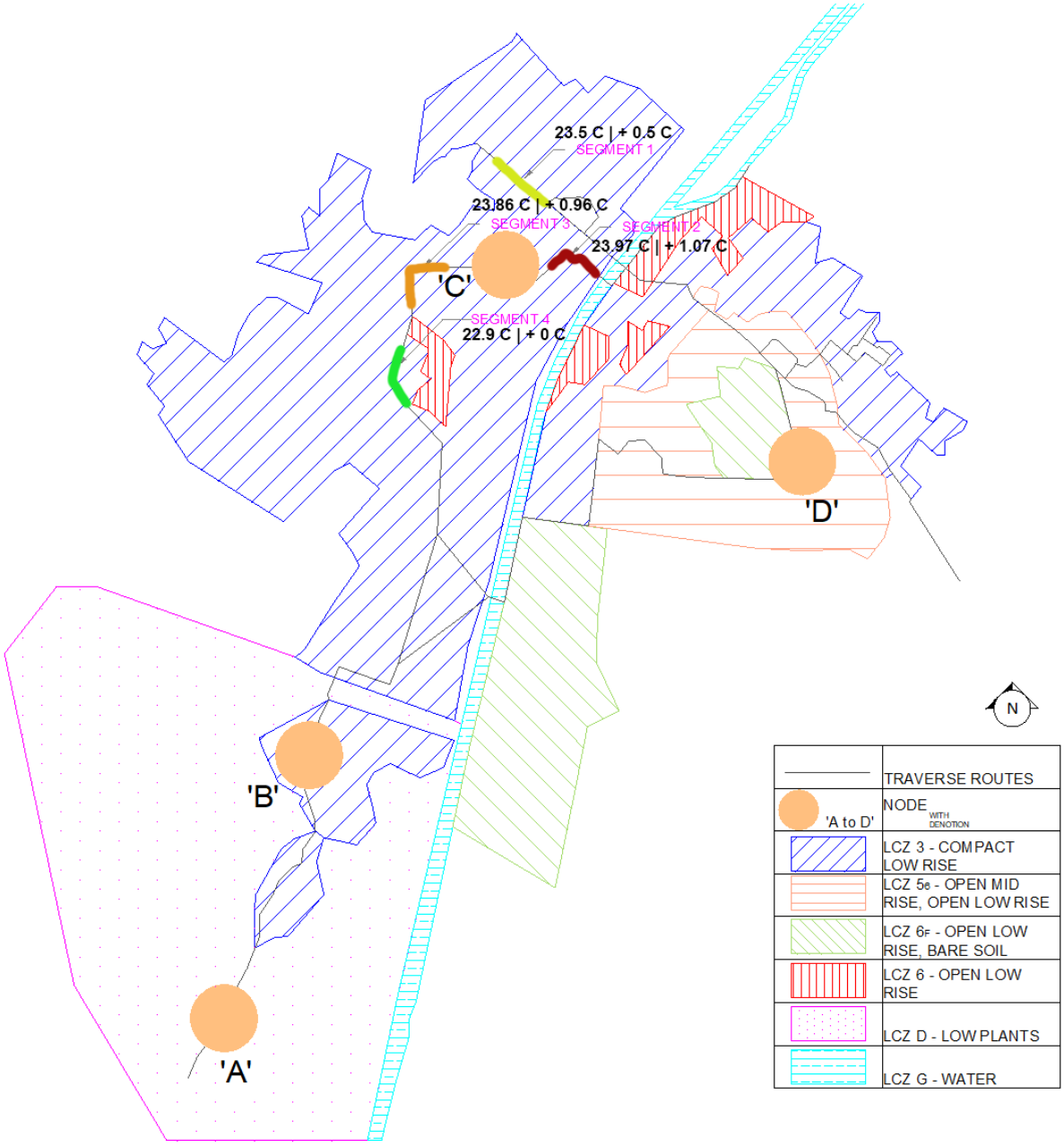


Figure 11- The nodes and Segments within the respective local climate zones are marked out on the drawing

References

Bhagat, R. B. (2014) 'Urban Policies and Programmes in India: Retrospect and Prospect', *Urban Planning, Yojana*, 58(January), pp. 4–8.

Census of India (2011) 'Census of India 2011', in *Census of India*. Available at: http://censusindia.gov.in/2011-prov-results/paper2/data_files/India2/1. Data Highlight.pdf (Accessed: 14 June 2018).

Ching, J. *et al.* (2018) 'WUDAPT: An Urban Weather, Climate, and Environmental Modeling Infrastructure for the Anthropocene', *Bulletin of the American Meteorological Society*, 99(9), pp. 1907–1924. doi: 10.1175/BAMS-D-16-

0236.1.

Government of India (2008) 'Sixth Central Pay Commission Report (No. 1/1/2008-I C)', *The Gazette of India*, pp. 28–57. Available at: https://doe.gov.in/sites/default/files/6cpcdecision %281%29.pdf.

Govindarajulu, D. (2014) 'Urban green space planning for climate adaptation in Indian cities', *Urban Climate*. Elsevier B.V., 10(P1), pp. 35–41. doi: 10.1016/j.uclim.2014.09.006.

Kotharkar, R. and Bagade, A. (2018) 'Evaluating urban heat island in the critical local climate zones of an Indian city', *Landscape and Urban Planning*. Elsevier, 169, pp. 92–104. doi: 10.1016/J.LANDURBPLAN.2017.08.009.

Mathew, A., Khandelwal, S. and Kaul, N. (2016) 'Spatial and temporal variations of urban heat island effect and the effect of percentage impervious surface area and elevation on land surface temperature: Study of Chandigarh city, India', *Sustainable Cities and Society*. Elsevier, 26, pp. 264–277. doi: 10.1016/J.SCS.2016.06.018.

Ministry of Finance (2008) 'Decision of the Government on the recommendations of the Sixth Central Pay Commission (No.1 (3)/2008-E-II(B))', *The Gazette of India*. Available at: http://dispur.nic.in/sixthpay/sixth-pay-allowances.pdf.

Ministry of Urban Development Government of India (2010) *National Mission on Sustainable Habitat*. Available at: http://www.indiawaterportal.org/sites/indiawaterportal.org/files/National-mission-on-sustainable-habitat-A-document-prepared-by-Ministry-of-Urban-Development %282011%29.pdf (Accessed: 19 July 2018).

Mohan, M. *et al.* (2009) 'Assessment of urban heat islands intensities over Delhi', *The Seventh International Conference on Urban Climate*, 3(July), pp. 3–6.

Oke, T. R. *et al.* (2017) *Urban climates*. Available at: https://www.barnesandnoble.com/w/urban-climates-dr-t-r-oke/1125125146 (Accessed: 15 May 2019).

Pandey, A. K. *et al.* (2014) 'Spatio – temporal variations of urban heat island over Delhi', *Urban Climate*. Elsevier, 10, pp. 119–133. doi: 10.1016/J.UCLIM.2014.10.005.

Stewart, I. D. *et al.* (2012) 'Local Climate Zones for Urban Temperature Studies', *Bulletin of the American Meteorological Society*. American Meteorological Society , 93(12), pp. 1879–1900. doi: 10.1175/BAMS-D-11-00019.1.

Stewart, I. D., Oke, T. R. and Krayenhoff, E. S. (2014) 'Evaluation of the "local climate zone" scheme using temperature observations and model simulations', *International Journal of Climatology*. John Wiley & Sons, Ltd, 34(4), pp. 1062–1080. doi: 10.1002/joc.3746.

The Hindu - Special Correspondent (2017) 'Climate change plan to get new missions', *The Hindu*, 25 January. Available at: http://www.thehindu.com/news/national/Climate-change-plan-to-get-new-missions/article17090498.ece (Accessed: 28 May 2018).

Thomas, G. *et al.* (2014) 'Analysis of Urban Heat Island in Kochi, India, Using a Modified Local Climate Zone Classification', *Procedia Environmental Sciences*. Elsevier, 21, pp. 3–13. doi: 10.1016/J.PROENV.2014.09.002.

United Nations (2014) *World Urbanization Prospects*. Available at: https://population.un.org/wup/Publications/ (Accessed: 15 May 2019).

RESILIENT DESIGN OF BUILDINGS IN RESPONSE TO CHANGING CLIMATES

Study of Adaptive City by Osaka Heat Island Countermeasure Technology Consortium

Hideki Takebayashi[1]*, Kobe University (Japan)*
Masakazu Moriyama, Osaka Heat Island Countermeasure Technology Consortium (Japan)

ABSTRACT

Osaka Heat Island Countermeasure Technology Consortium (Osaka HITEC) established in 2006, started the certification system of heat island measures technology in 2011, which contains 9 categories and has already certified 13 heat island measures technologies. A retroreflective high solar reflectance window film was first certified in 2018. Osaka HITEC is currently working on evaluation and implementation of adaptation measures against extreme heat. Several adaptation technologies have been developed by various companies and their evaluation methods were discussed so that they may be properly implemented in society. Adaptation measures for urban heat islands and their effects and associated evaluation indices are organized in a table. The cool spots and cool roads that exist in Osaka Prefecture area are aggregated to the web. The effect of shading by trees is dominant, and it combines the effects of evaporation and ventilation. The effects of adaptation measures obtained by demonstrative experiments are evaluated by SET*. Shielding of solar radiation to pedestrians is a more effective method of lowering MRT and SET*.

Overview of the efforts of Osaka local government

The following is a review of the measures taken by the local government for heat island measures in Osaka, the second largest urban area in Japan, and the most likely to be hotter due to local climatic characteristics.

Osaka heat island measures promotion plan established in 2004 (Osaka Prefecture 2004)

At the beginning of the plan, the current situation, causes and effects of urban heat islands were described based on statistical data. In Osaka, air temperature rises by 2.1 degrees in 100 years, which exceeds the national average of 1.0 degrees, and the difference of 1.1 degrees is considered to be the effect by urban heat islands. Looking at the change in the land use condition in Osaka area, forests and wild areas decreased by 11 % and farmland by 42 %, residential areas increased by 34 % and roads by 50 %, in the last 30 years. Simultaneously, the total energy consumption in Osaka area increased by 25 %. In Osaka city, the number of carriers due to heatstroke increased in the year the number of higher air temperature hours was large. The basic concepts of the plan are organized as follows.

- A town where we can comfortably live and walk
- A town full of green, water and natural winds
- A town where we can feel coolness and freshness
- A town where we can sleep without relying on air conditioner

[1] Corresponding Author: thideki@kobe-u.ac.jp, +81-78-803-6062.

- A town which does not waste energy
- A town where so much heat is not accumulated on buildings and roads

Plan period is until 2025, the objective area of the plan is the whole of Osaka Prefecture. The goals of the plan are the following two.

Goal 1: Reduce nighttime air temperature in residential areas and reduce the number of tropical nights by 30% by 2025. Tropical night is a night that minimum air temperature is 25 degrees Celsius or more.
Goal 2: Create cool spots in the outdoor space, improve the thermal environment during the summer daytime, and lower the sensational temperature of the human body.

The basic directions of measures are the following three.

1. Reduction of anthropogenic heat release by introduction of energy saving equipment and improvement of lifestyle
2. Control of surface temperature rise by improvement of surface coverage of lands and buildings
3. Utilization of the cooling effect of wind, green and water

Osaka heat island measures promotion plan revised in 2015 (Osaka Prefecture 2015)

According to statistical data, the number of tropical nights decreased slightly in recent years, but the number of heatstroke patients due to higher air temperatures during the day exceeded 4,000 in 2013, and daytime health damage became significant in recent years. Therefore, in addition to conventional summer nighttime measures, mitigation of daytime heat stress, that is, promotion of adaptation measures, was added to the plan. The basic concepts of the plan are organized as follows.

- Steady promotion of "mitigation measures", which include efforts to reduce the surface temperature of building and ground surfaces and reduce anthropogenic heat release
- In addition to "mitigation measures", promoting "adaptation measures", an effort to reduce the impact on human health, etc.
- Especially in the downtown area of Osaka, implementing various measures for redevelopment of urban areas and urban infrastructure
- In order to reduce the number of tropical nights, properly progress management by using appropriate indicators

Plan period is the same as before, until 2025. The goals of the plan are also the same as before, the following two.

Goal 1: Reduce nighttime air temperature in residential areas and reduce the number of tropical nights by 30% by 2025.
Goal 2: Create cool spots in the outdoor space, improve the thermal environment during the summer daytime, and lower the sensational temperature of the human body.

For the basic directions of measures, the fourth was added to the previous three.

1. Reduction of anthropogenic heat release
2. Control of surface temperature rise
3. Utilization of the cooling effect of wind, green and water
4. Promotion of adaptation measures

Osaka HITEC (Heat Island Countermeasure Technology Consortium) Activities

Certification system of heat island measures technology

Osaka HITEC was established in January 2006, for the purpose of the development and spread of heat island countermeasure technologies, implementation of measures and verification of their effects, and the collaboration between industry, academia, government and the private sectors. The consortium called on local governments, private companies, universities, research institutes, environmental NGOs and NPOs to participate. The consortium has five working groups; WG related to the materials, WG on heat utilization and reduction of anthropogenic heat release, WG on cool spot creation technologies, WG on thermal load evaluation method, and WG on urban design.

Osaka HITEC started the certification system of heat island measures technology in October 2011. In 2019, the category of certification technology increased to 9; high solar reflectance paint for roof, high solar reflectance pavement (excluding for roadways), high solar reflectance waterproof sheet (membrane), high solar reflectance roofing materials (tile, slate, metal, etc.), water retaining pavement block, external insulation specification for roof, external insulation specification for outer wall, retroreflective high solar reflectance outer wall material, retroreflective high solar reflectance window film. Three high solar reflectance paints for roof, five high solar reflectance pavements (excluding for roadways), three high solar reflectance roofing materials, one external insulation specification for outer wall, and one retroreflective high solar reflectance window film were certified (Osaka HITEC 2019).

Osaka HITEC has also held town planning ideas competition in consideration of the heat islands measures, recruitment and selection of cool spots and cool roads, and technology seminars.

Adaptation measures against extreme heat

Osaka HITEC is currently working on evaluation and implementation of adaptation measures against extreme heat. Several adaptation technologies have been developed by various companies and their evaluation methods were discussed so that they may be properly implemented in society. Adaptation measures for urban heat islands and their effects and associated evaluation indices are organized. A simple method to evaluate the adaptation measures is examined focusing on their appropriate introduction in urban space. Osaka HITEC is promoting the following three activities; organization of adaptation measures, examination of specific image of adaptive city, and examination of evaluation method of adaptive city.

Organization of adaptation measures

Research institutes such as universities that objectively evaluate the performance of each technology, and companies such as manufacturers that propose specific adaptation measures are working together. The adaptation measures for urban heat island listed in the heat countermeasure guidelines established by Japanese Ministry of Environment (Japanese Ministry of Environment 2018), the report by Japanese Ministry of Environment (Center for environmental information science 2017), and the town planning idea competition considering the urban heat island presented at the Osaka Heat Island Countermeasure Technology Consortium (Osaka Heat Island Countermeasure Technology Consortium 2015) are shown in Table 1. The mechanisms by which these methods work and the evaluation index governing their effects are also presented. Heat is mainly mitigated by solar shading, solar reflection, and evaporation. Therefore, solar transmittance, solar reflectance, and evaporative efficiency (evaporative rate) are the primary evaluation indices. The increase in the convection heat transfer coefficient is the cause of cooling by fractal-shaped sunshades, and artificial cooling is the cause of cooling by ceiling cooling systems and water cooling benches.

Table 1. Adaptation measures for urban heat islands and their effects and associated evaluation indices (Takebayashi 2018)

Menu	Evaluation index	Main effect mechanism
from the heat countermeasure guidelines by Japanese Ministry of Environment		
Green shade	Solar transmittance, Evaporative efficiency	Sun shade, Evaporative cooling
Solar radiation shade	Solar transmittance, Convection heat transfer coefficient	Sun shade, Convection heat transfer
Retroreflective surface	Downward solar reflectance	Solar reflection
Water retentive pavement	Evaporative efficiency	Evaporative cooling
Cool pavement	Solar reflectance	Solar reflection
Green pavement	Evaporative efficiency	Evaporative cooling
Green wall	Evaporative efficiency	Evaporative cooling
Water-retentive wall	Evaporative efficiency	Evaporative cooling
Fine mist spray	Evaporation rate	Evaporative cooling
from the report by Japanese Ministry of Environment		
Awning	Solar transmittance	Sun shade
Fractal-shaped sunshade	Solar transmittance, Convection heat transfer coefficient	Sun shade, Convection heat transfer
Mesh shade and water supply	Solar transmittance, Evaporative efficiency	Sun shade, Evaporative cooling
Evaporative cooling louver	Evaporative efficiency	Evaporative cooling
Greening cooling louver	Evaporative efficiency	Evaporative cooling
Tree pot	Solar transmittance, Evaporative efficiency	Sun shade, Evaporative cooling
Water-retentive block	Evaporative efficiency	Evaporative cooling
Water surface	Evaporative efficiency	Evaporative cooling
Fine mist spray with blower	Evaporation rate	Evaporative cooling

Ceiling cooling system	Surface temperature	Artificial cooling
Water cooling bench	Surface temperature	Artificial cooling
from town planning idea competition by Osaka HITEC		
Water surface	Evaporative efficiency	Evaporative cooling
Watering	Evaporative efficiency	Evaporative cooling
Fine mist spray	Evaporation rate	Evaporative cooling
Shading	Solar transmittance	Sun shade
Tree planting	Solar transmittance, Evaporative efficiency	Sun shade, Evaporative cooling
Roof and ground greening	Evaporative efficiency	Evaporative cooling
Wind use	Convection heat transfer coefficient	Convection heat transfer
Traffic mode control	Anthropogenic heat release	Reduction of heat release
Unused, natural energy use	Anthropogenic heat release	Reduction of heat release
ICT use	Human body physiological amount	Reduction thermal load

Examination of specific image of adaptive city

Local government provides boundary conditions for examination, such as selection of the objective urban area, population, infrastructure, etc. Research institutes such as universities that present ideas for the future image, and companies such as design offices and consultants that draw specific future images are working together.

The local government has carried out the following things; monitoring of weather and energy consumption at detailed spatio-temporal resolution, development of heat island measure plan as administration. Air temperature measurements have been conducted at 70 locations in the city with a city area of 225 km^2, and air temperature distribution influenced by the sea breeze in the daytime and that influenced by the urbanization in the nighttime were analyzed in detail. In addition, the actual situation of local high air temperature around the outdoor units of the air conditioners in the downtown commercial area was analyzed based on field measurement results (Masumoto et al. 2006, Nishimura et al. 2006, Oku et al. 2014). Currently, the spatial distribution of heat stroke occurrence is being analyzed in Osaka city area.

Working group on urban design mainly composed of university researchers have organized the cool spots and cool roads that exist in Osaka Prefecture area (Masuda 2019). Display of cool spots and cool roads on the map is shown in Figure 1. 119 cool spots and 121 cool roads were selected as a result of investigation based on information from citizen. As each point is selected on the Web, photos and descriptions of cool spots or cool roads will be introduced. The components and function of cool spots and cool roads are shown in Tables 2 and 3.

Regarding cool spots, several forests are left in the suburbs, and there are several parks such as Osaka Castle Park, Tennoji Zoo Park. Generally, there are a lot of green in the sites of shrines and temples. Street trees are placed on the side of several roads. The effect of shading by trees is dominant, and it combines the effects of evaporation and ventilation.

Promenade along the green and water, in the green area and covered by street trees are recognized as cool roads. As same as cool spots, the effect of shading by trees is dominant, and it combines the effects of evaporation and ventilation.

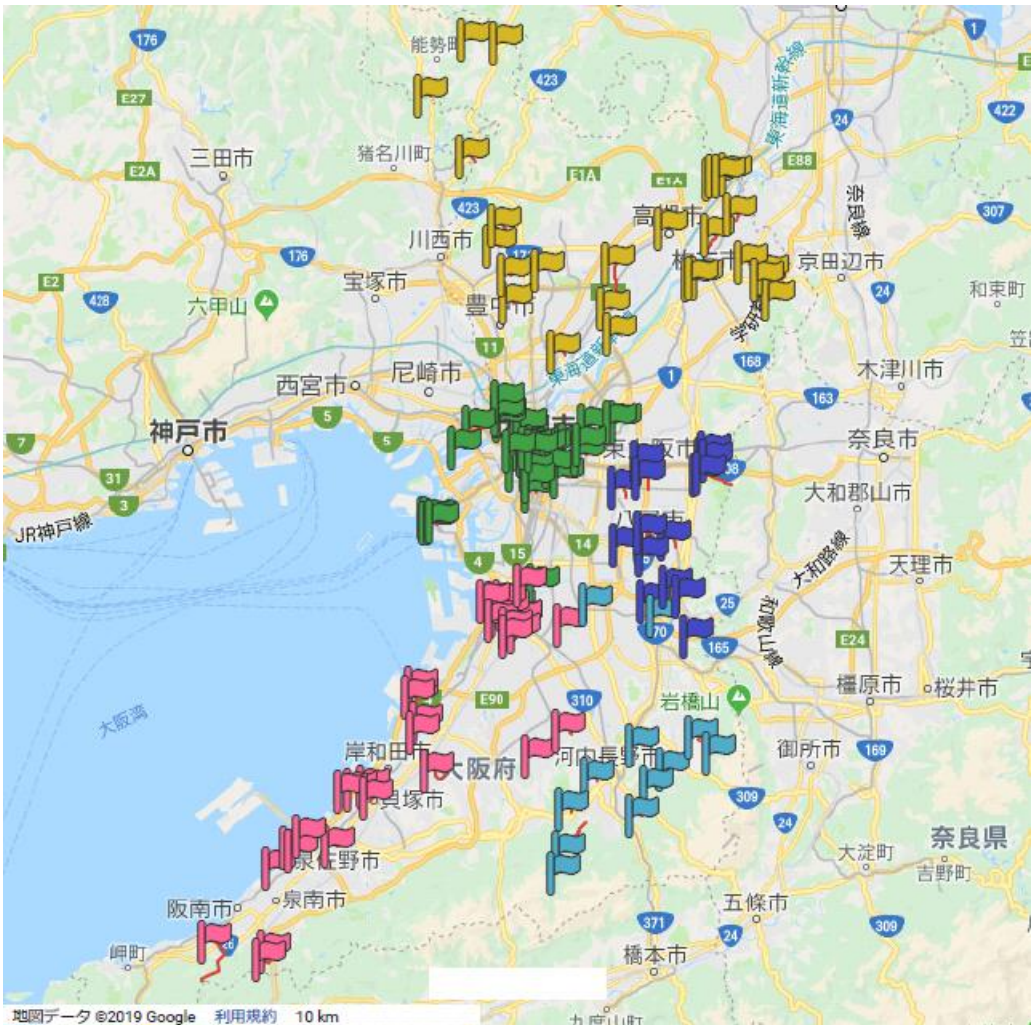


Figure 1. Display of cool spots and cool roads on the map (The color indicates an administrative area indicated by Osaka HITEC). *Source*: Osaka HITEC 2015.

Table 2. The components (left) and mechanism of measures effect (right) of cool spots. *Source*: Osaka HITEC 2015.

Forest	26.1 %
Green park	22.7 %
Open space	16.8 %
Temple or shrine	13.4 %
Street	10.1 %
Street trees	3.4 %
Shopping mall	2.5 %
Others	5.0 %

Tree shade	28.6 %
Tree shade and evaporation	15.1 %
Tree shade and ventilation	14.3 %
Evaporation by mist	9.2 %
Evaporation from surface	8.4 %
Tree shade, evaporation and ventilation	6.7 %
Evaporation and ventilation	5.0 %
Ventilation	4.2 %
Altitude	4.2 %
Building shade	3.4 %
Others	0.9 %

Table 3. The components (left) and mechanism of measures effect (right) of cool roads.
Source: Osaka HITEC 2015.

Green or water side walkway	24.8 %
Approach to temple or shrine	21.6 %
Walkway in park	20.8 %
Walkway with street trees	20.8 %
Others	1.9 %

Tree or building shade	40.0 %
Tree or building shade and ventilation	16.0 %
Tree or building shade and evaporation	15.2 %
Ventilation and evaporation	8.8 %
Ventilation	8.0 %
Others	12.0 %

Examination of evaluation method of adaptive city

Research institutes such as universities that organize boundary conditions for evaluation and present ideas of evaluation methods, and companies such as consultants that practice concrete evaluations are working together.

In Japan, Standard Effective Temperature (SET*) and Wet Bulb Globe Temperature (WBGT) are mainly used for the evaluation of outdoor human thermal comfort. WBGT, which is a stress index worldwide accepted as a preliminary tool for the assessment of hot thermal environments (ACGIH 2011, d'Ambrosio et al. 2014, ISO 2017), is often used under more severe conditions to warn of the risk of heat stroke, and SET* defined as the equivalent dry bulb temperature of an isothermal environment at 50% RH in which a subject, while wearing clothing standardized for activity concerned, would have the same heat stress and thermo-regulatory strain as in the actual test environment (Gagge et al. 1986), is used to evaluate the thermal environment. SET* is desirable as an index from the viewpoint of appropriately introducing adaptation measures in urban areas and developing a more comfortable outdoor space as it exhibits a good relationship with outdoor thermal comfort (Nakano 2004).

Examples of the effects of adaptation measures obtained by demonstrative experiments are shown in Figure 2. As MRT was measured by a globe thermometer, the solar absorptance was set to 1.0, which was much larger than that of the human body. The measurements were taken at various places and times under typical summer weather condition, therefore, a simple mutual comparison was not appropriate. It was, however, possible to qualitatively recognize the characteristics of each adaptation measure. Shielding of solar radiation to pedestrians was a more effective method of lowering MRT and SET*.

The decrease of MRT by the solar radiation shielding technology such as mesh shade, awning, fractal shape sunshade, is the largest, and SET* is also greatly reduced. While these technologies are installed horizontally on the upper part of the human body, cooling and greening cooling louvers are installed vertically on the side of the human body. They lower MRT due to the evaporative cooling effect, but the effect is smaller than the effect of solar radiation shielding. Fine mist spray with blower and ceiling cooling system work artificially and lower air temperature, but they cannot get so large SET* reduction. The decrease of MRT due to the improvement of coverage such as tree pot, water retentive block is smaller than the effect of solar radiation shielding.

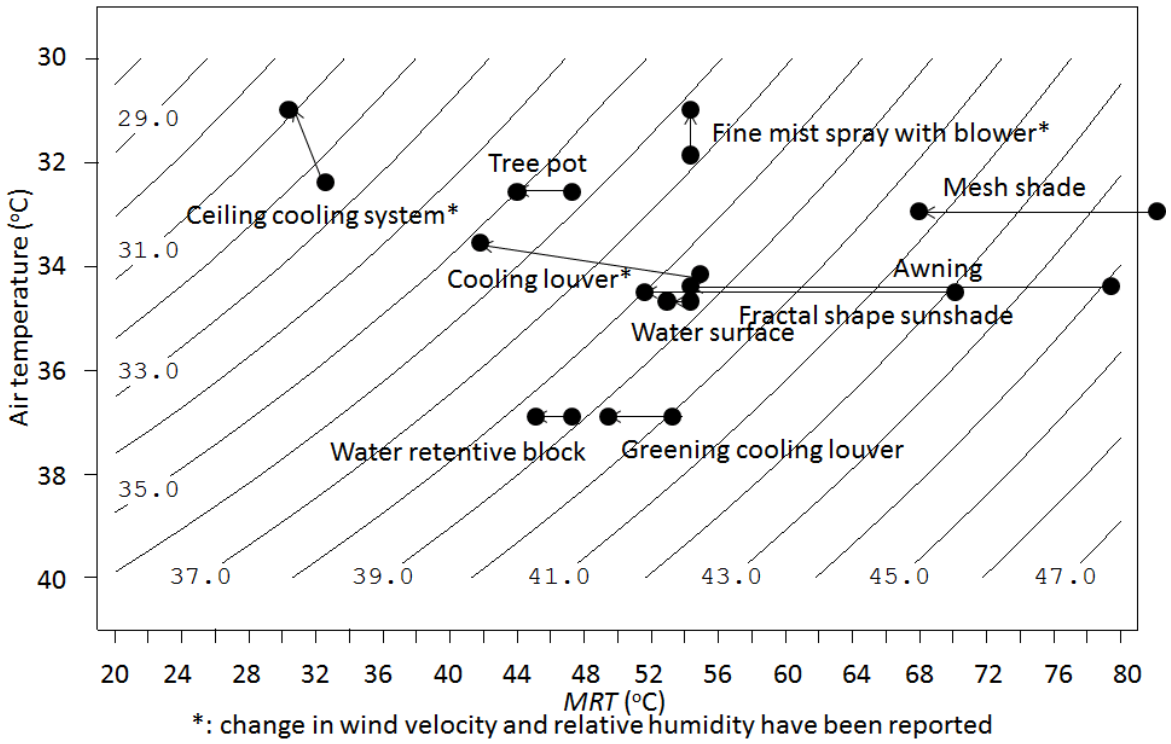


Figure 2. Examples of the effects of adaptation measures obtained through demonstrative experiments. SET* is indicated by a contour line. The relative humidity is 50 %, wind speed is 1 m/s, clothing insulation is 0.6 clo, and metabolic rate is 2 Met. (Takebayashi 2018)

Conclusions

The outline of Osaka heat island measures promotion plan is explained. The goals of the plan are to reduce the number of tropical nights by 30% by 2025 and to create cool spots in the outdoor space for improving the thermal environment of human body during the summer daytime. The specific methods of the plan are reduction of anthropogenic heat release, control of surface temperature rise and utilization of the cooling effect of wind, green and water. Promotion of adaptation measures was added in the revision of the plan in 2015. Osaka Heat Island Countermeasure Technology Consortium (Osaka HITEC) established in 2006, started the certification system of heat island measures technology in 2011, which contains 9 categories and has already certified 13 heat island measures technologies. Osaka HITEC is currently working on evaluation and implementation of adaptation measures against extreme heat. Adaptation measures for urban heat islands and their effects and associated evaluation indices are organized in a table. The cool spots and cool roads that exist in Osaka Prefecture area are aggregated to the web. The effect of shading by trees is dominant, and it combines the effects of evaporation and ventilation. Shielding of solar radiation to pedestrians was a more effective method of lowering MRT and SET*.

Acknowledgments

The authors would like to thank all members participating in Osaka HITEC's activities.

References

ACGIH. 2011. *Threshold limit values for chemical substances and physical agents and biological exposures indices.* Cincinnati, OH: American Conference of Governmental Industrial Hygienists.

Center for environmental information science. 2017. *Report on consignment work of survey and verification for the creation of a low-carbon city using surplus groundwater etc., Report entrusted by the Ministry of the Environment in 2016 fiscal year*. Accessed April 2019. http://www.env.go.jp/air/life/heat_island/guidelineH30/gudelineH30_all.pdf

d'Ambrosio Alfano FR., J. Malchaire, BI. Palella, and G. Riccio. 2014. "The WBGT index revisited after 60 years of use." *Annals of Occupational Hygiene*, 58(8), 955-970.

Gagge A., P. Fobelets and L.Bergland. 1986. "A standard predictive index of human response to thermal environment." *ASHRAE Transactions*, 92, 709–731.

ISO 2017. *Ergonomics of the thermal environment - Assessment of heat stress using the WBGT (wet bulb globe temperature) index - ISO Standard 7243*. International Organization for Standardization, Geneva.

Japanese Ministry of Environment. 2018. *Heat countermeasure guideline in the city*. Accessed April 2019. http://www.env.go.jp/air/life/heat_island/guidelineH30/gudelineH30_all.pdf

Masuda N. "Characteristics of cool spots and cool roads in Big City Osaka." Unpublished manuscript, last modified April 3, 2019. Microsoft Word file.

Masumoto K., I. Taniguchi and T. Nomura. 2006. "Characteristics of Air Temperature Distribution in 2005 and Situation of Heat Island in Osaka City." *Journal of Heat Island Institute International*, 1, 30-35.

Nakano J. and S. Tanabe. 2004. "Thermal comfort and adaptation in semi-outdoor environments." *ASHRAE Trans.*, 110, 543–553.

Nishimura M., M. Nabeshima, M. Nishioka, I. Taniguchi, K. Masumoto and T. Nomura. 2006. "Space-Time Characteristics of Energy Supply in Osaka City from Heat Island Viewpoint." *Journal of Heat Island Institute International*, 1, 15-22.

Oku Y. and K. Masumoto. 2014. "An Observational Study of the Difference on Urban Heat Islands between Summer and Winter in Osaka City." *Journal of Heat Island Institute International*, 9, 1-12.

Osaka Heat Island Countermeasure Technology Consortium. 2015. *Town planning idea competition considering urban heat island*. Accessed April 2019. http://osakahitec.com/result/index.html

———. 2015. *100 cool roads and 100 cool spots in Osaka.* Accessed April 2019. http://www.coolspot-osaka.jp/

———. 2019. *Outline of activities of Osaka Heat Island Countermeasure Technology Consortium.* Accessed April 2019. http://www.osakahitec.com/active/index.html

Osaka Prefecture. 2004. *Osaka Heat Island Measures Promotion Plan.* Accessed April 2019. http://www.pref.osaka.lg.jp/chikyukankyo/jigyotoppage/heat_mati.html

———. 2015. *Revised Osaka Heat Island Measures Promotion Plan.* Accessed April 2019. http://www.pref.osaka.lg.jp/chikyukankyo/jigyotoppage/osakaheatkeikaku.html

Takebayashi, H. 2018. "A Simple Method to Evaluate Adaptation Measures for Urban Heat Island." *Environments*, 5, 70, 1-13.

"Cradle to Gate" assessment of material related embodied carbon: A design stage stratagem for mid-rise housing in Sri Lanka

Ashan S Jayawardana, University of Moratuwa (Sri Lanka)
Narein G R Perera, University of Moratuwa (Sri Lanka)
L S Ranjith Perera, Sri Lanka Institute of Information Technology (Sri Lanka)

ABSTRACT

Achieving low carbon buildings is seen as a key concept in order to reduce carbon emission and mitigate climate change. In contrast to operational emission, material related embodied carbon (EC) in the built environment plays a pivotal role, with the continuous consumption of high carbon emitting materials. This research relates to the 'Cradle-to-Gate' system boundary, while limiting its focus on building design stage decisions. A hybrid analysis approach was adopted - a bottom-up process with steps encompassing mass analysis, EC calculation, highlighting carbon hotspots, and ultimately the identification of critical building components. As a case study, multi-storey housing was selected as a critical building typology, in Sri Lanka. The results reveal 'walls' as a carbon hotspot that needs to be explored in strategies for mitigation. Substantial EC savings were seen in the selection of fly ash blocks as an alternate material to clay brick or cement block. Changes to the configuration of walls, specifically, bonding patterns and non-inclusion of a plaster layer, also showed savings. This paper, contributes to the understanding of material selection implications - in the cradle-to-gate stage - for the reduction of carbon emissions in mid-rise housing, in the context of Sri Lanka.

Special Issue Journal	:	Energy and Buildings
DoI	:	https://doi.org/10.1016/j.enbuild.2020.110542
Citation	:	Jayawardana, A., Perera, N., & Perera, L. (2021). "Cradle to Gate" assessment of material related embodied carbon: A design stage stratagem for mid-rise housing in Sri Lanka. Energy And Buildings, 230, 110542.

The resilient design for traditional residential building in Northern Shaanxi of China

Sunwei Liu[1], *Yupeng Wang*[2], *Yitong Kang*[1]
1Master Student, Department of Architecture, Xi'an JiaoTong University
2Professor, Department of Architecture, Xi'an JiaoTong University

ABSTRACT

The indoor lighting environment and energy consumption is a big issue for traditional residents of Yaodong in Yan'an city in China. In order to promote the living environment of Yaodong, the retrofitted scheme uses passive ecological measures such as natural lighting and attached sunspace to make full use of solar energy during the winter. In summer, facing to the problem of high indoor air temperature, the building uses a wall with thermal insulation and a roof that draws on the traditional residence of Yaodong. In addition, the added windows can improve indoor ventilation and reduce the excessive indoor temperature and humidity in summer. Besides, this design is entirely using renewable energy. In this research, simulation software BESTenergy, Ecotect and RETScreen are used to evaluate the effects of the comprehensive design method for improving indoor lighting, thermal comfort, and annual energy consumption. All of the additional building resilient design will be based on the adaptation to traditional building design and living style of the local people. From the overall analysis of the whole year, these retrofit measures will be conducive to the improvement of indoor lighting and thermal comfort and reduce the energy consumption. It's demonstrated that the resilient house has better adaptability to UHI, compare to local ordinary urban dwellings.

Keywords: Resilient Building Design; Yaodong; Indoor thermal environment; Building Simulation

Introduction

The IPCC's fifth assessment report shows that the surface temperature has increased by 0.12 ℃ per decade for nearly 60 years, which is about twice the temperature increase rate of the past 100 years. Compared with global warming, urban areas have experienced more intense warming, forming UHI with significantly higher urban temperatures than surrounding rural and suburban areas. Shaanxi province is located in a high latitude area of China, which is experiencing hot summers. In 2018, the averaged summer air temperature reached up to 24.7℃, which is 1.2℃ higher than the standard averaged summer air temperature during June to August. Yan'an is located in the hilly and gully region of the Loess Plateau in northern Shaanxi. It belongs to the plateau continental monsoon climate, with the semi-arid region in the north and the semi-humid region in the south. There is a large annual temperature difference and a large daily temperature difference, which is characterized by hot days and cold nights, hot summers and cold winters. The influence of Yan'an urban development on the annual average temperature has appeared since 1993. From 1993 to 2002, the urban impact was lighter, and the annual average temperature contribution rate of heat island effect was 38.1%. From 2003 to 2008, the

Corresponding Author: Yupeng Wang, [wang-yupeng@mail.xjtu.edu.cn]

heat island effect was obvious. The temperature increasement is above 1°C, which is close to the UHI of the big city, and the temperature difference (heat island intensity) between Yan'an and the suburbs is gradually increasing. The effect of heat island effect on the temperature of the four seasons is basically the same.

In order to improve the indoor thermal comfort environment, Yan'an residents widely use indoor air condition and heating systems to adjust the indoor environment, resulting in a sharp increase in building energy consumption. Artificial heat source is one of the important reasons for UHI. Reducing building energy consumption and using clean energy to reduce greenhouse gas emissions have a positive effect on UHI mitigation. With the acceleration of urbanization, the intensity of UHI has increased year by year. Therefore, the adaptation of building design to the outdoor climate is becoming to be an important issue. On the other hand, in rural areas of northern Shaanxi in China, many people are still living in traditional Yaodong, which is a traditional residential style. The natural ecological advantages of Yaodong are cultivated land saving, low cost, low technique requirement for construction and high thermal insulation properties, and the disadvantages could be raised such like the lack of safety, waterproof, lighting and ventilation problems. The concept of adaption to local climate conditions and their regional characteristics make Yaodong of high protection value, but as China's urbanization process, many peasants abandoned Yaodong living forms, and new buildings styles are taking it over. The aim is to develop a transformation method for traditional Yaodong in northern Shaanxi to meet the needs of modern life without losing their original ecological nature and further improve its indoor thermal comfort, reduce building energy consumption, and improve its adaptability to the more severe UHI phenomenon that may occur.

Methodology

Determination of building model

In order to analyze whether the resilient design for traditional residential building is superior to most local urban dwellings and improves the shortcomings of traditional Yaodong, including its actual energy consumption and adaptability in UHI, lighting and humidity, two control groups of traditional Yaodong and ordinary urban dwellings with equal areas were set up for simulation and comparative analysis to study their indoor thermal comfort in the same climatic conditions in Yan'an in this research.

The first is a typical traditional Yaodong (model A). A typical three-cave Yaodong was selected as a prototype in Nanniwan Town, Yan'an City. It is oriented from north to south, with three caves and each with a width of 3.5m and a depth of 9m. The total construction area is 94.5m² and the volume is 302.61m³. In addition to the south side wall of the selected Yaodong, the other exterior walls and roof are rammed earth, and the inner walls between the three caves are brick walls of 240mm. The building has only windows on the south wall, and the window material is 6mm double-layer insulating glass. In the simulation, the exterior walls and the roof are regarded as 50cm thick rammed earth, and the U-value of window material is set to 2.7 W/m²K.

The second is a local ordinary single-storey urban dwelling (model B). According to the general practice of urban residence in Yan'an, a single-storey house with the same area and internal space as the traditional three-cave Yaodong is designed. The height of the house is 3.5m and the volume is 330.75m³. It has three windows on the south wall and three windows on the north wall. The window-wall ratio of the south wall is 20.38%. The exterior walls of the house

mainly consist of 250mm concrete and 40mmEPS insulation layer. The inner walls are also brick walls of 240mm. The roof consists of 20mm cement board, 40mm EPS insulation layer and 260mm concrete, and the glass is the same as Yaodong.

For the new single-layer resilient house based on Yaodong, the width, depth and area are the same as the former two, with the height of 4m and the volume of 378 m^3. On the south side of the building, a sunspace with a depth of 1.5m and a height of 4m is set as a buffer zoon to reduce building energy consumption. The north wall of the building has three small windows for improving the natural daylighting. The window-wall ratio of the north wall is 4.01%. The glass adopts 6mm+12mm+6mm double-layer low-e glass with U-value of 1.72 W/m^2K, visible transmittance of 0.74 and solar heat gain coefficient of 0.67. The exterior walls of the building are composed of cement board, 30mm timber board, 40mm polyurethane foam, 30mm timber board and 15mm Plywood from the outside to the inside. The roof of the building is covered with the same material as Yaodong. In the summer, the shading device is introduced on the south side of the building. The software model of the three buildings is shown in Figure 1.

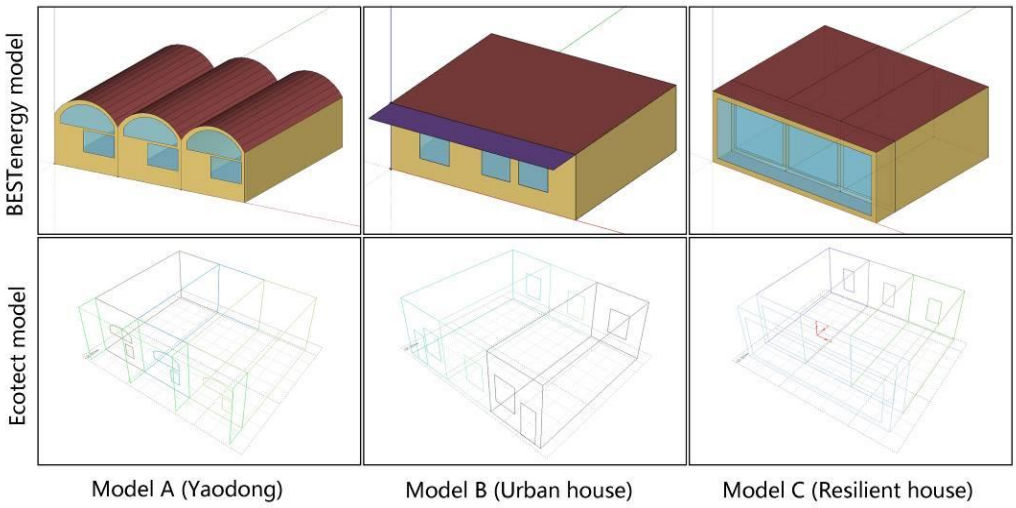


Figure 1. Images of three simulation models.

Simulation software

This research used BESTenergy to simulate building cooling energy demand (CED) and heating energy demand (HED), Ecotect to simulate building lighting and RETScreen to simulate the use of renewable energy.

BESTenergy is an open-source, free-redistributable building energy simulation software. It provides a SketchUp-based interface which runs dynamic building energy simulation by running EnergyPlus 8.9 calculation engine.

Ecotect uses the finite difference method and uses the grid to divide the analysis plane into multiple analysis units according to user needs and analyze each node. The software can analyze the lighting of the model based on the solar radiation intensity, building thermal parameters, etc.

RETScreen is a clean energy management software system for energy efficiency, renewable energy and cogeneration project feasibility analysis as well as ongoing energy performance analysis. The RETScreen software used in this study includes GSHP (Ground Source Heat Pump), PV (Photovoltaic) and SWH (Solar Water Heating). RETScreen and BESTenergy can work well together, because the important input parameters of RETScreen such

as annual heating or cooling energy load and design heating or cooling load can be calculated from the simulation results of BESTenergy.

Parameters setting for simulation

Through the BESTenergy simulation of three building models, this research calculates the annual CED and HED and the growth rate in winter and summer when the temperature rises, to see if the resilient house based on Yaodong can reduce building energy demand and their temperature sensitivity of UHI effects. In the evaluation of building energy demand, the ratio of energy demand and the corresponding building volume. Energy demand coefficient (λ) is used as a measure of building energy efficiency. The calculation method is shown in Eq.1, where i is the start hour of the calculation, n is the end hour of the calculation, EDn is the nth hour of building energy demand, and V is the building volume.

$$\lambda = \frac{\sum_i^n ED_n}{V} \quad (1)$$

According to the weather data of Yan'an City, continuous warming dates in winter and summer are selected and shown in Table 1. The λ_{HED} and λ_{CED} of the three models are calculated respectively. Linear regression is performed to investigate the correlation between air temperature, λ, and the growth rates, to determine the adaptability of each model to the UHI or enhanced UHI intensity. The details of input for BESTenergy simulation is shown in Table 2.

Table 1. Selected days for the air temperature-daily λ correlation analysis

Summer days	July 8	July 9	July 10	July 11	July 12	July 13
Air temperature	23.5℃	24℃	25.5℃	26℃	27℃	28℃
Winter days	Jan. 9	Jan. 10	Jan. 11	Jan. 12	Jan. 13	Jan. 14
Air temperature	-3.5℃	-3℃	-2℃	-0.5℃	0.5℃	1.5℃

Table 2. Details of the input parameters for the BESTenergy simulation

People Occupancy Rate	Activity Level	Electric Equipment Thermal Load	Ventilation Airflow Rate	Zone heating, Variable temperature	Zone cooling, Variable temperature
0.04 people/m²	Seated at rest	4W/m²	0.3/h	18:00-08:00, constant 20℃	18:00-08:00, constant 26℃

In addition, Ecotect was used to simulate daylighting of three building models, analyzing if the resilient house can use natural daylighting to reduce lighting energy consumption. BESTenergy was used to simulate the relative humidity inside the building throughout the year to analysis the differences of humidity, and uses RETScreen to simulate the use of geothermal energy and solar energy, and calculate the energy consumption and CO_2 emissions reduction. The ground source heat pump was introduced to provide energy for the whole year, and the solar energy was used to provide the energy required for the ground source heat pump, lighting, equipment and the hot water. Among them, the lighting electricity is calculated according to the residential building as 3KWh/m²year and the equipment electricity as 15KWh/m²year, so the lighting energy demand is 1.134MWh/year and the equipment energy demand is 5.67MWh/year.

The selected ground source heat pump is the horizontal one, with low cost and no water pollution. The parameters of the selected solar photovoltaic panel are: mono-Si PV module type, 19.2% Nominal PV module efficiency and one PV panel's power with 60 cells that is 0.315 KW. The parameters of the selected solar thermal panel are: glazed collector type, gross area of one collector is 2.42 m², aperture area of one collector is 2.26 m², Fr coefficient is 0.76, Fr UL coefficient is 3.74 (W/m²)/°C, and the slope of solar collector is 25°. Water heating load is considered for a house of 3 occupants, and the desired water temperature is 60°C. The estimated hot water use is 180L/d. RETScreen can calculate reduced CO_2 emissions based on the current state of China's energy structure. In 2017, China's energy structure was composed by 68.6% coal, 7.6% oil, 5.5% natural gas and 18.3% clean energy.

Results

Building cooling and heating energy demand

Simulation results are shown in Table 3. The CED of model A is 55.1 KWh lower than model B, and 148.1 KWh higher than model C. The HED of model A is 2.23 MWh higher than model B, and is 6.05 MWh higher than model C. The energy demand coefficient (λ) is calculated to provide more accurate total energy consumption.

Table 3. Statistical results of annual CED and HED for three simulation models

	Annual CED and HED	Annual CED	Annual HED
model A	13273.0KWh	3702.8KWh	9570.1KWh
model B	11095.1KWh	3757.9KWh	7337.2KWh
model C	7071.0KWh	3554.7KWh	3516.3KWh

The Annual $\lambda_{CED\ and\ HED}$ are shown in Table 4. The λ_{CED} of model A is 0.8KWh/m³ higher than model B, 2.8KWh/m³ higher than model C. The λ_{HED} of model A is 9.4KWh/m³ higher than model B, 22.3KWh/m³ higher than model C. This is to say, local urban single-story house is more energy-efficient than traditional Yaodong, in both of summer and winter, and the energy performants of resilient house is the best. In the energy consumption differences in summer is lower than that in winter. This is because the actual roof of the Yaodong is usually thicker than 500mm, and even some of the exterior wall of Yaodong is embedded in the mountain. Therefore, the simulation results are higher than the reality. On the other hand, the insulation layer of residential walls in Yan'an is generally thick, while Yaodong has no insulation layer. The resilient house, which draws on the experience of traditional Yaodong and improved, is superior in all respects to original Yaodong and local urban house of equal area.

Table 4. Calculation results of annual $\lambda_{CED\ and\ HED}$ for three simulation models

	Annual $\lambda_{CED\ and\ HED}$	Annual λ_{CED}	Annual λ_{HED}
model A	43.9KWh/m³	12.2KWh/m³	31.6KWh/m³
model B	33.5KWh/m³	11.4KWh/m³	22.2KWh/m³
model C	18.7KWh/m³	9.4KWh/m³	9.3KWh/m³

The daily λ of three models are shown in the Figure 3. The data of model A is relatively scattered. In the daily $\lambda_{CED\ and\ HED}$ comparison chart, the median, lower quarter and minimum values of model A are similar to model B. In the comparison diagram of daily λ_{CED}, the lowest value is even lower than model B and model C. This may be because the wall of traditional Yaodong is more thermally inert, although the overall thermal insulation effect is not as good as that of an urban residential building with thermal insulation, but it is more resistant to temperature fluctuations. The CED of the three models were calculated separately from July 8 to July 13. The results are shown in Table 5. It can be seen that the CED increases with increasing temperature, and the calculation of its daily λ value is shown in Table 6.

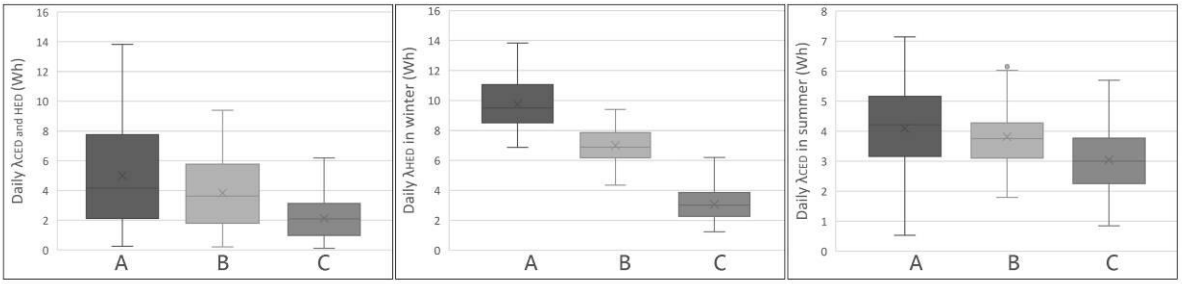


Figure 3. Statistical results of annual daily $\lambda_{CED\ and\ HED}$ comparison for three simulation models.

Table 5. Part simulation results of summer daily CED for three models

Daily CED (Wh)	July 8 (23.5℃)	July 9 (24 ℃)	July 10 (25.5℃)	July 11 (26℃)	July 12 (27℃)	July 13 (28℃)
Model A	40438.3	40432.1	42419.5	43062.0	42302.6	42574.6
Model B	33913.0	37131.4	40935.6	43908.5	46762.6	47843.8
Model C	35575.4	39601.9	43524.5	45205.0	48463.7	46926.5

Table 6. Calculation results of Daily λ_{CED} for three models

Daily λ_{CED} (Wh/m³)	July 8 (23.5℃)	July 9 (24 ℃)	July 10 (25.5℃)	July 11 (26℃)	July 12 (27℃)	July 13 (28℃)
Model A	133.6	133.6	140.2	142.3	139.8	140.7
Model B	102.5	112.3	123.8	132.8	141.4	144.7
Model C	94.1	104.8	115.1	119.6	128.2	124.1

Regression analysis was performed on these days in summer between λ_{CED} values and air temperature, and the results are shown in Figure 4. The R^2 of the daily λ_{CED} growth rate fitting lines of the three models were respectively 0.67, 0.97 and 0.87, indicating that the air temperature and daily λ_{CED} in summer have a high correlation. The growth rate of daily λ_{CED} of model A increases with air temperature to 1.79 KWh/m³ ℃, model B is 9.46 KWh/m³ ℃, and model C is 6.93 KWh/m³ ℃, indicating that model A will has the strongest adaptability under the intensity of UHI, model C is the second, and model A is the worst. It proves that the main material of Yaodong, loess, is a weather-adapted building material, and the concrete used in urban houses is highly sensitive to temperature rise. The renovation scheme only uses loess

roofing, so λ_{CED} grows faster than Yaodong when summer temperatures rise, but is slower than urban dwellings. The HED of the three models were calculated separately from J January 9 to January 14. The results are shown in Table 7. It can be seen that the HED decreases with increasing temperature, and the calculation of its daily λ value is shown in Table 8.

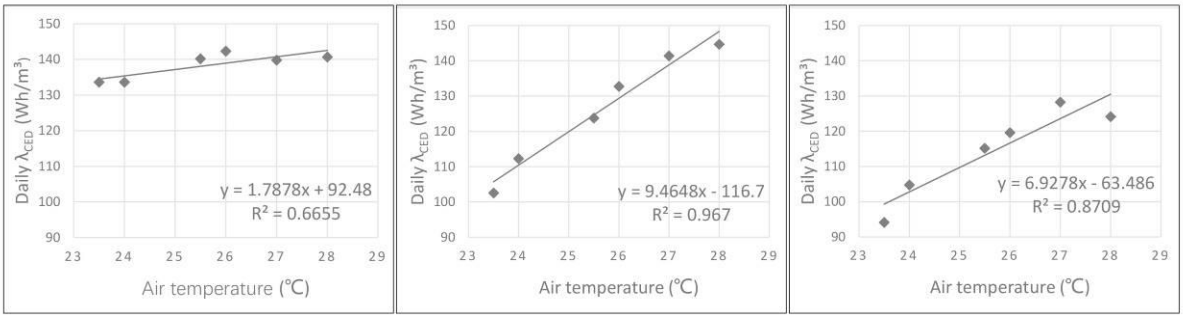


Figure 4. Air temperature-daily λ correlation analysis comparison of 6 select summer days for three simulation models.

Table 7. Part simulation results of winter daily HED for three models

Daily HED (Wh)	Jan. 9 (-3.5℃)	Jan. 10 (-3℃)	Jan. 11 (-2℃)	Jan. 12 (-0.5℃)	Jan. 13 (0.5℃)	Jan. 14 (1.5℃)
Model A	88752.7	88555.2	79895.5	66677.0	55149.8	85406.4
Model B	67995.8	66656.2	61691.0	55597.0	48594.0	62549.5
Model C	41528.9	39559.4	32623.2	21967.5	15269.6	44323.7

Table 8. Calculation results of Daily λ_{HED} for three models

Daily λ_{HED} (Wh/m³)	Jan. 9 (-3.5℃)	Jan. 10 (-3℃)	Jan. 11 (-2℃)	Jan. 12 (-0.5℃)	Jan. 13 (0.5℃)	Jan. 14 (1.5℃)
Model A	293.3	292.6	264.0	220.3	182.2	282.2
Model B	205.6	201.5	186.5	168.1	146.9	189.1
Model C	109.9	104.7	86.3	58.1	40.4	117.3

A regression analysis of the λ_{CED} value and air temperature is shown in Figure 5. It can be seen from the figure that the R^2 of the three regression lines are all lower than 0.43, and the degree of the deviation of the point of January 14 (1.5 ℃) is large. This may be because the change of indoor temperature lags with the outdoor temperature, resulting in the trend of energy consumption and outdoor air temperature are inconsistent.

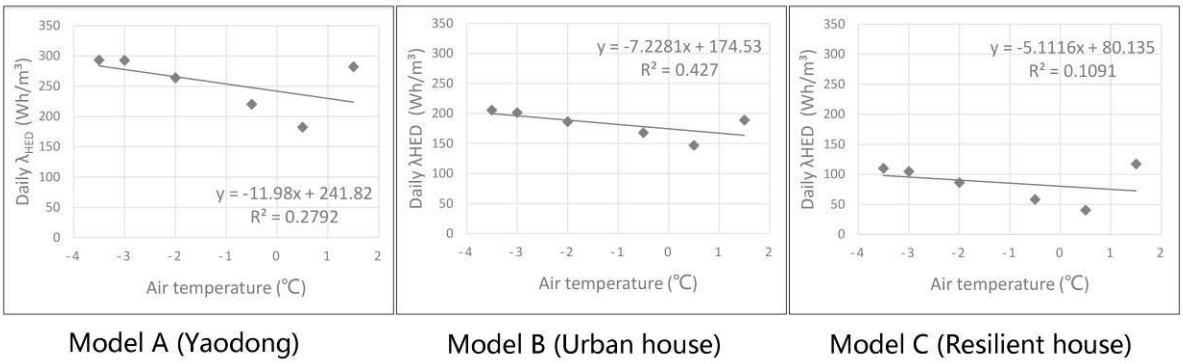


Figure 5. Air temperature-daily λ correlation analysis comparison of 6 select winter days for three simulation models.

In order to accurately observe the daily λ_{HED} with the increasement of temperature, the last point was removed. The results are shown in Figure 6, in which all three models showed high correlation (R^2 greater than 0.98). Among them, model A has a linear slope of -28.51, model B is -14.43, and model C is -17.80. This indicates that in winter, Yaodong's energy consumption decreases rapidly with increasing temperature, followed by the resilient house, and urban residence showed the slowest speed.

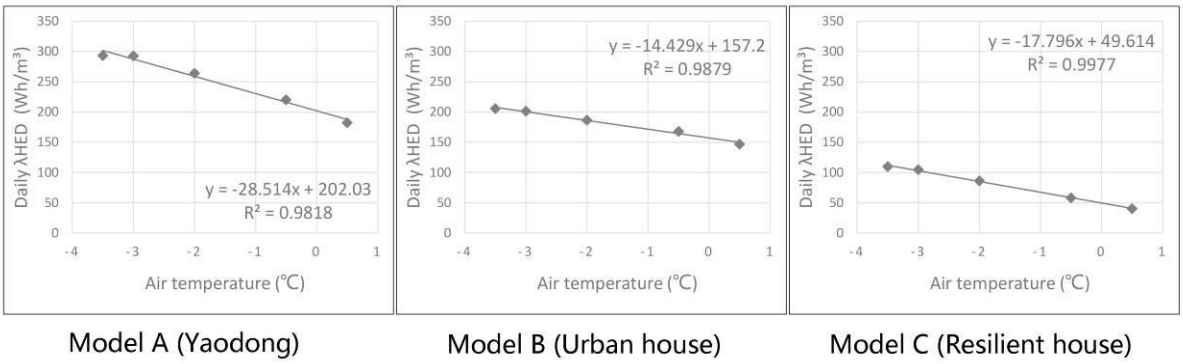


Figure 6. Air temperature-daily λ correlation analysis comparison of 5 select winter days for three simulation models.

Daylighting and humidity analysis

The daylighting simulation results are shown in Figure 7. The indoor natural lighting environment of model C is better than the others, thus reducing lighting energy consumption.

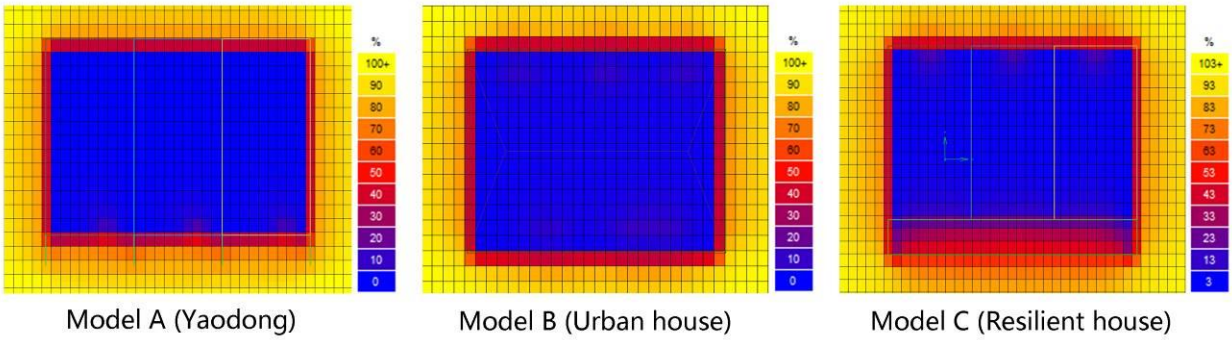


Figure 7. Simulation results comparison of natural daylighting for three models.

The relative humidity simulation of different schemes (Figure 8) shows the average relative humidity of model A is 33.1%, model B is 32.5% and model C is 32.0%. The numbers of comfortable days in humidity (30%-70%) of three models are all 191 days. The image shows that the humidity of the three models in winter is not much different. In the summer, model A has the highest humidity, which is close to the threshold of the comfort zone. Model C is similar to model B and is lower than model A. Therefore, retrofit scheme improves the indoor thermal comfort environment by improving the humidity.

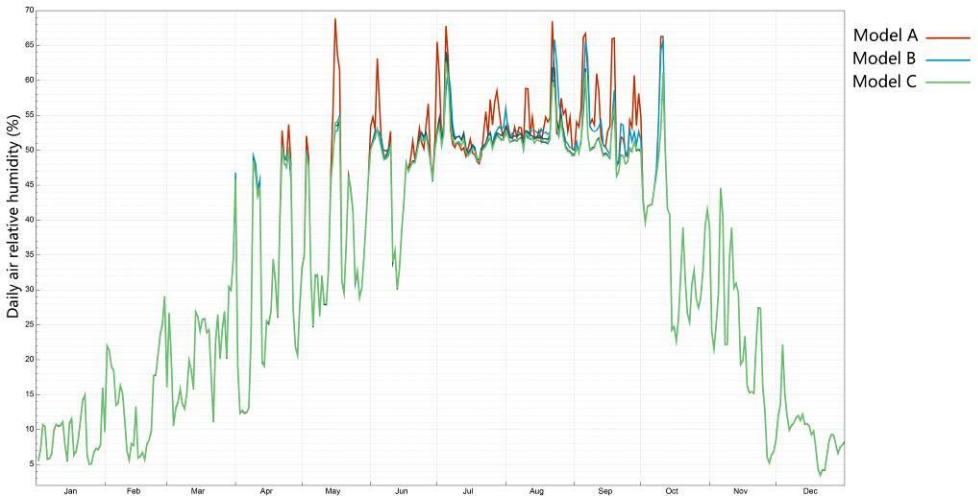


Figure 8. Simulation results comparison of daily air relative humidity for three models.

The usage of clean energy

According to the simulation results using BESTenergy, the annual HED is 3.52MWh and annual CED is 3.56MWh. Combined wiht RETScreen GSHP, the energy use with ground source heat pump for the resilient house is 1.2MWh/yr for space heating, and 0.9MWh/yr for cooling, 2.1 MWh/yr in total, which is only 29.7% of energy demand without GSHP. The total energy use for lighting, equipment and ground source heat pump is 8.91 MWh/yr, and 24 solar panels are required. Nominal PV array power is 7.56KWp, which can deliver 9.24 MWh/yr renewable energy and PV array area is 39.4m².The energy demand for hot water in resilient house is 3.8 MWh/yr. A total of 8 solar thermal collectors are needed, which can deliver energy of 3.8MWh/year and total gross collector area is 19.4m². This is to say, the net building energy consumption of our house is near zero.

In addition, the net GHG emission reduction is 1.84t CO_2/yr on heating system, 0.24t CO_2/yr on cooling system, 6.86t CO_2/yr due to the usage of photovoltaic panels, 1.17t CO_2/yr due to the adoption of solar hot water, and its 10.12t CO_2/yr in total.

Conclusion

This paper takes the transformation of Yaodong, a traditional residential building of China as an example, explored the climate adaptive design scheme for increasingly UHI environment in cities. Three simulation methods are used for evaluation. BESTenergy is used to simulate the three-year CED and HED, comparing the total energy demand and examining the

changes in energy demand during climate changes in winter and summer. The indoor relative humidity was simulated by using BESTenergy, and the indoor natural lighting was compared by using Ecotect simulation. RETScreen software is used to optimize the design of clean energy including geothermal energy and solar energy for reducing building energy consumption, improving indoor thermal comfort, and reduce CO_2 emissions.

The Annual CED and HED showed the energy consumption coefficient λ_{CED} and λ_{HED} of traditional Yaodong are both larger than those of local ordinary urban residence. These two coefficients of local urban residence are both larger than those of transformation based on Yaodong. It shows that the retrofit scheme has greatly reduced the energy consumption level of the original Yaodong, especially for heating. The air temperature-daily λ correlation analysis showed during UHI period, Yaodong has the best adaptability, because the rise speed of CED in summer is slower than the other models, and the reduce speed of HED in winter is faster. It is demonstrated the advantages of the proposed transformation scheme.

The natural lighting and indoor relative humidity of resilient house provides insufficient lighting and excessive humidity in summer. The renewable energy usage bases on the above optimization scheme, the use of ground source heat pump saves energy consumption of 4.97 MWh per year, the use of PV panels saves 8.90 MWh per year, the use of solar thermal collectors can save energy by 3.8 MWh per year, and saving 17.68MWh in total. Meanwhile, the CO_2 emissions reduction is 10.12 t CO_2/yr.

Some of the limits should be studied in the further. Firstly, the building model volume of BESTenergy software is usually larger than the reality, leads to a larger simulation results of energy consumption. Secondly, the setting of indoor structure in the model is simple, and the practicality of the single-storey house in the city is insufficient. Therefore, the resilient design that explores more practical residential types should be carried out in the future.

References

Huang Q, Lu Y. (2015). The effect of urban heat island on climate warming in the Yangtze River Delta urban agglomeration in China. International journal of environmental research and public health, 12(8): 8773-8789.

Lin B. (2018). China Energy Outlook 2018. Peking University Press. Beijing (China).

Ma R, Sun Z Cao X, Liu Z, Lei Y. (2011). The heat island effect of the loess in Yan'an. Journal of the Meteorological Sciences, 31(01):87-92.

Stocker T F, Qin D H, Plattner G K. (2013). Climate change 2013: The physical science basis. Working Group I Contribution to the Fifth Assessment Report of the Intergovernmental Panel on Climate Change. Cambridge University Press. Cambridge (UK).

Xie X, Wu M, Yuan R. (2015). Comparative study of natural daylighting simulation of Ecotect Analysis and Radiance. Low Carbon World, 2015 (1).

The Resilient Design for Small Commercial Building – A Case in City Center of Gifu, Japan

Yitong Kang[1], Dian Zhou[2], Yupeng Wang[2], Sunwei Liu[1]
[1]Master Student, Department of Architecture, Xi'an JiaoTong University
[2]Professor, Department of Architecture, Xi'an JiaoTong University

ABSTRACT

In recent years, the urban heat island (UHI) effects has caused many environmental problems, which is attracting attention from scientists and governments. As one of Japan's major cities, Gifu's UHI is becoming serious. Building energy consumption is greatly effected by UHI. It is important to design resilient buildings to reduce their energy consumption to alleviate UHI effects. In addition, in order to face to the UHI effects in the future, it is also important to reduce the growth rate of building energy consumption when the temperature rises.

This research takes the resilient design of a small commercial building in Gifu City, Japan as an example. By using BESTenergy software, the four design parameters of building volume, window-wall ratio, window shade ratio and envelope material were evaluated. Three evaluation criteria, the annual energy consumption, the annual cooling energy consumption and the daily increase of cooling energy consumption during the UHI phenomenon, evaluate the building design, and the optimal solution of each impact factor is obtained, so that the building design can reduce the building energy consumption and adapt to the extreme weather. This research supports new policies and design strategies for resilient building design.

Keywords: Resilient building design; Building simulation; Commercial Building; UHI; Gifu

1. Introduction

The UHI phenomenon means the temperature in urban areas is higher than that in the suburbs. The UHI effect higher the annual average temperature in the city of 1 °C to 6 °C than that in the suburbs. The main factors contribute to UHI are: hard urban surfaces (asphalt and concrete) with low albedo and high admittance; less of vegetation and permeable surfaces which limit shade and evapotranspiration; deep urban canyons modify overall wind environment; concentration of heat-generating activities released from fuel combustion (including cars), HVAC systems, and other anthropogenic processes.

Gifu is a prefecture in the Chubu region of central Japan. Gifu's climate varies from humid subtropical climate in the south, eventually making the transition to humid continental climate in the north. The Mino region is surrounded by low mountains, the temperature fluctuates through the year, with hot summers, with average air temperature of 27 degrees, which is 3.5℃ higher than the standard averaged summer air temperature in Japan. In addition, the meteorological data from 1985 to 2015 (30 years) shows that the average annual temperature in Gifu City is increasing year by year, with average annual increase of about 0.75 °C.

Building energy consumption refers to the building usage, including hot water, heating, air conditioning, cooking, lighting, household appliances, and office equipment. Release of heat from indoor environments to the local air is an important cause of the UHI effect. The UHI phenomenon

Corresponding Author: Yupeng Wang, [wang-yupeng@mail.xjtu.edu.cn]

has both positive and negative impacts on urban building energy consumption. Under the influence of the UHI phenomenon, the high air temperature in winter reduces the urban heating load. The UHI in summer increases the cooling load. Among these effects, the main impact on residents' living and consumption is the summer UHI. For example, 1/6 of the US's electricity consumption is used for cooling, and China's building energy consumption has accounted for 27.5% of the total energy consumption. Most of these energy sources are finally discharged into the environment in the form of heat, thus exacerbating the UHI, leads to the interaction between UHI phenomenon and building energy consumption. Therefore, reducing building energy consumption contributes to UHI mitigation.

Currently, few researches studied about the relationship between UHI and building energy consumption, especially the adaptability of building to the hot summer temperature. This research focused on annual energy consumption (AEC) and annual cooling energy consumption (CEC) of the building, and proposed the term of daily increment consumption (DIC) to consider the effects from climate change, and comprehensively consider the performance of various design factors in this aspect. Moreover, this paper starts from the design of a small commercial building in the city, evaluates and optimizes the four factors of building volume. The high speed simulation tool of BESTenergy was used for simulation. Thereby reducing the energy consumption of the building and improving the adaptability of the energy consumption of building to climate change, which will be important to the building design in the future.

Commercial building is a typical type of building in the city. Based on BESTenergy software simulation, this research takes the resilient design of a small commercial building in Gifu City, Japan as an example, demonstrated measures for reducing building energy consumption and UHI effects. Meanwhile, when the temperature rises, the DIC is reduced to cope with the increasingly extreme heat.

2. Methodology

2.1 Selected Urban Area



1.1 Gifu location map *1.2 Site location map*

Figure 1. Research area location map.

As shown in Figure 1, the site is located in the downtown area of Gifu, in the central part of Japan (35°25'N 136°45'E). The site is a 23m*24m rectangular area, now a temporary parking lot, surrounded by low-rise residential buildings, with convenient transportation and developed commercial facilities, as shown in Figure 2. This area has high building density, large population density and obvious UHI effect. Therefore, it is representative to choose this region as the resilient

building design under the background of UHI effect. Moreover, the design represents the main types of public buildings in the surrounding area and is instructive for other similar designs.

2.2 BESTenergy Software

BESTenergy is an open-source, free-redistributable building energy simulation software. It's SketchUp-based, runs dynamic building energy simulation by running EnergyPlus 8.9 calculation engine. The sharpness and reliability of a state-of-the-art simulation engine is coupled with SketchUp modeling. This energy tool provides following main advantages: reliable dynamic building energy simulation, that is the only method which ensures a correct evaluation in cooling-dominated buildings and in tropical climates, where dynamic paths heavily affects buildings' thermal behavior and energy performance; the intuitive interface based on Sketchup compiling the building energy model easily, it's the easiness in geometric modeling of the modeling tool with the reliability and accuracy of EnergyPlus.

2.3 Design and Simulation

In order to compare the influence of different building volume, window-wall ratio, window shade ratio and envelope structure material on building energy consumption and its temperature sensitivity, this study used BESTenergy to evaluate different schemes (Figure 2, 3, 4) with different factors (Table 1, 2, 3, 4). The influence from each factor on the building energy consumption of AEC and CEC were compared and discussed.

The impact of different factors on the climate adaptability was studied using Gifu's weather data. The typical summer day (August 1, daily air temperature is 26 °C) and the hottest day (August 16, daily air temperature is 31 °C) were selected for DIC, the influence of each factor on the sensitivity to climate change. The ratio λ (Energy consumption coefficient) of energy consumption to building volume is used as the standard for measuring building Energy efficiency (Equation 1). The λ_{AEC}, λ_{CEC} and λ_{DIC} are used for different schemes.

$$\lambda = \frac{\sum_i^n EC_n}{V} \quad (1)$$

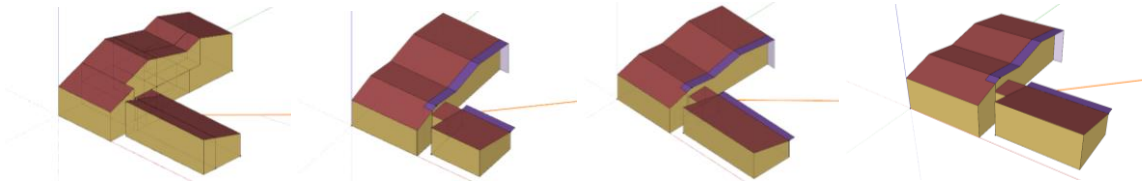
Where i is the calculation start hour, n is the calculation termination time, ECn is the nth hour building energy consumption, and V is the building volume.

Firstly, four building volumes (Figure 2) were compared and analyzed in this paper. The volume of the scheme 1 is 1042.6 m^3, with a large slope of the west side roof. The length and width of the main building is 7.7m*19.5m, and the length and width of the small building is11.5m*5.5m. The roof area of the building is 206.2 m^2, the main roof of the large building has a slope of 30 degrees, and the roof of the small building has a slope of 15 degrees; the volume of the scheme 2 is 1653.35m^3, with a smaller slope of the roof compare to that in scheme 1; the volume of the scheme 3 is 1868.6 m^3, the length of the sub-building is broadened to 15.5m; the volume of the scheme 3 is 1745.6 m^3, the length of the sub-building is 11.5m.

Secondly, based on the optimal volume scheme, window-wall ratio of each scheme is shown in Table 1, and the image of the design is shown in Figure 3.

Thirdly, three schemes with different window shade ratios are designed for evaluation, as shown in Figure 4. Scheme 1 has no special shading measures, the window shade ratio is 0; scheme 2 adds sunshade to the glass of the west wall and the south wall, and the window shade ratio is 56.25%; scheme 3 adds sunshade to the windows of the main building atrium and skylight, and the window shade ratio is 74.4%.

What's more, The effects of four different glasses on building energy consumption and temperature sensitivity are simulated and compared. The details of glass material is shown in Table 2. The effects of four different exterior wall materials on building energy consumption and its temperature sensitivity are simulated and compared. The details of exterior wall material schemes are shown in Table 3. The effects from three roof materials on building energy consumption and its temperature sensitivity are evaluated. The details of roof material schemes are shown in Table 4.

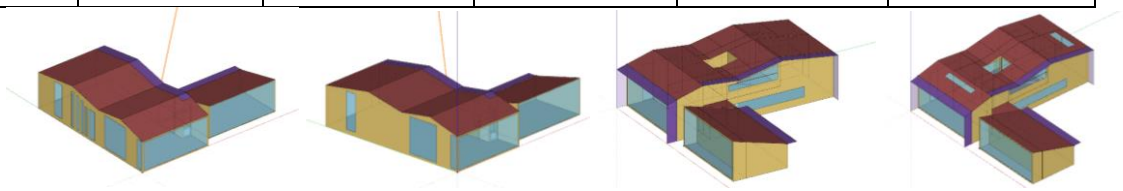


Scheme 1 *Scheme 2* *Scheme 3* *Scheme 4*

Figure 2. BESTenergy models of 4 volume schemes.

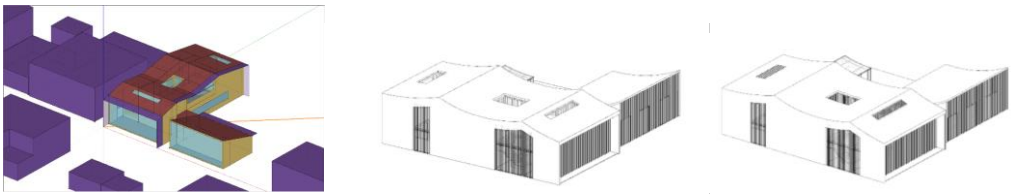
Table 1 Four different window-wall ratio schemes

Scheme number	Window-wall ratio (%)	North window-wall ratio (%)	East window-wall ratio (%)	South window-wall ratio (%)	West window-wall ratio (%)
1	49.04	72.82	64.68	90.29	18.50
2	46.29	72.82	64.68	90.29	12.94
3	38.24	58	30.37	73.33	11.91
4	46.65	65.93	51.74	80.78	17.59



Scheme 1 *Scheme 2* *Scheme 3* *Scheme 4*

Figure 3. BESTenergy models of 4 window-wall ratio schemes.



Scheme 1 *Scheme 2* *Scheme 3*

Figure 4. BESTenergy models of 3 window shade ratio schemes.

Table 2 Details of glass material schemes

Glass material types	U value (W/m^2°C)	Visible Transmittance	Solar Heat Gain Coefficient
4mm+16A+4mm Ordinary insulating glass	3.3	0.82	0.88
6mm+12mm+6mm Ordinary insulating glass	2.8	0.79	0.87
6mm+12mm+6mm Low-e insulating glass	1.8	0.73	0.75
6mm+12mm+6mm Low-e kryptone-filled glass	1.3	0.75	0.65

Table 3 Details of exterior wall material schemes

	Material layers	U-Value (W/m^2°C)
1	Aquapanel, 4cm EPS thermal insulation, 25cm reinforced concrete, external rendering	0.778
2	Aluminum Panel, Waterproof barrier, 10cm EPS thermal insulation, Plywood	0.328
3	Aluminum Panel，5 cm Air Gap, 10cm EPS thermal insulation, Plywood	0.311
4	Aluminum Panel，5 cm Air Gap, 10cm EPS thermal insulation, Plywood	0.311(winter), 0.328 (summer)

Table 4 Details of exterior roof material schemes

	Material layers	U-Value (W/m^2°C)
1	Aluminum Panel, 5cm Air Gap, 8cm EPS thermal insulation, 7.5cm Celenit (Wood wool) and Plaster Board	0.442
2	Aluminum Panel, 5cm Air Gap, 10cm EPS thermal insulation, 7.5cm Celenit (Wood wool) and Plaster Board	0.231
3	Aluminum Panel, 5cm Air Gap, 10cm EPS thermal insulation, 10cm Celenit (Wood wool) and Plaster Board.	0.212

2.4 Energy Load and Indoor Space Usage

The building spaces are divided into two types in the model: commercial and auxiliary areas, and different energy load design parameters are shown in Table 6. The commercial room section includes tea bar, workshop, front hall, reception hall, bathrooms, connecting hall, tea room, exhibition room, mediating room, staff room, preparing room and lounge. The auxiliary room part includes equipment room and buffer zoon.

Table 6. Details of the input parameters for the BESTenergy simulation

Building type	People Occupancy Rate		Activity Level	Electric Equipment Thermal Load	Ventilation Airflow Rate	Zone heating	Zone cooling
Commercial	0.85 people/m²	Seated eating	7.4W/m²	0.8/h	Variable temperature (09:00-20:00, constant 20℃)		Variable temperature (09:00-20:00, constant 26℃)
Auxiliary	0.05 people/m²	seated at rest	3.1W/m²	0.8/h	/		/

3. Results

3.1 Building Volume

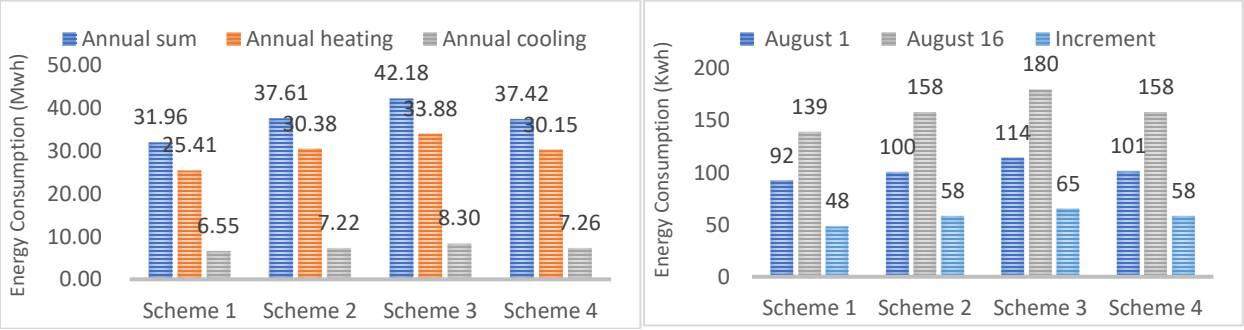


Figure 5. Simulation results of 4 volume schemes, from BESTenergy simulations.

The simulation results of energy consumption are shown in Figure 5. The λ_{AEC} of scheme 1 is the largest, and scheme 4 is the smallest, which is 30.0% lower than that of scheme 1. The λ_{CEC} of scheme 1 is the largest, and scheme 4 is the smallest, which is 33.7% lower than that of scheme 1. The AEC and CEC of scheme 4 is the most energy efficient. This is because scheme 4 is more gradual, and the ratio of the width of the building to the depth of the building is larger, which is more conducive to reducing the building energy consumption per unit volume.

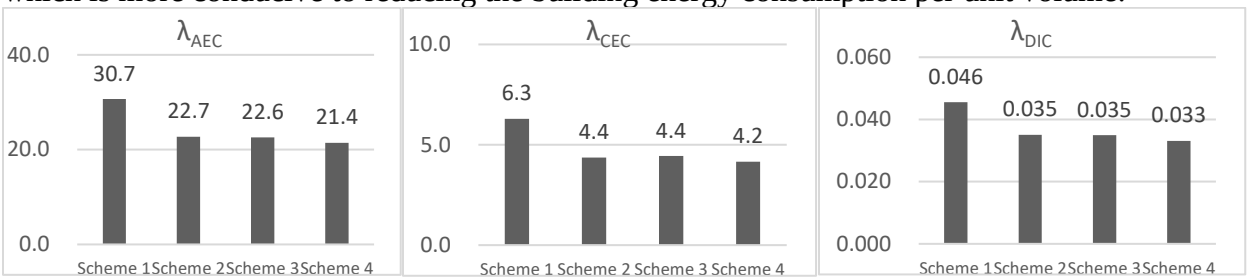


Figure 6. Comparison diagram of λ parameters of 4 volume schemes.

The values of λ_{AEC}, λ_{CEC} and λ_{DIC} of the four schemes are shown in Figure 6. The λ_{DIC} of scheme 1 is the largest, scheme 2 and scheme 3 is equal, and the minimum λ_{DIC} of scheme 4 is 28.3% lower than that of scheme 1. This is to say, when the hot summer temperature increases, the DIC of scheme 4 is the lowest, and the scheme 4 is the optimal scheme.

3.2 Window-wall Ratio

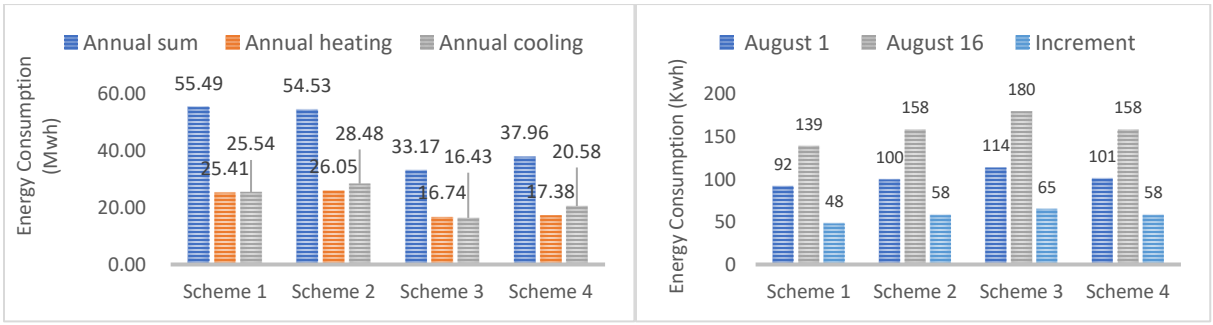


Figure 7. Simulation results of 4 Window-wall ratio schemes, from BESTenergy simulations.

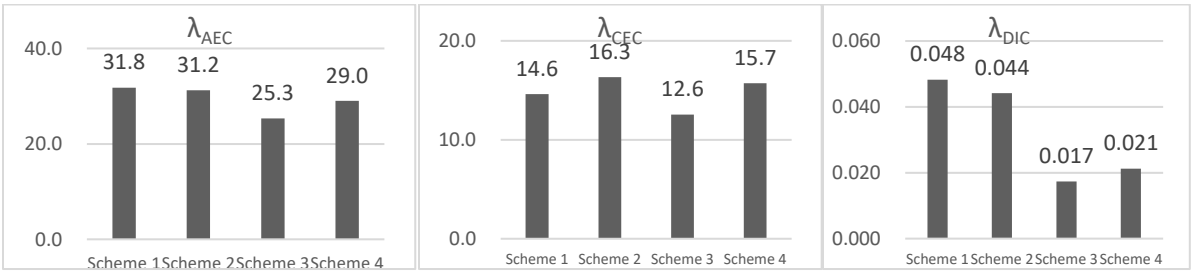


Figure 8. Comparison diagram of λ parameters of 4 window-wall ratio schemes.

The energy consumption of different window-wall ratios are shown in Figure 7. The λ_{AEC} of scheme 1 is the largest, and scheme 3 is the lowest, which is 20.4% lower than that of scheme 1. The λ_{CEC} of scheme 2 is the largest, and scheme 3 is the lowest, which is 22.7% lower than that of scheme 2. The window-wall ratio of scheme 3 is the most energy efficient for AEC and CED.

The values of λ_{AEC}, λ_{CEC} and λ_{DIC} of the four schemes are shown in Figure 8. The λ_{DIC} of the scheme 1 is the largest, the scheme 2 is the second, and the scheme 3 and the scheme 4 are similar, which is 64.6% lower than that of scheme 1. When the temperature increases in summer, the DIC of scheme 3 is the smallest. Therefore, the scheme 3 is the optimal scheme.

3.3 Window Shade Ratio

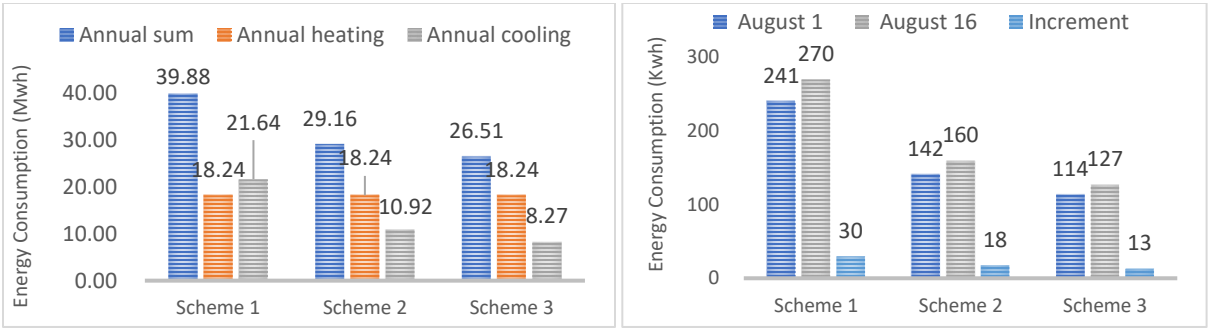


Figure 9. Simulation results of 3 window shade ratio schemes, from BESTenergy simulations.

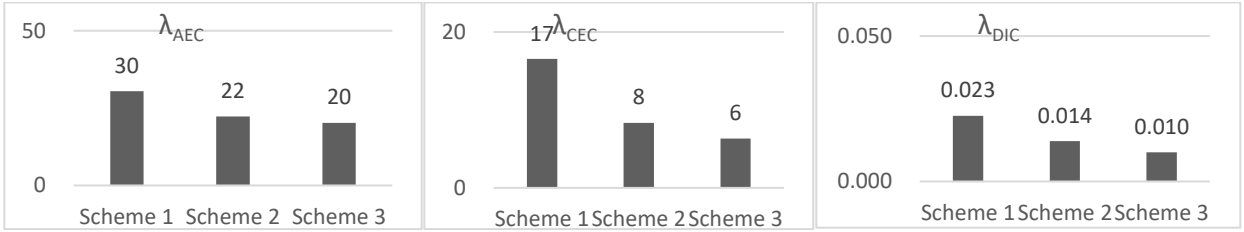


Figure 10. Comparison diagram of λ parameters of 3 window shading ratio schemes.

The energy consumption of different window shade ratios are shown in Figure 9. The λ_{AEC} of scheme 1 is the largest, and the scheme 3 is the lowest, which is 33.3% lower than that of the scheme 1. The λ_{CEC} of scheme 1 is the largest, and scheme 3 is the smallest, which is 64.7% lower than that of scheme 1. The scheme 3 is the most energy efficient for AEC and CED. This is because of the high shade ratio of windows.

The values of λ_{AEC}, λ_{CEC} and λ_{DIC} of the three schemes are calculated as shown in Figure 10. The λ_{DIC} of the scheme 1 is the largest, and scheme 3 is the lowest, which is 56.5% lower than that of scheme 1. The DIC of scheme 3 is the lowest. Therefore, the scheme 3 is the optimal scheme.

3.4 Envelope Materials

3.4.1 Glass material.

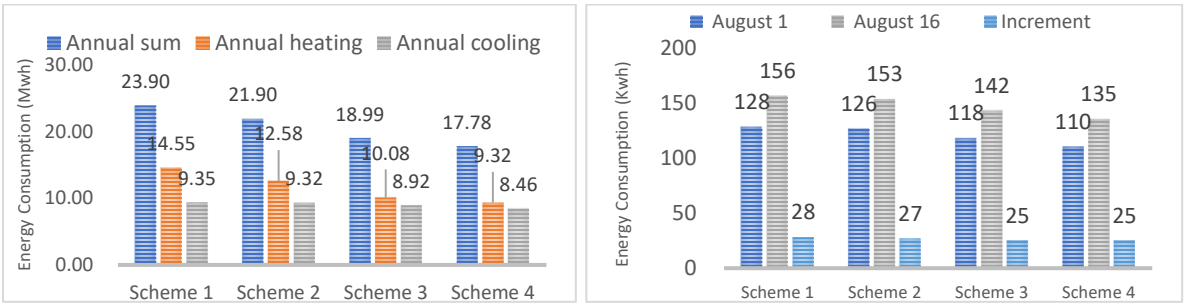


Figure 11. Simulation results of 4 glazed material schemes, from BESTenergy simulations.

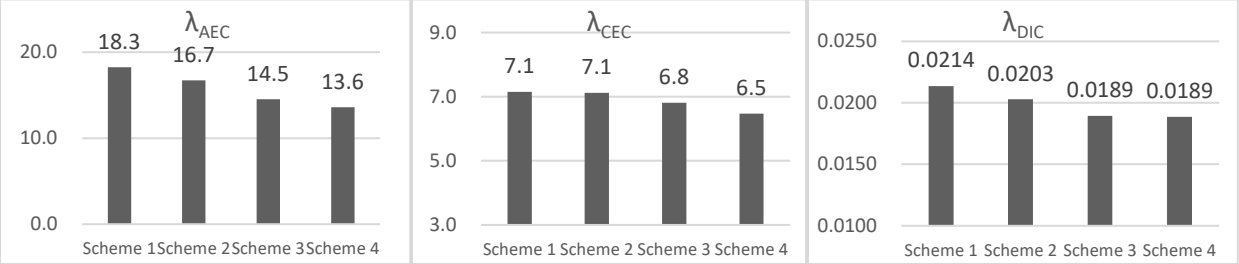


Figure 12. Comparison diagram of λ parameters of 4 glass material schemes.

The energy consumption of different glass materials are shown in Figure 11. The λ_{AEC} of scheme 1 is the largest, and scheme 4 is the smallest, which is 25.7% lower than that of scheme 1. The λ_{CEC} of scheme 1 and scheme 2 are the largest, and scheme 4 is the lowest, which is 8.5% lower than that of scheme 2. This is to say, the scheme 4 is the most energy efficient. This is because of the lowest U-value in scheme 4.

The values of λ_{AEC}, λ_{CEC} and λ_{DIC} of the 4 schemes are shown in Figure 12. The λ_{DIC} of the scheme 1 is the largest, and the scheme 3 is equal to the scheme 4, which is 11.7% lower than that of scheme 1. The DIC of scheme 4 is the smallest. Therefore, the scheme 3 is the optimal scheme.

3.4.2 Exterior wall material.

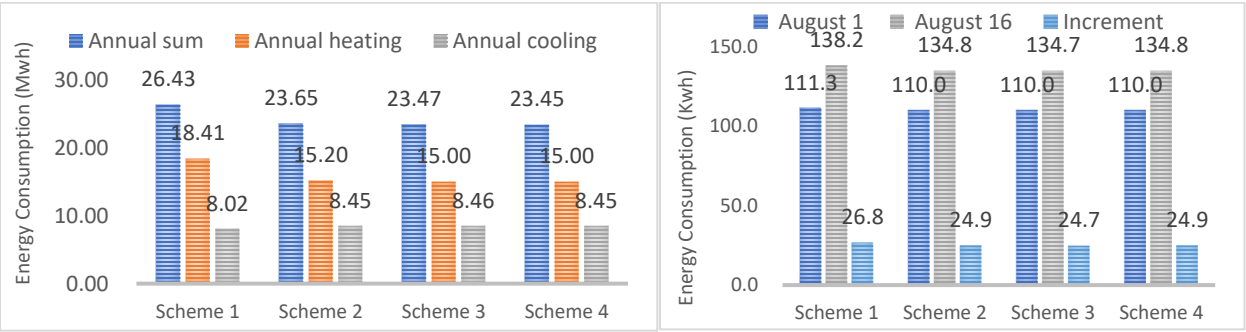


Figure 13. Simulation results of 4 exterior wall material schemes, from BESTenergy simulations.

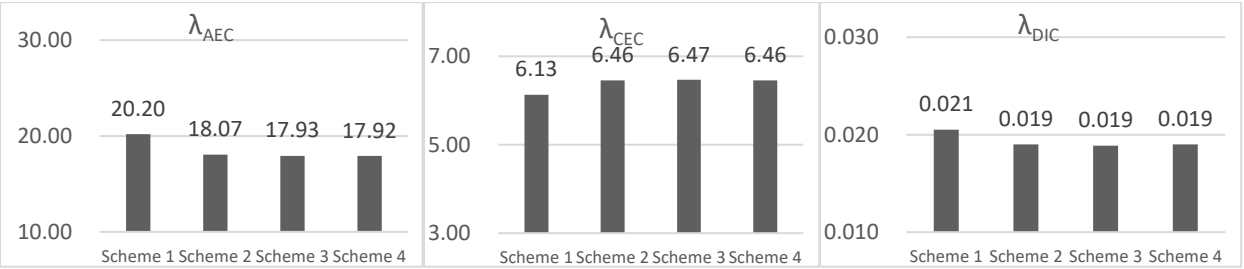


Figure 14. Comparison diagram of λ parameters of 4 Exterior wall schemes.

The energy consumption of different exterior wall materials are shown in Figure 13. The λ_{AEC} of scheme 1 is the largest, and scheme 4 is the smallest, which is 11.3% lower than that of scheme 1. The λ_{CEC} of scheme 2, scheme 3 and scheme 4 are similar. The λ_{CEC} of scheme 1 is the lowest, which is 5.7% lower than other schemes. The scheme 1 has the largest AEC, and the lowest CED. The scheme 4 has the lowest AEC, and high CED. This is because of the high thermal insulation performance of exterior wall in scheme 4.

The values of λ_{AEC}, λ_{CEC} and λ_{DIC} of the 4 schemes are shown in Figure 14. The λ_{DIC} of the scheme 1 is the largest, and that of schemes 2, 3, and 4 are equal, which is 9.5 % lower than that of scheme 1. The DIC of scheme 1 is the largest. The AEC and DIC of the scheme 1 are the highest in the four schemes. Schemes 2, 3, and 4 are similar, and scheme 3 is more adaptable when the hot summer temperature increases, and scheme 3 is the optimal scheme.

3.4.3 Roof material.

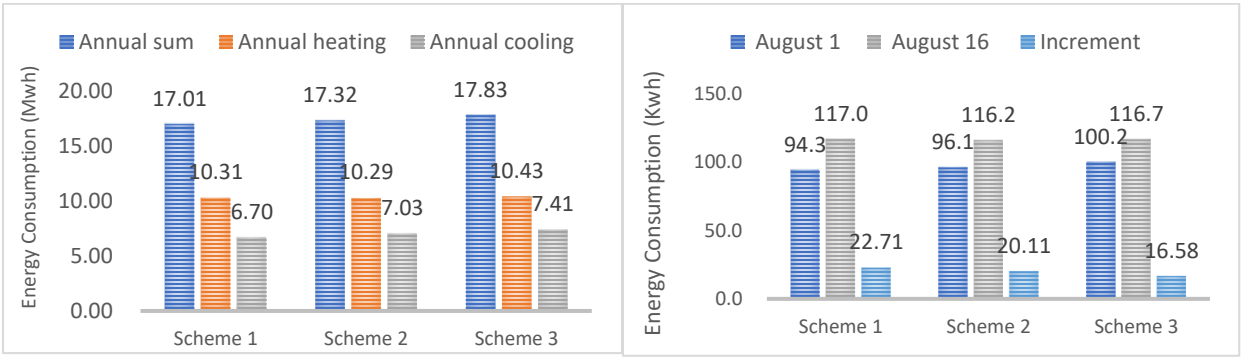


Figure 15. Simulation results of 3 roof material schemes, from BESTenergy simulations.

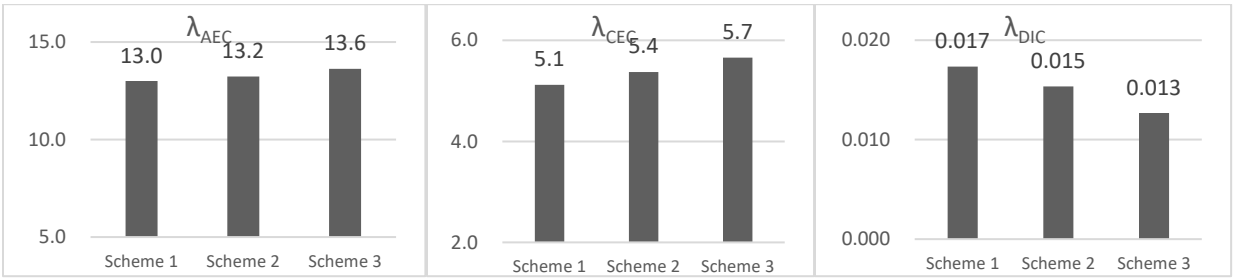


Figure 16. Comparison diagram of λ parameters of 3 Roof schemes.

The energy consumption of different roof materials are shown in Figure 15. The λ_{AEC} of scheme 3 is the largest, and scheme 1 is the smallest, which is 4.4% lower than that of scheme 3. The λ_{CEC} of scheme 2, scheme 3 and scheme 4 are similar. The λ_{CEC} of scheme 1 is the smallest, which is 5.7% lower than other schemes. The unit volume AEC and CEC of scheme 1 are the lowest, and the AEC and CEC of scheme 4 are the largest in four schemes. This is because the site is hot in summer, and the higher U-value of the roof of scheme 3 leads to an increase in CED.

The values of λ_{AEC}, λ_{CEC} and λ_{DIC} of the 3 schemes are shown in Figure 16. The λ_{DIC} of the scheme 1 is the largest, and scheme 3 is the smallest, which is 23.5% lower than that of scheme 3. The DIC of scheme 3 is the least, which is more adaptable to climate change. The AEC and CEC of scheme 1 are the lowest in the four schemes, and scheme 1 is the optimal scheme.

4. Conclusion

This research takes the resilient design of a small commercial building in Gifu City, Japan as an example. Exploring a climate-adaptive resilient building design to reduce building energy usage and adapt to urban climate change. Using BESTenergy simulation, the four different factors of building volume, window-wall ratio, window shade ratio, and envelope material are simulated and compared. Three evaluation criteria of AEC, CEC, and DIC were used to evaluate the building design, and the optimal schemes of each factor, so that the building design can reduce the building

energy consumption and adapt to climate change. This research supports new policies and design strategies for resilient building design.

Firstly, the larger the volume of the building, the smaller its λ_{AEC}, λ_{CEC} and λ_{DIC}. The building volume has a strong correlation with λ_{AEC}, λ_{CEC} and λ_{DIC}. Therefore, the volume of the building can be appropriately increased in the architectural design. Secondly, the smaller the window-wall ratio of a building, the smaller it is for λ_{AEC}, λ_{CEC} and λ_{DIC}. Therefore, the window-to-wall ratio of the building should be minimized in the architectural design. Thirdly, the larger the window shading ratio of a building, the smaller it is for λ_{AEC}, λ_{CEC} and λ_{DIC}. The size of the building volume is affecting to λ_{AEC}, λ_{CEC} and λ_{DIC}. Therefore, the building windows should be shaded during the summer. In the analysis of the glass material, it shows that the larger the U-value of glass materials, the larger it is for λ_{AEC}, λ_{CEC} and λ_{DIC}. Therefore, U-value of glass materials should be reduced as much as possible. Finally, the larger the U-value of exterior wall or roof, the larger the λ_{AEC}, λ_{CEC}, but the smaller the λ_{DIC}. The U-value of exterior wall and roof materials have a strong correlation with λ_{AEC}, λ_{CEC} and λ_{DIC}. Therefore, in order to reduce the energy consumption of the building, the U-value of the exterior wall and roof materials should be reduced. However, for urban climate change adaptation, the U-value of exterior wall and roof materials should be increased.

For energy simulation in this paper, BESTenergy has some shortcomings in accuracy, such as failure to consider the airtightness of the glazed structure and the actual construction of the doors and windows. In addition, modeling approach of BESTenergy increases the envelope materials beyond the actual volume, so the calculated energy consumption might be higher than the reality. What's more, this paper does not consider the influence of combinations of different system on the results. Many of the factors will have different effects when used in combination. Finally, the number of experiments performed by each design factor in this study was not sufficient, and the results could be haphazard. In the future, the number of cases for comparisons should be increased, as well as to develop resilient design for the other types of buildings.

References

Huang Yongbo. Research on the impact of UHI effect on building energy consumption [D]. Tianjin university,2005.

M. Giguere, UHI Mitigation Strategies, The Institut national de santé publique du Québec (INSPQ), 2009.

M. Hart, D. Sailor, Quantifying the influence of land-use and surface characteristics on spatial variability in the UHI, Theor. Appl. Climatol. 95 (3–4) (2009) 397–406.

Rahmat, Ali & Mutolib, Abdul. (2016). Comparison of Air Temperature under Global Climate Change Issue in Gifu city and Ogaki city, Japan. Indonesian Journal of Science and Technology. 1. 37-46. 10.17509/ijost.v1i1.2212.

Tian Zhe. Analysis of UHI effect and its effect on energy consumption of building air-conditioning [D]. Tianjin university,2005.

Yupeng Wang, Umberto Berardi, Hashem Akbari, Comparing the effects of UHI mitigation strategies for Toronto, Canada, Energy and Buildings, Volume 114, 2016, Pages 2-19, ISSN 0378-7788

Zhai Xiaoyan. UHI phenomenon and building energy conservation [J]. Journal of xiangtan normal university (natural science edition),2007(01):106-109.

Yuan ruiyang, Huang fengrong, Tang shuo. Review of urban heat island effect [J]. Research on land and natural resources,2019(01):11-12.

Assessing resilience to summertime overheating in modern low energy flats in UK

Rajat Gupta[1]*, Low Carbon Building Research Group, Oxford Institute for Sustainable Development, Oxford Brookes University, Oxford, UK, rgupta@brookes.ac.uk*
Matt Gregg, Low Carbon Building Research Group, Oxford Institute for Sustainable Development, Oxford Brookes University, Oxford, UK

ABSTRACT

This paper investigates the influence of physical and occupancy factors on the prevalence of summertime overheating in four new-built flats located in the same housing block in Southeast England. The dwellings were built to the same construction standards (building fabric thermal performance) and occupied by residents with similar economic status (high income). In-situ monitoring of indoor environment was carried out in the four flats using Hobo data loggers. Data on occupant behaviour were gathered using questionnaire surveys along with physical monitoring of opening-closing of windows. The paper focusses on the month of July as representative of the summer season.

The indoor temperature measurements in the summer revealed potential issues with overheating in the flats, especially those on the top floor. The maximum temperature in the southern exposed top-floor flats reached over 30°C, higher than the maximum outdoor temperature recorded over the same period. The lower level flats had more stable temperature and less overheating. Data on window opening showed that windows were regularly opened during the summer across the four flats, implying that occurrence of overheating could be due to lack of shading devices, as well as the high levels of insulation that prevented indoors to cool down in the night. Given the prevalence of summertime overheating found across the flats, it is necessary to carefully consider this risk during the design of homes, to avoid the growth of energy intensive and localized heat producing domestic air-conditioning in the future especially in a warming climate.

Introduction

The UK is legally committed to an 80% greenhouse gas emissions (GHG) reduction target for 2050 and to five-year carbon budgets in the interim set by the Committee on Climate Change (HM Government 2011). This has directed the need for new dwellings to be built with higher standards of insulation and greater air-tightness with managed ventilation. In addition, exploratory research projects and standards (Palmer et al. 2016, Gupta et al. 2015) are successfully driving the development of more advanced levels of fabric and system efficiency in housing beyond UK building regulations. Alongside this effort, there is growing evidence of overheating in UK homes (Lomas and Kane 2013, Beizaee, Lomas, and Firth 2013), particularly in newer homes built to satisfy more demanding standards of energy efficiency (ZCH no date). Though the term overheating is used to describe when higher temperatures make building

[1] Corresponding Author: rgupta@brookes.ac.uk, + 44 (0) 1865 484049, School of Architecture, Oxford Brookes University, Headington Campus, Gipsy Lane, Oxford OX3 OBP

occupants uncomfortable or heat stressed, it also has specific temperature thresholds. With consecutive days of hot weather (including warmer than average nights), internal temperatures in some homes, particularly newer efficient homes, can start to exceed external temperatures and may no longer provide protection from the heat. These conditions can cause discomfort and heat-related effects on health (Armstrong et al. 2010, Hajat et al. 2014).

Overheating can occur in homes as a result of several causes acting alone or together. These can include heat gain from high external temperatures (Haggag, Hassan, and Elmasry 2014), higher localised temperatures exacerbated by the urban heat island effect (Österreicher and Sattler 2018), direct solar gain on the exterior surface or penetrating glazing, and internal heat gains. Home characteristics such as dark surface materials, rooms in the roof, skylights, inability to ventilate due to location, predominately dark hard surface surroundings, single aspect flats on upper floors (Vellei et al. 2017), and orientation that allows late solar gain in windows can all contribute to overheating (Gupta and Gregg 2012). For more vulnerable occupants, such as infants, the elderly or sick, the risk of severe heat stress, including potentially fatal heat stroke, is greater. The cause of overheating is complex and not a simple measure of maximum temperatures; therefore, long continuous periods of above-average indoor temperatures in homes are used to evaluate this condition (CIBSE 2013).

Much research has set out to establish the risk of overheating by simulating the current and future risk in older dwellings (Gupta and Gregg 2013) and in newer dwellings (McLeod, Hopfe, and Kwan 2013). A number of studies have also demonstrated present-day monitored overheating or summer 'discomfort' in existing dwellings and newly built dwellings (Sameni et al. 2015, Lomas and Kane 2013, Gupta, Gregg, and Bruce-Konuah 2017, Gupta and Gregg 2017, Roberts, Allinson, and Lomas 2018) in the UK and abroad, in Denmark (Larsen and Jensen 2011), Austria (Österreicher and Sattler 2018), Sweden (Ruud et al. 2005), and Estonia (Maivel, Kurnitski, and Kalamees 2015). Within these studies the propensity to overheat is much greater in newer dwellings, e.g. Passivhaus designed dwellings, and particularly in flats. It is important to note that overheating is defined slightly differently from region to region, however, there is roughly an agreement that surpassing hours at 26-27°C is problematic. To contribute to this body of knowledge, the objective of this study is to investigate the extent of overheating in four flats located in the same building in southeast England. The flats were completed and occupied in 2017 and were built to exceed the UK building regulations in fabric efficiency standards.

Methodology

Case study dwellings

The four case study flats are a part of a recent housing development built in southeast England; completed and occupied in 2017. The complex is composed of a mix of housing typologies – townhouses, cottages, apartments and penthouses - which surround a central courtyard lawn (figure 1). The flats are occupied by residents with similar economic status (high income) and have all been designed with the same performance standards: wall U-value: 0.16 W/m^{2}K; roof U-value: 0.10 W/m^{2}K; floor U-value: 0.16 W/m^{2}K; window U-value: 1.4 W/m^{2}K; air permeability: 4 m^3/h.m^2@50 Pa. External walls are composed of one layer of concrete blocks and one inner layer of insulation (mineral wool) and plaster. The external surface is either plastered or with brick claddings and windows are double glazed. The flats differ in size, orientation and location within the four storey buildings (table 1&2). All the flats are rated B in

their Standard Assessment Procedure (SAP) documents, with primary energy ranging from 75.7 – 85.2 kWh/m^2/year.



Figure 1. View of the development from the courtyard.

Table 1. Case study physical characteristics

No.	Total floor area (TFA) (m^2)	Ratio of ext. surface area to TFA	Ratio of windows to TFA	SAP energy efficiency rating	Air perm. (m^3/h.m^2 @ 50 Pa)
N31	67	1.40	0.18	83 (B)	4.64
N15	72	0.39	0.10	84 (B)	3.03
N33	86	1.48	0.19	83 (B)	3.95
N06	95	1.43	0.15	84 (B)	3.31

Table 2. Case study occupancy details

No.	Beds / floor	Glazed orientation	Occ. no. and age range
N31	2 bed / 4th (top)	Facing adjoining building roof: NW (bedroom 2) – SW (living room & bedroom 1)	1: 46-55
N15	2 bed / 2nd	Facing street NW (all rooms)	2 (often 3): 16-25 and 26-35
N33	3 bed / 4th (top)	Facing street: NE (bedroom 1) - NW (bedroom 2 & 3) - SE (living room)	1: over 65
N06	3 bed / ground	Facing courtyard & sheltered: SE (all rooms)	1: 56-65

The tenant in flat N31 worked from home, using many office/electric appliances (monitors, desktop computer, laptops, amplifiers etc.) and was at home most of the time during both weekdays and weekends. In flats N15 there were two tenants plus one guest staying regularly on weekends. The tenant of flat N33 spent most of the time at home, but mostly in the living room/kitchen in which he would cook an relax occasionally with visitors. The tenant of

N06 lived alone but frequently had guests staying overnight (normally 1-3 days per week). Figure 2 shows the plans with installed environmental logger locations (explained later).



Figure 2. Plans and data logger locations.

Overheating assessment methods

For the overheating assessment, two methodologies were used. These are the *static method* and the *adaptive method*. The static method defines overheating as when in living areas, 1% of occupied hours is >28°C and in bedrooms, 1% of occupied hours >26°C (Humphreys and Nicol 2006). The adaptive method is a dynamic threshold based on changes in external temperature which also includes levels of occupant sensitivity. The adaptive method defines overheating as when two of the following three criteria are failed: 1) hours of exceedance, 2) daily weighted exceedance, and 3) upper limit temperature (Nicol and Spires 2013).

Table 3 lists the occupancy details for the flats. The greatest occupancy potential was used for the analysis in these models; i.e., a single pattern is applied to everyday, for example, though N15 works from home only 1-3 days per week, the days that the occupant works from home are used in the model to capture the worst-case potential.

Table 3. Case study occupancy details

No.	Living room	Bedroom 1	Bedroom 2	Occupancy details
N31	8:00 – 17:00 19:00 – 21:00	Not measured	Not measured	Works at home; away from home 5-10% of year: modelled as away 2 hours per day.
N15	8:00 – 17:00 19:00 – 21:00	22:00 – 7:00	22:00 – 7:00 (freq. guest)	1 works at home 1-3 days per week; away from home 5-10% of year: modelled as away 2 hours per day.
N33	8:00 – 21:00	22:00 – 7:00	Not measured	Most of the time at home; goes to gym on Wednesdays
N06	12:00 – 21:00	22:00 – 7:00	22:00 – 7:00 (freq. guest)	Works at home / out mornings and evenings on weekends

Performance evaluation

In-situ monitoring of indoor environment (air temperature and CO_2 levels at five-minute intervals) was carried out in the four flats using Hobo and Tinytag data loggers. Data loggers were placed in the rooms listed in table 3; figure 2 shows the plans and data logger locations. Data on occupant behaviour were gathered using questionnaire surveys along with physical monitoring of opening-closing of windows. Monitoring and survey data for the summer were gathered from 26 June – 26 July 2017 and BUS surveys where carried out at the end of May 2018. Window opening ratio (WOR) was calculated by multiplying the percentage of open (from 0 – 100%) by the number of seconds the window is open for every hour. This paper focusses on the month of July as representative of the summer season. A limitation of the study is the short period of monitored data as most overheating methods recommended assessing the period from 1 May – 30 September. The original purpose of this study was an annual energy consumption evaluation; however, some learnings can be taken from this regarding overheating in flats.

Results

The indoor temperature measurements in summer revealed overheating concerns in most of the flats, especially in the penthouses. Table 4 shows the overheating results for the flats. The only room to overheat using the adaptive method was the living room of N31. N31 also had the greatest maximum temperature reading (detailed later). Bedrooms generally tend to overheat more than living rooms though the living rooms were open to the kitchen, potentially providing more internal gains. Figure 3 shows the temperature ranges in the living rooms and bedrooms. The magnitude of static overheating can be seen here. The bedrooms show a much larger period (orange) where temperatures remained between the recommended temperature (23°C) and overheating (26°C) (CIBSE 2015).

Table 4. Overheating results *(OH = overheating)*

No.	Room	Window orientation / floor	Static method (occupied hours)	Static method (All hours)	Adaptive method (failed)
N31	Living room	Southwest / 4th floor	**34% - OH**	**21% - OH**	Criterion 2
N15	Living room	Northwest / 2nd floor	0%	0%	-
	Bedroom 1	Northwest / 2nd floor	**16% - OH**	**12% - OH**	-
	Bedroom 2	Northwest / 2nd floor	**23% - OH**	**14% - OH**	-
N33	Living room	Southeast / 4th floor	**11% - OH**	**9% - OH**	-
	Bedroom 1	Northeast / 4th floor	**33% - OH**	**30% - OH**	-
N06	Living room	Southeast / gr. floor	0%	0%	-
	Bedroom 1	Southeast / gr. floor	0%	**5% - OH**	-
	Bedroom 2	Southeast / gr. floor	0%	0.6%	-

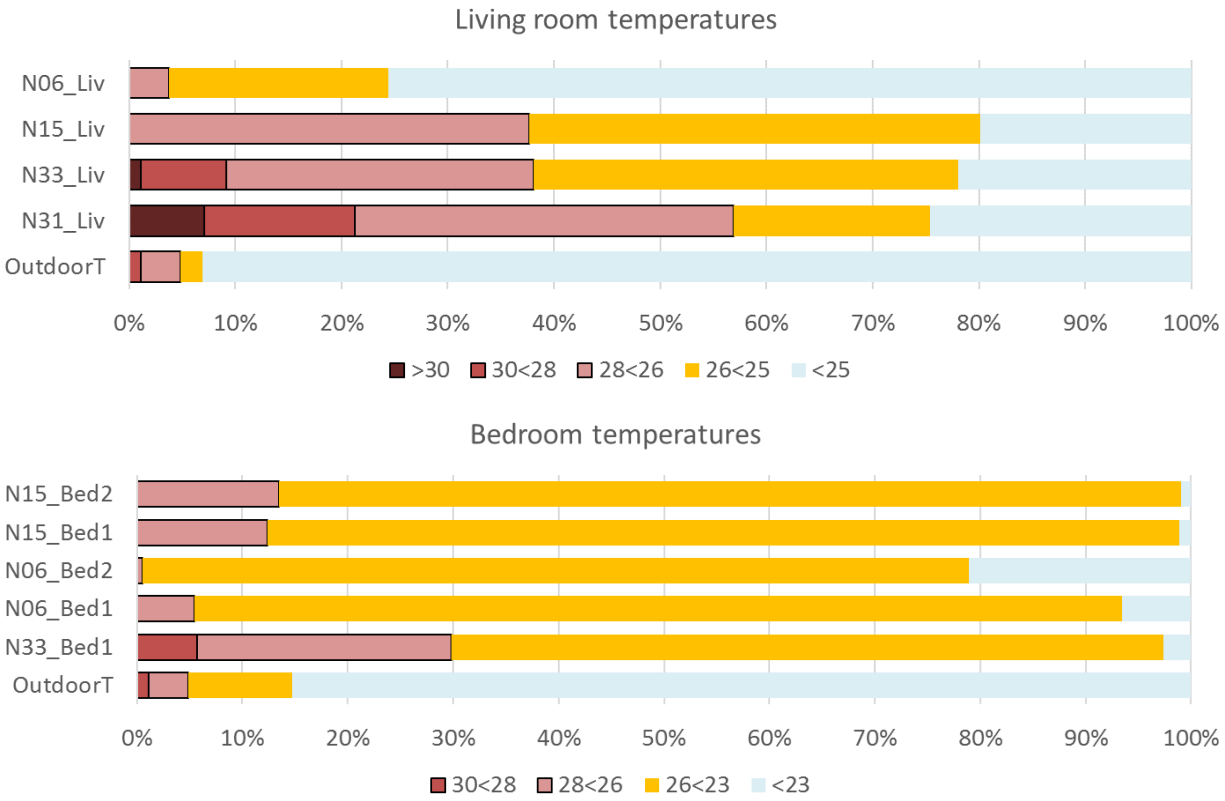


Figure 3. Temperature ranges in living rooms (top) an bedrooms (bottom).

The maximum temperature in the southern exposed top-floor flat, N31, reached up to 32°C, more than the maximum outdoor temperature recorded over the same period (30.3°C), while in N33 (northern exposure), indoor temperature reached up to 30.7°C. The mean indoor temperatures varied from 26.5°C in N33 and N31 to 23.9°C in N06, while the outdoor mean temperature was only 19.9°C. This means that indoor environments were generally warmer than outdoors in summer. As can be seen in figure 4, indoor temperatures were more stable in N15 and N06 and more variable in N31 and N33.

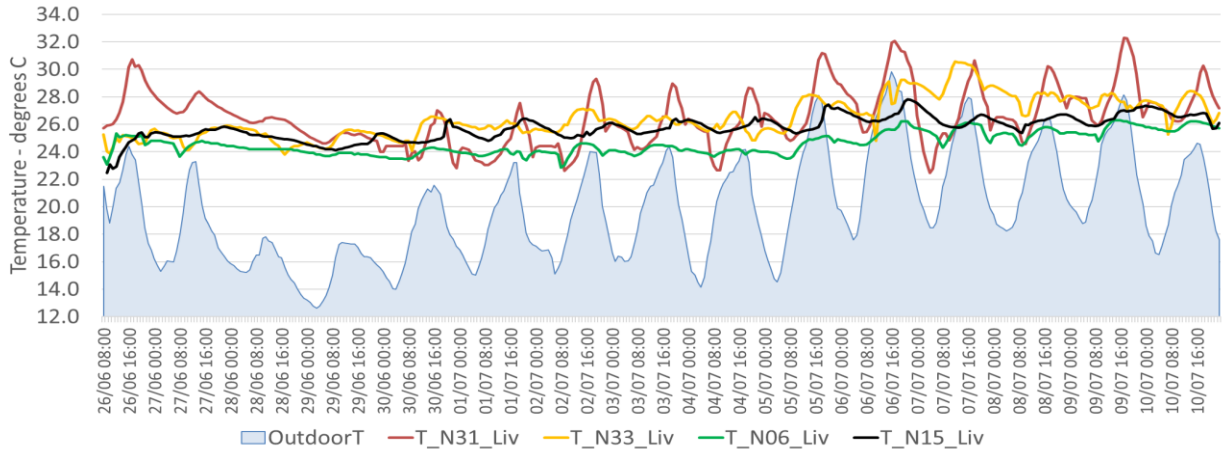


Figure 4. Living room temperatures during period of maximums (26 Jun – 10 Jul 2017).

Indoor air quality

Air quality in summer was good. As expected, CO_2 levels in summer were lower than in winter and spring, due to an average higher ventilation of the rooms in all the flats. The results showed a good air quality in all the flats. The mean CO_2 levels varied from 429 ppm in the living room of N33 to 725 ppm in the bedroom of the same flat. The 2000 ppm threshold was surpassed only once in one bedroom of flat N15.

Occupant survey

Building Use Studies (BUS) questionnaire showed that the occupants found the temperature and air in summer to be overall comfortable and satisfactory. These ratings were however at the higher end of the BUS benchmark for like-dwellings. When asked specifically about the range from too hot to too cold, occupants rated the dwellings as just a little on the hot side of neutral. This was again with in the benchmark range. Additional comments regarding comfort corroborated the findings with occupants of flat N06 showing higher levels of satisfaction with the indoor thermal environment. On the other hand, there were no comments from N31 and N33, and N15 concluded that the worst aspect about the flat is that it 'gets very warm in the summer'.

Discussion

Three characteristics were reviewed for their impact on overheating potential in the flats. These were floor level, glazing orientation, and window opening behavior.

Temperature maximums and overheating are clearly most significant in N33 and N31. These flats are located on the top floor of the building. Though four case studies are not able to conclude statistical significance, the findings are in agreement with previous studies that found that roof-exposed rooms have statistically significantly higher mean daily temperatures than lower-floor rooms and that top-floor flats are at a higher overheating risk than lower-floor flats (Beizaee, Lomas, and Firth 2013, Vellei et al. 2017). Glazing orientation also appears to fit the hypothesis that south facing glazing leads to greater overheating; however, there are too few flats and many variables to consider. As examples, N33 and N31 have south facing glazing in their most overheated rooms; however, they are located on the top floor which may have greater influence. N06, located on the ground floor, demonstrates little to no overheating. N06 has south facing glazing but is facing garden courtyard and is in a corner of the building where the building is shading the glazing for much of the morning and late afternoon. Nonetheless, Vellei et al. (2017) found that south-facing rooms were not found to have statistically significantly different mean temperatures than north-facing rooms in their study.

Another variable to complicate matters is window opening behavior. Window opening appeared to have little to no influence on the internal temperatures of the flats. As examples, N33 had an average window opening ratio (WOR) of 761 and N31 = 0.18. Though the windows were used far more in N33 the correlation (r) between external and internal temperature were the same. The WOR in N15 was much higher at 1,116 but the external and internal temperature r = 0.37. Though data showed that windows were regularly opened during the summer across the four flats, it appears that the high levels of insulation prevented indoors from cooling down at night, due also in part to the lack of cross ventilation. High levels of direct solar radiation could be to blame which would suggest the need to for shading devices especially in the most exposed

top floor flats. The lack of occupant comment of overheating could likely be attributed to the timing of the BUS survey. As the BUS surveys where carried out at the end of May 2018, this was almost a year after the environmental monitoring, long after the experience of the summer.

As can be seen in the image of the courtyard above, the site is surrounded by green space and light-colored surfaces, which though not measured, are expected to have moderated the microclimate and reduced the incident heat on the flats. Though the environmental surroundings of the flats are likely influential, a study of the impact of the UHI in London showed that the effects of built form and other dwelling characteristics appear to be more important determinants of variation in high indoor temperatures than the location of a dwelling within London's UHI (Oikonomou et al. 2012). The results of this study also show that design and occupancy factors are more influential than external temperature.

Conclusion

This study is based on data collected during the summer of 2017 in four flats located in a new low-energy development in southeast England. Analysis of the results showed that in general, overheating is prevalent in most flats, but most pronounced in upper level flats, particularly those with roof exposure. Bedrooms were more prone to overheating than living rooms; however, overheating depended more on the location of the flat in the building. The penthouses also showed much higher variability of indoor temperature compared to flats on lower levels. The mean indoor temperatures in summer varied from 26.5 °C to 23.9 °C, while the outdoor mean temperature was only 19.9 °C. The CO_2 levels were good throughout the summer in all the flats indicating enough ventilation for air quality. Windows were opened much more regularly in the summer than other times in the year.

Overheating occurrence was more prevalent using the static method as opposed to the adaptive method. This would suggest that the adaptive method is providing more leniency in high temperatures through the external temperature variation. Though not evaluated here, one aspect of this apparent leniency may stem from the fact that the adaptive method was designed for use in non-domestic environments.

Design has substantial influence on overheating. Passive design strategies such as integrated shading, ventilation, light-coloured surfaces as well as the use of green and blue spaces can help to avoid the risk of summertime overheating. Lack of such measures may encourage occupants to turn to air-conditioning for cooling as the climate warms.

Acknowledgments

We are grateful to Innovate UK for sponsoring the I-life research project. Thank you to the occupants of the flats for allowing us to study their homes for over a year. We are also grateful to Dr Agnese Salvati and Luka Oreskovic for their work in gathering the data used for this study.

References

Armstrong, B. G., Z. Chalabi, B. Fenn, S. Hajat, S. Kovats, A. Milojevic, and P. Wilkinson. 2010. "Association of mortality with high temperatures in a temperate climate: England and Wales." *Journal of epidemiology and community health* 65 (4):340-345.

Beizaee, A., K. J. Lomas, and S. K. Firth. 2013. "National survey of summertime temperatures and overheating risk in English homes." *Building and Environment* 65 (0):1-17. doi: http://dx.doi.org/10.1016/j.buildenv.2013.03.011.

CIBSE. 2013. *TM52 The limits of thermal comfort: avoiding overheating in European buildings*: CIBSE.

CIBSE. 2015. Environmental design: CIBSE Guide A. CIBSE.

Gupta, Rajat, and Matt Gregg. 2013. "Preventing the overheating of English suburban homes in a warming climate." *Building Research & Information* 41 (3):281-300.

Gupta, Rajat, and Matt Gregg. 2017. "Care provision fit for a warming climate." *Architectural Science Review* 60 (4):275-285.

Gupta, Rajat, Matt Gregg, and Adorkor Bruce-Konuah. 2017. "Assessing the occurrence of summertime overheating in occupied and unoccupied low energy homes." PLEA, Edinburgh, 3-5 July.

Gupta, Rajat, Matt Gregg, Stephen Passmore, and Geoffrey Stevens. 2015. "Intent and outcomes from the Retrofit for the Future programme: key lessons." *Building Research & Information* 43 (4):435-451.

Gupta, Rajat, and Matthew Gregg. 2012. "Using UK climate change projections to adapt existing English homes for a warming climate." *Building and Environment* 55 (September):20-42. doi: http://dx.doi.org/10.1016/j.buildenv.2012.01.014.

Haggag, M., A. Hassan, and S. Elmasry. 2014. "Experimental study on reduced heat gain through green façades in a high heat load climate." *Energy and Buildings* 82:668-674.

Hajat, Shakoor, Sotiris Vardoulakis, Clare Heaviside, and Bernd Eggen. 2014. "Climate change effects on human health: projections of temperature-related mortality for the UK during the 2020s, 2050s and 2080s." *Journal of epidemiology and community health* 68 (7):641-648.

HM Government. 2011. The carbon plan: Delivering our low carbon future. London: Department of Energy and Climate Change.

Humphreys, Michael , and Fergus Nicol. 2006. "Environmental criteria for design." In *Environmental Design: CIBSE guide A*, edited by Derrick Braham, 37. London: The Chartered Institution of Building Services Engineers.

Larsen, Tine Steen, and Rasmus Lund Jensen. 2011. "Comparison of measured and calculated values for the indoor environment in one of the first Danish passive houses." 12th Conference of International Building Performance Simulation Association, Sydney, 14-16 November.

Lomas, K. J., and T. Kane. 2013. "Summertime temperatures and thermal comfort in UK homes." *Building Research & Information* 41 (3):259-280. doi: 10.1080/09613218.2013.757886.

Maivel, Mikk, Jarek Kurnitski, and Targo Kalamees. 2015. "Field survey of overheating problems in Estonian apartment buildings." *Architectural Science Review* 58 (1):1-10.

McLeod, Robert S, Christina J Hopfe, and Alan Kwan. 2013. "An investigation into future performance and overheating risks in Passivhaus dwellings." *Building and Environment* 70 (December):189-209.

Nicol, Fergus, and Brian Spires. 2013. *The limits of thermal comfort: avoiding overheating in European buildings: CIBSE TM52: 2013*. Edited by Bonnie Craig. London: The Chartered Institution of Building Services Engineers.

Oikonomou, E., M. Davies, A. Mavrogianni, P. Biddulph, P. Wilkinson, and M. Kolokotroni. 2012. "Modelling the relative importance of the urban heat island and the thermal quality of dwellings for overheating in London." *Building and Environment* 57:223-238.

Österreicher, Doris, and Stefan Sattler. 2018. "Maintaining Comfortable Summertime Indoor Temperatures by Means of Passive Design Measures to Mitigate the Urban Heat Island Effect—A Sensitivity Analysis for Residential Buildings in the City of Vienna." *Urban Science* 2 (3):66.

Palmer, J, D Godoy-Shimizu, A Tillson, and I Mawditt. 2016. Building Performance Evaluation Programme: Findings from domestic projects Making reality match design. Innovate UK.

Porritt, Stephen Michael, Paul C Cropper, Li Shao, and Chris I Goodier. 2012. "Ranking of interventions to reduce dwelling overheating during heat waves." *Energy and Buildings* 55:16-27.

Roberts, Ben M, David Allinson, and Kevin J Lomas. 2018. "A matched pair of test houses with synthetic occupants to investigate summertime overheating."

Ruud, Svein H, L Lundin, M Sandberg, J Nielsen, A Wahlström, T Törnström, and P Kovacs. 2005. "Houses without a traditional heating system–results from two years of measurement." World Sustainable Building Conference, Tokyo, Tokyo, 27-29 September.

Sameni, Seyed Masoud Tabatabaei, Mark Gaterell, Azadeh Montazami, and Abdullahi Ahmed. 2015. "Overheating investigation in UK social housing flats built to the Passivhaus standard." *Building and Environment* 92 (October):222-235.

Vellei, Marika, Alfonso P Ramallo-Gonzalez, David Coley, Jeehang Lee, Elizabeth Gabe-Thomas, Tom Lovett, and Sukumar Natarajan. 2017. "Overheating in vulnerable and non-vulnerable households." *Building Research & Information* 45 (1-2):102-118.

ZCH, Zero Carbon Hub. no date. Overheating in Homes—An Introduction for Planners, Designers and Property Owners. Zero Carbon Hub.

URBAN ECONOMY

Health and energy benefits of urban overheating mitigation counteracting climate change

Riccardo Paolini[1], UNSW (Australia)
Samira Garshasbi, UNSW (Australia)
Shamila Haddad, UNSW (Australia)
Mattheos Santamouris, UNSW (Australia)

ABSTRACT

In many areas of the world, the population concentrates along the coastal regions, benefitting from the sea breeze, with warmer inland areas. However, increasing population is driving the explosion of urbanization in traditionally low-density areas, enhancing the impacts of climate change. A typical case is that of Australian capital cities. Here we show that local climate mitigation can reduce the impacts of climate change, with the analysis of a new development area in Sydney, 50 km from the coast. With meso-scale climate modelling, we computed that by 2050 the peak summer temperature will increase by 0.8 °C and the daily average summer temperature by 1.6 °C. Mitigation with cool materials, greenery, and irrigation will lower the peak and average daily temperatures respectively by 2.2 °C and 1.5 °C with respect to the unmitigated condition under the future climate. Moreover, mitigation can reduce the annual building energy demand (heating and cooling) by 14% for offices and 30% for residential buildings. The heat-related mortality rate also would be reduced by 27%, and still increasing from the current level of 10 to 12 deaths per 100,000 people. Our study indicates the need for improved mitigation technologies to tackle urban overheating in future climate scenarios.

Introduction

Global warming is not impacting all world areas in the same way (Arnell et al., 2016), with complex phenomena at the regional scale. In particular, population increase and consequent urbanization and land-use change produce synergies with global climate change (Solecki, Leichenko, & O'Brien, 2011), with still unclear dynamics concerning biodiversity, for instance (Clavero, Villero, & Brotons, 2011). Population growth together with global warming will drive an increase in electricity demand (Santamouris, 2016) and anthropogenic heat emissions mostly contributing to an increase in turbulent sensible heat fluxes (Wang et al., 2015). The impacts of the local climate on the energy needs of buildings are well known, as the possibility to mitigate the urban overheating with high albedo materials, greenery and other technologies (Akbari et al., 2016). These, on average, may reduce the summer ambient temperature by approximately 2.5 °C, depending on the context of application (Santamouris et al., 2017). Whether the available mitigation technologies will be sufficient to counteract both urbanization and climate change is to be demonstrated.

Here we discuss the case of the Greater Sydney Area, Australia, where the average demographic projections forecast the population to exceed 8.5 million by 2050, thus with an increase of 3.3 million with respect to the current value (Australian Bureau of Statistics, 2017).

[1] Corresponding Author: r.paolini@unsw.edu.au, +61 (02) 9385 5627.

The urban expansion is taking place towards west and south-west of Sydney, where the population density is of approximately 400/km^2, namely significantly lower than in the coastal Eastern Suburbs (~ 4,200/km^2). Moreover, in Sydney, the circulation types induce advection from inland, dragging warm air from the hot desert areas, while urbanization reduces the penetration of the sea breeze (Santamouris et al., 2017). The result is a more complicated situation than a single urban heat island, as per Oke's definition (Oke, 1982). In the Greater Sydney, there is the development of a cluster of three cities (i.e., the original Sydney on the coast, Parramatta inland, and a third city in the western portion of the Greater Sydney), each generating its heat island interacting with the regional climate dynamics. Here, we assess the present climate in the South Creek catchment in Western Sydney - where 1.2 million people will live - and we compute the ambient temperature reductions that may be achieved with high albedo roofing, tree plantation, greenery and optimized irrigation. Then, we assess the consequences on the energy demand of buildings and heat-related mortality.

Methods

Climate analysis and simulation

The Weather Research and Forecasting model (WRF) - Version 3.9.1 (Skamarock et al., 2008) - was used to simulate current and future climatic conditions, including a single-layer urban canopy model to represent the urban tile. The simulated domain was centered over the Greater Sydney Area, with a grid of 500 m × 500 m for the area of interest (Tombrou, 2019). The NSW Department of Planning and Environment provided the current land use, while the Greater Sydney Commission indicated the projected land uses for 2050. Simulations were performed for the whole summer period of 2050 with emphasis on February. The considered climate change scenario is RCP4.5. The results of the simulations have been compared to existing climatic data measured by several stations in the area managed by the Australian Bureau of Meteorology (Australian Bureau of Meteorology, 2017), with a good agreement (Tombrou, 2019). We used the climate data from the Horsley Park meteorological station (at the edge of the domain) as the reference case to represent the conditions in 2017 (Australian Bureau of Meteorology, 2017).

Building performance simulations

To estimate the impact of the different mitigation strategies on energy, the weather data given by WRF for 2050 have been modified considering the mitigation functions i.e., the function between the average temperature in each mitigated scenario predicted by WRF modelling and the ambient temperature in the reference case in 2050, producing the relative weather file. Then, the heating and cooling energy needs of representative residential, office, and school buildings were calculated for all of the above scenarios, through dynamic simulations performed with EnergyPlus V8.5 (US Department of Energy, 2016). The simulations have been performed for uninsulated buildings with poor energy performance, that are representative of the existing building stock (Table 1). The modelled residential building is a 2.4-star (brick veneer) single-story building with a total floor area of 218 m^2. The office building is a nine-story building with a total floor area of 11,450 m^2. The school building is three-story building with a total floor area of 4500 m^2. We then modelled building improvements, including increased ventilation and solar reflectance of the building envelope, window shading, and natural ventilation (Table 2).

Table 1. Design features applied in the modelled buildings (uninsulated case)

Building Type	Residential, Office and School building
Roof	Brick, Aerated Concrete Slab, Plasterboard U-Value = 0.464 W/(m^2 K). Solar Absorbance = 0.6
External wall	Brick, Plasterboard U-Value= 1.315 W/(m^2 K). Solar Absorbance = 0.6
Windows	3mm Single Clear Glazing U-Value = 5.894 W/(m^2 K) UPVC Window Frame U-value = 3.476 W/(m^2 K)
Internal Floor	Brick, Aerated Concrete Slab, Plasterboard U-value = 0.464 W/(m^2 K)
Ground Floor	Carpet, Reinforced Concrete, Cement Concrete U-value = 1.267 W/(m^2 K)
Cooling Setpoint Temperature (°C)	25 °C
Heating Setpoint Temperature (°C)	21 °C
Internal Gain (W/m^2)	Residential: 3.58 W/m^2 Office: 11 W/m^2 School: 15 W/m^2
Mechanical Ventilation	Night ventilation: 1 ac/h. No daytime ventilation
Infiltration Rate (ac/h)	1
Density (People/m^2)	Residential: 0.02 Office: 0.05 School: 0.2
Shading	No Shading
Natural Ventilation	No Natural Ventilation

Table 2. Design features of the modeled buildings in the energy conservation scenarios

Scenario	Scenario description
1	Reference Scenario
2	External Walls U-Value = 0.287 W/(m^2 K). Flat Roof U-Value = 0.182 W/(m^2 K)
3	Dbl LoE (e2=1) Clr 6mm/13mmArg. U-value = 1.5 W/(m^2 K)
4	Reflective Roof. Solar Absorbance = 0.25
5	Natural Ventilation=15 ac/h from 10 pm to 7 am; 5 ac/h from 7 am to 10 pm (no natural ventilation during cold periods)
6	Shading 1 m Overhang + 1 m Side fins (no shading during cold periods)
7	Combined scenario (5 and 6 not activated for the heating season).

Heat-related mortality

To compute the heat-related mortality, we used a correlation with the ambient temperature, which was validated for Sydney for the period 1988-2003 (Gosling, McGregor, & Páldy, 2007). As defined in Eq. (1), the heat-related daily mortality rate (MR) per 100,000 people is a function of the maximum daily outdoor temperature (Tmax, in °C), an r-squared of 0.917. For Sydney, the time lag between peak temperature and mortality tends to zero.

$$MR = e^{4.898-241.2/Tmax} \quad (1)$$

Simulations scenarios

We considered four combinations of climate and land-use:

- Scenario 1: Present climate and land-use (2018), without local climate mitigation.
- Scenario 2: future climate (2050) and current land-use (2018), without mitigation.
- Scenario 3: future climate and future land use (2050) with increased dwelling density based on future projections, new urban growth areas, increased anthropogenic heat flux, planting of 670,000 non-irrigated trees in the inner domain and 3 million non-irrigated trees in the rest of Sydney. Additional mitigation technologies were not considered.
- Scenario 4: future climate and land use (2050) with mitigation. As before, but with 2 million irrigated trees in the Parkland and 3 million irrigated trees in the rest of Sydney with increased albedo of urban impervious surfaces and with water in the landscape (3.5% of the catchment is water bodies).

Results and discussion

Climate analysis and simulation

The combination of climate change and urbanization (which includes the plantation of 670,000 urban trees in the area) will lead to an increase of the maximum ambient temperature by 0.7 °C (Table 3).

Table 3. Ambient temperature variations in the South Creek catchment in the four scenarios.

Temperature statistic (°C)	S1. 2018 climate & land use	S2. 2018 land use & 2050 climate	S3. 2050 land use & climate + 670 K trees	S4. 2050 land use & climate w/ mitigation
Max. summer daily max.	43.4	44.2	44.1	42.0
Average summer daily max.	30.4	32.0	31.8	30.3
Min. summer daily max.	18.8	24.2	22.8	22.4
99th percentile of summer daily max.	43.2	43.1	43.3	41.4

The most striking increase relates to the minimum summer daily maximum (by ~ 4 °C), which already outlines a scenario of more frequent use of air conditioning, with even the coolest summer days nearing the temperature set-point for cooling. Mitigation can reduce the maximum ambient temperature by 2 °C, but it cannot contain to the present values the minimum daily maximum temperatures, as it mostly relies on the reduction of solar gains.

Building energy performance results

The cooling demand of the representative residential, office, and school buildings increased by 123%, 77% and 65%, respectively, in 2050 compared with that under the current climate (Figure 1). Local climate mitigation (S4) reduces the cooling demand of the representative buildings (Table 4). Notwithstanding the higher cooling demand of buildings in general in 2050 compared to 2017, the climate mitigation strategies offset the future increment of cooling demand in 2050 by 37%. The climate mitigation scenario (S4) was found to reduce the sensible cooling load of the representative buildings by 11-21% compared to the 2050 reference condition (S2).

The total cooling load saving based on the mitigation scenario compared to the non-mitigated scenario in 2050, varied between 6 and 10 kWh/m^2. Because of climate change and higher ambient temperature in 2050, the heating demand of buildings by 2050 decreased by 25% and 28% in scenario 2 and scenario 3a compared to 2017 (scenario 1), respectively.

The building energy conservation measures decrease the total cooling load of buildings by 69-89%; by 38-41 kWh/m^2, 30-32 kWh/m^2, and 32-34 kWh/m^2 for the residential, office and school buildings, respectively, under scenario 2. When the climate mitigation scenario and building adaptation strategies were combined, the total cooling demand of the residential, office and school buildings reduced significantly by 92%, 84%, and 79% in 2050 compared to S2. This result highlights the important effects of the combination of adaptation and mitigation strategies to counterbalance the effects of climate change in future.

The sensible (and total) cooling demand of residential buildings by 2050, (S2), was found to increase up to 123% (93%) compared to 2017 reference (S1). The corresponding increase for S3 was 129% and 100% for the sensible and total cooling demand, respectively. Mitigation techniques (S4) decreased the sensible cooling load of residential buildings by 11.4% - 18%. Compared to scenario 2, the mitigation techniques (S4) increased the heating demand of residential buildings by 11% - 16%.

Under the current climate and land use, the application of building energy conservation techniques was found to decrease the total cooling load of residential, office and school buildings up to 86% (20.5 kWh/m^2), 76% (22.8 kWh/m^2) and 72 % (24.4 kWh/m^2) compared to the cooling load of each reference building with no building measures. Under the current climate (2017) and land use, adaptation techniques decreased the heating load of buildings up to 41.4% (4.6 kWh/m^2) compared to the reference building (without conservation) in 2017.

Under 2050 climate, the combined application of climate mitigation scenario (S4) and building energy conservation strategies in residential buildings reduced the total cooling load by 92.2% (39.3 kWh/m^2) compared to scenario 2 (2050). The application of both climate mitigation (S4) and energy conservation technologies in 2050 reduces the sensible (and total) cooling load of the residential, office and school buildings by 83% (86%), 71% (76%) and 66% (73%), respectively, compared to their actual energy consumption (2017).

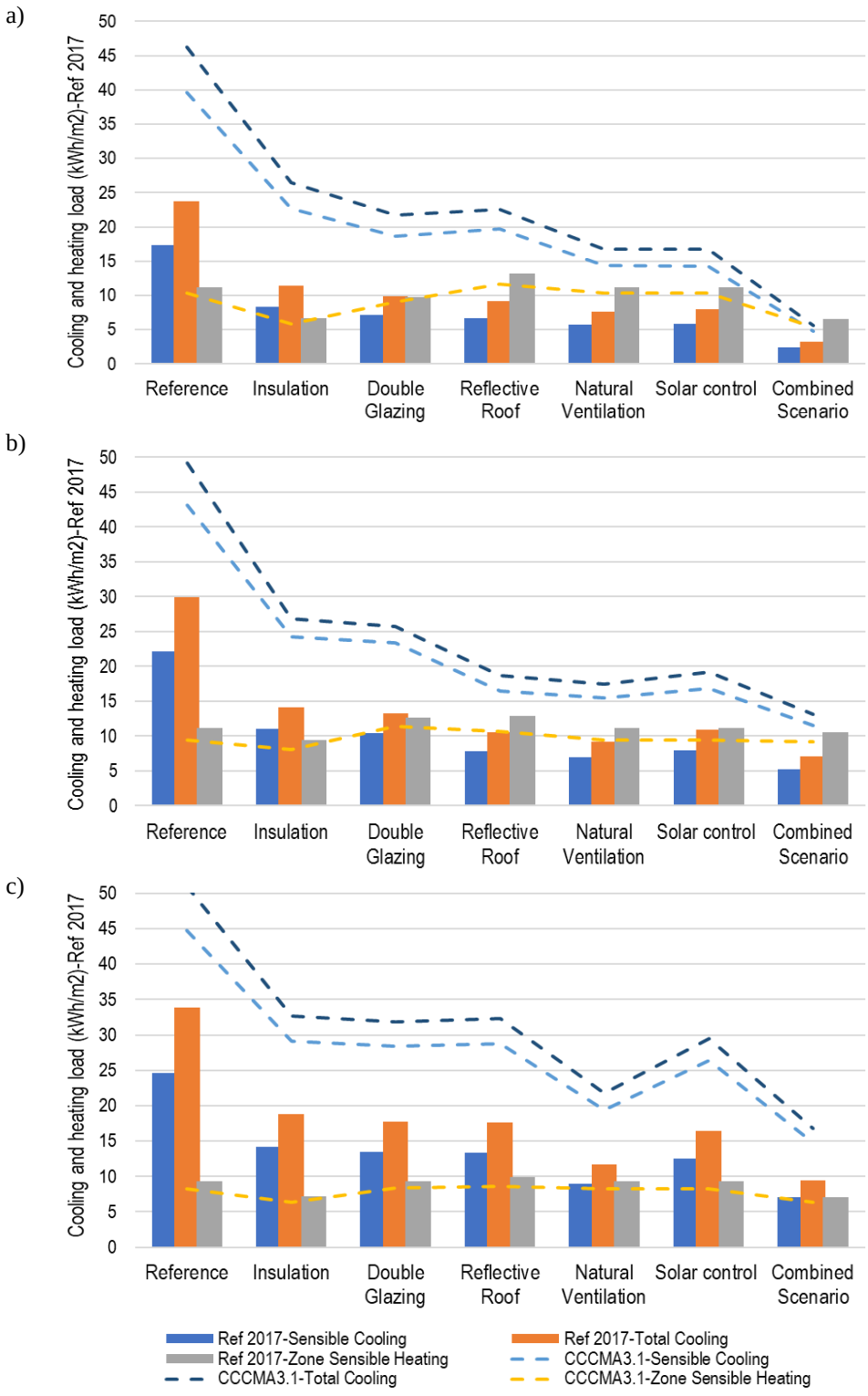


Figure 1. Residential building: sensible and total cooling and zone sensible heating load (kWh/m^2) for the reference case and each of the building scenarios in 2016-2017 and with future climate (CCCMA3.1), without mitigation for the simulated a) residential building, b) office, and c) school.

Table 4. Heating and cooling energy needs of the modeled buildings in all the climate scenarios.

Energy needs density (kWh m^{-2} y^{-1})	Building	S1. 2018 climate & 2018 land use	S2. 2018 land use & 2050 climate	S3. New land use, 2050 climate & 670 K trees in South Creek	S4. New land use, 2050 climate & mitigation
Residential - Cooling	Ref	23.8	43.5	44.8	29.0
	Comb	3.3	4.8	5.0	2.9
Residential - Heating	Ref	11.2	10.1	10.0	9.2
	Comb	6.6	5.2	5.2	4.8
Office - Cooling	Ref	30.0	42.7	42.8	33.4
	Comb	7.1	13.0	10.6	7.4
Office - Heating	Ref	11.2	10.7	10.8	12.2
	Comb	10.6	10.2	10.3	11.5
School - Cooling	Ref	33.8	35.6	35.7	28.1
	Comb	9.4	10.8	10.8	7.1
School - Heating	Ref	9.3	7.5	7.7	8.6
	Comb	7.1	5.8	5.8	6.5

Heat-related mortality

The computed peak daily mortality rate at Horsley Park was almost three times the coastal site of Observatory Hill, and even during a hot year like 2017, the mortality rate dropped after February. In the future, heatwaves (and high temperatures in general) will have health impacts for a more extended period under any scenario (Figure 2).

Scenario 3 with the new land use and the plantation of 670,000 trees lowered the mortality rate compared to scenario 2, but not homogeneously within the domain. Some differences can be attributed to increased thermal inertia with increased urbanization, which contributes to shift and dampen the peaks. The combined mitigation (S4) was found to reduce the peaks of the daily mortality rate in all precincts by approximately 0.1-0.2 deaths per 100,000 people (Table 5).

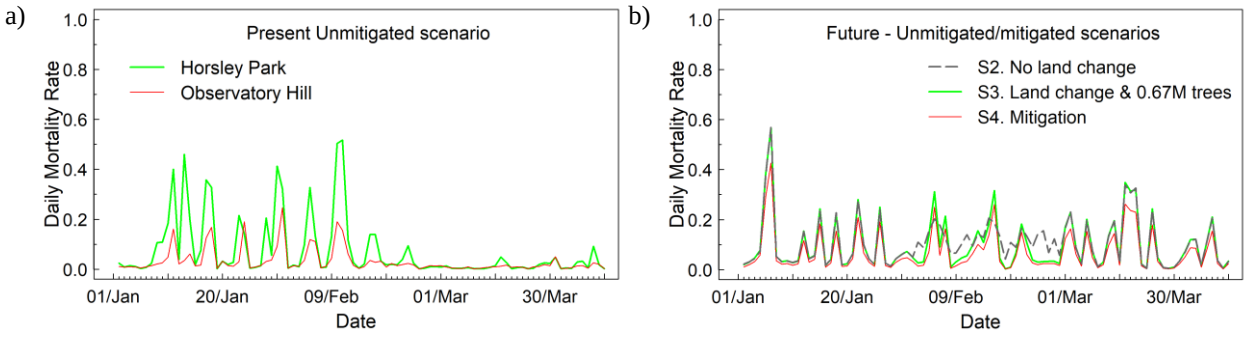


Figure 2. Daily mortality rate. a) present and b) future scenarios.

Table 5. Heat-related mortality per annum per 100,000 people in the four climate scenarios

Quantity	S1. 2018 climate & land use	S2. 2018 land use & 2050 climate	S3. New land use, 2050 climate & 670 K trees in South Creek	S4. 2050 climate & land use w/ mitigation
Computed number of heat-related deaths per annum per 100,000 people	10.67	17.44	16.74	12.09

With mitigation, mortality in the future is contained, but still showed an increase of 20% with respect to current levels, corresponding to approximately 12 deaths / 100,000 people per annum (10 today). The specificity for cities like Sydney the mortality is connected only to the maximum daily temperature with no time lag (Gosling et al., 2007), as temperatures drop during the night when the sea breeze penetrates inland (Santamouris et al., 2017). This is different from what occurs in European cities, where the peak of mortality has a time lag (Santamouris et al., 2017) and is induced by the persistence of heatwave conditions (Michelozzi et al., 2005). A relation with just maximum temperature may seem too simplistic, but other studies highlighted the fuzzy contribution of other environmental parameters as specific humidity (Fouillet et al., 2006), that may increase mortality both at high and low levels, impairing transpiration or causing dehydration (Semenza et al., 1999). Mortality occurs indoors in unconditioned buildings for which indoor and outdoor temperatures are related, and a bulk approach is the only viable when considering city-scale health impacts.

Limitations of the study

Building energy simulations. One of the limitations of this study is the consideration of a limited number of archetypes to represent the building stock. We can expect uncertainty in the absolute value of the cooling energy savings at the urban scale (Caputo, Costa, & Ferrari, 2013). However, our results are relative to the unmitigated case, and we consider the perturbing factors as invariants.

Heat-related mortality. The analysis presented here applied a parametrization based on the epidemiologic data of the population in the Greater Sydney Area for the period 1988-2003. By 2050 the demographics could be very different in terms of age distribution, general health conditions, country of origin and tolerance to extreme heat, socio-economic status. Moreover, the building stock quality and consequent response to heatwaves, market penetration of air conditioning, health infrastructure, medical and emergency procedures can also be different. Therefore, this analysis is only representative of the impact of climate (global and local) on heat-related mortality, while it cannot include the other important scenario variations and co-factors. Moreover, being exponentially related to the peak ambient temperature, the cumulative mortality per annum is probably the metric which is mostly subject to the propagation of uncertainty in climate change scenarios.

Conclusions

Here we considered the present (2018) and future (2050) climate and land-use scenarios in Western Sydney. With meso-scale simulations, we computed the air temperature reductions that may be achieved with increased albedo of roofs and pavements, significant tree planting, and improved irrigation. We computed that the total energy demand for representative buildings - with residential, office school uses - are reduced with climate mitigation, which is, however, to be complemented with improved building energy efficiency.

The cooling demand of residential, office and school buildings by 2050 climate (and 2018 land use), scenario 2, will increase up to 123%, 77% and 65% respectively compared to 2017 climate and 2018 land use. The corresponding increase based on 2050 climate and land use (scenario 3) is 129% for residential buildings, while it remains unchanged in office and school buildings. Mitigation techniques when applied in the whole Sydney area, decrease the sensible cooling load of residential buildings by 11% - 18% compared to scenario 2 (2050 climate and 2018 land use). Local climate mitigation can contain the cumulative mortality to 12 heat-related deaths per annum per 100,000, namely to 20% more than current levels (instead of 70% without mitigation). However, mitigation will be insufficient to minimize heat-related health risks. Adaptation countermeasures, including a radical improvement of the building quality and indoor environmental conditions, will be fundamental to manage the issue. The statistical impact of improvements of the building stock hygrothermal and energy performance of buildings on heat-related mortality cannot be analyzed with the approach used in this study, and further basic research would be required to support a similar development.

Acknowledgements

We thankfully acknowledge Infrastructure New South Wales and Sydney Water for supporting this study and the Greater Sydney Commission for granting access to present and future land-use scenarios. We kindly acknowledge Prof Maria Tombrou Tzella and her group (National Kapodistrian University of Athens) who performed the WRF simulations.

References

Akbari, H., Cartalis, C., Kolokotsa, D., Muscio, A., Pisello, A. L., Rossi, F., … Zinzi, M. (2016). Local climate change and urban heat island mitigation techniques – the state of the art. *Journal of Civil Engineering and Management*, *22*(1), 1–16. https://doi.org/10.3846/13923730.2015.1111934

Arnell, N. W., Brown, S., Gosling, S. N., Gottschalk, P., Hinkel, J., Huntingford, C., … Zelazowski, P. (2016). The impacts of climate change across the globe: A multi-sectoral assessment. *Climatic Change*, *134*(3), 457–474. https://doi.org/10.1007/s10584-014-1281-2

Australian Bureau of Meteorology. (2017). Climate Data. Retrieved August 24, 2017, from http://www.bom.gov.au/climate/data/

Australian Bureau of Statistics. (2017). Estimated Resident Population (ERP), Local Government Areas, New South Wales. Retrieved from http://www.abs.gov.au/AUSSTATS/abs@.nsf/DetailsPage/3218.02015-16?OpenDocument

Caputo, P., Costa, G., & Ferrari, S. (2013). A supporting method for defining energy strategies in the building sector at urban scale. *Energy Policy*, *55*, 261–270. https://doi.org/10.1016/j.enpol.2012.12.006

Clavero, M., Villero, D., & Brotons, L. (2011). Climate Change or Land Use Dynamics: Do We Know What Climate Change Indicators Indicate? *PLoS ONE*, *6*(4), e18581. https://doi.org/10.1371/journal.pone.0018581

Fouillet, A., Rey, G., Laurent, F., Pavillon, G., Bellec, S., Guihenneuc-Jouyaux, C., … H?mon, D. (2006). Excess mortality related to the August 2003 heat wave in France. *International Archives of Occupational and Environmental Health*, *80*(1), 16–24. https://doi.org/10.1007/s00420-006-0089-4

Gosling, S. N., McGregor, G. R., & Páldy, A. (2007). Climate change and heat-related mortality in six cities part 1: model construction and validation. *International Journal of Biometeorology*, *51*(6), 525–540. https://doi.org/10.1007/s00484-007-0092-9

Michelozzi, P., De Donato, F., Bisanti, L., Russo, A., Cadum, E., De Maria, M., … team, E. C. for D. P. and C. (ECDC)-H. C. U.-E. editorial. (2005). The impact of the summer 2003 heat waves on mortality in four Italian cities. *Euro Surveillance: Bulletin Europeen Sur Les Maladies Transmissibles= European Communicable Disease Bulletin*, *10*(7), 161–165. Retrieved from http://www.eurosurveillance.org/images/dynamic/EQ/v05n03/v05n03.pdf

Oke, T. R. (1982). The energetic basis of the urban heat island. *Quarterly Journal of the Royal Meteorological Society*, *108*, 1–24. https://doi.org/10.1002/qj.49710845502

Santamouris, M., Ding, L., Fiorito, F., Oldfield, P., Osmond, P., Paolini, R., … Synnefa, A. (2017). Passive and active cooling for the outdoor built environment – Analysis and assessment of the cooling potential of mitigation technologies using performance data from 220 large scale projects. *Solar Energy*, *154*, 14–33. https://doi.org/10.1016/j.solener.2016.12.006

Santamouris, Mat, Haddad, S., Fiorito, F., Osmond, P., Ding, L., Prasad, D., … Wang, R. (2017). Urban Heat Island and Overheating Characteristics in Sydney, Australia. An Analysis of Multiyear Measurements. *Sustainability 2017, Vol. 9, Page 712*, *9*(5), 712. https://doi.org/10.3390/SU9050712

Santamouris, Mattheos. (2016). Cooling the buildings – past, present and future. *Energy and Buildings*, *128*, 617–638. https://doi.org/10.1016/j.enbuild.2016.07.034

Semenza, J. C., McCullough, J. E., Flanders, W. D., McGeehin, M. A., & Lumpkin, J. R. (1999). Excess hospital admissions during the July 1995 heat wave in Chicago. *American Journal of Preventive Medicine*, *16*(4), 269–277. https://doi.org/10.1016/S0749-3797(99)00025-2

Skamarock, W. C., Wang, W., Klemp, J. B., Dudhia, J., Gill, D. O., Barker, D. M., … Powers, J. G. (2008). *A Description of the Advanced Research WRF Version 3*. *NCAR Tech Note*. https://doi.org/10.5065/D68S4MVH

Solecki, W., Leichenko, R., & O'Brien, K. (2011). Climate change adaptation strategies and disaster risk reduction in cities: connections, contentions, and synergies. *Current Opinion in Environmental Sustainability*, *3*(3), 135–141. https://doi.org/10.1016/J.COSUST.2011.03.001

Tombrou, M. (2019). *Urban Cooling analysis of the South Creek sector. Simulation of the Current and Future Climatic Scenarios*. Sydney, Australia.

US Department of Energy. (2016). EnergyPlus Engineering Reference: The Reference to EnergyPlus Calculations. *US Department of Energy*. https://doi.org/citeulike-article-id:10579266

Wang, X., Sun, X., Tang, J., & Yang, X. (2015). Urbanization-induced regional warming in Yangtze River Delta: potential role of anthropogenic heat release. *International Journal of Climatology*, *35*(15), 4417–4430. https://doi.org/10.1002/joc.4296

Use Urban Green as a Mitigation Strategy to Combat Urban Heat Island Effect: A Case of Puri-Cuttack Road, Bhubaneswar, Odisha

Sukanya Dasgupta[1], [1]B.Arch., MA (Urban Design), Asst. Professor, KIIT DU (India)
Nilanjana Roy[2], B.Arch., Design Head, A&N Architects & Designers, (India)
Dr.Dudam Bharath Kumar[3]. , PhD (Atmospheric Science), Asst. Professor, KIIT DU (India)

ABSTRACT

Environmental issues destabilize sustainable development of cities. In urban setting today urban greenery, vegetation and plants fall prey to the perils of increased levels of pollution. Roads and pavements constitute a major portion of the urban areas and are one of the highest contributors to the development of heat island effect in its tussle against the menace of imprudent urbanization; the go-green movement is a combatant that requires further reinforcement with regards to roads and pavements. Besides being a resource for the city, the urban green is a key player in countering the heat island effect.

The Puri Cuttack road in Bhubaneswar spans between two important nodes: The Rasulgarh Square and Kalpana Square. This stretch of 5.1 kms is abutted by a palette of commercial, industrial, healthcare, hospitality and residential settlements. The road also gives way to a secondary entrance to the Bhubaneswar Railway Station. The heat generated from structures, road materials and related anthropogenic activities has modified the neighborhood's natural state of vegetation and greenery.

The primary aim of this paper is to arrive at mitigation strategies for combating UHI at the Urban Design level. The paper uses the strategies of how one of the coolest cities in the world (Stuttgart, Germany) has been able to mitigate the effects of industrialization and improved the air quality issues in spite of its geographical set up. A set of recommendations to develop the urban environment of the Puri Cuttack road is prescribed based on the concepts comprehended from Stuttgart.

Introduction

History is testimony to the fact that gentrification and urbanization have had negative impacts on the environment owing to the changes it brings about in the physical and chemical properties of the existing atmosphere. A cumulative result of these impacts is called urban heat island (UHI). Due to the contribution to the green-house effect, primarily felt as temperature rise in manmade areas; UHI's have been indirectly a part of the global warming process.

The Research Question

Rapid urbanization has increased the whole range of urban infrastructure, services, housing and land. The increase in the traffic levels is the most unsustainable repercussion of this

development. There is hence an urgent need to respond to mitigate the indicators of the increased UHI. Figures3 and 4 refers to the traffic volumes in the 2 nodes of the paper's case. This paper makes an attempt to answer the following questions:

- What are the notable consequences of UHI on roads which are a highway but cut across a portion of the city?
- How best can the design principles deduced from Stuttgart be implemented to diminish the UHI on stretches like Puri Cuttack Road?

Research Objectives

Optimizing the UHI effect on urban stretches using Urban Design and Planning measures is the main aim of this paper as discussed earlier. A series of objectives act as a guide to achieve the primary aim.

1. Arrive at mitigation measures that can reduce the UHI effect on the 5.1 km stretch of Puri Cuttack Road.
2. Increase the resilience of the stretch against global warming by using green corridors at the urban design level.
3. Apply green infrastructure principles to improve the air quality of the vicinity.
4. Formulate generic measures that can be applied to a particular stretch that can improve the micro climate with focus on the heat mitigation strategies.

Methodology Adopted

A three-step approach is adapted for this paper. In the first step, which is analytical, a study for the city of Stuttgart is carried out to understand the measures that have been taken in order to mitigate the UHI. Based on the inferences from the analytical study of Stuttgart, the results are formulated into a framework and then applied to the context of Puri –Cuttack road in the second step. The last step is to suggest recommendations for developing the urban environment with special emphasis on roads.

UHI Mitigation using Stuttgart as a Precedence Concept

What Is UHI ?

This is a phenomenon in which predominance of dark, impermeable surfaces and concentrated human activity cause urban surface, air, and atmospheric temperatures to be several degrees hotter than those in the suburban or rural surroundings (Akbari 2005). UHI has major and varied effects on public health, air quality, energy consumption, climate adaptation, quality of life, storm water management, and environmental justice.

Primary Aim of Stuttgart in Mitigating UHI

The concepts applied by Stuttgart are one of the sustainable urban solutions for the city of tomorrow that depends on the application of the principles of urban heat management. It is the

key factor to diminishing the urban heat release, creating solutions of future climate change by reducing the volume of global emissions and creating smart growth and cool community scenarios' (Rehan,2016).

Applications of the Concepts in Urban Design and Planning

Europe and USA have been actively developing mitigation strategies and risk prevention measures concerning UHI phenomenon since many years. "UHI Project is developed in 8 of the most relevant metropolitan areas and Mega Urban Regions of the Central Europe cooperation program; one of them is Stuttgart city. UHI Project aims at developing mitigation and risk prevention and management strategies concerning the Urban Heat Island (UHI) phenomenon. This activity is supported by the Central European Programme and the European Regional Development Fund". The time span of this project was from 1st may 2011 to 30th April, 2014.(*Available Online at* https://www.met.hu/en/omsz/palyazatok_projektek/uhi/)

Amongst the 8 cities, Stuttgart was chosen as a case study for the paper since in spite of 60% of the city being covered by green, the industrial belt of the city is a major contributor to the UHI generated. Also, since the city lies in the valley basin, the heat generated remains trapped within the city itself. Similar to Bhubaneswar, Stuttgart also has numerous parks. The governing bodies have been instrumental in being able to mitigate the effects of UHI of this industrial town by applying effective climate planning strategies in the city's Urban Design and Planning interventions. Some of the interventions are described below:

Protection of Green Spaces

In order to achieve resilience against global warming, Stuttgart with the help of detailed local climatic maps has stopped construction activities in the recent years on land parcels which are green. These land parcels have been identified as green corridors and any construction in these areas would hinder wind movement and add to the UHI. As a result, at night, clean air sweeps down from the surrounding hills, runs through a series of 'ventilation-corridors' which have been kept open as wide, tree-flanked arteries within the city's street infrastructure.

Provision of Green Infrastructure

Cities have less vegetation than their surrounding rural areas. The UHI effect is exacerbated by this lack of vegetation because of reduced natural cooling potential from shade and plant evapotranspiration (Akbari 2002). During evapotranspiration, plants take in ambient carbon dioxide and other inputs and release oxygen and water vapor. The water vapour cools the leaves and when the wind blows, the surrounding area cools. Hence the provision of green infrastructure is a mandate to mitigate and combat UHI effects. For Stuttgart, "A new method for the strategic planning of green investments was directed towards the improvement of essential linkages between green spaces and places of employment and living. The essential linkages for commuters within Stuttgart Region are the 'development axes' mainly along the river valleys like the Neckar, the Rems and the Fils." Also, the city has 65,000 trees in parks and 35,000 along streets. Since the 70's, the city has integrated green areas into a large green 'U,' which now makes it possible to go through park environments all the way from the central royal gardens to the forests at the city's edge.

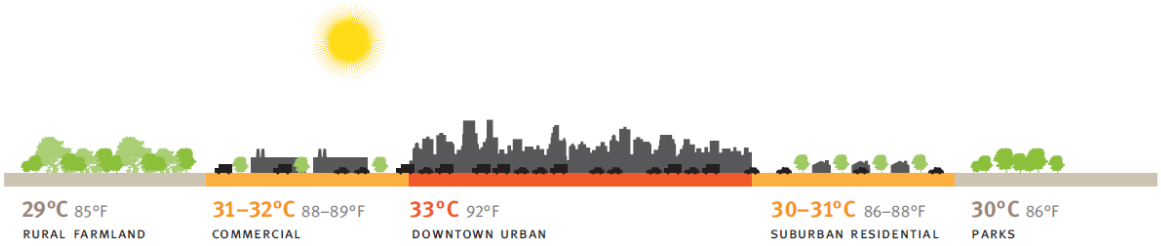


Figure 1: Indicating the effect of UHI in various neighborhoods highest being indicated by orange in Downtown Urban. *Source:UHI Mitigation Strategies, The institute national de santé publique,2009*

Materials

At least two of the three main causes of the urban heat island effect—dark surfaces and lack of vegetation- can be mitigated through policies and programs related to buildings and city planning. Installing reflective and lighter-coloured surfaces on city roadways, walkways and roofs is a primary UHI mitigation strategy. Surfaces store solar energy as latent heat and release it through contact (conduction) or slowly into the air (convection). The darker a surface, the more potential it has to store heat. A light-colored or reflective surface has a very small potential to store heat because of its high albedo, or reflective power. Surfaces that reflect solar energy stay cooler themselves, release less heat into the surrounding air, and allow for night-time cooling in a city. The EPA (2013a) reports that conventional asphalt pavements can reach summertime temperatures of 120-150°F. In contrast, a "cool" pavement can be 50-70°F cooler. In Stuttgart, not only at the surface, but also in the third dimension- facades, the heat is absorbed. That's where most of the facades in Stuttgart benefit from light colours.

Compact Urban Green

Stuttgart's land-use plan is urban-compact-green, of which a good example is the project of Stuttgart 21: ''The Stuttgart 21 project was a sustainable vision in urban design and planning due to its objectives of making the city more sustainable and cooler through maintaining the continuity of Rosenstein Park by transforming the present rail tracks into green urban spaces It is also possible to link the green areas of the park through passages of so-called green connections'' (Rehan 2016). Also, most of streets in Stuttgart are scarcely planted; sometimes trees have been planted just on one side of the street, sometimes not at all, or with a lot of space in between. Thus, urban compact green is a key factor to diminishing the urban heat release.

Water

Water has been a successful medium in reducing the temperature and water applications generally, are more effective when water is moving or dispersed as done by a fountain. The temperature reduction happens by evaporation which causes cooling. In case of Stuttgart, the use of fountains in the urban area and numerous lakes are visible along the Rosenstein Park (green U park), which is located in central Stuttgart. The two massive fountains that grace the park in front of the New Palace in central Stuttgart are quite beautiful (Wells et all 2017).

Framework for Urban Heat Management

As discussed earlier, the second step is to formulate framework based upon the inferences drawn from the interventions at Stuttgart. The strategies and interventions summarized from the previous section are vegetation, water, green infrastructure and the materials.

Case of Puri Cuttack Road

Benefits/Gains	Interventions/ Strategies	Actions	Scale
Improve the visual image of the environment.	Develop the Urban Green	Green Infrastructure, Urban Parks and green and water installations	Neighborhood
Improve the water quality.			
Reduce the temperature with the intent of betterment of the lives of the residential communities along this stretch.	Albedo	Reflective materials	Neighborhood
	Environmental Management	Develop strategies	City Level- Statutory body

Table 1: Analytical Framework

The Puri Cuttack road faces major issues that are caused by the rise in the micro temperature of this stretch. The main goal of this paper is to reduce the UHI effects on the stretch of 5.1 kms through a set of sub targets. They are:

- To improve the air quality by oxygen production and vegetation.
- To reduce the temperature with the intent of betterment of the lives of the residential communities along this stretch.
- To improve the water quality.
- To develop the visual image of the environment.

Role of air pollution in UHI

Recent studies on climate change issues suggest that air pollution is one of the significant factors, which influences the Earth's radiation budget through perturbing radiation balance (IPCC, 2017). A major research focus has been on the high levels of urban air pollution (e.g. particulates, aerosols, and ozone and volatile organic compounds) that emanated from various emission sectors including fossil fuel (coal of oil or gas) combustion from vehicles, industry and house-hold usages and open burning from waste burning from road-side or from dumping yard (Roth, 2007). Taking into account the seasonal mean day- (8:00 am-8:00 pm, IST) and night-time (8:00 pm to 8:00 am, IST) wherein observations were obtained from KIIT-DU station, an experiment using regression analysis was carried out at the 5 - study nodes (Rasulgarh node, Kalpana Node, Jharpada Node, New Bomikhal Flyover and old station road

crossing). It involves the analysis of effect of vehicular volume on air pollution (e.g. particulate matter of aerodynamic size less than 10 µm) levels in the ambient air.

Results reveal that regression coefficient of noise and air pollution levels are to be 0.44, which represents the moderate correlation between the levels of noise (L_n) and air pollution (PM_{10}). Due to the unavailability of ground-based air pollution (PM_{10}) data at the study nodes, we used statistical equation from regression curve of KIIT-DU station observations in order to estimate air pollution levels (PM_{10})at the corresponding nodes.

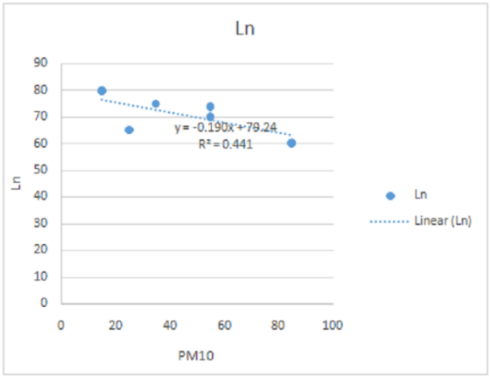


Figure 3: Computation of the regression coefficient

KIIT	PM10	Ln	T	RH
Monsoon (D)	15	80	30	86
Monsoon (N)	25	65	27	98
Winter (D)	55	70	32	40
Winter (N)	85	60	11	98
Summer (D)	35	75	40	50
Summer (N)	55	74	26	80

Figure 2: seasonal mean readings (day and night). *Source: KIIT(DU) station*

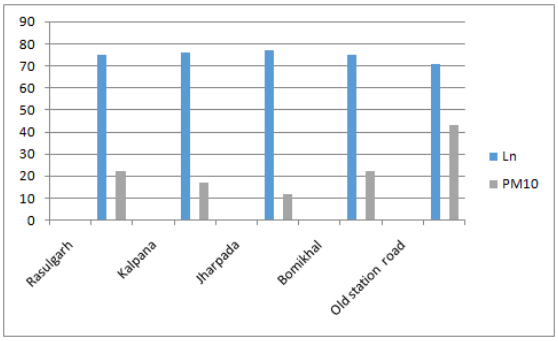


Figure 4: Computation of night time pollution levels

Inference

It is clearly visible from both the graphs that Kalpana node and the old station area have the maximum pollution levels which are imperative due to the anthropological heat and the vehicular movement in these 2 zones.

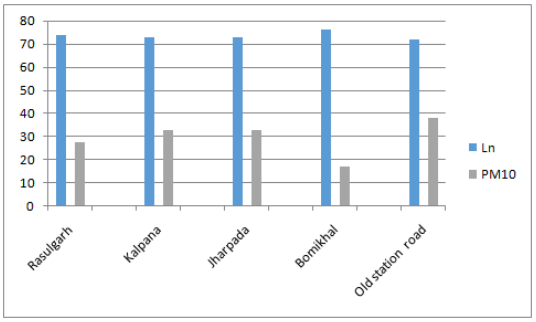


Figure 5: computation of day time pollution levels

Bomikhal and Jharpada have residential projects with urban green which reduces the values of pollution.

Rasulgarh as indicated in the photograph below has a larger expanse than all of the other nodes. This could probably be the reason for the pollution levels being lower than station road which is narrow and cluttered.

Documentation of the Important Junctions/Stops on the Stretch


Node 1


Node 2


Junction 4


Junction 3


Junction 5

Node 1: Rasulagarh Node: A major transit point and an entrance to Bhubaneswar from Kolkata via Cuttack. Since this area houses industrial estates, a huge mall, residential zones the generation of urban heat island effect is but inevitable. However, as the picture denotes, there is no sign of vegetation or water in spite of the fact that there is ample scope for placing the same.

Node 2: Kalpana Chowk: This is the one end of our paper's case, the Puri Cuttack Road, the other being the Rasulgarh Node. This is one of the exit/entrance gateways to Bhubaneswar while going to Puri, Konark and further regions in coastal Odisha. Plantation is scanty and mainly in the median.

Junction 3: Old Station Road Crossing: A busy node which gives way to a secondary entrance of the Bhubaneswar railway Station lacks any form of vegetation. Cluttered roads and archaic infrastructure are the identity of this connection. The junction of the connecting road and the main Puri Cuttack road is always a traffic bottleneck due to the inadequacy of its width. The air quality in this junction is the worst in the entire 5.1kms stretch.

Junction 4: Jhadpara Junction: As discussed earlier, the stretch of Puri Cuttack road, is home to several and important connecting roads of Bhubaneswar. The Jharpada flyover is one such junction. In spite of the traffic volume at this crossing being one of the highest in Bhubaneswar, no vegetation is witnessed in this area.

Junction 5: New Bomikhal Flyover: The newest chip of the block, this flyover is an additional connection to the prime vehicular spine of Bhubaneswar-The Janpath.

Inferences stemming from the Stuttgart clearly indicated that in response to local climate characteristics, areas of vegetation have an important effect on the local climate, due to cooling and shading, in particular by trees. Therefore, vegetation should be provided to surrounding developments and larger, connected green spaces should be created or maintained throughout developed areas. Also, the material used for the roads throughout is bitumen. An alternate finish for the roads, on the stretch abutting residential areas in particular with a higher solar reflective value would be recommended.

Implementing the Initiative

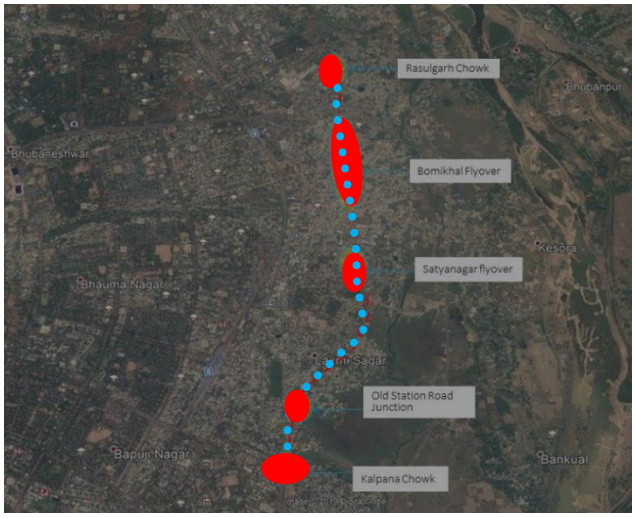


Figure 6: Five locations for implementation

As indicated in figure 6, the five area locations have been identified for implementation. In addition to the recommendation given, the patch of the road between any of the aforesaid locations will comply to the concept of connected green spaces as in Stuttgart.

In areas where there is a vehicular or pedestrian crossover, interventions indicated in figure 7 is to be followed. Each recommendation mentioned below has precedence in India and are supported with images for the same.

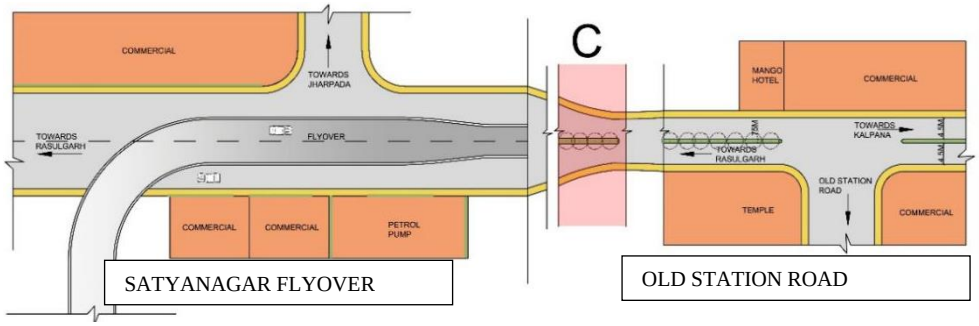


Figure 7: Satyanagar Flyover, Old station road and connection





Recommendation 1: Figure 7 represents the Satyanagar flyover and the old station road wherein the traffic volume is maximum. These two junctions are also the secondary entrance to the Janpath and the Bhubaneswar Railway station respectively. Hence the intervention proposed in these areas is minimal. Trees are proposed in the median and the underside of the flyover will be treated in the same manner as that proposed below the Bomikhal flyover.

However as discussed earlier, the idea is to propose a compact and connected green. Hence the median of the roads between any two junctions per say the old station road and Satyanagar flyover have also been proposed to have trees in the median indicated in the area marked C in figure 7. The adjoining images represent precedence in Lajpatnagar, Delhi where these practices have been implemented.

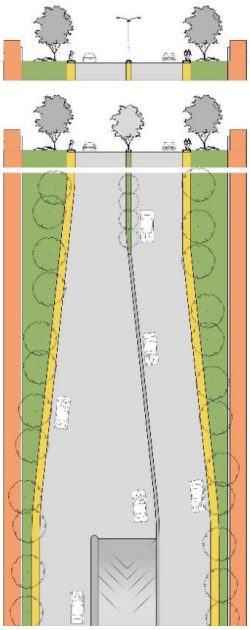


Figure 7 :Rasulgarh Node

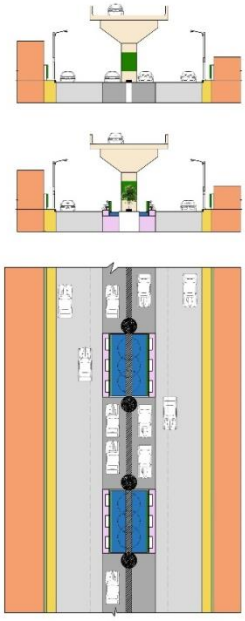


Figure 8: Bomikhal Flyover

Recommendation 2: Refer Figure8: New Bomikhal Flyover: As inferred from Stuttgart's study introduction of water and green reduced the micro temperature. Hence the area beneath the flyover which is currently being only for parking is proposed to have:

- Alternate pockets of water flanked with seating and the columns of the flyover to be covered with green.
- The following images wherein this intervention has been done in New Delhi.



Recommendation 3: Refer Figure7 for Rasulgarh Chowk: Unpaved Areas flanking the road to have native canopy trees planted. This will not only give the area the avenue look and feel but the augmented vegetation will reduce the temperature



CONCLUSION:

Studies on urban heat island and its effects have been happening since decades by urban climatologists, but the concern from the community and the statutory bodies has been recent. This interest is triggered due to heat related health issues. Development of heat island reduction strategies, mainly trees and vegetation, green roofs, and cool roofs are no more confined to the research fraternity. Literature reveals that the apparent strong influence of vegetation and water availability on the energy partitioning irrespective of the climate type, however, is an important result from the experiments carried out so far. Vegetation seems to be a useful way to reduce heat storage uptake during daytime and hence has the potential to effectively mitigate the nocturnal heat island.

The experiment conducted at the 5 study locations also reveals that the pollution levels are low in the zones with green sprawl available in the residential pockets. The most cluttered zone with the maximum anthropological and vehicular movement records the hightse level of pollution.

The aforesaid paper discussed and recommends enough possibilities to implement the design principles that can reduce the accumulation of the urban heat. Any renovation activity wherein mitigation of heat issues is involved, calls in for combined implementation of measures that are necessary to improve the social, physical or economical condition with urban heat island reduction strategies. If we take green as an example, besides cooling it has a positive effect on the human psyche in preventing depressions, etc. Green also produces oxygen and filters particulate matter and ozone out of the air.

BIBLIOGRAPHY:

Gunawardena, K.r., M.j. Wells, and T. Kershaw. "Utilizing Green and Blue space to Mitigate Urban Heat Island Intensity." Science of Total Environment 584-585 (2017): 1040-055. doi: 10.1016/j.scitotenv.2017.01.158

Kleerekoper, Laura, Marjolein Van Esch, and TadeoBaldiri Salcedo. "How to Make a City Climate-proof, Addressing the Urban Heat Island Effect." Resources, Conservation and Recycling 64 (2012): 30-38. doi: 10.1016/j.resconrec.2011.06.004.

Rehan, Reeman Mohammed. "Cool City as a Sustainable Example of Heat Island Management Case Study of the Coolest City in the World." HBRC Journal 12, no. 2 (2016): 191-204. doi: 10.1016/j.hbrcj.2014.10.002.

Roth, M. (2007). Review of urban climate research in (sub) tropical regions. International Journal of Climatology: A Journal of the Royal Meteorological Society, 27(14), 1859-1873.

Santamouris, M. "Cooling the Cities – A Review of Reflective and Green Roof Mitigation Technologies to Fight Heat Island and Improve Comfort in Urban Environments." Solar Energy 103 (2014): 682-703. doi: 10.1016/j.solener.2012.07.003.

Spatiotemporal Characteristics of Anthropogenic Heat and Its Impact on Outdoor Thermal Environment in a University in Chongqing

Zhongyu Hao[1], Yang Xu, Dachuan Shi, Yu Liu, Yafeng Gao
Chongqing University (China)

ABSTRACT

The research on the influence of anthropogenic heat on the outdoor micro-environment has not received enough attention, which leads to great differences in the prediction and evaluation of the outdoor thermal environment. This study is to obtain the spatiotemporal characteristics of anthropogenic heat on the campus of Chongqing University, and compare the total anthropogenic heat of the campus with solar radiation to evaluate its impact on urban energy balance and outdoor thermal environment. The results show that under winter conditions, the total amount of anthropogenic heat on working days and non-working days is 38.2% and 35.3% of solar radiation respectively. Under summer conditions, the total amount of anthropogenic heat on working days and non-working days is 15.8% and 17.1% of solar radiation respectively.

Keywords: Anthropogenic heat; Campus; Energy consumption simulation; Solar radiation; Outdoor thermal environment

INTRODUCTION

The Urban anthropogenic heat refers to the part of heat generated by human activities and discharged into the atmosphere. According to its source, it can be divided into human metabolic heat, industrial heat, traffic heat and building heat (Sailor 2011). In recent years, with the development of cities and the enhancement of human activities, the impact of anthropogenic heat on urban thermal environment is also increasing.

Over the past few decades, a large number of studies have been conducted on anthropogenic heat at different spatial scales. On the urban scale, calculation methods can be divided into three categories: Energy list method (Sailor and Lu 2004; Fan and Sailor 2005), the surface energy balance method (Offerle, Grimmond and Fortuniak 2005; Kato and Yamaguchi 2005; Zhou et al. 2012), the building energy simulation method (Heiple and Sailor 2008; Chow et al. 2014; Assimakopoulos, Mihalakakou and Flocas 2007).

In terms of the impact of anthropogenic heat on urban thermal environment, different models including mesoscale models (Kikegawa et al. 2003; Kikegawa et al. 2014) and urban canopy models (Bueno et al. 2011) were used to simulate different scales of research objects. It shows that urban anthropogenic heat is an important factor affecting climate change, and different regions and cities are affected by climate, environment and energy utilization, the warming effect is also different.

Through literature review, it is found that the current research on anthropogenic heat is concentrated on the large environmental scale of a single city, while the research on

[1] Corresponding Author: [zhongyuhao3704@126.com], [+86-13251325669].

anthropogenic heat for small regional scale is less. And due to the lack of relevant data, there are a lot of rough assumptions in many studies.

In this study, HuXi campus of Chongqing University was selected as the research object to calculate the average anthropogenic heat flux in its area. The spatial distribution and time variation of anthropogenic heat release from different sources are given in detail.

METHODOLOGY

Research area

Chongqing is located at 105°11'~110°11' east longitude and 28°10'~32°13' north latitude. It is located in the southwestern part of China and the upper reaches of the Yangtze River. It is affected by the high pressure of the Qinghai-Tibet Plateau and the surrounding mountains. The air has a high humidity and a small wind speed, forming a unique climatic feature and a subtropical monsoon humid climate.

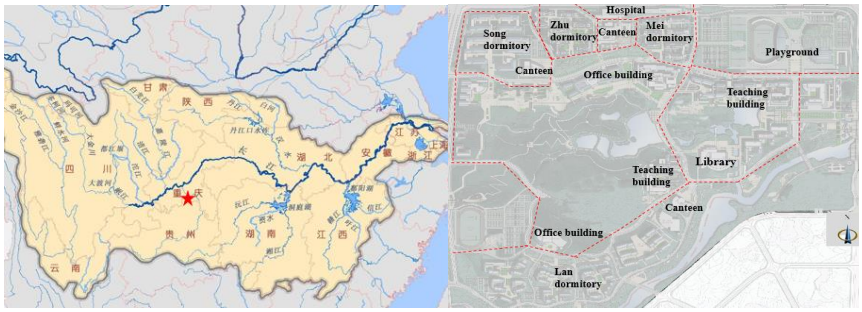


Fig 1. The geographical location of Chongqing and architectural distribution map of HuXi campus

The experimental research area was selected at the HuXi campus of Chongqing University. The campus is located in the university town of the western suburbs of Chongqing. The campus has a shallow hilly terrain with an open view. The overall planning of the school district is 1.55 million square meters and 35,000 students are enrolled. The total completed school building area is 600,000 square meters and more than 15,000 students are enrolled.

Calculation method

Since there is no waste heat from industrial production on campus, the sources of anthropogenic heat can be divided into three main categories: human metabolic heat, transportation exhaust heat, and building heat. The sum of them is the anthropogenic heat on campus.

Human metabolic heat. Human metabolic heat is related to population size and activity intensity:

$$Q_M = \frac{(P_1 t_1 + P_2 t_2) N}{A(t_1 + t_2)} \quad (1)$$

Where P_1= 75 W and P_2 = 175 W are the metabolic rates during sleep and active periods respectively these numbers are adopted from previous research results. t_1 = 8 h and t_2 = 16 h,

which represent the time for sleep and active periods, respectively, N the total number of people within the region during the day, S the total area of region.

The activity characteristics of students were obtained by questionnaire survey. The questionnaire mainly involves: basic information of students, time off class, meal time, etc. The information of opening hours of all kinds of buildings in the campus and the number of people living in each dormitory were obtained through investigation, and the building area was calculated. Then, the class schedule of students is summarized, and the hourly distribution of students in the campus is obtained based on the questionnaire survey results in the previous section. The metabolic heat release flux of human body is calculated according to equation (1).

Transportation exhaust heat. The road conditions and monitoring points in the campus were investigated to determine the main roads and measuring points in the study. The section numbering situation and the arrangement of each measuring point are shown in **Fig 2**. The monitoring video data acquisition technology is used to calculate the road traffic volume in the study area according to different vehicle types, and the heat release is calculated according to the fuel consumption of different types of vehicles. Since the types of cars that travel on the road are different and the heat release is not the same, a classification of the car types must be made. According to the actual situation of motor vehicles in the campus, motor vehicles on the road are divided into six categories: car, SUV, bus, van, truck (heavy truck, light truck) and tricycle.

Table 1. The motor vehicle gasoline heating value of each model

Categories	Car	SUV	Bus	Van	Truck		Tricycle
					Heavy truck	Light truck	
Gasoline consumption per 100 kilometers O (L/100km)	8.5	14.5	26.0	7.0	40.0	11.0	5.0
Gas calorific value G (kJ/g)	46						
Gasoline density ρ(kg/L)	0.74						



Fig 2. The main road numbering map of HuXi campus and the measuring point layout of the main road traffic flow

The anthropogenic heat flux calculation formula for the vehicle exhaust heat is as follows:

$$Q_V = \frac{V \times O \times \rho \times G}{360W} \quad (2)$$

Every hundred kilometres fuel consumption index O, gasoline calorific value G, gasoline density ρ are determined by Table 1, hourly traffic flow V and road width W are obtained according to the actual measurement statistics.

Building heat. In this study, the campus buildings were classified, and a typical building was selected in each type of building to simulate with the DesignBuilder energy simulation software. Then, the actual energy consumption of the building and the simulation results were compared and verified.

By obtaining the hourly energy consumption value of the building, the hourly heat output intensity of the building is obtained. Here, like other studies (Quah and Roth 2012; Nie, Sun and Ni 2014), the lag time between real energy consumption and calorific value emission is ignored, assuming that all energy consumption is converted to sensible heat and directly discharged into the atmosphere. Finally, the results were extended to other buildings of the same type in the campus to obtain the characteristics of building heat.

The total construction area of the campus is about 589,200 m^2. According to the functions, campus buildings are mainly divided into five types: office buildings, teaching buildings, dormitory buildings, library buildings and life service buildings. The building of foreign language institute, the first teaching building, the second building of Song dormitory, the library and the canteen were selected as the representatives. The typical meteorological year of Chongqing in China standard meteorological data CSWD was adopted as the typical meteorological year data file for DesignBuilder energy consumption simulation to dynamically simulate the annual energy consumption of the building.

Solar radiation. The solar radiation was detected by trm-zs2 automatic weather station. The instrument was located on the roof of the student dormitory in the northwest corner of the campus (with a height of 20.2m relative to the ground).

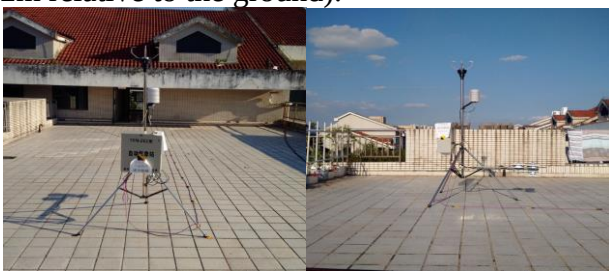


Fig 3. The overview of TRM-ZS2 automatic weather station

RESULT

Energy consumption simulation test verification

Since the current conditions limit only monthly energy consumption monitoring data, this study checks the monthly energy consumption data. In this study, the simulated energy consumption data output is compared with the existing energy consumption statistics in the simulation process. In order to make the simulation result more representative of the actual situation, and reference to the error control selection in IPMVP (IPMVP 2001), 20% is adopted.

Control error, that is, when the error between the simulation result and the measured data is found to exceed 20%, even if the feedback is adjusted, the error between the simulation result and the measured data is controlled within 20%. Typical building energy consumption simulation results and measured energy consumption statistics results, for example Table 2 Shown. S is simulation data; M is measured data.

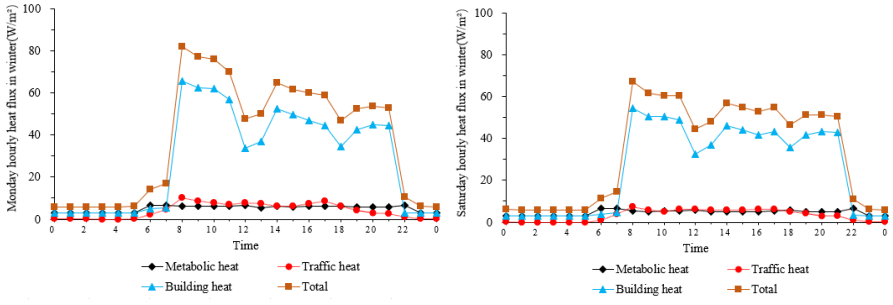
Table 2. The comparison between simulation results and measured results of typical buildings(kW·h)

Month	First teaching building		Foreign language institute building		Song dormitory		Canteen		Library	
	S	M	S	M	S	M	S	M	S	M
June	98132	83300	18006	16667	23897	20320	42455	50400	189923	234000
December	53023	61035	15313	13836	17398	15700	33261	31920	155238	174000

Comparing the energy consumption simulation results with the measured energy consumption data, The error range of energy consumption simulation calculation and measured data is 4.2%-18.8%.

Time variation characteristics

The human metabolic heat, traffic heat and building heat are summarized into the total anthropogenic heat of the campus. It can be seen in Fig 4 that in the daily change, the total anthropogenic heat has similar changes to the building heat. The building heat plays a leading role in the total anthropogenic heat, accounting for the largest proportion, followed by traffic heat, and the proportion of metabolic heat is the smallest. In the winter working days, building heat, traffic heat and metabolic heat accounted for 77.3%, 11.7% and 11.0% respectively, while in non-working days, 78%, 12.2% and 9.8% respectively; in summer working days, building heat, traffic heat and metabolic heat accounted for 82.1%, 9.4% and 8.5% respectively, while in non-working days, 82.7%, 10.1%, and 7.2% respectively. By comparing the daily variation characteristics of winter and summer, it can be seen that human heat also has significant seasonality, and peaks appear at different times. Specifically, the maximum total anthropogenic heat in winter appears at 8:00, and the maximum total anthropogenic heat in summer appears at 17:00.The inconsistency in the peak time of anthropogenic heat may have a complex impact on the regional climate. In addition, non-working day heat flux will decrease significantly.



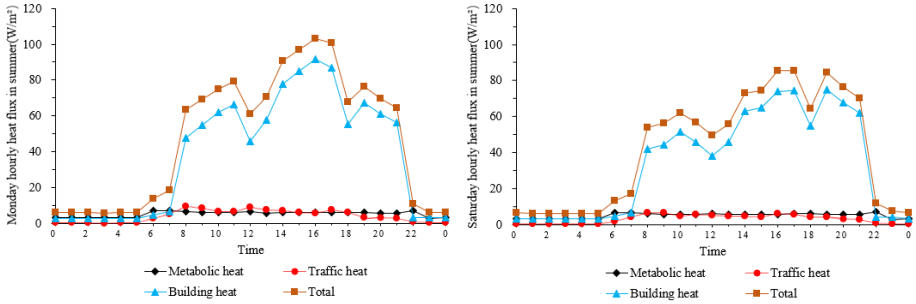


Fig 4. The daily changes of different sources of anthropogenic heat in winter and summer

Spatial distribution characteristics

As shown in Fig 5 , the daily heat flux distribution pattern during the working day is generally the same, the teaching area and the canteen area are at a larger value, while the dormitory area is smaller. The daily average heat flux distribution pattern changed during non-working days. In general, the heat flux in the teaching area decreases significantly, while the dormitory area increases. This is mainly due to the decrease in the number of students on non-working days and the significant decrease in the number of students. It can be seen that the metabolic heat release has extremely unevenness. Summer metabolic heat is similar to winter and still has very unevenness.

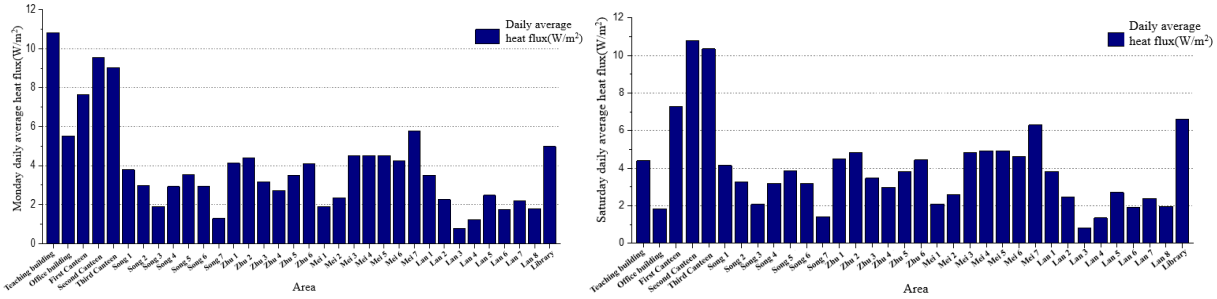


Fig 5. The spatial distribution of human metabolic heat on Monday and Saturday of winter

As can be seen from Fig 6, the daily average heat flux of the 25# section on Monday is 11.0W/m^2, while the daily average heat flux of the 19# section is about 0.6W/ m^2. The daily average daily heat flux appeared on the 14# section up to 8.0W/m^2, which is nearly 10 times different from the 23# section with the lowest daily heat flux. Due to the traffic control of the school, the average daily heat flux of the 23# section is small. It can be seen that the winter traffic heat is extremely uneven, and the summer traffic heat is similar to winter.

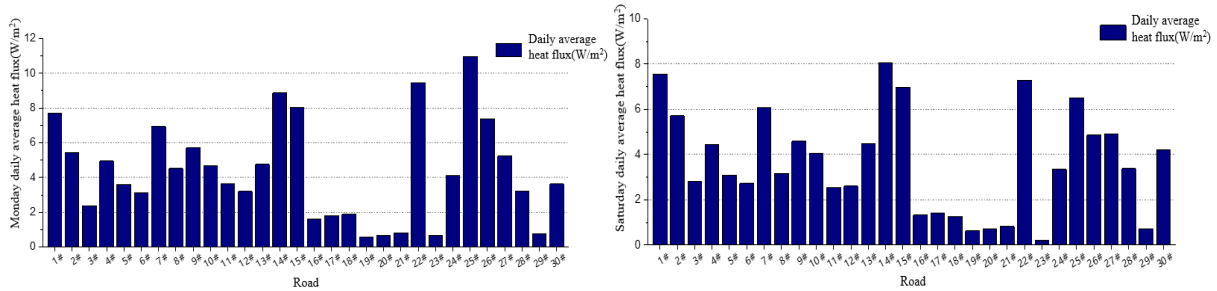


Fig 6. The spatial distribution of traffic heat of campus on Monday and Saturday of winter

According to the calculation results of campus building heat, the human metabolic and traffic heat are added in the same period. By using ArcGIS software, the spatial heterogeneity of total anthropogenic heat in the campus during typical working days and non-working days in winter is shown in Fig 7.

In the winter, 8:00 on Monday, the teaching area, canteen area and office area are mostly in high value area, up to 119.1W/m^2, while the dormitory area is relatively small, ranging from 16.2 to 23.2W/m^2. In the early peak period, the traffic heat intensity is between 1.1 and 25.6 W/m^2; at 12:00 and 17:00, the canteen area is in the high value area, ranging from 56.9 to 160.4 W/m^2. Traffic heat release at the midday and evening peaks is between 0.5 and 27.8 W/m^2; at 21:00, the dormitory and library area are at a large value, ranging from 28.0 to 81.2 W/m^2, and other areas are smaller. The heat release at night is basically the same and low, ranging from 0.3 to 7.6 W/m^2.In the winter, the office area is at a small value in winter, and the anthropogenic heat intensity in other areas will be correspondingly weakened, but the dormitory area will be strengthened than the working day, because the weekend does not go to work and the teaching arrangement is reduced. The distribution pattern in summer is generally similar to that in winter, but the total anthropogenic heat intensity is significantly enhanced, with a maximum of 160.4 W/m^2.

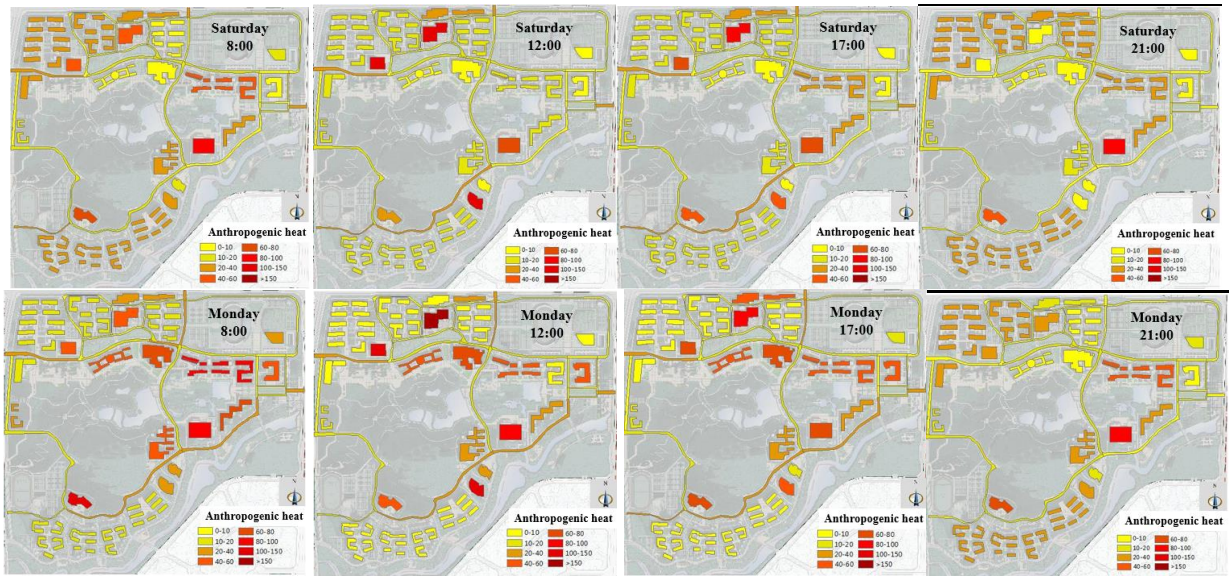


Fig 7. Spatial distribution of anthropogenic heat on Monday and Saturday of winter

Comparison of campus anthropogenic heat and solar radiation

From Fig 8, by comparing solar radiation with total anthropogenic heat, the average anthropogenic heat flux for winter working days and non-working days are 39.0 W/m^2 and 35.0 W/m^2 respectively, the average intensity of solar radiation is 102.1 W/m^2 and 99.0 W/m^2 respectively, accounting for 38.2% and 35.3%. The average anthropogenic heat flux for summer working days and non-working days was 48.8 W/m^2 and 43.1W/m^2 respectively, the average intensity of solar radiation was 309.2W/m^2 and 252.5W/m^2 respectively, accounting for 15.8% and 17.1%. Therefore, anthropogenic heat plays an important role in urban energy balance. In addition, the anthropogenic heat is not the same as the peak of solar radiation. The peak of solar

radiation usually appears between 12:00 and 14:00, while the peak of anthropogenic heat in winter appears at 8:00, and the peak of anthropogenic heat in summer appears at 17:00. This will extend the heating time of the urban thermal environment as a whole. It can be seen that anthropogenic heat has become an important part of urban energy balance. Especially in winter, anthropogenic heat may have a major impact, which cannot be ignored in the numerical simulation of climate environment.

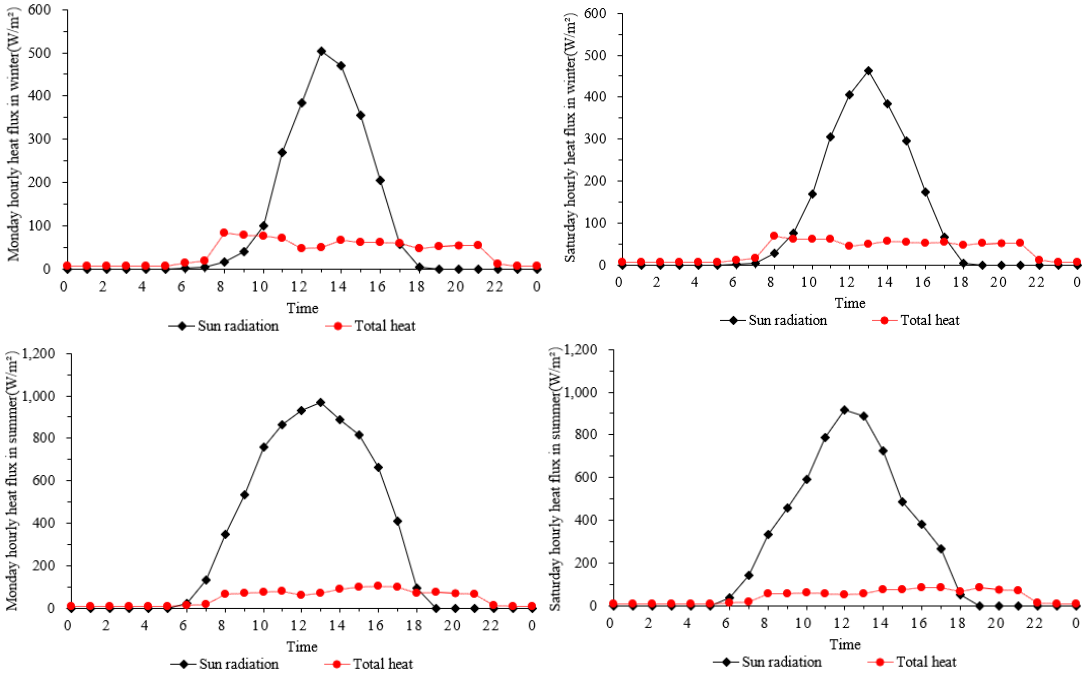


Fig 8. Comparison of solar radiation and total anthropogenic heat in winter and summer

CONCLUSION

In this study, we obtain hourly human metabolic heat, traffic heat and building heat. Then add up to get the anthropogenic heat on campus. Finally, the total anthropogenic heat and solar radiation are compared, and the conclusions are as follows:

(1) During the daytime, the average heat flux in winter showed a downward trend, while the average heat flux in summer showed an overall upward trend, which was mainly related to outdoor meteorological conditions. In addition, non-working day heat flux will drop significantly.

(2) The distribution of anthropogenic heat space on campus is very uneven. The high-value areas of total anthropogenic heat at different times are mainly related to the running time and building function of the building. The total anthropogenic heat intensity in summer will be significantly enhanced to 160.4 W/m^2, indicating that outdoor climate factors have an important impact on human heat. The intensity of heat exhaust at night is basically the same and low, which is related to the school's traffic control and personnel activity time.

(3) Building heat in the total anthropogenic heat accounted for the largest proportion, followed by traffic heat, the proportion of metabolic heat is the smallest.

(4) By comparing solar radiation with total anthropogenic heat, the total anthropogenic heat in winter working days and non-working days is 38.2% and 35.3% of solar radiation, respectively; in the summer working days and non-working days, the total anthropogenic heat is sun. 15.8% and 17.1% of radiation. In addition, the difference between the anthropogenic heat

and the peak time of solar radiation will extend the heating time as a whole, which has a complicated impact on the outdoor thermal environment.

ACKNOWLEDGMENT

This research work was supported by the China National Key R&D Program (No.2017YFC0702903), and the National Natural Science Foundation of China (No.51578086).

References

Assimakopoulos, M. N. , Mihalakakou, G. , & Flocas, H. A. (2007). Simulating the thermal behaviour of a building during summer period in the urban environment. Renewable Energy, 32(11), 1805-1816. https://www.sciencedirect.com/science/article/pii/S0960148106002515

Bueno, B. , Norford, L. , Grégoire Pigeon, & Britter, R. . (2011). Combining a detailed building energy model with a physically-based urban canopy model. Boundary-Layer Meteorology, 140(3), 471-489. https://link.springer.com/article/10.1007/s10546-011-9620-6

Chow, W. T. L. , Salamanca, F. , Georgescu, M. , Mahalov, A. , Milne, J. M. , & Ruddell, B. L. . (2014). A multi-method and multi-scale approach for estimating city-wide anthropogenic heat fluxes. Atmospheric Environment, 99, 64-76. https://www.sciencedirect.com/science/article/pii/S1352231014007468

Fan, H. , & Sailor, D. J. . (2005). Modeling the impacts of anthropogenic heating on the urban climate of philadelphia: a comparison of implementations in two pbl schemes. Atmospheric Environment, 39(1), 73-84. https://www.sciencedirect.com/science/article/pii/S1352231004008866

Heiple, S. , & Sailor, D. J. . (2008). Using building energy simulation and geospatial modeling techniques to determine high resolution building sector energy consumption profiles. Energy & Buildings, 40(8), 1426-1436. https://www.sciencedirect.com/science/article/pii/S0378778808000200

IPMVP Committee. (2001). International Performance Measurement and Verification Protocol: Concepts and options for determining energy and water savings, Volume I (No. DOE/GO-102001-1187; NREL/TP-810-29564). National Renewable Energy Lab., Golden, CO (US).

Kato, S. , & Yamaguchi, Y. . (2005). Analysis of urban heat-island effect using aster and etm+ data: separation of anthropogenic heat discharge and natural heat radiation from sensible heat flux. Remote Sensing of Environment, 99(1-2), 44-54. https://www.sciencedirect.com/science/article/pii/S0034425705001707

Kikegawa, Y. , Genchi, Y. , Yoshikado, H. , & Kondo, H. . (2003). Development of a numerical simulation toward comprehensive assessments of urban warming countermeasures including their impacts upon the urban buildings energy demands (in japanese). Applied Energy, 76(4), 449-466. https://www.sciencedirect.com/science/article/pii/S0306261903000096

Kikegawa, Y. , Tanaka, A. , Ohashi, Y. , Ihara, T. , & Shigeta, Y. . (2014). Observed and simulated sensitivities of summertime urban surface air temperatures to anthropogenic heat in downtown areas of two japanese major cities, tokyo and osaka. Theoretical and Applied Climatology, 117(1-2), 175-193. https://link.springer.com/article/10.1007/s00704-013-0996-8

Nie, W. S. , Sun, T. , & Ni, G. H. . (2014). Spatiotemporal characteristics of anthropogenic heat in an urban environment: a case study of tsinghua campus. Building and Environment, 82, 675-686. https://www.sciencedirect.com/science/article/pii/S0360132314003321

Offerle, B. , Grimmond, C. S. B. , & Fortuniak, K. . (2005). Heat storage and anthropogenic heat flux in relation to the energy balance of a central european city centre. International Journal of Climatology, 25(10), 1405-1419. https://rmets.onlinelibrary.wiley.com/doi/abs/10.1002/joc.1198

Quah, A. K. L. , & Roth, M. . (2012). Diurnal and weekly variation of anthropogenic heat emissions in a tropical city, singapore. Atmospheric Environment, 46(none), 92-103. https://www.sciencedirect.com/science/article/pii/S1352231011010685

Sailor, D. J. , & Lu, L. . (2004). A top–down methodology for developing diurnal and seasonal anthropogenic heating profiles for urban areas. Atmospheric Environment, 38(17), 2737-2748. https://www.sciencedirect.com/science/article/pii/S1352231004001529

Sailor, D. J. . (2011). A review of methods for estimating anthropogenic heat and moisture emissions in the urban environment. International Journal of Climatology, 31(2), 189-199. https://rmets.onlinelibrary.wiley.com/doi/full/10.1002/joc.2106

Zhou, Y. , Weng, Q. , Gurney, K. R. , Shuai, Y. , & Hu, X. . (2012). Estimation of the relationship between remotely sensed anthropogenic heat discharge and building energy use. ISPRS Journal of Photogrammetry and Remote Sensing, 67(none), 65-72. https://www.sciencedirect.com/science/article/pii/S0924271611001171

Climate-Informed Decision-Making for Urban Design: Assessing the Impact of Urban Morphology on Urban Heat Island

Luis G. R. Santos, TUMCREATE (Singapore)
Ido Nevat, TUMCREATE (Singapore)
Gloria Pignatta, UNSW Sydney (Australia)
Leslie K. Norford, MIT (United States)

ABSTRACT

Urban growth is related to major environmental consequences and affects people's livability and economy. To address such impacts, stakeholders must evaluate different mitigation policies. Due to the complexity of those phenomena, such comparison process can be challenging, resulting in subjective and unclear interpretations, which consequentially limits the course of action for its implementation. To overcome this difficulty, we develop a novel framework that provides a statistical analysis of urban climate models. The high-dimensional data generated by the climate model is transformed into a low-dimensional scoring system, according to statistical metrics that reflect desired priorities of stakeholders. This allows for informed quantification of the quality of different scenarios by policy makers. We illustrate the applicability of the framework in an urban area of Singapore. Different urban morphologies are analysed, estimating their environmental impact on Urban Heat Island and their potential for population allocation, while considering operational energy costs. The result is a matrix of scores per scenario, highlighting the optimal design according to the pre-defined metrics. The scenarios with the highest building height (81 m) and medium (40%) or low (30%) density offer a good balance between the environmental impact and its external trade-offs, evaluated by the number of people allocated per site area and the cost of energy to operate the district.

Special Issue Journal	:	Urban Climate
DoI	:	https://doi.org/10.1016/j.uclim.2021.100776
Citation	:	Santos, L., Nevat, I., Pignatta, G., & Norford, L. (2021). Climate-informed decision-making for urban design: Assessing the impact of urban morphology on urban heat island. Urban Climate, 36, 100776.

Climate change and infrastructure risk: Indoor heat exposure during a concurrent heat wave and blackout event in Phoenix, Arizona

Brian Stone, Georgia Institute of Technology (USA)
Evan Mallen, Georgia Institute of Technology (USA)
Mayuri Rajput, Georgia Institute of Technology (USA)
Ashley Broadbent, Arizona State University (USA)
E. Scott Krayenhoff, University of Guelph (Canada)
Godfried Augenbroe, Georgia Institute of Technology (USA)
Matei Georgescu, Arizona State University (USA)

ABSTRACT

Concurrent with a rapid rise in temperatures within US cities, the frequency of regional electric grid system failures is also rising in recent decades, resulting in a growing number of blackouts during periods of extreme heat. As mechanical air conditioning is a primary adaptive technology for managing rising temperatures in cities, we examine in this paper the impact of a prolonged blackout on heat exposure in residential structures during heat wave conditions, when air conditioning is most critical to human health. Our approach combines a regional climate modeling system with a building energy model to simulate how a concurrent heat wave and grid failure event impacts residential building-interior temperatures across Phoenix. Our results find a substantial increase in heat exposure across residential buildings in response to the loss of electrical power and mechanical cooling systems, with such an event potentially exposing more than one million residents to hazardous levels of heat. We further find the installation of cool roofing to measurably lower the risk of extreme heat exposure for residents of single-story structures.

Special Issue Journal	:	Urban Climate
DoI	:	https://doi.org/10.1016/j.uclim.2021.100787
Citation	:	Stone, B., Mallen, E., Rajput, M., Broadbent, A., Krayenhoff, E., Augenbroe, G., & Georgescu, M. (2021). Climate change and infrastructure risk: Indoor heat exposure during a concurrent heat wave and blackout event in Phoenix, Arizona. Urban Climate, 36, 100787.

URBAN VEGETATION AND GREENERY

Influence of urban green on human thermal bioclimate – Application of thermal indices and micro scale models

Andreas Matzarakis[1], Research Centre Human Biometeorology, German Meteorological Service (Germany)
Marcel Gangwisch, Research Centre Human Biometeorology, German Meteorological Service (Germany)
Dominik Fröhlich, Research Centre Human Biometeorology, German Meteorological Service (Germany)

ABSTRACT

For the quantification of the atmospheric conditions and their impact on humans, methods from human biometeorology can be applied. For the thermal component air temperature, humidity, wind and radiation fluxes are the key factors, which are required. Most significant for urban areas and urban green is the quantification of heat stress, which can be estimated by thermal indices, e.g. the Physiologically Equivalent Temperature (PET), the Perceived Temperature (PT), or the Universal Thermal Climate Index (UTCI). For an overall assessment, different approaches can be applied based on measurements and models (e.g. RayMan, ENVI-met and SkyHelios) for single points (Points of Interest) within urban areas or neighborhoods and city quarters (Areas of Interest). The most relevant reduction of heat stress can be obtained by increasing shade with specific trees and by improving wind conditions. These two factors (radiation and wind modification) can be extremely helpful in the creation of optimized thermal comfortable urban places with green areas. The application of models, which focus on long term quantifications, can deliver valuable results and information for whole year assessment of the effect of urban green on human thermal bioclimate. In addition, models deliver additional basic parameters (sun paths, sunshine duration, aerodynamic roughness), which are important in the estimation of the effects of urban green on human thermal bioclimate. In particular, this information is available for future planning and construction.

Introduction

Nowadays, people are becoming increasingly aware of the local impact of global climate change, urban administrations as well as architects are forced to consider measures to counteract its negative effects. The public awareness thereby is supported by the fact, that the local effect of global climate change is increased by the effect of urban climate (Matzarakis, 2013), e.g. the urban heat island (Ketterer and Matzarakis 2016). At the same time, thermal conditions in urban environments at street level can be modified quite effectively by making use of the same effects that are causing the urban heat island. Urban bioclimate, thus, can be controlled by urban planning measures, e.g. by altering the building configuration (Hwang, Lin, and Matzarakis 2011; Fröhlich and Matzarakis 2013), by application of different surface materials (Shashua-Bar,

[1] Corresponding Author: andreas.matzarakis@dwd.de, +49 69 8062 9610, Research Centre Human Biometeorology, German Meteorological Service, Stefan-Meier-Str. 4, D-79104 Freiburg, Germany.

Pearlmutter, and Erell 2011) and by the urban green infrastructure (GI) (Song and Park 2015; Santos Nouri et al. 2018).

In order to evaluate the impacts of the ecosystem services of urban trees on the urban environment, it is necessary to quantify radiation fluxes modified by the urban morphology. The physiological processes of trees (e.g. transpiration and photosynthesis) are controlled by radiation fluxes and modify the local micro climate (increased humidity and decreased air temperature) (Bowler et al. 2010). Urban trees can be shaded by urban obstacles, e.g buildings and other trees, so that the absorption of direct and diffuse short-wave radiation and tree growth are limited (Kjelgren and Clark 1992; Ferrini, Bosch, and Fini 2017). Urban trees may be surrounded by surfaces with dark materials (e.g. paved surface, buildings and streets with small albedo), which are warmer compared to surfaces of the GI with higher albedo (Kjelgren and Montague 1998; Leuzinger, Vogt, and Körner 2010). This can lead to an increased exposure of urban trees to long-wave radiation (Kjelgren and Montague 1998).

The radiation fluxes (especially photosynthetically active radiation (PAR; 0.34 µm - 0.71 µm)), modified by the processes of absorption, emission, reflection and transmission in the complex urban environment, have great impact on the ecosystem services of urban trees (Dobbs, Escobedo, and Zipperer 2011; Ferrini, Bosch, and Fini 2017): microclimate regulation by shading and cooling by transpiration. Quantifying the impact of the ecosystem services on the urban microclimate as well as the assessment of ecological and financial benefits (Akbari, Pomerantz, and Taha 2001; Akbari 2002) is required for improved urban planning, architecture, human thermal comfort and health.

For the selection of appropriate measures, municipalities and architects require quantitative information about the effect of specific individual aspects in their designs. While this kind of information was hard to obtain in the past it can now be easily generated by numeric models. The model in question thereby should be fast and easy to use by non-experts so the respective planners in charge can apply them. At the same time, they need to generate all required information in an integral and intuitively understandable way.

For the case of thermal comfort and thermal stress, the latter can be best fulfilled by the application of thermal indices. Sophisticated modern thermal indices do consider the integral effect of the environment in terms of the meteorological parameters air temperature (T_a), vapor pressure (VP), wind velocity (v) and the different radiation fluxes. In addition, these indices incorporate personal parameters like weight, height, workload, metabolism, posture and clothing of a sample person and approximate its thermal perception by solving the human energy balance or the respective energy fluxes (Fanger 1972). The result thereby should be presented in a unit, that can be judged sufficiently by non-experts, e.g. the unit “°C” (Höppe 1999).

Methods

Thermal indices

The application of thermal indices based on the human energy balance provides detailed information on the effect of complex thermal environments on humans (Staiger, Laschewski, and Matzarakis 2019). Commonly used thermal indices, based on the human energy balance (Fanger 1972), are Physiologically Equivalent Temperature (PET, Höppe 1999; Matzarakis, Mayer, and Iziomon 1999), Perceived Temperature (PT, Staiger, Laschewski, and Grätz 2012), Universal Thermal Climate Index (UTCI, Jendritzky, de Dear, and Havenith 2012) and modified Physiologically Equivalent Temperature (mPET, Chen and Matzarakis 2018). All thermal

indices mentioned above require the same meteorological input parameters: air temperature, air humidity, wind speed, as well as short- and long wave radiation fluxes considered by their integral effect as the mean radiant temperature (T_{mrt}). These input parameters have a temporal and spatial variability that has a huge influence on the thermal indices. Wind speed and mean radiant temperature have the highest variability and are severely modified by surroundings and obstacles in complex urban areas.

RayMan model

The RayMan model is developed to calculate short- and long wave radiation fluxes affecting the human body. The model considers complex building structures and is suitable for the analysis of the effect of various planning scenarios in different micro to regional scales. The model calculates the mean radiant temperature (T_{mrt}), which is required for the human energy balance model and, thus, for the assessment of human thermal bioclimate (Matzarakis, Rutz, and Mayer 2007, 2010). The thermal indices Predicted Mean Vote (PMV), Standard Effective Temperature (SET), PET, UTCI, PT and mPET can be calculated (see Thermal indices).

In addition, information about urban structures (buildings, deciduous and coniferous trees) can be generated or imported. Based on the input possibilities, sunshine duration with or without SVF, estimation of the daily mean, max or sum of global radiation or shadows for existing or future complex environments can be calculated. For the estimation of thermal indices, meteorological data can be entered through manual input or by loading data files. The output is provided as graphs and text files. RayMan offers the opportunity of importing long-term data sets of meteorological parameters allowing statistical assessments.

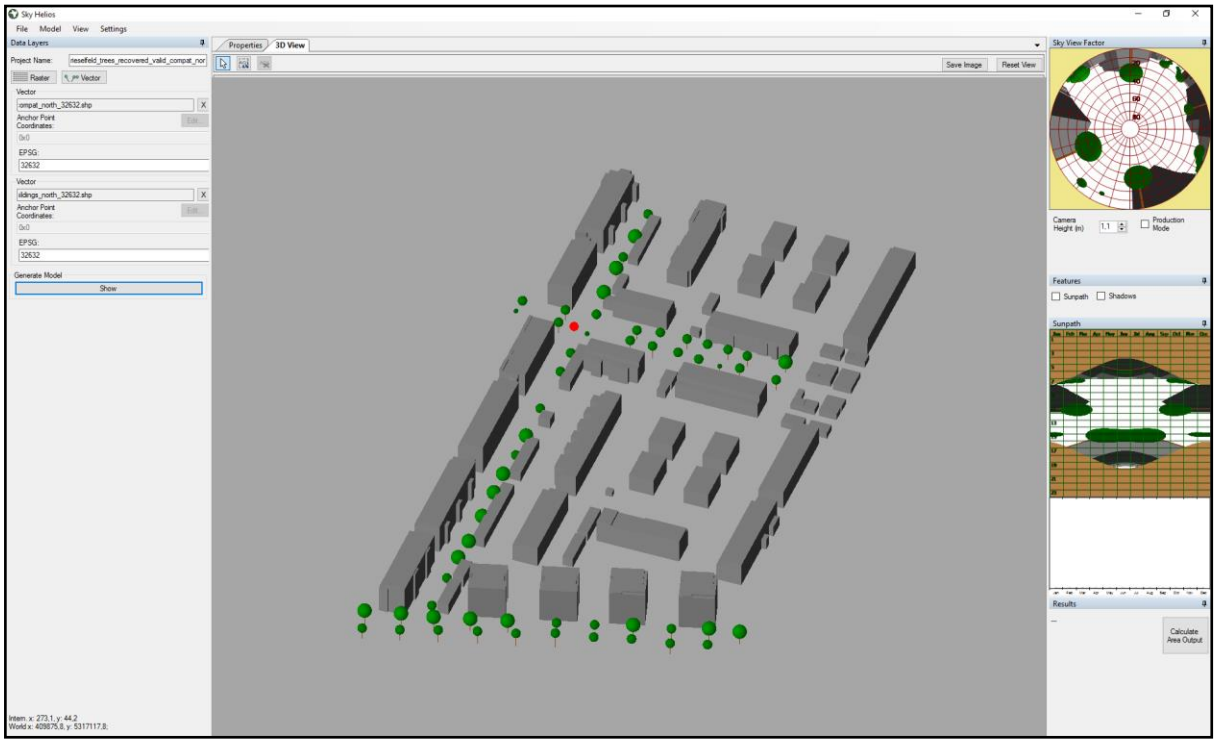


Figure 1. Main window of SkyHelios showing a 3D-scene of Rieselfeld, an urban district in Freiburg, Germany. The scene covers the footprint of all buildings in combination with urban trees.

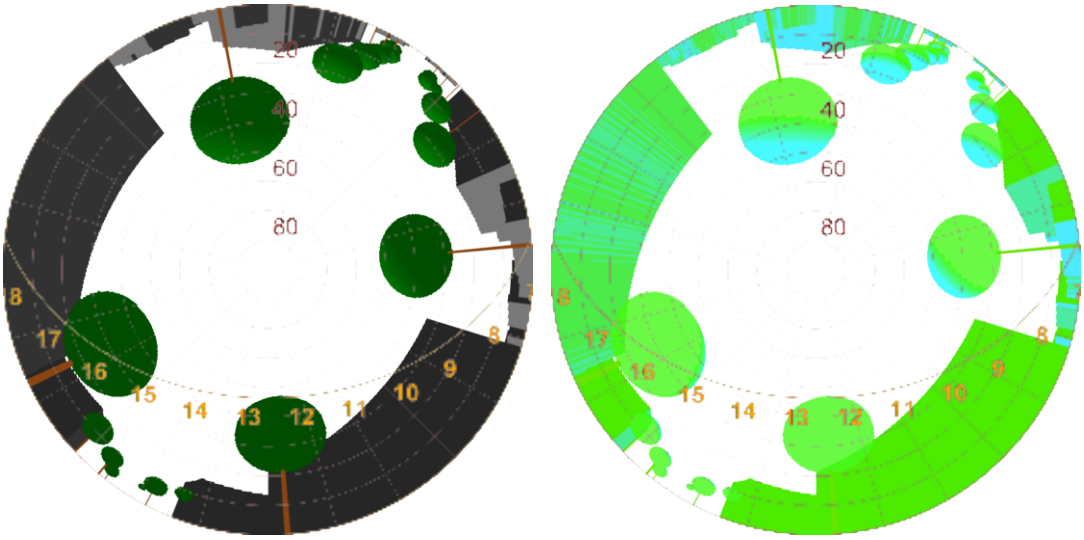


Figure 2. The Fisheye images show the obscuration of the upper hemisphere by buildings and vegetation (left). The surface properties (albedo, emissivity, extend of lighted surface) are encoded in RBG color space (right).

SkyHelios model

SkyHelios (Matuschek and Matzarakis 2010; Matzarakis and Matuschek 2011) is an urban micro scale model, having the ability to estimate crucial parameters of the urban environment spatially resolved (Figure 1). It is a steady-state, time-independent model, capable of estimating several thermal indices (Fröhlich and Matzarakis 2018): PET, UTCI and PT. Furthermore, SkyHelios is able to compute different environmental factors: sunshine duration, shading, wind speed and direction for areas of interest (AOIs) as well as points of interest (POIs).

By creating virtual, three-dimensional (3D) scenes from 3D urban geoinformation (e.g. CityGML LOD 0, 1 and 3D-Shapefiles), SkyHelios can be classified as a 3D city model. All 3D entities in the 3D scene are based on vectorial geodata, allowing for the specification of spatial resolution for all results on demand. The 3D scene is managed by the Object-Oriented Graphics Rendering Engine (Ogre Development Team 2019). The surfaces of the entities in the 3D scene are rendered according to the surface radiational material properties: shortwave transparency, shortwave albedo and longwave emission coefficient (Figure 2). Another color band is utilized to determine to which extent a surface is exposed to direct solar irradiation (Fröhlich and Matzarakis 2018). This is not only used for 3D display, but allows for the rendering of fisheye images containing the necessary input to estimate spatially resolved short- and longwave radiation fluxes, that are finally summarized in terms of the mean radiant temperature (T_{mrt}). Reflections are thereby not considered uniformly for one surface, but estimated individually for any pixel of a fisheye image rendered by the graphics engine. The pixels are weighted in accordance to spherical angles to calculate the radiation fluxes (Fröhlich and Matzarakis 2018).

SkyHelios does comprise a diagnostic wind model after (Röckle 1990) with modifications after (Singh et al. 2008) to estimate wind speed (v) and -direction (WD).

Using all this information together, SkyHelios is capable of estimating the thermal indices PET, PT and UTCI spatially resolved in high spatial resolution of e.g. 1 m on 1 m.

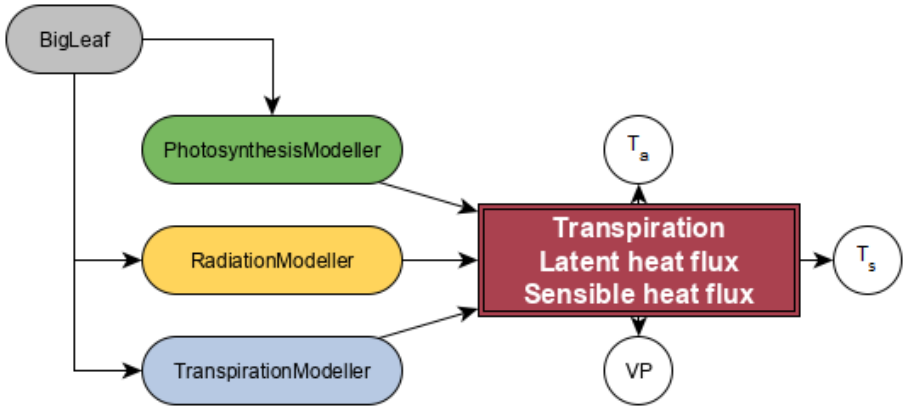


Figure 3. Controlling mechanism of urban green on physiological response, as planned for SkyHelios.

Further development of SkyHelios

In order to analyze the influence of urban green within the complex urban morphology on thermal bioclimate, it is necessary to quantify the physiological response of urban trees to prevailing weather conditions (especially PAR). The physiological response is modelled by a PhotosynthesisModeller, which is triggered by a RadiationModeller. The physical outcome (i.e. transpiration rate, latent and sensible heat fluxes), based on the energy balance for urban trees, is calculated with a TranspirationModeller which is coupled to given atmospheric conditions (i.e. gradient of humidity, wind-speed and -direction and air temperature) (Figure 3). The spatial extend of the vegetational impact on the urban environment depends on the wind field,

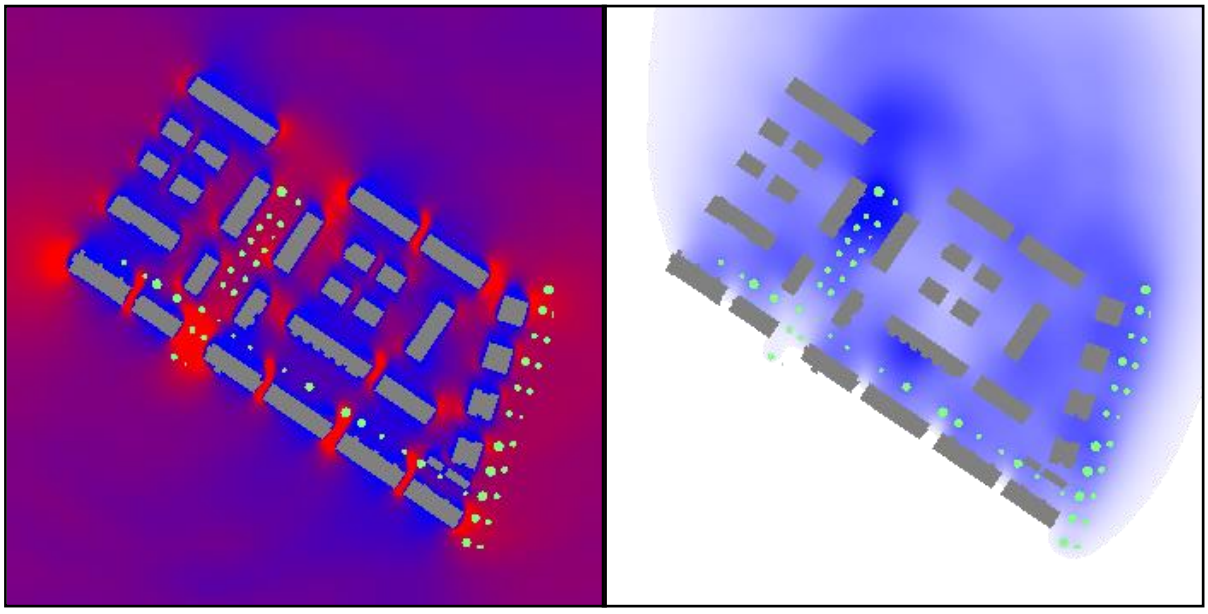


Figure 4. Left: Prognostic wind model based on the Lattice Boltzmann Method. Right: Production of water vapor by urban trees and spatial dispersion based on the wind model. Incident wind from left south.

characteristics of dispersion of humidity and convective and advective heat transfer.
Beside the existing diagnostic wind model, a new prognostic wind model after (Succi 2009; Lallemand and Luo 2000; Obrecht et al. 2015) is under current development. This new wind model will be implemented based on computational fluid dynamics by Lattice Boltzmann. The prognostic model will allow for the assessment of spatial dispersion of water vapor, which is transpired by urban trees as well as heat transfer from leafs (i.e. leaf surface temperature) to the atmosphere (i.e. air temperature) (Figure 4).

Results

To analyze the effect of urban green on human thermal comfort, the thermal index PET, was calculated for the sample study area Rieselfeld in Freiburg, Germany. PET was calculated and mapped for the 1st of April and 1st of July at 13:00 LST. The scenario is set up with constant air temperature of 20 °C, constant vapor pressure of 11.7 hPa, incident wind speed of 2.0 m/s from south (180 °) and constant cloud cover of 0.0 octas. The solar azimuth (φ, °) and solar altitude angle (θ, °) are determined by date and time (in April: φ = 222 °, θ = 38 °; in July: φ = 162 °, θ = 64 °).

The wind speed varies between 0.0 m/s and 2.8 m/s throughout the study area with 0.8 m/s on average (Figure 5).

PET varies in April between 18.7 °C and 44.6 °C with an average of 29.2 °C and in July between 19.6 °C and 47.6 °C with an average of 30.0 °C (Figure 6). The effect of shading and the impact of decreased wind speed on PET is observable on the lee side of each building.

In April, an area of 9796.19 m^2 of 78659.98 m^2 is shaded (12.45 %, 1052.06 m^2 by trees (1.33 %) and 8744.13 m^2 by buildings (11.11 %)). In July, an area of 5430.05 m^2 of 78659.98 m^2 is shaded (6.90 %, 981.36 m^2 by trees (1.24 %) and 4448.69 m^2 by buildings (5.65 %)). The shaded area by trees is decreased by 70.70 m^2 (6.72 %) while by buildings by 4295.44 m^2 (49.12 %), due to raise of the solar altitude angle from April to July.

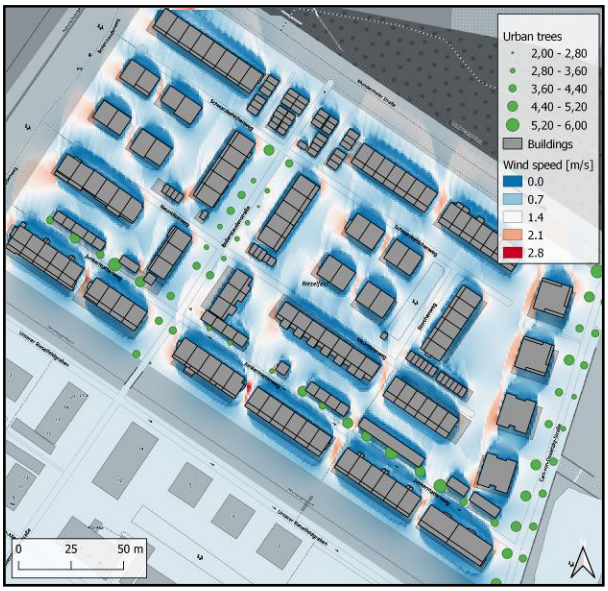


Figure 5. Diagnostic wind model showing wind speed with incident wind from south.

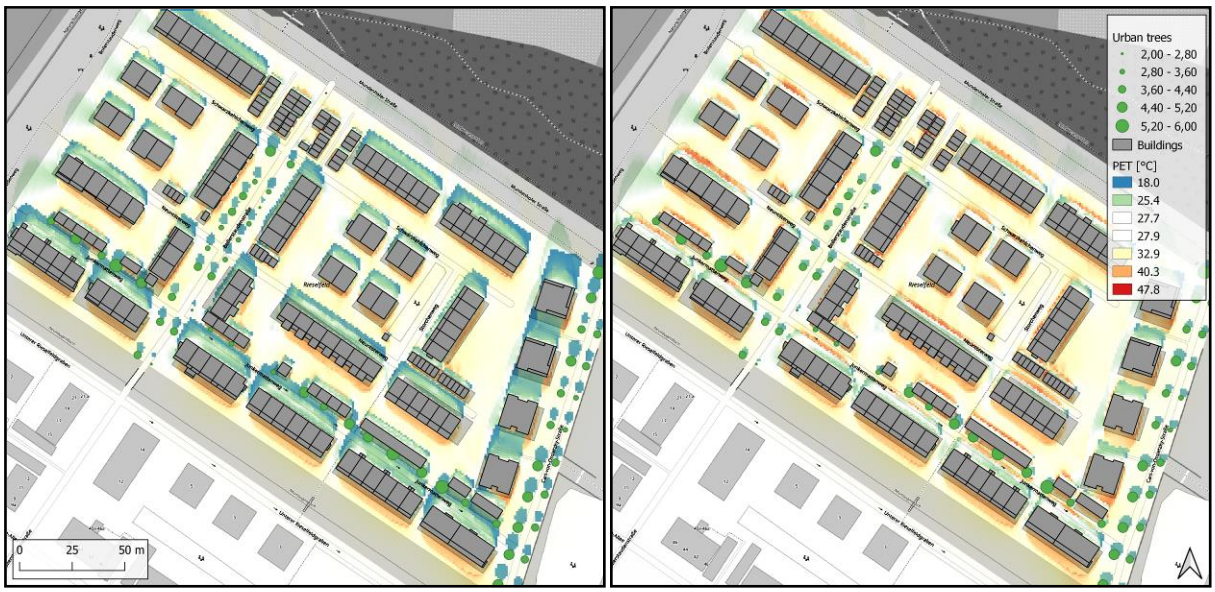


Figure 6. Thermal comfort, based on PET in 1.1 m above ground level for a residential neighborhood in Freiburg, Germany at 13:00 LST, 1st of April (left) and 1st of July (right)

Discussion

Spatially resolved thermal indices visualized as thermal comfort maps can help to identify areas that need to be improved in terms of thermal comfort. As they can be calculated very fast by the SkyHelios model, several scenarios can be analyzed to support urban planning as shown in this study. The rapid assessment method also allows for the calculation of long time series.

The results of the case study presented here indicate that thermal (heat) stress can be reduced most effectively by providing shade. Shaded areas can be generated by buildings, as well as by urban trees. While both are shown to reduce PET quite effectively, areas shaded by trees are found to be slightly more comfortable in terms of PET in this case study. This is in very good agreement with various other studies investigating the impact of urban green on heat stress represented by some thermal index, e.g. (de Abreu-Harbich, Labaki, and Matzarakis 2015; Santos Nouri et al. 2018). In addition, urban trees provide shade in the outdoor areas, where people are typically residing in residential neighborhoods: pavements, playgrounds. The shade of trees, compared to buildings, occurs mostly below the trees due to high solar altitude angle during midday in summer. The impact of outdoor shading by buildings is therefore of significant minor magnitude compared to trees, especially in midday of the summer time and in low latitude regions. This means, urban trees are more effective in providing shade in summer compared to buildings, while buildings are more effective in seasons with low solar altitude angle.

It must be noted, that the SkyHelios model currently does not consider spatial variations in T_a and VP for the calculation of thermal indices. Surfaces in the model domain are not coupled to the atmosphere with respect to heat transfer and mass transfer. The cooling effect by transpiration on leaf surface temperature is (Fröhlich, Gangwisch, and Matzarakis 2019).

Conclusion

Using all this information together, SkyHelios will be capable of estimating the thermal indices PET, PT and UTCI spatially resolved in high spatial resolution of e.g. 1 m on 1 m under consideration of the physiological processes of urban vegetation. Overall, it is shown that micro scale models like SkyHelios can provide valuable information for architects and urban planners.

Acknowledgments

MOSAIK: One of the authors wants to acknowledge the funding by the German Federal Ministry of Education and Research through the MOSAIK (Model-based city planning and application in climate change) Project.

GreenLung: One of the authors wants to acknowledge the funding by the German Federal Ministry of Education and Research through the GreenLung Project ("Inter- and transdisciplinary approaches to develop strategies for increasing the resilience of trees in growing cities and urban regions").

References

Abreu-Harbich, L. V. de, L. C. Labaki, and A. Matzarakis. 2015. "Effect of Tree Planting Design and Tree Species on Human Thermal Comfort in the Tropics." *Landscape and Urban Planning* 138 (June): 99–109.

Akbari, H. 2002. "Shade Trees Reduce Building Energy Use and CO2 Emissions from Power Plants." *Environmental Pollution (Barking, Essex: 1987)* 116 Suppl 1: S119-126.

Akbari, H., M. Pomerantz, and H. Taha. 2001. "Cool Surfaces and Shade Trees to Reduce Energy Use and Improve Air Quality in Urban Areas." *Solar Energy* 70 (3): 295–310.

Bowler, D. E., L. Buyung-Ali, T. M. Knight, and A. S. Pullin. 2010. "Urban Greening to Cool Towns and Cities: A Systematic Review of the Empirical Evidence." *Landscape and Urban Planning* 97 (3): 147–55.

Chen, Y.-C., and A. Matzarakis. 2018. "Modified Physiologically Equivalent Temperature—Basics and Applications for Western European Climate." *Theoretical and Applied Climatology* 132 (3–4): 1275–89.

Dobbs, C., F. J. Escobedo, and W. C. Zipperer. 2011. "A Framework for Developing Urban Forest Ecosystem Services and Goods Indicators." *Landscape and Urban Planning* 99 (3–4): 196–206.

Fanger, P. O. 1972. *Thermal Comfort: Analysis and Applications in Environmental Engineering*. New York: McGraw-Hill.

Ferrini, F., C. van den Bosch, and A. Fini, eds. 2017. *Routledge Handbook of Urban Forestry*. London ; New York: Routledge/Taylor & Francis.

Fröhlich, D., M. Gangwisch, and A. Matzarakis. 2019. "Effect of Radiation and Wind on Thermal Comfort in Urban Environments - Application of the RayMan and SkyHelios Model." *Urban Climate* 27 (March): 1–7.

Fröhlich, D., and A. Matzarakis. 2013. "Modeling of Changes in Thermal Bioclimate: Examples Based on Urban Spaces in Freiburg, Germany." *Theoretical and Applied Climatology* 111 (3–4): 547–58.

———. 2018. "Spatial Estimation of Thermal Indices in Urban Areas—Basics of the SkyHelios Model." *Atmosphere* 9 (6): 209.

Höppe, P. 1999. "The Physiological Equivalent Temperature - a Universal Index for the Biometeorological Assessment of the Thermal Environment." *International Journal of Biometeorology* 43 (2): 71–75.

Hwang, R.-L., T.-P. Lin, and A. Matzarakis. 2011. "Seasonal Effects of Urban Street Shading on Long-Term Outdoor Thermal Comfort." *Building and Environment* 46 (4): 863–70.

Jendritzky, G., R. de Dear, and G. Havenith. 2012. "UTCI—Why Another Thermal Index?" *International Journal of Biometeorology* 56 (3): 421–28.

Ketterer, C., and A. Matzarakis. 2016. "Mapping the Physiologically Equivalent Temperature in Urban Areas Using Artificial Neural Network." *Landscape and Urban Planning* 150 (June): 1–9.

Kjelgren, R. K., and J. R. Clark. 1992. "Microclimates and Tree Growth in Three Urban Spaces." *Journal of Environmental Horticulture* 10 (3): 139–45.

Kjelgren, R., and T. Montague. 1998. "Urban Tree Transpiration over Turf and Asphalt Surfaces." *Atmospheric Environment*, Conference on the Benefits of the Urban Forest, 32 (1): 35–41.

Lallemand, P., and L.-S. Luo. 2000. "Theory of the Lattice Boltzmann Method: Dispersion, Dissipation, Isotropy, Galilean Invariance, and Stability." *Physical Review E* 61 (6): 6546–62.

Leuzinger, S., R. Vogt, and C. Körner. 2010. "Tree Surface Temperature in an Urban Environment." *Agricultural and Forest Meteorology* 150 (1): 56–62.

Matuschek, O., and A. Matzarakis. 2010. "Estimation of Sky View Factor in Complex Environment as a Tool for Applied Climatological Studies." *Berichte Des Meteorologischen Instituts Der Albert-Ludwigs-Universität Freiburg* 20: 534–539.

Matzarakis, A., and O. Matuschek. 2011. "Sky View Factor as a Parameter in Applied Climatology Rapid Estimation by the SkyHelios Model." *Meteorologische Zeitschrift* 20 (1): 39–45.

Matzarakis, A., H. Mayer, and M. G. Iziomon. 1999. "Applications of a Universal Thermal Index: Physiological Equivalent Temperature." *International Journal of Biometeorology* 43 (2): 76–84.

Matzarakis, A., F. Rutz, and H. Mayer. 2007. "Modelling Radiation Fluxes in Simple and Complex Environments—Application of the RayMan Model." *International Journal of Biometeorology* 51 (4): 323–34.

———. 2010. "Modelling Radiation Fluxes in Simple and Complex Environments: Basics of the RayMan Model." *International Journal of Biometeorology* 54 (2): 131–39.

Obrecht, C., F. Kuznik, L. Merlier, J.-J. Roux, and B. Tourancheau. 2015. "Towards Aeraulic Simulations at Urban Scale Using the Lattice Boltzmann Method." *Environmental Fluid Mechanics* 15 (4): 753–70.

Ogre Development Team. 2019. "OGRE - Open Source 3D Graphics Engine."

Röckle, Rainer. 1990. "Bestimmung der Strömungsverhältnisse im Bereich komplexer Bebauungsstrukturen." Darmstadt.

Santos Nouri, A., D. Fröhlich, M. Matos Silva, and A. Matzarakis. 2018. "The Impact of Tipuana Tipu Species on Local Human Thermal Comfort Thresholds in Different Urban Canyon Cases in Mediterranean Climates: Lisbon, Portugal." *Atmosphere* 9 (1): 12.

Shashua-Bar, L., D. Pearlmutter, and E. Erell. 2011. "The Influence of Trees and Grass on Outdoor Thermal Comfort in a Hot-Arid Environment." *International Journal of Climatology* 31 (10): 1498–1506.

Singh, B., B. S. Hansen, M. J. Brown, and E. R. Pardyjak. 2008. "Evaluation of the QUIC-URB Fast Response Urban Wind Model for a Cubical Building Array and Wide Building Street Canyon." *Environmental Fluid Mechanics* 8 (4): 281–312.

Song, B., and K. Park. 2015. "Contribution of Greening and High-Albedo Coatings to Improvements in the Thermal Environment in Complex Urban Areas." *Advances in Meteorology* 2015: 1–14.

Staiger, H., G. Laschewski, and A. Grätz. 2012. "The Perceived Temperature – a Versatile Index for the Assessment of the Human Thermal Environment. Part A: Scientific Basics." *International Journal of Biometeorology* 56 (1): 165–76.

Staiger, H., G. Laschewski, and A. Matzarakis. 2019. "Selection of Appropriate Thermal Indices for Applications in Human Biometeorological Studies." *Atmosphere* 10 (1): 18.

Succi, S. 2009. *The Lattice Boltzmann Equation: For Fluid Dynamics and Beyond*. Reprinted. Numerical Mathematics and Scientific Computation. Oxford: Clarendon Press.

Assessment of Terrace Gardens as Modifiers of Building Microclimate

Chitra Chidambaram[1]*, Sharda University (India)*
Pranjali Varshney, Sharda University (India)
Sakshi Kumar, Sharda University (India)
Surabhi S. Nath, IIIT Delhi (India)

ABSTRACT

With rampant urbanization, permeable and soft grounds with vegetation are being replaced by impervious hard concrete surfaces that cause heat islands and floods, adversely impacting the quality of urban living. Terrace garden, reducing heat gain from the roofs and promoting greening at higher levels of built structures is seen as one of the key mitigating strategies for modifying building microclimate and improving urban health. We have undertaken a research project to quantitatively assess the value of a terrace garden to a building microclimate and explore its potential for organic farming. For the experimental research, a garden patch of about 15 m^2 in area, a typical size available in most urban terraces is developed on the terrace of an eight floored building. As conduction is the principal mode of heat gain in top floors, surface temperatures are measured on and below the roof, with and without a terrace garden, using thermocouples connected to a data logger. The data of surface temperature and the vegetable harvest is collected for one year from July 2018 to June 2019 and the paper presents the analysis. The results show that the terrace garden does stabilize and reduce the ceiling temperature of a concrete roof from 2°C in February to 7°C in the hottest month of June and provide nearly 400 grams of fresh monthly harvest per m^2 of garden. The study quantitatively demonstrates the benefits of a terrace garden in enhancing building microclimate and mitigating urban heat islands otherwise caused by bare concrete building roofs.

Introduction

Cities today are built jungles with very little greenery in their landscape. Besides, serious consequences like heat island effect and urban flooding, multi-storeyed concrete structures consume enormous amount of energy for air conditioning. Further, with growing demands on urban land, the farmlands in the urban fringe areas are lost, impacting the daily life of urban dwellers without fresh garden produce. This has led urban planners and builder community to look for solutions that can provide gardens within city precincts and enhance built urban environments (EMPRI 2017, USEPA 2008).

Architects and sustainable building professionals greatly promote rooftop gardens for their heat insulating value to the building (Hussain, Nizarudin, and Tukiman 2014). There have been many studies on terrace garden in an urban setting from different parts of the world available in literature (Chow 2016, Kamarulzaman 2014). These studies mostly focus on some aspect of environmental benefit from roof top greening or review of the field at large. It is felt that terrace gardens must be scientifically researched to study their potential as modifiers of building microclimate locally and explore the feasibility for gardening on terraces to contribute towards urban vertical farming (Barecca 2016). Towards this end, we initiated an experimental research project at our institute in Greater Noida, U.P. in 2018-19 for quantitative assessment of

[1] Corresponding Author: [chitra.chidambaram@sharda.ac.in], [9810977814].

conductive heat transfer mitigation in and out of a building, and additionally record the amount of fresh vegetable harvested by the terrace garden.

Background

Terrace gardens are gardens on building roofs or parts thereof. They are developed in many ways from the casual arrangement of few potted plants placed on the terrace to laying sophisticated gardens with integrated water proofing, root barrier, drainage layers, filter membrane and drip irrigation (Patel, Yadav, and Singh 2019). The growing medium again vary from normal soil to compost and specialized mixes of nutrients and light fibers like coir, cocopete etc. While any green on terrace would contribute to modifying building microclimate, the casual ones are often surmounted by issues of drainage, dampness and structure loads (Wang 2018).

A simple well laid out terrace garden bed consists of growing medium held by a fabric over a drainage mat and bounded by open brickwork all around for adequate air movement. Such terrace gardens can be easily maintained and seasonal vegetables and herbs required for a small family consumption can be conveniently harvested.

The thermal properties of the roofs are greatly modified by the gardens due to the growing medium and vegetation it holds. While conduction is the primary heat exchange process through a conventional roof, terrace gardens demonstrate convection, scattered radiation, evapo-transpiration and thermal mass property to modify the building microclimate. Figure 1 demonstrates these various processes involved.

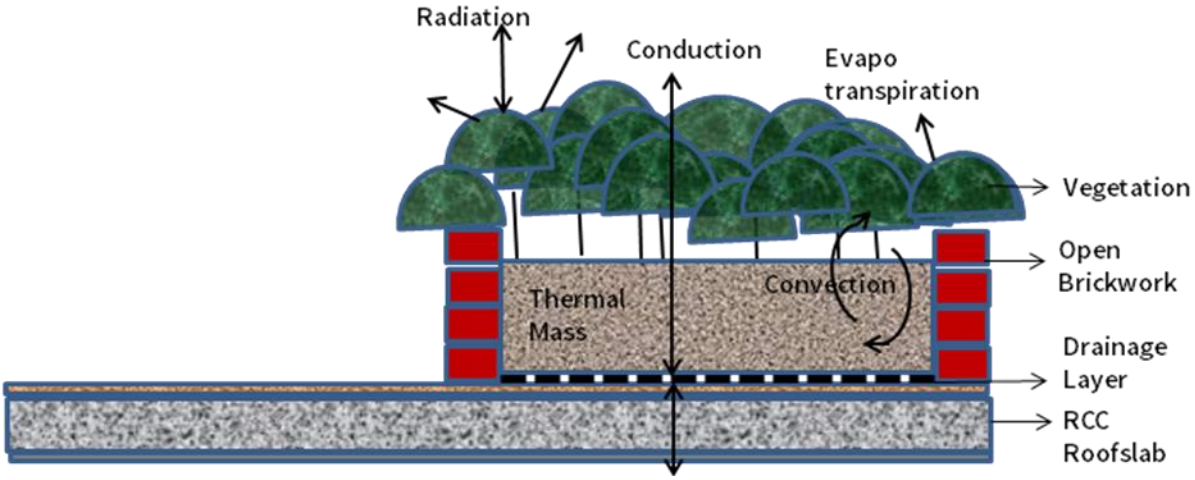


Figure 1. Terrace Garden as a thermal system

Conduction is the heat transferred through a solid medium and the direction and rate of transfer depends on the temperature gradient, material thickness and conductivity. RCC roofs with good weather proof course and appropriate surface treatment do modify and regulate heat transfer. Terrace gardens on RCC roofs add thickness and enhance the thermal performance due to its lesser conductivity. Convection is the heat transferred through liquid and gaseous medium and the flow of air and water in the growing medium and vegetation of the terrace garden demonstrates this phenomenon. The texture and massing of foliage of the vegetation scatter and shade reducing the intensity of incident solar radiation on the roof. The thermal mass of the

garden with the growing medium stores heat and reduces the variability of the roof temperature. Also, the evaporation and evapo-transpiration through the vegetation takes away heat from the built environment and cools the surface.

Experimental Set-Up

The terrace garden was set up on the terrace of an eight floor building in Sharda University Campus at Greater Noida. The location for setting up the garden was based on the orientation, availability of access for maintenance, access control and facility for water supply and drainage. South facing location on the terrace was preferred for sustenance of the garden in the winter months. The scope and scale of the project was kept small to fit the low budget and also demonstrate the effectiveness of laying such gardens on terraces of residential apartment blocks with limited budget and free space.

The experimental set-up consisted of four thermocouple sensor modules, two on the terrace and two fixed to the corresponding positions on the ceiling below. The two positions were within the ceiling of the same room. The room has a single window which is kept mostly closed to measure primarily the conductive heat. The radiation from the window pane has very little effect as they are well shaded. The room was unoccupied and the set-up remained undisturbed through the experimental study.

The garden is planned in an area of 15 m^2, laid in three beds of about 5 m^2 each, separated by walkways 0.6 m wide to water and maintain the garden (Figure 2a). The garden bed was outlined by 300 mm high open brickwork to permit air circulation. The drainage layer, about 35 mm thick, was laid on top of the finished terrace surface. The fine filter fabric was spread on the drainage layer to hold the growing medium consisting of soil, compost, nutrients and cocopeat. Cocopeat reduces the weight but adds bulk and provides a good hold for the roots. The first planting consisted of seasonal vegetables like spinach, chulai, coriander, radish, brinjal, and carrots. Subsequent planting included other seasonal vegetables like zucchini, gourd, spring onion, fenugreek and cherry tomatoes (Figure 2b).



a b

Figure 2a, 2b. Terrace Garden planting and harvest

The temperature recording equipment consisted of two sets of surface module fixed to the roof surface on the terrace and on the ceiling of the room below. One sensor module was fixed below one of the garden beds while the second sensor module which served as control module

(to compare the surface temperature below the garden to that of normal roof) was fixed outside the garden, about 5 m away from the other sensor. The exact positions of these sensors were located on the ceiling below and sensor modules were fixed at those points to measure corresponding surface ceiling temperature. The connections from the sensors were drawn to a data logger placed in the room below. The data logger was connected to a power supply and had the start and stop facility, real time digital display and a USB for storing data set to any time period. The data was retrieved periodically from the USB and analysed.

Data Recording and Analysis

The equipment was initially set to record the data at the pulse rate of every 5 minutes. The setting was subsequently changed to every 15 minutes for easier handling. The data was available in .csv format with date, time and the four surface temperatures (t1, t2, t3 and t4) in ^{o}C. (Table1). The data was compiled and analysed every month.

Table 1. Sample of recorded surface temperature data from the four sensors

TIME	DATE	t1	t2	t3	t4
$13:38:50	03/07/2018	0	0	0	0
$13:43:02	03/07/2018	32.5	32.4	41.3	41.9
$13:48:03	03/07/2018	32.5	32.4	40.2	40.8
$13:53:02	03/07/2018	32.5	32.5	39.2	40.4
$13:58:03	03/07/2018	32.5	32.5	38.8	39.3
$14:03:04	03/07/2018	32.6	32.5	38.8	39.2
$14:08:03	03/07/2018	32.7	32.6	38	39.2
$14:13:04	03/07/2018	32.6	32.6	38.5	39.3
$14:18:03	03/07/2018	32.8	32.6	38.5	39.6
$14:23:04	03/07/2018	32.9	32.6	39.4	40.4
$14:28:03	03/07/2018	32.9	32.6	40.1	41.1
$14:33:04	03/07/2018	33.1	32.6	39.6	40.9
$14:38:03	03/07/2018	33.1	32.6	42.3	43.7

While the experimental set-up was simple, there were issues like intermittent power cuts, resulting in some missing data. Due to the severed cable connection and malfunctioning of sensors, the data from the months of December and January were not recorded. Further, mishandling of equipment by terrace users and brief clearing of garden due to pests in February have also impacted the recording of data.

For the data analysis, a code was written in Python to handle over 40000 temperature data entries recorded during the year. As the arithmetic mean of such data gave erroneous values due to outliers and missing data, the median values were used for the analysis. For observing the trend, the monthly median values for every hour was obtained. Surface temperature curve for data from each sensor was plotted against the time of the day for all months for which the data was available. The garden harvest was also weighed and the records maintained as in Table 2.

Table 2. Terrace garden planting and harvest details

PLANTING DETAILS		HARVEST DETAILS		
Date	Item	Date	Item	Harvesting quantity (kg)
24.09.18	Palak	18.10.18	Palak	2.5
	Chulai		Chulai	1
	Daniya		Daniya	0.1
	Red Raddish	25.10.18	Palak	2.5
	White Raddish		Chulai	3
	Red Carrot		Daniya	0.1
	Beet root		Red Raddish	1.2
	Garlic chives	30.11.18	Brinjal	2
	Lemon Grass		Red Raddish	0.25
	Curry leaves		White Raddish	1.5
5.10.18	Methi		Beet root	1
	Turnip		Lemon Grass	0.1
	Brinjal	25.12.18	Carrot	2.5
	Tomato		Palak	3
	Saraso		Lettuce	0.7
	Celery		Turnip	0.75
	Mint		Tomato	1.2
25.10.18	Tomato		Sarso	1.5
15.11.18	Lettuce	17.02.19	Palak	1.5
	Dhania		Methi	0.5
	Brinjal		Lettuce	0.3
12.01.19	Palak		Brinjal	2
	Lettuce	19.3.19	Mint	0.3
	Cherry Tomato		Cherry tomato	0.5
13.2.19	Chulai		Lettuce	0.2
	Brinjal	25.3.19	Chulai	2.2
	Cherry Tomatoes	28.4.19	Cherry tomato	0.25
30.4.19	Brinjal		Brinjal	2.5
	Common Grass	12.6.19	Brinjal	1.5
		Total		**36.65**
Note: No new plantation and harvesting was done in the month of May. Only Green bed was maintained till June.				

Results and Discussion

Surface temperature analysis. The analysis of thermal performance of the terrace garden was based on thermocouple recordings of surface temperature data t1, t2, t3 and t4. The difference in temperatures with and without garden is a suitable indicator that can demonstrate the effect of the terrace garden. Extension to heat flux or heat gain/loss calculations would be possible if the thermal resistivity factor of the roof and the number of operational hours is known. For the discussion, the following nomenclature is used:

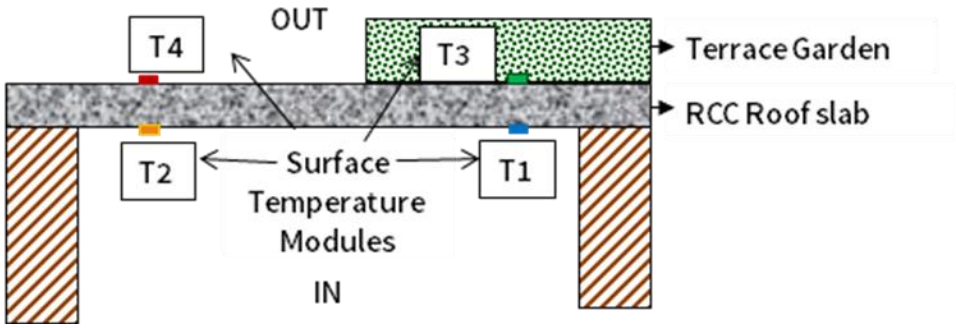


Figure 3. Graphical representation of location of the surface temperature module

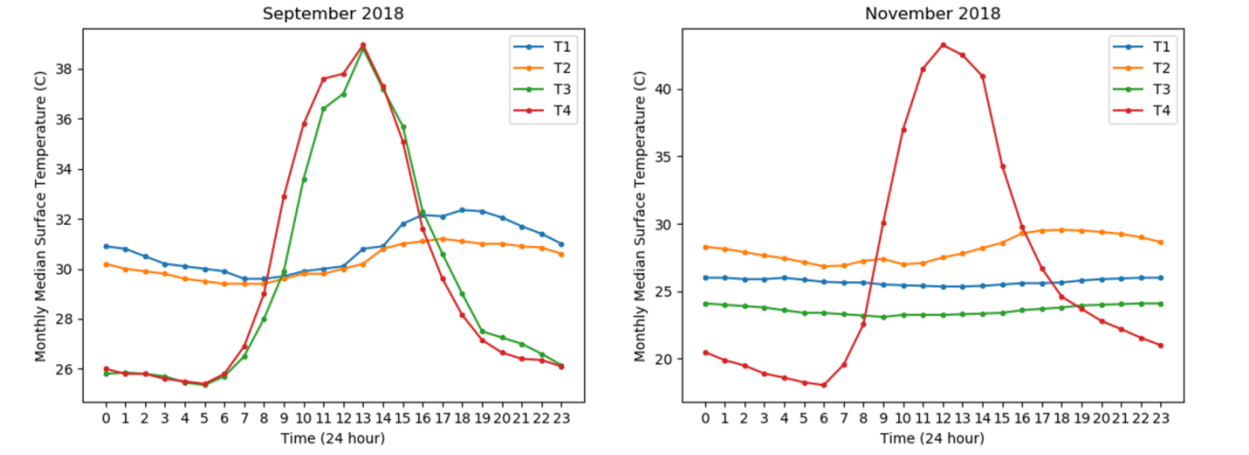
- T1 represents the monthly median surface temperature t1, Inside below garden (blue)
- T2 represents the monthly median surface temperature t2, Inside outside garden (orange)
- T3 represents the monthly median surface temperature t3, Outside below garden (green)
- T4 represents the monthly median surface temperature t4, Outside outside garden (red)

The four temperatures T1, T2, T3 and T4 are coded in four colours of blue, orange, green and red respectively as indicated above.

Before the garden was laid: In the months of July to September 2018 (Figure 4a), T3 and T4 clearly showed the highly variable surface temperatures through the day ranging from 25°C to 40°C peaking at 13 hours. The corresponding T1 and T2 showed significantly lesser variation in temperatures ranging between 30°C to 33°C peaking at 18 hours. A lag of 5 hours observed in peak temperatures can be attributed to the thermal mass of the RCC roof. The insignificant variation in T2 and T1 through the time may be due to the closing of the windows in the room preventing convective transfers which could affect the recorded conductive surface temperatures.

After the garden was laid: In November 2018 (Figure 4b), at the peak hour of 12 hours the temperature T4 outside garden was 44°C when temperature T3 outside below garden dropped down to around 24°C through the day. The significant reduction in temperature and variation in T3 may be attributed to the garden and the various processes of heat exchange like convection, evapo-transpiration and thermal mass it entails. T2 varied from 27 to 30°C peaking at around 18

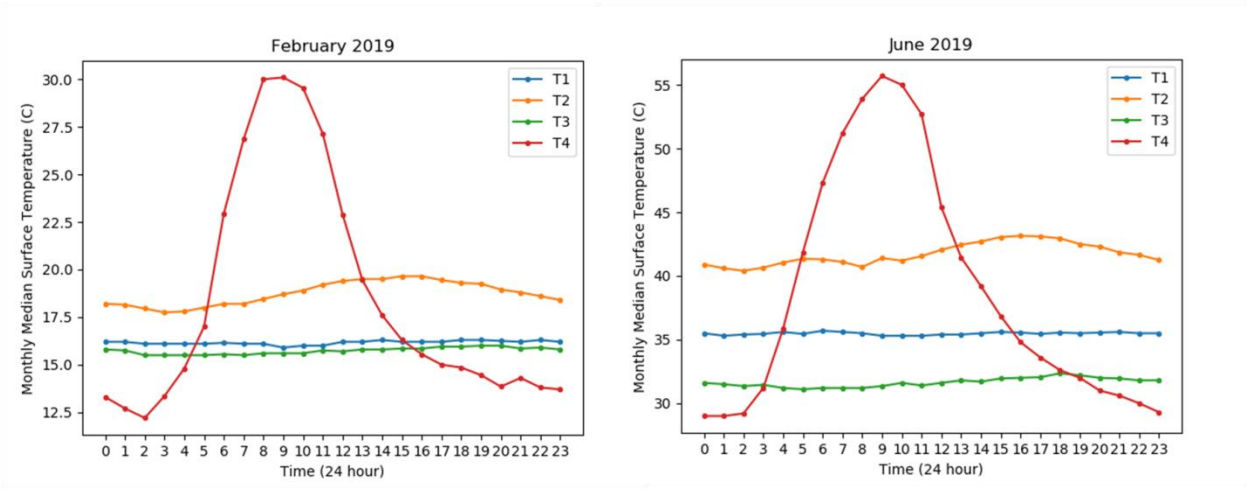
hours whereas T1 remained constant at 26°C, due to the moderating influence of the terrace garden.



a b

Figure 3a, 4b. Plots of the monthly median surface temperature vs time of the day for September and November 2018

In December and January there was no data recorded due to the malfunctioning of the sensors. In the colder month of February 2019 (Figure 5a), T4 showed a monthly average value varying from 11 to 30°C through the day, peaking as early as at 9 hours in the morning. T3 recorded 16°C through the day while T1 recorded 16.5°C, maintaining the marginal thermal gradient and drawing heat away from the room. T2 was slightly higher and varied from 17 to 19.5°C showing that the terrace garden had induced a cooling effect of about 0.5 to 3°C on the inner ceiling temperature.



a b

Figure 5a, 5b. Plots of the monthly median surface temperature vs time of the day for February and June 2019

In the hotter months of April and May, T4 showed higher temperatures and peaked around 12 hours with 53°C while inside T2 varied between 34 to 37°C. Terrace garden induced cooling to a greater extent and T1 recorded around 31°C, nearly 3 to 6 degrees below T2.

In June 2019, the hottest month on our record (Figure 5b), the outside surface temperature T4 varied from 28 to 56°C in the day while T3 remained constant at nearly 32°C through the day. The inside ceiling temperature T2 varied between 40 and 42°C peaking at 4 PM but T1 temperature inside below the garden was uniform at 35°C, almost 5 to 7°C cooler than T2. The effectiveness of the garden is felt most in this period.

The heat flux generated by the difference in surface temperatures after the laying of the garden (T3 is always lower than T1) demonstrate that throughout the hot months, the direction of heat transfer below the garden is from the ceiling surface T1 to T3, the roof surface, ensuring cooling of the inside space.

Vegetable harvest: The data from the harvest of vegetable produce also varied with the different months. While the first planting of October-November had very rich yield, the cold months were not as much. In February, the pest attacked the brinjal variety and had to be replanted. In March-April the garden was at its best and gave the maximum yield. In May-June, due to hot weather not many vegetables were planted. The garden beds were maintained green through common grasses and some brinjal planting nearly 500 mm tall. The total harvest obtained from October to April of all different vegetables in all six months on record, from the total garden area of 15 m^2 was close to 36.65 kilograms. This gives a net productivity of 2.44 kgs per m^2 of garden for 6 months and 400 gm per m^2 per month. While this figure is rather modest, the benefits of health and joy of growing one's own garden cannot be quantified.

Conclusion

Hard concrete roofs absorb solar radiation and transfer through conduction and convection to the surrounding area thus contributing to urban heat island effect. Terrace gardens reduce heat island effect by replacing heat absorbing surfaces with plants and shrubs that shade the roof from solar radiation, cool the air through evapotranspiration and also provide insulating effects to the building. The study focuses on assessment of terrace garden as modifier of building microclimate based on the analysis of surface temperatures on the roof and below at the ceiling in the presence and absence of the terrace garden. It also captures the harvest potential and aesthetic appeal of such terraces.

The surface temperature data clearly shows the cooling effect of the terrace garden during the summer months. The inside ceiling surface temperature below the garden during the month of March and April was between 3 – 6°C lower than at a point below the RCC roof without the garden. In the month of June, the hottest month recorded in our data, the ceiling below the garden was cooler by nearly 5 – 7°C. The garden also equalized and significantly reduced the variation in inside surface temperatures throughout the day. As the data of the coldest months are not available, it would be interesting to determine if the terrace garden would exert a cooling effect and to what extent or prevent cooling and add heat to the inside space in these months. That would be an objective of study for the coming winter months. The net monthly harvest obtained from the terrace garden was about 400 grams per m^2 per month. Clean air and lively terrace ambience are concomitant merits. As a further extension to this study, it is proposed to measure the ambient air temperatures and humidity, above the terrace garden and outside, to

assess the impact on ambient air, and demonstrate its mitigating influence on the heat island effect.

Thus, the ongoing study has, on a small scale, quantitatively assessed and brought out effectively the role of terrace garden in modifying building microclimate and mitigating heat island effect.

Acknowledgement

The authors are grateful to Sharda University for funding and supporting this research work.

References

1. Environmental Management and Policy Research Institute. (2017). Urban Planning Characteristics to Mitigate Climate Change in context of Urban heat island effect.
2. U.S. Environmental Protection Agency. 2008. "Green Roofs." In: Reducing Urban Heat Islands: Compendium of Strategies. Draft.
3. Hussain, M.R.M., Nizarudin, M.D., Tukiman, I., (2014). Landscape Design as Part of Green and Sustainable Design. Advanced Materials Research Vol (935). 277-280.
4. Chow, M. F., Abu Bakar M. F., (2016). A Review on the Development and Challenges of Green Roof Systems in Malaysia. World Academy of Science, Engineering and Technology International Journal of Architectural and Environmental Engineering 10 (1).16-20.
5. Kamarulzaman, N, et al (2014) Green Roof Concepts as a Passive Cooling Approach In Tropical Climate – An Overview. E3SWeb of Conferences (3). DOI 10.1051/e3sconf/20140301028
6. Barreca, F. (2016). Rooftop Gardening – A Solution for Energy Saving and Landscape Enhancement in Mediterranean Urban Areas. Procedia – Social and Behavioural Sciences 223. 720 – 725
7. Patel, A., Yadav, R., Singh, B., (2019) Study on Terrace Garden. International Journal of Trend in Research and Development. 6(1). 71 – 74.
8. Wang, W. (2018) Problems and Solutions in the Construction of Roof Garden in the Old Buildings. Proceedings from 8th International Conference on Social Network, Communication and Education (SNCE 2018). Advances in Computer Science Research Vol (83) 102-106

The seasonal thermal environment in urban park and surrounding urban spaces: A case study in Xi'an, China

Dixuan Ma, Xi'an Jiaotong University (China)
Yupeng Wang[1]*, Xi'an Jiaotong University (China)*
Zongzhou Zhu, Xi'an Jiaotong University (China)

ABSTRACT:

Urban parks are providing favorable conditions for sustainable urban planning, which is beneficial to the urban microclimate in different seasons. However, few studies have focused on the seasonal differences and comparisons between different urban spaces. In this research, air temperature, wind speed and wind direction of three seasons in the Xingqing Palace Park and its surrounding urban areas were measured in 2018. Through the analysis of air temperature, the actual seasonal thermal environment of park and surrounding urban spaces in different seasons is clarified. The temperature of high-rise building space and multi-story campus space in winter park is higher, but the temperature change of the multi-story residential building space is opposite to that of the park; the temperature difference between the inside and outside of the park is small and the fluctuation is diverse in spring; the internal temperature of park is slightly lower than the surrounding space in summer. In terms of application, surrounding urban spaces can be optimized in the future based on analysis results, so that the urban park can better exert its function by combining with the surrounding urban space, to mitigate the urban heat island (UHI) effect.

Introduction

With rapid growth of population and urban expansion, the urbanization process has led to significant modifications in the urban climate (Kalnay and Cai 2003). The most obvious feature is urban heat island (UHI), which is defined as the temperature difference measured in urban areas and surrounding rural areas (Oke 1982). As early as in 1978, this phenomenon was recognized in central business district and southern industrial district of Nagoya, Japan (Shionoya et al. 1978), which has continued to today. This phenomenon leads to the rise of temperature, which affects the outdoor thermal comfort of urban residents (Grimmond 2007).

Outdoor thermal comfort in urban area is known as an important contributor to the urban resident's well-being. It is affected by many factors, especially urban green areas, which can be used to mitigate UHI. Urban green areas such as shrines and parks are cooler than surrounding city areas, so that climatic conditions of urban areas can be improved and environmental stress produced by heat islands can be reduced, based on these urban green areas (Shionoya et al. 1978). It can greatly improve the outdoor thermal environment, as well as mitigate UHI effect by reducing air temperature in summer (Yan et al. 2018). As an important part of urban green areas, urban parks play an active role in mitigating UHI effect and improving the thermal environment. Akbari.

[1]Yupeng Wang: [wang-yupeng@mail.xjtu.edu.cn]

H. has found that an urban forest or park can ameliorate UHI and improve the climatic conditions of urban areas, by cooling air temperature in virtue of evapotranspiration and preventing incoming solar radiation from heating surfaces of surrounding buildings (Akbari 2002). Potchter et al. conducted a research on three different types of urban park with different greenbelt and forestland in summer in the Mediterranean city of Tel Aviv, Israel. The air temperature differences reached up to 3.51°C during the day between the built-up area and the urban park containing mature trees with a wide canopy (Potchter et al. 2006). Wong explored both the severity of UHI effect and cooling effect of green areas at the macro-level in Singapore, indicating a strong correlation between the temperature decrease and the appearance of urban parks in the city (Wong and Yu, 2005). Therefore, the urban park is an important factor to alleviate UHI effect and improve thermal environment.

However, the mitigation of UHI effect depends not only on the ecological effect of parks, but also on the diffusion of surrounding urban spaces. Howard first suggested considering the impact of urban form on microclimate (Howard 1833). In a study of Mohammad. T., the impact of different urban spatial forms, such as singular, linear and courtyard on microclimate with different comfort situations for pedestrians were demonstrated (Mohammad 2015). Steemers et al. proposed six archetypal generic urban forms for London, based on comparing the incident of solar radiation, built potential and daylight admission (Steemers et al. 1997). It is seen that the impact of urban space on the thermal environment cannot be ignored.

Similarly, in order to alleviate UHI, China’s urban green space construction has made great progress in the process of rapid urbanization (Song 2008). In China, most urban parks aim to meet the needs of urban beauty, so the construction of these parks lacks of the technical guidance for ecological function (Song and Binyi 2010). And accurate thermal comfort assessment is critical for the improvement of urban park and urban spaces (Chiru and Minghuang 2014). Therefore, it is necessary to understand the thermal environment difference between urban parks and surrounding urban space, so as to resolve environmental problems of urban sites and play the role of urban parks better.

Methodology

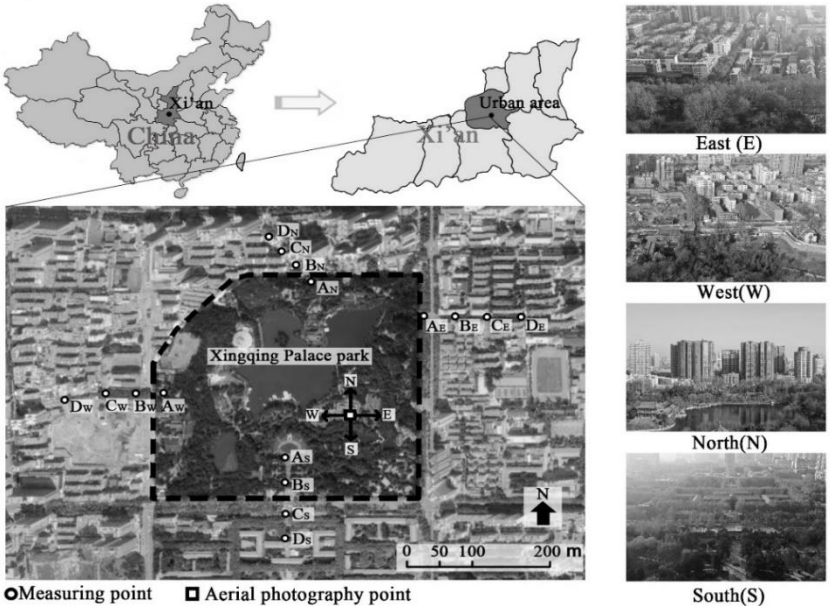
Study area

Xingqing Palace Park is the largest urban park in Xi'an, which covers an area of 520,000 square meters (including 100,000 square meters of water surface). The green area in the park is about 290,000 square meters, and the green coverage rate is up to 90% (according to Xi’an Xingqing Palace Park official website). The urban spatial forms around the park are different in spaces and functions. There are high-rise residential building spaces in the north, multi-story residential building spaces in the east, low-rise campus buildings in the south, and low-rise commercial building and multi-story residential building spaces as well as open spaces in the west (Figure 1).

Measurement

The hand-held mobile meteorological station is a portable meteorological observation instrument that is easy to carry, simple to operate, and integrates multiple meteorological elements (Figure 2). It can accurately measure five meteorological elements such as wind direction, wind speed, air pressure, air temperature and air humidity. On the top of the instrument, there are a wind vane measuring wind direction and a sensor recording wind speed. A temperature and humidity sensor in the small groove on the side of the instrument is used to record relevant values. Air temperature is the main analysis factor in this research. The measurement accuracy of instrument for air temperature is ± 0.2 °C.

According to the diversity of urban spatial forms around the park, field measurement has been carried out in this research. The measuring points are located in four directions of Xingqing Palace Park, with four measuring points in each side of the park. The distance between each measuring point is about 50 meters. A day of winter in 2017 (January 17, 2018), a day of spring (March 16, 2018) and a day of summer in 2018 (June 20, 2018) were selected for field measurement, which was conducted from 6 a.m. to 8 p.m. (9 p.m. in summer). The measurement was performed in four points per hour. Each measuring point in each direction was held for five minutes. And then, the instrument was moved to the next point at a constant speed. The measured environmental factors were recorded at the same height (1.5m).



a) Measuring point location b) Aerial photos of surrounding urban space

Figure 1. Location of Xingqing Palace Park and photos images around the park



Figure 2. Measuring point and measuring tools photos

In Figure 3, the Sky View Factor (SVF) images is listed as an auxiliary analysis of whether the measuring point is affected by the sun. In the SVF images, the visible sky range in the east and west of the park is smaller than that in the south and north of the park. One of the most visible image of the sky is the measuring point of the campus in the south, which makes the temperature affected by the sun. Moreover, the various urban parameters around each selected measuring point within 100 m are shown in Table 1.

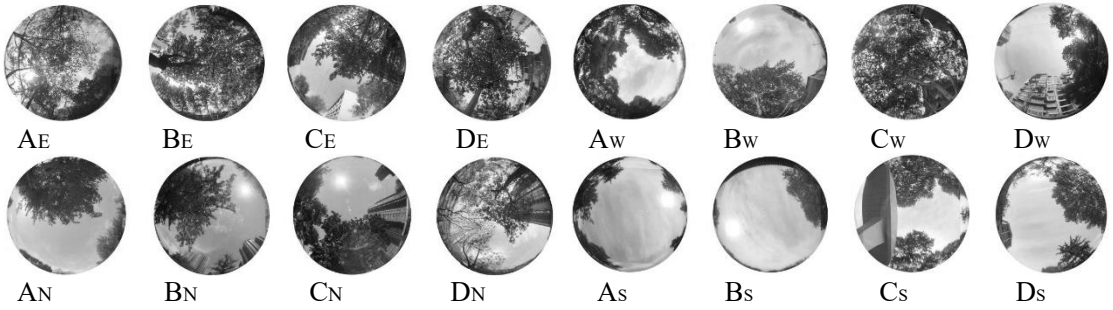


Figure 3. Sky View Factor (SVF) images of the measuring point (1.5m height)

Table 1. Detailed urban parameters within 100m around the measuring point

Direction	Measuring point	Centered on the measuring point, the radius of 100m				
		Building density	Average height of buildings(m)	Main building surface materials	Green coverage (%)	Road area ratio (%)
East	AE	0.14	18.64	Brick/Concrete	60.41	18.67
	BE	0.27	16.18	Brick/Concrete	14.74	7.96
	CE	0.26	15.92	Brick/Concrete	17.84	7.96
	DE	0.26	18.9	Brick/Concrete	22.99	7.96
West	AW	0.07	5.04	Brick	47.08	13.54
	BW	0.08	10.03	Brick	20.54	19.71
	CW	0.12	15.7	Brick/Concrete	13.37	5.73
	DW	0.22	10.82	Brick/Concrete	3.78	5.17
North	AN	0.23	15.08	Brick/Concrete	61.84	4.68
	BN	0.2	16.43	Brick/Concrete	44.62	10.76
	CN	0.15	64.76	Concrete	20.82	17.77

	DN	0.29	42.63	Concrete	9.5	10.82
South	AS	0.01	4	Brick	89.75	4.5
	BS	0.04	4	Brick	37.34	14.04
	CS	0.09	10.5	Brick	31.58	18.73
	DS	0.23	14	Brick	24.41	7.03

Source: The author organized factors according to Google Maps.

Data and analysis

Winter (January 17, 2018)

On the day of measurement, it was cloudy and foggy. The trend of air temperature changed in each measuring point of four directions can be seen from Figure 4.

In the east, the temperature at point AE is the lowest throughout the whole day. And the temperature at point BE is the highest between 11 a.m. and 5 p.m., which is up to 14.2°C at 3 p.m.. Although the SVF is high (Figure 3), the measuring points are affected by the midday sun. The same fluctuations are also visible at point Bw. All-day temperature changing trends of point CE and DE are similar. The maximum temperature difference between these two measuring points is 0.56°C (3 p.m.), and the minimum difference is only 0.03°C (10 a.m.). In addition, it can be seen from Table 1 that detailed urban parameters of the two measuring points are similar, which have an approximate impact on temperature. There is also a similar trend in the west. In the west, the temperature changes at four points before 11 a.m. are basically the same as the east. And the temperature at point AW in the park is also the lowest. The temperature trends of the other three points are similar to those in the east. But the maximum temperature at point BW (12.23°C) is lower than that of point BE (14.2°C). Although the SVF of point BW is lower (Figure 3), the green coverage is higher (Table 1). The results show that greening has a certain cooling effect on temperature. From the space of the low-rise and multi-story buildings in the east and west, the overall change is that the temperature of external park is higher than that in the internal.

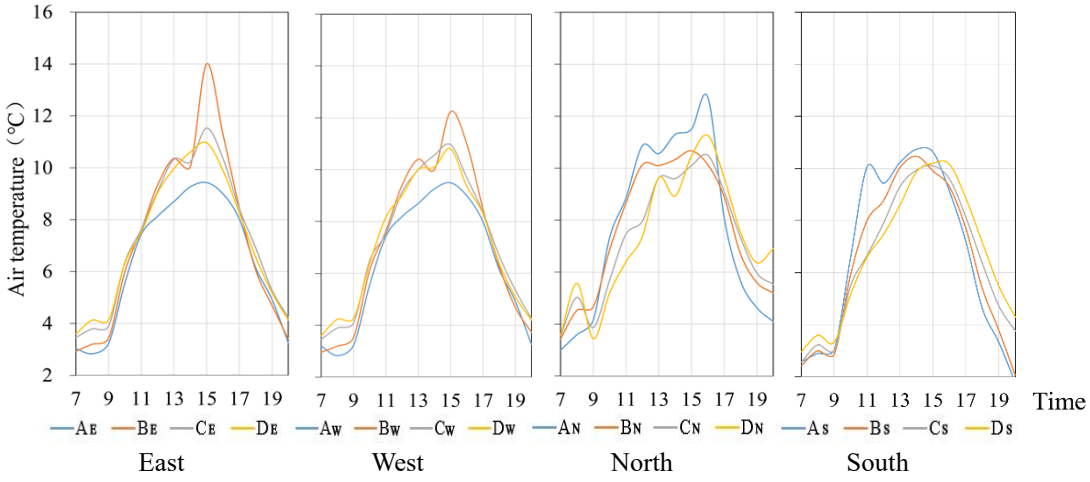


Figure 4. The temperature changes of measurement points in winter

But in the north and south, the temperature changing at the measuring points of the park is opposite to those outside the park. In the north, the building materials (Table 1) around point BN, CN and DN absorb heat during the day and release heat at night. In the south, the temperatures at point CS and DS are affected not only by the building materials, but also by trunks shadow. So, the temperature at these points are lower than other points in the park during the day. At noon, the overall temperature at point AN and AS are also higher than that of the other measured points. The highest temperature at point AS (10.74°C) is lower than that of point AN (12.73°C), because the green coverage at point AS is higher. The two points are both located on the open square inside the park. Although the green coverage rate is high, it is greatly affected by the sun.

In the surrounding urban spaces, the temperature at measuring point of the park is the lowest before sunrise and after sunset. Before 9 a.m., the temperature outside the park is higher than that inside the park. At noon, the temperature in the park is higher than that outside the park in the north and south spaces. After 5 p.m., the temperature in the park drops faster than that in the surrounding space. Although the trees are deciduous, with less shadow in winter, the shadow of trunks and branches still can affect the temperature inside and outside the park obviously. The temperature difference between the park and its surrounding area is beneficial to the local air circulation in Xi'an.

Spring (March 16, 2018)

On the day of measurement, it was sunny in the morning and became windy and cloudy in the afternoon. The changing trend of air temperature in four directions can be seen from Figure 5.

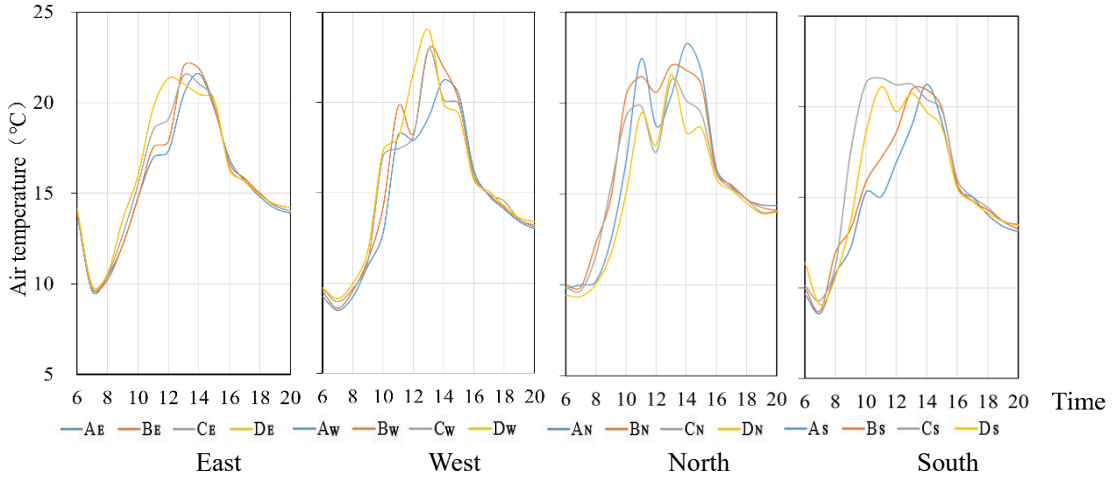


Figure 5. The temperature changes of measurement points in spring

In the east, from 8 a.m. to 1 p.m., the temperature at point AE near the park is the lowest. The changing trend at point BE and CE are similar. The maximum temperature difference between two points does not exceed 1°C. However, the temperature at point BE near the park is lower than that of point CE during this period. The SVF at point BE is higher than that of point CE (Figure 3), which can reduce the influence of sunlight. Temperature at point DE heats up fastest and may also be affected by the sun. After 2 p.m., point AE cools fastest, and the temperatures of other three

points drop slightly slower due to the factors of surrounding buildings and roads (Table 1). In the west, the temperature at point AW is the lowest before 2 p.m.. The maximum difference is 4.87 ℃, which appears at 1 p.m.. And then, the temperatures at point CW (from 22.93°C to 20.17°C) and DW (from 24.03°C to 19.93°C) drop quickly from 1 p.m. to 2 p.m., but the temperature at point BW falls (from 21.93°C to 20.17°C) slowly. Among them, SVF at point CW is higher (Figure 3) and the average building height at point DW is higher (Table 1), which can form shadows to block sunlight. These can have the temperature dropped. Although point BW has a high green coverage, its road area is also very large. It can be concluded that human factors play an important role in the temperature change, which suppresses the temperature reduction. After 3 p.m., the temperature changing trends at four points are similar.

While, in the north, the temperature at point DN is lowest, compared with most measurements, and the temperature fluctuation varies greatly. This is because the dominant wind direction on the day of measurement is northeast, which is very strong. Concomitantly, many high-rise residential buildings are in the north space. The wind speed direction are affected by the urban space, which has a significant impact on the temperature. Such effect can also be seen from the temperature fluctuations at four measuring points at 12 a.m.. In the south, temperatures at point AS and BS near the park rise slowly after 7 a.m., while it heats up quickly at point CS and DS. The temperature at point AS (21.26°C) and BS (21.02°C) reach the highest value at 2 p.m., while it is up to the highest value at point CS (21.12°C) and DS (21.14°C) at 11 a.m.. After 4 p.m., as the sun gradually set, the crowd activities decrease. Temperatures at point AN and AS in the park drop faster. But the temperatures at point CS and DS drop more slowly due to the influence of surrounding buildings and other factors. After 3 p.m., changing trends at four points are basically similar.

Due to the warm, windy and high wind speed in spring in Xi'an, measuring points are greatly affected by the urban space, with a great temperature fluctuation. Before sunrise and after sunset, the temperature changes in all direction are basically similar. In spring, the temperature changes inside and outside the park are affected by the urban climate. Consequently, the temperature fluctuates greatly in daytime and the temperature difference before and after sunrise is small.

Summer (June 20, 2018)

It was sunny on the day of measurement. The temperature changing trend in four directions can be seen from Figure 6.

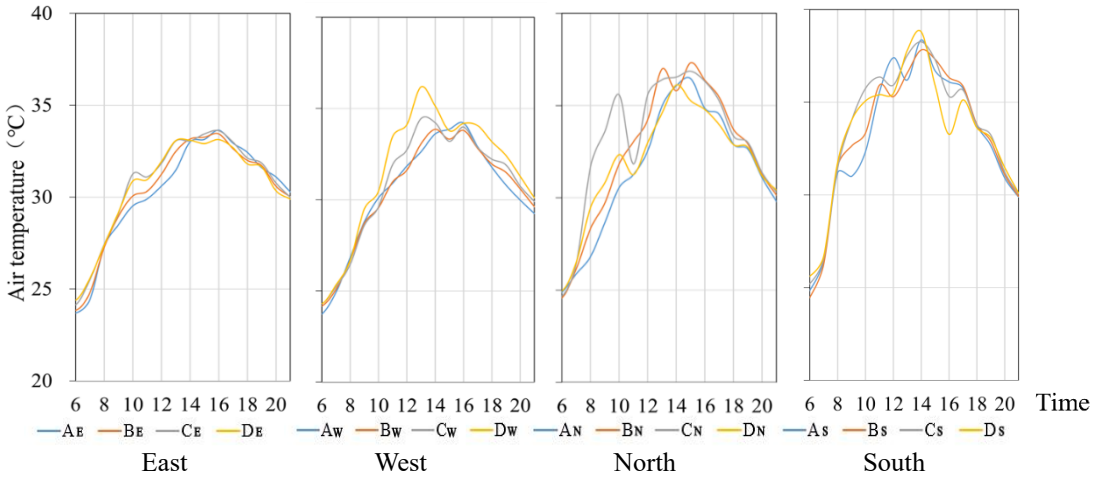


Figure 6. The temperature changes of measurement points in summer

In the east, the temperature at point AE is lowest before 3 p.m., and the temperature at point BE is higher than that at point AE. And then, the temperature changing trends at four sites are basically similar after 3 p.m., and the temperature differences between four measuring points do not exceed 1°C. The park inhibits the rate of temperature rise after sunrise. At 7 a.m., the maximum temperature difference between four measuring points is 0.12 °C. However, the maximum temperature difference between four measuring points is 1.34 °C at 12 a.m.. After 4 p.m., the temperature at point AE closest to the park declines slowly, which is due to leaves on the trees blocking the long-wave radiation from the ground, resulting in a slow temperature fall. The temperature at point BE, CE and DE are slightly higher during the day. The reason for that is three measuring points are located in the space of the multi-story building. Meanwhile, there are urban road areas which have an influence on the temperature (Table 1). However, all three measuring points have a certain green coverage (Table 1), which is conducive to the temperature fall. In the west, the temperature at point AW is the lowest in most measuring time, especially after 6 p.m., when the temperature drops from 31.78 °C to 29.24°C. It is the lowest value of four points at 9 p.m., followed by lower temperatures at point BW, CW and DW. Among them, temperature changes at point BW is close to that of point AW. But there is a big difference on the temperature changes between point BW and other two points (point CW and DW) from 10 a.m. to 2 p.m.. At 1 p.m., the temperature at point CW (34.44°C) and DW (36.18°C) reach the highest value, but it doesn't at point AW and BW. The temperature at point AW in the park drops fastest after 4 p.m..

But in the north and south, temperature fluctuations are more frequent, and overall temperature trends are higher, by comparison of temperature in the multi-story building spaces of the east and west. In the north, the temperature at point AN in the park is the lowest before 1 p.m. and after 6 p.m.. Point BN is close to the park, showing a slightly higher temperature, compared with temperature at point AN. As seen in Table 1, the detailed urban parameter of point BN is similar to that of point AN. Since point BN is located at the south gate of the park, with a higher building density and a lower green coverage, by reference to point AN. In addition, increased road area, as human factors, also has a considerable influence on temperature. The temperature at point CN and DN are variable, because the north space is mainly dominated by high-rise buildings in the

upwind direction. In the south, although there is a high green coverage, the measuring points are located in open spaces with low SVF (Figure 3), thus leading to highest temperature risen by 0.48 °C in the north due to the influence of the sun. The maximum temperature difference between four measuring points at 8 a.m. is 4.89 °C. However, the maximum temperature difference between four measuring points at 10 a.m. is 5.37 °C. This is because point AS and BS are located in the park, which have a high green coverage, and is less affected by architectural factors. Temperature varies greatly at four points from 12 a.m. to 5 p.m.. This is because the four measuring points are located in the open spaces with less occlusion, so they are susceptible to wind and the sun. During the measurement, point BS and CS are close to the road, so the temperatures are higher in most time periods.

Before sunrise and after sunset, the temperature in the park is basically lower than that in the surrounding urban spaces. While, at noon, the temperature at some measuring points in the park is slightly higher than that in the surrounding spaces, which is due to the heat absorption and building cooling during the daytime. In summer, the temperature at the measuring point in the park or near the park is lower, which is partly the result of greenbelt. It plays a good role in inhibiting the temperature rise and rapid temperature fall after sunset.

Discussion

Urban parks have a cooling effect on urban space, contributes to reducing the urban heat island effects, improving air circulation and providing physical and mental pleasure for human activities. The results of the research indicated that the temperatures change inside and outside the park were different in different seasons, which are affected by surrounding environmental factors.

In winter daytime, the average temperature of multi-story building space around the park with a radius of 50 meters rises by 1.37 ℃. Accordingly, the average temperature of high-rise building space is up by 0.72℃. The average temperature difference of multi-story building space inside and outside the park is 0.2 ℃ at night, while the difference of high-rise building space around the park is 0.63 °C at night. It is indicated that the temperature of multi-story building space around the park drops faster than that of the high-rise building space after sunset, which is more conducive to the spread of the cooling effect in park. In spring, there is little difference in temperature between the inside and outside of the park before sunrise and after sunset. The temperature difference between the multi-story building space and park is 0.08℃, and that between the high-rise building space and park is 0.5℃. It is the evidence of better cooling effect of multi-story building space, which is superior to high-rise building space. In summer, the average temperature outside the park is 0.61℃ higher than that inside the park, especially in the high-rise building space and in the space with city's main roads outside the park. The temperature difference between the two spaces and the park can be more than 1 °C. It can be seen that the two spaces have higher temperatures during the day, but the temperature difference inside and outside the park is 0.08℃, lower than that of the multi-story building space at night. Therefore, the cooling effect of these two spaces is similar to that of a multi-story building space. Based on the results measured in three seasons, the multi-story building space around the park is more conducive to temperature reduction.

However, there are some limitation in the result of field measurements. The weather conditions on the day of measurement, such as the wind speed and direction, will have an impact on temperature changes. In future research, the impact of weather conditions and surrounding environment on temperature changes will be further analyzed to make the results more accurate.

Conclusion

In this research, the weather conditions in 16 locations inside and close by a large scaled urban park are measured, and the measurement data are analyzed in order to investigate the effects from urban greening and urban building typology on urban micro-scaled climate. The actual data differences between the park and the surrounding urban spaces in different seasons were compared in this research, using field measurements. The temperature in the park during the daytime is higher than that in the surrounding urban spaces. The temperature differences between inside and outside of the park are greatly influenced by the type of surrounding building spaces, as well as in different seasons. On the whole, the multi-story building space with the tree-lined urban road has a more obvious cooling effect, which could be built around the park. Therefore, the space around the park should not be planned to build high-rise buildings and major urban roads with large traffic flows. Such space planning can better support the park's cooling effect and play a more effective role in improving the temperature change of local urban space. The three seasonal temperature relationships between the park and the surrounding urban spaces are different, which can be used as a basis for space planning to improve urban microclimate. This research laid a foundation for further research on the relationship between the surrounding urban space and the ecological effect of the park, and provided a reference for the urban park and the surrounding urban space planning.

Acknowledgments

This research is supported by the Young Scientists Fund of the National Natural Science Foundation of China (Grant No. 51608439).

Reference

Akbari, H. 2002. "Shade trees reduce building energy use and CO2 emissions from power plants." *Environmental pollution* 116: S119-S126.

Chang, C. R., and Li, M. H. 2014. "Effects of urban parks on the local urban thermal environment." *Urban Forestry & Urban Greening* 13(4): 672-681.

Grimmond, S. U. E. 2007. "Urbanization and global environmental change: local effects of urban warming." *Geographical Journal* 173(1): 83-88.

Howard, L. 1833. "The climate of London: deduced from meteorological observations made in the metropolis and at various places around it, vol 2. Harvey and Darton."*J. and A. Arch, Longman, Hatchard, S. Highley [and] R. Hunter*.

Hamada, S., and Ohta, T. 2010. "Seasonal variations in the cooling effect of urban green areas on surrounding urban areas." *Urban forestry & urban greening* 9(1): 15-24.

Kalnay, E., and Cai, M. 2003. "Impact of urbanization and land-use change on climate."*Nature*423(6939): 528.

Oke, T. R. 1982. "The energetic basis of the urban heat island."*Quarterly Journal of the Royal Meteorological Society* 108(455): 1-24.

Potchter, O., Cohen, P., and Bitan, A. 2006. "Climatic behavior of various urban parks during hot and humid summer in the Mediterranean city of Tel Aviv, Israel." *International journal of climatology* 26(12): 1695-1711.

Steemers, K., Baker, N., Crowther, D., Dubiel, J., Nikolopoulou, M. H., and Ratti, C. 1997. "City texture and microclimate." *Urban Design Studies* 3: 25-50.

Song, L. 2008, "Problems and countermeasures of urban green space system planning in transition period."*Urban Planning Journal* (6):79-82. [In Chinese]

Song, L, and Binyi, L.2010. "Coupling research on urban green space and urban development——taking Wuxi as an example." *Chinese Garden* 26(3): 14-18. [In Chinese]

Shinoya, K., Umeno, M., Ohata, T., Hattori, H., Nohara, T., Matsubara, T. and Shibayama, M. 1978. *Observation of urban heat island dynamics in Nagoya and its mechanisms through computer simulations.* Japan: Chubu region Development Research Center. [In Japanese]

Taleghani, M., Kleerekoper, L., Tenpierik, M., and van den Dobbelsteen, A. 2015. "Outdoor thermal comfort within five different urban forms in the Netherlands." *Building and environment*83: 65-78.

Wong, N. H., and Yu, C. 2005. "Study of green areas and urban heat island in a tropical city."*Habitat international* 29(3): 547-558.

WC (Weather China)."Xi'an climate background analysis." Accessed January15, 2019.http://www.weather.com.cn/cityintro/101110101.shtml.

Xi'an Xingqing Palace official website. "Landscape Overview." Accessed February 28, 2019.http://www.xingqinggong.com/page.asp?id=8.

Yan, H., Wu, F., and Dong, L. 2018."Influence of a large urban park on the local urban thermal environment." *Science of the Total Environment* 622: 882-891.

Study of the thermal behaviour of unplanted extensive green roof sample according to the nature of the substrat.

Chaumont Maxime,
Univ Paris Diderot, Sorbonne Paris Cité, LIED, UMR 8236, CNRS (France)
Parison Sophie,
Paris City Hall (France)
Univ Paris Diderot, Sorbonne Paris Cité, LIED, UMR 8236, CNRS (France)
Hendel Martin,
Univ Paris Diderot, Sorbonne Paris Cité, LIED, UMR 8236, CNRS (France)
Université Paris-Est, ESIEE Paris, département SEN (France)
Royon Laurent, Univ Paris Diderot, Sorbonne Paris Cité, LIED, UMR 8236, CNRS (France)

ABSTRACT

In this study we are interested in the influence of substrate composition on the thermal behavior unplanted extensive green roof structures. We also focus on the impact of on substrate water content on roof behavior. Two kinds of substrates are studied: the first is a compost-based gardening soil, while the second is sampled taken from a Parisian park (urban soil). It appears that the sample with the compost stores much less heat than the one with the urban soil. This trend is valid whether the substrates are dry or saturated with water. It should be noted, however, that the near-surface temperature is 5°C higher in the case of compost, and that the presence of water increases the thermal conductivity of the latter.

Keywords: Urban heat island, green roofs, heat storage

Introduction

The urban heat island (UHI) phenomenon, characterized by a temperature difference between the center of an urban area and its periphery, is due to various factors such as the use of low albedo materials, high building density, lack of vegetation and anthropogenic heat (Oke 1982). During heat waves, this phenomenon implies an increase in energy needs and poses health problems, especially for the most vulnerable people (Robine et al., 2008). Different strategies, including urban greening, are therefore being studied and developed to moderate the intensity of this phenomenon. Indeed, vegetated surfaces have several advantages: they often have a higher albedo than traditional urban surfaces, they absorb and store rainwater and cool the ambient air thanks to evapotranspiration.

One way to increase the proportion of plants in urban areas is to green building roofs and façades. There are three main types of green roofs: intensive, semi-intensive and extensive, that principally differ in substrate thickness and type of vegetation. Several studies have been conducted to quantify the impact of these last two parameters on roof thermal behavior (Bevilacqua et al 2015), but few have focused on the influence of substrate composition or on their thermal behavior during heat waves.

The objective of this study is therefore to characterize the thermal behaviour of an extensive green roof sample in the lab. We will only focus on the influence of two parameters: the nature of the substrate that makes up the sample and its water content. For this purpose, the tests are carried out on samples of unplanted roofing under heat wave-like conditions.

Methodology

The cylindrical samples used, representative in composition to extensive green roof structures, are 16 cm in diameter and 32 cm high. This shape and its 5 cm thick thermal insulation ensure unidirectional and axisymmetric heat transfer conditions, thus limiting edge effects. The samples are composed of 22 cm of concrete and 10 cm of substrate with a geotextile and a waterproofing film at the concrete/substrate interface. Vapour barrier, root protection, etc. layers are neglected. Three thermo-flowmeters are placed within the samples at different depths: near the surface at 0.5 cm depth, at the concrete/substrate interface (10 cm deep) and 17 cm below the surface (see Figure 1).

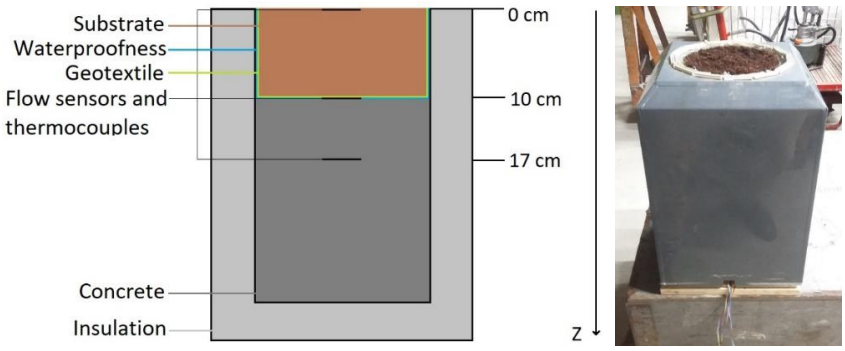


Figure 1. Left: sample composition and instrumentation of samples; Right: photograph of insulated sample

The unit is placed in a climate chamber controlling relative humidity and ambient temperature. The 24-hour test cycle includes an 8-hour daytime phase during which the relative humidity is set to 35% and the temperature to 35°C with artificial insolation. This phase is followed by a 16-hour night phase, with relative humidity set to 70% and temperature to 25°C (see Figure 2).

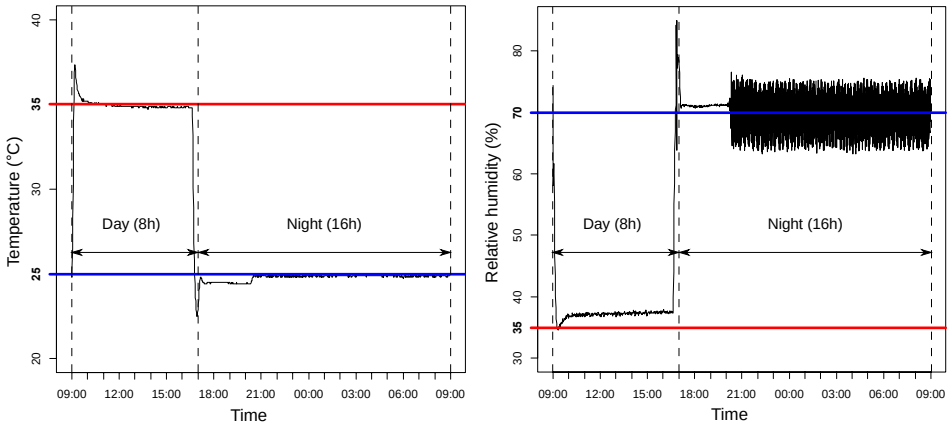


Figure 2. Temperature and relative humidity conditions inside the climate chamber.

Artificial sunlight is provided by a lamp composed of seven dichroic halogen bulbs with a colour temperature of 6500 K (see Figure 3). Substrate surface irradiance is 1320 $W.m^{-2}$.

Compared to the spectral power density of the standard AM1.5 spectrum, that of the halogen lamp is stronger in the infrared band and slightly lower in the UV and visible bands. Temperature and heat flux measurements are recorded every ten seconds.

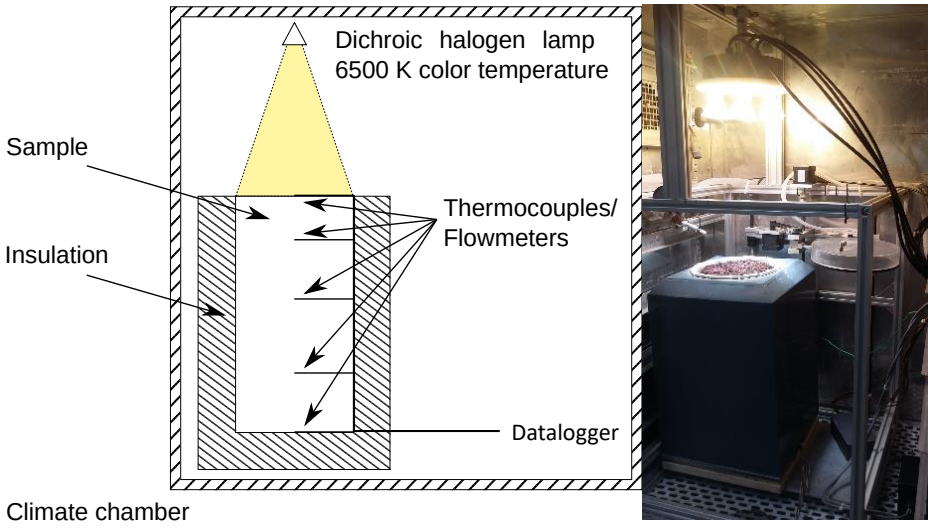


Figure 3. Inside the climatic chamber during the daytime phase.

Due to the insulation, the energy exchanges take place only through the upper surface of the samples and are decomposed as shown in Figure 4.

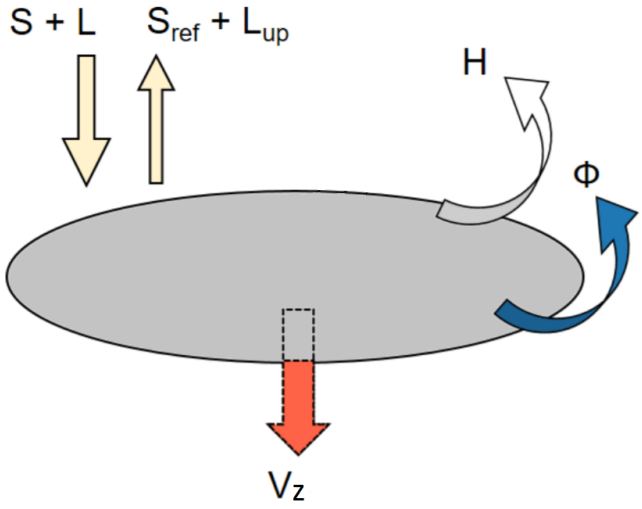


Figure 4. Schematic diagram of heat balance at the surface. S is downward shortwave (SW) radiations, L longwave (LW), Sref and Lup, respectively the reflected SW and upward LW radiations, H the upward atmospheric convective heat flux, Vz the absorbed heat flux, Φ the cooling flux due to watering.

Two kinds of substrate are compared. The first substrate is a vegetable compost composed of 80% organic matter and has a water retention capacity of 80% by volume. The second is soil sampled from a Parisian park (see Figure 5).



Figure 5. Urban soil on the left, compost on the right.

The two samples do not have the same density: the density of the compost is 185 $kg.m^{-3}$ while that of the urban soil is about 1145 $kg.m^{-3}$ (uncompacted and dry). The thermal conductivity of a compost substrate depends on several parameters such as density, water content, porosity or the raw material used to make it. According to the literature, for this type of substrate the thermal conductivity is between 0.03 and 0.89 $W.m^{-1}.K^{-1}$ (Laurent, 1987). For raw earth substrates (such as our urban soil), the parameters that determine their thermal conductivity vary and are essentially the same, except for the composition, which will depend on the type of minerals. According to the literature, their thermal conductivity is between 0.3 and 2 $W.m^{-1}.K^{-1}$ (Ahn et al, 2009). In both cases, the factor that has the greatest impact on the thermal conductivity of substrates is their density (i.e. their compactness). Each substrate is subjected to two 24-hour cycles: first totally dry and second saturated with water. To humidify our samples, we pour water to saturation, the excess being drained using a device shown in Figure 6.



Figure 6. Device used to saturate substrates with water.

Results

Surface Thermal Behaviour

Figure 7 illustrates near-surface temperatures for both samples and under both the dry and saturated conditions, while Figure 8 illustrates near-surface heat flows. As can be seen, near-surface temperatures reach up to 57.6°C for urban soil and 64.1°C for compost when the substrates are dry, while it only reaches 34.9°C and 39.3°C when the substrates are saturated with water (a difference of 22.7°C and 24.8°C between dry and wet trials). It is also noted that in both conditions the near-surface temperature is lower for the urban soil than for the compost (6.5°C when the

substrates are dry and 4.4°C when they are wet). For compost, the heat flows near the surface are essentially the same whether the substrate is dry or wet (see Figure 8 b). On the other hand, for the urban soil, there is a clear difference. The heat flux decreases more quickly and is much less important when the substrate is wet (see Figure 8 a).

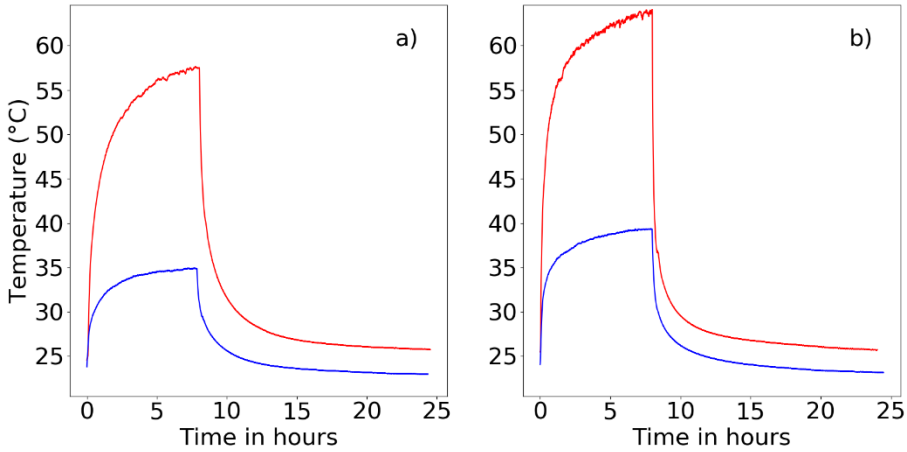


Figure 7. Evolution of the near-surface temperature for dry (red) and water-saturated (blue) samples. a) Urban soil b) Compost.

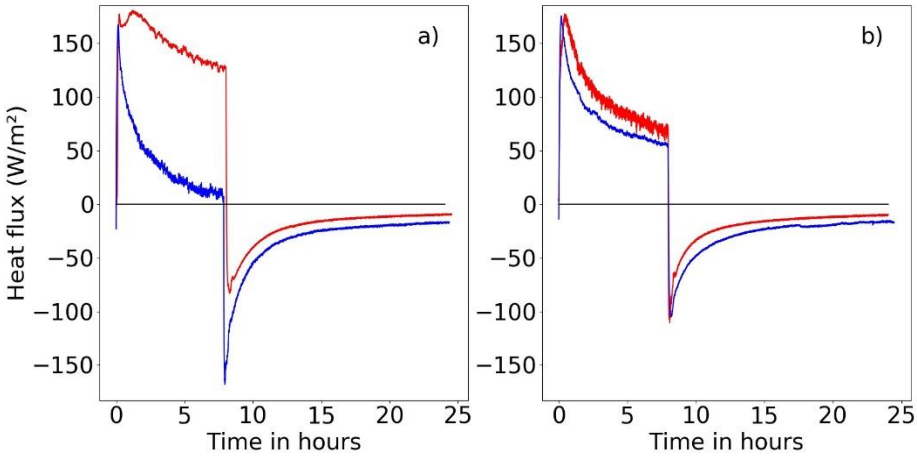


Figure 8. Evolution of the heat flow near the surface for dry (red) and water saturated (blue) samples. a) Urban soil b) Compost

Behaviour 10 cm deep

Figure 9 illustrates temperatures measured at the substrate/concrete interface, 10 cm deep. Figure 10 illustrates heat flow measurements at that depth. As can be seen in Figure 9 the previous trend is reversed. Temperatures are higher this time in the case of urban soil, whether the substrates are dry or saturated with water. It is also noted that the temperature difference between dry and wet samples is only 1.1°C for the urban soil and that there is almost no difference in the case of the compost.

Figure 10 shows that the heat flow through the interface is three times greater for the urban soil than for the compost when the substrates are dry and twice as much when the substrates are

saturated with water. It can be assumed that this is due to the difference in density of the two substrates. Indeed, the urban soil is almost 8 times denser, so it conducts heat better. The difference in density and therefore in conductivity is due to the composition of the two substrates. Urban soil is composed of minerals, stones and is not aerated unlike compost which is composed of organic matter and is very aerated. For the compost, Figure 10 b) shows that the heat flow through the interface is greater when the compost is saturated with water; this is not the case for urban soil. It would therefore seem that the presence of water increases the thermal conductivity of the soil.

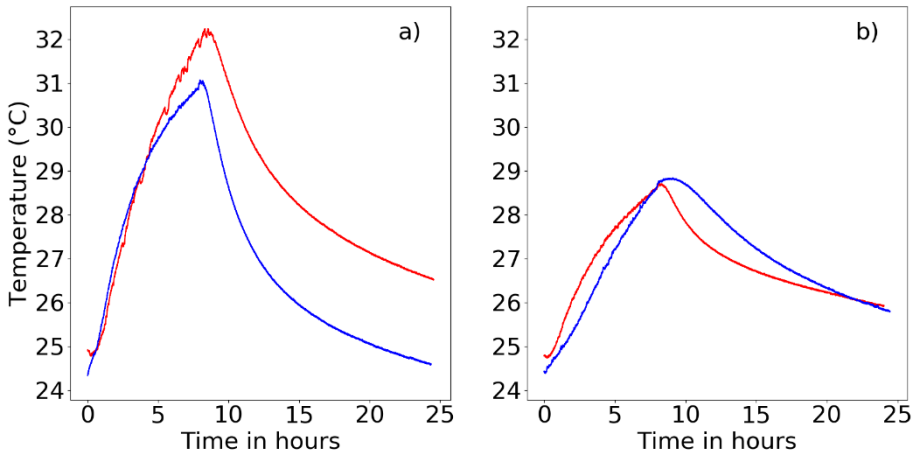


Figure 9. Temperature evolution at the interface for dry (red) and water saturated (blue) samples. a) Urban soil b) Compost

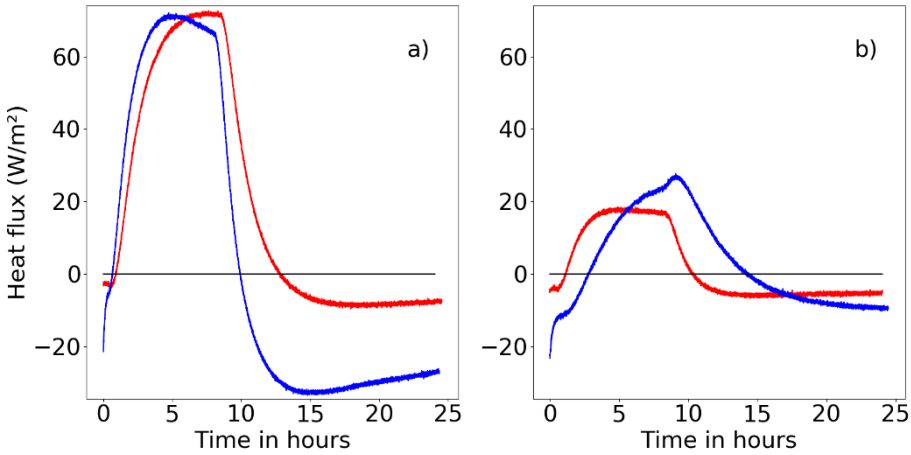


Figure 10. Evolution of the heat flow at the interface for dry (red) and water saturated (blue) samples. a) Urban soil b) Compost

Behaviour at a depth of 17 cm

At a depth of 17 cm, in concrete, temperatures are slightly higher by about 1 to 2°C for urban soil (see Figure 11). There is no longer any significant temperature difference between dry and water-saturated substrates (less than 1°C for urban soil and almost zero for topsoil). When the substrates are dry, the heat flux is four and a half times higher for urban soil, while it is only two and a half times higher when the substrates are saturated with water (see Figure 12). For the soil, as at the interface, the heat flow is greater when the substrate is wet.

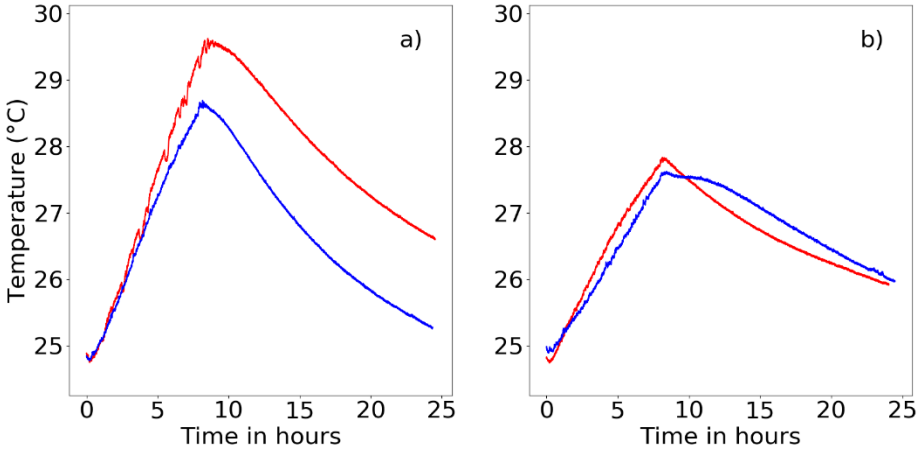


Figure 11. Temperature evolution in concrete (at a depth of 17 cm) for dry (red) and water-saturated (blue) samples. a) Urban soil b) Compost

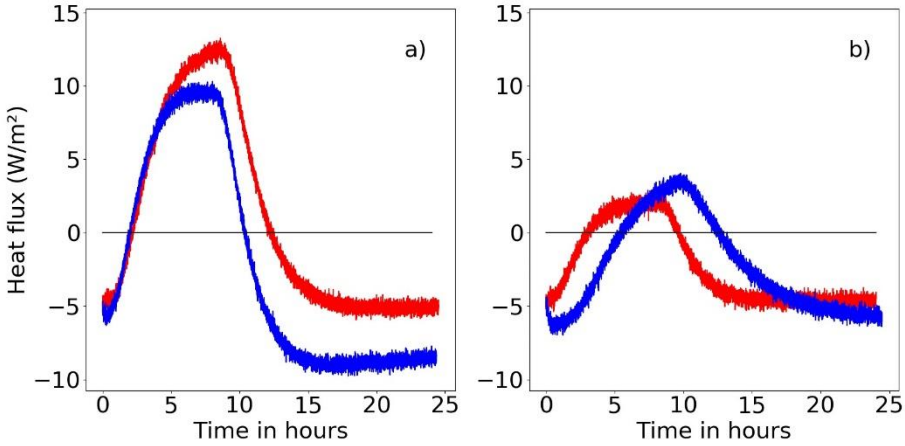


Figure 12. Evolution of the heat flow in the concrete (at 17 cm) for dry (red) and water-saturated (blue) samples. a) Urban soil b) Compost

The maximum temperatures are summarized in Table 1 below and those of the heat fluxes in Table 2.

Table 1. Maximum temperature (°C) observations

	Urban soil		Compost	
	dry	wet	dry	wet
Near the surface	57,6	34,9	64,1	39,3
10 cm depth	32,2	31,1	28,7	28,8
17 cm depth	29,6	28,7	27,8	27,6

Table 2. Maximum heat flux (W/m²) observations

	Urban soil		Compost	
	dry	wet	dry	wet
Near the surface	180,4	167,4	177,4	175,5
10 cm depth	72,7	72,1	18,5	27,7
17 cm depth	13,3	10,3	2,9	4,1

Conclusion

In this study we were therefore interested in the thermal behaviour of unplanted extensive green roof structures according to the substrate they are made of and their water content.

These initial results indicate that compost stores and releases much less heat than urban soil. However, it should be noted that the near-surface temperature, at 0.5 cm depth, is higher for compost by 6.5°C when the substrates are dry and by 4.4°C when the substrates are saturated with water. The presence of water does not have much influence on the behaviour of the urban soil sample, particularly on the amount of heat stored in the deep layers. On the other hand, for the compost, it appears that the presence of water increases its conductivity and thermal inertia since it stores (and releases) more heat when saturated. As we do not yet know the thermo-physical properties of our two substrates, it is difficult to determine the causes of this difference in behaviour.

However, we can make some assumptions. The difference in temperature near the surface is probably due to the difference in albedo of our two substrates: the compost is much darker than the urban soil. Additional measurements of spectral reflectivity are planned in future studies to this end. On the other hand, the fact that urban soil stores and releases more heat than compost is certainly related to their difference in density and thermal capacity. Compost is less dense and more aerated than urban soil, so it conducts heat less well. The change in the behaviour of the compost between the two configurations (dry vs. wet) is probably due to the fact that part of the air contained in the pores of the substrate is replaced by water.

The objective of this study was to measure the amount of heat stored during the day and then released during the night. This allows us to evaluate the role of these two substrates in the urban heat island phenomenon process. For both dry substrates, the near-surface temperature is high, so there will be significant heat transfer (because H, on Figure 4, depends on the temperature difference between the air and the substrate surface). The dry configuration will therefore tend to amplify the urban heat island phenomenon by heating the air near the roof. On the contrary, the wet configuration, due to the lower surface temperatures (about 20°C lower), will have a lower impact on UHC than the dry configuration or conventional roofs. We also note that the heat fluxes at a depth of 17 cm (V_{17cm} Figure 4) are quite low in both configurations (dry and wet) while our roof sample does not contain any insulating layers (normally present in all types of roofs). It can therefore be assumed that by adding an insulating layer, the heat flow to the inside of the building will be very low. Extensive green roofs are therefore a good solution for insulating roofs (this result has already been demonstrated with in situ experiments). It should be noted that the heat flux at a depth of 17 cm is 3 times less important for compost than for urban soil, so the composition of the substrate has a significant influence on the thermal behaviour of the roof.

Subsequently, it would be interesting to reproduce this experiment by varying different parameters such as the composition of the substrates (more or less organic/mineral matter), their

compactness, their water content (intermediate between dry and water-saturated) or the height of the substrate. It would also be relevant to conduct the same experiment over several consecutive cycles to measure the impact of the duration of a heat wave on the behaviour of this type of roof.

Acknowledgements

The authors would like to acknowledge the technical support of the Laboratoire des Essais des Matériaux (LEM) of the City of Paris. This study was funded by the ANR Urban Materials for Cool Cities (UMat4CC) project (ANR-18-CE22-015-01).

References

Oke, T. R. (1982). The energetic basis of the urban heat island. Quarterly Journal of the Royal Meteorological Society, 108(455), 1-24. https://rmets.onlinelibrary.wiley.com/doi/epdf/10.1002/qj.49710845502

Robine, J.-M., Cheung, S. L. K., Le Roy, S., Van Oyen, H., Griffiths, C., Michel, J.-P., & Herrmann, F. R. (2008). Death toll exceeded 70,000 in Europe during the summer of 2003. *Comptes Rendus Biologies*, *331*(2), 171–178. https://doi.org/10.1016/j.crvi.2007.12.001

Bevilacqua, P., Coma, J., Pérez, G., Chocarro, C., Juárez, A., Solé, C., ... & Cabeza, L. F. (2015). Plant cover and floristic composition effect on thermal behaviour of extensive green roofs. Building and Environment, 92, 305-316.

Ahn, H. K., Sauer, T. J., Richard, T. L., & Glanville, T. D. (2009). Determination of thermal properties of composting bulking materials. Bioresource technology, 100(17), 3974-3981. https://lib.dr.iastate.edu/cgi/viewcontent.cgi?article=1256&context=abe_eng_pubs

Laurent, J. P. (1987). Propriétés thermiques du matériau terre. Cahiers du CSTB, 279, 2156.

Study Of Urban Morphology And Its Impact On Microclimate Of Surrounding Area
Case Study – S.B. Road, Pune

Ar.Prathama Jhaveri[1], D.Y.Patil School of Architecture, Lohegaon, Pune (India)
Ar.Namrata Dhamankar, Dr.Bhanuben Nanavati College of Architecture, Pune (India)
Dr.Sujata Karve, Dr.Bhanuben Nanavati College of Architecture, Pune (India)

ABSTRACT

The aim of this paper is to study the impact of the urban morphology for its effectiveness to climate response through the analysis of its microclimate. To this end, the context of urban morphology is studied for streets, buildings, open spaces and vegetation. The rapidly growing population combined with rapid urbanization has led to unplanned and uncontrolled expansion of Pune leading to changes in land use, urban form and settlement.

This study takes a simulation approach to analyze the impact in an urban settlement in Pune, India of mixed use through Envi-met -3.1software. Three environmental factors of mean temperature, wind speed and relative humidity have been selected to quantify the outdoor micro-climate with a single constant indoor temperature.

Need for the study:

Urban form, land use, presence of natural geographical structures etc have significant effects on microclimate of an area. The Urban morphology includes the street pattern, built density, insufficient green space as responsible enough in creating urban heat island effect within a city (Smith & Levermore,2008). Urban vegetation influences urban climate as it helps to control heat gain, mitigate urban heat islands, produce shadow and also reduce noise levels. The proportion, of the street and building geometry, controls the solar heat gain (Smith & Levermore, 2008).

The intra-urban temperature rises, the wind and ventilation characteristics are greatly modified by the surroundings. The daytime canopy layer of heat island is of most interest to urban designers as it is largely due to design and hence is within the scope of control of the planners. Only In the last 20 years the transfer of knowledge from climatologic and biometeorology studies to urban & architectural design tools has begun to take place. Air temperature, relative humidity and wind speed are the environmental parameters that primarily affect thermal comfort of a human being. In urban areas, the great variety of different surfaces and sheltering obstacles produces a pattern of distinct microclimate.

Hence, a look into the changing morphology of the city and the effect it is creating on its microclimate is the need of the hour.

[1]Ar.Prathama Jhaveri: prathama.kapil@gmail.com, 7276382828.

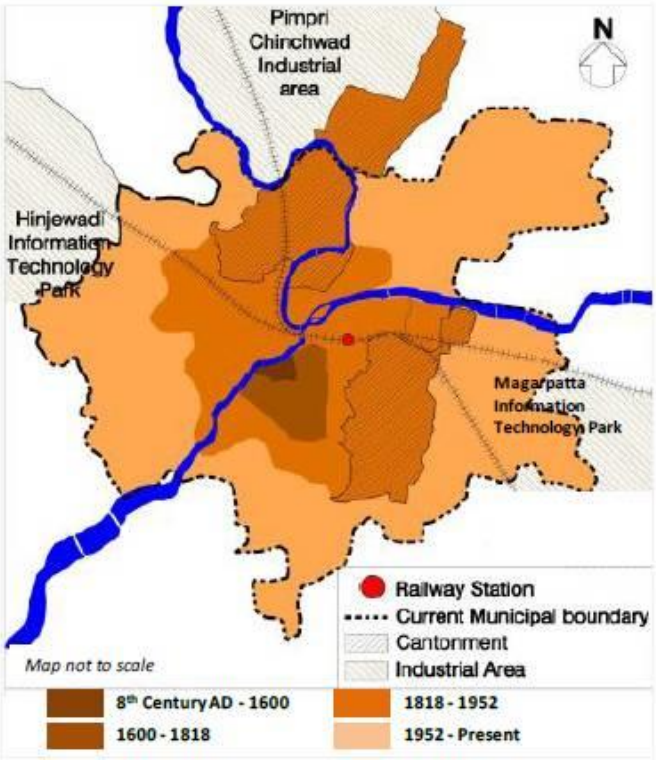


Figure 1: Chronological growth of Pune city
Source: Final draft CPD, Pune Municipal Corporation

Objectives of the study:

This research aims to analyze urban morphology with respect to the climate parameters and its effect on the urban microclimate. This study comprises of climate parameters of wind speed, potential temperature and relative humidity and studied for the city of Pune and hence covers one type of climate. Streets, open spaces, vegetation and buildings constitute the urban morphology for the study. The area was restricted to 600 m X 600 m for the feasibility of simulation. Hence, the study does not cover all urban scenarios and building typologies and configuration.

The research objectives are:

- To analyze the relation between climate parameters and its effect on the urban microclimate
- To explore the nature of urban morphology and its effect on the climate parameters.
- To explore the width and orientation of the streets for its effect on the climate parameters.
- To explore the height, orientation, and form of the buildings for its effect on the climate parameters.
- To explore the nature and type of vegetation and open spaces for its effect on the climate parameters.
- To prepare a basis for further study to investigate the consequences of urban canyon and urban microclimate.

Area of study:



Figure 2: The study area
Source: Google earth

An area covering a mix of form, height and usage with S.B. Road running along as a spine was selected for the study. The road starts at the BMCC (Brihan Maharashtra College of Commerce) Road and terminates off at Pune University Circle on the Ganesh Khind road.
A 600 m x 600 m of area was selected encompassed between Pawar road on the east, Kalu Tamanna Kusalkar road, Janawadi road on the south, Baburao Ramji Bahirat marg on the west. The east side of the area comprised of Durga nagar majorly having two and three storied bungalows and internal roads of 6m with new development of G+3 mix use buildings running on Dothre road and Harihareshwar having Maharashtra state institute of hotel management and catering technology, few two storied bungalows and few 5 -7 storied apartments having commercial use at the ground. Notable building was the Sai chambers along the road at the junction of S.B. road and Dothre road. The west side of the road comprised of Shivaji co-operative housing society and Bhageerath with bungalows at the back and prominent J.W. Marriott five star hotel along the road. Other notable buildings are the Cognizant and Persistent.
A field survey was conducted on 21st March 2015 which included visual survey, records through photographs and videos, measurements of prominent roads and buildings with the help of measuring tape and distance meter. The required information about initial temperature of atmosphere, wind speed and wind direction for 21st March 2015 was obtained from the Pune meteorological department.



Figure 3: Field survey of the study

Envi-met configuration:

The model prepared was simulated for 21st March 2015. The simulation was carried out for the entire day and output was obtained at an interval of every three hours. Hence, the model output was obtained for eight slots of time namely 06:00, 09:00, 12:00, 15:00, 18:00, 21:00, 00:00 and 03:00 hrs.

Sr. No.	Simulation parameters	Values
1	Start Simulation at Time (HH:MM:SS)	06:00
2	Total Simulation Time in Hours	24:00
3	Save Model State each	180
4	Wind Speed at 10 m above ground [m/s]	5
5	Wind Direction (0:N.90:E.180:S.270:W..)	270
6	Roughness Length z0 at Reference Point	0.1
7	Initial Temperature of Atmosphere [K]	303
8	Specific Humidity in 2500 m [g Water/kg air]	68

Table 1 : ENVI-met configuration information for simulation (source: author)

The analysis for the study area was done at two levels:
1) Generic level and 2) Specific level.

1) Generic level:

This was done by selecting 10 data points on the study area in line with its position with respect to streets, buildings and open spaces.
The analysis was done for the following cases:
Case 1: For different times with respect to height.
Case 2: For different data points with respect to height
Case 3: For different heights/data points with respect to time.
Case 4: For data point on a street parallel and perpendicular to wind direction.



Map 1: Data point's map (source: author)

Sr. No.	Data Point	Description
1	A	Inside park
2	B	At T junction near park
3	C	At mid length on first road perpendicular to wind direction
4	D	At mid length on second road perpendicular to wind direction
5	E	Behind J.W. Marriot
6	F	On S.B. Road in front of J.W. Marriot
7	G	Cross junction of S.B. Road
8	H	At T junction on road parallel to wind direction
9	I	On road perpendicular to wind direction along H
10	J	On end of road perpendicular to wind direction

Table 2: List of data points and their position in study area (source: author)

Findings:

Wind speed: The wind speeds (m/s) found are comparatively represented on Y axis with respect to the above four cases.

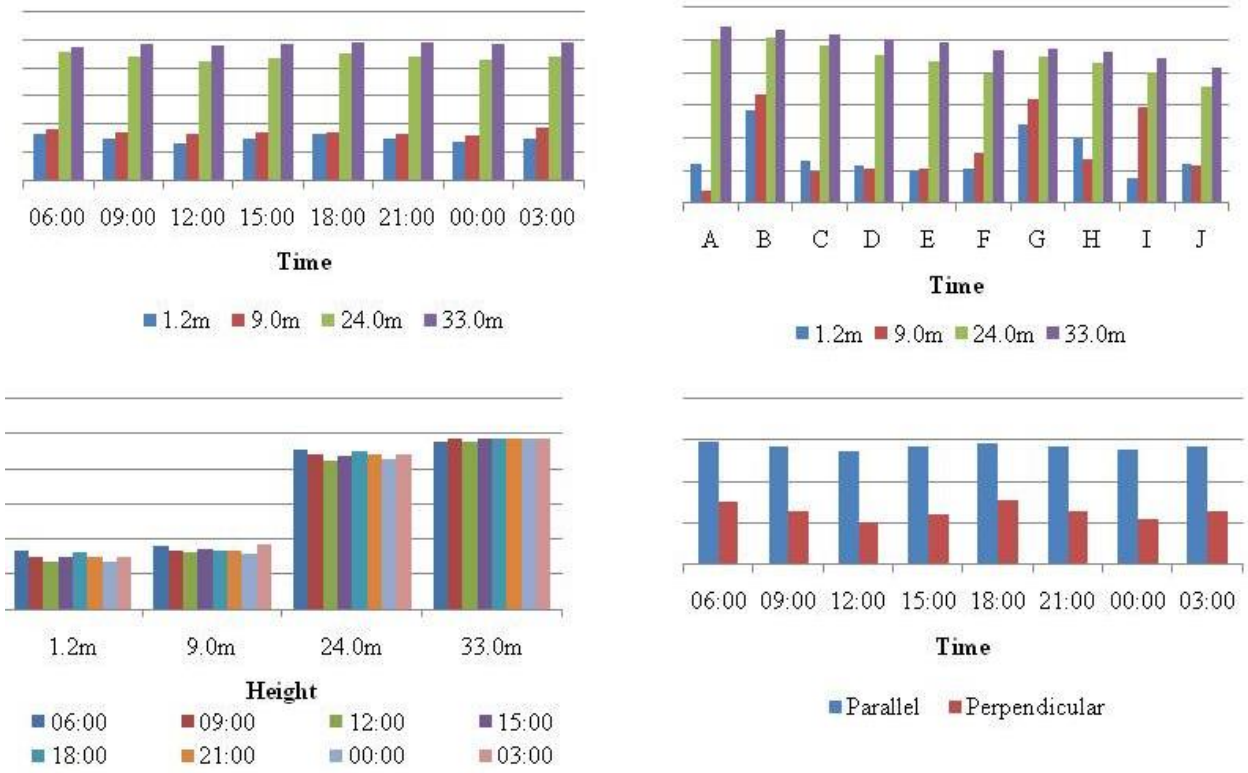


Figure 4: Wind speed analysis for Case 1, Case 2, Case 3 and Case 4

Case 1: At any given time of the day, the wind speed increased with increase in height. There is a notable increase in wind speed from 9m to 24 m and above since most of the buildings are less than 9.0 m in height.
Case 2: All the data points showed a increase in wind speed with increase in height except for points A, C, D, H at 9.0 m height since these points are with trees having canopy above 10m- 15 m. There is notable decrease at point A i.e. inside park since it has heavy vegetation. Wins speeds are higher at road junctions and loses speed as it travels a longer distance.
Case 3: At all the levels the wind speed did not show noticeable increase or decrease and was least at 12:00 and maximum during 06:00 and 03:00
Case 4: The wind speed on a data point on a street parallel to wind direction was noticeably higher than that of data point on a street perpendicular to wind direction.

Potential temperature: The potential temperature (K) found is comparatively represented on Y axis with respect to the above four cases.

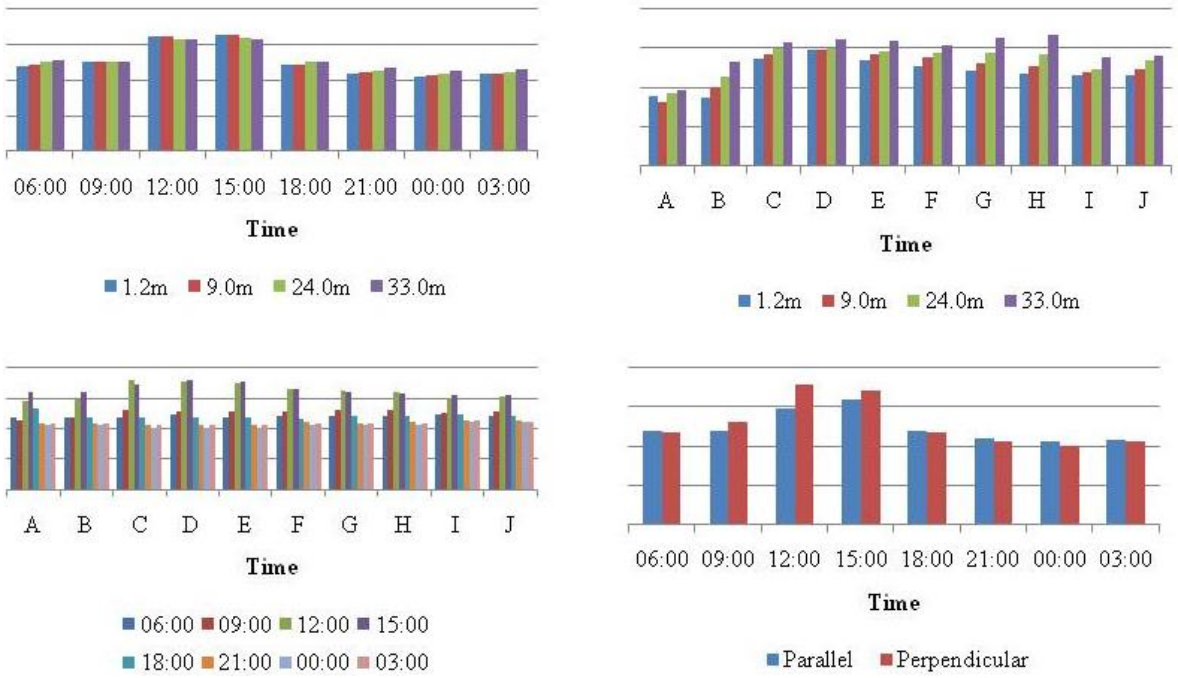


Figure 5: Potential temperature analysis for Case 1, Case 2, Case 3 and Case 4

Case 1: The area started heating up gradually from 09:00 to being noticeable at 12:00 onwards and started cooling from 18:00. There was no noticeable difference in temperature at any given time with increase in height.
Case 2: At most heights, the temperature of data point inside the park and near the park is the lowest. At any height the temperature is highest at the mid length of the road perpendicular to the wind direction. At the height after 33 m, there is not notable difference in the temperature of the data points except that of the point inside the park.
Case 3: The data points on the road junctions heated up more quickly and cooled more quickly.
Case4: The data point on the street parallel to wind direction had noticeable decrease in temperature at 12:00 and 15:00 hrs.

Relative humidity: The relative humidity (%) found is comparatively represented on Y axis with respect to the above four cases.

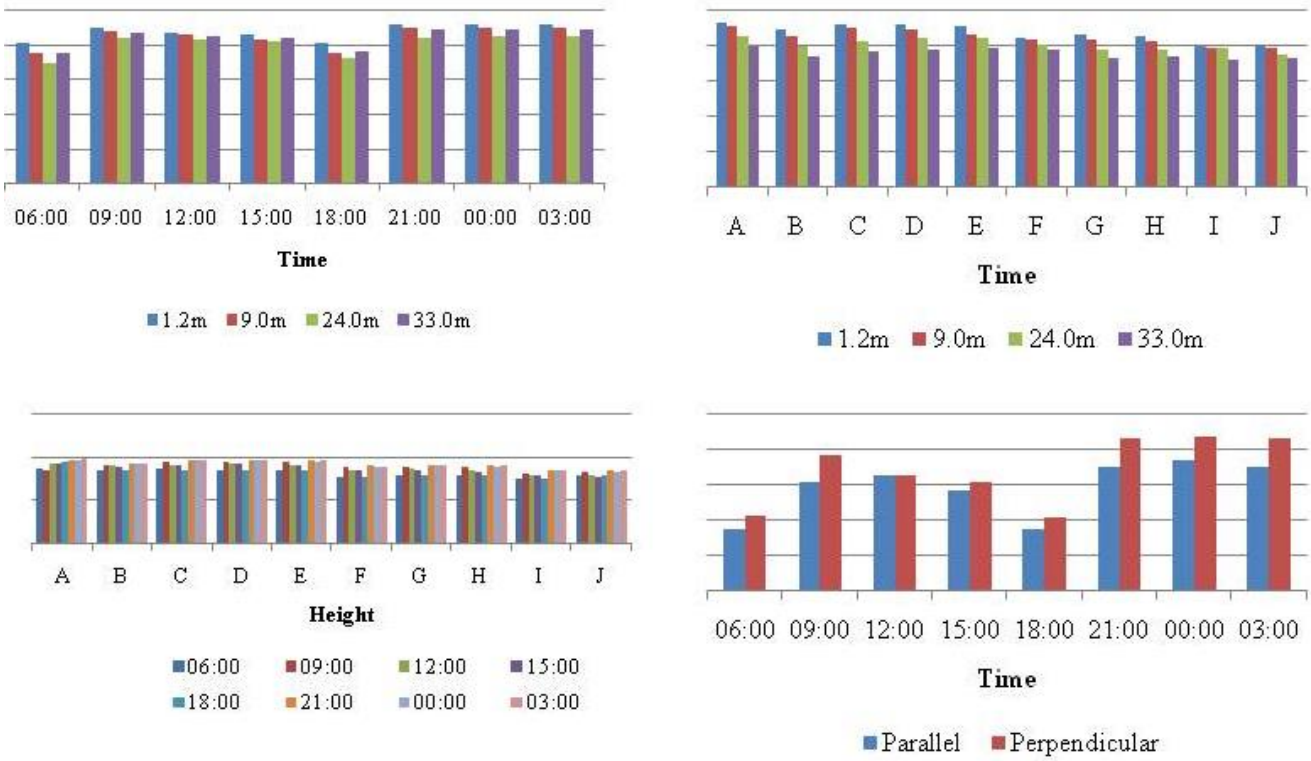


Figure 6: Relative Humidity analysis for Case 1, Case 2, Case 3 and Case 4

Case 1: At any time of the day, there is a gradual decrease in the relative humidity with the increase in height
Case 2: At any height, the data points with vegetation have notable higher relative humidity than the streets junctions with no vegetation. At the height of 9.0m there is a higher relative humidity than other heights since it is the crown area of a 10 m height tree.
Case 3: All the data points show a higher relative humidity during night hours and comparatively lower during the day.
Case 4: At any time of the day, the data point on the street parallel to wind direction had lower humidity than that of the point on street perpendicular to the wind direction.

2) Specific level:

After the analysis of the area on a generic level of the above four cases was done few specific scenarios were found to be of prominent study 1) relation of the climate parameters at the cross junction of streets and inside the park and 2) relation between potential temperature and humidity. This study involves the analysis with respect to these specific scenarios.

Specific Level:

Case 1: Relation of the climate parameters at the cross junction of streets and inside the park

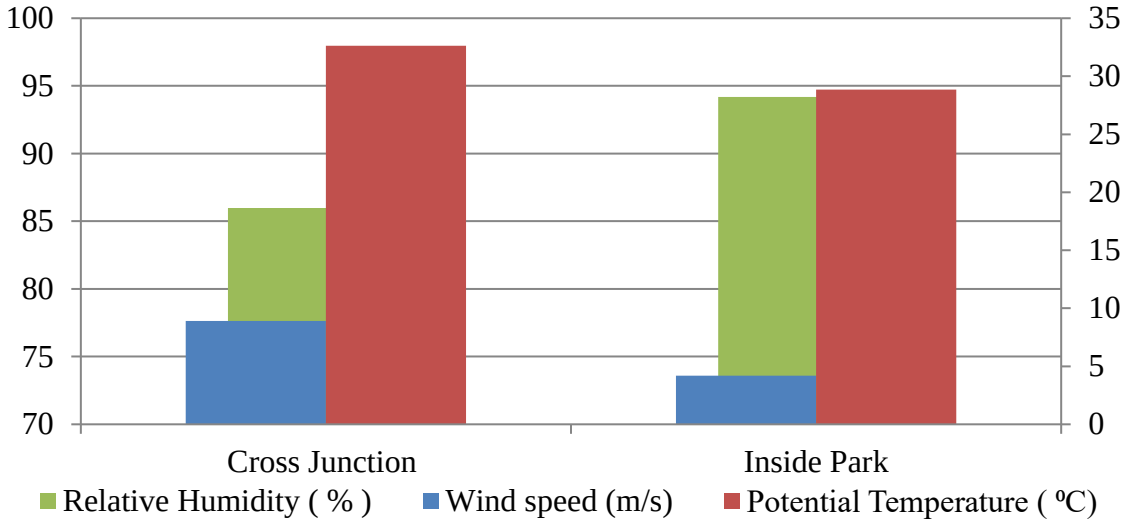


Figure 7: Cross junction/Inside the park

The data point inside the park has low temperature (3-4ºC) and wind speed with higher relative humidity

Case 2: Analyzing relation between potential temperature and humidity

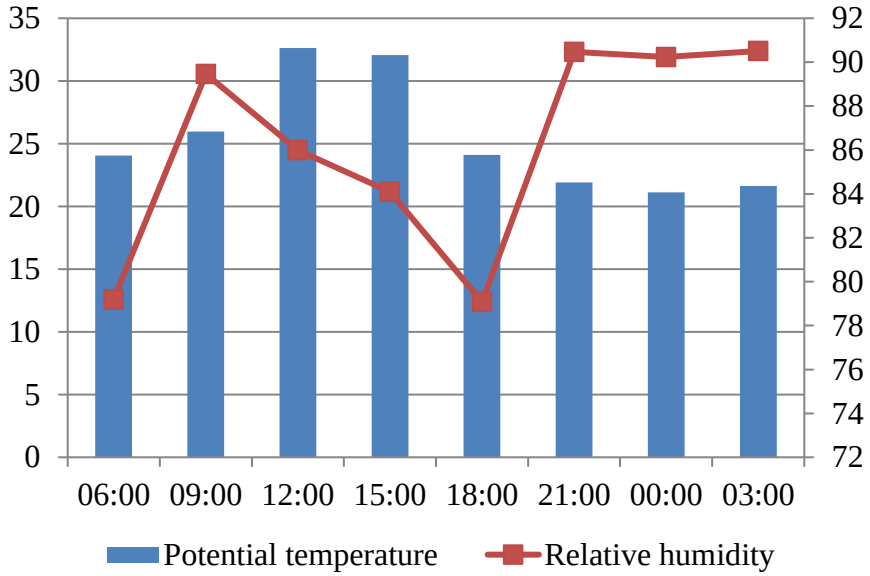


Figure 8: Relation between potential temperature and relative humidity

As the potential temperature increases, the relative humidity decreases at any time of the day.

Conclusion:

- Buildings obstruct the wind flow at their height and tress at a higher rate at the crown area.
- Wind speed is higher on streets oriented along the wind direction.
- Vegetation affects the microclimate of an urban area by reducing the potential temperature by 3-4°C.
- Large and dense trees create shade. It affects the microclimate of an urban area since the potential temperature of shaded area is less than that exposed to Sun by 1-2°C.
- Density, type and configuration of herbs, shrubs and trees are important components in effecting (reducing potential temperature) of an urban area.
- Relative humidity of areas having dense vegetation is higher.
- Area with vegetation has low temperature (3-4°C) and wind speed with higher relative humidity.
- As temperature increases, relative humidity decreases.

Suggestions:

- Since buildings obstruct the wind flow at their height and abrupt changes in building height significantly impact wind speed on the streets, an urban zoning policy could be implemented for allowable height transition to have gradation along the prevailing wind direction.



Figure 9: Schematic section to represent height gradation (source: sun, wind and light, G.Z.Brown and Mark Dekay)

- Since at most heights, the temperature of data point inside the park and near the park is the lowest hence if pockets of green are intermediately and regularly placed, it would play an important role in the balance of the overall microclimate of the urban area.
  In India , for the 10% open space rule ,the safest option adopted by developers is leaving that area together at one place in the development area. If a minimum and maximum area is prescribed in the guidelines, it would facilitate even distribution of green and open spaces.

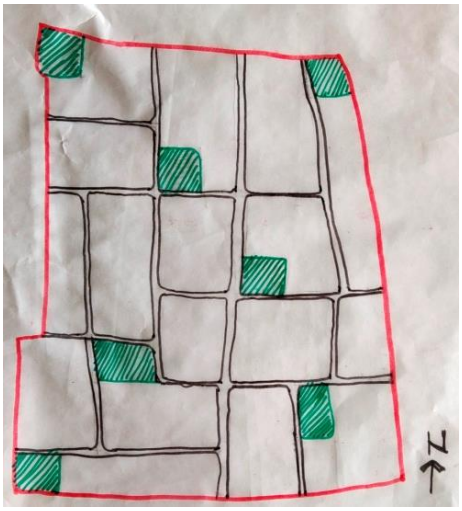


Figure 10: Representative plan of study area showing intermediate green pockets (source: author)

References:

1) .Krishnan Arvind, Nick Baker, Simos Yannas, SV Szokolay, Climate responsive Architecture, Tata McGraw-Hill Publishing Company Limited, New Delhi,2001.(pgs 84-93)
2).Koenigsberger, Ingersoll, Mayhew,Szokolay, Manual of tropical housing and buildings. Orient Longman 2001.
3)Givoni B. (1976), Man, Climate and Architecture, Van Nostrand Reinhold Company, London.(pgs 243- 293)
1) www.mdpi.com/2071-1050/6/11/7894/pdf (accessed on 18n febrauary 2015)
2) http://mnre.gov.in/solar-energy/ch2.pdf (accessed on 18n febrauary 2015)
3) http://www.urbanclimate.net/matzarakis/papers/BMIUF_18_2009_MzMa_SVF.
pdf((accessed on 18n febrauary 2015)
7)Using ENVI-met to simulate the impact of global warming on the microclimate in central European cities, Berichte des Meteorologischen Instituts der Albert-Ludwigs-Universität Freiburg Nr. 18 (2008):Helmut Mayer and Andreas Matzarakis (eds.): 5th Japanese-German Meeting on Urban Climatology,October 2008, pgs. 307-312
8)Street Design and Urban Microclimate: Analyzing theEffects of Street Geometry and Orientation on Airflow and Solar Access in Urban Canyons, Journal of Clean Energy Technologies, Vol. 1, No. 1, January 2013
9)A Study on Micro-climate of URBAN CANYON and Its Impact on Surrounding Urban Area, PLEA 2014
9)Tall Buildings and the Urban Microclimate in the City of London, PLEA 2014
10)An ENVI-met Simulation Study on Urban Open Spaces of Dhaka, Bangladesh, PLEA 2014
11)The Impact of Vegetation on Urban Microclimate to Counterbalance Built Density in a Subtropical Changing Climate,PLEA 2014
12)Sun, Wind and Light ,Architectural design strategies, Mark Devay and G.Z. Brown. (pg 83-92)

A study on Park Cooling Island Effect on Surrounding Urban Area, in Urban Design Perspective

Tong Wu, Department of Urban Planning and Design, Nanjing University, No. 22, Hankou Road, Nanjing 210093, (China)
Shuowen Chi, Department of Urban Planning and Design, Nanjing University, No. 22, Hankou Road, Nanjing 210093, (China)
Youpei Hu[1]*, Department of Urban Planning and Design, Nanjing University, No. 22, Hankou Road, Nanjing 210093, (China)*

ABSTRACT

Previous studies have shown that urban green space has a cooling island effect, which is beneficial to mitigate urban heat island, especially in the hot-summer region. However, Researchers' interest is mostly concentrated on the green space itself, and there are a few researches on the phenomenon of the spread of cooling island to surrounding urban areas under the influence of urban wind, which could have a more positive and broad meaning for mitigating UHI. This study focuses on the latter, and aim to identify the key factors which are manipulatable in urban design perspective among various factors influencing the diffusion of green cooling island.

The city of Nanjing is selected as the background city, because of its long-time and high-temperature summer. Two green spaces with different characters are chosen to conduct field measurement, from which the first-hand meteorological data are obtained, and then used to adjust the micro-climate simulation platform, ENVI-met, to ensure the reliability of simulation. Various factors, including green space own factors, meteorological factors, and surrounding urban fabric are parametric analyzed own to simulation method, from which, qualitative conclusions are drawn on the co-relation between factors and the diffusion distance of cooling islands. In the third part, we applied the knowledge obtained in this research to optimize the downwind urban fabrics of a test case. The result shows that with the knowledge, feasible urban design strategies could be applied to maintain and enlarge cooling island effect on surrounding urban area.

Keywords: Park cooling island, urban fabric, urban green space, urban design strategy

1. Introduction

As is well-known, the process of the urbanization has made a large number of artificial structures represented by concrete materials in the city replace the natural underlying surface, which makes the city form a local high temperature zone relative to the surrounding suburban environment, namely “urban heat island” (J.A. Voogta et al. 2003). The heat island effect brings great harm to urban life and development. It directly affects temperature and precipitation, and greatly harms human health (Tan, J et al. 2007).

1 Corresponding Author: [youpei.hu@nju,edu.cn].

Trees and green space could help in improving urban microclimates and mitigating urban heat islands. Trees not only reduce the high temperature caused by solar radiation through shading, but also affect air movement and heat exchange, absorb solar radiation and cool the air by evapotranspiration to achieve local cooling, forming a so-called green space cold island (Barradas, V. L. 1991). Many studies have proved that green space brings valuable practical effects to alleviate heat islands (Fanhua K et al. 2016) (H. Taha et al. 1991) (H Akbari et al. 1997).

The earlier researchers in the world about the phenomenon of green space cold islands are represented by T.R.Oke and R.A. Spronken-Smith. Through a large amount of data measurement and mathematical model establishment, it is confirmed that the urban public green space represented by the green-covered park has local low-temperature airflow phenomenon in both daytime and nighttime (Oke, 1989). Later, Jauregui, E, Barradas VL, Taha, H., Tsuyoshi Honjo and others conducted study on the cold island strength and influencing factors of park green space of different scales, shapes and configurations in cities (Spronken-Smith 1998.1999) (Ca et al. 1998) through the measurement of meteorological data of specific park green space and the application of satellite photo remote sensing technology. The research on the influencing factors of the green space cold island intensity is also deeper. It is believed that the size, shape and internal planting types of urban parks are several important internal factors affecting the cold island effect of urban parks (Wardoyo et al. 2012) (Chen Yu et al. 2006) (X Cao. 2010) (Chang et al. 2007) (Du. 2018). After decades of development, a large number of researchers have already produced meticulous and fruitful research results on the green space cold island itself. However, for the green space cold island under the movement of the urban wind field, there is relatively little research, especially the green space of urban area that is down the wind. The diffusion effect of the cold island is obviously more positive for mitigating the heat island phenomenon in the larger urban environment.

Since the 1990s, scholars have made early speculations and assumptions about the spread of urban green space cold islands. Representatives such as Victor L. Barradas, Tsuyoshi Honjo, RASpronken-Smith, etc., through the establishment of mathematical model simulation, data measurement and satellite remote sensing photo analysis and other technical methods, verified that under the action of the urban wind field, the green space cold island will spread to the outer wind. (Upmanis et al. 1998) (Spronken-Smith. 1994). More scholars believe that this diffusion can affect the range of a few hundred meters downwind. (Feng et al. 2012) (Su et al. 2010) (Hamada et al. 2010) (Gudina et al. 2014).

Most of the existing research on the spread of green space cold islands is based on measured cases. Limited by the sample size of the cases, the uniqueness of the individual cases, and the factors affecting the diffusion, it is difficult to analyze the performance of a single factor and draw universal conclusions (Bowler et al.2010). This study adopts the methodology of parametric modeling and microclimate simulation, and intends to make up for the weakness of research in the case study, so that the utility of single factor can be clearly manifested.

This study consists of three main parts. Firstly, the reliability of the ENVI-met simulation platform is tested in the first part, and the accuracy of the simulation data is improved by correcting the ENVI-met parameter setting based on the measured data. The second part simulates the single factor change of the ideal green space model. The qualitative conclusions of the influence of each factor on the diffusion distance of the cold island are obtained by means of quantitative analysis. The third part is the case study. Based on the qualitative conclusions drawn from the second part, from the perspective of urban design, under the premise of not changing

the floor area ratio and building type, the design of a case of architectural form layout of urban green space that is down the wind. The simulation results shown that the urban shape optimization strategy based on the development of qualitative knowledge of influencing factors can effectively expand the diffusion of park cooling islands, thus generating positive ecological value on a wider scale.

2. Methodology

2.1 Test cases and measurements

The city selected for this data survey is Nanjing, the capital of Jiangsu Province, China (east longitude 118°22'-119°14', north latitude 31°14'-32°37'). Its extreme temperature in summer can reach 39.2 °C. Summer in Nanjing is hot and humid with poor comfort.

This survey selected two urban parks green (Fig.1), namely: Beiji Ge Park and Longjiang Moonlight Plaza, where Beiji Ge Park is a municipal park green space. It is a small mountain with an area of about 10ha, an altitude of 60m and a green rate of 85.8%. The trees in the site are represented by tall cedar, camphor tree, and firmiana simplex, and the vegetation coverage is high. Longjiang Moonlight Plaza is a community-level small park. Its site is flat, with an area of about 1ha, and the arbor coverage of the square is high, represented by cedar and metasequoia.

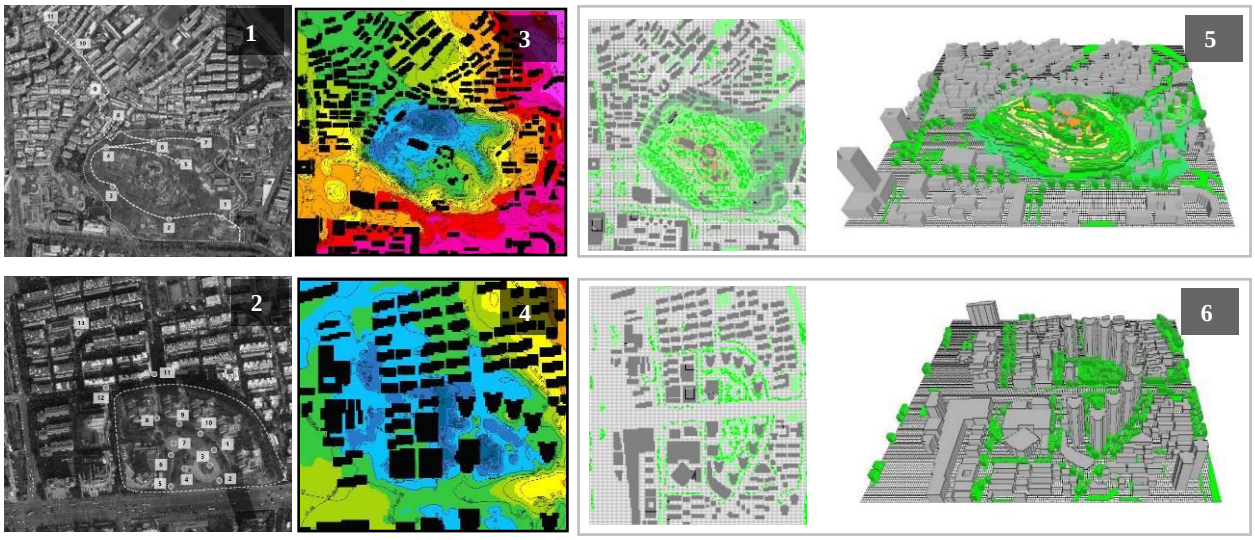


Fig. 1. 1 is Beiji Ge. 2 is Longjiang. 3 is simulation model. 4 is simulation results. 5 and 6 are site plan and 3D view of two cases.

This case measurement was conducted in the summer of 2018. Site 1 (Beiji Ge Park) is measured from 6 am to 8 pm on July 28th. Ten observation points are set in the measured site and another three points are set in the northwest of the site, because the dominant wind directions in Nanjing in summer are east and southeast wind.The measured time of Site 2 (Longjiang Moonlight Plaza) is from 6 am to 8 pm on July 21. Seven observation points are set in the measuredsite, and four points are set in the northwest direction of the site.Set the meteorological data collection point in the measured site and collect the temperature with the XIMA AS847 measuring instrument.And the modes of transportation to record data are cycling and walking respectively, the cycling time through all observation points is within 20 minutes, ensuring the timeliness of data.All the observation points of the two measured sites are set under the architectural projection or vegetation cover, and the data is re-recorded every hour.

2.2 Calibration of ENVI-met

In ENVI-met V_4.4.1, the input parameters required for the model simulation are set in SPACES and ENVI-guide respectively. Model size, model location, nested grid parameters, vegetation parameters, building material parameters, and underlying surface parameters are set in SPACES. The simulation duration, weather parameters, and simulated boundary condition parameters are set in the ENVI-guide (Table. 1).

Table 1. ENVI-met simulation condition setting

Steps of parameter input	Parameter option	Input value
Model grid	X, Y coordinate grid	180×180 (5m resolution) Longjiang 180×180 (5m resolution) Beiji Ge
	Z coordinate grid	25 (2m resolution, B2) Beiji Ge 25 (2m resolution, B2) Longjiang
Simulation location	Latitude and longitude	118.72，32.05
	Time zone	China Standard Time/GMT+8
Simulation duration	Start time	2018.07.21，06:00 (Longjiang) 2018.07.28，06:00 (Beiji Ge)
	Simulation duration (hours)	72 h
Meteorological parameters	Wind speed (10 meters height)	2.2 m/s
	Wind direction (0:N 180:S)	135°
	temperature	26-34℃ (Longjiang) 27-36℃ (Beiji Ge)
	humidity	75% (Longjiang) 79% (Beiji Ge)
Vegetation parameter	3D Plants Trees	K1 Koelreuteria paniculata
	Simple Plants Meadows	XX (25cm high meadows)
Building material parameters	Exterior wall	MI (moderate insulation)
	roof	MI (moderate insulation)
Underlying surface parameters	Main road	ST (Asphalt Road)
	Residential road	PG (gray concrete road)
Nested grid parameters	Quantity	5

Steps of parameter input	Parameter option	Input value
	Material	PG (gray concrete road)
Boundary condition parameter	Temperature and humidity boundary	Open (open type)
	Turbulent boundary	Forced (closed type)

Comparing the measured data with the simulated data, it was found that the highest temperature of the simulated data appears at 4 pm, which was inconsistent with the highest measured temperature at 2 pm. After the careful checking the setting in ENVI-met, we found that the default maximum temperature of ENVI-met was 4 pm. After reset the maximum temperature at 2 pm, the simulation data was in better agreement with the actual measurements (Fig. 2. Fig.3).

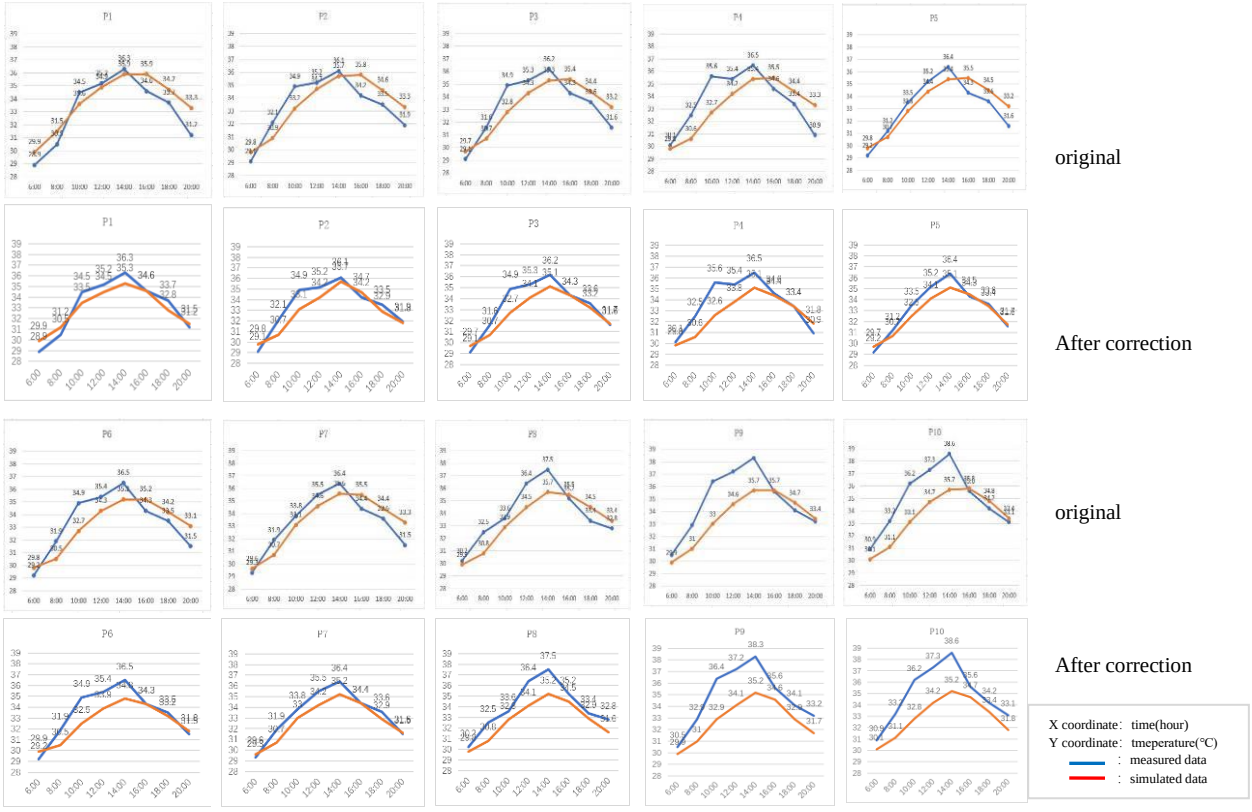


Fig. 2. Comparison of measured and simulation temperature (observation points) of park of Beiji Ge.

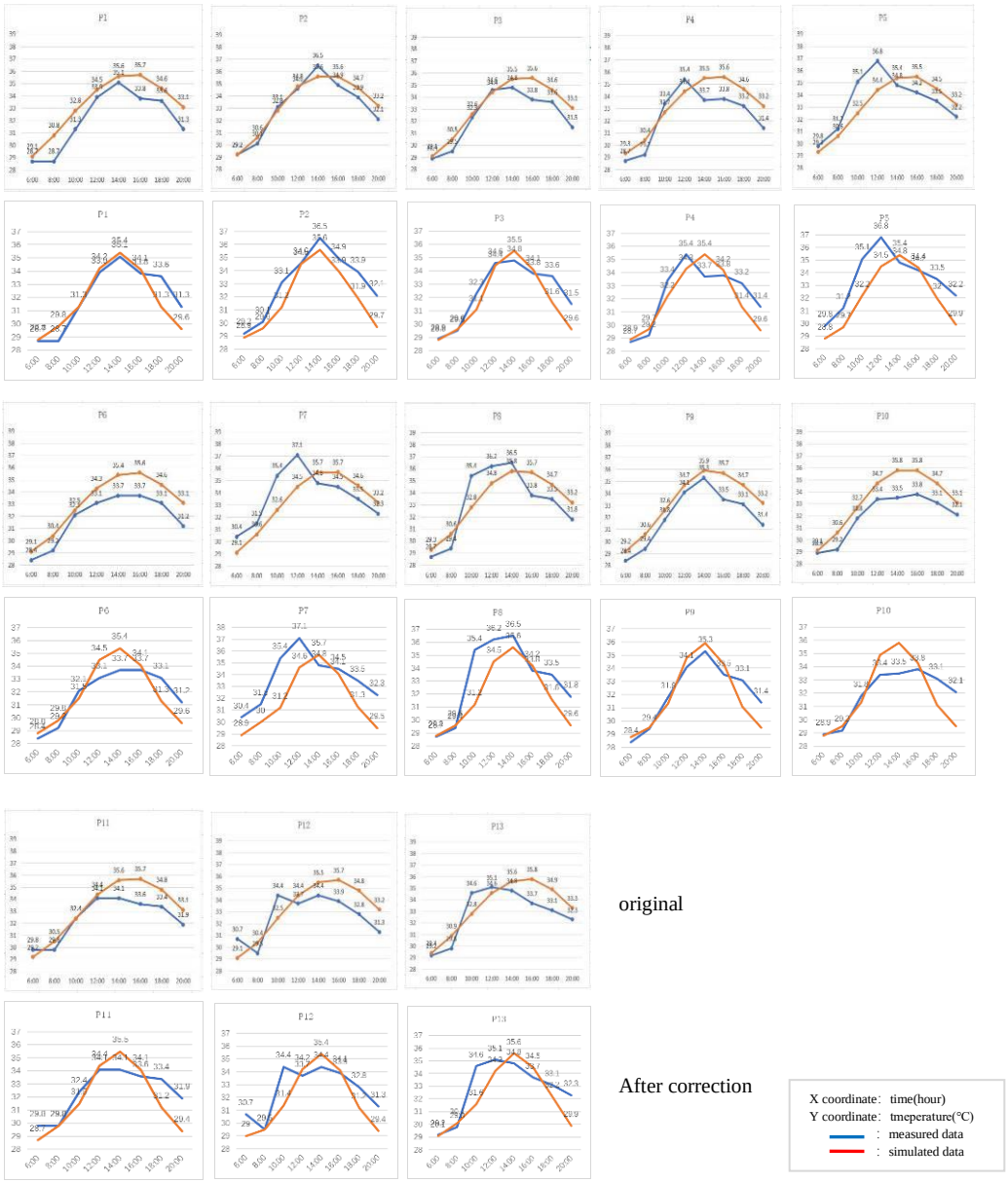


Fig. 3. Comparison of measured and simulation temperature (observation points) of Longjiang plaza.

Although there are detail inconsistent in some points, due to the complicated local context disturbing, like turbulence, anthropogenic heat, but the general trend and magnitude of temperature are the same. This result proved that ENVI-met is reliable as the simulation platform for our study.

2.3 ENVI-met Simulation

The ENVI-met parameter input used in the ideal model simulation is similar with the input value of the case simulation in the previous section. The simulation starts on July 21, 2018, and the duration is 48 hours. The temperature, wind speed and humidity are taken from the typical summer day weather data of Nanjing. See (Table 1) for model input parameters.

Systematic simulation of single factors include the factor of greenland,the factor of meteorological and the factor of urban fabrics. Greenland factors including the size,shape, plants,topography of the greenland. And meteorological factors including wind speed and direction,air humidity,cloudage change,and season.Urban fabric factors mainly focus on the windward area , building interval and orientation.

3. Simulation Results

3.1 Park Own Factors

3.1.1 Size

Set several groups of ideal square green space (1ha green, 2ha green, 5ha green, 10ha green, 20ha green, 40ha green, 80ha green and 160ha green). Under the premise of not changing the software basic simulation parameters and initial meteorological parameters and other factors that may affect the results of the green space cold island experiment, simply increase the green space size by multiples to directly study the relationship between the green space size and the green space cold island diffusion range.

The value of the isotherm temperature at the edge of the cold island diffusion distance is 0.2 °C lower than the average ambient temperature. Through the research results, it is found that the 1ha green space and 2ha green space model have weaker cold islands and the diffusion phenomenon is not obvious. The 5ha green space is the starting threshold for the apparent spread of cold islands. In the 5ha to 10ha interval, the diffusion distance of the cold island increased by nearly 130 meters, and the growth trend was obvious. The diffusion distance of the cold island increased by 30 meters from 10ha to 40ha, and the growth trend slowed down noticeably. In the 40ha to 160ha interval, the green area has expanded by 120ha and the cold island diffusion distance has increased by nearly 50m. The growth trend is more gradual than the previous stage (Fig. 4). Therefore, the cold island diffusion effect and benefit of the 5ha to 10ha green space is the best, which is also the scale of most small and medium green areas in Chinese cities.

3.1.2 Shape

Some researchers have done a qualitative study on the relationship between the spread of green space cold islands and the green space shape index, and draw different conclusions. Some scholars have proved that there is a positive correlation between the green space shape index and the cold island intensity, while some scholars believe that it is a negative correlation (Chen et al. 2012). However, there are few studies on the shape index and the diffusion distance of cold islands.

Setting a 10ha green space model of the same area and associated with different morphological index (land surface index) values. The LSI (morphological index) value ranges from 1.13 square green to 1.81 aspect ratio 1:8 strip green, and there are four sets of models. The simulation is performed without changing other conditions. The following figure extracts the peak temperature of 14 points on the second day of simulation (2018.7.22) as an example to compare the difference between the intensity and diffusion range of cold islands in different green space patterns.

The research found that as the green form index (land surface index) ncreases, the diffusion distance of the green space cold island gradually decreases (Fig.4). We noticed that with the increasing of LSI, the depth of the green space in wind direction decreases. So, we

speculate that the depth of the green space in wind direction are the latent factors behind LSI which affecting the diffusion distance of the cold island.

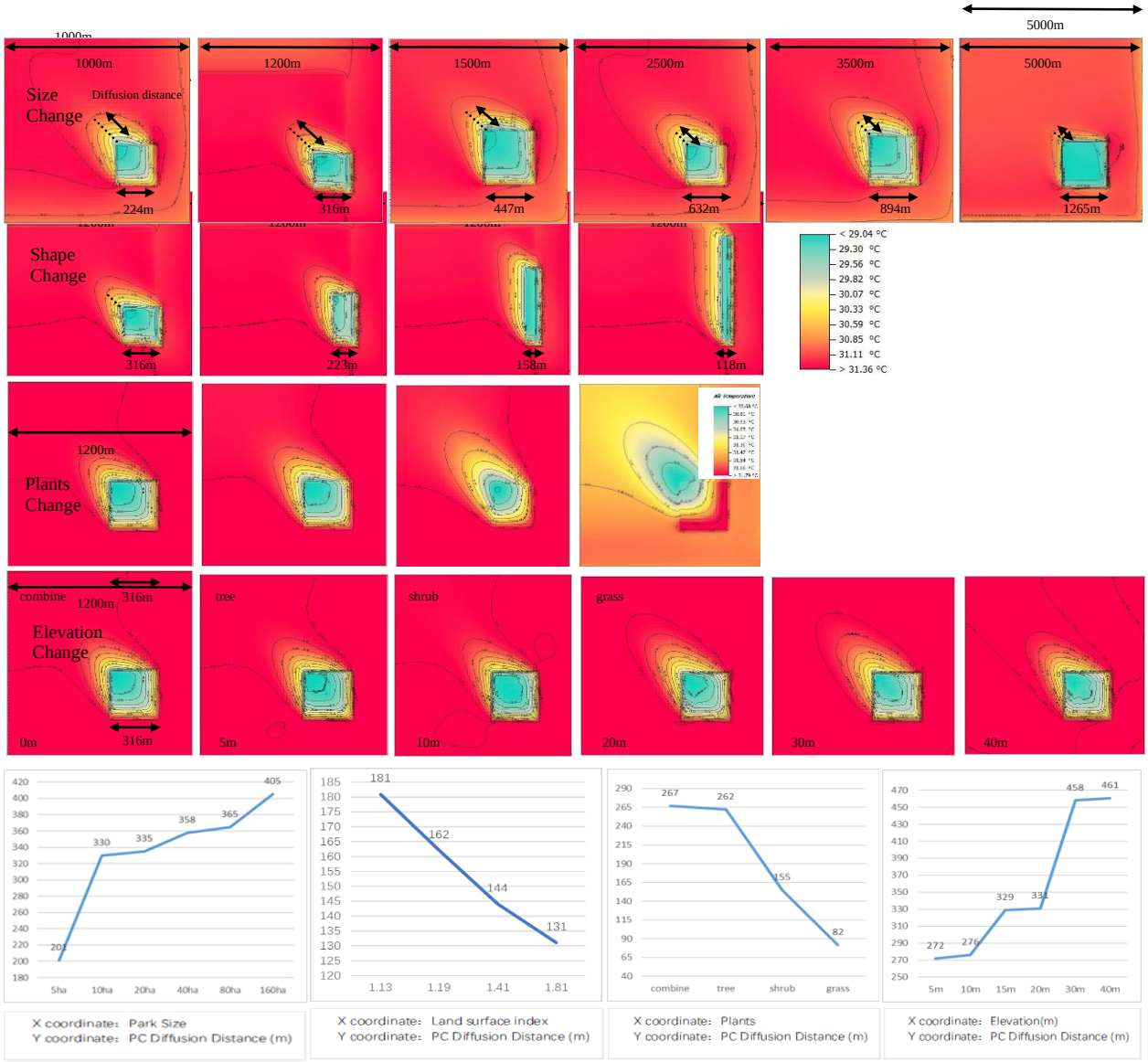


Fig. 4. ENVI-met simulation results about park own factors. First row represents size change. Second row represents shape change. Third row represents plants change. Fourth row represents topography change.

3.1.3 Plants

Setting up four groups of 10ha green space of the same size and shape, and only the green space planting is different. Arbors, shrubs, meadows and integrated planting were planted in four groups of models. The study found that the contribution of arbors to the diffusion distance of cold islands is greater than that of shrubs and meadows. The combination of arbors, shrubs and meadows model has the longest diffusion distance. (Fig. 4).

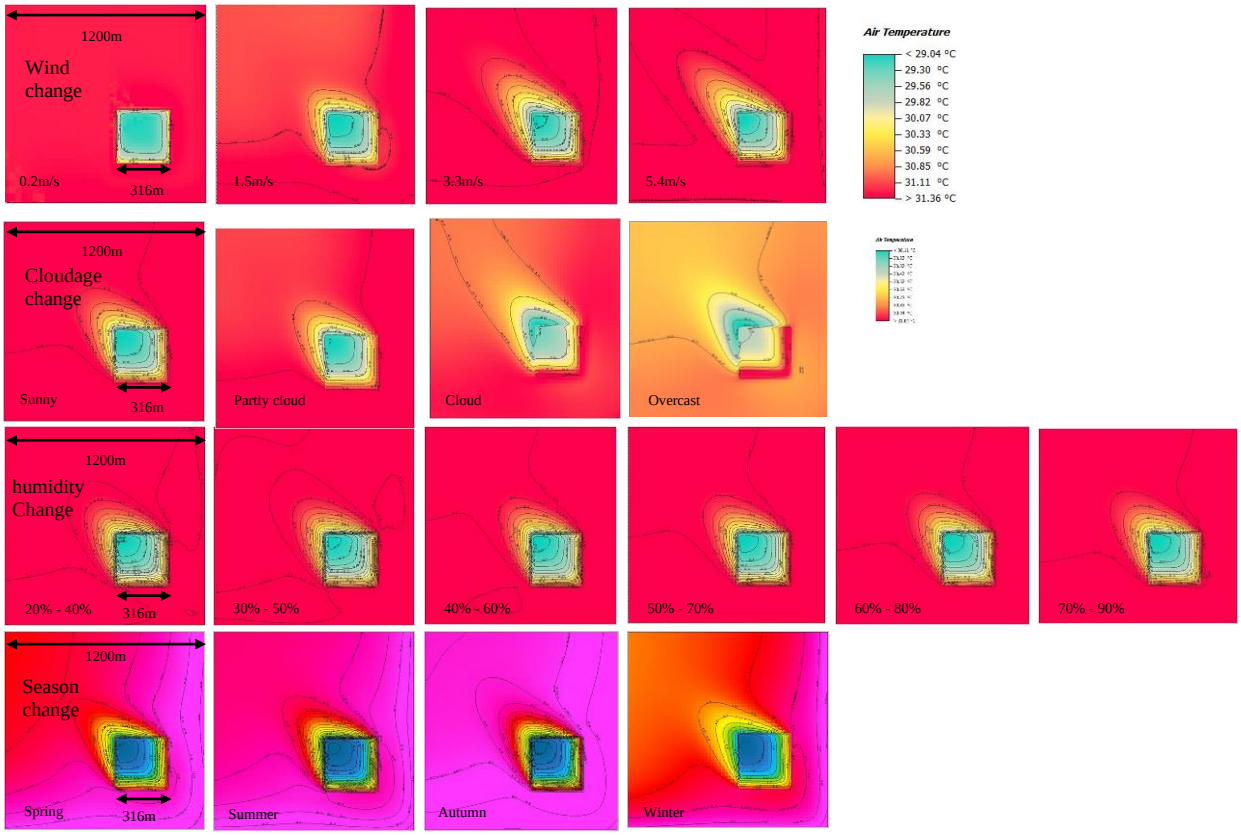
3.1.4 Topography

The height changes of the green space itself is an important factor affecting the spread of green space cold islands, but it has been neglected in previous studies. Setting 7 groups of 10ha green space model, letting the height increased from 0 meters to 40 meters. The simulation found that the 40m elevation green space cold island diffusion range nearly doubled than 0m green space. (Fig.4).

3.2 Meteorological Factors

3.2.1 Wind Speed and Direction

The wind exchanges the local cold airflow of the green space to the downwind to the surrounding environment. Setting four groups of 10ha green space models, letting the wind speed increase from 0.2m/s to 5.4m/s. The simulation results showed that the cold island diffusion distance increases from 18 meters to 355 meters, which indicated that the diffusion of green space cold islands was positively correlated with the wind speed. This shows that the existence of the wind field is a prerequisite for the formation of the diffusion effect of the green space cold island. (Fig. 5)



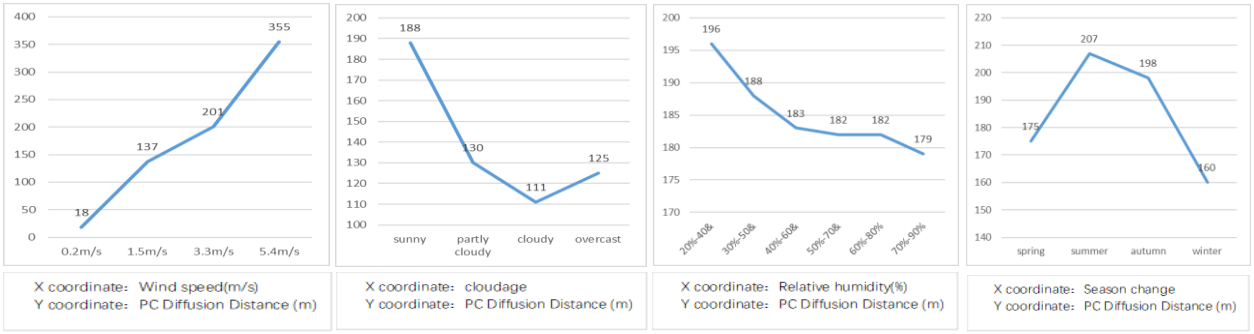


Fig. 5. ENVI-met simulation results about mteorological fctors. First row represents wind change. Second row represent cloudage change. Third row represents humidity change. Fourth row represents season change.

3.2.2 Air Humidity

Setting six sets of 10ha green space models, letting the relative air humidity increase from 30% to 80%. The simulation results showed that as the humidity increases, the diffusion distance of the cold island decreases. Therefore, in the hot and humid regions in summer, considering the dehumidification is a feasible way to improve the strength of the green space cold island. (Fig. 5)

3.2.3 Cloudage Change

Setting four groups of 10ha green space models, letting the cloud parameters be sunny, less cloud, cloudy and overcast. The simulation found that as the traffic volume increases, the cold island diffusion distance gradually decreases. The main reason is that cloud cover is one of the important factors affecting the amount of radiation. When the amount of radiation is affected by the cloud layer, it will reduce the cooling capacity of the plant transpiration endotherm. (Fig. 5)

3.2.4 Season

Setting four groups of 10ha green space, inputting the average temperature of spring, summer, autumn and winter without changing other influencing factors. The simulation found that the cold island has the largest diffusion distance in summer, followed by spring and autumn, and the smallest in winter. The reason for this phenomenon is that vegetation shows differences in transpiration endothermic ability in different seasons. The vegetation types used in this simulation were the ENVI-met model koelreuteria paniculata and the 25 cm high meadows. (Fig. 5)

3.3 Downwind Urban Fabric Factor

Setting the urban fabric around a 10ha green space, which is divided into three types: block, pavilion and slab. With the slab type, changing the orientation of buildings, two more cases are built. The simulation result shows (fig. 6). The sloping slab building has obvious wind guiding properties and the cold island spreads the farthest distance, while the vertical wind direction slab-type building obviously hinders wind diffusion and the cold island diffusion is the smallest. This observation suggests that the frontal area of the fabric in wind direction is a key morphological factor positively affecting the diffusion of the green space cold island. Reducing the frontal area of the building and increasing the building spacing can effectively increase the range of the green underground wind to the cold island.

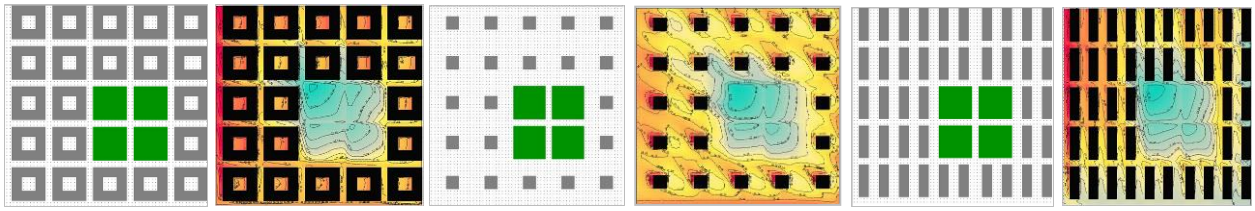


Fig. 6. ENVI-met simulation results about downwide fabric factor. which is divided into three types: block, pavilion and slab.

In summary, the single factor affecting the diffusion of green space cold islands can be divided into controllable factors and uncontrollable factors from urban design perspective. The controllable factors mainly include green space size, shape, planting and downwind urban fabrics. Uncontrollable factors are mainly green space elevation and climate parameters represented by temperature, humidity and wind speed. Therefore, increasing the size of green space, reducing the green form index and enriching the vegetation allocation in green areas are the main internal strategy for increasing the diffusion range of green space cold islands. Reducing the frontal area of the building and increasing the building spacing are the main external design strategy that increase the spread of the cold island.

4. Case study of park cooling island diffusion

The (Beiji Ge Park) area in the previous test case is used as the case study area. This part focuses on the urban fabric factor and explores the urban strategy to expanding the affected area. Based on the original simulation results verified by the measured data, under the premise of not changing the original building volume ratio and building type, we developed two urban design strategies. 1. Reducing the frontal area of fabrics and increasing the building spacing. 2. Setting up a wind corridor. Applying these two strategies, and the premise constraints to the test case, we re-design the downwind fabrics. The simulation is performed again without changing the other parameters of the model. The results are shown in the figure 7. Compared with the control case, it is found that the diffusion range of the cold island is increased by about 200 meters compared with the original site diffusion range, and the diffusion area increased nearly doubled to 10ha. The increased area is the area of light blue and medium green. The cooling zone brought by the cold island spreads to the urban area farther away from the green underground wind, which proves that the optimization strategy is effective (Fig. 7).

The above cases show that the large-scale green space is a valuable source of cold for the city. In reality, the value of this resource is usually limited by the improper urban forms downwind. By applying the optimal urban design strategy in downwind urban area (1, 2), the diffusion zone of the cold island can be expanded to benefit the surrounding urban areas, to a greater extent.

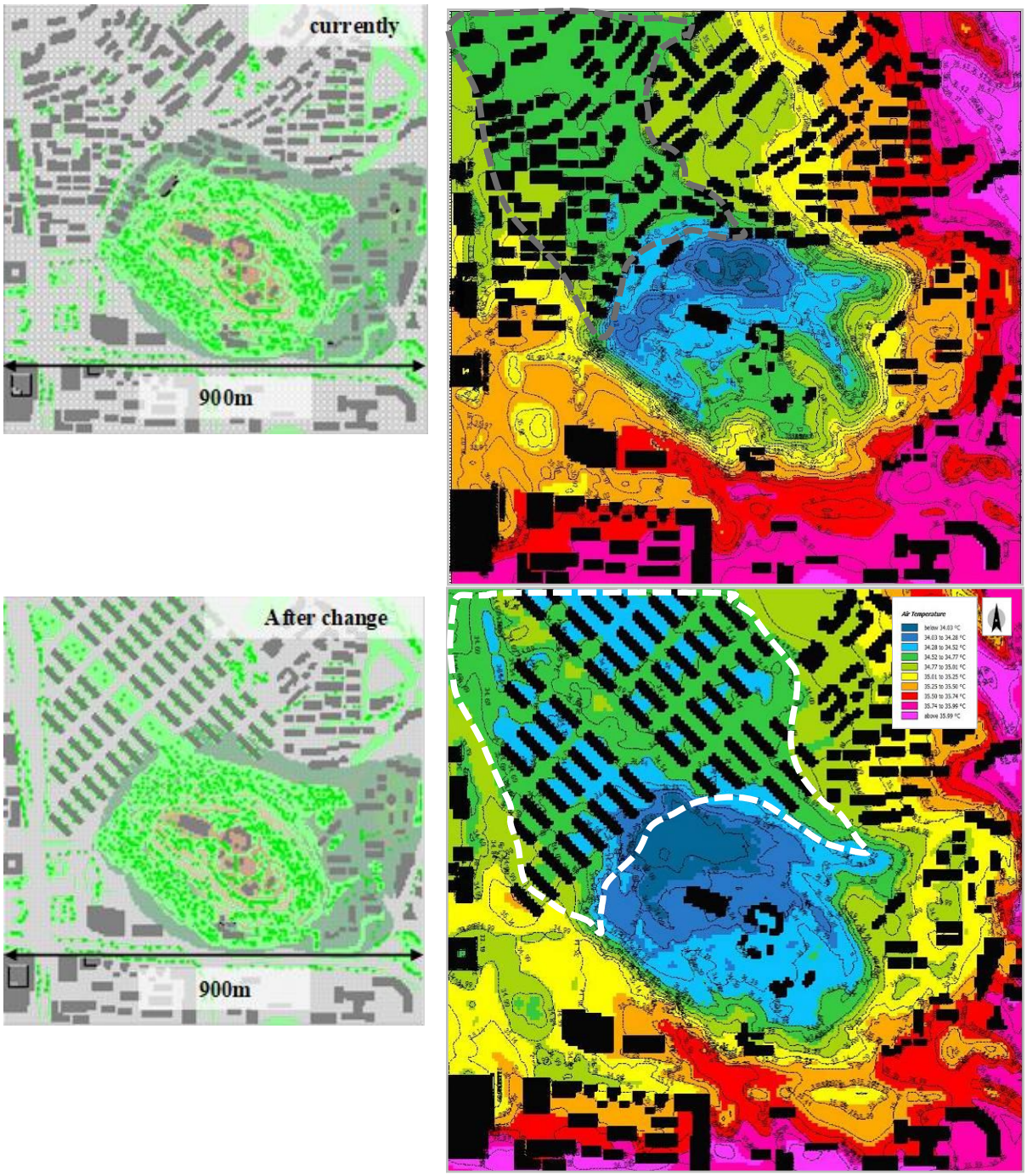


Fig. 7 Redesign of downwind urban fabric of the park Beiji Ge. First two graphics represents the model of Beigi Ge, last two graphics represents simulation results of currently model and redesigned model.

5. Conclusions

This study systematic and comprehensive tests three categories of factors, which might have influences on the diffusion of cooling island to surround urban area. And identify the mainpulatable and sensible factors to urban planning and design. Although the cases we studied was selected in Nanjing, the co-relationship between the factors revealed in this study and the diffusion results is universal. Under different climatic conditions in different locations, the specific diffusion scope will change to some extent, but the influence mode of factors on the diffusion effect is regular.

The first category are the park own factors, including park size, park form, plants in parks, and topography of the park. The green space size and the cold island diffusion distance have a nonlinear positive correlation, and the primitive judgment is an exponential function relationship. As a consequence, 5ha to 10ha green space have the most efficiency to produce cooling island effect. The shape of green space is another factor. More compact shape produce stranger cooling island and thus spread to further urban area. We speculate that the depth of the green space in wind direction are the latent factors behind park shape. Green space planting also plays an important role in the intensity and spread of green space cold islands. The larger the leaf area index, the better the shade of the green space and the stronger the cold island will be. This suggest that increasing the proportion of arbor in green areas is a key to increasing the intensity and diffusion range of cooling islands. The topography of green space is the forth factor, the greater the gradient change, the better the formation of cold island diffusion.

The second category of factors are meteorological factors, including urban wind speed, air humidity, cloudage, and day and night season changes. There is a wind speed and air temperature that are positively correlated with the diffusion of the cold island. The negative correlation is the air humidity and cloudage. The spread of cold islands during the day is greater than at night and the diffusion distance of cold islands in summer is greater than that in spring, autumn and winter.

The third category factors are urban fabrics in downwind area. The study identified frontal area of fabric in wind direction, is the key morphological parameter affecting the diffusion distance of the cold island, there is a negative co-relation between frontal area and diffusion distance.

From urban design perspective, among all these factors, only part of them are manipulatable. They are park own factors and urban fabrics in downwind area. Optimal design strategies could be applied to park design, such as optimizing the shape and size of green space according dominant wind. On the other side, reducing the frontal area of urban fabric, enlarging building spacing, or leave open space as wind corridor would be the feasible ways when concern on the downwind urban area.

Acknowledgments

This research was supported by National Natural Science Foundation of China (51538005) and National Natural Science Foundation of China (51578277).

References

Barradas, V. L, (1991), Air Temperature and Humidity and Human Comfort Index of some City Parks of Mexico City. International Journal of Biometeorology, 35, 24-28.

Bowler, D. E, Buyung-Ali, L. Knight, T. M, & Pullin, A. S, (2010). Urban greening to cool towns and cities: A systematic review of the empirical evidence. Landscape and Urban Planning, 97(3), 147–155.

Chen, X. Z., Su, Y. X., Li, D, Huang, G. Q, Chen, W. Q., & Chen, S. S. (2012). Study on thecooling effects of urban parks on surrounding environments using Landsat TMdata: A case study in Guangzhou, southern China. International Journal of RemoteSensing, 33, 5889–5914.

Chen Yu, Wong Nyuk Hien, (2006). Thermal benefits of city parks. Energy and Buildings 38 (2006) 105–120.

Chi-Ru Chang, Ming-Huang Li, Shyh-Dean Chang, (2007). A preliminary study on the local cool-island intensity of Taipei city parks. Landscape and Urban Planning 80 (2007) 386–395.

Du Hongyu, (2018), The Cool Island Effect of Urban Blue-green Spaces and Impact Factors in Mega City: A Case Study of Shanghai. East China Normal University.

Gudina Legese Feyisa, Feyisa, Klaus Dons, Henrik Meilby, (2014). Efficiency of parks in mitigating urban heat island effect: An example from Addis Ababa. Landscape and Urban Planning 123 (2014) 87– 95.

Hashem Akbari, Dan M. Kurn, Sarah E. Bretz, et al, (1997). Peak power and cooling energy saving of shade trees. Energy and Buildings, 1997, 25: 139-148.

H. Taha, H. Akbari, A. Rosenfeld, 1991), Heat Island and Oasis Effects of Vegetative Canopies: Micro-Meteorological Field-Measurements. Theoretical and Applied Climatology Theor. Appl. Climatol. 44, 123-138 (1991).

J.A. Voogta, T.R. Oke, (2003). Thermal Remote Sensing of Urban Climates. Remote Sensing of Environment 86 (2003) 370–384.

Jono Wardoyo, Atiek Suprapti, Hermin Wediningsih, (2012). Vegetation Configuration as Microclimate Control Strategy in Hot Humid Tropic Urban Park. Journal of Applied Sciences Research, 8(11): 5306-5310.

Oke, T. R, (1989), The Micrometeorology of the Urban Forest. Phil. Trans. Roy. Soc. Lond. B324,335–349.

R. A. Spronken-Smith, (1994), Energetics and cooling in urban parks. Vancouver: The University of British Columbia.

R. A. Spronken-Smith, T.R. Oke, (1998). The thermal regime of urban parks in two cities with different summer climates. int. j. Remote Sensing, 1998, vol. 19, no. 11, 2085- 2104.

R. A. Spronken-Smith, T.R. Oke, (1999). Scale Modelling of Nocturnal Cooling in Urban Parks. Boundary-Layer Meteorology 93: 287–312, 1999.

Shuko Hamada, Takeshi Ohta, (2010). Seasonal variations in the cooling effect of urban green area surrounding urban areas. Urban Forestry & UrbanGreening9(2010)15–24.

Tan, J, Zheng, Y, Song, G, Kalkstein, L.S, Kalkstein, A.J, Tang, X, (2007). Heat wave impacts on mortality in Shanghai,1998 and 2003, Int. J. Biometeorol. 51, 193–200.

Upmanis. H, Eliasson. I, Lindqvist. S, (1998). The influence of green areas on nocturnal temperatures in a high latitude city (Goteborg, Sweden). International Journal of Climatology, 18(6), 681–700.

Victor L. Barradas, (1991). Air temperature and humidity and human comfort index of some city parks of Mexico City. Int J Biometeorol (1991) 35:24-28.

Vu Thanh Ca, Takashi Asaeda, Eusuf Mohamad Abu, (1998). Reductions in air conditioning energy caused by a nearby park. Energy and Buildings 29 (1998) 83-92.

Xiaogang Feng, Hui Shi, (2012), A Study on “Cold Island Effect” of Xi’an Urban Park in Summer based on Remote Sensing. Journal of Ecology, 32(23):7355-7363.

Xin Cao, Akio Onishib, Jin Chena, Hidefumi Imura, (2010). Quantifying the cool island intensity of urban parks using ASTER and IKONOS data. Landscape and Urban Planning 96 (2010) 224–231.

Yongxian Su, Guangqing Huang, Xiuzhi Chen, Shuisen Chen, (2010), The Cooling Effect of Guangzhou Urban Park on Surrounding Environment. Journal of Ecology, 30(18):4905-4918.

Surface Temperature Reduction by Tree Shade: Influence of Tree Characteristics

Andrew Speak [1a], Leonardo Montagnani [1], Camilla Wellstein [1], Stefan Zerbe [1]
[1] Faculty of Science and Technology, Free University of Bozen-Bolzano, Bolzano, Italy
[a] corresponding author – email: andyspeak33@gmail.com

ABSTRACT

The shade provided by trees in cities can help to counteract Urban Heat Islands (UHI). This study used a thermal camera to record the surface temperatures of three common urban surfaces – asphalt, porphyry, and grass – in the shade of single tree crowns, of multiple species, during the peak temperature period of summer days. By subtracting from the temperature of adjacent unshaded ground, measures of the degree of cooling were made. The cooling was related to a multitude of tree traits, of which Leaf Area Index (LAI) and crown width were the most important. Median average cooling of 16.4, 12.9 and 8.5 ^{o}C was seen in the western edge of the tree shade for asphalt, porphyry and grass, respectively. Maximum temperatures were reduced by roughly 19 ^{o}C for all surface types. Strategic planning of single trees in cities can have significant impacts on the absorption of solar radiation by ground surface materials and thus the magnitude of the UHI.

Introduction

Urban centres are subject to a higher mean annual temperature compared to their rural hinterlands, with resulting urban heat island (UHI) magnitudes of 5 – 6 ^{o}C (Oke, 1982). Nature-based solutions such as tree-planting are being sought to tackle the threats to human health and economy which result (Roy et al., 2012). The leaves transpire, a process which utilises heat energy to convert water to vapour (Gkatsopoulos, 2017), and the interception of sunlight by the tree canopy prevents it reaching, and heating, adjacent urban surfaces. This direct shading has important effects on human thermal comfort, as it is the radiation exchange with the surrounding environment which most influences a person's perceived thermal comfort (Matzarakis et al., 2007). Research in cities has so far tended to focus on the effect of shade trees on building energy use (Akbari, 2002; McPherson and Dougherty, 1989) rather than the outdoor thermal environment.

Tree canopies have a range of efficiencies related to reduction of shortwave radiation with average transmissivities through foliated tree crowns of 1.3 to 5.3 % of direct radiation and 8 – 15 % of total radiation (Konarska et al., 2014). Shade factors of trees in the US typically range from 70 – 90 % and there are large species differences with *Gleditsia triacanthos* providing low shade with 62 % while *Tilia cordata* can have a shade factor up to 93 % (McPherson, 1984). Several studies have focussed on the cooling effect that tree shade has on urban surfaces. Armson et al. (2013) recorded asphalt surface temperature reductions of 12 ^{o}C in Manchester, UK, and species and Leaf Area Index (LAI) were both significant factors. Higher cooling of up to 19 ^{o}C was revealed in parks in Manchester, where larger trees in continuous canopy stands can be found

(Armson et al., 2012). A study in the hotter climate of Serbia showed shaded asphalt can be over 20 ^{o}C cooler than sunlit asphalt, however no data on tree height or species were presented (Đekić et al., 2018).

Sanusi et al. (2017) linked measured thermal comfort indices to Plant Area Index (PAI), a photographically estimated vertical canopy density index, for three tree species. They found air temperature, solar radiation, mean radiant temperature, and Physiologically Equivalent Temperature (PET) all decreased significantly with increasing PAI but species differences in leaf and canopy characteristics did not appear to be significant, only the PAI. Lin and Lin (2010) attempted to link multiple tree traits to the sub-surface soil cooling effect seen in a park in sub-tropical Taipei City, Taiwan. Regression analysis revealed foliage density to have the greatest contribution to cooling, followed by leaf thickness, leaf texture and then leaf colour lightness.

These studies hint at the role that different tree traits, such as LAI and leaf colour lightness, play in the cooling of urban areas by trees, and hence the importance of species choices for tackling elevated summer temperatures in built up areas. The unique dimensions of each tree crown will also play a large role in the magnitude of cooling that can be expected, as they dictate the area of ground that will be shaded. Differences among and within species in attenuation of solar radiation is something which is under-researched (McPherson et al., 2018) and this study addresses that gap by using thermal imaging to quantify the effect of solitary shade trees on the surface temperatures of three common urban floor materials. Specifically, we aim to address the following research questions:

- What is the magnitude of surface temperature reductions that can be observed on three urban surface types as they pass through the tree shadow?
- Which tree traits are more important in the control of this cooling effect?

Methodology

The study was conducted in the city of Bolzano (population 107,000) in northern Italy between August and September 2018. Bolzano has a moist, continental climate (Köppen classification ‘Cfb’) characterised by hot summers. Fieldwork was undertaken on eight clear, sunny days with low winds, and all measurements were taken between 11:00 and 16:00 hours to capture the time-period with maximum sun-shade surface temperature differences. Walking transects were pre-arranged with the goal of covering as much of the city as possible and including a wide range of tree species and sizes for three common floor surface types - asphalt, porphyry and grass. Trees were included in the study if they stood alone without any shade interference on the adjacent ground from buildings or other trees for at least two hours before measurements were taken. Solitary trees are chosen as a basis for determining the direct effects of a single tree canopy, which avoids the more complex effects from multi-tree canopies. A total of 332 trees were sampled.

Thermal images were taken at a height of 1 m with the field of view pointed perpendicular to the ground using a thermal camera (T640, FLIR systems, USA). Three images were taken in

each tree shadow, one at the western edge of the tree shadow where the ground has been in shadow the longest, one in the centre, and one at the eastern edge. A reference image was then taken on the same surface material as under the tree shade where the surface has been out of shade for at least two hours, as close to the tree as possible to avoid changes in surface properties. The maximum and mean average temperatures were subsequently obtained from all images using the FLIR Tools software (FLIR, 2009). The area analysed in each image is 25 cm x 15 cm. Emissivity values of 0.97, 0.98 and 0.96 were used for asphalt, porphyry and grass, respectively. Cooling (ΔT) is calculated as the mean temperature of the exposed surface (reference image) minus the mean temperature of the tree-shaded surface. For some trees, more than one surface type was able to be sampled within the same shadow, providing a few extra data, giving a total of 1,005 ΔT records.

At the same time as the thermal images were taken, solar radiation in the same three locations within each tree shadow, and externally, was measured with an AccuPAR LP-80 ceptometer (METER group Inc., USA). After correcting for solar zenith angle, LAI is calculated using Campbell and Norman's method (1988). A summary of all the additional tree measurements, environmental data and their respective codes and measurement techniques is presented in Table 1. Variables will be referred to by the codes found in this table from here on.

Table 1. Summary of all tree measurements and codes

Measurement	**Units**	**Code**	**Technique**
Cooling	^{o}C	ΔT	Mean surface temperature reference image minus mean surface temperature shaded image
Leaf Area Index	m^{-2} m^{-2}	LAI	Ceptometer
Tree height	m	H	Hypsometer
Crown height	m	C_H	Hypsometer
Crown diameter	m	D	Tape measure
Diameter at Breast Height	cm	DBH	Tape measure
% Canopy missing	%	MISS	Visual appraisal (i-Trees)
% Condition	%	COND	
Gap fraction vertical	%	GAP1	Image analysis of vertically taken hemispherical photos
Log volume	m^3	LOGVOL	Natural logarithm taken of volume
Air temperature	^{o}C	AIRT	Weather Station data
Relative Humidity	%	HUM	
Wind Speed	m s^{-1}	WIND	
Radiation	W m^{-2}	RAD	
Albedo	-	ALB	Photographic estimation
Grass cover	%	GRASS	
Categorisations			
Tree order	-	ORD	Literature
Tree crown shape	-	Cshape	Visual appraisal of horizontal images

Leaf shape	-	Lshape	Literature / visual appraisal of images
Leaf area	cm^2	Larea	Small (0 – 12), Medium (12 – 44), Large (44 +), Needle
Leaf arrangement	-	Larrange	Compound or Simple leaf arrangement
DH ratio	-	DHratio	D / C_H
Tree height factor	-	H_fact	Jenks natural breaks data clustering method
Crown width factor	-	D_fact	

Results

Study Characteristics

The 332 trees sampled in the study comprised 85 species. The weather on the eight sampling days was uniform with an average windspeed of 1.46 m/s (SD 0.24), peak solar radiation between 748 and 909 and average peak air temperature of 28.5 ºC (SD 2.3 ºC). The albedo of asphalt ranged from 0.13 to 0.28 (average 0.22 (SD 0.03)) and that of porphyry ranged from 0.13 to 0.29 (average 0.22 (SD 0.03)). The most common tree height for all surfaces was 5 m.

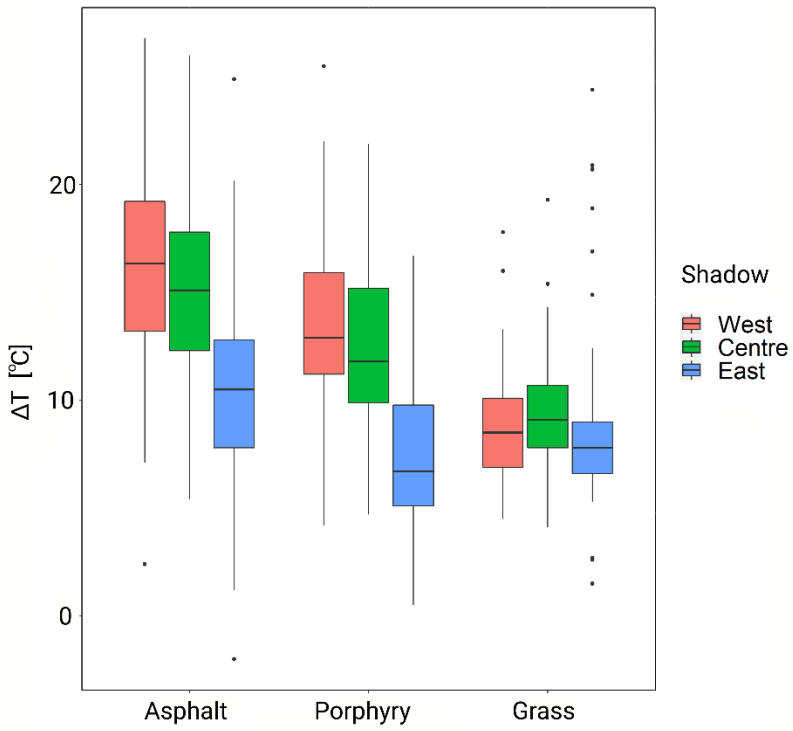


Figure 1. Cooling effect (ΔT) at the three locations (west, centre, east) within the tree shadows for the three surface types.

Cooling Magnitude

Figure 1 shows the different ΔT measured in the three locations in the tree shadow. It is clear that the eastern edge has the lowest cooling as it represents the ground that has only become shaded recently. The cooling in the centre of the tree shadow and at the western edge are more similar (higher at the western edge) and, while they do not differ significantly for grass (ANOVA, F=2.78, p=0.1) or porphyry (F=3.53, p=0.06), they do differ significantly for asphalt (F= 8.67, p=0.003).

The highest cooling of 26.8 ºC was seen at 14:00 on an asphalt surface under an 8m tall *Carpinus betulus* tree with a LAI of 3.92 in the western edge of the shadow and crown width of 6 m. The highest ΔT in general was seen on asphalt (Figure 1), and grass had the lowest ΔT and the least difference between shadow regions. Table 2 shows the effect of tree shade on the surface temperatures, with average maximum temperatures falling by around 19 ºC for all surfaces in the western edge. Maximum temperatures recorded in the sun are 60.8, 62.0 and 63.7 ºC respectively for asphalt, porphyry and grass, and 41.1, 46.4 and 52.9 ºC in the western shade.

Table 2. Maximum and average surface temperatures and the median average cooling for the three surfaces

	Median Maximum surface temp ºC				**Median average surface temp ºC**				**Delta T ºC**		
	West	Centre	East	Sun	West	Centre	East	Sun	West	Centre	East
Asphalt	28.3	30.2	36.5	46.3	26.3	28.5	33.6	43.6	16.4	15.1	10.5
Porphyry	29.7	30.9	36.4	49.4	25.9	27.7	32.2	39.8	12.9	11.8	6.7
Grass	25.3	24.1	26.0	43.2	21.9	21.4	22.6	30.5	8.5	9.1	7.8

Influence of Tree Traits

The bar-charts in Figure 2 show how the cooling varies with various tree characteristics. Leaf size shows that there is some evidence of higher cooling for trees with needles i.e. order Pinales, however more for porphyry and not evident for grass. Leaf arrangement shows that the median cooling is slightly higher for simple versus compound leaves for all surface types. The needle leaf shape has also the highest cooling when compared to other leaf types, with no other patterns apparent between leaf shapes. Tree order also has no clear patterns apart from higher cooling for the Pinales and lower cooling for the Saxifragales. The bar-chart for DHratio shows that ratios above 1, i.e. trees with a greater crown diameter than crown height provide slightly higher cooling on average, however these were only significant for asphalt and grass (ANOVA: F = 11.75, p = 0.0007 asphalt; F = 4.44, p = 0.04 grass; F = 1.12, p = 0.29 porphyry). Using categorical tree height and crown width figures (Figure 3) reveals similar ranges and medians of cooling over the three tree height factors with only porphyry showing markedly lower cooling for

smaller trees. The pattern for crown width is slightly different with small increases in the median cooling in the western and central shadows for asphalt and porphyry.

Correlations of LAI with ΔT were all significant and positive (Table 3) apart from with the grass surface.

Table 3. Correlations of Leaf Area Index (LAI) with ΔT for the three shadow locations on the three surfaces. ** = significance $p < 0.01$

	Shadow		
Material	West	Centre	East
Asphalt	0.19**	0.29**	0.27**
Porphyry	0.49**	0.44**	0.47**
Grass	0	0.02	0.21

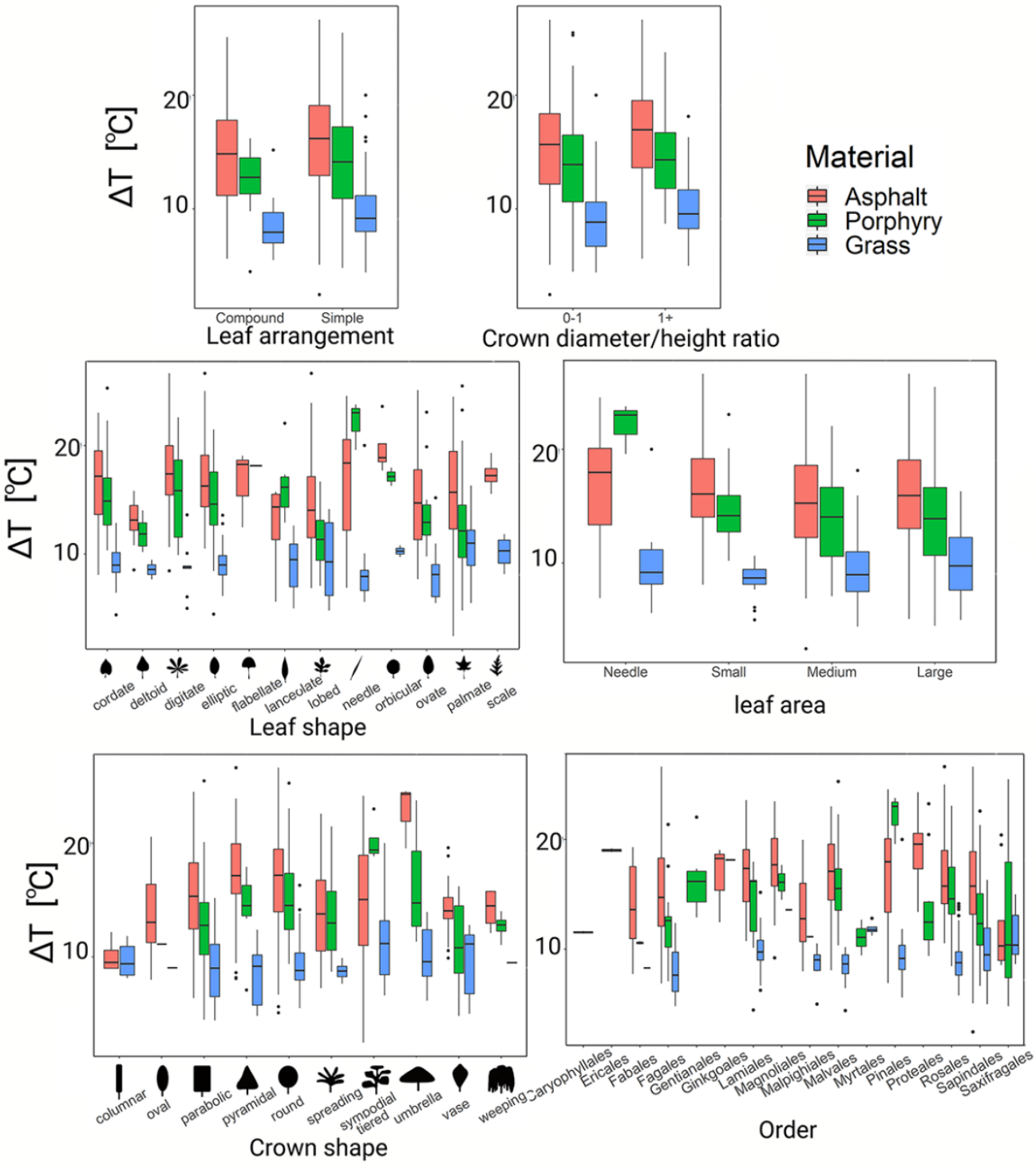


Figure 2. Barcharts to show the trends in cooling for different categoric tree characteristics for the three surface types. For the pooled data of western and central shadows.

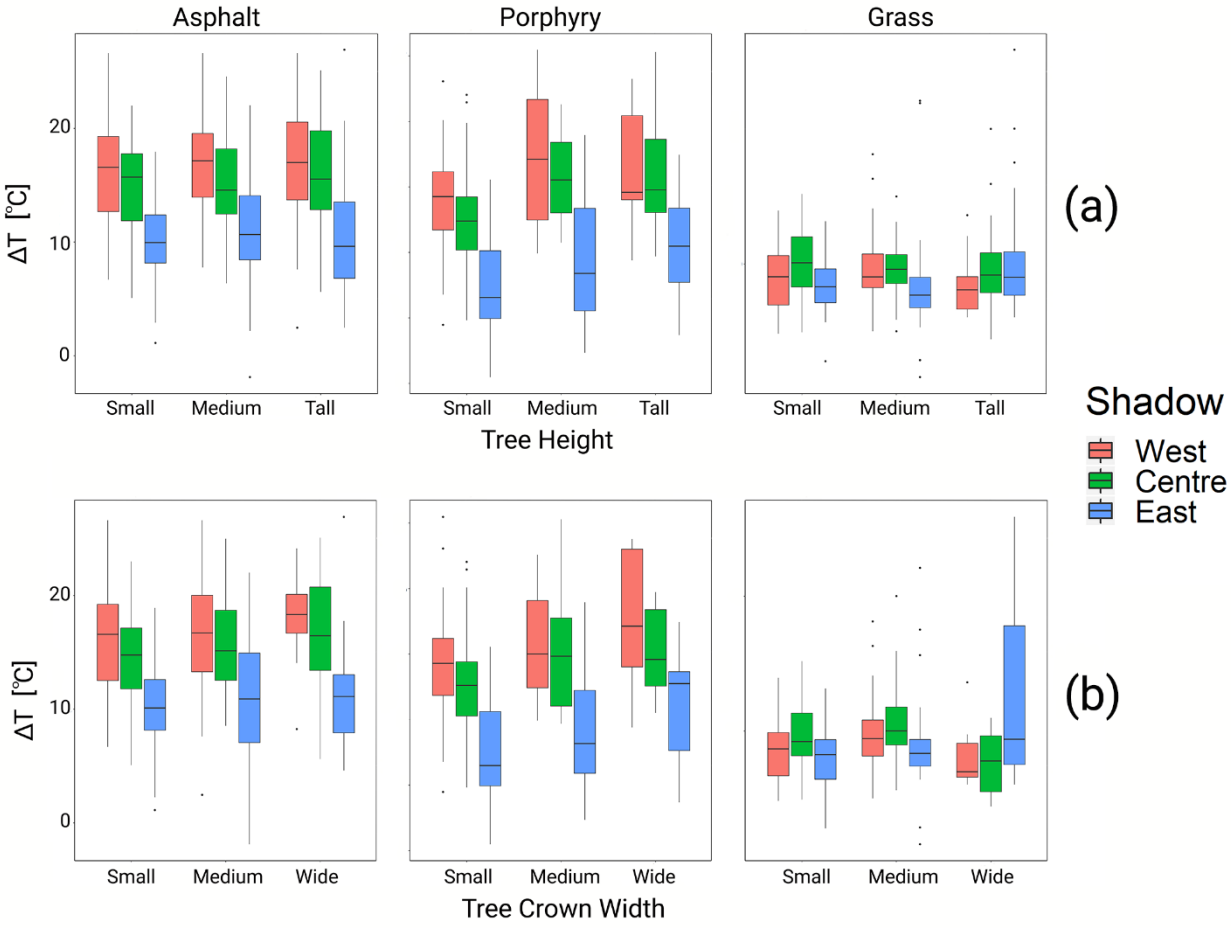


Figure 3. Cooling differences between the three categorical tree height (a) and crown width (b) factors for the three shadow locations on the three surfaces using the adjusted delta T data.

Discussion

Cooling magnitude

The thermal image data confirm that tree shade can reduce the surface temperatures of different urban surfaces by a considerable amount during the peak solar radiation period of summer days. Shortly after the surface has entered the shadow it loses accumulated heat by radiation, convection, and downwards conduction, and rapidly becomes cooler than the surfaces remaining in the sun by around 10 ^{o}C (Figure 1). As the ground enters the centre of the shadow, even higher ΔT is achieved which then starts to level off towards the western edge of the shadow. Here also, the average difference between maximum temperatures can be around 19 ^{o}C for all surfaces, i.e. reducing maximum temperatures from the high 40 degrees to the high 20 degrees. Eventually, there will come a point within the tree shadow, for dense crowns, where the surface temperature is no longer a function of the loss of stored heat but is linked solely to air temperature. Maximum

relative cooling therefore occurs at a crucial point where the unshaded ground reaches maximum temperatures and before the shaded ground temperatures rise in line with air temperature. This cooling process will of course be counteracted by radiation penetration through the canopy, linked to the unique LAI of each tree, which prevents the shade being complete.

The differences in thermal response between asphalt and porphyry are due to inherent thermal properties of the materials. The cooling trends for the grass surface are less clear-cut. This is due to the added impact of transpiring vegetation, and the facilitation of convection by a higher surface roughness, on surface temperature. One might expect grass to have a more rapid thermal response to any sunlight penetrating the canopy than the hard, higher thermal capacity surfaces. This happens more at the canopy edges due to canopy morphology, which may explain why ΔT appears to fall at the western edge of the shadow for grass surfaces, meaning, in contrast to the other two surfaces, the centre of the tree shade is coolest on grassed surfaces.

Influence of Tree Traits

Different canopy characteristics have subtle effects on the ΔT measured. Simple leaf arrangement, as opposed to compound, gave higher ΔT, presumably from a higher LAI resulting from this particular leaf organisation. Leaf shape did not appear to strongly influence ΔT, however the needle leaf type gave higher ΔT for porphyry. This trend repeated in the order classification with Pinales having higher ΔT for porphyry, and in the leaf size classification. The latter also showed no real differences between the broad-leaved size brackets. For surface temperatures, then, small-leaved trees appear not to have the same higher cooling trend seen for air temperatures in a previous study (Kong et al., 2016). The umbrella and columnar crown shapes gave the highest and lowest ΔT respectively for asphalt. This shows the influence of crown width on ΔT, which was also demonstrated by the increased ΔT from canopies with a DHratio greater than 1. Trees with a sympodial tiered structure include *Sophora japonica* L. and *Cedrus deodara*. The large gaps between clusters of branches in the canopy prevent the shade being complete, and trees with this structure, and the weeping structure, should perhaps be avoided when high surface cooling is a goal. LAI, as for other studies (Armson et al., 2013; Sanusi et al., 2017), is an important factor controlling the penetration of radiation through the canopy.

Conclusion

It is interesting that tree height does not appear to be as important as crown width for cooling. This is an important result and implies there is no need to choose tall-growing species to maximise cooling in the current study conditions. Trees with a broad canopy and high LAI should start providing a high level of surface temperature cooling, over a large area, just a few years after planting, with individuals reaching their maximum shade factor after 20 years (diameter at Breast Height (DBH) of 30 cm) (McPherson et al., 2018). Trees in the Pinales order often have dense crowns, providing a high LAI and high ΔT, however the commonly-occurring narrowness of the crowns limits the duration of the shadow on the surface.

This study considered single trees only, for simplicity, however the next step would be to determine what additional benefit is provided by trees clustered into canopies. The results from this study can aid in the vegetation parameterisation of urban thermal comfort models which rely on the accurate calculation of mean radiant temperature, such as ENVI-met or RayMan (Matzarakis et al., 2007). With these models the clear benefits provided by trees in terms of surface temperature reduction can be translated into thermal comfort mapping analyses to inform better urban planning. Sanusi et al. (2017) stated that trees with the same PAI give the same microclimate benefit, regardless of other leaf and canopy characteristics, however they only looked at three species. The current study confirms the importance of LAI, however reveals the added importance of crown characteristics, namely width and structure. Leaf size and shape do not appear to influence the effectiveness of tree shade. The significant temperature reductions seen in the western edge of the single tree shades confirm the role of trees in intercepting solar radiation and preventing the build-up of sensible heat in cities. Both day and night Urban Heat Island effects can be counteracted with strategic planting of shade trees.

References

Akbari, H. (2002) Shade trees reduce building energy use and CO2 emissions from power plants Environmental Pollution, 116 (2002), pp. 119-126

Armson, D., Stringer, P., Ennos, A.R., 2012. The effect of tree shade and grass on surface and globe temperatures in an urban area. Urban For. Urban Green. 11, 245–255.

Armson, D., Rahman,M.A., Ennos, A.R., 2013. A comparison of the shading effectiveness of five different street tree species in Manchester, UK. Arboricult. Urban For. 39, 157–164.

Campbell, G.S., and J.M. Norman (1988) The description and measurement of plant canopy structure, pp 1-19. In Russell, G., B. Marshall, and P.G. Jarvis (Eds.). Plant Canopies: Their Growth, Form and Function (ed. G. Russell), Society for Experimental Biology, Seminar Series 29, Cambridge University Press, Cambridge, England.

Đekić, J.P., Mitković, P.B., Branković, M.M.D., Igić, M.Z., Đekić, P.S. & Mitković, M.P. (2018) The study of effects of greenery on temperature reduction in urban areas. Thermal Science 22(4): 988 - 1000

FLIR (2009) FLIR Tools. Retrieved from https://www.flir.com/products/flir-tools/

Gkatsopoulos, P. (2017) A Methodology for Calculating Cooling from Vegetation Evapotranspiration for Use in Urban Space Microclimate Simulations. *Procedia Environmental Sciences* 38: 477 – 484

Konarska, J., Lindberg, F., Larsson, A., Thorsson, S. & Holmer, B. (2014) Transmissivity of solar radiation through crowns of single urban trees – application for outdoor thermal comfort modeling. *Theoretical Applied Climatology* 117 : 363 – 376.

Kong, F., Yan, W., Zheng, G., Yin, H., Cavan, G., Zhan, W., Zhang, N., & Cheng, L. (2016) Retrieval of three-dimensional tree canopy and shade using terrestrial laser scanning (TLS) data to analyze the cooling effect of vegetation. Agricultural and Forest Meteorology 217: 22 – 34

Lin, B.S. & Lin, Y.J. (2010) Cooling effect of shade trees with different characteristics in a subtropical urban park. HortScience 45(1): 83 – 86

McPherson, E.G., 1984. Solar control planting design. In: McPherson, E.G. (Ed.), Energy-Conserving Site Design. American Society of Landscape Architects, Washington, D.C, pp. 141–164.

McPherson, E.G. and Dougherty, E. (1989) Selecting trees for shade in the southwest. Journal of Arboriculture 15(2): 35 - 43

McPherson, E.G., Xiao, Q., van Doorn, N.S., Johnson, N., Albers, S. & Peper, P.J. (2018) Shade factors for 149 taxa of in-leaf urban trees in the USA. *Urban Forestry & Urban Greening* 31: 204 – 211.

Matzarakis, A., Rutz, F., Mayer, H., 2007. Modelling radiation fluxes in simple and complex environments – application of the RayMan model. *International Journal of Biometerology* 51 (4), 323–334.

Meteo Altoadige (2018) Weather station 83200MS data. Retreived from http://weather.provinz.bz.it/weather-stations-valley.asp?stat_stid=1242

Oke, T. R. (1982). The energetic basis of the urban heat island. *Quarterly Journal of the Royal Meteorological Society*, 108(455), 1-24

Roy, S., Byrne, J. & Pickering, C. (2012) A systematic quantitative review of urban tree benefits, costs, and assessment methods across cities in different climatic zones. Urban Forestry and Urban Greening 11: 351 – 363

Sanusi, R., Johnstone, D., May, P. & Livesley, S.J. (2017) Microclimate benefits that different street tree species provide to sidewalk pedestrians relate to differences in Plant Area Index. Landscape and Urban Planning 157: 502 – 511

USDA (2019) United States Department of Agriculture Forest Service Southern Research Station – UrbanCrowns software. Retreived from https://srs.fs.usda.gov/wood/software/urbanCrowns/

https://doi.org/10.37285/bsp.ic2uhi.48

Sustainable Landscaping Initiatives in Three Educational Institutions in India

Mohan Kotamrazu[1]*, School of Architecture, GITAM (Deemed to be University), (India)*

ABSTRACT

Green landscaping, environmentally friendly landscaping or sustainable landscaping is a way of designing gardens and larger landscapes which reduce harm to the environment. Green landscaping lowers maintenance which results in cost reduction. By treating water (both rainwater and water used for domestic or landscaping purposes) as a valuable resource and not as a waste product it aims to conserve water by reusing it or reducing its use. Plants, shrubs, ground covers and vines are used passively for improving environmental quality, modifying microclimates, reducing temperatures in and around buildings which ultimately result in improvement in environmental quality and in energy conservation.

Educational campuses can serve as a laboratory where the application of sustainable landscaping principles can be directly seen by students using the spaces in the campus. The present paper presents some of the landscaping strategies adopted by three different campuses in the country namely Piloo Mody College of Architecture, Cuttack, Kits Ramtek, Maharashtra and GITAM (Deemed to be University), Visakhapatnam.

Keywords: Sustainable landscaping, indigenous vegetation, drought tolerant plants, groundcovers, microclimate modification.

Introduction

Educational institutions are places of learning and should provide a serene environment that stimulates the pursuit of knowledge. Landscaping acts as a link between the built environment in a campus and nature. Educational campuses can serve as a laboratory where the application of sustainable landscaping principles can be directly seen by students and faculty using the spaces in the campus. Sustainable campus landscapes can enhance learning and contribute to mental and physical health of the students, other users and the surrounding community. A well landscaped campus with its aesthetic appeal helps in promoting the intake of students more than any other form of advertisement. A green campus that enhances pedestrian movement and is walkable helps in increasing the physical health and well being of its inhabitants. One important role of green landscaping in campus design is that it promotes energy and resource conservation and helps in mitigating the Urban Heat Island Effect that is today a major cause of concern in most cities.

[1]Corresponding Author: [profkmohan@gmail.com]

Benefits of Energy Efficient Landscaping

Today there is a paradigm shift in landscaping thought. Apart from the visual appeal of landscaping attention is being paid to the environmental benefits of landscaping. Extensive Literature exists on the way that trees and vegetation can help in energy conservation by modifying microclimatic conditions around buildings.

According to Oke (1979) the replacement of vegetation by hard impermeable surfaces such as asphalt and concrete is frequently mentioned as one of the causes for the summer heat island in the cities. Trees and other vegetation contribute to cooling the air by the evaporative process of transpiration. An urban shade tree can produce as much cooling as five room air conditioners running twenty four hours a day. The lack of transpiring vegetation in cities is one reason why cities often several degrees hotter than the surrounding countryside (Federer1976). Trees can be considered as nature's own air conditioners. An isolated 70 ft shade tree can transpire 100 gallons of water on a sunny day (Kramer and Kozlowski 1960). As pointed out by Huang et al. (1987), dramatic savings can be realized at the urban level through modification of the urban climate by increasing the total amount of vegetative cover and such a conservation strategy may be effective in counteracting the summer heat island evident in cities and may improve ambient conditions as well as reduce summertime air-conditioning requirements.

The popularity of green roofs and vertical greenery is growing because of their high potential to be used as sustainable solutions for enhancing the thermal performance of building envelopes and energy consumption in buildings. Like other forms of green infrastructure, they offer many ecosystem services like the mitigation of the urban heat island effect, the creation of natural habitats for improving urban biodiversity, noise attenuation, improved air quality and aesthetical impact of constructed areas (Shettini et al. 2016). Trees directly affect energy use in buildings by reducing solar heat gain from windows, walls and roofs by shading. Shading also reduces the radiant heat gain from the surroundings. Trees indirectly affect the energy use in buildings by lowering ambient wind speeds which reduces the outside air infiltration rate and reduces the heat gain into the buildings by lowering ambient temperatures through evapo- transpiration in summer (Huang et al.1987). Landscaping reduces cooling requirements by: blocking solar radiation from the building, the adjacent ground and the foundation, creating cool microclimates near the residence by evapo-transpiration, and either channeling or blocking air flows through and around the residence (Parker, 1983).

Landscaping Initiatives in Piloo Mody College of Architecture



(a) (b) (c)

Figure 1 (a) View of the Architecture building during construction (b) Architecture building with landscaping (c) View of the path connection g the Architecture and Engineering Building

The campus of Piloo Mody College of Architecture located in Cuttack , Orissa is spread over five acres. The two main buildings in the campus comprise of the Architecture College Building and the Engineering College Building. Figure 1(a) shows the Architecture Building the early stages of construction. From the year 2004 onwawrds various varieties of trees shrubs and ground covers have been introduced in the campus by the author. The present status of the campus with the landscaping in place is shown in Figures 1b and 1c respectively.



(a) (b)

Figure 2 (a) Medium height Mimumsops elengi variegated tree (b) Alstonia scholaris tree

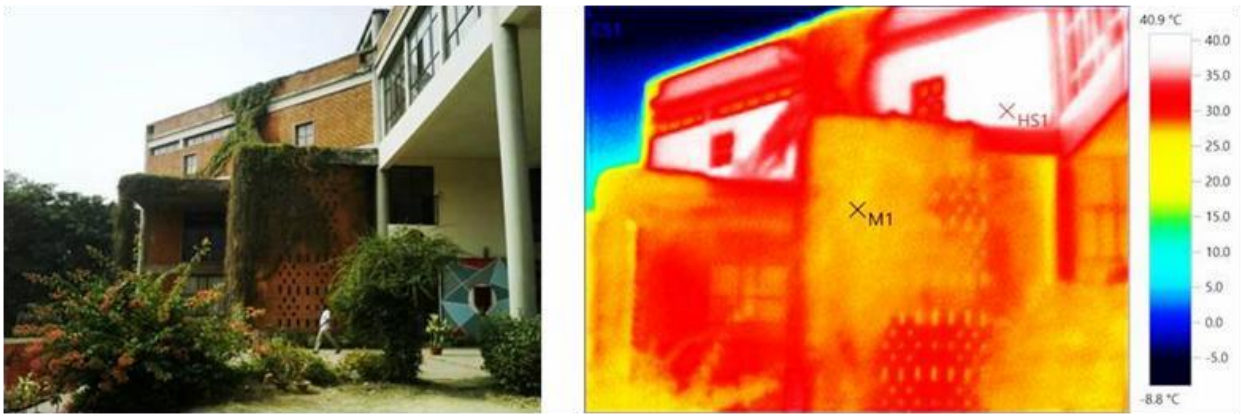


(a) (b) (c)

Figure 3 (a) Creeper Pyrestegia venusta on the wall (b) Ipomea chataruse groundcover (c) The Monarch butterfly on the flower of the ground cover Wedelia trilobata

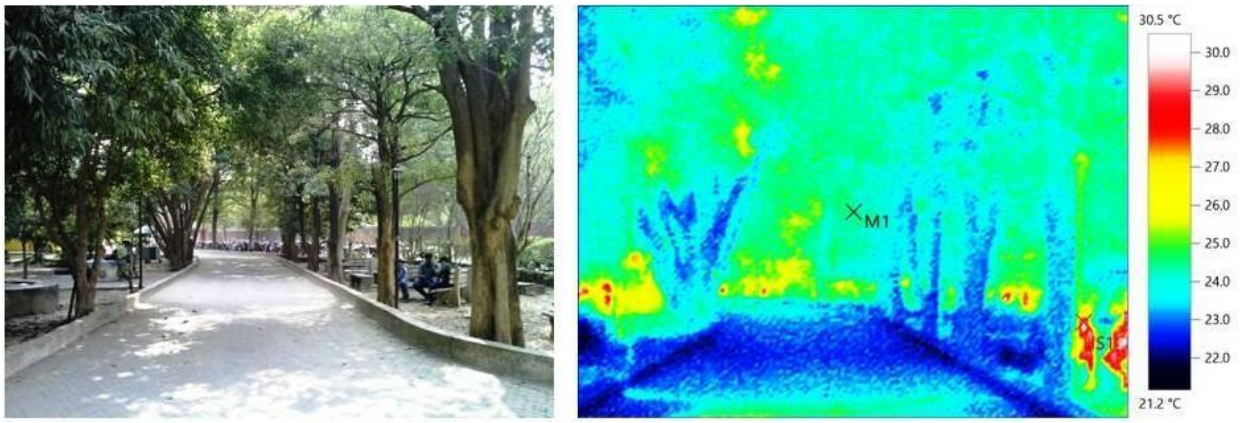
Prior to selecting the vegetation to be planted a careful survey of the existing trees in the neighbouring sites and localities was carried out. The following measures have been used for making the landscaping sustainable:

- Native plants such as Azadrachta indica that have higher chances of survival have been preferred over exotic varieties.
- For easy maintainence drought tolerant plants that consume less water such as Calliandra, Nerium oleander, Bougainvilleas, Agave species etc., have been planted.
- Flowering plants and groundcovers that attract butterflies such as Wedelia trilobata, Lantanas, Marigolds, etc., have been extensively planted, especially along the path connecting the Architecture and Engineering buildings.
- Hardy trees such as Alstonia scholaris, Bauhinea blackeana, Lagerstroemia-flos- reginae , Ficus nuda and medium height trees such as Mimumsops elengi variegated among others have been used for providing shade and modifying the microclimate.
- Flowering vines such as Pyrestegia venusta have been used to cover building walls to reduce heat transfer into the building walls as shown in Figure 3(a).
- Turf grass which consumes large amounts of water have been replaced with ground covers such as Ipoemea chataruse (Figure 3b), Ipomia tricolor and Wedelia trilobata (Figure 3c).
- Trees provide a habitat for birds, bees and other pollinators. Trees such as Callistemon lanceolatus have been planted which attract humming birds.
- Aromatic trees such as Plumeria alba and Plumeria rubra along with their attractive flowers increase the aesthetic appeal.



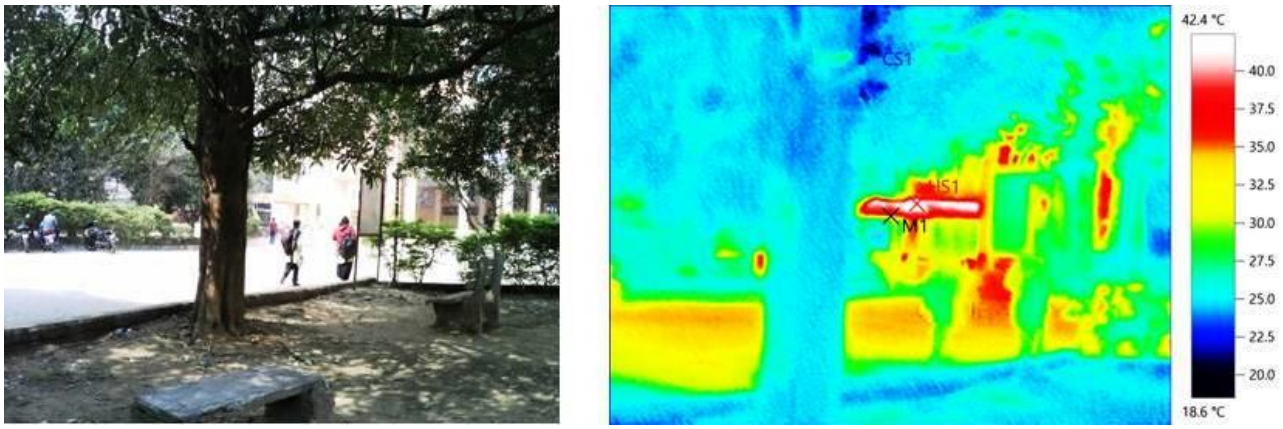
(a) (b)

Figure 4(a) Pyrestegia venusta vine at the entrance of the Architecture building (b) Thermal image of the building with the vine Pyrestegia venusta



(a) (b)

Figure 5 (a) View of the entrance road leading to the Engineering Building (b) Thermal image the tree road leading to the Engineering Building



(a) (b)

Figure 6 (a) View of the entrance load leading to the Engineering building without shade (b) Thermal image of the road leading to the Engineering Building without shade

The flowering vine Pyrestegia venusta has been used to cover some of the west facing south western walls of the Architecture building (Figure 4a). The thermal image of the building wall with the vine on the south-west wall at the entrance of the Architecture building is shown in Figure 4b. A temperature reduction of 5 degrees Celsius has been observed with the addition of the creeper. The Alstonia lined pathway leading to the Engineering building is shown in Fig 5a along with its thermal image which was recorded during a summer day in Figure 5b. The temperature recorded on the paved road due to the shade cast by the Alst0nia trees is around 23 degree Celsius. Figure 6a shows the same road without shade and Figure 6b shows the thermal image of the road without shade. The temperature recorded on the road is around 32 to 34 degree Celsius. This shows that around 8 to 10 degree Celsius reduction in temperature can be obtained due to shading of road by the Alstonia scholaris trees.

Landscaping Initiatives in KITS, Ramtek

The campus of KITS (Kavi Kulguru Intitute of Technology and Science), Ramtek is located at a distance of 48 km from Nagpur which has a hot and dry climate with

predominantly black cotton soil. Trees that provide shade, are drought tolerant and which help in soil stabilization were selected for planting in this campus. Sculptures made from construction waste and the recycled wood have also been installed in the campus.

Several Butea monosperma trees have been planted along with many varieties of shade giving trees as the roots of these trees hold the soil together and help in soil stabilsation (Figure 7a). Succulents and drought resistant plants like Calliandra have been planted extensively in the campus and rain water harvesting methods have also been adopted.

In the vacant site adjacent to the Triveni hostel the author designed a plantation comprising of the following trees: Cassia siamia, Bauhinea blakeana, Azadrachta indica, Delonix regia, Lagerstroemia flos reginae, Dalbergia sissoo, Calistemon lanceolatus and Pongamia glabra. The plantation has helped in providing shade and relief from the hot summer sun during summer. The Hostel Block without the plantation, with plantation after three years and after fifteen years is shown in Figures 8a, 8b and 8c respectively.



(a) (b) (c)

Figure 7 (a) Butea monosperma tree (b) Aurcarea orienalis shrubs help in purifying the air (c) Drought resistant succulents



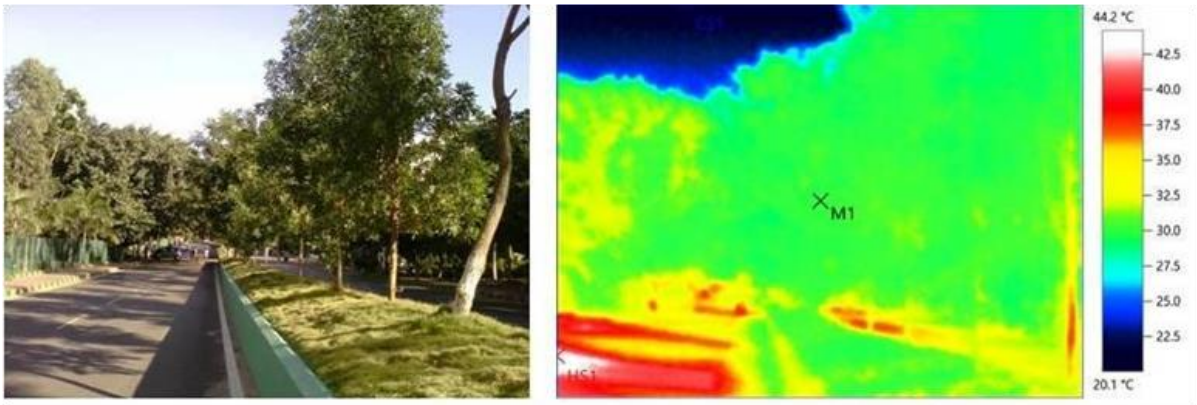
(a) (b) (c)

Figure 8 (a) View of the Triveni hostel block without plantation (b) View of the Triveni hostel block with plantation after three years (c) View of the plantation after fifteen years

Landscaping Initiatives in GITAM (Deemed to be University), Visakhapatnam

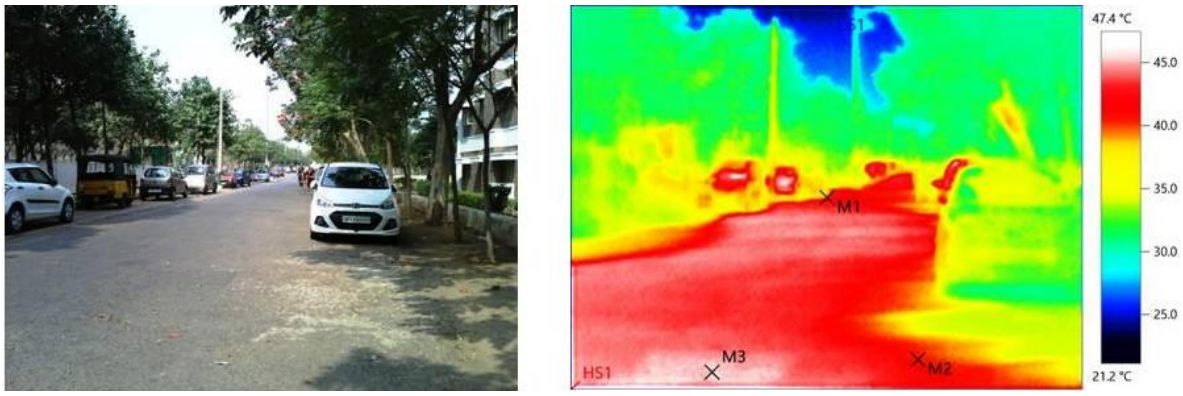
The GITAM (Deemed to be University) campus is located along the coastal corridor of Visakhapatnam, adjacent to the Rushikonda Hill. Spread over hundred acres the campus has extensive greenery with many indigenous and exotic varieties of trees, palms, shrubs and ground covers that have been introduced in the campus over the last three decades. Several parks such as the Nightingale Park, NTR Park, Gandhi Park and Ganesh Park, along with tree lined avenues help in moderating temperatures in the campus.

A view of the main thoroughfare of the campus lined with various species of trees such as Canocarpus erectus, Eucalyptus species, Pongamia pinnata trees among others is shown in Figure 9a and its thermal image taken during the summer is shown in Figure 9b. Temperatures on the grass covered median and the Canocarpus trees range from 28 to 32 degrees Celsius while the maximum temperature recorded on the black topped road is 44.2 degrees Celsius with a reduction of 8.2 degrees Celsius by the shadows cast by the trees. View of the road in front of the Architecture building without shade is shown in Figure 10a. The thermal image in Figure 10b shows that a maximum of 47.4 degrees Celsius is attained by the unshaded black topped road.



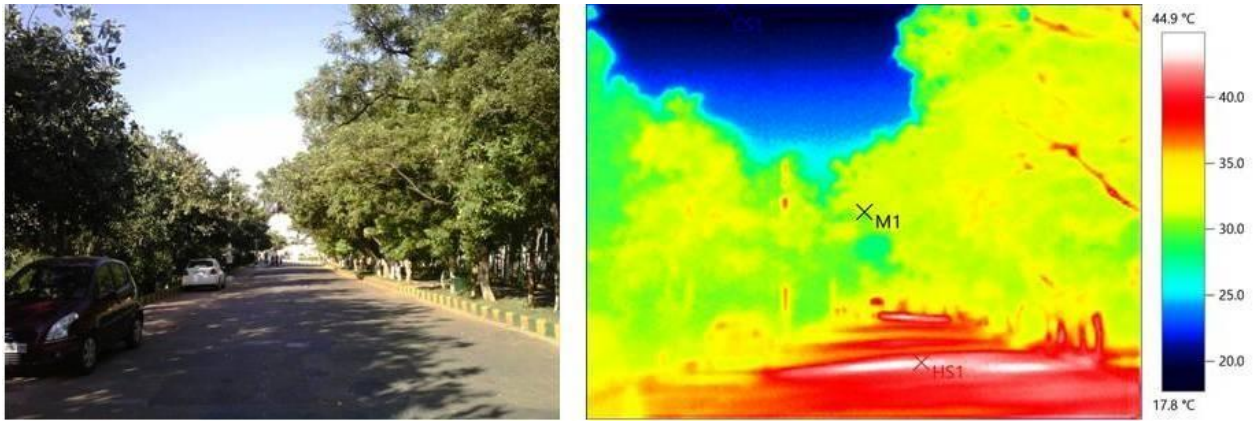
(a) (b)

Figure 9 (a) View of the tree lined main road of the campus (b) Thermal image of the shaded main road



(a) (b)

Figure 10 (a) View of the road in front of the Architecture Building without shade (b) Thermal image of the road in front of the Architecture building without shade



(a) (b)

Figure 11 (a) View of the shaded road in front of the Architecture School (b) Thermal image of the shaded road in front of the Architecture School

The road in front of the School of Architecture shaded by Ionophyllum callophyllum trees along with its thermal image is shown in Figures 11a and 11b respectively.



(a) (b)

Figure 12 (a) View of the rainwater harvesting pit adjacent to the Architecture School (b) View of the models of vertical greenery developed by students of the School of Architecture

A reduction of around 8.9 degrees Celsius on the black topped road by the shadows cast by the Callophyllum Ionophyllum trees is seen from the thermal image. The readings of the thermal images of the two roads show that on an average a reduction of around 8 degees Celsius can be obtained by shading the black topped roads with different types of vegetation. Figure 12a shows a rainwater harvesting pit located adjacent to the School of Architecture and Figure 12b shows models of vertical greenery developed by the students of the School of Architecture. Other green initiatives by the faculty and students of the School of Architecture include participation in debris removal from parks near the campus, documentation and listing of trees in the campus and imparting different methods of mulching to farmers in nearby villages for improving their crop yield.

Conclusion

Sustainable landscaping has today become an integral part of any educational campus design. Physical health benefits, social and environmental benefits accrue from a campus where the landscaping is designed with sustainability in mind. Various measures such as rainwater harvesting, green roofs and green walls, permeable pavements, adoption of water conservation measures, use of drought tolerant and native vegetation with a careful selection of softscape and hardscape material can go a long way in acting as counter measures for a reduction of the urban heat island in urban areas.

References

Federer,C.A. (1976). Trees modify the microclimate, Journal of Aboriculture 2,121-127.
Heisler, M.G. (1986). Energy savings with trees. Journal of Aboriculture 12, 113-125.

Huang, J.Y, Akbari, H, Taha, H and Rosenfeld, H (1987). The potential of vegetation in reducing summer cooling loads in residential buildings. Journal of Climate and Applied Meteorology 26, 1103-1116.

Kramer, P.J., and Kozlowski. (1960). Physiology of Trees, McGraw-Hill. New York (U.S.A)
Oke T.R. (1987). Boundary Layer Climates , Routeledge, London (U.K.). Parker, J.
H. (1983). Journal of Forestry 81, 82-105.

Shettini , E, Blanco, I, Campiotti, A,C, Bibiani C, Fantozzi, F and Vox, G (2016). Green control of microclimate in buildings. Agricultural and Agricultural Science Procedia 8, 576-582.

High albedo plant selection for mitigation of the urban heat island

Giulia Santunione, University of Modena and Reggio Emilia, Department of Engineering "Enzo Ferrari, Italy
Chiara Ferrari, University of Modena and Reggio Emilia, Department of Engineering "Enzo Ferrari, Italy
Alberto Muscio[1] University of Modena and Reggio Emilia, Department of Engineering "Enzo Ferrari, Italy

ABSTRACT

The use of greenery as countermeasure to Urban Heat Island phenomenon is one of the more efficient answers to urban warming since it provides significant benefits in terms of thermal comfort and air quality and, therefore, human health. The civil and environmental engineering research is rising the attention to the design of greenery in urban and surrounding areas in order to find out innovative strategies and technologies that can improve the urban climate. Different types of greenery usually exist in the city areas such as parks, green roofs, vertical gardens. The physical and physiological features of plant species involved in greenery systems lead to their effectiveness in terms of thermal mitigation. This study is aimed to investigate the surface radiative properties of green canopy with high albedo such as *Stachys bizantina*, a herbaceous plant characterized by an ashen color due to the presence of a white silky-lanate hair. Its albedo can be especially helpful during heat waves, when plants in green areas often close their stomata and thus reduce significantly evapotranspiration and, with that, their mitigation potential. The albedo of *Stachys b*. has been measured through ASTM E1918, then compared with the albedo of grass commonly used in green urban areas (*Lolium perenne*). Values obtained through field measurements have also been complemented with measurements through a WorldView-3 platform satellite image of the city of Modena, Northern Italy. Replacing partially the grass cover of green areas with high albedo plants like *Stachys b*., indeed representative of other useful species, can yield a non-negligible increase of the urban albedo on these green districts and their surroundings.

Introduction

Today, almost 60% of world's population is living inside cities, and the trend is going to increase (UN 2018). This is the reason why high attention is being paid to the potential influence of the urban environment on climate change. Building materials retain more solar energy during the day and have lower rates of radiant cooling during the night, compared with vegetated surfaces (Wilby 2007). Processes such as industrial manufacturing, building heating and air conditioning, and transport systems contribute to introducing additional heat sources into the urban environment. Moreover, heat dissipation due to wind-induced convective processes and plant evapotranspiration is less effective in densely built cities as a consequence of the lower wind speed and the smaller green areas. All these factors are responsible of the urban heat island (UHI) phenomenon, the most documented one related to climate change. UHI sensibly impacts on citizens' life, and on their health and quality of life. The high rate of energy consumption and pollutants emission for building cooling represents a serious problem also for the economy and the global environmental quality (Santamouris 2014).

[1] Corresponding Author: (alberto.muscio@unimore.it, 059 2056194)

Recently, the building engineering research has invested increasing resources to study and enable solutions for UHI mitigation through greenery (Ross et al. 2014). Urban forestry, parks, street trees, green roofs, gardens, vertical green represent efficient answers to urban warming, providing thermal benefits, air quality, and so human health (Akbari et al. 2001). A comprehensive review study by Santamouris et al. (2018) highlights how vegetation areas can reduce the peak ambient temperature by 1.2 K or 1.5 K by using grass or trees, respectively, while an average increase of the albedo of a given area by 0.2 may lead to an ambient temperature drop of 1.5 K.

The efficiency of greenery to create a cooler environment depends greatly on plants transpiration, which depends in turn on stomatal resistance, as well as on shading and albedo of the foliage canopy(Santamouris et al. 2018): the transpiration process relies upon the release of water vapor from leaves into the air, providing a temperatures drop of the leaves and the surrounding air thanks to the latent heat of the evaporated water (Akbari et al. 2002); this is influenced by parameters such as the leaf area index (LAI), a representation of the plan-form area coverage of the leaves with respect to the underlying ground area. The stomatal resistance controls the rate of moisture transpired by the plant, and therefore the rate of absorbed latent heat (Berardi et al. 2014). However, a non-negligible contribution to heat release can be obtained thanks to relatively high values of the effective albedo, that is the reflectance of the incident solar energy provided by the upper surface of the vegetation canopy layer.

Several research studies are showing how greenery selection is important to implement urban temperature mitigation (Hamada et al. 2010; Bowler et al. 2010). Species-specific morphologic and physiologic plant features influence the evapotranspiration rate of leaves and ground below, and the value of the albedo, two important factors that determine the cooling potential of greenery. This work is particularly focused on the enhancement of greenery albedo, or solar reflectance (ρ_{sol}), in order to improve the mean urban albedo. The albedo of a specific plant species, *Stachys bizantina*, potentially exploitable in most urban green areas and green roofs, has been measured and compared with *Lolium perenne*, representative of commonly used grass species. *Stachys b.* results especially interesting thanks to its morphology and physiology: its leaves are indeed covered by a white-colored hair, which can influence positively the albedo. Its higher albedo values and the cooler foliage canopy can contemporarily contribute to counter urban warming.

Three different standard test methods have been applied to study the solar reflectance of *Stachys b*. Two of them are used to measure the albedo of a single leaf: ASTM C1549, with a solar reflectometer, and ASTM E903, with a UV-Vis-NIR Spectrometer. The albedo of the canopy surface is instead measured according to ASTM E1918A with an albedometer consisting of a dual pyranometer. More details on the test methods can be found in (Muscio et al. 2018). The albedo of the *Lolium perenne*'s canopy layer was also measured on field by a pyranometer, and the acquired reflectance values were then compared with those obtained from a WorldView-3 platform satellite image on test areas in the city of Modena, Northern Italy. *Stachys b.* achieved higher values than those recorded over common grass according to all three standard test methods. Therefore, potential improvements that can be obtained in terms of average albedo increase and local temperature drop through a widespread plantation of whitish colored *Stachys b*. have been assessed. In this regard, the mitigation effect in smaller green area has already been recorded in previous study (Pisello 2016) and shown to be effective for microclimate zone in case of dense and low rising built areas. In fact, the application of high albedo greenery could be especially helpful against UHI on very dense urban areas and surroundings. It is worth to note that *Stachys b*. is not the only plant to have a potentially positive effect on albedo; other species with similar

morphology can be assessed: *Jacobaea maritima*, *Artemisia* spp. and *Helichrysum italicum* (Pisello 2016).

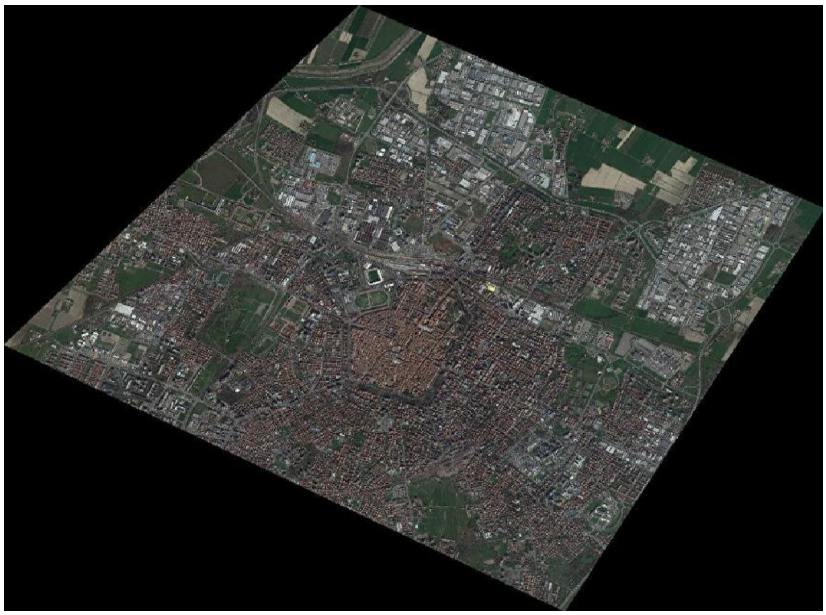


Figure 1: WorldView-3 Image on the urban area of Modena, Northern Italy.

An assessment of the albedo enhancement that can be obtained through the usage of a specific plant species such as the considered one has also been completed with the evaluation of its evapotranspiration potential, depending on its stomatal resistance (Vaz Monteiro et al. 2017; Blanusa et al. 2013). Indeed, several experiments performed under heat wave conditions suggested that the capability of physiological acclimatization and the response to extreme ambient temperature depend also to the reflectance of the leaves [Blanusa et al. 2013; Curtis et al. 2012]. Higher leaves reflectance means less solar radiation absorbed, and a better physiological process of vapor exchange and transpiration, thus a more persistent air cooling potential (Reich et al. 2016; Anderegg et al. 2012]. However, despite the key role of plants' characteristics in determining greenery benefits, the analysis of leaves reflectance and its impact on urban climate and temperatures still lacks (Pisello et al. 2016).

Materials and Methods

The albedo of two representative plants species, *Stachys bizantina* and *Lolium perenne*, have been measured. Three different standard test methods have been used to perform the measurements, and the results have been compared to assess differences between the test methods.

Laboratory characterizations were performed by using a UV-Vis-NIR spectrometer (Jasco V-670) with integrating sphere 150 mm (Jasco ILN-725) according to ASTM E903 (2012), and by a solar spectrum reflectometer (Devices and Services SSR v.6) according to ASTM C1549 (2009).

The spectrometer provides the spectral distribution of the reflectivity ρ_λ, defined as the ratio of reflected part and total amount of incident radiation at the considered wavelength λ [nm]. This is then averaged over the wavelength range relevant to solar radiation (300-2500 nm) to obtain the solar reflectance ρ_{sol}, weighting the spectral values with the standard spectral irradiance of the sun at the earth surface, $I_{sol,\lambda}$ [Wm^{-2} nm^{-1}]:

$$\rho_{sol} = \frac{\int_{300}^{2500} \rho_\lambda I_{sol,\lambda} d\lambda}{\int_{300}^{2500} I_{sol,\lambda} d\lambda} \quad (1)$$

The solar reflectometer calculates automatically the albedo as the average of measurements in several wavelength ranges of the solar spectrum, weighted by the reference solar irradiance.

For both measurements by spectrometer according to ASTM E903 (2012) and by reflectometer according to ASTM C1549 (2014), the tests were performed on a single leaf. Moreover, the irradiance spectrum is the most commonly used one as specified by ASTM E891 (1992) for beam normal solar irradiance (E891BN spectrum). Indeed, the reflectance relevant to solar radiation rejection is not that of leaves but that of the upper surface of the plant canopy layer. To analyze an area of such surface much larger than a single leaf, an albedometer (Kipp & Zonen CM6) has been used according to the so-called E1918A test method (Akbari et al. 2008) This one, indeed a modification of the commonly used ASTM E1918 test method (2015), covers the measurement of solar reflectance of various horizontal and low-sloped surfaces and materials in the field, and it allows reducing the minimum surface area to be analyzed from 4 m^2 as required by ASTM E1918 down to 1 m^2 by exploiting properly colored masks.

On-field measurements on *Stachys b.* canopy have been carried out in Spilamberto (Province of Modena, 44°32'00.5" N 11°01'25.3" E), on 18th July 2017. Laboratory measurement have been performed on leaves harvested on the same day, from the same plants. A *Lolium perenne* covered area has been tested successively through a Kipp&Zonen pyranometer on a 4 m^2 area at the Department of Engineering "Enzo Ferrari" (Modena, 44.628529, 10.948436), according to ASTM E1918.

Albedo data achieved through on-field measurements on *Stachys b.* and *Lolium p.* have subsequently been compared with data collected from earth observation satellite Landsat, which largely contributes to monitoring and extracting information on urban areas at high and very high resolutions. The analyzed satellite image comes from WorldView–3 (Digital Globe, 2018) on an area of 28.3 km^2 including the city of Modena, Northern Italy. The used image (Figure 1) was acquired on 15th March 2016, and the albedo has been calculated with ENVI 5.1 Software. The different types of surface have been then classified with Ecognition software. The data processing has been performed according to instruction by Kuester (2018). More specifically, the use of satellite images requires a preliminary classification work: each pixel has specific characteristics that define it into a specific area, called *object*, that has homogeneous properties. The *software* Ecognition Developer 9.1, whose license is provided by Trimble, is applied in order to classify the different objects of the image. The albedo of each object has been thus calculated according to the

simplified method proposed by Akdim et al., (2014). The equation introduces below solar reflectance values of the surfaces, with atmospheric corrections:

$$\rho_{sol} = \sum_{\Delta\lambda} w_{\lambda} r_{\lambda} \quad (2)$$

where $r_{ë}$ represents the spectral reflectance and $w_{ë}$ is the adjustment coefficient for each band, calculated as the ratio of solar spectral irradiance for one band ($I_{\Delta\lambda}$) and the sum of all irradiance values of all bands:

$$w_{\lambda} = \frac{I_{\Delta\lambda}}{\sum_{\Delta\lambda} I_{\Delta\lambda}} \quad (3)$$

The data of $I_{\Delta\lambda}$ have been deduced from the work by Kuester (2018).

Results

The values of solar reflectance measured on *Stachys b*. through the three different test methods are shown in Table 1. At least 3 repeated measurements have been performed for each method in order to achieve a representative standard deviation (SD). The UV-Vis-NIR reflectivity spectrum of *Stachys b.*'s leaf is reported in Figure 2. The measurements with the dual pyranometer according to ASTM E1918A are intended for use when the sun angle to the normal from a surface is less than 45°; this has been verified according to the day of the year and the time of measurements.

Table 1: Solar reflectance $ñ_{sol}$ of *Stachys b.* measured on the leaf surface according to ASTM E903 (UV-Vis-NIR spectrometer) and ASTM C1549-14 (solar reflectometer), and on the upper surface of the plant canopy layer according to ASTM E1918A (dual pyranometer). Standard Deviation is shown.

Standard Methods	δ_{sol}	SD
E903	0.390	0.009
C1549	0.422	0.004
E1918	0.410	0.005

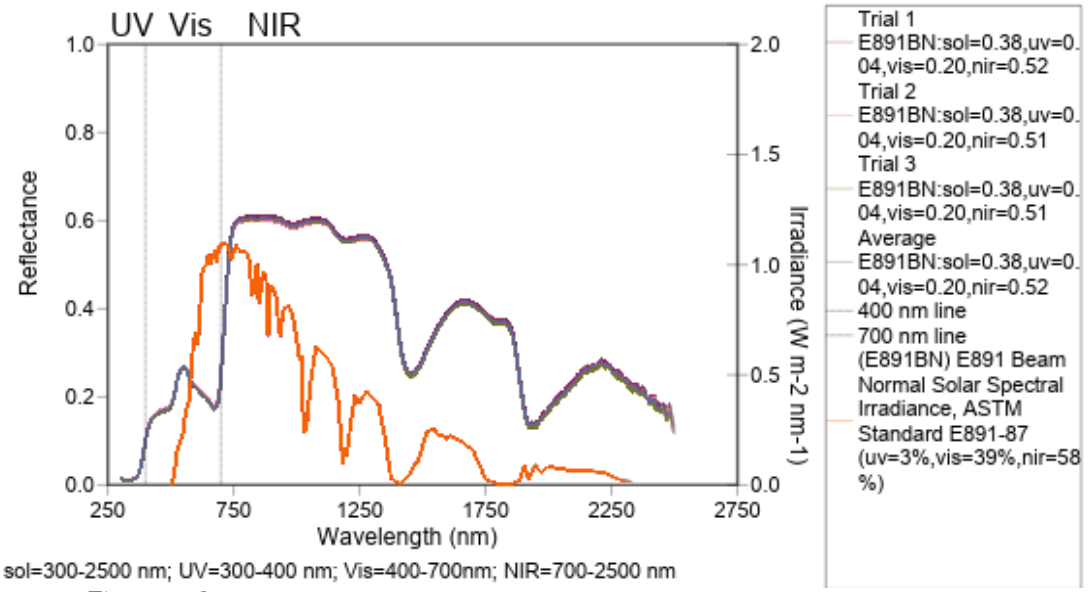


Figure 2: Solar reflectance of a *Stachys b*. leaf: UV-Vis-NIR spectral reflectivity (violet line, scale on the left) and E891BN standard spectrum of solar irradiance (orange line, scale on the right).

ASTM E1918 and its modification dubbed E1918A provide the reflectance value that is relevant in the energy balance of the city surface. The albedo of the single leaf measured by a reflectometer is slightly higher and can overestimate that of the canopy layer, therefore measurements made by albedometers should be preferred for the grass campy of on ground and on roof urban greenery.

Applying the software Ecognition Developer 9.1, through the algorithm “assign class”, different objects have been recognized as streets, buildings, parking and green areas. The algorithm takes in consideration the spectral features to divide the object in different classes. The identified classes in the urban area of Modena are: parking, streets, cool grey roofs, dark grey roofs, red roofs, green areas and other not identified (N.I.) surfaces. The total urban surface covered by vegetation has been calculated and reported in Figure 3, divided in three different “green types”. They involve “Green to natural evolution”, that includes urban forestation and the environmental recovery areas; “Service green”, which includes public parks and residential green areas, and “Others”, as the areas not detectable as one in the first two types. This is equivalent to 7.63 km^2 over the 28,3 km^2 examined. Applying equations (2) and (3), the mean albedo of each type of urban areas of Modena has been calculated and it is shown in Table 2.

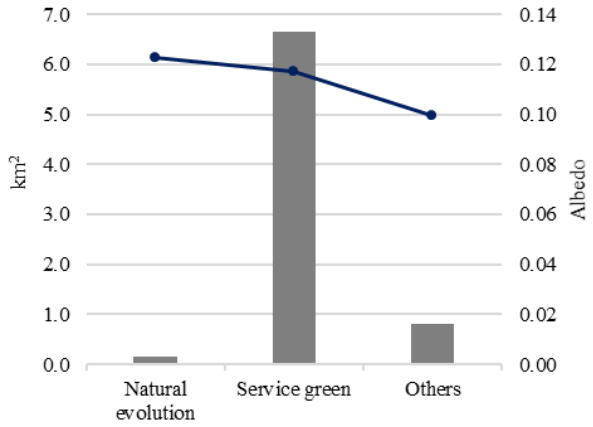


Figure 3: Green areas type and dimensions classified in "Natural evolution"; "Service Green" and "Others". Albedo (δ_{sol}) values from satellite data are reported for each area type.

Table 2: Mean solar reflectance values of different surface types: parking/streets, cool grey roofs, dark grey roofs, red roofs, green areas, and unidentified surfaces. Landsat satellite data are exploited.

Object type	δ_{sol}
Parking-streets	0.126
cool grey roofs	0.268
dark grey roofs	0.148
red roofs	0.142
green areas	0.116
N.I.	0.123

The average albedo δ_{sol} over the whole city has been evaluated to be 0.130. Focusing on the green areas, the mean satellite data return δ_{sol} equal to 0.116. A comparison was made between the albedo calculated from satellite data and that measured on ground in the green area of the Department of Engineering "Enzo Ferrari", covered with *Lolium perenne* sp., according to the ASTM E1918 test method. Values of 0.210 and 0.203 were measured, respectively. Since the variance is less than 0.01, the deviation between the two methods could be considered as irrelevant.

Discussion

The elaboration of WorldView-3 data provided a measure of the surface of public vegetated areas in Modena, which is equal 2.44 km^2. The fraction of this area that can potentially be replaced with high solar reflectance plants such as *Stachys b.* regards 50% of "Service green" zone. This deemed area doesn't contain surfaces covered by trees, as well as other green elements that cannot be replaced with herbaceous plants.

The albedo values recorded on *Stachys b.* according to E1918A modification of ASTM E1918 can allow a non-negligible increase of the albedo of urban green areas. Currently, a typical green surface covered with *Lolium perenne* has an albedo of 0.203, whereas that measured on the canopy layer of *Stachys b.* is as high as 0.410. This value has been used to estimate the average albedo on the green areas of Modena (Figure 4), then the mean improvements in term of

microclimate temperature on green zones. A non-negligible improvements of the average albedo were calculated. More specifically, assuming to replace 50% of the existing green areas with plants like *Stachys b.*, the albedo onto these areas would increase from 0.116 to 0.237. According to studies by Santamouris(2017), who reported a temperature decrease of urban area up to 1.5 K per 0.2 increase of the average albedo, the widespread adoption of high reflectance greenery can be extrapolated in a temperature decrease of 0.9 K. This value can be added to the potential temperature drop in the close surrounding of green areas due to evapotranspiration as described by several authors (Jonsson 2004; Ellis et al. 2017; Skoulika et al. 2013; Taha. 2015a), which can extend over a 1 km wide area and can range from 1 to 3.5 K (Ellis et al. 2017). With regard to this, the previously estimated 0.9 K temperature drop represents a further cooling potential that high albedo green areas may play on the microclimate of local urban areas.

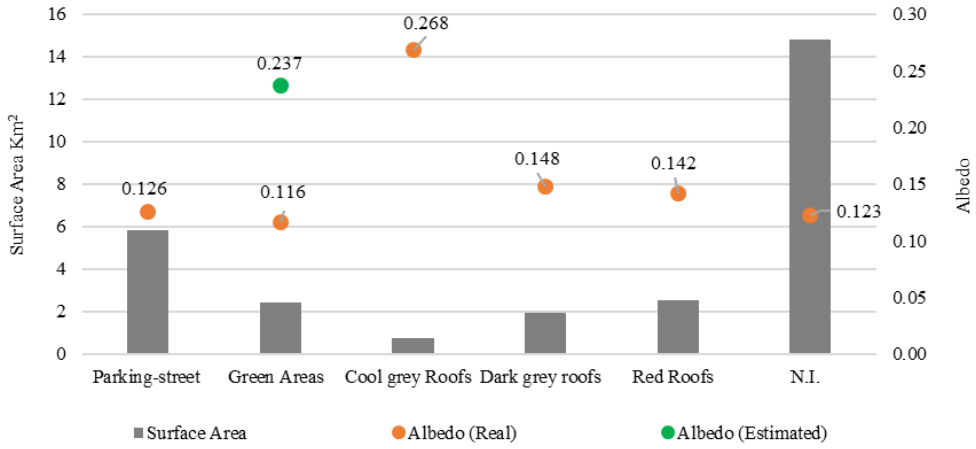


Figure 4: Whole surface area of Modena split in different kinds of surface: Parking-street; Green areas; Cool grey roofs; Dark grey roofs; Red roofs and Not identified (mixed) areas. The satellite data of albedo are reported for each surface type. The estimated albedo calculated replacing 50% of Green areas with *Stachys b.* is reported with the green dot.

The implementation of a higher albedo is not the only important factor involved in countering the heat island by means by plants like *Stachys b*. Its stomatal conductance, indeed, relates plant water use with surface temperature, then with the urban cooling potential (Kala et al. 2016)]. The phenomenon is due to the significant amount of solar heat that is dissipated by vaporization of water through the leaf stomata. A consequence is the lower surface and air temperatures above the green canopy. During heatwaves and, in general, in the summer period, a higher stomatal conductance can reduce heat transfer to the surfaces (Monterusso et al. 2015). In this regard, a comparison of the performance of albedo and stomatal conductance is made for *Stachys b*. and other high albedo plants such as *Helichrysum italicum* and with others species generally used in greenery infrastructures, well represented by *Sedum spp*. and *Heuchera sp.* (Table 3).

Table 3: Comparison of stomatal conductance (mmol $m^{-2}s^{-1}$) and albedo values for possible plant specie suitable to green roof or/and green areas.

Specie	Albedo (δ_{sol})	Stomatal conductance (mmol $m^{-2}s^{-1}$)
Sedum sp.	0.19 (Vaz Monteiro et al. 2017)	110.0 (Vaz Monteiro et al. 2017, Blanusa et al. 2013)
Stachys b.	0.410 (this work)	233.1 (Vaz Monteiro et al. 2017, Blanusa et al. 2013]
Helichrysum italicum	0.440 (Pisello et al. 2016)	n.a.
Heuchera sp.	0.140 (Vaz Monteiro et al. 2017)	200 (Vaz Monteiro et al. 2017)

Conclusions

Urban greenery represents a natural solution to counter the urban heat island effect. Because of the huge variability of available plants species, a deep knowledge on their cooling potential is needed according with their specie-specific morphological and physiological features. This study has investigated the radiative thermal properties of two representative types of urban herbaceous surfaces, *Stachys b*. and *Lolium p*, highlighting their differences in term of albedo. The albedo measured on *Stachys b*. leaves (according to ASTM C1549) and canopy (according to E1918A) is 0.422 and 0.410, respectively. Since the current average albedo measured on green areas of the city of Modena from Earth observation by satellite Landsat data is as low as 0.116, the potential enhancement provided by *Stachys b*. is considerable. Thereby, this work has underlined the importance of a specific and careful selection of plant species to be applied to green areas, particularly herbaceous ones. The replacement of 50% of current urban green surfaces with high albedo plant (*Stachys b*. in this case) could allow an additional decrease of temperature of 0.9 K. Further studies are needed to enlarge the set of high albedo species and understand their cooling potential, thus their contribute against UHI and hot waves in the urban climate.

Acknowledgments

The authors wish to thank Dr. Francesca Despini and Eng. Stefano Tommasone for their technical collaboration and support.

This research did not receive any specific grant from funding agencies in the public, commercial, or non-profit sectors. The authors declare no conflict of interest.

References

Akbari, H.; Pomerantz, M.; Taha, H. (2001). Cool Surfaces and Shade Trees to Reduce Energy Use and Improve Air Quality In Urban Areas. Solar Energy**,** 70, 295-310.

Akbari, H. (2002). Shade Trees Reduce Building Energy Use and CO_2 Emissions from Power Plants. Environmental Pollution, 116, 119–126.

Akbari, H.; Levinson, R.; Stern, S. (2008). Procedure for measuring the solar reflectance of flat or curved roofing assemblies. Solar Energy, 82, 648–655.

Akdim, N.; Alfieri, S.M., Habib, A.; Choukri, A., Cheruiyot, E.; Labbassi, K., Menenti, M. (2014). Monitoring of Irrigation Schemes by Remote Sensing: Phenology Versus Retrieval of Biophysical Variables. Remote Sens, 6, 5815–5851.

Anderegg, W.R.L.; Berry, J.A.; Field, C.B. (2012). Linking definitions, mechanisms, and modeling of drought-induced tree death, Trends in Plant Science, 17, 693–700.

American Society for Testing & Materials (1992). Tables for terrestrial direct normal solar spectral irradiance for air mass 1.5. Technical report, American Society for Testing and Materials, West Conshohocken, PA. (ASTM E891-87)

American Society for Testing & Materials (2012). Standard Test Method for Solar Absorptance, Reflectance, and Transmittance of Materials Using Integrating Spheres. (ASTM E903-12)

American Society for Testing & Materials (2014). Standard Test Method for Determination of Solar Reflectance near Ambient Temperature Using a Portable Solar Reflectometer. (ASTM C1549-09 -2014)

American Society for Testing & Materials (2015). Standard Test Method for Measuring Solar Reflectance Of Horizontal And Low-Sloped Surfaces In The Field. (ASTM E1918 – 06).

Berardi, U., Ghaffarianhoseini, A.; Ghaffarianhoseini A. (2014). State of the Art Analysis of the Environmental Benefits of Green Roofs. Applied Energy, 115, 411–428.

Blanusa, T.; Vaz Monteiro, M.; Fantozzi, F.; Vysini, E.; Li, Y.; Cameron, R.W.F. (2013). Alternatives to Sedum on green roofs: Can broad leaf perennial plants offer better 'cooling service'? Building Environment**,** 59, 99–106.

Bowler, D.E.; Buyung-Ali, L.; Knight, T.M.; Pullin, A.S. (2010). Urban greening to cool towns and cities: A systematic review of the empirical evidence. Landscape Urban Planning, 97, 147-155.

Curtis, E.M.; Leigh, A.; Rayburg, S. (2012). Relationships among leaf traits of Australian arid zone plants: alternative modes of thermal protection. Australian Journal of Botany, 60, 471–483.

Ellis, K.N.; Hathaway, L.; Mason, R.; Howe, D. A.; Epps, T. H.; Brown, V. M. (2017). Summer temperature variability across four urban neighborhoods in Knoxville, Tennessee, USA. Theoretical and Applied Climatology, 127, 701–710.

Hamada, S. & Ohta T. (2010). Seasonal variations in the cooling effect of urban green areas on surrounding urban areas. Urban For Urban Green, 9, 15 – 24.

Jonsson, P. (2004). Vegetation as an urban climate control in the subtropical city of Gaborone, Botswana. International Journal of Climatology, 24, 1307–1322.

Kala J; De Kauwe, M.G.; Pitman, A.J.; Medlyn, B.E.; Wang, Y.-P.; Lorenz, R.; Perkins-Kirkpatrick, S.E. (2016). Impact of the representation of stomatal conductance on model projections of heatwave intensity. Science Reports, 6.

Kuester, M. (accessed on 12th november 2018). Radiometric Use of Worldview-3 Imagery. Tech. Note 12. www.digitalglobe.com. Available online URL: https://dg-cms-uploads-production.s3.amazonaws.com/uploads/document/file/207/Radiometric_Use_of_WorldView-3_v2.pdf.

Monterusso, M.A.; Rowe, D.B.; Rugh, C.L. (2005). Establishment and persistence of Sedum spp. and native taxa for green roof applications. Horticultural Science, 40, 391-396.

Muscio, A. (2018). The solar reflectance index as a tool to forecast the heat released to the urban environment: Potentiality and assessment issues. Climate, 6, 12.

Pisello, A.L.; Piselli, C.; Cotana, F. (2016). Thermal-physics and energy performance of an innovative green roof system: The cool-green roof, Solar Energy, 116, 337–356.

Reich, P.B.; Sendall, K.M.; Stefanski, A.; Wei, X.; Rich, R.L. (2016). Boreal and Temperate Trees Show Strong Acclimation of Respiration To Warming Nature, 531, 633-636.

Ross, W.F., Cameron A,, Jane, E.; Taylor, B.; Martin, R.; Emmett, B (2014) What's 'Cool' In The World Of Green Façades? How Plant Choice Influences the Cooling Properties of Green Walls. Building Environment. 73, 198-207.

Santamouris, M., (2010). Mitigation Countermeasures to Face Urban Warming. International Journal of Low-Carbon Technology, 10, 1-2.

Santamouris, M.; Ding, L.; Fiorito, F.; Oldfield, P.; Osmond, P.; Paolini, R.; Prasad, D.; Synnefa, A. (2017). Passive and active cooling for the outdoor built environment – Analysis and assessment of the cooling potential of mitigation technologies using performance data from 220 large scale projects. Solar Energy, 154, 14–33.

Santamouris, M.; Ban-Weiss, G.; Osmond, P., Paolini, R.; Synnefa, A.; et al. (2018). Progress in Urban Greenery Mitigation Science – Assessment Methodologies Advanced Technologies and Impact On Cities. Journal of Civil Engineering Management, *In press*.

Skoulika, F.; Santamouris, M.; Kolokotsa, D.; Boemia, N. (2013). On the thermal characteristics and the mitigation potential of a medium size urban park in Athens, Greece. Landscape and Urban Planning, 123, 73–86.

Taha, H. (2015a). Cool cities: counteracting potential climate change and its health impacts. Current Climate Change Reports, 1, 163–175.

U.N., World Urbanization prospects, https://Population.Un.Org/Wup/ (accessed on 09/11/2018).

Vaz Monteiro, M.; Blanusa, T.; Verhoef, A.; Richardson, M.; Hadley, P.; Cameron, R.W.F. (2017). Functional green roofs: Importance of plant choice in maximizing summertime environmental cooling and substrate insulation potential, Energy and Buildings, 141, 56–68.

Wilby, R.L. (2007). A Review of Climate Change Impacts on the Built Environment. Building Environment. 33,31-45.

A Comparative empirical assessment of native deciduous and evergreen trees on carbon stock potential for regulating ecosystem services in tropical dry evergreen forest, Coromandel coast, Tamil Nadu, India

Parisutha Rajan Alphonse Marianadin[1],*School of Planning and Architecture, Vijayawada (India)*
Minakshi Jain, *School of Planning and Architecture, Vijayawada (India)*
Abdul Razak Mohamad, *School of Planning and Architecture, Vijayawada (India)*

ABSTRACT

Vegetation, particularly trees, provides a wide spectrum of regulating ecosystem services, which include up keeping of air quality, stabilizing temperature, reduction in ultraviolet radiation, oxygen generation, and carbon sequestration. Carbon Stock, called "C-stock", is one of the most common benefits of trees in today's scenario on climate change and anthropogenic disturbance all over the world. The purpose of this technical paper is to compare empirically and assess the total C-stock (TCS) of ten dominant native deciduous trees (NDT) and native evergreen trees (NET) for 10-ha area distributed 1-ha in each of ten tropical dry evergreen forest sites of Coromandel Coast of Tamil Nadu, India. The data obtained from a recent research publication is analyzed for total c-stock potential between NDT and NET trees through the application of the statistical tool. The **Chi-square, Goodness of fit between Above Ground Biomass of NDT and NET is 30733.80**, The p-value is < 0.00001. The result is significant at $p < .05$ (standard level for analysis). Hence, native evergreen trees have a higher c-stock capacity, when compared to native deciduous trees. Thus, prove the higher carbon sequestration potential of native evergreen trees.

Keywords: above ground biomass, below ground biomass, total biomass, carbon stock

Introduction

Forests, the largest carbon pool on earth, act as a major sink of carbon in nature. Woodland plays an important role in regulating ecosystem services, especially in carbon sequestration. Woody plant species sequester atmospheric carbon into their biological system during photosynthesis and storing excess carbon as "biomass". Especially, tropical forest ecosystems have the potential to hold and sequester large amounts of carbon than the other biomes. Living biomass of trees plays as main carbon pool in tropical forest ecosystem. Study of literature reveals that tropical forests comprise of 40% of the total terrestrial carbon stock on the planet. Carbon sequestration refers to the annual rate of Carbon-di-oxide storage, called as C-stock in above and below-ground biomass. The carbon stored in the AGB of trees is the largest pool. The estimation of AGB carbon is therefore, the most critical step in quantifying carbon stocks and fluxes from tropical forests. Increasing the number of trees can therefore slow the accumulation of atmospheric carbon, a contributor to climate change. The ability of a tree to sequester carbon changes over time as it grows. The key urban forest parameters reported to improve carbon sequestration and storage

[1] Corresponding Author: [parisutharajan@gmail.com]

are summarized in Table 1. Net oxygen production by trees is a function of the amount of oxygen produced during photosynthesis minus the amount of oxygen utilized during respiration. If the carbon dioxide uptake during photosynthesis exceeds carbon dioxide release by respiration during the year, the tree will accumulate carbon (carbon sequestration). Thus, a tree that has a net accumulation of carbon during a year (tree growth) also has a net production of oxygen. The net carbon sequestered is estimated as per the following expression:

Net Carbon sequestration (Kg/year) = Net Oxygen release (Kg/year) / 2.66

The aim of this technical paper is to address the following goals. First, through literature review identify the recorded values of ABG, BGB, TB and Total Carbon Stock of ten dominant native deciduous and evergreen trees. Second, analyze the values using statistical software Chi-square, Goodness of fit to perform comparative empirical assessment for carbon stock storage significance between ten dominant native deciduous and evergreen trees of Tropical Dry Evergreen Forest of Coromandel coast of Tamil Nadu, India.

Table 1: Forest parameters that are reported to improve the ecosystem service of carbon sequestration and storage

Scale and Management	The total amount of carbon-di-oxide stored and sequestered is influenced by the area of existing tree canopy (Mc Pherson,1998)
	Carbon storage increases with tree density; hence woodland are more effective than more sparsely planted urban land (Nowak and Crane, 2002). However thinning can encourage growth.
	Patch size of deciduous woodlands in an urban environment is positively correlated with carbon density (Godwin et al,2015)
Urban forest structure	On a per tree basis, carbon storage and sequestration is significantly greater is greater in urban areas than in forests due to large proportion of large trees and fastest growth rates resulting from the more open urban forest structure (Nowak and Crane, 2002).
	Ensuring diversity in species and canopy and understory layers will increases carbon sequestration (Zhao et al, 2010).
	Larger trees tend to sequester and store more carbon-di-oxide; indeed carbon-di-oxide storage is proportional to tree's biomass and diameter (McPherson,1998).
	Carbon storage and sequestration depends also on tree's growth rate and age class, with rates increasing to middle age and then diminishing towards post-maturity (Nowak and Crane, 2002).
	Trees with longer lifespan will have a greater positive effect on carbon-di-oxide uptake than short-lived trees as the frequency at which trees require planting, maintenance and removal (activities with associated fossil fuel carbon emission) will be reduced (Nowak and Crane, 2002).

	Healthy trees will sequester and store more carbon(Nowak and Crane, 2002).
	Evergreen broadleaved forests have been found to sequester more carbon-di-oxide than coniferous forest due to their faster growth rate (Zhao et al., 2010)
Location and proximity to people	Trees that are subject to a greater level of anthropogenic disturbances (eg. fragmented by roads) are found to store less carbon (Godwin et al,2015)
	Poor rooting conditions, exposure to air pollution and heat, and severe pruning can lower biomass accumulation and carbon storage (Jo and McPherson,1995)
Land use and ownership	Carbon-di-oxide by the urban forest in residential areas has been shown to be greater than for other urban land-use types due to the higher density of trees (McPherson,1998).

Source: Davies, H., Doick, K., Handley, P., O'Brien, L., and Wilson, J. (2017). Delivery of ecosystem services by urban forests, Forestry Commission Research Report, Forestry Commission, Edinburgh.

Methodology

1.0 Ten dominant NDT and NET trees biomass and carbon stock values from literature review :

The aboveground biomass (AGB) of trees was estimated following the Allometric equation of Chave et al. (2005) using two variables, the diameter and wood specific density (WSD):

$$\mathbf{AGB\ est = \rho \times exp\ (-1.499 + 2.148\ ln\ (D) + 0.207(ln\ (D))2 - 0.0281(ln\ (D))3)} \quad (1)$$

Where, **D** is the diameter and **ρ** is the wood specific density of tree species.

The belowground biomass (BGB) of trees was calculated by **multiplying the aboveground biomass value with 0.26** (Cairns et al. 1997, IPCC 2003).

The total carbon stock (TCS) was estimated to be **50 % of the total biomass** (AGB + BGB) (IPCC 2005).

Table 2 : AGB, BGB, TB and TCS values of ten dominant Native Deciduous Trees (NDT)

S.No	Native Deciduous Trees	AGB (Kg/tree)	BGB (Kg/tree)	TB (Kg/tree)	TCS (Kg/tree)
1	Abizia amara (Roxb.) Boivin	374.80	97.45	472.25	236.12
2	Bauhinia racemosa Lam.	213.50	55.50	269.00	134.50
3	Cassia fistula L.	180.87	47.02	227.9	113.95
4	Chloroxylon sweitenia DC.	155.23	40.36	195.59	97.79
5	Commiphora caudata (Wight & Arn.)	279.56	72.68	352.25	176.12
6	Dalbergia paniculata Roxb.	1775.07	461.51	2236.59	1118.29
7	Ficus religiosa L.	84.40	21.90	106.30	53.10
8	Gardenia resinifera Roth	202.45	52.63	255.08	127.54
9	Lannea coromandelica (Houtt.) Merr.	96.71	25.14	121.85	60.92
10	Ochna obtusata DC.	150.22	39.05	189.27	94.63
	Total	**3512.81**	**913.24**	**4426.08**	**2212.96**

Source: Vivek P & Parthasarathy N (2015) Diversity and carbon stock assessment of trees and lianas in tropical dry evergreen forest on the Coromandel Coast of India. *Tropical Plant Research 2(3): 230–239*

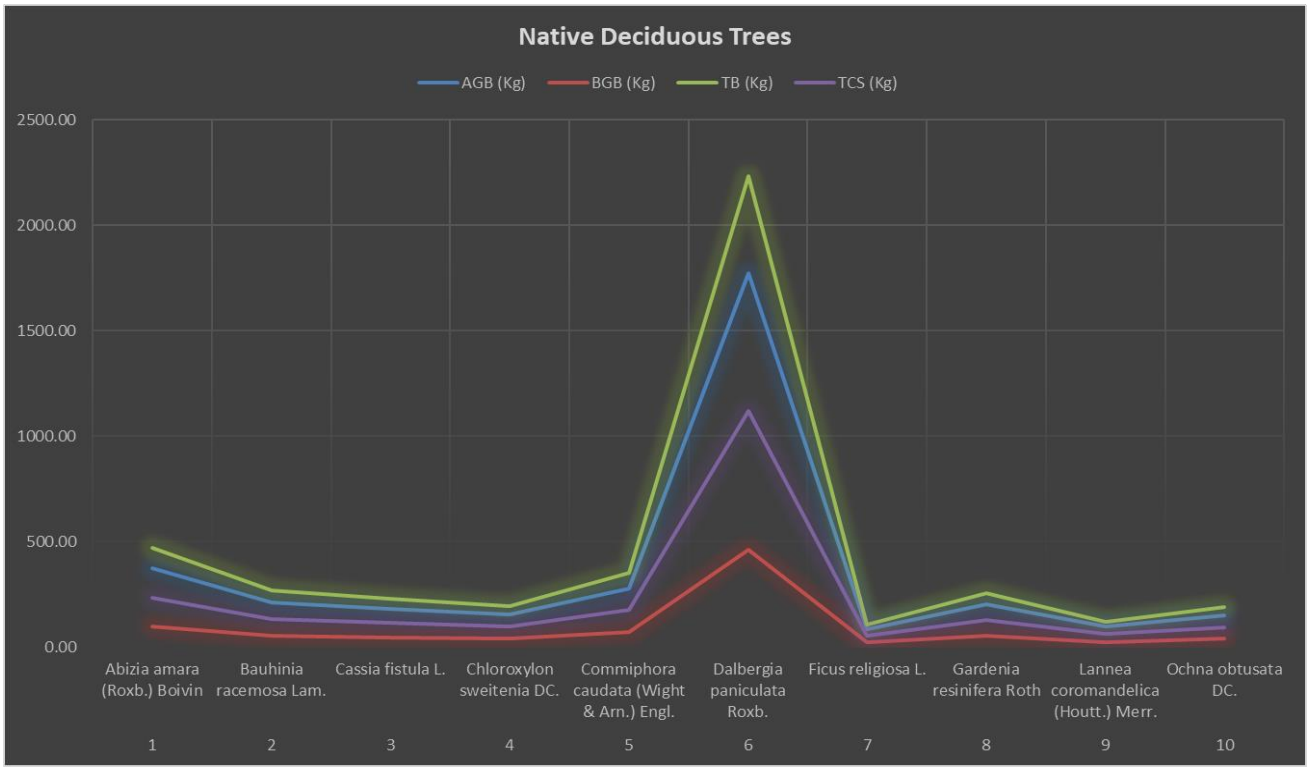


Figure 1: Graphical representation of AGB, BGB, TB and TCS values of ten dominant Native Deciduous Trees (NDT)

Table 3: AGB, BGB, TB and TCS values of ten dominant Native Evergreen Trees (NET)

S.No	Native Evergreen Trees	AGB (Kg/tree)	BGB (Kg/tree)	TB (Kg/tree)	TCS (Kg/tree)
1	Azadirachta indica A.Juss.	839.98	218.39	1058.37	529.18
2	Ficus amplissima Sm.	4238.40	1102.00	5340.40	2670.20
3	Ficus benghalensis L.	10122.22	2631.78	12754	6377.05
4	Ficus microcarpa L.f.	1278.65	332.44	1611.1	805.55
5	Lepisanthes tetraphlla (Vahl.)Radlk	490.75	127.59	618.35	309.17
6	Manilkara hexandra (roxb.) Dubard	1318.17	342.72	1660.89	830.44
7	Pongamia pinnata (L.) Pierre	1325.53	344.64	1670.17	835.08
8	Syzygium cumini (L.) Skeels	4153.87	1080.00	5233.88	2616.94
9	Tamarindus indica L.	15600.52	4056.12	19656.65	9828.32
10	Vitex altissima L.f.	773.47	201.10	974.58	487.29
	Total	**40141.56**	**10436.78**	**50578.39**	**25289.22**

Source: Vivek P & Parthasarathy N (2015) Diversity and carbon stock assessment of trees and lianas in tropical dry evergreen forest on the Coromandel Coast of India. *Tropical Plant Research 2(3): 230–239*

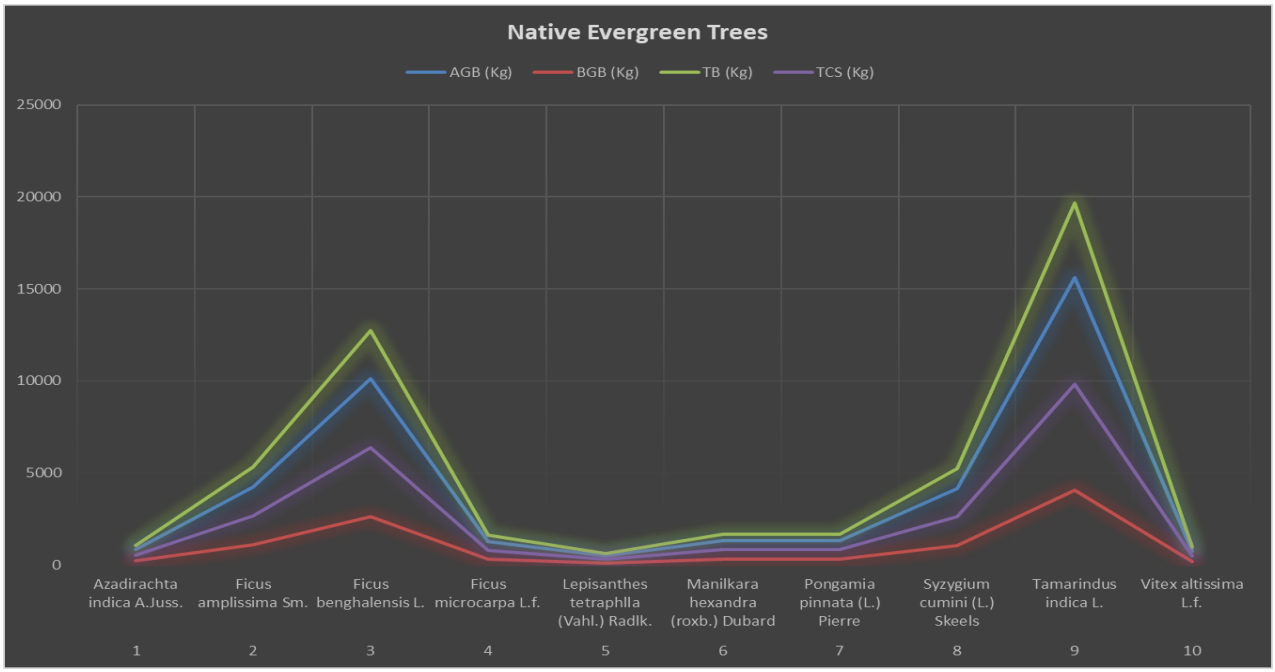


Figure 2: Graphical representation of AGB, BGB, TB and TCS values of ten dominant Native Evergreen Trees (NET)

2.0 Chi-square, Goodness of fit between AGB's of the ten dominant NDT and NET for carbon stock potential:

The chi-square, Goodness of fit is performed using the Equation – 2. The Table 4, reveals BGB, TB and TCS are 0.26, 1.26 and 0.63 times AGB. *(BGB=0.26xAGB, TB=1.26xAGB, TCS=0.63xAGB).*

Table 4 : Tabulation of AGB, BGB,TB and TCS

Species	Above Ground Biomass (Kgs)	Below Ground Biomass (Kgs)	Total Biomass (Kgs)	Total Carbon Stock (Kgs)
Native Deciduous Trees	3512.81	913.24	4426.08	2212.96
Native Evergreen Trees	40141.56	10436.78	50578.39	25289.22

Equation :

$$X^2 = \sum_{i=1}^{r} \sum_{j=1}^{c} \frac{(O_{i,j} - E_{i,j})^2}{E_{i,j}}. \qquad (2)$$

Where, **O** stands for the Observed frequency, **E** stands for the Expected frequency

Table 5 : Tabulation of Chi -square Goodness of fit between AGB of NDT and NET

Species	Observed	Expected	Difference	Difference Sq.	Difference Sq./Expected Fr.
AGB (NDT)	3513	21827.50	-18314.50	335420910.25	15366.90
AGB (NET)	40142	21827.50	18314.50	335420910.25	15366.90
					30733.80

3.0 Conclusion:

The **Chi-square,** Goodness of fit between **Above Ground Biomass of NDT** and **NET** is **30733.80,** The ***p*- value** is **< 0.00001. The result is significant at *p* < .05** (standard level for analysis). Hence, native evergreen trees have higher c-stock capacity, when compared to native deciduous trees. Thus, prove the higher carbon sequestration potential of native evergreen trees for regulating ecosystem services.

References

Cochran, William G. (1952). "The Chi-square Test of Goodness of Fit". The Annals of Mathematical Statistics. 23 (3): 315- 345. doi: 10.1214 / amos 1177729380.JSTOR 2226678

Davies, H., Doick, K., Handley, P., O'Brien, L., and Wilson, J. (2017). Delivery of ecosystem services by urban forests, Forestry Commission Research Report, Forestry Commission, Edinburgh

Vivek P & Parthasarathy N (2015) Diversity and carbon stock assessment of trees and lianas in tropical dry evergreen forest on the Coromandel Coast of India. Tropical Plant Research 2(3): 230–239

Organized By

INTERNATIONAL INSTITUTE OF INFORMATION TECHNOLOGY
HYDERABAD

Sponsored By

Gold Sponsor

COOL TOPS
Panache
Creating Cool Green Cities!

Silver Sponsor

DUPONT™

Supported By

asci
Leadership through Learning

IBPSA-INDIA

Indian Green Building Council

Global Cool Cities Alliance

NRDC

ISHRAE